UNIVERSAL
LIBRARY

OU_160300

UNIVERSAL
LIBRARY

V. SADANAND,
POST BOX No. 2447,

OSMANIA UNIVERSITY LIBRARY

Call No. 539.76/In61P Accession No. 36088

Author International Conference -- Peaceful uses of Atomic Energy.

Title Proceedings. Vol. 2. 1956

This book should be returned on or before the date last marked below.

V. SADANAND,
POST BOX No. 2447,
MADRAS-2.

PROCEEDINGS
OF THE
INTERNATIONAL CONFERENCE ON THE PEACEFUL USES OF ATOMIC ENERGY

Volume 2

PHYSICS; RESEARCH REACTORS

Proceedings of the International Conference on the Peaceful Uses of Atomic Energy

Held in Geneva
8 August-20 August 1955

Volume 2

Physics; Research Reactors

UNITED NATIONS
New York
1956

UNITED NATIONS PUBLICATION

Sales No.: 1956. IX.1. Vol.2

A/CONF.8/2

PREFACE

The Proceedings of the International Conference on the Peaceful Uses of Atomic Energy are published in a series of 16 volumes, as follows:

Volume Number	*Title*	*Sessions Included*
1	**The World's Requirements for Energy; The Role of Nuclear Power**	**2, 3.2, 4.1, 4.2, 5, 24.2.**
2	**Physics; Research Reactors**	**6A, 7A, 8A, 9A, 10A.1.**
3	**Power Reactors**	**10A.2, 3.1, 11A, 12A, 13A, 14A.**
4	**Cross Sections Important to Reactor Design**	**15A, 16A, 17A, 18A.**
5	**Physics of Reactor Design**	**19A, 20A, 21A, 22A, 23A.**
6	**Geology of Uranium and Thorium**	**6B, 7B.**
7	**Nuclear Chemistry and the Effects of Irradiation**	**8B, 9B, 10B, 11B, 12B, 13B.**
8	**Production Technology of the Materials Used for Nuclear Energy**	**14B, 15B, 16B, 17B.**
9	**Reactor Technology and Chemical Processing**	**7.3, 18B, 19B, 20B, 21B, 22B, 23B.**
10	**Radioactive Isotopes and Nuclear Radiations in Medicine**	**7.2 (Med.), 8C, 9C, 10C.**
11	**Biological Effects of Radiation**	**6.1, 11C, 12C, 13C.1.**
12	**Radioactive Isotopes and Ionizing Radiations in Agriculture, Physiology and Biochemistry**	**7.2 (Agric.), 13C.2, 14C, 15C, 16C.**
13	**Legal, Administrative, Health and Safety Aspects of Large-Scale Use of Nuclear Energy**	**4.3, 6.2, 17C, 18C.**
14	**General Aspects of the Use of Radioactive Isotopes; Dosimetry**	**7.1, 19C, 20C.**
15	**Applications of Radioactive Isotopes and Fission Products in Research and Industry**	**21C, 22C, 23C.**
16	**Record of the Conference**	**1, 24.1, 24.3.**

These volumes include all the papers submitted to the Geneva Conference, as edited by the Scientific Secretaries. The efforts of the Scientific Secretaries have been directed primarily towards scientific accuracy. Editing for style has been minimal in the interests of early publication. This may be noted especially in the English translations of certain papers submitted in French, Russian and Spanish. In a few instances, the titles of papers have been edited to reflect more accurately the content of those papers.

The editors principally responsible for the preparation of these volumes were: Robert A. Charpie, Donald J. Dewar, André Finkelstein, John Gaunt, Jacob A. Goedkoop, Elwyn O. Hughes, Leonard F. Lamerton, Aleksandar Milojević, Clifford Mosbacher, César A. Sastre, and Brian E. Urquhart.

The verbatim records of the Conference are included in the pertinent volumes. These verbatim records contain the author's corrections and, where necessary for scientific accuracy, the editing changes of the Scientific Secretaries, who have also been responsible for inserting slides, diagrams and sketches at appropriate points. In the record of each session, slides are numbered in numerical order through all presentations. Where the slide duplicates an illustration in the submitted paper, appropriate reference is made and the illustration does not appear in the record of the session.

Volume 16, "The Record of the Conference," includes the complete programme of the Conference, a numerical index of papers and an author's index, the list of delegates, the records of the opening and closing sessions and the complete texts of the evening lectures.

TABLE OF CONTENTS

Session 6A: Special Topics in Nuclear Physics

			Page
P/714	Pasechnik	Inelastic Neutron Scattering	3
P/581	Day	Gamma Rays from Inelastic Scattering	9
P/588	Walt	Angular Distribution in Inelastic Scattering	18
P/830	Weisskopf	Theory of Neutron Cross Sections	23
P/650	Spivak *et al.*	Neutron Decay	33
P/651	Groshev *et al.*	Neutron Capture Gamma Rays	39
P/941	Janik	Structure of Molecules and Liquids	54
P/870	Singwi, Kothari	Thermal Inelastic Neutron Scattering	56
P/579	Wollan, Shull	Neutron Diffraction Research	66
P/643	Nikitin *et al.*	Neutron Scattering by Deuterium	81
P/654	Nemirovski	Theory of Semitransparent Nucleus	86
P/807	McReynolds	Physics Research with Reactors	93
P/945	Wilhelmi	Cross Section of (n,p) Reaction	102
P/950	Green, Lee	Eigenvalues for Spherical Well	107
P/951	Lee, Green	IPM Mass Surface	113
P/1033	Huber, Seitz	Cross Section O^{16} $(n,\alpha)C^{13}$	121
P/1076	Ferreira, Waloschek	Excitation Levels of Be^8	124
P/1091	Ausländer *et al.*	Mass Determination in Nuclear Emulsions	132
P/1094	Titeica, Iusim	High Order Multipolar Radiation	135
P/1128	Chaudhri	High Energy Particle Accelerator	138
Record of Session			143

Session 7A: Fission Physics

P/911	Bohr	Theory of Nuclear Fission	151
P/593	Wheeler	Fission and Nuclear Theory	155
P/993	Popović	Time Involved in Fission	164
P/1089	Ausländer, Visky	Photographic Fission Tracks	165
P/897	Santos *et al.*	Nuclear Photoeffect	169
P/884	Skarsvåg	Angular Correlation of Fission Neutrons	185
P/891	Lundby *et al.*	Gamma-Rays from Fission Products	191
P/592	Leachman	Fission Quantities	193
P/652	Geilikman	Theory of Nuclear Fission	201
P/653	Nossoff	Fission Near Threshold	205
P/836	Huizenga	The Fission Process	208
P/913	Lassen	Energy Loss of Fission Fragments	214
Record of Session			220

Session 8A: Research Reactors

			Page
P/946	Kowarski	Report on Research Reactors	233
P/484	Snell	The Reactor in Basic Science	248
P/401	Bretscher *et al.*	Research Reactors	254
P/888	Barendregt *et al.*	Experience with JEEP	259
P/762	Jackson	Experience with B.E.P.O.	266
P/485	Doan, Huffman	MTR, Program and Operation	270
P/486	Ramsey, Cagle	ORNL Reactors, Program and Operation	281
P/859	McCorkle, Zinn	ANL Reactors, Program and Operation	304
P/487	Beck	Operation Raleigh Research Reactor	314
P/804	Johnson	Need for Basic Research	318
Record of Session			322

Session 9A: Research Reactors and Descriptions

P/623	Alichanov *et al.*	Heavy Water Research Reactor	331
P/387	Yvon	Saclay Reactor	337
P/915	Alder *et al.*	Swiss Research Reactor	351
P/860	Fox	Brookhaven Reactor	353
P/488	King	Water Boiler Reactors	372
P/621	Nikolaev	Reactor with Ordinary Water	392
P/622	Nikolaev	2000 kw Research Reactor	399
P/490	Weinberg *et al.*	MTR and Similar Reactors	402
P/489	Breazeale *et al.*	Swimming Pool Reactor	420
Record of Session			428

Session 10A.1: Research Reactors, Descriptions

P/620	Kruzhilin	RPT Reactor	435
P/402	Grout, Fenning	E.443	449
P/861	Zinn	ANL Reactors	456
Record of Session			471

Session 6A

SPECIAL TOPICS IN NUCLEAR PHYSICS

LIST OF PAPERS

Page

P/714 Inelastic scattering of fast neutrons by atomic nuclei .... M. V. Pasechnik 3

P/581 Gamma rays from neutron inelastic scattering .... R. B. Day 9

P/588 Angular distributions and non-elastic neutron scattering .... M. Walt 18

P/830 The theoretical prediction of neutron cross-sections of non-fissionable elements for energies up to 10 Mev .... V. F. Weisskopf 23

P/650 Investigation of neutron β decay .... P. E. Spivak *et al.* 33

P/651 Thermal-neutron capture gamma rays .... L. V. Groshev *et al.* 39

P/941 Investigation of the structure of molecules and the structure of liquids by scattering of thermal neutrons .... J. Janik 54

P/870 Thermal inelastic scattering of cold neutrons in polycrystalline solids .... K. S. Singwi and L. S. Kothari 56

P/579 Neutron diffraction research in the United States .... E. O. Wollan and C. G. Shull 66

P/643 Scattering of slow neutrons by ortho- and para-deuterium .... S. J. Nikitin *et al.* 81

P/654 The theory of semitransparent nucleus with a diffuse boundary .... P. E. Nemirovski 86

P/807 Physics research with reactors .... A. W. McReynolds 93

P/945 Cross sections of atomic nuclei for the (n,p) reaction .... Z. Wilhelmi 102

P/950 The energy eigenvalues for a spherical well with an exponentially diffuse boundary .... A. E. S. Green and K. Lee 107

P/951 The IPM mass surface .... K. Lee and A. E. S. Green 113

P/1033 $O^{16}(n,\alpha)C^{13}$ cross-section for neutrons in the energy range 3.6–4.2 Mev .... P. Huber and J. Seitz 121

P/1076 Determination of neutron spectra with nuclear plates and its application to the measurement of the Be^8 excitation levels .... E. P. Ferreira and P. J. Waloschek 124

P/1091 On mass estimation of non-relativistic charged particles in nuclear emulsions .... J. Ausländer *et al.* 132

P/1094 Notes on higher order multipolar electromagnetic radiation: Applications to nuclear physics .... S. Titeica and Ch. Iusim 135

P/1128 A high energy particle accelerator and its application to peaceful uses of atomic energy in Pakistan .... R. M. Chaudhri 138

Inelastic Scattering of Fast Neutrons by Atomic Nuclei

By M. V. Pasechnik,* Ukrainian SSR

INTRODUCTION

The process of inelastic scattering of fast neutrons has been investigated by J. I. Frenkel and V. Weisskopf by means of statistical theory nearly twenty years ago.[1] Nevertheless, due to the practical problems as well as to some reasons mentioned below, this phenomenon still attracts much interest and attention.

Firstly, most of the investigations made up to now dealt with measurements of total effective cross sections for interaction of fast neutrons with nuclei, while separate processes were not so carefully studied.

Only recently Barshal's laboratory[2] succeeded in obtaining some important data on inelastic scattering of 1-Mev neutrons by many nuclei separate from other interaction processes. Other experiments referred only to a few nuclei.[3]

Secondly, recent investigations have shown that certain difficulties involved in neutron inelastic scattering experiment resulted in contradictory data which could not be interpreted unambiguously.

A further important fact should be mentioned: the single particle model, with addition of spin-orbit coupling, is known to account well for various properties of nuclei in the ground state.[4,8,9] Simple relation between nuclear shell structure and excited energy levels near the ground state can be established from this model.[5]

Unfortunately there are very few data on the behaviour of closed shell nuclei in nuclear transformations. When our experiments were started, only data obtained by M. G. Mescherjakov and D. Hughes were at our disposal. Mescherjakov measured effective neutron capture cross sections in the region 1.5 to 2 Mev; in Hughes' experiments the neutron energy was 1 Mev. There investigations have shown that strong anomalies occurred in cross sections for nuclei with magic numbers of 82 and 126 neutrons.

Nuclear shell effects may therefore influence the probability of nuclear process even at high excitations. The problem arises how significant these effects are in other nuclear processes and at what excitation energies they vanish.

To solve this problem, systematic studies of inelastic scattering of fast neutrons in the region 2.5–14 Mev have been made in our laboratory since 1951. The results obtained by a Nuclear Physics Group of the Institute of Physics of the Academy of Science of the Ukrainian SSR (M. V. Pasechnik, V. I. Stryzak, O. F. Nemets *et al.*) are presented below.

1. EXPERIMENTAL METHOD AND APPARATUS

The analysis of the energy spectra of neutrons scattered by atomic nuclei is considered the best method for separate study of elastic and inelastic processes. The interpretation of these spectra can, in principle, give many data on these processes, including the effective cross-section values.[10] It is well known, however, that fast neutron spectrometry appears to be still in a very early stage of development.

Threshold detectors can be used to measure inelastic cross sections. Such detectors measure the probability of processes resulting in decreasing neutron flux falling upon the detector or changing its spectral composition: the latter is due to inelastic scattering of neutrons.

Neutrons with energy lower than reaction threshold will not activate the detector. Under given experimental conditions, the decrease of detector activation can serve as a measure for the probability of inelastic scattering.

Let us denote the neutron flux, falling upon N scattering centres per surface unit by $I_0(E_0)$, while the flux of neutrons scattered into unit solid angle per unit energy interval will be denoted as $I(\vartheta,E,E_0)$. The differential scattering cross section then will be given by

$$\sigma(\vartheta,E,E_0) = \frac{I(\vartheta,E,E_0)}{N I_0(E_0)}$$

The total inelastic scattering cross-section σ_{in} is obtained by integrating the differential cross-section data over angles and energies.

Practically, the measurements of inelastic scattering cross sections can be simplified by proper choice of scatterer and detector geometry as well as their arrangement. The problem is to choose the proper experimental conditions with the scatterer between the source and the detector measuring only unscattered and elastically scattered neutrons. These are achieved when the scatterer has the form of a spherical layer and the detector is a point detector. A good approximation to these conditions is achieved by a thin spherical scatterer with a spherical detector of finite size.

In the real measurements, a thick spherical layer is used with inner radius equal to the detector radius. In

---

Original language: Russian.

* This paper is based on work done in 1951 54 by M. V. Pasechnik, W. Stryzak, O. Nemets, B. Wertebny and V. Batalin.

this case the attenuation of the neutron flux as well as asymmetry of elastic scattering must be taken into account. Corrections for these effects are found by means of calculations. Figure 1 shows the experimental arrangement under various conditions of monitoring the neutron flux.

The threshold detector must have the following properties:

1. The reaction threshold must be lower than the source neutron energy but very close to it in order to detect a minimum number of inelastically scattered neutrons; this is especially important in the case of a continuous spectrum of inelastically scattered neutrons.

2. The reaction cross section must grow rapidly with neutron energy near the threshold. For neutron energy higher than energy threshold of the reaction, the reaction effective cross section must be constant.

We have used the reactions $P^{30}(n,p)$; $Al^{27}(n,p)$ and $S^{32}(n,p)$ as well as $Cu^{63}(n,2n)$.

These detectors fulfil the aforementioned requirements better than any others. They are especially suitable for our measurement procedure. The half-lives were measured in order to check the purity of the detectors. The effect of the activities induced by slow neutrons was eliminated by surrounding the detector with a thin cadmium shield.

The activity measurements were made with Geiger-Müller counters. The counting rate was taken before and after the measurements in order to verify the stability of counter performance.

The scatterers were made in the form of spherical layers consisting of two hemispheres. Most of the scatterers were machined of a solid piece of metal. Liquid and powdered materials were placed in 0.02-in. thick copper containers. Strongly oxidizing substances (sodium, barium) were enclosed in airtight containers. The thickness of the scattering layer was 0.8 to 1 inch.

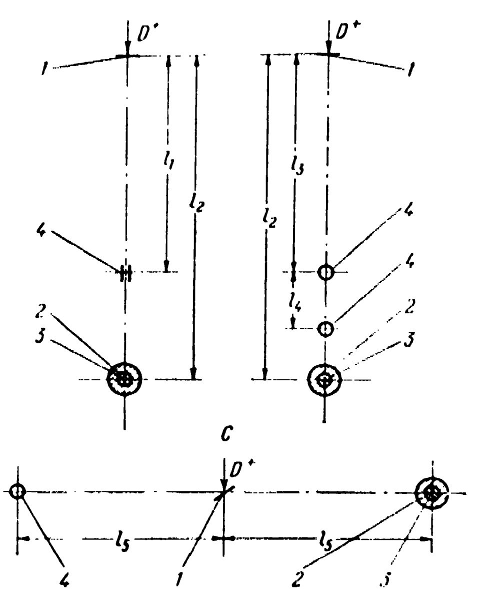

Figure 1. The experimental arrangements for measuring inelastic scattering cross sections: (1) target; (2) scatterer; and (3) detector; (4) monitor; (5) $l_1 = 18$, $l_2 = 30$, $l_3 = 19$, $l_4 = 24$, $l_5 = 18$ for 2.5-Mev neutrons and $l_3 = 30$ for 14-Mev neutrons

The $D(d,n)He^3$ and $D(T,n)He^4$ reactions served as neutron sources. The deuterons were accelerated in the accelerating tube of an electrostatic generator and in a low voltage neutron generator. Voltage stability was within 1%. The deuterium ions accelerated in the ion tube were focused on a heavy ice target. Heavy ice was obtained by precipitating heavy water vapour on silver backing, cooled with liquid nitrogen. The tritium target was prepared by absorption of tritium on a zirconium foil at high temperature. The composition of the primary beam was checked by means of nuclear emulsions.

2. CROSS SECTIONS FOR INELASTIC SCATTERING OF 2.5, 3.3, 4.1 AND 14-MEV NEUTRONS

The effective inelastic scattering cross sections of neutrons of various energies were measured for many elements by means of the above described method. As is known, the cross section σ_{in} is given by

$$\sigma_{in} = -\frac{1}{Nx}\ln\frac{A}{A_1}$$

where N is the number of atoms per cm^3 of the scatterer, x is the mean neutron path in the scatterer, which is determined by the geometry of the experimental arrangement, while A and A_1 are the detector activities with scatterer in position and without scatterer respectively.

Phosphorus was used as a threshold detector to measure the inelastic cross section of 2.5-Mev neutrons. The effective energy threshold for the reaction $P^{30}(n,p)Si^{30}$ is 1.7 Mev. Radioactive silicon from the reaction has a half-life equal to 170 min, with an end point of the beta spectrum of 1.8 Mev.

The measurements were done as follows: Two detectors (with and without scatterer) were placed in the holders in symmetric positions with respect to the target. After 45–90 min exposure the activity of each detector was measured. The next run of experiments was made with the positions of the first and second detector interchanged so as to eliminate the error due to a difference in the distance between source and detector. Then counter positions were interchanged to exclude a possible difference in the counter efficiencies.

An aluminium detector was used in the experiments with 3.3 and 4.1-Mev neutrons. The half-life of the Mg^{27} resulting from the (n,p) reaction is 10 minutes.

For each element from 8 to 20 measurements were performed, depending on the attenuation of the neutron beam. This procedure reduces the statistical errors to less than 1.5%.

The reaction $Cu^{63}(n,2n)Cu^{62}$, with a 12.5-Mev effective threshold, was used as detector in experiments with 14-Mev neutrons.

The experimental results are presented in Table 1 on the following page.

Table 1. Cross Sections for Inelastic Scattering of Neutrons

Scatterer 1	*2.5 Mev*† 2	*2.5 Mev** 3	*3.3 Mev* 4	*4.1 Mev* 5	*14 Mev* 6
Carbon	—	—	—		0.63 ± 0.05
Sodium	0.53 ± 0.26	—	—	0.57	—
Magnesium	0.77 ± 0.25	—	—	0.78 ± 0.20	1.08 ± 0.09
Aluminium	0.96 ± 0.17	—	0.81 ± 0.20	0.78 ± 0.20	1.13 ± 0.07
Phosphorus	0.7 ± 0.2	—	—		—
Sulphur	0.54 ± 0.21		—		—
Chlorine	0.6 ± 0.3	—	—	0.90 ± 0.3	—
Calcium	0.4 ± 0.2	—	—	—	—
Chromium	1.4 ± 0.3	—	—	—	—
Iron	1.16 ±	—	1.51 ± 0.21	1.58 ± 0.30	1.29 ± 0.07
Cobalt	1.40 ± 0.11	—	—	—	—
Nickel	0.83 ± 0.12	—	1.35 ± 0.25	—	1.38 ± 0.05
Copper	1.58 ± 0.15		1.67 ± 0.24	1.68 ± 0.25	1.35 ± 0.05
Zinc	2.18 ± 0.5		2.18	1.58 ± 0.3	1.37 ± 0.07
Selenium	1.88 ± 0.17	—	—	—	1.40 ± 0.23
Molybdenum	1.9 ± 0.3	—	—	—	—
Silver	2.13 ± 0.18	—	—	—	
Cadmium	2.21 ± 0.20	2.1 ± 0.2	2.35 ± 0.35	2.3 ± 0.3	1.83 ± 0.13
Tin	—	1.65 ± 0.3	1.73 ± 0.15	2.11 ± 0.3	1.81 ± 0.13
Antimony	1.88 ± 0.20	2.11 ± 0.20	2.11 ± 0.20	2.13 ± 0.3	1.90 ± 0.16
Tellurium	2.0 ± 0.35	—	—		1.97 ± 0.27
Iodine	1.96 ± 0.25		—		1.88 ± 0.16
Barium		0.8 ± 0.5	1.3 ± 0.4	2.2 ± 0.4	
Tungsten	2.6 ± 0.25	—			2.35 ± 0.14
Mercury	2.6 ± 0.3	—	2.99 ± 0.3	3.36 ± 0.3	—
Lead	1.69 ± 0.32		—	1.72 ± 0.3	2.42 ± 0.09
Bismuth	0.62 ± 0.29	—	0.62 ± 0.5	1.14 ± 0.40	2.44 ± 0.13

* Second run of measurements. † See reference 10.

3. SPECTRA OF SCATTERED NEUTRONS AT $E_n = 2.75$ Mev

The energy spectrum of fast neutrons scattered by atomic nuclei was investigated by means of several methods based on the measurements of the energy distribution of recoil protons. It is known that *n-p* scattering is isotropic in the centre-of-mass system for energies up to about 10 Mev and nearly isotropic for energies up to 20 Mev. The neutron spectrum can be found by differentiating the recoil proton energy distribution $P(E)$.

Let $N(E)\,dE$ be the number of neutrons having energies in the interval E, $E + dE$, and $P(E)\,dE$ the number of protons in the same energy interval. Then

$$N(E) = -\frac{E}{n\sigma(E)x}\frac{dP(E)}{dE}$$

where n is the number of nuclei per cm^3, $\sigma(E)$ the *n-p* scattering cross section, and x the mean path of neutrons in the scatterer.

The basic measurements were performed by using a fast neutron spectrometer with a pulse ionization chamber as the detector of fast neutrons. Its output pulses were fed through a preamplifier and linear amplifier to a 50-channel pulse height analyzer. A mechanical register counted the number of pulses in each channel.

The ionization chamber was filled with the mixture of hydrogen (1 atm) and argon (4 atm). To obtain complete electron collection, careful chemical purification and long-term testing were performed. Corrections for induction and wall effects were calculated theoretically.[11]

The preamplifier was mounted together with the chamber on a cylindrical chassis. The preamplifier band width was 1.5 Mc, chosen in accordance with the duration of the chamber output pulses. This band width gave the most favourable signal-to-noise ratio with minimum pulse distortion.

The main amplifier was a three-stage unit with cathode followers at the input and output. It delivered undisturbed pulses up to 100 volts.

To investigate the pulse height distribution, multichannel pulse height analyzers of the amplitude-time transformation type were used. Being relatively simple, these analyzers possess good discrimination level stability, satisfactory linearity and a great number of channels.

The alpha-spectrum of natural uranium was measured in order to test the resolution of the whole unit. The 4.76-Mev and 4.18-Mev lines are the most intense lines in that spectrum. As seen from the spectrogram in Fig. 2(*a*), these two lines are well resolved, the half-width of the 4.76-Mev line being 3.1%. This alpha-spectrum was measured repeatedly to check both reliability of the apparatus and its resolution for each set of measurements of the proton spectrum.

The resolution of the neutron spectrometer was determined by measuring the spectrum of the neutron beam leaving the target at 90 degrees with respect to the direction of the incident deuteron beam. Figure 2(*b*) shows one of these spectrograms. The half-width of the peak is 150 kev at 2.5-Mev neutron energy; the

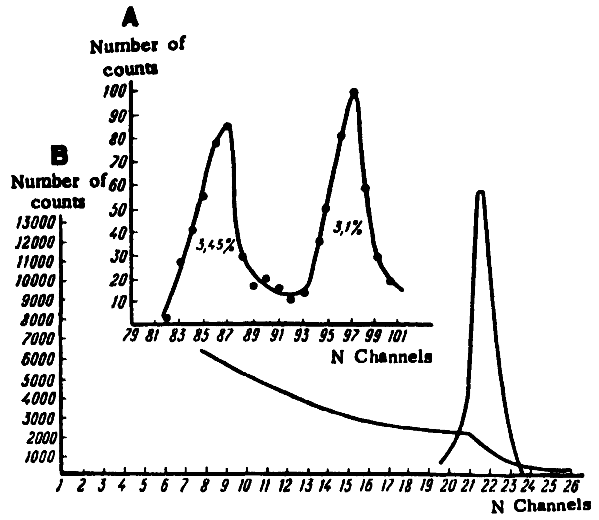

Figure 2. Alpha-particle spectrum (a), and direct neutron beam spectrum (b)

energy spread of the primary neutron beam is 120 kev. The resolution of the spectrometer at 2.5-Mev neutron energy is therefore 6%.

Figure 3 shows the arrangement of scatterer and chamber. The torroidal shape of the scatterers ensures the maximum number of scattering centers receiving the same energy range of incident neutrons and minimum multiple-scattering as compared with other scatterer shapes.

We were also interested in partial inelastic scattering cross section. Consequently three runs of measurements were made in each series: (*a*) measurement of the neutron flux falling from the source on the chamber; (*b*) measurement of the scattered neutrons with the direct beam being intercepted by the paraffin shield inserted between source and chamber; and (*c*) measurement of background neutrons.

The scattering angle was 90 degrees in almost all measurements.

If the neutron spectrum consists of several groups, the ideal recoil proton spectrum should be a well-pronounced step curve. Induction and wall effects in the chamber, however, smooth out the curve. Figure 4 shows one of the spectrograms (for iron) as an example, the experimental data being given by a broken curve and the corrected ones by a solid curve.

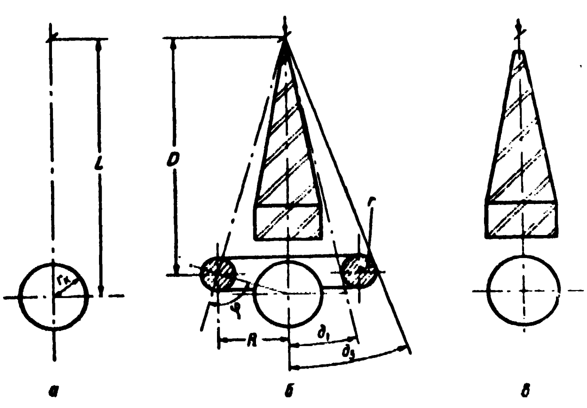

Figure 3. The experimental arrangement for observing scattered neutron spectra

Besides proton recoils, argon recoil nuclei as well as gamma-ray pulses were observed in the low-energy region. The initial part of the experimental curve was therefore especially distorted. In evaluating the experimental data the initial part of the curve had to be cut off up to 600 kev.

The principal results for a number of nuclei are given below. The investigation of other spectra is still in progress.

Magnesium

Three levels, at 0.8 ± 0.12; 1.29 ± 0.12 and 1.55 ± 0.12 Mev, have been identified from the inelastically scattered neutron spectrum, which was obtained as the result of 16 series of measurements. The energy values are confirmed to within the experimental accuracies by other investigators.[12,13,14]

Aluminium

Three levels have been found, at 1.00 ± 0.12; 1.36 ± 0.12 and 1.60 ± 0.12 Mev. These data are in agreement with the data obtained by other authors.

Sulphur

The scattered neutron spectrum does not differ from that of the direct beam neutrons. This result is in good agreement with other data according to which the 2.25-Mev level is the lowest excited level of the principal isotope S^{32}. Lower levels observed by other methods are due to isotopes S^{33} and S^{34}, but their natural abundance is too small (0.75 and 4.2%, respectively) to expect a noticeable change in the scattered neutron spectrum.

Iron

The spectrum of scattered neutrons consists of two sharply defined groups with energies of 1.87 ± 0.12 and 2.75 ± 0.10 Mev, which indicate the existence of one level 0.9 ± 0.12 Mev. This level can be assigned to the isotope Fe^{56}, the natural abundance of which is 91.6%.

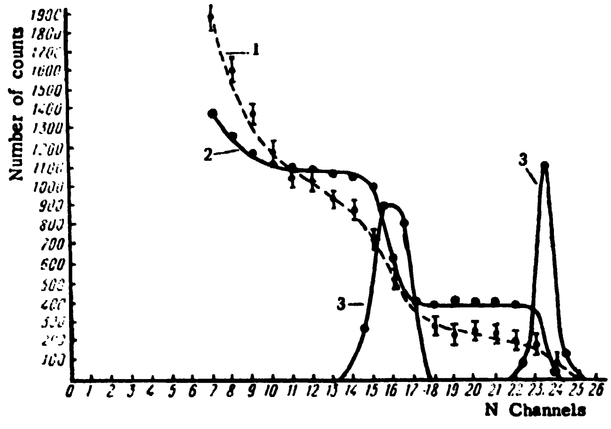

Figure 4. The spectrogram for iron: (1) experimental curve; (2) theoretical curve; and (3) neutron groups

The 2.75-Mev group is the result of elastic scattering of neutrons. The value for the level energy 0.90 ± 0.12 Mev agrees well with the data obtained by other methods, in particular by studying gamma-ray spectrum accompanying inelastic scattering of neutrons.

Copper

The recoil proton spectrum obtained in studying neutron scattering by copper has three steps, corresponding to two nuclear levels and elastically scattered neutrons. In addition to the 1-Mev level observed by other authors, a level at 1.40 ± 0.12 Mev was also found. This level was not known before; therefore the measurements were repeated several times. Similar results were reported[13] soon after our measurements.

Zinc

The spectrum of scattered neutron was not resolved in separate groups.

Cadmium

The spectrum of neutrons scattered by cadmium was never measured before. Energy levels have been found at 0.86 ± 0.12, 1.27 ± 0.12, 1.63 ± 0.12, and 1.84 ± 0.12 Mev.

Lead

The spectrum of the scattered neutrons consists of one group of 1.7 Mev energy. Above this energy lines are not resolved. By comparing the spectrum of the scattered neutron with the direct beam spectrum, the number of inelastic scattering events was shown to be a negligible fraction of that of elastic collisions.

Bismuth

The recoil proton distribution curve shows four well-defined steps. By differentiating we obtain four groups of neutrons. The first three of them correspond to inelastic scattering of neutrons (levels at 1, 1.5, and 1.9 Mev). Our data were confirmed by the investigations of other authors.[16]

This result proves once again that the nuclei with magic numbers of neutrons have high first excited levels as well as large level spacing.

The fact that this was not observed in the case of lead can be explained by the isotopic composition of the natural material. The natural abundance of isotope with neutron number 126 is known to amount to only 52.3%.

4. NEUTRON INELASTIC SCATTERING AND THE NUCLEAR SHELL MODEL

The analysis of experimental data permits drawing of some preliminary conclusions.

1. The effective cross sections for inelastic scattering of 2 to 4 Mev neutrons by all nuclei, except those having magic numbers of nucleons, increase smoothly with mass number approximately according to the $\sigma_{in} \sim A^{2/3}$ law.

The theoretical treatment of this dependence has been given by P. E. Nemirovsky, who extended the Feschbach-Porter-Weisskopf semitransparent nucleus model by introduction of a potential well with rounded edges instead of rectangular ones.

2. The inelastic scattering cross sections of nuclei with neutron numbers of 50, 82, and 126 are considerably lower than those of other nuclei in the same neutron energy region.

3. The data obtained cannot prove definitely a similar deviation for nuclei having a proton number of 50 in the neutron energy range from 2 to 3 Mev. In inelastic scattering, as elsewhere, the effects of closed proton shells are probably weaker than those of closed neutron shells.

4. In the intermediate neutron energy region (1 Mev) effective inelastic scattering cross sections show strong variation from one group to another. In this region there is no simple dependence of σ_{in} on mass number, but in this case too cross sections of magic number nuclei are small.

5. The higher the mass number, the stronger the anomalies in inelastic scattering cross sections values. This means that the nuclear shell effects are stronger for nuclei with a great number of nucleons, in agreement with data on neutron binding energies for nuclei with neutron numbers of 51, 83 and 127.

6. Cross sections for magic nuclei increase with neutron energy. For example, the effective inelastic scattering cross section of bismuth at 1 Mev is several tens times lower than that of the neighbouring nuclei, while at 2.5 Mev it is only 5 times lower, and at an energy of 4 Mev only 1.5 to 2 times.

7. The inelastic scattering of 14-Mev neutrons shows no deviation from smooth dependence within the experimental accuracy. It would be of great interest to perform measurements on inelastic scattering cross sections for magic nuclei in the neutron energy region from 5 to 10 Mev. It would make possible the determination of the excitation energy at which the effect of closed shells on neutron inelastic scattering vanishes.

8. The measurements of energy distributions of scattered neutrons confirm the spectroscopic data on nuclear energy levels. The first excited level of nuclei with magic numbers of neutrons and/or protons is higher than that of other nuclei. This conclusion is confirmed by the direct measurements of level position by studying gamma-ray spectra accompanying the inelastic scattering of neutrons.

It must be stressed that the above data do not stand by themselves in nuclear dynamics. Closed shell effects have been found recently in other phenomena. Among those must first of all be mentioned the anomalies in fast and slow neutron radiative capture cross sections. These anomalies must be explained in terms of nuclear level distribution.[16]

REFERENCES

1. Frenkel, Y. I., Sov. Phys. *9*, 533, (1936); Weisskopf, V., Phys. Rev., *52*, 295, (1937).
2. Barschall, H. H. and Walt, M., Phys. Rev., *93*, 1063 (1954); *90*, 714, (1955).

3. Barschall, H. H., *et al.*, Phys. Rev., *72*, 875, 881, (1947); Grace, M. and Beghian, L., Phys. Rev., *82*, 965, (1951); Stelson, P. H. and Preston, W. H., Phys. Rev., *86*, 132, (1952); Poole, M., Phil. Mag., *43*, 1060, (1952), *44*, 1398 (1953).

4. Korsunsky, M. I., Ach. phys. sci., *52*, b. 1, (1954); Mayer, M. G., Phys. Rev., *74*, 235, (1948), *75*, 1969 (1949); *78*, 16, 22, (1950); Feenberg, E., Hammak, K. C., Phys. Rev., *75*, 1877, (1949) *77*, 771, (1950).

5. Sliv, A., *et al.*, Reports Ac. Sci. USSR, *88*, 781, (1953), *92*, 277, (1953), *94*, 849, (1954).

6. Meshcheryakov, M. G., Reports Ac. Sci. USSR, *48*, 583, (1945).

7. Hughes, D., Phys. Rev., *91*, 1423, (1953).

8. Ivanenko, D. D., Reports Ac. Sci. USSR, *100*, 37, (1955).

9. Bohr, A., Dan. Mat. Fys. Medd. *26*, 14, (1952); Bohr, A., Mottelson, B. R., Dan. Mat. Fys. Medd. *27*, 16, (1953).

10. Strizhak, V. I., Dissertation, Inst. Phys. Ukr. SSR, (1952).

11. Nemets, O. F., Dissertation, Inst. Phys. Ukr. SSR, (1954).

12. Nemilov, U. A., Gedeonov, L. I., Reports Ac. Sci. USSR, *63*, 115, (1948).

13. Grace, M., *et al.*, Phys. Rev., *82*, 969, (1951); Beghian, L., *et al.*, Phys. Rev., *77*, 286, 1950.

14. Littl, R. N., Long, R. W., Mandeville, C. E., Phys. Rev., *69*, 414 (1946).

15. Pool, M., Phys. Mag. *43*, 1060 (1952), *44*, (1936), (1953).

16. Groshev, L. V., Reports Ac. Sci. USSR, *100*, 651, (1955); Kinsey, B. B., Bartholomew, G. A., Phys. Rev., *80*, 918, (1950); *89*, 375, 386, (1953).

Gamma Rays from Neutron Inelastic Scattering

By Robert B. Day,* USA

Until the very recent development of time-of-flight techniques for the millimicrosecond range[1] there has been no really satisfactory way of measuring the neutron spectra from inelastic scattering reactions. Photographic plates have provided a means of doing this, but they have a low efficiency and have, in addition, the disadvantage that a great deal of labor is involved in the plate reading. Other methods, which generally depend on the detection of proton recoils produced in a hydrogenous radiator, also have very low efficiency. An exception is the use of an organic crystal scintillation counter, which has good efficiency, but here one obtains an integral spectrum and it has proved difficult to get good neutron spectra from differentiating its pulse-height distribution.

In view of the difficulties involved in measuring fast neutron spectra one might look for alternative ways of measuring cross sections for neutron inelastic scattering. In many cases the states of a target nucleus that are excited by inelastic scattering decay by gamma emission. Since the NaI gamma-ray scintillation spectrometer provides fair resolution and good efficiency, its use is suggested in measuring the gamma-ray spectra accompanying neutron inelastic scattering. If one knows, or can measure, the decay scheme of the levels involved, then it is possible to deduce the neutron spectrum from the gamma-ray spectrum. In addition, the gamma-ray spectrum is of great importance in the design of reactor shields because of the gamma rays produced in the shields by inelastic scattering of fast neutrons.

For levels that are high enough to be unstable to particle emission this method is of little value since the relative probability of gamma emission is generally so low that the gamma rays will not be detected above the background. There are, of course, examples of unbound levels where particle emission is forbidden, but these are few. An additional difficulty occurs for low-lying levels that may be highly internally converted. Since the internal conversion electrons are largely absorbed in the neutron scatterer, transitions of this type are difficult to detect. These considerations indicate that the usefulness of gamma-ray spectra in deducing the spectra of inelastically scattered neutrons will be greatest in the lighter elements and for incident neutron energies below the neutron binding energy.

In the succeeding sections a description is given of the various experimental methods that have been used in the United States for the detection of gamma rays accompanying neutron inelastic scattering. This is followed by a discussion of the problems involved in measuring the cross sections for gamma-ray production and examples of some of the results obtained.

EXPERIMENTAL METHODS

In all of the experiments being reported a NaI(Tl) scintillation spectrometer has been used as the gamma-ray detector. In the most common experimental arrangement this detector is shielded from the direct flux from the neutron source by a cone of suitable material, such as Pb, W, etc., and is surrounded by a ring of the element to be investigated (Fig. 1). When the ring is bombarded by neutrons, the gamma rays emitted are detected with good efficiency in the NaI counter. The advantage of this arrangement is that a greater mass of the scatterer can be used than is possible in the other methods to be described, while still maintaining a good gamma-ray detection efficiency and minimizing gamma-ray absorption in the scatterer.

A second method has utilized the "associated-particle" technique.[2] Here the associated particle that is produced in the source at the same time as the neutron, e.g., the alpha particle in the reaction $H^3(d,n)He^4$, is used to define a beam of neutrons falling on the scatterer. A coincidence between the associated particle detector and gamma-ray detector indicates that the inelastic event has been induced by a neutron coming directly from the source. This method is very useful in reducing the background from room-scattered neutrons and from neutrons produced in other places than the source reaction. Its usefulness where these are not the important sources of background is correspondingly reduced.

Since the associated particle method is difficult to use with the reactions $H^3(p,n)He^3$ or $Li^7(p,n)Be^7$ as as the neutron sources, a collimator, such as the one described by Stelson and Preston,[3] can be used to obtain a well-defined beam of neutrons. The difficulty here is that the collimator may alter the primary neutron spectrum; however, experiments indicate that the number of neutrons degraded in energy is less than

---

* Los Alamos Scientific Laboratory. This paper is based on work by: G. L. Griffith, Westinghouse Research Laboratories; T. M. Hahn, University of Kentucky; F. L. Hereford, University of Virginia; R. M. Kiehn and A. Wattenberg, Massachusetts Institute of Technology; D. A. Lind, University of Wisconsin; C. E. Mandeville, Bartol Research Foundation; J. R. Risser, The Rice Institute; V. E. Scherrer, Naval Research Laboratory; and R. B. Day, Los Alamos Scientific Laboratory.

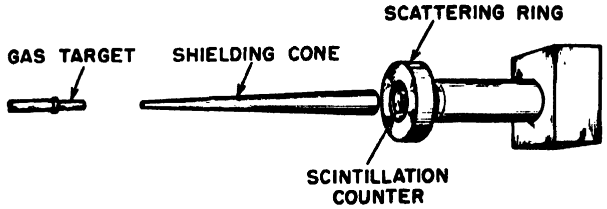

Figure 1. A typical experimental arrangement employing the ring geometry

10 per cent. It is also necessary in measuring cross sections to consider the increase in neutron flux produced by scattering from the walls of the collimator, but this can be measured rather easily.

In many cases the greatest contribution to the background of the gamma-ray detector arises from neutrons that are scattered from the scattering sample into the detector, where they produce gamma rays by inelastic scattering, capture, etc. One way of eliminating this effect is to use a second counter to detect the inelastically scattered neutrons and to require a coïncidence between these neutrons and the gamma rays accompanying them.[4] Although this procedure greatly reduces the detection efficiency, it may prove necessary in cases where the NaI background has a peak at the same energy as the element under investigation. Cranberg has suggested that a modification of the time-of-flight technique might also be used in eliminating this type of background.

With high neutron bombarding energies the pulse-height spectra are often so complicated that their interpretation is very difficult. Battat[5] has attacked this problem by employing a three-crystal pair spectrometer in investigations of the gamma rays from neutron inelastic scattering at 14 Mev. Since with this instrument one obtains just a single peak in the pulse-height distribution for each gamma ray, the interpretation of the pulse-height spectrum is much simpler than it is for the single-crystal NaI spectrometer; however, this method suffers the disadvantage of having a much lower efficiency than that for the single-crystal spectrometer.

Because of the backgrounds produced by neutrons, it is possible to get information on the gamma-ray spectrum from inelastic scattering only by a detailed examination of the pulse-height spectrum produced by the counter. An example of the background effects to be found[6] is shown in Fig. 2, which gives the pulse-height distributions produced in a NaI counter by neutrons of various energies. The counter was set up as shown in Fig. 1 and surrounded by a graphite ring, which for these neutron energies will produce no gamma rays. Thus, the spectra of Fig. 2 are due entirely to the room background and to effects produced by neutrons scattered into the NaI crystal by the ring. From a comparison of the two curves for a neutron energy of 2.64 Mev it can be seen that over half the background is caused by neutrons from the scatterer.

When a scattering sample of the element to be investigated is substituted for the graphite ring, the pulse-height spectrum produced by the inelastic scattering gamma rays is superimposed on the background spectrum discussed above. An example[6] is shown in Fig. 3, which gives the pulse-height distribution for Teflon (CF_2). The characteristic photopeaks produced by gamma rays from F^{19} are identified; the other peaks are background or Compton peaks. It will be observed that for strong gamma rays, such as the two low-energy ones shown in Fig. 3a, the signal to background ratio is fairly good, hence the intensity of those lines can be easily measured.

The question of the optimum size NaI crystal re-

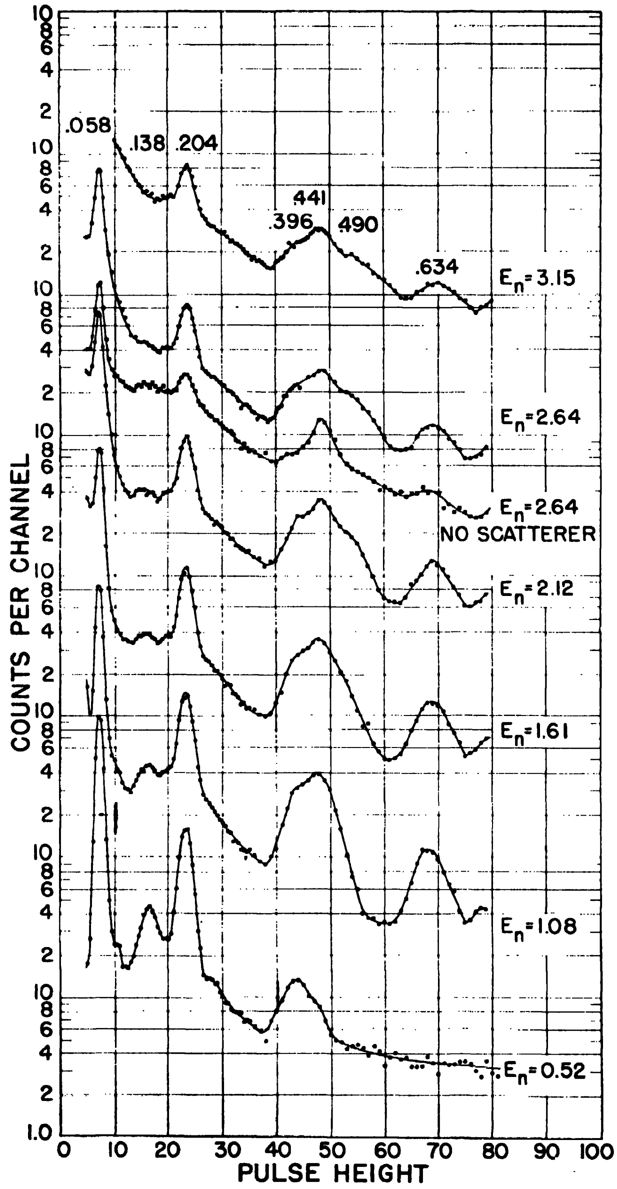

Figure 2. Low-energy background pulse-height distribution produced by neutrons of the energies shown, normalized to a constant neutron flux incident on the scatterer. A carbon ring scatterer was used in the arrangement illustrated in Fig. 1. Photopeak energies are given in Mev just above the top curve. The ordinate changes by a factor of 10 for each energy; however, the same scale is used for the two curves at $E_n = 2.64$ Mev

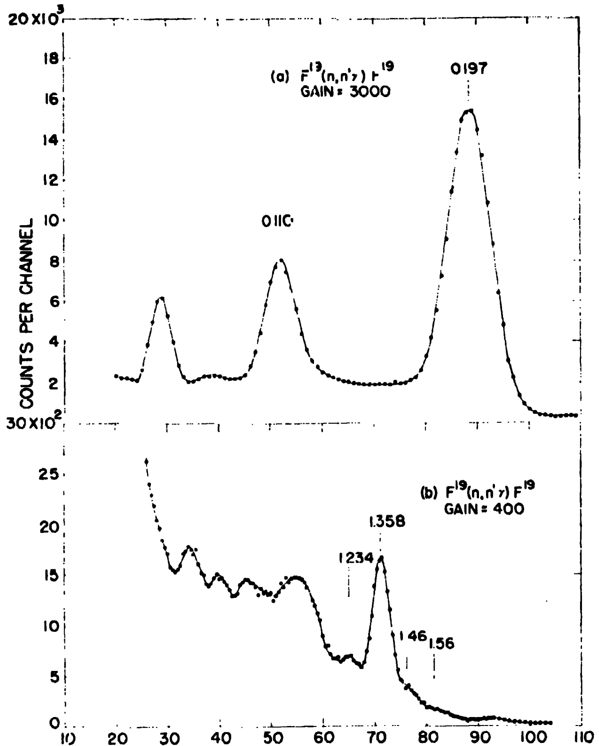

Figure 3. Pulse-height distributions obtained with a Teflon ring scatterer (CF_2). The photopeaks of the gamma rays produced in F^{19} are identified by their energies in Mev. The amplifier gain has been changed in the two pulse-height distributions

quired to maximize the signal to background ratio has not been completely settled. Since the gamma-ray cross section of NaI is greater than the total neutron cross section, one would think that a small crystal would be best. This is undoubtedly true at low gamma-ray energies; however, at higher energies the enhancement of the photopeak by multiple Compton scattering in the crystal may be great enough for large crystals to overcome their disadvantage of relatively larger neutron absorption In most cases it appears that large crystals have been preferred, perhaps because of their higher detection efficiency.

GAMMA-RAY ENERGY MEASUREMENTS AND ENERGY LEVELS

With NaI scintillation spectrometers used in experiments on radio-nuclides it has been possible to measure gamma-ray energies to better than one per cent accuracy. Although the background conditions are less favorable in neutron inelastic scattering experiments, this accuracy is often possible here because the high counting rates often found for neutron excitation of gamma rays permit good statistical accuracy to be obtained in the pulse-height distribution. It has been found possible for many gamma rays occurring in neutron inelastic scattering reactions to reproduce the position of the photopeak to within a few tenths of a per cent; thus the determination of the energy of the gamma ray is limited by the accuracy with which the pulse-height *versus* energy calibration is known. Techniques for eliminating the effects of any non-linearity in the amplifier and pulse-height analyzer are easily applied. In addition, one must also consider the possibilities of non-linear effects in the crystal and photomultiplier. These effects can be taken into account by a careful pulse-height calibration with gamma rays of known energy.

From a comparison of the measured gamma-ray energies with level energies already known from other experiments it is often possible to identify the levels that are excited by neutron inelastic scattering, and thus to deduce the neutron spectrum. For those elements where the spectrum is complicated because of the existence of several isotopes or many levels this identification is greatly aided by accurate energy measurements. The availability of separated isotopes in quantities of the order of ten grams or more is also of value here. For example, Sinclair[7] has been able to show by using an iron sample enriched in Fe^{54}. That the 1.41-Mev gamma ray observed in iron originates in Fe^{54}. This had already been suspected from the systematics of the energy levels in even-even nuclei.[8]

As an example of the results obtained, Table I lists the gamma rays observed for a number of elements.[6] Most of these gamma rays were excited by neutrons of 2.56 Mev, although in several elements where the energy of the first level was known to be higher than 2.56 Mev, neutrons of energy up to 7 Mev were used. Note that a few cases of $(n,p'\gamma)$ and $(n,\alpha'\gamma)$ reactions have been observed here.

The results on Bi are particularly interesting since it has not previously been possible to obtain information on the excited states of Bi^{209} from other reactions or from radioactive decay. The accuracy of the measurements is such as to exclude the possibility that the two lower-energy gamma rays are in cascade from a 2.6 Mev level. Furthermore, the excitation functions for these gamma rays, to be discussed later, show that they originate in the decay of excited states at 0.9 and 1.6 Mev. The energies of the inelastically scattered neutrons are obtained by subtracting the gamma-ray energies from the incident neutron energy, while the cross sections for producing these neutron groups are equal to the cross sections for exciting the gamma rays.

Some results[6] on inelastic scattering in Ca are also of considerable interest. Among other gamma rays observed (Fig. 4) is one of 0.508 ± 0.005 Mev, whose energy is so close to that for annihilation radiation that there is a strong presumption that it arises from positron annihilation. Its intensity is of the order of one hundred times too great to come from external pair formation by high-energy gamma rays. Experiments have shown that the half-life of the gamma ray is less than 0.5 second; furthermore, no positron-emitting nuclides are known that can be formed by neutrons of the energy used in these experiments on calcium. Thus it seems quite likely that this radiation comes from the decay of positrons emitted in the de-excitation of a state of Ca^{40} by nuclear pair emission. This conclusion is strengthened by the fact that the

Table 1. Gamma Rays from Neutron Inelastic Scattering. In the Second Column the Isotope Emitting the Gamma Ray Is Given, Where It Can Be Identified. A Comparison with the Energies Obtained from Other Reactions and from Radioactive Decay Is Given in the Fourth Column

Element	*Isotope*	*Eγ (Mev)*	*Comparison*	*Reference*
Beryllium	Be^9	None		
Boron	Li^7	0.478 ± 0.004	0.477	a
	B^{10}	0.717 ± 0.007	0.719	b
Carbon	C^{12}	4.42 ± 0.03	4.43	a
Nitrogen	N^{14}	2.30 ± 0.05	2.31	a
Oxygen	O^{16}	6.094 ± 0.06	6.14	a
Fluorine	F^{19}	0.110 ± 0.001	0.110	a
	F^{19}	0.197 ± 0.002	0.197	a
	F^{19}	1.234 ± 0.020		
	F^{19}	1.358 ± 0.010	1.35	a
	F^{19}	1.46 ± 0.03		
	F^{19}	1.56 ± 0.03	1.57	a
Magnesium	Mg^{24}	1.368 ± 0.01	1.368	c
	Mg^{25}	1.616 ± 0.016	1.612	c
	Mg^{26}	1.820 ± 0.018	1.825	c
Aluminum	Al^{27}	0.166 ± 0.003		
	Al^{27}	0.840 ± 0.008	0.843	c
	Al^{27}	1.017 ± 0.010	1.013	c
	Al^{27}	2.21 ± 0.020	2.211	c
Sulfur	P^{32}	0.077 ± 0.002	0.077	c
	S^{32}	2.23 ± 0.020	2.25	c
Calcium	K^{40}	0.0275 ± 0.0015	0.032	e
	Ca^{40}	0.508 ± 0.005	0.51094	d
	K^{40}	0.767 ± 0.007	0.768	e
	K^{40}	0.877 ± 0.017	0.861	e
	Ca^{44}	1.152 ± 0.020	1.16	e
	Ca^{40}	3.74 ± 0.03	3.731	e
	Ca^{40}	3.9 ± 0.1	3.900	e
Iron	Fe^{57}	0.123 ± 0.0012	0.1228	e
	Fe^{56}	0.847 ± 0.008	0.845	f
	Fe^{56}	1.241 ± 0.012	1.24	f
	Fe^{54}	1.405 ± 0.010	1.413	g
Nickel	Ni^{60}	0.827 ± 0.008	0.85	h
	Ni^{60}	1.329 ± 0.010	1.3325	i
	Ni^{58}	1.453 ± 0.014	1.453	i
	Ni^{60}	2.18 ± 0.04	2.13	h
Copper	Cu^{65}	0.365 ± 0.005	0.37	k
	Cu^{63}	0.651 ± 0.006	0.669	j
		0.764 ± 0.010		
	Cu^{63}	0.958 ± 0.010	0.968	j
	Cu^{65}	1.110 ± 0.010	1.12	k
	Cu^{63}	1.325 ± 0.010	1.326	j
	Cu^{63}	1.41 ± 0.03	1.410	j
	Cu^{65}	1.47 ± 0.03	1.49	k
	Cu^{63}	1.55 ± 0.03	1.549	j
	Cu^{63}	1.88 ± 0.04	1.89	l
		2.07 ± 0.02		
	Cu^{63}	2.52 ± 0.03	2.60	l
Tantalum	Ta^{181}	0.137 ± 0.002	0.137	m
	Ta^{181}	0.164 ± 0.004	0.166	m
	Ta^{181}	0.350 ± 0.004	0.344	n
	Ta^{181}	0.485 ± 0.005	0.481	n
Lead	Pb^{206}	0.533 ± 0.005	0.5375	o
	Pb^{207}	0.570 ± 0.010	0.570	p
	Pb^{206}	0.661 ± 0.010		
	Pb^{206}	0.802 ± 0.008	0.8033	o
	Pb^{207}	0.888 ± 0.010	0.880	q
	Pb^{206}	1.43 ± 0.03		
	Pb^{206}	1.73 ± 0.03		
	Pb^{208}	2.620 ± 0.020	2.61425	r
Bismuth	Bi^{209}	0.904 ± 0.009		
	Bi^{209}	1.615 ± 0.016		
	Bi^{209}	2.600 ± 0.020		

[a] Ajzenberg, F., and Lauritsen, T., Revs. Mod. Phys., 27: 77, (1955).

[b] Craig, Donohue, and Jones, Phys. Rev. 88: 808, (1952).

[c] Endt, P. M., and Kluyver, J. C., Revs. Mod. Phys. 26: 95, (1954).

[d] Muller, Hoyt, Klein, and DuMond, Phys. Rev. 88: 775, (1952).

[e] Alburger, D. E., and Grace, M. A., Proc. Phys. Soc. (London) 67A; 280, (1954).

[f] Sakai, Dick, Anderson, and Kurbatov, Phys. Rev. 95: 101, (1954).

[g] Phillips, Gossett, Schiffer and Windham, Bull. Am. Phys. Soc. 30: No. 3, 55 (1955).

[h] Nussbaum, Van Lieshout, Wapstra, Verster, Ten Haaf, Nijgh, and Ornstein, Physica 20: 555, (1954).

[i] Lindstrom, Hedgran, and Alburger, Phys. Rev. 89: 1303, (1953).

[j] Schiffer, Windham, Gossett, and Phillips, Bull. Am. Phys. Soc. 30: No. 3, 55, (1955).

[k] Siegbahn, K., and Ghosh, A., Phys. Rev. 76: 307, (1949).

[l] Huber, Medicus, Preiswerk, and Steffen, Helv. Phys. Acta 20: 495, (1947).

[m] Huus, T., and Bjerregaard, J. H., Phys. Rev. 92: 1579, (1953).

[n] Burson, Blair, Keller, and Wexler, Phys. Rev. 83: 62, (1951).

[o] Alburger, D. E., and Pryce, M., Phys. Rev. 95: 1482, 1954.

[p] Alburger, D. E., and Sunyar, A. W., Bull. Am. Phys. Soc. 29: No. 8, 28, (1954).

[q] Mihlich, Schardt, and Segre, Phys. Rev. 95: 1508, (1954).

[r] Lindstrom, G., Phys. Rev. 87: 678, (1952).

threshold for this line has been found to be at a neutron energy of 3.45 ± 0.05 Mev, corresponding to a center of mass energy of 3.36 Mev. Since the energy of the first excited state of Ca^{40} found by Buechner *et al.*,[9] by proton inelastic scattering was 3.35 ± 0.01 Mev, these results form a strong argument that this state has zero spin and even parity, in agreement with the original suggestion of Scharff-Goldhaber[8] concerning the nature of this level. These results are also confirmed by Bonner *et al.*,[10] who found nuclear pairs of 3.46 ± 0.1 Mev from proton bombardment of Ca.

CROSS-SECTION MEASUREMENTS

The problem of obtaining cross sections for reactions of the type discussed here is considerably more complicated than in many other neutron reactions, where all one often needs to know is the relative sensitivity of the detector as a function of neutron energy. The reason is that one has to make absolute measurements of both the neutron flux incident on the scatterer and the gamma-ray yield. Since entirely different problems are involved in making absolute measurements of neutrons and gamma rays they will be discussed separately.

GAMMA-RAY YIELD MEASUREMENTS

There are two approaches that have been followed in making gamma-ray yield measurements in neutron inelastic scattering reactions. The first is to calculate the efficiency of the NaI counter as a function of

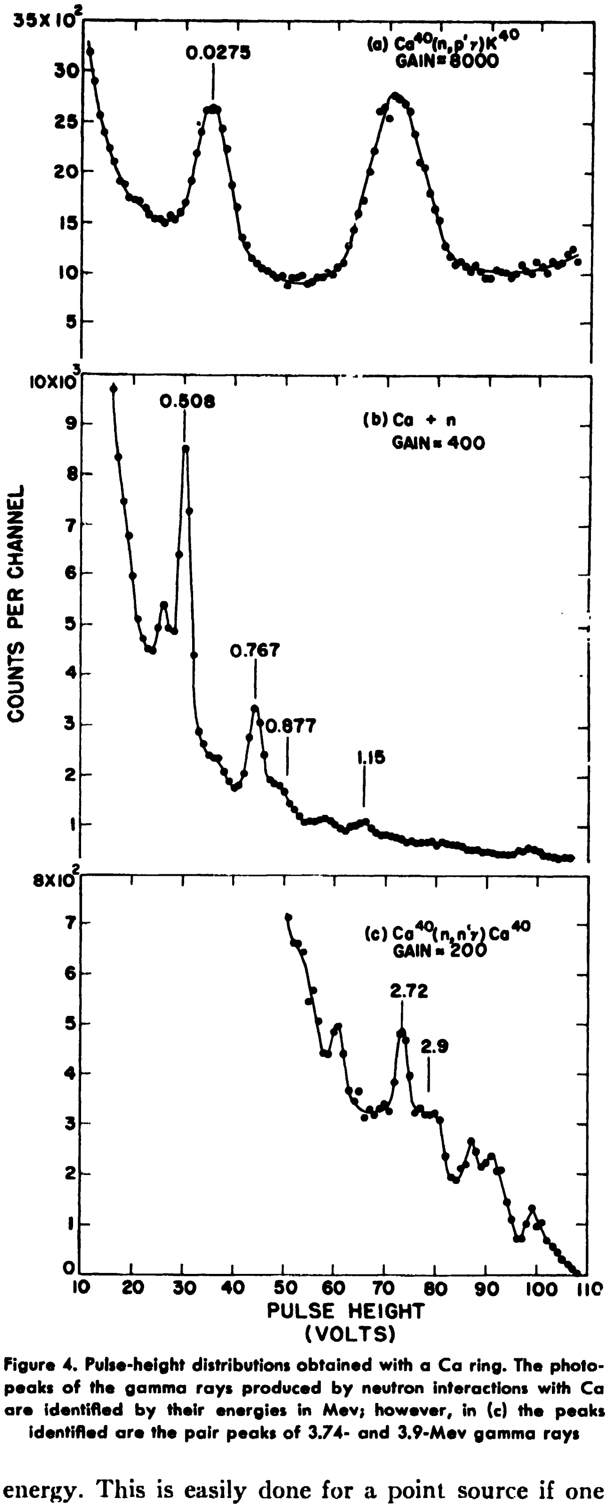

Figure 4. Pulse-height distributions obtained with a Ca ring. The photopeaks of the gamma rays produced by neutron interactions with Ca are identified by their energies in Mev; however, in (c) the peaks identified are the pair peaks of 3.74- and 3.9-Mev gamma rays

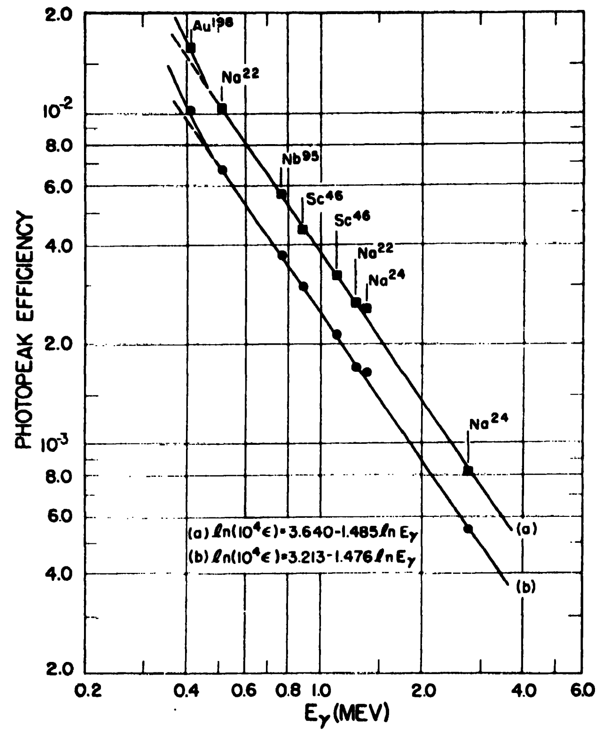

Figure 5. Photopeak efficiency of a NaI crystal 2.57 cm long and 2.54 cm in diameter for ring sources placed symmetrically about the crystal as in Fig. 1. The sources were enclosed in toroids of rectangular cross section with the following dimensions: (a) od = 7.08 cm, id = 5.08 cm, thickness = 1.00 cm; (b) od = 10.16 cm, id = 5.08 cm, thickness = 1.27 cm. The curves have been corrected for self-absorption in the sources

energy. This is easily done for a point source if one wishes the probability for a count to be produced in the detector. However, because of the background problems one can generally use only the photopeaks in measuring gamma-ray yields, hence it is necessary to multiply the calculated total efficiency by the ratio of the area under the photopeak to the total area under the pulse-height distribution. This ratio is generally obtained experimentally, although some calculations on it have been performed.[11] If one has an extended source of gamma rays, which is generally the case in neutron inelastic scattering measurements, the calculation of the total crystal efficiency is more tedious, although no more difficult in principle than for a point source.

The second method is to obtain the counter efficiency experimentally by employing gamma-ray sources of known strength. A number of radionuclides with simple decay schemes are suitable for this purpose; e.g., Au^{198}, Nb^{95}, Sc^{46}, Na^{24}. It is possible to measure the absolute decay rate of these by coincidence or 4π counting. A calibrated source of this kind can be put in solution and placed in a container having the same size as the scattering sample used in the neutron experiments. The efficiency of the NaI counter for an extended source can then be obtained directly without further calculation. An accuracy of five per cent or better can easily be obtained by this method. Figure 5 shows the results obtained for a crystal 2.57 cm long and 2.54 cm in diameter for two different source sizes.[6] The fortuitous circumstance that the photopeak efficiency *versus* gamma-ray energy is linear on a log-log plot makes interpolation between the calibration points quite reliable over the energy range from 0.5 to 2.8 Mev. At higher and lower gamma-ray energies one must resort to the semi-empirical procedure described first.

In order to get reasonable counting rates one is usually forced to use scattering samples for which the self-absorption of the gamma rays is not negligible. Calculation of this is made difficult by the uncertainty in how much to modify the Compton scattering cross section because of the "poor geometry." To a first approximation one might consider the Compton scattering as inelastic scattering which degrades the gamma-ray energy below the region accepted in the photopeak of the NaI counter. Gamma-ray transmission experiments[6] in a geometry close to that used in the neutron inelastic scattering experiments give effective Compton cross sections that agree within a few per cent with the cross sections calculated from this consideration. From this work it appears that corrections of 25–50 per cent can be calculated with an uncertainty of about 1–2 per cent. At low gamma-ray energies (<200 kev) this simple way of considering Compton scattering as inelastic scattering no longer holds, and it is easier to determine the absorption coefficients experimentally.

Kiehn and Goodman[12] have measured the counter efficiency and scatterer self-absorption simultaneously in an ingenious way. After first measuring the yield of 850-kev gamma rays produced by neutron inelastic scattering from iron shot placed in a suitable container, they then coated the shot with a known amount of Mn^{54}. Since the gamma ray from Mn^{54} is very close in energy to that observed in iron inelastic scattering, they were able to get the product of counter efficiency times self-absorption directly. Extrapolation to other energies and other materials was made by applying first-order corrections.

NEUTRON FLUX MEASUREMENTS

The problem of making absolute measurements of fast neutron fluxes is treated in detail in another paper here.[13] Therefore, only a brief discussion of the ones that have been used in connection with inelastic scattering measurements will be given. The most accurate is the "associated particle" method. This method not only aids in reducing the neutron background but also gives the neutron flux directly. However the problem of detecting the associated particle has thus far limited its use to the $H^3(d,n)He^4$ reaction.

The second method of flux measurement depends on a knowledge of the cross section for the neutron source reaction. Then if one knows the target thickness and the intensity of the bombarding ion beam, the number of neutrons is easily calculated. Because of the uncertainties in the published cross sections, the accuracy of this method is probably not better than 10 per cent.

The third method makes use of a neutron detector that can be calibrated or whose efficiency can be calculated. Examples here are the "counter telescope," hydrogen recoil proportional counter, and "long counter."[13] Of these the long counter is the easiest to use. Since its efficiency is very nearly constant over a wide energy range, it can be quickly calibrated with the aid of a neutron source (such as RaBe) of known strength.

Closely allied with the problem of neutron flux measurement is that of correcting for neutron multiple scattering in the scatterer. Ordinarily one assumes an exponential neutron flux distribution in the scatterer; however, after being scattered once there is often a good chance that a neutron will be scattered again. The probability for this depends on the dimensions of the scatterer and the scattering cross sections. If one assumes that a plane wave of neutrons is normally incident on the scatterer, the gamma-ray yields resulting from the first and second scatterings can be written

$$Y_1 = N_0(1 - e^{-\mu d})\frac{\sigma_{in}}{\sigma_t} \tag{1}$$

$$Y_2 = \frac{\sigma_{in}}{\sigma_t} k \frac{N_0(1 - e^{-\mu d})}{\int e^{-\mu z}\,dV} \int e^{-\mu z} \int \frac{1}{\sigma}\frac{d\sigma}{d\Omega} \times (1 - e^{-\mu l})\,d\Omega\,dV \tag{2}$$

where N_0 is the number of neutrons incident on the scatterer, σ_t and σ_{in} are the total and inelastic scattering cross sections, μ the total attenuation coefficient, d the scatterer thickness, $d\sigma/d\Omega$ the differential scattering cross section, l the neutron path length to the surface of the ring after the first scattering, and k the fraction of neutrons that can produce an inelastic event after their first interaction. Calculations of successive scatterings become increasingly tedious by this method; however, detailed Monte Carlo calculations have shown that P_{i+1}/P_i is very nearly constant in many cases (P_i is the probability of the ith collision). Thus the two equations above are sufficient for one to calculate the entire effect due to multiple scattering in small samples.

In order to test the accuracy of the calculations outlined above, the cross section for producing the 850-kev gamma ray in Fe has been measured[6] for a number of scattering rings of different sizes. Figure 6 shows the cross section* calculated from Equation 1 plotted against ring thickness, along with this cross section after correction for multiple scattering. The agreement of the corrected cross sections is remarkably good and indicates that the multiple scattering problem is well understood. An interesting result of this experiment is the fact that the correction is appreciable even for the smaller rings. This indicates that it is not worth while to sacrifice gamma-ray intensity by making a sample small in an attempt to avoid the problem of multiple scattering corrections.

With sufficient care it is possible in some cases to measure the cross sections for excitation of gamma rays in neutron inelastic scattering to an accuracy of 5 per cent. However, the subtraction of backgrounds often introduces the greatest uncertainty, hence in most cases a more reasonable figure for the accuracy of these cross-section measurements is 10 per cent. This figure applies to the stronger lines that are well resolved from other gamma rays in a pulse-height

---

* Since the measurements were made at only one angle, this cross section is really 4π times the differential cross section at 95 degrees.

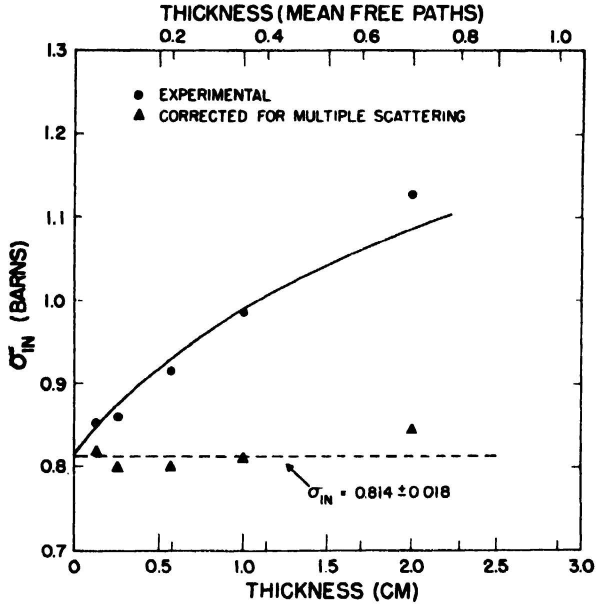

Figure 6. Cross section for excitation of the 850-kev gamma ray in Fe by neutron inelastic scattering as measured with rings of different sizes. The inner and outer diameters were 5.08 cm and 7.08 cm, respectively, with only the axial thickness being varied. The circles give the cross sections calculated from Equation 1, while the triangles give these cross sections after correction for multiple neutron scattering. The solid curve shows the theoretical variation of the gamma-ray yield caused by multiple scattering

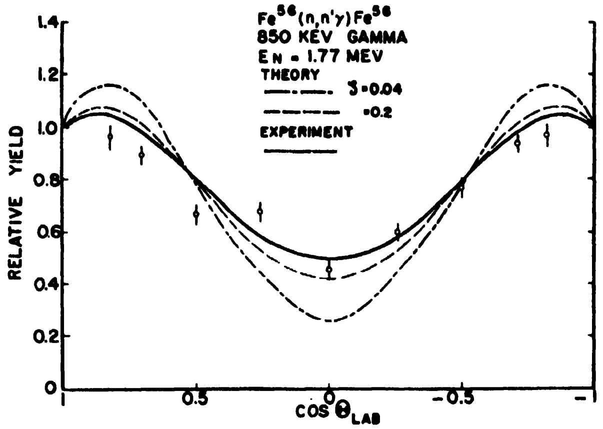

Figure 7. Angular distribution of the 850-kev gamma ray produced by inelastic neutron scattering in Fe. The solid curve is a least squares fit to the experimental data, corrected for the finite size of the scatterer and the detector crystal. The theoretical curves were calculated from the Hauser-Feshbach theory, using a complex square well potential with V_0 = 42 Mev, ζ as shown, and $R = 1.45 \times 10^{-13}A^{1/3}$ cm

spectrum. The problem of separating out the background in a complicated spectrum and obtaining the contributions of the less intense gamma rays is often so difficult that uncertainties as great as a factor of two can occur.

ANGULAR DISTRIBUTIONS

In order to get the total cross section for exciting a level by neutron inelastic scattering one must measure the angular distribution of the gamma rays emitted during the de-excitation of the level. An exception to this occurs if one knows that the level has a spin of 0 or ½, in which case the radiation is isotropic. The problem of measuring the angular distribution is simplified by the fact that it must be symmetric about 90 degrees. The reason is that the gamma-emitting levels are sufficiently narrow so that there is no overlapping, hence interference effects cannot occur. However, in practice it is customary to measure the angular distribution over as wide a range as possible in order to be sure that no asymmetries are being introduced by the experimental technique.

One method of measuring angular distributions is to use the ring geometry (Fig. 1) and move the detector along the axis of the ring to obtain the different scattering angles. The two disadvantages of this method are that the angular resolution varies with the angle of observation and corrections must be applied for the change of detector efficiency with angle. However, the method has the advantage over the one described below of providing higher counting rates except at small angles. This method has been used by Day and Walt to measure the angular distribution of several gamma rays, including the 850-kev gamma ray from Fe^{56}. The angular distribution of the latter

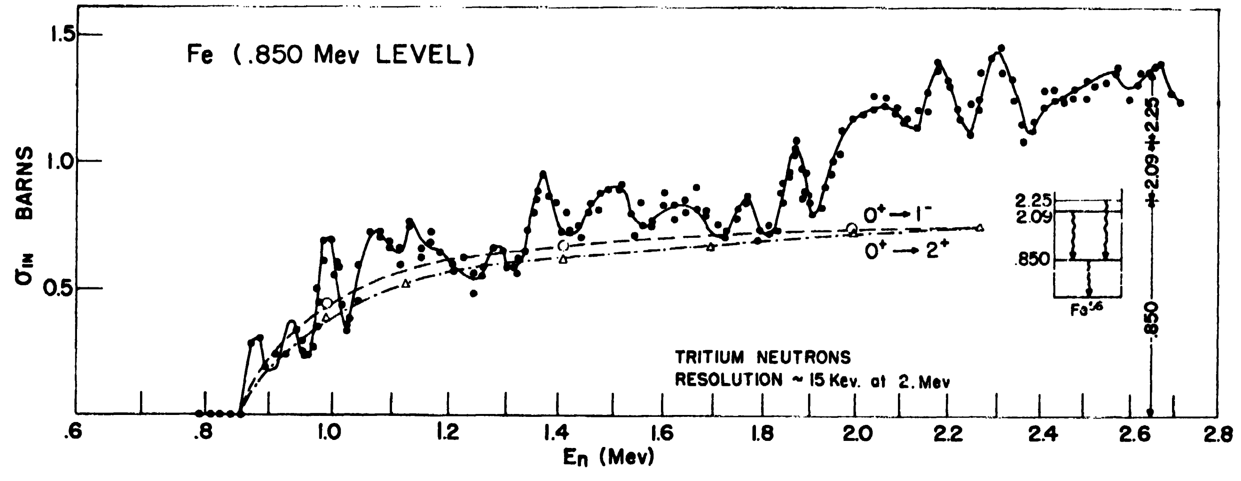

Figure 8. Neutron inelastic scattering by iron as a function of energy. The dashed curves were calculated using the Hauser-Feshbach theory

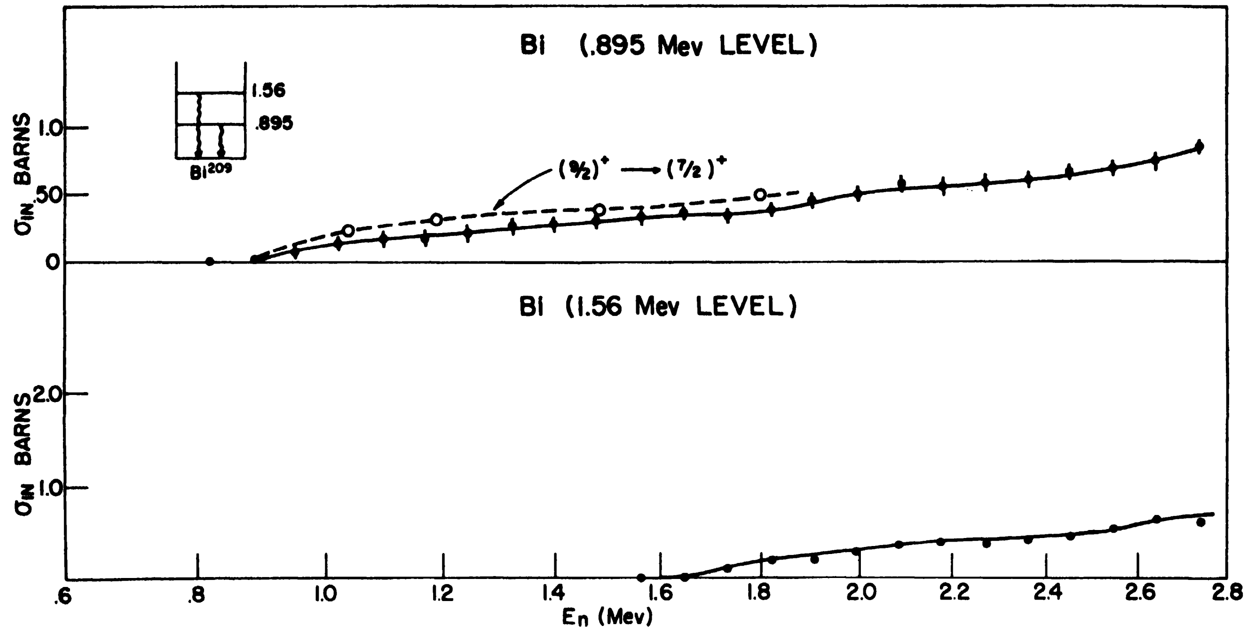

Figure 9. Neutron inelastic scattering by Bi as a function of energy. The dashed curve was calculated from the Hauser-Feshbach theory

exhibits terms up to cos^4 θ, which demonstrates that the spin of the level is ≥ 2.

A second way of measuring angular distributions is to rotate the detector about the scatterer. With a collimated beam of 1.7-Mev neutrons incident on an iron scatterer, Lind and Van Loef[14] have used this method to investigate the angular distribution of the 850-kev gamma ray. Their results are shown in Fig. 7. The theoretical curves shown here are calculated from the theory of Hauser and Feshbach,[15] modified for a complex square well potential with $V_0 = 42$ Mev, and $R = 1.4 \times 10^{-13}A^{1/3}$ cm. It is interesting to note that the best fit is obtained for $\zeta = 0.2$, which is much larger than the value of ζ used by Weisskopf *et al.*[16] to fit the neutron total cross section data up to 3 Mev.

EXCITATION FUNCTIONS

In contrast to reactions involving charged particles, neutron inelastic scattering usually has an observable threshold that agrees with the one calculated from the energy of the level that is excited. This fact is of use in understanding the decay scheme of various nuclei, since the approximate energy of the level emitting a particular gamma ray can be obtained from the threshold for the gamma ray. An example of this was given previously for Ca^{40}.

While most of the results on gamma rays from neutron inelastic scattering have been obtained for neutron energies near 3 Mev, there has been some work as a function of neutron energy. Figures 8–9 give the excitation curves obtained by Kiehn and Goodman[12] for Fe and Bi. Although they used scatterers of the order of a mean free path thick, no corrections were made for multiple neutron scattering. Therefore, the cross-section scale for these curves is expected to be in error by perhaps 50 per cent. In addition, it is possible that spurious resonances could appear in the inelastic

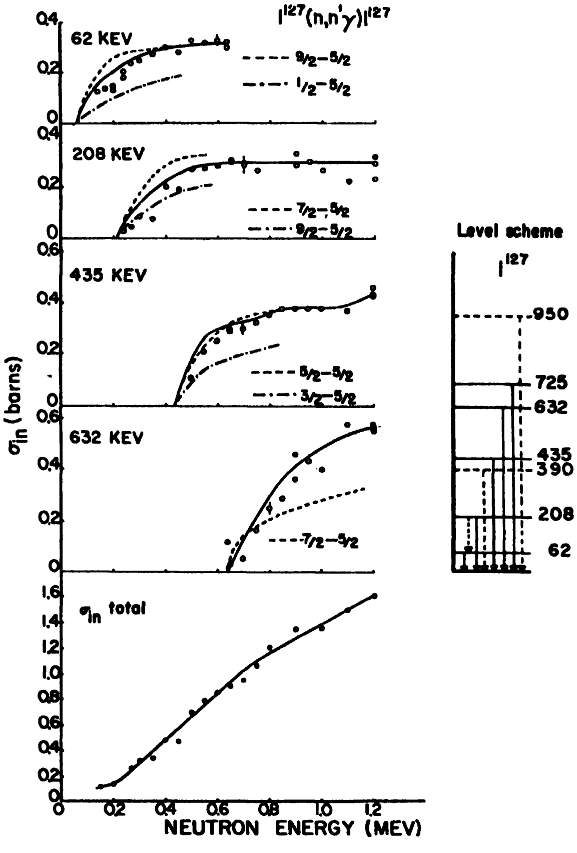

Figure 10. Neutron inelastic scattering by iodine as a function of energy. The bottom curve gives the sum of the cross sections for the 62-, 208-, 435-, and 632-kev gamma rays. The dashed curves were calculated from the Hauser-Feshbach theory, using a complex square well potential with $V_0 = 42$ Mev, $\zeta = 0.2$, and $R = 1.45 \times 10^{-13}A^{1/3}$ cm

scattering excitation curve as a result of increased multiple scattering at elastic scattering resonances. The shape of the curves, however, can probably be used as a guide to the behavior of the inelastic cross section with neutron energy.

Some work of this type has also been carried out by Lind and Van Loef[14] using smaller scatterers than those used by Kiehn and Goodman. Figure 10 shows their results on the excitation of the low excited states of I^{127}. The dashed curves are theoretical excitation functions, based on the Hauser-Feshbach theory, for several assumed values for the spin of these states. In these calculations a complex square well potential was used, with $V_0 = 42$ Mev, $\zeta = 0.2$, and $A = 1.45 \times 10^{-13} A^{1/3}$ cm.

REFERENCES

1. Cranberg, L., P/577, *Time-of-Flight Techniques Applied to Fast Neutron Measurements*, Volume 4, session 15A, these Proceedings.
2. Barschall, H. H., Rosen, L., Taschek, R. F., and Williams, J. H., *Measurement of Fast Neutron Flux*, Revs. Mod. Phys. 24: 1–14, (1952).
3. Stelson, P. H., and Preston, W. M., *The Inelastic Scattering of Fast Neutrons from Iron*, Phys. Rev. 86: 132–3, (1952).
4. Garrett, R. E., Hereford, F. L., and Sloope, B. W., *Inelastic Neutron Scattering in Al, Fe, Mg, and Cu*, Phys. Rev. 92: 1507–8, (1953).
5. Battat, M. E., and Graves, E. R., *Gamma Rays from 14-Mev Neutron Bombardment of O^{12}*, Phys. Rev. 97: 1266–7, (1955).
6. Day, R. B., unpublished results.
7. Sinclair, R. M., *Gamma-Radiation from Interaction of 4.4-Mev Neutrons with Fe^{54} and Fe^{56}*, Bull. Am. Phys. Soc. 30, No. 1: 8, (1955).
8. Scharff-Goldhaber, Gertrude, *Excited States of Even-Even Nuclei*, Phys. Rev. 90: 587–602, (1953).
9. Endt, P. M., and Kluyver, J. C., *Energy Levels of Light Nuclei ($Z = 11$ to $Z = 20$)*, Revs. Mod. Phys. 26: 95–166, (1954).
10. Bonner, T. W., Bent, R. D., and McCrary, J. H., *Nuclear Pairs from Proton Bombardment of Ca^{40}*, Bull. Am. Phys. Soc. 30, No. 1: 59, (1955).
11. Maeder, D., Müller, R., and Wintersteiger, V., *Uber die Linienform Monochromatischer γ-Strahlungen in Szintillationsspektrographen*, Helv. Phys. Acta 27: 3–44, (1954). Berger, M. J., and Doggett, J. A., *Monte Carlo Calculation of the Response of NaI(Tl) Scintillation Spectrometers*, Bull. Am. Phys. Soc. 30, No. 3: 63, (1955).
12. Kiehn, R. M., and Goodman, C., *Neutron Inelastic Scattering*, Phys. Rev. 95: 989–92, (1954).
13. Diven, B. C., P/579 *Techniques for Measurement of Fast Neutron Flux*, Volume 4, session 17A, these Proceedings.
14. Van Loef, J. J., and Lind, D. A., *Inelastic Scattering of Neutrons by Fe, F, Mn, and I*, Bull. Am. Phys. Soc. 29, No. 7: 9, (1955).
15. Hauser, W., and Feshbach, H., *The Inelastic Scattering of Neutrons*, Phys. Rev. 87: 366–73, (1952).
16. Feshbach, H., Porter, C. E., and Weisskopf, V. F., *Model for Nuclear Reactions with Neutrons*, Phys. Rev. 96: 448–64, (1954).

Angular Distributions and Non-Elastic Neutron Scattering

By Martin Walt,* USA

In discussing the interaction of fast neutrons with nuclei it is convenient to consider separately the resonance and nonresonance energy regions. In the resonance region, which consists of energies below several Mev for very light elements and energies below several hundred kev for most heavy elements, observed quantities such as the total cross-sections, the non-elastic cross-sections, and the differential elastic cross-sections show rapid fluctuations with small changes in energy. The nature of these fluctuations is determined largely by the characteristics of the compound states responsible for the resonances. These rapid fluctuations make it difficult to discuss in general terms the interaction of neutrons with nuclei in the resonance region. At higher bombarding energies the widths of the resonances become comparable to the distances between resonances, and the observed cross-sections become slowly varying functions of energy. The energy range where this condition obtains is called the continuum region.

In the past few years many measurements have been made in the continuum energy region of the differential cross-sections for elastic scattering of fast neutrons[1-7] and of the non-elastic cross-sections.[8-11] These cross-sections showed the expected slow changes with energy: However, it was also found that the angular distributions at all energies so far investigated, and the non-elastic cross-sections at energies above a few Mev varied in a systematic way with the atomic number of the target nucleus. It is possible, therefore, to describe the differential elastic cross-sections and the non-elastic cross-sections in rather general terms, and in particular to determine the manner in which these cross-sections vary as a function of neutron energy and of atomic weight.

The present report will deal with the existing data on angular distributions of elastically scattered neutrons and on non-elastic cross-sections in the continuum energy region.

ANGULAR DISTRIBUTIONS OF ELASTICALLY SCATTERED NEUTRONS

At low neutron bombarding energies the curves of differential cross-section plotted as a function of the scattering angle are rather flat except for a single maximum in the forward direction. As the bombarding energy is increased this forward peak becomes more pronounced and secondary maxima appear at larger angles. These secondary maxima move to smaller angles as the bombarding energy is further increased. At bombarding energies of several Mev a large fraction of the elastic scattering is concentrated in the small forward angles. This behavior is illustrated for the case of a heavy element in Fig. 1. The differential

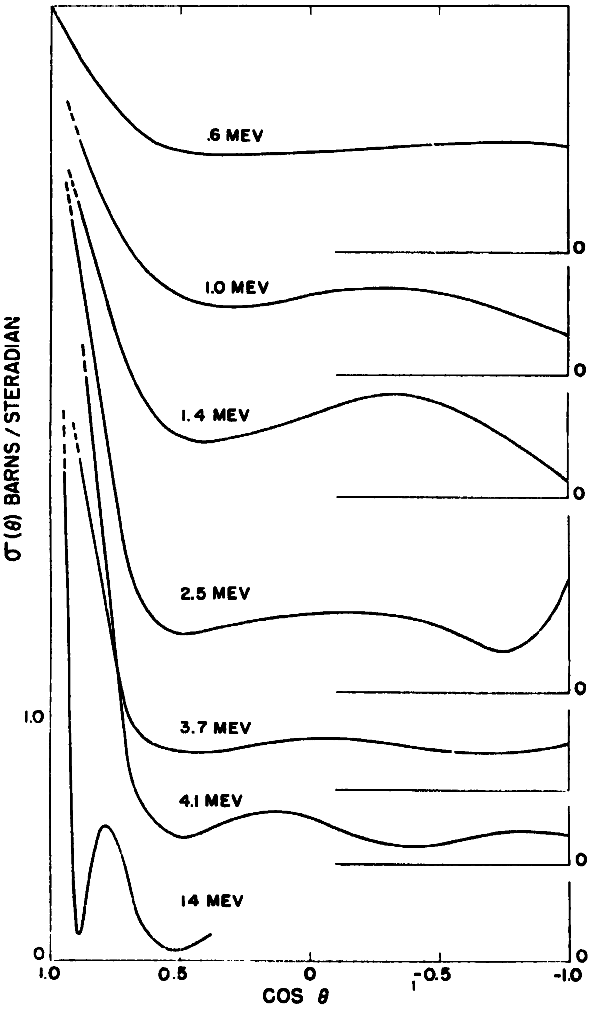

Figure 1. Differential cross section for elastic scattering of neutrons by a heavy element. The curve at 2.5 Mev is for Bi; the curves at all other energies were obtained using a Pb scatterer

---

* Los Alamos Scientific Laboratory. Including work by: H. H. Barschall, University of Wisconsin; T. W. Bonner, The Rice Institute; E. L. Hudspeth, University of Texas; A. S. Langsdorf, Argonne National Laboratory; S. C. Snowden, Bartol Research Foundation; J. R. Beyster, J. H. Coon, E. R. Graves, R. F. Taschek, and M. Walt, Los Alamos Scientific Laboratory.

cross-section is plotted as a function of the cosine of the scattering angle at a number of energies beginning with 600 kev at the top of the graph and ending with 14 Mev at the lowest curve. The vertical scale for each energy is displaced from those of the adjacent energies to minimize overlapping of the curves. The data shown in Fig. 1 have been obtained from several investigators[1–8] under a variety of experimental conditions. Since the angular resolution, energy resolution, and multiple scattering effects are not the same for the different experiments, the comparison of the curves should be limited to the general shapes rather than to absolute values of the cross-sections. Also, some of the results shown are still preliminary and further corrections may affect the absolute values. The curve for 2.5 Mev was measured using Bi as the scatterer; the curves at all other energies were obtained with Pb. For the present comparison the differences in the cross-sections of the two elements are not important. The variation in the shape of the curve with increasing energy can be seen to progress from a relatively flat distribution, peaked in the forward direction, at 600 kev to a more complicated distribution at higher energies. The measurements at 14 Mev did not extend beyond 68 degrees. However, from measurements of the total cross-section and the non-elastic cross-section of Pb it has been determined that probably less than 10 per cent of the elastic scattering takes place at angles greater than 68 degrees.

At a given energy the differential cross section curve of an element is closely related to the number of nucleons in the nucleus. Elements with nearly the same atomic weight have almost identical differential cross-section curves, while the curves of elements having very different atomic weights are quite dissimilar. In Fig. 2 the differential cross sections for elastic scattering of 1-Mev neutrons by a number of elements are plotted as a function of the cosine of the scattering angle. As the number o nucleons in the scattering nucleus increases, the shape of the differential cross-section curve undergoes variations similar to the slow changes in shape which accompany increasing bombarding energy. With increasing atomic number the shape of the differential cross section curve becomes more complex, the forward maximum increases in magnitude, and the secondary maxima move to smaller angles. Experiments carried out at 3.7 Mev[2,5] and at 4.1 Mev[3] show that the systematic changes illustrated in the curves at 1 Mev in Fig. 2 also occur at higher energies.

The regular variation of the angular distributions with energy and with atomic weight makes it possible to approximate the angular distribution of an element whose differential cross-section has not been measured by interpolating between curves of neighboring elements whose cross-sections have been measured at the same energy. Similarly an interpolation can be made to obtain a differential cross-section curve at any desired energy if the cross-section of that element or neighboring elements has been measured at nearby energies.

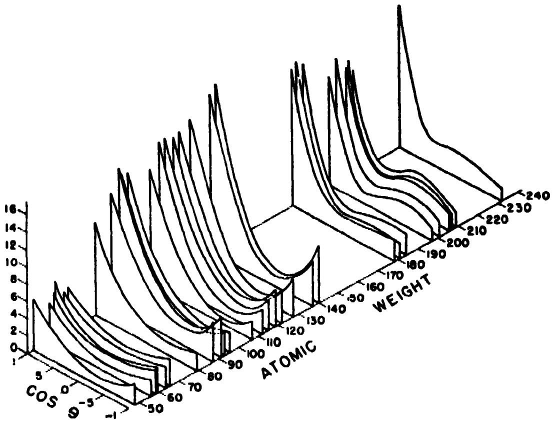

Figure 2. Differential cross sections for elastic scattering of 1-Mev neutrons by 28 elements

The angular distributions of neutrons elastically scattered from fissionable elements are of considerable importance in reactor calculations, and for this reason results are given in Figs. 3, 4, and 5.[7,8,15]

NON-ELASTIC CROSS SECTIONS

The non-elastic cross-section is the cross-section for all processes except elastic scattering. At low energies this cross-section is due primarily to reactions such as the (n,α) and (n,γ) reactions. However, at intermediate energies above several hundred kilovolts and below many Mev these reactions are in general small,

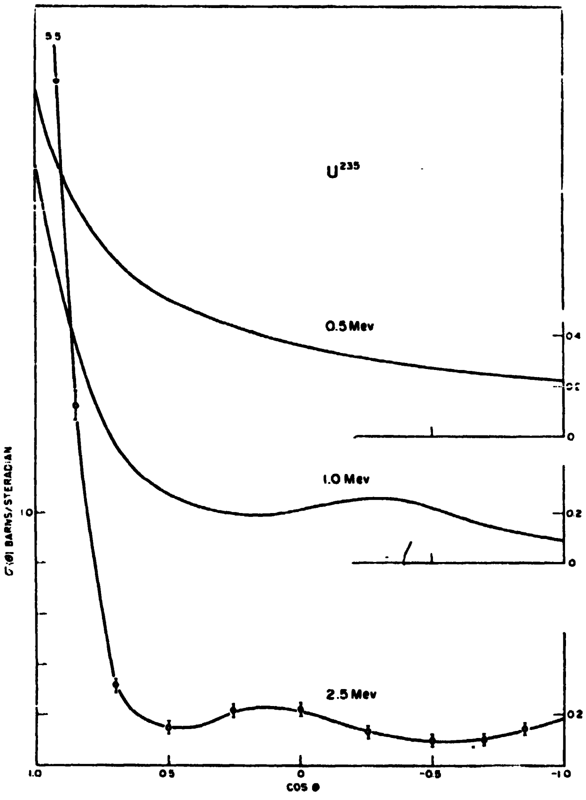

Figure 3. Differential cross sections for elastic scattering of 0.5-, 1.0-, and 2.5-Mev neutrons from U^{235}

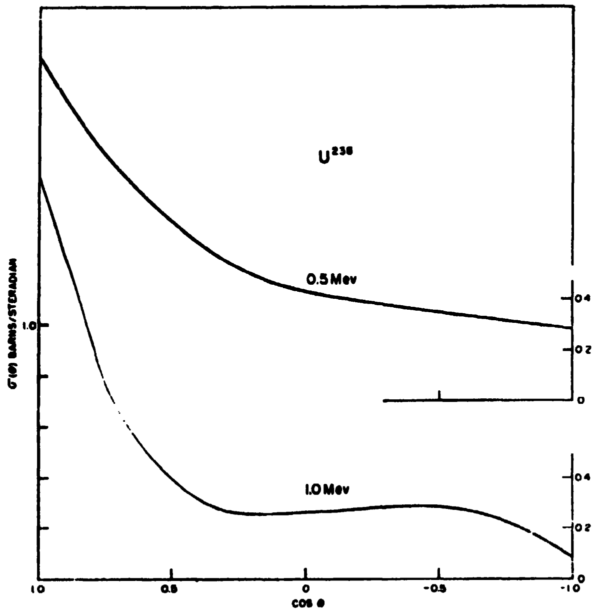

Figure 4. Differential cross sections for elastic scattering of 0.5- and 1.0-Mev neutrons by U^{238}

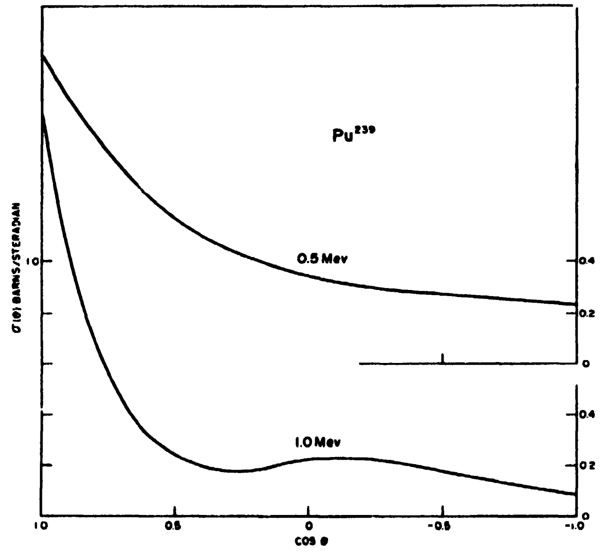

Figure 5. Differential cross sections for elastic scattering of 0.5- and 1.0-Mev neutrons from Pu^{239}

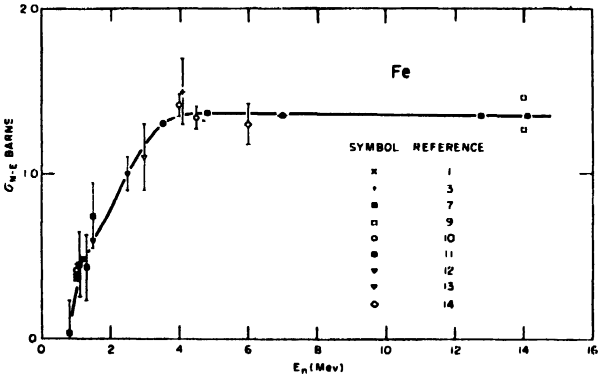

Figure 6. Non-elastic cross section (in barns) of Fe as a function of neutron energy

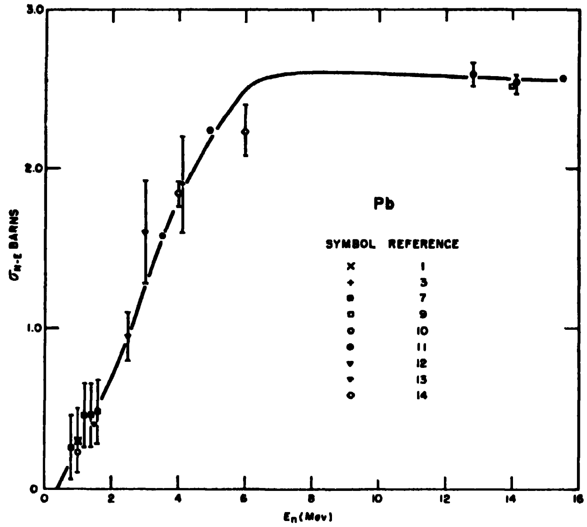

Figure 7. Non-elastic cross section (in barns) of Pb as a function of neutron energy

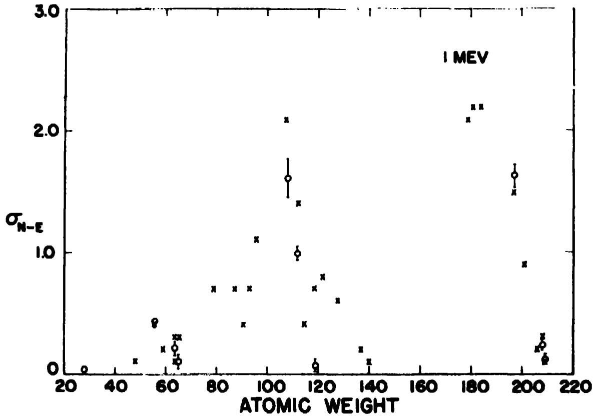

Figure 8. Non-elastic cross sections at 1-Mev neutron energy for 27 elements. The *x*'s denote cross sections obtained by subtracting measured elastic cross sections from the total cross sections and have rather large errors. The open circles were obtained from sphere transmission measurements

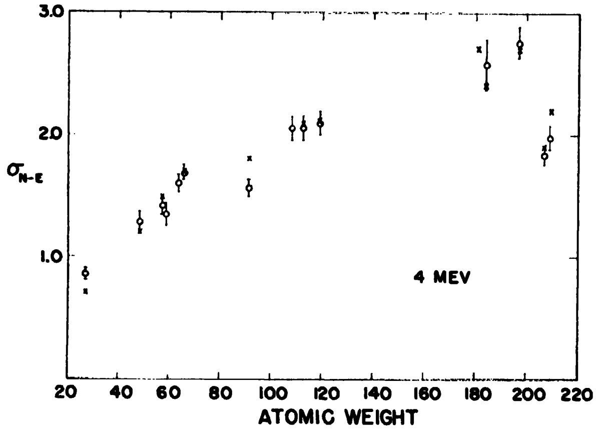

Figure 9. Non-elastic cross sections of fifteen elements at 4 Mev. The *x*'s denote cross sections obtained by subtracting measured elastic cross sections from the total cross sections and have probable errors of 0.2 to 0.3 barns. The cross sections indicated by open circles were obtained by sphere transmission measurements

and the non-elastic interaction consists almost entirely of inelastic scattering processes. Above many Mev processes such as the (*n*,2*n*) reaction become important.

Since an inelastic scattering event can occur only if the neutron energy is greater than the energy of the first excited state of the target nucleus, non-elastic cross-sections in the continuum region are small below a threshold determined by the energy of the first excited state of the target nucleus. As bombarding energy is increased above this threshold the non-elastic cross-section for a given element rises until it approaches a plateau where it is about one third to one half the total neutron cross-section at that energy. The energy at which this plateau is reached is usually between 3 and 6 Mev. In most of the cases for which data exists, the inelastic cross-section decreases slightly in absolute value as the energy is increased from about 6 Mev to 14 Mev.

Figure 6 illustrates the energy variation of the non-elastic cross section for a typical case, iron. These data have been collected from a number of experiments, the references to which are listed on the figure. Most of the values were obtained by sphere transmission measurements with monoenergetic neutron sources. The other points were measured by sphere transmissions with broad-energy-spectrum neutron sources, by subtracting measured elastic cross-sections from the total cross-sections, and by observing the gamma rays resulting from the decay of excited states of the residual nucleus following an inelastic scattering event. The first excited state of the principal isotope of iron is at 850 kev, so that below this value the non-elastic cross-section is expected to be very small. Above this threshold the cross-section rises to a plateau at about 5 Mev where the value is about 40 per cent of the total cross-section. The value near 14 Mev may be slightly lower than the values near 5 Mev although in this case the experimental errors are too large to make this decrease definite. Another example of the variation of the non-elastic cross-section with energy is shown in Fig. 7 where the non-elastic cross-section of Pb is plotted as a function of energy. The cross-section rises from a threshold at about 0.5 Mev and passes through a maximum near 7 Mev where it is about 45 per cent of the total cross-section.

Since the non-elastic cross-sections rise rapidly above a threshold energy determined primarily by the location of the first excited state, values of the non-elastic cross-section of different elements measured at an energy comparable to the threshold values for most elements would be expected to vary from element to element, depending upon whether the threshold for inelastic scattering is near to or far below the bombarding energy. Figure 8 is a plot of the non-elastic cross-sections at 1 Mev for 27 elements.[1,10] Most of the values, the ones represented by crosses, were obtained by subtracting the elastic cross-sections from the total cross-sections; and, due to large uncertainties in the measurements of the elastic cross-sections, these points may be considerably in error. However, they are accurate enough to illustrate the large differences in the non-elastic cross-sections of various elements. The values indicated by the open circles were obtained by sphere transmission measurements and are shown with their probable errors. It is interesting to note that the non-elastic cross-sections of the magic number nuclei Sn, Ba, Ce, Pb, and Bi at *A* equal to 119, 137, 140, 207, and 209, respectively, are considerably smaller than the cross-sections of their non-magic neighbors, a phenomenon which can be explained by the relatively high energies of the first excited states of these nuclei.

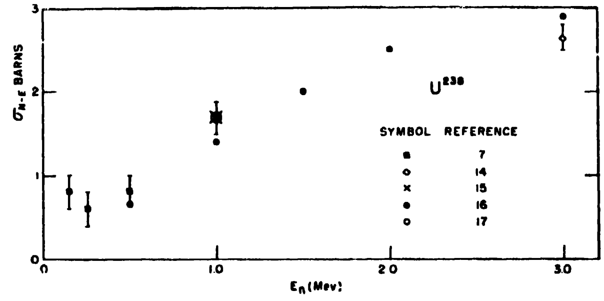

Figure 10. Non-elastic cross section of U^{238}

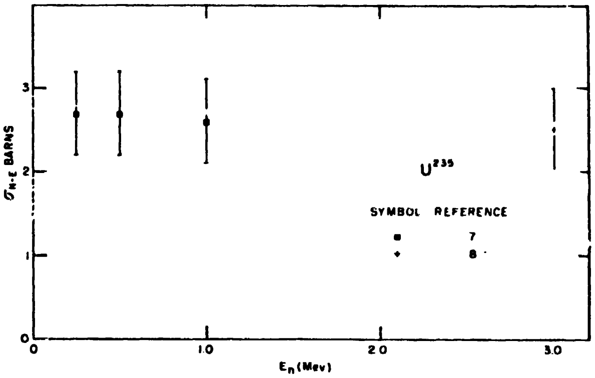

Figure 11. Non-elastic cross section of U^{235}

At energies of several Mev, where most elements have many levels available for inelastic scattering, the variation of non-elastic cross-section with atomic weight becomes much less rapid. Figure 9 shows the non-elastic cross-sections of 15 elements at 4 Mev neutron energy.[3,10] With the exception of Pb and Bi all observed points lie on a smooth curve, the non-elastic cross-section increasing with increasing atomic weight.

Figures 10 and 11 give the non-elastic cross-sections of U^{238} and U^{235} at several energies. The non-elastic cross-section of U^{235} is not expected to exhibit the threshold character shown by other elements since the fission cross-section, included in the nonelastic, does not decrease with decreasing energy.

REFERENCES

1. Walt, M. and Barschall, H. H., *Scattering of 1-Mev Neutrons by Intermediate and Heavy Elements*, Physical Review 93, 1062–8, (1954).

2. Whitehead, W. D. and Snowden, S. C., *Angular Distribution of Neutrons Scattered from Aluminum, Iron, and Lead*, Physical Review 92, 114–9 (1953). Also *Angular Distribution of Neutrons Scattered from Cadmium, Tin, and Bismuth*, Physical Review 94, 1267–72 (1954).
3. Walt, M. and Beyster, J. R., *Interaction of 4.1-Mev Neutrons with Nuclei*, Physical Review (1955) in press.
4. Langsdorf, A. and Lane, R. O., *Angular Distributions of Scattering of Moderate Energy Neutrons*, Bulletin of the American Physical Society, Volume 30, No. 3 (1955) and private communication.
5. Morgan, I. L., *Interaction of 3.7 Mev Neutrons with Al, S, Fe, and Cu*, Bulletin of the American Physical Society, Volume 30, No. 3 (1955) and private communication.
6. Coon, J. H. and Davis, R. W., *Elastic Scattering of 14-Mev Neutrons*, Bulletin of the American Physical Society, Volume 29, No. 6, (1954) and private communication.
7. Taschek, R. F. and Allen, R. C.. private communication.
8. Beyster, J. R. and Walt, M., unpublished.
9. Graves, E. R. and Davis, R. W., *Cross Sections for Nonelastic Interactions of 14-Mev Neutrons with Various Elements*, Physical Review 97, 1205–12, (1955).
10. Beyster, J. R., Henkel, R. L., Nobles, R. A., and Kister, J. M., *Inelastic Collision Cross Sections at 1.0-, 4.0-, and 4.5-Mev Neutron Energies*, Physical Review, in press.
11. Bonner, T. W., private communication.
12. Day, R. B., private communication.
13. Olum, P., *Evaluation of Scattering Data*, MDDC-353.
14. Carter, R. E. and Beyster, J. R., *Inelastic Collision Cross Sections for Fission Spectrum Neutrons*, Physical Review 90, 389 (1953).
15. Walt, M. and Barschall, H. H., unpublished.
16. Cohen, S., Olum, P., and Weisskopf, V., unpublished.
17. Beyster, J. R., private communication.

The Theoretical Prediction of Neutron Cross-Sections of Non-Fissionable Elements for Energies up to 10 Mev

By Victor F. Weisskopf,* USA

The exact theoretical calculation of neutron cross-sections must be based upon our knowledge of the interaction between nucleons within the nuclei. This knowledge is not available at present. A great deal of information is collected in regard to the interaction of two isolated nucleons. The properties of the deuteron are quite well understood and analyzed, and the proton-proton and neutron-proton scattering experiments have established the phase shifts from low energy up to any energy value which might conceivably play a role in a nucleus. However, one has not succeeded in finding a potential depending on the relative distance, spin and isotopic spin, and which reproduces the observed phase shifts. Although some promising progress was made in this direction, it is not possible at present to incorporate the observed dependence of the phase shifts on the polarization.

Even if we had a valid potential for the two-nucleon interaction, it would be far from sure that the same potential is active within the nucleus when more than two nucleons are at distances within the nuclear ranges. Almost any of the present meson "theories" of nuclear forces would give rise to a change of nucleon-nucleon interaction when a third nucleon or more are near by, simply because of the mutual disturbance of the meson clouds. Further indications of this effect are the difficulties encountered in trying to explain the saturation of nuclear binding energies and densities on the basis of the observed two-body interactions. It is not established yet whether the latter contain enough repulsion at the correct range in order to account for the observed saturation.

The apparent lack of nucleon interaction within the nucleus, as observed in the shell structure of nuclei and related phenomena, should not be considered as an argument for changed (weakened) nuclear forces within the nucleus. It is possible, though not yet shown, that these phenomena are consequences of the peculiar properties of low excited states of strongly interacting systems of Fermions.

Because of our ignorance in respect to the nature of nuclear forces within the nucleus, any theory of nuclear cross sections must necessarily be phenomenological and semi-empirical. It must be based upon some general properties of obstacles placed in the way of the incident beam, and any more specific theoretical predictions will of necessity be based upon generalizations of empirical material.

We define the cross-sections as follows. We consider a neutron reaction:

$$n + X = Y + b \tag{1}$$

where X is the target nucleus, Y is the residual nucleus, and b the emerging particle. Y and b are identical to X and n in the case of scattering. We introduce the total cross-section σ_t, which includes every effect that removes a neutron from the parallel incident beam. We subdivide it into two parts:

$$\sigma_t = \sigma_{el} + \sigma_r \tag{2}$$

the elastic scattering cross-section σ_{el}, and the reaction cross-section σ_r. The former includes the processes in which the residual nucleus is identical to the target nucleus and also is left in the same quantum state as the target. This quantum state is always the ground state. In case the latter is degenerated, because of non-vanishing nuclear spin, one introduces a channel spin, which is the combined angular momentum of the intrinsic spin ½ of the incoming neutron and the spin of the target nucleus. The elastic scattering then contains all processes in which the channel spin is unchanged. The reaction cross-section then contains all genuine nuclear reactions, the inelastic scattering and also the scattering in which the channel spin changes, but the energy of the neutron remains unchanged.

The cross-sections defined in Equation 2 will be called "the bulk cross-sections," in contrast to the cross-sections of the different special reactions. The reaction cross-section σ_r plays the role of an absorption cross section since it describes the amount of neutrons which are removed from the entrance channel of the reaction.

The detailed cross-sections of the different nuclear reactions are all contained in σ_r, which can be split into the sum of special reaction cross-sections:

$$\sigma_r = \sigma_{inel} + \sum_b \sigma(n,b) \tag{3}$$

Here σ_{inel} is the cross-section for inelastic scattering, and $\sigma(n,b)$ corresponds to the (n,b) reaction for $b \neq n$, as indicated in Equation 1. Obviously each of these cross-sections can be subdivided again into the parts corresponding to different excitations E_r of the residual nucleus:

---

* Massachusetts Institute of Technology. Including work by C. E. Porter, Brookhaven National Laboratory, and H. Feshbach, Massachusetts Institute of Technology.

$$\sigma_{inel} = \sum_r \sigma_{inel}(E_r), \qquad \sigma(n,b) = \sum_r \sigma(n,b,E_r) \tag{4}$$

and each cross-section represents an integral over the differential cross-sections for a given angle of escape of the secondary particle.

All cross-sections are, of course, functions of the energy ϵ of the incident neutron. The most characteristic feature of this dependence is the existence of resonances. The widths Γ and distances D of these resonances are strongly energy dependent and vary much from nucleus to nucleus. In general, the heavier the nucleus, the smaller the widths and distances. The widths increase with higher ϵ and, when Γ becomes of the order of D, the resonances disappear. For heavier nuclei, this happens at energies of several Mev.

Apart from the very light nuclei, the distances between resonances are small enough (say $D < 10^4$ ev), so that it appears practicable to introduce average values of the cross-sections over energy intervals I, which contain many resonances. In this case it turns out to be advantageous to define these averages as follows:

$$\langle\sigma\rangle = \overline{k^2} \int_I \sigma(\epsilon)\, \frac{d\epsilon}{k^2} \tag{5}$$

where k is the wave number of the incident neutron: $\epsilon = \hbar^2 k^2/2m$ and $\overline{k^2}$ is the average k^2 in the energy interval I. These averages and their energy dependence will be called the *gross structure* of the cross-sections. The actual resonance behavior will be referred to as the *fine structure*. This distinction is important, since much more can be predicted theoretically about the gross structure than about the fine structure.

The introduction of the gross structure suggests a division of the elastic cross-section into two parts. As is well known, the amplitude of the elastic scattering in a subwave of given angular momentum is proportional to $(1 - \eta_l)$, where

$$\eta_l = e^{2i\delta_l}$$

and δ_l is the (complex) phase shift. The gross structure of the elastic scattering, therefore, is proportional to $\langle|1 - \eta_l|^2\rangle$, where the symbol $\langle\ \ \rangle$ signifies an average over resonances within the previously used interval I. We write:

$$\langle|1 - \eta_l|^2\rangle = |1 - \langle\eta_l\rangle|^2 + \langle|\Delta\eta_l|^2\rangle$$

where $|\Delta\eta_l|^2$ is the absolute mean square fluctuation of η_l:

$$|\Delta\eta_l|^2 = |\langle\eta_l\rangle|^2 - \langle|\eta_l|^2\rangle$$

This split suggests a corresponding split in the elastic cross section:

$$\begin{aligned} \langle\sigma_{el}^{(l)}\rangle &= \sigma_{se}^{(l)} + \sigma_{ce}^{(l)} \\ \sigma_{se}^{(l)} &= C_l|1 - \langle\eta_l\rangle|^2 \\ \sigma_{ce}^{(l)} &= C_l\langle|\Delta\eta_l|^2\rangle \end{aligned}$$

Here C_l is the proportionality constant between the elastic cross-section $\sigma_{el}^{(l)}$ of the lth subwave and the factor $|1 - \eta_l|^2$. We call $\sigma_{se}^{(l)}$ the shape elastic cross-section and $\sigma_{ce}^{(l)}$, the fluctuation elastic, or compound elastic cross-section. One can easily show that σ_{ce} corresponds to that part of the average elastic scattering which goes via compound state formation; this is shown by substituting the Breit-Wigner expression for η_l. In discussing gross structure cross-sections, it is then useful to combine this part of the scattering with the average reaction cross section:

$$\sigma_{ce} + \langle\sigma_r\rangle = \sigma_c \tag{6}$$

and one obtains a magnitude σ_c which is best described by the name "cross-section for the formation of a compound system." It must be emphasized, however, that σ_r includes any kind of nuclear reaction, also those which do not fit the orthodox picture of the formation of a compound nucleus and its independent decay.

There is an important parallel in the gross-structure and fine-structure relations. One can easily verify:

$$\left.\begin{aligned} \sigma_{el}^{(l)} &= C_l|1 - \eta_l|^2 \\ \sigma_r^{(l)} &= C_l(1 - |\eta_l|^2) \end{aligned}\right\}\text{fine structure}$$

$$\left.\begin{aligned} \sigma_{se}^{(l)} &= C_l|1 - \langle\eta_l\rangle|^2 \\ \sigma_c^{(l)} &= C_l(1 - |\langle\eta_l\rangle|^2) \end{aligned}\right\}\text{gross structure}$$

The gross structure cross-sections σ_{se} and σ_c can be represented as being the elastic scattering and the absorption cross-section of a new scattering problem whose scattering amplitudes are the slowly varying averages of the actual amplitudes.

The distinction between gross and fine structure is important only in the lower energy regions where resonances occur. When the resonances merge, the fluctuations of the cross-sections and of η_l become small and both structures become identical. As a consequence we get in that limit $\sigma_{ce} = 0$ and $\sigma_c = \sigma_r$.

3. Some success has been achieved in the theoretical prediction of the gross structure of neutron cross-sections. It has been assumed that the average scattering amplitudes $\langle\eta_l\rangle$ can be considered as equal to the scattering amplitudes of a model in which the effect of the nucleus upon the incident neutron is described by a complex potential:

$$V = V_0(r) + iV_1(r) \tag{7}$$

The real part is a representation of the average potential energy to which the neutron is subjected when passing through the nucleus; the imaginary part indicates the strength and location of those processes which lead to an energy exchange of the neutron with the target nucleus.

The representation of the nucleus by a complex potential, as in Equation (7) is called the optical model of the nucleus. It was first introduced by Serber, Fernbach and Taylor[1] for use at higher energies and later was extended to low energies by Feshbach, Porter and Weisskopf.[2]

The simplest possible form for the functions $V_0(r)$

and $V_1(r)$ is a square well. For $V_0(r)$ one would choose a potential which gives rise to the correct shell structure of the nucleus. This is a potential with a depth of 30 to 40 Mev and a radius $R \sim 1.40 \times 10^{-13}$ cm. This radius seems large compared to the recent electron scattering and μ-meson-spectroscopy results, which indicate a nuclear radius of about $1.2 \times 10^{-13} A^{1/3}$ cm. It must not be forgotten, however, that the latter experiments measure the extension of the proton distribution and perhaps the extension of the mass distribution, if it is allowed to assume that protons and neutrons occupy roughly the same volume. The nuclear potential $V(r)$, on the other hand, reaches further out because of the range of the nuclear forces, thus producing a larger radius for V than for the mass distribution.

The imaginary potential $V_1(r)$ should, in first approximation, have the same shape as $V_0(r)$. One can estimate its magnitude for $r < R$ by means of the following simple consideration:

The imaginary potential describes the probability of energy exchange of the incoming neutron with the nucleons in the target nucleus. In fact, one can express the mean free path Λ in nuclear matter of the neutron:

$$\Lambda = \left[\frac{2(E + V_0)}{m}\right]^{1/2} \left(\frac{\hbar}{V_1}\right)$$

This mean free path can be estimated in a very rough way by calculating the collision probability of the incoming neutron on the basis of the known scattering cross-sections between isolated nucleons.[3] The Pauli principle forbids any collisions in which the nucleons within the nucleus lose energy, since they must end up in unoccupied levels. A calculation on this basis gives rise to an imaginary potential as a function of energy which starts with about 2 Mev at low energy and rises slowly to reach a maximum at about 50 Mev, (see Fig. 1) then it slowly drops to smaller values. The increase is due to the fact that the Pauli principle is most prohibitive at low incident energies; it loses its effect with rising energy. The elementary scattering cross-sections decrease, however, with increasing energy, and this produces the final drop in V_1 at high energies.

The cross-sections calculated from the square well complex potentials reproduce fairly well the observed gross structure, especially at low energies. Evidently the sharp edge of the square well potential cannot be an accurate picture of the situation. It would be more reasonable to assume edges in which the potential drops smoothly to zero in a surface zone of the dimension of the range of nuclear forces. At low energy the difference between a sharp and a smooth edge will not be very significant. There are strong indications, however, that the results would be better if the sharp edge of the square well were rounded-off by some smoother function. Such rounding-off is more important for higher energies. The angular distributions of elastic scattering of 14 Mev neutrons and of protons around 20 Mev can be reproduced satisfactorily only with a smooth potential well, as will be shown later on.

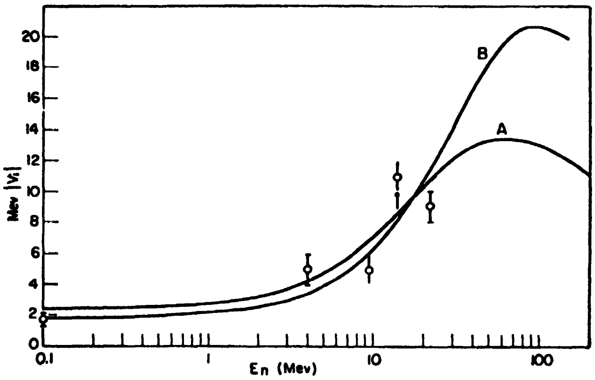

Figure 1. Imaginary part of nuclear potential calculated on the basis of nucleon-nucleon collisions. Curve *A* corresponds to a nuclear radius $R = r_0 A^{1/3}$, $r_0 = 1.45 \times 10^{-13}$ cm and curve *B* to $r_0 = 1.2 \times 10^{-13}$ cm

The best square well fit with the experiments in the first few Mev is at present:

$$\left.\begin{aligned} V_1 &= -42 \text{ Mev} \qquad r < R \\ V_1 &= 0 \qquad\qquad\quad r > R \end{aligned}\right\} (a) \tag{8a}$$

$$\left.\begin{aligned} V_2 &= \zeta V_1 \\ \zeta &= 0.03 - 0.05 \end{aligned}\right\} (b) \tag{8b}$$

$$R = (1.26 A^{1/3} + 0.7) \times 10^{-13} \text{ cm} \tag{8c}$$

We now compare the cross-sections derived from such a potential with the experimental material. There are three groups of data: (*a*) the total cross-sections σ_t as functions of the energy and atomic number; (*b*) the cross-sections for the formation of the compound nucleus; and (*c*) the angular dependence of the elastic scattering. The data of group (*a*) are represented in Figs. 2 and 3. They show the gross structure of the total cross sections in units of πR^2 as a function of the energy in units $x^2 = R^2/\lambda^2$ and of the radius R. Figure 2 shows the experimental material, and Fig. 3 shows the calculated values. The calculation seems to represent the most important features of the observed cross-sections. These graphs cover the region $0 < x^2 < 9$, which corresponds to the first few Mev, up to 9 Mev for Al and up to 4 Mev for Pb. The most characteristic maxima and minima occur at lower energy. This is why the fair agreement between Figs. 2 and 3 determines the constants of Equation 8 of the potential only for the first one or two Mev.

Although the over-all similarity between the theoretical and experimental curves is impressive, there are considerable differences in the details. The position and the magnitude of the maxima and minima are not exactly reproduced. Certainly the model is too crude for this. It was tried by R. G. Thomas[4] without success to improve the details by introducing a spin-orbit coupling. Calculations with rounded edges of the square well potential are now under way.

We now come to the cross-sections σ_c for the formation of the compound nucleus. The comparison with the experiment is sometimes made difficult by the fact

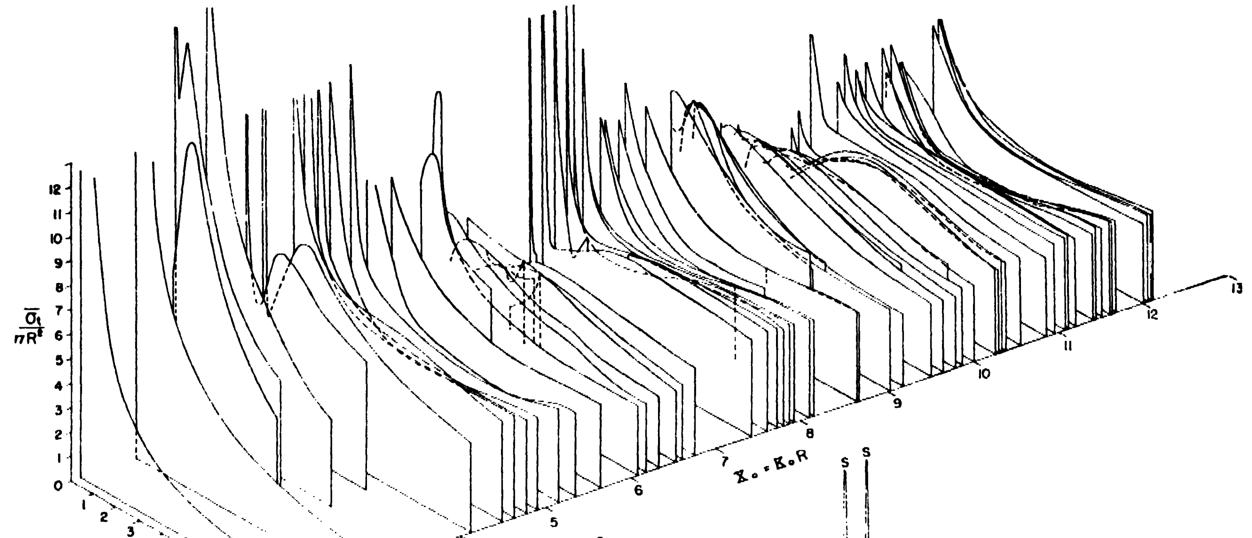

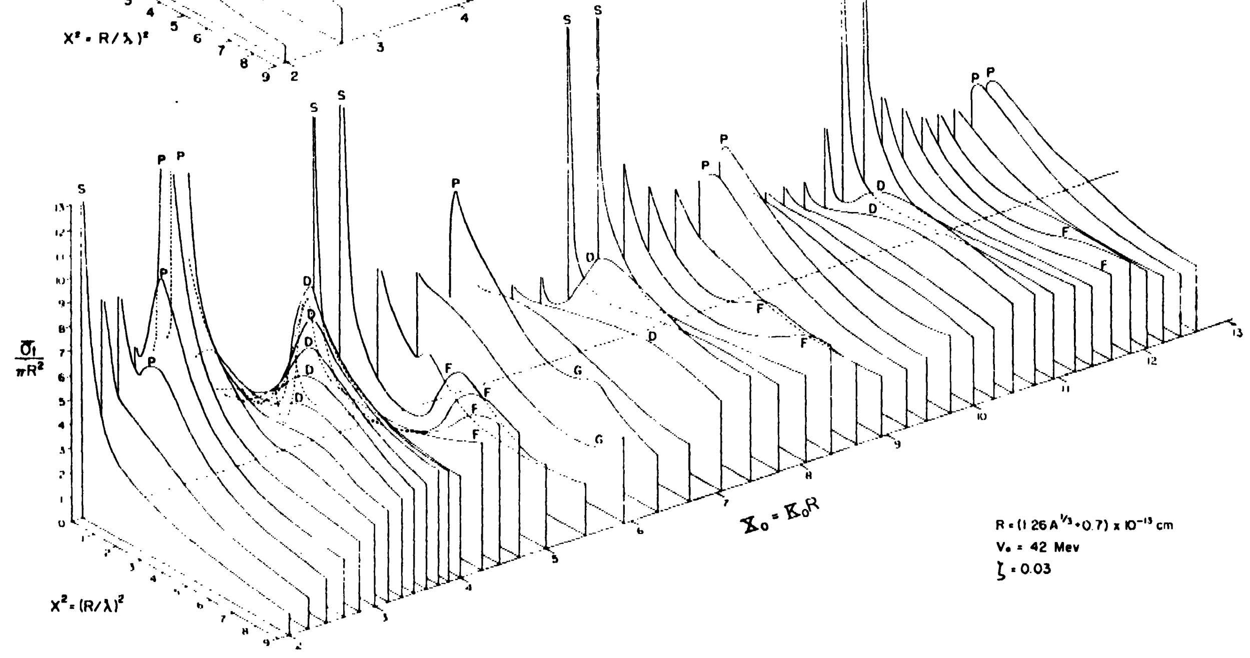

Figure 2 (Above). Observed neutron total cross section as a function of energy and radius R, with $R = (1.26A^{1/3} + 0.7)10^{-13}$ cm

Figure 3 (Below). Neutron total cross sections as functions of energy and nuclear radius R as calculated on the basis of the potential of Equation 8

that it also contains the compound-elastic scattering, which cannot easily be separated experimentally from the shape-elastic scattering. However, the theoretical predictions can be checked in the following way: The observed reaction cross-section must be smaller than σ_c: $\sigma_r \leq \sigma_c$, and the difference, the compound elastic cross section, should be appreciable only at relatively low energy and for nuclei for which little inelastic scattering is expected because of an insufficient number of excited states below the energy of the incident neutron.

A direct comparison between theory and experiment can be made, however, in the energy region where the resonance fine structure can be measured accurately. One uses the connection between σ_c, on the one hand, and the neutron width Γ_n and the average distance D of the resonances, on the other. From the Breit-Wigner expressions one can derive the following relation:

$$\sigma_c = 2\pi^2ƛ^2(\Gamma_n/D)(1 - \tfrac{1}{2}\pi(\Gamma_n/D))$$

and hence the determination of σ_c from the potential in Equation 8 gives a theoretical prediction for Γ_n/D, which can be tested directly. Figure 4 shows the predicted dependence of Γ_n/D upon A and the experimental values as determined by various authors. The predicted maxima occur for values of $R = [n + (\tfrac{1}{2})]L/2$, where L is the wave length of the neutron inside the potential well. The two maxima near $A = 50$ and 170 are borne out by the experi-

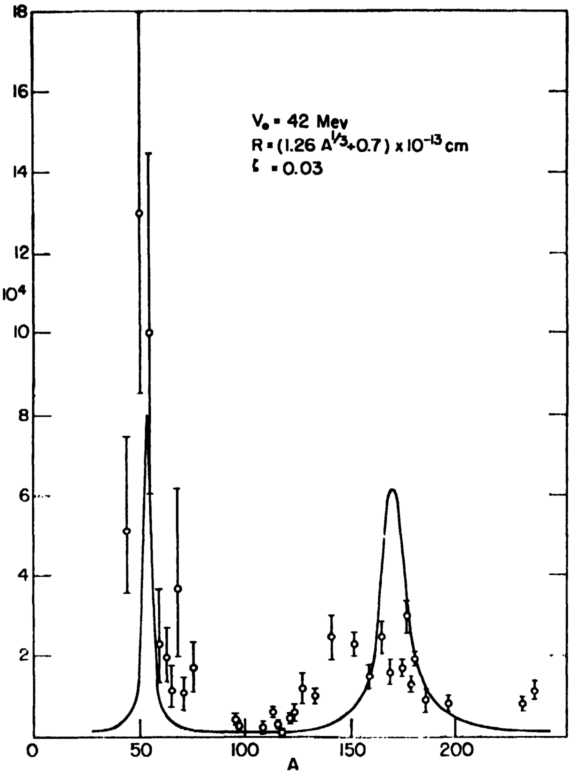

Figure 4. Γ_n/D as a function of A. The solid wave is the theoretical prediction on the basis of a square well with constants as listed. The experimental points near $A = 50$ are measurements by L. M. Bollinger, R. E. Cote, J. M. LeBlanc, D. A. Dahlberg, R. R. Palmer, all of Argonne National Laboratory. The points near $A = 150$ are measured by Carter, Harvey, Hughes, and Pilcher, Phys. Rev. 96, 113 (1954)

nents. The observed values between the maxima are igher than predicted. It can be shown that a smoothng of the edges of the potential removes this discrepancy. Quantitative data on this point are soon forthcoming. The low maximum and the large spread of the observed maximum at $A \sim 170$ has been explained by Bohr and Mottelson,[5] who ascribe it to the strong nuclear deformations which are found in that region. The observed value of Γ_n/D is expected to be some average of the expected value over the radii ranging between the smallest and largest radius of the deformed nucleus.

The comparison of the theoretical results for σ_c with the experiments at higher energy is subject to the difficulties mentioned before. Only parts of σ_c are directly subject to measurements. Figure 5 shows as a unction of A the inelastic cross sections at 1 Mev as determined by Walt and Barschall[6] and the theoretical curve for σ_c as determined[7] from Equation 8. The agreement is satisfactory if one bears in mind hat $\sigma_{in} \leq \sigma_c$ and that the difference—the compound elastic scattering—is expected to be especially strong n the lighter nuclei around $A = 50$ because of the carcity of excited levels below 1 Mev. In this respect ead and bismuth behave just like light nuclei because of their closed shells.

The measurements of inelastic and reaction cross ections at higher energy have not yet been evaluated on the basis of the optical model. It can be said, however, that they strongly indicate the ***increased*** absorption, which is predicted in Fig. 1. For example, the reaction cross sections measured at 14 Mev[8] are all very close to the geometrical maximum value $\pi(R + \lambda\!\!\!^{-})^2$, which is an indication of strong absorption. It points to an imaginary potential V_2 of at least 10 Mev.

A further group of experiments can be used to test the optical model of the gross structure of nuclear cross sections. It is the angular dependence of the elastic scattering. Also in this group the compound-elastic scattering introduces an element of uncertainty. The theory only determines the angular dependence of the shape-elastic cross-section. One observes, however, the sum of the shape-elastic and compound-elastic one. This difficulty is unimportant at higher energies, say $\epsilon > 4$ Mev, but at 1 Mev the compound-elastic scattering can amount to as much as 10 to 20% of the total. Its angular distribution has a tendency to be uniform because of the numerous possibilities of angular momentum changes.

Figures 6 and 7 show a comparison of the experimental data[6] at 1 Mev and theoretical data for that energy calculated from the potential in Equation 8. Again we find good qualitative agreement. Not much more should be expected because of the missing compound-elastic scattering in the theory.

Walt and Beyster[9] report good agreement of the observed angular dependence of neutron elastic scattering at 4.1 Mev with the data as given by Equations 8*a* and 8*c*. The imaginary part, however, had to be taken at least three times larger than Equation 8*b*, again supporting the theoretically predicted increase. At still higher energies one finds that the shape of the potential near the surface is of importance. Calculations by Culler, Fernbach and Sherman[10] were made in order to fit the angular distributions of elastic scattering of neutrons as measured by J. Coon.[10] They obtain a good fit with a potential whose real part is rounded-off. Actually they approximate the rounding-off by a step function and use:

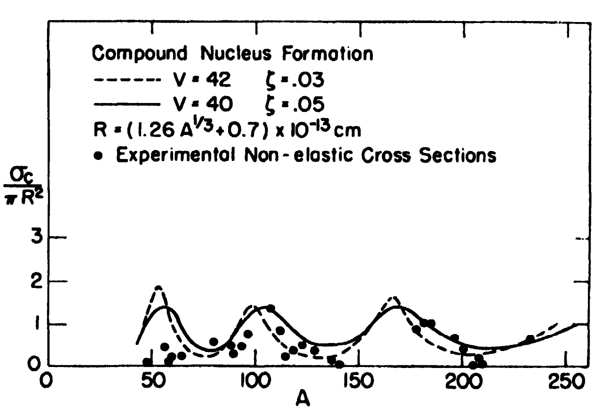

Figure 5. Observed reaction cross sections at 1 Mev as measured by Walt and Barschall, Phys. Rev. 93, 1062 (1954) and calculated cross section σ_c for compound nucleus formation. The calculations are done by W. S. Emmerich

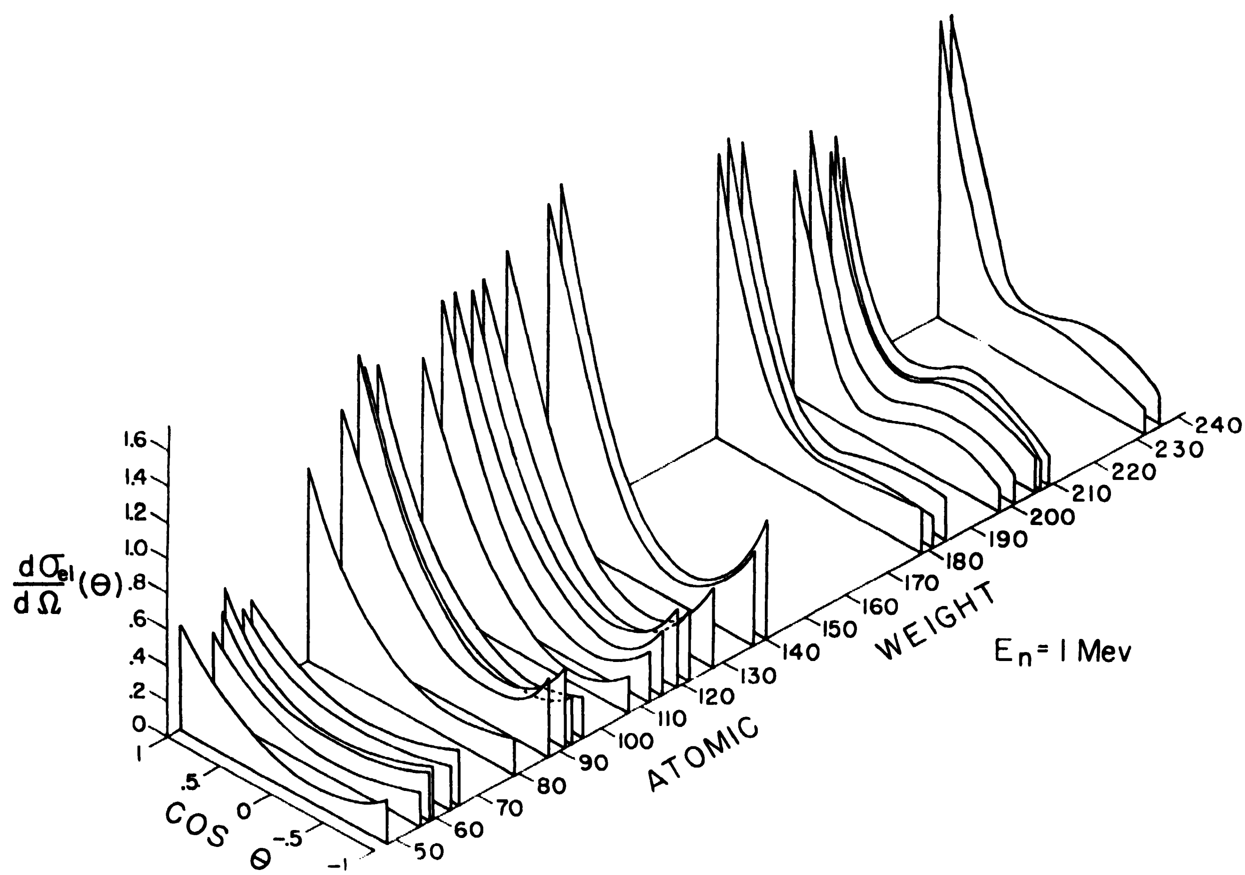

Figure 6. Angular dependence of elastic neutron scattering at 1 Mev as a function of cos θ and the radius as measured by Walt and Barschall, Phys. Rev. 93, 1062 (1954)

$$V = (42 + 11i)\ \text{Mev} \qquad r < R - d$$
$$V = 36\ \text{Mev} \qquad R - d < r < R$$
$$V = 0 \qquad r > R$$

with $d = 0.74 \times 10^{-13}$ cm and R almost identical to Equation 8*c*. Again they find a greatly increased imaginary potential at this high energy.

On the basis of the results discussed, it is safe to say that theoretical predictions of the *gross structure* of the *bulk cross-sections* are possible with a suitable optical model of the nucleus. The gross structure is the average over resonances, and the bulk cross-sections are the total, elastic and reaction cross-sections. The prediction of the fine structure and the prediction of the detailed cross-sections of different nuclear reactions, however, are much more complicated problems which, to a large extent, are unsolved as yet. The problem of the fine structure is a problem of the position and of the shape of individual resonances. The shape of the resonances can be predicted by theory. The Breit-Wigner[11] expressions determine the shape completely when two constants are given: The neutron width Γ_n and the total width Γ. There exists no theory which gives the individual values for these widths. However, the optical theory of the nucleus predicts the average values of Γ_n/D and can be used therefore to estimate Γ_n when the level distances are known. The total width Γ consists of the contributions of all possible modes of decay of the compound nucleus and, at low energies, is mainly determined by the radiation with Γ_γ. The theory of the radiation width is not very reliable, but experiments have shown that, in heavy nuclei, Γ_γ is always of the order of 0.1 ev. More detailed studies of this have been made recently by D. Hughes[12] and collaborators.

The actual position of the resonances cannot be predicted in general; the only exceptions are perhaps the cases of some light nuclei in which resonances can be ascribed to certain well-defined configurations of the shell model. In this case position and strength can be calculated.

Attempts have been made to obtain a theoretical or semi-empirical estimate of the density of resonances. Unfortunately these attempts were not too successful. One can, of course, construct expressions for the level density based upon some simple model of nuclear interaction. Bethe has used the independent particle model; others have used methods which take into account interactions.[13] It follows from general considerations that the level density $\omega(E)$ should increase with energy in an exponential way,

$$\omega \approx C \exp(aE^n) \tag{9}$$

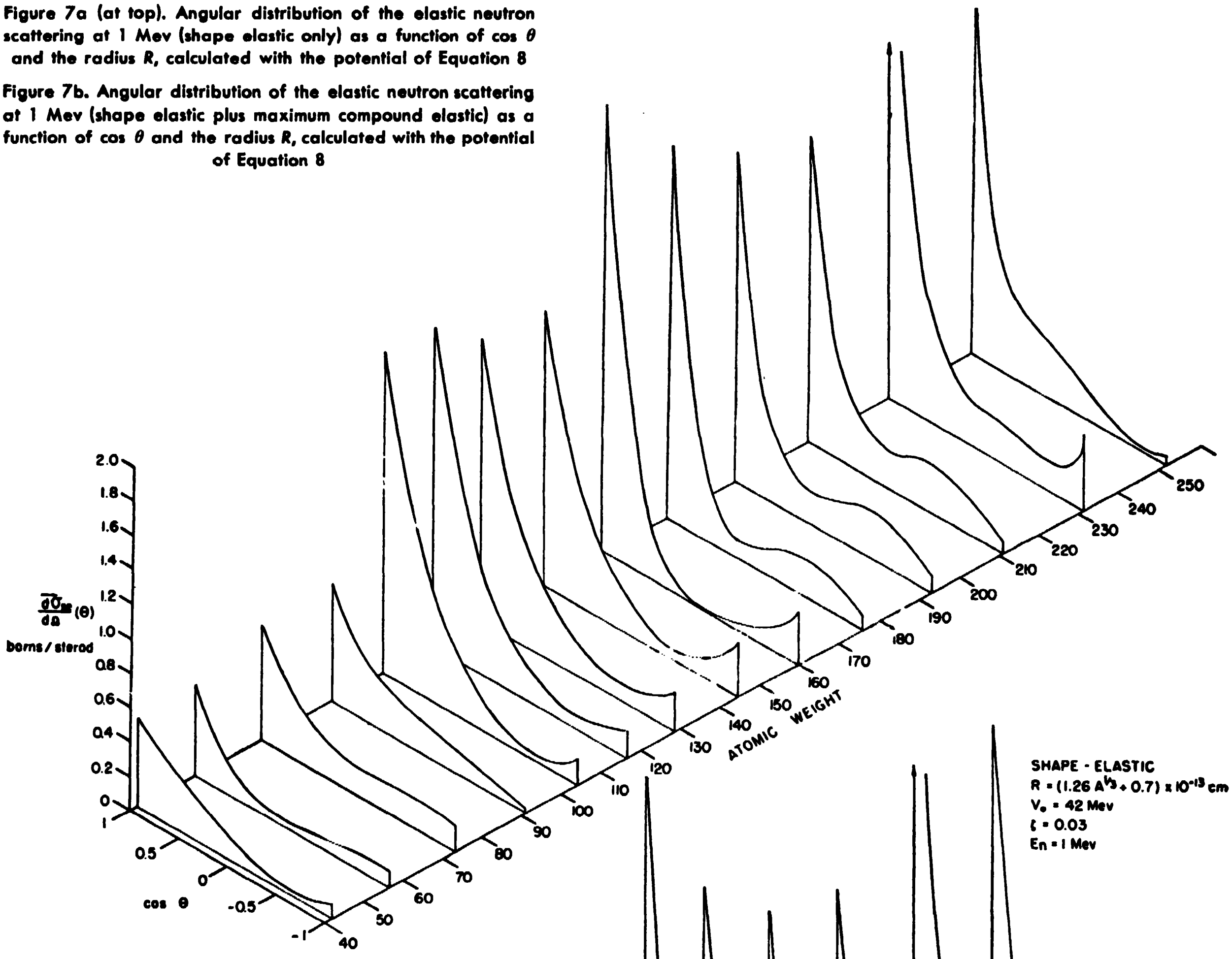

Figure 7a (at top). Angular distribution of the elastic neutron scattering at 1 Mev (shape elastic only) as a function of cos *θ* and the radius *R*, calculated with the potential of Equation 8

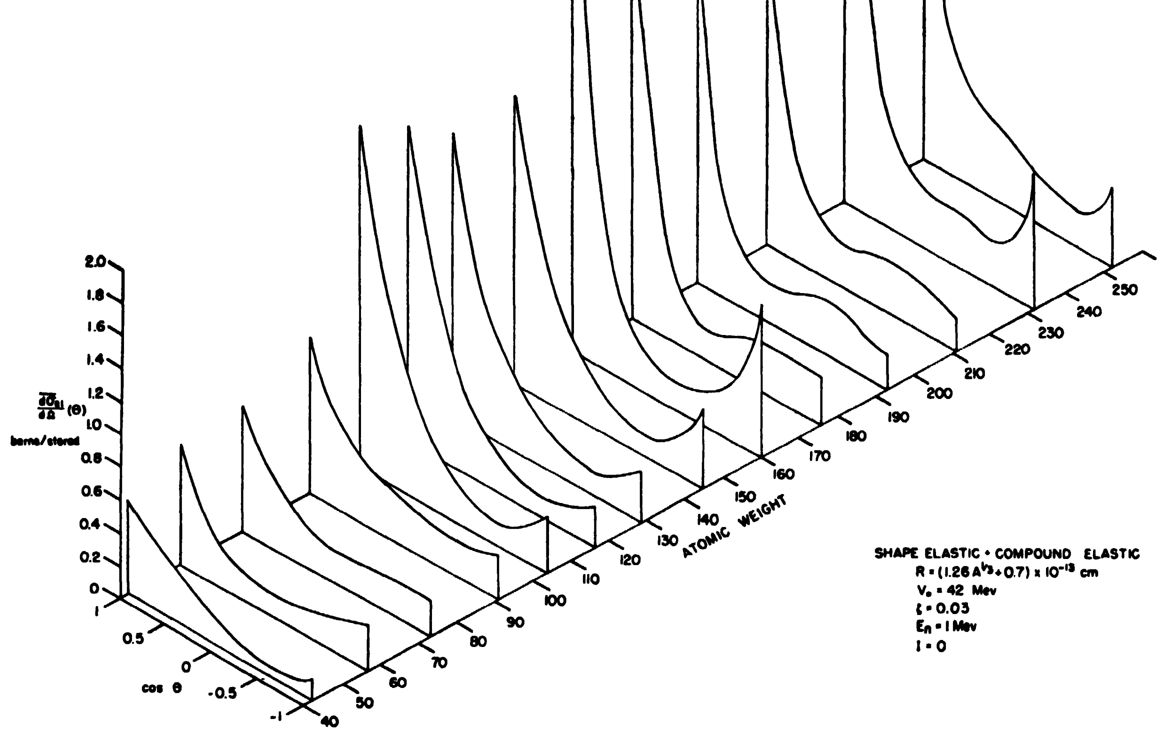

Figure 7b. Angular distribution of the elastic neutron scattering at 1 Mev (shape elastic plus maximum compound elastic) as a function of cos *θ* and the radius *R*, calculated with the potential of Equation 8

where $n < 1$. This relation is an asymptotic one only. Strong deviations, especially at low energy, are expected, and one must be very careful, therefore, in using this expression for the prediction of nuclear properties. Even cursory inspection of nuclear spectra reveals that the level density increases very slowly in the first few Mev. An adjustment of this initial increase to Equation 9 gives much too low a density at $E = B$, the binding energy of the neutron. This is the density observed with slow neutrons. Hence we have to assume a slow initial increase at low energy, which then turns into a rapid increase, in order to reach the observed value at B. The levels at lower excitation correspond to the ones expected on the basis of the shell theory from the single-particle excitations; whereas the subsequent increase reflects the large number of different kinds of motion (single-particle, many-particle excitation, surface oscillations, volume oscillations, etc.) which can be excited and which allow a statistical treatment of nuclear properties at higher excitation.

The quantitative behavior of level densities is still almost completely unpredictable and unexplained. For a fixed excitation energy the even nuclei have a lower density than the odd ones. This is not surprising since the greater stability of even nuclei increases the energies of the different modes of excitation. At low energy (first few Mev) this difference usually amounts to a factor less than 10; whereas at $E \sim B$ differences by a factor 1000 are not uncommon. One of the more surprising features is the behavior of the level density at $E = B$ as a function of A. The density increases rapidly by many orders of magnitude from low A up to about $A \sim 100$ and then stays roughly within one order of magnitude (if nuclei of the same character, even or odd, are compared) for all nuclei above $A \sim 100$. It is also surprising that no clear dependence of the density on the angular momentum of the level has been found.[14]

It must be the aim of any theory of nuclear structure to predict the cross sections of all nuclear reactions. The present state of theory is still very far from it. The most elaborate attempt is the theory of the compound nucleus which is based upon the assumption of independence of the compound nucleus from the way it was formed. Recent experimental material indicates that this independence hypothesis is somewhat questionable and represents a limiting case which is not often realized.[15]

On the basis of the independence hypothesis, the cross-section of a reaction which leads from an entrance channel α to a channel β can be written in the form

$$\sigma(\alpha,\beta) = \sigma_c(\alpha)G_c(\beta) \tag{10}$$

where $\sigma_c(\alpha)$ is the cross-section for the formation of the compound nucleus, and $G_c(\beta)$ is the relative probability (branching ratio) for the decay of the compound nucleus into the channel β. The gross structure of the cross-section $\sigma_c(\alpha)$ is directly given by the optical model as discussed earlier. The branching ratios $G_c(\beta)$ can be determined from formation cross sections by a reciprocity argument. The decay through a given channel is the inverse of the formation of a compound nucleus through the same channel. One gets:

$$G_c(\beta) = \frac{\Gamma(\beta)}{\Gamma} = \frac{k_\beta^2\sigma_c(\beta)}{\sum_\gamma k_\gamma^2\sigma_c(\gamma)} \tag{11}$$

where the k_γ are the wave numbers in the different decay channels, and $\sigma_c(\gamma)$ are the cross-sections for compound nucleus formation in the channel γ. In principle, these cross-sections could be calculated by the optical method. It is questionable, however, whether the imaginary potential that fits the ground state would be adequate to describe compound formation with excited nuclei. Very probably excited nuclei absorb particles somewhat easier, since the Pauli exclusion principle is not quite so effective to prevent interaction. Within the accuracy of these theories, it is sufficient to determine the $\sigma_c(\gamma)$ simply on the basis of a "black" nucleus (large imaginary potential). Equation 10 leads to the following expression for an (a,b) reaction, where a is the incident and b the emerging particle:

$$\sigma(a,b) = \sigma_c(a) \cdot \frac{F(b)}{\sum_c F(c)} \tag{12}$$

where $F(b)$ is given by

$$F(b) = \sum_\beta k_\beta^2\sigma_c(\beta) \tag{13}$$

and the sum is extended over all open channels β that lead to an emission of b. If the excited states in which the residual nucleus can be left are numerous, this sum can be expressed in terms of an integral:

$$F(b) = \frac{2M_\beta}{\hbar^2}\int_0^{\epsilon_{bY}} I_b(\epsilon)\,d\epsilon$$

with

$$I_b(\epsilon) = \epsilon\sigma_c(\epsilon)\omega(\epsilon_{bY} - \epsilon) \tag{14}$$

where M_b is the mass of the particle and ϵ_{bY} is the maximum energy with which it can be emitted, and $\omega(E)$ is the level density of the residual nucleus at the excitation E. The function $I_b(\epsilon)\,d\epsilon$ gives the energy distribution of the particle b emerging from the reaction.

The formulas described here do not include the effect of the conservation of angular momentum. One can refine the procedure by decomposing the reaction into the parts corresponding to a given angular momentum.[16] This refinement gives also predictions as to the angular distribution of the reaction products. This distribution depends upon the spins of the compound state and the residual nucleus. In a gross-structure problem, where averages are taken over the compound resonances, this theory uses a statistical average over the angular moments of the compound nucleus. All angular distributions which are derived from a compound nucleus theory have one feature in common: They are symmetric about 90 degrees. This is due to the fact that the independence hypothesis excludes any phase relations between the emissions from different states of the compound nucleus.

The compound nucleus theory enables us to predict the gross structure of any nuclear reaction cross-section when suitable assumptions are made in regard to the level densities of the residual nuclei. We quote a few important results of this theory.

INELASTIC SCATTERING

The re-emission of the neutron combined with the excitation of the target nucleus is by far the strongest reaction induced by neutrons. Exceptions to this rule occur only when the energy is insufficient to excite the target nucleus and also in the fissionable nuclei. When the incident energy ϵ is much higher than the first excited state of the target, the energy distribution of the secondary neutrons is strongly peaked at energies much lower than the incident energy ϵ. The distribution is similar to a Maxwellian, corresponding to a temperature $T(\epsilon) \ll \epsilon$. The function $T(\epsilon)$ is connected with the level density $\omega(E)$ of the target nucleus:

$$T^{-1} = (d \log \omega/dE)_{E=\epsilon}$$

The theory also gives the probability of excitation of a given state of the target nucleus as a function of the energy ϵ. This excitation function depends upon the spin of that state, and its comparison with the experiment can be used to determine the spin.[17]

OTHER REACTIONS

The theory gives definite results as to the yield of any reaction initiated with neutrons. This yield is based upon the competition of the particular decay with the re-emission of the neutron. Hence (n,p) and (n,α) reactions are predicted to be much weaker than inelastic scattering because of the effect of the Coulomb barrier. This effect is enhanced by the fact that the energy of the outgoing particle is peaked near the temperature T and not at the highest possible energy. The (n,γ) process can be calculated with this theory when suitable assumptions are made regarding the radiation width of the compound states and its energy dependence. The (n,γ) cross-section is predicted to decrease strongly with energy. Important at very low energy, the theoretical cross sections fall to about 0.1 barn at 1 Mev in heavy nuclei ($A > 100$). For higher energies it decreases rapidly because of the overwhelming competition of neutron emission.

Processes in which two particles are emitted, like $(n,2n)$ or (n,np), etc., are considered in this theory to be a succession of two emissions. The first reaction is a (n,n) or (n,p) reaction, which, in some cases, leaves the residual nucleus in a highly excited state so that it is able to emit another particle. From this consideration it follows that the $(n,2n)$ cross-section rises rapidly above its threshold at the expense of the (n,n') cross-section. This rise takes place within an energy interval of the order of the nuclear temperature.

The comparison with the experimental material reveals that the compound nucleus theory of nuclear reactions contains only part of the truth. It turned out to be correct that the inelastic scattering is the most important reaction. Also the energy distribution of the secondary neutron was found to have a low energy peak. In fact, the nuclear temperatures derived from the position of the maximum and from the general form of the distribution are somewhat lower than expected (0.75 — 1 Mev for $\epsilon = 14$ Mev) and were found for $\epsilon = 14$ Mev to be roughly the same for all heavier nuclei.[18] This equality of temperatures is surprising in view of the statistical interpretation of the process. One would expect that the same energy leads to lower temperatures for heavier nuclei.

The excitation of a given state of the target nucleus as a function of ϵ is well represented by the theory. The energy dependence of the cross-section and the absolute value agree fairly well with theory in almost all cases.[19]

The most striking disagreement with the compound nucleus theory lies in the fact that the inelastic scattering contains much more high-energy neutrons than the theory accounts for. The energy distribution deviates from Equation 14 when the energy ϵ exceeds the nuclear temperature. The excess is so strong that it cannot be accounted by any change in the assumptions regarding the level densities without contradicting other observations. Also these high-energy secondary neutrons have an angular distribution which is peaked in the forward direction, a feature which cannot occur in the theory of the compound nucleus.[20]

The yield of neutron-induced reactions is also often in disagreement with the compound theory. Paul and Clarke[21] have shown that at 14 Mev the (n,p) and (n,α) reactions are stronger than Equation 12 would admit. For very heavy nuclei the compound theory for these reactions predicts extremely small cross-sections which are several orders of magnitude smaller than the observed ones. It should be added that the observed values, though larger than the theoretical values, are still very much smaller than the cross-sections for inelastic scattering. The observed angular distributions of the secondary particles have maxima in the forward direction.

The (n,γ) cross-sections have been observed so far in the energy region from zero up to a few Mev.[22] They show essential agreement with the predictions of the compound theory.[23] Of course, the predictions contain certain assumptions as to the radiation width and its dependence upon the energy of the compound nucleus. Recent measurements of (p,γ) cross-sections by B. Cohen and P. Gugelot[24] indicate that at higher energies ($\epsilon > 5$ Mev) the (p,γ) cross-section is considerably larger than the theoretical value. It is probable that the (n,γ) cross-sections would also exceed the predicted value in that energy region.

The predictions of the compound nucleus theory in regard to the $(n,2n)$ processes are found to be well fulfilled. A slight discrepancy remains, since the nuclear temperatures derived from the $(n,2n)$ yield curves are somewhat higher than the temperatures derived from the inelastic scattering and its energy distribution. The yields of (n,pn) reactions are somewhat larger than the theory would predict.

The character of the deviations of the observed reaction cross-sections from the theoretical predictions indicates very strongly that the deviations might be explained by a direct momentum transfer from the incident neutron to a single nucleon in the nucleus. The optical model of the nucleus has shown that the mean free path of a neutron in nuclear matter, even at higher energies, is comparable to the nuclear radius. Hence the following processes must occur with reasonable probabilities:

(*a*) The incident neutron interacts with one nucleon by elastic collision and has enough energy left to leave the nucleus again and reaches the outside without further interaction.

(*b*) The struck nucleon acquires enough energy to leave the nucleus without further collisions with other nucleons. Both processes give rise to apparent inelastic scattering or to (n,γ) reactions and lead to cross-sections and angular distributions different from the compound nucleus theory. In these processes the secondary particles acquire an energy in excess of the nuclear temperature and are peaked in the forward direction. Some attempts have been made to calculate these effects and the results are encouraging.[25]

Also in the (n,γ) processes single-particle transitions can play a role if the cross-section as calculated with the compound nucleus theory becomes very small. A neutron can make direct radiative transitions in the potential well of Equation 8 before it is absorbed. These transitions give rise to (n,γ) cross-sections of the order of a few millibarns and might account for (n,γ) processes in heavy nuclei for neutrons with an energy above 5 Mev.

SUMMARY

For the theoretical prediction of neutron cross-sections, it is useful to distinguish between bulk cross-sections and detailed cross-sections. The former ones are total, elastic and reaction cross-sections; the latter ones are the actual cross-sections for specified reactions. The bulk cross-sections concern exclusively the incident beam; they are defined by the situation in the entrance channel. The detailed cross-sections reflect the effects of the mechanism of energy transfer from one channel to the other. The bulk cross-sections are therefore more accessible to theoretical discussion by simple nuclear models. In particular, the gross structure can be reasonably well represented by the optical model of the nucleus.

The problem of the theoretical prediction of the detailed cross-sections is much harder. There are two "complementary" descriptions of nuclear reactions which can be used for the calculation of the cross-sections. One is the theory of the compound nucleus which assumes that a nucleon shares its energy completely with the whole nucleus upon entering the interior. The other is the individual particle theory which assumes that, in an (a,b) reaction, the incident particle a directly interacts with the particle b and transfers its energy by an elastic collision.

It is very probable that both aspects play an important role in nuclear reactions. At present it is not yet possible to predict in each case the limits of validity of the two aspects. However, the concept of mean free path in nuclear matter, which is introduced by the optical model, could be helpful in estimates of the validity of the individual particle aspect. It is to be expected that the compound nucleus aspect will become valid if the individual particles have been "absorbed" before reaching the surface of the nucleus. We have reason to hope that the theory of nuclear reactions will be more successful when the enormous amount of new experimental material has been better understood and analyzed.

REFERENCES

1. Fernbach, Serber, and Taylor, Phys. Rev. *75*, 1352 (1949).
2. Feshbach, Porter, and Weisskopf, Phys. Rev. *96*, 448 (1954).
3. Morrison, Muirhead, and Rosser, Phil. Mag. *44*, 1326 (1953). Lane, A. M. and Wandel, C. F., Phys. Rev. in print.
4. Thomas, R. G., personal communication.
5. Bohr, A. and Mottelson, B. R., private communication.
6. Walt, M. and Barschall, H. H., Phys. Rev. *93*, 1062 (1954).
7. Calculation made by W. S. Emmerich.
8. Gittings, Barschall, and Everhart, Phys. Rev. *75*, 610 (1949). Phillips, Davis, and Graves, Phys. Rev. *88*, 600 (1952).
9. Walt, M. and Beyster, J. R., to be published in Phys. Rev.
10. Culler, Fernbach, and Sherman, unpublished communication. Coon, J., unpublished communication.
11. Breit, G. and Wigner, E. P., Phys. Rev. *49*, 519 (1936). Bethe, H. and Placzek, G., Phys. Rev. *51*, 450 (1937).
12. Hughes, D. J. *et al.*, Brookhaven National Laboratory, to be published soon.
13. Bethe, H., Revs. Mod. Phys. *9*, 71 (1937). Bloch, C., Phys. Rev. *93*, 1094 (1954).
14. Harvey, Hughes, Carter, and Pilcher, Phys. Rev. in print.
15. See Friedman, F. L. and Weisskopf, V. F., *Niels Bohr and the Development of Physics*, Pergamon Press, London, to appear October, 1955.
16. Hauser, W., and Feshbach, H., Phys. Rev. *87*, 366 (1952).
17. See Reference (16).
18. Gugelot, P. C., Phys. Rev. *81*, 51 (1951). Graves, E. R. and Rosen, L., Phys. Rev. *89*, 343 (1953).
19. Margolis, B., Phys. Rev. *93*, 204 (1954).
20. Eisberg, G. and Igo, R. M., Phys. Rev. *93*, 1039 (1954).
21. Paul, E. B. and Clarke, R. L., Can. J. Phys. *31*, 267 (1953).
22. *Neutron Cross Sections*, US AEC Report 2040, Washington (1952). Dementi and Timoshuk, Dokhl. Akad. Nauk. USSR *27*, 929 (1940). Mescheryakov, M. G., Dokhl. Akad. Nauk *48*, 555 (1945).
23. Blatt, J. M. and Weisskopf, V. F., *Theoretical Nuclear Physics*, Chapter 12, John Wiley and Sons, 1952.
24. Cohen, B. and Gugelot, P. C., personal communication of unpublished work.
25. McManus, H. and Sharp, W. T., Phys. Rev. *87*, 188 (1952).

Investigation of Neutron Beta Decay

By P. E. Spivak, A. N. Sosnovsky, A. Y. Prokofiev and V. S. Sokolov, USSR

Measurements of the neutron half-life, and preliminary experiments in angular electron-proton recoil correlation have been made on a pile neutron beam. The first measurements gave the half-life in the range 8–15 minutes. Further measurements, in which the proton collecting efficiency factor was eliminated, gave the value 12 ± 1.5 minutes for the half-life of the neutron. The results of the preliminary measurements of the angular correlation are in agreement with theory but are not sufficiently accurate for determining the particular form of the beta interaction.

PART I. MEASUREMENT OF THE NEUTRON HALF-LIFE*

The experiment was set up to detect the decay of the neutron and to measure its half-life.

The method used was based on observing neutron decay by registering the resulting protons and the procedure was as follows:

An intensive neutron beam was passed through a vacuum tank at some distance from the proton detector placed inside the tank. Between the tank and the detector an accelerating potential (10–20 kv) was applied, sufficient to collect a large part of the protons formed in the beam (boundary energy of proton spectrum ~750 v).

As the indicator had to count protons accelerated to an energy as low as 10–20 kev, was in close proximity to the neutron beam and badly shielded against radiation, a small proportional counter was used as an indicator. The results proved that this choice was justified. A film placed between the counter and the vacuum tank did not stop the protons, which lost only 2.5–3 kev in the film, but kept heavy ions from getting into the counter.

Work on the experiment began in April 1946. The measurements, however, began much later, in October 1949, when the opportunity presented itself to carry out the experiment on a sufficiently intensive beam of neutrons.

Description of Arrangement and Proton Counter

Figure 1 shows an over-all view of the apparatus. The tank *A* was pumped out to a high vacuum of ~1 to 2×10^{-6} mm Hg. The protons were focused by means of a radial electric field applied between the tank and the central electrode *C*. The tank served as the high-voltage electrode, and the central electrode was grounded. An additional electrode *B* was used to improve the shape of the electric field in the active volume of the tank. The windows through which the neutron beam passed were made of thin aluminum and were at some distance from the active volume.

Figure 2 shows a section through the central electrode head. The aperture in the head is covered with a spherical thin tungsten wire mesh. Inside the electrode is the proportional counter.

The counter window was covered with a film 0.06–0.07 micron thick made with ordinary medical collodion from which a large part of the ether had been removed and which had then been diluted with butyl-acetate. The film was formed on a water surface and was lifted up on the edge of a kind of spatula with a hole in the middle of the blade. Thus, over the hole the film was double.

The thickness of the film was judged from the interference color. The film with which the counter window was covered was black; four such films, in optical contact, were green. The film thus formed was placed

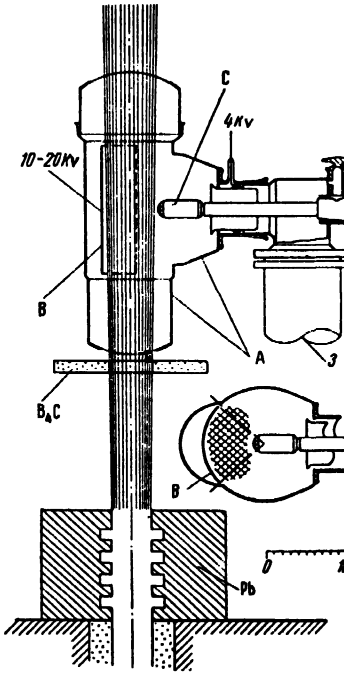

Figure 1. Over-all view of the apparatus: (A) vacuum tank; (B) auxiliary electrode; (1) to glass reservoir; (2) to amplifier; and (3) to pump

---

Original language: Russian.

* This report is based on the results of an investigation made in 1950.

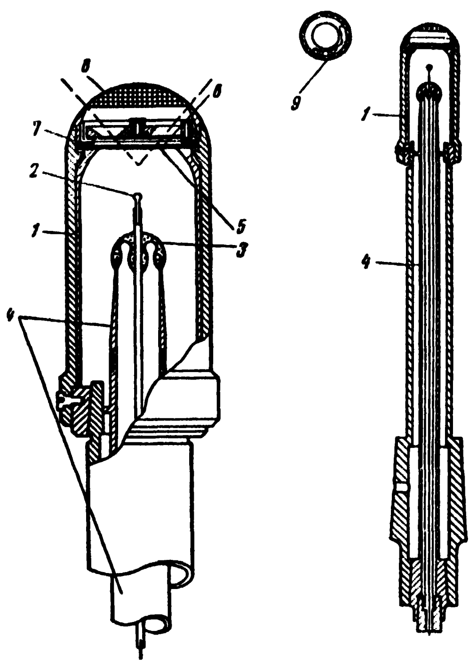

Figure 2. Cross section through central electrode: (1) outer electrode of counter; (2) collecting electrode; (3) insulator; (4) pin of collecting electrode; (5) film; (6) film supporting wire mesh; (7) spring; (8) spherical mesh; and (9) alpha-particle source

on an auxiliary ring and from there on the counter window. After that the head of the central electrode was put on the counter and the wire mesh for supporting the film pressed on to it by a flat spring.

The counter was connected to a small glass tank filled with a mixture of 75% A and 25% CF_4 to a pressure of about 12 mm Hg.

The size of the counter and the pressure of the gas in it were chosen in accordance with the proton range at energy 15-17 kev. The gas leakage through the film was so small that it permitted to ensure a high vacuum in the tank, a stable gas amplification and long performance without adding more mixture.

The collecting electrode of the counter, to which a working potential was applied, was connected to the recording system which consisted of a linear amplifier with a gain of about 10^5, a pulse-height discriminator and a scaler.

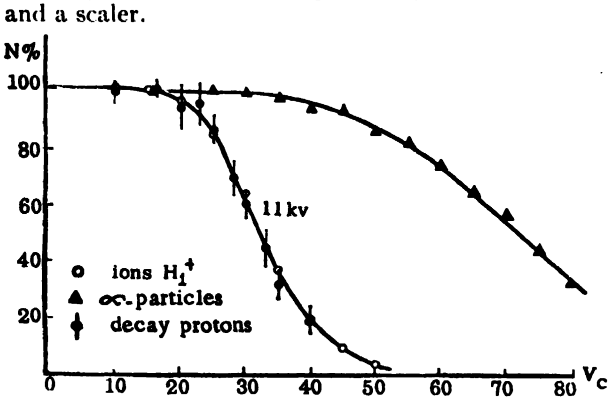

Figure 3. Pulse height distribution. Open circles, ions H_1^+; triangles, α-particles, closed circles, decay protons

The first testing and calibration of the counter was done by means of alpha particles. Figure 3 shows the pulse-height distribution of polonium alpha particles.

Figure 4 shows the set-up for measuring the proton pulse-height distribution and energy loss in the film. In this set-up the protons were drawn from the hydrogen discharge region, accelerated and separated by a magnetic spectrograph. The hydrogen entered through a palladium tube, from which the necessary pressure to create a discharge between the electrodes 1 and 2 may be obtained by heating. The ions passed through the 30-micron aperture in the electrode 2, were accelerated and selected by the diaphragms D_1 and D_2 of chamber 4 located in the magnetic field.

When the discriminating cut-off voltage was set close to the noise level, H_1^+ ions could be counted from an accelerating potential as low as 2.7 kv. When the potential was higher, H_2^+ ions also passed through the film, but their pulse-height distribution was broader and their pulse-heights smaller. The pulse height-distribution of H_1^+ ions accelerated to 11 kev is illustrated in Fig. 3 (open circles).

Quick adjustment of the counter gas amplification necessary for proton registration was achieved in the neutron beam measurements, by means of an alpha-particle source. The discriminator potential cut-off was then set to ensure 100% proton counting efficiency.

Measurements and Results

First of all measurements were done to show whether protons were produced in the tank if a neutron beam passed through it.

It was indeed observed that the number of pulses above counter background (measured with the accelerating potential switched off) increased when a potential sufficient to accelerate the protons and to collect a significant part of them in the counter was applied.

To be sure that this effect was really due to the decay of the neutrons, it was necessary to prove that the detected particles were protons and that they were caused by the presence of thermal neutrons in the tank. Since this effect should show up as the

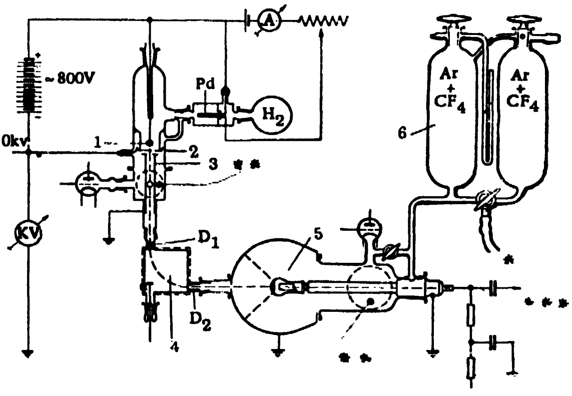

Figure 4. Set-up for measuring proton pulse height distribution: (1, 2, 3) electrodes; (4) chamber of magnetic spectrograph, (D_1 and D_2) diagrams; (5) counter; and (6) glass reservoir; * to f.v. pump, ** to h.v. pump,*** to amplifier

difference between the number of counts with and without the accelerating potential, it was necessary to show that the background did not depend on the electric field.

For this purpose three control experiments were performed. In the first the neutron beam was cut off by a boron shutter. In the second the tank was moved to such a position relative to the neutron collimator, that the beam would strike the tank walls, greatly increasing their irradiation, the active volume of the tank being shielded by a boron shutter. In the third, a cadmium shutter intercepted the beam near the tank, to increase the irradiation of the tank by gamma rays.

In all three cases the number of pulses did not depend on the accelerating potential in the tank, as long as it did not exceed 20 kv. At potentials $V > 20$ kv the number of pulses increases and rises sharply with the increase of the potential, depending on the intensity of the tank irradiation.

This effect had been observed already in the process of setting up the apparatus. If a high potential was applied to the electrodes, the counting system registered pulses, the number of which increased with potential as well as with irradiation of the tank with gamma rays from a radioactive source. It did not change with the degree of vacuum over a wide range, but greatly depended on the material of the tank and the finish of its interior surface. Measurement of the pulse-height distribution at different values of the accelerating potential showed that the pulses were due to hydrogen ions arising in the tank and focused upon the counter window.

The appearance of ions not due to neutron decay was observed also by other investigators.[1,2,3] Evidently, just because it is hard to distinguish the background caused by such ions, these investigators were for a long time unable to conclude with certainty what part of the observed effect was due to neutron decay. This difficulty was overcome in one study by registering the coincidences between the decay proton and electron.[3]

We succeeded in greatly reducing this effect by using an aluminum tank with a well-polished interior surface, oxydized with a 3% chromic acid solution.

Thus from our control experiments it follows, firstly, that when a neutron beam passes freely through the thin aluminum windows of the tank the number of background pulses does not depend on the accelerating potential if the latter is less than 20 kv; and, secondly, that the observed effect is caused by particles originating in the tank and in the thermal neutron beam.

To ascertain the nature of these particles, the distribution of the heights of the pulses created by them in the counter was investigated. The pulse-height distribution measured at various values of the accelerated potential coincided well with the corresponding data for H_1^+ ions. (Comparison for the value 11 kv is given in Fig. 3). The experiments showed that the effect depends strongly on the potential, which means that the initial velocities of the investigated particles were much lower than the velocities they attained after acceleration. The agreement between the pulse-height distribution curves shows that the investigated particles lose the same energy in the film and create the same ionization in the counter as do H_1^+ ions. Hence it definitely follows that the particles causing the effect are really protons.

The results of these experiments leave no doubt that the protons originated in the beam of neutrons, whose decay has thus been fully established.

The next problem was to measure the neutron half-life. For this it was necessary to determine the number of neutrons in the active volume of the tank and the number of protons arising in this volume.

To determine the number of neutrons, the distribution of neutron density over the beam cross section was measured by a small boron chamber. The absolute density was measured by activation of a gold foil. The maximum density was 260 ± 15 cm^{-3}. Using the data of these measurements one can calculate the total number of neutrons N_n in the active volume of the tank, which in our case was 10.4×10^4.

The number of neutrons N_p registered by the counter was measured at an accelerating potential of 17 kv and a discriminator cut-off corresponding to the plateau of the curve $N_p(V_c)$, i.e., at 100% efficiency of the counter.

At this discrimination cut-off the background, which owing to the small size of the counter and low pressure of the gas in it, was not too large, still exceeded the effect several-fold and depended strongly on the discrimination cut-off. The effect, therefore, was measured repeatedly: in each series, the accelerating potential was switched on and off alternately every 5–10 minutes. This eliminated the error that could arise from a slow drift of the counter's gas amplification.

The measurements showed that under the given conditions the proton counting rate was 1024 per minute. The ratio of the number of protons collected in the counter to the number of protons formed in the tank volume (collection factor k) was calculated by Y. A. Smorodinsky and co-workers. The calculations showed that in these experiments the value of this factor is between 0.16 and 0.26, depending on the assumption one makes regarding the proton initial velocity spectrum.

Substituting the above values in the expression

$$T_{1/2} = \ln 2 \frac{N_n}{N_p} k\eta$$

where $\eta = 0.7$ is the penetrability of the wire meshes in front of the counter window, we obtain a value of 8–15 minutes for the half-life $T_{1/2}$.

A More Accurate Neutron Half-Life Measurement

This value for the neutron half-life, 8–15 minutes, derived from our above measurements is, of course, not quite satisfactory because of the rather wide limits. Similar results were obtained by Snell and co-workers[1,2,3] who found 10–30 minutes. Robson[4,5] obtained 9–25 minutes, and in 1951[6] got a more accurate value of $T_{1/2} = 12.8 \pm 2.5$ minutes. The error is due mainly to the uncertainty in the collection factor.

In an attempt to obtain better results we rearranged our experiments somewhat and succeeded in eliminating altogether the dependence of the collection factor on the proton spectrum.

Suppose the neutrons in the tank uniformly fill a certain spherical layer around the central electrode. In this case, the recoil proton distribution along the surface of the electrode will likewise be uniform and, beginning with a certain value of the accelerating potential $V = V_{min}$, all protons arising in the tank volume will reach the central electrode.

It is then obvious that the number of protons striking any area of the central electrode, defined by a solid angle ω, is equal (due to the spherical symmetry) to the number of protons formed in the cone volume V_ω within this solid angle (this cone is shown in Fig. 5 by dashed lines). Thus the number of protons striking any area S, such as the window of the central electrode, for example, increases with the potential until V becomes equal to V_{min}, and reaches its saturation value equal to the number of decays occurring in volume V_ω, and upon a further rise of the accelerating potential remains constant. At the same time, with the increase of the potentials (that is, at $V > V_{min}$) the decays that occur in the region far outside the region V_ω cease to contribute to the number of protons striking the area S. Therefore, if the potential is sufficiently high, there is no need to fill the entire volume of the tank with neutrons. It is sufficient to fill the volume V_ω and a certain adjacent region. It is readily seen that the neutron density in the beam likewise need not be uniform; it is enough if the surfaces of uniform density coincide with the equipotential surfaces.

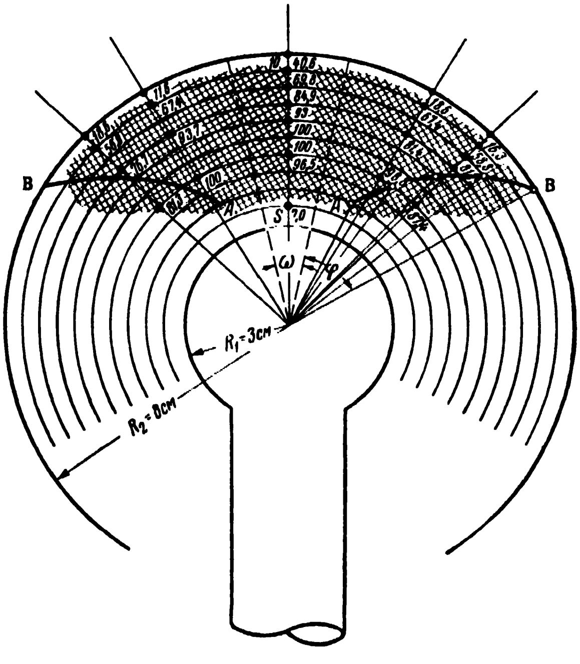

Figure 5. Schematic cross section through vacuum tank

In practice the region occupied with neutrons is determined by the neutron beam cross section. The neutron beam in our case had a diameter of approximately 130 mm. The calculation, which we are not giving here, shows that in this case, if the tank radius is 80 mm and the radius of the central electrode 30 mm, and the opening of the cone 23 degrees, the count of the protons reaches its stationary value at an accelerating potential of 15 kv.

In Fig. 5 the calculated boundaries of the active region are indicated by the lines AB, and the neutron beam cross section by the shaded part. The figures are the relative neutron densities at the corresponding points.

The apparatus used in these experiments is quite similar to that described in our previous experiments. A detailed cross section of the central electrode head is shown in Fig. 6. Its aperture is 12 mm in diameter and is covered with a spherical thin tungsten wire mesh. As in the previous case, the proton detector is a proportional counter. It is mounted inside the central electrode so that its window, 14 mm in diameter, is as near as possible to the electrode aperture. All protons focused on the electrode aperture, except those stopped by the meshes, enter the counter and are registered with 100% efficiency.

Results of the Measurements

The maximum neutron density ρ_{max} was determined in the same way as in our previous experiment and was

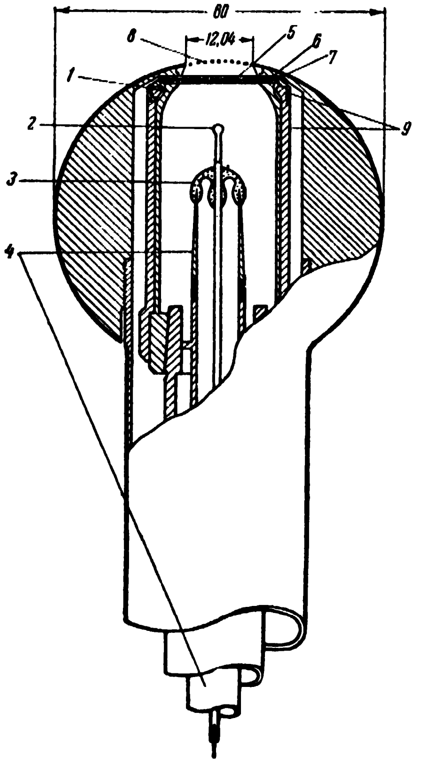

Figure 6. Cross section through central electrode: (1) outer electrode of counter; (2) collecting electrode; (3) insulator; (4) pin of collecting electrode; (5) film; (6) film supporting mesh; (7) spring; (8) spherical mesh; and (9) cylinder

equal to 290 ± 15 cm^{-3} and the total number of neutrons in the volume $N_n = (15.2 \pm 0.5) \times \rho_{max}$.

The measurements too were performed as in the previous work, that is, the number of decay protons was determined as the difference of counts with and without collecting voltage. The results of the measurements are shown in Fig. 7. From 15 to 16 kv on, the number of decay protons N_p reaches a stationary value of 180 ± 10 per minute. The error of this number, due to a certain fraction of the protons falling on the surface of the tank, is small, about 1 1.5%. The geometric transmission of the grids η is 0.7 (the transmission of each separately is 0.86 and 0.81, respectively). The error due to the dependence of the transmission on the angle of proton incidence does not exceed 1%.

Substituting the above values in the expression

$$T_{1/2} = \ln 2 \cdot \frac{N_n}{N_p} \cdot \eta$$

we get the value 12 ± 1.5 minutes for the neutron half-life.

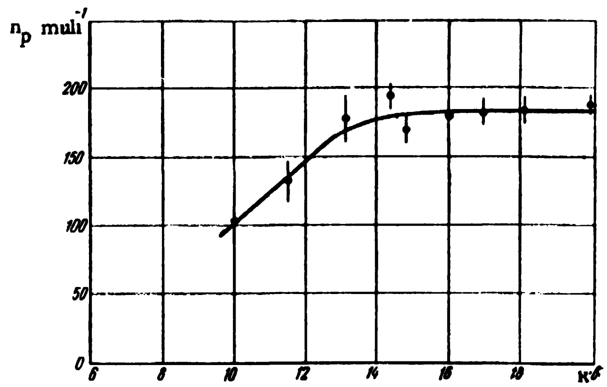

Figure 7. Decay proton counting rate, plotted against accelerating potential

In the future we intend, by using the apparatus built for investigating the electron-proton angular correlation in neutron beta decay (preliminary results of which are described below), to repeat the experiment for determining the neutron half-life. In our planned experiment, the decay protons will be collimated so that they will be totally focused on the counter. In this case, the registration efficiency of the recoil protons originating in the active part of the neutron beam can be calculated quite accurately. Thus, the errors of the previous measurements will be avoided, and we may hope that the error in these experiments will be mainly due to errors in neutron density measurements, and will not exceed 3–4%.

PART II. ANGULAR CORRELATION IN NUCLEAR DECAY

The exact form of the beta interaction law may be found, as is known, by experimental investigation of electron-recoil nucleus correlation.[7] Results of such experiments with P^{32}, He^6, Y^{90}, and Ne^{19} have already been published[8–12]. These results, together with discussions of other experimental facts, lead one to assume with high probability that the beta interaction law is determined by a linear combination of tensor (T) and scalar (S) invariants.[13,14]

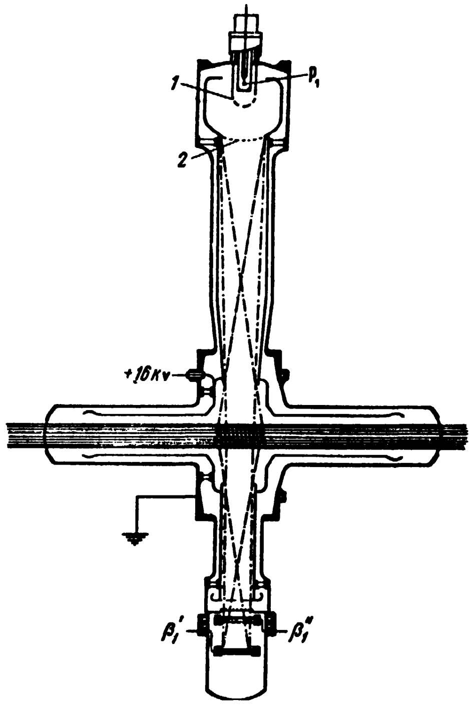

Figure 8. Over-all view of apparatus for studying angular correlation: (P_1) proton counter; (1, 2) grids between which accelerating potential is applied, (β_1' and β_1'') electron counters

We have begun an experimental study of electron-proton angular correlation in neutron beta-decay. A brief description of the set-up and preliminary results of the measurements, which are still going on, is given below. These measurements are conducted on the pile thermal neutron beam. The coincidences are recorded between the delayed pulses of three electron and three proton detectors, situated in the plane perpendicular to the axis of the beam passing through the vacuum tank. The detectors are arranged to register simultaneously the effect at several angles.

This work encounters certain difficulties due primarily to the small effect (7 coincidences per hour at an angle of 162 degrees), proportional to the detector solid angles. For our purpose these angles must, naturally, be small, and are 10^{-3}. On the other hand, the background of the accidental coincidences, even with a thick lead, boron, and paraffin shield, likewise amounts to about 5 coincidences per hour at each angle. This large background is chiefly due to the high rate of the beta located near the beam and to the resolving time of the coincidence circuit (4 microseconds), chosen in accordance with the time-of-flight of the decay protons.

Figure 8 shows a schematic cross section of the apparatus through the proton (P) and electron (β_1' and β_1'') detectors set at 180 degrees to each other.

To reduce the background, the electrons are registered by means of two banks of self-quenching

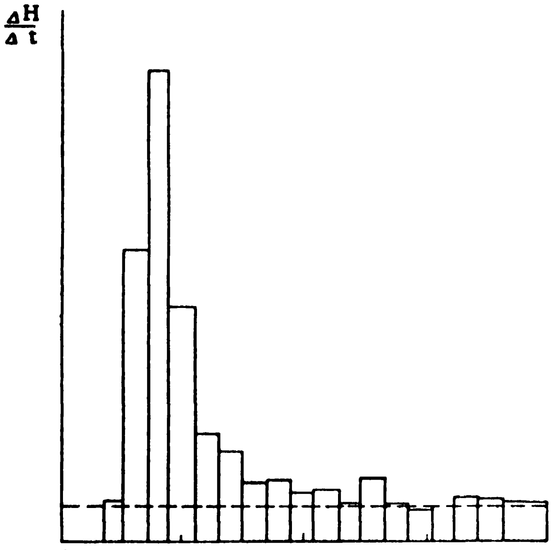

Figure 9. Proton time-of-flight distribution at 180 degrees

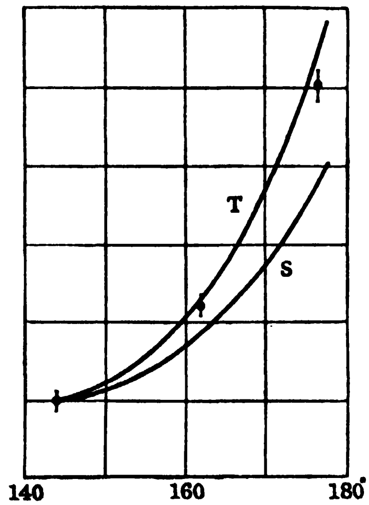

Figure 10. Results of angular correlation measurements and theoretical curves for *T* and *S* interactions

counters in coincidence and placed in a common chamber. The window of the chamber, 70 mm in diameter, is covered with a film 4–5 microns thick, which separates the chamber from the vacuum tank. To avoid absorption of the electrons in the counter walls the cathodes were made of thin wire. Both banks, together with the mesh supporting the film, have 65% penetrability.

The recoil protons, after passing a field-free space, enter a spherical electric field applied between grids 1 and 2, are accelerated in it to 16 kv and are focused on the window of the proportional counter. This window is 16 mm in diameter and is covered with a film about 0.07 microns thick.

The decay electron pulses are fed into a 6-microsecond delay line which, starting from 2 microseconds (maximum energy proton time-of-flight), has taps spaced 0.4 microseconds apart and leading to proton-electron pulse coincidence circuits. A tape recording device registers the coincidences and in which pair of indicators (i.e., at which angle) they occurred. Simultaneously, the counting rates of each proton and electron indicator are registered.

Thus the set-up makes it possible to record proton time-of-flight simultaneously with counting the coincidences at various angles, and measure the background of accidental coincidences. Figure 9 gives a histogram of one series of measurements obtained in our experiments, showing the proton time-of-flight distribution at 180 degrees between the detectors, and the relation between the background (dashed line) and the effect at this angle. The results of the measurement, which lasted altogether about 120 hours, are shown in Fig. 10 together with the theoretical curves for the (*T*) and (*S*) interactions, calculated by A. G. Afanasyev. The theoretical curves have been fitted to our experimental point at 144 degrees. The graph gives only the statistical errors of measurement.

The data does not yet include corrections for systematic errors, which are now being determined. Such corrections are to take into account the angular width due to the finite dimensions of the detectors and the source (the beam diameter is 70 mm), as well as the efficiency of electron and proton counting, which depends upon the energy of these particles and differs for different angles. The preliminary experiments and calculations show that these corrections will not be very large and can be determined with the required accuracy.

Thus, the angular distribution obtained in our experiments generally agrees with theory, though we still cannot choose or reject any particular form of beta interaction. The work will be completed in the near future, and we then hope to reach more definite conclusions.

REFERENCES

1. Shrader, E. F., Saxon, D. and Snell, A. H., Phys. Rev., *70*, 791, (1946).
2. Snell, A. H. and Miller, L. C., Bulletin of the American Phys. Soc., *23*, 2, (1948).
3. Snell, A. H., Pleasonton, F. and McCord, R. V., Phys. Rev., *78*, 310, (1950).
4. Robson, J. M., Phys. Rev., *77*, 747, (1950).
5. Robson, J. M., Phys. Rev., *78*, 311, (1950).
6. Robson, J. M., Phys. Rev., *83*, 349, (1951).
7. Blatt, D. M. and Weiskopf, V., Theoretical Nuclear Physics, Moscow, (1953).
8. Sherwin, C. W., Phys. Rev., *73*, 1173, (1948).
9. Sherwin, C. W., Phys. Rev., *82*, 52, (1951).
10. Rustad, B. M. and Ruby, S. L., Phys. Rev., *89*, 880, (1953).
11. Allen, J. S. and Jentschke, W. K., Phys. Rev., *89*, 902, (1953).
12. Alford, W. P. and Hamilton, D. R., Phys. Rev., *95*, 1351, (1954).
13. Mahmoud, H. M. and Konopinski, E. J., Phys. Rev., *88*, 1266, (1952).
14. Yamada, M., Progr. Theoret. Phys., *10*, 252, (1953).

Thermal-Neutron Capture Gamma Rays

By L. V. Groshev, B. P. Adyasevich, and A. M. Demidov, USSR

Thermal-neutron capture gamma radiation from nuclei was investigated with the aid of a Compton-electron magnetic spectrometer. The sample under investigation was irradiated with thermal-neutron flux from the RTP reactor. Spectra of beryllium, sodium, sulphur and chlorine gamma rays have been measured in the energy range from 0.3 to 10 Mev. The treatment of results obtained made it possible to deduce the intensities of some spectral lines in terms of photons per neutron capture. For a number of transitions experimental radiation probabilities were compared with theoretical ones calculated from Weisskopf's formulas. Spins of some of the lower levels of Cl^{36} and Na^{24} were determined.

INTRODUCTION

The present work is aimed at the investigation of thermal-neutron capture gamma radiation from nuclei. A nucleus which captures a thermal neutron is excitated up to the neutron binding energy of about 8 Mev. Particle emission under such an excitation (excluding the cases of some light nuclei) is of little probability and therefore the nucleus is de-excited by emission of gamma quanta. Studies of gamma-ray spectrum from the (n,γ) reaction make it possible to find level energy differences as well as relative probabilities of gamma transitions which occur between levels at energies lower than the neutron binding energy.

This, with the addition of data on nuclear characteristics of excited levels obtained from charged particle and neutron reactions, enables one to establish the most probable decay scheme of capturing states as well as characteristics of gamma transition (their multipole type and order).

Total radiative widths Γ_r are known for certain nuclei which, together with the experimentally measured relative gamma-ray intensities, permit one to determine the absolute probabilities of the corresponding gamma transitions and thus to get some knowledge of the radiative properties of nuclei. The knowledge of these properties may provide a check of a particular nuclear model because the theory of nuclear radiative properties is essentially connected with the internal structure of atomic nuclei. On the other hand, the accumulation of experimental data and the search for empirical regularities connected with nuclear radiative properties may form the basis for constructing a nuclear model.

At present abundant material is available on radiative properties of nuclei at excitation energies up to 2 Mev (excited states following $\beta^{\pm}$ decay or K-capture).

The study of neutron capture gamma-rays considerably increases the number of energy states which can be investigated.

Since 1948 thermal-neutron capture gamma-rays have been studied by Kinsey *et al.* (Canada). They have investigated almost every element of the periodic system. For studying the gamma-ray spectra they used a magnetic pair spectrometer and measured only the gamma-rays with energies exceeding 3 Mev. However, for energies below 4.5 Mev, only very intense gamma lines were measured. This group of authors analysed the results obtained for a large number of elements. They have established a number of empirical regularities for thermal-neutron capture gamma-rays.[1]

Some attempts have been made to measure neutron capture gamma radiation by means of scintillation spectrometers. Several intense lines for some elements have been measured by this method but no extensive results have been obtained so far.

In view of the impossibility of measuring gamma-ray energies lower than about 3 Mev with the aid of a magnetic pair spectrometer, we used a Compton-electron magnetic spectrometer to study the thermal-neutron capture gamma-rays. The efficiency of this instrument is less dependent on gamma-ray energy and thus it is possible to measure gamma-ray intensities and energies within the range of 0.3 to 12 Mev. Besides, the calculation of efficiency of this instrument is easy and reliable as compared with the case of a magnetic pair spectrometer.

1. THE SPECTROMETER AND THE METHOD FOR THE MEASUREMENT OF γ-RAY SPECTRA

Thermal-neutron capture gamma-ray spectra were measured with samples placed into the thermal column of the RTP reactor. Figure 1 shows the experimental arrangement. The sample under investigation enclosed in a graphite container was placed into the hole of the reactor thermal column near the reflector. Gamma rays emitted by the sample were collimated by three bismuth diaphragms inside the hole and two external lead diaphragms placed in front of the spectrometer. A shutter of boron carbide or of lithium bicarbonate was installed for absorbing neutrons at the outer end of the thermal column. A bismuth block

---

Original language: Russian.

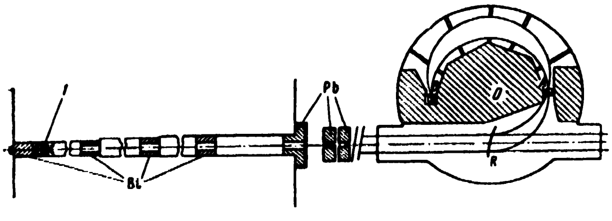

Figure 1. General arrangement of experiment, 1 is sample

7 1/3 inches thick was placed at the inner end of the hole in front of the sample to reduce the gamma-ray background from the reactor and reflector. The distance between the irradiated sample and the spectrometer was approximately 16 ft. The amount of material in the irradiated samples varied over a wide range (from several grams to several kilograms) depending on thermal-neutron absorption cross-section.

In our experiments we used a gamma-ray spectrometer using the principle suggested by Gelepov and Orbeli.[2] The principle of the spectrometer is shown in Fig. 1. Compton electrons are ejected by photons falling on a wide radiator *R* (area 40 × 50 mm, thickness 50 or 100 microns of polystyrene), situated in a homogeneous magnetic field (point *O* marks the symmetry axis of the magnetic field). The Compton electrons ejected into an angle of about 1 degree in the forward direction are focused on slit *A* by the homogeneous magnetic field for a certain energy of electrons. A suitably curved radiator is used to achieve optimum focusing of electrons. After passing slit *A*, the divergent electron beam is focused on the diaphragm *B*. Improved 180-degree-focusing in a radially falling off magnetic field is applied. The coincidence pulses in beta-counters placed at points *A* and *B* are counted at different magnetic field strengths *H*. The energy of the Compton electrons, and therefore the gamma-ray energy, is determined from the magnetic field strength and the distance between the counters.

The advantages of this gamma-ray spectrometer compared with other Compton-electron magnetic spectrometers are the following:

1. The use of a wide radiator makes it possible to have, at the same time, a small Compton electron acceptance angle (1 degree) and a good transmission. Under these conditions a gamma-ray spectrum can be measured with good resolution in the wide energy range of 0.3 to 12 Mev. Even in the worst case of 12 Mev, the broadening of the spectral line resulting from the dependence of the Compton-electron energy on the angle is about 0.5%.

2. The coincidence pulses in counters placed far from each other are measured, which is especially important in the case of the high background near the reactor. In this spectrometer, the background of occasional coincidence pulses was negligible, being less than one coincidence pulse per 30 minutes and could practically be ignored. It should be mentioned that it was impossible to measure the spectrum with one counter *B* only, as then the background was several times the observed effect.

In the spectrometer used, the diameter of the magnet pole pieces was 1.5 ft. The radial fall-off of the magnetic field necessary for improved focusing was provided by a fringing magnetic field at the edge of the magnet. By shimming we managed to obtain a fall-off of the magnetic field which differed by less than 0.5 per cent from the theoretically calculated one.

The radius of the principle orbit r_0 (inside of which the field is homogeneous and outside falls off radially) was 6 inches.

The magnetic field was measured by the induction method by means of a dc generator rotor rotating at constant speed, in the fringing field of the magnet. This magnetic field meter also provided the signal for the magnet-coil current regulation circuit. The magnetic field stability was within ±0.05 per cent at high strengths and within 0.1 per cent at low strength.

The spectrometer chamber was a brass cylindrical box (Fig. 1), 19 inches in diameter and 4 inches high, with windows for the entrance and exit of gamma-rays. The windows were closed with brass 0.02 in. thick. Two diaphragms, with slits 0.12 in. and 0.2 in. wide were placed in front of counters *A* and *B*, respectively. The counters were shielded with lead to the maximum degree. We used beta-counters with thin windows of Zapon film covered with a semi-transparent copper layer deposited in vacuum. The film was about 1 mg/cm^2 thick. Continuous change of gas filling was necessary for stable operation of the counters in the Geiger region. To this effect the counters were connected with a vessel in which the gas pressure was automatically maintained at 90 ± 1 mm Hg. The gas was pumped out of the counters through a capillary copper pipe. The counters were filled with the mixture of 80 per cent argon and 20 per cent alcohol.

One of the main characteristics of the spectrometer is its resolution. The resolution of the half-maximum width of the spectral line was measured in studying both capture gamma rays and gamma rays from Co^{60} and Na^{24}. Table I shows half-maximum widths of lines as a function of gamma-ray energy.

This table shows that the half-maximum width of the spectral line is essentially constant for the gamma-ray energies exceeding 1.5 Mev. In this energy region it is mainly determined by the ratio of diaphragm width to the radius of the path. At energies below approximately 1.5 Mev multiple scattering and the slowing down of electrons in the radiator and the counter windows becomes noticeable. This probably causes the decrease of resolution at low energies.

The data given in Table I were obtained for a radiator 100 microns thick. As the thickness is diminished to 25 microns the half-maximum widths of lines

Table I

Gamma-ray energy in Mev	0.48	0.78	0.84	1.14	1.37	2.74	4.4	5.4	8.56
Half-maximum width in per cent	8.3	4.0	3.3	2.9	2.7	2.3	2.3	2.3	2.3

down to about 500 kev is 2.3%, the luminosity being decreased by the factor of 3.

The knowledge of the instrumental line profile is highly essential for reliably resolving a measured gamma-ray spectrum into partial spectra due to separate monochromatic lines in the true spectrum. This problem is still under investigation. In analysing the gamma-ray spectra from S^{33}, Na^{24}, and Cl^{36} discussed below we used preliminary data on instrumental line shapes.

As has been mentioned above, the half-maximum widths of peaks are energy-independent for gamma-ray energies exceeding about 1.5 Mev. It appeared from the comparison of peaks for various energies that to the first approximation they also have similar shapes. Based on this, we split up the spectrum into separate components. Figure 2 shows an example of such an analysis. It shows a part of the gamma-ray spectrum from chlorine discussed below. In the energy region below 1.5 Mev the peak shape to a certain extent depends on energy. We used some well-defined lines of the neutron capture gamma-ray spectrum as reference peak shapes at various energies.

It should be noted that even in the case of a relatively small number of lines in the spectrum it was not always possible to define all the lines well. A part of the spectrum was left unresolved. In the discussion of corresponding spectra we shall investigate what fraction of the neutron binding energy carried away by gamma-rays goes into the unresolved part of the spectrum.

The gamma-ray energy for each peak was found by extrapolating its high-energy side to intersection with the abscissa or with the level of the unresolved background. The magnetic field intensity corresponding to this value of the abscissa was then determined. A calibration curve was constructed which gives the dependence of the gamma-quantum energy on the magnetic field intensity obtained by this extrapolation. To this end the best known gamma rays both in thermal neutron capture gamma-ray spectra and those from radioactive sources were used. The accuracy of this method of measuring the gamma-ray energy is determined by the uncertainties of measuring the field strength and of the calibration curve, as well as by the possibility of resolving the peak from the spectrum.

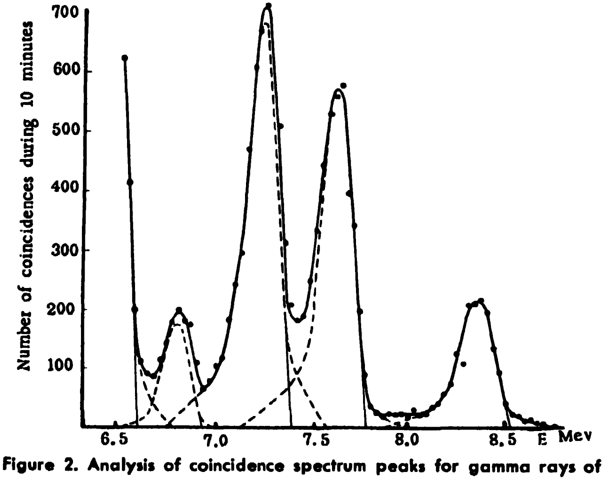

Figure 2. Analysis of coincidence spectrum peaks for gamma rays of chlorine

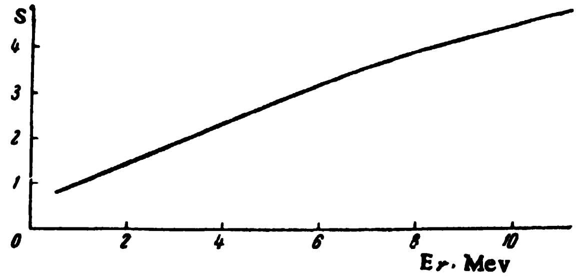

Figure 3. Gamma-spectrometer efficiency as a function of energy

The second important feature of the spectrometer is its spectral sensitivity S, i.e., the dependence of the peak area of the spectral line on gamma-quantum energy. [We mean the peak area obtained after corrections for self-absorption of gamma-rays in the sample, for absorption in the walls of container, chamber, boron cover, and air, and after normalizing to equal intervals of $\Delta(H\rho)$]. The spectral sensitivity was calculated theoretically and is shown in Fig. 3. (It has been made unity at a gamma-quantum energy of 1 Mev). The experimental verification was made with gamma rays from Co^{60} and Na^{24}. A satisfactory agreement with theoretical calculations was obtained to within the experimental accuracy. The transmission of the spectrometer could be evaluated from the experiments with a source of known strength. If the transmission of the instrument is defined as the number of counts in the peak per quantum falling on the radiator, then for a gamma-quantum energy of 1.33 Mev it is 2.5×10^{-7}.

2. DETERMINATION OF RELATIVE AND ABSOLUTE INTENSITY OF GAMMA-RAYS

The determination of the number of photons per capture can be made by the following method. As we measure gamma rays in a wide energy range beginning with 0.3 Mev, the following relationship applies rather well for the spectrum one obtains:

$$\sum_i p(E_i)E_i = B \qquad (1)$$

where $p(E_i)$ is the number of photons per capture, E_i is the photon energy and B is the binding energy of the neutron in the nucleus under investigation.

Equation 1 can be conveniently used for determining the number of photons per capture if relative intensities of all the gamma-rays in the spectrum have been measured. It should be stressed that Equation 1 is valid only where the energy contribution in form of photons of energy $h\nu$ less than 0.3 Mev, of the conversion electrons, and of internal conversion pairs is negligible.

The second method of determining the number of photons per capture consists in comparing the intensities of two gamma-rays for one of which the number of photons per capture is known. These gamma-rays can be from one and the same element or from two different elements In the latter case it is necessary to measure the gamma-ray spectrum from a mixture of these substances and to know the percentage or weight contents of the mixture as well as the thermal neutron capture cross-section ratio for the two components. The determination of the number of photons per capture for the "reference" gamma-ray can be done as follows: For many elements thermal neutron capture results in the formation of radioactive isotopes decaying with the emission of gamma-rays of a known spectral composition. If the irradiation time considerably exceeds the half-lives of these isotopes, a saturation is reached at which one disintegration of a new nucleus occurs per each neutron capture in an original nucleus.

This method of determining the intensities was used by Kinsey, *et al.* In this case Na was the only element suitable for these purposes. In the present work both methods can be used to determine the number of photons per capture; the first, that of normalizing the spectrum to binding energy, and the second, just described, the one which can in principle be applied for many elements.

In some cases the measured spectrum cannot be resolved into separate components corresponding to different lines in the original spectrum. In this case Equation 1 can be generalized easily and written as

$$\int_{0.3\ \text{Mev}}^{\infty} E \cdot \nu(E)\, dE = B \qquad (2)$$

where $\nu(E)$ is the number of photons per capture per unit energy interval. $\nu(E)$ can easily be deduced from Equation 2, again provided the neutron binding energy B is known. One other method of determining $\nu(E)$ is the following: Let us denote by $n(E)$ the coincidence counting rate at a given energy E. Then

$$n(E) = C(E) \int_{E}^{\infty} S(E') \cdot \nu(E') \cdot f(E' - E)\, dE' \qquad (3)$$

where $S(E')$ is the spectral sensitivity, while $f(E' - E)$ is the function which describes the instrumental line shape (the area under the curve being normalized to unity for all energies). The lower limit of integration is fixed by the fact that only photons with $E' \geq E$ contribute to $n(E)$. The constant $C(E)$ takes care of the self-absorption in the sample, the absorption in the walls of chamber, container etc., as well as the normalization of the spectrum to equal intervals $\Delta(H\rho)$. Assume that $S(E')$ and $\nu(E')$ do not vary much within the width ΔE of the spectral line. We then get

$$n(E) = C(E)S(E)\nu(E) \qquad (4)$$

On the other hand, let the spectrum have a peak due to photons of energy E_0 and of intensity $p(E_0)$ photons per capture. Denote peak coincidence rate by $n(E_0)$. In that case

$$n(E_0) = C(E_0)S(E_0)p(E_0)f_{max}(E_0) \qquad (5)$$

where $f_{max}(E_0)$ is the value of the function $f(E' - E)$ at its maximum at $E' = E_0$. From Equations 4 and 5 we get

$$\frac{n(E)}{n(E_0)} = \frac{S(E)\nu(E)C(E)}{S(E_0)p(E_0)f_{max}(E_0)} \qquad (6)$$

From Equation 6 it is easy to find $\nu(E)$, i.e., the number of photons per capture per unit energy interval, provided the spectrum contains at least one monochromatic line of known strength.

The following point should be made: The first method of determining the number of photons per capture requires a knowledge of neutron binding energy in the product nucleus, whereas the second method requires that of the cross section for thermal-neutron capture. By applying *both* methods one can determine cross sections, if the neutron binding energy is known, or neutron binding energies, if the cross section is known. The accuracy of these methods of determining the thermal-neutron capture cross section or the binding energy cannot compete with other known methods of determining these values, but they may be useful in analysing gamma-ray spectra produced by thermal-neutron capture.

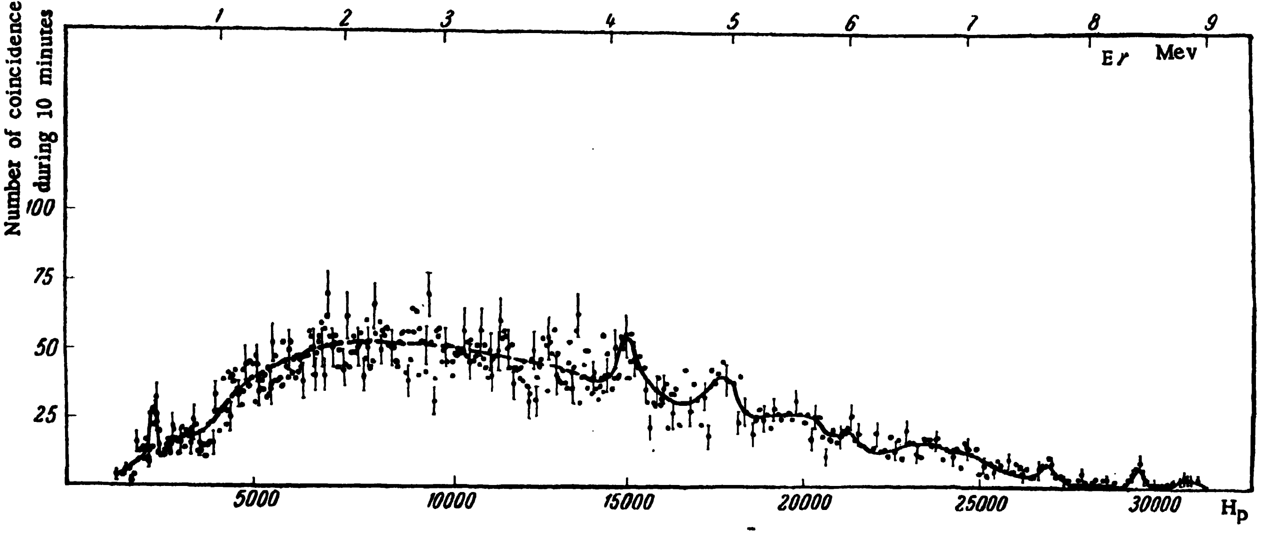

Figure 4. Coincidence background gamma-ray spectrum

3. GAMMA-RAY SPECTRA FROM Be, Na, S, AND CL

Before we discuss the results of measuring the thermal neutron capture gamma-rays from a particular substance let us consider the problem of background.

When there is no sample in the sample holder the spectrometer measures a background gamma radiation. It consists of (1) gamma-rays from the reactor which penetrate the bismuth shielding block, (2) gamma-rays from the thermal column scattered by the bismuth block into the spectrometer, and (3) neutron capture gamma-rays from bismuth and sample holder.

The measurement of the gamma-ray background was performed as follows: The sample under investigation was replaced by another one made of the same substance but slightly smaller. This sample was surrounded with a boron carbide layer 1 cm thick and placed in the same holder. The capture gamma-rays from the substance do not appear now, while the background gamma-rays are not changed. Figure 4 shows the measured background. It is practically independent of the substance (for approximately equal densities), placed in the position of the sample. For each element, the relevant background spectrum was subtracted from the measured gamma-ray spectrum.

In what follows the results of the measurements of the thermal-neutron capture gamma-ray spectra from sodium, chlorine, sulphur, and beryllium are presented.

Beryllium

We studied thermal-neutron capture gamma rays emitted by beryllium first of all in order to investigate the peak shape at gamma-ray energy of about 7 Mev. The results obtained could then be compared with Kinsey's data[3] on intensity measurement.

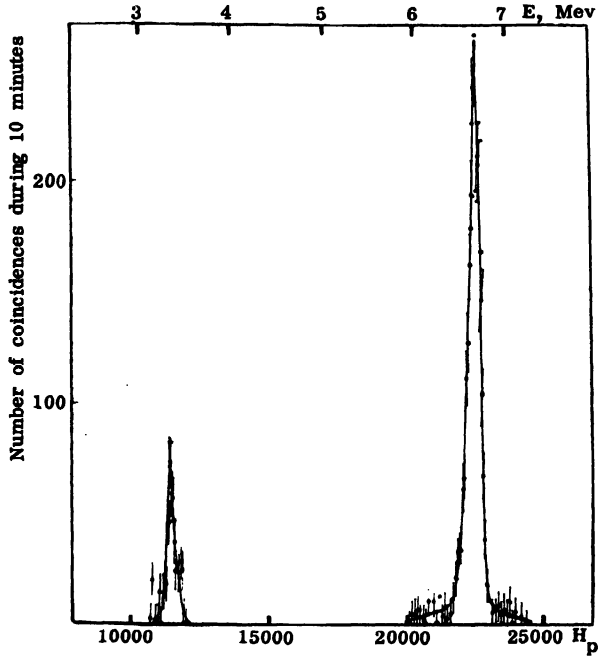

Figure 5. Coincidence gamma-ray spectrum from beryllium

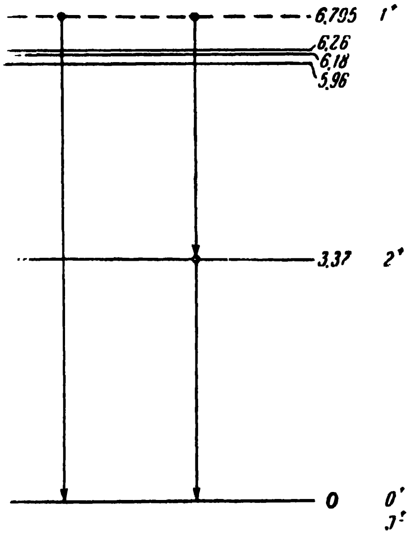

Figure 6. Decay scheme for capture gamma rays of Be^{10}

A 790-gram sample of spectroscopically pure metallic beryllium was used. According to Kinsey's data and in accordance with the level diagram of beryllium (see Fig. 5), only two lines can be observed in the gamma-ray spectrum. Therefore we limited ourselves to measurement of these two lines.

Figure 6 shows the results of our measurements. The 6.80-Mev gamma-ray arises from the transition from the excited capturing state to the ground state, whereas the 3.40-Mev gamma-ray represents the transition to the 3.37-Mev level and from the latter to the ground state of Be^{10}. The last two transitions are accompanied by the emission of gamma-rays with only slightly differing energies. It is obvious, therefore, that we observe only one peak for them.

The determination of intensities by normalizing the measurements to neutron binding energy in Be^{10} resulted in 0.73 photons per capture for 6.8-Mev gamma-rays and in 0.54 photons per capture for 3.40-Mev gamma-rays. These values are in good agreement with Kinsey's data of 0.75 and 0.50 photons per capture for gamma-rays of the higher and lower energies respectively.

Sodium

The sodium sample consisted of 750 grams of chemically pure sodium fluoride powder. The energy range from 0.4 to 7 Mev was examined. Figure 7 shows a so-called coincidence spectrum. The coincidence counting rate is plotted against $H\rho$. Figure 8 shows the corrected gamma-ray spectrum, $\nu(E)$ versus gamma-ray energy in Mev, obtained from the coincidence spectrum after all corrections are made and the spectral sensitivity of the spectrometer taken into account.

Sodium is one of the elements for which the determination of number of photons per capture can be made by both available methods; by the method of normalizing the spectrum with respect to binding energy as well as by comparison with a "reference" gamma-ray of known strength. The neutron binding energy of Na^{24} is known to be 6.955 ± 0.007 Mev.[4]

The capture of thermal neutrons by Na^{23} results in formation of a beta-emitting isotope with a half-life of 15 hours.[5] Mg^{24}, the product of Na^{24} beta-decay, is formed in the 4.122 = Mev excited state which is de-excited by two successive gamma rays with energies of 2.754 Mev and 1.368 Mev. These gamma rays serve as "reference" rays after saturation is obtained and their intensity has become one photon per capture.

The application of both methods for determining the number of photons per capture in sodium furnished close results, which differ from each other by 7%, the greater number of photons per capture being obtained by the second method. This relatively good agreement between two independent determinations of gamma-ray intensities justifies each of the suggested methods and the calculation of the spectral sensitivity of the spectrometer.

The accuracy in the determination of gamma-ray intensities is within ±15 per cent for strong and well-defined peaks and ±50 per cent for gamma-rays of low intensity. It should be mentioned that the unresolved part of gamma-ray spectrum from sodium amounted to 6%.

Table 2 gives the gamma-ray intensities in numbers of photons per capture, expressed in per cent. They are obtained by averaging the intensities determined by both methods. Table 2 also shows the gamma-ray energies. Doubtful energy values are in brackets. The results obtained by Kinsey, Bartholomew, Walker[6] and other authors[8,23,24] are given in Table 2 for comparison. The comparison with our results clearly shows the main advantage of our method, which permits measuring the gamma-rays in a wider energy range. We have observed three times as many gamma-transitions in sodium as those observed by the authors of reference 6. The comparison of gamma-ray energies in the two cases indicates a satisfactory agreement within experimental accuracies.

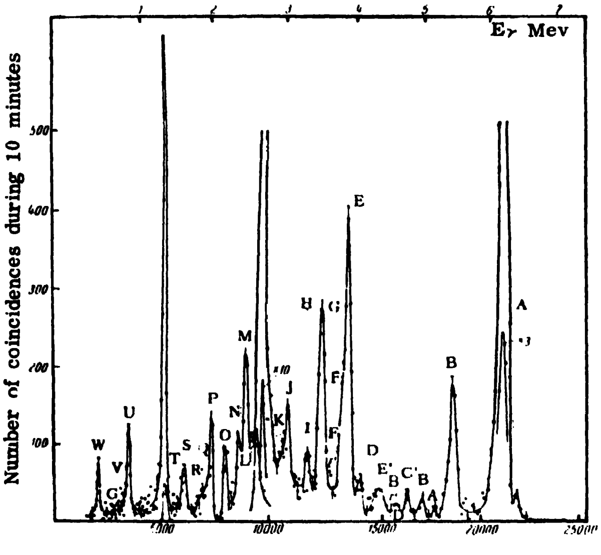

Figure 7. Coincidence gamma-ray spectrum from sodium

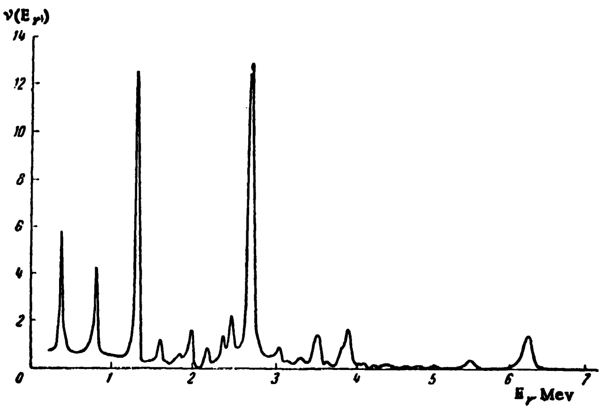

Figure 8. Corrected gamma-ray spectrum from sodium

Comparison of gamma-ray intensities shows a noticeable discrepancy. It is, however, also within the limits of error which are rather considerable here. It should be pointed out that for energies below 4 Mev the accuracy of determining gamma-ray intensities with the aid of a pair spectrometer is not better than 40 to 50%.

We have also established a decay scheme for capture gamma-rays of sodium and tried to meet two evident requirements:

1. The gamma-ray energy must fit to within the experimental accuracy into the difference between level energies in Na^{24} which are well known from the study of the (d,p) reaction.[4]

2. The number of photons emitted in nuclear transition to a given level must be equal to the number of photons emitted in transition from that same level. The fulfilment of these requirements considerably reduces the number of combinations possible for positioning gamma-rays between the known levels, though it does not permit to establish the decay scheme quite unambiguously. Figure 9 shows a possible decay scheme for capture gamma-rays of sodium.[4]

In working out the decay scheme for sodium we met a difficulty resulting from lack of information between 4.56 Mev and the neutron binding energy.

Thus, with our data on gamma-ray energies and intensities, it was impossible to work out the decay scheme so that the total number of photons emitted from excited state at 6.955 Mev would be one photon per capture. This means that in sodium a considerable number of transitions from the 6.955 Mev state terminate at the excited levels above 4.56 Mev. We have assumed, therefore, that a part of the transitions lead to 4.75 and 5.30 Mev levels.

We especially looked for the 6.955 Mev transition and failed to find it. If it takes place its intensity does not exceed 0.1% per capture.

It can be seen from Fig. 9 that the level at 0.56 Mev is excited in the decay with great probability but that the 0.47 Mev gamma-ray is emitted. In view of this we made a detailed measurement near 0.5 Mev to prove the absence of a transition from the 0.56 Mev level to the ground state. Figure 10 shows this part of the spectrum on an enlarged scale. The 0.56-Mev transition is seen not to show up noticeably. We estimate the upper limit of intensity of this transition to be 0.03 photon per capture.

As we used sodium fluoride to measure the gamma-ray spectrum from sodium we also observed the fluorine gamma-rays with an energy of 6.63 ± 0.05 Mev (see Fig. 7). If we take the thermal-neutron capture cross section of sodium to be 0.5 barn, and that of fluorine to be 9 millibarn, then our data show the intensity of the fluorine capture gamma-rays to be 0.20 ± 0.1 photon per capture, in agreement with the result obtained by Kinsey.

Some weak lines at lower energies may also be due to strong gamma-rays of fluorine.

Sulphur

The sample was a 1150-gram cylinder of chemically pure melted sulphur. The gamma-ray spectrum was investigated within the energy range of from 0.4 to 9.0 Mev.

Figure 11 shows the coincidence spectrum, and Fig. 12 the corrected gamma-ray spectrum.

Table 3 shows the abundances, cross sections, and binding energies of the various sulphur isotopes.[7]

Table 3

Target	*Abundance, %*	*Contribution to total capture cross section in barns*	*Binding energy of product nucleus in Mev*
S^{32}	95.1	0.49	8.645 ± 0.012
S^{33}	0.74		10.90 ± 0.25
S^{34}	4.2	0.011	7.16 ± 0.45
S^{36}	0.016	2×10^{-6}	5.78 ± 0.60

These data show that the main contribution to the capture cross section is due to the S^{32} and S^{33} isotopes. To prove that the absorption by S^{33} is insignificant, Kinsey *et al.*[7] especially investigated the gamma-ray spectrum above 9 Mev. No gamma-rays were detected in this region. No gamma rays corresponding to transitions from the 10.9-Mev state to the known levels in S^{34} were found either. Also, in our own measurements, no gamma-rays arising from transitions from the first excited levels in S^{34} to the ground state were found. Thus the conclusion can be drawn that S^{32} is the principal absorbing isotope and that the absorption by S^{33} is inconsiderable and makes no noticeable contribution to the capture gamma-rays from sulphur isotopes.

We determined the number of protons per neutron capture by means of normalization with respect to the

Table 2

	Magnetic spectrometers				*Lens spectrometer, Motz*[23]	*Scintillation spectrometer, Braid*[8]	*Photoplates loaded with D_2O, Miller, Cameron, Glicksman*[21]	
	Our measurements		*Kinsey's data*[6]					
Gamma ray	*Gamma ray energy (Mev)*	*Intensity in photons per capture (per cent)*	*Gamma-ray energy (Mev)*	*Intensity in photons per capture (per cent)*	*Gamma-ray energy (Mev)*	*Gamma-ray energy (Mev)*	*Gamma-ray energy (Mev)*	*Relative intensity*
1	*2*	*3*	*4*	*5*	*6*	*7*	*8*	*9*
A	6.40 ± 0.03	22	6.41 ± 0.03	20				
B	5.61 ± 0.03	6	5.61 ± 0.03	7.5				
A′	(5.30 ± 0.05)	0.3					5.37	31
B′	(5.12 ± 0.05)	0.8	5.13 ± 0.03	1.8				
C′	(4.90 ± 0.05)	1.2					4.82	100
D′	(4.70 ± 0.05)	0.9						
C	4.50 ± 0.04	2.1						
E′	(4.30 ± 0.05)	0.5					4.35	89
D	4.18 ± 0.04	2.1						
E	3.98 ± 0.04	17.2	3.96 ± 0.03	20			3.92	39
F	3.86 ± 0.04	5.9	3.85 ± 0.03	11				
F′	3.68 ± 0.05	1.3						
G	3.60 ± 0.03	18	3.60 ± 0.03	10				
H	3.56 ± 0.03		3.56 ± 0.03	20			3.55	70
I	3.30 ± 0.02	5					3.25	56
J	3.08 ± 0.02	9.5					3.05	61
K	2.84 ± 0.02	7					2.79	45
L	2.68 ± 0.02	8.5						
M	2.52 ± 0.02	21						
N	2.41 ± 0.03	10.5						
O	2.21 ± 0.03	7.5						
P	2.02 ± 0.015	11.5				2.0		
Q	(1.95 ± 0.03)	4						
R	(1.87 ± 0.03)	5.5						
S	1.66 ± 0.01	7.5				1.66		
T	1.35 ± 0.01	6.5				1.34		
U	0.86 ± 0.01	44				0.877 ± 0.010		
V	0.79 ± 0.015	4.3				0.86		
G′	(0.71 ± 0.015)	5						
W	0.47 ± 0.015	74				0.475 ± 0.010 0.48		

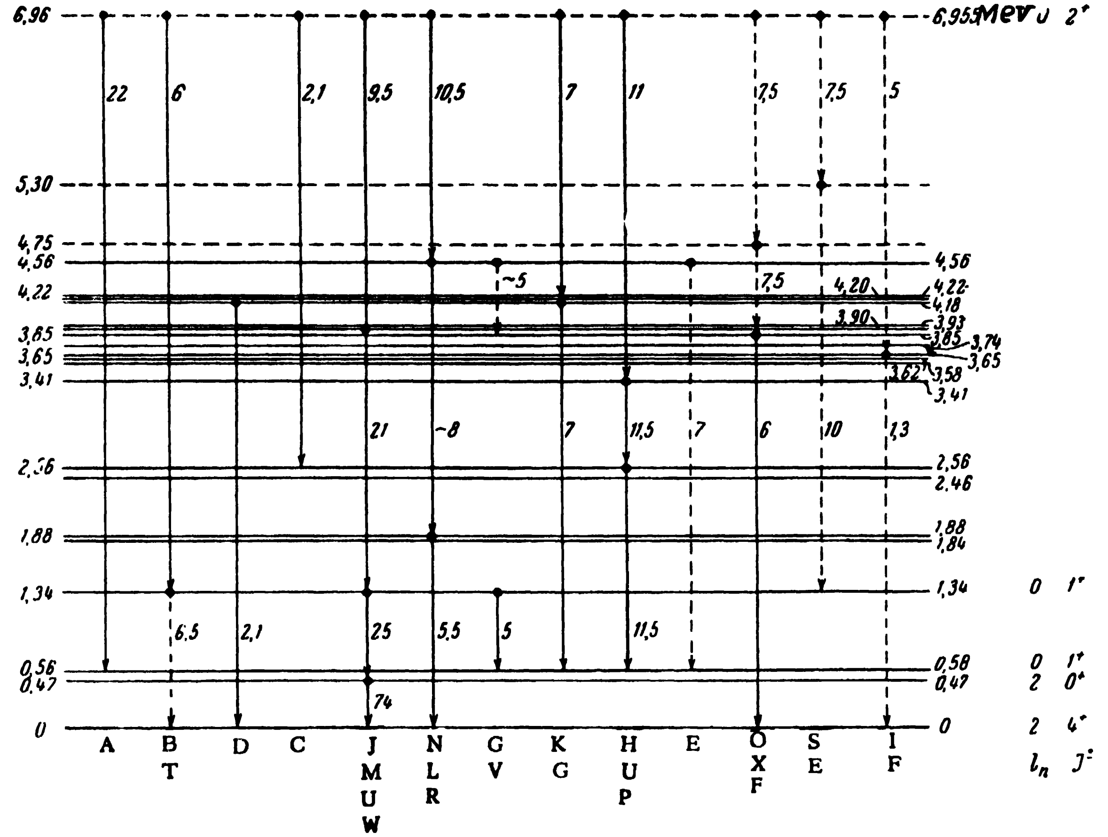

Figure 9. Decay scheme for capture gamma rays of Na^{24}

neutron binding energy of S^{33}. Table 4 shows the results of measuring the gamma-ray energies and intensities obtained that way. It also shows, for comparison, the results of measurements by Kinsey, Bartholomew, and Walker,[7] made with the aid of a pair spectrometer, and Braid's data,[8] obtained with a scintillation spectrometer. Our measurements of gamma-ray energy agree well with the data of Kinsey *et al.* and somewhat less well with Braid's data. The gamma-ray intensities do not agree so well but the discrepancy is within the experimental accuracies.

Figure 13 shows a possible decay scheme for S^{33}. In constructing the decay scheme we used the system of levels for S^{33} obtained from the (d,p) reaction by Holt, Marsham,[9] and Davison.[10] Level energies determined by the authors are given on the right. The energies of protons from the (d,p) reaction were found by measuring their range in foils and were determined with an accuracy to within 50 kev. Holt and Marsham[9] also studied the angular distributions of protons from the (d,p) reaction. The scheme also gives for each level the values of the captured neutron orbital angular momentum l_n, as well as possible spin values.

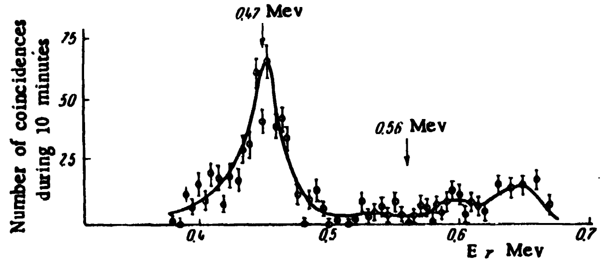

Figure 10. Coincidence gamma-ray spectrum from sodium near 0.5 Mev

The transitions corresponding to the 7.20 ± 0.05 Mev energy could not be fitted into the decay scheme. The energy of this transition is close to the neutron binding energy in S^{34}. If this gamma-ray represents the ground-state transition in S^{34}, its intensity must be about 0.25 photon per capture.

The positions of most strong gamma rays of high energies fit unambiguously in the proposed decay scheme for the capture gamma-rays of S^{33}. The figures on the arrows give the intensities of the gamma-rays in number of photons per capture in per cent. A small number of gamma-rays corresponding to transitions of low energy and intensity could not be fitted into the level scheme with certainty. They are indicated with dotted arrows. This resulted from an inadequate knowledge of the level energies of S^{33}.

Chlorine

The sample consisted of 470 grams of powdered $PbCl_2$.

Figure 14 shows the "coincidence spectrum" of chlorine and Fig. 15 the corrected gamma-ray spectrum.

The thermal neutron absorption cross section of chlorine (32 barns) is much greater than that of lead, therefore the capture gamma-rays from lead could not

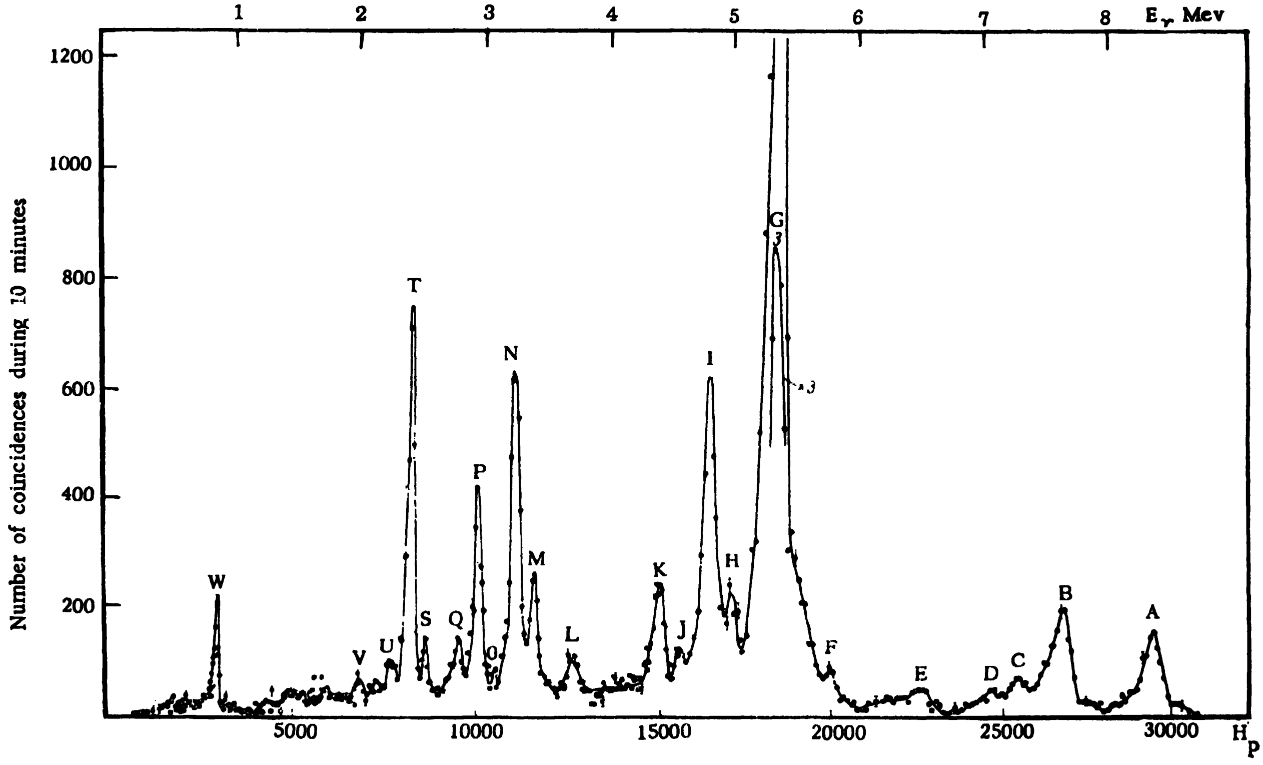

Figure 11. Coincidence gamma-ray spectrum from sulphur

contribute noticeably to the spectrum obtained. Also, the neutron capture cross section of Cl^{37} is $\frac{1}{250}$ of that of Cl^{35}, therefore the measured neutron capture gamma-ray spectrum was due to the Cl^{35} isotope.

We determined the gamma-ray intensities in the spectrum of chlorine by means of normalization with respect to the neutron binding energy of Cl^{36}.

Table 5 shows the gamma-ray intensities and energies thus measured. The unresolved part of the spectrum was 16%. Table 5 also gives the results of Kinsey *et al.*[7] and the data obtained with scintillation spectrometers.[8,11,12] Our values of gamma-ray energies agree well with the results obtained by other authors.[7,8,11,12] However, comparison of our measurements of gamma-ray intensities with the data obtained by Kinsey points to a considerable discrepancy for a number of gamma-rays, which can be explained neither by experimental nor by statistical errors. The reason for this discrepancy is still uncertain.

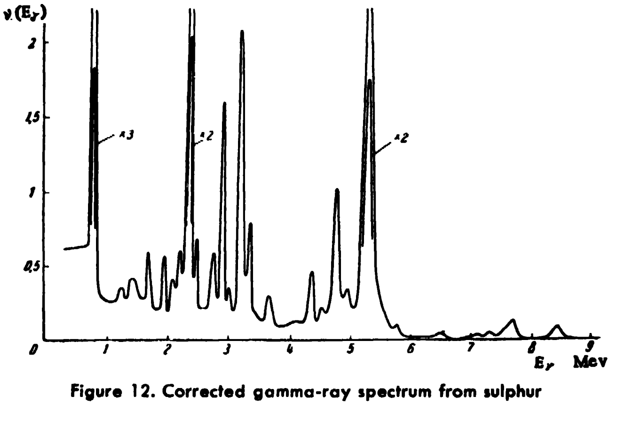

Figure 12. Corrected gamma-ray spectrum from sulphur

Figure 16 gives a decay scheme based on our measurements of gamma-ray energies and intensities and on the level scheme of Cl^{36} obtained from (d,p) reaction studies.[13,14]

The energy-level positions found from a study of the (d,p) reaction are given on the right hand side of Fig. 16. As the decay scheme indicates, double-cascade transitions occur in Cl^{36} in many cases. For the first four levels this is confirmed by Recksiedler and Hamermesh.[15] The equality between the sum of energies of gamma-rays in each cascade and the neutron binding energy in Cl^{36} confirms the correctness of the decay scheme. Table 6 shows this for 12 cascades. As may be seen from the table, the sums agree rather well with the value of the neutron binding energy.

Results in Table 6, and the fact that gamma-ray intensities in the cascades agree between themselves, strongly support the proposed decay scheme.

DISCUSSION OF RESULTS

Some data are available on spins and parities, obtained from the study of the angular distribution of protons from the (d,p) reaction for a number of levels in Be, Na, S and Cl. Such studies permit the values of the captured neutron orbital angular momentum l_n to be obtained. The knowledge of l_n enables one to find possible values of the total momenta for these levels. Besides the level energies, the decay schemes also give the values of l_n and, where possible, the total momenta. Making use of these data it is possible to

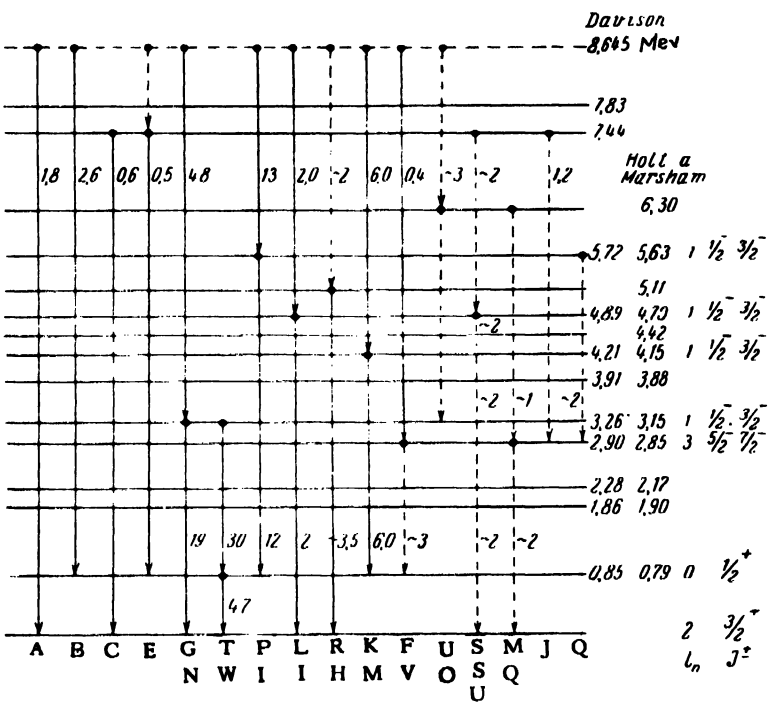

Figure 13. Decay scheme for capture gamma rays from S^{33}

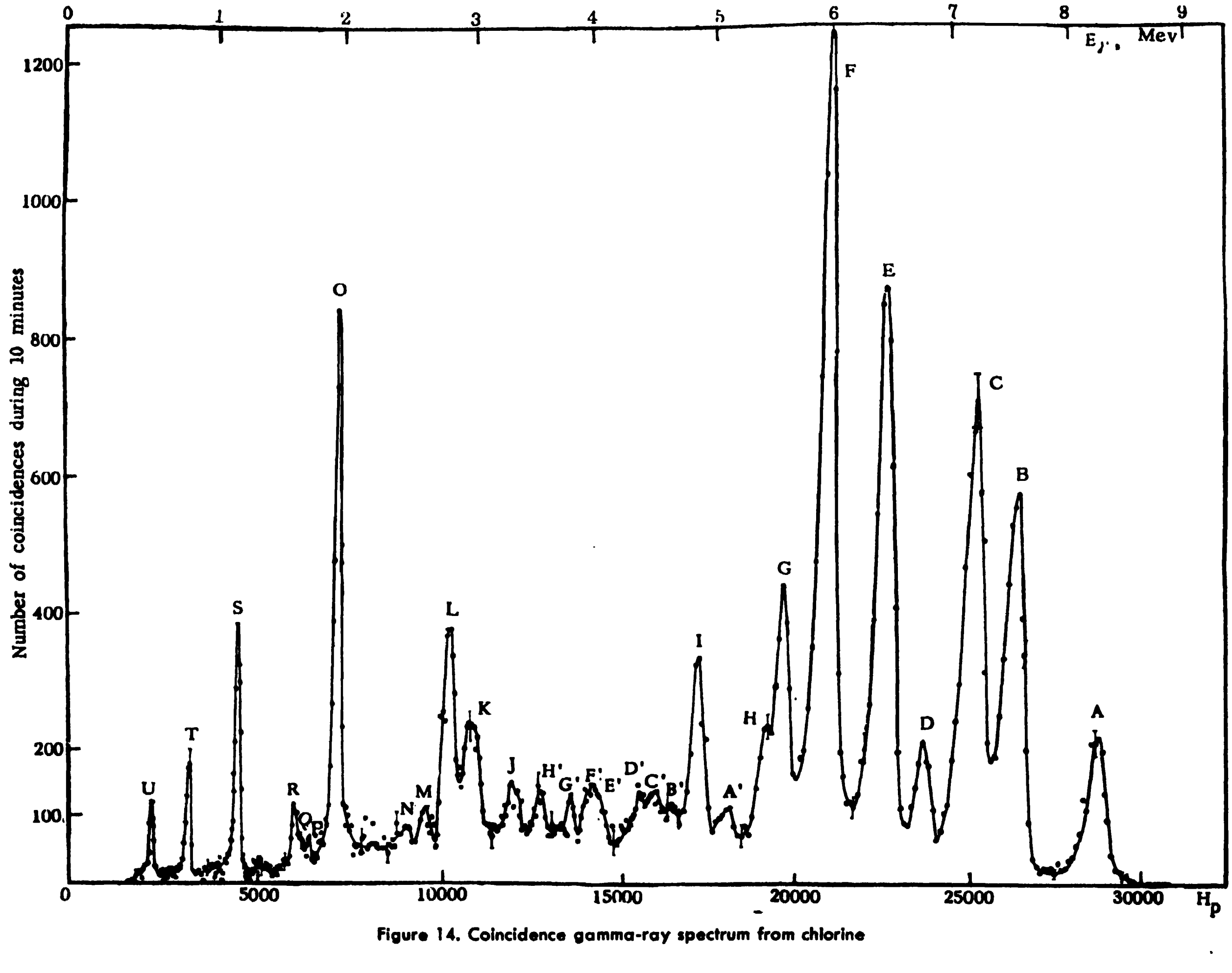

Figure 14. Coincidence gamma-ray spectrum from chlorine

Table 4

	Magnetic spectrometers					Scintillation spectrometers Braid[8]	
	Our measurements		Data of Kinsey, Bartholomew, Walker				
Gamma-ray	Gamma-ray energy (Mev)	Number of photons per capture (%)	Gamma-ray energy (Mev)	Intensity in photons per capture (%) from[7]	Intensity in photons per capture (%) from[1]	Gamma-ray energy (Mev)	Number of photons per capture (%)
1	2	3	4	5	6	7	8
A	8.63 ± 0.04	1.8	8.64 ± 0.02	3	1.2		
B	7.80 ± 0.04	2.6	7.78 ± 0.03	4	1.6		
C	7.42 ± 0.05	0.6	7.42 ± 0.03	0.7			
D	7.20 ± 0.05	0.5	7.19 ± 0.03	0.5			
E	6.62 ± 0.05	0.5	6.64 ± 0.03	0.7	0.25		
F	5.88 ± 0.05	0.4	5.97 ± 0.06	1			
G	5.44 ± 0.02	48.0	5.43 ± 0.02	84	60		
H	5.07 ± 0.03	3.5	5.03 ± 0.06	5			
I	4.87 ± 0.02	12.0	4.84 ± 0.06	20	11		
J	4.58 ± 0.03	1.2	4.60 ± 0.03	5			
K	4.40 ± 0.02	6.0	4.38 ± 0.03	13	7		
L	3.66 ± 0.05	2.0	3.69 ± 0.05	5	4		
M	3.41 ± 0.01	7.1	3.36 ± 0.05	7	7		
N	3.27 ± 0.01	19.0	3.21 ± 0.03	30	20		
O	3.10 ± 0.03	2.0					
P	2.975 ± 0.01	13.0	2.94 ± 0.05	19	20		
Q	2.82 ± 0.02	4.0					
R	2.70 ± 0.05	2					
S	2.550 ± 0.02	4.4					
T	2.415 ± 0.01	30				2.34	
U	2.29 ± 0.03	5					
V	2.00 ± 0.02	3				1.52	
W	0.84 ± 0.01	47				0.84	60

deduce the multipole order of some gamma-ray transitions.

If also the total radiative width Γ_γ is known for a given nucleus, we shall be able to find partial radiative widths Γ_r for the transition of interest from the relationship $\Gamma_r = p(E)\Gamma_\gamma$, where $p(E)$ is the number of photons of given energy per capture. The partial radiative widths thus obtained can be compared with the results of calculations of radiation probabilities based on Blatt and Weisskopf's formulas.[16]

Weisskopf gives the following expressions for the probabilities of electric and magnetic type transitions accompanied by 2^L-pole quantum emission:

$$W_{EL} = \frac{4.4(L+1)}{L[(2L+1)!!]^2}\left(\frac{3}{L+3}\right)^2\left(\frac{h\nu}{197\text{ Mev}}\right)^{2L+1} R^{2L}10^{21}S\text{ sec}^{-1} \quad (7)$$

$$W_{ML} = \frac{1.9(L+1)}{L[(2L+1)!!]^2}\left(\frac{3}{L+3}\right)^2\left(\frac{h\nu}{197\text{ Mev}}\right)^{2L+1} R^{2L-2}10^{21}S\text{ sec}^{-1} \quad (8)$$

where R is the nuclear radius in units of 10^{-13} cm and S is a statistical factor which depends on the spins of the original and final states and on the multipolarity of the radiation.

The transition probabilities of Equations 7 and 8 have been calculated for the lower levels, which in many cases can be described as one-nucleon excitation levels. The radiation probabilities for excitation energies of the order of the neutron binding energy, as shown by Weisskopf,[16] are obtained by multiplying Equations 7 and 8 by the factor $D(E)/D_0$, where $D(E)$ and D_0 are the average level spacing at the excitation energy E and the level spacing for the lower levels, respectively.

The quantity $|M|^2 = W_{exp}/W_{theor}$ is usually calculated for making comparisons between experimental and theoretical data, where W_{exp} and W_{theor} are the transition probability obtained experimentally, and that calculated with Equations 7 and 8, respectively. In the present case it is more useful to calculate the value $|M|^2D_0/D(E) = |M|^2/2D(E)$ because D_0 for sulphur, sodium, and chlorine is ~0.5 Mev. The departure of this value from unity is a measure for the discrepancy between experimental and theoretical data.

Gamma Rays from S^{33}

We have determined multipolarities of six gamma-ray transitions (four $E1$ and two $M1$) from the capturing state = of S^{33}. This state has spin ½ and even parity. Holt and Marsham[9] assumed that some levels in S^{33} can be ascribed to the excitation of the odd neutron. To this type belong all the levels which are the final states for $E1$ transition from the capturing state. We assume in calculations that radiation of $E1$ type represents the transition of one odd neutron. In this case Equation 7 must be multiplied by the factor $(Z/A)^2$. The statistical factor S can also be easily calculated for the transitions of the $E1$ type.

In S^{33} two transitions of $M1$ type from the capturing state to the ground and first excited states can be identified aside from the transitions of $E1$ type. If we

Table 5

	Magnetic spectrometers				*Scintillation spectrometers*			
	Our measurements		*Kinsey's et al. data*[7]		*Hamermesh*[11]	*Reardon et al.*[12]		*Braid*[8]
Gamma ray	*Gamma-ray energy (Mev)*	*Number of photons per capture (%)*	*Gamma-ray energy (Mev)*	*Number of photons per capture (%)*	*Gamma-ray energy (Mev)*	*Gamma-ray energy (Mev)*	*Relative intensity*	*Gamma-ray energy (Mev)*
1	*2*	*3*	*4*	*5*	*6*	*7*	*8*	*9*
A	8.55 ± 0.04	2.8	8.56 ± 0.03	3				
B	7.78 ± 0.03	7.8	7.77 ± 0.03	10	7.7 ± 0.2			
C	7.41 ± 0.03	14	7.42 ± 0.03	8				
D	6.96 ± 0.04	1.9	6.98 ± 0.03	1				
E	6.64 ± 0.04	14.4	6.62 ± 0.06	4				
F	6.12 ± 0.03	21.4	6.12 ± 0.03	6	6.2 ± 0.2			
G	5.72 ± 0.03	5.6	5.72 ± 0.03	2				
H	5.49 ± 0.04	2	5.51 ± 0.03	1				
A′	(5.28 ± 0.05)	1.6	5					
I	5.01 ± 0.04	6	5.01 ± 0.03	4				
B′	(4.79 ± 0.05)	1.9						
C′	(4.64 ± 0.05)	2.3				4.67 ± 0.10		
D′	(4.50 ± 0.05)	2.2	4.46 ± 0.04	2				
E′	(4.15 ± 0.05)	2.3						
F′	(4.05 ± 0.05)	2.1	4.06 ± 0.04	3				
G′	(3.90 ± 0.05)	1.8						
H′	(3.63 ± 0.05)	2.9	3.62 ± 0.05	2		3.71 ± 0.10	23	
J	3.40 ± 0.05	3.6						
K	3.09 ± 0.02 3.02 ± 0.03	8.0						
L	2.87 ± 0.02	9.5						2.84
M	2.68 ± 0.02	2.0				2.68 ± 0.10	10	
N	2.51 ± 0.03	1.0				2.40 ± 0.10	14	2.45
O	1.97 ± 0.01	29			2.00 ± 0.025	2.03 ± 0.10		
P	1.72 ± 0.02	1				1.77 ± 0.10	19	
Q	1.67 ± 0.02	1.0						
R	1.60 ± 0.02	2.4			1.59 ± 0.013			
S	1.165 ± 0.01	36			1.15 ± 0.01	1.12 ± 0.10	29	1.14
T	0.77 ± 0.01	23			0.784 ± 0.01	0.70 ± 0.10	35	0.75
U	0.485 ± 0.01	26						0.48

assume that this radiation is also due to a single-neutron transition, these are the transitions of type $s_{1/2} \rightarrow s_{1/2}$ and $s_{1/2} \rightarrow d_{3/2}$. Such transitions are forbidden in the independent-particle nuclear model. They become allowed, however, in case of the introduction of spin-orbit interaction, as was shown by Jensen and Mayer.[19] The fact that the selection rules for the independent-particle model are not satisfied in case of a transition to the first excited level, is in agreement with the fact that probably the state of at least two particles is changed in this transition. This is the conclusion drawn by Holt and Marsham from the "perforated" nature of the first excited state. In view of this, Equation 8, in fact, cannot be applied to predict the probabilities of these transitions. Therefore the comparison of experimental results with Weisskopf's predictions of probabilities of magnetic type transitions is ambiguous. To take into account the fact that the radiation is due to a neutron transition, Equation 8 must be multiplied by the factor $(\mu_n L)^2/[\mu_p L - (L/L+1)]^2$. The statistical factor S may also be calculated.

Table 7 gives the results of the comparison between the calculations and the experimental values of the transition probabilities. Of the two possible values of the spin in the final state we choose the one which gives the lowest spread in the $|M|^2$ values for all gamma rays of the same multipolarity.

From the decay scheme of S^{33} we can draw a conclusion about the parity and the spin of the 7.44 Mev state. As transitions from higher states probably terminate at this level, they must be of $E1$ type in order to compete with other transitions. Thus the 7.44 Mev excited state must have a spin of $1/2$ or $3/2$ and be of odd parity.

Gamma-Rays from Chlorine

The ground state of Cl^{35} having a spin of $3/2$ and even parity, it follows that after capturing a thermal neutron with zero orbital angular momentum, Cl^{36} is formed in the state 1^+ or 2^+. The transition to the ground state, which is the state 2^+,[20] will produce gamma-rays of $M1$ type and possibly $E2$ type, the probability of the latter being considerably smaller.

Studies of the angular distributions of protons from the (d,p) reaction on Cl resulted in the captured neu-

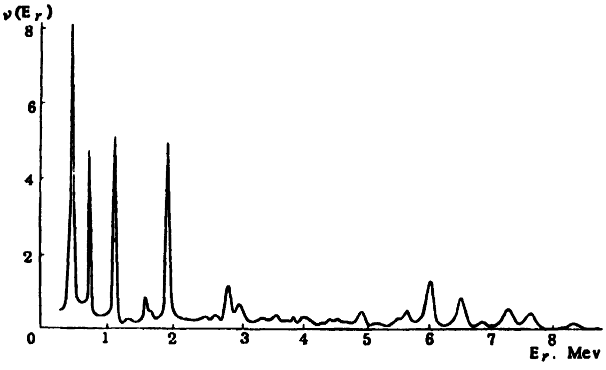

Figure 15. Corrected gamma-ray spectrum from chlorine

tron orbital angular momenta l_n.[14] However, with the exception of two cases of capture, which led to the 1.15 and 1.59 Mev excited states, the angular distributions of protons showed several l_n values which in some cases correspond to states of different parities. This makes the determination of l_n uncertain and results in uncertainty of probable spin and parity assignments for Cl^{36}. The neutron is captured to give the 1.15 and 1.59 Mev levels with zero orbital angular momentum; consequently Cl^{36} may be formed in states 1^{+} and 2^{+}. The observed gamma transitions to the ground state as well as to the levels at 1.15 and 1.59 Mev are of magnetic dipole type. We assume that the radiation emitted as in case of S^{33} is due to a single neutron transition, and, in the calculation of transition probabilities introduce an additional statistical factor as in reference 27, bearing in mind that the nucleus has a momentum. The comparison of intensities of the transitions leading to 1.15 and 1.59 Mev levels permits assigning the spins both to these levels and to the capturing state of Cl^{36}. Consistent results for experimental-to-theoretical intensities ratio can be obtained with the assignments of 2^{+}, 1^{+}, for the 1.15 and 1.59 Mev levels, and 1^{+} for the neutron capturing state.

The results of the comparison between experimental and predicted radiation probabilities for the three transitions are presented in Table 7.

We can draw the following conclusion concerning spins and parities of some states: As the transition from the 2.51 Mev level leads mainly to the 1.97 Mev level there must be either a great difference between the spin of the 2.51 Mev level and that of all the other levels (except 1.97 Mev level), or the transition to the 1.97 Mev level must be of *E*1 type to compete successfully with transitions to other levels.

Gamma-Rays from Sodium

The transition from the capturing state to the ground state has not been observed in the spectrum of sodium. Na^{24} in its ground state has spin 4 and even parity. The lowest neutron resonance of sodium is at 3 kev leading to a 2^{+} state.[25] It is likely that this state is mainly formed in thermal-neutron capture. Then, using the results of studies of angular distributions of protons from the (*d,p*) reaction as well as our decay scheme for the capture gamma-rays we can make the assignments of 0^{+}, 1^{+}, and 1^{+} for the first, second, and third excited levels in Na^{24} respectively. It then becomes uncertain whether the observed 1.35-Mev transition can proceed from the third level to the ground state. This gamma-ray may, however, correspond to a transition between some higher levels. The second and third excited states being 1^{+} states, the transitions from the 6.96-Mev state to them are of magnetic dipole type.

The results of comparison between calculated and experimental probabilities for these two *M*1 transitions in Na^{24} are included in Table 7.

Column 9 of Table 7 gives the data obtained by Kinsey and Bartholomew. The slight difference between our comparison of experimental and theoretical data and that of Kinsey can be explained by the different use of the statistical factor.

Many transitions seem to occur from the state at 6.96-Mev to high levels in sodium. It should be pointed out that these transitions are of electric dipole type and that they terminate at levels which have spins of 1, 2, and 3 and odd parities.

Gamma-Rays from Beryllium

The levels at 3.37, 5.96, 6.18 and 6.26 Mev are known to exist in Be^{10} between its ground state and the capturing state. According to the shell model Be^{9} in its ground state has odd parity. It follows from the study of the (*d,p*) reaction that the ground state and the 3.37-Mev state of Be^{10} have parities different from that of the ground state of Be^{9}. This means that the thermal neutron capture gamma rays must be of *E*1 or *M*2 type. The spin of Be^{9} in its ground state is $3/2$. The state of Be^{10} formed upon thermal neutron capture may be 1^{-} or 2^{-}. The ground-state transition and the transition to the 3.37-Mev level are probably of *E*1 type.

The ground state of Be^{10} is 0^{+} whereas the 3.37 Mev state is 1^{+}, 2^{+}, or 3^{+}. If the capture radiation were of

Table 6

Gamma ray	$B + T$	$C + S$	$D + R$	$E + O$	$G + L$
Sum of gamma-ray energies (Mev)	8.55 ± 0.03	8.57 ± 0.04	8.56 ± 0.05	8.63 ± 0.05	8.59 ± 0.04
	$K + H$	$O + H'$	$C' + G'$	$E' + D'$	$A' + N + T$
	8.58 ± 0.01	8.64 ± 0.08	8.54 ± 0.07	8.65 ± 0.07	8.56 ± 0.05
				$J + M + U + O$	$F + U + T + S$
				8.54 ± 0.05	8.54 ± 0.05

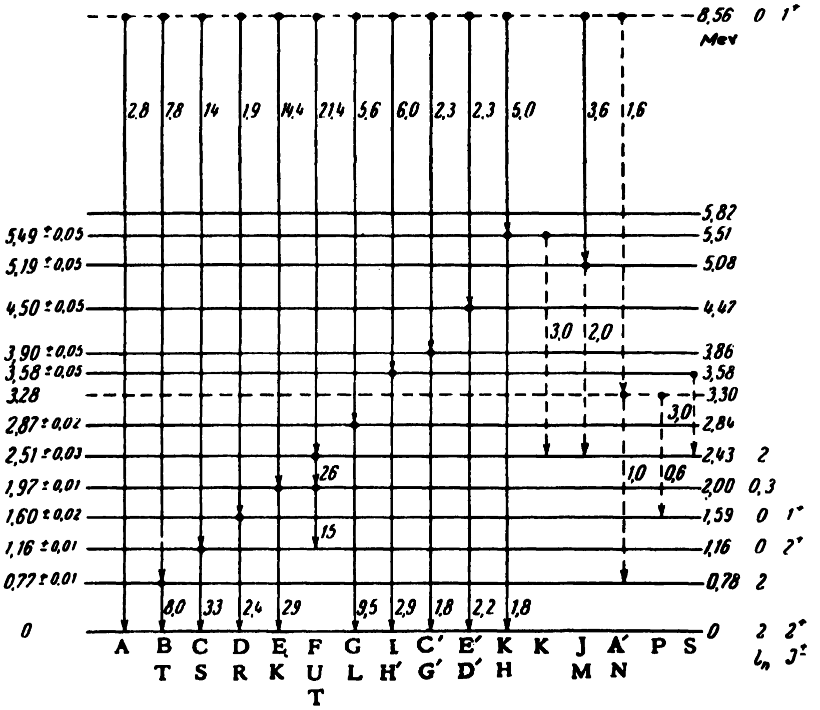

Figure 16. Decay scheme for capture gamma rays from Cl^{36}

Table 7

Product nucleus	Γ_γ (ev)	$D(E)$ (Mev)	Gamma-ray energy (Mev)	Type	Spin and parity of state		$S\frac{\|M\|^2}{2D}$	$\frac{(2J_f + 1)\|M\|^2}{2D}$
					Original	Final		
1	2	3	4	5	6	7	8	9
Be^{10}	15		6.80	E1	1−	0+	1.3	
Be^{10}	15		3.40	E1	1−	2+	1.5	
S^{33}	26[18]	0.3[18]	5.44	E1	½+	3/2−	0.2	0.3
S^{33}	26	0.3	4.40	E1	½+	½−	0.1	
S^{33}	26	0.3	3.66	E1	½+	½−	0.06	
S^{33}	26	0.3	2.9	E1	½+	3/2−	0.3	
Na^{24}	0.19	0.13[26]	6.4	M1	2+	1+	0.08	
Na^{24}	0.19	0.13	5.61	M1	2+	1+	0.035	
S^{33}	26	0.3	8.64	M1	½+	3/2+	0.1	0.08
S^{33}	26	0.3	7.80	M1	½+	½+	0.2	0.14
Cl^{36}	0.3[21]	0.04[22]	8.56	M1	1+	2+	0.01	0.03
Cl^{36}	0.3	0.04	7.41	M1	1+	2+	0.1	
Cl^{36}	0.3	0.04	6.96	M1	1+	1+	0.1	

$M2$ type the difference between the two possible transitions would be much greater because of stronger dependence of quadrupole type transitions on energy. As therefore transitions to the ground state and to the level at 3.37 Mev are of the electric dipole type the intensities of possible gamma transitions to higher levels are lower by several orders of magnitude. Therefore they cannot be detected with our apparatus, and can be neglected in determining the number of photons per capture. The total radiative width for Be^{10} was found by extrapolating the empirical curve obtained in reference 28 to $A = 10$. This extrapolation, however, seems to be not quite valid. It is possible that due to this fact the experimental radiation probability is overestimated as can be seen from Table 7. As to the relative probabilities of ground-state transitions and transitions to the 3.37 Mev level, they are well predicted by the Weisskopf formulas provided an additional neutron is taken into account.

It is seen from Table 7 that $(|M|^2/2D)S$ is nearly constant. This means that the Weisskopf formulas give correctly the variation of partial widths with gamma-quantum energy for $E1$ and $M1$ transitions, as well as correct relative probabilities for these transitions. The fact that $(|M|^2/2D)S$ is close to unity indicates that despite the crude approximations made by Weisskopf the formulas do give absolute widths quite well.

CONCLUSIONS

These results of measurements of the gamma-ray spectra produced by thermal-neutron capture in nuclei, show that the application of a Compton-electron

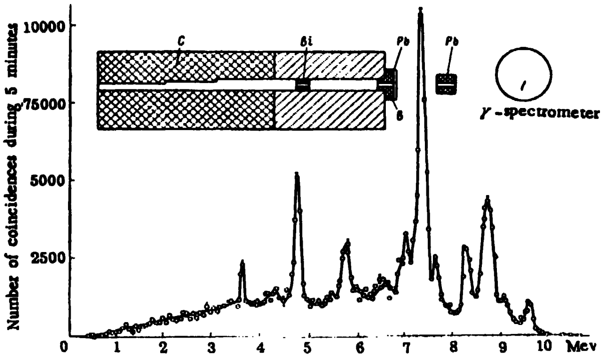

Figure 17. Coincidence gamma-ray spectrum from graphite thermal column

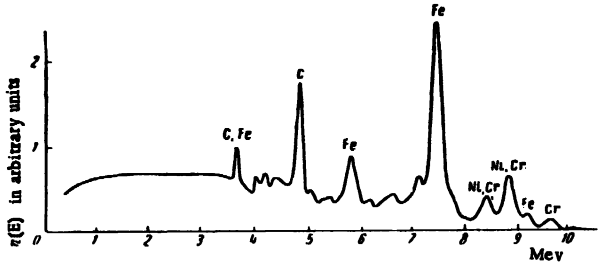

Figure 18. Corrected gamma-ray spectrum from graphite thermal column

spectrometer widens the possibilities of getting information on nuclear properties.

The study of gamma-ray spectra for Be, Na, S and Cl allowed the determination of the emission probabilities of γ-radiations of various multipolarities for a number of gamma transitions in these nuclei. The theory is in quantitative agreement with the experimental data.

The measurements of gamma-rays in a wide energy range lead to a reliable decay scheme of Cl^{36} and a considerable refinement of the level system of this nucleus. The spins of the first three excited states of Na^{24}, the spins of the second and third excited levels of Cl^{36} and the spin of the thermal neutron capturing state of chlorine were deduced.

APPENDIX

The study of thermal-neutron capture gamma-rays makes it possible to analyse the chemical composition of the material irradiated with neutrons. The spectrum of gamma-rays escaping from the channel of the graphite thermal column is given below as an illustration. The spectrum was measured with the spectrometer described above* with the arrangement shown in the top of Fig. 17. Gamma-rays from the reactor core, from the graphite reflector and from the reactor shield fall upon the radiator of the spectrometer, the gamma-rays from the core passing through the reflector. Figures 17 and 18 give the spectra obtained, the first showing the coincidence spectrum and the second a corrected gamma-ray spectrum.

Analysis of this spectrum shows that the main contribution at $E_\gamma > 3.5$ Mev is due to gamma-rays arising from neutron capture in the steel which is used as a structural material in the reactor, and in the graphite. The steel contains iron, nickel, and chromium. Accordingly, the spectrum shows gamma-rays from iron with $E_\gamma = 9.3$, 7.6, 6.0, and 3.5 Mev, from nickel with $E_\gamma = 9.0$, 8.6, and 6.8 Mev, and from chromium with $E_\gamma = 9.7$, 8.9, and 8.5 Mev. The capture gamma-rays from graphite lie at $E_\gamma = 4.9$ and 3.6 Mev.

In the energy region of $E_\gamma < 3.5$ Mev the spectrum is not resolved because of many overlapping lines of various substances and because of scattered radiation.

REFERENCES

1. Kinsey, B. B. and Bartholomew, G. A., Phys. Rev. *93*, 1260 (1954).
2. Dzhelepov, B. and Orbeli, M., Proc. Acad. of Sci., *62*, 615 (1948); Dzhelepov, B., Zhukovsky, N. and Kholnov, Y., Proc. Acad. of Sci. *77*, 233 (1950); Annals Acad. of Sci, USSR, Phys. Series, XVIII, 5, (1954).
3. Kinsey, B. B., Bartholomew, G. A. and Walker, W. H., Canad. Journ. of Phys. *31*, 1 (1953).
4. Sperdoto, A. and Buechner, W. W., Phys. Rev. *88*, 574 (1952).
5. Selinov, I. P., Atomic Nuclei and Nuclear Transformations, 1, (1951).
6. Kinsey, B. B., Bartholomew, G. A. and Walker, W. H., Phys. Rev. *83*, 519 (1951).
7. Kinsey, B. B., Bartholomew, G. A. and Walker, W. H., Phys. Rev. *85*, 1012 (1952).
8. Braid, T. H., Phys. Rev. *90*, 355 (1953).
9. Holt, J. R. and Marsham, T. H., Proc. Phys. Soc. A, *66*, 258 (1953).
10. Davison, P. W., Phys. Rev. *75*, 757 (1949).
11. Hamermesh, B. and Hummel, V., Phys. Rev. *88*, 916 (1952).
12. Reardon, W. A., Krone, R. W. and Stump, R., Phys. Rev. *91*, 334 (1954).
13. Ennis, W. W., Phys. Rev. *82*, 304 (1951).
14. Teplov, I., Dissertation (1954).
15. Recksiedler, A. L. and Hamermesh, B., Phys. Rev. *96*, 109 (1954).
16. Blatt, D. M. and Weisskopf, V. F., Theoretical Nuclear Physics, Moscow (1954).
17. Moszkowski, S. A., Phys. Rev. *89*, 474 (1953).
18. Adair, R. K., Bockelman, C. K. and Peterson, R. E., Phys. Rev. *76*, 508 (1949).
19. Jensen, J. H. O. and Mayer, M. G., Phys. Rev. *85*, 1040 (1952).
20. King, J. S. and Parkinson, W. C., Phys. Rev. *88*, 145 (1952).
21. Hibdon, C. T. and Muehlhause, C. O., Phys. Rev. *79*, 44 (1950).
22. Kiehn, R. M., Goodman, C. and Hausen, K. F., Phys. Rev. *91*, 66 (1953).
23. Motz, H. T., Phys. Rev. *90*, 355 (1953).
24. Millar, Cameron and Glicksman, Canad. Journ. Res. *28* A, 475 (1950).
25. Hibdon, C. T., Muehlhause, C. O., Selowe and Woolf, Phys. Rev. *77*, 730 (1950).
26. Barkov, L. M. and Gurevich, I. I., Width and Density of Nuclear Levels, Review (1953).
27. Satchler, G. R., Proc. Phys. Soc. *67*, 1024 (1954).
28. Heidmann, J. and Bethe, H. A., Phys. Rev. *84*, 274 (1951).

---

* The spectrum was obtained at the first stage of the investigation with a poorer resolution than that quoted in the paper.

Investigation of the Structure of Molecules and the Structure of Liquids by Scattering of Thermal Neutrons

By J. A. Janik, Poland

1. INTRODUCTION

It is well known that the cross-section for scattering of slow neutrons by hydrogen-containing molecules depends on the geometrical structure of these molecules. The theory of the scattering of slow neutrons by rigid molecules of gases was given by Sachs and Teller.[1] They obtained the following formula for the cross-section for scattering of a slow neutron by a proton bound in a rigid molecule:

$$\sigma = \sigma_\infty(\mu_1\mu_2\mu_3\mu)^{1/2}(T_0 + T_1 + T_2 + \cdots)$$

where $\sigma_\infty = 80 \times 10^{-24}$ cm^2, $T_0, T_1 \cdots$ are terms which depend on the energy of the neutrons and on the energy of the translational motion of the molecules, $\mu = \frac{1}{3}(\mu_1 + \mu_2 + \mu_3)$ and μ_1, μ_2, μ_3 are factors defined in the following manner:

A so-called "mass-tensor" M of a molecule is introduced. It is defined by:

$$(M^{-1})_{ii} = \left(\frac{r_j^2}{J_k} + \frac{r_k^2}{J_j} + \frac{1}{M_0}\right), \qquad (M^{-1})_{ij} = -\frac{r_i r_j}{J_k}$$

where r_1, r_2, r_3 are the co-ordinates of the atom considered with respect to the principal axes of inertia of the molecule, J_1, J_2, J_3 are the moments of inertia of the whole molecule with respect to these axes, and M_0 is the mass of the molecule.

A dimensionless tensor $n = mM^{-1}$ is introduced, where m is the mass of the proton. The characteristic values of this tensor are n_1, n_2, n_3. Then

$$\mu_1 = \frac{1}{1 + n_1}, \quad \mu_2 = \frac{1}{1 + n_2}, \quad \mu_3 = \frac{1}{1 + n_3}$$

It may be supposed that the theory of Sachs and Teller (valid for molecular gases) also may be applied to many liquids. In this case it is necessary to replace the bracket $(T_0 + T_1 + \cdots)$ by 1. This corresponds to neglecting the energy of the translational motion of the molecules in comparison to the energy of the neutrons.

It is evident that from the theory of Sachs and Teller we cannot obtain values for the cross-sections in full agreement with the experimentally obtained ones, because in practice we never have to deal with rigid molecules. The internal motions existing in molecules may be divided into two categories: (1) valence vibrations, and (2) free or hindered rotations.

The influence of valence vibrations on the scattering of slow neutrons by molecules was theoretically considered by Messiah. He showed that the result of this influence is a lowering of the cross-section values in comparison to the theory of Sachs and Teller.[2] This lowering is experimentally observed.

The influence of hindered rotation of two-atom groups in a molecule with respect to each other on the scattering of slow neutrons was theoretically considered by Kołos.[3] This influence also causes a lowering of the cross-section (in comparison to a rigid molecule), depending on the potential barrier of the hindered rotation.

In the light of these considerations it seems to be interesting to test experimentally the theory of Kołos for several different molecules, as well as to prove the possibility of investigating the association in liquids containing hydrogen bonds based on a semiquantitative treatment of the theory of Sachs and Teller. This experimental work was done in recent years in the Laboratory of Nuclear Physics of the Polish Academy of Sciences in Kraków.

2. APPARATUS

The apparatus consisted of a source of slow neutrons, flat vessels for the scatterers, and a detector of neutrons. All measurements were made with a very weak source of photoneutrons (200 mg Ra surrounded by about 1 kg of Be powder) slowed down in a layer of paraffin wax, 6 cm thick.

The neutron detector was a boron lined ionisation chamber connected to a linear amplifier.

3. INVESTIGATION OF THE INFLUENCE OF HINDERED ROTATION IN MOLECULES ON THE SCATTERING OF THERMAL NEUTRONS

Experimental work on this problem was carried out by Janik in 1953.[4,5]

The substance used was methyl alcohol. It is well known from spectroscopic data that the proton of the OH-group in the CH_3OH molecule can rotate around the CO-axis. This rotation, however, is not free, but is rather a torsional oscillation on account of the relatively high potential barriers formed by the three protons of the CH_3-group. The frequency of this torsional oscillation (known from spectroscopical measurements) is about 250 cm^{-1}.[6]

Measurements of the cross-section of the CH_3OH molecules for the scattering of neutrons were made using neutrons with Maxwellian velocity distributions corresponding to the temperatures of 300°K and 80°K. The 80°K-neutrons were obtained by cooling the paraffin wax, which was used to slow down the neutrons, by liquid air. The results are:

Cross-section of CH_3OH molecule for 300°K-neutrons: 180 ± 7 barns.

Cross-section of CH_3OH molecule for 80°K-neutrons: 227 ± 10 barns.

Cross-section of CH_3OH molecule theoretically evaluated from the theory of Sachs and Teller: 247 barns.

These results are in good agreement with the theory of Kołos. The lowering of the cross-section, especially for 300°K-neutrons, in comparison to that of the rigid molecule (247 barns) is much greater than that caused by the valence vibrations in the CH_3OH molecule.[7]

In this interpretation, however, the influence of molecular association in methyl alcohol was not taken into account, and it is well known from many physical and physico-chemical data that the methyl alcohol is strongly associated by the hydrogen bonds. There are experimental facts, however, from which one can deduce the existence of a hindered rotation in liquid CH_3OH analogous to that in the gas phase, but still it seems to be necessary to perform some further experiments on the scattering of neutrons on the molecules which are known not to be associated. In this connection measurements of the cross-section for the scattering of thermal neutrons by the CH_3SH molecule were recently made. The results are in agreement with the theory of Kołos.

4. INVESTIGATION OF THE MOLECULAR STRUCTURE OF LIQUIDS BY THE SCATTERING OF SLOW NEUTRONS

In 1951 experiments were carried out by Janik,[8] which suggest the possibility of investigation of the molecular structure of liquids by measurement of the scattering of neutrons. In this work the scattering of neutrons on aqueous solutions of sulphuric acid of different concentrations was investigated. If in the solutions of sulphuric acid only H_2SO_4 molecules were present, the attenuation coefficient (for scattering) for every concentration could be easily evaluated from the coefficients for pure H_2O and H_2SO_4. The experimentally measured neutron attenuation coefficient, however, is lower than that estimated in this manner, for low concentrations of sulphuric acid (up to 40%), and greater than that for higher concentrations.

The interpretation might be that the result for low concentrations is caused by the influence of the electrolytic dissociation of the H_2SO_4 molecules. The increase in scattering for greater concentrations of the acid, however, is caused by hydration of H_2SO_4 molecules, i.e., by attaching of the H_2O to the H_2SO_4 molecules.

In terms of the theory of Sachs and Teller this fact may be interpreted as follows:

The H_2O molecule if attached to another molecule loses the possibility of rotation. This has the same effect as that of increasing the moments of inertia of this molecule, which means increasing the values μ_1, μ_2, μ_3 and μ, and hence increasing the cross-section.

These experiments suggest the possibility of investigating association in other liquids containing hydrogen bonds by scattering of thermal neutrons. In this, the neutron method could supplement other methods generally used in these investigations (optical, ultrasonic, etc.).

REFERENCES

1. Sachs, R. G. and Teller, E., *The Scattering of Slow Neutrons by Molecular Gases*, Phys. Rev. *60*, 18–27 (1941).
2. Messiah, A. M., *Scattering of Slow Neutrons by* H_2 *and* CH_4, Phys. Rev. *84*, 204–214 (1951).
3. Kołos, W., *The Influence of Hindered Rotation on the Scattering of Slow Neutrons by Bound Protons*, Acta Physica Polonica *13* 67–75 (1954).
4. Janik, J. A., *Investigation of the Molecular Structure of Methyl Alcohol by the Scattering of Thermal Neutrons*, Acta Phys. Polon. *12*, 45–50 (1953).
5. Janik, J. A., *Scattering of 80°K-Neutrons by* CH_3OH *and* CH_3I*-Molecules*, Acta Phys. Polon. *13*, 167–173 (1954).
6. Burkhard, D. G. and Dennison, D. M., *The Molecular Structure of Methyl Alcohol*, Phys. Rev. *84*, 408–417 (1951).
7. Kołos, W., *The Influence of Hindered Rotation on the Scattering of Slow Neutrons by Bound Protons*, Bull. Ac. Pol. Sc. *2*, 423–427 (1954).
8. Janik, J. A., *Influence of the Electrolytic Dissociation and the Hydratation of* H_2SO_4*—Molecules on the Scattering of Slow Neutrons*, Acta Phys. Polon. *11*, 146–153 (1951).

Thermal Inelastic Scattering of Cold Neutrons in Polycrystalline Solids

By K. S. Singwi and L. S. Kothari,* India

1. INTRODUCTION

The theory of the influence of thermal motion on the scattering of cold neutrons in crystals was first worked out as early as 1944 by Weinstock.[1] Using the Fermi pseudo-potential and the Born approximation, he calculated the temperature variation of the inelastic scattering cross-section of cold neutrons in polycrystalline solids. His theory was found to be in reasonable agreement with experiments, until it was noticed by Cassels[2] that for aluminium at a temperature of about 700°K, which is nearly twice its Debye temperature, the observed value of the total inelastic cross-section was 15% greater than that calculated on the basis of Weinstock's theory. Similar discrepancies have since been observed by Squires[3] in magnesium and nickel and by Hughes[4] in beryllium.

At temperatures close to or greater than the Debye temperature of a solid one would naturally expect deviations from the simple Weinstock theory, since it takes account of only those processes in which a single phonon is exchanged and neglects the contribution of multi-phonon processes. This contribution becomes appreciable at high neutron energies and also for high temperatures of the scatter, since in the former case a neutron can emit while in the latter it can absorb many phonons. A calculation of the contribution of these multi-phonon processes has been attempted by Squires[3] and discussed more recently and somewhat in greater detail by Placzek.[5] Since from our experience in solid state physics we know that even very near the melting point of a solid the amplitude of the atomic vibrations is only a fraction of the lattice distance, it seems reasonable to suppose that once the multi-phonon contribution has properly been taken into account, the theory should hold good almost right up to the melting point of a solid.

The total inelastic scattering cross-section can be expressed as a sum of two terms, the coherent and the incoherent parts. The former is the interference part of the slow neutron scattering whereas the latter is the diffuse scattering arising due to spin and isotope disorder (we shall not be concerned here with magnetic diffuse scattering). Squires has attempted to calculate the contribution of the multi-phonon processes to both the coherent and the incoherent parts. He decomposes the total cross-section σ into partial cross-sections σ_l, corresponding to the emission or absorption of l phonons—a procedure the convergence of which becomes progressively poorer with increasing neutron energy and also with higher temperatures of the scatterer. For example, he finds that in the particular case of magnesium he has to consider processes involving the exchange of as many as five phonons to account for the observed total inelastic scattering cross-section. To overcome this difficulty, Placzek[5] expands the total incoherent cross-section in inverse powers of M, the ratio of nuclear to neutron mass, and shows that on account of certain compensation effects the new series is very rapidly convergent for M moderately large compared to both unity and T/Θ, Θ being the Debye temperature of the solid. It, therefore, becomes a simple matter to calculate the total incoherent cross-section. To get the total inelastic cross-section Placzek makes what he calls the "incoherent approximation." As we shall show, it is possible to extend his method to an exact calculation of the coherent part as well. It will be seen that Placzek's incoherent approximation is not always justified.

The present paper is divided into four main sections. In section 2, unlike Weinstock[1] who uses oscillator wave functions to represent the temperature displacements of the lattice points, we use the field theoretical method and represent the temperature displacements by a sum of emission and absorption operators. The calculation of the transition probability then became an easy matter involving simple algebraic operations of these operators. We have also generalized Weinstock's theory to take account of multi-phonon processes. Our method provides an alternative proof of the Debye-Waller factor, which in our notation is the expectation value of a certain operator. We believe this derivation is simpler than that given by Born and Sarginson[6] in the analogous case of temperature scattering of X-ray.

In section 3 general expressions for both the incoherent and coherent cross-sections, using the usual Debye frequency spectrum of a solid, are derived. The coherent cross-section hitherto not treated rigorously, is examined in detail. It is shown that the coherent part is a sum of two terms arising as a result of the replacement of a sum by an integral. The magnitude of the correction term is different for different order processes and also depends upon the wave-length of the incident neutrons and upon the crystal symmetry.

---

* Atomic Energy Establishment, Trombay.

The main as well as the correction terms of the total coherent inelastic cross-section are put in "Placzek" form and for cold neutrons explicit expressions are derived under two approximations (1) $M \gg 1$, $T/\Theta \geq 1$, and (2) M small (~ 10) and $T/\Theta \geq 0.5$.

In the last section numerical results obtained from the above theory are discussed in the case of magnesium, aluminium, iron, lead and beryllium. The correction term in the case of magnesium is -4% whereas in lead it is on the average $+22\%$. Agreement between theory and experiment for magnesium and aluminium is fairly good. On account of the extra magnetic scattering of neutrons in iron it is not possible to verify the theory of thermal inelastic scattering from measurements on this element. Nevertheless, the calculation is of importance in estimating the magnetic contribution to the total scattering. So far no experimental results are available to us for lead and for beryllium the one experimental result that is known within the temperature range we have considered agrees well with theory.

2. GENERAL MATHEMATICAL THEORY

We shall express all quantities in dimensionless units. Our unit of length would be $(\hbar^2/2m_0k_0\Theta)^{1/2}$ and that of energy $k_0\Theta$; where k_0 is the Boltzmann constant, m_0 is the neutron mass, $\hbar$ is Planck's constant divided by 2π, and Θ the Debye temperature of the solid.

Let the position of the σth nucleus at any instant be

$$\vec{R}_\sigma = \vec{\sigma} + \vec{u}_\sigma \tag{1}$$

where $\vec{u}_\sigma$ is its displacement from the equilibrium position $\vec{\sigma}$. The displacement $\vec{u}_\sigma$ is decomposed as

$$\vec{u}_\sigma = \frac{1}{(MN)^{1/2}} \sum_{j,s} \xi_j^{-1/2} \epsilon_s (a_j e^{i\vec{f}_j\cdot\vec{\sigma}} + a_j{}^* e^{-i\vec{f}_j\cdot\vec{\sigma}}) \tag{2}$$

where $M = m/m_0$ is the ratio of nuclear to neutron mass, N is the total number of nuclei in the crystal, ξ_j is the energy of the phonon corresponding to the wave vector $\vec{f}_j$, $\vec{\epsilon}_s$ is a unit polarization vector and $a_j{}^*$, a_j are respectively the emission and absorption operators for phonons of wave vector $\vec{f}_j$. The summation in Equation 2 extends over both j and s ($s = 1, 2, 3$, corresponding to the three directions of polarization of the phonon). The matrix elements of the operators $a_j{}^*$ and a_j are

$$\langle n_j + 1 | a_j{}^* | n_j \rangle = (n_j + 1)^{1/2} \tag{3a}$$

$$\langle n_j | a_j | n_j + 1 \rangle = (n_j + 1)^{1/2} \tag{3b}$$

where n_j is the number of phonons of type $\vec{f}_j$. They also satisfy the following commutation relation

$$[a_j, a_k{}^*] = \delta_{jk} \tag{4}$$

We assume a slow neutron to interact with a nucleus according to the pseudo-potential $V(r)$ discussed by Fermi.[7]

$$V(\vec{r}) = 4\pi a \delta(\vec{r}) \tag{5}$$

where a is the scattering length of the nucleus. In general the scattering length is different for different nuclei in the crystal depending upon their spin and isotopic mass. For nuclei with zero spin and no isotope

$$a = (\sigma_s/4\pi)^{1/2}$$

σ_s being the bound scattering cross-section.

The matrix element for the transition of a neutron from the initial state corresponding to the wave vector $\vec{k}_1$, to the final state corresponding to wave vector $\vec{k}_2$ is evaluated by using the pseudo-potential of Equation 5 and the Born approximation, the validity of which has been discussed by Fermi.[7] The wave function of a neutron inside a crystal is taken to be

$$\psi(\vec{r}) = e^{i\vec{k}\cdot\vec{r}} \tag{6}$$

The wave function of the phonon field is represented by $|n_j, n_k, \ldots\rangle$ Making use of Equations 1, 5 and 6 we have for the matrix element

$$\langle \vec{k}_2 | V | \vec{k}_1 \rangle = 4\pi \sum_\sigma a_\sigma \langle n_j', n_k', \ldots | e^{i(\vec{k}_1 - \vec{k}_2)\cdot(\vec{\sigma} + \vec{u}_\sigma)} \\ | n_j, n_k, \ldots \rangle \tag{7}$$

where a_σ is the scattering length of the σth nucleus, and n_j' is the number of phonons of the type $\vec{f}_j$ in the final state. The phonon wave functions have not been written down explicitly on the left hand side of Equation 7 for reasons of simplicity.

Single Phonon Process

For the transition of a neutron from the initial state $\vec{k}_1$ to the final state $\vec{k}_2$ in which only single phonon $\vec{f}_1$ is absorbed, Equation 7 becomes

$$\langle \vec{k}_2 | V | \vec{k}_1 \rangle = 4\pi \sum_\sigma a_\sigma e^{i(\vec{k}_1 - \vec{k}_2)\cdot\vec{\sigma}} \langle n_1 - 1 | e^{i(Q_{1.\sigma} a_1 + Q_{1.\sigma}{}^* a_1{}^*)} | n_1 \rangle \\ \times \prod_{j=2}^{3N} \langle n_j | e^{i(Q_{j.\sigma} a_j + Q_{j.\sigma}{}^* a_j{}^*)} | \eta_j \rangle \tag{8}$$

where we have put

$$Q_{j.\sigma} = \frac{1}{(MN)^{1/2}} \sum_s (\vec{k}_1 - \vec{k}_2) \cdot \vec{\epsilon}_s \xi_j{}^{-1/2} e^{i\vec{f}_j\cdot\vec{\sigma}} \tag{9}$$

Now consider F_{n_j-1,n_j}, which is defined as

$$F_{n_j-1,n_j} = \langle n_j - 1 | e^{i(Q_{j.\sigma} a_j + Q_{j.}{}^*{}_\sigma a_j{}^*)} | n_j \rangle \\ = n_j{}^{-1/2} \langle n_j | a_j{}^* e^{i(Q_{j.\sigma} a_j + Q_{j.}{}^*{}_\sigma a_j{}^*)} | n_j \rangle \tag{10}$$

On simplification we obtain

$$F_{n_j-1,n_j} = -in_j{}^{-1/2} Q_{j.\sigma} F_{n_j,n_j} + \left(\frac{n_j + 1}{n_j}\right)^{1/2} F_{n_j,n_j+1} \tag{11}$$

This recurrence relation leads to

$$F_{n_j,n_j+1} = i(n_j+1)^{-\frac{1}{2}}Q_{j,\sigma}|F_{n_j,n_j} + F_{n_j-1,n_j-1} + \cdots + F_{0,0}) \qquad (12)$$

Starting from

$$F_{n_j,n_j} = \langle n_j|e^{i(Q_{j,\sigma}a_j+Q_{j,}{}^{*}{}_{\sigma}a_j{}^{*})}|n_j\rangle$$

one also gets the result

$$F_{n_j,n_j} = in_j^{-\frac{1}{2}}Q_{j,\sigma}{}^{*}F_{n_j-1,n_j} + F_{n_j-1,n_j-1} \qquad (13)$$

Substituting F_{n_j,n_j} from Equation 13 in Equation 11 and comparing the result with Equation 11 we find that provided terms of the order $1/N$ are neglected in comparison with unity,

$$F_{n_j,n_j} = F_{n_j-1,n_j-1}$$

This when applied to Equation 12 leads to the following result

$$F_{n_j-1,n_j} = in_j^{\frac{1}{2}}Q_{j,\sigma}F_{n_j,n_j} \qquad (14)$$

Substituting Equation 14 in Equation 8 we obtain the following

$$\langle \vec{k}_2|V|\vec{k}_1\rangle = 4\pi i\sum_{\sigma} a_\sigma n_1{}^{\frac{1}{2}}Q_{1,\sigma}e^{i(\vec{k}_1-\vec{k}_2)\cdot\vec{\sigma}} \times \prod_{j=1}^{3N} F_{n_j,n_j} \qquad (15)$$

Multiphonon Process

It is simple to generalize the above one phonon treatment to the case of multiphonon processes. The matrix element corresponding to the absorption of say l different phonons is given by

$$\langle \vec{k}_2|V|\vec{k}_1\rangle = 4\pi i^l\sum_{\sigma} a_\sigma\left(\prod_{j=1}^{l} n_j{}^{\frac{1}{2}}Q_{j,\sigma}\right)e^{i(\vec{k}_1-\vec{k}_2)\cdot\vec{\sigma}}$$
$$\times\prod_{j=1}^{3N} F_{n_j,n_j} \qquad (16)$$

It may be mentioned here that the probability for the absorption of two phonons of the same type is N^{-1} times the probability for the absorption of two different types of phonons.

The average value of the square of the matrix element, on using Equation 9, is

$$\overline{|\langle k_2|V|k_1\rangle|^2} = \frac{16\pi^2}{(MN)^l}\sum_{n_1=0}^{\infty}\cdots\sum_{n_{3n}=0}^{\infty}\left(\prod_{j=1}^{3N}\omega(n_j)\right)$$
$$\overline{\times\left|\sum_{\sigma} a_\sigma e^{i\left(\vec{k}_1-\vec{k}_2+\sum_{j=1}^{l}\vec{f}_j\right)\cdot\vec{\sigma}}\right.}$$
$$\overline{\left.\times\left\{\prod_{k=1}^{l}\left(\frac{n_k}{\xi_k}\right)^{\frac{1}{2}}\sum_{s}(\vec{k}_1-\vec{k}_2)\cdot\vec{\epsilon}_s\right\}\prod_{j=1}^{3N}F_{n_j,n_j}\right|^2} \qquad (17)$$

where $\omega(n_j)$ is the probability that there are n_j phonons of the type $\vec{f}_j$ in the field at temperature T and is given by

$$\omega(n_j) = \frac{e^{-(n_j+\frac{1}{2})\xi_j/T}}{\sum_{n_j=0}^{\infty}e^{-(n_j+\frac{1}{2})\xi_j/T}} = (1-e^{-\xi_j/T})e^{-n_j\xi_j/T} \qquad (18)$$

T being the temperature of the scatterer in units of Θ.

To evaluate the various sums over the phonon numbers in Equation 17 we consider

$$F = \sum_{n=0}^{\infty}\omega(n)\langle n|e^{i(\eta a+\eta^{*}a^{*})}|n\rangle \qquad (19)$$

where η is any complex c-number. Making use of Weyl's[8] identity

$$e^{i(\eta a+\eta^{*}a^{*})} = e^{i\eta a}e^{i\eta^{*}a^{*}}e^{\frac{1}{2}\eta\eta^{*}} \qquad (20)$$

a simple algebraic proof of which has also been given by Nanda[9] and Equation 18, we obtain

$$F = (1-e^{-\xi/T})\sum_{n=0}^{\infty}e^{\frac{1}{2}\eta\eta^{*}}e^{-n\xi/T}\langle n|e^{i\eta a}e^{i\eta^{*}a^{*}}|n\rangle \qquad (21)$$

The matrix element in Equation 21 is easily evaluated by expanding the exponentials involving the operators a and a^{*}, and we get

$$\langle n|e^{i\eta a}e^{i\eta^{*}a^{*}}|n\rangle = \sum_{r=0}^{\infty}\frac{(-\eta\eta^{*})^r(n+r)!}{(r!)^2 n!} \qquad (22)$$

Substituting Equation 22 in Equation 21 and noting that the series in n is just the binomial expansion of $(1-e^{-\xi/T})^{-r-1}$, we obtain

$$F = (1-e^{-\xi/T})e^{\frac{1}{2}\eta\eta^{*}}\sum_{r=0}^{\infty}\frac{(-\eta\eta^{*})^r}{r!(1-e^{-\xi/T})^{r+1}}$$
$$= \exp -\frac{1}{2}\eta\eta^{*}\coth\frac{\xi}{2T} \qquad (23)$$

We can similarly show that, provided terms of the order $\eta\eta^{*}$ can be neglected in comparison to unity

$$\sum_{\eta=0}^{\infty}n\omega(n)\langle n|e^{i(\eta a+\eta^{*}a^{*})}|n\rangle = (e^{\xi/T}-1)^{-1}e^{-\frac{1}{2}\eta\eta^{*}\coth\frac{\xi}{2T}} \qquad (24)$$

Making use of results of Equations 23 and 24 with $\eta = Q_{j,\sigma} - Q_{j,p}$ we find that the sums over n_j in Equation 17 when averaged over all lattice points are independent of σ to within our approximation. Using Cassel's[10] result

$$\left|\sum_{\sigma} a_\sigma \exp i\left(\vec{k}_1-\vec{k}_2+\sum_{j=1}^{l}\vec{f}_j\right)\cdot\vec{\sigma}\right|^2 = N(\overline{a^2}-\bar{a}^2)$$
$$+\bar{a}^2\left|\sum_{\sigma}\exp i\left(\vec{k}_1-\vec{k}_2+\sum_{j=1}^{l}\vec{f}_j\right)\cdot\vec{\sigma}\right|^2$$

to simplify the summation over σ and p, we obtain finally

$$\overline{\langle\vec{k}_2|V|\vec{k}_1\rangle|^2}=\frac{4\pi}{(MN)^l}\left(\sum_s(\vec{k}_1-\vec{k}_2)\cdot\vec{\epsilon}_s\right)^2\prod_{j=1}^{l}\xi^{-1}(e^{\xi_j/T}-1)^{-1}$$

$$\times\exp-\frac{1}{MN}\sum_{j,\sigma}\xi_j^{-1}(\vec{k}_1-\vec{k}_2\cdot\vec{\epsilon}_s)^2\coth\frac{\xi_j}{2T}$$

$$\times\left[Ns+S\left|\sum_\sigma\exp i\left(\vec{k}_1-\vec{k}_2+\sum_{j=1}^{l}\vec{f}_j\right)\cdot\vec{\sigma}\right|^2\right]\quad(25)$$

where we have put

$$s=4\pi(\overline{a^2}-\bar{a}^2);\qquad S=4\pi\bar{a}^2\quad(26)$$

In Equation 25 the terms proportional to s and S represent respectively the incoherent and coherent scattering. The factor

$$\exp-\frac{1}{MN}\sum_{j,s}\xi_j^{-1}(\vec{k}_1-\vec{k}_2\cdot\vec{\epsilon}_s)^2\coth\frac{\xi_j}{2T}$$

is the well-known Debye-Waller factor and under the usual Debye approximation reduces to

$$\exp-\frac{6F}{M}(\vec{k}_1-\vec{k}_2)^2\quad(27)$$

where

$$F=\frac{1}{2}\int_0^1\xi\,d\xi\coth\frac{\xi}{2T}=\frac{1}{4}+T^2Q(T^{-1}),$$

$$Q(z)=\int_0^z\frac{\beta\,d\beta}{e^\beta-1}\quad(28)$$

3. INCOHERENT AND COHERENT SCATTERING CROSS-SECTIONS

The inelastic scattering cross-section is obtained on multiplying Equation 25 by $k_2/16\pi^2Nk_1$. We have seen that the total scattering divides into two parts, the incoherent and the coherent part. We shall now discuss each of them separately.

Incoherent Scattering Cross-Section

In the general case when l phonons are absorbed, the incoherent cross-section per unit solid angle per scattering nucleus is given by

$$d\sigma_{incoh,+l}=\frac{s}{4\pi k_1l!}\left(\frac{1}{MN}\right)^l\sum_{\xi_j=0}^{1}k_2(\vec{k}_1-\vec{k}_2\cdot\vec{\epsilon}_s)^{2l}$$

$$\times\exp-\frac{6F}{M}(\vec{k}_1-\vec{k}_2)^2\times\prod_{j=1}^{l}\xi_j^{-1}(e^{\xi_j/T}-1)^{-1}\quad(29)$$

where k_2 is related to k_1 and ξ through the energy conservation condition

$$k_2^2=k_1^2+\sum_{j=1}^{l}\xi_j\quad(30)$$

Replacing the sums over ξ by integration and using the usual Debye approximation, we obtain after some simplification

$$\sigma_{incoh,+l}=\frac{s}{2k_1^2l!}\left(\frac{3}{2M}\right)^l\prod_{j=1}\int_0^1\xi_j\left(\coth\frac{\xi_j}{2T}-1\right)d\xi_j$$

$$\int_{k_2-k_1}^{k_2+k_1}e^{-\frac{6F}{M}t^2}t^{2l+1}\,dt\quad(31)$$

where we have replaced $(\vec{k}_1-\vec{k}_2)^2$ by t^2.

If formally we let ξ_j take both positive as well as negative values, we can combine the scattering cross-section for the absorption of l phonons with that for the emission of l phonons in one single formula and obtain

$$\sigma_{incoh,l}=\frac{s}{2k_1^2l!}\left(\frac{3}{2M}\right)^l\prod_{j=1}^{l}\int_{-1}^1\xi_j\left(\coth\frac{\xi_j}{2T}-1\right)$$

$$d\xi_j\int_{k_2-k_1}^{k_2+k_1}e^{-\frac{6F}{M}t^2}t^{2l+1}\,dt\quad(32)$$

The total incoherent cross-section is

$$\sigma_{incoh}=\sum_l\sigma_{incoh,l}\quad(33)$$

Coherent Cross-Section

The contribution of the coherent part to the total inelastic scattering cross-section has been estimated by Squires[3] in a rather unsatisfactory manner. We shall, therefore, discuss this in a little more detail.

The coherent part of the scattering is proportional to the second term on the right-hand side of Equation 25. Now

$$\left|\sum_\sigma e^{i\left(\vec{k}_1-\vec{k}_2+\sum_{j=1}^{l}\vec{f}_j\right)\cdot\vec{\sigma}}\right|^2$$

$$=\frac{(2\pi)^3N}{B}\,\delta\left(\vec{k}_1-\vec{k}_2+\sum_{j=1}^{l}\vec{f}_\delta-2\pi\vec{\tau}\right)\quad(34)$$

where $\vec{\tau}$ is a reciprocal lattice vector. The vectors in the argument of the δ-function are in cartesian co-ordinate space. B is the volume per nucleus in ordinary space and represents the Jacobian of transformation from the reciprocal to the cartesian system of co-ordinates. Equation 34 is valid for a cubic crystal, and a suitable change has to be made for any other crystal symmetry. For example, for a close-packed hexagonal structure the right-hand side of Equation 34 has to be multiplied by $\frac{1}{2}(1+\cos\varphi)$, where φ is a function of the components of $\vec{\tau}$.

From Equations 25, 27 and 34 it follows that the coherent cross-section per unit solid angle per scattering nucleus, corresponding to a process in which l different phonons are absorbed or emitted, is

$$d\sigma_{coh,l} = \frac{2\pi^2 S k_2}{B k_1 l!}\left(\frac{1}{MN}\right)^l \sum_{\xi_j=-1}^{1} \delta\left(\vec{k}_1 - \vec{k}_2 + \sum_{j=1}^{l} \vec{f}_j - 2\pi\vec{\tau}\right) e^{-\frac{6F}{M}(\vec{k}_1 - \vec{k}_2)^2}$$
$$\times \prod_{j=1}^{l} \xi_j^{-1}(e^{\xi_j/T} - 1)^{-1}(\vec{k}_1 - \vec{k}_2 \cdot \vec{\epsilon}_s)^2 \quad (35)$$

To get the total cross-section $\sigma_{coh,l}$ for a poly-crystal, Equation 35 has to be integrated over all directions of $\vec{k}_2$ and averaged over all directions of $\vec{k}_1$. Fortunately the angle dependence is contained only in the argument of the δ-function in Equation 35. Using the result (see Weinstock[1])

$$\frac{1}{4\pi}\int_0^{\pi} \sin\theta_{k_1}\, d\theta_{k_1} \int_0^{2\pi} d\varphi_{k_1}\, 2\pi \int_0^{\pi} \sin\theta_{k_2}\delta(\vec{k}_1 - \vec{k}_2 + \sum_{j=1}^{l} \vec{f}_j - 2\pi\vec{\tau})\, d\theta_{k_2} = \frac{1}{2k_1k_2\left|2\pi\vec{\tau} - \sum_{j=1}^{l} \vec{f}_j\right|} \quad (36)$$

and replacing the summation over the phonon wave vectors by integrals and making the usual Debye approximation, we obtain

$$\sigma_{coh,l} = \frac{\pi^2 S}{B k_1^2 l!}\left(\frac{3}{2M}\right)^l \prod_{j=1}^{l} \int_{-1}^{1} \xi_j\left(\coth\frac{\xi_j}{2T} - 1\right) d\xi_j$$
$$\times \sum_{\tau} e^{-\frac{6F}{M}\left|2\pi\vec{\tau} - \sum_{j=1}^{l}\vec{f}_j\right|^2} \left|2\pi\vec{\tau} - \sum_{j=1}^{l} \vec{f}_j\right|^{2l-1} \quad (37)$$

In Equation 37 the sum over $\vec{\tau}$ extends over all possible values of τ consistent with the energy conservation condition (Equation 30) and the momentum conservation condition:

$$\vec{k}_1 - \vec{k}_2 + \sum_{j=1}^{l} \vec{f}_j = 2\pi\vec{\tau} \quad (38a)$$

which may also be written as

$$k_2 - k_1 \leq \left|2\pi\vec{\tau} - \sum_{j=1}^{l} \vec{f}_j\right| \leq k_2 + k_1 \quad (38b)$$

It is laborious to evaluate Equation 37 since one has to sum over a large number of $\vec{\tau}$ values, even for a single phonon process. We, therefore, replace the summation by an integration over $\vec{\tau}$ (Squires).[8] However, this needs a little care, for one may easily drop terms that give an appreciable contribution to the final result.

Consider

$$\sum_n f(\vec{\tau}_n) = \sum_n \int f(\vec{\tau})\delta(\vec{\tau} - \vec{\tau}_n)\, d\vec{\tau} \quad (39)$$

Making a Fourier expansion of $\sum_n \delta(\tau - \tau_n)$ and using the result $\exp(2\pi i\vec{\tau}_n \cdot \vec{\sigma}) = 1$, where $\vec{\sigma}$ is any lattice vector, we obtain

$$\sum_n f(\vec{\tau}_n) = B\sum_{\sigma} \int f(\vec{\tau})e^{2\pi i\vec{\sigma}\cdot\vec{\tau}}\, d\vec{\tau}$$

The first term for $\sigma = 0$, is $B\int f(\vec{\tau})\, d\vec{\tau}$

The other terms are

$$B\sum_{\sigma} Z_{\sigma} \int f(\vec{\tau})\langle \exp 2\pi i\vec{\sigma}\cdot\vec{\tau}\rangle_{avg}\, d\vec{\tau}$$

where Z_{σ} is the number of nuclei at the lattice distance σ. The quantity $\langle \exp 2\pi i\vec{\sigma}\cdot\vec{\tau}\rangle_{avg}$, which represents the average over various directions, can readily be evaluated and we obtain

$$\sum_n f(\vec{\tau}_n) = B\int f(\vec{\tau})\, d\vec{\tau} + B\sum_{\sigma} Z_{\sigma} \int f(\vec{\tau})\frac{\sin 2\pi\sigma\tau}{2\pi\sigma\tau}\, d\vec{\tau} \quad (40)$$

Making the substitution

$$2\pi\vec{\tau} - \sum_{j=1}^{l} \vec{f}_j = \vec{t}$$

we find from Equations 37 and 40 that we can write

$$\sigma_{coh} \equiv \sum_{l=1}^{\infty} (\sigma_{coh,l}{}^0 + \sigma_{coh,l}{}^1) = \sigma_{coh}{}^0 + \sigma_{coh}{}^1 \quad (41)$$

where

$$\sigma_{coh,l}{}^0 = \frac{S}{2k_1^2 l!}\left(\frac{3}{2M}\right)^l \prod_{j=1}^{l} \int_{-1}^{1} \xi_j\, d\xi_j\left(\coth\frac{\xi_j}{2T} - 1\right)$$
$$\times \int_{k_2-k_1}^{k_2+k_1} \exp\left(-\frac{6F}{M}t^2\right) t^{2l+1}\, dt \quad (42)$$

and the correction term is

$$\sigma_{coh,l}{}^1 = \frac{S}{2k_1^2 l!}\left(\frac{3}{2M}\right)^l \sum_{\sigma} \frac{Z_{\sigma}}{\sigma} \prod_{j=1}^{l} \int_{-1}^{1} \xi_j\, d\xi_j$$
$$\left(\coth\frac{\xi_j}{2T} - 1\right) \times \int_{k_2-k_1}^{k_2+k_1} \exp\left(-\frac{6F}{M}t^2\right) t^{2l} \sin\sigma t\, dt \quad (43)$$

In Equations 42 and 43 it should be remembered that k_2 is related to the phonon energy ξ through the energy conservation condition of Equation 30.

If we compare Equations 42 and 32 we find that the two expressions are the same apart from the constant factors S and s. Thus Placzek's[5] assumption of incoherent approximation is justified only so long as the correction term of Equation 43 is small. As we shall show later, Equation 43 in most cases makes an appreciable contribution to the final result.

Consider the main term of the coherent cross-section as given by Equation 42. For $M \gg 1$, and T, we can expand the function exp $(-6Ft^2/M)$, and integrate term by term over t, obtaining

$$\sigma_{coh.l}{}^0 = \frac{S}{2k_1{}^2 l!}\left(\frac{3}{2}\right)^l \sum_{r=0}^{\infty} \frac{(-6F)^r M^{-l-r}}{2(l+r+1)r!}$$

$$\prod_{j=1}^{l} \int_{-1}^{1} \xi_j \left(\coth \frac{\xi_j}{2T} - 1\right)$$

$$\times \{(k_2 + k_1)^{2(l+r+1)} - (k_2 - k_1)^{2(l+r+1)}\}\, d\xi_j \quad (44)$$

The total cross-section $\sigma_{coh}{}^0$ is obtained by summing Equation 44 over all values of l from 1 to ∞. ($l = 0$ would correspond to elastic scattering and is left out of present considerations.) The final result can be expressed as a series in $1/M$.

$$\sigma_{coh}{}^0 = \sum_{n=1}^{\infty} \frac{A^{(n)}}{M^n} \quad (45)$$

where

$$A^{(1)} = \frac{3S}{2k_1{}^2} \int_{-1}^{1} \xi(k_1{}^2 + k_2{}^2)k_1k_2 \left(\coth \frac{\xi}{2T} - 1\right) d\xi$$

To integrate this we expand coth $(\xi/2T)$ and change the variable of integration from ξ to k_2, by using the energy conservation condition

$$k_2{}^2 = k_1{}^2 + \xi$$

For $T \geq 1$, we get

$$A^{(1)} = \frac{3S}{k_1}\left[\left(+\frac{2T}{5} - \frac{1}{7} + \frac{1}{54T}\right)\right.$$
$$+ k_1{}^2\left(\frac{5T}{3} - \frac{1}{2} + \frac{5}{84T}\right) + k_1{}^4\left(\frac{7T}{4} - \frac{7}{24} + \frac{7}{240T}\right)$$
$$\left. + k_1{}^6\left(\frac{3T}{8} + \frac{3}{16} - \frac{1}{96T}\right)\right] \quad (46)$$

For all the cases that we have considered here, except that of beryllium, $A^{(2)}/M^2$ is negligible, being about ½% of $A^{(1)}/M$.

We can obtain a similar expansion in the inverse powers of M for $\sigma_{coh}{}^1$. Straightforward, though a little lengthy, calculation leads to the result

$$\sigma_{coh}{}^1 = \sum_{n} \frac{B^{(n)}}{M^n} \quad (47)$$

where

$$B^{(n)} = \frac{3S}{k_1{}^2} \sum_{\sigma} \frac{Z_\sigma}{\sigma^6}\left(A_\sigma + B_\sigma T + \frac{C_\sigma}{T}\right) \quad (48)$$

with

$$A_\sigma = \sin\left(\sigma(1 + k_1{}^2)^{1/2}\right)\left[\left\{-\frac{180}{\sigma^2} + 90 - 7\sigma^2\right.\right.$$
$$\left. + k_1{}^2(89 - 12\sigma^2) - 4\sigma^2k_1{}^2\right\} \sin \sigma k_1$$
$$\left. + \left\{\left(\frac{60}{\sigma} - 30\sigma + 2\sigma^3\right)k_1 + (2\sigma^3 - 24\sigma)k_1{}^3\right\} \cos \sigma k_1\right]$$
$$+ \sigma(1 + k_1{}^2)^{1/2} \cos\left(\sigma(1 + k_1{}^2)^{1/2}\right)\left[\left\{\frac{180}{\sigma^2} - 30 + \sigma^2\right.\right.$$
$$\left. + k_1{}^2(2\sigma^2 - 24)\right\} \sin \sigma k_1 + \left\{\left(10\sigma - \frac{60}{\sigma}\right)k_1\right.$$
$$\left.\left. + 4\sigma k_1{}^3\right\} \cos \sigma k_1\right] \quad (49a)$$

$$B_\sigma = \sin\left(\sigma(1 + k_1{}^2)^{1/2}\right)[\{-14 + 10\sigma^2 + 12\sigma^2k_1{}^2\} \sin \sigma k_1$$
$$+ \{(12\sigma - 4\sigma^3)k_1 - 4\sigma^3k_1{}^3\} \cos \sigma k_1]$$
$$+ \sigma(1 + k_1{}^2)^{1/2} \cos\left(\sigma(1 + k_1{}^2)^{1/2}\right)[\{24 - 2\sigma^2 - 4\sigma^2k_1{}^2\}$$
$$\sin \sigma k_1 - 12\sigma k_1 \cos \sigma k_1] \quad (49b)$$

$$C_\sigma = \sin\left(\sigma(1 + k_1{}^2)^{1/2}\right)\left[\left\{-\frac{1120}{\sigma^4} + \frac{560}{\sigma^2} - \frac{140}{3} + \frac{3}{2}\sigma^2\right.\right.$$
$$\left. + k_1{}^2\left(\frac{520}{\sigma^2} - \frac{220}{3} + 3\sigma^2\right) + k_1{}^4\left(-\frac{155}{6} + \frac{4}{3}\sigma^2\right)\right\}$$
$$\sin \sigma k_1 + \left\{k_1\left(\frac{280}{\sigma^3} - \frac{140}{\sigma} + \frac{350}{3}\sigma - \frac{1}{3}\sigma^3\right)\right.$$
$$\left.\left. + k_1{}^3\left(-\frac{120}{\sigma} + \frac{40\sigma}{3} - \frac{\sigma^3}{3}\right) + \frac{8}{3}\sigma k_1{}^5\right\} \cos \sigma k_1\right]$$
$$+ \sigma(1 + k_1{}^2)^{1/2} \cos\left(\sigma(1 + k_1{}^2)^{1/2}\right)\left[\left\{\frac{1120}{\sigma^4} - \frac{560}{3\sigma^2} + \frac{28}{3}\right.\right.$$
$$\left. - \frac{\sigma^2}{6} + k_1{}^2\left(-\frac{440}{3\sigma^2} + 12 - \frac{\sigma^2}{3}\right) + \frac{8}{3}k_1{}^4\right\} \sin \sigma k_1$$
$$+ \left\{\left(-\frac{280}{\sigma^3} + \frac{140}{3\sigma} - \frac{7}{3}\sigma\right)k_1\right.$$
$$\left.\left. + \left(\frac{80}{3\sigma} - \frac{4\sigma}{3}\right)k_1{}^3\right\} \cos \sigma k_1\right] \quad (49c)$$

the other terms in the expansion of Equation 47 being small.

In the case of beryllium, on account of its small mass and high Θ, apart from certain other terms that become important in $A^{(1)}/M$, $A^{(2)}/M^2$ also makes a significant contribution. $A^{(3)}/M^3$ should also be calculated and seen that it is small. We have not done this so far as the calculations become extremely lengthy. But we hope that $A^{(3)}/M^3$ is very small since our calculated values agree well with experiment. Correction is applied only to $A^{(1)}/M$, since any correction to $A^{(2)}/M^2$ is beyond the accuracy we claim for our results. Putting $\eta = 4T$ for simplicity, the various expressions for the case of beryllium become

$$A^{(1)} = \frac{3S}{k_1}\left[\left(\frac{\eta}{10} - \frac{1}{7} + \frac{2}{27\eta} - \frac{8}{585\eta^3}\right)\right.$$
$$\left. + k_1{}^2\left(\frac{5}{12}\eta - \frac{1}{2} + \frac{5}{21\eta} - \frac{4}{99\eta^3}\right)\right] \quad (50)$$

$$
\begin{aligned}
A^{(2)} = & -\frac{9\eta FS}{2k_1}\left[\left(\frac{2}{7}-\frac{4}{9\eta}+\frac{8}{33\eta^2}-\frac{32}{675\eta^4}\right)\right. \\
& \left. + k_1^2\left(\frac{7}{3}-\frac{10}{3\eta}+\frac{140}{81\eta^2}-\frac{112}{351\eta^4}\right)\right] \\
& + \frac{9\eta^2 S}{4\sqrt{2}\,k_1}\left(1+\frac{3}{4}k_1^2\right)\bigg[\frac{4}{3}a_0k_1^2 \\
& + \sum_{n=0}^{7}\frac{2^{n+2}}{2n+7}\bigg\{a_n + k_1^2\bigg(b_n+\frac{(n+2)}{2}a_n \\
& + \frac{10}{3}a_{n+1}\bigg)\bigg\}\bigg]
\end{aligned}
\tag{51}
$$

where F in this approximation is

$$
F = \frac{\eta}{4}+\frac{2}{9\eta}-\frac{4}{225\eta^3}
\tag{52a}
$$

and

$$
\begin{aligned}
a_0 &= 2-\frac{8}{9\eta^2}+\frac{32}{75\eta^4}-\frac{256}{945\eta^6} \\
b_0 = -a_1 &= 1+\frac{4}{\eta}-\frac{4}{3\eta^2}-\frac{16}{9\eta^3}+\frac{16}{15\eta^4} \\
&\qquad +\frac{65}{75\eta^5}-\frac{128}{135\eta^6} \\
b_1 = -2a_2 &= -\frac{4}{\eta}-\frac{16}{3\eta^2}+\frac{16}{3\eta^3}+\frac{64}{135\eta^4}-\frac{64}{15\eta^5} \\
&\qquad +\frac{1792}{675\eta^6}-\frac{2048}{4725\eta^8} \\
b_2 = -3a_3 &= \frac{14}{3\eta^2}-\frac{64}{15\eta^4}+\frac{256}{45\eta^5}-\frac{128}{45\eta^6}+\frac{1024}{2025\eta^8} \\
b_3 = -4a_4 &= -\frac{16}{9\eta^3}+\frac{128}{45\eta^4}-\frac{128}{45\eta^5}+\frac{512}{405\eta^6} \\
&\qquad -\frac{2048}{10125\eta^8} \\
b_4 = -5a_5 &= -\frac{56}{135\eta^4} \\
b_5 = -6a_6 &= \frac{64}{225\eta^5} \\
b_6 = -7a_7 &= -\frac{128}{2025\eta^6} \\
b_7 = a_8 &= 0
\end{aligned}
\tag{52b}
$$

$$
B^{(1)} = \frac{3S}{k_1^2}\sum_{\sigma}\frac{Z_\sigma}{\sigma^6}\left(A_\sigma + B_\sigma T + \frac{C_\sigma}{T}+\frac{D_\sigma}{T^3}\right)
\tag{53}
$$

where A_σ, B_σ, C_σ are given by Equation 49 and

$$
\begin{aligned}
D_\sigma = & -\frac{1}{360}\bigg[-\sigma Q\left(1+\frac{11}{2}k_1^2\right)\cos\sigma(1+k_1^2)^{1/2} \\
& + \{11Q(1+5k_1^2)+\sigma R(1+k_1^2)\} \\
& \times \sin\sigma(1+k_1^2)^{1/2} \\
& + \sigma^2\left(P-\frac{110Q}{\sigma^2}-4k_1^2Q-\frac{10R}{\sigma}\right) \\
& \times \bigg\{-\frac{1}{\sigma}\left(1+\frac{9}{2}k_1^2\right)\cos\sigma(1+k_1^2)^{1/2} \\
& + \frac{9}{\sigma^2}(1+4k_1^2)\sin\sigma(1+k_1^2)^{1/2}\bigg\} \\
& + \frac{504}{\sigma^2}\bigg\{-\left(1+\frac{k_1^2\sigma^2}{18}\right)P+\left(\frac{110}{\sigma^2}+4k_1^2+\frac{\sigma^2k_1^4}{12}\right)Q \\
& + \left(\frac{10}{\sigma}+\frac{4}{9}\sigma k_1^2\right)R\bigg\} \times \bigg\{\bigg(\bigg(\bigg(-\frac{\sigma}{7}+\frac{6}{\sigma}-\frac{120}{\sigma^3}+\frac{720}{\sigma^5}\bigg) \\
& - k_1^2\bigg(-\frac{\sigma}{2}+\frac{15}{\sigma}-\frac{180}{\sigma^3}+\frac{360}{\sigma^5}\bigg)\bigg)\cos\sigma(1+k_1^2)^{1/2} \\
& + \bigg(1-\frac{30}{\sigma^2}+\frac{360}{\sigma^4}-\frac{720}{\sigma^6}+k_1^2\bigg(3-\frac{60}{\sigma^2}+\frac{360}{\sigma^4}\bigg)\bigg) \\
& \times \sin\sigma(1+k_1^2)^{1/2}\bigg\}\bigg]
\end{aligned}
\tag{54}
$$

$$
\begin{aligned}
\text{with}\quad P &= 2\sigma k_1\cos\sigma k_1 + (\sigma^2k_1^2-2)\sin\sigma k_1 \\
Q &= \sigma^2\sin\sigma k_1 \\
R &= 2\sigma\sin\sigma k_1 - 2\sigma^2k_1\cos\sigma k_1
\end{aligned}
\tag{55}
$$

It may be noted that the correction term of Equation 47, under both the approximations that we have considered, is a function of k_1 as well as T.

4. DISCUSSION

On the foregoing theory we shall now discuss the inelastic scattering of cold neutrons by polycrystal-

Table 1

Crystal	$M = \frac{m}{m_0}$	*Debye temperature* Θ *°K*	S *(barns)*	s *(barns)*	k_1 *Wavelength in Å of the neutrons used is indicated within brackets*	σ_a *(barns) (for the particular wave-length)*	*Crystal symmetry*
Mg	24.12	305	3.6	0.1	0.2827 (6.25)	0.2	Close-packed hexagonal
Al	26.72	398	1.5	0	0.1933 (8.0)	1.02	Face-centred cubic
Fe	55.34	420	11.4	0.4	0.215 (7.0)	9.9	Body-centred cubic
Pb	205.3	88	11.5	0.1	0.3963 (8.3)	0.78	Face-centred cubic
Be	8.937	1000	7.54	0	0.0976 (10.0)	0.056	Close-packed hexagonal

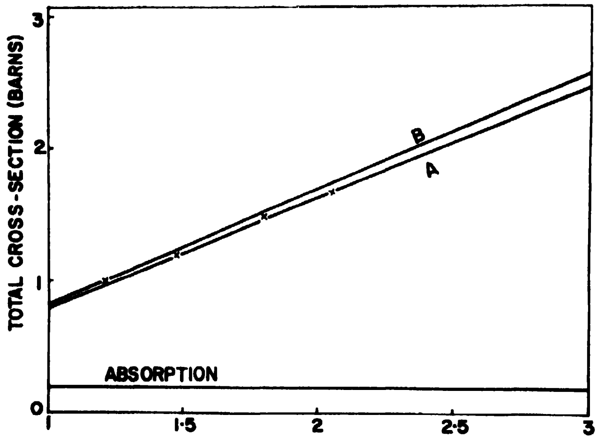

Figure 1. Magnesium, total cross section against temperature: curve *B*, total theoretical cross section using incoherent approximation of Placzek; curve *A*, total theoretical cross section with correction included; *X*, experimental points (Squires)

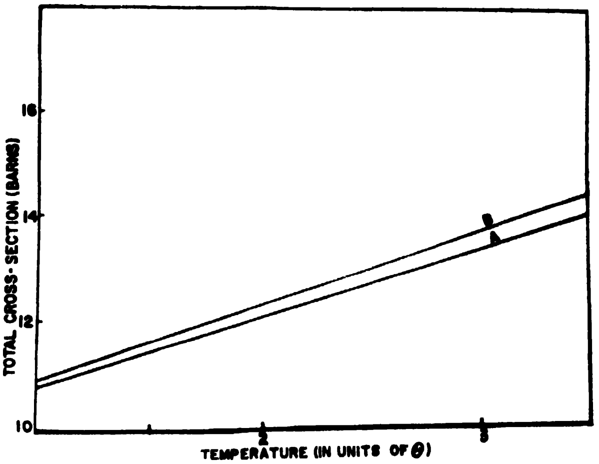

Figure 3. Iron, total cross section against temperature: curve *B*, total theoretical cross section using incoherent approximation of Placzek; curve *A*, total theoretical cross section with correction included; *X*, experimental points (Squires) including magnetic scattering

line magnesium, aluminium, iron, lead and beryllium. The values of the various constants used in the present calculations are given in Table 1.

Magnesium

In Fig. 1 we have plotted the total cross-section which is the sum of the observed absorption cross-section and the calculated scattering cross-section. Curve *B* is got by adding to the coherent contribution given by Equations 45 and 46, the incoherent contribution obtained by substituting *s* for *S* in the same two expressions. It includes the absorption cross-section σ_a which is also shown separately in the figure. The result of adding to curve *B* the correction term $\sigma_{coh}{}^1$ obtained from Equations 47, 48 and 49 is shown by curve *A*.

We find that to get the final result correct to within 1%, six terms of the series in Equation 48 have to be considered. The experimental points indicated in Fig. 1 are those of Squires.[3]

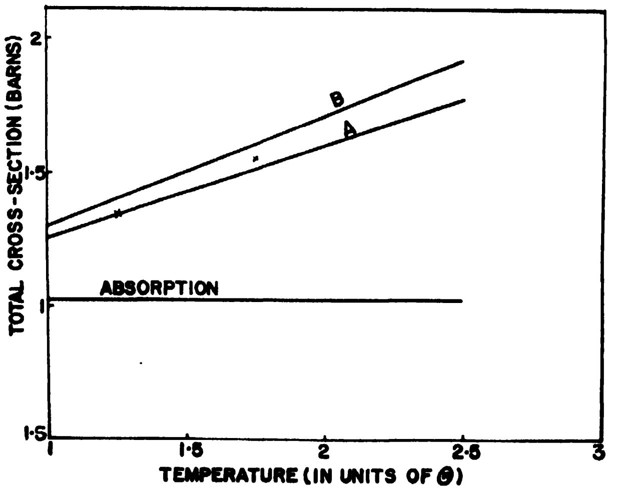

Figure 2. Aluminium, total cross section against temperature: curve *B*, total theoretical cross section using incoherent approximation of Placzek; curve *A*, total theoretical cross section with correction included; *X*, experimental points (Cassels)

The net correction is negative and contributes about 4% to the total scattering cross-section for all temperatures of the solid that have been considered. It may be remarked that the series of Equation 48 converges very slowly. One would wish for a more rapidly convergent series but so far as calculations go, Equation 48 serves fairly well because the expressions involved are purely algebraic.

The agreement between theory and experiment is fairly good. But it should be borne in mind that all calculations involve the assumption of the Debye frequency spectrum for the solid. One would indeed be surprised if the experimental values could be explained exactly on the above theory. For the few crystals for which the frequency spectrum has been calculated from force constants, it is found that the spectrum deviates markedly from the usual smooth Debye curve. However, since we are interested only in the integrated properties, the error involved in assuming the Debye frequency spectrum appears to be comparatively small as is shown by the fact that our results agree well with experiment.

Aluminium

Cassels[2] has obtained some experimental results on the scattering of cold neutrons by aluminium and has tried to fit a one phonon theory. We have also calculated on the basis of the foregoing theory the scattering of 8 Ångstrom neutrons by aluminium at various temperatures.

The results are plotted in Fig. 2. Curves *A* and *B* have the same meaning as in the case of magnesium. The correction to the total scattering cross-section is again negative and its contribution varies from about 13.9% at $T = 1$ to 15.5% at $T_k = 2.5$. Four terms in the series of Equation 48 were necessary to obtain the result correct to within 1%.

Iron

Palevsky and Hughes[11] and Squires[12] have reported some experiments on the scattering of cold neutrons by iron. In this case besides the scattering due to lattice vibrations, there is also present a magnetic scattering. An exact calculation of the contribution of lattice vibrations to the total scattering, is of importance in order to estimate the magnetic contribution and to verify its theory. The results of our calculations are shown in Fig. 3. The correction term $\sigma_{coh}{}^1$ is negative and its contribution varies from 7.9% at $T = 1$ to about 10.0% at $T = 3.5$. To obtain the final result correct to within 1% seven terms were considered in the series of Equation 48.

Lead

The results of calculations for lead are presented in Fig. 4. The correction in this case is rather large and positive. It contributes about 22% in the temperature range from $T = 3$ to $T = 7$. Six terms in Equation 48 suffice for a result correct to within 1%. It would be interesting to compare our results with experimental values when they become available.

Beryllium

On account of its low nuclear mass and high Debye temperature, beryllium has to be treated separately from the other elements that we have considered. The total scattering cross-section was calculated from Equations 41, 45, 47 and 50 to 55. The various important quantities are shown in Table 2. The final results are plotted in Fig. 5. It will be seen from Table 2 that the correction (which is $B^{(1)}/M$) to $A^{(1)}/M$ is of the same order though opposite in sign to $A^{(2)}/M^2$. Both these terms are nearly 10% of the main term $A^{(1)}/M$. To be sure one should also calculate $A^{(3)}/M^3$ and $B^{(2)}/M^2$ but we have not done so because the lack of accurate experimental results on beryllium does not warrant the extreme labour involved in the calculations. We expect that these higher order terms would not contribute more than a few per cent. The only experimental result available on beryllium is that given by Hughes.[13] The one experimental point at $T = 0.9$ which falls within our calculated range lies quite close to the corrected curve.

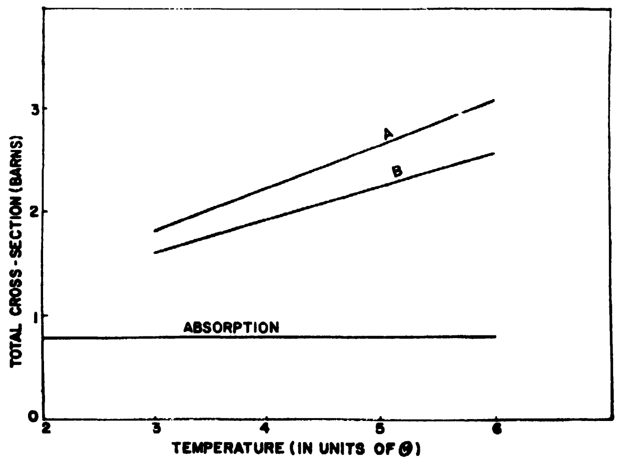

Figure 4. Lead, total cross section against temperature: curve B, total theoretical cross section using incoherent approximation of Placzek; curve A, total theoretical cross section with correction included

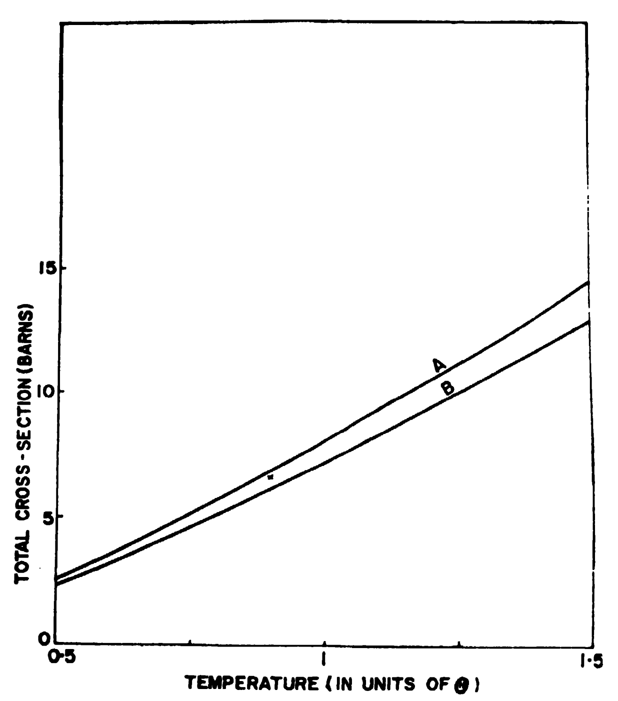

Figure 5. Beryllium, total cross section against temperature: curve B, total theoretical cross section using incoherent approximation of Placzek; curve A, total theoretical cross section with correction included; X, experimental points (Hughes)

ACKNOWLEDGEMENT

Part of this work was done during the authors' stay at Service Physique Mathematique, C.E.N., Saclay, France, and we are grateful to Professor Yvon and Dr. Horowitz for making the facilities of their department available to us. We wish to thank Professor R. Peierls for interesting discussions and to Professor G. Placzek for valuable correspondence on the subject and for sending to us in advance his unpublished

Table 2

T	0.50	0.625	0.75	0.875	1.00	1.50
$A^{(1)}/M$	2.509	3.681	4.911	6.172	7.451	12.681
$B^{(1)}/M$	0.212	0.354	0.509	0.678	0.852	1.580
$A^{(2)}/M^2$	−0.270	−0.349	−0.370	−0.361	−0.320	+0.109
σ_{coh} (barns)	2.45	3.68	5.05	6.49	7.98	14.37
σ_{total} (barns)	2.51	3.74	5.11	6.54	8.04	14.43

results. Thanks are also due to Mr. Udgaonker for his help in the present investigation. The experimental values for Mg and Fe sent to us by Dr. Squires are gratefully acknowledged. We are also thankful to Drs. Hughes and Palevsky for communicating to us the experimental value of σ_{scat} for beryllium. We wish to acknowledge the numerical work done by the personnel of bureau du calcule, C.E.N., Saclay. Finally, we wish to thank Dr. H. J. Bhabha, F.R.S., for his kind interest in our work.

REFERENCES

1. Weinstock, R., *Inelastic scattering of slow neutrons*, Phy. Rev. *65*, 1–20 (1944).
2. Cassels, J. M., *The inelastic scattering of very slow neutrons by aluminium*, Proc. Roy. Soc. A, *208*, 527–34 (1951).
3. Squires, G. L., *Multi-oscillator processes in the scattering of neutrons by crystals*, Proc. Roy. Soc. A., *212*, 192–206 (1952).
4. Hughes, D. J., *Pile neutron research*, (Addison-Wesley Pub. Co., Cambridge, Mass.), 254 (1953).
5. Placzek, G., *Incoherent neutron scattering by polycrystals*, Phy. Rev., *93*, 895–6 (1954).
6. Born, M. and Sarginson, K., *The effect of thermal vibrations. on the scattering of x-rays*, Proc. Roy. Soc. A., *179*, 69 (1941).
7. Fermi, E., *Motion of neutrons in hydrogenous substances*, Ricerca Scientifica, 7, Part 2, 13–52 (1936).
8. Weyl, H., *Quanten mechanik und Grupp-entheorie*, Zeits. F. Physik, *46*, 1–46 (1927).
9. Nanda, V. S., *A note on Weyl's inequality*, Indian J. Phys., *24*, 181–4 (1950).
10. Cassels, J. M., *Progress in nuclear physics 1*, (Butterworth-Springer Ltd., London), 185–215 (1950).
11. Palevsky, H. and Hughes, D. J., *Magnetic inelastic scattering of slow neutrons*, Phy. Rev., *92*, 202–203 (1953).
12. Squires, G. L., *The scattering of slow neutrons by ferromagnetic crystals*, Proc. Phy. Soc. A, *67*, 248 (1954).
13. Hughes, D. J., *Pile neutron research*, (Addison-Wesley Pub. Co., Cambridge, Mass.) (1953).

Neutron Diffraction Research in the United States

By E. O. Wollan and C. G. Shull,* USA

I. INTRODUCTION

Neutron diffraction as a practical research tool is a product of the so-called atomic age since it depends for its successful application on the high thermal neutron fluxes obtainable from nuclear reactors. An increase in the availability of reactors will undoubtedly result in an increase in the number of research groups who will become actively engaged with neutron diffraction techniques and it is with this hope in mind that a review of work in this field is presented.

The first efforts in this field were concerned primarily with basic neutron scattering phenomena but it has become apparent that the long range possibilities of this new technique lie in solid state studies of magnetism and of crystal and molecular structure. It will be principally with this aspect of the subject that this review will be concerned and the work to be reported here will include illustrative examples of that carried out in the USA. Up to the present, research in this field in this country has been supported in the three national laboratories, Argonne, Brookhaven and Oak Ridge in which several independent research groups have been involved. We are especially indebted to Drs. L. M. Corliss, J. M. Hastings, H. A. Levy, R. Pepinsky, W. L. Roth and S. S. Sidhu for contributions used in the preparation of this survey report.

The work is reported in three sections, the first of which deals with the methods, the types of problems which can be studied and with a few general principles of neutron scattering as compared with the corresponding X-ray case. In the last two sections the results and conclusions from a number of specific studies in the fields of crystallography and magnetism are briefly surveyed. For the reader who is interested in the theory and the experimental details there is included a brief bibliography in addition to the references to papers herein discussed.

II. PRINCIPLE METHODS AND SCOPE

Thermal neutrons such as those obtained from slow neutron reactors have wave lengths comparable to atomic dimensions and the diffraction patterns from molecules and crystals are similar to those obtained by the more common X-ray technique. There are, however, significant differences between the interaction of neutrons and X-rays with matter and it is these differences which have made neutron scattering such an important new tool in studies of solid state phenomena.

X-rays interact primarily with the atomic electrons, whereas for neutrons there are two important scattering interactions, one with atomic nuclei and the other with the atomic moments in magnetic systems. These two types of interaction are the bases of the two major fields of application of neutron scattering to the study of solid state problems. For the one, neutron diffraction is supplementary to X-ray diffraction in the study of molecular and crystal structure problems, the other which involves the unique magnetic interaction furnishes a completely new method of attack for the study of magnetic problems on the atomic level.

For the basic theory of neutron scattering as applied to these fields the reader is referred to the original papers. A brief survey will be given in this section of the methods and type of problems to which the new techniques can be applied.

For crystal and molecular structure problems the nuclear scattering properties must be considered. For X-rays the coherent atomic scattering cross section per unit solid angle in the near forward direction is equal to $Z^2e^4/(m^2c^4) = 0.73\ Z^2$ barns per steradian where Z is the atomic number, the barn is a cross section unit equal to 10^{-24} cm^2 and the other quantities have their usual significance. The X-ray cross section of hydrogen is thus seen to be near one barn whereas for a heavy element such as lead it is about 6000 barns. The X-ray scattering cross sections vary monatomically with atomic number whereas for the coherent scattering of neutrons by atomic nuclei the cross sections have no regular trend, and their values except for a few cases lie in the much narrower range from about 1 to 10 barns. With X-rays the scattering is by the atomic electrons, and hence for wave lengths of the order of atomic dimensions interference effects within the atom give rise to a form factor fall off with angle of the effective scattering power of the atom whereas with neutrons the nucleus being effectively a point scatterer relative to the wave lengths of thermal neutrons the scattering cross section will be independent of angle.

There are also other effects associated with the scattering of neutrons which are not encountered with X-rays. Different isotopes of a given element, for example, may have quite different neutron scattering properties. The spins of nuclei can interact with the neutron spin, and there may be two comparable cross sections for the same nucleus, one for neutron and nuclear spins parallel and one for the antiparallel case.

---

* Oak Ridge National Laboratory.

The neutron wave scattered by nuclei can either be in phase or 180 degrees out of phase with the incident neutron wave; in fact these two situations may obtain for the two spin states of a given nuclide as is actually the case for the scattering of neutrons by hydrogen. These effects can alter the effective coherent scattering by the atoms in crystals and molecules. Some of these effects will be illustrated later for specific cases. It will be well first, however, to look briefly at the technical aspects of neutron scattering.

The thermal neutrons from a reactor have a Maxwell energy distribution. A typical distribution curve is shown in Fig. 1 as a function of neutron wave length. In the same curve there is shown also a typical X-ray spectrum with the characteristic monochromatic line radiation, which is so important for the X-ray technique and for which there is no counterpart in the neutron source. A monoenergetic beam of neutrons is obtained by Bragg reflection from a crystal of a relatively narrow band of neutron wave lengths in the Maxwell distribution of the thermal neutrons from a reactor shown in the figure. Such a band gives a much less well defined monochromatic beam than is realized in the X-ray case from a spectral line and as a result the resolution obtained in neutron experiments will be inferior to the corresponding X-ray case. This has, however, not proved to be a really serious obstacle to progress with the neutron methods.

Neutron spectrometers are basically the same as their X-ray counterparts, but they are in general much more bulky because (*a*) rather massive shields are required to protect the personnel and the counting equipment from stray neutrons and gamma rays emerging from the reactor, (*b*) larger beams are required for sufficient intensity, and (*c*) the BF_3 counters which are usually used for detecting the scattered neutrons are much larger than X-ray counters, and they also require considerable shielding for background reduction.

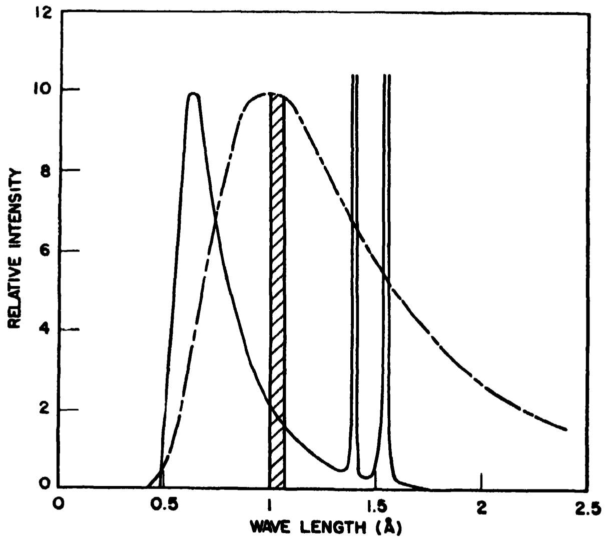

Figure 1. Wavelength distribution of the thermal neutrons from a reactor and a typical spectrum from a copper target X-ray tube

A schematic drawing of a neutron spectrometer unit is shown in Fig. 2. The monochromating crystals in use at present are usually metal crystals, lead, copper or aluminum, since they are less perfect and hence reflect a broader energy band for greater intensity than could be obtained from the more perfect compound crystals. The beam hole from the reactor is usually made quite large ~4 cm in diameter and the beam collimator after the crystal is in a typical case for powder diffraction experiments about 1 in. high by ⅜ in. wide. A corresponding acceptance slit in front of the counter would be about 1 in. × ¼ in. For improved resolution smaller slits are used or preferably multiple Soller type slits can be used in front of the counter and also in conjunction with the first crystal.

For efficient operation in this field reliable amplifiers and scalers and automatic beam monitoring and data recording devices are essential.

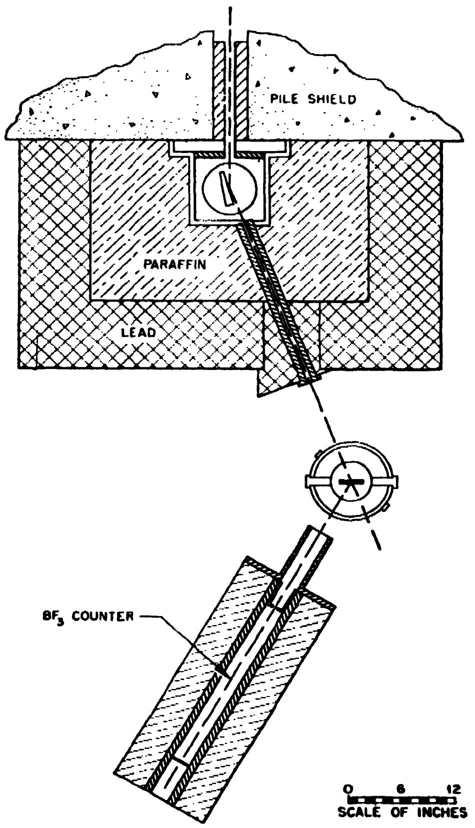

Figure 2. Diagrammatic sketch of neutron spectrometer

The scattering by nuclei in the neutron case and by the distributed electron cloud in atoms for the X-ray case is well illustrated by the curves of Fig. 3 for a diatomic molecule. The details of the interatomic interference effects are more pronounced with neutrons for which there is no form factor fall off of intensity. In crystals this is also apparent but here the temperature motions of the atoms introduce a statistical spacial extent to the nuclear positions which introduces a fall off with angle of the neutron scattering

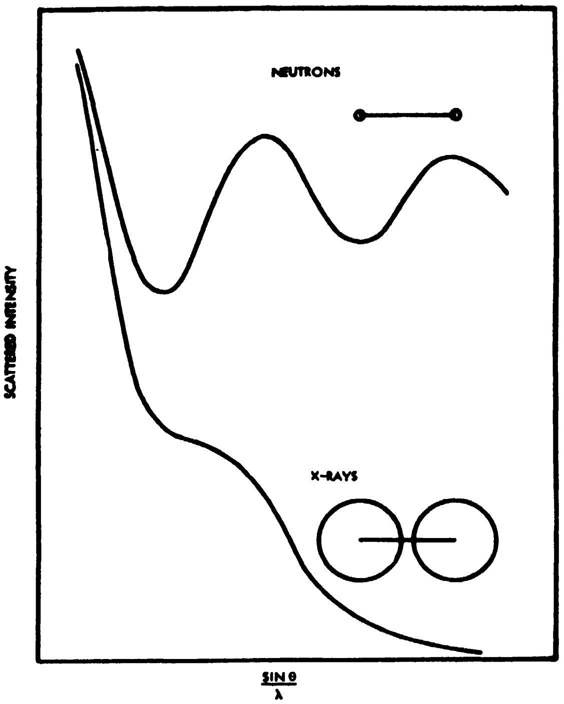

Figure 3. Angular dependence of scattering of X-rays and neutrons from a diatomic molecule

also. In the neutron case, however, this fall off arises from the temperature motion and thus this effect can be more easily recognized than in the X-ray case.

Some typical neutron powder crystal diffraction patterns will be shown to illustrate some of the more important neutron scattering characteristics.

Figure 4 shows the first two diffraction peaks for samples of normal NiO and samples for which the nickel has been highly enriched in one of its constituent isotopes.[1] The curves have been normalized so that the intensities can be directly compared. The intensities of the (200) reflections in these patterns are proportional to the square of the sum of the scattering amplitudes of the nickel and oxygen nuclei and the (111) reflections represent the square of the difference. One observes that Ni^{58} has a large scattering cross section (~26 barns) and the scattering is in phase with the scattering from oxygen (positive phase). For Ni^{60} the cross section is small (~1 barn) and of positive phase whereas for Ni^{62} the (200) reflection is nearly absent, and hence this nucleus must scatter with negative phase to cancel the oxygen scattering to this line.

The scattering by hydrogen is also of negative phase while that from deuterium is of positive phase. Patterns[2] for the scattering by ThH_2 and ThD_2 in which one sees the opposite phases in hydrogen and deuterium are shown in Fig. 5. The very large diffuse scattering for the ThH_2 case is also apparent. This arises from the fact that there are two spin states in hydrogen with comparable amplitude values one of which scatters with positive phase and one with negative phase. This reduces the coherent cross section of hydrogen to about 2 barns from the total cross section value of about 80 barns. These patterns are a striking illustration of the value of neutron diffraction in observing a hydrogen atom in the presence of very heavy elements. For X-rays the scattering amplitude of hydrogen would be only about one per cent of that of thorium, and hence interference effects between them

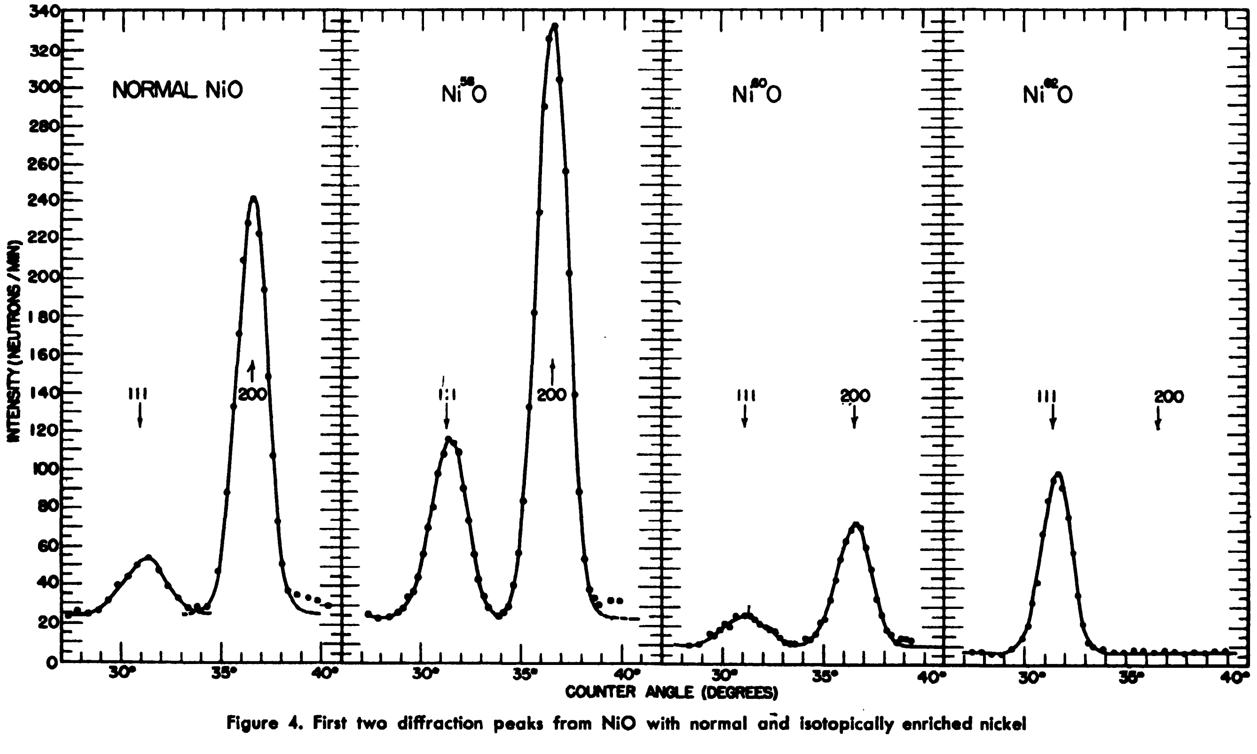

Figure 4. First two diffraction peaks from NiO with normal and isotopically enriched nickel

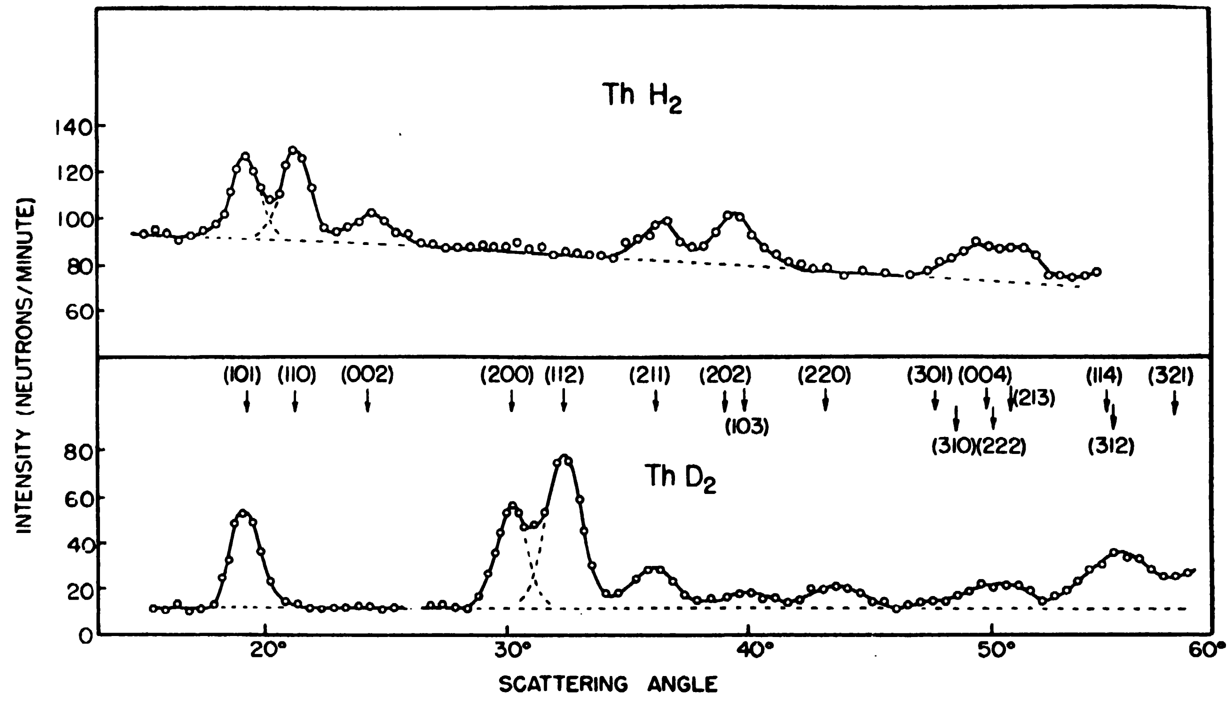

Figure 5. Diffraction patterns for ThH_2 and ThD_2

could hardly be expected to be observed. For neutrons the scattering amplitudes are quite comparable and in addition, use can be made of the fact that the scattering by the hydrogen and deuterium is of opposite phase.

Studies of hydrogen positions in complicated systems cannot be profitably made by the powder technique alone. With single crystals the lower resolution as compared to the X-ray case is of less significance. With single crystals the Bragg reflections can be studied to high orders of reflection, and hence much more data becomes available for the analysis. Studies of this type will be taken up in the next section.

When two atoms have very nearly the same scattering power, they become indistinguishable. With X-rays for example it is difficult without resorting to special devices to distinguish Fe from Co. For neutrons, however, these elements have very different scattering amplitudes and hence, for example, superstructure lines in an FeCo alloy[3] can be distinguished as shown in Fig. 6.

The other important interaction of neutrons with atomic systems involves the spins or magnetic moments of the neutron and the atom. Since these magnetic moments are associated with the electron spins and also in some cases with the orbital currents in the atom the moment distributions will extend over the atom, and in this case there will be intra-atomic interference effects which will lead to a form factor angular dependence of the neutron scattering. The scattering arising from the interaction of the neutron with the moments in magnetic atoms will, of course, be accompanied by and can interfere with scattering by the atomic nucleus of these atoms. The different properties of these two interactions do, however, in most cases allow the scattering contributions from the two effects to be identified and separately studied.

For a paramagnetic crystalline solid, in which the spin moments are randomly oriented, the magnetic scattering by the atoms in the crystal will be incoherent and will appear as a diffuse scattering, whereas the nuclear contribution will for most cases be primarily confined to the Bragg peaks. In the diffuse scattering, besides the magnetic contribution, there will be contributions from multiple scattering from the thermal motion of the atoms and possibly from other sources. It has, however, been found possible to make corrections for these nonmagnetic contributions and thus to determine the residual magnetic part only.

The paramagnetic scattering of neutrons[4] by several paramagnetic salts containing Mn^{+2} ions is shown in Fig. 7. The MnF_2 curve corresponds very closely

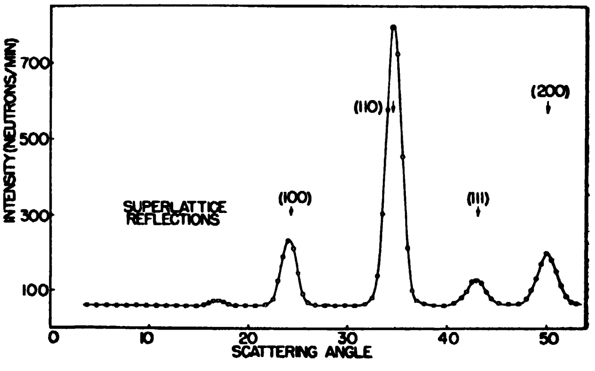

Figure 6. Diffraction pattern for ordered FeCo showing superstructure lines

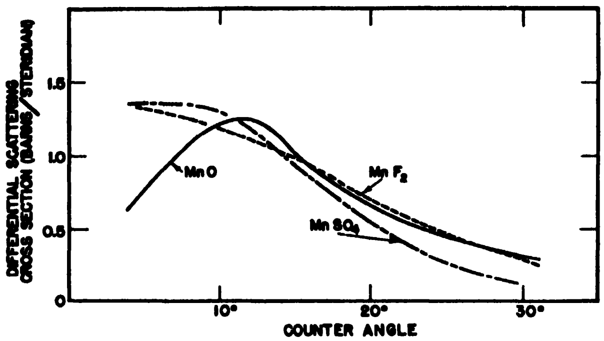

Figure 7. Paramagnetic scattering by several salts containing divalent manganese

to the scattering by individual Mn^{+2} ions, the interference effects leading to the decrease of intensity with angle being ascribable entirely to the spacial distribution of the magnetic electrons in the atom, in this case the five $3d$ electrons of Mn^{+2}. One thus has here a technique for determining the electron distribution function for specific electron groups in an atom whereas with X-rays it is the atom as a whole which is observed. From the scattering curve illustrated in Fig. 7 the radial density distribution for the electrons in the $3d$ shell can be obtained as shown in Fig. 8. The paramagnetic scattering curve for MnO in Fig. 7 shows an intensity distribution characteristic of a liquid. This is ascribed in the magnetic case to short range order in the orientation of the spin moments which introduces some coherence between the scattering by groups of atoms in the solid.

When all the moments in a magnetic crystallite are aligned parallel as in a ferromagnetic material the magnetic scattering will be in phase with the coherent nuclear scattering, and both will appear as contributions to the Bragg peaks. Here also it is possible in most cases to separate the magnetic and the nuclear scattering effects; in fact there are several means by which this can be accomplished. Considering for example the case of α-cobalt, if one evaluates the differential scattering cross sections associated with the Bragg peaks of a powder pattern,[5] one obtains the points shown as circles in Fig. 9. Since it is known that the nuclear scattering is isotropic except for a small temperature effect correction, it is evident that the fall off of the cross-section values with scattering angle are to be associated with the form factor of the magnetic moment distribution of the $3d$ electrons in this element. An example of another more powerful approach to the problem of separating the magnetic and nuclear scattering effects is shown[5] in Fig. 10. From the theory it is found that the magnetic scattering contribution to a given reflection depends on the angle α between the atomic moment vector k and the unit scattering vector e, the intensity contribution

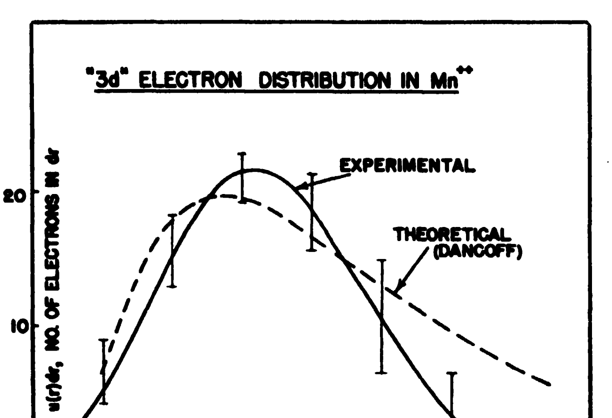

Figure 8. Distribution of $3d$ electrons in the Mn^{+2} ion as determined from the angular dependence of the paramagnetic scattering by MnF_2 or the antiferromagnetic reflections in MnO, for example

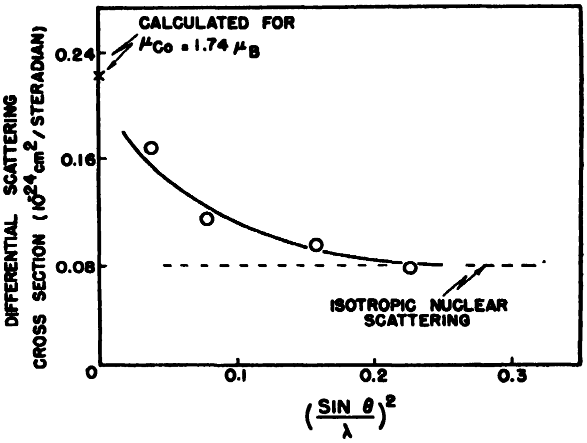

Figure 9. Differential scattering cross section of α-Co showing magnetic form factor dependence of ferromagnetic reflections

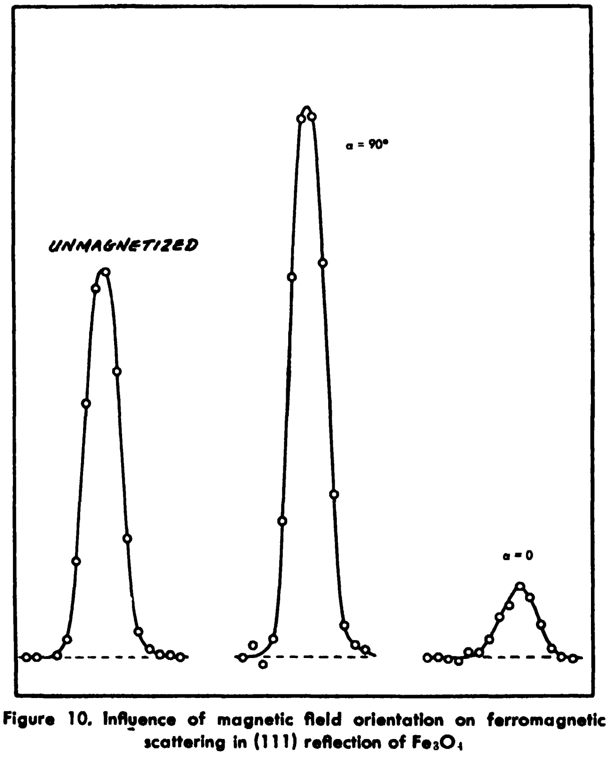

Figure 10. Influence of magnetic field orientation on ferromagnetic scattering in (111) reflection of Fe_3O_4

being proportional to $\sin^2 \alpha$. The figure shows the (111) reflection from Fe_3O_4 for (*a*) unmagnetized, (*b*) magnetized perpendicular to the scattering vector, and (*c*) magnetized parallel to the scattering vector. In the latter case the magnetic scattering should be zero, and the residual peak is due to nuclear scattering only.

Probably the most significant contribution of neutron diffraction to the study of magnetic phenomena is that associated with antiferromagnetic and ferrimagnetic systems. In antiferromagnetic systems the spins of the magnetic ions in a crystal are arranged on two or more interpenetrating lattices for which the spins of one will be parallel, and of another they will be antiparallel to a given direction in the crystal so that the magnetic moments completely cancel on an atomic scale. In systems referred to as ferrimagnetic there are similar ordered arrangements of parallel and antiparallel spins, but the net moment of one sublattice does not cancel that of the other in a two sublattice system. A considerable amount of information regarding the nature of these types of magnetic systems was obtained in an indirect way from specific heat and susceptibility data, and much credit must go to the early workers in this field for the excellence of the deductions regarding them. With the neutron diffraction techniques it has, however, now become possible to directly determine the magnetic structure of such systems, and as a consequence a completely new approach to problems of this type is possible.

One of the earliest such systems to be studied[4] was α-Fe_2O_3 for which a neutron diffraction pattern is shown in Fig. 11 together with an X-ray pattern of the same sample. The two innermost lines in the neutron pattern fall at superstructure positions for which there is no contribution in the X-ray case or from nuclear scattering in the neutron case. These lines originate from the antiferromagnetic structure, the nature of which is shown on the left in Fig. 12 where the circles represent the iron atoms only. The transition temperature or Neel point at which the antiferromagnetic ordering sets in is for this case well above room temperature at which the pattern was taken. An additional magnetic transition in α-Fe_2O_3 was found to occur at low temperatures which was ascribed to a rotation of the direction of the magnetic axis as shown on the right in Fig. 12.

In many cases the ordering transitions are found to occur at low temperatures. The antiferromagnetic ordering[4] which has developed at 80°K is shown for MnO in Fig. 13 where the room temperature pattern is included for comparison. Several such antiferromagnetic systems have now been studied, some of which will be discussed in the last section.

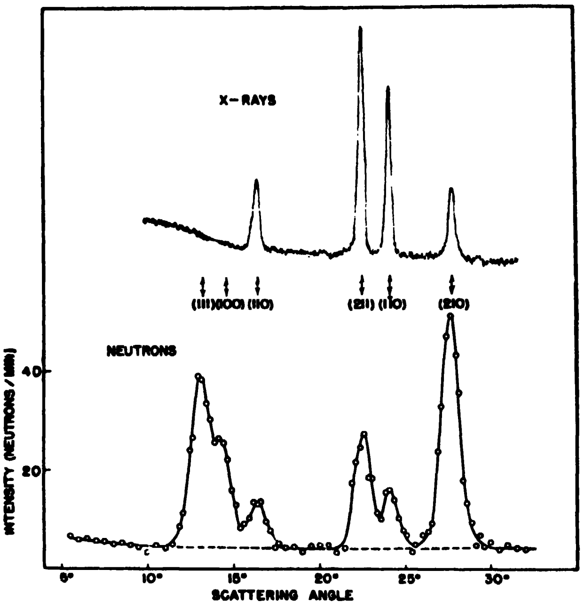

Figure 11. Neutron diffraction pattern of α-Fe_2O_3 showing antiferromagnetic superstructure reflections, and X-ray pattern included for comparison

Ferrimagnetism in which the atomic magnetic moments do not completely cancel, and the substance shows strong ferromagnetic properties is well illustrated by members of the ferrite series of compounds of which magnetite Fe_3O_4 is a special case. Several members of this group of compounds have been studied. Figure 10 showed the (111) line from an Fe_3O_4 pattern and the magnetic field effects previously mentioned for this pattern showed the ferromagnetic character of the reflection. The more complete studies of this and other ferrite compounds have given the magnetic structure and the distribution of moments on the lattice sites.

III. CRYSTALLOGRAPHIC APPLICATIONS

The application of the neutron diffraction techniques to crystallographic problems has its greatest

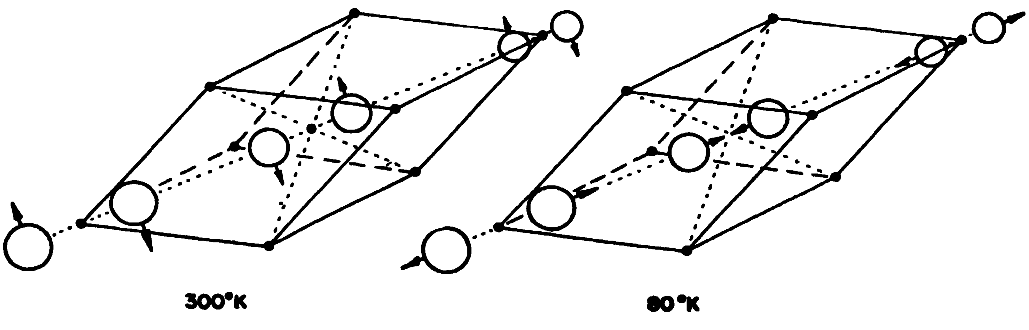

Figure 12. Antiferromagnetic structures for Fe_2O_3 observed at room temperatures and at 80°K

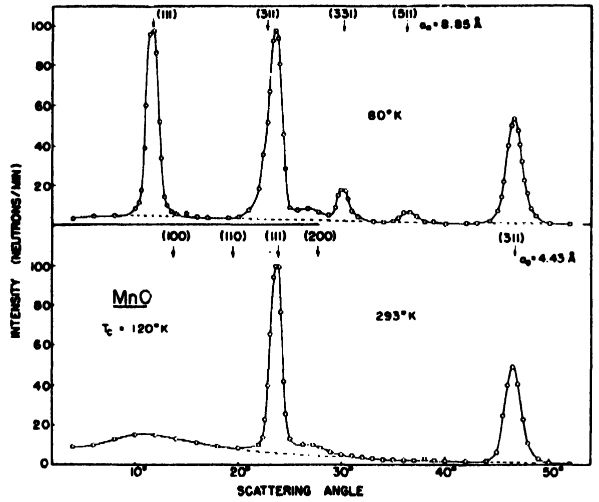

Figure 13. Room temperature and low temperature patterns for MnO showing antiferromagnetic superstructure lines which have developed at the lower temperature

value in cases where the neutron scattering amplitudes are more favorable than the equivalent X-ray or electron amplitudes.

Foremost in this classification of problems are those dealing with the location of hydrogen atoms in crystal structures. As mentioned earlier, the neutron scattering by hydrogen or deuterium nuclei is quite comparable to that of other nuclei, and hence the neutron intensities diffracted by a hydrogen-containing crystal are sensitive to the hydrogen positions in the crystal lattice. With the exception of the simple hydrides, most hydrogen-containing crystals are fairly complex structures, and these have been attacked by single crystal techniques rather than by the powder or polycrystalline method.

In addition to the problems of hydrogen-containing crystals, the neutron scattering methods have proven useful in settling structural ambiguities in such cases as heavy metal oxides and ordering in metallic alloys. Because of the absence of a form factor in nuclear scattering, the neutron method has been successfully applied in obtaining additional structure information on amorphous materials and liquids.

A number of these structural and crystallographic investigations will be discussed in the following with only brief mention of the results in each case.

Alkali Hydrides

The first demonstration of the coherent scattering of hydrogen and deuterium came in the early powder diffraction studies[6] on NaH, NaD, LiH, LiD and KH. These results confirmed the suspected NaCl-type structure for these hydrides and gave the first values for the sign and magnitude of the coherent scattering amplitudes of H and D.

ThH_2-ThD_2-ZrD_2-UD_3

These heavy-element hydrides represent extreme cases of heavy-light atom combination and the polycrystalline scattering data[2,7] showed the hydrogen atom positions in the different lattices. The powder patterns for ThH_2 and ThD_2 have already been given in Fig. 5, and the pronounced difference between these two patterns illustrates strikingly the effect of the reversed sign of the hydrogen scattering amplitude relative to that for deuterium.

Ice

Early neutron diffraction data[8] for polycrystalline samples of frozen D_2O had suggested the correctness of the Pauling picture of the hydrogen structure in ice as deduced from thermodynamic data. In this model, each hydrogen atom was considered to reside in disordered fashion at either of two positions along an O-O linkage bond. A more extensive investigation has recently been carried out by Levy and Peterson[9] using the single crystal technique, and one of their Fourier projections is shown in Fig. 14. The contour lines in this figure connect regions of uniform scattering density and an oxygen scattering center is seen close to the center of the figure and deuterium centers surrounding it. Another oxygen atom is to be found at the top of figure (but not shown) along the vertical line connecting O-½D-½D-O. At the points labelled ½D, there is equal probability of finding the deuterium atom at either of two ½D positions along any one O-O bond.

Potassium Bifluoride

Using single crystal techniques, Peterson and Levy[10] were able to demonstrate that the hydrogen atom in KHF_2 occupies the central position along the F-F linkage bond. This is in contrast to the situation in ice described above wherein the hydrogen atom was to be found in disordered positions along the O-O bond. These two examples illustrate the importance of the neutron scattering data in an understanding of the mechanism of hydrogen bonding in crystals.

Ammonium Halides

Various crystallographic transitions have been known to occur in NH_4Cl, NH_4Br and NH_4I, and these have been considered to represent the development of different degrees of order in the orientation

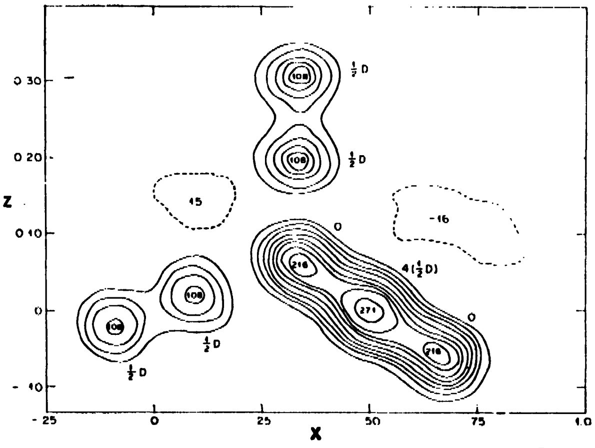

Figure 14. Fourier projection plot of the distribution of scattering power in ice (Levey and Peterson)

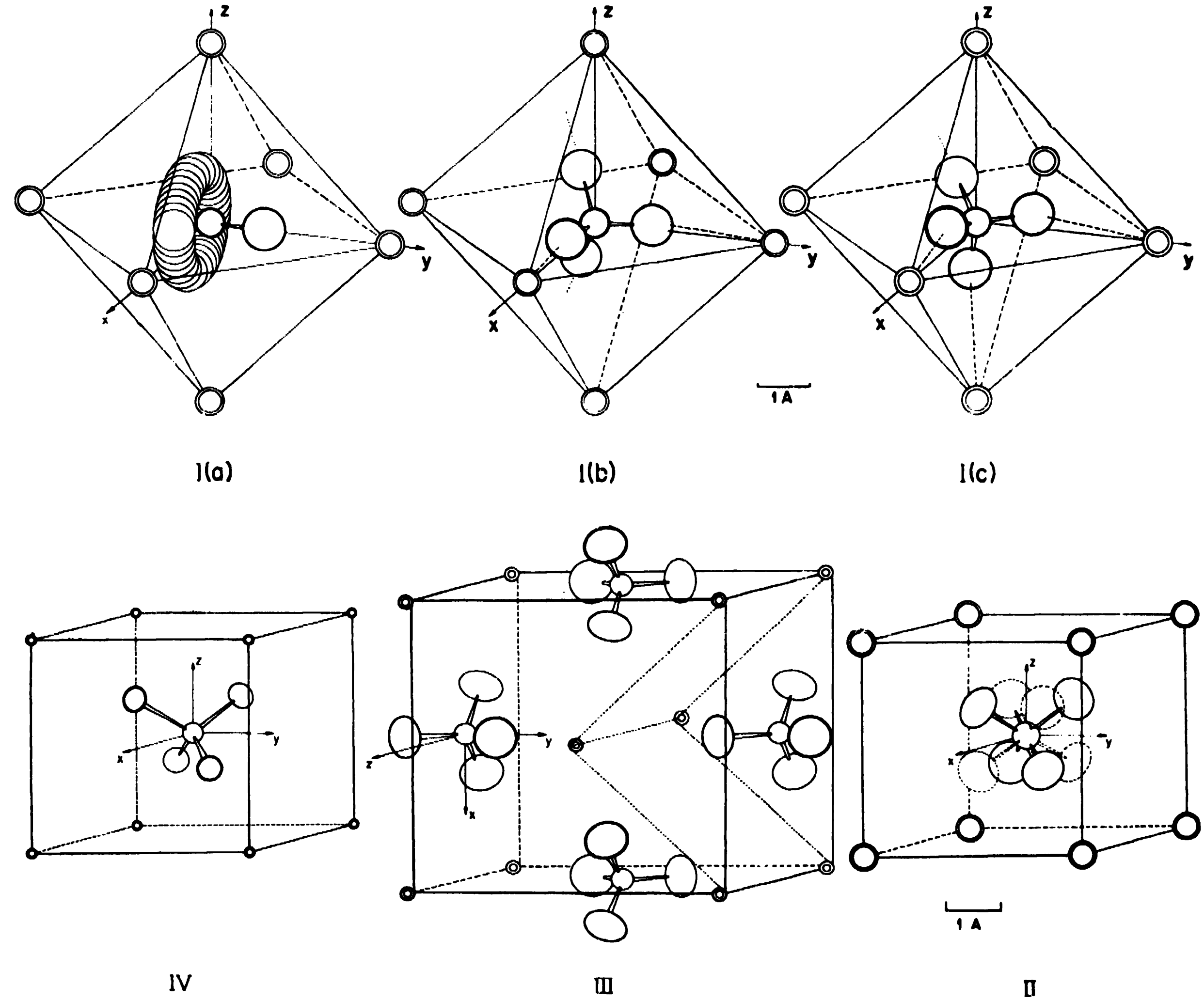

I(a) I(b) I(c)

IV III II

Figure 15. Diagrammatic representation of various structure modifications in ND_4Br (Levy and Peterson)

of the ammonium group in the crystal structure. In a series of papers,[11] Levy and Peterson report the results of investigations on many of these transitions, and Fig. 15 summarizes the findings for the four phases which exist in ND_4Br. In ND_4Br (for which most of the results were obtained) three transition temperatures of 125, −58 and −104°C separate the different structural regions. Phase I exists above 125°C and Fig. 15 shows three alternative structures which would account for the neutron scattering observations. Each of these, I(*a*), I(*b*) and I(*c*) represents only a single orientation among a group of six, twelve and eight, respectively, occupied at random, so in the high temperature phase there exists a very considerable orientation disorder. In Phase II the disorder has been reduced to a two-fold degree and in Phases III and IV orientational disorder is absent except for the effects of temperature disorder. Various theories of these different transitions have been given in the literature and the neutron scattering data have been instrumental in clarifying the general picture.

Hafnium and Titanium Hydrides

A recent study of the phases produced when hydrogen is occluded into hafnium and titanium has been made by Sidhu, Heaton and Zauberis.[12] For the composition $HfH_{1.6}$, they find a CaF_2-type structure with only a fraction of the fluorine sites occupied by hydrogen atoms. For higher hydrogen concentration, the number of vacant fluorine sites decreases and at the same time the cubic unit cell splits tetragonally. Patterns for TiD_2 showed a face-centered cubic lattice, again of the CaF_2-type.

Potassium Dihydrogen Phosphate

This material has been of interest to crystallographers because of its transition to the ferroelectric state below a temperature of 121°K. The development of ferroelectricity below this temperature implies that unbalanced electric dipole moments exist in the unit cell of the crystal structure, and this has been thought to be caused by a repositioning of the hydrogen atoms in the lattice. In order to establish this, neutron diffraction studies have been carried out by Levy, Peterson and Simonsen[13] and by Pepinsky and Frazer[14] and by Bacon and Pease[15] at temperatures above and below the transition temperature. These studies show that the hydrogen atom resides at or around the center of the oxygen-oxygen linkage bond at high temperatures whereas at low temperatures it moves to a new equilibrium position near one or the other of the oxygen atoms at the ends of the bond. This is shown diagrammatically in Fig. 16.

Along with these hydrogen atom conclusions, the neutron scattering data as well as improved X-ray scattering data have shown some previously unsuspected potassium and phosphorus atom displacements below the ferroelectric transition. The significance of this is not established as yet, but it may be that these displacements are of importance in explaining the electrical properties.

$BaTiO_3$-$PbTiO_3$-Rochelle Salt-$NH_4H_2PO_4$

Interest in these structures follows closely that in KH_2PO_4 since all of these structures exhibit ferroelectric transitions. Making use of more favorable neutron scattering amplitudes, Pepinsky, Frazer and Danner have been studying all of these structures with the goal of determining the ionic displacements which are responsible for ferroelectric and antiferroelectric transitions.

Rare-Earth Sesquioxides

X-ray diffraction investigations of rare-earth sesquioxides such as La_2O_3, Pr_2O_3, etc. had left unsettled the oxygen positions because of the low relative scattering power of the oxygen atoms. In their studies of magnetic scattering effects in these compounds, Koehler and Wollan[16] were able to establish the oxygen positions without ambiguity from the powder patterns obtained with neutron radiation.

Ordering in Alloys

Many alloys of interesting properties exist as combinations of transition elements and neutron diffraction data have been instrumental in showing the presence or absence of chemical order in these. Thus Shull and Siegel[8] have shown that long range order in FeCo and Ni_3Mn can be studied effectively by this technique, and very recently, Kasper[17] has reported on ordering in the Fe-Cr-Mo system.

The structure of UBe_{13} represents an interesting case in that the alloy contains elements at extreme ends of the periodic system. By combining neutron scattering data with X-ray results, Koehler, Singer and Coffinberry[18] were able to describe the structure completely.

Extinction effects in the scattering of neutrons by cold-worked brass were studied by Weiss, Clark, Corliss and Hastings.[19]

Amorphous Solids and Liquids

Because of the absence of a form factor in the nuclear scattering of neutrons, it is possible to determine extra coherent scattering effects in amorphous solids and liquids over that usually obtained by X-ray methods. Figure 17 illustrates this for the case of amorphous silica as obtained by Milligan, Levy and Peterson in unpublished work. Several liquids have been studied in this fashion, including lead and bismuth and Sharrah and Smith[20] and mercury by Vineyard.[21]

Very interesting small angle scattering observations were made by Weiss[22] on materials existing in a fine state of subdivision. Using highly collimated neutron beams he was able to demonstrate a number of salient features implicit in the small angle scattering theory.

IV. MAGNETIC SCATTERING APPLICATIONS

Application of neutron scattering to magnetic problems which depends on the interaction of the magnetic moment of the neutron with the moment of atoms in magnetic systems has no counterpart in X-ray and electron scattering and hence the neutron method has unique aspects for the study of magnetic phenomena at the atomic level. The results and conclusions from some of the problems which have been

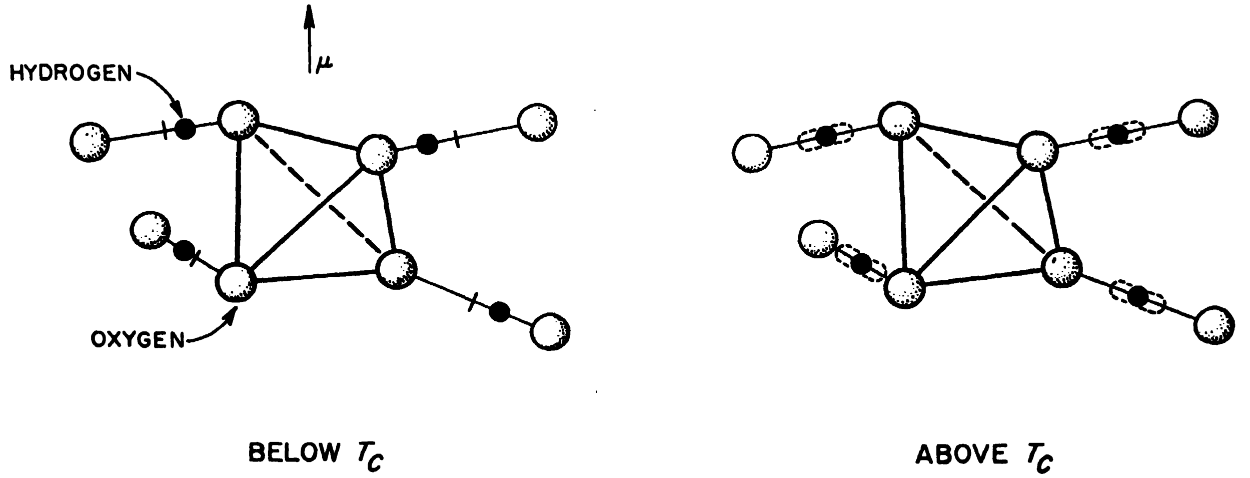

Figure 16. Diagrammatic representation of hydrogen atom locations in potassium di-hydrogen phosphate

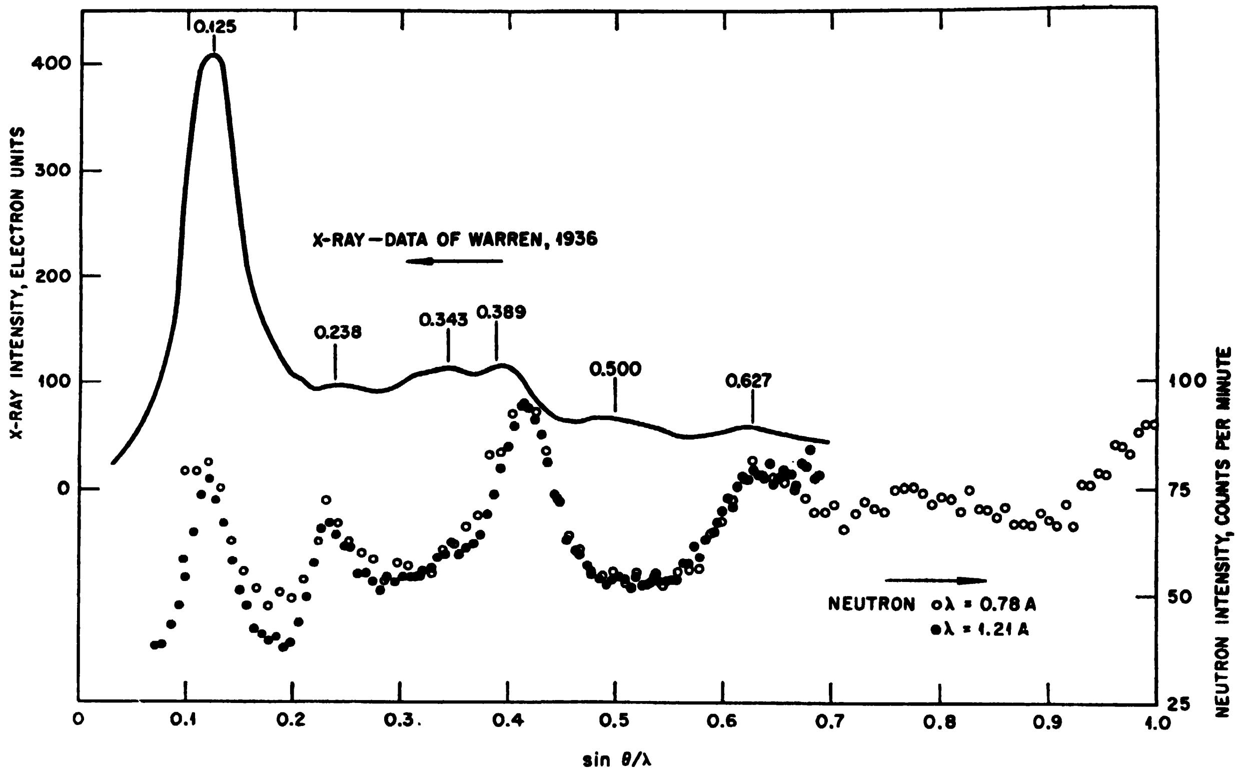

Figure 17. Scattering pattern for amorphous silica (Milligan, Levy, and Peterson)

investigated by this method are briefly surveyed in this section.

Ferrites and Chromites

Ferrites, of which magnetite (Fe_3O_4) is a special case are a class of compounds which have become of increasing practical importance for their unique magnetic properties. The ferrites and chromites are members of an even larger group of compounds having the general formula $X^{+2}Y_2^{+3}O_4$ which crystallize with the spinel structure. This structure is cubic but it is somewhat complicated having eight molecules per unit cell. There are two forms of this structure, regular and inverted spinels, both represented in Fig. 18.

The first ferrite to be studied by neutron methods was magnetite[5] for which the formula is most descriptively written as $Fe^{+3}(Fe^{+2}Fe^{+3})O_4$. This was found to have the inverted ferrimagnetic structure proposed by Neel, the ferromagnetic moment being due to the Fe^{+2} ions only.

Neutron diffraction studies of many more such compounds have now been made in which in addition to describing the magnetic structures which exist in these compounds, these studies have furnished complete information on the degree of inversion (whether they are of regular or inverted type) and on the crystallographic parameters which define the atomic positions. Corliss and Hastings and colleagues[23] have studied Ni, Mg, Zn and Mn ferrites and Zn and Mn chromites, the formulae being of the form $NiFe_2O_4$ and $ZnCr_2O_4$, and Wilson and Kasper[24] have investigated the structure of $Ni_{0.5}Zn_{0.5}Fe_2O_3$ in which they find the Ni moments to be randomly oriented. A neutron diffraction pattern obtained by Corliss and Hastings with a high resolution instrument for the case of $MgFe_2O_3$ is shown in Fig. 19. The magnetic

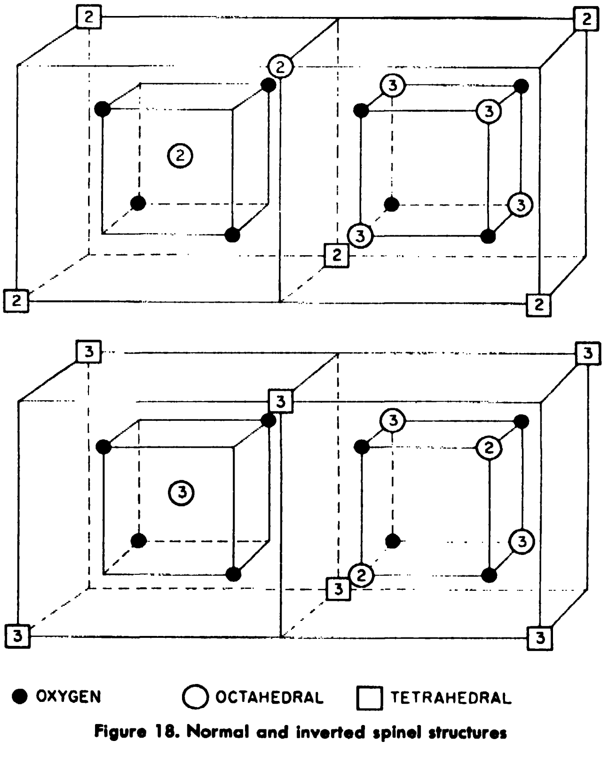

Figure 18. Normal and inverted spinel structures

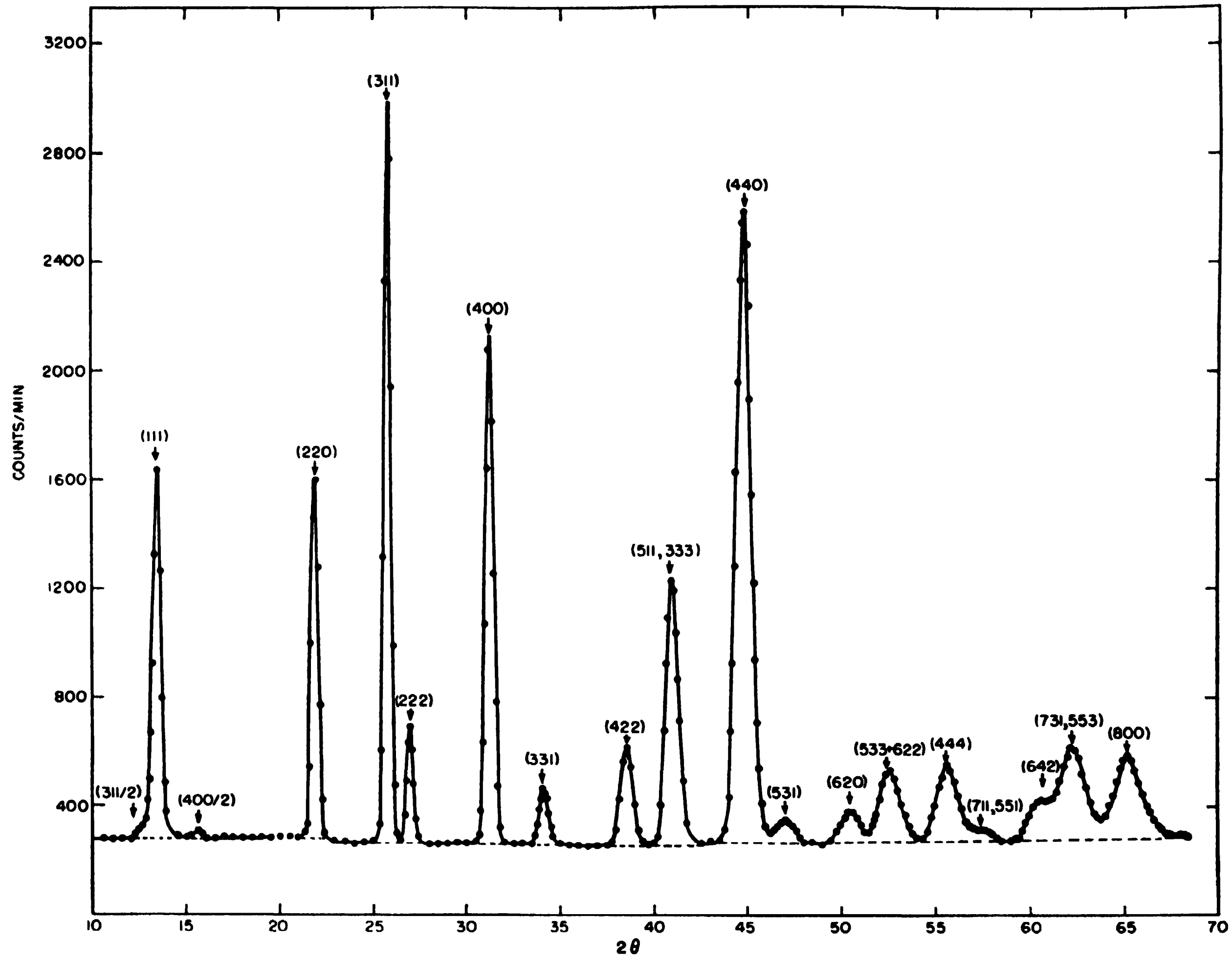

Figure 19. High resolution diffraction pattern for $MgFe_2O_4$ (Corliss and Hastings)

contributions to the coherent peaks are measured with the aid of a magnetic field.

In the case of $ZnFe_2O_4$ which is paramagnetic at room temperature, Corliss and Hastings find an antiferromagnetic transition at 9°K. The unusual pattern obtained for this compound is shown in Fig. 20 in which the nuclear scattering contributions are designated by N and the remainder of the pattern is of magnetic origin. The structure deduced for this compound is of a complicated type. It can be qualitatively described as consisting of antiferromagnetic alternations of ferromagnetic bands, each of which is several atoms wide.

Aside from accounting for the observed magnetization in the ferrites and chromites, the neutron scattering conclusions have offered very valuable information as to the various interactions which exist between the ionic states and positions in the lattice.

Some Elements of Transition Groups

Shull and Wilkinson[25] have applied neutron scattering methods to the study of several transition group elements. Their magnetic scattering data show that the ferromagnetic elements iron and cobalt possess simple ferromagnetic structures with no evidence for more complicated magnetic superstructure or for magnetic disorder. Moreover the strength of the ferromagnetic scattering seems to be accounted for by the magnetization moment and the magnetic form factor obtained by theoretical calculation for the $3d$ shell.

Manganese and chromium, however, were found to be antiferromagnetic with Neel temperatures of 100°K and 475°K, respectively, but with very small associated atomic moments. The observed moment for chromium, for example, is only $0.4\mu_B$ whereas for the free ion it would be $5\mu_B$. Vanadium was found to have no observable moment. The data for V, Cr and Mn and saturation moments of Fe, Co and Ni are plotted as the points in Fig. 21 and the line shows the predictions of the theories of Slater and of Pauling with which the measurements are in good accord. As examples of other transition element groups, in the case of molybdenum with five ($4d$) electrons and of tungsten with four ($5d$) electrons, no neutron magnetic scattering effects were observed.

In the rare earths the two elements neodymium and erbium have been studied by Koehler and Wollan.[26] Both these elements show susceptibility anomalies

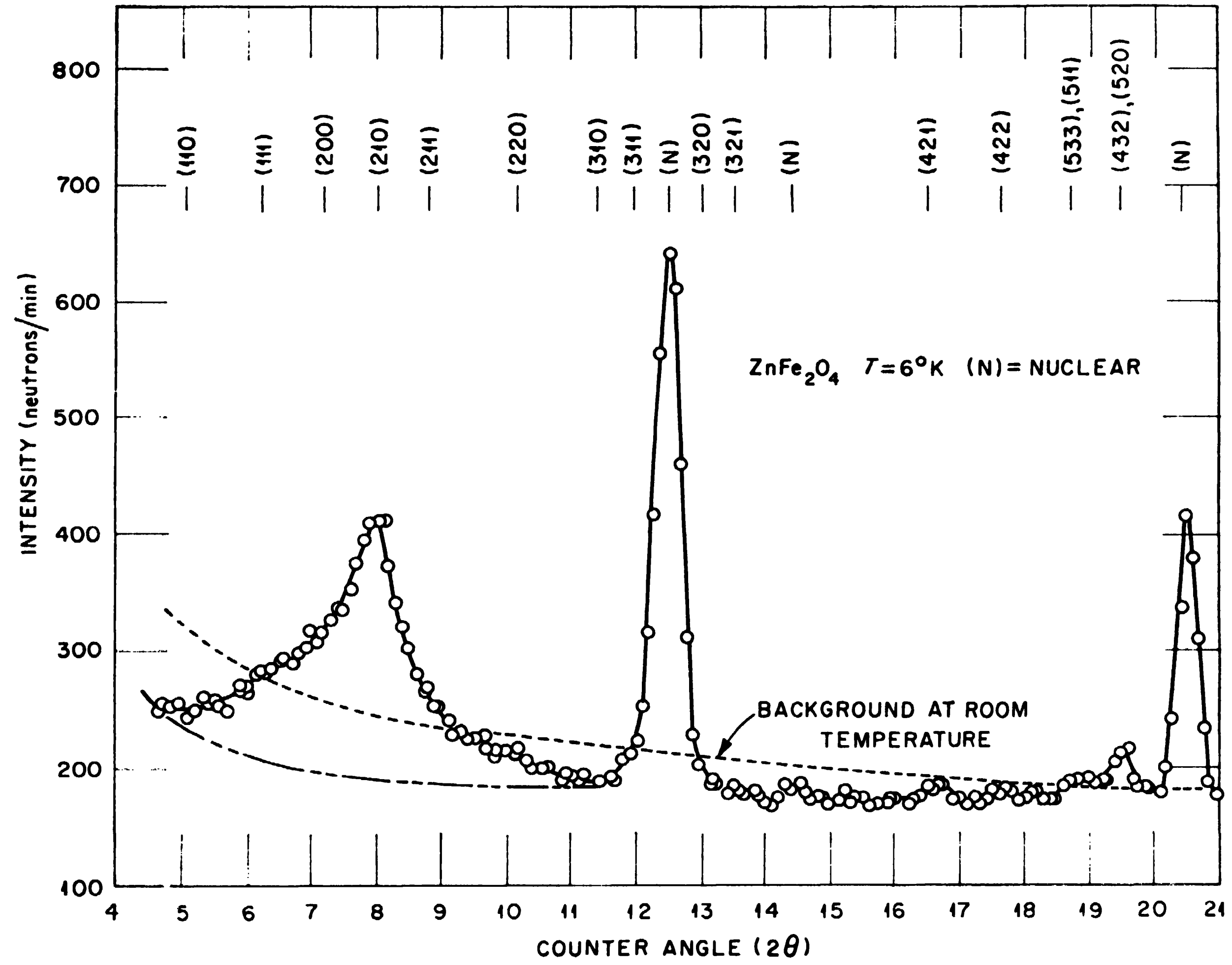

Figure 20. Low temperature pattern for $ZnFe_2O_4$ representing a complicated antiferromagnetic phase (Corliss and Hastings)

which suggest ordered magnetic behavior. In the case of neodymium there is if any only the slightest indication of ordering at very low temperatures. Erbium on the other hand becomes strongly ferromagnetic below about 30°K, and it shows ferrimagnetic or antiferromagnetic behavior between 80°K and about 30°K. The nature of this phase has not yet been determined.

Alloys of the Iron Group

Alloys of various compositions in the Fe-Cr, Ni-Fe, Ni-Mn and Co-Cr systems have also been studied by Shull and Wilkinson[27] and the Cu-Mn system has been investigated by Meneghetti and Sidhu.[28] In the disordered alloys of the first groups (all ferromagnetic), a rather pronounced magnetic disorder scattering was found which indicated that the different chemical components possessed different magnetic moments. For the ordered alloys, magnetic superstructure scattering was observed. By combining these neutron scattering results with magnetization data, information on the individual atomic moments in the alloy was obtained, and these moments were found to differ from those of the pure elements as a function of the alloy composition.

In the Cu-Mn system ferromagnetic properties are observed to appear at a manganese concentration of about 13%. Above about 70% manganese the neutron patterns show antiferromagnetic scattering properties with a transition temperature of about 380°K. It is suggested that the observed antiferromagnetism is to be associated with a negative exchange coupling be-

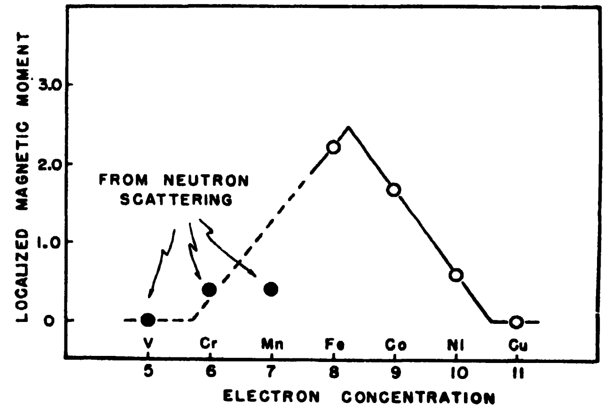

Figure 21. Observed atomic moments for the iron group elements compared to Slater-Pauling curve

tween the manganese ions as the manganese content becomes dominant.

The Iron Group Monoxides and Similar Compounds

The compounds of this group which were among the first to be studied by neutron diffraction methods by Shull, Strauser and Wollan[4] include MnO, FeO, CoO, NiO, MnS and MnSe. These compounds were all found to be antiferromagnetic and to possess magnetic unit cells which were larger than the chemical unit cells. The antiferromagnetic coupling was established as being between second nearest neighbors or through an intermediate oxygen ion, and this represented the first demonstration of the important "super-exchange" interaction.

Associated with the antiferromagnetic ordering transitions which take place at different temperatures for the various compounds there is observed in general an anomalous behavior in other properties of the crystals. Maxima are observed in the susceptibility and the specific heat and the thermal expansion, the lattice dimensions and the crystal symmetry are sometimes observed to change near the transition temperatures. A set of curves obtained by Foex[29] of the variation in thermal expansion coefficients with temperature for the iron group oxides is reproduced here in Fig. 22. The temperatures at which these compounds show the expansion anomalies agree closely with specific heat and susceptibility anomalies and with the Neel temperature of antiferromagnetic ordering as observed in the neutron diffraction experiments.

Rare-Earth Oxides

The neutron magnetic scattering properties of some rare-earth oxides have been studied by Koehler and Wollan.[30] No magnetic ordering was observed in these compounds, and this is understandable since the magnetic moments are associated with the 4*f* shell of electrons which is deeply buried in the atom and hence the aligning interactions between neighbors should be very weak.

The magnetic scattering amplitudes for erbium and neodymium in these oxides are shown in Fig. 23. In these elements there is a strong orbital contribution to the moments. In the case of erbium the magnetic moment is the sum of orbital and spin contributions whereas for neodymium the moment is given by the difference. Since both these elements have approximately the same orbital and spin moments, the individual contributions can be obtained approximately from the sum and difference of the erbium and neodymium amplitudes as shown in the figure. The theory for the scattering of neutrons by these compounds has been given by Trammell and by Kleiner.

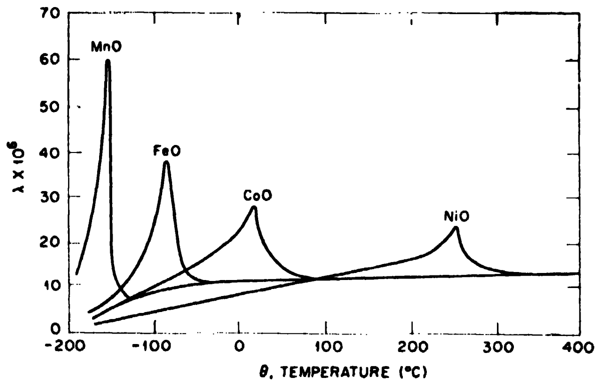

Figure 22. Thermal expansion of various oxides in the temperature regions of the antiferromagnetic transitions (Foë)

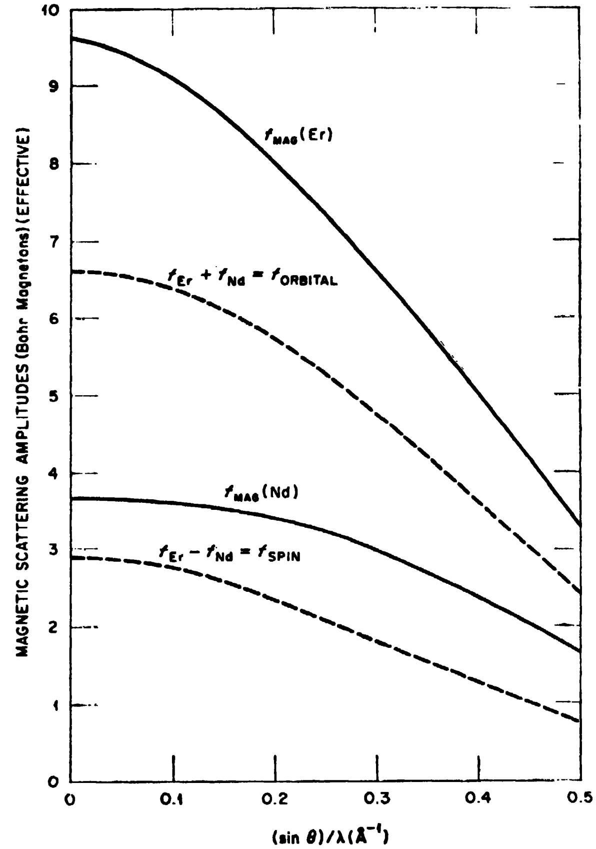

Figure 23. Paramagnetic scattering amplitudes for neodymium and erbium showing spin and orbital contributions

Perovskite Type Compounds

There is a large class of compounds of the so-called perovskite type, some of which exhibit some remarkable electrical and magnetic properties. $BaTiO_3$, for example, is one of these compounds which is well known for its electrical properties. These compounds are ideally of cubic symmetry with one molecule of the form ABO_3 per unit cell, where A is a large ion such as La^{3+}, Nd^{3+}, Ca^{2+}, etc. located at the cube center; B is a small ion like Mn^{3+}, Co^{3+}, Ti^{4+}, Mn^{4+}, etc. situated at cube corners and the three oxygens are at the midpoints of the cube edges.

Certain mixed perovskite type compounds containing elements of the iron group were shown by Jonker and Van Santen to be ferromagnetic with Curie points ranging from about room temperature downward. A series of mixed compounds of the form $(1 - x)$La, xCa MnO_3 has been studied by neutron diffraction methods by Wollan and Koehler[31] and a complicated series of antiferromagnetic structures and ferro- and antiferromagnetic transitions with sample composition has been observed. The magnetic structures and transition depend to a great extent on the types of indirect exchange coupling between the Mn^{3+} ions, the Mn^{4+} ions and between the Mn^{3+} and Mn^{4+} ions. Some antiferromagnetic structures observed in this system of compounds are shown in Fig. 24. A theory for the magnetic and ionic coupling in these compounds based on a semicovalent concept of exchange has been developed by Goodenough.

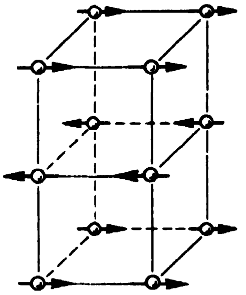

$La^{+3}Mn^{+3}O_3$
ANTIFERROMAGNETIC

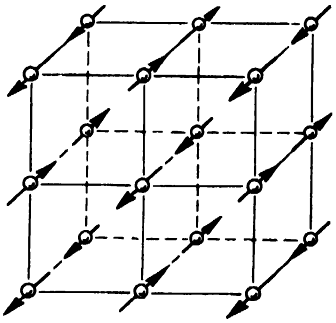

[0.20 La-0.80 Ca] MnO_3
ANTIFERROMAGNETIC

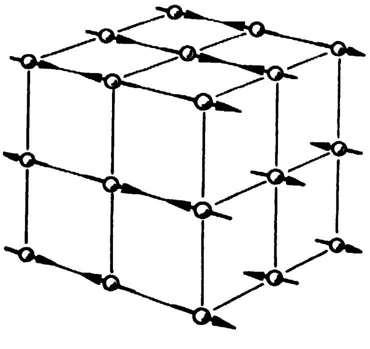

$Ca^{+2}Mn^{+4}O_3$
ANTIFERROMAGNETIC

Figure 24. Some magnetic structures observed in the (La, Ca)MnO_3 series of compounds

Other compounds in this group some of which show magnetic ordering effects and others which show no ordering have been investigated by Roth[32] and by Koehler and Wollan.

High Temperature Studies on Iron and Magnetite

The magnetic susceptibility data above the Curie temperature for ferromagnetic metals of the transition group is invariably anomalous with respect to the ferromagnetic data. As an investigation of this, Wilkinson and Shull[32] have studied the neutron scattering from iron in the paramagnetic region above the Curie temperature of 770°C. The presence of paramagnetic scattering was established although it still exhibited considerable short range characteristics even at the highest temperature studied, namely 1000°C. Additionally this study showed the development of an intense small angle scattering in the diffraction pattern which grew to a maximum at the Curie temperature and then decreased and merged into the short range order paramagnetic scattering above T_c. This was attributed to the disruption of the coherently scattering regions in the magnetic structure as the Curie temperature was approached.

In a somewhat related study, McReynolds and Riste[34] have studied both the magnetic coherent reflections in Fe_3O_4 and the inelastic scattering around these reflections in the vicinity of the Curie temperature. Again this inelastic scattering was found to maximize itself at T_c.

Other Compounds and Alloys

Neutron diffraction studies have been made on a number of other magnetic systems.

The two types of magnetic structures obtained for hematite, Fe_2O_3 were shown in Fig. 12. The isomorphous compound Cr_2O_3 was shown by Brockhouse[35] and by Kasper[36] to have a single magnetic structure similar to the 300° type in Fe_2O_3 but with the spin sequence (⇅ ⇅).

Pyrrhotite FeS_{1+x} in the NiAs crystalline form was shown by Sidhu[37] to be antiferromagnetic with a structure consisting of oppositely aligned ferromagnetic sheets perpendicular to the long axis of the unit cell. In this compound the magnetic moments were found to be parallel to the ferromagnetic sheets. Snow[38] investigated CrSb which has the same crystal structure, and he found a similar magnetic cell but in this case the spin moments were observed to be a perpendicular to the ferromagnetic planes.

Wilkinson, Gingrich and Shull[39] have shown that Mn_2Sb is ferrimagnetic, there being two sets of manganese atoms of different spin moments aligned antiparallel. They observed also a transition in which the spin moments changed orientation from parallel to perpendicular to the C-axis of the crystal as the temperature was lowered below about 250°K.

The magnetic scattering by UH_3 and UD_3 has been investigated by Wilkinson, Shull and Rundle.[40] These compounds are found to be ferromagnetic with a Curie point of 175°K. From the magnitude and an angular dependence of the magnetic scattering it was also possible to show that an appreciable part of the magnetic moment in uranium is associated with the 5*f* electron shell although there may be some contribution from the 6*d* shell.

REFERENCES

1. Koehler, Wollan and Shull, Phys. Rev. 79: 395, (1950).
2. Rundle, Shull and Wollan, Acta Cryst. 5: 22, (1952).
3. Shull, C. G. and Siegel, S., Phys. Rev. 75: 1008, (1949).
4. Shull, Strauser and Wollan, Phys. Rev. 83: 333, (1951).
5. Shull, Wollan and Koehler, Phys. Rev. 84: 915, (1951).
6. Shull, Wollan, Morton and Davidson, Phys. Rev. 73: 830, (1948).
7. Rundle, R. E., J. Am. Chem. Soc. 73: 4172, (1951).
8. Wollan, Davidson and Shull, Phys. Rev. 75: 1348, (1949).
9. Levy, H. A. and Peterson, S. W., (unpublished).
10. Peterson, S. W. and Levy, H. A., J. Chem. Phys. 20: 704, (1952).
11. Levy, H. A. and Peterson, S. W., Phys. Rev. 83: 1270, (1951), Phys. Rev. 86: 766, (1952), J. Chem. Phys. 21: 366, (1953), J. Am. Chem. Soc. 75: 1536, (1953).
12. Sidhu, Heaton and Zauberis (in press).
13. Levy, Peterson and Simonsen, J. Chem. Phys. 21: 2084, (1953), Phys. Rev. 93: 1120, (1954).
14. Pepinsky, R. and Frazer, B. C., Science 117: 1, (1953).
15. Bacon, G. E. and Pease, R. S., Proc. Roy. Soc. (London) A220: 397, (1953).
16. Koehler, W. C. and Wollan, E. O., Acta. Cryst. 6: 741, (1953).
17. Kasper, J. S., Acta. Metallurgica 2: 456, (1954).
18. Koehler, Singer and Coffinberry, Acta. Cryst. 5: 394, (1952).
19. Weiss, Clark, Corliss and Hastings, J. Appl. Phys. 23: 1379, (1952).
20. Sharrah, P. C. and Smith, G. P., J. Chem. Phys. 21: 228, (1953).
21. Vineyard, G. H., J. Chem. Phys. 22: 1665, (1954).
22. Weiss, R. J., Phys. Rev. 83: 379, (1951).
23. Corliss, L. M., Hastings, J. M., *et al.*, Phys. Rev. 90: 1013, (1953), Rev. Mod. Phys. 25: 114, (1953), also unpublished results.
24. Wilson, V. C. and Kasper, J. S., Phys. Rev. 95: 1408, (1954).
25. Shull, C. G. and Wilkinson, M. K., Rev. Mod. Phys. 25: 100, (1953).
26. Koehler, W. C. and Wollan, E. O., Phys. Rev. 97: 1177, (1955).
27. Shull, C. G. and Wilkinson, M. K., Phys. Rev. 97: 304, (1955).
28. Meneghetti, D. and Sidhu, S. S., Phys. Rev. 95: 666, (1954).
29. Foex, M., Compt. Rend. 227: 193, (1948).
30. Koehler, W. C. and Wollan, E. O., Phys. Rev. 92: 1380, (1953).
31. Wollan, E. O. and Koehler, W. C., Phys. Rev. (in press)
32. Roth, W. L., Pittsburgh Diffraction Conference (1954).
33. Wilkinson, M. K. and Shull, C. G., Phys. Rev. 94: 1439, (1954).
34. McReynolds, A. W. and Riste, T., Phys. Rev. 95: 1161, (1954).
35. Brockhouse, B. N., J. Chem. Phys. 21: 961, (1953).
36. Kasper, J. S., (unpublished).
37. Sidhu, S. S., Pittsburgh Diffraction Conference (1954).
38. Snow, A. I., Phys. Rev. 85: 365, (1952).
39. Wilkinson, Gingrich and Shull, Pittsburgh Diffraction Conference (1954).
40. Wilkinson, Shull and Rundle, APS Meeting, Washington (1955).
41. Halpern, O. and Johnson, M. H., Phys. Rev. 55: 898, (1939).
42. Wollan, E. O. and Shull, C. G., Nucleonics 3: 8, (1948).
43. Shull, C. G. and Wollan, E. O., Naturwissenschaften 10: 291, (1949).
44. Bacon, G. E. and Lonsdale, K., Reports on Progress in Physics XVI: 1, (1953).
45. Bacon, G. E., *Neutron Diffraction*, Oxford, (1955).

Scattering of Slow Neutrons by Ortho- and Para-Deuterium

By S. J. Nikitin, W. T. Smolyankin, W. Z. Kolganow, A. W. Lebedew and G. S. Lomkazy, USSR

The scattering cross-sections of neutrons on ortho- and para-deuterium with the effective energy 0.0047 ev, filtered by beryllium, were measured.

The measurements were carried out with gaseous samples, cooled by liquid hydrogen. The values of the scattering cross-sections obtained, $\sigma_{ortho} = 15.95$ barns and $\sigma_{para} = 14.63$ barns, are in close agreement with the theory of Hamermesh and Schwinger.[1]

The amplitudes obtained from the measured cross-section values,

$$\left.\begin{array}{lcl} a_{1/2} = 0.843 \pm 0.024 & & 0.057 \pm 0.014 \\ & \text{or} & \\ a_{3/2} = 0.253 \pm 0.005 & & 0.647 \pm 0.014 \end{array}\right\} \times 10^{-12}\text{ cm}$$

are in accordance with the results obtained by Hurst and Alcock.[2]

I. INTRODUCTION

The study of the scattering of slow neutrons by ortho- and para-deuterium is of considerable interest, as such experiments may give important information of the spin-dependence of the nuclear forces.

When the wavelength of the neutrons, scattered by molecular deuterium, exceeds the distance between the deuterons, interference of the waves, scattered on each of the nuclei occur. If the nuclear forces depend on the spin-orientation of the neutron and of the nucleus, the observed interference will be different when the neutrons are scattered by ortho-deuterium (even rotational quantum number I, even spin) or by para-deuterium (odd I, odd spin). The observed scattering-cross sections will be different.

The analysis of the experimental data on the scattering of neutrons on ortho- and para-deuterium will be complicated, as there are possible elastic and inelastic processes. But when choosing the experimental conditions so that the energy of the neutrons is insufficient for the excitation of the first rotational level of the deuterium molecule ($E_1 = 0.007416$ ev) and the deuterium molecules are in their lowest energy states ($I = 0$, $v = 0$ for ortho-deuterium, $I = 1$, $v = 0$ for para-deuterium, where I and v are rotational and vibrational quantum numbers respectively), a simple interpretation of the results is possible. In this case only the following transitions are possible:

$$I = 0 \rightarrow I = 0$$

$$I = 1 \rightarrow I = 0$$

$$I = 1 \rightarrow I = 1$$

The $I = 0 \rightarrow I = 0$ transition determines the scattering cross-section on ortho-deuterium (σ_o) the other two transitions the para-deuterium cross-sections (σ_p).

The theoretical treatment of the scattering of neutrons by ortho- and para-deuterium was given by Hamermesh and Schwinger.[1] These authors evaluated the scattering cross-section, using Born-approximation and the δ-function interaction-potential. The results do not account for the vibration of the nuclei in their lowest energy states and can be used at low temperatures of deuterium and low neutron energies.

According to reference 1 the scattering cross-sections σ_o and σ_p contain the quartet and doublet-amplitudes in the two following combinations $(2a_{3/2} + a_{1/2})^2$ and $(a_{3/2} - a_{1/2})^2$. So from the experimental cross-section values it is possible to evaluate only two sets of amplitude values.

The scattering amplitudes of deuterium were measured by several authors.[2,3,4]

Hurst and Alcock[2] measured the differential neutron scattering cross-section of deuterium at several scattering angles. The target used, contained gaseous deuterium of ⅔ of ortho- and ⅓ of para-modification content, cooled by liquid nitrogen. The energy of the scattered neutrons equaled to 0.0724 ev. They obtained the following values of the scattering-amplitudes

$$\left.\begin{array}{lcl} a_{1/2} = 0.826 \pm 0.012 & & 0.07 \pm 0.03 \\ & \text{or} & \\ a_{3/2} = 0.26 \pm 0.02 & & 0.638 \pm 0.006 \end{array}\right\} \times 10^{-12}\text{ cm}$$

In the present work the total scattering cross-sections of ortho- and para-deuterium were measured by transmission method. Sutton *et al.*[5] measured the scattering cross-sections of ortho- and para-hydrogen. The unreliable determination of the ortho- and para-concentrations leads to some uncertainties in the interpretations of their experimental results. Because of this we deemed it necessary to repeat these experiments.

II. METHOD AND APPARATUS

We determined the scattering cross-sections of ortho- and para-deuterium by transmission method

---

Original language: Russian.

using targets with various ortho- and para-deuterium composition.

The transmission T is determined by

$$T = e^{-nl\sigma_t}$$

where n is the number of molecules per cm^3, l is the length of the scattering layer, and σ_t is the total scattering cross-section of deuterium.

If f_0 and f_p are the relative concentrations of the ortho- and para-modifications of deuterium, then neglecting capture we have

$$\sigma_t = f_o\sigma_o + f_p\sigma_p$$

Measuring σ_t for two various concentrations of ortho- and para-modifications we can get the values of σ_o and σ_p.

The scheme of the experimental arrangement is given by Fig. 1.

The thermal column of the heavy-water research reactor, from which all graphite blocks were removed, served as the source of slow neutrons.

The neutrons emerging from the reactor passed through the reflector (100 cm of graphite) and through the vacuum-collimator, with a diameter 5 cm and 250 cm long. The collimated beam was filtered through 26 cm of metallic beryllium powder. In order to reduce the losses of neutrons the beryllium filter was cooled by liquid nitrogen.

It was shown by special absorption measurements of the filtered neutrons in Be that the effective energy of the filtered neutrons equaled 0.0047 ev. The neutron beam was additionally collimated and passed into the scattering chamber. The scattering chamber consisted of two concentric tubes. The inner tube was 200 cm long and 5 cm in diameter, and contained gaseous deuterium. The annular space between the inner and the outer tubes was filled with liquid hydrogen.

In order to reduce the evaporation rate of hydrogen, the scattering chamber was surrounded by a protection mantle, filled by liquid nitrogen. The details of the scattering chamber are shown at the Fig. 2.

The neutrons that suffered collisions within the scattering chamber, passed through the third collimator to the neutron counter, filled with BF$_3$ enriched in B^{10}.

The primary intensity of the beam was controlled by two monitor counters.

One of the main parts of the experimental arrangement was the ortho-para-convertor with the gas analyzer. The schematic arrangement of this part of the apparatus is shown at Fig. 3.

Gaseous deuterium was obtained by electrolytic decomposition of heavy water. The gas used contained, according to mass-spectroscopic analysis, 99.2 ± 0.05% of deuterium (D).

The gaseous deuterium was chemically bound with uranium powder. The filling of the scattering chamber was achieved by heating the container with uranium-deuteride. By heating, the uranium-deuteride decomposed accompanied by the reducing of the gaseous deuterium, which filled the scattering chamber. In order to remove the gas from the scattering chamber, the uranium container held at room temperature was connected with the scattering chamber, and deuterium was absorbed by uranium. The filling and evacuating of the scattering chamber lasted not more than 15 min.

In equilibrium the relative ortho-para-content is determined by the temperature of the gas only. But a simple cooling or heating of deuterium to a certain temperature without a catalyst does not bring rapidly the gas to the equilibrium state, corresponding to the given temperature.

In the present work the catalyst used consisted of a mixture of metallic nickel and chromium-oxide. It was shown that the catalyst was rather effective in the temperature interval 20–450°K and leads to the establishing of the equilibrium state in 0.5–1 sec. The scattering chamber was filled with deuterium of two different compositions: 66.7% ortho- and 33.3% para-deuterium, and 97.79% ortho- and 2.21% para-deuterium.

The first composition was obtained by passing the gas through the catalyst, held at room temperature, the second by passing it through the catalyst cooled with liquid hydrogen.

The gas analysis was accomplished by measuring the heat conductivity of deuterium, as the ortho- and

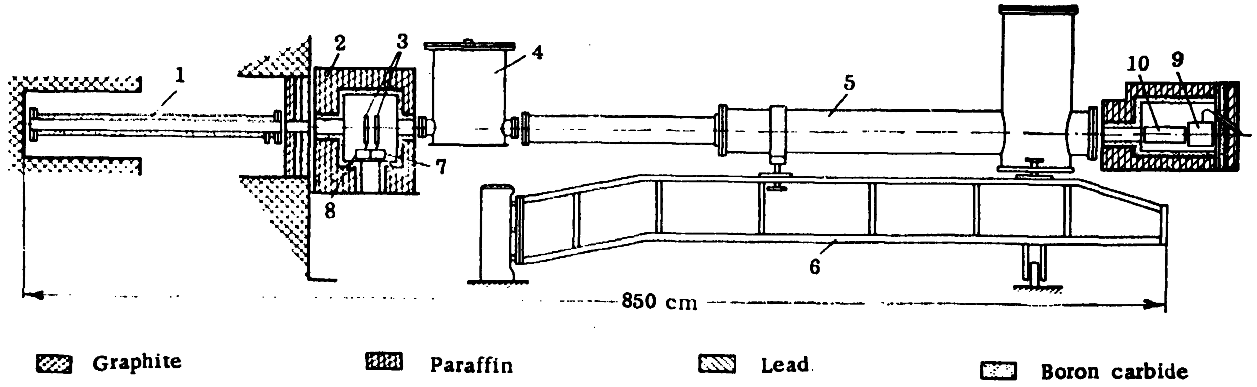

Figure 1. Diagram of installation: (1) collimator; (2) monitor shield; (3) monitor counters; (4) beryllium filter; (5) scattering chamber; (6) movable table; (7) cathode followers I; (8) cathode followers II; (9) cathode followers of the main counter; and (10) main counter

para-modifications show different heat conductivity.

The gas-analyzer consisted of four platinum resistance-thermometers, connected in a Wheatstone bridge. Two of them were filled with the etalon-gas, two others were filled with the gas under analysis. As the maximal difference in the heat conductivity is observed at 70–80°K, the gas analyzed was held at this temperature.

The content of ortho- and para-modifications was measured with an accuracy up to 0.1%.

The deuterium, containing $\frac{2}{3}$ of ortho- and $\frac{1}{3}$ of para-modification is unstable at the liquid-hydrogen temperature. This concentration was held constant during the experiment by continuous pumping of the gas through the catalyst, held at the temperature corresponding to the ratio of the concentrations of ortho- and para-modifications equal to 2:1.

The gas was analyzed several times during the series of the measurements, and it was shown that no changes of the concentration ratio of ortho- and para-modifications were observed.

III. EXPERIMENTS AND RESULTS

After the cooling of the system by liquid hydrogen the intensity of the direct beam was measured during 60–90 min. The scattering chamber then was filled with deuterium up to the pressure 200–250 mm Hg. During the following 90–120 min, the intensity of the transmitted beam was measured. Then the deuterium was removed from the scattering chamber; again the intensity of the direct beam was measured. The background due to spuriously scattered neutrons was measured with the filled and with the empty scattering chamber; the spurious counting-rate did not exceed 0.3% of the counting-rate of the direct beam.

The counting-rates were normalized by the monitor counting-rates, and from the normalized data the transmission T was obtained.

The measurements of the ortho- and para-scattering cross-sections were performed in 19 independent series. In nine series, the scattering cross-section σ_1 of the gas, containing $\frac{2}{3}$ of ortho- and $\frac{1}{3}$ of para-deuterium was obtained. In ten other series the scattering cross-section σ_2 corresponding to 97.79% of ortho- and 2.21% para-deuterium was obtained. The mean values of the measured cross-sections σ_1 and σ_2 obtained, were

$$\sigma_1 = 16.00 \pm 0.03 \text{ barns}$$

$$\sigma_2 = 16.41 \pm 0.02 \text{ barns}$$

The errors given are determined by the statistical errors and by the errors in pressure measurements. The corrections accounting for the scattering on small angles and for the scattered neutrons getting into the counting system, as well as corrections accounting for double scattering, turned out to be negligibly small and were not introduced. With our beryllium-filter the number of unfiltered neutrons with $E > 0.0093$ ev did not exceed 0.5% of the number of neutrons with $E < 0.0093$ ev. The small number of the infiltered neutrons made it unnecessary to introduce any corrections accounting for the non-elastic scattering of neutrons. When evaluating the σ_o and σ_p cross-sections from the measured σ_1 and σ_2 cross-sections, we introduced a correction accounting for the presence of 1.6% of HD molecules.

The following values of σ_o and σ_p were obtained:

$$\sigma_o = 15.95 \pm 0.03 \text{ barns}$$

$$\sigma_p = 14.63 \pm 0.1 \text{ barns}$$

The values of σ_o and σ_p allow to determine the quartet ($a_{3/2}$) and doublet ($a_{1/2}$) scattering amplitudes.

The evaluation of the scattering amplitudes was performed for neutrons with effective energy equal to 0.0047 ev and deuterium temperature equal to 20.35°K

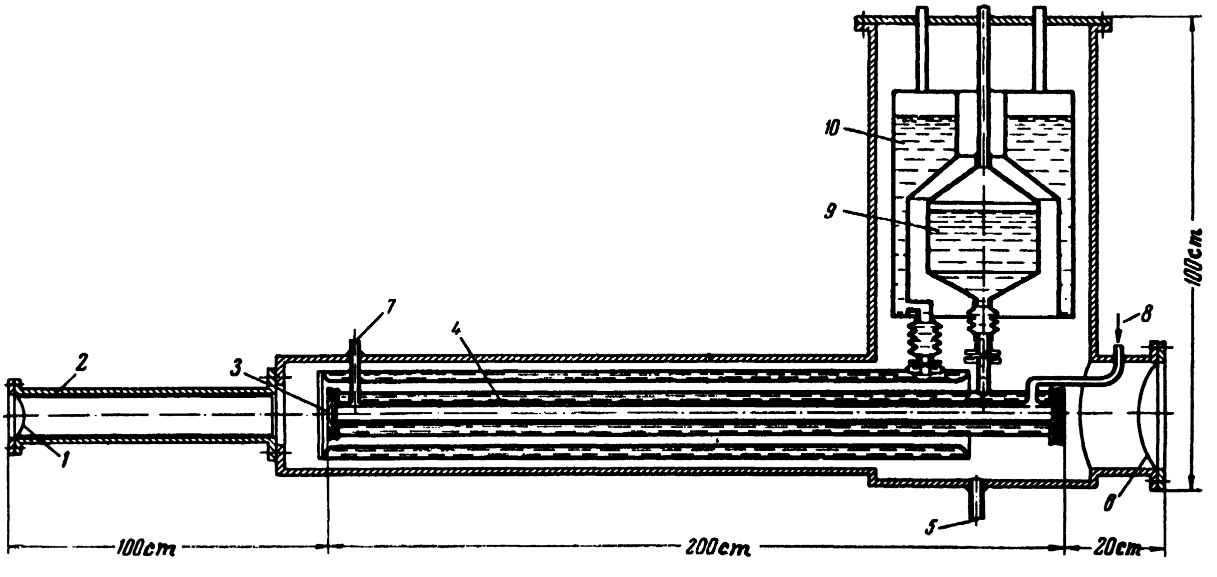

Figure 2. Scattering chamber: (1) aluminium window, 0.2 mm thick; (2) cadmium; (3) aluminium window, 0.2 mm thick; (4) cadmium; (5) diffusion pump; (6) aluminium window, 0.2 mm thick; (7) and (8) filling system; (9) liquid hydrogen; and (10) liquid nitrogen

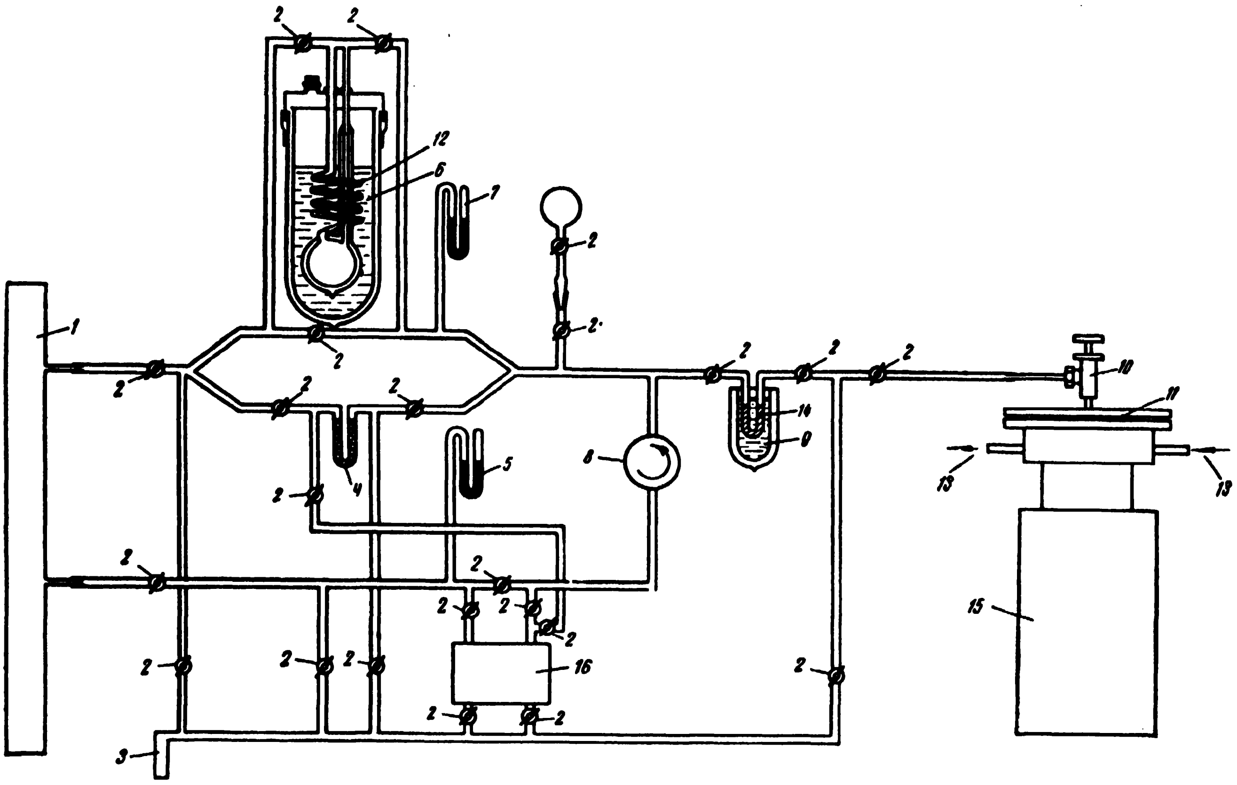

Figure 3. Scheme for filling scattering chamber: (1) scattering chamber; (2) stopcock; (3) to pump; (4) catalyst; (5) manometer; (6) liquid hydrogen; (7) manometer; (8) mixer; (9) liquid nitrogen; (10) valve; (11) copper washer; (12) catalyst; (13) cooling water; (14) cold trap; (15) electrical heater of container; and (16) gas-analyzer

according to the results of the paper of Hamermesh and Schwinger.[1] We obtained the following amplitude values:

$$\left.\begin{array}{lcl} a_{3/2} = 0.253 \pm 0.005 & & 0.647 \pm 0.014 \\ & \text{or} & \\ a_{1/2} = 0.843 \pm 0.024 & & 0.057 \pm 0.014 \end{array}\right\} \times 10^{-12}\ \text{cm}$$

The comparison of the obtained amplitude values with the results of Hurst and Alcock[4] shows a near agreement within the limits of experimental errors.

The measured cross-sections of neutron scattering on ortho- and para-hydrogen were:

$$\sigma_o = 104.1 \pm 0.7 \text{ barns}$$

$$\sigma_p = 3.91 \pm 0.1 \text{ barns}$$

When evaluating these data, corrections were introduced accounting for absorption of neutrons by hydrogen.

The values of hydrogen cross-sections obtained lie higher than could be expected for the energy 0.0047 ev from the results of Sutton *et al.*[5]

Using the results of Hamermesh and Schwinger[6] one can calculate the singlet (a_0) and triplet (a_1) scattering amplitudes from the measured cross-sections σ_o and σ_p for hydrogen.

These calculations lead to four sets of values of a_1 and a_0.

The existence of the bound triplet state of deuterium ($a_1 < 0$) and the range of the nuclear forces lead to a single-valued choice of the amplitudes:

$$a_1 = -0.542 \pm 0.005 \times 10^{-12} \text{ cm}$$

$$a_0 = 2.49 \pm 0.005 \times 10^{-12} \text{ cm}$$

The value of a_1 found allows to obtain a more correct value of the range of the nuclear-forces equal to

$$a = 2.0 \pm 0.1 \times 10^{-13} \text{ cm}$$

which exceeds the value obtained by Sutton *et al.*[5]

IV. CONCLUSION

The results obtained with hydrogen and with deuterium show the spin dependence of the nuclear forces.

The following scattering amplitudes for scattering of neutrons by hydrogen were obtained:

$$a_1 = -0.542 \times 10^{-12} \text{ cm}$$

$$a_0 = 2.49 \times 10^{-12} \text{ cm}$$

The range of the nuclear forces found from these data

$$a = 2.0 \times 10^{-13} \text{ cm}$$

is in reasonable accordance with the value 2.8×10^{-13} cm obtained from the experiments on proton-proton scattering.

The measurements of the neutron cross-sections of ortho- and para-deuterium confirm closely the results of theoretical evaluations of Hamermesh and Schwinger.[1]

The following values of scattering amplitudes for deuterium were obtained:

$$\left.\begin{array}{lcl} a_{3/2} = 0.253 & & 0.647 \\ & \text{or} & \\ a_{1/2} = 0.843 & & 0.057 \end{array}\right\} \times 10^{-12}\ \text{cm}$$

REFERENCES

1. Hamermesh, M. and Schwinger, J., Phys. Rev., *69*, 145, (1946).
2. Hurst, D. and Alcock, N., Canadian Journ. Phys., *29*, 36, (1951).
3. Shull, R. B. *et al.*, Phys. Rev., *73*, 842, (1948).
4. Wollan, E. O. *et al.*, Phys. Rev., *75*, 1343, (1949).
5. Sutton, R. B. *et al.*, Phys. Rev., *72*, 1147, (1947).
6. Hamermesh, M. and Schwinger, J., Phys. Rev., *71*, 678, (1947).

The Theory of Semitransparent Nucleus with a Diffuse Boundary

By P. E. Nemirovski, USSR

INTRODUCTION

It has usually been believed that the cross-section of all inelastic neutron-nucleus interactions is equal to πR^2, if the neutron wave length λ is smaller than the nuclear radius R. But experiments with high-energy neutrons[1] (100 Mev) have shown that not every neutron colliding with the nucleus causes an inelastic process. To explain this effect, it has been supposed that high energy neutrons have a finite mean free path in the nuclear matter.[2]

For low-energy neutrons, however, the assumption that the nucleus is completely absorbing has been conserved.

The schematic theory[3] of nuclear cross-sections, which uses the idea of a completely absorbing nucleus with a sharp boundary, leads to a monotonous decrease of the cross-sections with increasing energy. This cross-section dependence has been found to be in contradiction with the experimental data. Experiments have shown that total neutron cross-sections have maxima and minima at some values of neutron energy.[4] To explain the experimentally observed regularities, the model of a semi-transparent nucleus has been proposed.[5]

In this model the neutrons with energies in the 1–3 Mev region have a large mean free path in the nuclear matter.

At low energies the collisions of the incident neutrons with inner nucleons are rare, because of the exclusion principle. The latter restricts the possibilities of the momentum transfer between colliding particles, which results in the large mean free path. Thus there are two models. Both models use the assumption that the absorption of the nucleus is finite, but differ in some essential features.

For low energies the sharp boundary model has been proposed and for high energies the optical one.

In the sharp boundary model of the nucleus there is a fictitious reflection, but it does not exist in the optical model.

Indeed, the sharp boundary model can be applied only when the condition $\lambda \gg R$ is fulfilled. But in this region there is no inelastic scattering. In this paper a diffuse boundary model of the nucleus with a finite absorption is considered. At high energies this model coincides with the optical model, but for low energies its results are essentially different from those obtained by means of the square-well model.

1. THE STATEMENT OF THE PROBLEM

Let us suppose that the neutron interaction with the nucleus may be described by a complex potential $U + iW$, depending only on r (spin orbital coupling is neglected).

For simplicity, we shall assume that the dependence of the real and imaginary part on r is the same. For $r < r_0$ the function $U + iW$ is constant and it varies chiefly, in the region with the thickness $1.5\text{–}2 \times 10^{-13}$ cm.

The Schrödinger equation for the neutron is:

$$\Delta\psi + \frac{2m}{\hbar^2}[E + U(r)(1 + i\zeta)]\psi = 0 \qquad (1)$$

where $\zeta U(r) = W(r)$

One can expand the function $\psi_l(r)$ in spherical functions as follows:

$$\psi = \sum_{l,m} \psi_l(r)\Phi_{l,m}(\vartheta,\varphi) \qquad (2)$$

Then denoting $k = (2mE)^{1/2}/\hbar$ and $k_0 = [2mU(0)]^{1/2}/\hbar$ one can obtain the following equation for the radial function $\psi_l(r)$:

$$\frac{d^2(r\psi_l)}{dr^2} + [k^2 + k_0^2 f(r)(1 + i\zeta)](r\psi_l) - \frac{l(l+1)}{r^2}(r\psi_l) = 0 \qquad (3)$$

For $r \leq r_0 f(r) = f(r_0) = 1$ at $r \to \infty$ $f(r) \to 0$, [$f(r)$ is assumed to tend to zero, faster than by power law]. To solve Equation 3 it is convenient to make the substitution:*

$$\psi_l(r) = \frac{1}{r^{1/2}}[v_l^{(2)} H_{l+1/2}^{(2)}(kr) + \eta_l v_l^{(1)} H_{l+1/2}^{(1)}(kr)] \qquad (4)$$

Then for the functions $v_l^{(1)(2)}$ the following equation is obtained:

$$\frac{d^2 v_l^{(1)(2)}}{dr^2} + 2\,\frac{d \ln r^{1/2} H_{l+1/2}^{(1)(2)}(kr)}{dr}\,\frac{dv_l^{(1)(2)}}{dr} + k_0^2 f(r)(1 + i\zeta) v_l^{(1)(2)} = 0 \qquad (5)$$

Original language: Russian.

* $H_{l+1/2}^{(1)(2)}(kr)$ is the Hankel function of the first and second kind with a half-integer index.

When $r \to \infty$, Equation 4 should become a common expression for the sum of the convergent and divergent waves, consequently

$$\lim_{r \to \infty} v_l^{(1)}(r) = \lim_{r \to \infty} v_l^{(2)}(r) = 1$$

Equation 5 is more conveniently expressed in nondimensional coordinates $X = kr$

$$\frac{d^2 v_l^{(1)(2)}}{dr^2} + 2\,\frac{d \ln r^{1/2} H_{l+1/2}^{(1)}(kr)}{dr}\,\frac{dv_l^{(1)(2)}}{dr} + k_0^2 f(r)(1 + i\zeta) v_l^{(1)(2)} = 0 \qquad (6)$$

It is necessary to note that the function v_l is finite at $X = 0$ (if $U(r)$ has no singularity). Indeed, near $X = 0$ the variation of the centrifugal energy $l(l+1)/r^2$ is much faster than the variation of $U(r)$.

Expanding $U(r) = U(O) + U'(O)r$ and neglecting the second term in the series for $U(r)$, we obtain the equation for a free particle with the energy $E + U(O)$.

Its general solution has the form:

$$\psi = a\,\frac{1}{\sqrt{x}}\,H_{l+1/2}^{(1)}\left(\frac{K_0'}{k}\,x\right) + b\,\frac{1}{\sqrt{x}}\,H_{l+1/2}^{(2)}\left(\frac{K_0'}{k}\,x\right) \qquad (7)$$

where $K_0' = (k^2 + k_0^2)^{1/2}$.

Therefore near $X = 0$ the solution $v_l^{(1)} H_{l+1/2}^{(1)}(x)$ must turn into Equation 7 and so for small x we obtain the equation

$$v_l^{(1)}(x) = \frac{aH_{l+1/2}^{(1)}\left(\frac{K_0'}{k}\,x\right) + bH_{l+1/2}^{(2)}\left(\frac{K_0'}{k}\,x\right)}{H_{l+1/2}^{(1)}(x)}$$

The functions

$$x^{1/2} H_{l+1/2}^{(1)}\left(\frac{K_0'}{k}\,x\right)$$

and

$$x^{1/2} H_{l+1/2}^{(2)}\left(\frac{K_0'}{k}\,x\right)$$

have at $x = 0$ the poles of the same order, and hence the function v_l is finite at $x = 0$.

For high energies Equation 6 may be solved without any difficulty.

2. HIGH ENERGIES

If the energy is high, it is convenient to write the function v_l in the form:

$$v_l^{(1)} = e^{-\int_x^\infty U_l^{(1)} dx} \qquad (8)$$

Then the following equation for the function $U_l^{(1)}$ is obtained:

$$\frac{dU_l^{(1)}}{dx} + U_l^{(1)2} + 2\,\frac{d \ln x^{1/2} H_{l+1/2}^{1}(x)}{dx}\,U_l^{(1)} + \frac{k_0^2}{k^2} f(x)(1 + i\zeta) = 0 \qquad (9)$$

Similarly to the one-dimensional semiclassical problem one can neglect dU/dx.

Then we obtain:

$$V_l^{(1)}(x) = \exp\left\{ \int_x^\infty \left[\frac{d \ln x'^{1/2} H_{l+1/2}^{(1)}(x')}{dx'} - \left\{ \left(\frac{d}{dx} \ln x'^{1/2} H_{l+1/2}^{(1)}(x') \right)^2 - \frac{k_0^2}{k^2} f(x')(1 + i\zeta) \right\}^{1/2} \right] dx' \right\} \qquad (10)$$

The function ψ is finite at $x = 0$ when the condition:

$$\eta_l = \frac{v_l^{(2)}(0)}{v_l^{(1)}(0)} \qquad (11)$$

is fulfilled.

The integrand in Equation 9 is finite on the real axis, and the integral may be easily evaluated.

The following notations are introduced

$$\operatorname{Re} \frac{d \ln x^{1/2} H_{l+1/2}^{(1)}(x)}{dx} = a_l \qquad (12a)$$

$$\operatorname{Im} \frac{d \ln x^{1/2} H_{l+1/2}^{(1)}(x)}{dx} = b_l \qquad (12b)$$

If the real part of the potential is much larger than the imaginary one (such a situation arises for a fairly transparent nucleus) then the integrand may be expanded in powers of

$$[(a_l + ib_l)^2 - c^2(1 + i\zeta)]^{1/2} = i[(b_l - ia_l)^2 + c^2]^{1/2} - \frac{c^2 \zeta}{2[(b_l - ia_l)^2 + c^2]^{1/2}}$$

where $c^2 = (k_0^2/k^2) f(r)$.

Then η may be written as follows:

$$\eta = \exp\left[-2i \int_0^\infty \{ b_l(x) - \operatorname{Re}[(b_l - ia_l)^2 + c^2]^{1/2} \}\, dx - \zeta \int_0^\infty c^2(x)\, \frac{\operatorname{Re}[(b_l - ia_l)^2 + c^2]^{1/2}\, dx}{[(b_l^2 + c^2 - a_l^2)^2 + 4a_l^2 b_l^2]^{1/2}} \right]$$

where

$$\operatorname{Re}[(b_l - ia_l)^2 + c^2]^{1/2} = \frac{1}{2^{1/2}} [b_l^2 - a_l^2 + c^2 + \{(b_l^2 - a_l^2 + c^2)^2 + 4a_l^2 b_l^2\}^{1/2}]^{1/2}$$

Now for the total and absorption cross-sections the following expressions result:

$$\sigma_{tot} = \sum_{l=0}^{\infty} (2l + 1)\pi \lambdabar^2 (1 - |\eta_l|^2) = \sum_{l=0}^{\infty} (2l + 1)\pi \lambdabar^2 \left(1 - \exp\left\{ -\frac{2k_0^2}{k^2}\,\frac{\zeta}{2^{1/2}} \int_0^\infty f(x) \times \frac{[\{(b_l^2 - a_l^2 + c^2)^2 - 4a_l^2 b_l^2\}^{1/2} + b_l^2 - a_l^2 + c^2]^{1/2} dx}{\{(b_l^2 - a_l^2 + c^2)^2 + 4a_l^2 b_l^2\}^{1/2}} \right\} \right) \qquad (13)$$

$$\sigma_{tot} = \sum_{l=0}^{\infty} 2(2l + 1)\pi \lambdabar^2 (1 - \operatorname{Re} \eta_l) = \sum_{l=0}^{\infty} 2l + 1) 2\pi \lambdabar^2$$

$$\times\left[1-\cos 2\int_0^\infty\left\{b_l(x)-\frac{1}{2^{1/2}}\left[(b_l^2-a_l^2+c^2)\right.\right.\right.$$
$$\left.\left.+\{(b_l^2-a_l^2+c^2)^2+4a_l^2b_l^2\}^{1/2}\right]^{1/2}\right\}dx$$
$$\times\exp\left\{-\frac{k_0^2}{k^2}\frac{\zeta}{2^{1/2}}\right.$$
$$\left.\left.\int_0^\infty f(x)\frac{[b_l^2-a_l^2+c^2+\{(b_l^2-a_l^2+c^2)^2+4a_l^2b_l^2\}^{1/2}]^{1/2}}{[(b_l^2-a_l^2+c^2)^2+4a_l^2b_l^2]^{1/2}}dx\right\}\right] \quad (14)$$

Thus the cross-section computation reduces in this case to quadratures for any shape of the potential. But the corresponding integrals may be calculated only numerically and therefore it is more convenient to expand the integrand in powers of $K_0^2/K_0 \ll 1$, that can be made always.

In the K_0^4/K_0 approximation Equations 13 and 14 may be written in the form:

$$\sigma_{tot}=\sum_{l=0}^{\infty}(2l+1)\pi\bar{\lambda}^2\left[1-\exp\left\{-\frac{2k_0^2}{k^2}\right\}\right.$$
$$\left.\times\int_0^\infty f(x)\left[\frac{b_l}{b_l^2+a_l^2}-\frac{k_0^2}{2k^2}f(x)\frac{b_l^3-3a_l^2b_l}{[b_l^2+a_l^2]^3}\right]dx\right] \quad (15)$$

$$\sigma_{tot}=\sum_{l=0}^{\infty}(2l+1)2\pi\bar{\lambda}^2\left[1-\cos\frac{k_0^2}{k^2}\int_0^\infty f(x)\frac{b_l}{b_l^2+a_l^2}\right.$$
$$\left[1-\frac{k_0^2}{4k^2}f(x)\times\frac{b_l^2-3a_l^2}{[b_l^2+a_l^2]^2}\right]dx\Big\}\exp\left\{-\frac{k_0^2}{k^2}\zeta\right.$$
$$\left.\left.\int_0^\infty f(x)\frac{b_l}{b_l^2+a_l^2}\times\left[1-\frac{k_0^2}{2k^2}f(x)\frac{b_l^2-3a_l^2}{(b_l^2+a_l^2)^2}\right]dx\right\}\right] \quad (16)$$

When the absorption in the nuclear matter is large, the quantity ζ is of the order of unity, and then the integral in Equation 10 cannot be expanded in powers of $U(O)\zeta$.

If $\zeta U(r) > 2a_lb_l$ in the point where

$$a_l^2-b_l^2-U(r)=0$$

then for the ingoing wave solution, difficulty arises. Indeed the solution which satisfies the boundary condition at $x\to\infty$ turns out to be zero at $x = 0$. Thus r in this case would be zero. This difficulty, which is due to the approximation made at solving the problem, may be avoided if one assumes, that near the point x', where x' is the root of the equation $a_l^2 - b_l^2 = U = 0$, the potential $U = \text{const}$. (This is true for all waves with $l < (k_0^2 + k^2)^{1/2}R$.)

Then the exact solution of Equation 6 in this region is equal to

$$\chi(x)=\frac{AH_{l+1/2}^{(1)}\left(\frac{K}{k}x\right)+BH_{l+1/2}^{(2)}\left(\frac{K}{k}x\right)}{H_{l+1/2}^{(1)}(x)}$$

where $\quad K = [k_0^2(1 + i\zeta) + k^2]^{1/2}.$

Because $\chi(x)$ must become Equation 10 at $x > x'$ where x is solution of $a_l^2 - b_l^2 - U = 0$, the factor B must be equal to zero.

Therefore $v_l(r)$ may be written as follows:

$$v_l^{(1)}(x)=v_l^{(1)}(0)\left(\frac{K}{k}\right)^{l+1/2}\frac{H_{l+1/2}^{(1)}\left(\frac{K}{k}x\right)}{H_{l+1/2}^{(1)}(x)}$$
$$=\exp\left[\int_x^\infty\left\{\frac{d\ln x''^{1/2}H_{l+1/2}^{(1)}(x'')}{dx''}\right.\right.$$
$$\left.\left.-\left[\left(\frac{d\ln x''^{1/2}H_{l+1/2}^{(1)}(x'')}{dx''}\right)^2-U\right]^{1/2}\right\}dx''\right]$$

Hence

$$v_l^{(1)}(0)=\exp\left[\int_{x_1}^\infty\left\{\frac{d\ln x''^{1/2}H_{l+1/2}^{(1)}(x'')}{dx''}\right.\right.$$
$$\left.-\left[\left(\frac{d\ln x''^{1/2}H_{l+1/2}^{(1)}(x'')}{dx''}\right)^2-U\right]^{1/2}\right\}$$
$$\left.dx''\right]\cdot\left(\frac{k}{K}\right)^{l+1/2}\frac{H_{l+1/2}^{(1)}(x_1)}{H_{l+1/2}^{(1)}\left(\frac{K}{k}x_1\right)} \quad (17)$$

x_1 is assumed to be larger than x^1. Such a consideration is not valid if the point x^1 is in the boundary region.

It must be noted that when Equation 17 for $v(0)$ is substituted in Equation 11, the result coincides with one, which may be obtained, if the lower limit in Equation 10 is taken as $x = x^1$ instead of $x = 0$. Therefore in those cases when x^1 is in the boundary region and $\zeta U(x) > 2a_lb_l$, a good estimate may be obtained from the formula $\eta = v_l^{(2)}(x^1)/v_l^{(1)}(x^1)$.

When the term k_0^4/k^4 in Equations 15 and 16 may be neglected, the integrand for $l < kR$ is equal to the mean free path of the neutron with the angular momentum l in the nucleus (calculated by means of the optical model).

Let us suppose that the potential energy decreases at the nuclear boundary as $l^{-\alpha r}$.

Then determining the nuclear radius as $R = r_0 + (1/\alpha)$ we see from Equation 15 that the geometric path of the neutron with the angular momentum $l < kR$ is equal to $R - [l(l + 1)/2k^2R^2]$ and does not depend on $1/\alpha$ for constant R.

The boundary is essential only for terms with $l \geq kR$. When $1/\alpha \ll \bar{\lambda}$ and the term with k_0^4/k^4 is neglected, only the waves with $l \leq kR$ penetrate into the nucleus.

If $1/\alpha \geq \bar{\lambda}$ then the waves with $l > kR$ penetrate into the nucleus also.

In distinction from the geometrical optics, in our model the wave with $l = kR$ is scattered. Its contribution to the scattering cross-section tends to zero as $\bar{\lambda}$ (when the absorption is supposed to be constant). If the width of the boundary region is larger than the wave length, the influence of the boundary on the cross-section depends upon the relation between the wave length and the nuclear radius. For heavy nuclei with $R \sim 7\text{–}8 \times 10^{-13}$ a 10% increase of the cross-section is obtained, comparing with the case $1/\alpha \ll \bar{\lambda}$ provided the value of $r_0 + (1/\alpha)$ is the same.

For light nuclei the cross-section increases strongly. However, if the quantity $U(r)$ is assumed to be proportional to the density of the nuclear matter, then the nuclear density in the center of the nucleus decreases with increasing $1/\alpha$ and provided $r_0 + (1/\alpha) = \text{constant}$.

If the density of the nuclear matter in the center remains constant, then the dependence of the absorption cross-section upon the boundary shape is rather weak (cross-section variation is within several per cent).

On the contrary the assumption that the potential has a shape different from the shape of the nuclear density, will give a strong dependence of the light nuclei absorption cross-section upon the boundary shape.

When the second term in the exponent in Equation 15 cannot be neglected, the waves with $l > kR$ penetrate into the nucleus even for $1/\alpha \ll ƛ$. In this case the absorption cross-sections can be 15 to 20% larger than πR^2 even for heavy nuclei provided the neutron mean free path in the nuclear matter is small.

A more detailed study of the absorption cannot be made now because of the scarcity of experimental data on the absorption cross-sections at energies $E > U(0)$.

An important conclusion can be made from Equation 16. It is evident that the function under cosine in Equation 16 decreases with the increase of the energy. For some energy it becomes the value 2π that corresponds to a minimum in the total cross-section for this l.

For still larger energy a maximum appears at $\cos \varphi_l = 1$, i.e., $\varphi_l = \pi$. Thereafter the cross-section decreases monotonously.

For the sum of the total cross-sections for all l the maxima and minima are also obtained (although they are less pronounced). For heavy nuclei these maxima must be observed at higher energies, than for light ones. The reason for this is that the phase φ_l is larger for larger R. The dependence of this maximum displacement on the atomic weight is confirmed by the experiment. From the minimum position for lead ($E = 55$ Mev) it is possible to estimate the real part of the potential, assuming that $R = 1.2 \times 10^{-13} A^{1/3}$.

In the case of lead the boundary shape has little influence on the cross-section.

This estimate gives $U(0) = 35$–40 Mev.

It must be pointed out, that the Fermi energy is equal to 31 Mev, for $R = 1.2 \times 10^{-13} A^{1/3}$. Therefore, with account of the binding energy, the potential energy $U(0)$ must be equal to 38 Mev. Similar values of $U(0)$ may be obtained for small energies also. At energies larger than 100 Mev the simple model with a complex potential is probably not correct.*

3. THE VALIDITY RANGE OF THE HIGH ENERGY APPROXIMATION

The second approximation for the function is looked for similarly to the one dimensional problem. Let us expand U in the form $U_0 + U_1 + U_2$.

Then the equation for U_1 may be written as at the bottom of this page in Equations 18 and 19.

As is well known, the substitution in Equation 19 into the formula for v_0 gives for the S-wave the factor $1/\sqrt[4]{k_0^2 + k^2}$, which is real and drops out in calculating the scattering phase. For waves with $l > 0$ but $l \ll kr_0$, i.e., for waves entering into the region of constant potential, the substitution of Equation 19 into Equation 8 gives also a real factor:

$$[(k^2 + k_0^2)^{1/2} + k]^{1/2}$$

The contribution of the second approximation in r is essential only for waves with $l \sim kr_0$. For $1/\alpha \ll ƛ$:

$$v_2(0) = [\{1 + c^2(1 + i\zeta)[b_l(R) - ia_l(R)]^{-2}\}^{1/2} + 1]^{-1/2} v_1(0)$$

As the quantity a_l is small for all $l < kR$, the second approximation gives no contribution in r; for $l \geq kR$, the quantity a_l is larger and the factor at $v_1(0)$ is complex.

In this case the phase is changed proportionally to k_0^2/k^2.

The correction to r_l does not exceed, however, $e^{-0.4i}$ even for $l = kR$. The correction to the absorption cross-section is not large (at $\zeta = 0.2$ and $kR = e$, r_l^2 is increased by a factor $e^{0.16}$).

$$\frac{dU_0}{dx} + 2U_0U_1 + 2\,\frac{d \ln x^{1/2} H_{l+1/2}^{(1)}(x)}{dx}\, U_1 = 0 \tag{18}$$

Hence

$$U_1 = -\frac{\dfrac{dU_0}{dx}}{2U_0 + 2\,\dfrac{d \ln x^{1/2} H_{l+1/2}^{(1)}(x)}{dx}} = \frac{1}{2\left[\left(\dfrac{d \ln x^{1/2} H_{l+1/2}^{(1)}(x)}{dx}\right)^2 - c^2(1 + i\zeta)\right]^{1/2}} \cdot \left\{\frac{d^2 \ln x^{1/2} H_{l+1/2}^{(1)}(x)}{dx^2}\right.$$

$$\left. - \left[\frac{d^2 \ln x^{1/2} H_{l+1/2}^{(1)}(x)}{dx^2}\,\frac{d \ln x^{1/2} H_{l+1/2}^{(1)}(x)}{dx} - \frac{1}{2}\frac{\partial c^2}{\partial x}(1 + i\zeta)\right] \times \left[\left(\frac{d \ln x^{1/2} H_{l+1/2}^{(1)}(x)}{dx}\right)^2 - c^2(1 + i\zeta)\right]^{-1/2}\right\} \tag{19}$$

---

* It is stated in reference 6 that for the angular distribution of protons, scattered by *Pt* nuclei, an agreement with experiment may be obtained with the following set of parameters:

$$U(r) = 38 \text{ Mev } (1 + e^{\frac{r-r_1}{\alpha}})^{-1},\ a_0 = 0.49 \times 10^{-13},$$
$$r_0 = 8.24 \times 10^{-13} \text{ and } \zeta = 0.24.$$

It seems that the value or r_0 in reference 6 is too high. If we take $r_0 = 8.24 \times 10^{-13}$ for neutrons $\sigma_{abs} = 3.2$ and $\sigma_{tot} = 6.5$ that is 20% to 25% larger than the experimental values. Therefore, it is more probable that $r_0 = 7.5 \times 10^{-13}$ cm (the proton and neutron radius of the nucleus are supposed to be equal). It is possible, that in calculating the angular distribution of the protons the nonsphericity of *Pt* nucleus must be taken into account.

When $1/\alpha \geq \lambda$ the correction to the function with $l = kR$ decreases and for other l increases. The correction in the absorption cross-section will be of the same order as for $\frac{1}{2} \sim \lambda$.

The next approximation contributes a term of the order of $k_0^2\alpha/8k^3$ and is therefore essential for $1/\alpha \ll \lambda$ at $U \sim E$.

Equations 15 and 16 can be applied, therefore, at $U < E$, but a stronger condition $U \ll E$ is not required, because the corrections are not too large if $1/\alpha \sim \lambda$, even at $U = E$.

4. LOW-ENERGY REGION

If $E < U(0)$ then the semiclassical calculation method breaks down. In this case the solution of the Equation 3 is to be found numerically for a definite boundary shape.

In the latter calculations, the assumption that $(x) = l^{a(x-x_0)}$ for $x \geq I_0$ is made. Then at $r = r_0$ the boundary conditions

$$\frac{1}{\psi_i}\frac{d\psi_i}{dr} = \frac{1}{\psi_a}\frac{d\psi_a}{dr} \tag{20}$$

must be satisfied.

At $r \leq r_0$ the potential $U = \text{const}$ and therefore the solution of Equation 3 may be written in the form

$$\psi = r^{-\frac{1}{2}} J_{l+\frac{1}{2}}(\varkappa r) \tag{21}$$

where

$$\varkappa = [k^2 + k_0^2(1 + i\zeta)]^{\frac{1}{2}} \tag{22}$$

For the region where the potential is not constant, the solution is to be looked for in the form of Equation 4. Then the solution of Equation 6 is found in the form of a series of powers of k_0^2/k^2. The condition $v_l = 1$ at $r \rightarrow \infty$ is used. In the first approximation we assume that in Equation 6 $v_l = 1$.

An equation of the first order for the derivative dv_l/dr is obtained

$$\frac{d^2v_l^{(1)}}{dy^2} + 2\,\frac{d \ln y^{\frac{1}{2}} H_{l+\frac{1}{2}}^{(1)}\left(\frac{k}{\alpha}y\right)}{dy}\,\frac{dv_l^{(1)}}{dy} + \frac{k_0^2}{\alpha} f(y)(1 + i\zeta) = 0 \tag{23}$$

Equation 23 is solved for $dv_l^{(1)}/dy$. Then integrating once more we obtain

$$v_l^{(1)}(y) = 1 - \frac{k_0^2}{\alpha^2}(1 + i\zeta)\int_y^\infty \left[y'^{\frac{1}{2}} H_{l+\frac{1}{2}}^{(1)}\left(\frac{k}{\alpha}y'\right)\right]^{-2} \times \int_{y'}^\infty f(y'')\left[y''^{\frac{1}{2}} H_{l+\frac{1}{2}}^{(1)}\left(\frac{k}{\alpha}y''\right)\right]^2 dy'\,dy'' \tag{24}$$

Equation 24 may be transformed into a more convenient form

$$v_l^{(1)}(y) = 1 - \frac{k_0^2}{\alpha^2}(1 + i\zeta)\int_y^\infty y'\left[H_{l+\frac{1}{2}}^{(1)}\left(\frac{k}{\alpha}y\right)\right]^2 f(y') \times \int_y^{y'}\left[y''^{\frac{1}{2}} H_{l+\frac{1}{2}}^{(1)}\left(\frac{k}{\alpha}y\right)\right]^{-2} dy'\,dy''$$

Evaluating the inner integral we obtain finally:

$$v_l^{(1)}(y) = 1 - \frac{i}{2}\frac{k_0^2}{\alpha^2}(1 + i\zeta)\frac{\alpha}{k}\left\{\int^\infty \left(\frac{k}{\alpha}y'\right)^{-2l} \left|P_l\left(\frac{k}{\alpha}y'\right)\right|^2 f(y')\,dy' - \frac{P_l^*\left(\frac{k}{\alpha}y\right)}{P_l\left(\frac{k}{\alpha}y\right)}\int_y^\infty e^{2i\frac{k}{\alpha}(y'-y)} \left(\frac{k}{\alpha}y'\right)^{-2l}\left[P_l\left(\frac{k}{\alpha}y'\right)\right]^2 f(y')\,dy'\right\} \tag{25}$$

In Equation 25

$$P_l\left(\frac{k}{\alpha}y\right) = e^{-i\frac{k}{\alpha}y}\left(\frac{k}{\alpha}y\right)^{l+\frac{1}{2}} H_{l+\frac{1}{2}}^{(1)}\left(\frac{k}{\alpha}y\right)$$

If $\alpha^{-1} = 1.5\text{–}2 \times 10^{-13}$, the first approximation is bad.

For the energy region 3–10 Mev three or four terms of the series must be computed. However the integrals depend only on one parameter k/α, which makes numerical calculations easier (the parameters $k_0\zeta$ and r_0 may be varied arbitrarily).

The expression for the n-approximation is obtained when the $(n - 1)$-approximation is substituted in Equation 6.

It has the form:

$$v^{(1)[n]}(y) = 1 - \frac{i}{2}\frac{k_0^2}{\alpha^2}(1 + i\zeta)\frac{\alpha}{k}\left\{\int_y^\infty \left(\frac{k}{\alpha}y'\right)^{-2l} \left|P_l\left(\frac{k}{\alpha}y'\right)\right|^2 \times f(y')v_l^{(1)[n-1]}(y')\,dy' - \frac{P_l^*\left(\frac{k}{\alpha}y\right)}{P_l\left(\frac{k}{\alpha}y\right)}\int_y^\infty e^{2i\frac{k}{\alpha}(y'-y)}\left(\frac{k}{\alpha}y'\right)^{-2l}\left[P_l\left(\frac{k}{\alpha}y'\right)\right]^2 f(y')v_l^{(1)[n-1]}(y')\,dy'\right\} \tag{26}$$

It may be noted that such cumbersome calculations are necessary only for small l waves (smaller than 5–6) for which the virtual levels may exist.

The condition of the existence of a virtual level may be obtained from a semiclassical consideration. This condition is $\cos \varphi_l = -1$ at $E \rightarrow 0$ in Equation 14.

For a well with $c(1/\alpha) \ll R$, we obtain

$$[k_0^2R^2 - l^2]^{\frac{1}{2}} = (2n + 1)\frac{\pi}{2} + l \arctan\frac{[k_0^2R^2 - l^2]^{\frac{1}{2}}}{l} \tag{27}$$

in good agreement with the exact solution. It may be noted that for a diffuse boundary with $c(1/\alpha) \sim R$, the agreement between the exact condition and the semiclassical is worse. Nevertheless for estimates and particularly for heavy nuclei (i.e., $1/\alpha < R$) the semiclassical condition may be used.

5. COMPARISON WITH EXPERIMENTS

The inelastic cross-section data for the Mev region are not numerous. At energies smaller than 2–3 Mev the number of nuclear levels, which can be excited is small and therefore, especially for magic nuclei, the decay of the compound nucleus can go elastically. We have used the last unpublished data on the inelastic scattering of neutrons at energies 2.5 Mev and 4.3 Mev. For comparison with these experiments a calculation of the dependence of the absorption cross-section on the nuclear radius has been made for both values of the energy. The exponential shape of the boundary $e^{-\alpha r}$ with $1/\alpha = 1.45 \times 10^{-13}$ cm has been assumed. The depth of the well has been taken equal to 20 Mev but the situation is little altered when $u(0) = 40$ Mev.

At $E = 2.5$ Mev the imaginary part of the potential $u(0)\zeta$ is taken equal to $0.053\ u(0)$.

At $E = 4.3$ Mev, two values of the imaginary part are taken: $u(0) = 0.055$ and $u(0) = 0.11$.

On Fig. 1 the results of the absorption cross-section $\sigma/\pi R^2$ calculation are given. The radius R is taken equal to $r_0 + 1/\alpha$ (the solid curve). The results of a calculation with rectangular boundary and the same values of u and ζ are given also (broken curve).

The experimental points obtained by means of a threshold detector are shown by open circles. The nuclear radius R is taken equal to $1.25A^{1/3} \times 10^{-13}$.

The absorption cross-section in the diffuse boundary model is seen to be about two times larger than in the square well model. The maxima and minima appear to be rather weak (the cross-section ratio in maximum and minimum is equal to 1.3, while in the square well model this quantity exceeds 2). The experimental points fall at both sides of the diffuse boundary model curve. The magic nuclei are not included into the set of comparison points, because they have few levels accessible for inelastic scattering and therefore their inelastic cross-section is small.

Only the point for the Zn nucleus is far from the theoretical curve; the experimental value for this nucleus is too large. On Fig. 2 the calculated data for 4.3 Mev neutrons are given. The solid curves give the values of the absorption cross-sections in the diffuse boundary model for two imaginary parts of the potential $0.055\ U(0)$ and $0.11\ U(0)$; the broken curve corresponds to the absorption cross-section for a square well model with $\zeta = 0.055$. For comparison the experimental points are given. The nuclear radius R is taken equal to $1.25A^{1/3} \times 10^{-13}$. The experimental points are seen to be in better agreement with the upper curve than with the lower. Thus, the comparison with experimental data shows that the mean free path of the neutron in the nuclear matter for low energies is fairly large, but it decreases rapidly when the energy increases.*

The agreement between the values of nuclear radius obtained from other data (the scattering of fast electrons) and the neutron cross section in the diffuse boundary model of the nucleus can be obtained.

On the contrary, for the square well model the absorption cross-section is equal to $1–1.2\pi R^2$ even for the case of large absorption. The enormous values of the radius ($R = 1.6 \times 10^{-13}A^{1/3}$) are obtained from the comparison of this model with experimental data. These values of R differ very strongly from the other experimental values. The absorption cross-section maxima disappear in the diffuse boundary model at energies $E = 5$ Mev.

At higher energies the absorption cross-section is a monotonic function of the radius. The experimental data on the inelastic cross-sections for 14 Mev neutrons do not contradict to the assumption that $R = 1.25A^{1/3} \times 10^{-13}$. For lightest nuclei ($A \sim 10$) the radius may be somewhat larger.

The mean free path for this energy must be of the order of $3–4 \times 10^{-13}$ cm; that is, the nucleus is completely absorbing for waves with $l < KR$. On the contrary the total cross-sections will have maxima and minima for all l for which the nucleus is not completely absorbing, because the phase of the scattered wave varies with R and E.

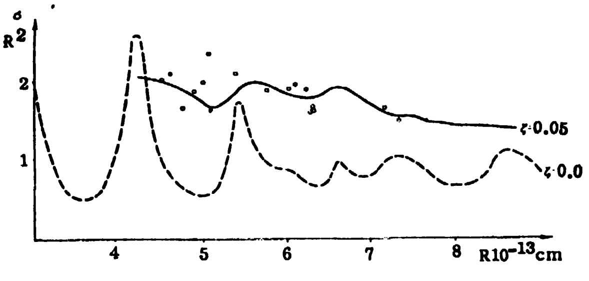

Figure 1. Inelastic scattering cross section dependence on the radius of the nuclei at energy 2.5 Mev: the solid curve has been calculated according to the model of diffuse boundary; the broken curve, according to the model of square boundary; the circles represent the experimental points

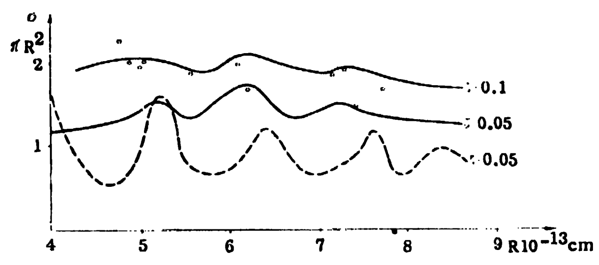

Figure 2. Inelastic scattering cross section dependence on the radius of the nuclei at energy 4.3 Mev: the solid curves have been calculated according to the model of diffuse boundary; the broken curve, according to the model of square boundary; the circles represent the experimental points

---

* Recently new data concerning the inelastic cross-section for energies 1.4 and 4.5 Mev are published.[7] The cross-sections for 4 Mev and 4.5 Mev neutrons are somewhat smaller than that mentioned above. Therefore the quantity S can be somewhat lower than 0.11.

The 1 Mev data cannot be compared with the theory because for some nuclei the inelastic scattering for this energy is impossible as they have no low energy levels.

It is also possible that only one level is excited at this energy, and the transition to the ground state with an elastic scattering of the neutron has a large probability.

CONCLUSION

For the calculation of neutron scattering cross-section a method of modulated spherical waves is proposed. At energies $E > U(0)$ this method is a generalization of the semiclassical one. The solution, contrary to the usual semiclassical one, satisfies the exact boundary conditions.

The higher approximations can be obtained easily and in this way a transition to the limit at exact solution of the problem of phase analysis can be realized. At $E > U(0)$ a simple explanation of maxima in the total cross-section is given. The difference of the total cross-section from $2\pi R^2$ is explained. The absence of sharp maxima in the absorption cross-section at function of radius for small energies is also explained.

In the diffuse boundary model an agreement between neutron radius of the nuclei and the values of radius calculated from other experiments may be obtained.

REFERENCES

1. Cook, McMillan, Peterson and Sewel, Phys. Rev., *75*, 7, (1949).
2. Fernbach, Serber and Taylor, Phys. Rev., *75*, 1352, (1949).
3. Feshbach and Weisskopf, Phys. Rev., *76*, 1550, (1949).
4. Miller, Adair, Bockelman and Darden, Phys. Rev., *88*, 83, (1952).
5. Feshbach, Porter and Weisskopf, Phys. Rev., *90*, 166, (1953); Phys. Rev., *96*, 448, (1954).
6. Woods and Saxon, Phys. Rev., *95*, 577, (1954).
7. Beyster, Henkel and Nobles, Phys. Rev., *97*, 563, (1955).

Physics Research with Reactors

By Andrew W. McReynolds,* USA

The research reactor can be regarded as a general research instrument for application to various branches of science. An important part of its function is in deriving technological information and experience of value in development of further reactors. That is covered elsewhere, however, and is discussed here only incidentally. Rather its use as a general physics research instrument is outlined by a survey of certain recent and current experiments in the various fields to which it is applicable. Generally these fall into two classes, nuclear, including properties of the neutron and its interactions with nuclei, and atomic or solid-state, including interactions of the neutron with bound aggregates of atoms in crystals, liquids or molecules. The topics discussed are: (1) fundamental properties of the neutron, (2) neutron-nuclear interaction cross-sections, (3) gamma rays from (n,γ) reactions, (4) nuclear spin alignment in crystals, (5) neutron diffraction crystal structure analysis, (6) neutron scattering, refraction, and depolarization, (7) energy exchange between thermal neutrons and crystal lattice vibrations, (8) slow neutron transmission studies in solids, and (9) fast neutron radiation damage. Those topics which relate more directly to reactor technology, such as cross-section measurements, are adequately discussed elsewhere, as is neutron diffraction, and need be discussed only briefly here for completeness. Such subjects as the determination of integral quantities and observations on reactor kinetics have not been included for similar reasons. Those experiments which are discussed have been chosen rather to be illustrative of the variety of recent uses of reactors, rather than an exhaustive survey of recent work.

In all of the experiments above, the reactor serves primarily as a source of a strong flux of neutrons, and in all but the last a collimated neutron beam is used. This illustrates that in a reactor for physics research, the important considerations are a high flux, and as many independent beam holes as possible.

1. FUNDAMENTAL PROPERTIES OF THE NEUTRON

The most fundamental studies made possible by the concentrated neutron flux from reactors are those relating to the properties of the neutron itself. The half-life for decay of the free neutron has been measured both by Snell[1] and by Robson.[2] Another recent work is the determination of the neutron magnetic moment. Previous experiments[3] had established this quantity, or more precisely, the gyromagnetic ratio, to an accuracy of about 1 part in 10^4 by measurement of the resonant frequency for precession in a static magnetic field. Principal limiting factors were in strength of neutron flux, degree of neutron polarization attainable by transmission through magnetized iron, and short path-lengths in the static magnetic field. Improvements in these three factors in an experiment by Cohen, Corngold, and Ramsey have made possible improvement of the precision of measurement by one or two orders of magnitude.

A high degree of polarization was attained by using the total reflection, rather than transmission technique. Total reflection from a magnetic surface depends on a scattering amplitude, a, which is the sum or difference of nuclear and magnetic components, $a = a_n \pm a_m$, depending on whether the neutron magnetic moment is parallel or anti-parallel to the magnetic field in the mirror. Since for saturated Co the magnetic component is larger than the nuclear, $a_m > a_n$, only one component of the beam is reflected, and complete polarization results. The finely collimated beam was therefore reflected successively at small angles from two Co mirrors 1.25 × 14 inches, the first serving as a polarizer and the second as an analyzer. Final mirrors were made of a 94% Co-6% Fe alloy to facilitate magnetic saturation. Since this alloy is face-centered-cubic, rather than hexagonal like pure Co, magnetic anisotropy is considerably decreased without significant increase of the nuclear amplitude. In practice polarization was around 90%. The experimental arrangement is shown in Fig. 1.

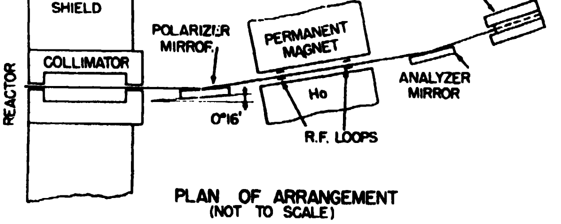

Figure 1. Apparatus for measurement of the neutron magnetic moment with a beam polarized by Co mirrors and passed through a long static field

---

* Brookhaven National Laboratory, Upton, New York. Based on work by J. Antal, R. Carter, V. F. Cohen, N. Corngold, G. J. Dienes, N. Holt, D. J. Hughes, A. W. McReynolds, H. T. Motz, H. Palevsky, R. J. Weiss, Brookhaven National Laboratory; S. Bernstein, L. D. Roberts, Oak Ridge National Laboratory; N. F. Ramsey, Harvard University; and F. Gould, W. W. Havens, B. Rustad, Columbia University.

Between the two mirrors the neutron beam passed through a 60-inch long uniform field between magnet pole pieces. The average static magnetic field was determined by a number of measurements with a proton resonance probe at points along the same path. Near the beginning and end of the path were radio-frequency field sources in the form of loops of copper tube, which were tuned to resonance near 25 megacycles. The phase of voltage in a particular loop could be shifted 180 degrees by means of a switch. It is the study of the resonant absorption of radio frequency energy by neutron moments in a known static field which yields the value of the neutron magnetic moment. The dynamics of moments in such an arrangement, with separated oscillating fields, has been discussed by Ramsey[4]. His analysis shows that the resonance width, which is the determining factor for precision, is only 0.6 as wide for such separated fields as for an oscillating field extended over the entire path. Further, resonance depends only on the average magnetic field over the path, and is not broadened by fluctuations in the field. It is just this average which was measured by the proton resonance probe. Figure 2 shows a typical resonance pattern, the bottom curve representing the difference between "in phase" and "out of phase" curves. The center of the neutron resonance peak could be determined to an accuracy of about 10 cycles (in 24 megacycles) within a period of a few minutes. Proton resonance, which had to be measured at a number of points, required somewhat longer, and introduced such experimental difficulties as slow drift of magnet field by temperature drift. Both resonances could be measured to higher accuracy than the absolute value of the proton moment, so that the quantity actually measured in this experiment is not the magnetic moment of the neutron but its ratio to the magnetic moment of the proton. The values found for this ratio in two separate series of experiments were 0.6850492 ± 0.0000018 and 0.6850680 ± 0.0000011, where the indicated errors are average deviations between individual runs.

Some other fundamental properties of the neutron which have been verified include a possible quadrupole moment, which Smith and Ramsey[5] have, in experiments at Oak Ridge showed to be zero within very close limits. Observations by McReynolds[6] on the deflection of a slow neutron beam in the earth's gravitational field showed that a free neutron interacts in the same way with a gravitational field as bulk matter. Furthermore from the absence of deflection of the same beam by the application of an electrostatic field, an upper limit of 5×10^{-12} electronic units of charge could be deduced for the neutron.

2. NEUTRON-NUCLEAR INTERACTION CROSS-SECTIONS

A rather large quantity of data on neutron nuclear cross-sections, particularly on total cross-sections as measured by transmission, has been accumulated and compiled. There still remains, however, an at least equally large quantity to be obtained, particularly in the epithermal and resonance regions. Recent developments in technique such as high resolution crystal spectrometers for the region up to 10 ev and fast choppers for higher energies have made possible the satisfactory resolution of resonances over much of this range. This subject is discussed in a number of papers, however, comprising a large part of the reactor physics sessions Q, and covering both instrumental techniques and results.

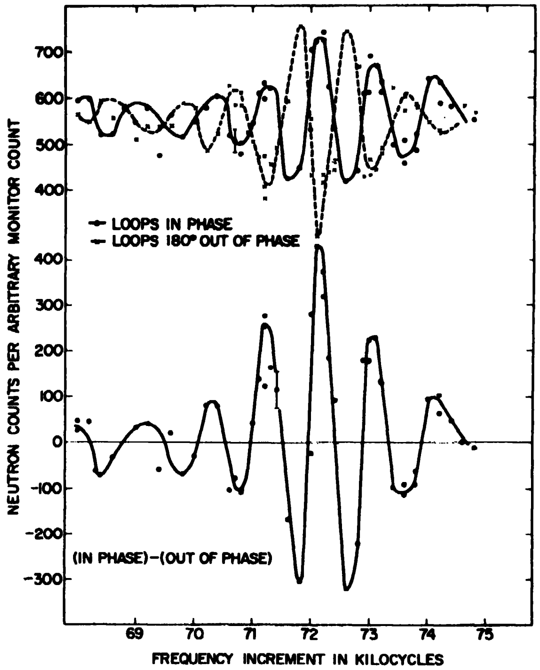

Figure 2. Resonance curve of neutron intensity as a function of radio frequency in coils. Pattern is characteristic of the "separated RF loop" method

A particularly elemental and therefore interesting interaction is that between neutron and electron, which was measured by Rainwater, Havens and Rabi[7] by neutron transmission through liquid Bi, as a function of energy. The very small neutron-electron interaction is separable from the larger neutron-nuclear interaction, because the space distribution of the electrons leads to a form factor dependence of scattering on angle or on wave-lengths. More recently Hughes, Harvey, Goldberg and Stafne[8] used a reactor beam and the technique of total reflection at very small angles from the interface between a bismuth mirror and liquid oxygen. Another experiment is currently in progress by Havens, Melkonian and Rustad using the monochromatic beam from a crystal spectrometer to measure transmission as a function of energy from 0.1 to 10 ev through liquid bismuth at 300 and 500°C.

3. GAMMA RAYS FROM (n,γ) REACTIONS

A thin lens beta-ray spectrometer is being used by Motz[9] at the Brookhaven Reactor to observe the prompt gamma-rays emitted by elements capturing slow neutrons. The gamma-ray energies and intensities in the range of 400 kev to 3 Mev are measured by means of the photoelectric effect in thorium and

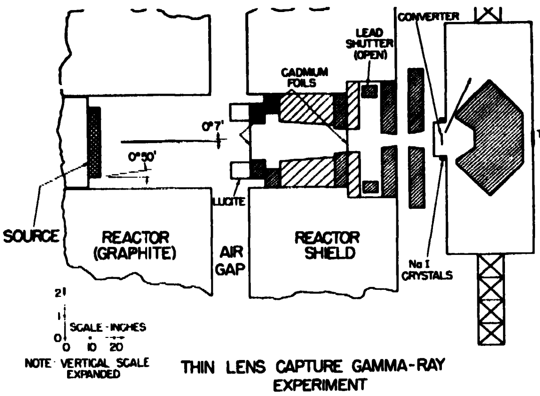

Figure 3. Experimental arrangement for prompt gamma-ray experiment with thin lens β spectrometer. The gamma rays are collimated by lead apertures and pass into the spectrometer vacuum, through a converter and into the beam catcher. Two NaI crystals outside the direct beam but near the converter are used to detect the K X-rays of the converter

uranium converters. (This energy range complements that of the 3 to 10 Mev region studied by Kinsey and Bartholomew at the Chalk River Reactor.) The experimental arrangement is shown in Fig. 3. Because the gamma-ray beam is so well collimated, it is possible to locate two NaI crystal detectors near the converter without counting much of the direct or scattered beam. The K X-rays of the converter are easily seen above this background. These X-rays are emitted isotropically and have a half-life of about 10^{-15} sec and serve as excellent coincidence pulses for the K photoelectrons detected by the spectrometer crystal detector. By means of the K X-ray coincidence requirement the background of Compton and pair electrons is greatly reduced and the L photopeaks completely eliminated. This results in a much higher relative yield for the K photopeaks and a much easier interpretation of complex spectra.

The spectra shown in Fig. 4 were obtained from a 325 gram sample of polyethylene and an array of thin cadmium foils. The $H^1(n,\gamma)H^2$ spectrum shows the absence of the L photopeak, the suppression of the Comptons and the low background from the reactor. The yield observed from Cd^{113} (n,γ) Cd^{114} consists almost entirely of K peaks though most of the observed yield is actually in unresolved peaks. It is to be expected that the cascading of gamma rays from the capturing state (9.0 Mev for Cd) will allow the excitation of low-lying excited states in Cd^{114} that might not be seen in other methods of excitation. Because of this, several gamma rays believed to be associated with low-lying levels are seen in the capture spectrum that are not present (or have not yet been detected) in the In^{114} K-capture branch to Cd^{114}. An interesting feature of the capture spectrum is the intense line at 556 kev which indicates that 89% of the disintegrations result in the excitation of the first excited state of Cd^{114}. Most of the observed lines[9] fit well with the high energy data of Kinsey and Bartholomew.[10]

The source intensity is limited by self-absorption and so the minimum absorption cross section required is a function of Z. The lower limit of source strength is $I \sim k\sigma/Z$. Results for Na ($\sigma/Z \sim 0.05$) indicate that 1 barn cross sections are just sufficient up to $Z = 25$ and correspondingly larger ones are required for heavier nuclei.

4. NUCLEAR SPIN ALIGNMENTS IN CRYSTALS

The interaction between a neutron and nucleus is dependent on whether the nuclear spin I and neutron spin $\frac{1}{2}$ are parallel or antiparallel, that is, whether the compound nucleus has $J = I + \frac{1}{2}$ or $J = I - \frac{1}{2}$. In the absence of resonances the cross-section for the two interactions is nearly equal but as a resonance is approached, one becomes much larger while the other remains constant. The quantity usually measured in

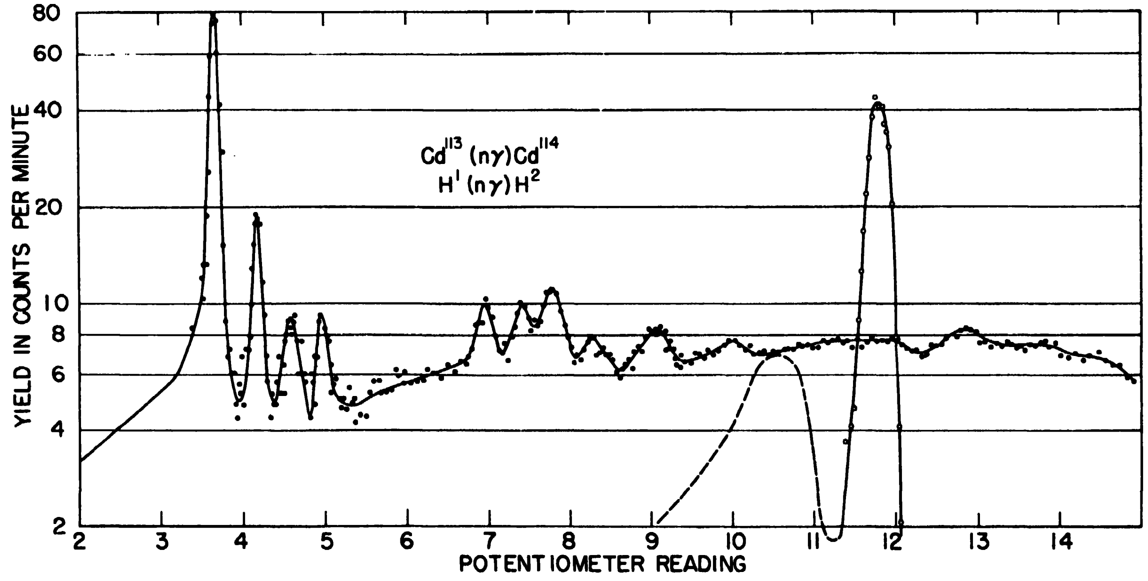

Figure 4. Spectra of $H^1(n,\gamma)H^2$ and $Cd^{113}(n,\gamma)Cd^{114}$. The abscissa is proportional to electron momentum and is approximately linear in energy from 0.3 to 2.9 Mev. The 2.23 Mev line from hydrogen is normalized to that of cadmium for the same energy. The energy sensitivity is roughly E_γ^{-1} for comparison of other energies

cross-section measurements is an average of the two, since both nuclei and neutron beams are unpolarized. Polarization of neutron beams is possible however, and in principle the nuclear moments can also be aligned by application of a suitably high magnetic field.

For polarization, energy of the nucleus in the magnetic field, μH, must be greater than the thermal vibration energy kT which tends to disorient nuclei. Because of the small value of the nuclear moment, this requires high magnetic fields and temperatures well below 1°K. A number of measurements have been made at Oak Ridge in the past few years to produce polarization by adiabatic demagnetization cooling, and to detect it by variation in the neutron cross-section. Experiments by Bernstein *et al.*[11,12] on Mn^{55} and by Roberts *et al.*[13] on Sm took advantage of the hyperfine coupling between the nuclei and electronic system by using paramagnetic salts of the metals. Polarization of Mn nuclei in manganous ammonium sulfate at 0.2°K and 2350 gauss was detected by the dependence of induced activity on the polarization of a bombarding thermal neutron beam. In an experiment on Sm in samarium ethyl sulfate the magnetic field was 11,000 gauss and temperature 0.13°K. Nuclear polarization was detected in this case by allowing an initially unpolarized neutron beam to fall on the sample and analyzing polarization of the transmitted portion, from which one component had been selectively absorbed by the Sm thermal resonance.

The most recent experiment has been the direct or "brute force" polarization of indium in metallic form, by low temperature and high magnetic fields only, without recourse to the hyperfine coupling. Indium was a favorable choice for several reasons. It has a large magnetic moment, is suitable for cryogenic work because of its metallic heat conductivity, and has a resonance at 1.458 ev which results in a high thermal neutron capture cross section for one spin state. As had been pointed out by Rose[14] it is possible from such polarization experiments to determine which spin state has the resonance.

In the experimental arrangement, the sample, in the form of 20 indium foils 0.025 cm thick, was cooled by conduction through silver wires to a salt, $Fe(NH_4)(SO_2)_2$-12 H_2O, which in turn was cooled by adiabatic demagnetization to around 0.035°K. A field of 11,150 gauss was then applied to the indium. A polarized neutron beam was obtained by diffraction from the 220 planes of a magnetized Fe_3O_4 crystal,[15] and transmission through the indium was measured for the neutron polarization either parallel or antiparallel to the applied field. Figure 5 shows on the left scale the per cent difference of transmission for the two cases as a function of time after application of the field. Per cent nuclear polarization is shown on the right scale. Time delay represents a relaxation time for establishment of thermal equilibrium in the system. Transmission was highest for antiparallel relative spin orientation, leading to the conclusion that the compound state corresponding to the 1.458 ev resonance in In is $J = I + \frac{1}{2} = 5$. Minimum temperature reached was computed from the formula for polarization

$$f_n = \tfrac{1}{3}\,\frac{I+1}{I}\,\frac{\mu H}{kT}$$

to be 0.043° ± 0.005°K.

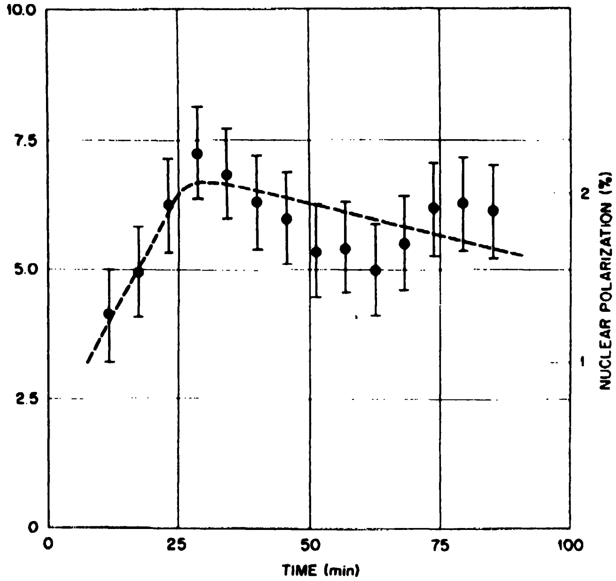

Results of Experiments IV. Average of 4 Runs.

Figure 5. Variation of neutron transmission due to polarization of nuclear magnetic moments in In metal at low temperature and high applied field. Per cent polarization is shown at right

5. NEUTRON DIFFRACTION CRYSTAL STRUCTURE ANALYSIS

The diffraction of thermal neutrons in crystals has proved to be a widely applicable reactor research method, which has been developed particularly by Wollan and Shull. Work in this field is surveyed by them[16] in the reactor physics sessions, and only some general comments are made here. Initially neutron diffraction served the purpose of determining nuclear scattering cross-sections in the thermal energy range,[17] where total cross-section as measured by transmission is too dependent on crystal diffraction effects to be readily interpretable as a nuclear property. Although cross-sections for almost all natural elements and a number of isotopes have now been measured, there still remain a large number of separated isotopes to be done.

Recently, however, the role of neutron diffraction has been not so much in nuclear as in solid-state research, where it is similar and complementary to X-ray and electron diffraction. One of the principal applications has been magnetic structures. Unlike X-rays, the neutron, in virtue of its magnetic moment, interacts with atomic magnetic moments. In magnetic crystals, diffraction is therefore by a combination of the nuclear and magnetic scattering from each atom. It is therefore possible to determine not only the space arrangement of the atomic lattice, but also the magnitude and orientation of magnetic moments associated with the various lattice positions. A number of reports on ferromagnetic and anti-ferromagnetic materials are to be found in the recent literature.[18,19] Another particular field of application has been the investigation of structures involving atoms whose X-ray scattering powers are either too nearly equal (e.g., iron and cobalt) or too different (e.g., hydrogen and carbon) to be readily amenable to X-ray detection. There is particularly wide potential application in the large class of hydrogenous crystals, including of course all organics. Although a few hydrogenous crystals, such as Rochelle salts[20] and potassium dihydrogen phosphate, have been intensively investigated, work in this field has hardly started.

Most of the initial work with neutron diffraction was done by the Debye-Scherrer, or powder diffraction method. With refinement of techniques and increasing complexity of the problems attacked, single crystal diffraction techniques have become increasingly useful and necessary. Figure 6 shows the most recent neutron spectrometer developed for this purpose by Frazer, Pepinsky, and others at Brookhaven Laboratory. The BF_3 detector, operating at 1 or 2 atmospheres pressure, has been reduced in size enough to be used with a standard GE X-ray goniometer. The goniometer was also modified by the addition of an arc mounting to permit counter rotation about a horizontal axis to study upper layer lines without change of the sample crystal. Perhaps the most complex structure investigated so far by neutron diffraction is the work on Rochelle salts by Frazer.[20] This has established the structure with considerably more precision than by X-ray methods and demonstrated the applicability of neutrons to crystallographically complex structures.

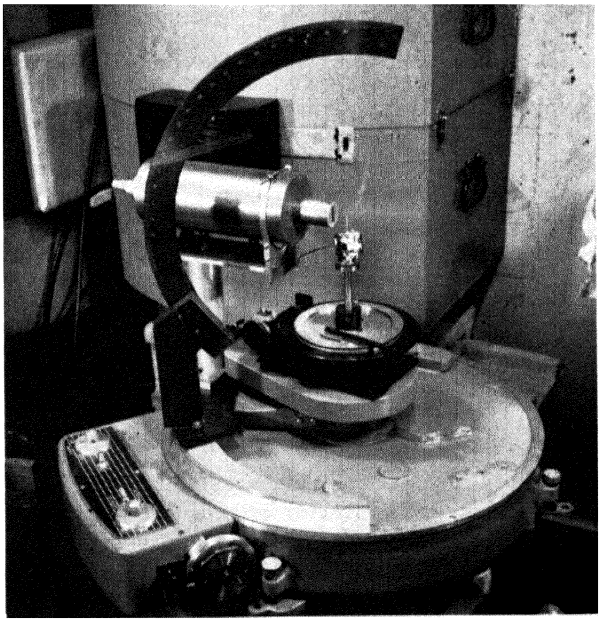

Figure 6. Neutron diffraction spectrometer for single crystals. Small high pressure BF_3 counter is adjustable on arc mounting added to GE X-ray unit. Sample crystal is $BaTiO_3$

6. NEUTRON SCATTERING, REFRACTION AND DEPOLARIZATION

A number of experiments, although perhaps properly classified as neutron diffraction, are of a slightly different character. The preceding section dealt with studies of the arrangement of atoms and their magnetic moments in the crystal lattice, that is, the structure of the lattice unit cell for a perfect crystal. This section deals briefly with one or two experiments which bear on the larger scale structure of crystalline materials, such as grain and mosaic structure, magnetic domains, distortions, and imperfections. These can be investigated partly through the characteristics of the diffraction pattern, but also through such effects as refraction and total reflection at boundaries, or depolarization of a neutron beam under action of local magnetic fields.

In diffraction studies on the anti-ferromagnetic oxides NiO and CoO, Shull and collaborators[21] found that, whereas anti-ferromagnetic ordering exists only below the Neel temperature, there was some evidence of residual intensity in the diffraction peaks just above the Neel temperature. Later experiments by McReynolds and Riste[22] on Fe_3O_4, and by Shull and Wilkinson[23] on Fe, both near the Curie points, have established more clearly the interpretation. Figure 7 shows some results for Fe_3O_4 indicating that around the usual Bragg (111) peak a weaker diffuse peak arises as temperature approaches the Curie temperature of 580°C. With further decrease of the temperature below T_C the diffuse peak diminishes. Shull and Wilkinson[23] had observed a related phenomenon of small angle scattering of a beam transmitted through iron, the scattering being maximum near the Curie temperature. Both results are explained by the interpretation that although the long-range ordering, and therefore the domain structure, disappears above the Curie temperature, a short-range correlation between spins, representing a sort of transient sub-domain structure, persists. In fact the short-range correlation is at a maximum just at the critical point. Van Hove has shown theoretically that just such behaviour is to be expected. Results similar to those for the Fe_3O_4 have been found for a CoO single crystal. CoO is a somewhat

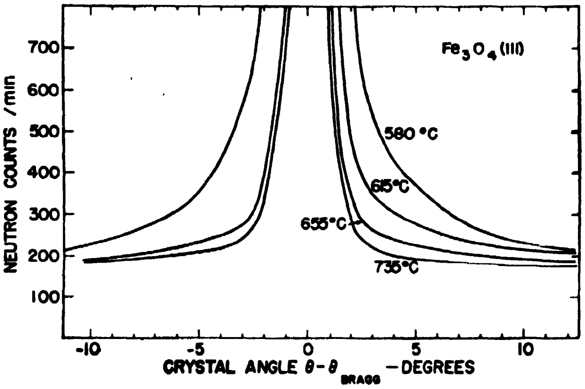

Figure 7. Diffuse peak around the (111) Bragg diffraction arises from short range spin correlation which is at a maximum at the Curie temperature of 580°C

more favorable case because the peak is entirely antiferromagnetic, with no nuclear component. Further quantitative measurements have been carried out to investigate the correlation function of distance and temperature.

Another feature of interest in magnetic domains is the nature of the "Bloch wall," or transition layer, between two differently oriented domains. Figure 8 shows an Fe-Si single crystal specially prepared by Williams and Nesbitt to contain a single domain wall as shown. Experiments on the effects on a neutron beam transmitted through such a single domain wall have been carried out by Holt and McReynolds. Two expected effects are directly observed. Since the neutron has its magnetic moment parallel to the internal field on one side of the boundary and anti-parallel on the other side (if it retains the same polarization) its energy is slightly different. This means that it has a slightly different index of refraction on the two sides of the boundary, and if incident at small angles is refracted slightly. A second effect is that, depending on the transit time of the neutron through the wall as compared with its Larmor precession frequency, it may or may not have its polarization reversed in transit. Using highly collimated beams and the polarizing and analyzing mirrors shown in Fig. 1, both effects of refraction and depolarization have been observed. It is hoped that further investigation of these effects as a function of neutron velocity and incident angle can lead to an evaluation of the Bloch wall thickness.

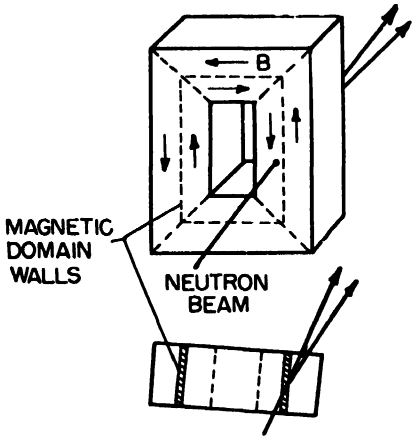

Figure 8. Experimental arrangement for direct observation of refraction and depolarization of neutron beams at a single magnetic domain boundary. Beam polarization arrangement is shown in Fig. 1

7. ENERGY EXCHANGE BETWEEN THERMAL NEUTRONS AND CRYSTAL LATTICES

A neutron of near thermal energy scattered in a crystal can lose energy by exciting lattice vibrations or can gain energy from the lattice vibrations. That is, it can be inelastically scattered with either emission or absorption of quanta of lattice energy called phonons. From the practical viewpoint this process is of interest because it constitutes the mechanism of thermalization of neutrons in a moderator. From a theoretical viewpoint it provides a means of investigating crystal lattice dynamics. The objective is to determine the energy spectrum of lattice vibrations. X-rays, which serve to some extent this purpose, have wave-lengths comparable to lattice dimensions but have much higher energy than the phonons. With neutrons it is possible to observe directly the energy exchange since neutrons of thermal energy have a wave-length of the order of an Ångstrom unit.

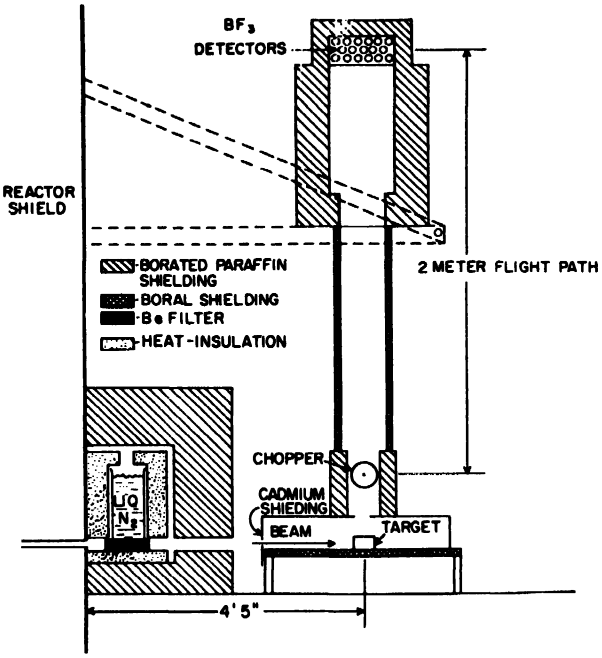

Figure 9. Apparatus for observation of the energy spectrum of Be filtered slow neutrons after scattering in a crystal lattice

One experimental approach to the problem is to introduce neutrons of essentially zero energy, then study the energy distribution of the scattered neutrons as a function of crystallographic direction. Apparatus set up for that purpose at Brookhaven Laboratory by Carter, Palevsky, and Hughes[24] is shown in Fig. 9. The reactor beam is filtered through fine grained Be to remove all neutrons except those of wave-length 4 Å and greater. Liquid nitrogen cooling of the filter increases transmission. Energy analysis of the beam scattered at right angles is accomplished by a chopper time-of-flight apparatus. Figure 10 shows the energy distribution of neutrons inelastically scattered in polycrystalline Be. As shown, the energy spectrum can be predicted theoretically by the Debye approximation and from the known constants of the crystal. Whereas the energy of the maximum of the distribution is in good quantitative agreement with the theoretically predicted one, the predicted double peak shows up only as a slight asymmetry of the peak. In order to obtain more detailed information about vibrational modes it is desirable to use a single crystal as scatterer, and such experiments are in progress with an Al single crystal. The energy peaks in the scattered beam show strong dependence on the orientation of the scatterer, as would be expected from the crystalline anisotropy. Rather detailed calculations have in fact been made by Squires[25] on the basis of a more detailed model than the Debye model for zero energy incident neutrons. These lead to the prediction of three energy surfaces in reciprocal space defining the possible energy absorption as a function of crystallographic direction. The right-angle scattering direction used is very useful for comparison with these predictions, since in that direction the effect of non-zero energy of the incident beam is very small. By measurement of the scattered beam energy peaks in various directions, one could determine the energy surfaces experimentally, and, to the extent to which this has been done, agreement with Squires' calculated peaks is satisfactory.

An alternative approach to measurement of lattice dynamics has been taken by Brockhouse[26] at the Chalk River Canadian Reactor. Rather than a zero energy beam, he has used a monochromatic beam in the much higher flux thermal energy range. This beam, obtained from a crystal spectrometer, is scattered from the crystal sample, and the scattered beam is energy analyzed by a second crystal spectrometer. A diagram of the apparatus used is shown in Fig. 11. In studies on the energy exchange through the coupling forces in paramagnetic crystals, he reports appreciable effect in Mn_2O_3 with transition temperature 80°K, but no observable effect in the more weakly coupled $MnSO_4$, with transition temperature 14°K.

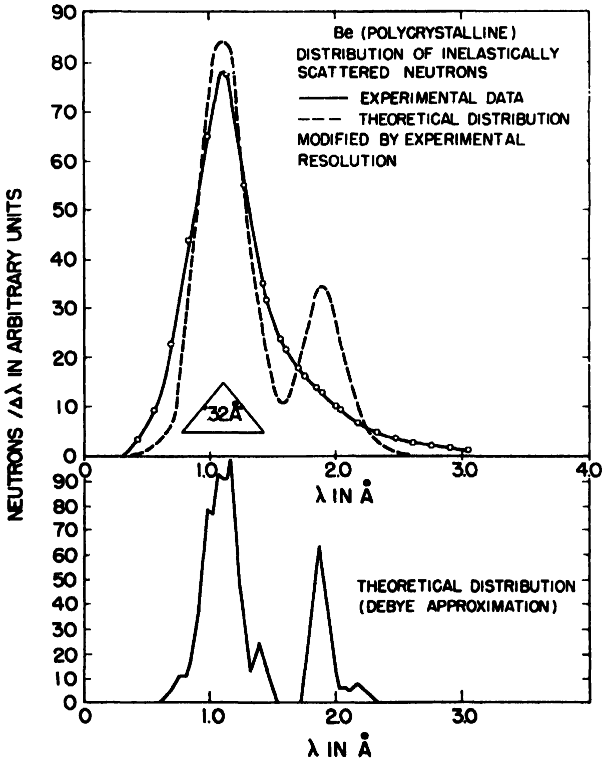

Figure 10. Wave-length spectrum of neutrons after scattering in polycrystalline Be, measured as shown in Fig. 9. Incident neutrons were beryllium filtered (λ > 4.4 Å)

8. SLOW NEUTRON TRANSMISSION STUDIES IN SOLIDS

In the thermal energy range, neutron scattering in solids depends in a rather complicated way on the crystal and grain structure. It is just this dependence in fact which enables one to investigate the crystal structure by neutron diffraction, as discussed in a previous section. Consequently most of the published data on total neutron cross-sections vs energy through the thermal range are strongly dependent on unknown details of the grain structure of the particular sample used and have little fundamental significance. This is true except in the cases where capture cross-section is large compared to scattering. At lower energies, however, when the neutron wave-length becomes greater than twice the largest lattice spacing, Bragg diffraction is no longer possible, and the crystal becomes relatively transparent. Neutron transmission studies in this simpler range lead to both nuclear and solid-state data of interest. The transparence of crystals in this range is in fact an aid in obtaining slow neutron beams for such experiments.

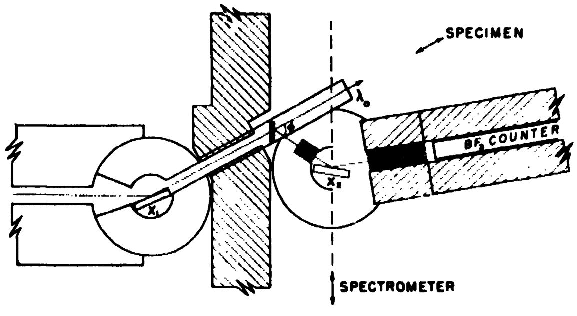

Figure 11. Crystal spectrometer arrangement at Chalk River, Canada, for study of energy change of monochromatic neutron beam of near-thermal energy in crystal lattices (courtesy B. N. Brockhouse)

Slow neutron beams may be obtained by several methods—crystal filters, crystal spectrometers, chopper time-of-flight instruments, mechanical velocity selectors or combinations of these. Passage of the neutron spectrum from a reactor through a crystalline filter in the shield causes the higher energies to be selectively scattered out, leaving in the transmitted beam only the long wave-length part of the Maxwellian distribution, which lies beyond the Bragg cut-off. With a Be filter this means λ > 4Å, E < 0.005 ev. For some purposes a filtered beam is sufficient, but further selection of a monochromatic beam can be accomplished by a crystal spectrometer or mechanical selector. Alternatively, the beam can be sorted into intervals by a chopper time-of-flight apparatus. A combination of filters and suitable crystal monochromators has been used by McReynolds[27] for transmission studies over the range λ = 3.6 to 9 Å, E = 0.006 to 0.001 ev. A diagram of the apparatus is shown in Fig. 12. A preliminary Pb filter attenuates fast and thermal neutrons and gamma rays. An external Be or BeO filter further attenuates neutrons up to 4.4 Å, which would otherwise appear as higher order diffracted beam from

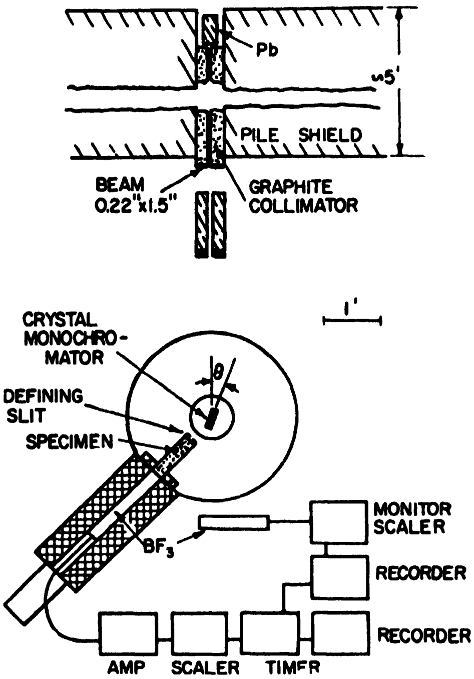

Figure 12. Arrangement of crystal spectrometer for studies of long wave-length neutrons (4–10 Å) through crystal lattices

the crystal. Selection of the monochromatic beam is then by diffraction from the (111) planes of an Fe_3O_4 crystal set at the appropriate angle for the desired energy. Further improvements by Antal, particularly the substitution of mica for Fe_3O_4, with different filter crystals, promises to extend the range to around 14 Å.

A recent application of long wave-length transmission studies is the measurement of imperfections in the crystal lattice. Attenuation of the neutron beam arises from three effects: (1) nuclear absorption, (2) inelastic scattering by lattice thermal vibrations, and (3) incoherent scattering, in which the atoms act individually as scatters. The three effects are separable, since the nuclear component depends linearly on wavelength but not on temperature, the inelastic component is temperature dependent, and the incoherent component depends on neither temperature nor wavelength. Neglecting for the moment the effects of spin and of random isotopic distribution, it may be said that the atoms in a perfect lattice cause no incoherent scattering. However, each atom displaced from its normal lattice site into an interstitial position scatters just as a single isolated atom. Similarly, a vacant lattice site in an otherwise perfect lattice has a scattering cross-section equal to that of the missing atom. Thus the difference in attenuation between a perfect and imperfect lattice, if the imperfections are only interstitials and vacancies, is a direct measure of the number of imperfections. Figure 13 shows the results of transmission measurements by Antal, Dienes, and Weiss[28] of the comparative transmissions of two graphite samples identical except that one had been subjected to fast neutron irradiation in the Brookhaven reactor of about 1.1 × 10^{20} neutrons/cm². Attenuation of the two samples can therefore be expected to be identical except for the effect of lattice damage by irradiation. As seen in the figure, transmission of the irradiated sample is decreased by a factor of 0.6, corresponding to a fraction 0.026 of displaced atoms. Since the carbon cross section is well known, this is an absolute figure and may be compared with the predictions of Seitz's theory, which gives a fraction 0.021. In view of the rather large uncertainty in calibration of the number and energy distribution of the bombarding fast neutrons, this agreement is satisfactory.

The effects on slow neutron transmission of inelastic scattering by lattice thermal vibrations have also been extensively investigated by Palevsky, Hughes and collaborators,[29] who used the slow chopper technique. The total inelastic scattering as thus measured is an integral quantity, including all directions and energies of scattering. It is therefore not subject to as detailed interpretation in terms of the lattice vibration spectrum as is the energy analysis of scattered neutrons, discussed in the preceding section. The experimentally measured inelastic cross-section as a function of crystal temperature and neutron wave-length can nevertheless be compared with approximate theoretical calculations based on the assumption of a Debye frequency spectrum. Measurements have been carried out on polycrystalline samples of Be, C, Mg, Al, Fe, Cu, Zr, Pb, and Bi. For a few of these cases the agreement between experiment and theory is good, but in most of the cases it is poor. Besides its interest in solid-state theory, measurement of the temperature-dependence of slow neutron scattering beyond the Bragg cut-off allows one to eliminate from the total cross-section that part which arises from thermal inelastic scattering, and thus to determine the nuclear capture cross-section.

9. FAST NEUTRON RADIATION DAMAGE

Although the most immediate interest in radiation damage is in its technological considerations, the controlled introduction of crystal lattice defects by nuclear particle bombardment offers an opportunity to

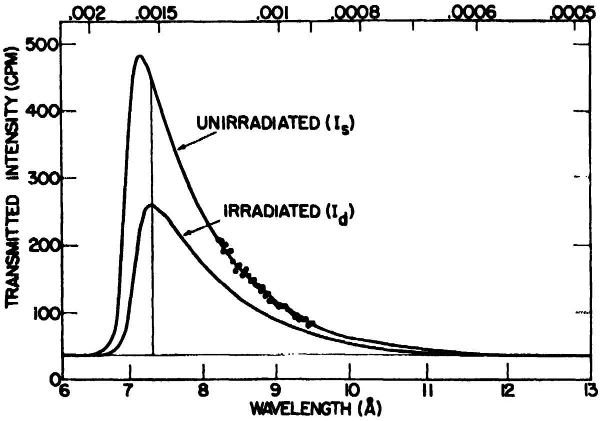

Figure 13. Decrease in slow neutron transmission of graphite by scattering from lattice defects created by fast neutron radiation damage in a reactor

gain further insight into fundamental processes in crystals. Radiation damage both from the standpoint of reactor materials and of solids in general is surveyed by a number of authors in Sessions 11B and 13B, (Vol. 7), and need not be further discussed here.

CONCLUSIONS

It may be concluded that besides the obvious technological applications of a research reactor, there remain a variety of problems in basic physics research to which it is applicable. Nuclear measurements of cross-sections and both (n,γ) and fission reactions can be expected to continue to be important for some time. Neutron diffraction and other solid-state applications including radiation damage constitute an increasingly large part of physics research with reactors, and can be expected ultimately to outweigh the nuclear applications.

REFERENCES

1. Snell, A. H., *Neutron Decay: The Problem and the Experiments*, Nucleonics 8, 3–13 (1951).
2. Robson, J. M., *The Radioactive Decay of the Neutron*, Phys. Rev. 83, 349–58 (1951).
3. Bloch, F., Nicodemus, D. and Staub, H. H., *A Quantitative Determination of the Magnetic Moment of the Neutron in Terms of Proton Magnetic Moment*, Phys. Rev. 74, 1025–45 (1948).
4. Ramsey, N. F., *A Molecular Beam Resonance Method With Separated Oscillating Fields*, Phys. Rev. 695–9 (1950).
5. Smith, J. H. and Ramsey, N. F., unpublished.
6. McReynolds, A. W., *Gravitational Acceleration of Neutrons*, Phys. Rev. 83, 172–3 (1951).
7. Havens, W. W., Rainwater, L. J. and Rabi, I. I., *Interaction of Neutrons with Electrons in Liquid Bismuth*, Phys. Rev. 82, 345 (1951).
8. Hughes, D. J., Harvey, J. A., Goldberg, M. D. and Stafne, Marilyn J., *The Neutron Electron Interaction*, Phys. Rev. 90, 497–8 (1953).
9. Motz, Henry, *Gamma-Ray Spectrum of* Cd^{113} (n,γ) Cd^{114}, Phys. Rev. 99 (1955).
10. Kinsey and Bartholomew, *Neutron Capture Gamma Rays from Cd*, Can. Jour. of Phys. 31, 1051 (1953).
11. Bernstein, S., Roberts, L. D., Stanford, C. P. and Dabbs, J. W. T., *Interaction of Polarized Neutrons with Polarized* Mn^{55} *Nuclei*, Phys. Rev. 94, 1243–1251 (1954).
12. Dabbs, J. W. T. and Roberts, L. D., *Polarization of* Mn^{55} *Nuclei-Cryogenic Aspects*, Phys. Rev. 95, 970–74 (1954).
13. Roberts, L. D., Bernstein, S., Dabbs, J. W. T. and Stanford, C. P., *Capture of Polarized Neutrons by Polarized* Sm^{149} *Nuclei*, Phys. Rev. 95, 105–10 (1954).
14. Rose, M. E., *On the Production of Nuclear Polarization*, Phys. Rev. 75, 213 (1949).
15. Shull, C. G., *Production of Highly Polarized Neutron Beams by Bragg Reflection from Ferromagnetic Crystals*, Phys. Rev. 81, 626 (1951).
16. Wollan, E. O. and Shull, C. G., *Neutron Diffraction Research in the United States*, Conference paper 579.
17. Shull, C. G. and Wollan, E. O., *Coherent Scattering Amplitudes as Determined by Neutron Diffraction*, Phys. Rev. 81 527–35 (1951).
18. Shull, C. G. and Smart, J. S., *Detection of Antiferromagnetism by Neutron Diffraction*, Phys. Rev. 76, 1256–7 (1949).
19. Corliss, L. M. and Hastings, J. M., *A Neutron Diffraction Study of Magnesium Ferrite*, Phys. Rev. 90, 1013–19 (1953).
20. Frazer, B. C., McKeown, Marilyn, and Pepinsky, Ray, *Neutron Diffraction Studies of Rochelle-Salt Single Crystals*, Phys. Rev. 94, 1435 (1954).
21. Shull, C. G., Strausser, W. A. and Wollan, E. O., *Neutron Diffraction by Paramagnetic and Antiferromagnetic Substances*, Phys. Rev. 83, 333–45 (1951).
22. McReynolds, A. W. and Riste, T., *Magnetic Neutron Diffraction from* Fe_3O_4, Phys. Rev. 95, 1161–67 (1954).
23. Wilkinson, M. K. and Shull, C. G., *Neutron Diffraction Observations on Fe at High Temperatures*, Phys. Rev. 94, 1439 (1954).
24. Carter, R. S., Hughes, D. J. and Palevsky, H., *Energy Distribution of Cold Neutrons Scattered by Lattice Vibrations*, Phys. Rev. 99 (A) (1955).
25. Squires, G. L., private communication.
26. Brockhouse, B. N., *Energy Distributions of Neutrons Scattered by Paramagnetic Substances*, submitted to Phys. Rev. (1955).
27. McReynolds, A. W., *Neutron Monochromator Crystals,* Fe_3O_4 *and Ge*, Phys. Rev. 88, 958 (1952).
28. Antal, J. J., Dienes, G. J. and Weiss, R. J., *Long Wave-Length Neutron Transmission as an Absolute Method for Determining the Concentration of Lattice Defects in Crystals*, submitted to Phys. Rev. (1955).
29. Palevsky, H., Hughes, D. J. and Zimmerman, R. L., *Inelastic Scattering of Cold Neutrons by the Lattice Vibrations of Crystalline Solids*, Phys. Rev. 99 (A) (1955).

Cross Sections of Atomic Nuclei for the (*n,p*) Reaction

By Z. Wilhelmi, Poland

The statistical theory of nuclear reactions has been in the crossfire of different types of experiments for many years. It emerges triumphantly from some experiments, showing agreement between the theoretical cross-sections, and the results of experiment;[1] sometimes, however, it conflicts with such experimental results, as it does for example, in the case of reactions produced by photons of average energy.[2] Finally, in several cases, the results of the measurements made by one author,[3] disagree with those obtained by another author.[4]

In view of the fact that this question is of a complex nature, it is necessary to gather a wealth of experimental material concerning new nuclear reactions, which not only would be a criterion for the statistical theory, but also would strengthen the experimental basis for the development of more perfected theoretical concepts.

Bearing these broad requirements in mind, this paper deals with the measurement of effective cross-sections for the (*n,p*) reaction and their interpretation on the basis of statistical theory. For these investigations, incidentally, use was made of the nuclei of elements which have a bearing on reactor design.

I. METHOD OF MEASUREMENT

In order to determine the cross section of nucleus $X_Z{}^A$ in the reaction:

$$X_Z{}^A(n,p)Y_{Z-1}{}^A \qquad (1)$$

it is necessary to know: (*a*) the intensity, I, of the neutron flux impinging on the sample of known content of isotope $X_Z{}^A$; (*b*) the number of nuclei, n, which react during a period of one second of irradiation.[1] The intensity, I, of the neutron beam, was determined by counting the proton tracks in a photographic emulsion. The number of nuclei, n, was determined from the number of β-radioactive nuclei produced by reaction (1); i.e., $Y_{Z-1}{}^A$.

Measurements were made in the following manner: we placed a ground sample of $X_Z{}^A$ in a ring-shaped container (Fig. 1); this chamber was rotated around the shield of the accelerator used as a source of fast neutrons with a known spectral distribution[5] by the (*d,n*) reaction; the energy of the neutrons was 750 kev. A photographic plate placed on a suitable holder was rotated with the container and served to measure the intensity of the neutron flux.

A rotating container was used because the neutron source could not be assumed to be a point source, as the design of the accelerator tube did not make it possible to have a highly concentrated beam of deuterons.

The measurement of neutron intensity with the aid of a photographic emulsion was done only once, namely for the determination of the (*n,p*) cross-section of Fe^{56}. For other isotopes, the cross-sections were determined relative to Fe^{56}. For this, the substance under investigation and an iron powder sample, which served as reference, were placed in separate sections of the container.

After neutron irradiation over a certain period of time during which the intensity was kept constant, the irradiated samples were transferred, in suitable standard trays, to Geiger counters and their activity measured. Analysis of the radioactive decay curves enabled us to single out the product of the reaction, $Y_{Z-1}{}^A$.

The question of corrections to account for backscattering and absorption of the electrons in thick irradiated samples; i.e., samples for which neglecting these phenomena might lead to significant errors, deserves special mention. If one wishes to know accurately the number of nuclei subject to the reaction under investigation (1) it is necessary to know what portion of the total number of β-particles emitted from nuclei $Y_{Z-1}{}^A$ in the direction of the Geiger counter actually reaches it. It is known that a portion of these electrons going in the direction of the counter window is absorbed by the mass of the sample itself, and does not reach the window. However, on the other hand, several β-particles which are moving in the direction opposite to the window are thrown back, thanks to backscattering, and enter the counter. The coefficient of electron absorption, and the coefficient of backscattering (which sometimes is simply ignored) are usually determined separately; afterwards, a correction is made utilizing a semi-empirical relationship between these quantities and the sample thickness.

Such a method is not very accurate. This is borne out, at the very least, by the large difference in results in measuring the coefficient of absorption obtained by different authors.[3,4]

We have therefore developed a method with which it is possible to determine, in one measurement on a thick sample, the effects both of the absorption and of the backscattering of electrons. Using this method, all assumptions regarding the nature of absorption and backscattering are unnecessary; especially in the case

---

Original language: Russian.

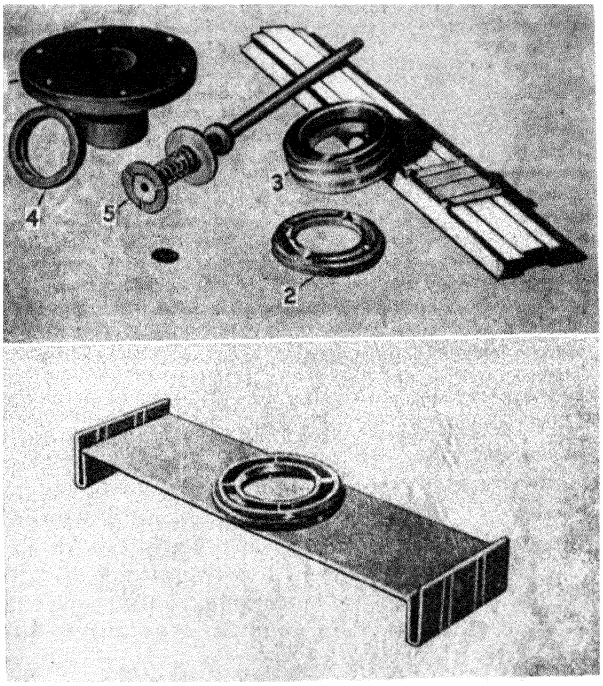

Figure 1

when the spectrum of the isotope being investigated is a complicated one, these assumptions could lead to serious errors, and, at any rate, would require very complicated calculations.

In our investigations, we prepared a thin sample (i.e., a sample with negligibly small absorption and backscattering) of the isotope $Y_{Z-1}{}^A$ which is yielded in sufficiently large quantity by some reaction [not necessarily (n,p)] with as good an efficiency as possible. The thin sample consisted of a thin layer applied to a thin cellophane base.

After measuring the activity a_1 of this thin sample, the radioactive material was thoroughly scraped or washed from it; it was then mixed with a powder consisting of the same material and in the same quantity as the sample irradiated during the cross-section investigation (for instance, iron powder). This mixture was placed on a standard tray on the counter, and its activity, a_2, was measured. The separately measured activity, a_3, of the tracks remaining on the cellophane base of the thin sample after scraping, permitted us to determine the per cent ratio of active material transferred from it to the thick sample. Of course, in view of the decrease in activity during the time required for the three measurements, the counts had to be corrected for the difference in time. a_1, a_2 and a_3 are the activities so corrected.

The quantity $$b = \frac{a_1 - a_3}{a_2} \qquad (2)$$

is the so-called "thick sample correction coefficient;" if one wishes to find the number of β-disintegrations taking place over a certain period of time in the thick sample, the number of counter pulses must be divided by the efficiency and multiplied by b.

It must be noted that the accuracy of this method depends on the activity of the thin sample, and therefore on the possibility of obtaining the given isotope in sufficiently large quantities and with a sufficiently high activity. In some cases, this entails great difficulties.

In these cases, in place of the given isotope $Y_{Z-1}{}^A$, it is possible to use for the thin sample another isotope readily available in considerably larger quantities; however, this may be done only on the condition that the "replacement isotope" have exactly the same spectrum as the isotope $Y_{Z-1}{}^A$. In the described measurements, we used our "replacement method" with Ge^{75}; it was replaced by N^{13}, obtained by the reaction $C^{12}(d,n)N^{13}$ in a concentration a thousand times higher than Ge^{75}.

It should be pointed out that when the half-life of isotope $Y_{Z-1}{}^A$ was very short (for instance, of the order of some seconds), we used photographic detection; individual counter pulses flashed a neon lamp, and the flashes were recorded on a film moving at constant speed. Another lamp, fed by a stabilized frequency generator, recorded a time scale on the same film. This is the method we used in measuring the cross-sections for the new reaction discovered by us $Sn^{116}(n,p)In^{116}$.[6]

II. RESULTS

Our measurements of effective cross-sections include the (n,p) reactions in Table I.

Table I

1. $Mg^{25}(n,p)Na^{25}$
2. $Al^{27}(n,p)Mg^{27}$
3. $Cr^{52}(n,p)V^{52}$
4. $Fe^{56}(n,p)Mn^{56}$
5. $As^{75}(n,p)Ge^{75}$
6. $Sn^{116}(n,p)In^{116}$
7. $Sn^{118}(n,p)In^{118}$

The cross-section of the reaction $Fe^{56}(n,p)Mn^{56}$ was determined on the basis of the cross section of hydrogen for neutron scattering, which is known to an accuracy of about 5%.[7,8,9]

For these measurements, we used an Ilford C 250 photographic plate placed in the rotating container, as was described above (Fig. 1). It turned out that it is convenient to arrange this plate in such a way that the neutrons impinge on the surface of the emulsion. Taking into account a whole series of corrections, it was found that the effective cross section of Fe^{56} for the (n,p) reaction is:

$$\sigma_{Fe} = 3.1 \times 10^{-26}\ \text{cm}^2 \pm 12\%$$

For the remainder of the reactions in Table I, the effective cross sections were measured using the nucleus of Fe^{56} as a standard of comparison.

The results of the measurements are shown in Table II.

Table II also contains the results of theoretical calculations based on the statistical theory of nuclear reactions of Weisskopf and Ewing.[10,11]

According to the statistical theory, the effective cross-section of a nucleus to the reaction (n,p) may be determined from the following equation:

Table II

Nucleus	*Z*	*N*	*Reaction threshold used in calculations, in Mev*	*Experimental cross-section of (n,p) reaction in millibarns*	*Error in measurement in %*	*Theoretical cross-section of (n,p) reaction in millibarns*
Mg^{25}	12	13	2.95	62	12	53.9
Al^{26}	13	14	1.83	42	8	136
Cr^{52}	24	28	2.73	20	10	29.2
Fe^{56}	26	30	2.92	31	12	13.4
As^{75}	33	42	0.42	5.2	9	14.3
Sn^{116}	50	66	2.17	1.6	18	0.12
Sn^{118}	50	68	0.72	11.3	18	0.75

$$\sigma(n,p) = \sigma_c(E_n) \frac{F_p(E_n - T_{n,p})}{F_n(E_n) + F_p(E_n - T_{n,p}) + F_\alpha(E_n - T_{n,\alpha}) + \cdots} \tag{3}$$

where F_p, F_n, F_α, etc., give the probability of emission of proton, neutron, α-particle, etc. from the compound nucleus.

$\sigma(E_n)$ is the effective cross-section of the primary nucleus for the formation of the compound nucleus upon collision with a neutron with energy E_n. $T_{n,p}$ is the threshold of the (n,p) reaction which, according to the theory of the compound nucleus, is equal to the difference in binding energy of a proton and a neutron in the compound nucleus; $T_{n,\alpha}$ is the threshold of the (n,α) reaction.

For high energy neutrons, the de Broglie wave length of which is significantly smaller than $2\pi R$ (where R is the radius of the nucleus, and σ is equal to the geometric cross section of the nucleus, πR^2), the function F_p, F_n, F_α or, in the general case, F_β is given by the following equation:

$$F_\beta(E_n - T_{n\beta}) = \frac{2M}{\hbar^2} \int_0^{E_n - T_n} E_\beta \sigma_c(E_\beta) W_y(E_n - T_{n\beta} - E_\beta)\, dE \tag{4}$$

where E_β is the energy of the proton (neutron, α-particle, etc.) leaving the compound nucleus; M_β is the mass of the proton (neutron, α-particle, etc.); σ_c (E) is the cross-section for the formation of a compound nucleus by collision between a proton (neutron, α-particle, etc.) of energy E_β, and the nucleus which is the end product of the (n,p), (n,n), (n,α) etc., reaction, excited to an energy $E_n - T_{n\beta} - E_\beta$; W_y is the density of levels in the final nucleus.

The theoretical cross-sections in Table II, were calculated on the assumption that the geometric radius of the nucleus is given by

$$R = r_0 \cdot A^{1/3} \tag{5}$$

where A is the mass number and $r_0 = 1.3 \times 10^{-13}$ cm. The ratio between the level density W_y, and the excitation energy E, was calculated according to statistical theory, as follows:

$$W_y/E = ce^2 \sqrt{aE} \tag{6}$$

where a is the constant relating the excitation energy E to the temperature of the nucleus:

$$E = a \cdot \theta^2 \tag{7}$$

This constant was used by us in calculations in accordance with Weisskopf.[10]

We determined the functions F_n and F_p for each of the investigated isotopes; and, on that basis, we calculated $\sigma_{n,p}$ for different energies. As an illustration we give $\sigma_{n,p}(E_n)$ for Fe^{56}, Cr^{52} and Sn^{116} (Fig. 2).

In view of the fact that, in our measurements, we determined the average cross-sections of the neutron spectrum all the way up to 15 Mev, we also had to average the theoretical cross-sections for purposes of comparison. The results of these calculations are shown in Table II; according to statistical theory, theoretical cross sections of double-even nuclei (Z and N-even) were multiplied by two.[11]

A comparison of experimental and theoretical values shown in Table II indicates that, although the order of magnitude and general nature of changes of the investigated cross-sections $\sigma_{n,p}$ with the atomic number Z is in accordance with the predictions of statistical theory, there still are large deviations in individual cases. Thus, we see that the cross-sections of Sn^{116} and Fe^{56} actually are larger than the theoretical values, whereas As,[75] Cr^{52} and Al^{27} have a cross-section smaller than expected. This last case is difficult to handle with the statistical theory of nuclear reactions in view of the small number of neutrons. As to the others, it is necessary to decide whether these deviations violate statistical theory or whether they are compatible with it. Let us review, briefly, the possible reasons for the lack of agreement:

1. First of all, it must be noted that the theoretical cross section depends to a very great extent on the assumed geometric cross-section, and therefore on r_0 in Equation 5. Unfortunately, however, in many

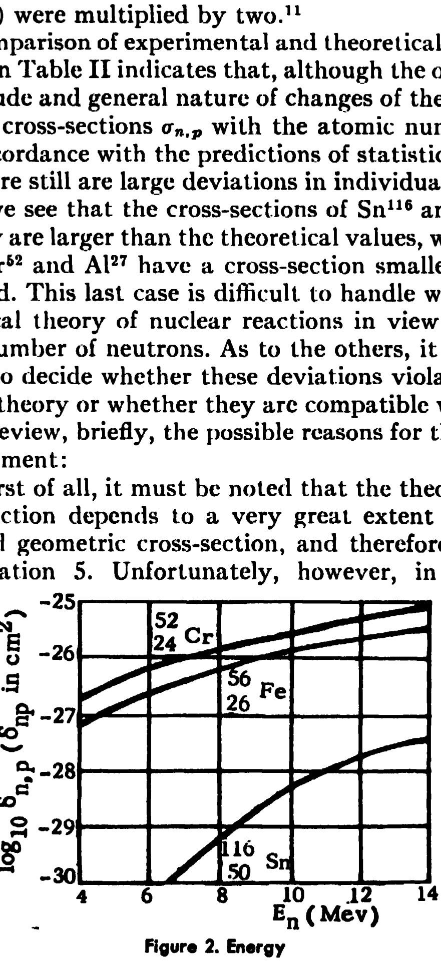

Figure 2. Energy

papers on the experimental determination of the radius of a nucleus (such as references 12 and 13) different values of r_0 are given, depending on the method of measurement and on the particular element involved. From this, there arises some possibility of incorrect evaluation of the (n,p) cross section which, as our calculations have shown, is very sensitive to the choice of r_0.

As an illustration, we give the results of computations of $\sigma_{n,p}(E_n)$ performed for the nucleus Sn^{116} for different values of r_0, viz., $r_0 = 1.3 \times 10^{-13}$ cm and $r_0 = 1.5 \times 10^{-13}$ cm (curves 1 and 2 in Fig. 3) at equal nuclear temperatures. It turns out that $\sigma_{n,p}$ with $r_0 = 1.5 \times 10^{-13}$ is 3–4 times larger than the corresponding value for $r_0 = 1.3 \times 10^{-13}$ cm. Because of this, assuming that for Sn^{116} the coefficient $r_0 = 1.5 \times 10^{-13}$ (which, by the way, is in accordance with the results of Amaldi's work on the scattering of 14 Mev neutrons,[14] thus work whose conditions were close to ours), we obtain a theoretical average cross-section for the spectrum used of 0.33 mb, considerably closer to the experimental value. Proceeding in a similar fashion in the case of Fe^{56} using the larger value of r_0 we obtain results in conformity with experiment.

Things are different for Cr^{52} and As^{75}. Since the value of $r_0 = 1.3 \times 10^{-13}$ cm, which was assumed in the calculations, is probably the smallest among measured r_0 values, the theoretical values of σ will not be reduced but rather increased. Thus, the differences between the experimental and theoretical values of σ for Cr^{52} and As^{75} must be sought elsewhere, and not in the choice of r_0.

2. Apart from r_0, a large influence upon the theoretical value of σ is exerted by the assumptions made with regard to nuclear temperature. To establish this dependence, Fig. 3 shows, in curve 3, the effective cross-section calculated for the same nucleus radius as curve 2, $r_0 = 1.5 \times 10^{-13}$, but at a temperature 8% lower. It turns out that even such an insignificant decrease in the assumed nuclear temperature causes a considerable decrease of $\sigma_{n,p}$. The average cross-section of Sn^{116} over the range 3–15 Mev became 3.5 times smaller (from 0.32 mb to 0.092 mb). A suitable temperature correction with regard to nuclei Cr^{52} and As^{75} could, of course, make their theoretical effective cross-sections equal to the observed cross-sections. However, this would cause a change in the cross-section of other reactions such as $(n,2n)$, etc., and also a change in the energy spectrum of the reaction products. These investigations must be carried out as broadly as possible. However, since at present there is not enough experimental material, we cannot offer proposals for changing the present assumptions about the temperature of nuclei. We can confidently state, however, that the very need to make such a change in the heretofore assumed temperatures with regard to only a few nuclei, would throw doubt on the power of statistical theory, and it would at the very least indicate that, in addition to the mechanism by means of which this theory explains nuclear behavior, there exist other processes as well; that even at such low neutron exciting energies as were used in our measurements, these do affect the course of the reaction.

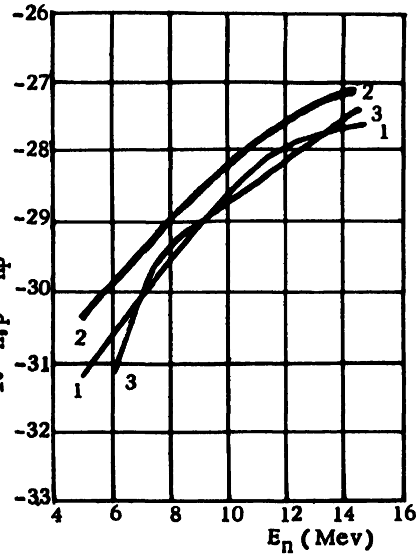

Figure 3. Energy

3. Finally, we must turn our attention to the relation between $\sigma_{n,p}$ and the threshold of reaction, $T_{n,p}$, since disagreements between the results of experiments and theory may partly be explained by an insufficient knowledge of this threshold. Its value is not known from independent experiments; it must be inferred. In the case of light nuclei, the mass of which is known with great accuracy (to the sixth and even to the seventh decimal),[15] in calculating $T_{n,p}$ we used the mass balance, while for heavy nuclei we determined the threshold on the basis of product nucleus disintegration. Here we utilized the fact that the nuclei appearing as the product of the (n,p) reaction are as a rule β-emitters, and that their disintegration, therefore, leads back to the primary nucleus.

$$X_Z{}^A(n,p)Y_{Z-1}{}^A \xrightarrow{\beta^-} X_Z{}^A \tag{8}$$

It is easily noted that, as a result of this, the threshold of the (n,p) reaction is:

$$T_{n,p} = E_x + m_{\mathrm{H}} - m_n \tag{9}$$

where E_x is the energy of disintegration, m_{H} is the mass of hydrogen atom, and m_n the mass of a neutron.

In this way, we determined the thresholds for Cr^{52}, Fe^{56}, As^{75}, and Sn^{116} as accurately as is permitted by the accuracy of measuring E. In the case of the Sn^{118} isotope which, at the present time, has had a very short history since observations on it took place only in the (γ,n) reaction[16] and the (n,p) reaction,[6] the energy of the γ-photon is altogether unknown. In view of this we were only able to determine the lower limit of the threshold (assuming the photon energy is zero) and so the corresponding upper limit of the cross-section. For this example we performed observations on the effect of the threshold height on cross-section. Assuming different values of $T_{n,p}$ (0, 1, 2, 3, 4 Mev) it turned out that this influence is tremendous,

Table III

E_n	$\sigma_{n,p}$ for $T_{n,p}$ (in Mev) = 0	1	2	3	4
6 Mev	6.95×10^{-29}	4.30×10^{-30}	1.20×10^{-32}		
8 Mev	1.94×10^{-28}	3.63×10^{-29}	6.2×10^{-30}	3.74×10^{-31}	1.07×10^{-33}
10 Mev	6.25×10^{-28}	1.17×10^{-28}	2.30×10^{-29}	4.25×10^{-30}	7.20×10^{-31}
14 Mev	7.05×10^{-27}	2.14×10^{-27}	3.60×10^{-28}	7.40×10^{-29}	1.62×10^{-30}
Average for 3 to 15 Mev	1.83×10^{-27}	4.5×10^{-28}	7.35×10^{-29}	1.66×10^{-29}	4.70×10^{-30}

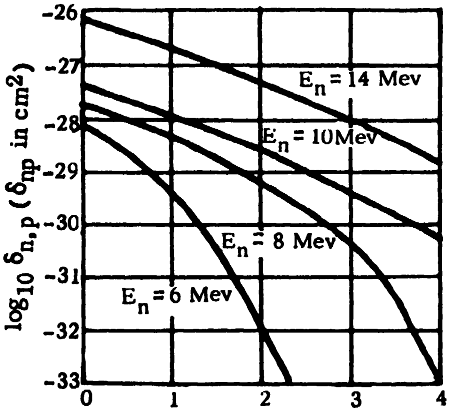

Figure 4. Threshold of reaction (n,p), in Mev

(Table III, Fig. 4). Thus we see, for instance, that increasing the threshold energy from 3 Mev to 3.5 Mev, i.e., by 17%, reduces the effective cross-section six-fold.

From this, it becomes obvious how important it is to know the disintegration energy for calculating $\sigma_{n,p}$. It is possible that the reason for disagreement between experiment and predictions of the statistical theory in the case of As^{76} and Cr^{52} is the poor evaluation of E_x. Calculating $T_{n,p}$ for As^{76} we were basing ourselves on the work of McGowan and others[17] who did not detect radiations of Ge^{76} which was the product of the (n,p) reaction. In the earlier work of Seaborg and others,[18] the presence of γ-rays is mentioned in the spectrum of this isotope, although their energy is not given. And so, if Ge^{76} actually does radiate γ-photons, in accordance with Seaborg's observations, then its disintegration energy E_x would be larger than the one which we assumed for our calculation in accordance with McGowan's work, the threshold energy would be higher, and the theoretical cross-section closer to the cross-section observed.

With regard to the $\sigma_{n,p}$ cross-section of tin, we should mention that no special peculiarities appeared here in connection with the magic atomic number $Z = 50$; the cross-section for the (n,p) reaction did not turn out to be smaller than that expected on the basis of the statistical theory. However, here one must take into account the fact that the theoretical cross-section depends to a considerable extent on the threshold energy $T_{n,p}$, and therefore on the binding energy of nucleons in the compound nucleus, since, the greater the proton binding energy, the higher the reaction threshold. Since nuclei with a magic number have an especially large proton binding energy, applying the experimental value of $T_{n,p}$ to the calculation of $\sigma_{n,p}$ we take into account, to some extent, the "magic" character of the nucleus. A more thorough solution of this problem would require comparing the measured cross-section of tin with cross-sections of nuclei whose Z is close to 50 (especially with the cross-section of antimony 1-50), as well as similar investigations of cross-sections of nuclei with other magic atomic numbers together with their neighbors.

REFERENCES

1. Temmer, G. M., Phys. Rev. 76, 424, (1949).
2. Hirzel, O. H. and Wäffler, G. H. P. A. 20, 373, (1949).
3. Wäffler, G., H. P. A., 23, 248, (1950).
4. Cohen, B. L., Phys. Rev. 81, 184, (1951).
5. Staub, H. and Stephens, W. E., Phys. Rev. *55* 845 (1949).
6. Wilhelmi, Z., Brusz, R. and Dabrowski, C., Bul. Acad. Pol. Sc. Cl. III, Vol. 1, 105, (1953).
7. Lampi, E. E., Freier, G. D. and Williams, J. H., Phys. Rev. 80, 853, (1950).
8. Sleator, W., Phys. Rev. 72, 207, (1947).
9. Staub, H. and Stephens, W. E., Phys. Rev. *55*, 845, (1949).
10. Weisskopf, V. F. and Ewing, D. H., Phys. Rev. 57, 472. (1940).
11. Blatt, J. M. and Weisskopf, V. F., *Theoretical Nuclear Physics*, John Wiley, 1952.
12. Feshbach, H. and Weisskopf, V. F., Phys. Rev. 76, 1550 (1945).
13. Blaser, J. P., Boehm, F., Marmier, P. and Peaslee, D. C., H. P. H. 24, 33, (1951).
14. Amaldi, E., Bocciarelli, D., Cacciapute, C. and Trabacchi, G., Nuovo Cim., 3, 203 (1946).
15. Dzelepow, B. C. and Zyrienowa, L. H., Y. H., XLVIII, 465 (1949).
16. Duffield, R. B. and Knight, J. D., Phys. Rev. 75. 1967 (1949).
17. McGowan, D. A., Woodward, L. L. and Pool, M. L., Phys. Rev. 74, 1311, (1948).
18. Seaborg, G. T., Livingood, J. J. and Friedlander, F., Phys. Rev. 59, 320, (1941).

The Energy Eigenvalues for a Spherical Well with an Exponentially Diffuse Boundary*

By Alex E. S. Green,† and Kiuck Lee,†‡ Republic of Korea

ABSTRACT

The discrete energy eigenvalues of a spherical well with an exponentially diffuse boundary are obtained to a good approximation for a range of well parameters of interest in nuclear physics. The method used involves replacing the centrifugal energy in the exponentially diffuse region by an approximate expression which leads to analytic solutions of the wave equation. The matching of the internal and external wave functions is then accomplished by the use of specially prepared graphs and tables. The eigenvalues and eigenfunctions are thought to be of interest in connection with studies of the independent particle model of the nucleus.

1. INTRODUCTION

A number of recent studies have stimulated interest in the problem of a single particle in a central field with a diffuse boundary. While most of this interest has been in connection with the positive energy states of the continuum, nevertheless the bound states are also of considerable importance. In this paper an approximate method is developed which appears to be adequate for the range of well parameters encountered in nuclear physics.

The solution of the square spherical well eigenvalue problem is an essential preliminary phase of the approximate method of solution of the diffuse boundary problem. Accordingly, this older problem, which has been solved earlier in the literature,[1] will be considered briefly first.

2. EIGENVALUES FOR THE SQUARE SPHERICAL WELL

The radial equation for the lth state of orbital angular momentum for a central field characterized by the potential $V(r)$ may be placed in the form

$$d^2G/dr^2 + (2m/\hbar^2)[W - V(r) - \hbar^2 l(l+1)/2mr^2]G = 0 \tag{1}$$

where $G = rR$ and R is the radial wave function. For the study of the spherical well of depth V_o and radius a it is convenient to let a serve as a unit of length, $E_o = \hbar^2/2ma^2$ serve as a unit of energy and to define the dimensionless parameters

$$\epsilon_w{}^2 = -W/E_o \tag{2}$$

$$\epsilon_o{}^2 = V_o/E_o \tag{3}$$

and

$$\epsilon'^2 = \epsilon_w{}^2 \tag{4}$$

Letting $\rho = r/a$, the radial wave equation becomes

$$\frac{d^2G}{d\rho^2} + \left[\epsilon'^2 - \frac{l(l+1)}{2}\right]G = 0 \qquad \rho \leq 1 \tag{5}$$

and

$$\frac{d^2G}{d\rho^2} - \left[\epsilon_w{}^2 + \frac{l(l+1)}{2}\right] = 0 \qquad \rho \geq 1 \tag{6}$$

The internal solution which is well behaved at $\rho = 0$ is

$$G_i = A_i\rho^{1/2}J_{l+1/2}(\epsilon'\rho) \tag{7}$$

where J denotes the usual Bessel function and A denotes a normalization constant. The external solution which is well behaved as $\rho \rightarrow \infty$ may be expressed in terms of Hankel functions of imaginary argument also called modified Hankel functions or Basset functions. Denoting these functions by $K_{l+1/2}$ the external solution may be written as

$$G_e = A_e\rho^{1/2}K_{l+1/2}(\epsilon_w\rho) \tag{8}$$

The ϵ_w eigenvalues are obtained without consideration of the normalization constants by imposing the requirement that at the boundary, $\rho = 1$

$$-\frac{1}{G_i}\frac{dG_i}{d\rho} = -\frac{1}{G_e}\frac{dG_e}{d\rho} \qquad \text{or} \qquad I_l(\epsilon') = E_l(\epsilon_w) \tag{9}$$

where $I_l(\epsilon')$ and $E_l(\epsilon_w)$ are defined as the negatives of the logarithmic derivatives of the internal and external radial functions.

To facilitate the solution of these transcendental equations subject to the condition imposed by Equation 4, tables and graphs of I_l and E_l are exceedingly helpful. These may be compiled using

$$I_l(\epsilon') = -\frac{1}{G_i}\frac{dG_i}{d\rho}\bigg|_{\rho=1} = -\frac{\tfrac{1}{2}J_{l+1/2}(\epsilon')}{J_{l+1/2}(G')} \tag{10}$$

Using the familiar recurrence relations for Bessel functions it follows that readily that

---

* This investigation was supported by grants from the US Atomic Energy Commission and Florida State University Research Council.

† Department of Physics, the Florida State University, Tallahassee, Florida, USA.

‡ On leave from the Seoul University, Seoul, Korea.

$$I_l(\epsilon') = \frac{\epsilon' J_{l+3/2}(\epsilon')}{J_{l+1/2}(\epsilon')} - (l+1) \tag{11}$$

and

$$I_l(\epsilon') = l - \frac{\epsilon' J_{l-1/2}(\epsilon')}{J_{l+1/2}(\epsilon')} \tag{12}$$

Using these equations, these functions may be calculated for integral values of l by the use of tables of half-integral Bessel functions or tables of spherical Bessel functions (since ratios of Bessel functions are involved). Alternatively I_l values may be generated for various orders by means of the recurrence relationship

$$I_l(x) = l - \frac{x^2}{I_{l+1} + l} \tag{13}$$

providing I_l values for orders between $-\frac{1}{2}$ and $\frac{1}{2}$ are first calculated using tables of elementary functions. The use of I_l functions of nonintegral order will arise in the next section.

Figure 1 contains graphs in which the ordinates represent the values of I_l at the abscissas corresponding to the square of the arguments. Such a graph will prove helpful in connection with the problem in the next section.

Using the recurrence relationships for modified Bessel functions, the external function E_l can readily be shown to satisfy

$$E_l(\epsilon_w) = \frac{1}{G_e}\frac{dG_e}{d\rho}\bigg|_{\rho=1} = -(l+1) + \epsilon_w \frac{K_{l+3/2}(\epsilon_w)}{K_{l+1/2}(\epsilon_w)} \tag{14}$$

and

$$E_l(\epsilon_w) = l + \frac{\epsilon_w^2}{E_{l+1} + l} \tag{15}$$

This latter equation in conjunction with

$$E_0(\epsilon_w) = \epsilon_w \tag{16}$$

may be used to generate the external functions of integral order.

For the application of the square well eigenvalue to nuclear physics a functional relationship between ϵ_w^2 and ϵ_0^2 for various states is desired. These functions can now readily be generated by means of Figs. 1 and 2 in the following way: (1) for a given l chose ϵ_w^2 and go to Fig. 2 to find $E_l(\epsilon_w)$; (2) read the ϵ'^2 values corresponding to $I_l(\epsilon') = E_l(\epsilon_w)$ from Fig. 1; (3) calculate ϵ_0^2 using Equation 7. The process is then repeated for a larger ϵ_w^2 until the entire desired range of ϵ_0^2 is covered. For a given ϵ_w^2 and hence $E_l(\epsilon_w)$ there are usually several ϵ'^2 roots within the range of ϵ_0^2 values of interest. These higher roots correspond to the higher vibrational states for a given l.

Figure 3 contains the results of the work with the square well potential. The form of presentation of the eigenvalues follows that of Moskowski[5] who has prepared a similar graph for a somewhat narrower range of the well range parameter. Essentially Fig. 3 represents the energy eigenvalue measured relative to the bottom of the well. For a given state this parameter has a far smaller range of variation as ϵ_0^2 is changed than ϵ_w^2 which corresponds to the actual energy. Furthermore, these ϵ'^2 values go over to the results of the infinite spherical well as ϵ_0^2 goes to infinity. The ϵ'^2 eigenvalues for the infinite spherical well case are obtained simply by imposing the requirement that

$$J_{l+1/2}(\epsilon') = 0 \tag{17}$$

These ϵ'^2 eigenvalues for the infinite case results are also shown in Fig. 3. Since the range of ϵ_0^2 values of interest in nuclear physics certainly does not exceed 200, the large differences between the finite and infinite results are quite noteworthy. It clearly points to the fact that results based upon either the spherical or cubic box approximations should be treated with great care in application to nuclear physics.

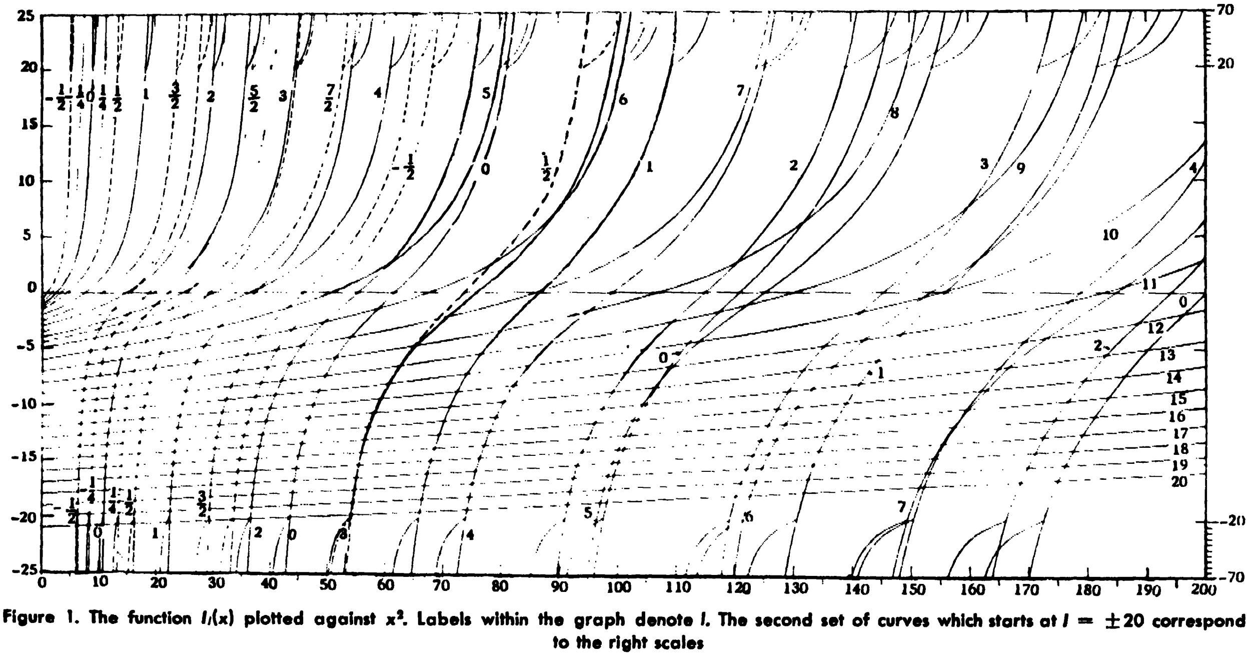

Figure 1. The function $I_l(x)$ plotted against x^2. Labels within the graph denote l. The second set of curves which starts at $l = \pm 20$ corresponds to the right scales

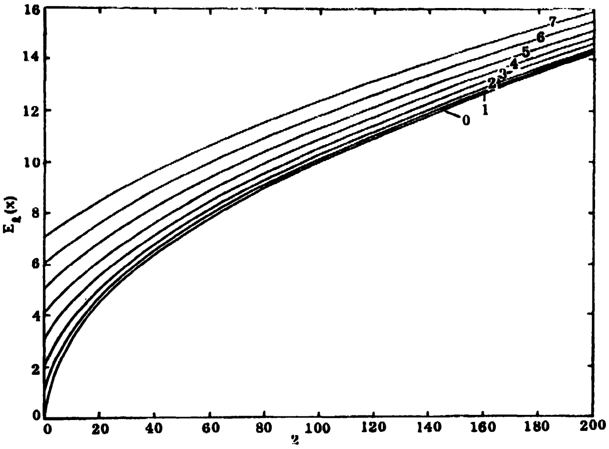

Figure 2. The function $E_l(x)$ plotted against x^2. Labels within the graph denote l

The results described here are naturally limited in accuracy by virtue of the graphical method employed. However, for the most part the accuracy obtained is more than is necessary at the present stage of nuclear physics. However, should the occasion arise, the results for the finite square well can be refined considerably by the direct use of a table of $E_l(\epsilon_w)$ and a table of spherical Bessel function.[6] Accordingly we may write Equation 9 in the form

$$\frac{\epsilon' J'_{l+\frac{1}{2}}(\epsilon')}{J_{l+\frac{1}{2}}(\epsilon')} = l + 1 + E_l(\epsilon_w) \tag{18}$$

Using the graphical results to locate the appropriate ϵ' neighborhood it is relatively simple to refine the ϵ' root (for a chosen ϵ_w) to four or even five significant figures by careful interpolation. Should the need arise, these methods could probably be programmed into digital computer for still more accurate results.

3. SPHERICAL WELL WITH AN EXPONENTIALLY DIFFUSE BOUNDARY

In this section, a continuous central potential is assumed which changes at $r = a$ from a constant $-V_0$ to

$$V(r) = -V_0 \exp\left(-\frac{r-a}{\delta a}\right) \qquad r > a \tag{19}$$

The dimensionless parameter δ characterizes the "shortness" of the exponential "tail." The case $\delta = 0$ is simply the case discussed in the previous section. The form of the interior radial wave equation and its solutions are of course unaltered from those developed in the previous section; however, the dimensionless radial equation for $\rho > 1$ in this case is

$$\frac{d^2G}{d\rho^2} + \left[\epsilon_0^2 \exp\left(-\frac{\rho-1}{\delta}\right) - l\left(\frac{l+1}{\rho^2}\right) - \epsilon_w^2\right] G = 0 \tag{20}$$

Because of the presence of both the exponential and ρ^{-2} terms Equation 20 does not have any analytical solutions, nor is any transformation known which will reduce it to a differential equation with analytical solutions. It is, however, known that for s states, i.e., when the ρ^{-2} term vanishes, Equation 20 can be transformed into Bessel's equation.[7] One approximate procedure which has been used[8] to overcome the difficulty for other than s states is equivalent to replacing ρ^{-2} by 1. The centrifugal energy can then be taken together with ϵ_w^2 and solutions can be obtained in terms of Bessel functions. This approximation, however, is fairly crude and the chief concern here shall be to improve upon it. The improvement considered here is based upon the assumption that

$$\frac{1}{\rho^2} \approx \alpha^2 + (1 - \alpha^2) \exp\left(-\frac{\rho - 1}{\delta}\right) \tag{21}$$

where the constants α^2 are chosen to accomplish the best match of the function on the right to the function on the left over the external region of importance. Thus, the "centrifugal" energy in the external region is absorbed into the exponential tail and the total energy. The external radial wave equation now becomes

$$4\delta^2 \frac{d^2G}{d\rho^2} + (k^2 e^{-\frac{\rho-1}{\delta}} - n^2)G = 0 \tag{22}$$

where

$$k^2 = 4\delta^2[\epsilon_0^2 - l(l+1)(1-\alpha^2)] \tag{23}$$

$$n^2 = 4\delta^2[\epsilon_w^2 + l(l+1)\alpha^2] \tag{24}$$

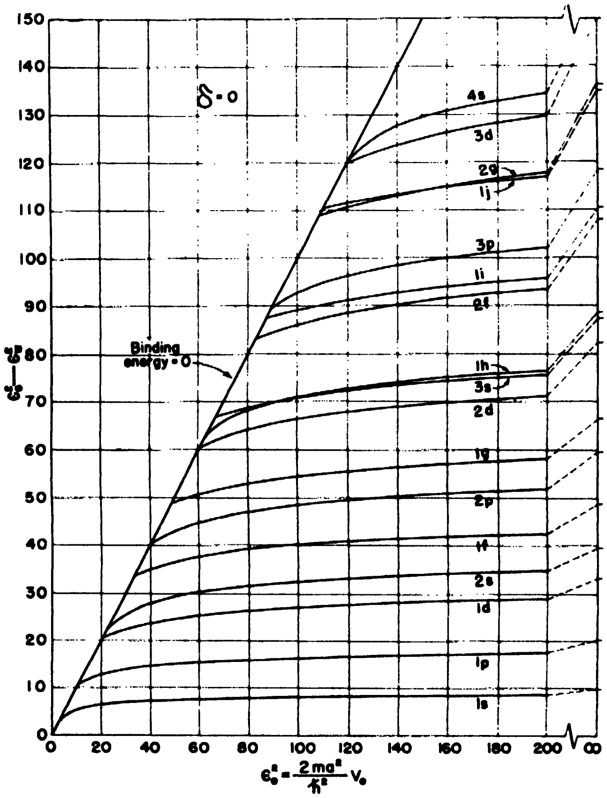

Figure 3. Energy eigenvalues for the square spherical well (i.e., $\delta = 0$). The right scale gives the infinite spherical well eigenvalues

Letting

$$x = \exp((1-\rho)/2\delta) \tag{25}$$

the radial equation becomes

$$x^2G'' + xG' + (k^2x^2 - n^2)G = 0 \tag{26}$$

where the prime here denotes differentiation relative to x. The solution of this equation which is well behaved as $\rho \rightarrow \infty$, i.e., as $x \rightarrow 0$ is

$$G_e = A_e J_n(kx) = A_e J_n\{k \exp[(1-\rho)/2\delta]\} \tag{27}$$

The negative of the logarithmic derivative of the exterior function at $\rho = 1$ is thus

$$\begin{aligned} -G_e'/G_e &= kJ_n'(k)/2\delta J_n(k) \\ &= \tfrac{1}{2}[n - kJ_{n+1}(k)/J_n(k)] \end{aligned} \tag{28}$$

Introducing $\nu = n - \frac{1}{2}$, the negative of the external logarithmic derivative takes the form

$$E_\nu(k,\delta) = -I_\nu(k)/2\delta - 1/4\delta \tag{29}$$

where $I_\nu(k)$ is precisely the function introduced in Equation 9. The eigenvalue equation for the present case thus becomes

$$I_l(\epsilon') = -[I_\nu(k)/2\delta] - (1/4\delta) \tag{30}$$

The parameters involved in this equation are subject to the requirements imposed by Equations 4, 23 and 24. These may be combined into

$$\epsilon'^2 = [k^2 - (\nu + \tfrac{1}{2})^2]/4\delta^2 + l(l+1) \tag{31}$$

For a given δ, l, and k^2, Equations 30 and 31 may be regarded as two simultaneous equations for the determination of ϵ' and ν. Actually, for the application to which these solutions have been applied, δ and l are first chosen in accord with the states under study and ν is taken in accord with the orders of tabulated or graphed I functions. Then, Equations 30 and 31 are solved simultaneously for ϵ'^2 and k^2. Since ν^2 fixes ϵ_w^2, and ϵ'^2 in conjunction with ϵ_w^2 determines ϵ_0^2, it is possible to generate the curves relating ϵ'^2 to ϵ_0^2 throughout the range of interest.

For the purposes of solving Equations 30 and 31 for ϵ'^2 and k^2, the graph of the values of I functions may be utilized in the following way. According to Equation 31, ϵ'^2 is a linear function of k^2 with the slope $(1/4\delta^2)$. If a compressed scale is prepared such that one unit on the ϵ'^2 scale corresponds to $(1/4\delta^2)$ units of ϵ'^2 on the compressed scale, then for chosen values of ν and l the compressed scale may be positioned so that any ϵ'^2 on the compressed scale corresponds directly to k^2 on the basic scale. This may be accomplished simply by aligning the value of $(\nu + \frac{1}{2})^2$ on the regular scale next to $l(l+1)$ on the compressed scale. Next, a compressed vertical scale is prepared with an offset index so that as the index point is slid along the center axis of the horizontal scale the readings of the curve correspond directly to $E_\nu(k,\delta)$ given by Equation 29. Now to solve simultaneously for the values of ϵ'^2 and k^2 the special vertical scale is moved in relation to ϵ'^2 values listed on the horizontal scale and readings of the νth curve are taken. At the same time, values of $I_l(\epsilon')$ are read at the corresponding ϵ'^2 of the basic scale. Proceeding in this way, one finds readily the ϵ'^2 eigenvalues. Having generated all the ϵ'^2 (and k^2) values for a given ν and l, one next advances to the next ν for the same l and repeats the procedure. In this way, a series of relationships between ϵ'^2 vs ν^2 for each l is developed. Again, by appeal to tables of Bessel functions, the approximate graphical results may be refined quickly.

It is noteworthy that the values of ϵ'^2 so obtained do not depend upon the constant α^2. However, to translate from ϵ'^2 and k^2 into ϵ_0^2 and ϵ_w^2, a value of α^2, must be established.

4. ADJUSTMENT OF α^2

The form chosen for Equation 21 insures the agreement of the right and left sides at $\rho = 1$. Clearly, therefore, α^2 may be related to a second point at which agreement between these functions is imposed. Denoting this point by ρ_1, Equation 21 may be placed in the form

$$\alpha^2 = \frac{\rho_1^{-2} - e^{-\frac{\rho_1 - 1}{\delta}}}{1 - e^{-\frac{\rho_1 - 1}{\delta}}} \tag{32}$$

Thus, the adjustment problem has been reduced essentially to the problem of arriving at a prescription for the second cross-over point between the functions characterized in Equation 21.

The procedure used in this study takes advantage of the fact that the case $\delta = 0$ can be solved exactly as well as by the approximation method. Therefore, this case was studied carefully in an effort to find how best to accomplish the adjustment of α^2 for the small values which may be of interest in nuclear physics.

Equations 23 and 24 indicate that as $\delta \rightarrow 0$ both the order, n, and the argument, k, of the external radial function vanish. Since $J_1(0) = 0$ and $J_0(0) = 1$, it follows immediately from Equation 28 that

$$-G_e'/G_e = [\epsilon_w^2 + l(l+1)\alpha^2]^{1/2} \tag{33}$$

To obtain a reasonable value for α^2, the right side of this equation was equated to the function $E_l(\epsilon_w)$ derived in Section 2. When solved for α^2, Equation 33 then becomes

$$\alpha^2 = [E_l^2(\epsilon_w) - \epsilon_w^2]/l(l+1) \tag{34}$$

Substituting into this for a range of values for ϵ_w^2 and l it became clear that the values of α^2 so obtained varied only slightly (in the range from 0.8 to 0.9). The final constant,

$$\alpha^2 = 0.82645 \qquad \text{for} \qquad \delta = 0 \tag{35}$$

was chosen as an appropriate one. This corresponds to a second cross-over point at

$$\rho = 1.1 = 1 + 0.1 \qquad \text{for} \qquad \delta = 0 \tag{36}$$

This choice was made not only because of its convenience but also because it works particularly well for small values of ϵ_w^2, the region for which Equation 33

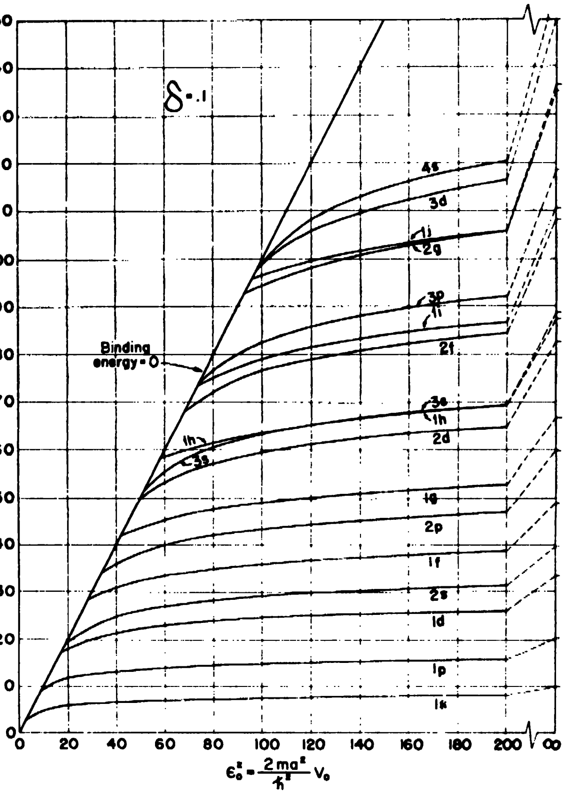

Figure 4. Eigenvalues for $\delta = 0.1$

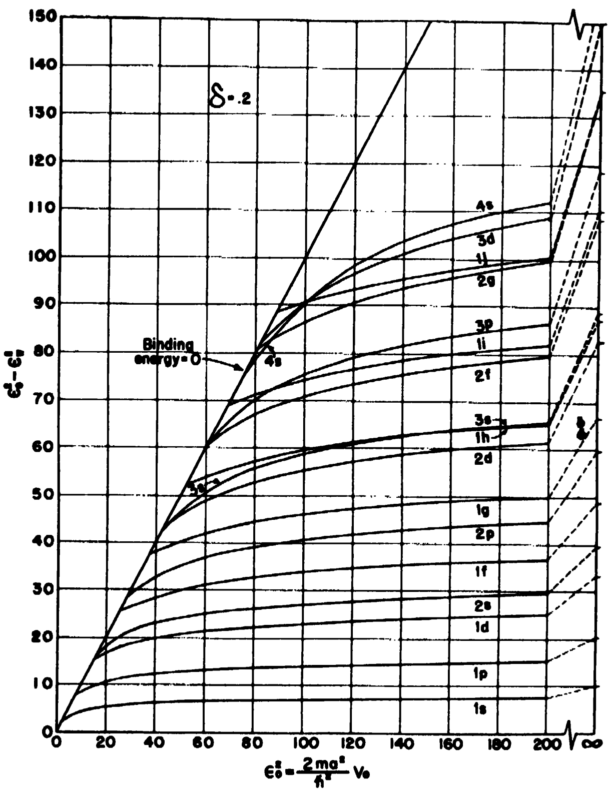

Figure 5. Eigenvalues for $\delta = 0.2$

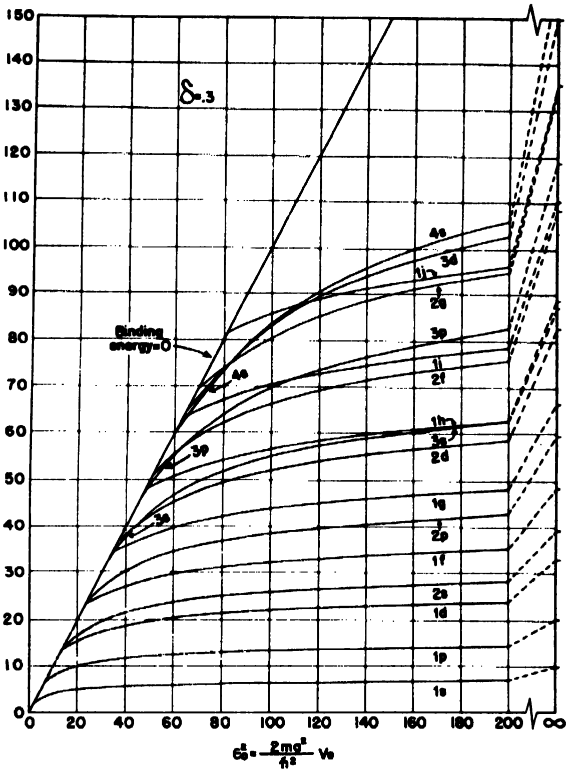

Figure 6. Eigenvalues for $\delta = 0.3$

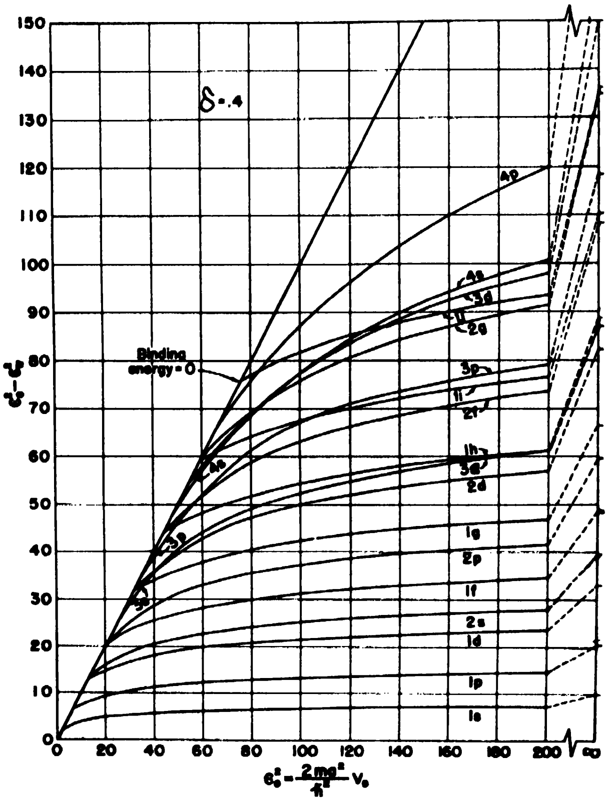

Figure 7. Eigenvalues for $\delta = 0.4$

is most sensitive to α^2. This region of $\epsilon_w{}^2$ values is particularly of interest in applications of these results to the study of particle binding energies and nuclear transitions. Accordingly, it would seem best to favor this region in an adjustment. For non-zero values of δ, the rule

$$\rho_1 = 1 + \delta + 0.1 \tag{37}$$

was chosen as the simplest result which goes over to Equation 36 for $\delta = 0$. This simple rule is admittedly somewhat arbitrary; however, since only a small correction is involved here, it is difficult to see how Equation 37 can lead to appreciable errors. Most certainly this procedure represents an improvement over the usual approximation of replacing ρ^{-2} by 1 which is equivalent to making the second point of agreement at infinity. Inserting Equation 37 into Equation 32 leads immediately to the function $\alpha^2(\delta)$. Values of this function are given in Table 1.

Table I. The Values of $\alpha^2(\delta)$

δ]	0.	0.1	0.2	0.3	0.4	0.4
α^2	0.8264	0.6466	0.4744	0.3349	0.2214	0.1280

5. RESULTS AND DISCUSSION

The ϵ'^2 *vs* ν and l, and k^2 *vs* ν and l relationships arrived at by the procedure described in Section 3 may now be translated into ϵ'^2 *vs* $\epsilon_0{}^2$ relationships for comparison with Fig. 3. These are shown in Figs. 4, 5, 6, and 7 for $\delta = 0.1$, 0.2, 0.3 and 0.4, respectively. For case $\delta = 0$, the eigenvalues arrived at by the approximate method rarely deviate by more than a line width from the curves shown in Fig. 3. It must be remembered that the results for $\delta \neq 0$ are exact for *s* states but are approximate for *p*, *d*, . . . *f*. By first-order perturbation theory the error of the energy eigenvalue in natural units may be estimated to be $\Delta\epsilon_w{}^2 = l(l + 1)$

$$\frac{\int_1^\infty G_e{}^2[\rho^{-2} - \alpha^2 - (1 - \alpha^2)\exp(1 - \rho/\delta)]\, d\rho}{\int_0^1 G_i{}^2\, d\rho + \int_1^\infty G_e{}^2\, d\rho} \tag{38}$$

By virtue of the vanishing of the perturbation at $\rho = 1$ and $\rho = 1 + \delta + 0.1$, the factor in the bracket is less than 0.05 in the intermediate region, which is the region within which the external wave function is significantly large. Accordingly the error is expected to be less than $0.05l(l + 1)f$, where f is the probability for the particle being found beyond $\rho = 1$. Since f is expected to be considerably less than 1 the error in $\epsilon_w{}^2$ due to the method of approximation is expected to be considerably less than a unity. Quantitative estimates using numerical integration substantiate this statement. At the present stage of our knowledge of the nucleus the approximate eigenvalues given in Figs. 3 to 7 should be sufficiently accurate so that their further refinement at this time is unnecessary. If these approximate eigenvalues and eigenfunctions prove helpful in resolving nuclear problems it should not be difficult to refine them further.

In conclusion it is important to note that the infinite spherical well eigenvalues provide a poor representation of the finite spherical well eigenvalues in the range of interest in nuclear physics. When the boundary is made diffuse to a moderate degree the infinite spherical well eigenvalues are hopelessly inaccurate. Even the finite square spherical well differ appreciably from the diffuse boundary eigenvalues, particularly in the region of small energies, which is the region of greatest interest in nuclear physics. Accordingly, one might expect that some of the well known difficulties of the IPM model based upon square well eigenvalues and eigenfunctions might be removed by the use of diffuse boundary eigenvalues and eigenfunctions.

REFERENCES

1. Woods, R. D., Dissertation, University of California, August, 1954.
2. Chase, D. M. and Rohrlich, F., Phys. Rev. *94*, 81 (1954).
3. Feshbach, H., Porter, C. E. and Weisskopf, V. F., Phys. Rev. *96*, 448 (1954).
4. Schiff, L. I., *Quantum Mechanics* (McGraw-Hill Book Company, Inc., New York), Chap. IV (1949).
5. Moskowski, S. A., Phys. Rev. *89*, 482 (1953).
6. Mathematical Tables Project, National Bureau of Standards, *Tables of Spherical Bessel Functions, Vol. 1 and 2,* Columbia University Press, New York, 1947.
7. Morse, P. M. and Feshbach, H., *Methods of Theoretical Physics, Part II.* (McGraw-Hill Book Company, Inc., New York), Chap. XII (1953).
8. Malenka, B. J., Phys. Rev. *86*, 68 (1952).

The IPM Mass Surface*

By Kiuck Lee and Alex E. S. Green,† Korea

ABSTRACT

An analytic expression is found which represents the sum of the energy eigenvalues for a finite spherical well rather accurately for the range of well radii, well depths, and occupancy numbers of interest in nuclear physics. Using this expression an analytic mass surface equation is derived which is quite similar to the semi-empirical equation. With reasonable choices based on scattering and other data of the two available parameters in the IPM surface it is found that the volume energy is much too large and the symmetry energy too small.

The approximate eigenvalues for a spherical well with an exponentially diffuse boundary are then applied to the study of the IPM mass surface. Again an analytical expression is found which represents the energy sums quite well for various degrees of diffuseness. The use of a diffuse boundary improves the mass surface obtainable from a strict IPM alleviating both the volume and symmetry energy difficulties. While some additional forces such as two body repulsive forces, exchange forces, velocity dependent forces or many body forces are still needed to derive a completely satisfactory mass surface, the demands upon such forces are much less for the case of the diffuse boundary than the case of the sharp boundary.

1. INTRODUCTION

The purpose of this study is to determine the extent to which the strict independent particle model (IPM) can account for the experimental nuclear mass surface. A number of earlier attempts in this direction have been made before.[1–5] The effort here is made in the light of recent successes of the IPM and, of course, with the hope of carrying the work further ahead.

To formulate the problem in a general way, it is assumed that the potential involves a range parameter given by

$$a = r_0 A^{1/3} = bA^{1/3} \text{ fermis} \qquad (1)$$

(a fermi is 10^{-13} cm) where b is a dimensionless number which probably lies between 1.0–1.5. The mass used in this work is taken to be the average mass of the neutron and proton

$$m = \tfrac{1}{2}(M_n + M_p) = 1008.288 \text{ mMU} \qquad (2)$$

All energies shall be referred to the natural energy unit

$$E_0 = h^2/2ma^2 = U_0/b^2A^{2/3} \qquad (3)$$

where

$$U_0 = 22.2669 \text{ mMU} \qquad (4)$$

The potential shall also be characterized by the depth constant V_0 and the dimensionless well strength parameter

$$\theta_0 = (V_0/E_0)^{1/2} = c_0 A^{1/3} \qquad (5)$$

where

$$c_0 = (2mV_0 r_0^2/\hbar^2)^{1/2} \qquad (6)$$

Thus the well depth constant may be expressed as

$$V_0 = c_0^2 E_0 A^{2/3} = c_0^2 U_0/b^2 \qquad (7)$$

For any type of well, allowed energy eigenvalues shall be characterized by a dimensionless parameter θ_{wnl}^2 defined by

$$\theta_{wnl}^2 = -W_{nl}/E_0 \qquad (8)$$

where W_{nl} denote the actual energy eigenvalues. Since each energy state in a central field is $(2l + 1)$-fold degenerate, according to the exclusion principle each state can admit $2l + 1$ nucleons of the same charge and spin. Thus a large number of identical nucleons will go into the lowest energy states with $2l + 1$ nucleons in each state. As the spin-orbit coupling energies tend to cancel in closed shell configurations one can for the purpose of initial studies and for convenience choose closed shell occupancy numbers in computing energy sums. The energy sum for A identical nucleons all in completed shells is

$$\begin{aligned} E(A) &= -(U_0/b^2A^{2/3})\Sigma_{n,l}(2l + 1)\epsilon_{wnl}^2 \\ &= -(c_0^2U_0/b^2)A \\ &\qquad + (U_0/b^2A^{2/3})\Sigma_{n,l}(2l + 1)\epsilon'^2_{nl} \qquad (9) \end{aligned}$$

where

$$\epsilon'^2_{nl} = \epsilon_0^2 - \epsilon_{wnl}^2 \qquad (10)$$

is the energy in natural units measured relative to the bottom of the well and is the counterpart of the classical kinetic energy of a particle in the well. The principal problem which remains is the determination of the eigenvalues ϵ'^2_{nl} for various types of central fields. Before undertaking this problem let us first consider briefly the Fermi gas model calculation of the mass surface.

2. THE FERMI GAS MODEL

The usual Fermi gas model approximations are based upon the relationship

---

* Supported by a grant from the US Atomic Energy Commission. Part of a dissertation to be submitted by Kiuck Lee in partial fulfillment of the requirements for the degree of Doctor of Philosophy at the Florida State University.

† The Florida State University, Tallahassee, Florida.

$$\Lambda = V(k_m^3/6\pi^2) \tag{11}$$

where V is the volume of the nucleus and k_m is the maximum propagation constant identifiable with the states associated with a given spin and isotopic spin. From this equation it follows that the kinetic energy sum is given approximately by[6]

$$\begin{aligned} T(\Lambda) &= (3\hbar^2/10mr_0^2A^{2/3})(9\pi/2)^{2/3}\Lambda^{5/3} \\ &= (U_0G_0/b^2A^{2/3})\Lambda^{5/3} \end{aligned} \tag{12}$$

where

$$G_0 = (3/5)(9\pi/2)^{2/3} = 3.5080 \tag{13}$$

If we identify Equation 12 with the energy sum in Equation 9, the total energy sum may be written as

$$E(\Lambda) = -(e_0^2U_0/b^2)\Lambda + (U_0/b^2A^{2/3})\Lambda^{5/3}G_0 \tag{14}$$

The occupancy numbers for up-spin neutrons, down-spin neutrons, up-spin protons, and down-spin protons shall be denoted by Λ_1, Λ_2, Λ_3, and Λ_4. For convenience this study will be carried out for even-even nuclei such that

$$\Lambda_1 = \Lambda_2 = \tfrac{1}{2}N = \tfrac{1}{4}(A + D) = \tfrac{1}{4}A(1 + D/A) \tag{15}$$

and

$$\Lambda_3 = \Lambda_4 = \tfrac{1}{2}Z = \tfrac{1}{4}(A - D) = \tfrac{1}{4}A(1 - D/A) \tag{16}$$

Adding the energy sums given by Equation 14 for each of the four types of particles and expanding combinations involving $(1 \pm D/A)^n$ by the binomial theorem, it follows that the net energy sum is approximately given by

$$\begin{aligned} \Sigma_iE(\Lambda_i) &= -(e_0^2U_0/b^2)A \\ &\quad + (U_0G_0/b^24^{2/3})A(1 + 5D^2/9A^2) \end{aligned} \tag{17}$$

where terms of the order of D^4/A^4 have been neglected·

An approximate correction for the coulomb repulsion of protons may be made by adding the energy

$$E_c = 3e^2Z^2/5r_0A^{1/3} = U_cZ^2/bA^{1/3} \tag{18}$$

where

$$U_c = 0.92779 \text{ mMU} \tag{19}$$

Comparing the results with the well-known semi-empirical equation one may identify

$$a_1 = U_0/b^2(e_0^2 - G_0/4^{2/3}) \tag{20}$$

$$a_2 = 0 \tag{21}$$

$$a_3 = U_c/b \tag{22}$$

and

$$a_4 = 20G_0U_0/9b^24^{2/3} \tag{23}$$

From these one may obtain the ratio

$$a_4/a_3 = 20G_0U_0/4^{2/3}9U_cb = 74.248/b \tag{24}$$

According to studies of the semi-empirical equation this ratio is the primary factor which determines the theoretical line of beta stability. If this theoretical line is to match the experimental line the ratio cannot deviate appreciably from the value

$$a_4/a_3 = 133 \tag{25}$$

In almost all discussions of the nuclear mass surface the extreme range for b is taken as 1 to 1.5. Thus it is apparent that the symmetry energy obtained from the usual Fermi gas treatment is much too small. A second and more obvious defect is the absence of a surface energy which, as is well known, is essential to the theory of fission.

Feenberg and Hammack[3,4] and Hill and Wheeler[5] have called attention to the fact that the usual k space summation procedure for obtaining the total number of states with propagation constants less than k_m neglects some rather large effects. When these effects are taken into account they find that

$$\Lambda = Vk_m^3/6\pi^2 - Sk_m^2/16\pi + Lk_m/8\pi^2 \tag{26}$$

where V, S, and L are the volume, surface, and characteristic length of the nucleus. On the basis of this expression it is found that

$$T(\Lambda) = U_0\Lambda^{5/3}(G_0 + G_1\Lambda^{-1/3} + G_2\Lambda^{-2/3})/b^2A^{2/3} \tag{27}$$

where

$$G_1 = (9\pi/10)(5\pi/16)(6/\pi)^{2/3} = 4.2727 \tag{28}$$

and

$$G_2 \approx 2.2140 \tag{29}$$

The last constant was obtained by Feenberg and Hammack by a rather involved adjustment procedure. If one pursues this function it is found that the total nuclear energy now may be written in the form

$$\begin{aligned} E_T &= -U_0/b^2\,(e_0^2 - G_0/4^{2/3})A + U_0/b^2\,G_1A^{2/3}/4^{1/3} \\ &\quad + (U_0G_2/b^2)A^{1/3} + U_cZ^2/bA^{1/3} + U_0/b^2[20\,G_0/4^{2/3}9 \\ &\quad + 8\,G_1/4^{1/3}9A^{1/3}]D^2/4A \end{aligned} \tag{30}$$

The occurrence of a surface energy and a length energy are the outstanding features obtained from this more careful treatment of the Fermi gas model. While Equation 30 is not strictly in the form of the usual semi-empirical expression it might for qualitative comparisons be compared with the usual form by rearranging it into the form

$$\begin{aligned} E_T &= -U_0/b^2(e_0^2 - G_0/4^{2/3})A + U_0/b^2[G_1/4^{1/3} \\ &\quad + G_2/A^{1/3}]A^{2/3} + U_cZ^2/bA^{1/3} + U_0/b^2[20\,G_0/4^{2/3}9 \\ &\quad + 8\,G_1/4^{1/3}9A^{1/3}]D^2/4A \end{aligned} \tag{31}$$

Replacing the $A^{1/3}$ value in the brackets by

$$A^{-1/3} = (130)^{1/3} \tag{32}$$

one may now set

$$a_1 = (22.2669/b^2)(e_0^2 - 1.3922) \tag{33}$$

$$a_2 = 69.666/b^2 \tag{34}$$

$$a_3 = 0.92779/b \tag{35}$$

$$a_4 = 79.4031/b^2 \tag{36}$$

The ratio a_4/a_3 is now

$$a_4/a_3 = 85.5830/b \tag{37}$$

This represents an improvement upon the previous value; however, it is an insufficient one for the purposes of accounting for the line of beta stability.

Furthermore the surface energy is much too large. It has been remarked that this excessive surface energy is related to the use of the eigenvalue for an infinite box in the Fermi gas treatment and the effect would be considerably reduced when finite well eigenvalues are used. It is in connection with the calculation of the effect of the finiteness of the well that this work begins its main departures from the work of Feenberg and Hammack.

3. THE FINITENESS CORRECTION

Rather than attempt to modify the Fermi gas model calculational procedure with its long chain of approximations it appears best to go directly to the set of eigenvalues calculated for a finite square well. These have been calculated by Green and Lee (in P/950, the preceding paper in this volume) for the complete range of well parameters of interest in nuclear physics (see Fig. 3 of P/950).

The results of the Fermi gas treatment suggest that the sum of the energies of Λ particles in the lowest states permitted by the exclusion principle is proportional to $\Lambda^{5/3}$. Thus, it might be expected that the actual energy sums involved in Equation 9 when divided by $\Lambda^{5/3}$ would yield a slowly varying function whose properties might be uncovered by empirical analysis. Accordingly, the sum function

$$G(\Lambda,\epsilon_0) = \Lambda^{-5/3}\Sigma_{nl}(2l + 1)\epsilon'^{2}_{nl} \qquad (38)$$

was computed for various values of ϵ_0 and Λ. After some experimentation it was found possible to represent these sums quite well by the analytical expression

$$G(\Lambda,\epsilon_0) = G_0 + G_1\Lambda^{-1/3} - k\epsilon_0^{-1} \qquad (39)$$

where an adjustment procedure which favored the range $\epsilon_0 = 5$–12 led to the constants

$$G_0 = 3.60 \qquad G_1 = 5.00 \qquad k = 10.00 \qquad (40)$$

Rounded constants were chosen to simplify the computation at a slight, but not significant, sacrifice of accuracy. The goodness of the fit achieved will be discussed in Section 4. Using Equations 39, 38, and 9 and adding the nuclear energy sums for the four spin-isobaric spin states it follows that the total nuclear energy of an even-even nucleus is given by

$$\begin{aligned} E_N = & -U_0/b^2(e_0^2 - G_0/4^{2/3})A + U_0/b^2(G_1/4^{1/3} \\ & - k/4^{2/3}e_0)A^{2/3} + U_0/b^2[5x4^{1/3}G_0/9 \\ & + 4^{2/3}/9A^{1/3}(2G_1 - 5k/4^{1/3}e_0)]D^2/4A \end{aligned} \qquad (41)$$

The correction for the coulomb interaction between protons here presents certain difficulties. In the first place the repulsion between protons might be expected to raise the effective potential for protons. The direct effect of this raising of the potential acts through the e_0 in the first of the two terms in Equation 9 and gives rise to the basic coulomb energy. However, this raising of the depth of the well also acts indirectly through the third term in Equation 39 and thereby gives rise to a smaller coulombic contribution. A third contribution arises by virtue of the "spilling out" of the nucleons outside the well radius constant b. The recent argument of Teller and Johnson[7] suggests that the neutron and proton distribution "tail off" somewhat differently. Furthermore by virtue of the coulomb interaction one might expect to have an additional exchange energy between protons over and above that embodied in the phenomenological nuclear potential. Since these last two effects cannot readily be handled simply by using a modified square well for the protons it appears best to proceed tentatively simply by using for the coulomb energy

$$E_c = 3e^2Z^2/5b_pA^{1/3} = U_cZ^2/b_pA^{1/3} \qquad (42)$$

where b_p is the dimensionless radius constant which characterizes the proton distribution. One might expect from recent μ-mesonic X-ray studies[8] as well as the analysis of the semi-empirical equation[9] that $b_p \approx 1.2$. Adding the coulomb energy given by Equation 42 to the nuclear energy given by Equation 41 one obtains an expression which, apart from the second and small term in the bracket of Equation 41, is identical with the well-known semi-empirical equation. It is sufficient for the purposes of comparing Equation 41 with the results of recent studies of the semi-empirical mass surface to replace $A^{1/3}$ in the bracket by $(130)^{1/3}$. Inserting numerical constants one obtains the semi-empirical constants

$$a_1 = \frac{22.267}{b^2}[e_0^2 - 1.42866] \qquad (43)$$

$$a_2 = \frac{22.267}{b^2}[3.1498 - 3.96850/e_0] \qquad (44)$$

$$a_3 = 0.92779/b_c \qquad (45)$$

$$a_4 = \frac{82.9998}{b^2}[1 - 0.46704/e_0] \qquad (46)$$

in terms of the parameters e_0, b, and b_c. Considerable light has been shed upon the constant e_0 by studies of neutron cross sections. It is well known in the study of potential elastic scattering by a square well that peaks in the zero velocity limit cross section associated with s waves occur whenever

$$\epsilon_0 = (n + 1/2)\pi \qquad (47)$$

where n is an integer. The recent interpretative work of Adair,[10] Feshbach, Porter,[11] and Weisskopf as well as the earlier work of Ford and Bohm[12] suggests that maxima observed by Barschall[13] in the low velocity limit of the total neutron cross sections at $A \approx 11$, 55, and 150 may be identified with the second, third, and fourth s-wave maxima. Letting $\epsilon_0 = e_0A^{1/3}$ it follows that

$$e_0 \approx 2.08 \qquad (48)$$

will account for the location of these maxima. Inserting this value into Equations 43, 44, 46 and letting $b \approx b_c \approx 1.2$ one obtains

$$a_1 = 44.81 \qquad (49)$$

$$a_2 = 19.20 \qquad (50)$$

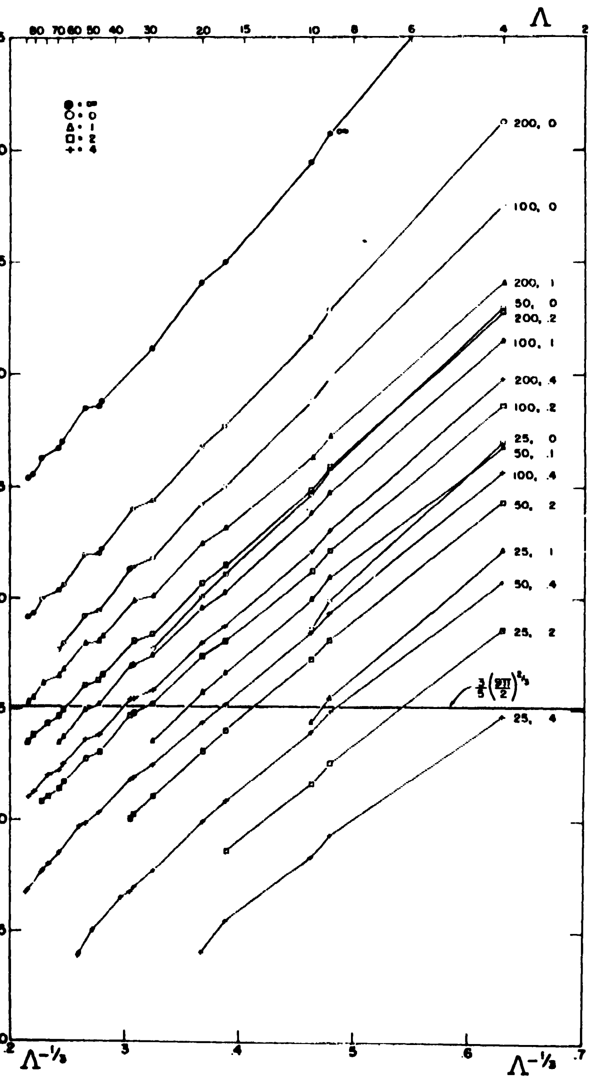

Figure 1. The D function obtained from the eigenvalues against A for ϵ_0 = 25, 50, 100, 150 and 200 and δ = 0.1, 0.2, 0.3 and 0.4

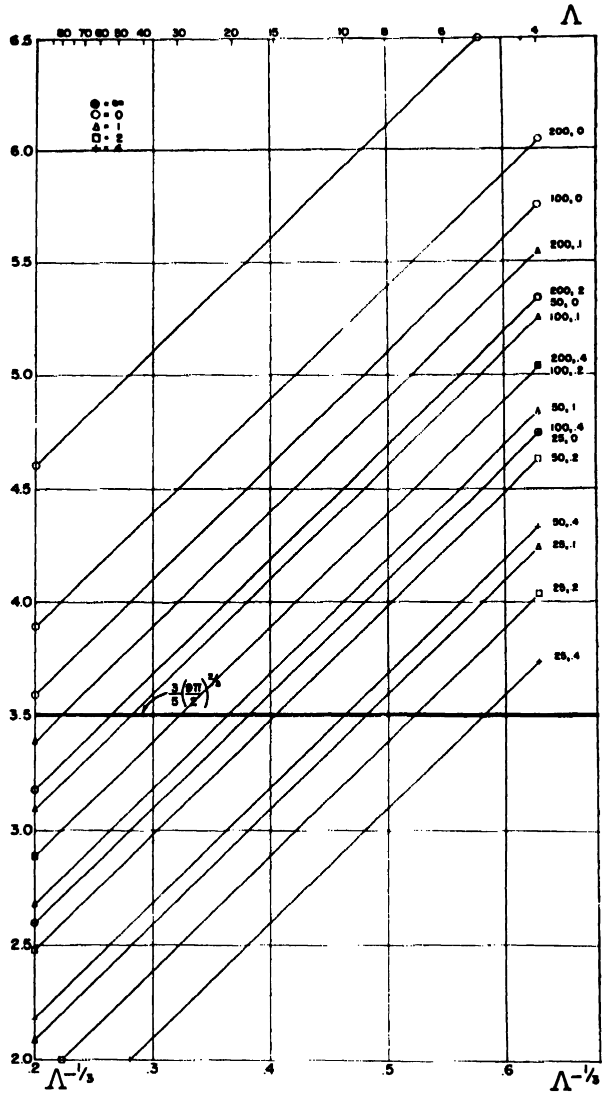

Figure 2. The analytic G functions against A for ϵ_0 = 25, 50, 100, 150 and 200 and δ = 0.1, 0.2, 0.3 and 0.4

$$a_3 = 0.773 \qquad (51)$$

$$a_4 = 44.70 \qquad (52)$$

From the standpoint of work with the semi-empirical equation the surface and the coulomb terms are now in a satisfactory range of magnitudes. However the volume energy constant is rather large and the symmetry energy constant is rather small.

To eliminate these difficulties we might attempt to: (*a*) modify the square well by adding a tail or diffused boundary or by shaping the core of the potential; (*b*) introduce an exchange force or correlation energy or many body force. It was decided first to attempt to exhaust the possibilities connected with modification of the first potential well.

4. THE DIFFUSENESS CORRECTION

In this section the eigenvalues for a square well with an exponential tail are used for the computation of energy sums. These eigenvalues have been calculated (see Figs. 4, 5, 6 of P/950).

Using these eigenvalues the energy sums were computed for various combinations of Λ, ϵ_0 and δ. It was found possible to represent the G functions corresponding to these sums by the approximate separated expressions

$$G(\Lambda,\epsilon_0,\delta) = 3.60 + 5.0\Lambda^{-1/3} - 10.0/\epsilon_0 - (2.5\delta)^{1/2} \qquad (53)$$

To indicate the nature of the agreement attained Fig. 1 represents the G functions obtained from the eigenvalues as a function of Λ for various combinations of ϵ_0 and δ. Figure 2 represents the analytic G functions for these energy sums. A careful comparison of these figures should indicate that Equation 53 is a good starting point for a study in which the effect of the diffuse boundary is considered. It might be mentioned that Equation 53 fails to satisfy one requirement; namely, that as $\epsilon_0 \to \infty$ the effect of the tail must also vanish. This shortcoming may be eliminated by multiplying the last term in Equation 53 by $(\epsilon_s/\epsilon_0)^{\frac{1}{n}}$

$$G_n = 3.60 + 5.0A^{-1/3} - 10.0/\epsilon_0 - (2.5\delta)^{1/2}(\epsilon_s/\epsilon_0)^{\frac{1}{n}} \tag{54}$$

where ϵ_s is a central value such as 10 and n is a large number such as 12. The resulting expression would then satisfy the desired requirement yet do just about as well in the region of interest. However, for simplicity, Equation 53 shall be used since it works well in the range of ϵ_0 from 2–15 which is the region of well strength parameters of interest in nuclear physics.

Before developing the mass surface based upon Equation 53, the G function which would be applicable to the proton sums must be considered. The addition of the coulomb potential energy for each proton to the nuclear potential energy for each proton might be approximately regarded as creating an effective potential of slightly altered V_0, a and δ parameters. Unfortunately, to arrive at the effective individual particle potential for each proton one must first make a reasonable assumption as to the resulting proton distribution. Thus in effect one must solve a complete self-consistent field problem for the nucleus. Since, however, here the coulomb potential energy is relatively small and rather insensitive to the fine details of the charge distribution one might proceed on the basis of almost any reasonable distribution of protons in arriving at an appropriate potential energy for a single proton.

The basis for finding the coulomb potential energy for a single proton is to let

$$\sum_{i=1}^{Z} V_{ci}(r_i) = \tfrac{1}{2}\sum_{ij}{}' e^2/r_{ij} \tag{55}$$

where the prime denotes the omission of the self energy terms. Thus the coulomb potential for the ith particle should be a central field which approximates

$$V_{ci} = \tfrac{1}{2}\sum_{j} e^2/r_{ij} \tag{56}$$

Accordingly, the appropriate individual particle coulomb potential energy is one-half the interaction energy of a single charge with all the other charges in the nucleus. If the single charge is regarded as small compared to $(Z - 1)e$ one may simply use one-half the potential energy of a small test charge in the field of a reasonable charge distribution. For example, if one assumes a proton distribution in which the proton density has the form

$$\begin{aligned} \rho(r) &= \rho_0 & r &\leq a \\ \rho(r) &= \rho_0 e^{(a-r)/\delta a} & r &\geq a \end{aligned} \tag{57}$$

the coulomb potential energy function for a single proton is

$$V_c(r) = [(Z - 1)e^2(\tfrac{1}{2} + \delta + \delta^2 - r^2/6a^2]/ 2a[\tfrac{1}{3} + \delta + 2\delta^2 + 2\delta^3] \quad r \leq a$$

$$V_c(r) = \frac{(Z-1)e^2}{2r}\left[1 - \frac{\delta^2 e^{-\frac{r-a}{\delta a}}\left(\frac{r}{a} + 2\delta\right)}{\tfrac{1}{3} + \delta + 2\delta^2 + 2\delta^3}\right] \quad r \geq a \tag{58}$$

To utilize the results for the neutron case the net potential for protons may be assumed to have the form

$$\begin{aligned} V(r) &= (g_1 - g_2)V_0 & r &\leq a \\ V(r) &= (g_1 e^{-\frac{r-a}{\delta' a}} - g_2)V_0 & r &\geq a \end{aligned} \tag{59}$$

where g_1, g_2 and δ' are constants. These constants can be determined by setting

$$4\pi\int_0^a \left[V_0 - \frac{(Z-1)e^2}{2a}\left(\frac{1}{2} + \delta + \delta^2 - \frac{r^2}{6a^2}\right)\Big/ \left(\frac{1}{3} + \delta + 2\delta^2 + 2\delta^3\right)\right] r^2\,dr = 4\pi(g_1 - g_2)V_0\int_0^a r^2\,dr \tag{60}$$

and by forcing the right and left sides of

$$V_0 e^{-\frac{r-a}{\delta a}} - \frac{(Z-1)e^2}{2r}\left[1 - \frac{\delta^2 e^{-\frac{r-a}{\delta a}}(r/a + 2\delta)}{\tfrac{1}{3} + \delta + 2\delta^2 + 2\delta^3}\right] = (g_1 e^{-\frac{r-a}{\delta' a}} - g_2)V_0 \tag{61}$$

to agree at two reasonable values of r. For example, by matching the external potentials at $r = a + \delta a$ and $r = a + 2\delta a$ and solving these three equations simultaneously one obtains

$$g_1 = k_1^2/(k_2 - 2k_1) \tag{62}$$

$$1 - g_1 + g_2 = e^2(Z - 1)(\delta + \delta^2 + \tfrac{2}{5})/ 2V_0 a(\tfrac{1}{3}\delta + 2\delta^2 + 2\delta^3) \tag{63}$$

and

$$\delta' = \delta/\log[k_1/(k_2 - k_1)] \tag{64}$$

where

$$k_1 = (e^{-1} - 1) - (Z - 1)e^2[\tfrac{1}{3} - \tfrac{2}{5} - \tfrac{2}{5}\delta + \delta^3 - \delta^2 e^{-1}(1 + 3\delta)]/ 2V_0 a(1 + \delta)(\tfrac{1}{3} + \delta + 2\delta^2 + 2\delta^3) \tag{65}$$

and

$$k_2 = (e^{-2} - 1) - (Z - 1)e^2[\tfrac{1}{3} - \tfrac{2}{5} - \tfrac{4}{5}\delta - \delta^2 - \delta^2 e^{-2}(1 + 4\delta)]/ 2V_0 a(1 + 2\delta)(\tfrac{1}{3} + \delta + 2\delta^2 + 2\delta^3) \tag{66}$$

In Fig. 3, the coulomb potential energy given by Equation 58 for a typical nucleus ($A = 130$, $Z = 50$) the nuclear potential energy corresponding to $V_0 = 40$ mMU, $b = 1.2$, and $\delta = 0.2$, and the sum of these energies for a typical nucleus are shown. In this case, Equations 62 and 63 give

$$g_1 = 0.953, \quad g_2 = 0.056, \quad \text{and} \quad \delta' = 0.197 \tag{67}$$

Also shown is the effective protonic potential energy given by Equation 59 for these constants.

It is noteworthy that the effective protonic potential

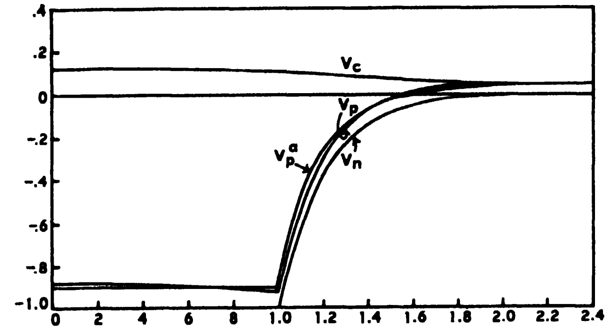

Figure 3. The effective proton potential $V_p{}^a$ for $A = 130$, $Z = 50$, $V_0 = 40$, $b = 1.2$ and $\delta = 0.2$

differs from the effective neutron potential not only by the raising of the level of the inner and outer regions but also by reduction in the extension of the diffuse region for protons.

Using the relations

$$\epsilon_{op}{}^2 = \epsilon_0{}^2 - \epsilon_0{}^2(1 - g_1 + g_2) \tag{68}$$

$$\delta' = \delta - \Delta\delta = (1 - \Delta\delta/\delta) \tag{69}$$

one may now write

$$G(A,\epsilon_{op},\delta') = G(A,\epsilon_0,\delta) - \frac{1 - (g_1 - g_2)^{1/2}}{(g_1 - g_2)^{1/2}} \frac{10.0}{\epsilon_0} + \frac{\Delta\delta}{2}\left(\frac{2.5}{\delta}\right)^{1/2} \tag{70}$$

Combining the neutron and proton sums and rearranging, the IPM mass surface becomes

$$\begin{aligned} E_T = &-\frac{U_0}{b^2}\left[e_0{}^2 - \frac{3.6 - (2.5\delta)^{1/2}}{4^{2/3}}\right]A \\ &+ \frac{U_0}{b^2}\left[\frac{5}{4^{1/3}} - \frac{10}{4^{2/3}e_0}\right]A^{2/3} \\ &+ \frac{5U_0}{9b}\left[4^{1/3}(3.6 - (2.5\delta)^{1/2}) - \frac{4^{1/3} \times 10}{e_0A^{1/3}} \right.\\ &\left. + \frac{4^{2/3} \times 2}{A^{1/3}}\right]\frac{D^2}{4A} \\ &+ \frac{3e^2Z(Z-1)}{5r_0A^{1/3}}\left[1 \right.\\ &- \left(1 - \frac{2 + 5\delta + 5\delta^2}{2 + 6\delta + 12\delta^2 + 12\delta^3}\right) \\ &- \frac{U_0Z^{2/3}}{2^{2/3} \times 0.92779b(Z-1)A^{1/3}}\left(\left(\frac{1}{(g_1 - g_2)^{1/2}}\right.\right. \\ &\left.\left.\left. - 1\right)\frac{10}{e_0A^{1/3}} - \frac{\Delta\delta}{2}\left(\frac{2.5}{\delta}\right)^{1/2}\right)\right] \end{aligned} \tag{71}$$

For a qualitative comparison with the known semi-empirical surface one may use $A = 130$ and $Z = 50$ in the brackets. The average semi-empirical constants then are

$$a_1 = \frac{U_0}{b^2}[e_0{}^2 - 1.42866 + 0.627488^{1/2}] \tag{72}$$

$$a_2 = \frac{U_0}{b^2}[3.14980 - 3.96851/e_0] \tag{73}$$

$$\begin{aligned} a_3 = &\frac{0.92779}{b}\left[1 - \frac{\delta + 7\delta^2 + 12\delta^3}{2 + 6\delta + 12\delta^2 + 12\delta^3}\right. \\ &- \frac{0.27698U_0}{b}\left(\left(\frac{1}{(g_1 - g_2)^{1/2}} - 1\right)\frac{1.34035}{e_0}\right. \\ &\left.\left. - 0.53679\frac{\Delta\delta}{\delta^{1/2}}\right)\right] \end{aligned} \tag{74}$$

$$a_4 = \frac{U_0}{b^2}[3.72752 - 1.39440\delta^{1/2} - 1.74088/e_0] \tag{75}$$

e_0 can be determined by identifying the observed maxima of the total low-velocity limit neutron cross sections at $A \approx 11$, 55 and 150 with the second, third and fourth s-wave maxima for diffuse potential well. The critical ϵ_0 values for the 1s, 2s, 3s and 4s states as obtained from the eigenvalue calculations in paper P/950 are shown in Fig. 4. For each of these ϵ_0 the corresponding $e_0 = \epsilon_0/A^{1/3}$ were calculated and the average of the 2s, 3s and 4s e_0's for each δ were determined. The function $e_0(\delta)$ so obtained is shown in Fig. 5. It is clear that to a good approximation the location of the scattering maxima imposes the relation

$$e_0 = 2.08 - 2\delta \tag{76}$$

One might also expect that as the diffuseness parameter δ grows larger the constant b necessary to account for various experimental radius constant determinations, such as the μ-mesonic X-ray radius constant, the nuclear masses coulomb radius constant, various nuclear scattering radius constants, etc., will grow smaller. As an exploratory approximation one might make the identification

$$b + \delta b = b^x \quad \text{or} \quad b = b^x/(1 + \delta) \tag{77}$$

where b^x is an experimental radius constant. By virtue

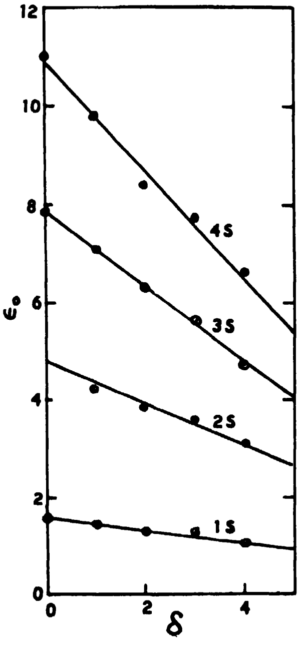

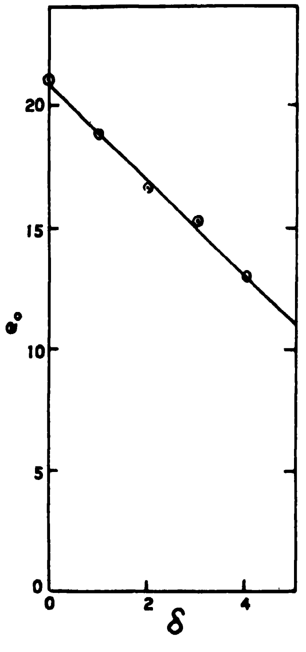

Figure 4. (At left) The critical ϵ_0 values for the 1s, 2s, 3s and 4s states obtained from the eigenvalues. Figure 5. (At right) The values of $\epsilon_0(\delta)$

of these relations Equations 72, 73, 74 and 75 can be expressed only in terms of the constants b^x and δ

$$a_1 = \frac{U_0}{b^{x^2}}(1+\delta)^2[2.89774 + 0.62748\delta^{1/2} - 8.32\delta + 4\delta^2] \quad (78)$$

$$a_2 = \frac{U_0}{b^{x^2}}(1+\delta)^2[3.14980 - 1.98426/(1.04-\delta)] \quad (79)$$

$$a_3 = \frac{0.92779}{b^x}(1+\delta)\left[1 - \frac{\delta + 7\delta^2 + 12\delta^3}{2(1+3\delta+6\delta^2+6\delta^3} - 0.27698\frac{U_0}{b^x}(1+\delta)\left(\left(\frac{1}{(g_1-g_2)^{1/2}} - 1\right)\frac{0.67018}{1.04-\delta} - 0.53679\frac{\Delta\delta}{\delta^{1/2}}\right)\right] \quad (80)$$

$$a_4 = \frac{U_0}{b^{x^2}}(1+\delta)^2[3.72752 - 1.394408\delta^{1/2} - 0.87044/(1.04-\delta)] \quad (81)$$

where g_1 and g_2 are functions of δ as given by Equations 62, 63, 65 and 66. The numerical values are the semi-empirical parameters as well as various functions of δ for $b^x = 1.0$, 1.2 and 1.4.

On the basis of studies of the semi-empirical equation it would appear that none of the combinations shown in Table 1 of the preceding paper are completely satisfactory.

5. THE HOLLOWNESS CORRECTION

In this section the effects of adding to the internal potential a repulsive potential given by

$$V_{ir}(r) = \frac{\lambda^2\hbar^2}{2Ma^2}(a^2/r^2 - 1) \quad (82)$$

is considered. The solution of the eigenvalue equation for the resulting combination of potentials can be solved by the techniques used in GLI. However rather than carry out the problem numerically, one might for the sake of orientation make use of the effect of an r^{-2} core upon the harmonic oscillator solutions. Since this potential is only influential near $r = 0$ where the harmonic oscillator potential resembles the square well, one might be guided by the analytical expression for the energy shift for this case. It is not difficult to show that this energy shift is given by

$$W = E_0\lambda^2\left[\frac{\hbar w_c/2E_0}{l + \frac{1}{2}} - 1\right] \quad (83)$$

when $\lambda^2 \ll (l + \frac{1}{2})$. These shifts might be applied to the square well diffuse boundary problem providing $(\hbar w_c/E_0)$ for a given l and v is identified on the basis of the unperturbed eigenvalues obtained from the diffuse boundary well. The sums of the energy shifts (apart from the factor $E_0\lambda^2$) may then be carried out directly for various values of $\epsilon_0{}^2$ for $\delta = 0.2$. The additional G functions associated with these sums was found to be fairly well represented by

$$G_h = 2.83\lambda^2(\epsilon_0)^{1/3}/A \quad (84)$$

This implies an additional energy sum for each type of particle of the form

$$E_h = 2.83\lambda^2\hbar^2(\epsilon_0)^{1/3}A^{2/3}/2Mr_0{}^2 \quad (85)$$

Ignoring the difference between the proton and neutron well strength parameter and letting $\epsilon_0 = e_0A^{1/3}$ the additional energy associated with the hollowness correction may be written as

$$E_h = \frac{2.83\lambda^2 e_0{}^{1/3}U_0}{2^{1/3}b_x{}^2}(1 - D^2/9A^2)A^{1/9} \quad (86)$$

Since the entire expression is based upon $\lambda^2 \ll \frac{1}{2}$ the approximate effect of the hollowness correction may be estimated by letting $\lambda^2 \approx 0.2$, $e_0 \approx 1.68$ and $b^x \approx 1.2$. The correction may be viewed as equivalent to the addition of a small approximately constant energy (14.2 mMU) plus a symmetry corresponding to a change in a_4 of about

$$\Delta a_4 = -0.046 \quad (87)$$

Accordingly, small degrees of hollowness change only slightly the symmetry energy and in the wrong direction. An attractive r^{-2} core would tend to increase the symmetry energy, however, since Equation 86 is only applicable when $\lambda^2 \ll \frac{1}{2}$ this effect would be insufficient to remove the difficulty.

6. DISCUSSION

Our studies indicate that one can derive a variety of combinations of semi-empirical parameters by the use of a diffuse boundary IPM model. Among these are cases ($b_x = 1.0$, $\delta = 0.3$ and 0.4) in which the symmetry energy may be sufficiently large to account for the line of beta stability. On the other hand the volume energy comes out too large in all cases. This latter difficulty, of course, is an intrinsic limitation which one can scarcely hope to eliminate with the strict IPM model since experiment has indicated that for light and medium weight the binding energy of the last particle frequently is greater than the average binding energy of all the particles. It is rather interesting to note that the energy

$$E = -\Xi L/A \quad (88)$$

where

$$\Xi = -\frac{A^2}{8} - \frac{D^2}{8} + 2A - |D| \quad (89)$$

which is associated with antisymmetric pairs in the Wigner model has the desirable property of reinforcing the symmetry energy and counteracting the volume energy. In view of the complexity and close proximity of the IPM levels in the diffuse boundary case one might well expect that a model which is intermediate between the strict IPM and the Uniform model would furnish a good description of the nucleus.

Alternatively one might look to two body forces which turn repulsive at short ranges, to velocity dependent forces, or to many body forces to provide the residual energy needed to derive a successful mass surface. In any event it is satisfactory to note that the IPM can provide a flexible first approximation to the actual mass surface.

REFERENCES

1. Von Weiszacker, C. F., Z. Physik *96*, 431 (1935).
2. Bethe, H. A. and Bacher, R. F., Revs. Modern Phys. *8*, 165 (1936).
3. Feenberg, E., Phys. Rev. *60*, 204 (1941).
4. Hammack, K. C., Dissertation, Washington University, June, 1951.
5. Hill, D. L. and Sheeler, J. A., Phys. Rev. *89*, 1102 (1953).
6. Rosenfeld, L., Nuclear Forces, Interscience Publishers, Inc., New York, 1948, Chap. IX.
7. Johnson, M. H. and Teller, E., Phys. Rev. *93*, 357 (1954).
8. Fitch, V. L. and Rainwater, J., Phys. Rev. *92*, 789 (1953).
9. Green, A. E. S., Phys. Rev. *95*, 1006 (1954).
10. Adair, R. K., Phys. Rev. *94*, 737 (1954).
11. Feshbach, H., Porter, C. E. and Weisskopf, V. F., Phys. Rev. *96*, 448 (1954).
12. Ford, K. W. and Bohm, D., Phys. Rev. *79*, 745 (1950).
13. Barschall, H. H., Phys. Rev. *86*, 431 (1952).

$O^{16}(n,\alpha)C^{13}$ Cross-Section for Neutrons in the Energy Range 3.6–4.2 Mev

By P. Huber* and J. Seitz,† Switzerland

Only one value is known for the cross section for $O^{16}(n,\alpha)$ at the present time,[1] namely the value $\sigma_\alpha = 310$ mb for a neutron energy of 14.1 Mev. The cross section for this reaction has a practical significance, aside from its interest from the point of view of nuclear theory, in relation to the use of water as a neutron moderator. According to Troyer and Tavernier,[2] neutron source-strength determinations for Ra-Be sources lead to different values depending on the use of water or paraffin as a moderating substance. This discrepancy is attributed to the absorption of fast neutrons in water by means of the $O^{16}(n,\alpha)C^{13}$ reaction.

NEUTRON SOURCE AND NEUTRON FLUX

We have used a *d-d* neutron source with a heavy ice target. The acceleration of the deuterons is accomplished by use of a 1 Mev cascade generator.[3]

The (n,p) scattering cross section has been used to determine the neutron flux. In the energy range of interest, this cross section is known to an accuracy of approximately 3%. For this purpose, the hydrogen recoil ionization chamber pictured in Fig. 1 has been employed. The chamber is equipped with a thick polyethylene radiator, the thickness being greater than the maximum range of the recoil protons. For a known range-energy relation for protons in polyethylene, the pulse-height distribution can be computed.[4] One then obtains a pulse-height distribution of the form

$$W(E) = \text{const.}\ (E/E_n)^{4/5}[1 - (E/E_n)^{3/2}]$$

where E_n is the neutron energy, and $W(E)\,dE$ is the number of recoil particles having an energy between E and $E + dE$.

The energy distribution of the recoil protons recorded with a 19-channel impulse spectrograph agrees well with this expression for neutrons observed in the forward direction (0 degrees) when a null-effect correction is made (Fig. 2). With increasing angle of emission the correspondence with theory becomes poorer on account of the increasing background of scattered neutrons. Agreement with theory can be obtained when correction is made for the contribution of the scattered neutrons (see Fig. 3).

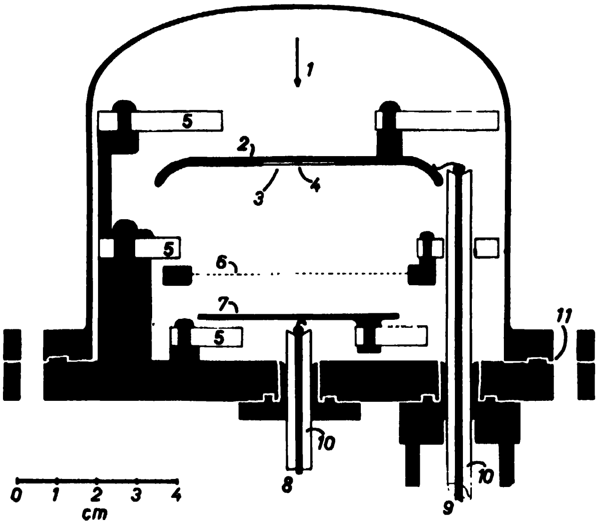

Figure 1. Section through H_2-recoil chamber: (1) direction of incident neutrons, (2) high-voltage electrode, (3) polyethylene layer, (4) polonium source for calibration purposes, (5) glass insulators, (6) grid, (7) collector electrode, (8) lead through to preamplifier, (9) high-voltage lead through, (10) steatite insulator, (11) lead gasket

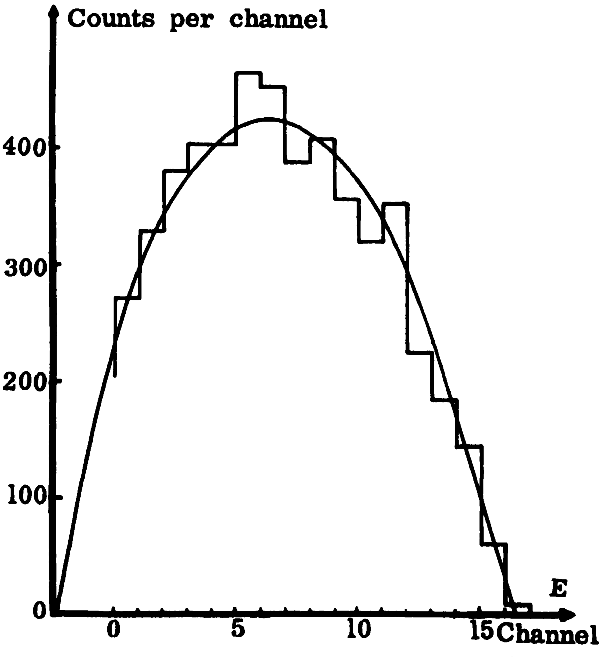

Figure 2. Recoil pulse spectrum due to forward neutrons, (E_n = 3.65 Mev): histogram, experimental curve; smooth curve, theoretical curve

---

* Physikalische Anstalt der Universität, Basel.

† i Fa. E. Haefely & Cie. A.-G., Basel.

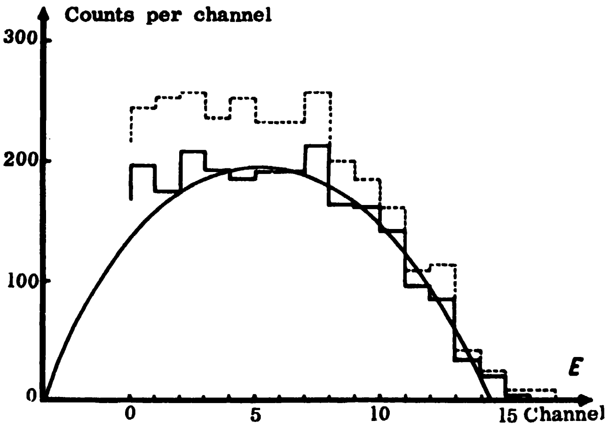

Figure 3. Recoil pulse spectrum for 105° neutrons (E_n = 2.38 Mev): punctuated curve (histogram), experimental result; smooth curve, corrected for scattered neutrons

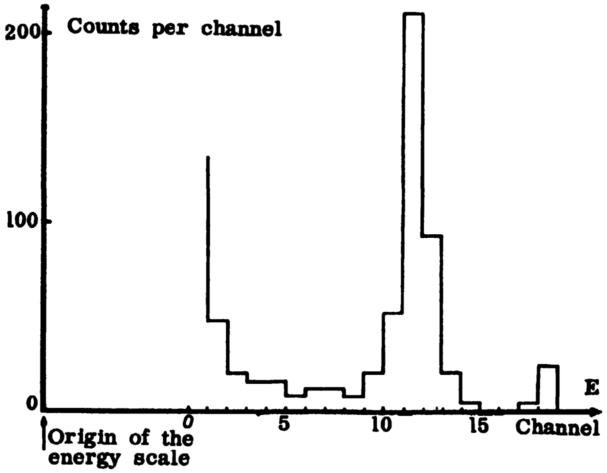

Figure 4. Pulse height distribution for the $O^{16}(n,\alpha)C^{13}$ reaction at E_n = 4.11 Mev

For the interpretation of the pulse spectra, the recorded and corrected spectrum is fitted with a theoretical curve which is then extrapolated to zero recoil energy. The area under the resulting curve corresponds to the total number N of recorded pulses per unit time. N divided by the neutron flux v is the efficiency of the chamber, for which we shall use the symbol μ_K. This can be computed to be

$$\mu_K = \frac{\int_0^{E_n} W(E)\,dE}{v} = (^{16}\!/_{13})n^*FR^*(E_n)\sigma_s(E_n)$$

where n^* = number of molecules of a gas per cm^3 at NTP; F = area of radiator (cm^2); R^* = range of a proton of energy E_n in ethylene at NTP; and $\sigma_s(E_n)$ = cross section for (n,p) scattering (cm^2).

From this expression the neutron flux can be determined for known σ_s since all other quantities are known.

Because of the large dimensions of the recoil chamber, it was used for an absolute calibration of a Hornyak counter. This counter was then employed in the cross-section determination.

CROSS SECTION FOR THE REACTION $O^{16}(n,\alpha)C^{13}$

The reaction was observed in an ionization chamber filled with oxygen to a pressure of 2886 ± 5 mm Hg. The pulses attributed to the disintegration alpha particles and the C^{13} recoils were amplified and displayed on the 19-channel pulse-height analyser. The neutron flux was determined by use of the calibrated Hornyak counter. A pulse-height distribution is shown in Fig. 4. The total number of alpha pulses in the pulse spectrum and the number of neutrons recorded with the Hornyak counter determine the reaction cross section. The variation of the total cross section with neutron energy is shown on Fig. 5. The statistical uncertainty of each point and the width of the neutron spectrum are indicated.

The variation of the cross section with energy observed here corresponds closely to what one would expect from the variation of the penetrability of the Coulomb barrier for the alpha particle. The dashed curve indicates the variation of penetrability with energy for $l = 0$ alpha particles calculated for a nuclear radius of 4.02 × 10^{-13} cm. The computed and experimental curves agree quite well. Two resonances are observed, namely at E_n = 3.90 Mev and E_n = 4.05 Mev. These correspond to excited

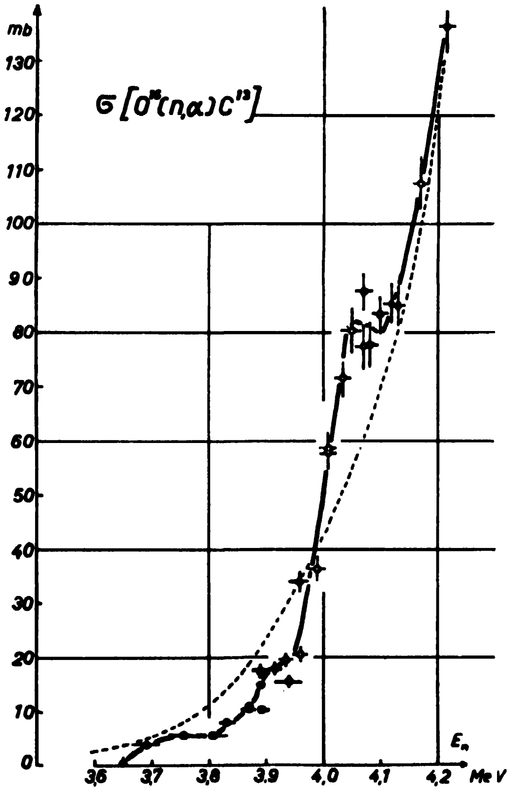

Figure 5. Cross section for $O^{16}(n,\alpha)C^{13}$; smooth curve, result of measurement; punctuated curve, penetrability of alpha-particle through Coulomb barrier

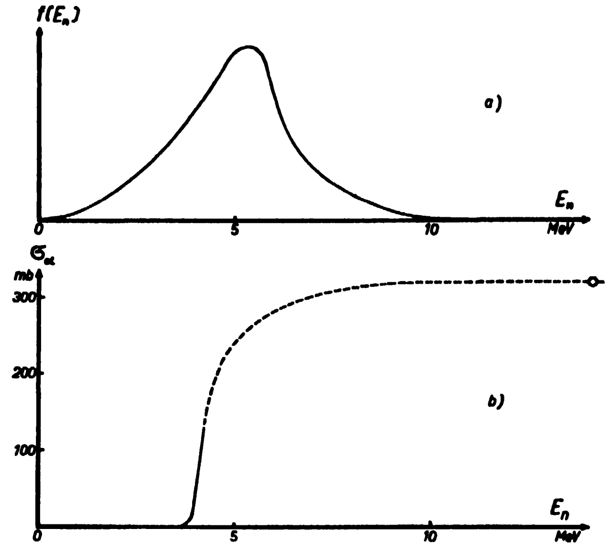

Figure 6. (a) Energy spectrum of Ra-Be neutrons (Racey *et al.*[5]); (b) cross section for $O^{16}(n,\alpha)C^{13}$. Smooth curve, our measurement; punctuated curve, arbitrary extrapolation; o, denotes Lillie's measurement

states of O^{17} at 7.81 ± 0.02 and 7.95 ± 0.02 Mev above the ground state.

H_2O AS MODERATOR FOR RA-BE NEUTRONS

We have mentioned that source strength determinations made with water and paraffin lead to different results, that is, for H_2O moderators a source strength 2.5 ± 0.3% smaller is determined than for paraffin moderators.[2] This is attributed to the $O^{16}(n,\alpha)C^{13}$ reaction. For a known energy spectrum of Ra-Be neutrons and known $O^{16}(n,\alpha)C^{13}$ cross section for the entire energy region, the loss of fast neutrons due to this reaction could be computed. Since σ_α values are known only for neutron energies up to 4.2 Mev, we have attempted a calculation of the loss under the following assumptions: (*a*) neutron spectrum has the form given by Racey *et al.*[5] (Fig. 6a); (*b*) cross section for $O^{16}(n,\alpha)C^{13}$ has the form shown on Fig. 6b; (*c*) scattering cross section for oxygen according to reference 6; (*d*) scattering cross section for hydrogen according to reference 7.

In the computation, we have employed the concept of "resonance escape probability," as defined by Glasstone and Edlund.[8] We then obtain for the proportion of the total number of neutrons captured by oxygen 3%. For the assumed neutron spectrum, this proportion is not strongly dependent on the type of extrapolation of the $O^{16}(n,\alpha)C^{13}$ reaction cross section (extrapolation shown in Fig. 6b).

REFERENCES

1. Lillie, A. B. Phys. Rev. 87, 716 (1952).
2. de Troyer, A. and Tavernier, G. C., Bull. Acad. Roy. Belg. Cl. Sci. 40, 150 (1954).
3. Delivered by Fa. E. Haefely & Cie. A.-G. Basel.
4. Seitz, J. and Huber, P., H.P.A. 28, 227 (1955).
5. Racey, E., Paine, R. W. and Goodman, C., Nuclear Shielding Studies III, Techn. Rep. 23, AEC File No. N.P. 1243 (1949).
6. "Neutron Cross-Section" AECU 2040, Suppl. 2 (June 1953).
7. "Neutron Cross-Section" AECU 2040, Suppl. 1 (Nov. 1952).
8. Glasstone, S. and Edlund, M. C., Nuclear Reactor Theory, Chapter VI.

Determination of Neutron Spectra with Nuclear Plates and Its Application to the Measurement of the Be^8 Excitation Levels

By Emma Perez Ferreira and Pedro J. Waloschek,* Argentina

I. EXPERIMENTAL TECHNIQUE

Introduction

Powell[1] called attention to the possibility of using nuclear plates for the determination of fast neutron spectra. Gibson and Livesey[2] subsequently developed a method for such determinations, which was followed by most of the later workers. Richards[3] also suggested a similar method which, while it was easier for experimental purposes, has the disadvantage of a low spectral resolution. A method used at the Los Angeles laboratory (California), and described in detail by Allred and Armstrong,[4] shows a similar disadvantage. Rosen[5] compiled over 60 references to publications on the subject.

Generally speaking, those methods entail the measurement of the angle of emergence θ and of the energy E_p of the recoil protons produced by impacts with the H nuclei of the emulsion of a plate so placed as to be grazed by the neutron beam (Fig. 1). These data serve as the starting point for computing the number of incident neutrons N and their energy E_n by means of equations:

$$dP = N(E) \cdot \sigma(E) \cdot A \cdot V \cdot \frac{\cos\theta}{\pi} \cdot d\Omega \cdot \Delta E \qquad (1)$$

$$E_p = E_n \cos^2\theta \qquad (2)$$

in which dP is the number of protons emitted by the neutrons in the energy interval ΔE, into the element of solid angle $d\Omega$. V is the volume and A the H content of the emulsion. $\sigma(E)$ is the neutron-proton scattering cross section.

Gibson and Livesey compute E_n by means of Equation 2, using, for each proton, its angle θ with the direction of incidence of the neutron beam; on the other hand, Richards, Allred and Armstrong measure only those tracks whose θ angle is so small that it may be assumed that the proton carries practically all the energy of the neutron which produced it, i.e., $E_n = E_p$, except for a correction factor obtained by averaging $\cos^2\theta$ over the whole of the solid angle containing the tracks. While this last method affords a great saving of time and work, since all the angular measurements are eliminated and the computations are simplified, its low resolving power makes the Gibson and Livesey method preferable.

Any high resolution method implies the computation of the energy of several thousands of protons, based on the microscopic measurement of one length and two angles for each of them. This means that in the measurement work it is important to apply criteria of selection which are sufficiently strict so as to avoid waste of time on proton tracks that would later be discarded for not being in the energy range in which it is intended to work, and also to simplify the computation of the energies and corrections using nomograms and tables in case electronic machines are unavailable.

This work was undertaken with that purpose in mind. Essentially the Gibson and Livesey method is followed, but the selection criteria are basically modified in order to obtain the greatest possible efficiency in the energy range for which information is sought, and to make a simple function available for the computation of the corrections for the efficiency of the method and for the emergence of tracks from the emulsion.

Selection of Tracks

The proton tracks to be measured are selected so that their projection along the direction of neutron incidence (x) is greater than a constant R_0, and that the angle with that same direction θ, is less than 45 degrees. This last criterion is applied, in part, during microscopic examination, and is completed after the computations have been made. Thus a fraction of the protons is selected, the energy of which is greater than $E_0 = (R_0/a)^{1/b}$, where a and b are constants of the emulsion.

Measurement

Measurements for each proton selected (Fig. 2) include: the angle α formed by the projection of the track on the plane of the plate with the direction x; the angle φ formed by the track and the plane of the plate; and the length L, of the projection of the track on the plane of the plate.

In order that the deviation of the track from its original direction, produced by scattering, distortion,

---

Original language: Spanish.

* Comisión Nacional de la Energía Atómica, Argentina.

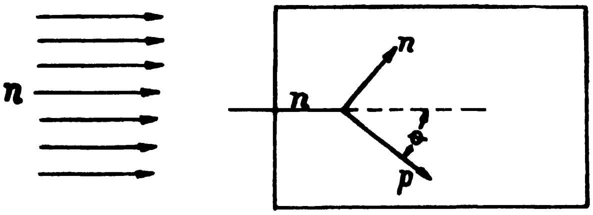

Figure 1

etc., should not affect the measurement, the angle α will be taken to be the one formed by the direction x and the tangent at the origin of the direction of the track. The angle φ is measured by taking the difference in depth (Δz) between the origin of the track and a point 100 divisions away from it on the optical scale.

The determination and recording of the data are carried out at a rate of about 10 protons per hour per person, using a binocular microscope (Ortholux) with a 100× immersion objective lens and a 10× eyepiece. (With this combination, the scale calibration gave: 100 divisions = 111 microns.) L is measured on the optical scale, following the track.

Computation of the Energy

The energy E_n of the neutron responsible for each recoil is derived from these data by applying formulae:

$$E_p = E_n \cos^2 \theta \qquad (2)$$

$$R = a \cdot E_p{}^b \qquad (3)$$

$$\cos \theta = \cos \alpha \cdot \cos \varphi \qquad (4)$$

where R is the range of the proton and E_p its energy.

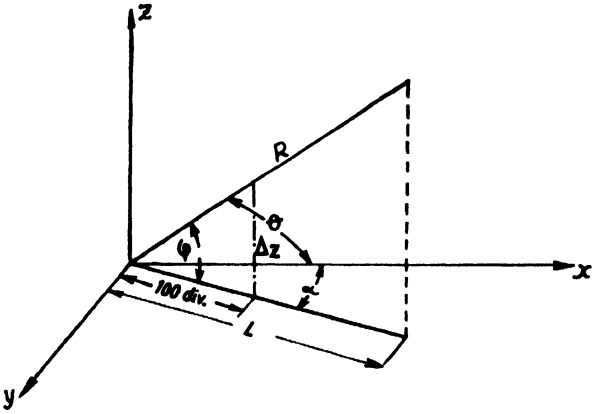

Figure 2

From Equations 2, 3 and 4, one can write:

$$a \cdot E_n{}^b = R(E) = \frac{L}{\cos^{2b+1} \varphi \cdot \cos^{2b} \alpha} \qquad (5)$$

The terms $\cos^{2b+1} \varphi$ and $\cos^{2b} \alpha$ are derived from Δz and α (in degrees) by means of a nomogram which also gives the value of θ (Fig. 3). This nomogram should be constructed especially for each plate, since the individual shrinkage factor modifies the scale on which Δz actually is measured.

For subsequent use of the data, and for checking purposes, a tabulation of the values for $\cos^{2b+1} \varphi$, $\cos^{2b} \alpha$ and θ is convenient.

The values for E are taken from a chart, or even better, from the 0.1 Mev tables of the US AEC (1953) corresponding to the Lattes *et al.* data of 1947.[6]

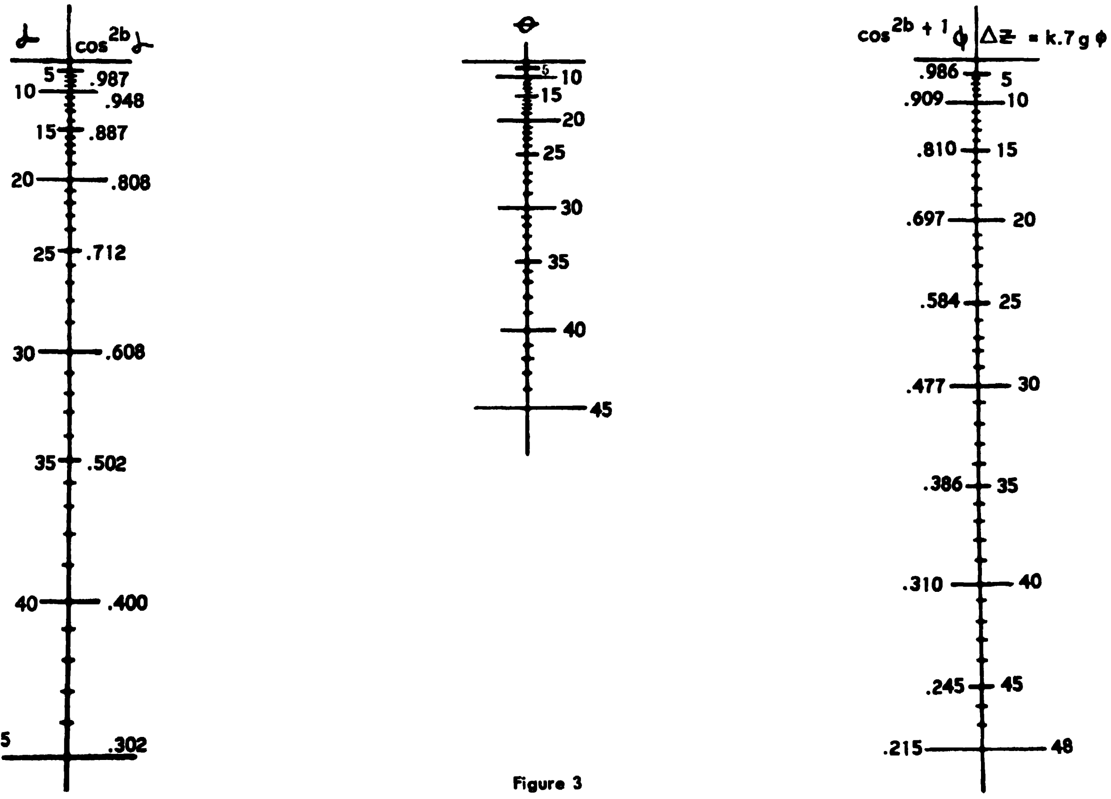

Figure 3

Evaluation of the Spectrum

Construct, with the E values obtained, an histogram $P(E_n)$, in which the interval ΔE is to be taken as small as possible, which, in this case, according to the resolution of the method, could be 0.1 Mev. In passing from the histogram to the curve $P(E_n)$ it is convenient, in order to avoid dispersion of the data, to increase the interval, for instance to $3\Delta E$.

In order to compensate for the consequent decrease in the number of points used for charting, it is convenient, instead of using the successive increased intervals, to have them partially overlap, in such a way as again to have data for each ΔE. The curve will be drawn through the points obtained by averaging the three possible ordinates which, in this case, will belong to each ΔE interval; this is the equivalent of a weighted average between the values for the interval in question and those adjacent to it.

In effect, the graphical method used yields:

$$P(\Delta E_i) = \frac{P(\Delta_3 E_{i+1}) + P(\Delta_3 E_i) + P(\Delta_3 E_{i-1})}{3}$$

$$= \frac{3P(\Delta E_i) + 2[P(\Delta E_{i+1}) + P(\Delta E_{i-1})] + [P(\Delta E_{i+2}) + P(\Delta E_{i-2})]}{3}$$

where $P(\Delta_3 E_i)$ is the ordinate corresponding to the increased interval which includes the simple intervals ΔE_{i-1}, ΔE_i and ΔE_{i+1}.

The resulting curve coincides, within less than 10^{-3}, with the one obtained by the usual method of polynomial approximation, in this case, of the second degree.

The errors of curve $P(E)$ also are easily obtained by joining the maximal and minimal values of consecutive intervals, as may be seen on Fig. 4.

The obtained $P(E)$ values are tabulated with 0.1 Mev intervals in order that the relevant corrections might be applied in passing from the proton to the neutron spectrum $N(E)$.

Corrections

The $P(E)$ curve, above, represents the neutron spectrum $N(E)$, multiplied by the (n,p) scattering cross section $\sigma(E)$, and a factor due to track suppression according to the selection criteria used, $A(E)$, and to emulsion emergence, $B(E)$ and $C(E)$:

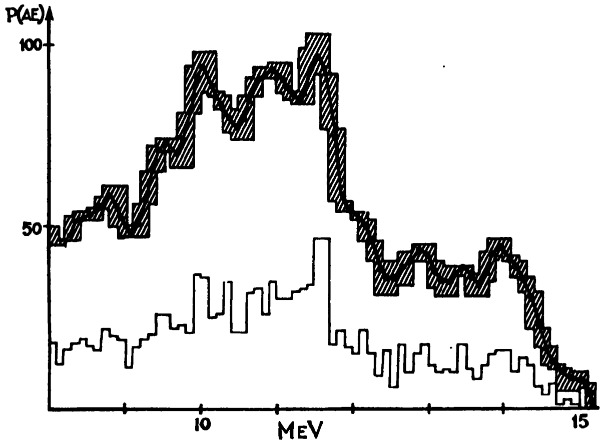

Figure 4

$$P_1(E) = V \cdot A \cdot N(E) \cdot \sigma(E) \cdot \Delta E[1 - A(E) - B(E)] \qquad (6)$$

where E is such that

$$R_0 \leq R(E) \leq \frac{R_0}{\cos^{2b+1} 45 \text{ degrees}}$$

and

$$P(E) = \tfrac{1}{2} A \cdot V \cdot N(E) \cdot \sigma(E) \cdot \Delta E[1 - C(E)] \qquad (7)$$

where E is such that:

$$R(E) > \frac{R_0}{\cos^{2b+1} 45 \text{ degrees}}$$

in which V is the revised volume of the emulsion, A the number of H atoms per cm^3 of emulsion, and

$$A(E) = \left[\frac{R_0}{R(E)}\right]^{2/2b+1} = \cos^2 \theta(E) \qquad (8)$$

$$B(E) = \frac{4R(E)}{\pi h} \int_0^{\theta(E)} \cos^{2b+1}\theta \sin^2 \theta \, d\theta$$

$$= \frac{4R_0}{\pi h} \left[\frac{R(E)}{R_0} \int_0^{\theta(E)} \cos^{2b+1} \theta \sin^2 \theta \, d\theta\right] = \frac{4R_0}{\pi h} B'E \qquad (9)$$

$$C(E) = \frac{0.1656}{h} \cdot R(E) \qquad (10)$$

All these corrections are applicable provided that (See Appendix):

$$h > 0.303R(E)$$

The integral given in Equation 9 was computed numerically and plotted with enough accuracy to obtain its values as a function of $R_0/R(E)$ through

$$\cos^{2b+1} \theta(E) = \frac{R_0}{R(E)} \qquad (11)$$

shown in the same graph (Fig. 5). The data obtained appear on Table I, together with the values for:

$$1 - A(E) = \sin^2 \theta(E) \qquad (12)$$

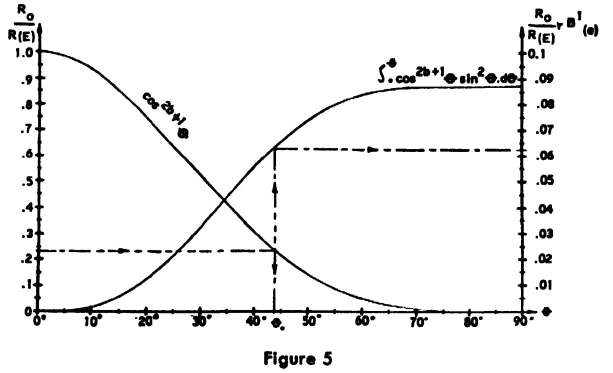

Figure 5

The total correction for selection and escape, for each energy interval in which Equation 6 holds good, is obtained, for a given R_0 and h, by computing first the corresponding $R_0/R(E)$, and then applying the values of Table I to Equation 6. We obtained the values appearing in Fig. 6 for $R = 111$ microns and $h = 400$ microns. A tabulation in function of $R_0/R(E)$ when Equation 7 should be applied was not deemed necessary, due to the simplicity of the relationship it expresses. Figure 6 also includes the resulting values of the aforementioned R_0 and h in this energy interval.

II. DETERMINATION OF THE NEUTRON SPECTRUM FOR THE Li(*d*,*n*)Be REACTION

Li(*d*,*n*)Be Reaction Neutrons

The bombardment of lithium with deuterium in the accelerator is one of the methods most used for obtaining neutrons over a spectrum extending up to 15 Mev. Richards[8] determined the energy of these neutrons in 1941, and Green and Gibson[4] improved the measurement in 1949; the spectrum produced by Li^6 and by Li^7 also was observed. Trumpy *et al.*[9] measured, in

Table I

$R_0/R(E)$	$0_0'$	B'	$1 - A$
0.00	90 00	∞	1.000
0.01	70 00	8.65	0.883
0.02	65 50	4.28	0.832
0.03	63 20	2.83	0.799
0.04	60 50	2.09	0.763
0.05	59 10	1.66	0.737
0.06	57 50	1.36	0.717
0.07	56 40	1.15	0.698
0.08	55 30	0.996	0.679
0.09	54 20	0.873	0.669
0.10	53 20	0.775	0.643
0.11	52 30	0.695	0.629
0.12	51 40	0.628	0.615
0.13	50 50	0.571	0.601
0.14	50 00	0.522	0.587
0.15	49 05	0.480	0.571
0.16	48 25	0.443	0.560
0.17	47 45	0.411	0.548
0.18	47 05	0.382	0.536
0.19	46 30	0.356	0.526
0.20	45 55	0.333	0.516
0.21	45 15	0.311	0.504
0.22	44 40	0.292	0.494
0.23	44 05	0.275	0.484
0.24	43 30	0.259	0.474
0.25	42 55	0.244	0.464
0.26	42 20	0.230	0.454
0.27	41 50	0.217	0.445
0.28	41 20	0.206	0.436
0.29	40 45	0.195	0.426
0.30	40 15	0.185	0.418
0.31	39 50	0.175	0.410
0.32	39 15	0.166	0.400
0.33	38 45	0.158	0.392
0.34	38 15	0.150	0.383
0.35	37 50	0.143	0.376
0.36	37 20	0.136	0.368
0.37	36 50	0.129	0.359
0.38	36 25	0.123	0.352
0.39	36 00	0.117	0.346
0.40	35 30	0.111	0.337
0.41	35 05	0.106	0.330
0.42	34 40	0.101	0.324
0.43	34 10	0.096	0.315
0.44	33 45	0.092	0.309
0.45	33 15	0.087	0.301
0.46	32 50	0.083	0.294
0.47	32 25	0.079	0.287
0.48	32 00	0.075	0.281
0.49	31 35	0.072	0.273
0.50	31 10	0.068	0.268
0.51	30 40	0.065	0.260
0.52	30 20	0.062	0.255
0.53	29 50	0.059	0.248
0.54	29 25	0.056	0.241
0.55	29 00	0.053	0.235
0.56	28 35	0.051	0.229
0.57	28 10	0.048	0.223
0.58	27 45	0.046	0.217
0.59	27 20	0.043	0.211
0.60	26 55	0.041	0.205
0.61	26 30	0.039	0.199
0.62	26 10	0.037	0.193
0.63	25 40	0.035	0.188
0.64	25 10	0.033	0.181
0.65	24 45	0.031	0.175
0.66	24 20	0.029	0.170
0.67	23 55	0.027	0.164
0.68	23 25	0.026	0.158
0.69	23 00	0.024	0.153
0.70	22 35	0.023	0.148
0.71	22 15	0.021	0.143
0.72	21 45	0.020	0.137
0.73	21 20	0.019	0.132
0.74	20 55	0.018	0.128
0.75	20 25	0.016	0.122
0.76	19 55	0.015	0.116
0.77	19 25	0.014	0.111
0.78	18 55	0.013	0.105
0.79	18 25	0.012	0.100
0.80	18 00	0.011	0.096
0.81	17 25	0.010	0.090
0.82	16 55	0.010	0.085
0.83	16 25	0.009	0.080
0.84	15 50	0.008	0.074
0.85	15 25	0.007	0.071
0.86	14 45	0.007	0.065
0.87	14 15	0.006	0.061
0.88	13 30	0.005	0.055
0.89	13 00	0.005	0.051
0.90	12 30	0.004	0.047
0.91	11 50	0.003	0.042
0.92	11 05	0.003	0.037
0.93	10 30	0.002	0.033
0.94	9 40	0.002	0.028
0.95	8 50	0.001	0.024
0.96	8 00	0.001	0.019
0.97	7 00	0.001	0.014
0.98	6 00	0.000	0.011
0.99	4 10	0.000	0.005

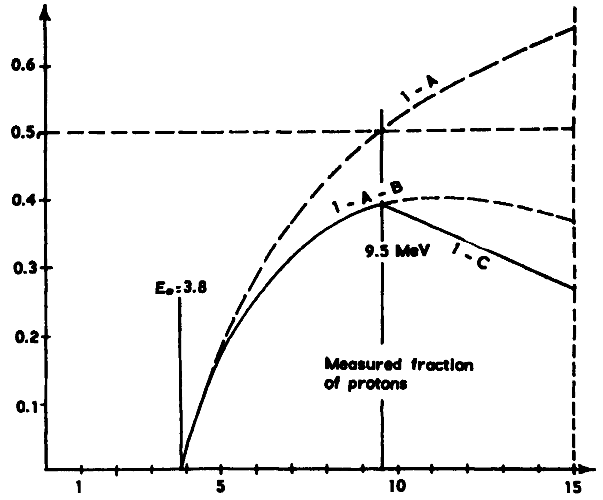

Figure 6

1952, the spectrum obtained with seven different angles relative to the direction of the deuterons, thus also obtaining the angular distribution. The energy values obtained for the peaks of the spectrum by the different authors (excepting Richards, whose resolution was poor) are in substantial agreement and give good information on the Be^8 and Be^7 excitation levels. However, the intensity of the peaks found shows differences due to several factors, particularly to the dependence on the geometry of the Li target and the criteria on selection of tracks used.

Exposure and Development of the Plates

Plates were exposed about the Li target of the C.N.E.A. cascade accelerator (Buenos Aires), in the positions shown in Fig. 7, between −150 and +150 degrees, for 12.9 μa-hr and at 900 kv. The distance from the source was 22 cm.

Ilford G5, 2 × 3 in., 400 micron plates were used; development was carried by the Dainton *et al.*[10] (1951; Bristol) hot-plate method. About nine days of processing are required before a plate ready for microscopy is obtained.

Notwithstanding the G5 plate sensitivity to electrons, the background produced by the exposure was not excessive, and, on the other hand, one had the advantage of good proton track visibility ("black" tracks). Previous trial exposures at 0 and 90 degrees had been made, from which the plates used for another determination of the spectrum of the same reaction were obtained, using a graphical method (1953).[11]

Leitz 24:1, 53:1 and 100:1 special nuclear plate objective lens sets were used for the measurements, particularly the latter, and 10 × eyepiece pairs, one with a scale, and the other with a grid.

Spectra at 0 and 90 Degrees

Among the plates exposed as above, those at 0 and at 90 degrees were selected while, at 0 ± 1 and 90 ± 1 degrees, respectively, the recoil protons were selected according to the criterion explained earlier, and in volumes 5 to 10 mm from the edge of the plate closer to the Li target.

Figures 8 and 9 show the results obtained in the determination of the neutron spectrum, including the emergence, efficiency and cross-section corrections.

In both cases, the applicability condition of the method ($h > 0.303\ R(E)$) applied, since the range of the protons of maximal energy obtained in the reaction under study (15 Mev), was about 1140 microns, and 400 micron plates were used.

III. CONCLUSIONS

Be^8 Excitation Levels

As already shown by Green and Gibson (1949)[7] the neutrons of over 5 Mev produced in lithium by the deuterium can only come from reactions:

$$Li^7 + d \rightarrow Be^8 + n$$

$$Li^7 + d \rightarrow \alpha + \alpha + n$$

The former produces neutrons in individual groups, since the Be^8 may remain excited, a condition which is in agreement with observations made in the course of other experiments, while the latter produces neutrons having energies showing the characteristic spectral distribution of disintegration into three particles.

The Q of the first reaction above may be computed for the neutron spectrum peaks, allowing for the neutron emission angle and the incident deuterium energy (where the loss of energy of the deuterium in the thick lithium target should be observed). Q was computed in this fashion for the measured spectra, to which were added those of the papers published by Green and Gibson,[7] and Trumpy *et al.*,[9] and all were

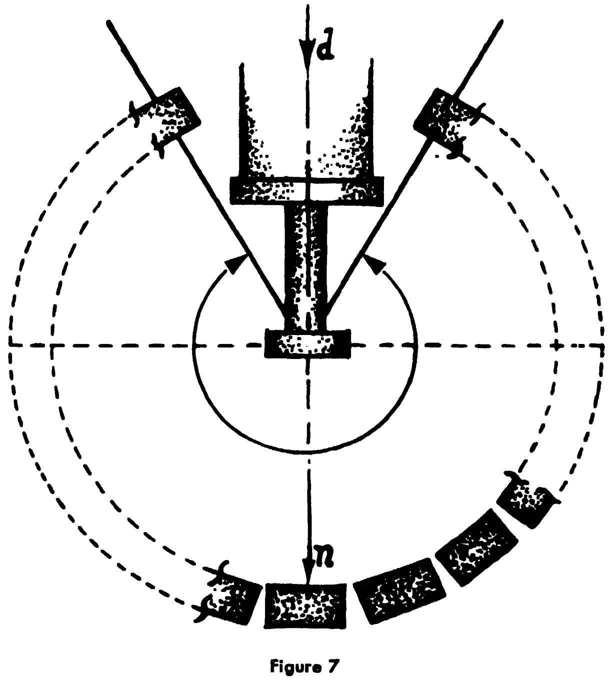

Figure 7

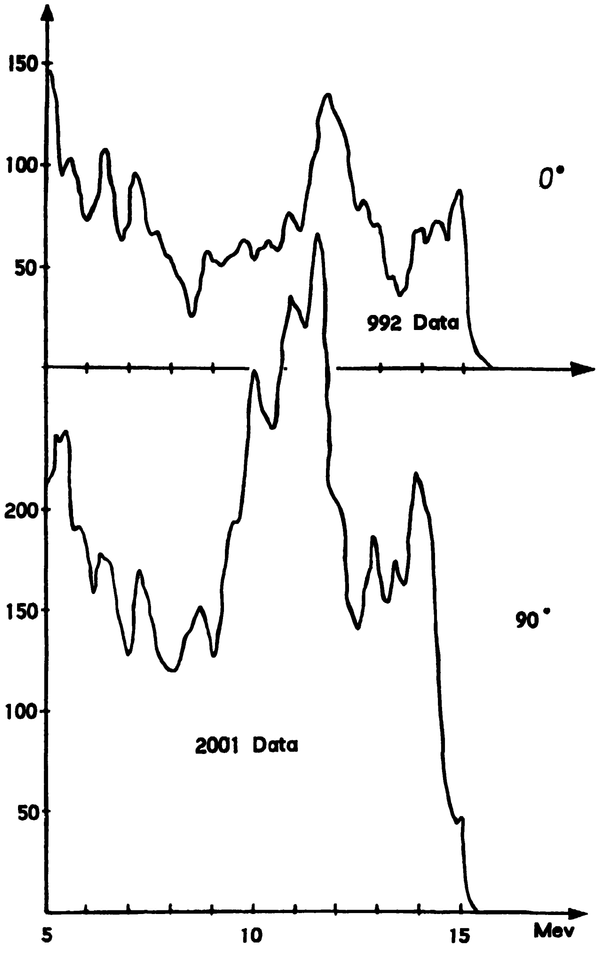

Figure 8. (Above) Figure 9. (Below)

grouped in Fig. 10. To the spectra given by these authors (solid line), we added a dotted line connecting the experimental data.

Perfect coincidence of the 15 Mev peak is observed in all the measurements.

The other observed peaks were those corresponding to 2.8, 3.4, 4.2 and 5.0 Mev Be^8 excitation energies, of which the 2.8 and 3.4 levels have not been resolved to date, although they are suggested by all the data gathered so far.

These peaks are verified by other reactions in which the Be^8 excitation levels come into play (see Green and Gibson[7]). This is not true of the other peaks that may be observed but, when computing the value of Q they do not coincide. These are probably due to impurities in the target or to mutual actions with the target holder.

Note:

The Richards (*R*) data of over 6 Mev are statistically poor, since they were measured from 2 Mev, and the greater part of the neutrons (⅘) are accumulated between 2 and 5.

The Trumpy *et al.* data (*B*) were taken from a short abstract published in *Nature* (1952). The complete data published in Bergen (1953), were not received at Buenos Aires.

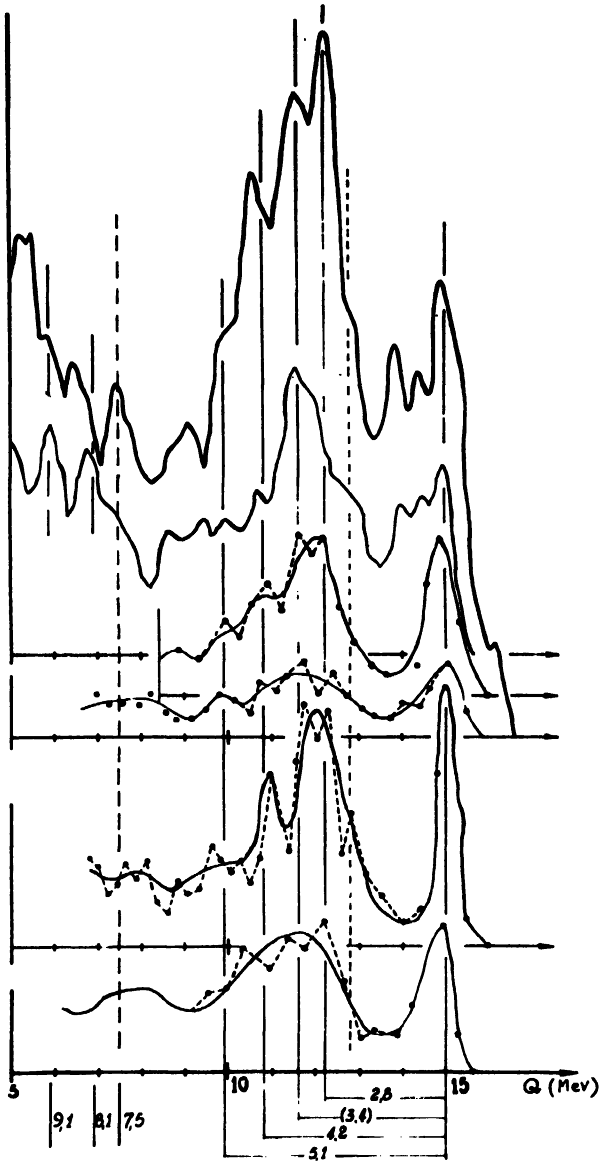

Figure 10

The Green and Gibson (G & G) data above 7.5 Mev are not corrected for emergence, so that the relevant ordinates are not comparable with other measurements. The small thickness of the plates used in most of the work (100 microns) greatly reduces the number of the protons between 11 and 15 Mev.

Method Used

It has been possible, by the selection criteria used in the high resolution method (chapter II) to map out the area of the spectrum in which measurements are taken (See efficiency curve, Fig. 6). This eliminates the superfluous data and greatly improves the statistics in the maximal efficiency zone which, on the other hand, may be selected according to the spectrum being studied, taking the appropriate R_0 and θ_{lim} parameters.

In this fashion the greater part of the measured data were obtained in the 8 to 13 Mev zone, giving great precision in the details of the peaks grouped about 11 Mev in the 90 degree spectrum. In these peaks, the data obtained within each 0.3 Mev interval are of the order of 50 in each 1000 measured protons while Richards, for example, gets some 5 per 1000 protons measured, over a 0.4 Mev interval.

With only two microscope operators some 1000 data are collected in about a fortnight by the high resolution method, which if they fall within a zone of the spectrum which is not unduly wide, do give good information on it.

APPENDIX

Computation of Corrections

From Equations 2 and 3 one can find out that the range of a proton produced by a neutron of energy E_n, which forms an angle θ with the direction of the incidence of the latter is:

$$R_p = a \cdot E_n^{\,b} \cdot \cos^{2b}\theta \qquad (13)$$

where $a \cdot E_n^{\,b}$ represents the range of a proton having the energy E_n of the incident neutron, which we shall express as:

$$a \cdot E_n^{\,b} = R(E)$$

Thus:

$$R_p = R(E)\cos^{2b}\theta \qquad (14)$$

It will be seen here that all the recoil proton tracks created in the same elementary volume by monoenergetic neutrons will end over surfaces defined by the $R = K(\cos^{2b}\theta)$ equation. Once they are drawn for the different energies, the cross sections of these surfaces will show the outline indicated in Fig. 11 (assuming that $b = 1.725$), serving as the base for the development of the graphical method for the determination of the neutron spectra mentioned in Section II.

On the other hand, the number of recoil protons originated in a $s \cdot dz$ volume of emulsion located at depth z, with A atoms of H per cm^3, crossed by $N(E)$ neutrons of an energy included in the interval ΔE, and which are emitted within solid angle $d\Omega$, forming angle θ with the direction of neutron incidence is:

$$dP = A \cdot s \cdot N(E) \cdot \sigma(E,\theta) \cdot d\Omega \cdot dz\,\Delta E \qquad (15)$$

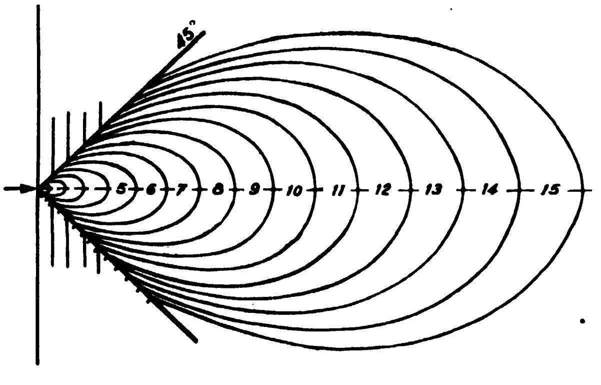

Figure 11

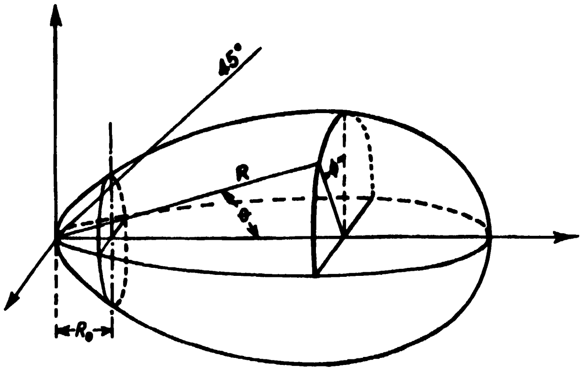

Figure 12

with $\sigma(E,\theta) = (\sigma(E)\cos\theta)/\pi$ the (n,p) differential cross section and $(d\Omega)$ the solid angle which, in our case, is $d\Omega = \sin\theta\, d\theta\, d\phi$ (Fig. 12), from which the total number of protons produced by the neutrons in interval ΔE will be:

$$P(E) = \frac{A}{\pi} \cdot s \cdot N(E) \cdot \sigma(E) \int_z\int_\theta\int_\phi \sin\theta \cos\theta\, d\theta\, d\phi\, dz\, \Delta E \qquad (16)$$

The limits for each one of the successive integrations will be deduced from the conditions resulting from the selection of the tracks for their measurements: (*a*) angle formed with the direction of incidence smaller than 45 degrees: $\theta < 45$ degrees; (*b*) projection of the track on direction x, greater than a constant value: $R(E)\cos^{2b+1}\theta > R_0$; and (*c*) trace totally contained in the emulsion: $R(E)\cos^{2b}\theta \sin\theta \cos\phi < z$.

In order to be able to judge the physical meaning of the integration limits thus derived, the following reasoning may be used (Fig. 13).

For a given energy, and for each θ direction, there is a boundary or limiting value z_0 such that, for each value $z < z_0$ a part of the relevant protons escape from the emulsion through its surface ($z = 0$); while on the other hand, for $z > z_0$, all the recoil protons produced with such an angle will have been counted since their tracks end within the emulsion.

Therefore, within the first zone, i.e., for $0 < z < z_0$, there will remain, within the emulsion, those protons

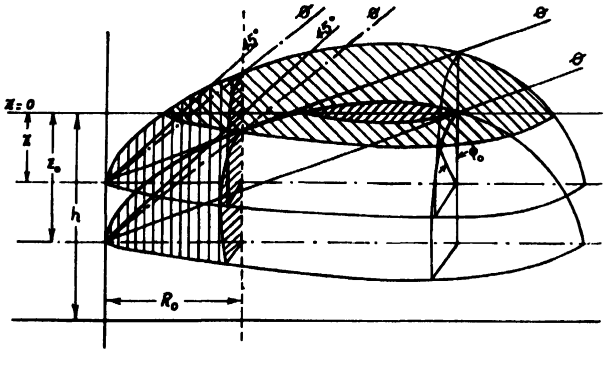

Figure 13

whose ϕ would be larger than a ϕ_0, minimum ϕ_0, which is the one deduced from condition (*c*)

$$\phi_0 = \text{arc cos}\,\frac{Z}{R(E)\cdot\cos^{2b}\theta\cdot\sin\theta} \qquad (17)$$

and, if we consider only the upper "half lobes" (related to the emergence through the surface of the emulsion), all those protons whose ϕ is such that $\pi/2 > \phi > \phi_0$ will have been counted.

On the other hand, for $z_0 < z < h$ (h is emulsion thickness) it was observed that all the protons would be counted regardless of their ϕ. The value z_0 is also deduced from conditions (*c*) for

$$\phi = 0, \qquad (\cos\phi = 1)$$

or, it is:

$$Z_0 = R(E)\cdot\cos^{2b}\theta\sin\theta \qquad (18)$$

Therefore the integration of Equation 16 should be carried out leaving the integral over ϕ for last, as follows:

$$P(E) = \frac{2A}{\pi}sN(E)\sigma(E)\int_\theta\left[\int_{z=0}^{z_0}2\int_{\phi=\phi_0}^{\pi/2}\sin\theta\cos\theta\, d\phi\, dz + \int_{z_0}^{h}2\int_0^{\pi/2}\sin\theta\cos\theta\, d\phi\, dz\right]d\theta\,\Delta E \qquad (19)$$

in which the factors 2, in the two terms within the bracket, complete the rear part of each half lobe, and the 2 applied to the expressions as a whole causes the contribution of the lower half lobes and resulting emergence through the lower surface of the emulsion to be taken into account.

Regarding the integral over θ, it will suffice to take it between 0 and a θ_0 deduced from condition (*b*)

$$\theta_0 = \text{arc cos}\left[\frac{R_0}{R(E)}\right]^{\frac{1}{2b+1}} \qquad (20)$$

provided this θ_0 is smaller than 45 degrees (case shown on Fig. 13). If not, it will be taken only between 0 and 45 degrees (case shown on Fig. 13). Therefore, it will be necessary to split Equation 19 in two parts, obtaining:

for $\quad R_0 < R(E) < \dfrac{R_0}{\cos^{2b+1}45\text{ degrees}}$:

$$P_1(E) = 2\frac{A}{\pi}sN(E)\sigma(E)\int_{\theta=0}^{\theta_0}\left[\int_{z=0}^{z_0}2\int_{\phi=\phi_0}^{\pi/2}\sin\theta\cos\theta\, d\phi\, dz + \int_{z_0}^{h}2\int_0^{\pi/2}\sin\theta\cos\theta\, d\phi\, dz\right]d\theta\,\Delta E \qquad (21)$$

and for:

$$R(E) > \frac{R_0}{\cos^{2b+1}45\text{ degrees}}:$$

$$P_2(E) = 2\frac{A}{\pi}sN(E)\sigma(E)\int_{\theta=0}^{\pi/2}\left[\int_{z=0}^{z_0}2\int_{\phi=\phi_0}^{\pi/2}\sin\theta\cos\theta\, d\phi\, dz + \int_{z_0}^{h}2\int_0^{\pi/2}\sin\theta\cos\theta\, d\phi\, dz\right]d\theta\,\Delta E \qquad (22)$$

After computing both integrals, we have, taking $V = s\,h$:

$$P_1(E) = AVN(E)\sigma(E)\left[1-\left(\frac{R_0}{R(E)}\right)^{2/2b+1} - \frac{4R(E)}{\pi h}\int_0^{\theta_0}\cos^{2b+1}\theta\sin^2\theta\, d\theta\right]\Delta E \qquad (23)$$

$$P_2(E) = \frac{A}{2}VN(E)\sigma(E)\left[1-\frac{0.1656}{h}R(E)\right]\Delta E \qquad (24)$$

in which one can see the correction terms due to intersection with a plane at distance R_0 and to the emergence of tracks from the emulsion in the first expression and only this last condition in the second.

An indispensable requirement yet has to be taken into consideration in order that this result be valid. When referring to the integration over z we said that there was no emergence from the emulsion for $z_0 < z < h$; this means that it is a necessary condition for this reasoning that $h > z_0$ and, since this should happen for all possible directions of θ, it is a necessary condition that $h > \max[z_0]$, a value easily obtained by making the z_0 differential equal to zero:

$$-2b\cdot R(E)\cos^{2b-1}\theta\sin^2\theta + R(E)\cos^{2b+1}\theta = 0$$

Solving:

$$\cos^2\theta - 2b\sin^2\theta = 0 \qquad \tan\theta = \sqrt{\frac{1}{2b}}$$

Therefore:

$$\max[z_0] = R(E)\cdot\frac{(1/2b)^{1/2}}{(1+1/2b)^{b+1/2}}$$

and:

$$\max[z_0] = 0.303\cdot R(E) \qquad (25)$$

REFERENCES

1. Powell, *Further applications of the photographic method in nuclear physics*, Nature, 145, 155, Bristol (1940).
2. Gibson and Livesey, *The neutrons emitted in the disintegration of nitrogen by deuterons*, Proc. Phys. Soc., 60, 523, Cambridge (1948).
3. Richards, *A photographic plate spectrum of the neutrons from the disintegration of lithium by deuterons*, Phys. Rev., 59, 796, Texas (1941).
4. Allred and Armstrong, *Laboratory handbook of nuclear microscopy*, Report of Los Alamos Scientific Laboratory, USAEC (1953).
5. Rosen, *Nuclear emulsion techniques for the measurement of neutron energy spectra*, Nucleonics, July and August (1953).
6. Lattes, Fowler and Cuer, *A study of the nuclear transmutations of light elements by the photographic method*, Proc. Phys. Soc. 59, 883, Bristol (1947).
7. Green and Gibson, *The neutrons emitted in the disintegration of lithium by deuterons*, Proc. Phys. Soc., 62, 407, Cambridge (1949).
8. Green and Gibson, *The neutrons emitted in the bombardment of Li^6 by deuterons* Proc. Phys. Soc., 63, 494, Cambridge (1950).
9. Trumpy, Grodtal and Graue, *Angular distribution of the neutrons from the reaction Li^7 (d,n) Be^8*, Nature, 170, 1118, Bergen (1952).
10. Dainton, Gattiker and Lock, *The processing of thick photographic emulsions*, Phil. Mag., Ser. 7, 42, 396, Bristol (1951).
11. Waloschek, Pérez Ferreira and Roederer, *Un método gráfico para la determinación de espectros de neutrones rápidos*, Communicación a la Asociación Física Argentina, Buenos Aires (1953).

On Mass Estimation of Non-Relativistic Charged Particles in Nuclear Emulsions

By J. Ausländer, C. Bercea and E. Friedländer,* Romania

In nuclear emulsion work, one is often confronted with one of the two following tasks: (*a*) to estimate the mass of an unknown particle which escapes from the emulsion; (*b*) to ascertain whether a particle with track ending in the emulsion has been stopped by ionization losses only.

In this paper we shall describe a method for settling these two problems with tracks of non-relativistic particles of unit charge.

We shall restrict ourselves to the case of particles such that the mass determination by grain-counting is rendered impossible by the blackness of the track. Though, in principle, such tracks may be analyzed by gap-measurements or photoelectric densitometry, the well-known difficulties concerning calibration diminish the practical value of these procedures.

The only track characteristic which does not depend on the processing of the emulsion and does not imply the presence of calibration tracks of special requirements, is the scattering sagitta D. Our method is based entirely on the variation of this quantity along the track, once the (RE) relation of the emulsion is known. In certain limits the method can be used inversely to estimate the exponent of the (D,R) relation from tracks of particles known by other means to be stopped in the emulsion by ionization losses only.

MASS ESTIMATE OF NON-STOPPED PARTICLES IN FIRST APPROXIMATION

Consider the track of a particle which leaves the emulsion (Fig. 1). At both ends of the track we chose the sections $A_0' A_0''$ and $A_1' A_1''$ of lengths Λ_0 and Λ_1 and determine the corresponding average values $\langle D_0 \rangle$ and $\langle D_1 \rangle$.

We make use of the well-known relation:[1]

$$D = Cm^{-\gamma} R^{\gamma - 1} \tag{1}$$

where

$$\gamma = 1/(k+1) \tag{2}$$

and k has the meaning given in reference 1.

By R_0 and R_1 we shall designate the residual ionization ranges which would appear if the emulsion were infinite. Then evidently

$$(R_0/R_1) = [\langle D_1 \rangle / \langle D_0 \rangle]^{\frac{1}{1-\gamma}} \tag{3}$$

Assuming R_0 and R_1 to refer to the centers a_0 and a_1 of Λ_0 and Λ_1, separated by the distance L (Fig. 1) we have

$$R_0 = \frac{Q}{Q-1} L, \qquad R_1 = \frac{1}{Q-1} L \tag{4}$$

where

$$Q \equiv \left[\frac{\langle D_1 \rangle}{\langle D_0 \rangle}\right]^{\frac{1}{1-\gamma}} \tag{5}$$

In this way, the usual (α,R) method can be applied to non-stopped particles.

A preliminary note on this subject has been communicated to the Academy of the Rumanian People's Republic on April 23, 1954.[2] Later we came to know that in his paper,[3] Beiser hinted at the possibility of such a way of mass estimate without going into details. The method has been applied by two of us[4] to the analysis of an unusual V^0 decay.

Preliminary tests—which do not take into account the rigorous considerations, to be exposed in the following section—were carried out on tracks of stopped cosmic-ray particles recorded in an Ilford G5 plate.

For tracks of sufficient length and near enough to the end of their range, the agreement with the values furnished by the usual (α_1,R) method is quite satisfactory. For instance, for the 2000μ track of a deuteron issued from a $4 + 0_p$ star we obtained

$$m = (1.98 \pm 0.16) m_p$$

MASS ESTIMATE AVOIDING APPROXIMATIONS

Rigourously speaking, the $\langle D \rangle$'s do not refer to the centers of the sections (Fig. 1), but to some points displaced with respect to these centers, since the (D,R) relation is not linear.

Taking into account that $\langle D_j \rangle$ (with $j = 0$, or 1) is defined as

$$\langle D_j \rangle \equiv \frac{1}{R_j'' - R_j'} \int_{R_i'}^{R_i''} D\,dR = \frac{C_m^{-\gamma}}{\gamma} \cdot \frac{R_j''^{\gamma} - R_j'^{\gamma}}{R_j'' - R_j'} \tag{6}$$

where R_j and R_j'' refer to Λ_j' and Λ_j'' (Fig. 1) and the evident relations:

$$R_j'' - R_j' = \Lambda_j \tag{7}$$

and

$$L \equiv R_0 - R_1 = \frac{R_0'' + R_0'}{2} - \frac{R_1'' + R_1'}{2} \tag{8}$$

---

* Institute of Physics, Academy of the Romanian People's Republic, Bucharest.

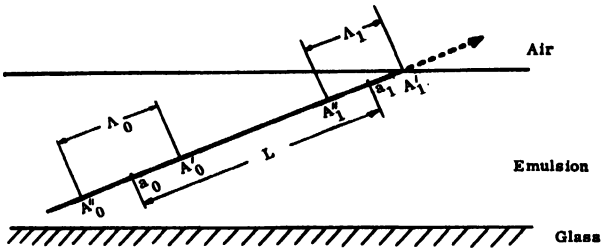

Figure 1

we have five equations which can be solved numerically with respect to the two pairs R_j' and R_j'' and the fifth unknown quantity m. It should be stressed that, for the purpose pursued, m is the only relevant quantity.

Computations by the rigourous method are under way.

A CRITERION FOR ABSENCE OF NON-IONIZATION ENERGY LOSSES

As to the second problem mentioned earlier, the following variant of the above method leads to some interesting results.

Let us consider a case in which the visible end of the track may not be identical with the end of the ionization range. For instance, such a doubt arises frequently in cases of spontaneous decay (decay in flight or at rest). Let r (Fig. 2) be the residual ionization range at the visible end of the track. The value $r = 0$ would be a particular case thereof. We chose the two sections Λ_0 and Λ_1 so that they cover the whole visible length of the track l, and divide it in the ratio $f:1-f$ (Fig. 2). We determine experimentally the average values $\langle D_f \rangle$ and $\langle D_{1-f} \rangle$ for different values of f. In this case, the system of Equations 6, 7 and 8 becomes:

$$\langle D_f \rangle = \frac{C_m^{\ \gamma}}{\gamma} \cdot \frac{R_f^{\gamma} - r^{\gamma}}{R_f - r} \tag{9}$$

$$\langle D_{1-f} \rangle = \frac{C_m^{-\gamma}}{\gamma} \cdot \frac{R_t^{\gamma} - R_f^{\gamma}}{R_t - R_f} \tag{10}$$

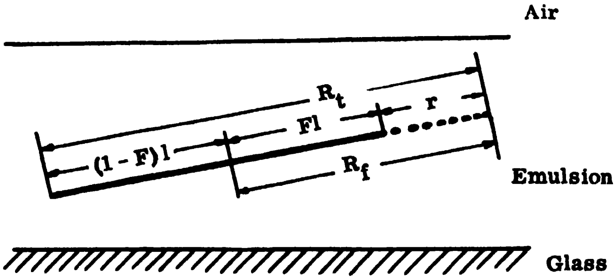

Figure 2

$$R_f - r = fl \tag{11}$$

$$R_t - R_f = (1+f)l \tag{12}$$

R_t and R_f can be found on Fig. 2.

If all ranges are expressed in terms of l as the unit of length, Equations 9-12 yield

$$Y_f \equiv \frac{\langle D_{1-f} \rangle}{\langle D_f \rangle} \cdot \frac{1-f}{f} = \frac{(r+1)^{\gamma} - (r+f)^{\gamma}}{(r+f)^{\gamma} - r^{\gamma}} \tag{13}$$

As all quantities of Equation 13 except r are known or can be measured directly, this equation can be solved numerically with respect to r.

In the particular case $r = 0$, Equation 13 takes the very simple form:

$$Y_f + 1 = f^{-\gamma} \tag{14}$$

The plot of log $(Y_f + 1)$ against log f, is a straight line of slope $(-\gamma)$.

It is important to point out that Equation 14 is independent of m and C, so that it can be applied to any particle, provided $r = 0$. Furthermore, if it can be made sure by other means that actually $r = 0$, the slope of the straight-line plot yields the value of γ.

In order to establish the efficiency of this criterion, preliminary measurements of $\langle D_f \rangle$ and $\langle D_{1-f} \rangle$, in function of f, have been carried out by the coordinate method[5] on eight tracks recorded in G5 plates. Of these tracks four (two deuterons d_1, d_2, and two protons p_1, p_2) were known to be stopped by ionization only, three (a pion π and two protons p_3, p_4) were

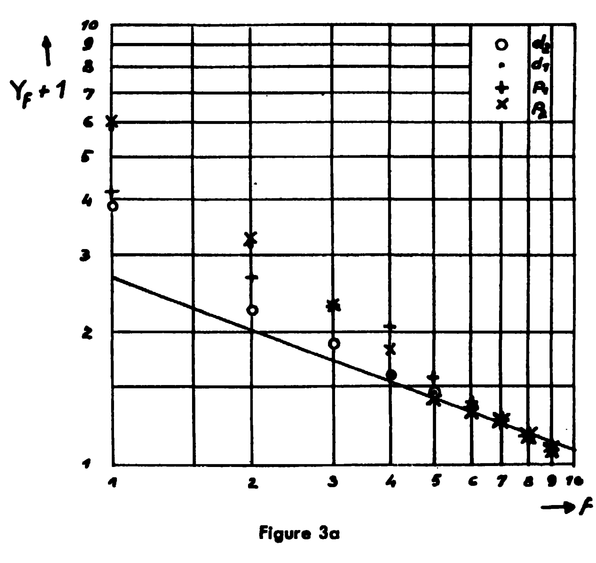

Figure 3a

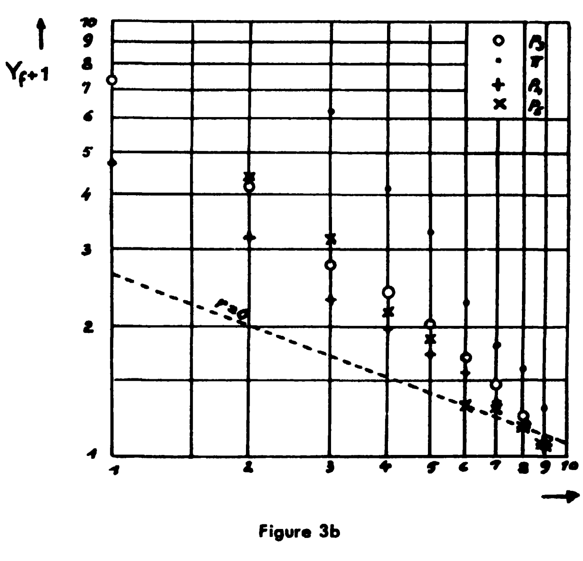

Figure 3b

known to have escaped from the emulsion, while one proton, p_6 was an uncertain case.

The results are plotted in Fig. 3a (stopped particles d_1, d_2, p_1, p_2) and Fig. 3b (π, p_3, p_4, p_6).

The straight line in Fig. 3a, of slope $|\gamma| = 0.42$ (i.e., $k = 1.37$) which is the generally accepted value for Ilford G5 plates,[1] has been traced in such a way as to fit best the experimental points in the interval $0.8 \geq f \geq 0.5$. Outside this interval, the influence of fluctuations can be expected to play a great role.

If more tracks with $r = 0$ are available, γ can be determined by the method of least squares according to Equation 14, as mentioned above.

As seen in Fig. 3b, different non-stopped particles give different plots. Even if there might be found some straight lines to fit these plots more or less, their slope would be sensibly different from γ. For comparison the straight line of slope γ is traced by dots.

CONCLUDING REMARKS

As far as we know, the method described in the preceding section, is the only quantitative criterion which enables one to ascertain whether the visible range is identical with the ionization range, or not. It is evident that Equations 9–12 yield also the mass m of the particle even if $r \neq 0$. This method, which could be conveniently called the method of averaged sagittas, has a common feature with the constant sagitta method,[6] viz., it uses the whole length of the track. As compared with this last method, it is much simpler in operation.

A detailed account of the measuring technique will appear elsewhere. The experiments are being continued.

REFERENCES

1. Fowler, P. H. and Perkins, D. H., *Fundamental Mechanisms of Photographic Sensitivity*. London, 1951, p. 266; quoted after Russian translation in Problemy Sovromennoi Fiziki Nr. 8, 125 (1953).
2. Ausländer, J., Bercea, C. and Friedländer, E., Communic. Acad. R.P.R. *5*, 343 (1955).
3. Beiser, A., Rev. Mod. Phys. *24*, 273 (1952).
4. Bercea, C. and Friedländer, E., Rev. Univ. Parhon (1955). In the press.
5. Fowler, P. H., Phil. Mag. *41*, 169 (1950).
6. Biswas, S., George, E. P., Lal, D., Pal Yash, Peters, B., Dilworth, C., Goldsack, S. and Hirschenberg, L., Bagnères Congr. p. 136 (1953), quoted after Russian translation in Problemy Sovremennoi Fiziki, Nr. 4, 145 (1955).

Notes on Higher Order Multipolar Electromagnetic Radiation Applications to Nuclear Physics

By Serban Titeica and Ch. Iusim, Romania

It is proposed to offer a solution to the problem of breaking down the electromagnetic field produced by a system of electrical charges in motion into its multipolar electrical and magnetic components. We shall assume, in so doing, that the charges do not leave the immediate vicinity of a certain fixed point in space, which we shall choose as the origin of the coordinate system; in addition, we shall assume that the distribution of the charges is continuous, so that it will be possible to go over immediately to the case of point charges by passing to the limit.

Let (x,y,z,t) and $\vec{j}(x,y,z,t)$ be the density of charge and that of electrical current respectively. The continuity equation will then be written as follows:

$$\frac{1}{c}\frac{\partial \rho}{\partial t} + \partial iv\vec{j} = 0 \qquad (1)$$

and we shall assume that functions ρ, $\vec{j}$, are substantially different from zero only for fairly small values of x, y, z, regardless of the value of t. The total charge of the system, which is independent of the time considered, is given by:

$$g = \int \rho \, dV \qquad (2)$$

The electromagnetic field of the charge system considered is given by the retarded potentials:

$$U(X,Y,Z,t) = \frac{\rho\left(x,y,z,t - \frac{r}{c}\right)}{r} dV$$

$$\vec{A}(X,Y,Z,t) = \frac{\vec{j}\left(x,y,z,t - \frac{r}{c}\right)}{r} dV \qquad (3)$$

wherein:

$$r = \sqrt{(x - X)^2 + (y - Y)^2 + (z - Z)^2} \qquad (4)$$

In order to break down the field (Equation 3) into its multipolar electrical and magnetic components, we shall make use of Taylor's formula, in the form:

$$f(r) = f(\sqrt{(x - X)^2 + (y - Y)^2 + (z - Z)^2})$$
$$= \sum_{n=0}^{\infty} \frac{(-1)^n}{n!}\left(x\frac{\partial}{\partial X} + y\frac{\partial}{\partial Y} + z\frac{\partial}{\partial Y}\right)^n f(R)$$
$$= \sum_{n=0}^{\infty} (-1)^n \sum_{\alpha+\beta+\gamma=n} \frac{1}{\alpha!\alpha\beta!\gamma!} \frac{\partial^n}{\partial X^\alpha \, \partial Y^\beta \, \partial Z^\gamma} x^\alpha y^\beta z^\gamma f(R) \qquad (5)$$

By applying this formula to the right-hand members of Equations 3, the following expression is obtained immediately:

$$U(X,Y,Z,t) = \sum_{n=0}^{\infty} (-1)^n \sum_{\alpha+\beta+\gamma=n} \frac{1}{\alpha!\beta!\gamma!} \cdot \frac{\partial^n}{\partial X^\alpha \, \partial Y^\beta \, \partial Z^\gamma}\left[\frac{1}{R}\int x^\alpha y^\beta z^\gamma \rho\left(x,y,z,t - \frac{R}{c}\right) dV\right]$$

$$\vec{A}(X,Y,Z,t) = \sum_{n=0}^{\infty} (-1)^n \sum_{\alpha+\beta+\gamma=n} \frac{1}{\alpha!\beta!\gamma!} \frac{\partial^n}{\partial X^\alpha \, \partial Y^\beta \, \partial Z^\gamma}\left[\frac{1}{R}\int x^\alpha y^\beta z^\gamma \vec{j}\left(x,y,z,t - \frac{R}{c}\right) dV\right] \qquad (6)$$

These formulae still do not give a solution to the problem raised. To solve it, we shall define Hertz's electrical and magnetic vectors by the formulae:

$$\vec{P} = \sum_{n=1}^{\infty} \frac{(-1)^n}{n+1} \sum_{\alpha+\beta+\gamma=n} \frac{1}{\alpha!\beta!\gamma!} \cdot \frac{\partial^n}{\partial X^\alpha \, \partial Y^\beta \, \partial Z^\gamma}\left[\frac{1}{R}\int x^\alpha y^\beta z^\gamma \vec{x}\rho\left(x,y,z,t - \frac{R}{c}\right) dV\right]$$

$$\vec{M} = \sum_{n=0}^{\infty} \frac{(-1)^n}{n+2} \sum_{\alpha+\beta+\gamma=n} \frac{1}{\alpha!\beta!\gamma!} \cdot \frac{\partial^n}{\partial X^\alpha \, \partial Y^\beta \, \partial Z^\gamma}\left\{\frac{1}{R}\int x^\alpha y^\beta z^\gamma \left[\vec{x}\,\vec{j}\left(x,y,z,t - \frac{R}{c}\right)\right] dV\right\} \qquad (7)$$

Original language French.

in which $\vec{x}$ is the vector having x, y, z, for its coordinates.

Direct computation makes it possible to check, by using the continuity relation, Equation 1, that:

$$U(X,Y,Z,t) = \frac{g}{R} - \nabla \cdot \vec{P}; \qquad \vec{A}(X,Y,Z,t) = \frac{1}{c}\frac{\partial P'}{\partial t} + \nabla x \vec{M} \quad (8)$$

in which ∇ is the vector having components: $\frac{\partial}{\partial X}$, $\frac{\partial}{\partial Y}$, $\frac{\partial}{\partial Z}$.

Equations 7 and 8 embody a complete solution of the problem. The multipolar electric radiation of order 2^{n+1} is given by the potentials:

$$U_n = -\nabla \cdot \vec{P}_n; \qquad \vec{A}_n = \frac{1}{c}\frac{\partial P_n}{\partial t} \quad (9)$$

in which $\vec{P}_n$ is the sum of terms which correspond to a given value of n in the expansion of Equation 7:

$$\vec{P}_n = \frac{(-1)^n}{n+1} \sum_{\alpha+\beta+\gamma=n} \frac{1}{\alpha!\beta!\gamma!} \cdot \frac{\partial^n}{\partial X^\alpha \, \partial Y^\beta \, \partial Z^\gamma} \left[\frac{1}{R}\int x^\alpha y^\beta z^\gamma \vec{x} \rho \left(x,y,z,t - \frac{R}{c}\right) dV\right] \quad (10)$$

Similarly, the multipolar magnetic component of order 2^{n+1} is given by:

$$U_n = 0, \; \vec{A}_n = \nabla x \vec{M}_n \quad (11)$$

in which:

$$\vec{M}_n = \frac{(-1)^n}{n+2} \sum_{\alpha+\beta+\gamma=n} \frac{1}{\alpha!\beta!\gamma!} \cdot \frac{\partial^n}{\partial X^\alpha \, \partial Y^\beta \, \partial Z^\gamma} \left\{\frac{1}{R}\int x^\alpha y^\beta z^\gamma \left[\vec{\alpha}\, \vec{j}\left(x,y,z,t - \frac{R}{c}\right)\right] dV\right\} \quad (12)$$

It will be seen at once that, when $n = 0$, there is a return to the classical formulae which give the radiation of an electrical or magnetic dipole.

One of our coworkers applied this breakdown method to a study of the radiation emitted by a charged liquid drop oscillating under the action of surface tension and electrostatic forces.

Let R_0 be the radius of the drop at rest and

$$R = R_0[1 + u(\theta,\varphi)] \quad (13)$$

the equation of the surface of the deformed drop in polar coordinates. Function $u(\theta,\varphi)$ may be developed as a series of spherical functions:

$$u(\theta,\varphi) = \sum_{l=0}^{\infty} \sum_{m=-l}^{+l} u_{l,m} = \sum_{l=0}^{\infty} \sum_{m=-l}^{+l} \alpha_{l,m} Y_{l,m}(\theta\varphi) \quad (14)$$

in which $Y_{l,m}$ is a normalized spherical function.

By assuming that the motion of the liquid which makes up the drop is irrotational, one can write:

$$\vec{v} = \text{grad}\,\frac{\partial \psi}{\partial t} \quad (15)$$

for the velocity vector $\vec{v}$ of any element of the fluid, in which ψ is a function which satisfies

$$\Delta\psi = 0 \quad (16)$$

and in the limit:

$$\left(\frac{\partial \psi}{\partial Y}\right)_{r=R_0} = \frac{dR}{dt} = R_0 u \quad (17)$$

The solution of the equation may be written as a series of spherical functions

$$\psi = \sum_{l=\partial}^{\infty} \sum_{m=-l}^{+l} \psi_{l,m} \quad (18)$$

in which

$$\psi_{l,m} = \frac{R_0^2}{l}\left(\frac{r}{R_0}\right)^l \alpha_{l,m} Y_{l,m}(\theta,\varphi) \quad (19)$$

The term in Equation 19 of the series in Equation 18 represents a multipolar component of order 2^l of the mechanical vibration of the drop.

The oscillations of the drop cause a distribution of variable electrical currents to appear inside it, as well as a distribution of variable electrical charges at its surface.

A separate study can be made of the electromagnetic field due to the charges and currents of each multipole of the mechanical vibration of the drop. It is further possible to break down the field into multipolar electric and magnetic components.

Let ω_l be the frequency of the mechanical multipolar vibration in Equation 19. One can write:

$$\alpha_{l,m} = a_{l,m}\, e^{-i\omega_l t} \quad (20)$$

in which $a_{l,m}$ is a constant amplitude, assumed small. Let us also introduce the wave number k_l of the radiation emitted by this vibration:

$$k_l = \frac{\omega_l}{c} \quad (21)$$

Then the intensity of the electric radiation of multipole order 2^{n+1} emitted by that oscillation is given by the expression

$$\left(-\frac{dW}{dt}\right)_{l,m;n,el} = \frac{9c}{4\pi}(k_l R_0)^{2n+1}\left(\frac{Ze}{R_0}\right)^2 [a_{l,m}]^2 \frac{l(l+1)}{(n+1)^2}\left[\frac{1}{(n+1-l)!!} \cdot \frac{1}{(n+l+2)!!}\right]^2 \quad (22)$$

in which Ze is the total charge of the drop.

Similarly, for the magnetic radiation of multipole order 2^{n+1} the following intensity is obtained.

$$F\left(-\frac{dw}{dt}\right)_{l,m;n,\mathrm{magn}} = \frac{9c}{4\pi}(k_l R_0)^{2n+1}\left(\frac{Ze}{R_0}\right)^2$$

$$|a_{l,m}|^2 \frac{l+1}{l(n+2)^2}\left[\frac{1}{(n-l)!!(n+l+3)!!}\right]^2 \qquad (23)$$

It will be seen that the intensity of the magnetic radiation of multipole order 2^n is of the same order of magnitude as the intensity of the electrical radiation of multipole order 2^{n+1}.

The selection rule for electrical radiation of multipole order 2^{n+1} is

$$n + 1 - l = 2p \qquad (24)$$

in which p is either a positive integer or zero. Similarly, the corresponding rule for magnetic radiation of order 2^{n+1} is

$$n - l = 2p \qquad (25)$$

A High Energy Particle Accelerator and Its Application to Peaceful Uses of Atomic Energy in Pakistan

By Rafi Muhammed Chaudhri,* Pakistan

THE HIGH TENSION ROOM

The accelerator is housed in a special building constructed for the purpose. The high tension room is 60 × 35 × 40 ft. Its interior is covered all around with chicken gauze embedded in plaster and is well grounded to earth. It has a lintelled floor about 1 ft thick. The metal parts of the lintel are well grounded. The room is provided with five exhaust fans and two inlet fans to circulate cold air in summer. Three windows with reinforced glass are provided to allow diffused light into the room when desired. It has a main door 12 × 9 ft. The high tension room is cooled in summer by using special khas grass kept wet all the time. A certain volume of air is enclosed within the khas grass structure outside the main door, windows and the inlet fans. By regulating the speed of the fans the temperature is brought down by more than 30°F and this enables the machine to function during the hottest part of the year. It may be mentioned here that Philips rectifiers work normally within a certain limited range of temperature. The humidity in the room rises to much higher value than that of the atmosphere outside by this arrangement but we have found that it is possible to work with the set under these conditions up to a voltage of about 800 kv quite satisfactorily.

Adjacent to the high tension room is an observation room wherefrom one can watch the performance of the set while it is functioning.

THE ACCELERATOR

The accelerator is a Philips set and consists of: (1) a 1.2-million-volt Cockcroft-Walton type six stage cascade generator; (2) a smoothing column; and (3) an accelerating tube with Oliphant type ion source.

The voltage to the generator is supplied by a 100 kv transformer which is fed by a 200-cycle ac generator. The transformer charges a condenser to a peak voltage of 100 kv through a Philips nine-ring Mercury rectifier. One of the six condensers, joined in series, of the dc column of the generator is charged to a peak voltage of 200 kv through a second similar rectifier. The other five condensers of the dc column are charged to 200 kv each in a similar way, thus giving a total voltage of 1.2 million volts on the top stage of the set with respect to earth. (Since the Cockcroft-Walton circuit is well-known, the details of its principle of operation are not described here.)

The filaments of the mercury rectifiers are heated by the secondaries of special dust core transformers whose primaries are joined in series with condensers of the set and are fed with rf current from a transmitter. The rectifiers are cooled by a special blower which circulates air through two hollow insulating supporting columns of the generator.

The surges in the output of the set are cut down by special oil-cooled wire-wound resistors connected between its two top spinnings. The ht voltage is stabilized by a smoothing column which consists of six condensers joined in series. Its each stage is connected on one side to the generator and on the other to the accelerating tube via special wire-wound oil-cooled resistors. The ripples may be further reduced by adjusting the amplitude and phase of the output of a transformer connected at the bottom of the smoothing column. The primary of this transformer is fed by the 200 cycles generator through a phase-shifter.

An electronic voltage stabilizer has been constructed to control the long period fluctuations of the ht voltage.

The Oliphant ion source is a discharge tube with two hollow metal cylindrical electrodes, whose anode is oil-cooled. The power to the Oliphant ion source is supplied from an ac generator placed in the top stage of the accelerating tube and which feeds a transformer whose output is rectified by a Philips five-ring mercury rectifier and stabilized by an RC circuit. The generator is run by a long insulating belt driven through a hollow supporting column by a motor placed on the floor. The current through the field coil of the ac generator is controlled through a variable resistance, whose value may be adjusted by a rotating insulating rod worked by a remote-controlled reversing motor kept at earth potential. An output voltage from 0–50 kv may be obtained with this device from the transformer. The ion source current and voltage are read by two meters which are placed on the side of the column and can be viewed from the observation room. The flow of the gas into the ion source is adjusted by a needle valve, which is also remote-controlled in a similar manner. The positive ions from the discharge tube are accelerated at six stages of the accelerating tube through suitably designed electrodes. A maximum target current of 250 micro-amperes with unanalysed proton beam has been obtained.

---

* Professor of Physics and Dean, Faculty of Science, Government College, Lahore.

The target assembly is separated from the accelerating tube by a special vacuum valve and can be evacuated independently. There is a provision to shift the position of the target with respect to the axis of the accelerating tube while the beam is on. The position of the beam is located with a quartz disc fixed with a Wilson seal in a glass chamber below the vacuum valve.

The target is placed on a copper backing silver-soldered to a hollow copper tube hermetically sealed into a Pyrex glass. The glass structure is joined to the accelerating tube through a flexible metal pipe.

The accelerating tube is exhausted by a fast oil diffusion pump backed by a Kinney pump. There is a baffle valve on the top of the diffusion pump which cuts it out from the accelerating tube and the target chamber when desired. The pressure in the vacuum system is indicated by Penning gauges whose currents are read by meters placed in various control panels. A separate Penning gauge works an automatic alarm when the pressure exceeds a certain value on account of failure of pumps or a leakage in the tube. The pumps are water-cooled and so are the ht transformer and the oil-pressure pump which circulates oil through the Oliphant ion source and measuring resistance column placed between the top bun of the accelerating tube and the earth. The failure of water supply is indicated by micro-switches which work automatic alarms placed in the control room. The target is cooled either by cold water or liquid air as desired.

The remote controls of the machine are fixed in a main control desk and three control panels. One of the switches of the main control desk operates the high-frequency transmitter, blower, oil-cooling pump and the 200 cycles ac generator. The second switch puts the power on the high tension set which will not be possible unless the transmitter, blower and the oil-cooling pump are on and the variac controlling the output of the transformer is set in a position to give its minimum output voltage. There is also a provision in the control desk for the very fine adjustment of the main voltage of the machine.

The meters in the control desk read the (*a*) total current passing through the set, (*b*) total output dc voltage of the set, (*c*) target current, (*d*) transmitter input current, (*e*) input voltage of the transformer and (*f*) current in primary of the ht transformer. There are also three safety relays fixed in the control desk which switch off the set if the current in the primary of the high tension transformer, the total load current of the set or the target current exceeds certain preset values.

The output voltage of the ht set is measured by a calibrated meter by tapping a known resistance put in series with the oil-cooled measuring resistance column. The remote controls which work the ion source power supply and gas flow are provided in control panels placed in the main control room and observation room. A separate control panel placed near the diffusion pump on the floor controls the power to the Penning gauge, backing and diffusion pumps. There is also a safety switch in this panel which cuts all power supplies to the top spinning of the accelerating tube when required.

DETECTING AND MEASURING INSTRUMENTS

The gamma radiations have been detected using a NaI(Tl) single crystal spectrometer with photo-multiplier types 6260 and 6262. The crystal and the photo-multiplier are placed in a light tight chamber close to the target. The position of the assembly is fixed with the help of two cross telescopes to repeat observation under similar conditions. The output pulses of the photo-multiplier are fed into an amplifier through a cathode follower and then to a five-channel pulse-height analyser or to a scaler (scale of 100) provided with a variable bias voltage (5–50 volts). In some measurements the output of the photo-multiplier is fed to the scaler through 1186 head amplifier. The neutrons have been detected with a BF_3 counter whose output is fed to the scaler through a head and main amplifier. The reactions of neutrons on boron have also been studied with photo-emulsion plates using a Cooke Troughton nuclear microscope. For counting alpha particles special counters were made with a filling of helium at atmospheric pressure. The output pulses of the counter are fed direct into the scaler through a probe unit.

The various counting devices like Geiger counters, alpha and beta end-window counters, and proportional counters for neutrons have been constructed in this laboratory.

MAGNETIC ANALYSERS

Two magnetic analysers for resolving and focusing the proton and deuteron beams at 15 and 30 degrees have been set up. The former consists of a permanent magnet and the latter of an electro-magnet. A target has been devised whose position from the magnet may be varied while the beam is on in order to locate the focus.

SAFETY DEVICES

(1) Pocket monitors are used by laboratory workers to indicate the total dose of radiation to which a person has been exposed during the day.

(2) Automatic gamma-ray and neutron monitors are installed at suitable places in the laboratory to give alarm when either the instantaneous flux or the total radiation dose exceeds safety limits.

(3) It is hoped that in the near future we shall have film badge service available as well in the laboratory.

THE RADIO-FREQUENCY ION SOURCE

The ion source consists of a Pyrex glass discharge tube with a tungsten anode 1 cm in length and 2 mm in diameter, fixed in a narrow capillary at its top. The cathode is of brass. An aluminium probe 1.8 cm long and having a bore 4.5 mm in diameter along its axis is screwed in the cathode. The surface of this

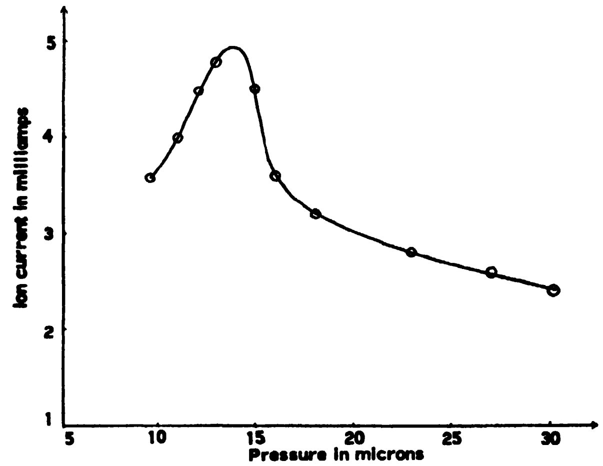

Figure 1. Curve showing variation of ion current with pressure keeping wattage input of the oscillator and extracting voltage constant. The probe current varies from 4.5 to 9 ma

electrode is shielded with a Pyrex disc with a hole in its centre. A fused silica tube 8 mm in internal diameter shields the probe. Its length over the tip of the probe is adjusted to be equal to the external diameter of the probe.

The circuit of the oscillator is of the Hartley type. The frequency of the oscillations used ranges between 8 and 10 megacycles. The transmitter tube used is an 805.

The positive ions from the discharge tube are extracted by applying a dc voltage on the probe. The ion current is found to depend upon: (1) power input in the oscillator; (2) probe extracting voltage; (3) pressure in the discharge tube. At fixed values of the input power and probe extracting voltage, the ion current is maximum at a certain critical pressure and falls on either side of it as shown in Fig. 1. It shows, however, a regular increase with power input keeping pressure and extracting voltage constant as given in Fig. 2. Using a discharge tube 24 cm in length and 5.4 cm in diameter an ion current of about 5 milliamperes was obtained below the cathode at a pressure of 13 microns with a probe extracting voltage of about 5 kilovolts. The tank current had a frequency of about 8 megacycles.

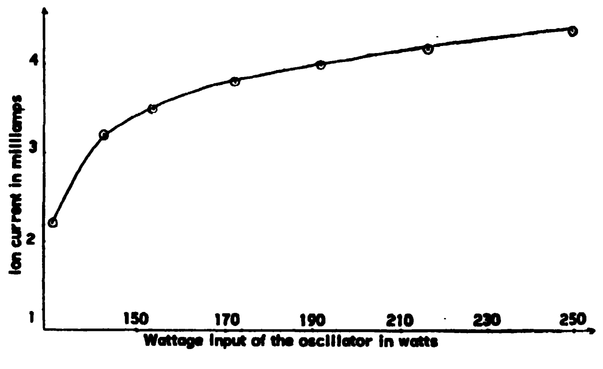

Figure 2. Curve showing variation of ion current with wattage input of the oscillator keeping the pressure and extracting voltage constant. The probe current varies from 5 to 8 ma

The presence of water vapour and other impurities was found to affect adversely the ion current under all conditions of the experiment studied. The hydrogen gas was, therefore, allowed to enter the discharge tube through a liquid air trap and a palladium leak to keep it as pure as possible.

With the increase in the diameter of the silica tube acting as the shield of the probe, the ion current was found to decrease. Under identical conditions the ion current with silica tubes of 8 and 10 mm diameter was 4.8 and 4.4 milliamperes respectively.

The tank coil consists of a few turns of Cu wire 4.5 mm in diameter. The position of the tank coil was found to have quite a considerable influence on the ion current. The maximum ion current was obtained with the coil as near to the cathode surface as possible. This current decreases as the position of the coil is removed away from the cathode.

The shape of the shield of the cathode, whether plane or convex had little effect on the ion current. The radius of curvature of the convex shield used is about 5 cm.

The effect of the oscillation frequency on ion current is shown in Figs. 3 and 4 for a discharge tube 27 cm in length and 5.4 cm in diameter using 8 and 10 megacycle frequencies.

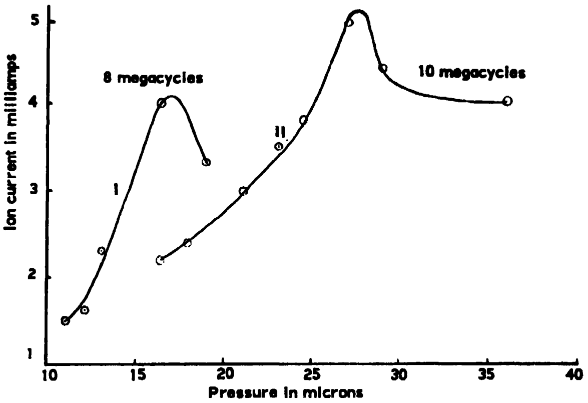

Figure 3. Curves showing variation of ion current with pressure at 8 and 10 megacycles frequency of the oscillator keeping the wattage input of the oscillator and extracting voltage constant. In curve I the probe current varies from 5 to 8 ma. In curve II the probe current varies from 5 to 9 ma

THE HEAVY HYDROGEN PLANT

It consists of a Pyrex glass " U " shaped electrolysing cell about 1.5 cm in diameter with platinum electrodes. The heavy hydrogen produced by electrolysis bubbles against atmospheric pressure through mercury in a narrow annular space between two glass tubes one slipping into the other; the outer tube dips in a mercury reservoir. A glass bulb with a narrow glass capillary hook sealed inside it is fixed at the top of the outer tube. This device avoids violent splashing of the mercury while hydrogen bubbles through it and prevents it from rushing into the pumping side of the system. As the heavy hydrogen bubbles in vacuum, the open oxygen delivery tube would allow air to rush

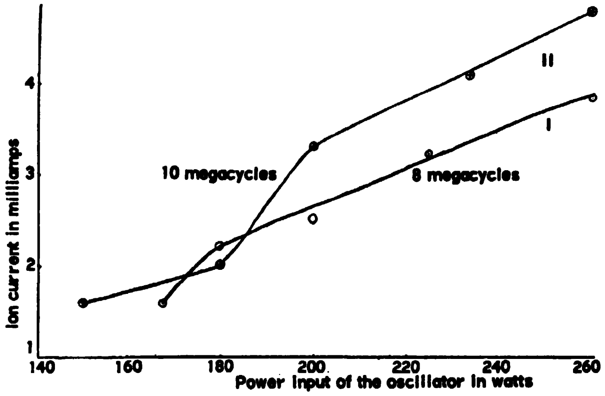

Figure 4. Curves showing variation of ion current at 8 and 10 megacycles frequency of the oscillator with power input of the oscillator keeping the pressure and extracting voltage constant. In curve I the probe current varies from 5 to 8 ma. In curve II the probe current varies from 4.5 to 9 ma

in and push the electrolyte in the hydrogen column which will break the electric circuit. The oxygen delivery tube is, therefore, dipped in a mercury cup which acts as a valve allowing oxygen to escape into the atmosphere and preventing air from rushing in.

A combined pressure and vacuum pump is employed to collect heavy hydrogen in a glass reservoir of about one litre capacity. An automatic device breaks the electric circuit when the reservoir is filled with heavy hydrogen to an atmospheric pressure.

RESULTS

With an Unanalysed Proton Beam on Al

(1) Definite resonance levels were found to exist in the $Al(p,\gamma)Si$ reaction. The gamma-rays emitted were studied using a single NaI(Tl) crystal spectrometer. Two pronounced resonance peaks at proton energies of about 400 and 500 kev were observed with an Al target $\frac{1}{10}$ mm thick (Fig. 5). (The Al foil was supplied by Messrs. Johnson Matthey Limited of London.) The target was liquid-air cooled. The emission of gamma-rays from the reaction at energies other than the above two resonance energies are under investigation. The half-width (full width at half height of the peak) of the 400 kv peak is about 7%.

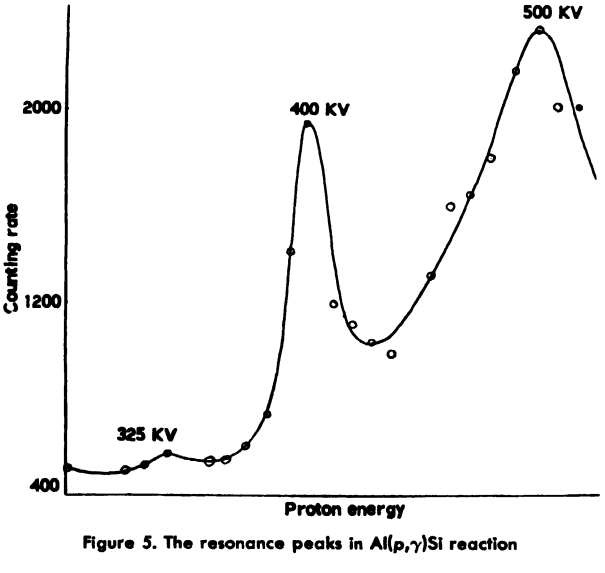

Figure 5. The resonance peaks in $Al(p,\gamma)Si$ reaction

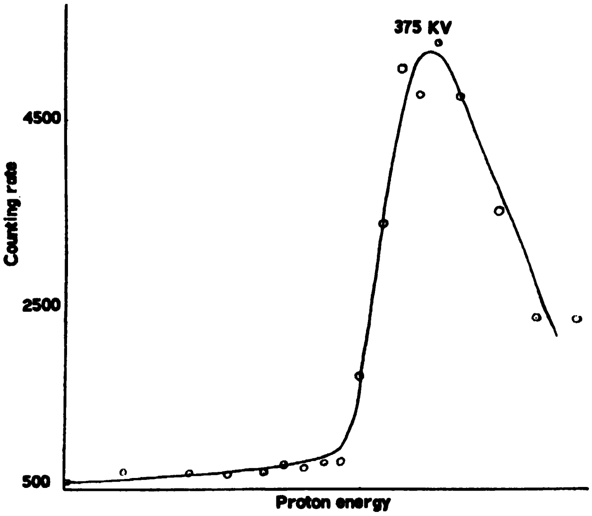

Figure 6. Gamma radiation from copper excited by proton bombardment

Now a plant has been set up to prepare thin metal films, by evaporation in vacuum, to serve as a target in future experiments.

(2) The yield of gamma-rays is found to be proportional to the proton current within the experimental error.

(3) It was also observed that at each of the above proton resonance energies, gamma-rays of various energies are emitted as detected by a single-crystal spectrometer using a five-channel pulse-height analyser.

The definite energies of the gamma-rays emitted will be investigated after improving the resolution of the spectrometer.

Experiments with an Unanalysed Proton Beam on a Cu Target

Experiments were done with a Cu target $\frac{1}{10}$ mm thick. The Cu foil was supplied by Messrs. Johnson Matthey. We have observed a fairly well-pronounced peak at about 370 kev proton energy (Fig. 6). We are, however, not yet certain of the reaction which produces these gamma-rays. It will be studied in detail in due course.

Experiments with Photographic Emulsion Plates

The reaction of neutrons on boron has been studied using photographic emulsion plates Type C 2 obtained from Messrs. Ilford, Ltd., London.

Experiments with D-D Reactions

An ice target was prepared by allowing a jet of water vapour to condense on a liquid-air cooled copper target. The resulting neutrons from the D-D reaction are to be studied with BF_3 counters, photographic emulsion plates, NaI(Tl) crystals and organic crystals like anthracene, stillbene and pamelon.

The neutrons from the D-D reaction and deuterons from the set will be used in preparing isotopes, particularly of short lives, which are required in medical and biological research.

It may be added at the end that the paper is primarily intended to give briefly a survey of the nuclear work now in progress in the laboratory and to indicate the scope of its extension in future and not a critical discussion of any particular aspect of it.

ACKNOWLEDGEMENTS

The entire electronic equipment for this laboratory has been procured from the Atomic Energy Research Establishment, Harwell (UK) and I wish to take this opportunity to express my sincere thanks to Sir John Cockcroft, Director of the Establishment and Dr. Denis Taylor, head of its Electronic Division, who provided all facilities for its supply.

My thanks are due to my old teachers and colleagues of the Cavendish Laboratory, Cambridge.

The work described in the paper has been carried out here in collaboration with Dr. Tahir Husain, Mr. A. L. Taseer and Mr. Mustafa Yar Khan, and I am grateful for their co-operation and assistance.

Record of Proceedings of Session 6A

WEDNESDAY AFTERNOON, 10 AUGUST 1955

***Chairman:* Mr. A. Bohr (Denmark)**
***Vice-Chairman:* Mr. T. Sigurgeirsson (Iceland)**
***Scientific Secretaries:* Messrs. J. Leite Lopes and A. Salam**

PROGRAMME

P/714	Inelastic scattering of fast neutrons by atomic nuclei	M. V. Pasechnik
P/581	Gamma rays from neutron inelastic scattering	R. B. Day
P/588	Angular distributions and non-elastic neutron scattering	M. Walt
	DISCUSSION	
P/830	The theoretical prediction of neutron cross-sections of non-fissionable elements for energies up to 10 Mev	V. F. Weisskopf
	DISCUSSION	
P/650	Investigation of neutron β decay	P. E. Spivak *et al.*
	DISCUSSION	
P/651	Thermal-neutron capture gamma rays	L. V. Groshev *et al.*
	DISCUSSION	
P/941	Investigation of the structure of molecules and the structure of liquids by scattering of thermal neutrons	J. Janik
	DISCUSSION	
P/870	Thermal inelastic scattering of cold neutrons in polycrystalline solids	K. S. Singwi and L. S. Kothari
	DISCUSSION	

Mr. M. V. PASECHNIK (Ukrainian Soviet Socialist Republic) presented paper P/714.

Mr. R. B. DAY (USA) presented paper P/581.

Mr. M. WALT (USA) presented paper P/588. With regard to elastic cross-sections he showed two slides that do not appear in the paper. They, and the relevant part of the presentation, are reproduced here:

In the past several years many measurements have been made of the angular distributions of neutrons elastically scattered by nuclei. The angular distribution of neutrons scattered by a given element changes slowly with energy as expected in the continuum energy region. However, it was also found that at a given energy the shape of the angular distribution varied in a systematic manner as one progressed from element to element in the periodic table.

The general dependence of the angular distribution with neutron bombarding energy can be seen in Slide 1. In this slide the differential cross sections for elastic scattering of neutrons by a heavy element are plotted as a function of the cosine of the scattering angle, the scattering angle going from 0 degrees on the left to 180 degrees on the right. Each curve is for a given energy, going from 0.6 Mev at the top to 14 Mev at the bottom of the graph. The vertical scale of each curve is displaced slightly from that of adjacent curves to prevent overlapping, the zero for each curve being given on the right-hand side of the figure. As the energy increases from 0.6 Mev at the top of the figure to 14 Mev at the bottom, the angular distribution changes slowly from a relatively flat curve, peaked in the forward direction, to a more complicated structure involving several secondary maxima and minima. The forward peak becomes much more pronounced and in general the cross sections at large angles decrease greatly in absolute value. For example, in going from 0.6 Mev to 7 Mev the forward peak increases by a factor of almost 10. The scattering near 180 degrees, on the other hand, decreases by a factor of roughly 20 in going from 0.6 Mev to 7 Mev. For purposes of reactor calculation, it should be noted that in general as the energy increases, the elastic transport cross section decreases.

Slide 2 (Fig. 2 of P/588) illustrates the regular variation of the shape of the differential cross-section curves with changing atomic weight. In this figure, the differential cross-section for elastic scattering of 1-Mev neutrons is plotted as a function of the cosine of the scattering angle for some 28 elements. Each curve is the differential elastic cross-section curve of the element whose atomic weight is indicated on the horizontal scale. As one moves to heavier elements, the forward peak in general increases, and the curve

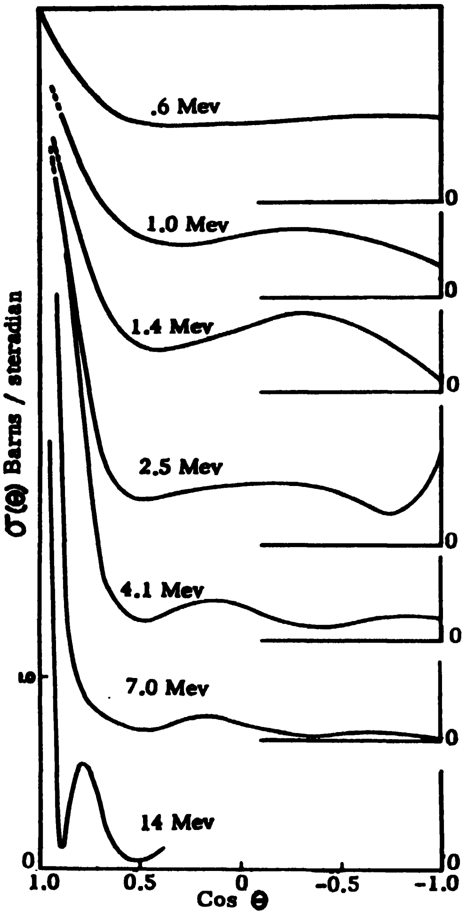

Slide 1

becomes more complicated, eventually showing secondary maxima and minima. Figure 2 of P/588 indicates the situation at 1 Mev bombarding energy.

Slide 3 is a similar figure for a neutron energy of 4 Mev. Note the much more pronounced forward scattering at this increased energy. Again, as in the last figure, one sees the increase in the forward peak with increasing atomic weight and the greater complexity of the curves for the heavier elements.

The regular variation of the angular distributions with energy and with atomic weight makes it possible to guess the angular distribution of an element whose differential cross-section has not been measured, by interpolating between curves of neighboring elements whose cross-sections have been measured at the same energy or nearby energies.

DISCUSSION OF PAPERS P/714, P/581 AND P/588

Mr. P. A. Egelstaff (UK): I would just like to comment on the inelastic scattering cross-section of U^{238} from work we have done at Harwell, and compare it with the results we have just seen. This work has involved the use of the He^3 neutron spectrometer which you have seen in the United Kingdom exhibition here, and it was carried out by R. Batchelor.

Slide 4 shows the spectrum of neutrons inelastically scattered by natural uranium for a bombarding energy

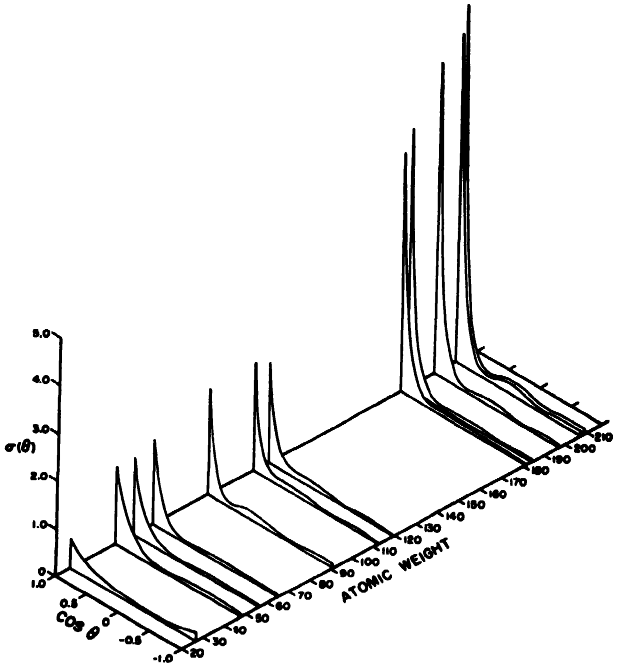

Slide 3

of 500 kv. The energy loss is on the whole about 100 kv, the peak of the spectrum coming at about 400 kv.

Slide 5 shows the spectrum of neutrons scattered inelastically for 900 kv bombarding energy, and in this case there is a peak at about 800 kv showing the same rather small energy loss, but now a larger peak has appeared at 200 kv corresponding to an energy level in U^{238} at 700 kv. We attribute this lower peak to a level other than the rotational levels and the peak at a loss of 100 kv to rotational levels.

Slide 6 shows the cross-section for this process. The circles show the total cross-section for inelastic scattering, and if you compare this with the similar curve in the last paper, you will see that the rise from 500 kv to 1.4 Mev is about of the same order, but that the absolute value of the cross-section in our case is about

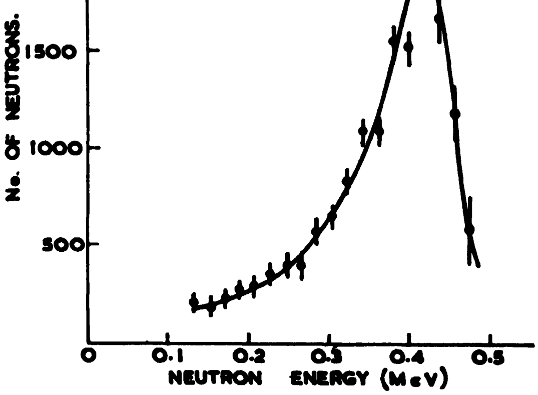

Slide 4. The spectrum of neutrons scattered inelastically by uranium at 500 kev bombarding energy

twice that found there. The crosses show the cross-section for an energy loss less than 500 kv and would correspond approximately to the part of the cross-section relating to the rotational energy levels.

Mr. WALT (USA): I would like to make a comment on the first paper. I notice that in the table of inelastic cross-sections, the inelastic cross-sections for lead and bismuth were quite different at all energies except at 14 Mev. I think this does represent a disagreement between our results and the results presented there, because at all energies above 1 Mev we have found the same inelastic cross-sections for both lead and bismuth.

I also have another question. Could the speaker describe briefly the manner in which his transmissions were corrected for the energy loss in inelastic collisions and for multiple scattering in order to arrive at inelastic collision cross-sections?

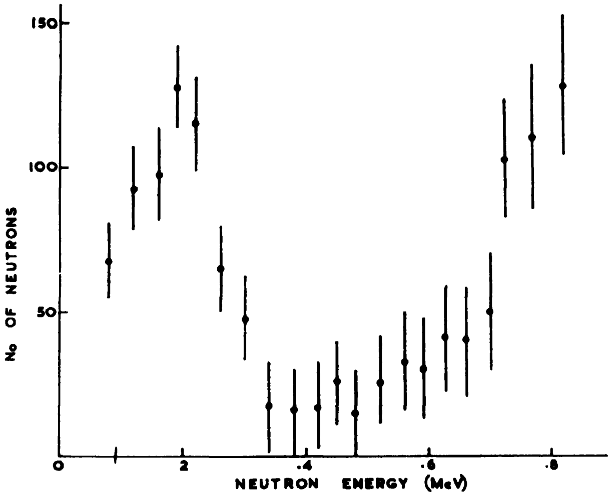

Slide 5. The spectrum of neutrons scattered inelastically by uranium at 900 kev bombarding energy

Mr. PASECHNIK (Ukrainian Soviet Socialist Republic): We noted the divergence in the data on the cross-sections for bismuth and lead some time ago and ran a special series of experiments in order to check our results. According to our data there is a divergence which may be explained by the fact that natural lead has over 48% of isotopes with a not-magic number of neutrons. It is because of this proportion of isotopes that we obtain a much larger cross section for lead than for bismuth. I have no reason to doubt Mr. Walt's data. However, I would like to ask him to recheck his data as we rechecked ours.

As for the second question I think it would be preferable if I discussed this matter in private with Mr. Walt, since the matter of introducing corrections to the experimental data is of rather special interest. Of course we introduced such corrections, and I will be glad to give Mr. Walt all the details.

Mr. WALT (USA): In regard to the angular distribution of inelastically scattered neutrons, in some of the experiments by which we obtained angular distribution of elastically scattered neutrons we could obtain a crude determination of the inelastic distribution by measuring this distribution with detectors having different thresholds, and we found that the angular distribution of the inelastic scattered neutrons was isotropic although our experimental errors were very large.

However, recently a colleague of mine, Mr. Granberg, using a time-of-flight technique which he will describe in a later session of this Conference,* has measured the angular distribution of inelastic scattered neutrons to considerably greater precision. Inasmuch as his results, at 2½ Mev in the case of iron, are quite applicable to the preceding paper, I will ask him to present these results now.

Mr. L. GRANBERG (USA): I would just like to comment on our results obtained for the angular distribution of neutrons scattered from iron. The primary neutrons had an energy of about 2.45 Mev. It is relevant particularly to this discussion to point out that we do observe a small anisotropy for the neutrons which excite the 850 kev level in iron. The weightiest points are the ratio of 90 to 155 and 167 degrees, and there the anistropy is about 17%. I believe that the uncertainty in that is only of the order of a few per cent. I believe this is quite consistent with the reports of isotropy taking account of the angular range which is covered in other work and the experimental uncertainties.

Mr. O. D. KAZACHKOVSKI (USSR): I would like to make two remarks regarding Mr. Walt's report.

1. Similar experiments, at least in the energy region above 1 Mev, can, in principle, be carried out by means of photographic plates, if one succeeds in reducing the background to a sufficient degree.

Such measurements were carried out in our laboratory by Sal'nikov for lead and iron with 2.3 Mev neutrons. The results for lead are given in Table I.

In the upper line are the angles of scattering: 30, 60, 90 and 135 degrees, and in the left column the energies of the scattered neutrons: 2.3 Mev, 1.8 Mev and 1.5 Mev. These correspond to elastically scattered neutrons and to neutrons non-elastically scattered at the

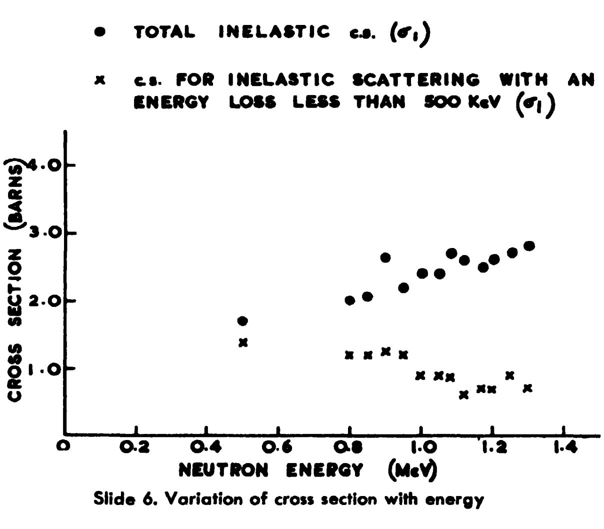

Slide 6. Variation of cross section with energy

---

* Session 15A, paper P/577, Vol. 4, these Proceedings.

Table I

Neutron energy	*Angle, degrees*			
	30	*60*	*90*	*135*
2.3 Mev	15 ± 1.24	2.75 ± 0.47	3.79 ± 0.43	2.57 ± 0.34
1.8 Mev	0.81 ± 0.5	0.76 ± 0.21	0.91 ± 0.19	0.77 ± 0.19
1.5 Mev	0.96 ± 0.48	1.06 ± 0.31	1.19 ± 0.29	1.03 ± 0.26

0.5 Mev and 0.8 Mev levels, respectively. The differential cross sections (referred to 4π) are given in barns.

As may be seen from Table I, the curve for the elastic scattering cross-section has the usual shape, with anisotropic scattering. In contrast to this, the non-elastic scattering cross-section remains constant within the limits of experimental error. In non-elastic scattering from iron nuclei, isotropy of scattering also occurs for the 0.85 Mev level. The corresponding cross-section is approximately one barn.

2. Extension of the investigation of non-elastic scattering into the region of lowest possible energies presents undoubted interest. Glazkov and other investigators in our laboratory have carried out measurements of the non-elastic scattering of photoneutrons with energies of 0.22, 0.7 and 0.9 Mev. Spherical ionization chambers with helium or hydrogen were used as detectors. The measurements were carried out in spherical geometry. The results are a number of measurements given in Table II.

Table II

Element	*220 kev*	*700 kev*	*900 kev*
Cu	0	0	0.2
Sb	0	0.4 ± 0.1	0.7 ± 0.1
W	0.4 ± 0.1	1.3 ± 0.2	2.6 ± 0.2
Hg	0.1 ± 0.5	0.8 ± 0.1	1.5 ± 0.1
Pb	0	0	0.2 ± 0.1
Bi	0	0	0

In the upper line we give the photoneutron energies and in the left column the investigated elements. The cross-sections are given in barns. As will be seen from Table II the heavy "non-magic" elements have a considerable non-elastic scattering cross-section even at a neutron energy of 220 kev. The cross-section values for 900 kev neutrons are apparently in agreement with the data given by Mr. Walt for 1 Mev neutrons.

Mr. V. F. Weisskopf (USA) presented P/830.

DISCUSSION OF PAPER P/830

Mr. Rudik (USSR): I have two remarks to make about Mr. Weisskopf's paper.

First, regarding the question of the diffuse boundary of the nucleus already mentioned by Mr. Weisskopf, consideration of a diffuse boundary leads to better agreement between theory and experiment. It seems to me that an investigation of non-spherical nuclei should also result in closer agreement of theory with experiment.

The second point I want to raise is that even at low neutron energies several mechanisms of the reaction may be suggested without recourse to the compound nucleus model. One of these possible mechanisms was investigated by Zaretski and Shut'ko ("Excitation of rotational nuclear levels by neutrons," forthcoming issue of the Journal of Experimental Theoretical Physics/ZHETF). They showed that the inelastic scattering of neutrons with an energy of several kev may be regarded as a process involving the excitation of rotational levels of an elongated nucleus, without formation of a compound nucleus.

Mr. Weisskopf (USA): I agree on both points. The first point is, I think, of great importance, and I think that work in this respect is going on now in Copenhagen.

With regard to the second point, we are also very interested in it; both at Copenhagen and at MIT they are trying to discuss the precise way a neutron comes in and sets a nucleus in rotation without forming a compound nucleus. I should like to say that calculations have also been carried out at Oxford. It seems that this is an important process for inelastic scattering at low energies.

Mr. M. S. Kozodayev (USSR) presented paper P/650.

DISCUSSION OF PAPER P/650

Mr. Snell (USA): I would like to compliment the Russian physicists on the daring use of the proportional counter so close to a heavy neutron beam. I am not quite clear as to the relative geometry of the spherical collecting chamber and the beam. Am I right in assuming that the spherical chamber poked partway into the neutron beam and, if so, about how far away was the sensitive part of the counter from the edge of the beam?

My second question is about the determination of the neutron density in the beam. I would like to ask this question: How accurately do you think you can measure absolute thermal neutron densities?

Mr. Kozodayev (USSR): In these measurements the neutron beam was rigorously defined and therefore did not graze the metal parts of the equipment. Special test measurements showed that the experimental conditions were satisfactory and that the equipment really registered the protons from neutron fission. The background in these measurements was of the same order of magnitude as the effect. Conditions in the second experiment were better and the background was appreciably weaker, which made it possible to attain accurate results.

With reference to the second question I can say the following: For determining the density of the neutron flux in this experiment we did not have to know the exact cross-section for boron; only the relative distribution of the flux density of the neutron beam was measured by means of a small boron chamber. The absolute magnitude of the neutron flux density was measured by means of activation of a gold foil. The neutron flux in the central part of the beam was 260 ± 15 per cm^2 per second. This is the exact value of the density.

Mr. Weisskopf (USA): I would like to congratulate the Russian group on these excellent measurements, which have opened up a very important new field of investigation. These measurements constitute a most interesting advance. I would like to ask the speaker what kind of results he has got in the measurement of heavy elements. You very probably got a continuous spectrum at low energies, and it would be especially interesting to know whether this continuous spectrum is in agreement with the theoretical predictions and whether it falls off in intensity at low energy.

Mr. Adjasevich (USSR): We have investigated the gamma-spectra of cadmium, samarium and mercury. The spectrum for samarium has the usual form predicted by theory. However, on the low energy side, as well as on the high energy side, we observed a number of peaks corresponding to gamma-rays emitted in the transitions between the lower levels of these nuclei and in transitions from the compound nucleus state for this level. In the case of mercury, the observed spectrum is closer to a line spectrum. This may be explained by the fact that the atomic number of mercury is almost a magic number.

The Chairman: Are there any other questions for Mr. Adjasevich? I myself would like to ask him a question. In the decay scheme of sodium-24, from your work, Mr. Adjasevich, it appears that there should be an intense transition of 90 kv which might even have a measurable lifetime. I wonder if Mr. Adjasevich has any information whether such a transition has been detected?

Mr. Adjasevich (USSR): Unfortunately, our spectrometer is not sufficiently sensitive at γ-ray energies of 90. We have no information whatsoever about these transitions.

Mr. H. Niewodniczanski (Poland) presented paper P/941.

DISCUSSION OF PAPER P/941

Mr. O. Simpson (USA): I should like to ask Mr. Niewodniczanski whether he has any data to present on the variation of the cross section with the temperature of the scattering material.

Mr. Niewodniezanski (Poland): Yes. Such measurements are being made now by one of my collaborators, who is measuring the scattering of neutrons by methyl alcohol molecules at different temperatures up to the critical temperature, in order that the influence of association can be measured. There are already some preliminary results, and the results will no doubt become more accurate as time goes on.

Mr. L. S. Kothari (India) presented paper P/870.

DISCUSSION OF PAPER P/870

Mr. P. A. Egelstaff (United Kingdom): We have heard from Mr. Kothari of the interaction of cold neutrons in polycrystalline solids involving exchange of an energy quantum. I would like to compare that interaction with the analogous interaction for a liquid, because we have had one curious result, and I would like an explanation of this. We have studied the scattering of cold neutrons of a temperature of 14° absolute from solid and liquid lead. We have shown that over the whole temperature range we have studied, and the whole angular range we have studied, there is an inelastic interaction involving an energy exchange of about 80° absolute, and so it corresponds to the single-phonon process discussed in Mr. Kothari's paper. This is true even in the liquid state.

Slide 7 is the differential cross-section for the scattering of 14° absolute neutrons by solid and liquid lead for angles of 35, 90, and 145 degrees. The solid line is a theoretical calculation based on the same theory as outlined in the previous paper, using a liquid model in which the liquid is treated as a crystal with the atoms placed at random positions. In the case of

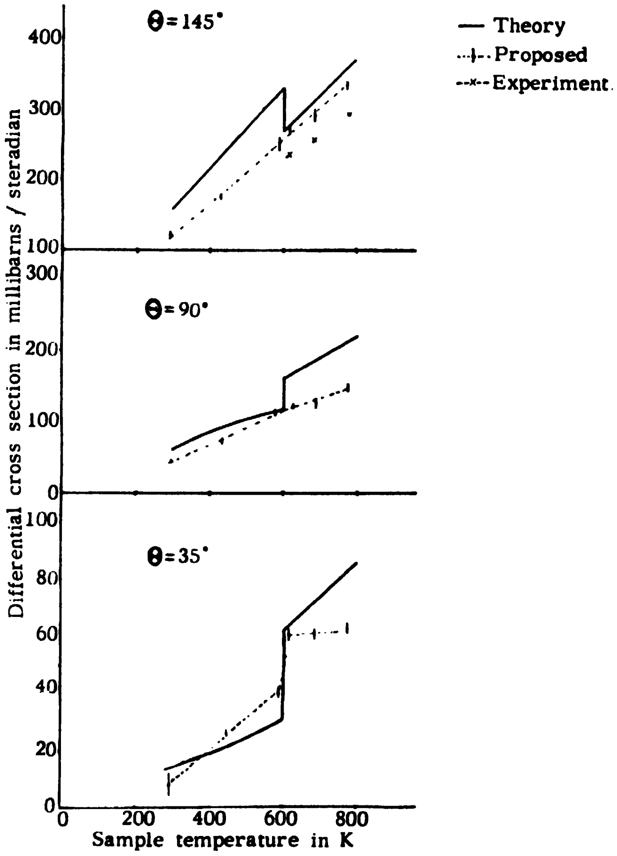

Slide 7. Differential cross section for scattering of 14°K neutrons by lead

145 and 90 degree scattering the points show a steady increase with temperature, but in the case of 35 degrees you can see there is a rise in the scattering by solid lead with increasing temperature. There is a sharp step at the melting point and then the scattering is about constant. This is in contrast to the theory, which indicates a rise in scattering with temperature. This rise of scattering with temperature is quite general for all cases of solid scattering and any case of liquid scattering where you treat the liquid by means of some sort of crystal model. The problem is how to relate this constant cross-section with temperature to all the other features of the scattering, which are analogous to solid type scattering.

The CHAIRMAN: I will now ask if anybody wishes to make any comments or observations on Mr. Kothari's paper or on what has just been said by Mr. Egelstaff.

Mr. E. P. WIGNER (USA): I should like to ask if you can measure the cross-sections up to very high temperatures, and how they go over into the cross section which one expects from a hot gas.

Mr. EGELSTAFF (United Kingdom): We have not measured the cross-section above a temperature of 800° absolute—that is about 200° above melting point—but we are hoping to extend measurements to a much higher temperature. However, at that temperature it is very much lower than the cross-section expected for a gas.

Session 7A

FISSION PHYSICS

LIST OF PAPERS

P/911 On the theory of nuclear fission . . . . A. Bohr 151

P/593 Fission physics and nuclear theory . . . . J. A. Wheeler 155

P/993 The time involved in the fission process . . . . D. Popovic 164

P/1089 Statistics of photographic fission tracks and range estimate of fragments . . . . J. S. Ausländer and T. Visky 165

P/897 Studies on the nuclear photoeffect . . . . M. D. de Souza Santos *et al.* 169

P/884 Angular correlation of fission neutrons . . . . K. Skarsvåg 185

P/891 High energy gamma-rays from short-lived fission products . . . . A. Lundby *et al.* 191

P/592 Determinations of fission quantities of importance to reactors . . . . R. B. Leachman 193

P/652 Some problems of the theory of nuclear fission . . . . B. T. Geilikman 201

P/653 On the theory of nuclear fission near threshold . . . . V. G. Nossoff 205

P/836 The nuclear fission process . . . . J. R. Huizenga 208

P/913 Energy loss and total charges of fission fragments passing through matter . . . . N. O. Lassen 214

On the Theory of Nuclear Fission

By Aage Bohr,* Denmark

ABSTRACT

The spectrum of quantum states of fissioning nuclei passing over the saddle point is discussed together with some of its consequences for the fission process. Thus, the effective fission threshold is found to depend significantly on the spin and parity of the compound nucleus. Moreover an interpretation is given of the observed anisotropies in the fragment distribution for photo fission and fission produced by fast particles.

INTRODUCTION

When a heavy nucleus captures a neutron or absorbs a high energy photon, a compound nucleus is formed in which the excitation energy is distributed among a large number of degrees of freedom of the nucleus.[1] The complex state of motion thereby initiated may be described in terms of collective nuclear vibrations and rotations coupled to the motion of individual nucleons.[2,3]

The compound nucleus lives for a relatively very long period, usually of the order of a million times longer than the fundamental nuclear periods, after which it decays by emission of radiation or of neutrons, or by fission. The latter process occurs if a sufficient amount of energy becomes concentrated on potential energy of deformation to enable the nucleus to pass over the saddle point shape, at which the repulsive coulomb forces balance the cohesive nuclear interactions.[4,5]

For excitation energies not too far above the fission threshold, the nucleus, in passing over the saddle point, is "cold," since the major part of its energy content is bound in potential energy of deformation. The quantum states available to the nucleus at the saddle point of the "fission channels" are then widely separated and represent relatively simple types of motion of the nucleus. These channels are expected to form a similar spectrum as the observed low-energy excitations of the nuclear ground state.

This ordered character of the motion of the nucleus at saddle point gives rise to a number of regularities in the fission phenomena. Thus, a fission process passing through a single channel may exhibit a marked anisotropy in the angular distribution of the fragments, depending on the angular momentum quantum numbers of the channel. Moreover, the wide spacing of the channels implies that the fission threshold may depend significantly on the spin and parity of the compound nucleus. Experimental data on these aspects of the fission phenomenon may thus provide valuable information on the structure of the fissioning nuclei at a crucial stage of the process.

FISSION CHANNEL SPECTRUM

The channel spectrum for fissioning nuclei refers to the sequence of potential energy surfaces $E(\alpha)$ considered as functions of the deformation parameter α characterizing the motion towards fission, and evaluated at the saddle point deformation.

In this section we briefly describe the channel spectrum expected on the basis of present knowledge of the low energy spectra of the nuclei in the region of the very heavy elements. These nuclei have already in their ground states a strongly elongated shape, and the ground state excitations therefore exhibit many similarities to those of the saddle point.

We shall assume that the nuclear shape during the passing of the saddle point remains axially symmetric, as is the preferred shape of the nuclear ground states. The channels can then be characterized by the quantum number K, representing the component of the nuclear angular momentum about the symmetry axis.

For even-even nuclei, the lowest state of the nucleonic structure has $K = 0$, corresponding to a paired nucleon configuration. With this intrinsic state is associated a rotational band with energies[6]

$$E_{I,K} = E_K + \frac{\hbar^2}{2J} I(I+1) \tag{1}$$

where I is the total nuclear angular momentum and J the effective moment of inertia. This latter quantity depends on the nuclear deformation. For the ground states of the very heavy elements, the value of $\hbar^2/2J$ is about 7 kev, and for the greater deformation at saddle point the value may be even smaller.

For nuclei, whose shape possesses reflection symmetry, the spectrum (1) contains, for $K = 0$, only the rotational levels with even I-values: 0, 2, 4, . . . , which all have positive parity. The observed mass ratio of the fission fragments indicates, however, that at the saddle point the nuclear shape in general does not possess reflection symmetry. The rotational band then also contains the odd I-values, having negative parity; however, the negative parity levels will be displaced with respect to the positive parity levels by an amount $\hbar\omega$, where ω is the frequency of the tunnelling motion between the mirror shapes of the preferred asymmetry. The more pronounced the asymmetry is, the smaller will be ω.

---

* Institute for Theoretical Physics, Copenhagen, Denmark (including considerations developed jointly by Dr. Ben R. Mottelson and the author).

In this connection it is of interest that low lying (1−) excitations of the nuclear ground states have been observed to occur systematically in the even isotopes of Ra and Th with energies in the region of 200 300 kev.[7] The energies increase as one goes to heavier elements. The interpretation of these states as collective modes of excitation associated with an asymmetry in the nuclear shape[8] is suggested by the fact that the lowest intrinsic excitations in even-even nuclei appear to have energies of the order of an Mev, and by the observed branching ratios for the $E1$ decay to the ground state and first excited (2+) state, which indicate a K-value of 0.[9]

At the saddle point shape one thus expects even-even nuclei to have a lowest state of $I = 0+$, and close lying collective excitations of 2+, 4+, . . . type as well as, although with somewhat higher energies, states of 1−, 3−, . . . type.

Apart from these collective rotational excitations, the nucleus possesses states involving the excitation of the nucleonic configuration. Since, however, these require the breaking of a nucleon pair, there will be a significant energy gap, estimated to be of the order of an Mev, between the lowest configuration (with $K = 0$) and the first excited configuration. After this gap the spacing between intrinsic excitations is expected to be only of the order of a hundred kev, corresponding to the average spacing of individual particle orbits. With each such intrinsic excitation, characterized by a definite K, there is associated a rotational band with $I = K, K + 1, K + 2, \ldots$ and both parities. The rotational energies are again given by (1).

In odd-A nuclei the lowest K-value is given by the component of angular momentum of the last odd particle in its lowest binding state. At saddle point this lowest K-value will in general differ from that of the nuclear ground state.[10] The spacing between the states of the last odd particle is of the order of a few hundred kev, and the intrinsic excitations in odd-A nuclei involve no energy gap similar to that characterizing the paired configuration in even-even nuclei. With each particle configuration is associated a rotational band with $I = K, K + 1, \ldots$ and both parities assuming a preference for an asymmetric shape at saddle point, or a softness towards deformations of this type (cf. reference 9). Similarly, in odd-odd nuclei, the intrinsic excitations may be closely spaced.

PHOTOFISSION

The case of photofission of even-even nuclei presents certain especially simple features, since in this case the compound nucleus is always produced in a (1−) state, assuming electric dipole absorption. As mentioned above, the lowest (1−) fission channel at saddle point corresponds to the $K = 0$ configuration, with the nuclear angular momentum taken up by rotational motion. For photon energies close to the fission threshold, the great majority of the fissioning nuclei are therefore expected to pass through this particular channel. This circumstance provides an explanation of the observed angular anisotropy of the fission fragments.[11,12]

Thus for the state involved, with $I = 1$, $K = 0$, and magnetic quantum number $M = \pm 1$ in the direction of the incident beam of photons, the probability for the nuclear symmetry axis to form an angle θ with the photon direction is of the form

$$W(\theta) = b \sin^2 \theta \tag{2}$$

After the saddle point has been passed, the coupling between rotational and intrinsic motion may to some extent weaken the anisotropy, but since this last stage of the fission process takes place rapidly, the angular distribution of the emitted fragments is expected to be mainly of the type expressed in Equation 2.

With increasing photon energy, other channels of (1−) type representing intrinsic nuclear excitations become available. Those having $K = 1$ give an anisotropy of opposite character to that in Equation 2 and on the average an approximately isotropic distribution is expected for the nuclei passing through the saddle point in a state of intrinsic excitation. Thus, the total angular distribution becomes

$$W(\theta) = a + b \sin \theta^2 \tag{3}$$

with the ratio b/a decreasing as the photon energy is increased. Assuming the first intrinsic excitations to have an energy of about one Mev (cf. above), the anisotropy would become small at an energy of a few Mev above threshold.

The experimentally observed angular distribution for photofission[11,13] of Th^{232} and U^{238} follows such a pattern. The distribution is found to be of the type in Equation 3, with the $\sin^2 \theta$ term dominating close to the threshold and becoming relatively small already a few Mev above threshold.

The anisotropy is observed to be somewhat larger in Th^{232} than in U^{238}, which might indicate a somewhat larger gap in the former nucleus between the first collective and intrinsic (1−) excitations at the saddle point. It is of interest to note, in this connection, that the energy of the collective (1−) excitations of the ground state appears to increase as one goes from Th to U (cf. above).

In odd-A nuclei several spin states may be formed by absorption of a dipole quantum, and the M-values extend from $-I$ to $+I$. Moreover, as mentioned above, the quantum states at saddle point lie denser than in the even-even nuclei. Even rather close to threshold, therefore, the photofission may proceed through several states, and no pronounced anisotropy is expected. The experiments on the photofission of U^{235} have also yielded an approximately isotropic distribution of the fragments.[13]

The photofission of odd-A nuclei should be more comparable to the part of the even-even photofission which passes through intrinsic excitations, where the level density is high. It has also been noted[13] that the isotropic part of the even-even photofission shows a similar yield curve as for the odd-A nuclei, while the anisotropic component appears as an additional contribution to the photofission process.

The interpretation of the anisotropic component in photofission as representing the nuclei which pass through the saddle point in the $(1-)$ collective excitation has a further interesting consequence for the mass distribution of the fragments. In fact, since the wave function for this state is antisymmetric in the co-ordinate describing the degree of asymmetry of the nuclear shape, a nucleus in this state cannot undergo symmetric fission. Such a discrimination against symmetric mass division has been observed experimentally in the photofission of Th^{232}.[14] It is found that the anisotropy vanishes for symmetric division and increases strongly with the ratio between the fragment masses.

SLOW NEUTRON INDUCED FISSION

Slow neutron capture by an even-odd nucleus of spin I_0 leads to a compound nucleus of even-even type with spin $I = I_0 \pm \frac{1}{2}$, and with same parity π as the target nucleus.

As follows from the above discussion of the spectrum at saddle point only one of these spin-parity combinations is contained in the rotational band associated with the lowest nucleonic configuration $(K = 0)$, viz., the state with $(-1)I = \pi$.

Therefore, the fission threshold is expected to differ appreciably, by as much as an Mev, for the two types of compound levels formed. This may imply a rather different ratio of fission to capture for the two level systems, especially if the neutron binding energy is smaller than the larger of the threshold values.

The circumstance that slow neutron fission is expected to proceed through one or a few channels also implies large fluctuations in the fission width among the levels of same I. The fluctuations should be similar to those observed for the neutron width, which likewise depends on the presence in the compound nucleus wave function of a definite component (representing the channel for elastic neutron scattering).

The parity of the target nucleus may further affect the mass distribution of the fission fragments. Thus for the levels with $(-1)I = \pi$, the nuclear wave function is symmetric or antisymmetric in the asymmetry co-ordinate, for $\pi = +1$ and -1, respectively. In the latter case, symmetric fission is expected to be inhibited, as in the case of the photofission (cf. above).

If slow neutron fission of aligned nuclei could be studied, large angular anisotropies of the fragments would be expected. For the states with $(-1)I = \pi$, which pass through the saddle point with $K = 0$, the distribution is directly related to the distribution of M-values of the compound states. For the other set of levels with $(-1)I = -\pi$, the distribution in addition depends on the K-value of the fissioning nucleus.

Some even-even target nuclei have also been observed to undergo slow neutron fission. For such targets the compound states all have $I = \frac{1}{2}$ and even parity, and the fission threshold depends on the energy of the lowest $K = \frac{1}{2}$ configuration at saddle point. If the intrinsic parity of this configuration is odd, symmetric fission should again be inhibited.

FISSION PRODUCED BY FAST PARTICLES

In the case of fission initiated by the impact of faster particles, there may be a correlation between the direction of the incident beam and of the fragment emission. This correlation depends on the distribution of the I- and M-values with which the compound nucleus is formed, as well as on the K-values of the states available to the fissioning nucleus at the saddle point. For a fission process proceeding through a channel with quantum numbers I, M, K, the orientation of the nuclear symmetry axis, representing the direction of fission, is distributed according to the corresponding symmetric top wave function.

For relatively small energies, at which a single angular momentum state of the incident particle may play an important role, or close to the fission thresholds, specific effects may occur associated with the dominance of a single or a few fission channels.

For larger energies of the incident particle, the fissioning nuclei may pass through a great number of different states at the saddle point, with different angular momentum quantum numbers. Nevertheless, a systematic tendency for anisotropy in the fragment emission results from the fact that the M- and K-values are not distributed uniformly from $-I$ to $+I$, but are concentrated towards numerically small values. Thus, assuming the incident particle to be a proton or a neutron, the M-values are restricted to the range $|M| \leq I_0 + \frac{1}{2}$, where I_0 is the spin of the target nucleus. Moreover, the channel spectrum is expected to exhibit a marked preference for small K-values; this is especially so for even-even nuclei, but also the density of K-values for additional individual nucleons decreases with increasing K.[15]

The tendency towards small values of M implies that for large I, the nuclear angular momentum vector points preferentially in a direction perpendicular to the incident direction. Moreover, for small K-values the nuclear axis is orientated predominantly perpendicular to the angular momentum vector. Consequently the distribution of the fission fragments per solid angle is peaked in the forward direction.

An anisotropy of this type has been found for fast neutron fission in a number of elements.[16] The dependence of the observed anisotropy on the even-odd character of the target nucleus can also be understood from the above line of argumentation. Thus, if the target is even-odd (even Z, odd N), so that the compound nucleus is even-even, the K-values at the saddle point are the smallest. On the other hand, the M-values are smallest for even-even targets, in which case the compound nucleus has $M = \pm\frac{1}{2}$. Therefore, the anisotropy should be relatively large for these two types of targets, and appreciably smaller for odd-even or odd-odd targets. The experiments[16] indicate comparable anisotropies in U^{233}, U^{235} and U^{238}, but only half the effect in Np^{237}.

For even-odd targets, the anisotropy is expected to be largest for small values of the target spin I_0, since the range of M-values is then most restricted. The observed small difference between the anisotropies of U^{233} ($I_0 = 5/2$) and U^{235} ($I_0 = 7/2$) is in this direction, but may not be significant in view of the experimental uncertainties. An especially large anisotropy should result for Pu^{239} with $I_0 = 1/2$.

In order to obtain a theoretical estimate of the order of magnitude of the anisotropy in the fission fragment distribution, we may employ the classical approximation to the angular distribution functions, which becomes valid for high angular momenta. Considering a particle incident on an even-even target and neglecting the spin of the particle, the compound nucleus has $M = 0$ and the angular distribution of the fragments is then, in the classical approximation, given by

$$W(\theta) = \int dI \int_{|K|<I\sin\theta} dK \quad f(K,I)\left(\sin^2\theta - \frac{K^2}{I^2}\right)^{-1/2} \qquad (4)$$

where $f(K,I)$ gives the distribution in K and I of the fissioning nuclei.

For simplicity, we shall represent the distribution in K at the saddle point by a constant for K less than some effective limit K_m. Moreover, in the classical approximation, the probability for formation of the compound nucleus in a state of total angular momentum I, is proportional to I up to a limiting value I_m, given by

$$\hbar I_m = R_0 M V \qquad (5)$$

where R_0 is the mean nuclear radius and MV the momentum of the particle. The distribution in Equation 4 then depends only on the ratio $x = I_m/K_m$. For $x < 1$, the distribution is isotropic, but for larger x it exhibits a forward peak, which increases with x. The ratio $W(0°)/W(90°)$ takes on values of about 1.15, 1.3 and 1.8 for $x = 1.25$, 1.5 and 2, respectively.

The observed anisotropy for fast neutron fission in U^{238} follows such a general trend increasing with the energy of the incident neutron.[17] A maximum anisotropy of $W(0°)/W(90°) \sim 1.4$ was obtained for a neutron energy of about 7 Mev. For this energy we have $I_m \sim 5$, so that the observed anisotropy corresponds to the above estimated, if we take $K_m \sim 3$, which is of the expected order of magnitude. For still larger neutron energies, fission processes occurring after neutron emission are expected to become increasingly important[18] and would seem to account for the observed decrease in the anisotropy of the fragment distribution. Similar anisotropies have also been observed in the fission of Th- and U-isotopes produced by protons of about 22 Mev.[18]

ACKNOWLEDGEMENT

The author wishes to thank Dr. David H. Frisch for many enlightening discussions.

REFERENCES AND NOTES

1. Bohr, N., Nature *137*, 344 (1936); Bohr, N. and Kalckar, F., Dan. Mat. Fys. Medd. *14*, No. 10 (1937).
2. Bohr, A., Dan. Mat. Fys. Medd. *26*, no. 14 (1952); Bohr, A. and Mottelson, B. R., Dan. Mat. Fys. Medd. *27*, No. 16 (1953).
3. Hill, D. L. and Wheeler, J. A., Phys. Rev. *89*, 1102 (1953).
4. Meitner, L., and Frisch, O. R., Nature *143*, 239 (1939).
5. Bohr, N. and Wheeler, J. A., Phys. Rev. *56*, 426 (1939).
6. For a discussion of nuclear rotational states, cf., e.g., Bohr, A. and Mottelson, B. R., chapter 17 of Beta- and Gamma-Ray Spectroscopy, edited by Siegbahn, K. (North-Holland Publishing Company, Amsterdam 1955) and Bohr, A., Rotational States of Atomic Nuclei (Einar Munksgaard, Copenhagen 1954).
7. Stephens, F., Jr., Asaro, F., and Perlman, I., Phys. Rev. *96*, 1568 (1954).
8. Such an interpretation was first suggested by R. F. Christy, private communication, Oct. 1954.
9. As an alternative to the interpretation of the (1 −) states as rotational excitations of asymmetric nuclei, one may also consider the possibility of an asymmetric vibration of the nuclear shape about an equilibrium which is symmetric but very soft towards asymmetric deformations.
10. This circumstance has been suggested as the explanation of the slower rate of spontaneous fission in odd-A nuclei as compared to that observed in even-even nuclei [Newton, J. O., Nuclear Properties of the Very Heavy Elements. Contribution to Progress in Nuclear Physics, vol. 4, ed. by Frisch, O. R. (1954)].
11. Winhold, E. J., Demos, P. T. and Halpern, I., Phys. Rev. *87*, 1139 (1952).
12. The observed anisotropy in photofission has been earlier discussed (ref. 3) in terms of a tendency for the absorbed photon to set up an oscillation of the nucleus preferentially in a direction perpendicular to the beam. From similar arguments an opposite anisotropy in fast neutron induced fission was predicted and later verified experimentally (cf. below). It would appear, however, that any such correlation in the initial stage of the process is quickly lost in the highly complex motion of the compound nucleus, since the quantum number K, which determines the direction of the nuclear axis with respect to the total angular momentum vector, is not a constant of the motion for the compound state. Thus, the anisotropy in the photofission depends on the fact that in the threshold region, the nucleus must pass through saddle point in a definite channel, having $K = 0$. In the fast neutron fission the situation is somewhat different. The high angular momentum values given to the nucleus here implies a tendency even in the complex motion of the compound nucleus to concentrate a large part of this angular momentum on collective rotational motion.
13. Winhold, E. J., Ph.D. Thesis, Mass. Inst. of Technology, Sept. 1953.
14. Fairhall, A. W., Halpern, I. and Winhold, E. J., Phys. Rev. *94*, 733 (1954).
15. Cf. e.g., Nilsson, S. G., Dan. Mat. Fys. Medd. *29*, No. 16, in the press.
16. Brolley, J. E., Jr., and Dickinson, W. C., Phys. Rev. *94*, 640 (1954).
17. Brolley, J. E., Jr., and Henkel, R. L., Bull. Am. Phys. Soc. *30*, No. 3, CA 3.
18. Bohr, N., Phys. Rev. *58*, 864 (1940).
19. Cohen, B. L., Jones, W. H., McCormick, G. H. and Ferrell, B. L., Phys. Rev. *94*, 625 (1954); Cohen, B. L., Ferrell, B. L., Coombe, D. J., and Hullings, H. K., Phys. Rev. *98*, 685 (1955).

Fission Physics and Nuclear Theory

By J. A. Wheeler,* USA

Fission physics has advanced in remarkable phase with nuclear theory. The compound nucleus picture[1] of 1935 and liquid drop model[2] of 1937 correlated[3] 1939's flood of observations on fission. Now new advances in nuclear theory shed light on newly recognized features of fission, including: (1) variations in fission to capture ratio from one neutron resonance to another,[4] (2) irregular variations in the cross section for neutron-induced fission for energies of the order of one Mev,[5] (3) correlation in direction between the line of fission and the line of incidence of gamma ray[6] or neutron[7] or proton,[8] (4) variations from one nucleus to another in heights of fission barriers; and fission thresholds for nuclei of odd mass systematically higher than those for neighboring even-even nuclei. This effect leads naturally to the consideration of spontaneous fission. The discovery of this phenomenon by Flerov and Petrjak in 1940[9] is one more reminder of the international character of fission physics, as of every other branch of science.

All four effects find a natural place in the unified nuclear model. The development of this picture from 1939 and earlier views of nuclear constitution may be briefly recapitulated in the following outline:

1932

Discovery of neutron; neutrons and protons identified as constituents of nucleus; first stage of shell model; nucleus compared to atom; nucleons compared to electrons; hypothesis of an effective average potential and of single particle orbits; calculated time for radiative transition from excited state to ground state of order of 10^5 times time for nucleon to cross nucleus; single nucleon sent in from outside expected to have extremely small probability to lose its energy traversing nucleus.

1934

Observations of high probability for radiative capture of slow neutron by typical heavy nuclei; quite incompatible with individual particle model in its existing form.

1935

Compound nucleus picture of nuclear reactions; emphasis placed on local character of nuclear forces contrasted with the smooth character of the long range electrostatic forces in an atom; rapid exchange of energy assumed to occur between one nucleon and another; energy of incoming nucleon or absorbed photon regarded as distributed over all accessible degrees of freedom of compound nucleus; method of disposal of excitation idealized as independent of mechanism of formation of compound nucleus; probability of dissipation of energy by kth mode of reaction (particle emission or radiation) measured by partial transition probability A_k and associated partial level with $\Gamma_k = \hbar A_k$.

1936

Analysis of behavior of cross-section in the neighborhood of a single isolated resonance; cross-section

$$\sigma_{12} = \pi \lambdabar_1^2 \frac{(2I_{comp} + 1)}{(2I_{initial} + 1)\begin{pmatrix}\text{number of}\\ \text{polarization}\\ \text{states}\end{pmatrix}} \times \frac{\Gamma_1 \Gamma_2}{(E - E_{res})^2 + (\Gamma/2)^2} \quad (1)$$

for reaction in which compound nucleus is formed by mode 1 and breaks up by mode 2.

1937

Compound nucleus compared to a liquid drop; system concluded to possess collective types of excitation analogous to capillary oscillations of a drop of liquid under restoring force of surface tension; density, ρ, of excitation levels estimated to increase with excitation, E, roughly as

$$\rho(E) \sim (\text{lowest excitation energy})^{-1} \exp (\text{const } E^{1/2}) \quad (2)$$

Probability of formation of compound nucleus by neutron bombardment idealized as of order of geometrical cross-section, πR^2, of nucleus when reduced wave length of nucleon, $\lambdabar$, is comparable to or smaller than R; emission of neutrons from a nucleus of high excitation compared with Maxwell-Boltzmann description of evaporation.

1938

Further development of statistical description of reactions of nuclei that contain large numbers of particles; simple arguments to determine excitation dependence of partial level widths Γ_r for radiation, Γ_p and Γ_α for proton and alpha emission, Γ_n for emission of a neutron of any energy and $\Gamma_{n'}$ for emission of a neutron with the maximum available energy; applications of this picture to account successfully for the principal features of many nuclear reactions.

---

* Princeton University.

1939

Discovery and interpretation of principal features of nuclear fission; mechanism compared with deformation and division of a uniformly charged droplet; rotation-symmetric shape specified by the radius function $R(\theta)$ or by the amplitudes α_2, α_3 . . . of various terms in the harmonic analysis of this periodic function; energy of deformation, $V(\alpha)$, regarded as a function of these or similar deformation coordinates, α; energy calculated by comparing the nucleus with a uniformly charged drop of incompressible liquid, with charge Ze, volume $(4\pi/3)r_0{}^3A$, and surface tension o, with r_0 and o estimated from the relevant terms,

$$4\pi r_0{}^2A^{2/3}o + 3Z^2e^2/5r_0A^{1/3} = 13 \text{ Mev } A^{2/3} + 0.585 \text{ Mev } Z^2/A^{1/3} \quad (3)$$

in the semi-empirical formula for nuclear binding energies; deformation energy expressible in the form

$$V(\alpha) = 4\pi r_0{}^2A^{2/3}of_s(\alpha) + (3Z^2e^2/10r_0A^{1/3})f_c(\alpha) \quad (4)$$

where f_s and f_c are dimensionless functions of the shape of the deformed droplet; minimum energy required to pass from original nucleus to a critical deformation defines the "saddle point energy," or minimax energy, or critical energy, or activation energy for fission, or the fission barrier, E_f; this energy and the associated critical form are uniquely specified by the dimensionless fissionability parameter, x:

$$x = \frac{Z^2e^2}{10Ao(4\pi r_0{}^3/3)} = \frac{Z^2/A}{(Z^2/A)_{crit}} = \frac{Z^2}{45A} \quad (5)$$

When this parameter has the value 1, the droplet is already unstable in its spherical form; for smaller x, the critical energy has the form

$$E_f = 13 \text{ Mev } A^{2/3}f(x) \quad (6)$$

The dimensionless function $f(x)$ has been calculated as a function of x; when the excitation of the compound nucleus is less than E_f, the nucleus has to penetrate a potential barrier to undergo fission; as E rises above E_f, fission becomes rapidly more probable; the partial width for fission, $\Gamma_f(E)$, then increases almost exponentially with energy; dependence of cross-section for fission upon neutron energy governed by relative magnitudes of total level width, Γ, and level spacing, $D = 1/\rho(E)$, as illustrated by Table 1; reasonable account given by nuclear theory for fissionability of natural uranium at thermal energies (U^{235}) and at Mev energies (U^{238}) and low fission cross section at intermediate energies; for the difference in fissionability of these two nuclei; for the magnitude of the energy release in fission; for the emission of prompt and delayed neutrons; and for other features of the experimental evidence.

It was not clear in 1939 whether predictions of the compound nucleus—liquid drop—statistical model as to level widths should apply to each level individually, or should be considered to represent average values for several levels. Recent observations of D. J. Hughes and collaborators suggest the following version of the relevant statistical arguments: (1) The partial width for transition from a single level, a, of the original compound nucleus to a specific level, b, either of the same nucleus (radiative transition) or of another

Table 1. Principle Regimes in the Dependence of Cross Section upon Energy. Neutron-Induced Fission is the Reaction Illustrated in the Table, but Radiative Capture Follows Similar Relations Obtained from the Simple Substitution $\Gamma_f \rightarrow \Gamma_{rad}$ for the Relevant Level Width

Level width narrower than level spacing. Cross-section curve shows well separated resonances	*Level breadth wider than level separation, D. Relatively smooth variation of cross section with energy expected on compound nucleus picture*
Low energy; particle wave length large compared to nuclear dimensions	
Case LN. Ideal cross section at resonance is of order of $\pi\lambda^2\Gamma_{n'}/\Gamma_{total} \gg \pi R^2$. Ideal cross section *away* from a single resonance of energy E_0 is of order $\pi\lambda^2\Gamma_{n'}\Gamma_{total}/(E - E_0)^2$ For slow neutrons λ^2 is proportional to $1/v^2$, and $\Gamma_{n'}$ to v, so both cross-section formulae go as $1/v$. Fraction Γ_f/Γ_{total} of cross section leads to fission	Case LW. Cross section for fission of order of $\sigma_f \sim \pi\lambda^2 \frac{\Gamma_{n'}}{\Gamma_{total}} \frac{2\pi\Gamma_{total}}{D} \frac{\Gamma_f}{\Gamma_{total}}$ Varies as $1/v$
High energy—of order 1 Mev to 10 Mev; particle wave length smaller than nuclear dimensions	
Case HN. Does not occur for uranium and other heavy nuclei but is familiar situation in many reactions of light nuclei. Cross sections for typical reactions still follow formulae like those above	Case HW. Product of first three factors above equal to some substantial fraction of πR^2 ("unit sticking probability"). Cross section for fission $\sigma_f \sim \pi R^2 \frac{\Gamma_f}{\Gamma_{total}}$
Still higher energies (above 10 Mev). Compound nucleus picture progressively less adequate.	

nucleus (such as the residue from a process of particle emission) varies from level to level in an irregular way. However, the average of the relevant partial width or transition probability over a number of levels has a reasonably well defined value, $\langle\Gamma_k\rangle$ or $\langle A_k\rangle$. The distribution of individual cases about this partial width follows a law not fully investigated either experimentally or theoretically. However, in the case of neutron emission at least the preliminary observations suggest a quite simple law: The fraction of levels, df, which have a neutron partial width between Γ_n and $\Gamma_n + d\Gamma_n$ is

$$df = \frac{d\Gamma_n}{\langle\Gamma_n\rangle} \exp - \frac{\Gamma_n}{\langle\Gamma_n\rangle} \tag{7}$$

Here the average width, $\langle\Gamma_n(E,I)\rangle$, is presumed to be a slowly varying function of excitation. (2) The average neutron widths, $\langle\Gamma_n(E,I)\rangle$ are such that the cross section for formation of the compound nucleus is equal to the geometrical cross section of the nucleus, πR^2, or to a reasonably large fraction thereof. This prediction, too, rests on the liquid drop model. (3) For a process such as radiation that leads from a given highly excited state to any one of an enormous number of states of lower energy, the totalized radiation width,

$$\Gamma_r = \Gamma_{r_1} + \Gamma_{r_2} + \cdots$$

has a value which is practically unaffected by small changes in the energy of the excited state. In such a case the width is represented by a smoothly varying function of energy, $\Gamma_r = \Gamma_r(E)$. (4) Another smooth function of energy, $\Gamma_n(E)$, will represent the probability per second of neutron ejection, $A_n(E)$, multiplied by $\hbar$, under conditions where emission processes leading to numerous states of the residual nucleus are energetically possible. When the excitation energy is less, and neutron loss can lead only to the ground state of the residual nucleus, or a very few low-lying levels, then one cannot predict in advance the partial width of the level in any given case, and one can only speak about the average value, $\langle\Gamma_{nk}(E)\rangle$, expected in an average over a number of such cases. Similar considerations apply to the emission of other particles and to fission. This analysis leads to the picture of the fission cross sections of U^{235} and U^{238} presented in Table 2.

1948

Rebirth of the shell model;[11] recognition of some approach to idealization of independent particles moving through a common nuclear potential, as evidenced by regularities in the spins and magnetic moments of nuclei in their ground states, and the extra stability of nuclei that contain 2, 8, 20, 28, 40, 50, 82 or 126 like nucleons; recognition that superposed on the background of the effective average potential there are corrections due to specific nucleon-nucleon couplings; estimate of strength of these couplings from magnetic moment corrections and the pattern of low-lying energy levels of light nuclei.

1953

Successful application of individual particle model

Table 2. General Character of Cross Sections of U^{235} and U^{238} in Their Dependence upon Energy in the Light of the Compound Nucleus—Liquid Drop—Statistical Model

Neutron energy	U^{235}	U^{238}
Thermal	$\sigma_{rad} = 101 \times 10^{-24}$ cm^2 $\sigma_{fiss} = 549 \times 10^{-24}$ cm^2 Cross sections perhaps due to single resonance close to thermal energy	$\sigma_{rad} = 2.8 \times 10^{-24}$ cm^2; $\sigma_{fiss} = 0$ Cross section due to one or more resonances separated from thermal energy by an amount of order of a few ev—large compared to the level width, $\Gamma_{total} \sim \Gamma_{rad}$, of the rough order of 10^{-1} ev
Few ev	Numerous characteristic cross-section resonances for which Γ_{rad} will be expected to be nearly the same, but $\Gamma_{n'}$ and Γ_f may vary from resonance to resonance as in Equation 7. In addition to such fluctuations $\Gamma_{n'}$ will show a general increase in proportion to v	Characteristic resonances with a spacing greater than that for U^{235} because of lesser excitation. Similar fluctuations in $\Gamma_{n'}$. This quantity of order of milli ev and therefore smaller than Γ_{rad}. Cross-section σ_{rad} at resonance less than $\pi\bar{\lambda}^2$ by a factor of order $\Gamma_{n'}/\Gamma_{rad}$.
Many kev	Level spacing has decreased and level width increased so that levels now overlap and fission cross section varies relatively smoothly with energy. Beginning to approach a value of order of $\sigma_f \sim \pi R^2 \sim 2 \times 10^{-24}$ cm^2. Radiative capture cross section obtained by multiplication with Γ_r/Γ_f	$\Gamma_{n'}$ becomes comparable with Γ_{rad}, and cross section at exact resonance σ_{rad} (res) $\sim \pi\bar{\lambda}^2$. With further increase in energy. $\Gamma_{n'}$ exceeds Γ_{rad}, and $\sigma_{rad}\ (\text{res}) \sim \pi\bar{\lambda}^2 \dfrac{\Gamma_{rad}}{\Gamma_{n'}}$ Ultimately level widths exceed level spacings and Γ_{rad} becomes a nearly smooth function of energy
Region 1 Mev to 10 Mev	$\sigma_f \sim \pi R^2 \sim 2 \times 10^{-24}$ cm^2 $\sigma_{rad} \sim \pi R^2 \dfrac{\Gamma_{rad}}{\Gamma_{total}}$ Latter becomes very small, not that Γ_{rad} decreases, but $\Gamma_{tot} = \Gamma_{rad} + \Gamma_n + \Gamma_f$ increases	Near 1 Mev the nuclear excitation becomes comparable to the fission barrier. Γ_f rapidly rises and overwhelms Γ_{rad}. The fission cross section approaches $\sigma_f \sim \pi R^2 \dfrac{\Gamma_f}{\Gamma_f + \Gamma_n} \sim 0.5 \times 10^{-24}$ cm^2 —only a fraction of geometrical because neutron emission is still more important than fission. When the energy of the bombarding neutron reaches 7 or 8 Mev, its re-evaporation with only 1 Mev leaves the residual nucleus with enough energy to have a second—and more hopeful—try at fission. Now σ_f approaches πR^2

to analysis of scattering of nucleons in effective average nuclear potential;[12] recognition that means free path of nucleon in nuclear matter is neither so short as implied by the primitive liquid drop model, nor so long as assumed in early independent particle picture, but comparable to nuclear dimensions; consequent distinction between nucleons that merely *taste* the nuclear potential, and those that exchange energy and become *assimilated* into a compound nucleus; in scattering of ~20 Mev protons by nuclei, consequent division[13] of scattered particles into nearly elastic group, and group that follows statistical predictions of evaporation picture; rough description of this division by way of a complex nuclear potential; imaginary part of potential measures the probability of absorption—assimilation into a compound nucleus, the subsequent fate of which can then be analyzed separately.

1954

Beginnings of a justification of concept of effective average potential for strongly interacting nucleons;[14] comparison of nuclear medium with optical medium; comparison of effect of scattering at individual centers to effect of refractive index; alteration in normal wave length-frequency relation interpreted in terms of change in effective mass of nucleon inside nucleus.[15]

1950

First combination of independent particle model with idea of collective displacement of all nucleons to explain extraordinarily large quadrupole moments of many nuclei;[16] those nucleons that are not balanced off against each other in closed shells create unbalanced pressure against nuclear wall; deform nuclear surface; cause bulk transport of charge and asymmetry in nuclear charge distribution of observed order of magnitude.

1951

Recognition[17] that deformation of nuclear surface can rotate; excitation associated with such collective rotation analyzable in terms of ideas familiar from molecular physics; extensive experimental evidence for such rotational excitations;[18] correlation of nuclear deformations as estimated from rotational energy levels, from quadrupole moments, and from isotopic shifts in optical spectra.[19]

1953

Formulation of collective or unified nuclear model;[20] common treatment for all nucleons, whether in completely filled or partially filled shells; nearly adiabatic adjustment of particle motion to changing configuration of nuclear surface; nucleus more nearly analogous to a molecule than to an atom (Table 3); analysis of fission phenomena in terms of unified nuclear model.

CONCLUSION

Certain features of nuclear physics depend principally on the properties of one nucleon—such as the

Table 3. Analogy Between the Collective Nucleus and a Molecule

Property	*Molecule*	*Nucleus*
Individual particle state occupied by	Electron	Nucleon
Slowly varying parameters that affect energy of individual particle states	Internuclear separations; $r_{12}, r_{13}, \ldots$ etc.	Parameter α and other parameters that describe in more detail the configuration of the nuclear wall
Oscillation period in an example	8×10^{-15} sec in H_2	$\sim 5 \times 10^{-21}$ sec in U
Fundamental period of motion of most energetic particle in same example	$\sim 10^{-15}$ sec	$\sim 0.3 \times 10^{-21}$ sec
Vibrational potential energy described as function of these one or more parameters by a curve or surface	$V(r_{12}, r_{13}, \ldots) =$ sum of energies of individual electron states plus electrostatic interactions not otherwise taken into account	$V(\alpha_2, \alpha_3 \ldots) =$ sum of energies of individual nucleon states calculated for a deformed wall plus other interactions not otherwise taken into account
Vibrational or rotational kinetic energy	Mainly localized in nuclei	Increment of kinetic energy of nucleons because wall is moving and nodes of individual particle wave functions are undergoing displacement
Quantum numbers required to specify state of excitation of system	Electronic quantum numbers; vibrational and rotational quantum numbers	Nucleonic quantum numbers; oscillation and rotational quantum numbers
Exchange of energy between individual particle excitation and general vibration of the system can take place at point of contact between one potential surface and an adjacent one, via a radiationless transition	Mechanism for excitation to be degraded into vibrational energy; important in polyatomic molecules, where the variation of two or more parameters ordinarily allows one to arrive at a point in configuration space where two successive potential surfaces make a cusp-like contact	Mechanism for nucleonic motion to be degraded into collective motion, and conversely for energy of collective vibration to be imparted to an individual nucleon, as for example in a nucleonic evaporation process. To be distinguished from direct energy exchanges between a pair of nucleons—an independent mechanism for capture and evaporation. Both contribute to the absorption component of the complex nuclear potential

spins and magnetic moments of certain nuclear ground states, and many transition probabilities, and the elastic or nearly elastic scattering of merely "tasted" nucleons. These features can be described to a first approximation in terms of the independent particle picture and more accurately by calculations that allow for perturbation of the individual nucleon orbit by other orbits and by wall deformations. In contrast, collective motions such as vibration and fission receive their first approximate description in the liquid drop model. An improved analysis combines the two points of view and has the following features: (1) the equilibrium configuration of the surface is ordinarily no longer spherical, but depends on the nucleonic state of the system, (2) the restoring force, or effective surface tension, associated with the vibrations also depends upon the nucleonic state, (3) the partition of the energy between nucleonic and collective excitation will ordinarily change slowly with time except as forbidden by a principle like the law of conservation of angular momentum. A more and more comprehensive view of nuclear constitution has evidently evolved and continues to develop hand in hand with the experimental and theoretical study of many nuclear phenomena, among which the center of interest here is fission.

In the light of nuclear theory as it stands today it is appropriate to consider four issues of fission physics.

Effect No. 1

The first is a striking variation in the fission to capture ratio between one slow neutron resonance and another. This effect shows in the U^{235} and Pu^{239} resonances analyzed elsewhere before this conference. This ratio not only influences neutron economy, chain reactivity, and reproduction of fissionable material in a chain reactor, but also gives the most direct measure for the ratio of the partial widths, Γ_f and Γ_r, with respect to fission and radiation. From the available evidence it is apparent that both Γ_r and Γ_f vary from level to level.

At the nuclear excitation, ~6 Mev, given by slow neutron capture, the number of lower-lying levels is very great, and the number of possible gamma-ray transitions is very large. Consequently it is not unreasonable to expect a radiation width, Γ_r, that is nearly constant from level to level, provided that the slow neutron is captured in an even-even nucleus to give always a compound nucleus of spin $\frac{1}{2}$. However, capture in either U^{235}, with spin $\frac{5}{2}$ or $\frac{7}{2}$, or Pu^{239}, with spin $\frac{1}{2}$, evidently leads to two different classes of levels of the compound nucleus. According as this system possesses one or the other of two distinct spin values, it will make radiative transitions to different families of lower-lying levels and will be expected to have an appreciably different width, which one may designate by Γ_r^+ and Γ_r^-.

Also dependent upon spin will be the fission probability. The deformation potential will differ from one nucleonic state of the nucleus to another. Consequently the height of the fission barrier will alter from the one spin value to the other. The probability of fission depends in a critical way upon the comparative values of the fission barrier and the nuclear excitation. Below the top of the barrier the partial width, Γ_f, will be an exponentially small fraction of the level spacing, D. A little above the top of the barrier the statistical theory of fission[3] predicts a ratio of average level width to level spacing given by

$$\langle \Gamma_f \rangle / D \sim N/2\pi \tag{8}$$

where N is the number of excitation levels of the nucleus in its critical form which are accessible with the given excitation of the compound nucleus. A rough estimate of the order of the spacing of the low-lying levels of the nucleus in its fission form is 0.1 Mev (all levels) or perhaps $\frac{1}{2}$ to 1 Mev (levels of a given spin). At excitations of the compound nucleus of the order of 0 Mev to $\frac{1}{2}$ Mev or 1 Mev above the fission barrier one therefore expects a width to spacing ratio of the order

$$\langle \Gamma_f \rangle / D \sim \frac{1}{6} \tag{9}$$

The ratio Γ_f/D is observed to be less than one for both U^{235} and Pu^{239} bombarded with epithermal neutrons. However, the ratio is not exceedingly small compared to one. Consequently one concludes from Equation 9 that $E - E_f$ for epithermal neutron irradiation is probably some reasonable fraction of 1 Mev.

An estimate of the difference in barrier height between one spin state and the other, $E_f^+ - E_f^-$, gives a number also of the order of $\frac{1}{2}$ Mev. Depending upon the precise value of the excitation energy, one can expect, from Equation 9, differences between $\langle \Gamma_f^+ \rangle$ and $\langle \Gamma_f^- \rangle$ varying from a factor 2 to a factor 10. In addition to these characteristic spin differences one has to expect statistical differences of the type described by Equation 7. In summary, one expects the slow neutron resonances of U^{235} and Pu^{239} to fall into two groups of spin values $I + \frac{1}{2}$ and $I - \frac{1}{2}$. In a given one of these groups one expects a fission to capture ratio, $R_\pm$, with a probability

$$d\,(\text{probability}) = \frac{dR_\pm}{\langle R_\pm \rangle} \exp\left[-R/\langle R_\pm \rangle\right] \tag{10}$$

Here the ratio

$$R_\pm = \langle \Gamma_f^\pm \rangle / \langle \Gamma_r^\pm \rangle \tag{11}$$

may have for the two groups values that are—accidentally—equal, or values that differ by a factor as much as possibly ten.

These predictions seem not to contradict the observations reported elsewhere at this conference. However, it appears too early to give a definite classification of each of the observed levels into the one class or the other, and too early to state specific values for the four relevant average widths, $\langle \Gamma_{f,r}^\pm \rangle$, for each of the two nuclear species under consideration.

Effect No. 2

As the energy of the bombarding neutron is raised, the average level width increases, and average level

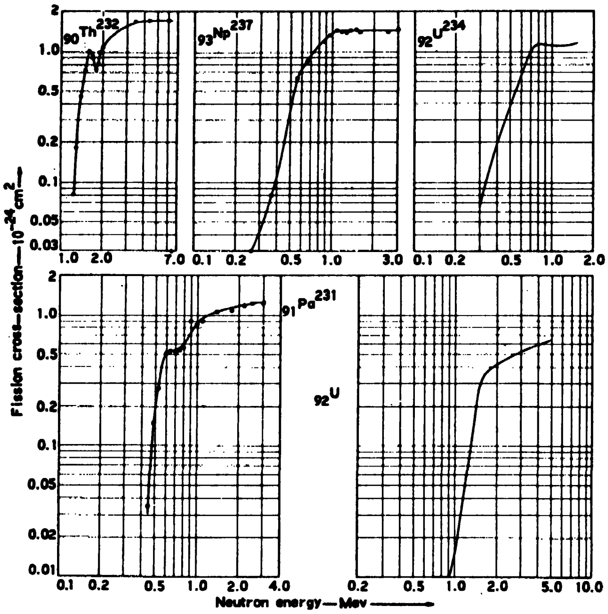

Figure 1. Observations[5] of cross section for neutron induced fission showing (a) regular variation of cross section with energy in continuum region as predicted by compound nucleus—liquid drop—statistical model; but (b) superposed on this incompletely resolved structure interpretable in analogy to Ramsauer effect in electron-atom encounters

spacing decreases. The spectrum becomes continuous. At higher energies the simple compound nucleus—liquid drop—statistical model leads one to expect[3] a relatively regular dependence of cross section upon energy. However, the recent observations[5] summarized in Fig. 1 show superposed on this regular variation in a few cases an irregular structure with a characteristic energy of the order of ¼ Mev. One is open to believe that increase in resolving power will show the same effect in the other cases illustrated.

The ¼ Mev energy is large compared to level spacings of the order of 1 ev. Consequently the structure of Fig. 1 can have nothing directly to do with the energy level pattern of the compound nucleus. On the other hand, ¼ Mev is of the right order to correspond to the spacing between energy levels of a single neutron in the average field of force of a deformed nucleus. Moreover, observation and theory of the scattering of neutrons by a nucleus show that there exist resonances in the neutron scattering. However, these neutron resonances are too broad to be easily compatible with the observed narrow widths. It is more reasonable, as Aage Bohr points out, to understand the rises in σ_f as due to the availability of a new fission channel in the transition state nucleus, and to understand the drops as due to the availability of a new channel for inelastic neutron scattering.

Effect No. 3

There should be no correlation between the direction of the fission fragments and the direction of the neutron, proton or gamma ray that initiates the fission, according to the liquid drop formulation of the compound nucleus model.[3] In contrast, the observations show a substantial directional correlation; and this correlation changes in a striking way with energy.[11] This effect has been discussed in considerable detail by A. Bohr.

Effect No. 4

The barrier against fission can be estimated for a number of nuclei from photofission thresholds, thresholds for neutron induced fission, or—where thermal neutron energy is already above the threshold—from partial level widths with respect to fission, as under effect No. 1 above. The results collected in Table 4 show (*a*) a good agreement of values for fission barrier from neutron threshold and from photofission threshold for the compound nucleus U^{236}, the only case where such a quantitative check appears to be available; (*b*) a qualitative check between photofission threshold and slow neutron fissionability in the other two cases where a test is possible, viz., the compound nuclei U^{233} and Pu^{239}; (*c*) an agreement between observation and liquid drop model as to general order of magnitude of fission barriers ($x = Z^2/45A$ predicted from liquid drop parameters of semi-empirical mass formula; $x = Z^2/47.61A$ to fit observed barrier height of U^{236}); (*d*) lack of agreement as to general trend with Z over the observed range, $Z = 90$ to $Z = 96$; and (*e*) fluctuations from nucleus to neighboring nucleus in barrier heights, of the order of ½ Mev to 1 Mev, as seen most clearly by comparing Th^{232} with Th^{233}, and comparing U^{233}, U^{235}, U^{238} and U^{239} with each other.

It is not surprising that the liquid drop predictions fail to give in detail the correct trend of E_f with Z and A. The calculations refer to a spherical nucleus, whereas the actual nuclei are strongly deformed, as evidenced by the pattern of low-lying rotational levels where known.[19,26] The equilibrium deformations are estimated to correspond to a fractional increase of the symmetry axis of the nucleus by an amount of the order of 25 per cent of the value for a sphere. This effect can be considered as evidence for the unbalanced pressure against the nuclear wall due to nucleons in unfilled shells. This pressure will be active, not only at equilibrium, but throughout the course of a deformation. It will produce a general lowering of fission barriers by a substantial fraction of the barrier height itself. This lowering has of course been completely overlooked in the liquid drop values listed in Table 4. It is reasonable to look to this lowering—and its trend with Z and A—superposed on the liquid drop effects—to account for broad general variation of barrier heights among the heavy nuclei. As more extensive information on nuclear quadrupole moments becomes available, it may become possible to analyze fission barrier expectations semi-quantitatively.

The pressure on the nuclear wall, coming from individual nucleons, will be expected to vary from nucleus to nucleus in an irregular way with the process of shell filling. Consequently one will expect fluctuations from nucleus to nucleus in the height of fission barriers, as observed. In addition, one will expect

Table 4. Fission Thresholds from Neutron Irradiation and Photofission Experiments Confronted with Liquid Drop Predictions*

Neutron-induced fission		*Compound nucleus*		*Fission barrier, E_f*		
Target	*threshold, E_n*	*Symbol*	*B(Mev)*	*Observed (photofission or $E_n + B$)*	*Calculated (droplet) (f = 0.0111)*	
${}_{90}\mathrm{Th}^{227}$	SNF	Th^{228}	7.1	$<\sim 7.1$	6.1	5.4
Th^{228}	not SNF	Th^{229}	5.4	$>\sim 5.4$	6.4	5.4
Th^{229}	SNF	Th^{230}	6.7	$<\sim 6.7$	6.7	5.4
Th^{230}	not SNF	Th^{231}	5.1	$>\sim 5.1$	7.0	5.4
Th^{231}		Th^{232}	6.3	PF 5.4 ± 0.22	7.3	5.5
Th^{232}	1.05	Th^{233}	5.1	6.2	7.6	5.5
Th^{234}	not SNF	Th^{235}	4.6	$>\sim 4.6$	8.3	5.5
${}_{91}\mathrm{Pa}^{230}$	SNF	Pa^{231}	6.8	$<\sim 6.8$	5.7	5.5
Pa^{231}	0.45	Pa^{232}	5.5	6.0	6.0	5.5
Pa^{232}	SNF	Pa^{233}	6.7	$<\sim 6.7$	6.2	5.5
Pa^{233}	not SNF	Pa^{234}	5.2	$>\sim 5.2$	6.4	5.5
${}_{92}\mathrm{U}^{232}$	SNF	U^{233}	5.9	PF 5.18 ± 027.	5.0	5.5
U^{233}	SNF	U^{234}	6.7	$<\sim 6.7$	5.3	5.5
U^{234}	0.28	U^{235}	5.3	$\left\{\begin{matrix} 5.6 \\ \text{PF } 5.31 \pm 0.27 \end{matrix}\right\}$	5.5	5.5
U^{235}	0 to ~1 Mev	U^{236}	6.4	~6 ?	5.8	5.5
U^{236}		U^{237}	5.4		6.0	5.5
U^{237}		U^{238}	6.0	PF 5.08 ± 0.15	6.3	5.6
U^{238}	0.92	U^{239}	4.8	5.7	6.5	5.6
U^{239}		U^{240}	5.9		6.8	5.6
${}_{93}\mathrm{Np}^{234}$	SNF	Np^{235}	7.0	$<\sim 7.0$	4.4	5.5
Np^{237}	0.25	Np^{238}	5.4	5.7	5.1	5.6
Np^{238}	SNF	Np^{239}	6.2	$<\sim 6.2$	5.3	5.6
Np^{239}	not SNF	Np^{240}	4.9	$>\sim 4.9$	5.6	5.6
${}_{94}\mathrm{Pu}^{238}$	SNF	Pu^{239}	5.7	PF 5.31 ± 0.25	4.3	5.6
Pu^{239}	0 to 1 Mev	Pu^{240}	6.4	5.4 to 6.9	4.5	5.6
Pu^{240}		Pu^{241}	5.5		4.7	5.6
Pu^{241}	SNF	Pu^{242}	6.1	$<\sim 6.1$	4.9	5.6
${}_{95}\mathrm{Am}^{241}$	not SNF	Am^{242}	5.5	$>\sim 5.5$	3.9	5.6
Am^{242}	SNF	Am^{243}	6.3	$<\sim 6.3$	4.1	5.6
Am^{243}		Am^{244}	5.1		4.3	5.7
${}_{96}\mathrm{Cm}^{242}$		Cm^{243}	5.7		3.2	5.6

* Neutron kinetic energy, E_n, required for appreciable fission cross sections ($\sim 0.03 \times 10^{-24}$ cm^2) estimated in the five listed cases from the smooth curves of cross section as a function of energy given in reference 5. The two negative values of ~0 −1 Mev originate in the text. The indications *SNF*— slow neutron fissionable—and its opposite in the second column come from G. T. Seaborg[22] and are defined by him to mean respectively σ_f greater than or less than about 10^{-24} cm^2. The estimates for neutron binding energies come from Glass, Thompson and Seaborg.[23] The photofission thresholds are designated by *PF* in the table and are due to Koch, McElhinney and Gasteiger.[24] The calculations of thresholds on the liquid drop model use the formula $E_f = 13$ Mev $A^{2/3} f(Z^2/47.61A)$, with the first constant taken from the semi-empirical mass formula, the second constant adjusted to give $E_f = 5.5$ Mev for U^{235} (for which one has two independent determinations of E_f), and $f(x)$ a smooth curve with the limiting behavior[3] $0.260 - 0.215x$ at small x, $(98/135)(1/x)^3 - (11368/34425)(1-x)^4$ near $x = 1$, passing through the points [25] $(x,f) = (0.9, 0.0007)$; $(0.81, 0.0050)$; $(0.77, 0.009_3)$; $(0.74, 0.0136)$; and $(0.65, 0.0400)$. The last column shows a better fit to the data with the constant value $f = 0.0111$. Additional evidence about fission barriers from spontaneous fission rates has not been considered.

systematically higher barriers for odd-A nuclei than for neighboring even-even nuclei, for a reason that is most simply visualized in the framework of the extreme independent particle picture. At one deformation of the nucleus those individual particle states that lie lowest will differ from those states that lie lowest at another deformation—will differ in respect to the quantum number, Ω, of rotation about the nuclear symmetry axis. This difference will be irrelevant for an even-even nucleus. One has only to fill the lowest available states, pairing off nucleons with quantum numbers Ω and $-\Omega$, in order always to get spin 0. However, when the number of neutrons, for example, is odd, then the unpaired neutron—if placed in the lowest unfilled state—will have for one deformation an Ω value different from what it has at another deformation. But the Ω value of the nucleus as a whole is a reasonably good constant of motion, and will not be expected to change during a deformation. Consequently an odd-A nucleus that is deformed, starting with its equilibrium deformation, will be promoted to a state of higher energy, as illustrated for example by the curve for $\Omega = 3/2$, even parity, in Fig. 2. On this account fission barriers will be expected to be higher for odd-A nuclei than for neighboring even-even nuclei by an amount estimated[27] to be roughly of the order of 0.7 Mev. This increase appears adequate[27] to account for the fact that half-lives with

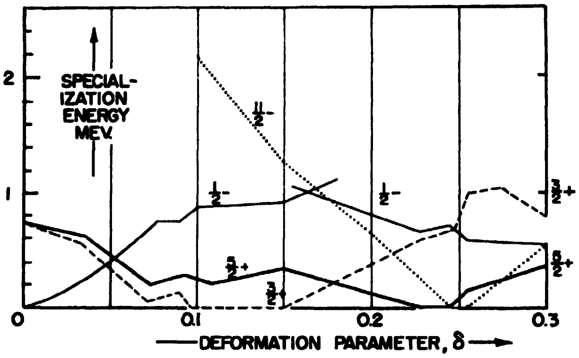

Figure 2. Approximate increment to be added to the energy of a nucleus with a given deformation in the lowest nucleonic state to achieve a state of *specified* spin and parity. This "specialization energy" gives an estimate of the increase of fission barrier for an odd-A nucleus compared to neighboring even-even nuclei. The curves for specialization energy are built up by addition from the single particle energies calculated on the idealized independent particle model[27] and therefore have illustrative value only

respect to spontaneous fission are longer[28] for odd-A nuclei than for neighboring even-even nuclei by a factor of the order of $10^{3\pm1}$.

Spontaneous fission rates and rates of other processes that limit nuclear stability have recently been projected[27] to the region of very large masses, with the results shown in Fig. 3. From this diagram one sees that fission and neutron emission dominate the stability analysis of very heavy nuclei. In so far as one can extrapolate the stability criteria for very heavy nuclei, one is led to expect the existence of nuclei twice as heavy as known nuclear species, that can be created by massive neutron irradiation, and that will live long enough to be studied in the laboratory.

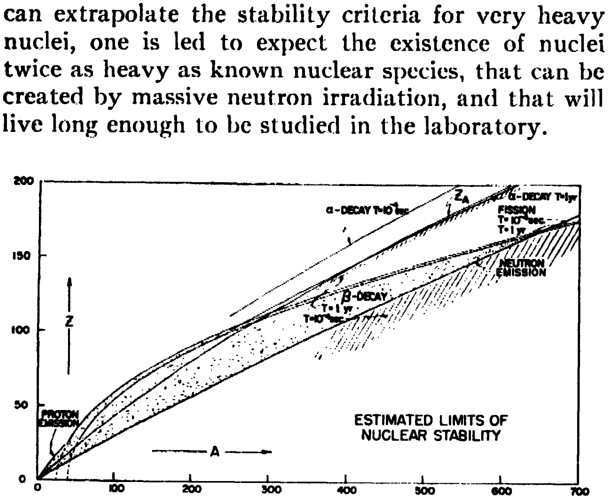

Figure 3. Estimated limits of nuclear stability. Diagram based on reference 27. In the dotted region a substantial fraction of the nuclei have estimated half-lives greater than 10^{-4} sec. One will expect a little way outside the dotted region occasional nuclei of high spin or of otherwise exceptional properties which will also live at least as long as 10^{-4} sec. The limits to the stability of superheavy nuclei are set primarily by neutron escape (too high a ratio of neutrons to protons) and by spontaneous fission (too high a ratio of Z^2 to A). Calculations of energies were based on the semiempirical mass formula and the rate of spontaneous fission was determined by a simple extrapolation procedure.[27] The extrapolations may be appreciably in error. However, it seems reasonable to look for nuclei with a well defined existence with masses perhaps two or more times heavier than the heaviest nucleus now known, 100^{256}. Massive neutron irradiation of existing heavy nuclear species is an appropriate means to build such superheavy nuclei

REFERENCES

1. Bohr, N., *Neutron Capture and Nuclear Constitution*, Nature 137: 344 (1936).
2. Bohr, N. and Kalckar, F., *On the Transmutation of Atomic Nuclei by Impact of Material Particles*, Kgl. Danske Videnskab. Selskab, Mat-fys. Medd. 14: No. 10 (1937).
3. Bohr, N. and Wheeler, J. A., *The Mechanism of Nuclear Fission*, Phys. Rev. 56: 426 (1939).
4. See other papers reported at this conference.
5. Cross-section compilation of the U. S. Atomic Energy Commission Neutron Cross-Section Advisory Group, Unclassified Document AECU-2040 (1952).
6. Winhold, E. J., Demos, P. T. and Halpern, I., *The Angular Distribution of Fission Fragments in the Photofission of Thorium*, Phys. Rev. 87: 1139 (1952).
7. Dickinson, W. L. and Brolley, J. E., *Angular Distribution of Fragments from Neutron-Induced Fission*, Phys. Rev. 90: 388 (1953).
8. Cohen, B. L., Jones, W. H., McCormick, G. H. and Ferrell, B. L., *Angular Distributions of Fission Fragments from 22 Mev Proton-Induced Thorium Fission*, Phys. Rev. 94: 625 (1954).
9. Flerov and Petrjak, *Spontaneous Fission of Uranium*, Phys. Rev. 58: 89 (1940).
10. Hughes, D. J. and Levin, J., Phys. Rev., to be published.
11. This development is summarized in Mayer, M. G. and Jensen, J. H. D., *Elementary Theory of Nuclear Shell Structure*, John Wiley, New York, 1955 as well as in Sachs, R. G., *Nuclear Theory*, Addison-Wesley Publishing Co., Cambridge 42, Mass. (1953).
12. See Feshbach, H., Porter, C. E. and Weisskopf, V. F., *Model for Nuclear Reactions with Neutrons*, Phys. Rev. 96: 448 (1954).
13. Seen in observations of Cohen, B. L., *The Statistical Theory of Nuclear Reactions*, Phys. Rev. 92: 1245 (1953); Gugelot, P. C., *Level Densities of Nuclei from the Inelastic Scattering of 18 Mev Protons;* Eisberg, R. M., *Energy Spectra of Neutrons Evaporated from a Compound Nucleus*, Phys. Rev. 94: 739 (1954); Schranck, G., Gugelot, P. C. and Dayton, I. E., *Direct Interaction in $Fe^{56}(p,P')Fe^{56*}$*, Phys. Rev. 96: 1156 (1954).
14. Brueckner, K. A. and Watson, K. M., *Nuclear Forces in Pseudoscalar Meson Theory*, Phys. Rev. 92: 1023 (1953); Brueckner, K. A., *Nuclear Saturation and Two-Body Forces. II Tensor Forces*, Phys. Rev. 96: 508 (1954); *III Details of the Structure of the Nucleus*, Phys. Rev. 97: 1353 (1955); Brueckner, K. A. and Levinson, C. A., *Approximate Reduction of the Many Body Problem for Strongly Interacting Particles to a Problem of Self Consistent Fields*, Phys. Rev. 97: 1344 (1955).
15. Wheeler, J. A., *Proceedings of the 1954 Glasgow Conference on Nuclear and Meson Physics*, Ed. by Bellamy, E. H. and Moorhouse, R. G., Pergamon Press, London and New York, 1955, p. 42; see also Johnson, M. H. and Teller, E., *Classical Field Theory of Nuclear Forces*, Phys. Rev. 98: 783 (1955).
16. Rainwater, J., *Nuclear Energy Level Argument for a Spheroidal Nuclear Model*, Phys. Rev. 79: 432 (1950); see also Bohr, A., *On the Quantization of Angular Momentum in Heavy Nuclei*, Phys. Rev. 81: 134 (1951).
17. Bohr, A., *On the Quantization of Angular Momentum in Heavy Nuclei*, Phys. Rev. 81: 134 (1951); *The Coupling of Nuclear Surface Oscillations to the Motion of Individual Nucleons*, Kgl. Danske Videnskab. Sels. Mat.-fys. Medd. 26: No. 14 (1952); *Rotational States of Atomic Nuclei*, Thesis, Copenhagen (1954).
18. See for example Temmer, G. M. and Heydenburg, N. P., *Coulomb Excitation Process in the Lighter Odd-Mass Nuclei*, Phys. Rev. 96: 426 (1954); *Coulomb Excitation of Nuclear States in the Light of the Collective Model* (to be published).

19. Ford, K. W., *The First Excited States of Even-Even Nuclei*, Phys. Rev. 90: 29 (1953); Wilets, L., Hill, D. L. and Ford, K. W., *Isotope Shift Anomalies and Nuclear Structure*, Phys. Rev. 91: 1488 (1953).

20. Hill, D. L. and Wheeler, J. A., *Nuclear Constitution and the Interpretation of Fission Phenomena*, Phys. Rev. 89: 1102 (1953); Bohr, A. and Mottelson, B. R., *Collective and Individual Particle Aspects of Nuclear Structure*, Kgl. Danske Viden. Sels. Mat.-fys. Medd. 27: No. 16 (1953).

21. Brolley, John, observations to be published, for the communication of which appreciation is here expressed.

22. Seaborg, G. T., *Activation Energy for Fission*, Phys. Rev. 88: 1429 (1952).

23. Glass, R. A., Thompson, S. G. and Seaborg, G. T., *Nuclear Thermodynamics of the Heaviest Elements*, J. Inorganic and Nuclear Chem. 1: 3 (1955).

24. Koch, H. W., McElhinney, J. and Gasteiger, E. L., *Experimental Photo-Fission Thresholds in* U^{235}, U^{238}, U^{233}, Pu^{239} *and* Th^{232}, Phys. Rev. 77: 329 (1950).

25. Frankel, S. and Metropolis, N., *Calculations in the Liquid Drop Model of Fission*, Phys. Rev. 72: 914 (1947); see also Businaro, V. L. and Gallone, S., *Saddle Shapes, Threshold Energies and Fission Asymmetry on the Liquid Drop Model*, Nuovo Cimento, to be published; also 1: 629 (1955).

26. Asaro, F. and Perlman, I., *Decay Properties of* Am^{243} *and Possible Rotational Bands in the Alpha Spectra of Odd-Even Nuclei*, Phys. Rev. 93: 1423 (1954).

27. Wheeler, J. A., *Nuclear Fission and Nuclear Stability*, chapter in *Niels Bohr and the Development of Physics*, Pergamon Press, London (1955).

28. Odd-even difference: Seaborg, G. T., *Some Comments on the Mechanism of Fission*, Phys. Rev. 85: 157 (1952); Whitehouse, W. J. and Galbraith, W., *Spontaneous Fission Rates*, Nature 169: 494 (1952). Implications for barrier height: Huizenga, J. R., *Spontaneous Fission Systematics*, Phys. Rev. 94: 158 (1954).

The Time Involved in the Fission Process

By Dragoslav Popović,* Yugoslavia

It was usually assumed that the time required for the fission process is short due to the high probability of fission when the excitation energy of the nucleus is higher than the fission threshold. Consequently the radiative capture probability in a fissionable nucleus should be low, since the time required for this process is relatively long.

The incomplete measurements of the time required for fission[1,2] did not give a definite experimental proof of the above assumption. On the other hand, Bohr and Wheeler[3] came to the conclusion, based partly on the measurements of Anderson *et al.*[4] which led to a $1/v$ dependence of the fission cross section of uranium-235 in the low energy region, that the fission width of U^{235} (Γ_f) is of the order of 100 ev, which led to the lifetime of the compound nucleus uranium-236 of $\tau_f \sim 10^{-17}$ sec.

Since the lifetime of heavy nuclei for the radiative capture should be longer than 10^{-14} sec ($\Gamma_\gamma < 0.1$ ev) the probability for the (n,γ) process should be 1,000 times smaller than that for fission in uranium-235.

The release of the thermal cross sections of uranium-235 ($\sigma_f \sim 550$ barns and $\sigma \sim 100$ barns)[5] contradicted the latter and led to the following conclusions:

(1) The lifetime of the compound nucleus uranium-236 is not too short.

(2) The fission width Γ_f is not extremely large so that the fission resonances are not smoothed off.

The measurements of the fission cross section of uranium-235 as function of energy[6] revealed pronounced resonances. The resonance at $E \sim 0.27$ ev shows the total absorption width and hence approximately the fission width of

$$\Gamma_f = 0.1 \pm 0.04 \text{ ev}$$

which leads to the lifetime of the compound nucleus uranium-236 for fission of

$$\tau_f = (7 \pm 3) \times 10^{-15} \text{ sec}$$

The level spacing found is of the order of 1 ev. Hence, the period of the wave function of the system or the time for which the distribution of energy among nucleons repeats is approximately

$$P = 4 \times 10^{-15} \text{ sec}$$

The above result means that the lifetime of the compound nucleus is of the same order of magnitude as the period of the system. Due to the high probability of fission the time required for it is short but has to remain within the limits of the period of the system.

REFERENCES

1. Feather, N., Nature, Lond. 143, 597 (1939).
2. Wilson, R., Phys. Rev. 72, 98 (1947).
3. Bohr, N. and Wheeler, J., Phys. Rev. 56, 462 (1939).
4. Anderson, H., Booth, E., Dunning, J., Fermi, E. and Glasoe, G., Phys. Rev. 55 (1939).
5. AEC Release (1951).
6. Popović, D., Journal of Nuclear Energy No. 1 and 2.

---

* Institute of Nuclear Sciences, "Boris Kidrič", Beograd, Yugoslavia.

Statistics of Photographic Fission Tracks and Range Estimate of Fragments

By J. S. Ausländer and T. Visky,* Romania

If a nucleus contained in a nuclear emulsion by impregnation, or otherwise, is fissioned by impact of a slow neutron,—e.g., in a reaction of the type $Li^6(n,\alpha)H^3$—the ranges of the fission tracks cannot be estimated directly, as, because of momentum conservation, the track must be a straight line, the origin of which is not distinguished from other points.

One of the indirect methods is that proposed by Chastel,[5] which we shall call henceforth the "length method." It is based on the fact that if only those tracks are selected which touch with one of their ends the glass-emulsion surface, the shortest total length which may appear is R_1, i.e., the shorter of the two fission fragment ranges, while the longest one is $R \equiv R_1 + R_2$, where R_2 is the longer of the two fission tracks. These sharp steps of the corresponding distribution function would appear, if there were no fluctuations of range. Actually the distribution is "broadened" by the fluctuations.

This method is cumbersome in manipulation, as it implies knowledge for each track of both its projections and the computation of its real length by aid of the shrinkage factor, which must be measured too.

We have proposed a variant of this method, which will be called henceforth the "projection method." It consists essentially in the substitution of the histograms of real length r by those of the horizontal projections ρ of the tracks.

The distribution function $F(\rho)$ of these projections has been calculated. The results were published in three papers.[1,2,3] A detailed account of the calculations leading to these results is in press.[4]

Firstly, the calculations were carried out under the simplifying assumption of absence of fluctuations, in order to obtain a general view of the different cases which may arise for different emulsion thicknesses H. The results for the case $H \geq R$ are published in reference 1; those for the cases $R \geq H \geq R_2$, $R_2 \geq H \geq R_1$ and $R_1 \geq H > 0$ and their subcases and variants are published in reference 2.

In the more important case, when the fluctuations of range are not neglected,[3] there appear a lot of computational difficulties (numerical integrations). For this reason in reference 3 it is always supposed that $H > R$.

The other assumptions are as follows:

(*a*) The fissionable atoms are distributed uniformly in the emulsion in all its depth.

(*b*) The incident neutron flux is distributed uniformly over the whole surface of the emulsion.

(*c*) The neutron intensity is constant over all the emulsion thickness, i.e., the neutron absorption is negligibly small.

(*d*) The fission fragments are emitted isotropically in all directions.

(*e*) The probability $\psi(L_j)\,dL_j$ of appearance of a real length L_j of the j branch of the track ($j = 1$ or 2) is assumed to be of the Gaussian type

$$\psi(L_j)\,dL_j = \frac{1}{a_j\sqrt{\pi}} \exp\left[-\left(\frac{L_j - R_j}{a_j}\right)^2\right] dL_j \qquad (1)$$

where $R_j = \langle L_j \rangle$ is the mean range of the j fragment.

We must also mention that the distribution function $F(r)$ of the real lengths was calculated too,[3] since in his paper Chastel[5] gives no explicit expression of this function. In the interval $0 \leq r \leq R_1$, we get, with the assumptions specified below, the following expression

$$F(r) = \frac{1}{8H}\left[2 - \operatorname{erf}\frac{R_1 - r}{a_1} - \operatorname{erf}\frac{R_2 - r}{a_2}\right] \qquad (2)$$

where the error function is defined, as usually, by

$$\operatorname{erf} t \equiv \frac{2}{\sqrt{\pi}} \int_0^t \exp(-Z^2)\, d_t \qquad (3)$$

In all other intervals of r the function $F(r)$ is expressed, too, by additive combinations of error functions of the type shown in Equation 2.

From Equation 2 there follows a limitation for the applicability of the length method. If there exists a large enough r interval, beginning with $r = 0$, in which practically $\operatorname{erf}[(R_2 - r)/a_2] =$ constant, then, but only then, $[dF(r)/dr]_{r=R_1} \neq 0$, while

$$[d^2F(r)/dr^2]_{r=R_1} = 0$$

i.e., $F(r)$ has an inflection point for $r = R_1$, the determination of which yields the value of R_1. The r interval must be large enough to enable one to choose a Gauss curve which fits the experimental histogram; such an interval will exist, if the ratio R_1/R_2 has a value far enough from unity. Otherwise the length method can yield no estimate of R_1 or R_2.

---

* Institute of Physics, Academy of the Romanian People's Republic, Bucharest.

In the calculation of the fluctuated distribution function $F(\rho)$ of the horizontal projections ρ, two more simplifying assumptions have been introduced which are not in agreement with reality.[4] It has been checked by test computations that their influence is negligible.[4]

Finally, the following expression of $F(\rho)$ is obtained

$$F(\rho) = \sum \int_{r_{min}}^{r_{max}} \Phi_i(r,\rho)\, dr \qquad (4)$$

where the summation extends over all functions $\Phi_i\,(r,\rho)$, defined below, which exist, i.e., are not naught, in the corresponding interval, and R_{min} and r_{max} are the extreme r values compatible with the given value of ρ.

In the following definition of $\Phi_i(r,\rho)$ the index $i (i = 1$ or $2)$ denotes the fragment directed outward to the glass and index $k(k = 2$ or $1)$ the fragment directed inwards toward the emulsion. Then we have in the intervals specified in each line:

$$0 \leq r \leq R_i \cdots \Phi_i(r,\rho) = \frac{1}{4H} \cdot \frac{\rho}{r^2}\left(1 + \operatorname{erf}\frac{r - R_k}{a_k}\right) \qquad (5)$$

$$R_i \leq r < \infty \cdots \Phi_i(r,\rho) = \frac{1}{4H} \cdot \frac{\rho}{r^2}\left|\operatorname{erf}\frac{r - R}{a_k} - \operatorname{erf}\frac{r - R_k}{a_k}\right| \qquad (6)$$

The integrals in Equation 4 have to be computed numerically or graphically; the limits of integration, r_{min} and r_{max}, depend not only on the ρ interval considered, but also on whether $\rho < r_{min}$ or $\rho > r_{min}$. Table 1 gives r_{min} and r_{max} for all pairs of r and ρ intervals; the last column contains a symbol, the meaning of which is defined, e.g., for the pair of intervals $0 \leq r \leq R_1$ and $0 \leq \rho \leq R_1$ by

$$(1a) \equiv \int_{\rho}^{R_1} \Phi_1(r,\rho)\, dr \qquad (7)$$

where $\Phi_1(r,\rho)$ is given, according to Equation 5, by

$$\Phi_1(r,\rho) = \frac{1}{4H} \cdot \frac{\rho}{r^2}\left(1 - \operatorname{erf}\frac{r - R_2}{a_2}\right) \qquad (8)$$

By aid of the symbols from Table 1, Equation 4 may be written explicitly for the different ρ intervals as follows:

$$0 \leq \rho \leq R_1 \cdots F(\rho) = (1a) + (1b_1) + (1c_1) + (1d_1) + (2a) + (2a_1) + (2b_1) + (2c_1) \qquad (9)$$

$$R_1 \leq \rho \leq R_2 \cdots F(\rho) = (1b_2) + (1c_1) + (1d_1) + (2a_2) + (2b_1) + (2c_1) \qquad (10)$$

$$R_2 \leq \rho \leq R \cdots F(\rho) = (1c_2) + (1d_1) + (2b_2) + (2c_1) \qquad (11)$$

$$R \leq \rho < \infty \cdots F(\rho) = (1d_2) + (2c_2) \qquad (12)$$

With these formulas we have computed $F(r)$ (Fig. 1) and $F(\rho)$ (Figs. 2 and 3) for the following two examples: $R_1/R_2 = 1/3$ and $R_1/R_2 = 9/11$. The encircled points in Figs. 2 and 3 show the peaks which would appear in $F(\rho)$, if it were calculated without fluctuations,[1] as a broken line. All these plots were computed under the most unfavourable presumption $a_j = 0 \cdot 1R_j$.

Figures 2 and 3 show that in both cases the maximum of the $F(\rho)$ plot yields an acceptable estimate of R_1. The errors implied by the projection method are illustrated by the following facts. The displacement of the maximum with respect to R_1 is ~8% for $R_1/R_2 = 1/3$ (Fig. 2) and ~7% for $R_1/R_2 = 9/11$

Table 1

i	Interval $a \leq r \leq b$		Interval $\alpha \leq \rho \leq \beta$		r_{min}	r_{max}	Symbol of line
	a	b	α	β			
1	0	R_1	0	R_1	ρ	R_1	$(1a)$
	R_1	R_2	0	R_1	R_1	R_2	$(1b_1)$
			R_1	R_2	ρ	R_2	$(1b_2)$
	R_2	R	0	R_2	R_2	R	$(1c_1)$
			R_2	R	ρ	R	$(1c_2)$
	R	∞	0	R	R	$\sqrt{H^2 + \rho^2}$	$(1d_1)$
			R	∞	ρ	$\sqrt{H^2 + \rho^2}$	$(1d_2)$
2	0	R_1	0	R_1	ρ	R_1	$(2a)$
	R_1	R_2	0	R_1	R_1	R_2	$(2a_1)$
			R_1	R_2	ρ	R_2	$(2a_2)$
	R_2	R	0	R_2	R_2	R	$(2b_1)$
			R_2	R	ρ	R	$(2b_2)$
	R	∞	0	R	R	$\sqrt{H^2 + \rho^2}$	$(2c_1)$
			R	∞	ρ	$\sqrt{H^2 + \rho^2}$	$(2c_2)$

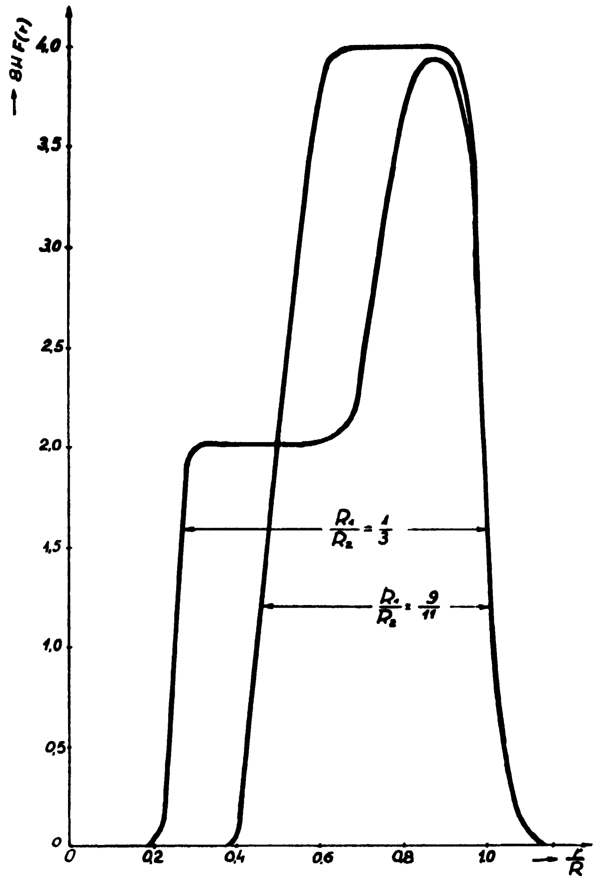

Figure 1

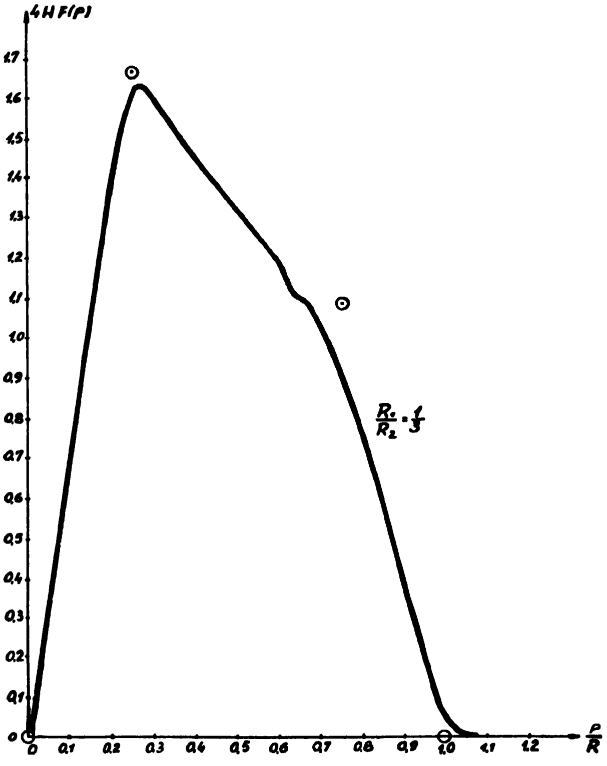

Figure 2

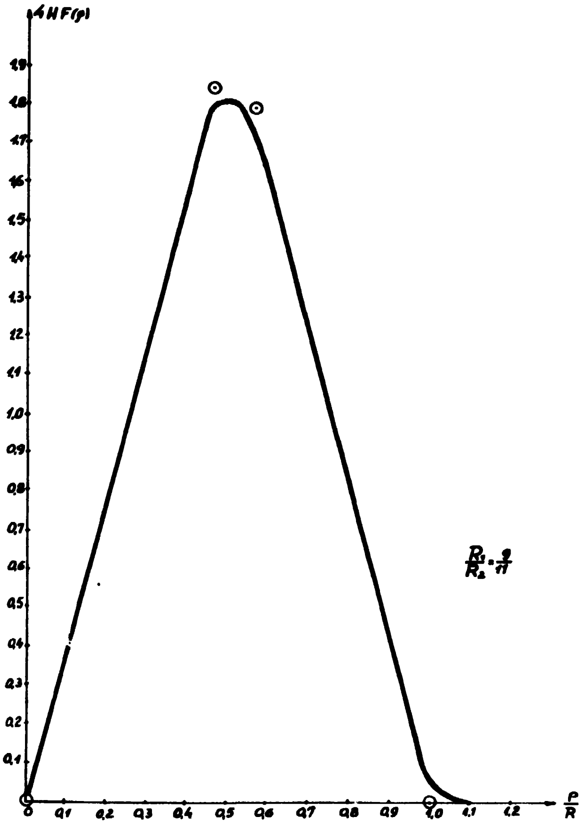

Figure 3

(Fig. 3). As can be seen from Fig. 1, in the second case the length method[6] is unable to yield any value of R_1 at all. In a case similar to $R_1/R_2 = \frac{1}{3}$, quoted by Chastel[6] as his only example, the experimental error is ±13.5%.

Even taking into account that the above displacements combine with "broadening" by experimental fluctuations in the histograms, we may infer that the experimental errors of both methods are of the same order.

Briefly, our conclusions are as follows:

(*a*) The length method is limited to not too small values of the ratio R_1/R_2. In this respect the projection method applies to a larger interval of R_1/R_2.

(*b*) The experimental errors are of the same order for both methods.

(*c*) The projection method has a series of advantages over the length method. It does not require the knowledge of the vertical track projections, nor of the shrinkage factor, and avoids the computations of the real length of each track. Furthermore, the situation is represented in a direct, visual manner; there is no need to carry out such operations as the choice of a Gauss curve which fits best to the experimental histogram and the determination of the inflection point co-ordinates. These operations, avoided by the projection method, involve by necessity a certain degree of arbitrariness.

It should not be left unmentioned that both the projection method and length method must compete with a number of other methods which might be more efficient or of wider application.

REFERENCES

1. Ausländer, J. and Visky, T., Com. Acad. R. P. R. *2*, 217 (1952).
2. Ausländer, J. and Visky, T., Rev. Univ. C. I. Parhon şi a Politehnicii Bucureşti, seria şt. naturii, *1*, 99 (1952).
3. Ausländer, J., Com. Acad. R. P. R., in press.
4. Ausländer, J. and Visky, T., Studii şi Cercetări de Fizică, in press.
5. Chastel, R., C. R. Acad. Sci. Paris, *228*, 1725 (1949).

Studies on the Nuclear Photoeffect

By M. D. de Souza Santos, J. Goldemberg, R. R. Pieroni, E. Silva, Ottavia A. Borello and Suzanna S. Villaça,* and J. Leite Lopes,† Brazil

ABSTRACT

Photonuclear reactions induced in several elements by the X-ray beam of the University of São Paulo 24 Mev Betatron were accurately measured by means of the residual activity technique.

Thresholds and cross-sections for different photonuclear processes were measured with a fairly high accuracy and are discussed in this paper.

Some influence of shell structure on the photoprocesses is presented.

INTRODUCTION

In the experiments described in this paper, the source of X-rays of a variable energy was a 24 Mev betatron of Kerst's design.[1,2,3] The magnet was made by Allis-Chalmers Mfg. Co., and the machine and auxiliary circuits were installed by the laboratory staff of the University of São Paulo.

Although the electronic circuitry is conventional in its main aspects and follows quite closely the University of Illinois' design,[2,3] some circuits, however, were developed at our laboratory in order to provide the machine with a long-term stability of the electron beam energy.

Our machine has been in operation since 1951; the experience accumulated during the first years of operation has shown that most of the difficulties connected with the energy stability of the beam were due to the energy control system which was similar to the precision device used at the University of Saskatchewan.[4]

Fundamentally, the energy control in an induction accelerator is obtained when the magnetic field, which determines the momentum of the electrons at the equilibrium orbit, reaches a pre-determined value. It is not easy, however, to measure directly this magnetic field so that use is made of a method developed at the University of Illinois.[2,3]

Although the magnetic induction B, which determines the electron momentum is not easily obtained, the applied emf across the magnet coils is immediately available. This emf determines the rate of change $\dot{B}$ of the guide field; its time integral represents, therefore, a measure of the magnetic induction B and, hence, of the momentum of the electrons at the equilibrium orbit. The voltage developed across the armatures of a condenser, charged by this emf through a large resistance, is a direct measure of the required instantaneous value of B and is available as a voltage of the same frequency of, and practically in phase with, B, provided that R/C is properly chosen.

In our energy control circuits this integrated emf is compared with a pre-determined adjustable emf in a double triode amplitude comparison circuit whose characteristics can be checked at any time. Whenever the variable voltage just equals the reference emf, a signal is delivered to the grid of the expander circuit and the beam is expanded on to the target. The circuits used for this purpose are illustrated in Figs. 1, 2, 3, 4 and 5.

Most of the work described in this paper was carried out with a pumped donut provided with a thin gold radiator which was attached to the injector structure and located at 1.2 cm from the equilibrium orbit. Previous experiments[5] have shown that no multiple passages did occur under the experimental conditions used.

The machine was excited by means of an alternator driven at a predetermined frequency by means of an electronically controlled magnetic clutch. This device allowed the machine to be driven at its resonant frequency under constant magnet excitation during the experiments: by this procedure, no frequency effects[6] on the energy scale were observed and the amplitude effect[6] was, under the most unfavorable conditions, smaller than 16.4 kev per a one volt change in magnet amplitude.

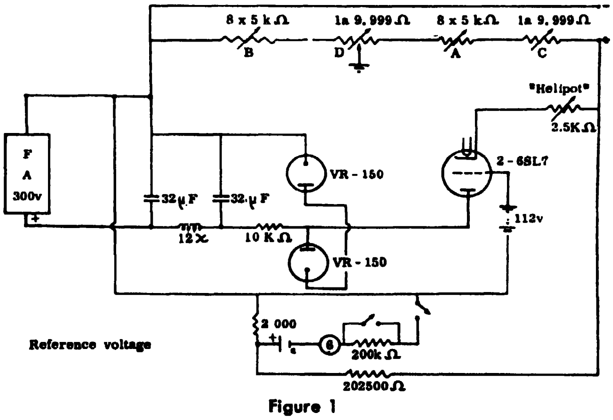

Figure 1

---

* Laboratories de Fisica Nuclear, Universidade de São Paulo, Brazil.

† Faculdade Nacional de Filosofia, Universidade do Brazil and Centro Brasileiro de Pesquisas Fisicas, Rio de Janeiro, D.F., Brazil.

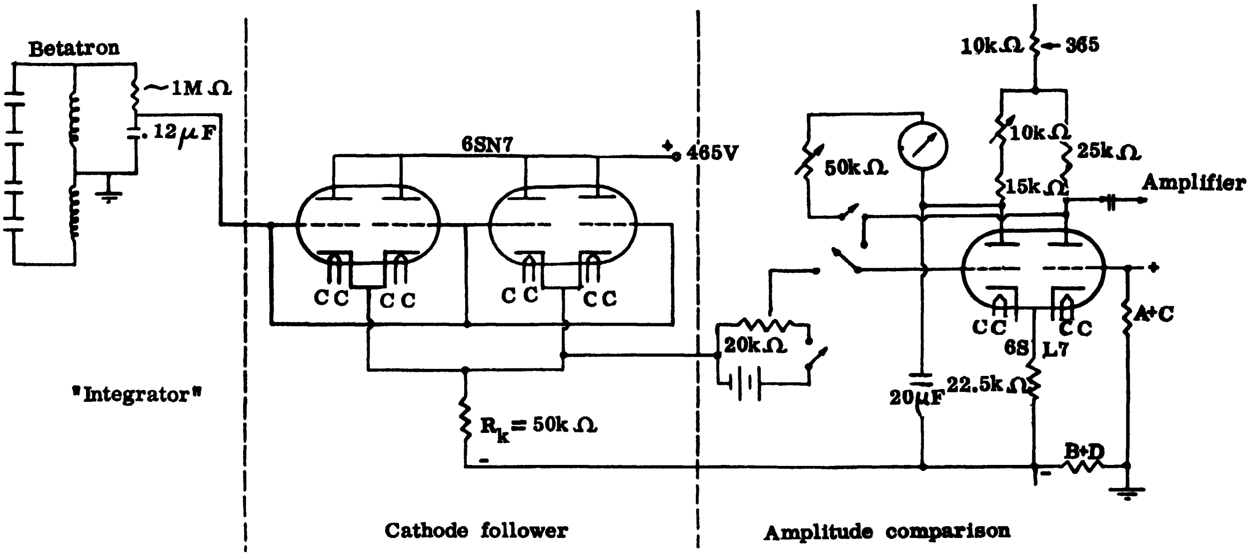

Figure 2

During a six-month period, in which most of the experiments were made, it was found that the most common cause of drift in the energy control was due to a temperature effect in the integrator resistance stack. This is a systematic error which was eliminated by immersing the *RC* network in a temperature controlled oil bath. A smaller temperature systematic effect could still be observed and was duly corrected by keeping the Weston standard cell, used to check the reference voltage of the energy control circuit under constant temperature. With these precautions, it was found that a very small effect (smaller than $\frac{1}{5000}$) could be attributed to a 40°C change in the magnet temperature. This systematic error, when required, can be corrected by measuring the magnet temperature at the different irradiations.

By using the procedure outlined above, it was possible to keep the energy stability of the machine within 3 kev (for an electron beam energy of 17.5 mev) in short periods, whereas the long term stability is of the order of 10 kev. A typical stability curve, for which the above discussed temperature effects were not corrected, is reproduced in Fig. 6.

The measurement of the machine energy stability

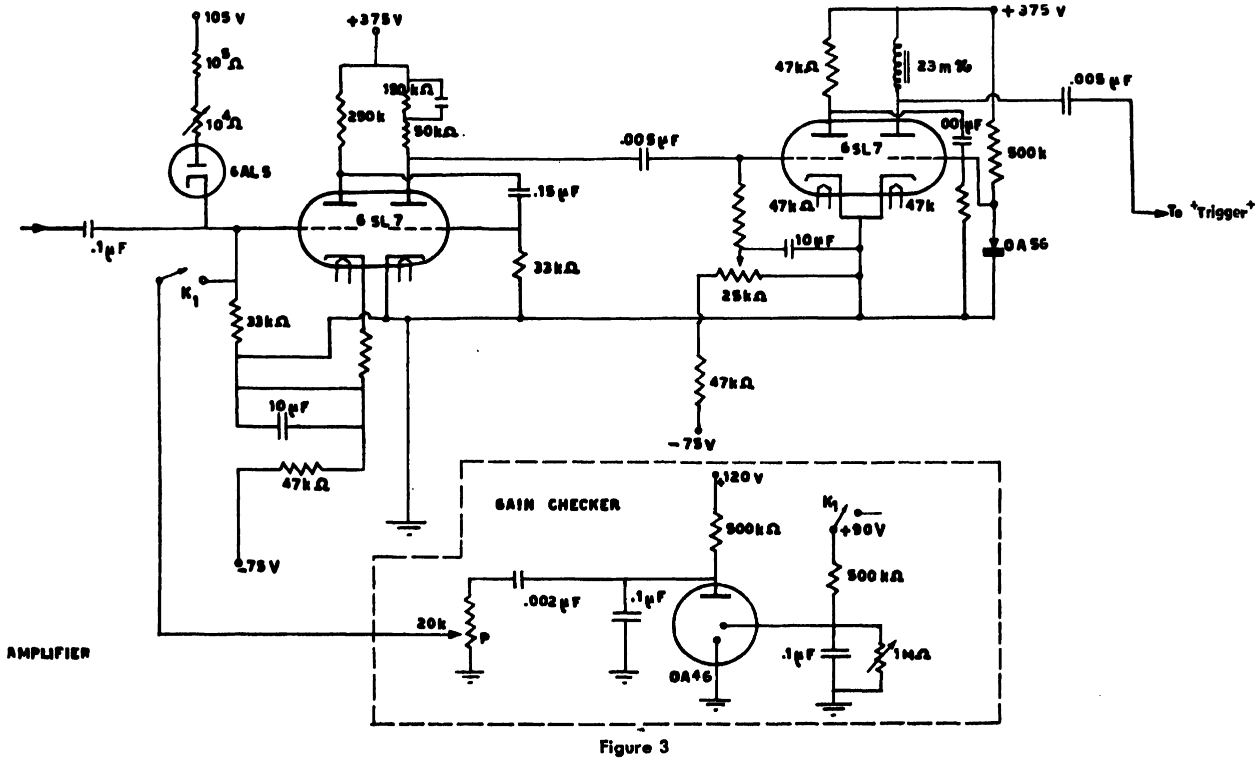

Figure 3

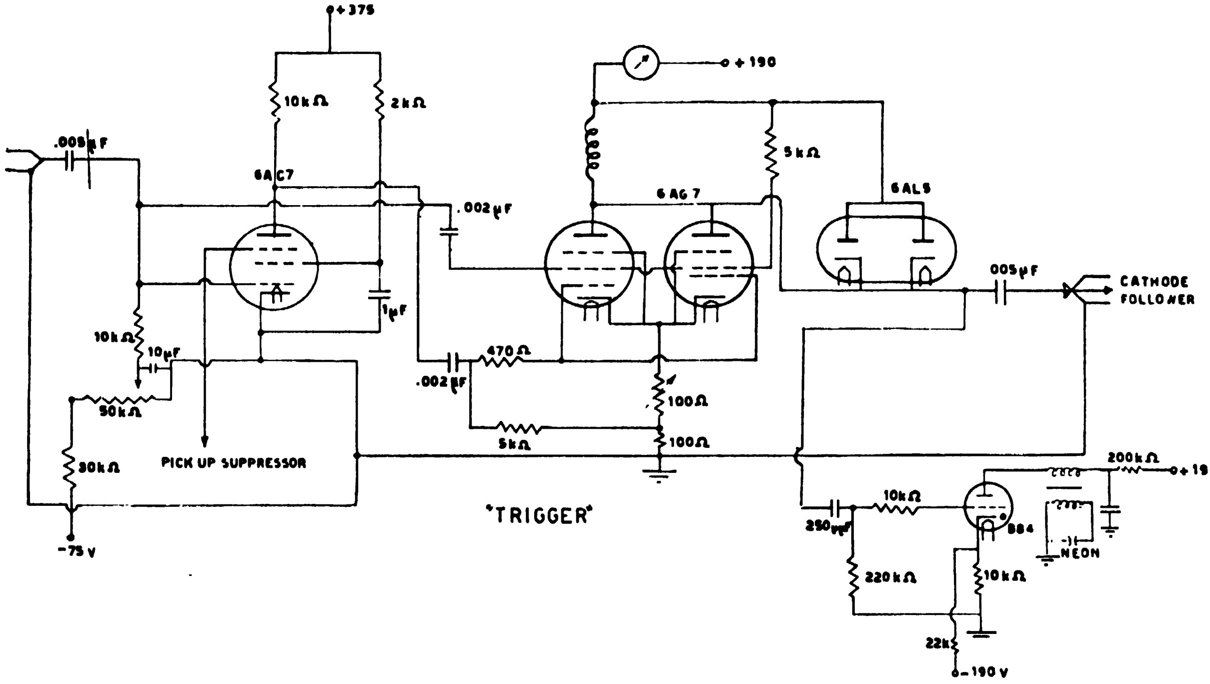

Figure 4

was made by means of repeated irradiations, at different times, of a boric acid pressed cylinder in a region of the activation curve of oxygen[15] for which the slope was 1.5% per a 10 kev change in energy.

THRESHOLD DETERMINATIONS

The excitation functions of photoinduced nuclear reactions show that as the peak energy of the bremsstrahlung spectrum is increased, the cross-section for photodisintegration rises slowly from zero at the threshold energy E_t and reaches a maximum in the region of the so-called giant resonance. Near the threshold, the behaviour of the excitation function depends on the disintegration process investigated, on the nature of the process responsible for the absorption of the bombarding photon and, in the particular case in which a single neutron is emitted, on the angular momentum of the outgoing particle.

At low energies (of the order of 10 Mev), magnetic dipole and electric quadrupole absorption are important and start to drop at about 20 Mev. At high energies, however, the absorption is strongly increased by the onset of dipole absorption.[7]

The examination of the behaviour of the excitation function near the threshold has been discussed by several investigators;[8,9,10] experimental data available show that although there are several instances in which the excitation function rises slowly due mainly to magnetic dipole and electric quadrupole absorption, there are several others for which a steep rise is observed and the cross-section analysis shows only the contribution due to the giant resonance (dipole absorption). A rapid rise in activity is thus expected whenever the energy of the incoming photons exceed the threshold energy.

In the instances, however, where the threshold for the process under consideration is located in the region of magnetic dipole and electric quadrupole absorption, a slow increase of activity with the excess energy of the bombarding photon over the threshold is to be expected.

The considerations sketched above show that an accurate experimental determination of the thresholds for photonuclear reactions can only be obtained through the extrapolation of an experimental curve whose shape cannot be predicted accurately (due, mainly, to the lack of precise knowledge of the shape of the tail of the bremsstrahlung spectrum); as the obtained curves are smooth in a small region and since in most cases its curvature cannot be significantly appreciated, a good fit is obtained by calculating the least squares straight line and extrapolating it to zero yield.

Sometimes a parabolic rise is observed at the threshold; in this case a least squares fit of a quadratic expression is the best criterion available; a point is then

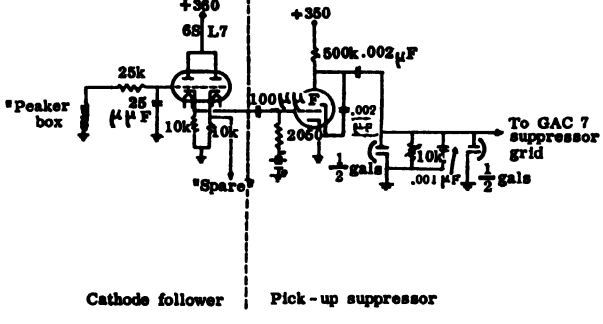

Figure 5

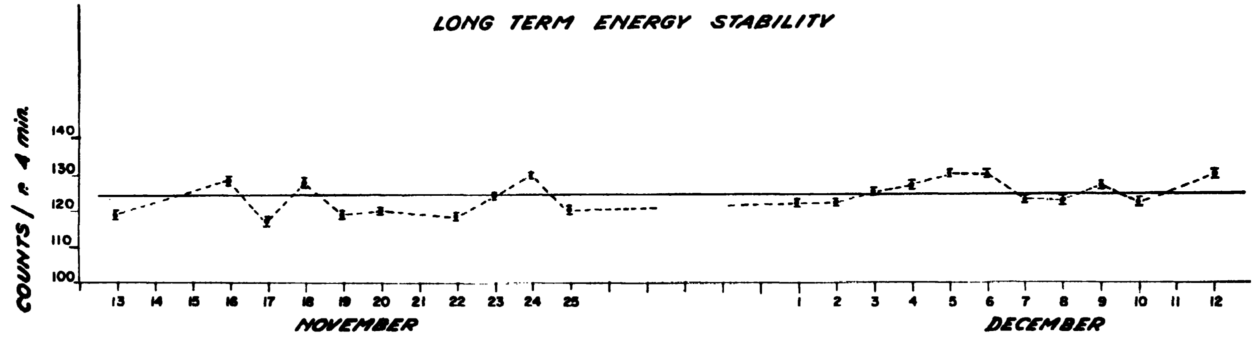

Figure 6

determined unambiguously and is considered as a measurement of the threshold energy. A further check on this value can be obtained by observing the induced yield for energies just slightly below or above this extrapolated energy. In some instances, this has turned out to be quite an accurate procedure to locate a threshold within an error of 0.1%. This is a tedious procedure, however, since the activities are usually just above the natural background.

Another procedure which can be used to determine unambiguously the extrapolation point was suggested by Parsons and Collie[9] and has been used widely by several investigators.[11,12] If one assumes that the yield Y' for a given process increases with some power n of the photon excess energy over the threshold, $(\Omega - \Omega_0)$, a plot in a double logarithmical scale of the expression $Y' = k(\Omega - \Omega_0)^n$ allows the value of the threshold to be calculated. Since however, an assumption is made on the behaviour of the excitation function near the threshold, this value, although unambiguously determined, may be different from the actual threshold.

The measured thresholds reported in this paper were obtained by means of the induced activity technique and the least squares extrapolation, as described above, was used in most instances.

Experimental Arrangement

Cylindrical samples of compressed material under about 8000 psi were used in most cases. They were designed to fit snugly over a Victoreen Thyrode counter encased in a lead castle. The thickness of the samples was chosen in every instance in order to get a source of infinite thickness. This procedure was chosen in order to get the maximum counting rate under a given irradiation.

The cylindrical samples were irradiated at 30 cm from the X-ray target and the irradiation dose was measured by means of a Victoreen thimble ionisation chamber immersed in a lucite block whose sides were 8 cm long.[13] Whenever high doses of irradiation were necessary, a Hammer dosimeter was used under the same experimental conditions.

Energy Scale

The energy control system of the University of São Paulo's betatron gives a linear dependence between the variable reference emf and the momentum of the electrons at the equilibrium orbit prior to the expansion of the beam towards the X-ray target. This dependence can be verified at any moment during irradiation by means of the checking controls incorporated in the circuit. In particular, it is possible to calibrate the energy scale by means of a dc variable emf connected to the input of the cathode follower tube. This circumstance has turned out to be a useful feature to provide a quick check on the working conditions of the whole energy control system.[6] It can be shown that the relationship between the kinetic energy of the electrons that strike the target at a pre-determined value of the reference voltage energy control is given by

$$[E_{max}(E_{max} + 1.02)]^{1/2} = A(R + B) \qquad (1)$$

where R is the variable arm of the reference emf potentiometer and A and B are constants. A depends upon the constants of the integrator and energy control circuits, the radius of the equilibrium orbit, the target radius, the true phase shift between the magnetic field and the integrated voltage across the con-

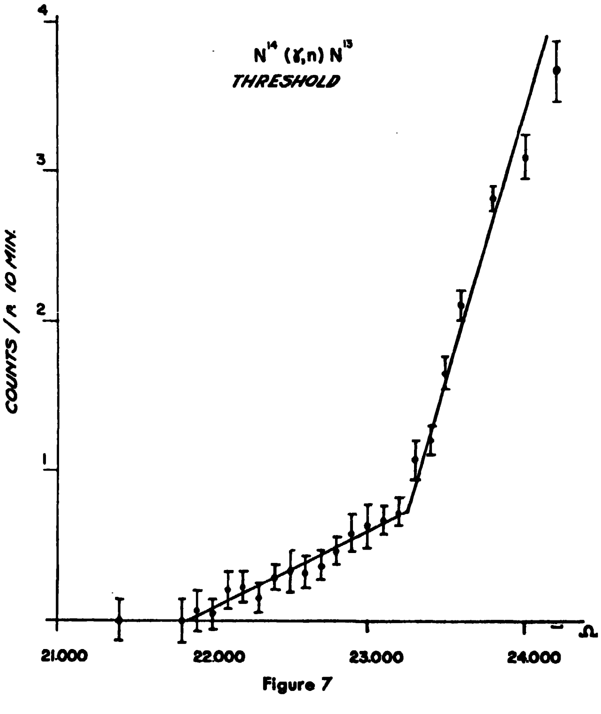

Figure 7

denser of the integrator stack and of the characteristics of the pulse applied to produce the expansion of the orbit towards the target.[14]

These constants could be both, in principle, calculated without difficulty since B represents the displacement of the reference voltage introduced by the standing current in the cathode follower dropping resistance; this voltage can be accurately measured by means of either a sensitive voltmeter or by a potentiometer.

The constants A and B were both determined experimentally by measuring the thresholds of (γ,n) reactions in light elements. Equation 1 was used then as an interpolation formula, and it will be seen that the linear relationship holds within the accuracy of the experimental data. Indeed, since nuclear masses are not yet well enough known to enable small systematic departures from Equation 1 to be detected, small departures from the ideal conditions assumed in the derivation of this equation are thus found to be smaller than the errors introduced by mass-differences.

The thresholds used in this calibration were:[15]

$N^{14}(\gamma,n)N^{13}$
$O^{16}(\gamma,n)O^{15}$
$C^{12}(\gamma,n)C^{11}$

which are, respectively, 10.543 ± 0.0168 Mev, 15.957 ± 0.012 Mev, and 18.707 ± 0.027 Mev. Those values should still be corrected by the energy of the recoiling nucleus after the photon capture

$$E_r = E_\gamma^2/2mc^2$$

and we get then 10.549 ± 0.017 Mev, 15.605 ± 0.012 Mev and 18.728 ± 0.027 Mev respectively.

Although the dc check on the energy scale calibration leads one to the certainty that there is a linear relationship between the reference voltage (as measured by the potentiometer arm R in ohms) and the momentum of the electrons at the equilibrium orbit, the introduction of a third point allows a better interpolation of Equation 1 in the experimental data.

EXPERIMENTAL RESULTS

I. Nitrogen

Cylinders of dicyandiamide ($N_4C_2H_4$) compressed under 8000 psi were used in these determinations. The samples used fit snugly over the thyrode counter used to detect the N^{13} activity induced by the (γ,n) process in N^{14}. The purity of the samples used was checked by measuring its decaying activity during several half-lives ($T_{1/2}$ = 10.1 min.).

The obtained activities as a function of the maximum energy of the betatron X-rays are illustrated in Fig. 7, where the points were obtained in integrator steps of 100 ohms. The extrapolated threshold occurs at 21,850 ohms. It can be observed that there is a sharp break at 23,200 ohms which corresponds to the contribution of an excitation level in the N^{14} excited nucleus and which had not been observed before by betatron irradiation. This level occurs at 11.38 Mev and has been observed by several investigators as quoted by Ajzenberg and Lauritsen.[16]

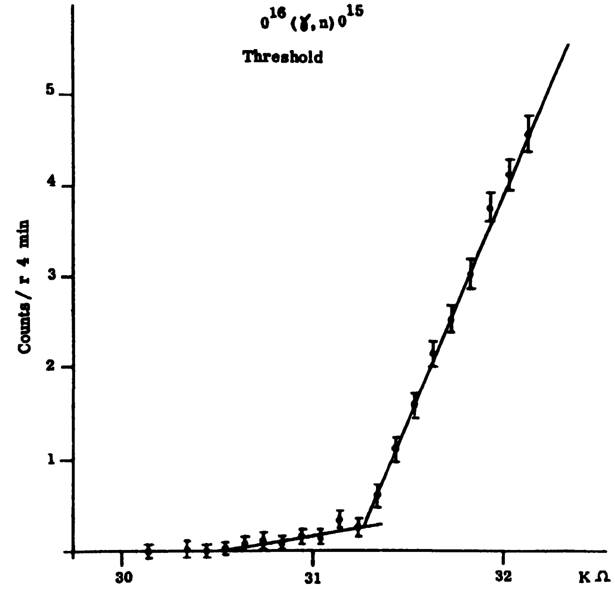

Figure 8

II. Oxygen

Samples of compressed boric acid, also under 8000 psi were used in this experiment. A purity test was made by following the induced activity due to O^{15} during several half-lives. The excitation function obtained is illustrated in Fig. 8. There is also a sharp break of the excitation function which is attributed to an excitation level in the O^{16} nucleus and which has been observed before.[10,17] The extrapolated threshold for this (γ,n) reaction occurs at 30,440 ohms.

III. Carbon: $C^{12}(\gamma,n)C^{11}$

In order to study the $C^{12}(\gamma,n)C^{11}$ reaction, pieces of polyethylene tubing were used. A check on their purity was made by irradiating the samples during one half-hour and following the induced activity for several half-lives; a pure C^{11} activity of 20.5-min half-life was observed.

The obtained extrapolated threshold lies at 35,600 ohms. The small activity, just above background was found to be a 10-munite half-life activity ascribed to the $N^{14}(\gamma,n)N^{13}$ reaction in N impurities (see Fig. 9).

With the data obtained on these three reactions, a least squares fit was made to Equation 1 which can then be written as

$$[E_{max}(E_{max} + 1.02)]^{1/2} = -2.428 + 0.593\,R$$

This equation has been used in the determination of the thresholds of the reactions which will be described below.

IV. Chlorine: $Cl^{35}(\gamma,n)Cl^{34}$

The threshold for this reaction can be computed by taking into account the known mass differences of both nuclides;[18] since the maximum energy of the

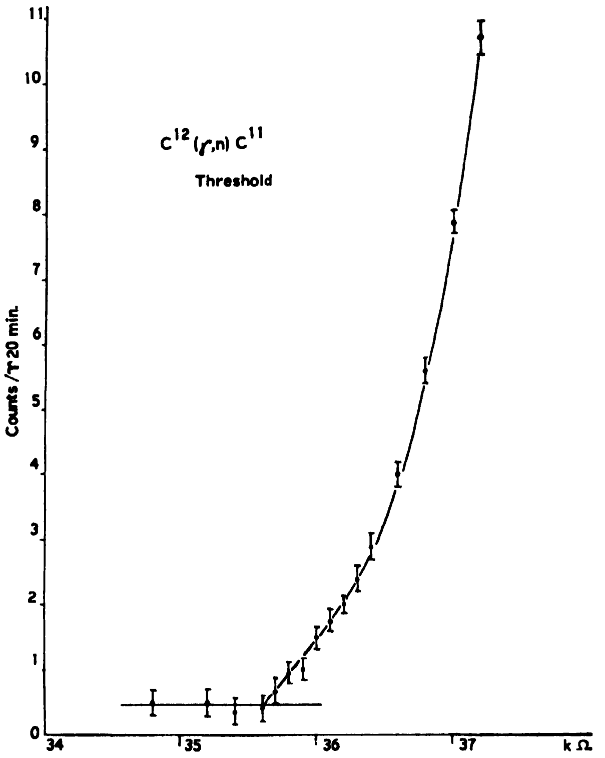

Figure 9

emitted positrons from Cl^{34} is known to be 4.5 Mev, the threshold for the process is found to be 12.58 ± 0.09 Mev.[19]

The threshold was determined by means of the induced activity in CCl_4 samples measured in a liquid counter. A pure 33-minute ($T_{1/2}$) activity was observed and constitutes an independent check on the purity of the CCl_4 employed in our measurements. The obtained results are represented in Fig. 10. The observed threshold for this reaction is found to be 12.35 ± 0.035 Mev.

V. Iron: $Fe^{54}(\gamma,n)Fe^{53}$

Cylindrical samples of iron were used in this experiment; their purity was known by chemical analysis and was further checked by the induced activity under betatron irradiation. The threshold is located at 24,150 ohms which corresponds to 11.90 ± 0.07 Mev (Fig. 11). The previous values for the threshold of this reaction were quoted as 14.2 ± 0.4 Mev[20] and 13.8 ± 0.2 Mev.[8] This value of the threshold corresponds to the rapid rise of the activity which is found in the region *C* of Fig. 11. One should expect this region to be the beginning of the contribution due to electric dipole absorption whereas the slow initial rise is a contribution of both magnetic dipole and electric quadrupole absorption. This region was missed by the investigators who examined this reaction before.

In order to examine whether this activity was not due to impurities, a very careful series of tests was made. The half-life of the induced activity in the region *BC* was measured in each point and was found to be typical of the Fe^{53} activity ($T_{1/2} = 9$ min). A chemical analysis of the samples showed no traces of copper in the amounts required to be responsible for the yields observed.

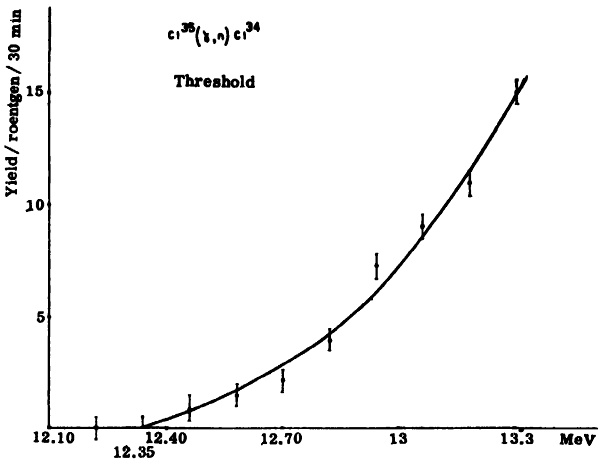

Figure 10

VI. Copper: $Cu^{63}(\gamma,n)Cu^{62}$

Electrolytic copper cylinders were used and their purity was examined by radioactive procedures. Special care must be exercised in this threshold determination owing to the fairly large capture cross-section of Cu^{65} for slow neutrons, leading to the 5-minute half-life activity of Cu^{66}.

The obtained results are illustrated in Fig. 12 where the extrapolated threshold occurs at 21,870 ohms which corresponds to 10.54 ± 0.04 Mev. This value agrees with Birnbaum's[12] observed threshold within the experimental errors. Previous measurements have located this threshold at 10.90 ± 0.2,[20] 10.90 ± 0.2 and 10.8 ± 0.2.[8,21]

Since it is usual to calibrate the betatron energy scale with the $Cu^{63}(\gamma,n)Cu^{62}$ threshold as a standard point, this error must have influenced a number of earlier threshold measurements.

The threshold value as calculated from mass differences gives 10.00 ± 0.10.[22] Since no cascade gamma rays between 350 and 650 kev have been observed,[23] the mass-difference must have an error of 540 kev.

VII. Zinc: $Zn^{64}(\gamma,n)Zn^{63}$

Cylinders of pure zinc were irradiated and the resid-

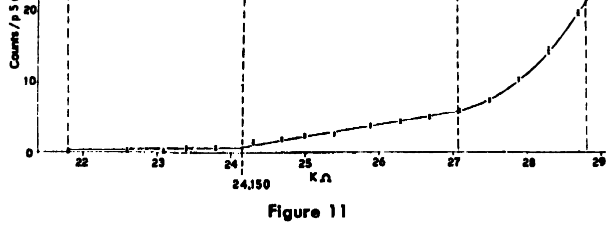

Figure 11

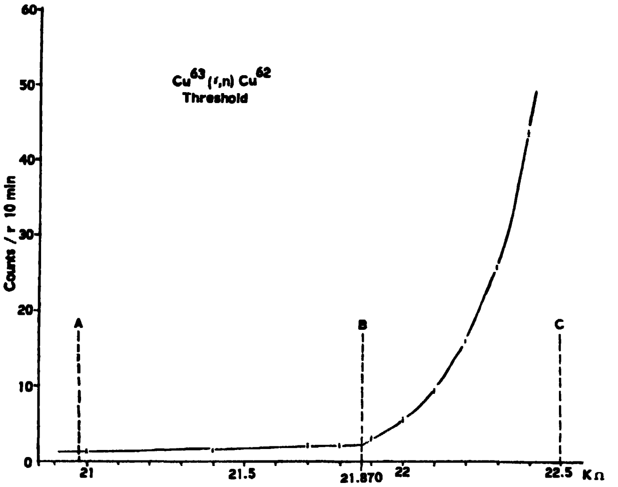

Figure 12

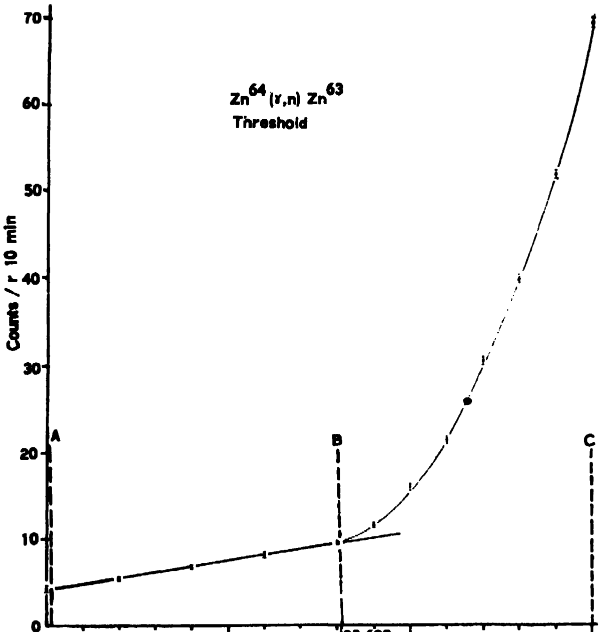

Figure 13

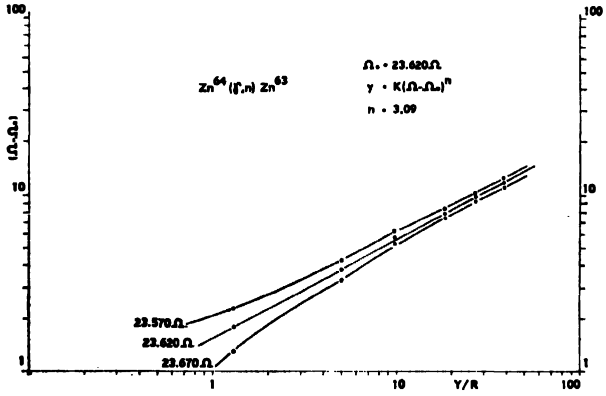

Figure 14

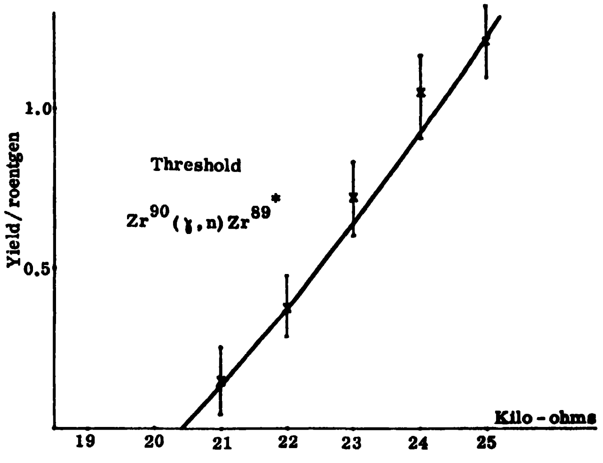

Figure 15

ual activity was measured in our standard arrangement for cylindrical samples. The obtained results are illustrated in Fig. 13. Below the threshold an activity of 5-minute half-life was detected and found to be due to $Zn^{67}(\gamma,p)Cu^{66}$. If the contribution of this activity is subtracted, the extrapolation gives for the threshold 23,620 ohms which corresponds to 11.58 ± 0.06 Mev.

The same extrapolated value was obtained by extrapolating to zero yield by means of the procedure described by Parsons and Collie[9] as illustrated in Fig. 14. This value agrees within the experimental errors with the threshold as calculated by using mass differences[22] as 11.435 ± 0.058 Mev.

VIII. Zirconium: $Zr^{90}(\gamma,n)Zr^{89*}$

Discs of pressed zirconium oxide were irradiated at several betatron energies and the decay of the 4.4-minute activity was followed by an automatic counting system; the results are presented in Fig. 15 which locates the threshold for this reaction at 24,100 ohms, which corresponds to 12.20 ± 0.06 Mev. The values previously obtained for this threshold by other investigators were: 12.1 ± 0.1[24] and 12.3.[25]

IX. Silver: $Ag^{109}(\gamma,n)Ag^{108}$

Silver cylinders were used as samples in these experiments and were irradiated at several betatron energies. Since Ag^{107} has a high cross-section for slow neutron capture, it is impossible to avoid some contribution of this process even for irradiation energies below the threshold and which is ascribed to neutrons originated both in the X-ray target and donut walls. By subtracting this contribution in the yield curve, the threshold can be located at 18,900 ohms which corresponds to 8.78 ± 0.04 Mev (Fig. 16). Previous values of this threshold were: 9.3 ± 0.5,[20] 9.05 ± 0.2[11] and 9.07 ± 0.7.[12]

X. Samarium: $Sm^{144}(\gamma,n)Sm^{143}$

Discs of pressed Sm_2O_3 were irradiated at different betatron energies and the induced 9.03-minute half-life activity measured in our standard counting arrangement. The obtained results located the threshold at 9.60 ± 0.05 Mev (Fig. 17).

Table 1

Element	Threshold (Mev)	$\sigma(E_{max})$	E_{max}	$\int\sigma\,dE$ (Mev-b)	Width (Mev)
Cl^{35}	12.35	7.4 mb	18.75 Mev	0.02	3.3
K^{39}	13.00	13.8 mb	18.25 Mev	0.04	2.6

CROSS-SECTIONS

In the course of the experiments carried out in our laboratory, cross-sections for several photonuclear reactions were computed by means of the photon difference method.[26]

In this paper, some typical or peculiar ones will be described.

I. Chlorine: $Cl^{35}(\gamma,n)Cl^{34}$ and II. Potassium: $K^{39}(\gamma,n)K^{38}$

Cylinders of compressed KCl at a pressure of 8500 psi were used in these experiments and irradiated by the betatron as shown in Fig. 18. The samples were irradiated for a period of time of the order of ten minutes and the decay of the induced activities was followed for three hours: the activities measured were the 33-minute half-life positron emitter Cl^{34} and 7.7-minute K^{38}. The dose to which the samples were submitted was measured by means of a Victoreen condenser r-meter.

Analysis of the decay curves obtained at several energies gave the initial saturated activity induced in the samples. The absolute rate of disintegration was determined by computing the number of active nuclei in an irradiated disc of compressed KCl, since for discs the determination of the geometric efficiency of the counting arrangement is less cumbersome. Corrections were made for self-absorption and self-scattering.

The disintegration scheme used in these computations for Cl^{34} is that given by King[19] and for K^{38} the one quoted by Low and Townes.[27] The results obtained for the activation curves are represented in Fig. 19. From these one can obtain the cross-sections for the (γ,n) reactions in Cl^{35} and K^{39}. The results are shown in Fig. 20.

The significant data obtained from these curves is presented in Table 1.

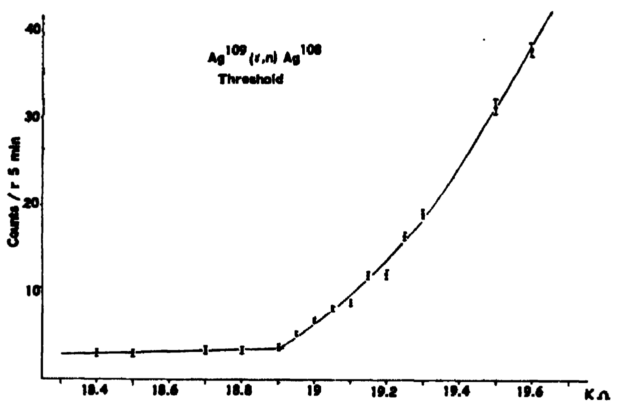

Figure 16

III. Zinc: $Zn^{64}(\gamma,n)Zn^{63}$, $Zn^{64}(\gamma,2n)Zn^{62}$, and $Zn^{66}(\gamma,n_p^d)Cu^{64}$

Cylinders of pure zinc were irradiated at a distance of 30 cm of the betatron target during times ranging from 5 to 20 min, and the activity induced was measured by a cylindrical counter for 72 hours; in this way it was possible to separate the activities originated in the following reactions:

$Zn^{64}(\gamma,n)Zn^{63}$ with a half-life of 38 minutes, emitting positrons of 2.36 and 1.40 Mev.

$Zn^{64}(\gamma,2n)Zn^{62}$ of half-life of 9.3 hours, emitting positrons of 0.66 Mev, in equilibrium with Cu^{62}.

$Zn^{66}(\gamma,n_p^d)Cu^{64}$ with half-life of 12.8 hours emitting positrons of 0.57 Mev and beta rays of 0.66 Mev.

The 9.3- and the 12.8-hour activities were separated by absorption techniques. Some activity due to Zn^{68} formed by neutron capture in Zn^{67} with 14-hour half-life had to be subtracted from the long lived isotopes mentioned above.

The absolute rate of disintegration of a Zn disc was determined by comparison with a copper sample irradiated in the same conditions; the other activities were determined by comparison with the 38-minute activity. It was possible in this way to obtain the activation curves for the reactions listed above; the results are shown in Figs. 21, 22, and 23. From those curves the cross-sections of Figs. 24 and 25 were obtained. The activation curve for the $Zn^{64}(\gamma,2n)Zn^{62}$ reaction determines the threshold for this reaction at 20.35 ± 0.35 Mev.

The results for the $Zn^{66}(\gamma,n_p^d)Cu^{64}$ are very interesting although measurements were not made above

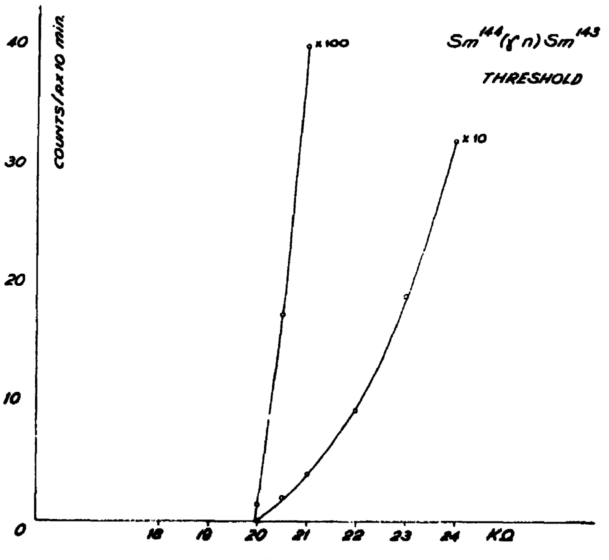

Figure 17

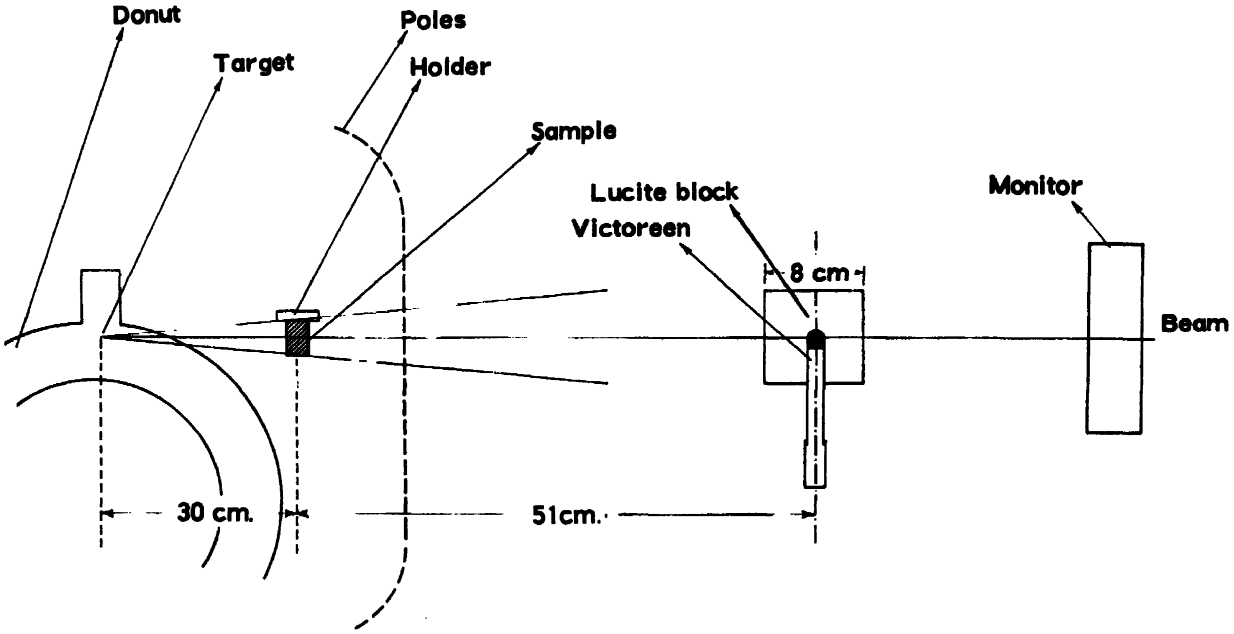

Figure 18. Experimental arrangement

22 Mev; at 21 Mev the ratio of the (γ,n) to the (γ,n_p^d) cross-sections is 1.6: the same ratio computed from the evaporation model gives $\sim 6 \times 10^3$.[28] The yields for those reactions at the same energy are 200; this constitutes a confirmation of the results obtained by Byerly and Stephens for the emission of photodeuterons from copper.[29] The need of a special mechanism to explain the emission of photo-deuterons is clearly necessary.

IV. Sulfur: $S^{32}(\gamma,n_p^d)P^{30}$

Pressed cylinders of sulfur powder were irradiated at different betatron energies in the same arrangement already described for zinc measurements. The residual nucleus P^{30} is a 2.5-minute (half-life) positron emitter.

The activities obtained were compared to the activity of a boric acid sample in order to obtain the absolute rate of disintegration. The known activation curve for the reaction $O^{16}(\gamma,n)O^{15}$ was used for that purpose. The resulting activation curves and cross-sections are shown in Fig. 26.

The results obtained in this measurement can be compared with those of Katz and Penfold[30] for the same reaction. The first interesting point to observe is that our samples were 10 times heavier than those of Katz and Penfold; one can then be fairly confident of the results obtained close to the threshold. As we can see, in Fig. 26, the activation curve rises slowly from the threshold of the (γ,d) reaction at 19 Mev up to 20.5 Mev where the (γ,np) reaction comes in, and then increases rapidly; this can be interpreted as the contribution of the (γ,np) process that adds to the (γ,d). At these energies the ratio of the cross-section for the reaction (γ,n) as measured by Summers-Gill *et al.*[31] to the (γ,n_p^d) is six. Using the evaporation model one gets for the same ratio $\sim$400. Here we have again, clearly stressed, the need of a special mechanism to explain the emission of photodeuterons by nuclei.

V. Iron: $Fe^{54}(\gamma,n)Fe^{53}$

Iron cylinders were used in a measurement of the activation curve of the (γ,n) reaction of the 9% abundant Fe^{54}. Special care was taken in the measurements of the energy region immediately above the threshold, since this region presents some peculiarities.

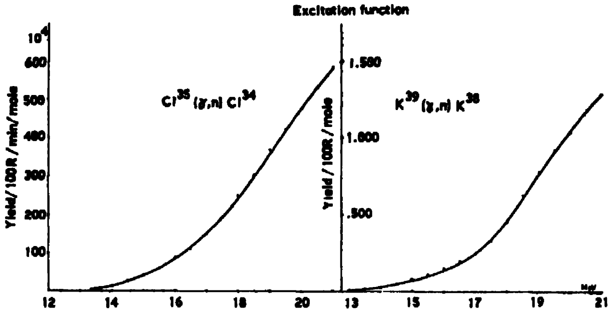

Figure 19

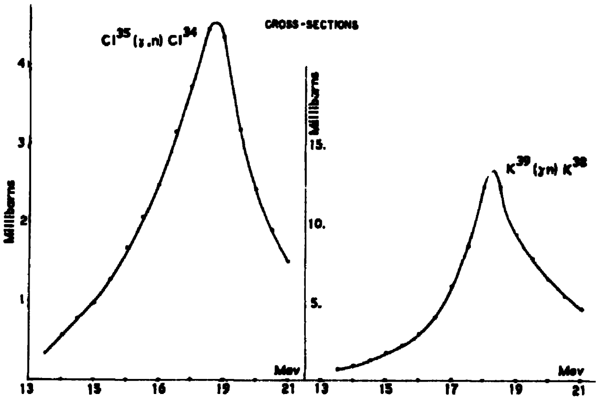

Figure 20

Table 2

Element	*Threshold*	E_{max}	$\sigma(E_{max})$	$\int \sigma\, dE$
Ge^{70}	12.1 Mev	20 Mev	0.125 b	0.59 Mev-b
Ge^{76}	9.3 Mev	18.9 Mev	0.243 b	1.5 Mev-b

The activation curve obtained in the form of counts per roentgen is shown in Fig. 27. The cross-section computed from it is shown in Fig. 28 normalized to the cross-section for the same process as measured at the University of Saskatchewan.[32] The agreement between the two curves is very good in the region of the dipole resonance, but, at lower energies our curve shows a knee typical of the contribution of magnetic dipole or electric quadrupole absorption. This behaviour has been found before in light nuclei, like oxygen and nitrogen.[33,34] It is interesting to find this peculiarity in such a middle *A* nucleus like iron ($A = 54$).

VI. Germanium: $Ge^{70}(\gamma,n)Ge^{69}$ and $Ge^{76}(\gamma,n)Ge^{75}$

Irradiation of natural germanium in the betatron beam allows the study of the following (γ,n) reactions: $Ge^{70}(\gamma,n)Ge^{69}$ which decays into Ge^{69} by positron emission with a half-life of 40 hours, and $Ge^{76}(\gamma,n)Ge^{75}$ which decays by beta ray emission into As^{75} with a half-life of 82 minutes.

A very small contribution to the activity is due to neutron capture reactions, but an analysis of the decay curves of irradiated germanium permits the separation of the activities of Ge^{69} and Ge^{75}.

Samples of two grams of germanium were irradiated during ten minutes close to the betatron X-ray target and their activity was measured with an end window counter. In order to obtain the absolute rate of disintegration, the usual corrections were applied and the disintegration schemes quoted by King[19] were utilized.

The activation curves so obtained are shown in Fig. 29, and the corresponding cross-sections are illustrated in Fig. 30. The yields obtained at 18 Mev for the above reactions fit quite well the yield data of Price and Kerst. The threshold obtained in our measurement for Ge^{70} at 12.1 ± 0.2 Mev indicates that the disintegration scheme for germanium-69 suggested by Way and Wood[35] is correct.

The cross-sections present the peculiarity of a maximum cross-section at an energy anomalously high; however, as the obtained data were limited to a maximum energy of 22 Mev, it was not possible to obtain the falling part of the giant resonance. The "shoulder" present in the part of the cross-section immediately above the threshold indicates the presence of absorption of photons due to magnetic dipole or/and electric quadrupole.

The characteristics of the determined cross-sections are shown in Table 2.

VII. Samarium: $Sm^{144}(\gamma,n)Sm^{143}$

Discs of pressed samarium oxide were irradiated at several energies in order to obtain the activation curve and cross-section for this reaction. Some effort was spent to obtain also more information on the characteristics of the radioactivity induced in Sm^{144} by betatron irradiation.

The irradiated samples were counted with an end window counter, and the decay curve was followed for approximately 3 hours; besides a long-lived activity present in the samples with a half-life of the order of 50 hours, an activity of the order of 10 min half-life was observed. This activity has been found before by Butement[36] and assigned tentatively to Sm^{143}. As will be shown this assignment is confirmed by our measurements.

The half-life of this activity was accurately measured to be 9.03 ± 0.02 min. The disintegration scheme was studied roughly by absorption methods and the information obtained that Sm^{143} decays by the emission of 2.6 Mev positrons; no other gamma-rays were

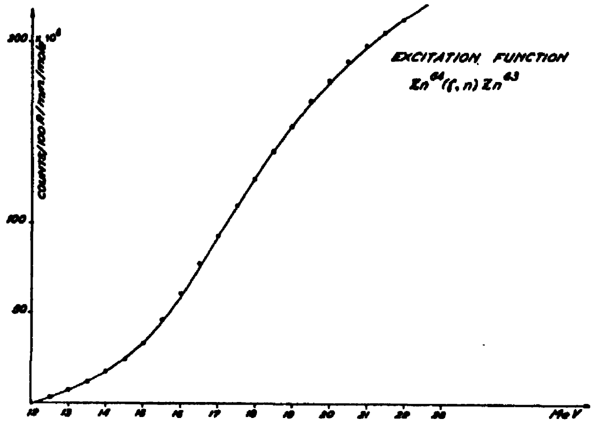

Figure 21

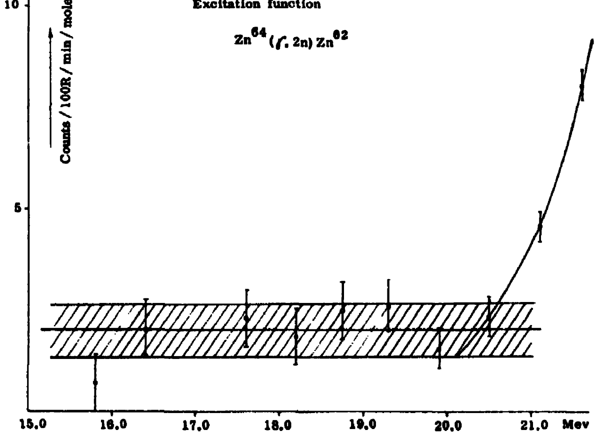

Figure 22

found besides the annihilation radiation. Using this data, the activities obtained at a number of energies were compared with a copper sample irradiated in the same conditions, and the absolute rate of disintegration computed.

The activation curves so obtained are shown in Fig. 31; from this curve the cross-section was obtained and is shown in Fig. 32. The yield per mole/r/min at 18 Mev is 0.24 × 10^7. Interpolating in the yield data

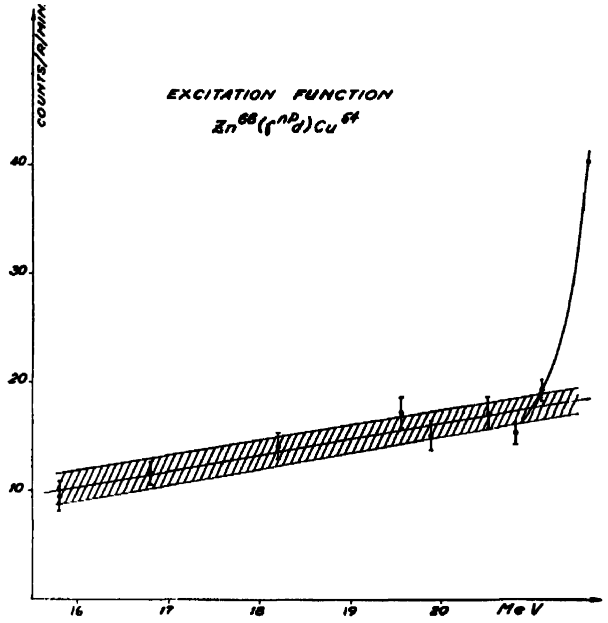

Figure 23

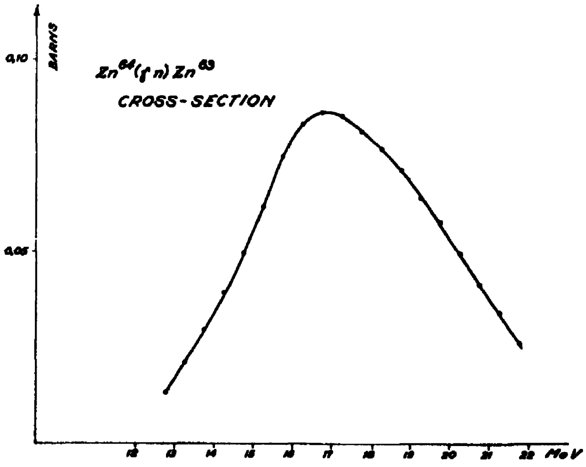

Figure 24

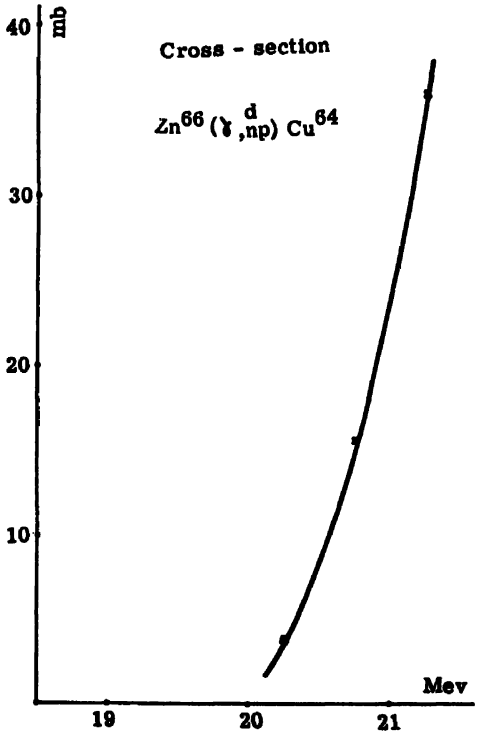

Figure 25

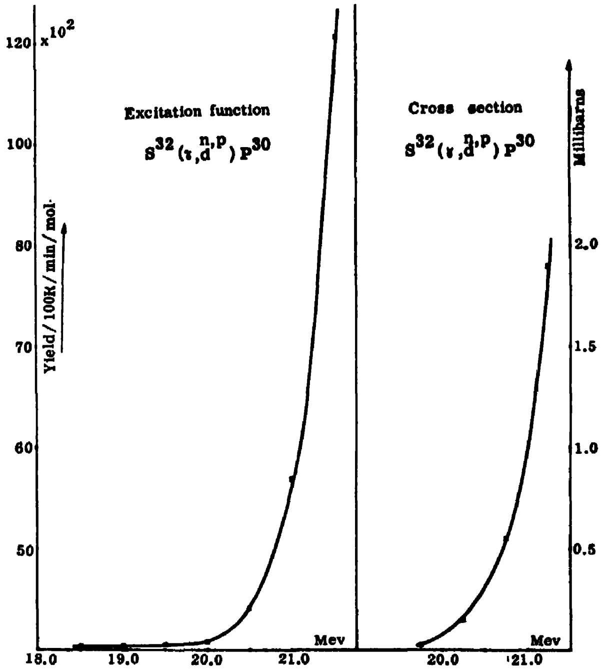

Figure 26

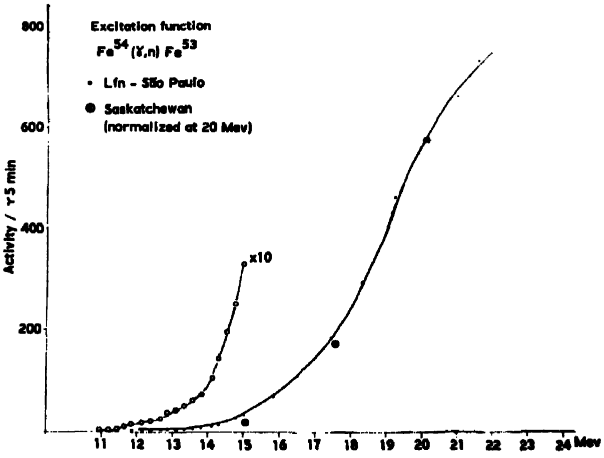

Figure 27

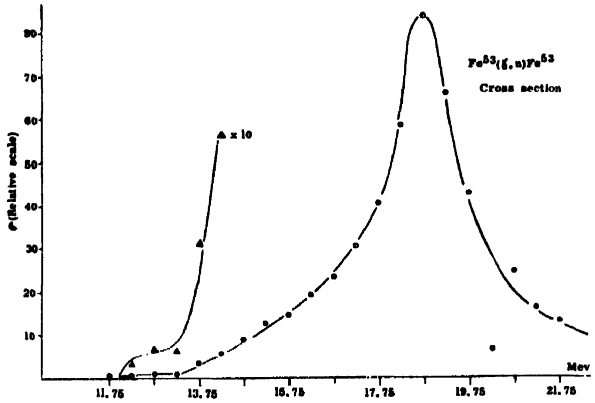

Figure 28

of Price and Kerst[37] one gets for the same nucleus 0.93×10^7; our result is then lower than the expected by a factor 4. If the reaction responsible for the 9.03-min activity is Sm^{147}, which is the other possible assignment for this activity, our yield would be lower, by a factor of 20, than Price and Kerst's; this seems very unlikely to be the case.

The remaining disagreement of a factor of 4 might be explained by the existence of an undetected isomeric transition state in Sm^{143}; Sm^{143} belongs to one of the "islands of isomerism" indicated by Goldhaber and Hill.[38]

VIII. Lead: $Pb^{207+208}(\gamma,p)Tl^{206+207}$

This reaction was studied in order to gain information on the validity of the evaporation model for the lead nucleus. Since the gamma-*n* cross-section has been measured before,[39] the knowledge of the gamma-*p* reaction in the above mentioned isotopes might permit a comparison with theory.

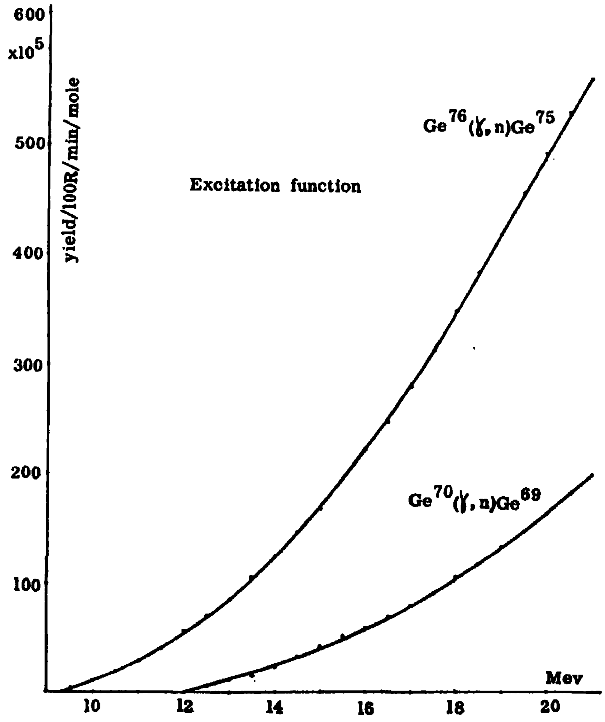

Figure 29

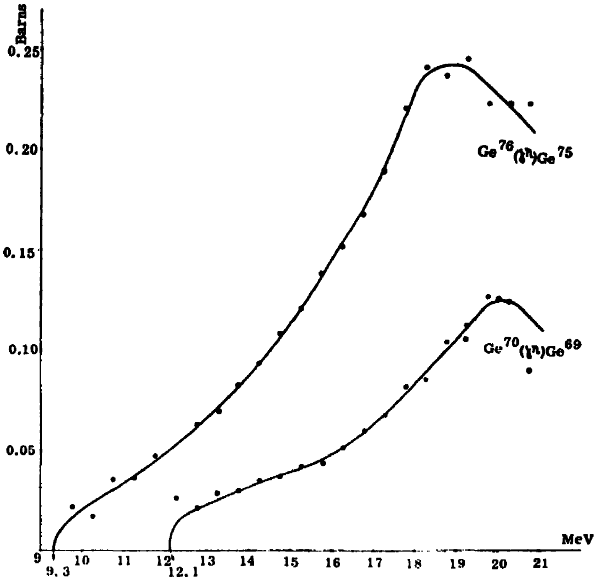

Figure 30

The experiment can be made easily by residual activity methods since both Tl^{206} and Tl^{207} decay by emission of beta rays of approximately the same energy, 1.51 and 1.45 Mev respectively; besides that, the half-lives of those isotopes is approximately the same, 4.23 and 4.76 min. Although a separation of the contributions from Tl^{206} and Tl^{207} was attempted using the fact that the first does not emit gamma rays whilst Tl^{207} emits some of 0.87 Mev, this attempt failed: a gamma-ray crystal spectrometer using a one-inch thick NaI scintillator was assembled but the relative intensity of the gamma-rays in Tl^{207} is so small[40] (0.005) that few counts were obtained.

The results of this work refer then to the sum of the contributions of Pb^{207} and Pb^{208}. Cylinders of natural lead were irradiated at several energies and counted in a cylindrical counter. Due to the high mass of the cylinders, it was possible to measure the activation curve down to 11 Mev; the thresholds for the reactions lie around 8 Mev.[41]

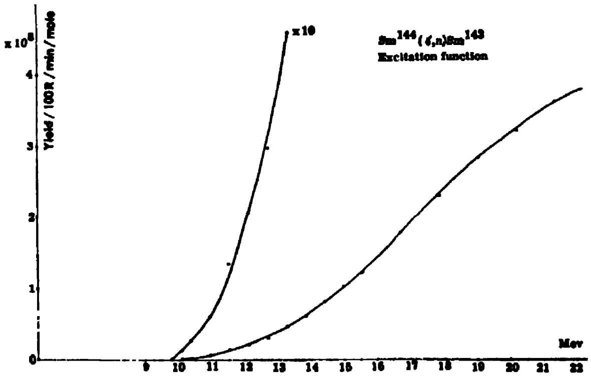

Figure 31

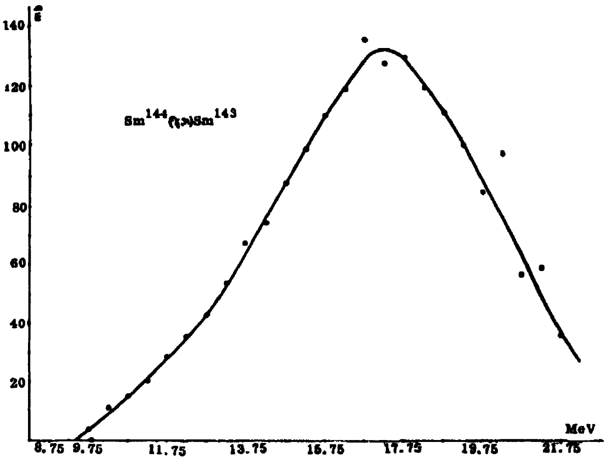

Figure 32

The absolute rate of disintegration was determined irradiating discs of Pb and Cu together and comparing their activities. After the usual corrections, the activation curve was obtained and is shown in Fig. 33; the cross-section computed from it is shown in Fig. 34.

Using this cross-section and assuming that the (γ,n) cross-section for the sum of the isotopes Pb^{207} and Pb^{208} is the same as the (γ,n) cross-section for natural lead, one can compute at each energy the ratio $\sigma(\gamma,n)/\sigma(\gamma,p)$. The same ratio was computed from the evaporation model, and the results are shown in Table 3 and in Fig. 35.

Table 3

E (Mev)	*Experiment*	*Evaporation model*
12	135,000	—
13	13,000	—
14	7400	$200{,}000 \times 10^4$
15	3350	$17{,}000 \times 10^4$
16	1470	3000×10^4
17	600	740×10^4
18	230	290×10^4
19	80	96×10^4
20	26	38×10^4

An analysis of this ratio shows that not only the evaporation model fails to account for the number of emitted protons by a factor 10^4 but, besides, it gets increasingly worse at low energies.

GENERAL DISCUSSION

The advent of the 24 Mev betatron has made it possible, in the last few years, to accumulate a wealth of information on the photonuclear processes in the intermediate energy range. It has turned out that, in most nuclides for which the different modes of decay of the compound nucleus have been examined, a valuable information on the behaviour of the processes responsible for the absorption of the electromagnetic radiation is obtained. In two particular instances in which the de-excitation of the compound nucleus by gamma-ray re-emission was studied, it has turned out that this effect is not larger than about 10% of the

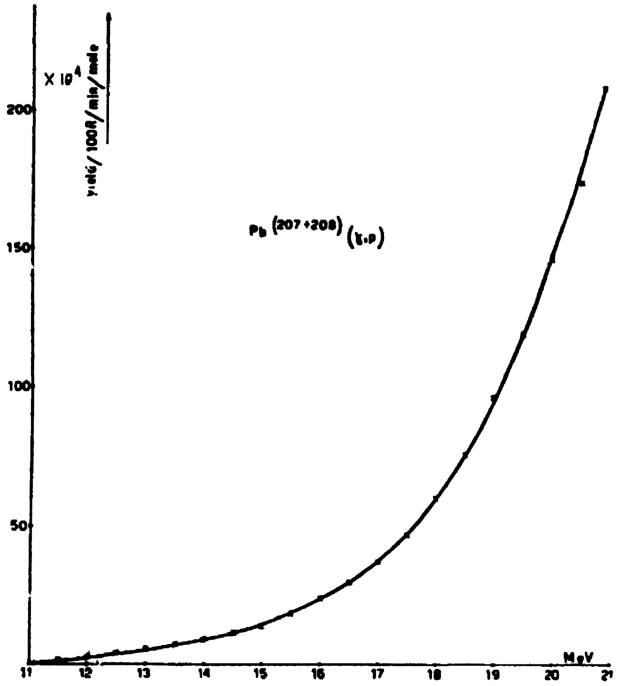

Figure 33

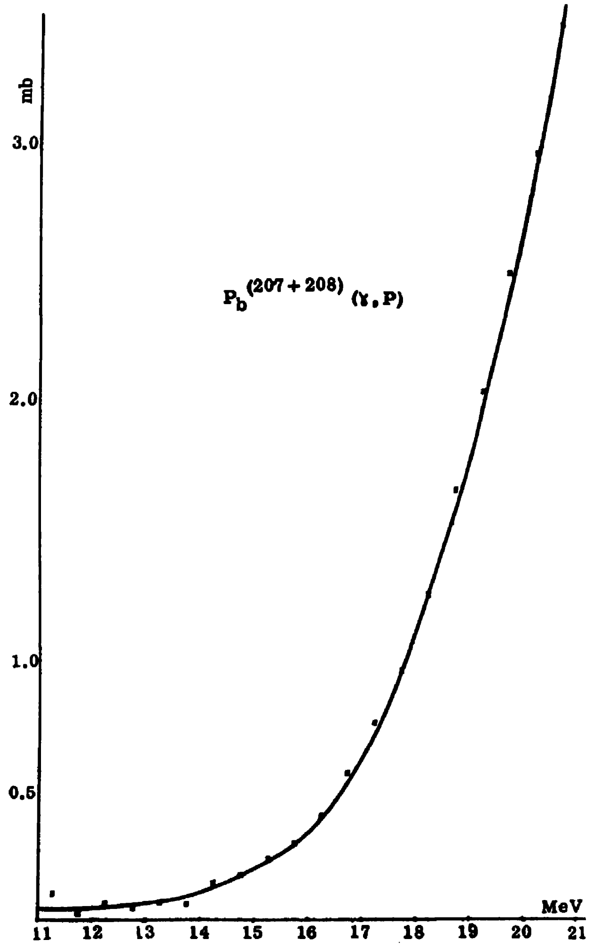

Figure 34

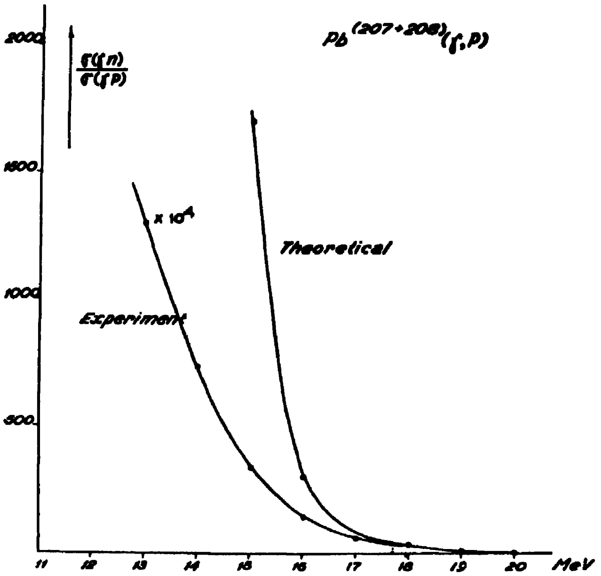

Figure 35

gamma-neutron mode of de-excitation.[42,43] On the other hand, it has been fairly well established that the de-excitation by a single neutron emission is the predominant mode of decay of the compound nucleus.

From the considerations outlined above it follows that a good estimate of the absorption processes of the electromagnetic radiation by the atomic nuclei is given by the analysis of gamma-neutron processes.

A common feature of the measured cross-sections for photonuclear reactions is that the cross-section rises slowly at threshold and stays practically constant for a while rising then in a typical bell-shaped curve which is often referred to as the "giant resonance."

Several theories have been put forward to explain the nature of this giant resonance;[44,45,46] amongst these theories Levinger and Bethe's is based on considerations which are quite independent of the nuclear model. In particular, the integrated cross-section for photon absorption, as calculated by these authors, makes use of the quantum mechanical sum rules, and gives predictions which are well verified by the experimental data available.[39,47]

Another result of this theory is that the harmonic mean energy W_H for photon absorption, in the region of the giant resonance, can be expressed as a function of the mean squared displacement $\langle r^2\rangle_\infty$ of a nucleon, in the nuclear ground state, as

$$W_H = \frac{\int\sigma(E)\,dE}{\int\sigma(E)\,dE/E} = \frac{3\hbar^2}{2M}\,\frac{1+0.8x}{\langle r^2\rangle_\infty}$$

Here, $\sigma(E)$ is the nuclear absorption cross-section of photons of energy E, x is the fraction of the neutron-proton force which is of exchange nature, and M is the nucleon mass.

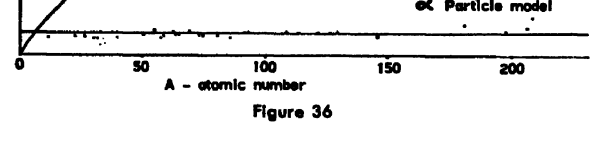

Figure 36

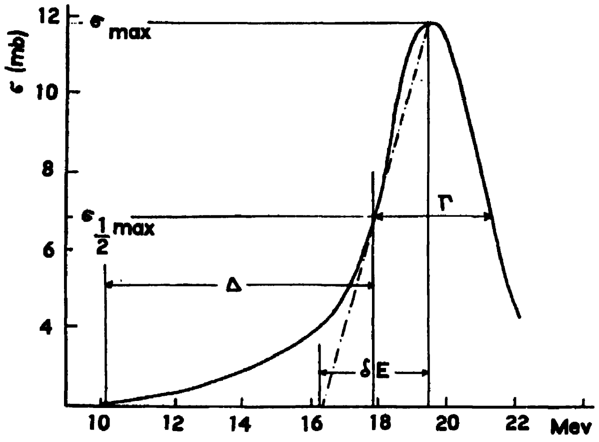

Figure 37

As the integrals that occur in the equation above can be obtained from the experimental data, it is possible to compute $\langle r^2\rangle_\infty$ and, therefore, to gain some insight on the sub-units which are responsible, in a nucleus, for the dipole absorption.

In Fig. 36 is illustrated the behaviour of $\langle r^2\rangle_\infty$ as a function of A for the experimental data available and from the measurements reported in this paper. In the same figure two theoretical curves are drawn, corresponding to a model in which the neutrons are free to move inside the nuclear boundary, as defined by its radius, and for a model in which the sub-units responsible for photon absorption are assumed to be alpha particles.

It seems that the available data strongly substantiate the model in which, most of the time, the nucleons are clustered as alpha particles.

An effect of closed shells on the photonuclear phenomena has been pointed out by Nathans and Halpern.[48] These investigators have found that magic nuclei show an anomalously narrow giant resonance half-width. The criterion used to evaluate the half-width, however, is not free from criticism since they consider in their measurements of the total neutron yield all the modes of de-excitation of the compound nucleus in which neutrons are emitted. As the thresholds for these processes are quite independent of the dipole absorption mechanism, fortuitous contributions may mask any effect that might be due to the shell structure. As, on the other hand, it is well established that the sudden rise of the cross-section of the giant resonance up to σ_{max} is in an interval of excitation for which the predominant mode of decay is by single neutron emission, a good criterion to avoid the difficulties just discussed could be to take into

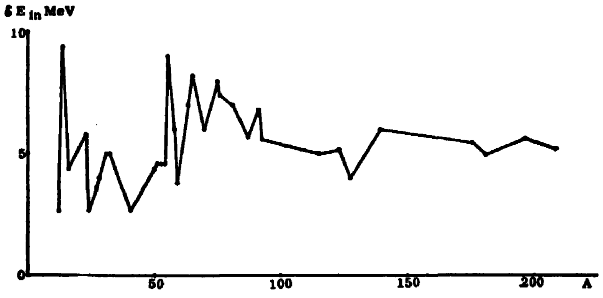

Figure 38

account the first half of the giant resonance curve to examine whether a magic number effect exists.

As one can see by examining Fig. 37, a good criterion to evaluate the onset of the dipole absorption for a given nucleus is to determine the point in which a straight line drawn through the points for which $\sigma_{½max}$ and σ_{max} intercepts the energy axis. The distance from this point to the energy at which σ is maximum is practically twice as large as one half of the half-width.

The results obtained by plotting δE against the atomic number are given in Fig. 38. The data used in these computations given in the references at the end of this paper. As one can observe, there is no clear evidence for a magic-number effect in this graph.

From very general considerations on the properties of magic-number nuclides, one should expect that neutrons in an excited compound nucleus should have a smaller chance of being emitted as compared with a non-magic one at the same excitation energy. Indeed, as follows from Bohr's concept of the compound nucleus[49] the level density in a heavy nucleus increases rapidly with the excitation energy; it is obvious, therefore, that the sudden drop in the neutron binding energy which is observed in nuclei beyond magic numbers cause a corresponding increase of level density for the same excitation energy. This argument suggests a criterion to put in evidence any effect that might be due to shell-effects.

If we consider a typical cross-section as represented in Fig. 37, one can define a parameter Δ which is a magnitude dependent on the level density, and, there-

Table 4

Element	*Z*	*N*	*A*	*Threshold*	*E*($½\sigma_{max}$)	Δ (*Mev*)	*Reference*
C	6	6	12	18.70	20.6	1.9	39, 51
M	7	7	14	10.54	19.3	8.8	34
O	8	8	16	15.60	21.8	6.2	34
Na	11	12	23	12.10	15.4	3.3	39
Mg	12	12	24	16.0	18.2	2.2	51
Al	13	14	27	14.0	17.5	3.5	39
Si	14	14	28	16.9	18.8	1.9	52
P	15	16	31	12.4	16.2	3.8	30
S	16	16	32	15.0	18.0	3.0	31
Cl	17	18	35	13.0	16.8	3.8	this paper
A	18	20	38	10.5	15.0	4.5	56
K	19	20	39	12.5	17.5	5.0	this paper
Ca	20	20	40	15.8	18.0	2.2	52
Cr	24	26	50	13.4	16.8	3.4	50
V	23	28	51	10.8	15.5	4.7	50
Mn	25	30	55	10.0	14.5	4.5	39
Fe	26	28	54	11.7	17.7	6.0	this paper
Co	27	32	59	10.2	15.0	4.8	39
Mi	28	30	58	12.0	15.5	3.5	32
Cu	29	34	63	10.6	14.5	3.9	13
Cu	29	36	65	10.2	14.1	3.9	13
Zn	30	34	64	11.6	14.5	2.9	this paper
As	33	42	75	10.1	13.0	2.9	39
Br	35	46	81	10.0	14.0	4.0	53
Rb	37	50	87	9.3	14.7	5.4	54
Nb	41	52	93	8.7	14.5	5.8	39
Mo	42	50	92	13.1	15.1	2.1	54
Ag	47	62	109	9.3	13.2	3.9	55
In	49	66	115	9.0	12.5	3.5	39
Sb	51	70	121	9.3	12.4	3.1	13
I	53	74	127	9.1	13.2	4.1	39
La	57	82	139	8.0	12.5	4.5	34
Ta	73	108	181	8.8	11.5	2.7	13
Au	79	118	197	7.9	11.4	4.1	39
Bi	83	126	209	7.4	11.6	4.2	39
U	92	146	238	6.0	9.5	3.5	56

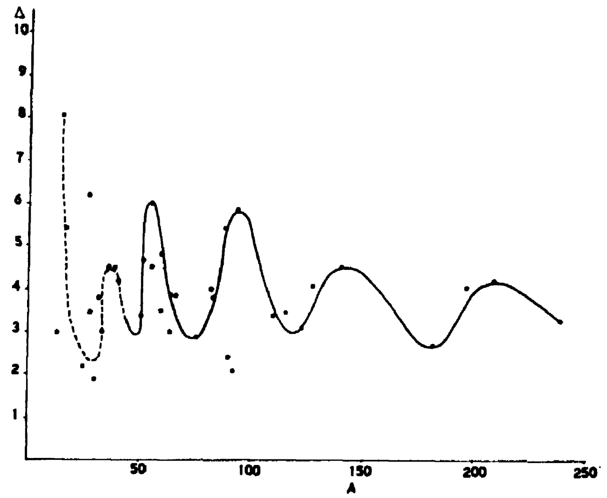

Figure 39. Shell effect in photonuclear reactions

fore, takes into account the steepness of rise of the cross-section.

For magic nuclei and neighbours one should expect Δ to be larger than for the others. The results obtained by computing this parameter for several nuclides are represented in Fig. 39 and in Table 4.

The shell structure is clearly exhibited in this curve at nuclides for which N is equal to 20, 28, 50, 82, 126 and the effect is neater for high mass-numbers.

The work described in this paper was supported with funds from the University of São Paulo, and, in part, by the Conselho Nacional de Pesquizas.

REFERENCES

1. Kerst, D. W., Phys. Rev., 58, 841 (1940).
2. Kerst, D. W., Phys. Rev., 59, 110 (1941).
3. Kerst, D. W., Phys. Rev., 60, 47 (1941).
4. Katz, L., McNamara, A. G., Forsyth, P. A., Haslam, R. N. H., and Johns, H. E., Can. Journal of Research A28, 113 (1950).
5. Goldemberg, J., Pieroni, R. R., Santos, M. D. S., and Silva, E., "Simposio sobre novas tecnicas de pesquisa em fisica," published by the Academia Brasileira de Ciencias, Rio de Janeiro, 1954.
6. Pieroni, R. R., Ph.D. thesis (University of São Paulo), 1955.
7. Blatt, J. M., and Weisskopf, V. F., Theoretical Nuclear Physics, p. 656, John Wiley & Sons, New York, 1952.
8. McElhinney, J., Hanson, A. O., Becker, R. A., Duffield, R. B., and Diven, B. C., Phys. Rev. 75, 542 (1949).
9. Parsons, R. W., and Collie, C. H., Proc. Phys. Soc. A 43, 839 (1950).
10. Collie, C. H., Santos, M. D. S., Pieroni, R. R., Silva, E., and Borello, O., Proc. of the 1954 Glasgow Conference on Nuclear and Meson Physics, Pergamon Press, Ltd., London, 1954.
11. Sherr, R., Halpern, J., and Stephens, W. E., Phys. Rev. 81, 154 (1951).
12. Birnbaum, M., Phys. Rev. 93, 146 (1954).
13. Johns, H. E., Katz, L., Douglas, R. A., and Haslam, R. N. H., Phys. Rev. 80, 1062 (1950).
14. Santos, M. D. S., "Energy control for magnetic induction accelerators," thesis, 1953 (University of São Paulo press).
15. Li, C. H., Wahling, W., Fowler, W. A., and Lauritsen, C. C., Phys. Rev. 83, 512, (1951).
16. Ajzenberg, F., and Lauritsen, T., Rev. Mod. Phys. 24, 321 (1952).
17. Spicer, B. M., Penfold, A. S., and Goldemberg, J., Phys. Rev. 95, 629 (1954).
18. Segré, E., Experimental Nuclear Physics, Vol. 1, John Wiley and Sons, 1953.
19. King, R. K., Rev. Mod. Phys. 26, 327 (1954).
20. Balwin, G. C., and Koch, H. W., Phys. Rev. 67, 1 (1945).
21. McElhinney, J., and Ogle, W. E., Phys. Rev. 78, 63 (1950).
22. Duckworth, H. E., and Hogg, B. C., Can. Journal of Physics, 32, 238, 1953.
23. Nassbaum, R. H., *et al.*, Physica XX, 8, 571 (1954).
24. Ogle, W. E., Brown, L. J., and Carson, A. N., Phys. Rev. 78, 63 (1950).
25. Axel, P., and Fox, J. D., Phys. Rev. 95, 613 (A) (1954).
26. Katz, L., and Cameron, A. G. W., Can. J. of Physics 29, 518 (1951).
27. Low, W., and Townes, C. H., Phys. Rev. 80, 608 (1950).
28. Blatt, J. M., and Weisskopf, V. F., Theoretical Nuclear Physics, p. 373, John Wiley and Sons, New York 1952.
29. Byerly, P. R., and Stephens, W. E., Phys. Rev. 83, 54 (1951).
30. Katz L., and Penfold, A. S., Phys. Rev. 81, 815 (1951).
31. Haslam, R. N. H., Summers-Gill, R. G., and Crosby, E. H., Can. J. Res. 30, 257 (1952).
32. Katz, L., Johns, H. E., Baker, R. G., Haslam, R. N. H., and Douglas, R. L., Phys. Rev. 82, 271 (1951).
33. Horsley, J., Haslam, R. N. H. and Johns, H. E., C. J. Phys., 30, 159 (1952).
34. Johns, H. E., Horsley, J., Haslam, R. N. H., and Quinton, R., Phys. Rev. 84, 856 (1951).
35. Way, K. and Wood, M., Phys. Rev. 94, 119 (1954).
36. Butement, F. D. S., Proc. Phys. Soc. A64, 395 (1951).
37. Price, G. and Kerst, D. W., Phys. Rev. 77, 806 (1950).
38. Goldhaber, M., and Hill, R. D., Rev. Mod. Phys. 24, 179 (1952).
39. Montalbetti, R., Katz, L., and Goldemberg, J., Phys. Rev. 91, 659 (1953).
40. Surugue, J., Comp. Rend. 212, 337 (1941).
41. Cameron, A. G. W., Harms, W., and Katz, L., Phys. Rev. 83, 1264 (1951).
42. Goldemberg, J., and Katz, L., Phys. Rev. 90, 308 (1953).
43. Del Rio, C. S., and Telegdi, V. L., Phys. Rev. 90, 439 (1953).
44. Goldhaber, M., and Teller, E., Phys. Rev. 74, 1046 (1948).
45. Levinger, J. S., and Bethe, H. A., Phys. Rev. 78, 115 (1950).
46. Levinger, J. S., and Kent, D. C., Phys. Rev. 95, 418 (1954).
47. Goldemberg, J., and Katz, L., Can. J. Phys., 32, 49 (1954).
48. Nathans, R., and Halpern, J., Phys. Rev. 93, 437 (1954).
49. Mayer, M. G., and Jensen, J. H. D., Elementary Theory of Nuclear Shell Structure, p. 35, John Wiley and Sons, New York, 1955.
50. Goldemberg, J., and Katz, L., Can. J. Phys. 32, 49 (1953).
51. Haslam, R. N. H., Johns, H. E., and Horsley, R. J., Phys. Rev. 82, 270 (1951).
52. Summers-Gills, R. G., Haslam, R. N. H., and Katz, L., Can. J. Phys. 31, 70 (1953).
53. Katz, L., Pease, L., and Moody, H., Can. J. Phys. 30, 476 (1952).
54. Katz, L., Baker, R. G., and Montalbetti, R., Can. J. Phys. 31, 250 (1953).
55. Diven, B. C., and Almy, G. M., Phys. Rev. 80, 407 (1950).
56. McPherson, D., Pederson, P., and Katz, L., Can. J. Phys. 32, 593 (1954).
57. Katz, L. and Cameron, A. G. W., Phys. Rev. 84 1115 (1951).

Angular Correlation of Fission Neutrons

By K. Skarsvåg,* Norway

INTRODUCTION

An experimental curve of the angular dependence of coincidences between fission neutrons can tell us how many neutron pairs are emitted by opposite fragments and by the same fragment. Since the average number of neutrons emitted per fission is 2.5 ± 0.1,[1] and the probability of emitting neutrons is about thirty per cent greater for the light fragment than for the heavy,[2] the mean square of the number of neutrons emitted per fission can be found by a neutron-neutron coincidence experiment. Previous measurements by De Benedetti *et al.*[3] were uncertain at small angles, and we have therefore attempted to perform more accurate measurements in this region.

EXPERIMENTAL PROCEDURE

A beam of collimated slow neutrons was taken out of an isotope channel in J. E. E. P. The outer part of the collimator was of steel (32 cm long) and the inner part of graphite (132 cm long). The diameter of the opening was at the outer end 1.35 cm, and the collimated beam had a semi-angle of 0.9 degrees.

A block diagram of the experimental arrangement is shown in Fig. 1. As U^{235} was not available, natural uranium metal was used. For slow neutrons (0.025 ev) the total cross section of uranium metal is $\sigma = 16$ b[4] which gives a mean free path of $\lambda = 1.3$ cm. For fast neutrons (1 Mev) the corresponding values are $\sigma = 7$ b and $\lambda = 3.0$ cm.

Measurements were made for three dimensions of the uranium: 4.2 cm in length and 2.54 cm in diameter; 2.5 cm in length and 1.5 cm in diameter; and 1.3 cm in length and 1.5 cm in diameter.

The detector consists of a cylinder or button used in conjunction with a 6260 E.M.I. photomultiplier tube. The button is molded of Kalden† powder mixed with ZnS‡ powder and Kalden liquid. The detector is therefore very similar to the Hornyak detector.[6] The diameter of the button is 35 mm. The button contains $1/9$ ZnS by weight. The efficiency of the detector for fission neutrons was measured for different thicknesses of the button. It was found that the optimum thickness of a button containing $1/9$ ZnS was 6–7 mm.

Pulses from the last dynode of the photomultiplier are fed to a cathode follower, amplified in a one loop linear amplifier and fed to an E.F.P. 60 circuit discriminator.[5] The anode pulses from this circuit are counted by a scale of 256 and the secondary emission grid pulses are fed to a 6 BN6 coincidence circuit. The coincidence pulses are selected by a Schmitt trigger circuit and counted by a scale of 16.

Pulses produced by gamma rays in the detector are of shorter duration than the neutron pulses.[7] The ratio between the fast neutron counting rate and the gamma counting rate depends therefore upon the value of the *RC* time-constant at the input of the photomultiplier cathode follower. With a grid resistor of 10 Ω a favourable neutron to gamma sensitivity was obtained. in the neutron-neutron coincidence measurements a photomultiplier voltage was used which corresponds to an efficiency of less than $2 \times 10^{-4}\%$ for Na^{24} gamma-rays and 0.8% efficiency for Ra-Be neutrons, the cylindrical side of the button facing the source.

The detector is not only sensitive to fast neutrons and gamma-rays, but also to slow neutrons. In the neutron-neutron coincidence measurements a sheet of cadmium was used for shielding against the slow neutrons scattered in the uranium piece. The gamma pulses being smaller than the slow neutron pulses, the background was reduced in this way.

Due to the variable delays resulting from the different sizes of the pulses accepted in the pulse height selector, genuine coincidences are lost. A curve showing the number of genuine coincidences as a function of the resolving time was recorded. For resolving times $2\tau = 10^{-7}$ sec and 2×10^{-7} sec respectively, 60% and 90% of the genuine coincidences are recorded. In order to keep the coincidence rate stable, the resolving time $2\tau = 2 \times 10^{-7}$ sec was chosen. The resolving time was then stable to a few per cent, and the stability of the coincidence rate was within statistics.

COINCIDENCE MEASUREMENTS

In the first series of measurements the uranium radiator was 4.2 cm in length and 2.54 cm in diameter. The distance between the collimator and the radiator was 70 cm. In order to obtain a reasonably good angular resolution the cylindrical side of the button was facing the uranium radiator. The distance between the radiator and the button was 7.5 cm. Measurements were done at 36 degrees, 45 degrees, 60 degrees, 90 degrees, 120 degrees, 150 degrees and 180 degrees. The background counting rate, due to uncollimated and scattered fast neutrons and gammas, was

---

* Joint Establishment for Nuclear Energy Research, Kjeller, near Lilleström.

† Imperial Chemical Industries, Ltd., Welwyn Garden City, Herts, England.

‡ RCA phosphor number 33-Z-20 A.

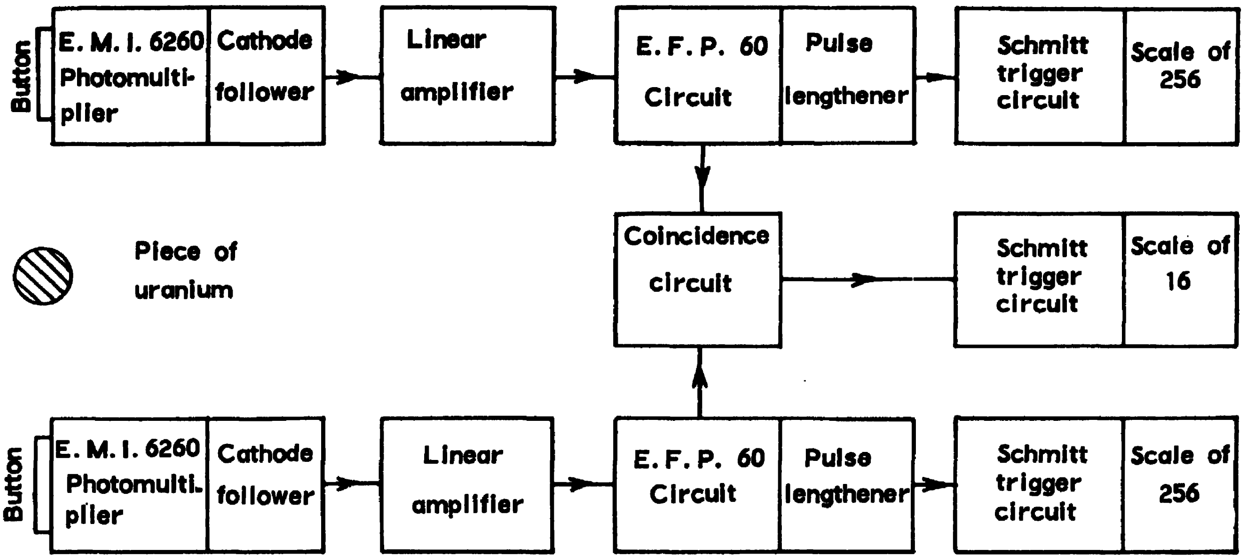

Figure 1. Experimental arrangement

found to be approximately given by the counting rate with the uranium radiator replaced by a lead scatterer of the same dimensions. The individual counting rate was 20,000 cpm and the background counting rate was 10% of this. The counting time for one angle was one day or one night. The points were recorded in such a sequence as to make it easy to detect any drift of the apparatus. The resolving time was measured by placing the detectors in the neutron beam, with a distance of 2 m between them, or alternatively, one of them in the beam from another channel. The resolving time was found to be independent of the counting rate. The resolving time was measured during the course of one night, with a standard error of less than 2%. One week was required to record a curve. Several curves were recorded in order to test the reproducibility. Fluctuations in the individual counting rates were assumed to be due to fluctuations in the efficiencies of the detectors. The genuine coincidence rate was therefore reduced to individual counting rates of 18,000 cpm by assuming the genuine coincidence rate to be proportional to the product of the individual counting rates.

Typical values recorded during one week are given in Table I.

The errors given are standard errors due to the counting statistics. It was considered possible that the shape of the curve could depend upon the discriminator level. A run with less amplification with a counting rate of 12,500 cpm was therefore performed. The background counting rate was 4%. The curve was normalized to the same counting rate as before. No appreciable difference was found.

Table I. Typical Values

Angle, degrees	*Coinc. per min.*
36	1.65 ± 0.11
45	1.48 ± 0.09
60	1.22 ± 0.08
90	1.07 ± 0.07
120	1.06 ± 0.08
150	1.39 ± 0.08
180	1.64 ± 0.08

For small angles a fast neutron can be detected by one detector and scattered into the other. De Benedetti *et al.*[3] corrected for this effect by replacing the U^{235} radiator by a Po-Be fast neutron source. As has been remarked in reference 3, the effect of scattering cannot be expected to be exactly the same for fission neutrons and Po-Be neutrons, due to the difference in energy distribution. Another approximation was therefore applied. The uranium piece was replaced by a Pb scatterer of the same dimensions. By putting a uranium slug in the centre of the channel a high flux of fast neutrons was obtained at the scatterer. The counting rate was 5000 cpm with the lead scatterer in position and 700 cpm without the lead scatterer. The coincidence rate was normalized to 18,000 cpm by assuming the coincidence rate to be proportional to the individual counting rates. A correction of 0.17 ± 0.05 cpm was found at 36 degrees, i.e., (10 ± 3)%. The fission spectrum is deformed by inelastic scattering, however. Due to this fact and due to the high counting rate without the scatterer in position, the uncertainty in the correction is somewhat larger.

In order to improve on the angular resolution and reduce errors due to the large size of the radiator a second series of measurements was performed with a piece of uranium 15 mm in diameter and 25 mm long. The distance between the collimator and the uranium piece was 13 cm. Measurements were made at 30, 60, 90, 120, 150 and 180 degrees. The curve was recorded for three photomultiplier voltages corresponding to counting rates of 9600, 12,800 and 16,000 cpm and a background of 4%, 5% and 6%, respectively. Each curve was repeated twice in order to check the stability and to improve the statistics. Measurements were performed at 0 degrees, one detector 13 cm behind the other, for the two highest photomultiplier voltages used. In order to avoid shielding of the farthest by the nearest button, a run was also made at 5 degrees (at the middle photomultiplier voltage). No appreciable difference was found between the curves at the three photomultiplier voltages. Measurements were also done in order to correct for coincidences due to scattering. Since the ratio between the elastic and inelastic scattering cross section is greater for bismuth than for lead,[8] the uranium radiator was replaced by a bismuth scatterer instead of a lead scatterer. The results were reduced to an individual counting rate of 12,000 cpm. A correction of 0.123 ± 0.022 coincidences/min was found at 30 degrees. The uncorrected value at 30 degrees being 0.761 ± 0.036 coincidences/min, the correction was (16 ± 3)% and the corrected value (0.638 ± 0.042) coincidences/min. The correction at 0 degrees cannot be found by simply placing the two detectors in a collimated fast neutron beam, as the neutrons from the uranium radiator are collimated. As an approximation the correction was taken to be that measured with one detector in the beam and the other at an angle of 10 degrees with the beam, as seen from the first detector. The correction was found to be 0.0193 ± 0.0058 coincidences/min when normalized to 12,000 cpm for the detector nearest the neutron source. The uncorrected value at 0 degrees being 0.0977 ± 0.0096 coincidences/min, the correction was (20 ± 6)% and the corrected value 0.0784 ± 0.0112 coincidences/min, and when normalized to 12,000 cpm for the other detector, 0.811 ± 0.116 coincidences/min. The values of the coincidence rates then become those shown in Table II.

Table II. Corrected Rates

Angle, degrees	*Coinc. per min.*
0	0.811 ± 0.116
30	0.638 ± 0.042
60	0.524 ± 0.036
90	0.455 ± 0.029
120	0.503 ± 0.036
150	0.681 ± 0.040
180	0.762 ± 0.032

As will be seen the minimum is slightly more pronounced in this series of measurements than in the first one.

As a Ra-Be source of the same dimensions as the uranium radiator was available, the coincidences due to scattering with this source were measured. A correction of 0.174 ± 0.020 coincidences/min was found at 30 degrees and 0.0452 ± 0.0063 coincidences/min at 0 degrees, i.e., (23 ± 3)% and (46 ± 8)%. This shows that the correction obtained with a Ra-Be source is too large, and since the energy distribution of Po-Be neutrons and Ra-Be neutrons is not very different it can explain the result of De Benedetti *et al.*

A third series of measurements was made with special care to reduce the coincidences due to scattering at 0 degrees. When a neutron is elastically scattered by a proton, the recoil proton energy E_p is given by

$$E_p = E_0 \sin^2 \theta$$

where θ is the angle of deflection and E_0 is the original energy of the neutron. Since the lowest detectable recoil proton energy is of the order of 0.2 Mev,[6] the coincidence rate due to scattering can be reduced by reducing the dimensions of the radiator and the detectors. The length of the uranium piece was therefore reduced to 1.3 cm and the sides of the button were cut as parallelopipeds with widths equal to the radius of the original buttons. Measurements were made at 0, 5, and 180 degrees, and the counting time for one angle was 5000 min. The measurements were normalized to 8400 cpm. The uncorrected values at 0 and 5 degrees were 0.0450 ± 0.0043 and 0.0495 ± 0.0044 coincidences/min. A run was made with one detector in the beam and the other at an angle of 0, 5 and 10 degrees with the beam as seen from the first detector. The coincidence rate is rather constant in this region of the angle and the corrections at 0 and 5 degrees were found to be 0.0090 ± 0.0020 and 0.0090 ± 0.0010 coincidences/min respectively. The corrected values at 0 degrees were then 0.0360 ± 0.0047 and 0.0405 ± 0.0045 coincidences/min respectively. When normalized to 8400 cpm in the second detector the values at 0, 5 and 180 degrees were as shown in Table III.

This is in good agreement with the measurements at 0 and 180 degrees in the second series of measurements.

THE THEORY OF THE EXPERIMENT

The choice of the model of emission of fission neutrons is guided by the fact that it must give the laboratory energy distribution of fission neutrons[9] and also the angular distribution, relative to the direction of motion of the fragments, of the fission neutrons as recorded by Fraser.[2]

The following assumptions are made:

1. Isotropic emission in the centre-of-mass system of fragment and neutron.
2. A Maxwell-Boltzmann energy distribution in the c.m. system

$$\Phi(\eta) = \frac{2\pi}{(\pi Q)^{3/2}} \eta^{1/2} e^{-\eta/Q} \qquad (1)$$

where Q is an energy which corresponds to the "temperature" of the fragment and η is the neutron energy in the c.m. system.

3. Fragment velocity at the time of neutron emission corresponding to the full kinetic energy.
4. The neutrons are all emitted in the most probable fission mode.

Table III

Angular separation, degrees	*0*	*5*	*180*
Coinc. per min	0.408 ± 0.053	0.390 ± 0.043	0.382 ± 0.013

5. The energy distribution of the neutrons in the c.m. system is the same for the light and heavy fragments and independent of the number of neutrons emitted, i.e., the values of the constants Q are set equal.

6. The ratio of the neutron emission probability of the light fragment to that of the heavy is R.

The values of the most probable velocities for the two fragments are taken from Leachman's velocity measurements[10]

$$v_1 = \begin{cases} 14.19 \times 10^8 \text{ cm/sec} \\ 9.65 \times 10^8 \text{ cm/sec} \end{cases}$$

Taking the mass of the neutron as the mass unit and Mev as the energy unit, we get:

$$\text{Velocity unit} = (\text{Mev/neutron mass})^{1/2} = 0.97858 \times 10^9 \text{ cm/sec}$$

and

$$v_1 = \begin{cases} 1.450 \text{ velocity units} \\ 0.986 \text{ velocity units} \end{cases}$$

Assumptions (1), (4) and (5) were also made by Fraser. As concerns assumption (3) Fraser could conclude from his experiment that the decrease in the kinetic energy of the fragment before neutron emission was not more than 5 Mev. The only difference between this model and that of Fraser is assumption (2), as Fraser uses a distribution given by Feld *et al.*[11] instead of the Maxwell-Boltzmann distribution. The two distributions are not very different and the Maxwell-Boltzmann distribution is preferred here, because it is simpler.

For R the value found by Fraser, $R = 1.3 \pm 0.1$, is used.

In Fraser's curve[2] with all fragments allowed, the ratio between the coincidence rate at 180 and 90 degrees is strongly dependent upon the value of Q and nearly independent of the value of R. This ratio can therefore be used to determine the value of Q, and $Q = 1.25$ Mev was found.

The laboratory fission neutron spectrum in terms of the fission neutron spectrum in the c.m. system is given by Feather.[12] For a Maxwell-Boltzmann distribution in the c.m. system Feather's formula gives

$$\Phi(E) = \frac{1}{(\pi Q)^{1/2}} \frac{1}{1+R} \left\{ R \left(\frac{M_L}{mE_L} \right)^{1/2} e^{-mE_L/M_LQ_c - E/Q} \sinh \frac{2}{Q} (EE_Lm/M_L)^{1/2} + \left(\frac{M_H}{mE_H} \right)^{1/2} e^{-mE_H/M_HQ_c - E/Q} \sinh \frac{2}{Q} (EE_Hm/M_H)^{1/2} \right\} \quad (2)$$

where M_L, M_H are the masses and E_L, E_H the kinetic energies of the light and heavy fragments respectively.

With the exception of the assumptions (4) and (6) the assumptions made are those of Watt. With the value of Q used by him, $Q = 0.875$ Mev, Equation 2 becomes

$$\Phi(E) = 0.1000e^{-E/0.875} \sinh 2.3436E^{1/2} + 0.2158e^{-E/0.875} \sinh 1.5936E^{1/2} \quad (2a)$$

This equation fits the experimental data of Watt quite well.

There seem therefore to be some discrepancies between the data of Watt and those of Fraser, as will also be seen from the experimental and computed points at 60, 90 and 120 degrees in Fraser's curve for U^{235} with only the light fragment allowed.[2]

The calculations are therefore made for two values of Q, $Q = 0.875$ Mev and $Q = 1.25$ Mev.

According to assumption (1) the probability per unit solid angle in the fragment system that neutrons of emission energy η will emerge is $1/4\pi$. Let $f(\eta,\theta)$ be the probability per unit solid angle in the laboratory system that neutrons of emission energy η emerge at an angle θ (in the laboratory system) between the direction of the neutron and that of the fragment. As the same number of neutrons emerge into the differential solid angle $d\Omega_f$ about ψ in the fragment system as into $d\Omega$ about θ in the laboratory system, we have

$$\frac{1}{4\pi} d\Omega_f = f(\eta,\theta)\, d\Omega$$

We have

$$d\Omega_f = 2\pi \sin \psi \, d\psi$$

$$d\Omega = 2\pi \sin \psi \, d\psi \, |\cos(\psi - \theta)| \frac{v_2^2}{v_3^2}$$

where v_2 and v_3 are the neutron velocities in the fragment and laboratory systems, respectively. We then have

$$f(\eta,\theta) = \frac{1}{4\pi} \frac{v_3^2}{v_2 |v_3 - v_1 \cos \theta|} \quad (3)$$

If we measure the angular distribution of the neutrons around the direction of the fragment by means of a neutron counter of efficiency $\epsilon(E)$, the number of counts per neutron and per unit solid angle will be:

$$F(\theta) = \int_0^\infty \Phi(\eta) f(\eta,\theta) \epsilon[E(\eta,\theta)]\, d\eta \quad (4)$$

as a function of the angle θ.[3] Let

$$F_f(\theta) = \Sigma a_{fl} P_l(\mu) \quad (5)$$

represent the expansion of $F_f(\theta)$ in series of spherical harmonics, where $\mu = \cos\theta$ and f means L or H, i.e., light or heavy fragment. Let ω be the solid angle covered by each of the two detectors, and λ the angular separation between the detectors, and let us define $\alpha = \cos\lambda$. Calculating along the same lines as De Benedetti it may be shown that in the case of emission of one pair of neutrons per fission, the number of coincidences per fission as a function of α is

$$c_f(\alpha) = 2\omega^2 \sum \frac{a_{fl}}{2l+1} P_l(\alpha) \quad (6)$$

Table IV

Angle, degrees	*0*	*30*	*60*	*90*	*120*	*150*	*180*
$\dfrac{c_L(\alpha)}{Q}$	10.3002	7.9611	3.8596	1.3517	0.4290	0.1699	0.1189
	8.7411	7.1828	4.1339	1.8526	0.7662	0.3705	0.2765
$\dfrac{c_H(\alpha)}{Q}$	3.6810	3.1904	2.1337	1.1911	0.6305	0.3764	0.3070
	3.6764	3.2982	2.4320	1.5673	0.9752	0.6684	0.5772
$\dfrac{c'(\alpha)}{Q}$	0.2325	0.3023	0.5905	1.3557	2.9147	4.9530	5.9828
	0.4639	0.5663	0.9422	1.7763	3.1874	4 7789	5.5204

if both neutrons are emitted by the same fragment, and

$$c'(\alpha) = 2\omega^2 \sum (-1)^l \frac{a_{L2}a_{H1}}{2l+1} P_l(\alpha) \qquad (7)$$

ff both neutrons are emitted by opposite fragments.

Finally, if $\bar{\pi}_L$ pairs of neutrons on the average are originating from the light fragment, $\bar{\pi}_H$ from the heavy fragment and $\bar{\pi}'$ from opposite fragments, the number of coincidences per fission becomes

$$c(\alpha) = \bar{\pi}_L c_L(\alpha) + \bar{\pi}_H c_H(\alpha) + \bar{\pi}' c'(\alpha) \qquad (8)$$

where the bars indicate average values.

Assuming no light absorption in the Hornyak button, the efficiency $\epsilon(E)$ may be calculated along the same lines as for a detector using a thick radiator[13]

$$\epsilon(E) = b\{E - \tfrac{5}{2}B^{3/2}E^{-1/2} + \tfrac{3}{2}B^{5/2}E^{-3/2}\} \qquad (9)$$

where b is a constant and B is the bias energy.

Hornyak measured the efficiency for 0.50-Mev neutrons, Po-Be neutrons and 14.2-Mev neutrons. According to his curves the efficiency for one discriminator setting may be approximated by

$$\epsilon(E) = bE$$

or

$$\epsilon(E) = \frac{\epsilon_0}{v_{30}^2} v_3^2 \qquad (9a)$$

where ϵ_0 is the efficiency at the neutron velocity v_{30}.

We then have for $F(\theta)$

$$F(\theta) = \frac{\epsilon_0}{v_{30}^2\pi}\left(\frac{2Q}{\pi m}\right)^{1/2} e^{-p}\left\{\frac{v_1}{2}\left[\frac{5}{2}\cos\theta + p\cos^3\theta\right] + e^{p\cos^2\theta}\left[\frac{3}{4} + 3p\cos^2\theta + p^2\cos^4\theta\right]\left[\left(\frac{\pi Q}{2m}\right)^{1/2} + \int_0^{v_1\cos\theta} e^{-\frac{m}{2Q}x^2}\,dx\right]\right\} \qquad (4a)$$

where $p = mv_1^2/2Q$.

$$\frac{\epsilon_0}{v_{30}^2\pi}\left(\frac{2}{\pi m}\right)^{1/2}$$

is in the following set equal to 1.

Using the first eight and seven terms respectively in Taylor's expansion of

$$e^{p\cos^2\theta} \text{ and } \int_0^{v_1\cos\theta} e^{-\frac{m}{2Q}x^2}\,dx$$

we expand $F(\theta)$ in series of spherical harmonics.

$c_f(\alpha)$ and $c'(\alpha)$ are then given by Equations 6 and 7 with good accuracy by eight terms.

The result is given in Table IV for $Q = 0.875$ Mev and $Q = 1.25$ Mev respectively.

For a fission accompanied by ν neutrons of which n_1 from the light fragment and n_2 from the heavy fragment, we have

$$\pi_L = \tfrac{1}{2}n_1(n_1 - 1)$$

$$\pi_H = \tfrac{1}{2}n_2(n_2 - 1)$$

$$\pi' = n_1 n_2$$

$$\pi_L + \pi_H = \tfrac{1}{2}\nu(\nu - 1) - n_1 n_2$$

On the average we have according to assumption (6):

$$\frac{\bar{n}_1}{\bar{n}_2} = R$$

$$\bar{n}_1 + \bar{n}_2 = \bar{\nu}$$

$$\bar{\pi}_L + \bar{\pi}_H = \tfrac{1}{2}(\overline{\nu^2} - \bar{\nu}) - \bar{n}_1\bar{n}_2$$

$$\bar{\pi}' = \bar{n}_1\bar{n}_2$$

Let us define

$$\beta = \frac{\bar{\pi}_L + \bar{\pi}_H}{\bar{\pi}'} \qquad (10)$$

$\overline{\nu^2}$ is then given by

$$\overline{\nu^2} = \bar{\nu} + 2(1 + \beta)\frac{R}{(1 + R)^2}\bar{\nu}^2 \qquad (11)$$

Since $\bar{\nu}$ and R are known, and β is found from this experiment, $\overline{\nu^2}$ can be found from Equation 11.

COMPARISON WITH EXPERIMENTS

A ratio of $\bar{\pi}_L$: $\bar{\pi}_H$: $\bar{\pi}'$ which gives a good fit of Equation 8 to the experimental curve of the second series of measurements is found by the method of least squares,[14] Fig. 2. The experimental curve has not been corrected for the angular resolution, and each point is given a weight inversely proportional to the square of the standard error. The value of β and $\bar{\nu}^2$ can then be found from Equations 10 and 11 respectively. The result for $Q = 0.875$ Mev and $Q = 1.25$ Mev is

Q (*Mev*)	$\bar{\pi}_L$	$\bar{\pi}_H$	$\bar{\pi}'$	β	$\overline{\nu^2}$
0.875	(−10±5)%	(78±11)%	(32±1)%		
1.25	(12±9)%	(41±17)%	(47±3)%	1.1±0.1	9.0±0.6

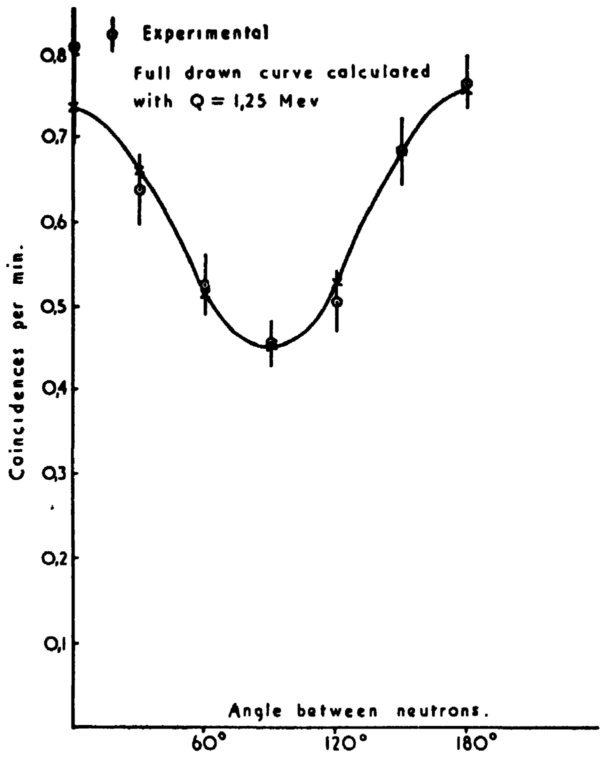

Figure 2. Comparison of the calculated and the experimental results

Since $\bar{\pi}_L$ comes out negative for $Q = 0.875$ Mev, the calculation was repeated with only $c_{II}(\alpha)$ and $c'(\alpha)$

Q (*Mev*)	$\bar{\pi}_{II}$	$\bar{\pi}'$	β	$\overline{\nu^2}$
0.875	(63 ± 3)%	(37 ± 1)%	(1.7 ± 0.1)	(10.8 ± 0.8)

It is interesting to see that if the number of neutrons had a Poisson distribution we would have for $\bar{\nu} = 2.5$,

$$\overline{\nu^2} = 8.75$$

$Q = 1.25$ Mev, which was in good agreement with Fraser's curve, gives a reasonable result. The result with $Q = 0.875$ Mev is not reasonable and seems therefore to be in disagreement with both this experiment and the data of Fraser.

The result in the experiment may, however, be influenced by the finite size of the neutron radiator, and of the roughness of the model used in the theory. Especially the assumptions (3) and (5) may influence the result.

It seems, however, justified to draw the conclusion that about equally many pairs of neutrons are emitted from opposite fragments as from the same fragment, since this conclusion is not so dependent upon the assumptions made.

ACKNOWLEDGEMENT

I wish to express my appreciation to Dr. Arne Lundby for valuable discussions, and to Messrs. T. Oistad, H. Hansen and J. Trana for numerical calculations.

REFERENCES

1. Nuclear Data for Low-power Reactors, Nucleonics, 8, No. 1, 78 (1951).
2. Fraser, J. S., *The Angular Distribution of Prompt Neutrons Emitted in Fission*, Phys. Rev. 88: 536–541, (1952).
3. De Benedetti, S., Francis, . E., Preston, W. M. and Bonner, T. W., *Angular Dependence of Coincidences between Fission Neutrons*, Phys. Rev., 74: 1645–50, (1948).
4. *Neutron Cross Sections*, A.E.C.U.—2040, May 15, (1952).
5. Lundby, A., Skarsvåg, K. and Andersen, E., Jener Report No. 13, (1952).
6. Hornyak, W. F., *A Fast Neutron Detector*, Rev. Sci. Instr., 23: 264–267, (1952).
7. Emmerich, W. S., *A Fast Neutron Scintillator*, Rev. Sci. Instr., 25: 69–70, (1954).
8. Mandeville, C. E. and Swann, C. P., *The Scattering of Fast Neutrons by Bismuth and Lead*, Phys. Rev., 84: 214–217, (1951).
9. Watt, B. E., *Energy Spectrum of Neutrons from Thermal Fission of U^{235}*, Phys. Rev., 87: 1037–41, (1952).
10. Leachman, R. B., *Velocities of Fragments from Fission of U^{233}, U^{235} and Pu^{239}*, Phys. Rev., 87: 444–447, (1952).
11. Feld, Feshbach, Goldberger, Goldstein and Weisskopf, A. E. C., Report NYO-636.
12. Feather, N., BR 335A (unpublished 1952) (see Ref. 2).
13. Barschall, H. H. and Bethe, H. A., *Energy Sensitivity of Fast Neutron Counters*, Rev. Sci. Instr., 18: 147, (1947).
14. Rose, M. E., *The Analysis of Angular Correlation and Angular Distribution Data*, Phys. Rev. 91, 610–615, (1953).

High Energy Gamma-Rays from Short-Lived Fission Products

By A. Lundby, B. Winther, E. Andersen, and H. Enger,* Norway

ABSTRACT

Short-lived gamma-rays from fission fragments are analyzed with a scintillation spectrometer. Measurements have shown that a gamma-ray with an energy of about 2.2 Mev is associated with the 0.5 sec period. Some low energy gamma-rays are found to follow a period of about 2 sec.

INTRODUCTION

Previous experiments have indicated that several high energy gamma-rays are emitted from the fission fragments with lifetimes of the order of seconds.[1] These gamma-rays have a great influence on the operation of a heavy-water moderated reactor. The energies, lifetimes and abundances of the gamma-rays are, however, not very well known. They follow beta-decays, but the genetic relationships may involve several beta-transitions before gamma-emission occurs. In this respect the periods of the delayed photoneutrons may differ from those of the delayed neutrons.

For longer periods (>1 hr) there is good agreement between measured photoneutron activities in Be and D_2O and those calculated with the known hard gamma-rays from fission products as sources.[2] These results have been verified in this laboratory by E. Germagnoli.† For periods less than one hour the agreement between the results of measurements of photoneutron periods in different laboratories is not very satisfactory.[3] Since more than 90% of the delayed photoneutrons seem to have lifetimes of less than one minute,[1] we have started experiments to measure the properties of the corresponding gamma-rays.

EXPERIMENTAL

Figure 1 shows the experimental arrangement. The "rabbit" consists of a piece of turbax shaped like a projectile, containing 18 gm natural uranium metal in the form of a cylinder 1 cm in diameter, 0.25 cm thick, and 1.5 cm long. The rabbit is pneumatically transferred from the surface of the reactor to the centre in 0.4 sec, irradiated for a variable time (0.7 sec in the experiments to be described here) and then ejected to the surface in 0.4 sec. The rabbit is locked into a fixed position when it reaches the lead block in which the scintillation detectors are located. Due to the shocks at the extreme positions the turbax projectile is damaged after a number of transfers. For this reason and in order to avoid build-up of activities in the uranium an arrangement is used so that the old rabbit can be changed with a fresh young rabbit in a few seconds.

The gamma-rays from the rabbit pass through a lead collimator with an opening 0.5 cm in diameter and 8.5 cm long. When the pair-spectrometer is used the central crystal has the dimensions 3 × 2.5 × 1.2 cm.[3] When a single Na(Tl) crystal is used this has a diameter of 3 cm and a length of 2.5 cm. The light from the crystals is detected with RCA 5819 photomultipliers and the pulses amplified in non-overload amplifiers. The pulses from the central detector are lengthened to about 5 microseconds and applied to the vertical deflection plates of a cathode ray oscillograph. The intensity of the oscilloscope beam is modulated with (*a*) the signals from the output of the triple coincidence circuit (see Fig. 1), (*b*) pulses from a pulse generator to indicate time, and (*c*) pulses triggered by a microswitch to indicate the time of arrival of the rabbit at the apparatus. The selected pulses are photographed on a moving film so that their magnitudes and time relationships can be derived.

RESULTS

Due to the finite resolving time of the electronic circuits the counting rates from the individual scintil-

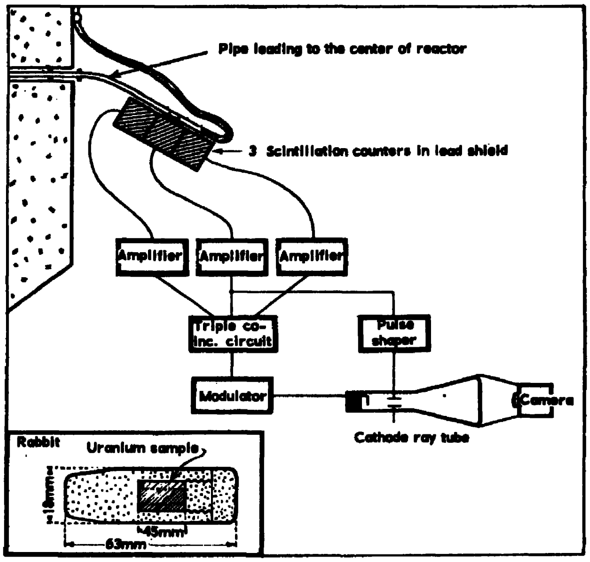

Figure 1. Experimental arrangement

---

* Joint Establishment for Nuclear Energy Research, Kjeller near Lilleström.

† Unpublished.

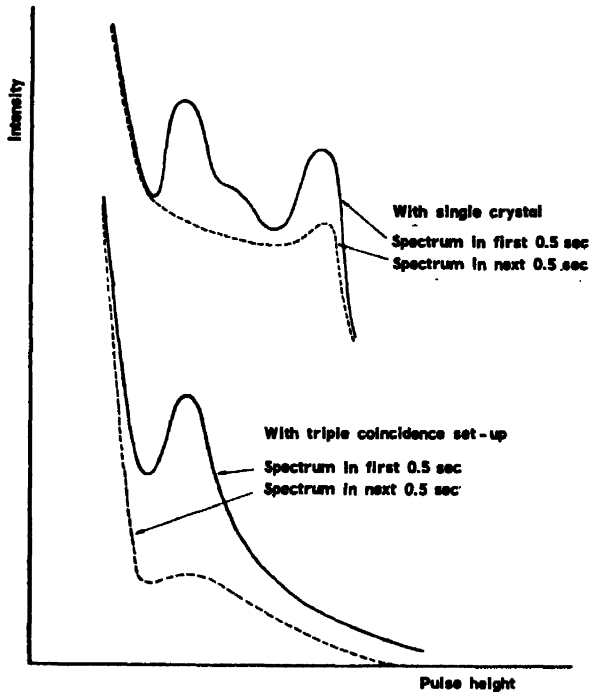

Figure 2. Delayed γ-rays from U^{235}

lation detectors has to be kept below about 5 × 10^3 per second. This condition is satisfied when the reactor is run at 3 kw. The central thermal neutron flux is then 9 × 10^9 cm^{-2} sec^{-1}.

When the rabbit is irradiated for 0.7 sec and the scintillation pair spectograph is used to observe the gamma-rays we obtain less than five pulses per run. The film moves in this case with a speed of 1 cm per second for 30 seconds. It takes another 20 seconds to change the old rabbit for a new. A complete run therefore takes about one minute.

Since we can only run the experiment one day per week it takes a long time to accumulate sufficient data. We hope in the near future to get a very large NaI(Tl) crystal so that we always can use a single-crystal spectrometer.

The results so far obtained are given in Fig. 2. In the upper part of the diagram the single-crystal results are shown and in the lower part the pair-spectrometer results. We have calibrated the horizontal scale with known gamma-ray lines. The gamma-ray responsible for the peaks in Fig. 2 is found to have an energy of 2.2 Mev ± 20%. We are therefore not yet able to say whether it is above the photodissociation threshold for the deuteron, and we have not yet calibrated the absolute intensity. The gamma-ray intensity decays with a period of about 0.5 sec.

The low energy component in Fig. 2 decays, on the other hand, with a period of about 2 sec. We are in the process of measuring the spectrum at somewhat longer irradiation times where this and other periods are more pronounced.

REFERENCES

1. Bernstein, S., Preston, W. M., Wolfe, G. and Slattery, R. E., *Yield of Photo-Neutrons from U^{235} Fission Products in Heavy Water*, Phys. Rev. 71: 573 (1947).
2. Ergen, W. K., *Hard Gamma Emitters among Fission Fragments*, ANP-59 (1951).
3. Johns, M. W. and Sargent, B. W. *Photoneutrons in a Heavy Water Pile*, Can. J. Phys. 32: 136 (1954).

Determinations of Fission Quantities of Importance to Reactors

By R. B. Leachman,* USA

INTRODUCTION

In recent months an increased knowledge of the fission process has been obtained through a series of extensive measurements and calculations that have not previously been reported. These studies were of the promptly emitted fragments, gamma rays, and neutrons from fission. These prompt radiations are to be distinguished from the neutrons, beta particles, and gamma rays emitted during the decay of the fission products. Both the prompt and delayed radiations from fission are of importance in reactor design and operation, but the prompt products are emphasized here because of their importance to an understanding of the fission process. The mass distribution of the fission products and the cross sections of neutron-induced fission are, similarly, quantities of importance to reactors and to fission studies, but are subjects which are discussed in other papers in this Conference.

Here, the new measurements of the energies of the fission fragments, gamma rays, and neutrons and also of the numbers of fission neutrons are discussed. Simple concepts of nuclear models are used in a calculation that results in values agreeing with these data. This satisfactory correlation is a result of the detail and accuracy of these recent measurements.

Finally, recent data of the angular relation between fragments and the neutrons inducing fission are discussed. These extensive new data have had only qualitative explanation by means of the collective model of fission.

FISSION FRAGMENT ENERGY

By far the greatest amount of the mass energy available in the fission process is liberated as the kinetic energy of the massive fission fragments. A study of the kinetic energy of the fission fragments is of importance for several reasons. First, an accurate measurement of this quantity is necessary for an evaluation of the total heat of fission, which is important in reactor power considerations. Second, the difference between the total prompt energy of fission (as determined from masses) and the kinetic energy of the fragments is the excitation energy of the primary fission fragments. This excitation energy appears in the emission of prompt neutrons and gamma rays from fission. Finally, it is of importance in reactor work to have knowledge of the processes by which this large amount of fission fragment energy is lost, particularly of the processes which lead to radiation damage of reactor fuel elements.

In the published literature are many reports[1] of the energy distributions of fission fragments as obtained by ionization chamber measurements. These measurements, particularly those made by double, "back-to-back," ionization chambers measuring simultaneously the energies of the fragment pairs, are easily made and provide a complete picture of the fragment energetics. Recently, however, measurements of the distribution of the fission fragment energies have been reported[2] by time-of-flight observations. This measurement provided less complete information on fragment energetics, but introduced considerably less dispersion in the data and provided data whose absolute accuracy could be readily determined. From this measurement and from other less direct determinations, the ionization chamber measurements of energy were shown to be low by about 7 per cent and to contain dispersions in the data amounting to roughly 8 Mev full width at half maximum.

The high neutron fluxes available in nuclear reactors have made possible recent direct determinations of the average energy of fission by calorimetry. A calorimetric measurement with a low neutron flux was made by Henderson[3] shortly after the discovery of fission. Shown in Fig. 1 is a schematic diagram of the essential parts of a fission calorimeter recently used by Leachman and Schafer at Los Alamos for measuring the average kinetic energy of the fission fragments from neutron-induced fission of U^{235}. The plate shown in this figure is the center plate of a back-to-back fission pulse counter for a twin determination of the fission rate in the U^{235} heater assembly. The heat is determined by substitution of electrical power in the heater for the fission power. The amount of electrical energy required for substitution is determined by temperature indications from the thermocouples. Measurements were made with this calorimeter in a thermal column of the Los Alamos Homogeneous Reactor as shown in Fig. 2. A value of 167 ± 2 Mev per fission was obtained, which agrees with the average from velocity measurements.

Determinations of the average heat of fission as observed in reactors must, in addition, take into account the neutron, gamma ray, and beta particle energies together with a consideration of the decay times of the delayed gamma rays and beta particles. These

---

* Including work by D. M. Barton, J. E. Brolley, Jr., J. E. Hammel, R. B. Leachman, N. G. Nereson, L. Rosen, H. W. Schmitt, and N. J. Terrell, Jr., Los Alamos Scientific Laboratory; R. L. Gamble, and J. L. Fowler, Oak Ridge National Laboratory; D. A. Hicks, J. Ise, Jr., and R. V. Pyle, University of California Radiation Laboratory.

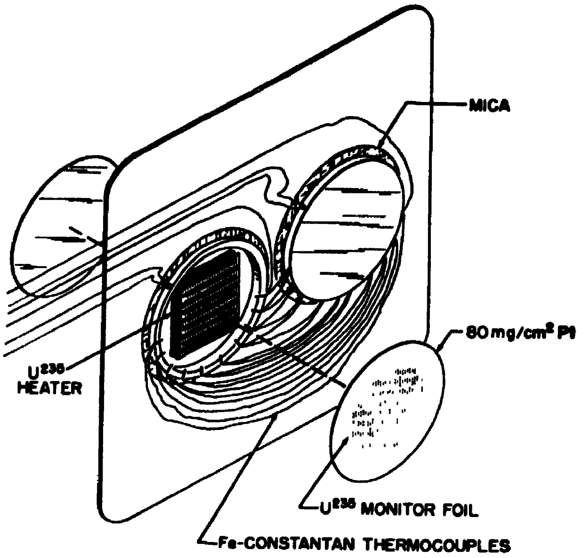

Figure 1. Center plate of the Los Alamos fission calorimeter. The cell on he right contains a heater of U^{238} similar to the U^{235} heater. Flux monitoring foils of U^{235} are on each side of the U^{235} heater

additional quantities can be determined from independent measurements and calculations. Meem[4] has recently reported a measurement of the average heat of fission as observed in the Oak Ridge Bulk Shielding Reactor which includes these quantities. When his results are corrected for recent cross sections of fission and of gold activation, the result of 186 ± 5 Mev for the equilibrium average energy of fission is in good agreement with the calorimeter results of kinetic energy and determinations of the other energies involved. The 19 ± 5 Mev difference between these calorimetric values is satisfactorily accounted for by the measured 5 Mev each for the prompt neutrons and the prompt gamma rays and the calculated[5] 11 Mev average of detectable decay energy of the fission products. From these recent measurements, the heat of fission is now a well established quantity that is about 7 per cent greater than previously established quantities from ionization chamber measurements.

Energy loss studies of fission fragments have recently been made by Schmitt and Leachman at Los Alamos that provide greater information on the methods by which this energy is lost. The measurements provide a confirmation of the nuclear recoil effect previously calculated by Knipp and Ling.[6] For these measurements, metal foils of various thicknesses were used to slow fission fragments into various energy groups. The average energy of each of these groups was determined by time-of-flight measurements. In separate measurements, the average ionization of each of these fragment energy groups when stopped in a gas was measured in an ionization chamber. In Fig. 3 are the results for stopping fragments in nitrogen. The positive intercepts of the energy-ionization curves on the energy axis for different stopping gases indicate that roughly 6–9 Mev of fission fragment energy is expended in nuclear recoils of the stopping material. In solid stopping materials these nuclear recoils lead to radiation damage in the materials.[7]

NUMBERS OF PROMPT NEUTRONS FROM FISSION

The number of neutrons from fission is of considerable concern in reactor design. This is especially true of $\bar{\nu}$, the average number of neutrons per fission. To a lesser extent this is true of the variation of ν from one fission event to another. The fluctuation in ν is closely related to the fluctuations in the neutron flux in subcritical reactors, but is not readily obtained from these flux fluctuations for the reason of complications in the neutron multiplication in the reactor. Recent measurements with large tanks of liquid scintillator provide data on ν with an accuracy and detail considerably greater than previously available. With regard to fission calculations, the number of fission neutrons is closely related to the excitation energy of fission as obtained from fission fragment energies. A correlation of these quantities is considered later.

The large tanks of liquid scintillator used in these recent measurements by Diven, Martin, and Terrell at Los Alamos and by Hicks, Ise, and Pyle at Berkeley are basically of the design published by Reines, *et. al.*,[8] but modified with the provision of a central tube containing the fission source and fission pulse counter. A similar tank of smaller size has been used at Los Alamos by Hammel and Kephart. As shown in Fig. 4, Diven, Martin and Terrell have given considerable attention to the neutron shielding of the large tank from the source of neutrons inducing fission. Only spontaneous fission has been studied by the other two groups. The number of neutrons for each of many thousands of fission events was observed on photographs of oscilloscope traces displaying the gamma ray pulses from neutron capture in the cadmium loading of the liquid scintillator. At Los Alamos, the efficiency of the large tank for detecting fission neutrons was accurately determined to be 82 ± 2 per cent by several independent means.

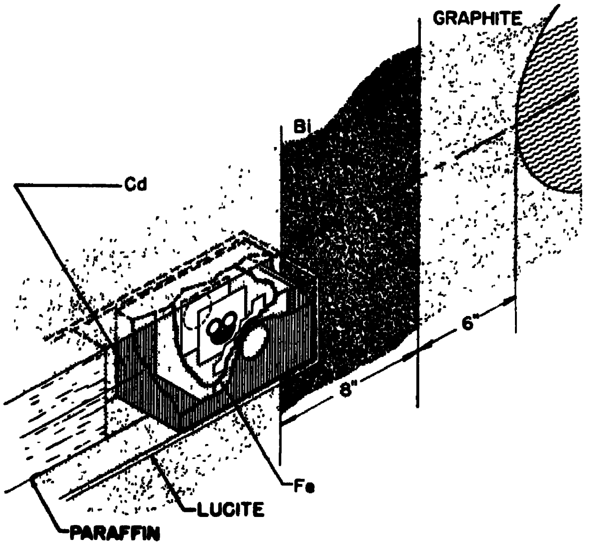

Figure 2. Position of the fission calorimeter in the south thermal column of the Los Alamos homogeneous reactor. The reactor sphere is on the right

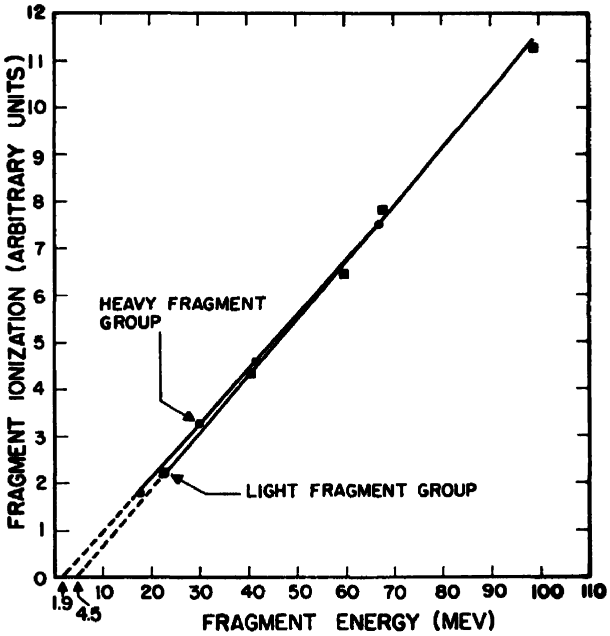

Figure 3. Energy-ionization relation of fission fragments in nitrogen

With such a high and accurately known detection efficiency for neutrons, this method of determining $\bar{\nu}$ and the fluctuation in ν has proved to be a valuable research instrument. It has been used for the study of fission neutrons from each of several nuclides that fission spontaneously and also from fission of several nuclides induced by neutrons of various energies. Some preliminary results from spontaneous fission of Cf^{252} have been published.[9] Examples of the results obtained from some Los Alamos measurements are shown in Fig. 5. Here the fluctuations in the number of neutrons emitted from fission of the compound nuclei U^{236} and Pu^{240} under different excitations are shown. Other such measurements are compared later with calculations of neutron emission.

Two additional measurements of the variation of $\bar{\nu}$ with the energy of neutrons inducing fission in U^{235} have recently been made by different methods. In these cases, the experimental arrangement did not allow a determination of the multiplicity of the neutrons. The results are of $\bar{\nu}(E_n)/\bar{\nu}_{th}$, where E_n is the energy of the neutrons inducing fission and $\bar{\nu}_{th}$ is for fission induced by thermal neutrons.

One of these measurements was made by Fowler at Oak Ridge with the method shown schematically in Fig. 6. In this measurement both the total number of fissions and the number of fissions in coincidence with detected fission neutrons were recorded. These data were taken with a source of thermal neutrons and, also, with a source of 1.0-Mev neutrons. The design of the neutron chamber provided a neutron detection efficiency that was nearly the same for various neutron energies. Cadmium was used to shield the fission chamber from scattered low-energy neutrons. From these measurements, Fowler obtained $\bar{\nu}(1\ \text{Mev})/\bar{\nu}_{th} = 1.15 \pm .14$ for U^{235}.

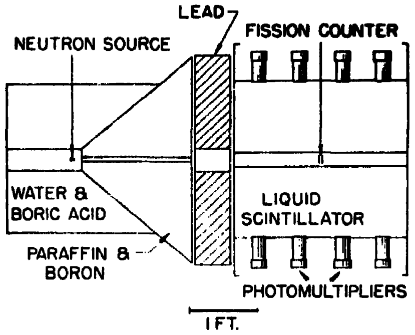

Figure 4. Schematic diagram of the scintillator tank used by Diven, Martin, and Terrell

The other measurement of $\bar{\nu}(E_n)/\bar{\nu}_{th}$ was made by Terrell at Los Alamos. He used a spherical shell of U^{235} surrounding a spiral fission counter of U^{238}. In one set of measurements, the sphere was bombarded by thermal neutrons. In the other set, 0.7-Mev neutrons were used. In each case, the numbers of fissions were determined by radio-chemical techniques from the amount of the Mo^{99} fission products in the U^{235}. The relative numbers of fission neutrons were measured by the U^{238} spiral counter. After correcting for background and other effects, Terrell found $\bar{\nu}(0.7\ \text{Mev})/\bar{\nu}_{th} = 1.02 \pm .02$ for U^{235}.

ENERGIES OF PROMPT NEUTRONS FROM FISSION

At Los Alamos, considerable attention has recently been given to a careful measurement of the energy distribution of neutrons from thermal-neutron induced fission of U^{235}. This has resulted in a somewhat different spectrum than previously measured.[10] Of convenience in reactor work are the semi-empirical expressions that accurately fit these new data. As discussed later, detailed calculations of this spectrum from over-all energy considerations of the fission processes are complicated by the large influence of the neutron-fragment angular correlation on the observed neutron energy.

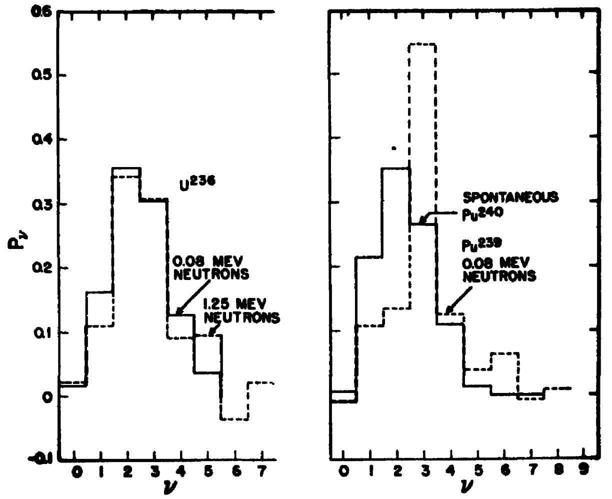

Figure 5. Observed fluctuations in ν as measured with a large tank of liquid scintillator a Los Alamos

Barton has used an expansion cloud chamber filled with low pressure hydrogen plus water vapor and has obtained the energy spectrum of the fission neutrons below 700 kev from proton recoil tracks in the chamber. In the intermediate region of neutron energies, Cranberg and Nereson have used a neutron time-of-flight measurement to obtain the energy spectrum of the fission neutrons in the 0.2 to 3 Mev interval. As shown in the schematic diagram of the equipment in Fig. 7, the time of the fission event is given by the fission pulse from a spiral fission counter, which also serves as the fission source. The time-of-flight between this pulse and a proton recoil pulse from a fission neutron in a plastic scintillator at 50-cm distance is measured on an oscilloscope trace. The high energy interval has been measured by Frye and Rosen by recoils in photographic emulsions. Their measurements are in the energy interval between 0.3 and 12 Mev. In these three sets of measurements of overlapping energy intervals, considerably improved statistics were obtained and more careful background measurements made than in the previously reported measurements of the neutron energy distribution.

A compilation of these three new sets of measurements is presented in Fig. 8 in which somewhat arbitrary normalizations of the sets of data to each other have been made. These data are compared with the semi-empirical expression $N(E) \propto [\exp(-E/0.965)]$ $[\sinh\sqrt{2.29E}]$, where $N(E)$ is the probability of a fission neutron with energy E. This convenient form has been used earlier by Watt[10] and is derived from simplest considerations of neutron emission and transformations of velocity frames. It has been used with both the nuclear "temperature" and the fragment energy as parameters that are adjusted to fit the experimental data. A further simplification of this semi-empirical expression results in the form $N(E) \propto \sqrt{E}$ $\exp(-E/1.29)$, which is shown in the figure similarly to provide a satisfactory fit with the experimental data. This fit with only the coefficient in the exponent as a parameter is regarded as fortuitous in view of the dependence of the neutron spectrum on the many variables such as fragment excitation, neutron binding energies and fragment energy.

PROMPT GAMMA RAYS FROM FISSION

After the primary fission products have emitted all the neutrons that are energetically possible, the residual excitation energy is expended in the emission of prompt gamma rays. With the distribution in the magnitude of the residual energy and with the energy level structure of the many primary fragments, the gamma ray spectrum is expected to be complex. Until the recent measurement to be described, little experimental or theoretical information on these gamma rays had been published. However, measurements of the prompt gamma rays have been reported[11] which have been made by Geiger counters with walls of medium atomic weight. This method of measurement of gamma rays in coincidence with the fission pulses provided a satisfactory measure of the average gamma ray energy, but the spectrum of the gamma rays could not be determined easily.

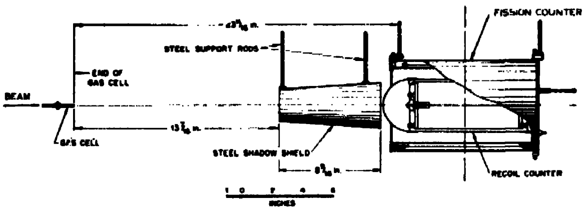

Figure 6. Schematic diagram of the fission neutron experiment made by Fowler. The neutron chamber in the center at the right detects proton recoils. Fissions are detected in the cylindrical, parallel plate ionization chamber. The neutron source is at the left

Recently, Gamble and Francis at Oak Ridge have observed the spectrum of the gamma rays in coincidence with fission by a NaI scintillation detector. Since the size of their detector resulted in distributions in pulse heights for the line sources of gamma rays used for calibration, the data obtained by Gamble and Francis were corrected for the response of the detector. The results, as shown in Fig. 9, indicate an exponentially decreasing probability with energy to a gamma ray energy of 7 Mev. However, the method of detection was sensitive to the inelastic scattering of prompt fission neutrons and so the average energy of the prompt gamma rays from fission is expected to be less than the 7.5 Mev obtained from the results in Fig. 9. Similarly, the average number of gamma rays per fission is expected to be less than the 7.5 from this measurement.

CORRELATION OF DATA ON PROMPT FISSION PRODUCTS

At Los Alamos, Leachman has investigated the correlation between calculations of these data of the

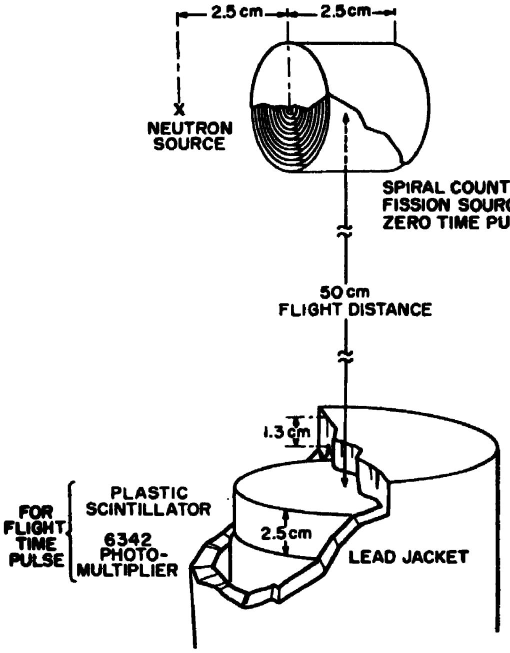

Figure 7. Schematic diagram of the time-of-flight equipment used for energy measurements of fission neutrons

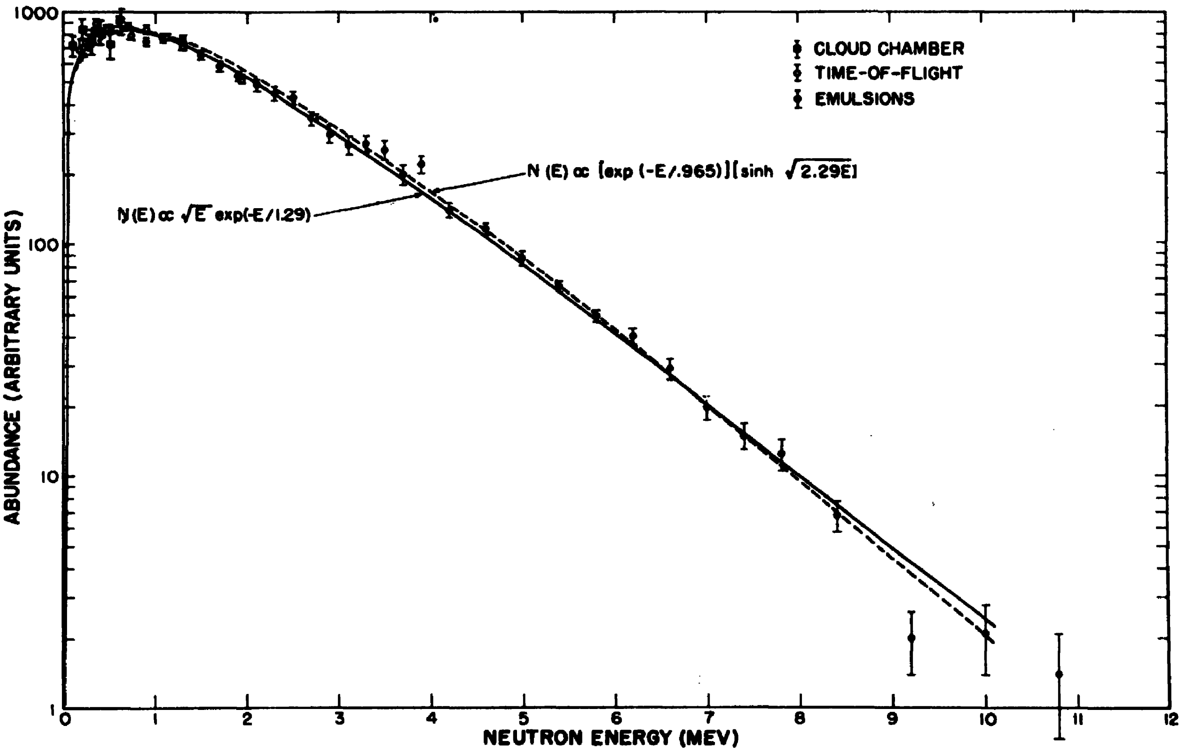

Figure 8. Comparison of semi-empirical expressions of the energy spectrum of fission neutrons with recent measurements of thermal-neutron-induced fission of U^{235}

promptly emitted fission products with results in satisfactory agreement with the recently measured quantities that are discussed above. The correlations have been based on simple concepts of: (1) the mass equation of fission, (2) neutron evaporation considerations, and (3) the mass surface of nuclides.

For each nuclide undergoing fission that is considered in this analysis, a separate analysis is made for several mass ratios of fission. For each mass ratio, the distribution in the total excitation energy shared by the fragment pairs is obtained by subtracting the distribution in the total kinetic energy of the fragment pairs from the total fission energy. The total fission energy is calculated from the mass equation of fission. After the dispersion in the data of the fragment kinetic energy has been removed mathematically and the distributions in the excitation energies of the individual fragments has been obtained by a convolution, the typical excitation energy distribution of the individual fragments shown in Fig. 10 is obtained. Also shown in Fig. 10 are the neutron emission probabilities based on the simple neutron emission concepts introduced by Weisskopf.[12] The neutron binding energies involved in this analysis are determined from the mass surface of nuclides as discussed by Coryell,[13] where attention is given to the effects of nuclear shells. The combination of the excitation and neutron emission data in Fig. 10 results in the distributions in the number of fission neutrons as shown in Fig. 11 for spontaneous fission and in Fig. 12 for neutron induced fission. For comparison, the experimental determinations of neutron emission obtained at Los Alamos and at Berkeley are also included.

Fowler, at Oak Ridge, has applied somewhat similar calculations to the variation of $\bar{\nu}$ with the energy of neutrons inducing fission. He first pointed out that the observed[1,14] constant average of the kinetic energy of the fission fragments results in an increasing excitation energy of the fragments with increasing energy of the incident neutrons. This fact has been applied to the above calculations to find the variation in $\bar{\nu}$. In this analysis, the absolute accuracy of the masses of the fission products have been corrected a few milli-mass units by a normalization to the $\bar{\nu}_{th}$ values from a recent compilation at the Brookhaven National Laboratory.[14]

The results of such calculations of the variation of $\bar{\nu}$ with the energy of neutron inducing fission are shown in Fig. 13 along with the experimentally measured values of Diven, Martin, and Terrell. The $\bar{\nu}(E_n)/\bar{\nu}_{th}$ values obtained by Fowler and by Terrell are in reasonable agreement with the results of Fig. 13. In the calculations of $\bar{\nu}$ the most sensitive parameter is the nuclear "temperature" used in the boil-off expression. The data in Fig. 13 are based on $T = 1.4$ Mev, a value obtained from $(n,2n)$ excitation functions. For U^{235}, a decrease of T from 1.4 Mev to 1.0 Mev in the calculations increases the slope $d\bar{\nu}/dE_n$ from 0.126 Mev^{-1} to 0.147 Mev^{-1}. Similarly an increase of T to 1.8 Mev decreases the slope to 0.116 Mev^{-1}. Even these large changes in T are seen to give calculated results in reasonable agreement with measured values.

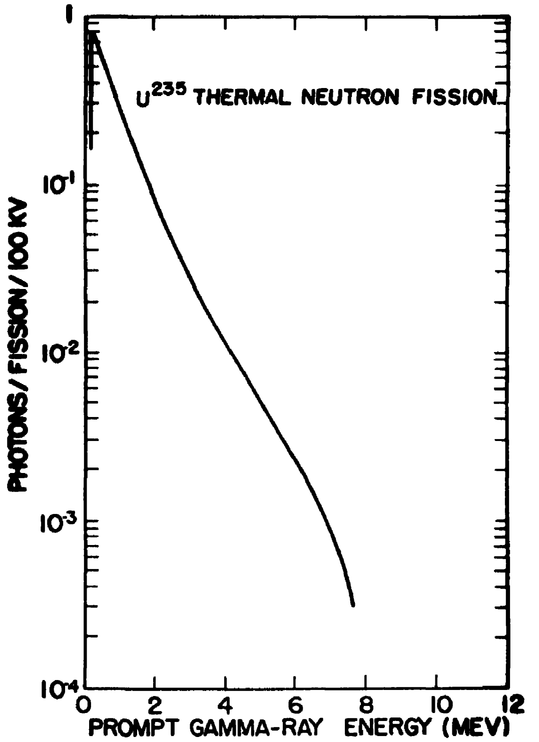

Figure 9. Prompt gamma-ray spectrum from fission of U^{235} as measured with a NaI crystal and coincidence techniques

Leachman has also made detailed calculations of the energy spectrum of the fission neutrons from thermal-neutron fission of U^{235} by a Monte Carlo method. These calculations were based on (1) the distributions shown in Fig. 10, (2) neutron energies with respect to the moving fragments based on neutron boil-off considerations, and (3) the assumption of an isotropic angular distribution of neutrons from the moving fragments. The resulting energy spectrum of the fission neutrons is, however, critically dependent upon assumption (3) at the low energy end of the spectrum and on the amount of the dispersion in the energy data (1) at the high energy end of the neutron spectrum. On the basis of the collective model of the nucleus the fission neutrons are, instead, expected to be preferentially emitted along the line of the fragment direction. In view of these difficulties, it is difficult to draw conclusions from the reasonable fit of the calculated energy distribution of the fission neutrons with the experimental values in Fig. 14.

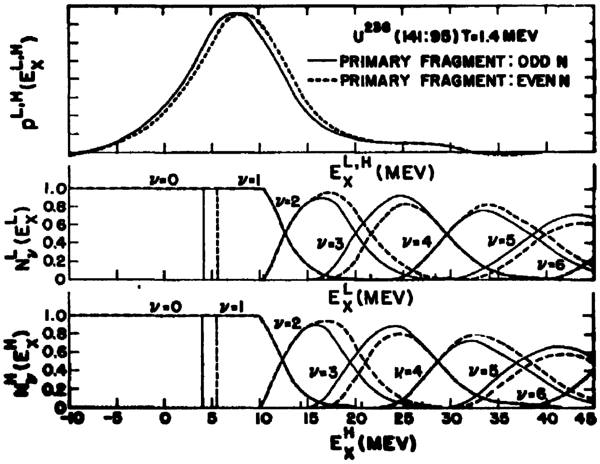

Figure 10. Calculated distributions for thermal-neutron fission of U^{235} into fragments in the regions of masses 141 and 95. At the top are the excitation energy distributions of the fragments. The distributions in the middle of the figure are the neutron emission probabilities of the mass 95 region as a function of the excitation energy $E_X{}^L$. Similar distributions for the mass 141 region are below. A "temperature" T = 1.4 Mev was used in the neutron emission calculations. Superscripts L and H refer to the light and heavy fragments, respectively

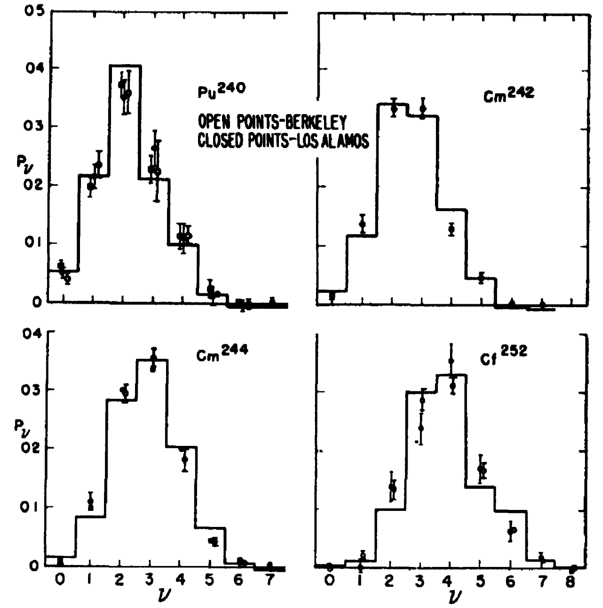

Figure 11. Calculated and observed variations in ν for spontaneous fission. Lines are calculated distributions. Data are: closed circles, Diven, Martin, and Terrell; closed squares, Hammel and Kephart; and open circles, Hicks, Ise, and Pyle

Also shown in Fig. 14 is the calculated energy spectrum of neutrons from 3.0-Mev neutron fission of U^{235}. For this calculation, an excitation energy distribution displaced to higher energy, as discussed above, is used. The increase of the energy of the incident neutrons is seen to increase the spectrum of fission neutrons to slightly higher energy.

The residual excitation energy appearing as prompt gamma ray energy from thermal-neutron fission of U^{235} is calculated by this analysis to be 3.9 Mev, which is in satisfactory agreement with the Geiger tube measurements[11] of 4.6 Mev and 5.1 Mev. Since the calculation of the gamma ray energy is independent of the neutron-fragment angle assumption (3), the agreement is considered significant. A calculation for 3-Mev neutron fission of U^{235} indicates a 0.2-Mev increase in the prompt gamma ray energy.

ANGULAR CORRELATION OF FRAGMENTS AND INCOMING NEUTRONS

Recent data of the angular correlation of the fission fragments with the neutrons of various energy inducing fission have been taken by Brolley, Dickenson, and

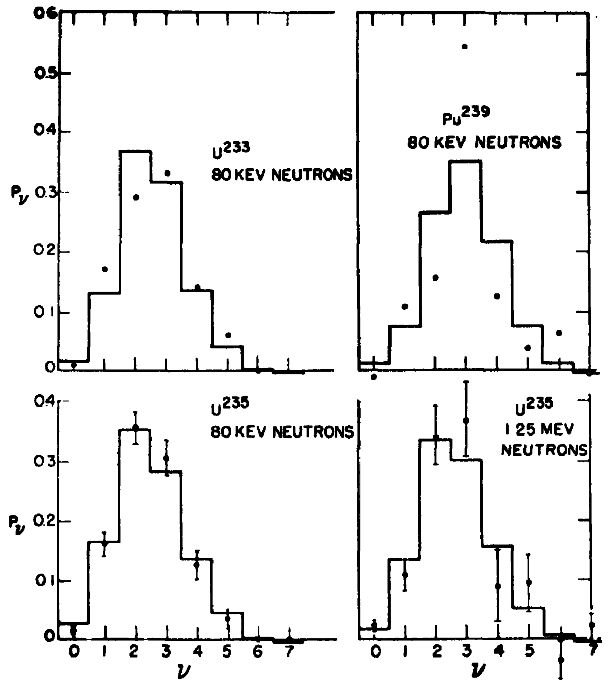

Figure 12. Calculated and observed variations in ν for neutron-induced fission. The statistical uncertainties in the U^{233} and Pu^{239} data are considerably greater than those indicated for the U^{235} data

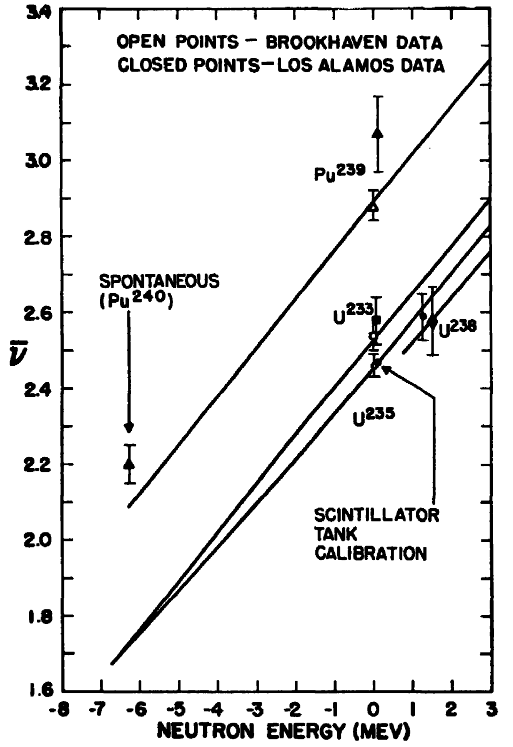

Figure 13. Observed and calculated variation of $\bar{\nu}$ with the energy of the neutrons inducing fission. The results of the calculations are given by lines

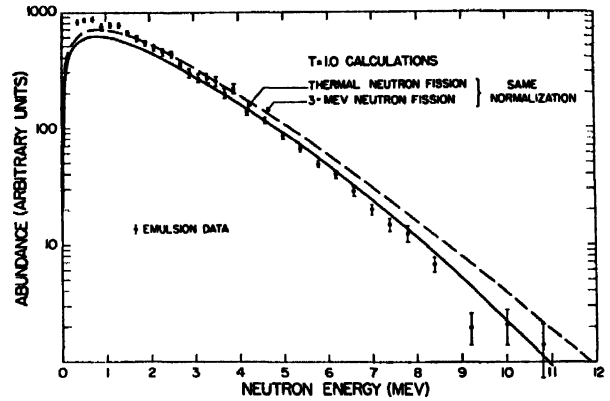

Figure 14. Comparisons of energy spectra of neutrons from U^{235} fission. Curves are of Monte Carlo calculations. Data are of thermal-neutron fission as observed by Frye and Rosen

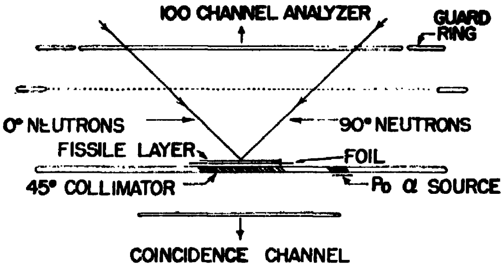

Figure 15. Schematic diagram of the fragment angular correlation experiment. Fission fragments in the upper ionization chamber are recorded only when in coincidence with complimentary fragments that go through the collimator into the lower ionization chamber

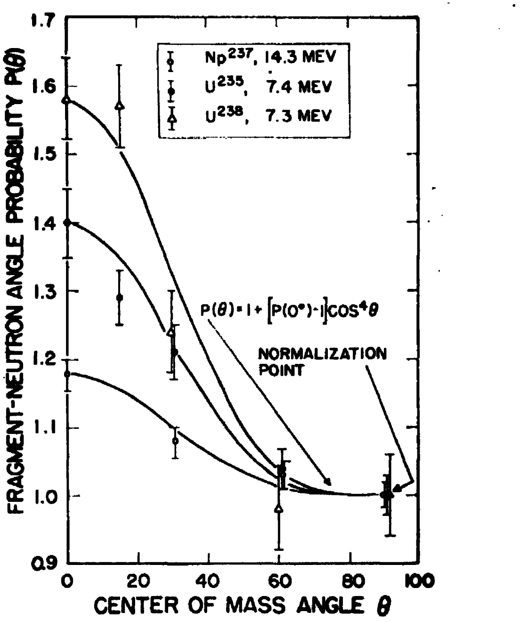

Figure 16. Angular relation of neutrons inducing fission and fission fragments

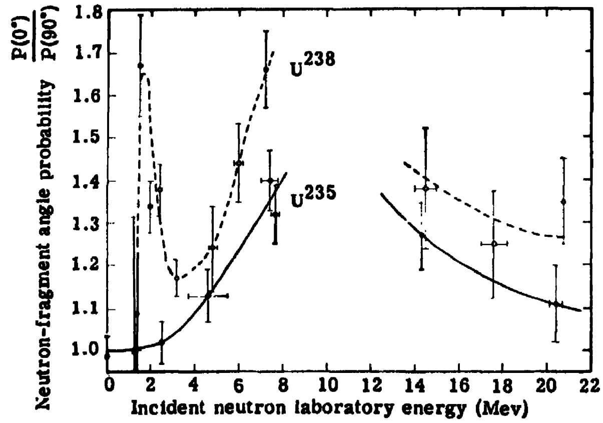

Figure 17. Observed anisotropies of fragments and incident neutrons as a function of the neutron energy

Henkel at Los Alamos. These new data provide considerably greater information than the preliminary data that have been published.[16] These results are closely related to the fission processes as described by the collective model of the nucleus. However, only qualitative explanations of these data have been made.

In Fig. 15 is shown a schematic diagram of the apparatus with which these angular correlation measurements have been made. By means of a rotation of the chamber assembly with respect to the direction of the incident neutrons, data of the angular distribution of the fission fragments as shown in Fig. 16 were obtained. These data are seen to fit an angular distribution with a strong $\cos^4 \theta$ dependence, where θ is the angle between the neutron and fragment directions. This angular relation is in agreement with the expectations from the collective model.

As the energy of the incident neutrons is varied, data of the anisotropy as a function of neutron energy as shown in Fig. 17 are obtained. The preference for fragments in the direction of the incident neutrons is in agreement with collective model considerations, just as similar published data from proton induced fission[17] and gamma-ray induced fission[18] are explained. Although it is not shown in the figures, additional data of fragment pulse heights, which are used to distinguish the heavy and light fragments, indicate a preference for the heavy fragment in the direction of the incident neutrons.

REFERENCES

1. Wahl, J. S., *Energy Distributions of Fragments from Fission of U^{235}, U^{238}, and Pu^{239} by Fast Neutrons*, Physical Review 95: 126–32 (1954), and earlier references listed in this paper.
2. Leachman, R. B., *Velocities of Fragments from Fission of U^{233}, U^{235}, and Pu^{239}*, Physical Review 87: 444–7 (1952).
3. Henderson, M. C., *The Heat of Fission of Uranium*, Physical Review 58: 774–80 (1940).
4. Meem, J. L., *Energy Released per Fission in the Bulk Shielding Reactor*, Nucleonics 12: No. 5, 62 (1954).
5. Way, K. and Wigner, E. P., *The Rate of Decay of Fission Products*, Physical Review 73: 1318–30 (1948).
6. Knipp, J. R. and Ling, R. C., *On the Ionization Yields of Heavy Particles*, Physical Review 82: 30–5 (1951).
7. Dienes, G. J., *Radiation Effects in Solids*, Annual Review of Nuclear Science 2: 187–220 (1953).
8. Reines, F., Cowan, C. L., Jr., Harrison, F. B. and Carter, D. C., *Detection of Neutrons with a Large Liquid Scintillation Counter*, Review of Scientific Instruments 25: 1061–70 (1954).
9. Hicks, D. A., Ise, J., Jr. and Pyle, R. V., *Multiplicity of Neutrons from the Spontaneous Fission of Californium-252*, Physical Review 97: 564–5 (1955).
10. Nereson, N., *Fission Neutron Spectrum of U^{235}*, Physical Review 85: 600–3 (1952). Bonner, T. W., Ferrell, R. A. and Rinehart, M. C., *A Study of the Spectrum of the Neutrons of Low Energy from the Fission of U^{235}*, Physical Review 87: 1032–4 (1952). Hill, D. L., *The Neutron Energy Spectrum from U^{235} Thermal Fission*, Physical Review 87: 1034–7 (1952). Watt, B. E., *Energy Spectrum of Neutrons from Thermal Fission of U^{235}*, Physical Review 87: 1037–41 (1952).
11. Kinsey, B. B., Hanna, R. C. and VanPatter, D., *Gamma Rays Produced in the Fission of U^{235}*, Canadian Journal of Research 26A: 79–98 (1948). Deutsch, M. and Rotblat, J., *Investigation of Fission Gamma Rays*, AECD 3179 (1944).
12. Blatt, J. M. and Weisskopf, V. F., *Theoretical Nuclear Physics*, John Wiley and Sons, New York (1952).
13. Coryell, C. D., Beta-Decay Energetics, *Annual Reviews of Nuclear Science* 2: 305–34 (1953).
14. Segrè, E. and Wiegand, C., *Energy Spectrum of Spontaneous Fission Fragments*, Physical Review 94: 157–8 (1954).
15. Hughes, D. J. and Harvey, J. A., *Neutron Cross Sections*, Brookhaven National Laboratory Report 325 (1955).
16. Brolley, J. E., Jr. and Dickinson, W. C., *Angular Distribution of Fragments from Neutron-Induced Fission*, Physical Review 94: 640–2 (1954).
17. Cohen, B. L., Coombe, D. J. and Ferrell, B. L., *Recent Progress in Fission Fragment Angular Distribution Measurements*, Physical Review 95: 303 (1954).
18. Winhold, E. J., Demos, P. T. and Halpern, I., *The Angular Distribution of Fission Fragments in the Photofission of Thorium*, Physical Review 87: 1139–40 (1952).

Some Problems of the Theory of Nuclear Fission

By B. T. Geilikman, USSR

I. THE SHAPE AND BARRIER AT THE FUSION OF TWO NUCLEI

In order to understand the peculiarities of the fission process (after the fission takes place) and the reverse process of the fusion of two nuclei, it is essential to determine the shapes of two contacting nuclei.

Let us consider only the variation of the shapes of two colliding nuclei, disregarding the variation of the charge distribution across the volume of the two nuclei.

This assumption is warranted since owing to the strong cohesion of protons and neutrons a greater energy is required for changing the charge distribution than for changing the shape of the nucleus. And truly, the energy of one quantum of the surface (quadrupole) oscillation for $A = 240$ is of the order of ~0.8 Mev whereas the energy of one quantum of the volume (dipole) oscillation is of the order of ~15 Mev.[1]

Let us assume that the shapes of the two nuclei differ little from the spherical one:

$$r_i(\theta_i) = R_i\left[1 + \sum_{n=0} \alpha_n^{(i)} P_n(\cos\theta_i)\right]; \qquad i = 1, 2$$

$$R_i = r_0 A_i^{1/3}; \qquad \alpha_n \ll 1 \tag{1}$$

Given a constant volume and the centre of inertia of each nucleus at rest, we can express α_0 and α_1 as a function of other α_n.*

Let us find the part of the energy of the nuclei that depends on their shape, i.e., the sum of surface and coulomb energy for a given value of the distance ar_0 between the centres of deformed spheres. The energy for each nucleus calculated by Bohr and Wheeler[2] and Frenkel[3] is:

$$U_i^{int} = 4\Pi r_0^2 A_i^{2/3}\sigma\left[1 + \sum_{n=2}\frac{(n-1)(n-2)}{2(2n+1)}(\alpha_n^{(i)})^2\right]$$
$$+ \frac{3}{5}\frac{Z_i^2 e^2}{r_0 A_i^{1/3}}\left[1 - \sum_{n=2}\frac{5(n-1)}{(2n+1)^2}(\alpha_n^{(i)})^2\right]; \qquad i = 1, 2 \tag{2}$$

where σ is the coefficient of the surface tension.

In our calculation of the coulomb energy of interaction for U_0 we shall retain only linear and quadratic terms in α_2 and α_3 (parameters, defining the symmetrical deformation and the asymmetrical one).

As a result of simple but rather long calculations we get the expression for U_{int} and then for the total energy $U = U_0 + U_{int}$:

$$\frac{U}{e^2/r_0} = \left[\frac{4\pi r_0^3\sigma A_1^{2/3}}{e^2} + \frac{3}{5}\frac{Z_1^2}{A_1^{1/3}} + \frac{4\pi r_0^3\sigma A_2^{2/3}}{e^2} + \frac{3}{5}\frac{Z_2^2}{A_2^{1/3}}\right]$$
$$+ \frac{Z_1Z_2}{a} + \frac{b_1}{2}(\alpha_2^{(1)})^2 + \frac{b_2}{2}(\alpha_2^{(2)})^2 + \frac{c_1}{2}(\alpha_3^{(1)})^2$$
$$+ \frac{c_2}{2}(\alpha_3^{(2)})^2 + d_1\alpha_2^{(1)} + d_2\alpha_2^{(2)}$$
$$+ e_1\alpha_3^{(1)} + e_2\alpha_3^{(2)} + f\alpha_2^{(1)}\alpha_2^{(2)} + h_1\alpha_2^{(1)}\alpha_3^{(2)}$$
$$+ h_2\alpha_3^{(1)}\alpha_2^{(2)} + g\alpha_3^{(1)}\alpha_3^{(2)} + k_1\alpha_2^{(1)}\alpha_3^{(1)}$$
$$+ k_2\alpha_2^{(2)}\alpha_3^{(2)}$$

$$b_i = \frac{6}{25}\left(\epsilon A_i^{2/3} - \frac{Z_i^2}{A_i^{1/3}} + \frac{10}{7}\frac{Z_1Z_2}{a^3}A_i^{2/3} + \frac{15}{7}\frac{Z_1Z_2}{a^5}A_i^{4/3}\right)$$

$$c_i = \frac{3}{7}\left(\epsilon A_i^{2/3} - \frac{4}{7}\frac{Z_i^2}{A_i^{1/3}} + \frac{8}{15}\frac{Z_1Z_2}{a^3}A_i^{2/3}\right.$$
$$\left. + \frac{6}{11}\frac{Z_1Z_2}{a^5}A_i^{4/3} + \frac{400}{429}\frac{Z_1Z_2}{a^7}A_i^2\right)$$

$$d_i = \frac{3}{5}Z_1Z_2A_i^{2/3}/a^3; \qquad e_i = \frac{3}{7}Z_1Z_2A_i/a^4$$

$$f = \frac{54}{25}Z_1Z_2(A_1A_2)^{2/3}/a^5; \qquad g = \frac{180}{49}Z_1Z_2A_1A_2/a^7$$

$$h_i = \frac{18}{7}Z_1Z_2(A_1A_2)^{2/3}A_i^{1/3}/a^6; \qquad k_i = \frac{Z_1Z_2}{a}\left(\frac{27}{70}\frac{A_i^{1/3}}{a}\right.$$
$$\left. + \frac{2}{7}\frac{A_i}{a^3} + \frac{5}{11}\frac{A_i^{5/3}}{a^5}\right); \qquad \epsilon = \frac{40\pi r_0^3\sigma}{3e^2}$$
$$i = 1,2$$

According to the estimates of Bohr and Wheeler[2] $\epsilon = 47.8$ and of Wöste $\epsilon = 45.5$.

The values of $\alpha_2^{(i)}$, $\alpha_3^{(i)}$, corresponding to the minimum U for a given distance a, are found through the system of four equations linear in $\alpha_2^{(i)}$ and $\alpha_3^{(i)}$:

$$\frac{\partial U}{\partial\alpha_2^{(i)}} = 0; \qquad \frac{\partial U}{\partial\alpha_3^{(i)}} = 0.$$

Original language: Russian.

* We shall later omit in Equation 1 the term $\alpha_1 P_1(\cos\theta)$, since we shall show below that $\alpha_3 \ll \alpha_2 \left(\alpha_3 \sim \frac{1}{10}\alpha_2\right)$. Then $\alpha_1 \ll \alpha_2$, since

$$\alpha_1 \simeq -9 \sum_{n=2}\frac{(n+1)}{(2n+1)(2n+3)}\alpha_n\alpha_{n+1}$$

This system was solved numerically for the value of a, which corresponds to the contact of two nuclei, i.e., for

$$a_c \simeq A_1^{1/3}(1 + \alpha_2^{(1)} + \alpha_3^{(1)}) + A_2^{1/3}(1 + \alpha_2^{(2)} + A_3^{(2)}).$$

Calculated values for $\alpha_2^{(i)}$, $\alpha_3^{(i)}$, a_c and barrier height for the fusion of nuclei $V = [(U)_{a=a_c} - (U)_{a=\infty}]$ for various values of Z_1, Z_2, A_1, A_2, and the value of the parameter $\epsilon = 47.8$ are given in Table 1 (with $\epsilon = 45.5$ the values practically coincide). For comparison we include in Table 1 the values of the height of the coulomb barrier, without deformation, this is $V_0/(e^2/r_0) = Z_1Z_2 \times (A_1^{1/3} + A_2^{1/3})^{-1}$ where $d = A_1^{1/3} + A_2^{1/3}$ is the distance between the centres of nondeformed spheres.

From Table 1 it follows that if the values Z_1, Z_2 are sufficiently large, the deviations, from the spherical shape are quite large $|\alpha_2| \sim 0.2 - 0.3$; we note that α_2 is always negative. The negative sign corresponds to the oblate shape of the nuclei (see Fig. 1). It is obvious that this shape (i.e., the "spreading" of the charge in the plane perpendicular to the line connecting the centres of the nuclei) corresponds to the minimum of the energy of the system.

Owing to the oblateness, the nuclei can draw closer than in the case of nondeformed nuclei, with the result that the barrier height increases markedly by about 15–20%. The values of α_3 are very small: $\alpha_3 \sim 0.02$–0.03. We can therefore hope, that the values obtained for the barrier height V are quite accurate. The values for α_3 are not so accurate because we have omitted the terms with α_1.

The main effect produced by the reduction of the distance a due to the oblate shape of the nuclei was overlooked in the paper of Breit *et al.*[5] This was indeed the main reason for the incorrect conclusion that the barrier is lowered by deformation. The dynamic effects, i.e., effects connected with the oscillation of nuclear shape during approach (which were considered[5] according to classical mechanics) are not essential because of the quasistatic character of the process (see section II below).

In our calculations of the equilibrium of nuclear shapes we did not take into account the influence of individual nucleons upon the nuclear shape, the effect indicated by A. Bohr.[6] If neither of fragments is heavy this effect is inessential. But even if there is only one heavy fragment it can be easily shown that if the nucleus is prolate the symmetry axis (owing to the action of individual nucleons is perpendicular to the line connecting the centres of the nuclei, and in the case of oblate nucleus the symmetry axis is parallel to this line. To see that it is sufficient to consider the value of the energy of the interaction of the charge and the quadrupole: $\frac{1}{2}eQP_2(\cos\gamma)/r^3$ (γ is the angle between $\vec{r}$ and the symmetry axis of the nucleus, and Q is the quadrupole moment). For $Q > O$ (prolate nucleus) the minimum of the energy corresponds to $\gamma = \pi/2$; for $Q < O$ the minimum corresponds to $\gamma = 0$.

In the case of the prolate nucleus the effect of the approach of the nuclei upon the rotation around the axis connecting the centres is small. Therefore the height of the barrier will increase, because of the coulomb oblateness and owing to the orientation of the prolate nucleus. In the case of the oblate nucleus, the axis of the rotation is perpendicular to the line connecting the centres. As the nuclei are approaching, their rotation will be transformed into small oscillations around the equilibrium orientation. Thus, in the case of the oblate nucleus too the effects —combined effect of the coulomb oblateness and of the orientation of nonspherical nuclei—raises the height of the barrier. The effect of orientation in the nonspherical case is however owing to the rate of the orientation process.

II. THE QUASISTATIC PROCESS OF FISSION AND EXCITATION OF THE FRAGMENTS

In the case of deformation of the fissionable nucleus, in order to determine the character of the fission after the descent from the top of the barrier, it is important to establish the degree to which this process is quasistatic.

The duration of the descent from the top of the barrier to a distance of about $2R$ (i.e., to the distance where the scission took place) is, in the case of the fission near the threshold, of the order

$$\tau_f \sim 2R/\sqrt{2(E - V_f)/M} \sim (1 - 3) \cdot 10^{-20} \text{ sec}$$

M — mass of the nucleus, $(E - V_f)$ is the difference

Table 1

	$Z_1 = Z_2 = 46$; $A_1 = A_2 = 118$; $\epsilon = 47.8$	$Z_1 = Z_2 = 46$; $A_1 = A_2 = 118$; $\epsilon = 60.2$ (ref. 5)	$Z_1 = 92$; $A_1 = 238$; $Z_2 = 6$; $A_2 = 12$; $\epsilon = 47.8$	$Z_1 = 47$; $A_1 = 109$; $Z_2 = 54$; $A_2 = 141$; $\epsilon = 47.8$	$Z_1 = 64$; $A_1 = 160$; $Z_2 = 38$; $A_2 = 98$; $\epsilon = 47.8$	$Z_1 = Z_2 = 31$; $A_1 = A_2 = 72$; $\epsilon = 47.8$	$Z_1 = Z_2 = 23$; $A_1 = A_2 = 54$; $\epsilon = 47.8$
$\alpha_2^{(1)}$	−0.20	−0.15	−0.23	-0.22_5	−0.32	-0.13_5	−0.09
$\alpha_3^{(1)}$	0.01	−0.005	−0.02	0.03	0.02	−0.01	−0.01
$\alpha_2^{(2)}$	−0.20	−0.15	−0.02	−0.25	−0.15	-0.13_5	−0.09
$\alpha_3^{(2)}$	0.01	−0.005	0.005	0.02	0.03	−0.01	−0.01
a_c	7.9	8.3	6.9	7.9	7.8_5	7.1	6.8_5
d	9.8	9.8	8.5	10.0	10.0	8.3	7.6
$V/(e^2/r_0)$	255.6	246.9	75.3	305.0	291.8	131.5	75.9_5
$V_0/(e^2/r_0)$	215.7	215.7	65.0	254.3	242.3	115.5	70.0
$(V - V_0)/V_0$	0.18_5	0.14_5	0.16	0.20	0.20_5	0.14	0.08_5

between the excitation energy and the height of the fission barrier,

$$(E - V_f \sim 1 \text{ Mev})$$

The characteristic time for the quadrupole oscillation of the surface is:

$$\tau_g \sim \frac{\hbar}{\hbar\omega} \sim 10^{-21} \text{ sec (as } \hbar\omega \sim 0.8 \text{ Mev)}$$

$$\tau_g \ll \tau_f$$

Thus the process of the fission after the descent from the top of the barrier is in general quasistatic, with respect to the oscillationary degree of freedom of the nucleus. The same is true for the single nucleon's degree of freedom for $\tau_n \sim \hbar/\Delta E_n \lesssim \tau_k$. ($\Delta E_n$ is the separation of the nucleon's level of the nucleus.) Since the deviation from the quasistatic state is small, the probability of the excitation of the oscillation and nucleon levels at the expense of the kinetic energy, in the process of fission is not great. (The same conclusion is true for the reverse process of the fusion of two nuclei; see section I.) The excitation of the rotational levels is of no importance, since the angular momentum of the nucleus near the fission threshold is small.

After the fission took place and in the reverse process of the impact of the nuclei, orientational oscillations become possible around the equilibrium orientation when the symmetry axes are directed along the line connecting the centres. At the impact of heavy nuclei, the oblateness may also be caused by the action of separate nucleons.[1] However the period of orientational oscillations $\tau_0 \sim \sqrt{(I_2R^3/Z_1eQ_2)}$ (where I is the moment of inertia, and Q is the quadrupole moment) is much smaller than the time of the approach of the nuclei τ_f. Therefore, there is no great probability of the excitation of the orientational oscillation.

There is, however, a stage in the fission when the quasistatic state is markedly disturbed. We have noted in I that the equilibrium shapes of two mutually gravitating nuclei correspond to oblate spheroids (Fig. 1). At the moment of fission, however, the fragments have an entirely different shape, with appendages left from the fission (Fig. 2). In consequence of this, the fragments acquire spheroidal shape soon after the scission and the appendages are drawn in. Owing to the nonquasistatic character of this process, the probability of excitation of the vibrational levels may be great at this stage. The amount of energy received by the fragments after fission determines the number and the energy of the secondary neutrons and γ-quantas. We assume, in accordance with the experiments of Wilson, de Benedetti and Fraser,[7,8,9] that the secondary neutrons are emitted principally by the excited fragments after the scission takes place.

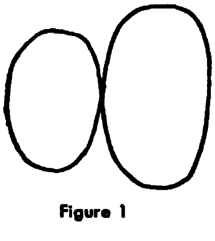

Figure 1

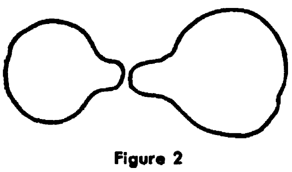

Figure 2

In the case of fusion of two nuclei (near the threshold) the process approximates the quasistatic up to the moment when the impact takes place. After the impact, the surface appears to be shrinking rapidly, since this reduces the energy of the system. We thus see that the course of the fission differs from that of the reverse process of fusion. This difference is demonstrated in simplified form in Fig. 3, where the potential energy of the nucleus and of the fragments is shown as parameter a, which characterises the symmetrical deformation of the initial shape before the fission, and the distance between the centres of fragments after the fission.

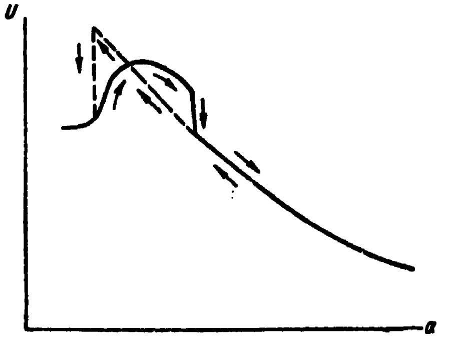

Figure 3

III. FISSION WIDTH AT HIGH EXCITATION

At high excitation ($E \sim 100$ Mev), the irreversibility of the process of fission is inessential and therefore the fission width may be evaluated from the principle of detailed balance. According to the principles of detailed balance there is a simple relation between the probability of the direct process $W_{A_1A_2}{}^A$ (the fission of the nucleus into fragments A_1 and A_2) and the reverse one (the building of the nucleus A out of the nuclei A_1 and A_2).

$$g_A W_{A_1A_2}{}^A = g_{A_1A_2} W_A{}^{A_1A_2} \qquad (4)$$

g_{A_k} is the statistical weight of the state.

$$g_{A_k} = (2i_k + 1)\rho(E_{A_k})\Omega\, dp \frac{1}{h^3}$$

Here i_k is the angular momentum of the nucleus, A_k, $\rho(E_{A_k})$ is the level density of the nucleus with the angular momentum, i_k, E_{A_k} is the excitation energy of the nucleus, A_k, and Ω is the normalisation volume.

Proceeding from p_A and p_A to ρ and ρ_A (ρ is momentum of the relative motion of the fragments) and using the relation

$$E_A + |\Delta E_{cB}| = E_{A_1} + E_{A_2} + E$$

(ΔE_{cB} is the binding energy of the fragments, and E is the energy of the relative motion of the fragments) we obtain from Equation 4:

$$\Gamma_f = \hbar W_{A_1A_2}{}^{A} = \frac{(2i_1+1)(2i_2+1)}{2i+1} D_i \frac{m\sigma_A{}^{A_1A_2}}{\hbar^2\pi^2} (E + |\Delta E_{cB}| - E_{A_1} - E_{A_2})_{cp} \frac{A_1A_2}{A} N_1N_2 \quad (5)$$

Here $\sigma_A{}^{A_1A_2} = W_A{}^{A_1A_2} \frac{\Omega}{v}$ is the cross-section of the fusion of the fragments, $D_i = 1/\rho(E_A)$; $N_1(E_{A_1})$ and $N_2(E_{A_2})$ is the average number of the levels of the fragments A_1 and A_2, with the excitation E_{A_1} and E_{A_2}. Owing to the exponential dependence $N(E_k) \sim \exp(a\sqrt{E_k})$ upon the energy E_k, at high excitations N_1N_2 are the most important factors in Equation 5. Thus at high values of E_1 and E_2 the width of the fission Γ_f is essentially determined in the main by the statistical weight of the final state. This estimation is similar to the estimation of the multiple meson production according to the Fermi theory.

Let us compare Equation 5 with the well known expression for a neutron width, likewise based upon the principle of detailed balance

$$\Gamma_n = \frac{2(2i'+1)}{2i+1} D_i \frac{\sigma_A{}^{nA'}m}{\hbar^2\pi^2} (E_A - \epsilon_n - E_{A'})_{op} N'(E_A)$$

$N'(E_{A'})$ is the number of the levels with the energy $<A'$ of the nucleus A left, after the neutron was irradiated.

ϵ_n is the binding energy of the neutron; $\sigma_A{}^{nA'}$ is the cross-section of the capture of the neutron by the nucleus A. Let us find Γ_f/Γ_n:

$$\frac{\Gamma_f}{\Gamma_n} = \frac{(2i_1+1)(2i_2+1)}{2(2i'+1)} \frac{\sigma_A{}^{A_1A_2}}{\sigma_A{}^{A'n}} \frac{(E + |\Delta E_{oB}| - E_{A_1} - E_{A_2})_{op}}{(E_A - \epsilon_n - E_{A'})_{op}} \frac{A_1A_2}{A} \frac{N_1N_2}{N'}$$

At high excitation, when there is sense in using Equation 5 the exponential factor N_1N_2/N' plays the principal part.

If the height of the fission barrier E_f is greater than the binding energy of the neutron ϵ_n, then $N_1N_2 \ll N'$; however in the case of medium nuclei $x = (Z^2/A)/(Z^2/A)_{cr} < 0.6$ the barrier height may be quite low for a strong asymmetrical fission.[10] It appears also, that at high excitation the barrier height decreases owing to the decrease of the surface tension with the rising temperature of the nucleus. Therefore for the medium nuclei at high excitation the ratio N_1N_2/N' may not appear very small. And yet, a simple fission (observed in the case of bismuth at excitation of about $E \sim$ 100–150 Mev) is impossible for sufficiently light nuclei.

In fact, even in the case when the total energy of excitation is carried away by neutrons, the ratio Z^2/A will not be so low as to bring the height of the fission barrier down to the magnitude of the binding energy of the neutron which is the necessary condition for emissional fission.[11]

Therefore, for medium nuclei as well as for the most heavy nuclei (like uranium), the fission at high excitation is apparently the fission of an excited nucleus and not the emissional fission, which takes place in the heavy nucleus of the bismuth type. The fission of medium nuclei was observed in subsequent experiments.

REFERENCES

1. Migdal, A. B., J. Exper. Theor. Phys., *15*, 81 (1945).
2. Bohr, N. and Wheeler, Y., Phys. Rev., *56*, 426 (1939).
3. Frenkel, Y. I., J. Exper. Theor. Phys., *9*, 641 (1939).
4. Wöste, K., Zs. Phys., *133*, 370 (1952).
5. Breit, G., et al., Phys. Rev., *87*, 74 (1952).
6. Bohr, A., Dansk. Kgl. Mat.-Fys. Medd., *26*, N 14 (1952).
7. Wilson, R., Phys. Rev., *72*, 189 (1947).
8. De Benedetti *et al.*, Phys. Rev., *74*, 1645 (1948).
9. Fraser, Y., Phys. Rev., *88*, 536 (1952).
10. Frankel, S. and Metropolis, N., Phys. Rev., *72*, 914 (1947).
11. Gockermann, R. and Perlman, Y., Phys. Rev., *73*, 1127 (1948); *76*, 628 (1949).

On the Theory of Nuclear Fission Near Threshold

By V. G. Nossoff,* USSR

THE ASYMMETRY OF FISSION

As is well known, the symmetric deformation of the liquid drop nucleus model[1,2] is energetically the most favourable in the case of small deviations from its spherical shape. Indeed, if the surface of the nucleus is given, as usual, by the equation

$$R(\mu) = R_0 \left\{1 + \sum_{n=0}^{\infty} \alpha_n P_n(\mu)\right\} \tag{1}$$

for the potential energy, we find up to the terms of the fourth approximation.

$$\begin{aligned} U = U_s^{(0)} \Bigg\{ & 1 + \frac{1}{2} \sum_{n=2}^{\infty} \frac{(n-1)(n+2)}{2n+1} \alpha_n^2 \\ & - \frac{1}{3} \sum_{l,m,n=2}^{\infty} I_{lmn}\alpha_l\alpha_m\alpha_n + \sum_{m,n=2}^{\infty} \frac{\alpha_n^2\alpha_m^2}{(2n+1)(2m+1)} \\ & + 36 \sum_{m,n=2}^{\infty} \frac{(m+1)(n+1)}{(2m+1)(2m+3)(2n+1)(2n+3)} \alpha_m\alpha_{m+1}\alpha_n\alpha_{n+1} \\ & - \frac{1}{128} \sum_{\substack{k,l,m,n=2 \\ i=0}}^{\infty} [k(k+1) + l(l+1) - i(i+1)][m(m+1) \\ & + n(n+1) - i(i+1)](2i+1) I_{ikl} I_{imn} \alpha_k\alpha_l\alpha_m\alpha_n \Bigg\} \\ + U_c^{(0)} \Bigg\{ & 1 - 5 \sum_{n=2}^{\infty} \frac{n-1}{(2n+1)^2} \alpha_n^2 \\ & - \frac{5}{12} \sum_{l,m,n=2}^{\infty} \frac{7n-10}{2n+1} I_{lmn}\alpha_l\alpha_m\alpha_n \\ & + 5 \sum_{m,n=2}^{\infty} \frac{n-4}{(2n+1)^2(2m+1)} \alpha_n^2\alpha_m^2 \\ & + 45 \sum_{m,n=2}^{\infty} \frac{(4n-7)(n+1)(m+1)}{(2m+1)(2m+3)(2n+1)^2(2n+3)} \alpha_m\alpha_{m+1}\alpha_n\alpha_{n+1} \\ & + \frac{15}{16} \sum_{\substack{k,l,m,n=2 \\ i=0}}^{\infty} \left(\left[i(i+1) - m(m+1) + \frac{1}{3}(n^2 - n + 1)\right] \frac{2i+1}{2n+1} \right. \\ & + \frac{2}{9}\left[2m(m+1) - \frac{9}{4} i(i+1) + n(n+1)\right](2i+1) \\ & \left. - \frac{1}{2}(i-1)(i+2)\right) I_{ikl} I_{imn} \alpha_k\alpha_l\alpha_m\alpha_n \Bigg\} \end{aligned} \tag{2}$$

Here $U_s^{(0)} = 4\pi R_0^2\sigma$ and $U_c^{(0)} = {}^{16}\!/_{15}\pi^2 e^2 \rho_p^2 R_0^5$ are the equilibrium values of the surface energy and coulomb energy respectively; σ is the surface tension, e the proton charge, ρ_p the number of protons per unit of nuclear volume, R_0 the equilibrium value of the nuclear radius. The integral of the product of three Legendre polynomials I_{klm} differs from zero if the sum of all three indices is equal to an even number and if no one of them exceeds the sum of the two others. In this case

$$\begin{aligned} I_{kln} &= \int_{-1}^{1} P_k P_l P_n \, d\mu \\ &= \frac{2}{k+l+n+1} \cdot \frac{(k+l-n-1)!!}{(k+l-n)!!} \\ &\times \frac{(n+k-l-1)!!}{(n+k-l)!!} \, \frac{(l+n-k-1)!!}{(l+n-k)!!} \\ &\qquad \frac{(k+l+n)!!}{(k+l+n-1)!!} \end{aligned} \tag{3}$$

where for a positive integer n the expression $n!!$ is equal to the product of all positive integers of the same parity as n, which does not exceed n. For $n = 0$ and -1, by definition $0!! = 1$; $(-1)!! = 1$.

We note that Equation 2 does not contain the coordinates α_0 and α_1, which are eliminated by means of the conservation conditions of nuclear volume and of its center of mass position.

The position of the saddle-point is determined from the equations:

$$\frac{\delta U}{\delta \alpha_n} = 0; \qquad n = 2, 3, 4 \ldots \tag{4}$$

Original language: Russian.

* V. G. Nossoff, "On the Problem of Asymmetry of Nuclear Fission," Acd. Sci. of the USSR (unpublished).

The expansion in Equation 2 permits solving these equations in the approximation of small α_n. It appears, that the solution obtained by the method of successive approximations is in fact an expansion in a power series of the quantity $1 - x$ where $x = U_c^{(0)}/2U_s^{(0)}$. It is easy to see also that α_2 is a small quantity of the order $1 - x$; α_4, a small quantity of the order $(1 - x)^2$, α_6, of the order $(1 - x)^3$, etc. All the α_n's with odd n-values are equal to zero, i.e., the shape of the nucleus at the saddle-point is symmetrical. Let us quote in the first non-vanishing approximation the well-known expressions[2] for α_2 and for the fission threshold $u(x) = U - U^{(0)}/U_s^{(0)}$ measured in $U_s^{(0)}$-units:

$$\alpha_2 = \tfrac{7}{3}(1 - x); \qquad u(x) = \tfrac{98}{135}(1 - x)^3 \tag{5}$$

In the region of the uranium group nuclei the quantity $1 - x$ is not small and the position of the saddle-point cannot be determined in the approximation of small deviations from spherical shape. So much the more one should not limit himself to a small deformation approximation in the investigation of the asymmetry of fission. In fact, it is natural to try to explain the asymmetry of fission observed experimentally as a result of the instability of the nuclear shape with respect to asymmetric deformation at some critical value of the symmetric deformation. It may appear that the point of stability loss lies beyond the saddle-point. Restricting ourselves in Equation 2 to terms of the form α_3^2 and $\alpha_2\alpha_3^2$ and determining the critical deformation α_2, at which the nucleus becomes unstable with respect to small asymmetric deformations α_3, we obtain:

$$\alpha_2 = \frac{75}{8} \cdot \frac{7 - 4x}{7 + 23x} \tag{6}$$

Thus even at $x = 1$ (a nucleus with $x > 1$ cannot exist because at $x = 1$ the spherical shape of the surface ceases to be stable) we get the value $\alpha_2 = {}^{15}\!/_{16}$ which lies evidently beyond the limits of applicability of the expansion in Equation 2. In order to account for the large deviations of the nuclear surface from spherical shape we shall roughly approximate the nucleus surface shape by a prolate ellipsoid. For the purpose of farther investigation, however, it is essential to account for some deviation from the ellipsoidal shape manifesting itself in a small "squeezing" in the equatorial plane. For this purpose we shall introduce the ellipsoidal coordinates by the formulae:

$$\begin{aligned} y &= c \cdot \sqrt{\nu^2 - 1}\,\sqrt{1 - \mu^2}\cos\varphi; \\ y &= c \cdot \sqrt{\nu^2 - 1}\,\sqrt{1 - \mu^2}\sin\varphi; \\ z &= c \cdot \nu \cdot \mu \end{aligned} \tag{7}$$

and let the deviation of the nucleus surface from an ellipsoid be described by the expression

$$\nu(\mu) = \nu_0\{1 + A_0 + A_2P_2(\mu)\}. \tag{8}$$

After some simple computation we obtain in the linear approximation the following expression for the potential energy:

$$\begin{aligned} u = {} & \frac{(1 - 3A)^{1/3}}{2}\left[\frac{1}{\sqrt{1 - 3A}}\,\frac{\arcsin\sqrt{3A}}{\sqrt{3A}} + 1\right] \\ & + 2x(1 - 3A)^{1/3}\,\frac{\operatorname{arth}\sqrt{3A}}{\sqrt{3A}} - 1 + 2x) \\ & + \left\{\frac{5/16}{A(1 - A)(1 - 3A)^{2/3}}\left[\frac{1}{\sqrt{1 - 3A}}\,\frac{\arcsin\sqrt{3A}}{\sqrt{3A}}\right.\right. \\ & \left(1 - \frac{29}{5}A + \frac{288}{25}A^2 - \frac{216}{25}A^3\right) \\ & \left. - \left(1 - \frac{19}{5}A + \frac{54}{25}A^2\right)\right] - \frac{x}{A(1 - 3A)^{2/3}} \\ & \left.\left(\frac{\operatorname{arth}\sqrt{3A}}{\sqrt{3A}} - \frac{1}{1 - A}\right)\left(1 - \frac{18}{7}A + \frac{27}{35}A^2\right)\right\} A^2. \end{aligned} \tag{9}$$

The coordinate A is given by the expression $A = 1/3\nu_0^2 = c^2/3a^2$, where c is the linear eccentricity of the ellipsoid, a its major semi-axis; the coordinate A_0 is eliminated due to the conservation condition of the nuclear volume.

Solving the equations $\delta u/\delta A = 0$; $\delta u/\delta A_2 = 0$, we obtain for the position of the saddle-point and the thresholds of fission the results listed in Table 1. For comparison, the values of the fission thresholds obtained by Frankel and Metropolis[3] by means of an electronic computer are given in the last column. As can be seen from the table, the condition $A_2 \ll 1$ is fulfilled everywhere, which means that the deviation from the ellipsoidal shape is not too great.

In order to determine the critical deformation at which the instability with respect to small asymmetric deformations appears, we assume for the nuclear surface shape the expression

$$\nu(\mu) = \nu_0\{1 + A_0 + A_1P_1(\mu) + A_3P_3(\mu)\} \tag{10}$$

Table 1

				Electronic computer
x	$A(x)$	$A_2(x)$	$u(x)$	$u(x)$
0.90	0.17	0.029	0.0009	0.0007
0.81	0.23	0.090	0.0068	0.0050
0.77	0.25	0.11	0.0126	0.0093
0.74	0.27	0.12	0.0187	0.0136
0.65	0.30	0.17	0.0529	0.0400

Table 2

x	A
0.90	0.280
0.81	0.290
0.77	0.293
0.74	0.296
0.65	0.300

Thus we have chosen A and A_3 as the symmetric and asymmetric coordinates respectively (the parameters A_0 and A_1 are eliminated due to the conservation conditions of nuclear volume and its center of mass position). After rather simple, but cumbersome computations, we obtain in the quadratic approximation:

$$
\begin{aligned}
u = {} & \frac{(1-3A)^{1/3}}{2}\left[\frac{1}{\sqrt{1-3A}} - \frac{\arcsin\sqrt{3A}}{\sqrt{3A}} + 1\right] \\
& + 2x(1-3A)^{1/3}\frac{\operatorname{arth}\sqrt{3A}}{\sqrt{3A}} - (1+2x) \\
& + \left\{\frac{875/3072}{A^3(1-A)(1-9/5A)^2(1-3A)^{5/3}}\right. \\
& \left[\frac{1}{\sqrt{1-3A}} - \frac{\arcsin\sqrt{3A}}{\sqrt{3A}} \times \left(1 - \frac{2309}{175}A\right.\right. \\
& + \frac{454599}{6125}A^2 - \frac{1411237}{6125}A^3 + \frac{90976608}{214375}A^4 \\
& \left. - \frac{3958848}{8575}A^5 + \frac{59082048}{214375}A^6 - \frac{3079296}{42875}A^7\right) \\
& - \left(1 - \frac{1959}{175}A + \frac{322369}{6125}A^2 - \frac{829711}{6125}A^3\right. \\
& + \frac{44491274}{214375}A^4 - \frac{41037432}{214375}A^5 + \frac{12528}{125}A^6 \\
& \left.\left. - \frac{1026432}{42875}A^7\right)\right] + 2x\frac{125/308}{A^3(1-9/5A)^2(1-3A)^{5/3}} \\
& \left[\frac{\operatorname{arth}\sqrt{3A}}{\sqrt{3A}}\left(1 - \frac{154}{15}A + \frac{332069}{7875}A^2 - \frac{77468}{875}A^3\right.\right. \\
& \left. + \frac{3088143}{30625}A^4 - \frac{1842534}{30625}A^5 + \frac{95013}{6125}A^6\right) - \frac{1}{1-A} \\
& \left(1 - \frac{154}{15}A + \frac{338369}{7875}A^2 - \frac{247244}{2625}A^3\right. \\
& \left.\left.\left. + \frac{31811567}{275625}A^4 - \frac{2343454}{30625}A^5 + \frac{137673}{6125}A^6\right)\right]\right\} A_3^2
\end{aligned}
$$

The position of the point of stability loss is determined by equating the coefficient of A_3^2 to zero. The results of the computation are given in Table 2 for five values of the parameter x.

There exist weighty reasons to suppose that the instability arising at the critical point is absolute, i.e., that the stability cannot be restored at any finite value of the asymmetric coordinate. In fact, the stability could be restored at the expense of the higher powers of the potential energy expansion in a power series of A_3. It appears, however, that the next term of the expansion proportional to A_3^4 is negative. The deviations from spherical shape being small: it is equal to $U_s^{(0)}[-0.569 + 0.217x]\alpha_3^4 < 0$ as can be obtained easily from Equation 2. In the opposite limiting case of an ellipsoid with a large eccentricity the coulomb energy is negligible, and the surface energy can be easily shown to assume the form:

$$
\begin{aligned}
U_s = \frac{\frac{\pi}{4}U_s^{(0)}}{(\nu_0^2-1)^{1/6}}\left\{1 - 0.0528\frac{A_3^2}{(\nu_0^2-1)^2}\right. \\
\left. - 0.0440\frac{A_3^4}{(\nu_0^2-1)^4}\right\} \quad (12)
\end{aligned}
$$

i.e., the term we are interested in also appears to be negative. It is highly improbable that the stability is restored at the expense of still higher terms of the expansion.

The absolute character of the instability permits to estimate approximately the ratio of the fragment masses in the following way: assuming the symmetrical coordinate to be equal to the value corresponding to the point of stability loss, we ought to increase the asymmetric coordinate up to the vanishing of the thickness of the neck. The ratio of volumes of the rotation bodies into which the nucleus breaks up gives an estimate of the fragment masses ratio. To account for the "squeezing" of the symmetric nuclear configuration we adopt the following equation for the nuclear surface shape

$$
\nu(\mu) = \nu_0\{1 + A_0 + A_1P_1(\mu) + A_2P_2(\mu) + A_3P_3(\mu)\} \quad (13)
$$

where the parameters A_0 and A_1 are eliminated due to the conservation conditions of nuclear volume and its center of mass position. Let the quantity A_2 be 0.10, according to Table 1. For the values $x = 0.81$; $A = 0.29$ the numerical computations show that with the increase of the asymmetric coordinate A_3 the quantity $\nu(\mu)$ turns into unity for the first time at $\mu = \mu_{cr} = 0.29$. At this point the rupture of the neck has to occur; for the fragment masses ratio we obtain $V_1/V_2 = 1.9$. Taking into account the rough character of the estimate the agreement with experiment is reasonably good.

In the foregoing we have not taken into account the effects of interaction of the single nucleons' motion with the vibration of the nuclear surface. It can hardly be supposed that taking into account of these effects could alter the result qualitatively.

ACKNOWLEDGEMENT

The author expresses his gratitude to B. T. Geilikman for interesting discussions.

REFERENCES

1. Frenkel, Y. I., J. Exper. Theor. Phys. *9*, 641 (1939).
2. Bohr, N. and Wheeler, J., Phys. Rev. *56*, 426 (1939).
3. Frankel, S. and Metropolis, N., Phys. Rev. *72*, 914 (1947).

The Nuclear Fission Process

By J. R. Huizenga,* USA

INTRODUCTION

The phenomenon of fission is probably the most characteristic property of the very heavy elements. In a study of the nuclear fission process one seeks to answer two general questions. First, how will the absolute fission yield, i.e., fission cross section, change with the initial kind of nucleus and bombarding conditions. Second, once fission has occurred how will its mass, charge, energy, etc., be divided, and how will these behaviors vary with the fissioning nucleus. Fong[1] has studied in some detail the second problem, i.e., how the nucleus fissions. In the present paper we will be concerned with the first problem, i.e., a study of the question of when a nucleus fissions.

We shall restrict this discussion of fission probability to spontaneous fission and induced fission with low-energy particles. Although nuclear fission is energetically possible for the intermediate nuclides, the probability for this process is not appreciable for the above kinds of fission except for the elements of atomic number $Z \geqslant 90$. The data discussed will necessarily, therefore, be limited to isotopes of elements thorium and above.

FISSION THRESHOLD ENERGIES

For the heavy nuclides it is a well known fact that nuclear fission is an exothermic process. The term fission threshold is, therefore, a misleading one, since a photofission threshold is not a threshold at all in the sense of a true threshold, e.g., photoneutron threshold. A photofission threshold is somewhat analogous to an activation energy for an exothermic chemical reaction. The numerical value of a fission threshold is related to the sensitivity of the fission cross-section measurement which is employed in the threshold determination, since in the limiting case a small fission cross section is observed even though no energy is added to the fissioning nucleus (spontaneous fission). The fission threshold energy therefore should not be considered an energy at which fission no longer takes place but an energy region in which a function of the fission probability (i.e., cross section) versus excitation energy curve changes its slope. Most of the information on fission thresholds has been obtained from experiments in which fission takes place in nuclear times comparable to those involved in gamma and neutron emission. Thus, for fission to be observed it must compete to a measurable extent with other nuclear processes.

Information about fission thresholds can be obtained from the following measurements:

1. Photofission thresholds: Koch *et al.*[2] measured the photofission threshold of the materials given in Table I.
2. Neutron-fission thresholds: Fission thresholds of nuclides which do not fission with thermal neutrons can be calculated from measured neutron-fission thresholds plus the appropriate neutron binding energies (Table II).
3. Fast-neutron-fission cross sections: The fission cross section of Np^{237} is almost constant at neutron energies from 2 to 5.5 Mev.[5,3] The ratio of the fission probability to neutron emission probability is independent of energy in the above region upon the assumption of constant total neutron-absorption cross section. The increase in the neutron-fission cross section of Np^{237} at neutron energies ≥ 5.5 Mev can be explained by assuming that at this energy the product nuclide after neutron emission begins to have sufficient excitation energy to undergo fission, i.e., the fission threshold for Np^{237} is 5.5 Mev.
4. Fission thresholds from spontaneous fission half-lives: Frankel and Metropolis[6] have derived an equation of the following form for the spontaneous fission half-life in seconds,

$$T = 10^{-21+kE_f} \tag{1}$$

where E_f (fission threshold) is the energy deficit at the saddle point in Mev and k is a constant for a particular nuclide. If one assumes that the general form of the Frankel and Metropolis equation is correct, some information on the variation of fission thresholds can be calculated by employing the experimental spontaneous fission half-lives. For this purpose we will assume the photofission threshold of 5.1 Mev for U^{238} to be correct. Employing a spontaneous fission half-life of 8.0×10^{15} years for U^{238} in Equation 1 gives a k value of 8.706. If one assumes further that k is constant for all heavy nuclides, fission threshold values of many nuclides can be calculated from existing spontaneous fission data (see Table III).

Table I. Photofission Thresholds

Target nucleus = compound nucleus	*Photofission threshold, Mev*
Th^{232}	5.40 ± 0.22
U^{233}	5.18 ± 0.27
U^{235}	5.31 ± 0.27
U^{238}	5.08 ± 0.15
Pu^{239}	5.31 ± 0.25

---

* Argonne National Laboratory.

Table II. Calculated Fission Thresholds

Target nucleus	*Compound nucleus*	*Neutron fission threshold*,[3] *Mev*	*Neutron binding energy*,[4] *Mev*	*Calculated fission threshold, Mev*
Th^{232}	Th^{233}	≤ 1	4.9	≤ 5.9
Pa^{231}	Pa^{232}	≤ 0.4	5.4	≤ 5.8
U^{238}	U^{239}	≤ 0.9	4.8	≤ 5.7
U^{234}	U^{235}	≤ 0.3	5.4	≤ 5.7
Np^{237}	Np^{238}	≤ 0.3	5.3	≤ 5.6

In those cases where the fission thresholds have been determined by more than one method, the agreement in all cases is within experimental error. It is especially interesting to compare the values obtained by photofission with those calculated from spontaneous fission half-lives since the agreement is excellent, thus giving some validity to the assumption of constant k over a limited number of nuclides. In addition, the values calculated from spontaneous fission half-lives support the conclusion drawn from other fission threshold determinations that fission thresholds do not change very fast with atomic number Z and mass number A. Theoretical predictions[6,7,8] of fission thresholds disagree quite markedly with the values discussed above in that theory predicts a much larger variation (see, for example, Figs. 2b and 3 in reference[6]) in thresholds than is observed.

SPONTANEOUS FISSION HALF-LIVES

Spontaneous fission has not been observed for elements with $Z < 90$. The probability for spontaneous fission is apparently associated with the parameter Z^2/A, in such a manner that the spontaneous fission half-life decreases rapidly with increasing atomic number.

In a discussion of spontaneous fission it is important to consider the heavy nuclides in two separate groups: (1) nuclides with an even number of protons and an even number of neutrons (even-even) and (2) nuclides containing an odd neutron and/or odd proton. The following empirical correlations will deal with the even-even nuclides. The first successful correlation of spontaneous fission half-lives was made by Seaborg[9] and by Whitehouse and Galbraith.[10] These authors plotted the logarithm of the spontaneous fission half-lives of several nuclides as a function of the parameter Z^2/A and observed that the logarithm of the spontaneous fission half-lives of even-even nuclides decrease with increasing Z^2/A values in a linear manner.

The spontaneous fission half-lives of the even mass sotopes of an element with even Z were expected to increase with increasing A, since from the Z^2/A parameter the charge per unit volume is diminished with increasing A. The even-even isotopes of uranium were the first observed exception to the above linear relationship.[11] The measured spontaneous fission half-life of U^{238} is smaller than that of U^{234}, whereas from the Z^2/A correlation one would have predicted the spontaneous fission half-life of U^{238} to be one hundred times larger than the value of U^{234}.

The recent production of several heavy nuclides by intense neutron irradiation in sufficient quantities for spontaneous fission half-life determinations[12] has made it possible to greatly extend the data on spontaneous fission stability. These new data reveal that the spontaneous fission half-lives of even-even isotopes of other elements also do not continue to increase with increasing A but behave in a way analogous to the even-even uranium isotopes. Thus, all of the data consistently show that the even-even spontaneous fission half-lives of a particular element when plotted against some function of A fall on a parabolic curve with a maximum at an A value which is in the neighborhood of maximum beta-stability.[11,13] Beyond this maximum the half-lives continue to decrease with increasing A. The experimental data are plotted in Fig. 1.

The fundamental nature of the spontaneous fission process and its direct relation to the understanding of nuclear structure make it worthwhile to discuss possible explanations of the shorter spontaneous fission half-lives beyond the maximum. This property may be associated with closed shells and thus result from changes in the nuclear deformation of the heavy nuclides.

It is generally accepted at present that many properties of the heavy nuclides, e.g., quadrupole moments, rotational levels, etc., can best be accounted for by collective nuclear motion.[14,15] The energies of the first excited states in even-even nuclides are closely related to closed shells. The rotational excitation energies decrease rapidly beyond the double closed shell at

Table III. Fission Thresholds (Mev) from Spontaneous Fission Half-Lives (Equation 1)

Nuclide	E_f	*Nuclide*	E_f	*Nuclide*	E_f	*Nuclide*	E_f	*Nuclide*	E_f
Ra^{226}	$\geqslant 4.9$	U^{234}	5.1	Pu^{236}	4.4	Cm^{241}	4.0	Cf^{249}	$\geqslant 4.0$
Th^{230}	$\geqslant 5.3$	U^{235}	5.3	Pu^{238}	4.5	Cm^{242}	4.1	Cf^{250}	3.8
Th^{232}	5.4	U^{236}	5.1	Pu^{239}	5.1	Cm^{244}	4.1	Cf^{252}	3.5
Pa^{231}	$\geqslant 5.1$	U^{238}	5.1	Pu^{240}	4.5	Bk^{249}	$\geqslant 4.2$	99^{253}	$\geqslant 3.9$
U^{232}	$\geqslant 4.8$	Np^{237}	$\geqslant 5.2$	Pu^{242}	4.5	Cf^{246}	3.7	99^{254}	$\geqslant 3.4$
U^{233}	$\geqslant 5.3$	Np^{239}	$\geqslant 4.7$	Am^{241}	$\geqslant 4.8$	Cf^{248}	3.7	100^{254}	3.2

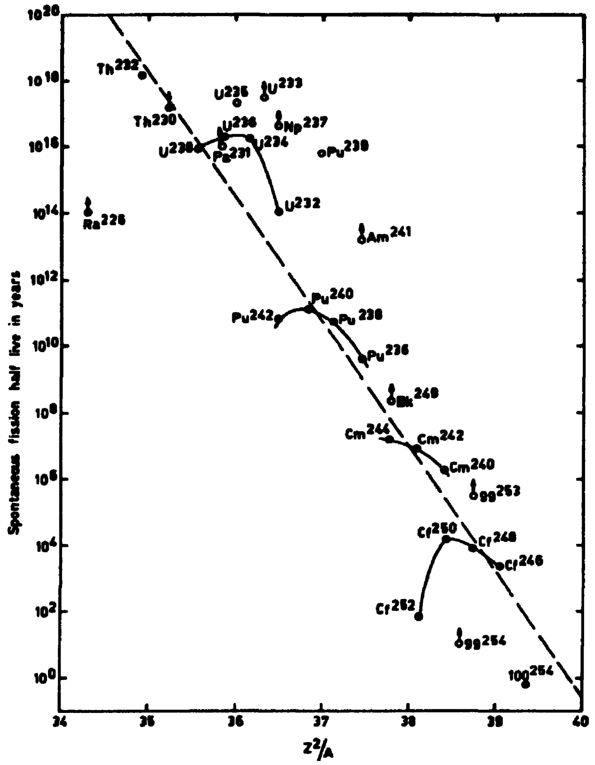

Figure 1. Spontaneous fission half-lives as a function of Z^2/A. Solid points represent even-even nuclides and the circles, odd nuclides. The arrow signifies a lower limit to the half-life.

lead, corresponding to an increasing nuclear deformation as one moves away from the closed shells. However, the magnitude of the energies of the first excited states in the even-even nuclides for $Z \geq 90$ are about equal, and the above criterion fails to distinguish between the nuclear deformations in the very heavy region. Due to the nature of the spontaneous fission process, one would expect that differences in the probabilities for spontaneous fission disintegration are a very sensitive measure of small changes in nuclear deformation. A study of the trends in spontaneous fission half-lives may therefore be an extremely sensitive method of determination of the nuclear deformations and thus give some information on the filling of nuclear subshells.

Bohr and Mottelson have suggested that the lifetimes of the M4 transitions in the odd A nuclei in the regions before the closed shells at 50, 82 and 126 can be understood in terms of nuclear deformation. The above authors calculated the ratios of the observed transition probabilities to that of the single particle transition probabilities between the appropriate single particle states (this ratio designated as the unfavored factor F). It is shown that the $M4$ transitions are consistently slower by a large factor than expected for an uncoupled particle. This reduction provides evidence that the particle transitions are associated with an appreciable readjustment of the collective field. Thus for nuclides near closed shells, the F-factors are the largest. Moreover, for a series of isotopes of the same element, the F-values decrease as one moves away from a closed shell nucleus. These trends can be correlated with the increased nuclear deformation away from closed shells, a property reflected in many nuclear properties.

It is possible to interpret the spontaneous fission half-lives in a way analogous to the $M4$ transitions. For example, Cf^{250} has 26 neutrons beyond the 126 neutron closed shell. These 26 neutrons may complete the $g_{9/2}$ and the $j_{15/2}$ levels. Pairs of nucleons would be expected to occupy these levels preferentially, since the pairing energy of nucleons in these high j orbits is probably large. Therefore, this supposition is in no way contradictory to the observed spins of $5/2$, $1/2$ and $5/2$ for U^{235}, Pu^{239} and Pu^{241}, respectively. The spins of U^{235} and Pu^{241} can be explained quite simply by assuming the $j_{15/2}$ level to be filled and the $d_{5/2}$ level containing one nucleon and one hole respectively for which in both cases the expected spin would be $5/2$. Pu^{239} would contain three nucleons outside the $j_{15/2}$ orbit and the individual spins of the three particles may couple in the ground state to give a resultant spin of $1/2$. Higher mass Cf isotopes, i.e., Cf^{252}, etc., would have extra nucleons outside the $g_{9/2}$ and $j_{15/2}$ orbits and as a result be more deformed, thus increasing the probability for spontaneous fission. It could also be argued that Cf^{246} and Cf^{248}, with holes in the uncompleted orbit, would also be more deformed than Cf^{250}, giving some reason for the maximum spontaneous fisson stability at Cf^{250}. The degrees of oblate and prolate distortions may also play a role in spontaneous fission. Hill and Wheeler have pointed out that for x particles outside a closed shell, oblate distortion is favored when $x < \frac{1}{2}j$ and prolate distortion when $x > \frac{1}{2}j$. Any quantitative analysis of the trends in the spontaneous fission half-lives of the even-even nuclides will have to consider some of the above effects in addition to the charge-volume effect discussed earlier.

No discussion of spontaneous fission half-lives is complete at present without some mention of the odd nuclides (class 2 defined previously). Sufficient spontaneous fission half-life measurements (in most cases lower limits) have been made on odd nuclides to make the following general statement. The odd nuclide spontaneous fission half-lives are much larger than one would predict by interpolation between the experimental data of the even-even nuclides (see Fig. 1). The odd nucleon decreases the probability for spontaneous fission by factors up to 10^6. This is analogous to the hindered ground state transitions of the odd nuclei in the alpha-decay. The odd nucleon may increase the spontaneous fission half-life by damping the collective motion of the nucleons and thus hindering the probability for critical deformation. One might explain this damping in the following way.

In an even-even nuclide all the nucleons are paired, resulting in a spin of zero, whereas in an odd nuclide there is always at least one odd nucleon in a certain level. The restrictions on the odd nuclide during the oscillation of the nuclear matter, e.g., conservation of spin, reduces the frequency with which it can reach the deformation shape, whereas pairs of nucleons can move into other levels with only the restriction required by the symmetry of the wave functions. Thus one might expect the fission threshold energy for odd nuclides to be greater than for even-even nuclides. The experimental evidence on this point is very uncertain. However, it is interesting to note that the measured photofission thresholds of U^{233} and U^{235} are slightly higher than that of U^{238}, although the experimental errors may render the difference unreliable.

INDUCED FISSION CROSS SECTIONS

Thermal-Neutron-Fission Cross Sections

An examination of thermal-neutron-fission cross sections reveals that a large number of the nuclides which undergo fission with slow neutrons contain an odd number of neutrons. This may be qualitatively explained by the fact that the resultant compound nucleus has more excitation energy than the compound nuclei formed from thermal-neutron capture on neighboring isotopic even-neutron nuclei. Actual values of σ_f (slow-neutron-fission cross section) are somewhat difficult to predict due to the uncertainty in the level density of different excited nuclei. For this reason it has been suggested[16] that the ratio σ_f/σ_γ (where σ_γ is slow-neutron-radiative capture cross section) is a better measure of the fissionability of a nuclide and should be used for comparative purposes rather than values of σ_f alone. This follows from the fact that the radiation width, Γ_γ, is expected to vary only slowly for the heavy nuclides in the energy range under consideration, whereas the fission width, Γ_f, should be a highly dependent function of the nuclear excitation energy. The ratios,[17] σ_f/σ_γ, of several nuclides are thus correlated with ΔE, where $\Delta E = E_n - E_f$, that is, the difference between the neutron binding energy and the fission threshold energy. The thermal neutron fission ratios, σ_f/σ_γ, are plotted in Fig. 2. against ΔE, where E_f has been assumed to be a constant, 5.3 Mev. Several interesting cross-section predictions can be made for nuclides which have had only their thermal-neutron-fission or radiative-capture cross sections measured. For example, one would predict rather large slow-neutron-fission cross sections for Cm^{245} and Cf^{251} since both have large radiative-capture cross sections.[18]

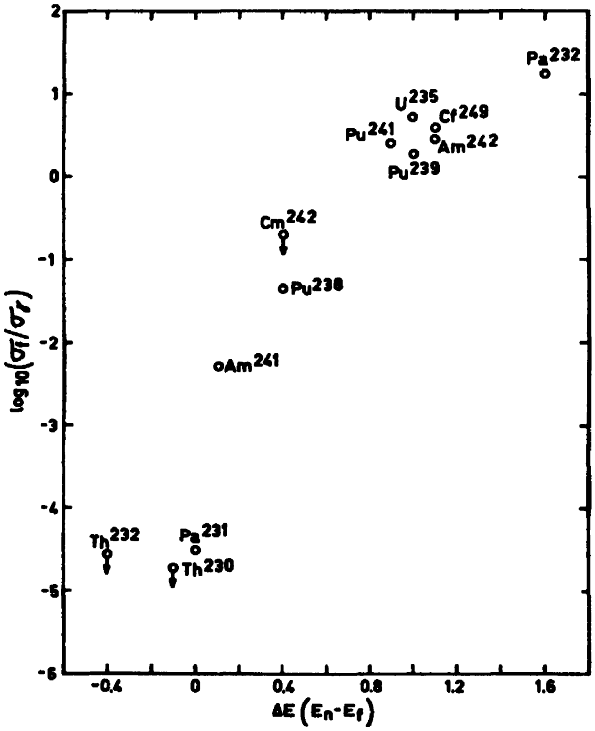

Figure 2. Logarithm (base 10) of the ratios, σ_f/σ_γ vs ΔE values which are equal to the differences between the appropriate neutron binding energies and fission threshold energy

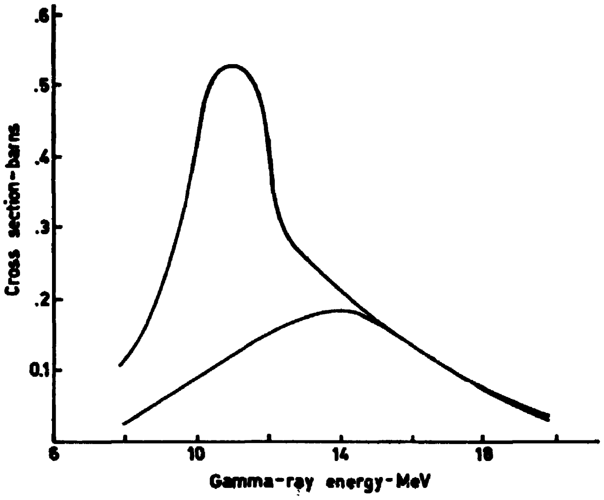

Figure 3. The cross sections for the reactions U^{238}(γ,n) U^{237} and U^{238}(γ,f) vs the energy of the gamma ray

Gamma Fission Yields

Nuclides excited with gamma rays can de-excite by fission, neutron emission, or re-emission of one or a cascade of gamma rays. The yields of the two reactions U^{238} (γ,n) U^{237} and U^{238} (γ,fission) produced by bremsstrahlung have been measured as a function of the maximum energy of the X-ray spectrum.[19] With the aid of the Schiff bremsstrahlung spectrum[20] the above yield curves were analysed to give cross sections as functions of discrete gamma-ray energies. The cross-section cuves calculated from the experimental data are shown in Fig. 3. At excitation energies between 6 and 11.3 Mev an excited U^{238} nucleus can either fission or emit one neutron (neglecting gamma emission). At energies above 11.3 Mev the product nucleus U^{237} after neutron emission begins to have sufficient energy to fission or emit a second neutron (since the neutron binding energy and fission threshold of U^{237} are both about 5.3 Mev and the neutron binding energy of U^{238} is 6.0 Mev). If we let $\sigma_{(\gamma,f)}$ represent the cross section for the (γ,fission) reaction and $\sigma_{(\gamma,n)}$ the cross section for the (γ,n) reaction, the calculated results from our U^{238} data show the branching ratio,

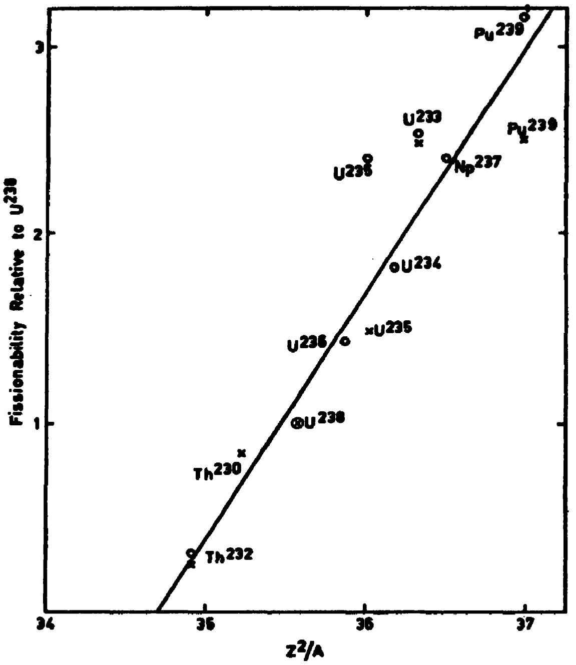

Figure 4. The fissionability of several materials relative to U^{238} are plotted as a function of the Z^2/A values of the bombarded nuclei. The circles represent an average of the data obtained from gamma rays at two betatron energies, 17 and 20 Mev. The crosses are data of McElhinney and Ogle (see reference 22)

$X = \sigma_{(\gamma,f)}/(\sigma_{(\gamma,f)} + \sigma_{(\gamma,n)})$ for U^{238} to be nearly constant at 0.2 in the excitation region 8 to 11 Mev. Thus the probability for fission relative to the probability for neutron emission is independent of the excitation in the above energy region. The next question is how the above branching ratio changes as a function of Z and A. Since an analysis similar to that made on U^{238} is not practical for a number of materials, a study of the relative photofission yields (U^{238} standard) of U^{236}, U^{235}, U^{234}, U^{233}, Th^{232}, Np^{237} and Pu^{239} were made.[21] These measurements extended the results of McElhinney and Ogle[22] and were obtained by a different experimental technique. The average of the data measured at 17- and 20-Mev betatron energies are plotted in Fig. 4 as a function of the Z^2/A values of the bombarded nuclei. To a first approximation, relative fissionability may be considered to be linearly dependent upon Z^2/A according to the relation

$$\text{relative fissionability} = 1.3[(Z^2/A) - 34.7] \qquad (2)$$

If one assumes that the gamma absorption cross sections of the above nuclides do not differ appreciably from that of U^{238}, it is possible to calculate the fission branching ratios for other nuclides by the relation

$$\text{relative fissionability} = X_{\text{nuclide}}/X_{U^{238}} \qquad (3)$$

where the relative fissionability is assumed to be a measure of the relative fission cross sections. For 20-Mev bremsstrahlung, it is necessary to modify equation (3) for higher order contributions to the fission process such as (γ,nf) and even (γ,nnf) reactions, but to a first approximation Equation 3 should be valid. By equating Equations 2 and 3 a relationship between the fission branching ratios and the parameter Z^2/A is obtained:

$$X_{\text{nuclide}}/X_{U^{238}} = 1.3[(Z^2/A)_{\text{nuclide}} - 34.7] \qquad (4)$$

Substituting a particular Z^2/A value into Equation 4 gives a measure of the branching ratio for that nuclide. For example, one calculates from Equation 4 an X value of 0.6 for Pu^{239}. This means that 60 per cent of the Pu^{239} atoms are destroyed by fission and 40 per cent by neutron emission. It can be seen from Equation 4 and Fig. 4 that fission competes favorably with neutron emission for elements $Z \geq 90$ and fission becomes more and more probable with increasing Z^2/A.

ACKNOWLEDGEMENT

It is a pleasure to acknowledge the interest of W. M. Manning in this work.

REFERENCES

1. Fong, P., Thesis, *A Theory of Nuclear Fission*, University of Chicago (1953); Phys. Rev. 89: 332 (1953).
2. Koch, H. W., McElhinney, J. and Gasteiger, E. L., *Experimental Photofission Thresholds in* U^{235}, U^{238}, U^{233}, Pu^{239}, *and* Th^{232}, Phys. Rev. 77: 329 (1950).
3. Neutron Cross Section Advisory Group, *Nuclear Cross Sections*, AECU-2040 (1952) and Supplements.
4. Huizenga, J. R., and Magnusson, L. B., "Masses, Neutron and Proton Binding Energies of the Heavy Elements," ANL-5158 (Nov., 1953).
5. Klema, E. D., *The Fission Cross Section of* Np^{237}, Phys. Rev. 72: 88 (1947).
6. Frankel, S., and Metropolis, N., *Calculations in the Liquid-Drop Model of Fission*, Phys. Rev. 72: 914 (1947).
7. Bohr, N., and Wheeler, J. A., *The Mechanism of Nuclear Fission*, Phys. Rev. 56: 426 (1939).
8. Hill, D., and Wheeler, J. A., *Nuclear Constitution and the Interpretation of Fission Phenomena*, Phys. Rev. 89: 1102 (1953).
9. Seaborg, G. T., *Some Comments on the Mechanism of Fission*, Phys. Rev. 85: 157 (1952).
10. Whitehouse, W. J., and Galbraith, W., *Spontaneous Fission Rates*, Nature 169: 494 (1952).
11. Huizenga, J. R., *Spontaneous Fission Systematics*, Phys. Rev. 94: 158 (1954).
12. For a summary of the recent spontaneous fission data see Studier, M. H., and Huizenga, J. R., *Correlation of Spontaneous Fission Half-Lives*, Phys. Rev. 96: 545 (1954).
13. Fields, P. R., Studier, M. H., Magnusson, L. B. and Huizenga, J. R., *Spontaneous Fission Properties of Elements 97, 98, 99 and 100*, Nature 174: 265 (1954).
14. Bohr, A., and Mottelson, B. R., *Collective and Individual-Particle Aspects of Nuclear Structure*, Dan. Mat. Fys. Medd. 27: No. 16 (1953).
15. Ford, K. W., *The First Excited States of Even-Even Nuclei*, Phys. Rev. 90: 29 (1953).
16. Huizenga, J. R., and Duffield, R. B., Fission-to-Capture Cross Section Ratio, Phys. Rev. 88: 959 (1952).
17. For cross-section values see review by Huizenga, J. R., Manning, W. M. and Seaborg, G. T., Chapter 20, in *The Actinide Elements* (Seaborg, G. T. and Katz, J. J.), NNES, Div. IV, Vol. 14A: McGraw-Hill Book Company Inc., New York, (1954).

18. Stevens, C. M., Studier, M. H., Fields, P. R., Mech, J. F., Sellers, P. A., Friedman, A. M., Diamond, H. and Huizenga, J. R., *Curium Isotopes 246 and 247 from Pile-Irradiated Plutonium, Berkelium and Californium Isotopes Produced in Neutron Irradiation of Plutonium*, Phys. Rev. 94: 974 (1954); Magnusson, L. B., Studier, M. H., Fields, P. R., Stevens, C. M., Mech, J. F., Friedman, A. M., Diamond, H., and Huizenga, J. R., *Berkelium and Californium Isotopes Produce in Neutron Irradiation of Pu.* Phys. Rev. 96: 1576 (1954).

19. Duffield, R. B., and Huizenga, J. R., *Photofission and Photoneutron Emission in Uranium*, Phys. Rev., 89: 1042 (1953).

20. For a discussion, see Adams, G. D., *The Absorption of High Energy Quanta*, I., Phys. Rev. 74: 1707 (1948).

21. Huizenga, J. R., Gindler, J. E. and Duffield, R. B., *Relative Photofission Yields of Several Fissionable Materials*, Phys. Rev. 95: 1009 (1954).

22. McElhinney, J., and Ogle, W. E., *Relative Photofission Cross Sections of Several Fissionable Materials*, Phys. Rev. 81: 342 (1951).

Energy Loss and Total Charges of Fission Fragments Passing through Matter

By N. O. Lassen,* Denmark

The fragments resulting from fission of a uranium nucleus fly apart from each other with velocities of about 10^9 cm per sec. Some of the electrons belonging to the mother uranium atom will probably follow the daughter nuclei. Meanwhile, in collisions with the atoms of the surrounding medium, exchange of electrons will take place. Sometimes the fragment will lose an electron, or maybe more electrons, sometimes it will capture electrons. Thus, a fragment is an ion with a total charge equal to the difference between the nuclear charge and the number of accompanying electrons. When passing through matter the fragment will very quickly reach a charge state for which the probabilities for electron capture and for electron loss are about equal. The total charge will fluctuate around this mean value, which in the beginning of the path is of the order of magnitude 15–20 ϵ, where ϵ is the electronic charge. The cross-sections for electron capture and loss vary with the velocity of the fragment, and the total charge decreases, when the fragment is slowed down.

This decrease in total charge along the path is a property of the fragments which is significant for their whole behaviour. In the beginning of the path, where the fragments have high charges, the energy loss per cm is high. As the fragments are slowed down, the decreasing total charge involves that the specific energy loss also decreases along the path. According to theoretical considerations as developed by Bohr[1] the range of the fragments may be divided into two parts over which the stopping mechanisms are essentially different. In the first part of the range the energy loss will, almost entirely, be due to excitation and ionization of the atoms, and here the energy loss decreases along the path, as just mentioned. Near the end of the range, when the fragments reach a velocity of the order of $V_0 = \epsilon_2/\hbar$, they will be almost completely neutralized, and the energy loss in electronic collisions becomes very small. However, here begins the second part of the range. The fragments still have a considerable kinetic energy of the order of a few Mev and they will travel an appreciable distance before being finally stopped. Along the second part of the range the stopping is due mainly to nuclear encounters, i.e., collisions in which the kinetic energy is imparted to the stopping atom as a whole. From the theory it follows that the specific energy loss due to such nuclear collisions increases towards the end of the path.

Some of the mentioned features are well illustrated by the cloud-chamber experiments by Bøggild, Brostrøm and Lauritsen.[2] The tracks are characterized by the many branches, and it can be directly seen on the photographs (Fig. 1), from the number of branch tracks, that the energy loss due to nuclear collisions increases with decreasing residual range and reaches a maximum near the very end of the range. Using statistical methods it was possible from the cloud-chamber experiments to derive the velocity-range curve for the whole range.

A more direct measurement of the specific energy loss in the first part of the range was undertaken by means of the apparatus sketched in Fig. 2.[3] To the left side in the box is placed a brass plate carrying a thin uranium layer supported on a mica sheet. In front of the uranium is placed another metal plate with a number of collimating holes. To the right side in the box is a shallow ionization chamber; the fragments enter through one of its electrodes which is a thin foil of gold supported on a framework. The uranium could be moved; thus, the specific ionization at various points of the range could be measured in rel-

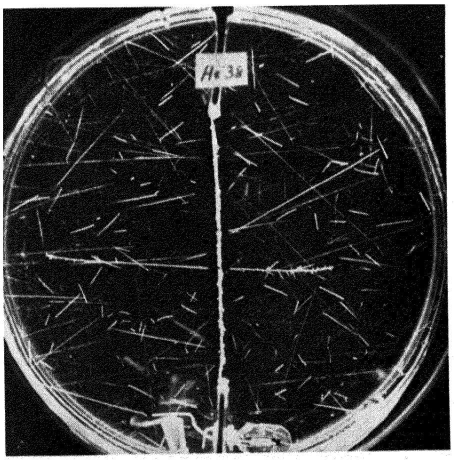

Figure 1. Tracks of fission fragments. (Photograph by Dr. J. K. Bøggild)

---

* Institute for Theoretical Physics, Copenhagen, Denmark.

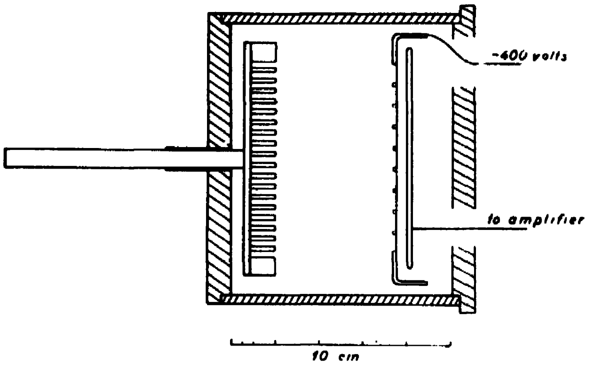

Figure 2. Arrangement for measuring the specific ionization by fission fragments along the path

ative units. The box was placed close to the cyclotron and irradiated with neutrons from an internal beryllium target. Figure 3 shows some ionization distribution curves obtained with deuterium in the box. The two lower curves correspond to distances between the uranium layer and the ionization chamber of 21.0 and 25.8 mm, respectively. In both cases the distributions clearly show the existence of the well-known two groups of fragments. It may also readily be seen that both peaks move to the left for increasing distances, the peak belonging to the heavy group moving faster than the other peak. For a distance of 16.2 mm the two peaks are rather close to each other, and for the still smaller distance of 11.5 mm they almost coincide. Figure 4 shows the distributions for higher values of the distance. The peaks move more and more to the left with increasing distance; the heavy group disappears in the background for a distance somewhere between 30 and 35 mm, while the light group may still be seen at a distance of 45 mm.

By plotting the abscissae for the peaks against the corresponding distances, curves shown in Fig. 5 are obtained. Due to the unavoidable background in the ionization chamber experimental points could be obtained only for the first part of the path. Here the stopping is due almost entirely to electronic encounters. It is satisfactory that the points corresponding to ordinary hydrogen (open circles) and to deuterium (full circles) fit the same curves. Along a considerable part of the range the specific ionization decreases almost linearly for both groups of fragments. By extrapolating the curves to zero ionization it is possible to define extrapolated ranges. The values so obtained are found to be much smaller than the values measured in cloud chamber studies by Bøggild, Arrøe, and Sigurgeirsson.[4] This is in conformity with the theory, since, as mentioned above, when the energy loss due to electronic interactions has become negligible, the fragments still have a considerable residual range.

In the figure an attempt has been made to derive the energy loss curve for the whole range. The end-points of the curves are the ranges given by Bøggild, Arrøe, and Sigurgeirsson. The end-parts of the curves show the energy loss per cm due to nuclear collisions, as calculated from the theory [reference 1, formula (5.1.2.)]. By fitting the two parts of the curves in a smooth way the result shown in the figure is obtained. While the curves for hydrogen and deuterium are identical in the first part of the range, they differ in the second part, due to the different nuclear masses. This gives rise to different total ranges in hydrogen and deuterium, as also found by Bøggild, Arrøe, and Sigurgeirsson.

Curves obtained in argon have a similar appearance (Fig. 6). Here the experiments seem to show rather definitely, that the curves cross over each other, the heavy group having the higher initial ionization.

From the specific ionization curves, energy-range and velocity-range curves may be calculated. In Fig. 7 these curves are given for argon; for comparison some velocity-points obtained by Bøggild, Brostrøm, and Lauritsen are shown; the agreement is fairly good.

Also the charges may be calculated. However, in other experiments the total charges have been directly measured by deflecting the fragments in a magnetic

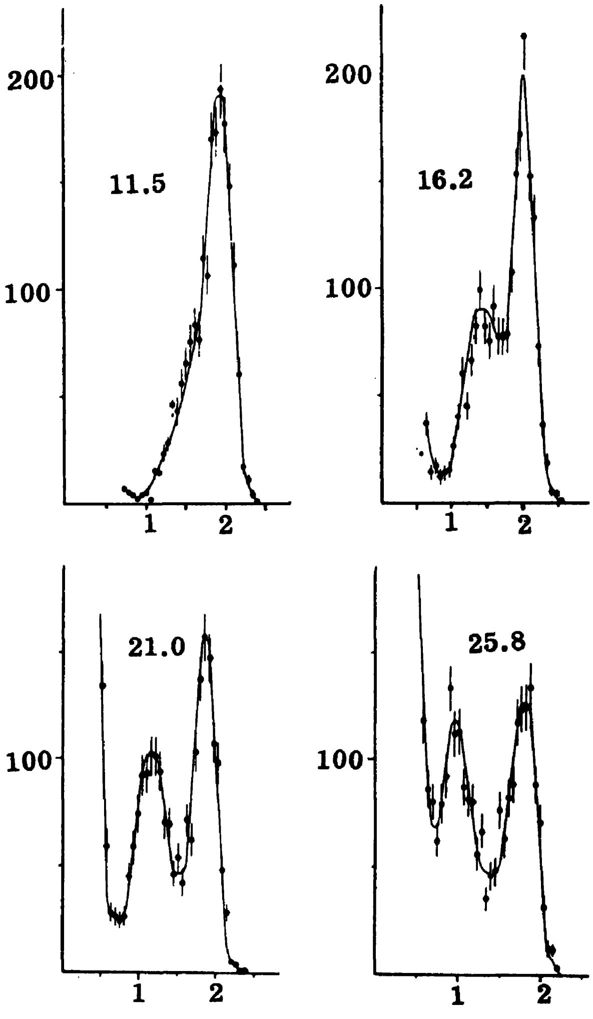

Figure 3. Ionization distributions in deuterium corresponding to distances between uranium layer and ionization chamber ranging from 11.5 to 25.8 mm D_2. Ordinate: number of fragments; abscissa: pulse size in Mev per mm D_2

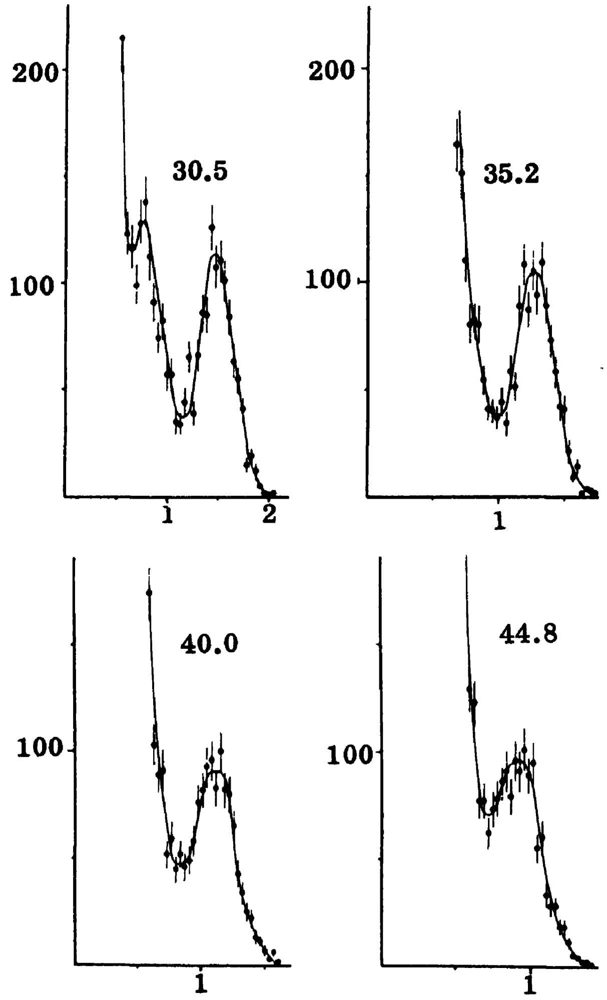

Figure 4. Further ionization curves in deuterium

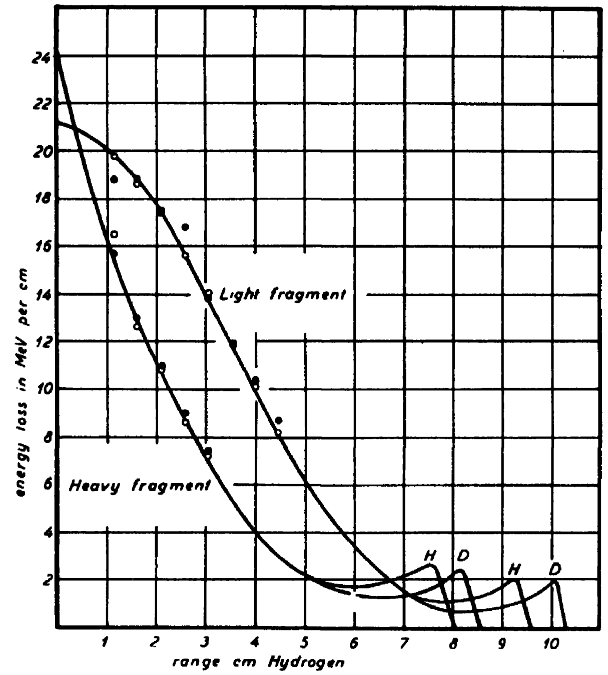

Figure 5. Energy loss along range in hydrogen and deuterium. Open and full circles correspond to H_2 and D_2, respectively

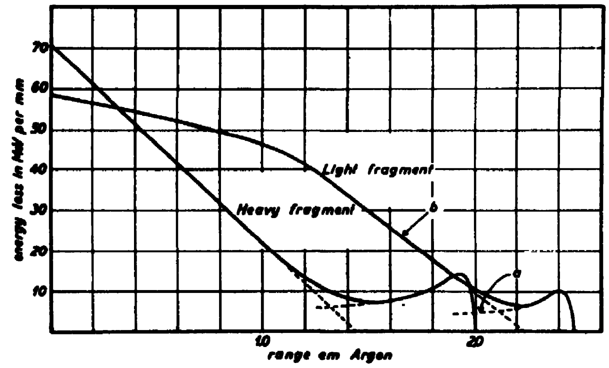

Figure 6. Energy loss along range in argon. Part a of the curves giving the energy loss due to nuclear collisions is theoretically calculated, while part b is experimentally measured

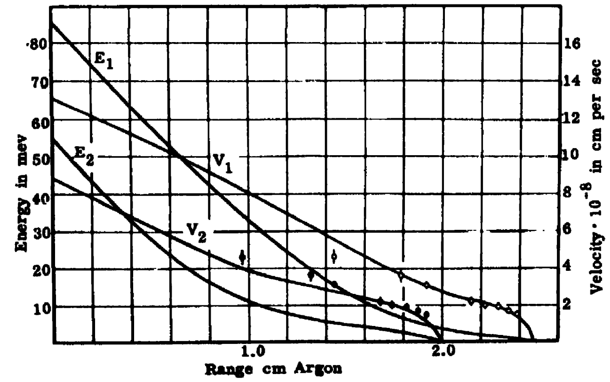

Figure 7. Energy vs range (scale to the left) and velocity vs range (scale to the right) in argon. Indices 1 and 2 refer to the light and heavy fragment, respectively. The points are the velocities given by Bøggild, Brostrøm and Lauritsen

field.[5] The arrangement shown in Fig. 8 was used. A thin strip-formed uranium layer (11) is placed close behind a beryllium plate (9) between the cyclotron dee's (10). Some of the fission fragments from the uranium layer pass through a movable slit (12); through a second slit (16) covered with a mica foil they enter an ionization chamber and are recorded. By counting for various positions of the movable slit, deflection distribution curves were obtained. The deflection chamber, i.e., the space between the uranium layer and the mica window, could be evacuated or filled with a gas to a low pressure. When it is empty, each fragment must possess the same charge along the whole deflection path, and the deflection distribution gives information about the charges with which the fragments leave the surface of the uranium layer. When a gas is admitted to the chamber, charge exchange processes will take place along the path. When the pressure is sufficiently high, the fragments will reach the state of equilibrium between electron capture and loss close to the uranium target, and the charge will fluctuate around the mean value along the whole path. In Fig. 9 the two curves to the right show the charge distributions for fragments having passed a thin Be-layer and emerging into vacuum. The two curves to the left show charge distributions obtained, when the fragments emerge into argon at a pressure of 0.9 mm Hg. White and black points correspond to the light and heavy group of fragments, respectively. In order to understand better the curves, let us for a moment assume each of the two groups of fragments to be homogeneous, that is, within each group all fragments have the same nuclear charge, mass and velocity. Along the path through matter the total charge fluctuates, the charge exchanges being randomly distributed. Hence at a definite point of their range, for instance when leaving the surface of the beryllium layer, the fragments will have a charge distribution which shows the magnitude and frequency of the fluctuations. This fluctuation distribution is measured when there is vacuum in the deflection chamber. With a high gas pressure in the chamber a high number of charge exchange processes also takes place along the deflection path and, consequently, the deflection will be determined solely by the mean charge. In agreement with this consideration the peaks obtained with argon in the chamber are much narrower than those corresponding to vacuum. The small residual widths may be accounted for partly by the geometry of the apparatus, partly by the inhomogeneity of the fragment groups.

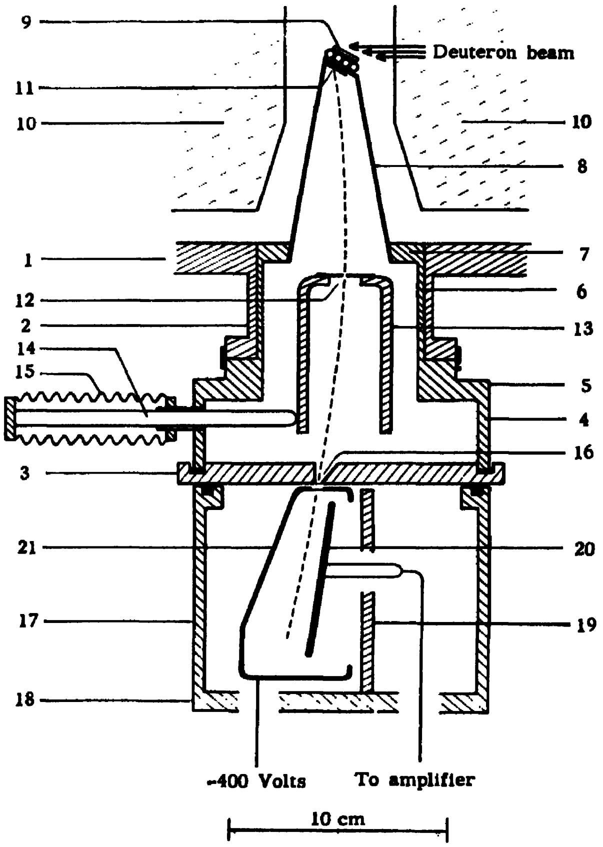

Figure 8. Apparatus for measuring the deflection of fission fragments in a magnetic field

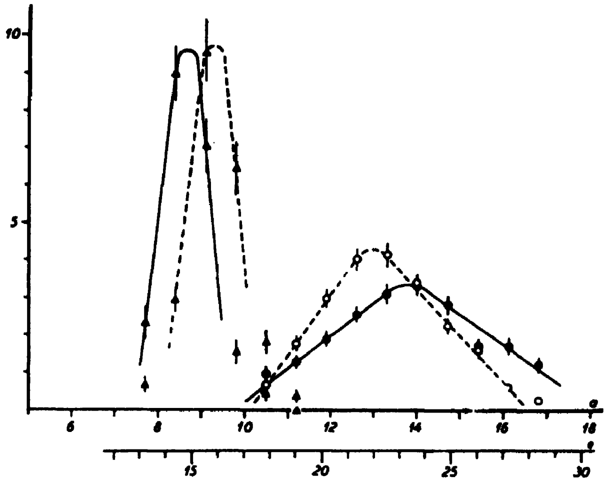

Figure 9. Charge distributions of fission fragments. The abscissa is the displacement a of the movable slit in the deflection apparatus. a is proportional to e/mv. Below is given the approximate charge scale corresponding to the mean value of mv. Circles refer to fragments having traversed a thin Be-layer and emerging into vacuum. Triangles refer to fragments emerging into argon at a pressure of 0.9 mm Hg. White and black points correspond to the light and heavy fragments, respectively

Besides in the widths, the curves differ in two other respects. Firstly, the charges are found to be much lower in argon than in beryllium. In beryllium, the mean charges are about 22 and 24 ϵ for the light and heavy fragment, respectively, while in argon the corresponding figures are 16 and 15 ϵ. Secondly, in beryllium the heavier fragment has the higher charge; in argon it is opposite, the lighter fragment has the higher charge.

Measurements in a number of materials have given the results shown in Fig. 10. As seen, the charges are about the same in all solids, though a slight variation with atomic number of the stopping medium is found. The same result applies to gases, and here the curves also show some anomalies for the lightest substances. The salient feature, however, is the considerable difference between the charges in solids and in gases.

This difference is again apparent in Fig. 11. Here the most probable deflections are plotted against the pressure of argon in the deflection chamber. For zero pressure the deflections correspond to the mean charges in uranium, for a pressure $\sim$1 mm they correspond to the mean charges in argon. For intermediate values of the pressure, intermediate values of the deflections are obtained, because at such low pressures the fragments do not reach the equilibrium charge state before having traversed a considerable path in the deflection chamber. The transition curves yield information about the length of this path and, hence, the cross-section for electron capture may be estimated. For the light fragment in argon a capture cross-section of the order of magnitude 10^{-16} cm^2 is found, in close agreement with theoretical estimates by Bohr and Lindhard[6] and by Bell.[7] The transition curves show clearly that the heavy fragment has a much higher capture cross-section ($\sim 10^{-15}$), which also agrees with theory.

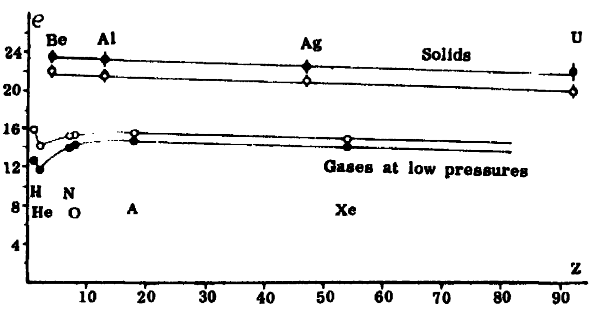

Figure 10. Equilibrium charges of fission fragments in various substances plotted against the atomic number. White and black points correspond to the light and heavy fragments, respectively

Another interesting feature exhibited by the curves in Fig. 11 is the increase in charge with increasing pressure for higher pressures. This increase may be understood by the following considerations. After a collision the fragment ion will often be left in an excited state. An electron is more easily removed from an excited state than from the ground state and the probability for loss of the electron depends on whether the ion has time to get rid of the excitation before the next collision. The time intervals between successive collisions are inversely proportional to the pressure. The higher the pressure is, the shorter are the intervals, the higher is the probability for finding the fragment in an excited state when a collision occurs, the higher is the loss cross-section and the higher is the balance charge.

With the experimental arrangement described, it was not possible to follow the charge increase beyond pressures of about 10–20 mm. Using the modified arrangement shown in Fig. 12 measurements could be made at somewhat higher pressures.[8] Here the ionization chamber is moved closer to the uranium layer and the mica window is omitted. Three spectrographs are used in parallel to increase the yield.

The results are given in Fig. 13. As seen, the rate of charge increase is highest for pressure below some 20 mm of argon or some 100 mm of the light gases. From the rate of increase the order of magnitude of the radiation life time may be estimated to be about 10^{-11} sec. At high pressures the charges seem to approach values some 3 or 4 units higher than the charges at very low pressures. Still, the charges are lower than in solids.

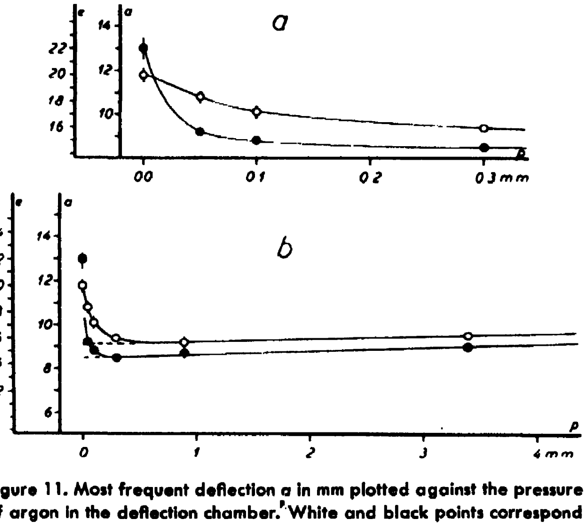

Figure 11. Most frequent deflection a in mm plotted against the pressure of argon in the deflection chamber. White and black points correspond to the light and heavy fragments

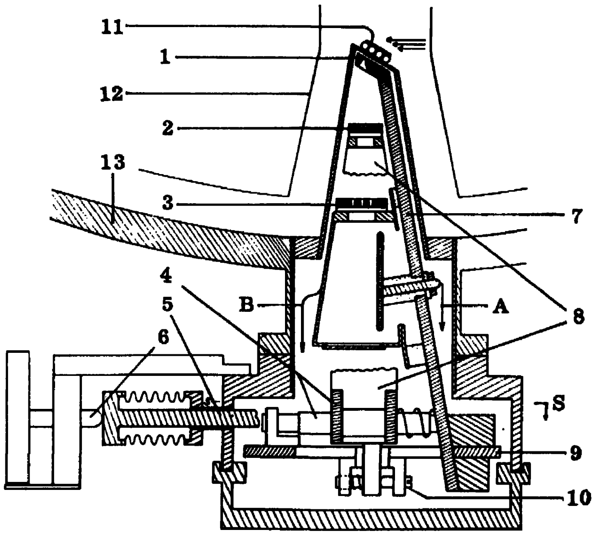

Figure 12. Modified deflection apparatus for measurements at high pressures

According to theoretical considerations by Bohr the total charge of fission fragments is approximately given by the formula

$$Z^* = \nu \cdot \frac{v}{v_0}$$

where v is the fragment velocity and ν is the effective quantum number for the outermost electron in the ion. For the heavy fragment ν is close to $Z^{1/3}$, where Z is the nuclear charge. The experimental value in argon at low pressure, 15ϵ, agrees closely with the formula. Using the relation $\nu = Z^{1/3}$ would lead to a charge of about 20ϵ for the light fragment. However, ν must, for the light fragment, be expected to be somewhat smaller than $Z^{1/3}$, which is in conformity with the experimentally observed value of 16ϵ. As mentioned, the charge increase with pressure may be accounted for by considering the competition between

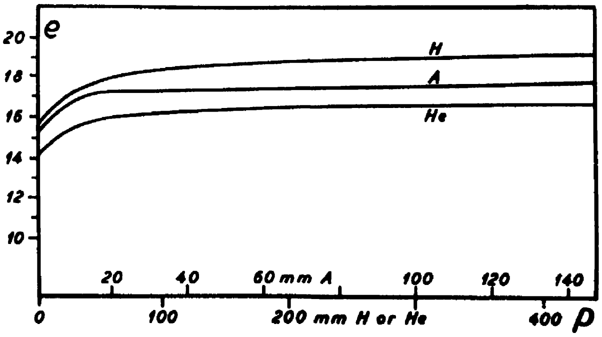

Figure 13. The total charge of the light fragment in hydrogen, helium and argon as function of the pressure

radiation from excited states and collisions. However, closer considerations show, that the phenomena may be even more complicated. If, for instance, an electron is captured in an excited state, the excitation energy will rapidly be shared among several electrons, and when the next collision occurs, the first electron will be found in a somewhat lower state. This sharing process will be independent of the pressure, since the time, τ_{dis}, for the distribution of the excitation energy is small compared with the time lapse τ_c, between successive collisions, even at high gas pressures. However, in very dense materials, such as solids, τ_c may be comparable with, or even smaller than τ_{dis}, and the considered electron may, until the next collision, remain in the highly excited state, from which it is easily removed. Such considerations would account for the higher charges in solids. Also, a qualitative argument can be given for the inverse ratio between the charges of the light and heavy fragment in gases and in solids, respectively. All these phenomena have been discussed in the paper by Bohr and Lindhard.[6]

REFERENCES

1. Bohr, N., Dan. Mat. Fys. Medd. *18*, No. 8 (1948).
2. Bøggild, J. K., Brostrøm, K. J., and Lauritsen, T., Dan. Mat. Fys. Medd. *18*, No. 4 (1940).
3. Lassen, N. O., Dan. Mat. Fys. Medd. *25*, No. 11 (1949).
4. Bøggild, J. K., Arrøe, H., and Sigurgeirsson, T., Phys. Rev. *71*, 281 (1947).
5. Lassen, N. O., Dan. Mat. Fys. Medd. *26*, No. 5 (1951).
6. Bohr, N., and Lindhard, J., Dan. Mat. Fys. Medd. *28*, No. 7 (1954).
7. Bell, G. I., Phys. Rev. *90*, 548 (1953).
8. Lassen, N. O., Dan. Mat. Fys. Medd. *26*, No. 12 (1951).

Record of Proceedings of Session 7A

THURSDAY MORNING, 11 AUGUST 1955

Chairman: **Mr. V. F. Weisskopf (USA)**
Vice-Chairman: **Mr. N. Ahmad (Pakistan)**
Scientific Secretaries: **Messrs. A. Salam and J. Leite Lopes**

PROGRAMME

P/911 On the theory of nuclear fission . . . . A. Bohr
P/593 Fission physics and nuclear theory . . . . J. A. Wheeler
P/993 The time involved in the fission process . . . . D. Popovic
P/1089 Statistics of photographic fission tracks and range estimate of fragments . . . . J. S. Ausländer and T. Visky
DISCUSSION

P/897 Studies on the nuclear photoeffect . . . . M. D. de Souza Santos *et al.*
P/884 Angular correlation of fission neutrons . . . . K. Skarsvåg
P/891 High energy gamma-rays from short-lived fission products . . . . . . A. Lundby *et al.*
DISCUSSION

P/592 Determinations of fission quantities of importance to reactors . . . . R. B. Leachman
DISCUSSION

Mr. A. BOHR (Denmark) presented paper P/911.

Mr. J. A. WHEELER (USA) presented paper P/593. As he included a certain amount of new material, his presentation is reproduced here in full:

We have just heard a most interesting and valuable account by Mr. A. Bohr of spin and parity effects in nuclear fission. We have seen a striking agreement between experiment and his theoretical conclusions. This agreement has to be taken as one more verification of the unified or collective nuclear model. Let me therefore briefly recapitulate some of the features of nuclear physics as embraced in this model. Let me then apply this point of view to consider five points: (1) slow neutron resonances, (2) fission barriers, (3) irregular variations in the fission cross-section for neutrons in the Mev range, (4) angular anisotropy in direction of fission, and (5) stability of superheavy nuclei.

	Molecule	**Nucleus**
1. Individual particle state occupied by	**Electron**	**Nucleon**
2. Slowly varying parameters affect particle states	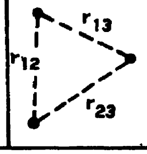	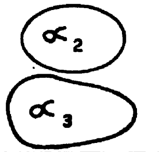

Slide 1

Some features of the nucleus are most economically described, as is well known, in terms of individual particle orbits, and others in terms of collective motions of the nucleus as a whole. The need for a unified model is clear. The possibility for such a picture follows from the circumstance that sufficiently heavy nuclei undergo collective oscillations with a period long in comparison with the time required for an individual nucleon to cross the nucleus. The time ratio is even longer in the case of a collective rotation. Consequently, it is a reasonable approximation to regard the individual nucleon motions as adjusting themselves adiabatically to the changing configuration of the nuclear surface. In this respect, it is appropriate to compare the nucleus with a molecule.

In the one case, as shown in Slide 1, the individual particle states are occupied by electrons; in the other case, by nucleons. In both cases these individual particle orbits are affected in wave function and in energy by the slowly varying co-ordinates that describe deformations and rotations. In the one case, these co-ordinates are the inter-nuclear distances, r_{12}, and so on; in the other case, they are the measures, α_2, α_3, and so on, of the various independent kinds of deformation—and rotation—of the nuclear surface.

Slide 2 estimates for a uranium nucleus and for a hydrogen molecule the comparative periods for collective oscillation and for motion of the most energetic individual particle—periods that are evidently consistent with the adiabatic approximation.

Slide 3 illustrates in a rough and schematic way, both for the molecule and for the nucleus, the difference between the two kinds of excitation of the system.

	Characteristic time, sec.	
	Molecule H_2	*Nucleus* *U*
3. Period of collective oscillation	8×10^{-15}	$\sim 5 \times 10^{-21}$
4. Fundamental period of motion of most energetic particle	$\sim 10^{-15}$	$\sim 0.3 \times 10^{-21}$
5. Ratio	8	15

Slide 2

The curves show energy of the system in a certain approximation as a function of deformation, both for the molecule and for the nucleus. This energy depends not only upon the deformation of the system but also upon the quantum numbers of the states occupied by the individual particles. Consequently, each curve is characterized by a different set of quantum numbers: the quantum numbers *n* for electronic excitation in the one case; or *n* for nucleonic excitation, in the other case. Collective motion is described in quite another way, for it is associated with a time rate of change of co-ordinates such as r_{12} or α. The corresponding excitations are described approximately not by a new set of curves, but by different amplitudes of motion along the curves already indicated. Associated with these collective excitations are vibrational and rotational quantum numbers, ν and *J* (or *I*).

It is one feature of the collective or unified description that it treats all nucleons in the same way, whether they are in completely filled or in partially filled shells. Also the unified model supplies a plan how to improve one's preliminary description of any given nuclear process, whether one starts with the individual particle picture or with the liquid drop model. It is appropriate to start with the individual particle picture when one is dealing with features of nuclear behavior that depend principally upon the properties of one nucleon. Among such features are the spins and magnetic moments of certain nuclear ground states, and many transition probabilities, and elastic or nearly elastic scattering of nucleons that are merely "tasted" by the nuclear potential without being "assimilated" into a compound nucleus. In such cases the unified model suggests as next step in the analysis allowance for the perturbation of the individual nucleon orbit by other orbits and by wall deformations.

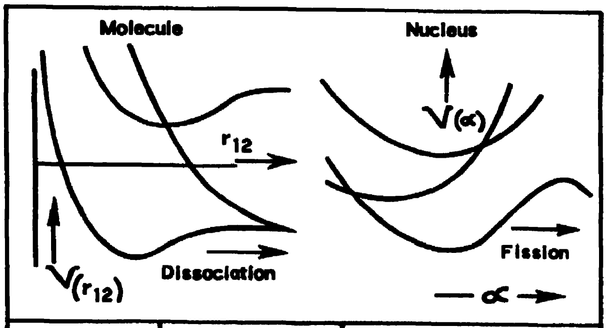

Particle states	**Electronic**	**Nucleonic**
Collective motion	**Vibration-rotation**	**Deformation-rotation**
Quantum numbers	**n** **v, J, K, Ω**	**n** **v, J, K, Ω**

Slide 3

In contrast, collective motions such as vibration and fission receive their first approximate description in the liquid drop model. In Slide 4, energy is calculated as a function of deformation, starting with the equilibrium spherical configuration of a uniformly charged liquid drop, and leading over a fission barrier to rupture and rapid separation of two fragments. Above is a contour diagram of the same deformation energy. Each curve is a line of constant energy. The principal deformation co-ordinate is plotted horizontally. Vertically is plotted another typical deformation co-ordinate, such as would correspond to an asymmetric distortion. *A* is a minimum and *C* a saddle point.

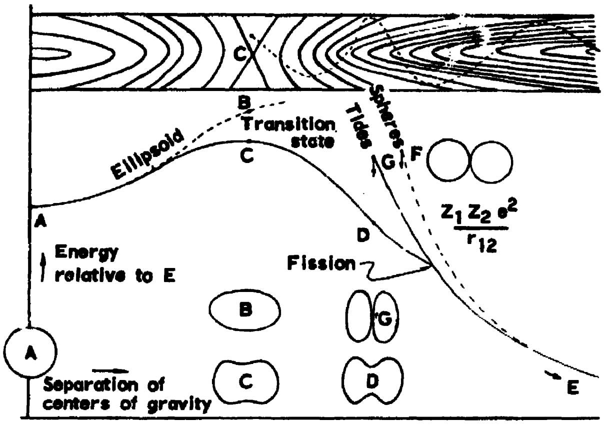

Slide 4

This picture of fission is only a crude first approximation, according to the unified model. First, there is not one energy surface, but a great number of energy surfaces, characterized by different values of the nucleonic quantum numbers. Second, the minimum of the typical surface will occur for a finite deformation, corresponding to the appropriate nuclear quadrupole moment, which will differ from one nucleonic state to another. Third, the height of the fission barrier above the minimum will differ from one nucleonic state to another, as already mentioned by Mr. Bohr. In particular, one has to expect a dependence of fission barrier upon nuclear spin and parity. Such changes in barrier heights will have their effect upon fission probability and partial level widths with respect to fission.

Slide 5 illustrates the levels of a given spin and parity belonging to a compound nucleus of an excitation up to *E*. In the center is a contour diagram of energy as a function of the principal deformation parameter plotted horizontally, and one other typical deformation parameter. With the energy *E*, all points are accessible that lie within the outer curve. The representative point of the system ultimately acquires enough velocity of collective motion to pass over the saddle point to fission. At the saddle point three nucleonic states of the given spin and parity are accessible; or $N = 3$. A simple statistical analysis of this problem leads one to expect, in the most primitive approximation, level width for fission proportional to the spacing of levels of the given spin and parity in the compound nucleus and proportional also to N. In a more nearly complete analysis one has to expect Γ_f to represent, not the width of any specific level of the compound nucleus, but the average of the width over a number of levels. Widths of individual levels of the given spin and parity will vary about this average in accordance with a statistical law like that for slow neutron widths, so long as N is one. They will show less variation when N is larger. This fluctuation is over and above any difference in Γ_f due to the two different spin values of the compound nucleus, $I \pm \frac{1}{2}$, and the marked differences in barrier heights and level widths that may be associated with these two values.

Now to pass from these expectations about fission widths to the observations, and what they tell about fission barriers. At other sessions of this Conference fission widths are reported for U^{235} bombarded by slow neutrons. The ratio of observed fission widths to level spacings is of the order of one tenth. It would not be unreasonable to assume that $N = 1$ or that only one nucleonic level is accessible in the saddle point configuration. This means an E value for U^{236} lying between the lowest level and the first excited level. A still lower excitation would call for barrier penetration and would greatly reduce the level width in disagreement with observation. The value $N = 1$ is also reasonable because the fission widths fluctuate about as much as the neutron widths—and the neutron widths themselves, of course, lead to only a single level of the residual nucleus. But to say $N = 1$ means a great uncertainty in our knowledge of the fission barrier height relative to E—an uncertainty of perhaps as much as 2 Mev, even greater than that proposed in the original text of this report. Now let us pass from level widths to barrier heights.

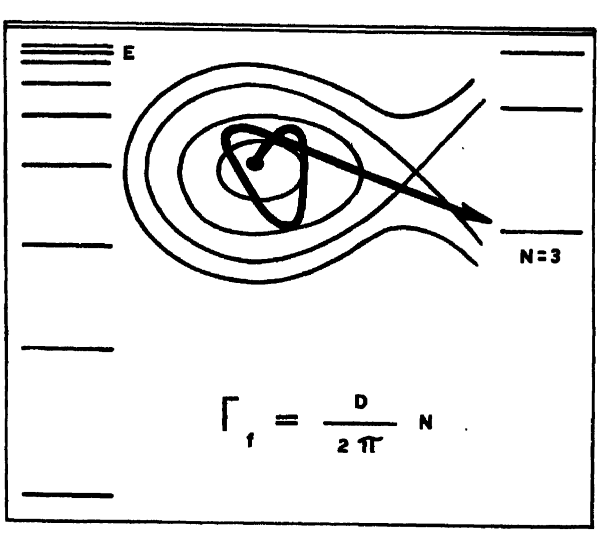

$$\Gamma_f = \frac{D}{2\pi} N$$

Slide 5

	(n,f)		Compound		E_f	
	Target	E_n	A	B(Mev)	(γ,f) or $E_n + B$	Drop
Th	232	1.05	233	5.1	6.2	7.6
	234	not SNF	235	4.6	> ~4.6	8.3
U	232	SNF	233	5.9	PF 5.18 ± 0.27	5.0
	233	SNF	234	6.7	< ~6.7	5.3
	234	0.28	235	5.3	5.6 PF 5.31 ± 0.27	5.5
	235	−1?	236	6.4	5.5?	5.8
	237		238	6.0	PF 5.08 ± 0.15	6.3
	238	0.92	239	4.8	5.7	6.5
Pu	238	SNF	239	5.7	PF 5.31 ± 0.25	4.3
	239	0 to ~ −1	240	6.4	~ 5.4 to 6.4	4.5

Slide 6

Slide 6 shows the case of the target nucleus U^{235}, the compound nucleus U^{236}, and the energy of excitation 6.4 Mev set free by binding of the extra neutron. The −1 Mev with the question mark symbolizes the depression of the fission barrier below this excitation by an amount anywhere from 0 to 2 Mev. The fission barrier is therefore expected to have a height anywhere from 4.4 to 6.4 Mev. The situation for U^{235} is almost exactly duplicated by the situation for Pu^{239}. There also the 5.5, with a question mark added, indicates a height anywhere from 4.4 to 6.4 Mev. The case of Th^{232} is much better defined, for the incoming neutron must have an energy a little over 1 Mev before it produces fission. Adding this to the neutron binding gives a barrier height of about 6.2 Mev. Other figures for barrier heights come from photo-fission measurements, as in the case of U^{233}, where the measured height is 5.2 Mev. This is consistent with the fact that U^{232} undergoes slow neutron fission, for the neutron binding of 5.9 Mev exceeds the barrier height. Apparently only in the case of the compound nucleus U^{235} does one have two independent measurements of barrier height, by thresholds for neutron-induced fission and for photo-fission. They agree.

The empirical values for barrier heights do not agree with the values calculated from the liquid drop model. One expects deviations on the basis of the unified nuclear model. Pressure on the nuclear wall will be expected to vary from nucleus to nucleus in an irregular way in the process of shell filling. Consequently, one will expect fluctuations from nucleus to nucleus in the height of fission barriers and strong departures from the liquid drop values, as observed. But we cannot yet predict the sense of the deviations, except for one effect—systematically higher barriers for odd-A nuclei than for neighboring even-even nuclei. The data in this table do not reveal this effect clearly; one has instead to go to spontaneous fission, which is also to be discussed elsewhere in this Conference.

One can expect in the future to get more data on barrier heights indirectly from observed rates of spon-

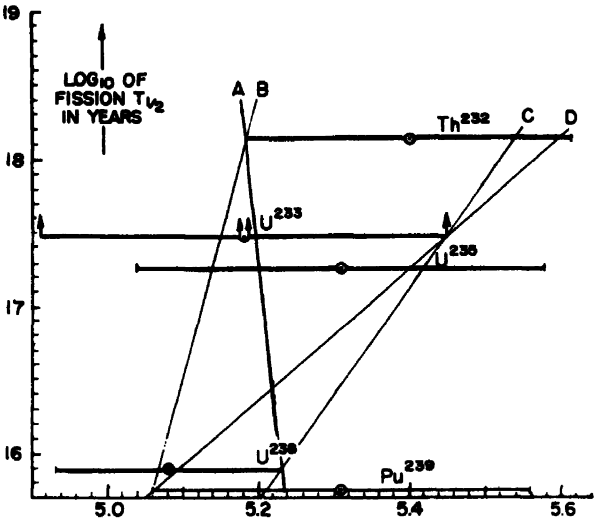

Slide 7

taneous fission. For this purpose one will need in a few cases a careful correlation between half-life against fission and fission barrier as measured directly. The available observations collected in Slide 7, with their great uncertainties suggest that a change in life time by a factor of 10^3 goes with a changing barrier height of the order of ½ Mev to 1 Mev. It is well known that half-lives against fission are longer for odd-A nuclei than for even-even nuclei by a factor of the order of 10^3, or sometimes very much more. This circumstance implies, then, a barrier height greater by anything from ½ to 2 Mev.

It is easy to see the foundation of an explanation for the lower barrier height of even-even nuclei. Slide 8, adapted from Nilsson, shows energies of individual nucleon states as a function of deformation. The numbers indicate the angular momentum Ω about the symmetry axis. With 94 protons one fills all states up to and including those marked by the dark line—2 protons to a state. The pairing means that the total spin is always zero. When the number of protons is odd, then placing the unpaired particle in the lowest unoccupied state results in an Ω-value that differs from one deformation to another deformation.

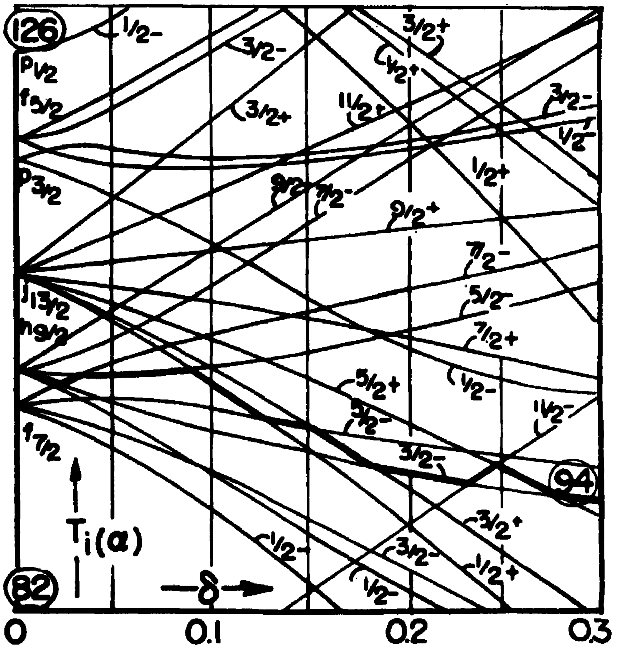

Slide 8

Slide 9 (Fig. 2 of P/593) shows what may be called the energy of specialization as a function of deformation. It is the energy increment to be added to the energy of a nucleus with a given deformation in the lower spin state to achieve a state of *specified* spin and parity. Of course, for an even-even nucleus the state of spin zero is expected always to be the lowest. Thus the "specialization energy" gives an estimate of the increase of barrier height of an odd-A nucleus compared to a neighboring even-even nucleus. The order of magnitude appears to be sufficient to account for the observed 1000-fold or longer fission half-lives.

Angular distribution of fission fragments has been so thoroughly discussed by Mr. Bohr that any comments in this report have been superseded. He takes into account not only the angular momentum brought in by the bombarding particle radiation but also the special features of the nucleonic energy level pattern when the nucleus is in its transition state.

Another effect that depends both on the pattern of transition state energy levels and on the incident nucleon energy levels is the cross-section for fission. Slide 10 (Fig. 1 of P/593) shows dips in the observed fission cross-sections for certain nuclei for neutron energies of the order of magnitude of a Mev.

Slide 11 shows still more recent results of Lamphere and Greene at Oak Ridge now in course of publication. The spacing of the peaks in the fission cross-section as a function of neutron energy can have nothing directly to do with the much finer energy level pattern of the compound nucleus. A quarter of a Mev spacing is of the right order of magnitude to correspond to the spacing between energy levels of a single neutron in the average field of force of a deformed nucleus. More-

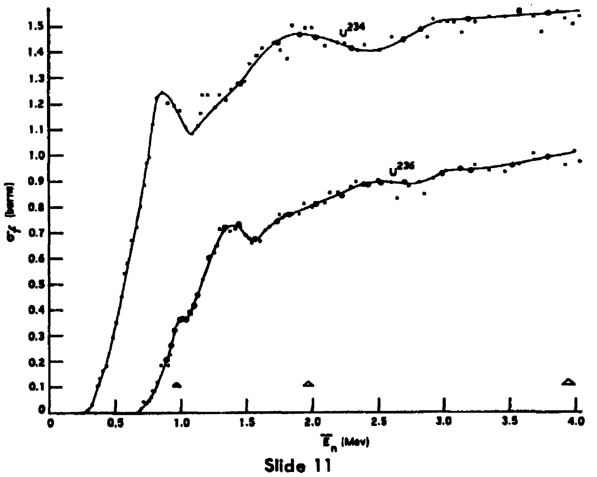

Slide 11

over, observation and theory of the scattering of neutrons by a nucleus show that there exist resonances in the neutron scattering. Otherwise stated, there are variations from energy to energy in the probability for the neutron to be in the nucleus, closely analogous to the Ramsauer effect in the scattering of electrons on atoms.

However, the observed neutron resonances are too broad to be compatible with the observed narrow widths. It is more reasonable, as Aage Bohr points out, to understand the rise in σ_f as due to the availability of a new fission channel in the transition state nucleus, and to understand the drops as due to the availability of a new channel for inelastic neutron scattering.

Slide 12 (Fig. 1 of P/593) uses what information is available about spontaneous fission and other stability limiting processes to estimate the stability limits for nuclei with half-lives greater than 10^{-4} sec. It is most difficult to extrapolate the fission half-lives reliably because superposed on the liquid drop trends there are individual nucleon effects, as already mentioned, but these have not yet been estimated. Subject to a very great deal of uncertainty on this account, one estimates that it should be possible to create and study nuclei in the dotted region, with masses perhaps twice as heavy as those of known nuclei.

CONCLUSIONS

1. Dependence of E_f on spin and parity.
2. N only 1 or 2 for $(E - E_f) \sim 1$ or 2 Mev.
3. Variations of Γ_f from level to level
   (a) Statistical, for given spin and parity
   (b) Difference in $\langle\Gamma_f\rangle$ for $I \pm \frac{1}{2}$
4. Rises in σ_f (E_n) when a new fission channel becomes energy-wise accessible; drop in σ_f when a new channel for inelastic neutron scattering becomes accessible (A. Bohr).
5. Directional correlation: (n,f) and (γ,f).
6. Odd-A nuclei: specialization energy; higher E_f, slower spontaneous fission.
7. Superheavy nuclei, $T_{1/2} > 10^{-4}$ sec.

Slide 13 is a brief recapitulation of the effects that we have just run over: the dependence of fission barrier on spin and parity; values of N that are small for slow neutron fission of U^{235} and plutonium; the variations of fission widths from level to level due to two quite different sources— one statistical for any given spin and parity; and the differences in the fission width depending upon the parity and spin itself; wiggles in the fission cross-section; directional correlations discussed by Mr. Bohr; for odd-A nuclei a fission barrier higher than for even-even nuclei and a slower spontaneous fission rate; and a set of limits for the stability of super-heavy nuclei.

Mr. D. Popovic (Yugoslavia) presented paper P/993.

Mr. J. S. Ausländer (Romania) presented paper P/1089.

DISCUSSION OF PAPERS P/911, P/593, P/993 AND P/1089

Mr. D. I. Blokhintsev (USSR): I listened with great interest to Mr. Wheeler's paper and would like to make a few observations.

It seems to me that the aspect of contemporary fission theory that relates to the adiabatic study of nuclear surface oscillations is weak. The period of these oscillations can be estimated to be of the order of 10^{-21} sec. The period of the individual transitions is several times greater than this period, and the fission time is still greater. It is therefore to be expected that during the fission time transfers of energy from surface oscillations to individual movements of the particles will frequently occur: the nucleus will remain part of the time in a state of collective oscillation, and the rest of the time in a state of individual excitation. This should have a considerable effect on the ratio of the fission width to the radiation width.

My second remark concerns Mr. Wheeler's views on nuclei of high atomic weight, which I find extremely interesting. I would like, however, to make a remark here originating from certain of our theorists who are not present here: no matter how nuclei of high atomic weight are obtained, they will consistently appear in the excited state. This circumstance may substantially alter the practical possibility of obtaining nuclei of high atomic weight.

Lastly, my third remark concerns heavily-charged nuclei. I would like to point out that it is customary to state that a consideration of the stability of motion of the electron shows that no nucleus having an atomic number above 137 can exist. It appears to me that these considerations fail to allow for the tremendous polarization in the vacuum surrounding such a nucleus. It is necessary to take into account the motion of the electron in the co-ordinate field. This may mean a substantial change in our conclusions about the motion of electrons round a heavily-charged nucleus.

The necessary calculations are already being made, but it is possible that in this problem electrodynamic theory will prove to have reached the limits of its usefulness.

The Chairman: Does Mr. Wheeler want to answer this now?

Mr. Wheeler (USA): There are three questions. The first question is about the theory. The point is only that the time for a vibration was compared with the time for motion of an individual nucleon across the nucleus, and this is the basis for the discussion of the *adiabatic* approximation. Of course, the time for fission itself is extremely long, merely because it takes such a very long time to concentrate energy in the particular body of deformation which leads to fission. But this time has otherwise no direct significance for the discussion of the *adiabatic* approximation.

I hope I have answered that point. Perhaps I could now go on to the second point about the formation of the super heavy nuclei, which will demand the addition of one neutron after another to an already heavy nucleus as one method of formation of a super heavy nucleus. Each neutron which is added will of course cause an excitation of the newly formed nucleus and this excitation must be dissipated by radiation. This time of dissipation will, of course, if the radiation occurs, be of the order of magnitude of 10^{-12} seconds as in typical radiative processes. This radiation is competing with processes of beta decay and of spontaneous fission of the newly formed nuclei which are estimated to have times which, in the ground state, are longer—10^{-4} seconds. In the excited state the time for fission will, of course, be shortened because of the excitation itself. Therefore, it is possible that one will be faced with limitations on how far one can go on this account. I have made no detailed calculations of the building-up process to see with what efficiency one can get to very heavy nuclei. It is, of course, very remarkable to how heavy nuclei one has already been able to go in the process of building up nuclei.

The third point, the limitations imposed on the stability of super heavy nuclei by electron theory itself, is a most interesting point because it is so often taken for granted that one cannot have a charge greater than 137 because the solutions of the Dirac equation failed to have the proper character beyond this point. However, we have done a numerical integration of the Dirac equation, changing from a point nucleus to a nucleus of a finite size. One finds that even with a nuclear charge of 170, the K electron has a perfectly reasonable wave function and orbit and has a binding energy of about 1.85 mc^2. There seems to be no difficulty on this account in accepting the possibility of super heavy nuclei.

Mr. R. E. PEIERLS (UK): My question is very similar to the first question which Mr. Blokhintsev has already asked, but perhaps I could put the point a little differently.

In his very interesting presentation Mr. Wheeler has in particular referred to the analogy with the motion of the molecules. Now, the difference seems to be, however, that in the energies with which one is involved in the fission process, one is not concerned with only one or two possible states of internal variables, but there are very many of them accessible, and this is perhaps brought out by the fact that Professor Wheeler's slide had, in addition to the quantum numbers written down, a little black block, and I think we have to remember that there are many quantum numbers hidden in that black block. We are really in analogy, not so much with the vibration of the molecule, but with similar problems in the theory of solids where, for example, the interaction between the excitation of an atom in a dielectric and the vibrations of the adjacent atoms leads to problems of somewhat similar structure, and I think we know from that field that one must be rather careful with the use of the simple analogy with the one degree of freedom in the molecule.

May I also make one point on the very interesting remark made by Mr. Wheeler on electron orbits around a heavy nucleus. I think it is certain that, as Mr. Wheeler points out, one should not take any notice of the divergence one gets from a point charge for a large atomic number. But, of course, whether to believe the solution of the Dirac equaton for a charge as high as this, is another question because, as Mr. Blokhintsev also indicated, at that point the correction becomes a complication due to vacuum polarization and will become so serious that it is doubtful whether the simple solution of the Dirac equation would represent the truth in such an academic case.

Mr. BOHR (Denmark): As to the first question, I think we would certainly agree that the fission process in the initial stage represents a situation where many degrees of freedom come in, and I think that the analogies with the molecules are only used in a statistical way in such cases. In the cases of the low lying spectra or of nuclei passing over the saddle point close to threshold one has however relatively few degrees of freedom to take into account, and it seems that one then makes a detailed description on the basis considered.

The question which I wanted to put to Mr. Wheeler is in regard to the interpretation of the hump in the fission cross-section. They seem to be sharper than the observed variations in the total cross section interpreted on the basis of the optical model.

I wanted to ask whether someone would care to comment on this. I also wanted to ask if one might not think of an alternative interpretation in terms of the effect of the competition between fission and neutron emission. Such an explanation has been advanced by Mr. Ben Mottelson.

For example, at the point where the fission cross section levels off or decreases some new inelastic channels may become available which would make the neutron emission strong and drive the fission cross section down.

Mr. V. V. VLADIMIRSKI (USSR): Mr. Wheeler's paper gives an interesting comparison of the available experimental data concerning the dependence of the fission threshold on the charge and on the number of nucleons in the nucleus with calculations based on the liquid-drop model. The work of Koch, MacAllen and Gasteiger on photofission thresholds has already shown that the close dependence of the fission threshold on the fission parameter x, proportional to Z^2/A, predicted by the liquid-drop model theory was not confirmed by experiment. The paper shows that merely substituting a constant factor for the function of the form $(1 - x)^3$ predicted by the theory gives better agreement between the calculated and observed thresholds.

The picture provided by the liquid-drop model is a rather rough approximation. In particular, it does not permit a description of the elongated form of the unexcited nucleus.

I wish to call attention to a point which may reduce considerably the dependence of the threshold on the nuclear charge, as predicted by the liquid-drop model, and give better agreement with the experiments. In the liquid-drop model the interaction energy of the nucleons is conventionally divided into volume and surface terms. Thus, the volume term in the Weizsäcker semi-empirical equation depends closely on the excess of neutrons in the nucleus, while the surface term is entirely independent of the mass number. It can now be considered as established that some of the excess neutrons are concentrated near the surface of the nucleus. Teller has given a qualitative explanation of this effect. It is necessary for a phenomenological description of the redistribution of the charge in the nucleus to introduce into the surface energy a term dependent on the excess neutrons. Consideration of the liquid-drop model as thus refined leads to the following results:

$$\frac{a\left(\frac{A}{2}-Z\right)^2}{A+\mu A^{2/3}}$$

The sign of the isotope component of the surface energy may be determined on the basis of stability considerations. It can be shown that the excess neutrons behave similarly to surface-active agents in solutions. They accumulate on the surface, and as the number of excess neutrons in the nucleus increases, the surface tension of the nucleus decreases.

As the nuclear charge increases, the neutron excess decreases and the surface tension increases. This compensates to a considerable extent for the lowering of the fission barrier, associated with the increase in the Coulomb energy.

The logarithm for spontaneous-fission probability depends principally on the fission parameter x, but systematic deviations from this rule have been observed. Isotopes with a small excess of neutrons are relatively long-lived. The isotope dependence of the surface tension affords a qualitative explanation of this phenomenon.

The **Chairman**: I do not know if you would like to reply to this, Mr. Wheeler.

Mr. **Wheeler** (USA): I would like to talk with Mr. Vladimirski individually, if I could.

Mr. **Leachman** (USA): I have to make a remark that has a bearing on the paper by Mr. Bohr. In the last paper of this session, new data of anisotropies from neutron-induced fission as obtained by Brolley and Henkle will be presented. It is of interest to note at this time that a large anistropy has been observed for U^{238} fission just above the threshold for fission. The second matter of interest in this new data—and here the data are for 7 and 14 Mev induced neutron fission—is the cosine to the fourth power relation between the fragments and the neutrons inducing fission. I was hoping that Mr. Bohr might be able to make a few remarks in regard to both these pieces of data.

The second question is to Mr. Ausländer. This is in regard to Mr. Ausländer's paper on the ranges of fission fragments, which gives a very nice method for simplifying the experimental difficulties in establishing ranges of fission fragments. The statement I have to make is that we should like to know whether the recently published data on the fission fragment ranges could be applied to the method developed in his paper, and thereby test the assumptions of this method and also the sensitivity of the method. An example of the range data of which I am speaking is the photographic emulsion work done by Demers in Canada and which appeared in the Canadian Journal of Physics about a year ago.

Mr. **Ausländer** (Romania): I thank Mr. Leachman for his intervention, the more so as the paper by Demers which he referred to had escaped my attention. I do not know the details of this paper but I suppose that surely the method proposed here may be applied competitively with other methods to give further information and to establish its accuracy.

The **Chairman**: Mr. Bohr, would you like to answer Mr. Leachman's question here or in private conversation?

Mr. **Bohr** (Denmark): I would say that these data brought out by Mr. Leachman are extremely interesting. The isotropy observed which is above the threshold may perhaps be related to the fact that the nucleus at this point passes over the saddle point under one particular configuration, and I think that one can draw conclusions from the observed isotropy as to the quantum numbers of this configuration, which must have a low K value. For fast neutron fission, one may expect higher multiples in the nuclear distribution but no very detailed analysis has been made so far. Certainly, there should be higher terms.

The **Chairman**: At this point, I would like to ask Dr. Mostovoi to make some remarks.

Mr. V. I. **Mostovoi** (USSR): I have some brief notes to offer about experimental work on the fission of nuclei into three parts.

Neutron-induced fission of nuclei into three parts has been studied by many investigators (Green, Livesey, Titterton, Louisa Marshall, Tsiang, Wigner, Allen and Devon, and others).

This particular research by T. A. Mostovoi determined the probability of emission of a long-range alpha particle during spontaneous and induced fission of the Pu^{240} nucleus.

An ionization chamber of special construction was used to study triple fission. The chamber is shown schematically in Slide 14. The system of electrodes (BAB') forms a chamber for detecting fragments. The long-range alpha particles are detected in the space between electrodes CB and $B'C'$.

A nylon mount transparent to the fragments was coated with a thin layer of plutonium and placed on the central electrode (A). The plutonium layer employed in the work contained 90 per cent Pu^{239} and approximately 10 per cent Pu^{240}.

The long-range alpha particles produced by fission in the target S entered the chamber (CB and $B'C'$) through electrodes B and B', which were made of aluminum foil 15 microns thick. The fact that triple fission had taken place was detected by the coincidence of the ionization pulse due to the fission fragment in chamber (BA, AB') with the pulse from the long-run alpha particle in chamber (CB and $B'C'$).

Measurements were made during fission of Pu^{239} by

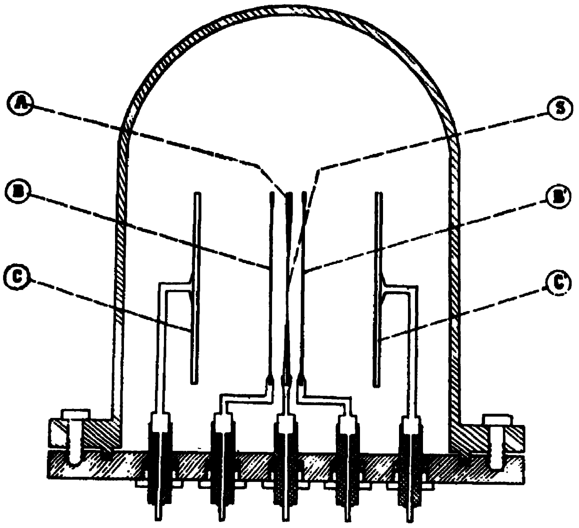

Slide 14

thermal neutrons and during spontaneous fission of Pu^{240}.

The measurement results show that the probability of triple spontaneous fission of the Pu^{240} nucleus is 1.60 ± 0.15 times greater than the probability of a triple fission of Pu^{239} by thermal neutrons. This result agrees with Tsiang and Wigner's hypothesis on the mechanism of triple fission. (Phys. Rev. *83*, 673, 1951).

Since the triple spontaneous fission effect is very infrequent (approximately three fissions per hour), a series of control experiments were performed. In particular, measurements were made with a polonium target having the same alpha activity as the plutonium target used in this work. Measurements were made with a U^{235} layer without a source of neutrons, etc.

All these control experiments have confirmed that the measured effect was produced by triple spontaneous fission.

The CHAIRMAN: I am afraid that we have to cut off the discussion at this point. I would ask the speakers who sent in additional questions to discuss them at the next discussion period, if there is time.

Mr. M. D. DE SOUZA SANTOS (Brazil) presented paper P/897.

Mr. A. LUNDBY (Norway) presented papers P/884 and P/891.

DISCUSSION OF PAPERS P/897, P/884 AND P/891

Mr. B. C. DIVEN (USA): I have a question for Mr. Santos.

In view of the fact that he has found some serious discrepancies in the (γ,n) thresholds that have been used for many years, I wonder if he plans to make any measurements on the photo-fission thresholds to check if those accepted now are correct?

Mr. SANTOS (Brazil): Many experimental determinations of (γ,n) thresholds were made assuming that the threshold for the (γ,n) process in Cu^{63} was 10.90 ± 0.2 Mev.

Since this value has been considered as a standard for betatron energy scale calibration and since, on the other hand, our measurements indicate that the correct value should be 10.54 ± 0.04 Mev, I think that some of the values which have been assumed for the thresholds of photoprocesses in many elements will have to be altered. Our determination of the Cu^{63} threshold agrees with the recent measurements of Birnbaum within the experimental errors.

As we think that the values which have been assumed for photofission thresholds may be affected by a small systematic error, it is a part of our program to measure their values.

Mr. WILKINS (USA): I have a question for Mr. Lundby. I wonder if you could comment in a little greater detail on the status of the comparison between the photo-neutron measurements and gamma-ray measurements?

Mr. LUNDBY (Norway): For periods longer than one hour, as I mentioned, the agreement was very good. For our measurements on short-lived gamma rays, we do not yet know the abundance of the gamma rays. We have not yet gotten that far in the experiment. Earlier experiments on short-lived neutron period would probably not be able to see the effect of our gamma-ray because they usually obtain the periods by a peeling-off process.

If you compare the results in Canada and the United States of America, we find that particularly in this low life-time region, there are insufficient experiments, or where there are experiments, they are not in agreement as regards periods.

The CHAIRMAN: Since we have some time left for the discussion, I should like to ask the speakers whom we had to cut off during the last period to speak now. I have a question here from Mr. Sanders of the United Kingdom.

Mr. J. E. SANDERS (UK): This question is directed to Mr. Bohr of Denmark. I would like to ask Mr. Bohr whether he considers that the mass distribution in fission and the number of neutrons emitted in fission, in the slow neutron fission region, might be a sensitive function of the spin and parity of the compound state which is formed; whether one may get different neutron emissions from various resonances due to this cause?

Mr. BOHR (Denmark): As to the mass distribution, a specific effect is expected regarding the possibility for symmetric fission. Some levels may give less symmetric fission than others. On the other hand, this would probably not affect the general trend of the whole mass distribution curve. Therefore, also, one hardly expects a major effect on the neutron number.

The CHAIRMAN: We have another question by Mr. Egelstaff of the United Kingdom which refers to the paper by Mr. Wheeler. I am sorry that Mr. Wheeler has left the room. Would you still like to present your problem?

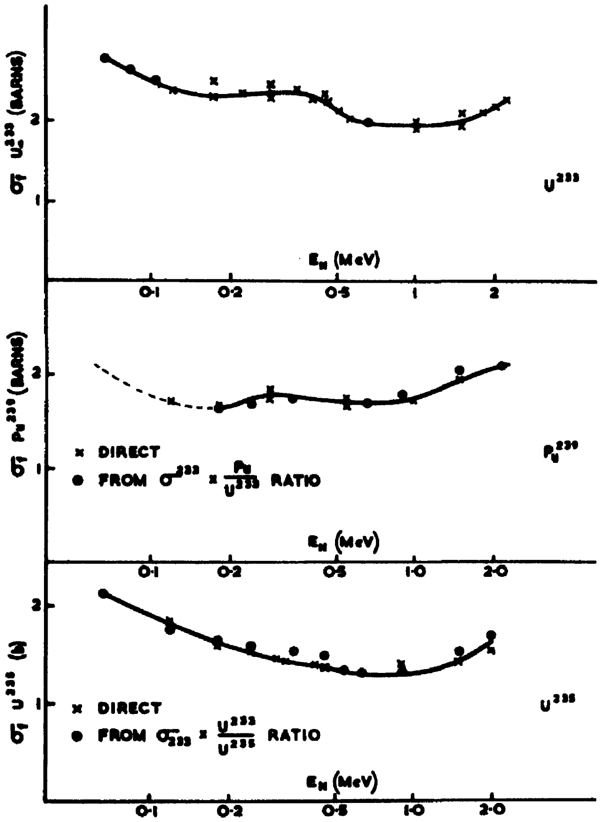

FISSION CROSS-SECTIONS.

Slide 15

Mr. P. A. **Egelstaff** (UK): The question refers to the variation of fission cross section with neutron energy in the fast fission of U^{233} and U^{235} and plutonium-239. We have observed variations in these cross sections similar to the variations shown in one of the slides for even-even target nuclei. The question is: could these variations be accounted for in the same way as suggested for an even-even target nuclei? Slide 1 shows the type of variation meant. There are two kinds of things which we observe. One type of variation is a rather sharp variation with energy. The other type is a rather slow variation.

One can see in the upper curve which is for U^{233} that there is a rather sharp drop in the cross-section at 0.4 Mev. On the other hand, there is a rather slow variation before it and a slow rise after it. Similarly, at 0.3 Mev for plutonium, you get a maximum and then a slow rise at 1.5 Mev. But for U^{235}, you get the form shown in the lower curve. The question is, can these rather slow variations be accounted for on the single particle model or perhaps can the sharp variations be accounted for by the presence of inelastic scattering levels coming in strongly at one point.

Mr. **Bohr** (Denmark): As you point out, there are the two mechanisms that have been discussed that can give rise to variations in the fission cross-section. One is the single particle resonance effects and the other is the competition with neutron emission, and it might be, as Mr. Egelstaff said, that the more sharp variation may be of the latter type, whereas the more smooth variations may be of the former. It will be very interesting, of course, to have data on the total cross-section to compare with. This could decide the question.

Mr. **Egelstaff** (UK): On the question of the variation of the total cross-sections, we have found and I think that a number of other laboratories are in agreement with us—that the total cross-section does also show a rise at about 2 Mev where you can see all three fission cross section curves show an increase of cross-section towards 2 Mev.

The **Chairman**: Are there any other comments on the paper before the discussion?

Mr. **Netter** (France): I would just like to say that we have found the same type of variation for the three isotopes U^{233}, U^{235} and plutonium-239 in our paper (P/355), which will be presented at a later session (17A).

Mr. R. B. **Leachman** (USA) presented paper P/592.

DISCUSSION OF PAPER P/592

Mr. M. S. **Kozodayev** (USSR): We have just had the pleasure of hearing a very interesting and informative paper by Mr. Leachman concerning the work of a large group of physicists. This paper dealt with the determination of important quantities that characterize fissionable materials. Mr. Leachman remarked that the data obtained by United States physicists on the dependence of ν on the excitation energy of the Pu^{240} nuclei agree very well with the data reported in the work of Spivak and his associates. In this connection, I should like to furnish some slightly more detailed information on the work of these Soviet physicists.

Using a method based on recording the *coincidence* between the fissions occurring in the investigated matter under the influence of thermal neutrons, and rapid fission neutrons, V. P. Zakharova, V. A. Kalashnikova, V. I. Lebedev, L. A. Mikaelian, and P. E. Spivak measured the relative values of ν for U^{233}, U^{235}, Pu^{239} and Pu^{241}.

The following results were obtained:

$$\frac{\nu(U^{233})}{\nu(U^{235})} = 1.03 \pm 0.01 \qquad \frac{\nu(Pu^{241})}{\nu(Pu^{239})} = 1.04 \pm 0.01$$

$$\frac{\nu(Pu^{239})}{\nu(U^{235})} = 1.19 \pm 0.01$$

In the same work, independent measurements were also made of the value of ν, using a calibrated source to reproduce the spectrum of the fission neutrons. It turned out that

$$\nu(U^{233}) = 2.6 \qquad \nu(Pu^{239}) = 3.0$$

$$\nu(U^{235}) = 2.5 \qquad \nu(Pu^{241}) = 3.1$$

The error in determining ν is approximately 4 per cent.

Other research dealt with the determination of the dependence of the quantity ν on the excitation energy of the nucleus that is being fissioned. In its purest form, this dependence should be shown by a comparison of the number of neutrons released by spontaneous fission of a certain nucleus (${}_{z}X^{A}$), and the number released by fission by thermal neutrons of a nucleus of the same element but with its atomic weight reduced by one (${}_{z}X^{A-1}$). In the case of spontaneous fission the nucleus is not excited and the fission process depends entirely on the probability of passing through the potential barrier. When the (${}_{z}X^{A-1}$) nucleus is fissioned by thermal neutrons, the excitation energy of the fissioned nucleus equals the binding energy of the last neutron in the formed nucleus (${}_{z}X^{A}$). To determine the dependence of ν on the excitation energy of the fissioned nucleus, the number of neutrons emitted by spontaneous fission of Pu^{240} and by induced fission of Pu^{239} by thermal neutrons was measured in an experiment performed by the same authors, and also performed by A. V. Krasnushkin and M. I. Pevzner.

It was found that the number of neutrons, ν, emitted by fission of the excited Pu^{240} nucleus exceeds by about 30 per cent the number of neutrons emitted by spontaneous fission of the same nucleus.

All the work mentioned here was reported at one of the meetings of the July session of the Academy of Sciences in Moscow.

Mr. SANDERS (UK): I would like to make one or two remarks about the very beautiful work reported by Mr. Leachman in his paper. At Harwell, we have made measurements on the relative neutron emission from the spontaneous fission of plutonium-240 and thermal neutron induced fission of plutonium-239 and we find that the average number of neutrons per induced fission of plutonium-239 is greater than the number of neutrons in spontaneous fission of plutonium-240. $\bar{\nu}$ in the spontaneous fission of plutonium-240 is 76 per cent of $\bar{\nu}$ for thermal neutron fission of plutonium-239. This result, I think, is in very good agreement with the result given by Mr. Leachman and also the result mentioned by Mr. Kozodayev.

I would like to ask Mr. Leachman one question about neutron spectra from fission. Has he any data on the neutron spectra from spontaneous fission of any nuclides?

One further question: could he comment on the gamma-ray sensitivity of the counters used in measuring neutron multiplicity and how compensation for the gamma rays emitted in fission was made in this case?

Mr. DIVEN (USA): With regard to the question about the gamma-ray sensitivity of the detector used for observing the neutron multiplicities from fission, the only gamma rays of interest are those which are emitted not promptly, but within about 30 microseconds after a fission occurs, because we observe all of the neutrons from fission in an interval of some tens of microseconds. We can see no prompt fission gamma rays and we see no delayed gamma rays beyond a few tens of microseconds. We have an efficiency for detection of gamma rays that is near 100 per cent for anything that comes out inside this interval of 30 microseconds. It is conceivable that some gamma rays get counted as neutrons, but very few.

Session 8A

RESEARCH REACTORS

LIST OF PAPERS

Page

P/946 Report on research reactors . . . . . . L. Kowarski 233

P/484 The nuclear reactor in basic science . . . . . . A. H. Snell 248

P/401 Research reactors . . . . . . E. Bretscher *et al.* 254

P/888 Practical experiences with the JEEP reactor . . . . . . T. J. Barendregt *et al.* 259

P/762 Experience with B.E.P.O. . . . . . . R. F. Jackson 266

P/485 Materials testing reactor experimental program and reactor operation . . . . . . R. L. Doan and J. R. Huffman 270

P/486 Research program and operating experience on ORNL reactors . . . . . . M. E. Ramsey and C. D. Cagle 281

P/859 Research program and operating experience on ANL reactors . . . . . . W. H. McCorkle and W. H. Zinn 304

P/487 Observations on operation, training and research experiences with the Raleigh research reactor . . . . . . C. Beck 314

P/804 The need for basic research in an atomic energy program . . . . . . T. H. Johnson 318

Report on Research Reactors

Prepared by L. Kowarski,* UNESCO

1. INSTITUTIONS INTERESTED IN RESEARCH REACTORS, AND THEIR FIELDS OF RESEARCH

This UNESCO sponsored survey aims at providing a technical basis for discussions as to whether a given institution should acquire a research reactor, and, if so, what type. Such decisions must often be made by non-specialists who sometimes stand in need of a quick orientation prior to calling for expert advice.

We start with a few definitions.

A research reactor may be defined as one which has been built for the purpose of gaining information, rather than for producing useful energy or transmuted substances. The information sought may be totally extraneous to the reactor itself, or to reactor technology; the reactor then serves as a tool and a source of radiations (chiefly neutrons). Or it may be used as an object of research; a line is to be drawn here between research and advanced development in the pre-production stage; some pilot versions of industrial reactors although—strictly speaking—of a mainly informative interest, are too closely connected with production programmes to be considered as research reactors.

Whether tools or objects, reactors built for research may also be used for demonstration or training purposes, in accordance with the traditional connection between higher teaching and original research. Experience also shows that a reactor built primarily for research may become quite useful to a research institution in a small-scale producer capacity; it may contribute to research activities by producing moderate quantities of radioactive material for local consumption.

A tool of such uncommon versatility may be found of interest to a wide variety of institutions. We may mention, as a matter of further definition:

(1) Science faculties, in which both the basic teaching of fundamental science (physics, chemistry, biology), and graduate work on original research subjects are taking place.

(2) Medical schools, chiefly for radiobiology and for radioactive tracers used in graduate research work.

(3) Technological schools and faculties, both for teaching and graduate work.

(4) Institutes and schools specialized in nuclear science and technology. (This category is likely to develop in the near future.)

(5) Government research establishments exploring the advanced regions of nuclear science in view of both civilian and military applications.

(6) Research establishments connected with power production (general-purpose electrical networks; in the future: railways, industrial combines, etc.)

(7) Testing stations (mostly governmental) of the Bureau of Standards type. (They may perform useful services for other institutions engaged in reactor work, by carrying out radioactive calibrations, purity tests and analyses by methods involving radiochemistry).

(8) Research institutes acting frequently as suppliers to other institutions (we shall probably see the development of specialized radioisotope stations, similar to the present Isotope Divisions of Oak Ridge or the Commissariat à l'Energie Atomique, and equipped for local supply of fairly short-lived isotopes; the supply function will develop from the station's own research activities, as in Institut Pasteur). Provision of irradiation facilities for outside institutions may also be considered as a supply service.

(9) Industrial institutes of applied research (metallurgy, ceramics, food, drugs, plastics, etc.—a very quickly developing category).

(10) Hospitals (diagnosis with the help of tracers and radiations; therapeutical possibilities as yet in their bare beginnings, but quick development may be expected to take place. Many hospitals are today in possession of nuclear accelerating machinery such as betatrons or linear accelerators; a reactor is potentially as useful as any of these).

It will be found that categories 4, 5 and 6 will tend to install research reactors of the most powerful and expensive types, whereas for most purposes of interest to the other categories, the medium-sized and medium-priced reactors developed during the last few years will be quite adequate.

The choice of research subjects for which a given reactor will be used will depend both on the character of the institution and on the type of the reactor. The present report may be of some help in reaching the very preliminary decisions relevant to a reactor project, i.e., whether a given institution should go into the reactor field at all, and if so, what type of reactor would be best suited to its aims and resources. For such a preliminary survey we think it useful to give a fairly comprehensive list of possible research subjects. Since new ways of using a reactor for research purposes are invented and tested, so to speak, every day, this list should not be considered as exhaustive. It is however diversified enough to necessitate some sort of a selection if used as a help to establish a research program for a single reactor. When attempting such a selection, the following remarks may be of use:

---

* Commissariat à l'Energie Atomique, Paris; and European Organization for Nuclear Research, Geneva. Paper submitted by the United Nations Educational, Scientific and Cultural Organization.

Original language: French.

(1) Is a substantial part of the time and space available around a reactor to be devoted to teaching, or is, on the contrary, advanced research to be considered as the main purpose of the project? If the former is true, stress will be laid on the chapter "Reactor Behaviour" and, in the other chapters, on basic techniques and on simple experiments, easy to repeat and to check. If advanced research is the aim, the behaviour of the reactor will be studied once for all in its early life, and study of the general techniques will be reduced to an indispensable minimum. Care will be taken to look for new items, and to create new combinations of items already named.

(2) Some groups of items are practically a must, whatever the specialization selected. This "common trunk" includes above all the reactor behaviour, and some specific items such as fast neutron techniques, chemical manipulations, production of short-lived isotopes, and radiation dosimetry.

(3) The chapter on Reactor Behaviour is of particular interest to technical universities which wish to train future reactor engineers, and to research stations attached to governmental or private power projects, In such institutions, this chapter, suitably expanded, and supplemented by some material testing, may constitute the whole programme.

(4) Institutions of the testing and supplying types will have to devote most of the time of its reactor to (*a*) items of research calculated to study and improve its performance as a supplier, (*b*) the supplying functions themselves. Experience shows that, if these functions have to be satisfied first, other items of research will have to be curtailed.

(5) As we have already stated, pilot versions of production reactors should not be considered as research reactors at all. Experimental reactor assemblies, built for the sole purpose of testing some new physical or technological principle, are more closely connected with research activities proper; they should, however, hardly be attempted by educational and scientific institutions other than the highly specialized establishments of the Argonne-Harwell-Saclay type.

(6) A reactor, as practically any other research tool, is subject to the following dilemma:

(*a*) If it aims at coming close to the ideal of "second to none" or "giving the most intense radiation available in the world," it will be very costly and difficult to build.

(*b*) The most powerful tools tend however to skim any research field to which they come to be applied; gross effects are spotted more easily, normal-type experiments can be performed in a shorter time and the most refined features of a phenomenon, on the limit of the powerful tool's possibilities, pass unnoticed by its weaker competitors.

To put it briefly, opportunities to make discoveries cost money. However, the finest apparatus cannot exhaust a whole science, if only because its very uniqueness reduces its availability. Possessors of second-line equipment, by dint of ingenuity, harder work, and preparedness to scrap, if necessary, a no longer promising opening have a good chance of producing brilliant work and providers of research reactors need not strain their financial backs to a breaking-point. Some quantitative indications as to the correlation of the reactor intensity with the extent of its usefulness for research will be given in the last chapter.

List of Research Subjects

I. Behaviour of the Reactor

11. Reproduction factor: rise and fall of the radiation level (amount of fuel burnt per second) according to the value of reproduction factor, including the subcritical values.

Effect of control rods and other absorbing bodies put in the reactor, on the reproduction factor.

Effect of temperature and pressure on the reproduction factor.

12. Exploration of neutron densities in and around the reactor core, with precision techniques (foils, wires, etc. . . .). Ratios of fast to thermal and resonance to thermal neutrons. Determination of characteristic lengths in various media in and around the core. Radiation densities inside and outside experimental holes and channels.

13. Attenuation of radiation in shields (fast neutrons and gamma rays).

14. Effect of the structure of the reactor on various aspects of its behaviour (e.g., radiation density gradients in or near a cooling or experimental channel).

15. Operation and safety routines. Radioactivity after shutdown.

16. Effects due to the accumulation of fission products and to the irradiation of reactor materials.

II. Physical Research

21. Behaviour of the reactor's control and measuring equipment; use of the reactor as a test bench for detecting and measuring instruments to be used elsewhere.

22. Standardization and calibration of reactor radiations in absolute and relative units.

23. Fission process: fission fragments (velocity, angular correlations . . .) delayed neutrons, excitation energies, etc. . . .

24. Creation of specialized neutron spectra: monochromatic neutrons (crystal monochromators and choppers; uranium slow-to-fast converters). Interaction of these neutrons with various substances: thermal cross-sections, fast cross-sections, migration in reproducing and non-reproducing media, interaction of slow neutrons with the molecular structure of medium.

25. Study of neutron resonance phenomena. Neutron optics (diffraction, refraction, polarization and reflection).

26. Gamma-ray, beta-ray and neutrino studies; nuclear spectroscopy of isotopes produced by irradiation in the reactor; neutrons produced by gamma-emitters (photoeffect).

27. Physical study of transmutation products (transuranic elements, fission products, radioisotopes).

28. Solid state physics: (*a*) Diffusion in solids, studied with the help of reactor-produced radioactive tracers.

(*b*) Effect of neutron irradiation on conductivity of semi-conductors.

(*c*) Effect of neutron irradiation on physical properties of alloys.

(*d*) General study of lattice defects, as produced by fast neutron irradiation.

III. Chemical Research

31. Use of the reactor as a test bench for the development of tele-manipulation and hot chemistry equipment.

32. Characterization of nuclear species, produced in the reactor, by radiochemical techniques.—Chemical study of transmutation products (cf. 27 above).

33. Radiation chemistry: effects of neutrons and gamma-rays (from gamma-emitters manufactured in the reactor) on chemical properties and reactions. Modifications of crystalline and plastic structure under neutron irradiation. Hardening of alloys. Speeding up of polymerization.

34. Phenomena involving both nuclear and chemical processes (e.g., Szilard-Chalmers effect).

35. Study of chemical reactions with the help of reactor-produced tracers and sources. Separation processes.

36. Quantitative analysis: (*a*) with the help of tracers; (*b*) by neutron irradiation. Search for very small admixtures of specific impurities (by neutron irradiation).

37. Determination of molecular structures by neutron diffraction: (*a*) substances containing hydrogen; (*b*) substances containing atoms with specific magnetic properties.

IV. Biology and Medicine

(Present uses rather than all possible uses have been listed.)

41. Effect of radiations on personnel; tolerances. Quantitative formulation of radiation doses, dosimetry, shielding. Civil defence.

42. Detailed studies of separate kinds of radiation: slow neutrons, fast neutrons, gamma rays. Effects on living beings (survival, fertility, mutations) studied individually or on whole populations. Delayed effects.

43. Pure and applied genetics. Production of useful mutations in plants.

44. Selective response to neutrons of tumours injected with neutron-capturing substances (this item is quoted as an example of diagnostic and therapeutic possibilities of a reactor; we may expect that a considerable number of other such possibilities will be discovered within the next few years).

45. Biological and physiological research with the help of reactor-produced tracers and sources.

46. Production of sterile media. Sterilization of food, drugs and medical supplies. Irradiation of fermentation agents.

47. Insect and fungus control.

V. Reactor Engineering

In addition to relevant subjects listed under "reactor behaviour" we first mention a very comprehensive item, followed by a few of a more particularized kind.

51. Comparative study of basic reactor designs. Tryouts of novel and unconventional designs under a more detailed approach.

52. Study of neutron-multiplying and neutron-reflecting properties of media containing fissile or moderating substances, or both. Exponential and critical experiments using a reactor as a neutron source.

53. Effects of radiation on proposed reactor materials (effects produced by fast neutrons and by gamma rays to be studied separately) as revealed by changes observed in (*a*) electrical conductivity; (*b*) thermal conductivity; (*c*) heat capacity; (*d*) viscosity; (*e*) material strength; (*f*) corrosion properties, etc.

54. Development and selection of new materials. Control of materials as regards neutron absorption, by the "danger coefficient" and oscillation methods.

55. Study of nuclear properties (interaction with radiation) of matter in general, to deepen the scientific background of items 53 and 54.

56. Shielding materials, shapes and designs.

VI. Other Branches of Applied Research

Most engineering research is carried out by specialized applied-research organizations which in due course may acquire reactors as standard research tools. In the present stage of development and use of such tools it would be premature and, at any rate, too long to list all possible specialized applications branching out of the basic physical, chemical and reactor-engineering subjects mentioned above. A "supplying type" research institution may find to be called upon to supply the following broad categories of services to engineering research establishments:

61. Manufacture of radioactive sources, used for instance: for radiography; for accelerated tests of corrosion, stress etc.; for thickness gauges by beta-ray absorption.

62. Manufacture of radioactive tracers used in the study of engineering processes (e.g., study of lubrication and wear by friction).

63. Study of radiation damage to materials likely to be exposed to radiation in the future atomic power stations, atomically propulsed vehicles, seacraft and aircraft, etc.

Applications in agricultural research and food and drug research will naturally grow out of the sections III and IV listed above. Among industries relying on advanced research, fine metallurgy, electronics (esp. semi-conductors) and organic chemistry may be expected to make an increasingly wide use of reactors for their research; others will follow.

2. TECHNOLOGICAL FACTORS AFFECTING THE CHOICE OF A RESEARCH REACTOR

Next to the question whether a given institution should acquire a research reactor comes the choice of a type. A definite decision can be taken, of course, only on basis of detailed knowledge of the proposed types, for which the descriptions given in the current declassified literature are usually adequate. This chapter, together with the next one, provide a common background for such a detailed study.

2.1 Performance Rating

For an overwhelming majority of the uses to which a research reactor may be put, it is important that inside its material assembly there should be volumes in which numerous free neutrons are present at any given moment.

Neutron density usually is measured as the aggregate length of track which the neutrons leave behind them as they traverse the unit volume in a given time. This total length (cm per cm^3 sec) is called "neutron flux"; it can be imagined as arrived at by counting each neutron multiplied by its velocity. Since neutrons of different velocities act on matter in a different way, it is customary to divide them in velocity classes and to count these partial fluxes separately. The two most important classes are: (*a*) neutrons which have yet all the original velocity with which they came out of a fission ("virgin flux"); sometimes this class is widened as to include all those whose velocity stays above a certain limit (corresponding to, say, 1 kev; "fast flux"). (*b*) In reactors using the slowing-down process (as is the case of nearly all reactors considered in the present report), by far the greater part of the useful life of a neutron is spent in a state close to the velocity equilibrium with the surrounding medium. The partial flux corresponding to this range of velocities ("slow"† or "thermal flux") is often considered as *the* "flux" characterizing a reactor. The most powerful research reactors existing at present produce a maximum slow flux of the order of 10^{14} n/cm^2/sec. Reactors run deliberately at very weak power levels may produce as little as 10^7 n/cm^2/sec.

High fluxes (useful for research) are connected with high powers (useful for most other purposes) but not coincident. In a given reactor, the flux observed at a given moment is directly proportional to the total power which the reactor produces at that moment. But two different reactors run at the same power may produce very different flux values. The other relevant factors are: the total volume of the reacting medium and the lifetime of the neutrons within the medium. It so happens that the incidence of these three factors on the slow flux can be combined in a single datum: power per unit weight of fissile element (U^{233} or plutonium, see below) present in the medium. Since power as such is of little interest for research purposes, the designer will seek to keep the necessary minimum amount of fissile element ("critical mass") as low as possible. Since fissile atoms have to compete for neutrons with neutron-absorbing bodies in the medium, the introduction of any such body increases the critical mass.

It appears from the foregoing that search for a high performance in the design of a research reactor is unseparable from a certain number of compromises. We may mention:

(*a*) The conflict between the highest power extraction rate (efficient cooling devices, see below) and the increase of the critical mass due to these devices;

(*b*) Every attempt to use the flux by inserting bodies to be irradiated, providing experimental facilities, or removing neutron beams outwards reduces the maximum flux; we have a choice between a higher flux available for fewer uses, and the contrary.

The last-mentioned dilemma exists also as regards the size of the reacting core. A very compactly designed research reactor gives more flux per unit power, but fewer experimental facilities than a more loosely-built one. The best way out of this contradiction is to build several compact reactors, but a community which for any reason decides to build only one reactor is somewhat less interested in compactness.

In a reactor designed for a high slow-neutron flux, fast neutrons present are considerably smaller in numbers but since their velocity is thousands of times higher, the fast flux is lower than the slow flux by a not very big factor (see figures in specialized descriptions below). The best conditions for reducing this gap are not the most favourable for maintaining a high slow flux; hence another compromise to be observed by designers who want both fluxes to be as high as possible. A high fast flux is, of course, useful whenever, in a given research item the interest is focussed on the interaction of fast neutrons with matter (such a bias can be given to solid state studies, cross-section research, preparation of radioactive isotopes—in fact, if one so chooses, to most of the items listed in Chap. I). In any reactor a high local value of fast flux can be obtained by using the "converter" device (a suitably shaped mass of uranium which gives off fast neutrons if subjected to a high slow flux).

2.2 Nature of Nuclear Fuel

All nuclear fuels used at present contain either U^{235} or plutonium. "Natural fuel" is the isotopic mixture of the two uraniums (7 kg of fissile U^{235} per ton of mixture), as it is found in nature; "pure fuel" is nearly pure U^{235} (as obtained by isotope separation), or plutonium (as obtained by transmutation of U^{238}). Intermediate fuels may be "slightly enriched" (say, 10 or 20 kg of U^{235} per ton), or "medium enriched" (such as the fuel made available under the International Pool Agreement and which may contain up to 200 kg per ton), or "highly enriched" (about 90% pure, as used in many American research reactors). Extraneous atoms are however present even in the pure fuel, whether U^{235} or Pu, since it has to be used in the form of a chemical compound, or an alloy, or in conjunction with a carrier substance.

The most commonly used types of fuel are at present:

(*a*) Natural uranium, usually in the form of pieces of chemically pure metal. They are usually cylindrical

---

† The term "slow flux" sometimes *also* covers the class of velocities immediately above the thermal; this distinction may be ignored in this brief survey.

(short or long, full or tubular) and wear a thin metallic sheath ("cladding").

Main advantage: availability in a nearly free market. Basic disadvantage: absorption of neutrons by the preponderant U^{238} leaves few neutrons available for other losses. The resulting increase in critical mass is considerable. In order to mitigate it, only the least neutron-absorbing materials, and those only in limited amounts, may be used for cladding and in the construction of the reacting vessel and of its internal cooling, controlling and experimental devices. However, the critical mass remains big enough to necessitate the extraction of great amounts of heat for a given flux; in fact for each kilowatt extracted from a current-type enriched-fuel reactor, we may have to take as many as a 100 kw out of a graphite-and-natural U reactor if we want to obtain the same flux in both cases.

This enormous increase in the necessary power level aggravates all safety problems and necessitates costly engineering structures outside the reactor proper. To sum up: compared to an enriched-fuel research reactor, a natural-uranium one is crude, costly and less safe. Nevertheless, many research reactors of this type have been, and probably yet will be, built; the advantages of availability may be decisive if the required flux is not too high. It should also be said that for various types of production reactors, the disadvantages of natural uranium are far less decisive and a community which wishes to combine research with a pilot-design for a producing system may well decide to make a start with natural fuel.

(*b*) Chemical compounds of highly enriched uranium. The most commonly used compound is uranyl sulfate dissolved in ordinary water.

(*c*) Highly enriched uranium alloyed with many times its weight of aluminium. This alloy, sandwiched between Al sheets, constitutes the "fuel plate" and several plates, held in an Al box, constitute a standard "fuel element."

Absorption by Al tends to thin out the available neutrons; with a minimum of Al, more flux is obtained per kilowatt of reactor power. Since tendency is towards higher fluxes, it may be expected that future designs of fuel elements will tend to reduce the Al content.

This type of fuel is likely to assume a preponderant place in the research reactor field. It has already this place in the US practice and, as enriched fuel becomes available to a greater number of nations, this preponderance will spread. Medium-enriched uranium (up to 20 per cent; see above) can be used in the same way, although the U^{238} atoms present in the fuel diminish the flux-generating efficiency in the same way as aluminium does. At 20 per cent enrichment this decrease is noticeable but in no way decisive for the reactor design. Plutonium, whenever available, may in principle be used in the same way, in similar fuel units, although the metallurgy of its mixing with the carrier may be in practice somewhat different.

(*d*) Slightly enriched uranium (15 kg or so, of total U^{235} per ton of U) may become available in the future as a first, and militarily innocuous, step of isotope separation. Its presentation must be different from that of richer sorts, since U^{238} is plentiful enough to act both as a carrier and as flux inhibitor.

As regards the disadvantages mentioned under (*a*) above, it will be found that slightly enriched uranium is intermediate between the natural and the rich grades. The intolerance of materials, on the other hand, is greatly attenuated even at the slightest enrichment. In other words, a reactor of this type, compared to a rich-fuel one, is still somewhat costly and less safe, but—contrary to a natural-uraniun one—it need not be technologically crude.

Two important aspects of the fuel question may be mentioned here. The cladding problem in research reactors is far less important than in productive ones, since there is little need for high temperatures, unusual mechanical stresses or corrosive liquids. Only in gas-cooled (see below) natural-U types are there serious difficulties to solve in connection with this problem.

The length of stay of a fuel element in the reactor depends on many causes of limitation, most of which are simply proportional to the flux. This goes for the radiation damage which tends to throw the element out of shape; for the mechanical, thermal and corrosional fatigue (chiefly in natural-U reactors); for the poisoning by fission products and finally for the simple depletion (which is the dominant cause in rich-fuel types). The following rule of thumb may be of some use: in low-energy reactors (those not requiring any cooling), the length of stay of the fuel is practically indefinite. In cooled reactors giving a flux under 10^{13}, the lifetime of the fuel may be counted in years (many, or at least a sizable fraction). Above 10^{13} the useful life is counted in months or weeks.

2.3 Moderators and Reflectors

In most research reactors, and certainly in all those which have been declassified to any marked degree, the chain reaction is propagated by thermal neutrons, which means that the reacting medium, in addition to fuel, must contain a high proportion of lightweight "moderating" atoms. The juxtaposition of fuel and moderator may be homogeneous (solutions of U salts), or arranged in a spatial lattice (a certain degree of spatial segregation is structurally convenient and moreover, whenever the fuel contains considerable amounts of U^{238}, becomes necessary for nuclear reasons).

Moderators used at present are:

H (light hydrogen) in the form of H_2O (other compounds, such as plastics, can be used only at lowest fluxes because of radiation damage).

D in the form of heavy water.

Be, usually in the form of beryllia BeO.

Carbon in the form of synthetic graphite.

The advantages of H_2O are: zero cost; highest slowing-down efficiency per cm of neutron path, hence the possibility of achieving the reaction in a minimum volume; possible use as a coolant, which makes possible a simplified reactor design; ability to maintain, in a given medium, a high ratio of fast to slow neutrons (see in chap. III the description of the highest-flux research reactors). Disadvantages: relatively high neutron absorption (thins out the thermal flux). The very compactness of the water-moderated reacting medium may become a disadvantage if one wishes to maintain the reaction in a fairly large volume in order to accommodate many experimental facilities.

The advantages of D_2O are: good slowing-down efficiency (not so good as H_2O, better than C or BeO); possible cooling function (like H_2O) and, above all, practically no neutron absorption (important in conjunction with poorer fuels; very important in techniques based on natural U). Disadvantage: high cost.

The advantages of graphite are: low cost; solidity (which is put to use in some very simple designs, as for instance in low-pressure air-cooled reactors); resistance to high temperatures. Disadvantages: appreciable neutron absorption (not as bad as H_2O, so that graphite is still usable with poor fuels); lowest slowing-down efficiency.

This balance of advantages and disadvantages points overwhelmingly to the use of graphite, as a moderator, in conjunction with cheaper fuels and least advanced technology. In the present research reactor technique, moderation by graphite occupies a rather unimportant place; it had a greater importance in the past when lower fluxes were aimed at, and refined materials were less easily obtainable, and may become important again if the trend in research reactors reverts towards higher temperatures.

Beryllia is on the whole comparable to graphite; its much higher cost offsets its somewhat greater efficiency as slower-down.

An additional layer of a moderating substance is usually provided around the reacting medium for the purpose of sending back some of those neutrons which tend to escape from the outer surface of this medium. Such a reflector exerts a beneficial effect on the flux to total power ratio since it improves the neutron economy and thereby decreases the critical mass.

For reflectors the high density (atoms per liter) is rather more important than for moderators; low atomic weight is somewhat less useful and appreciable neutron absorption somewhat less prohibitive; otherwise the requirements are similar. This shifts the balance in favour of beryllia, the other three competitors ranging in the order: heavy water, graphite, light water. Two other considerations are: cost (which makes beryllia particularly desirable for reactors moderated by light water, since in these the reacting volume is small, and therefore can be surrounded without expending too great an amount of reflecting substance); and simplicity of design, which confers an additional preference on using the same substance as both moderator and reflector. This structural unity of the "core" (reacting zone) with the reflector is customary in graphite-moderated, and in many types of water-moderated reactors: in the latter, the capacity of the tank containing H_2O or D_2O may considerably exceed the volume necessary to maintain the chain reaction and the fuel lattice occupies only a central zone of water-filled volume, so that the fuel-carrying core is surrounded on all sides by (at least) a few decimeters of water.

The device of composite reflection may be resorted to. Heavy water is an efficient but expensive reflector; it pays to use it in a fairly thin layer and to dispose, outside the water-tank, an additional and cheaper layer of graphite. In H_2O-moderated reactors the situation is reversed: cheap but inefficient, ordinary water is best used as a second (outer) reflector which means that the water tank is big, and that a hollow polyhedron build of BeO or C is immersed in it so as to surround the core on (if possible) all sides.

2.4 Cooling

The operation of a high-flux research reactor produces great quantities of heat in a small core volume; this heat has to be removed in order to avoid the disruption of the core. Contrary to what takes place in power-producing reactors, the removal of heat from research reactors is to be considered as a means rather than an end and can be carried out with little regard to the quality (temperature) of the outgoing heat flow. This indifference simplifies the construction of the circuits which carry the coolant through the reacting core; their low working temperature widens the choice of circuit materials; corrosion dangers are minimized and high coolant pressures can be more easily withstood. Only in the highest-flux reactors (around 10^{14}), where the rate of heat removal per unit volume approaches the ultimate possibilities offered by the contemporary engineering, does the necessity of maintaining high temperature gradients reappear in some designs.

Zero-power and low-power research reactors present no cooling problem; as the power approaches the 10-kilowatt range, or the flux some 10^{11}, the necessity for some fluid to move continuously through the reacting volume begins to appear. At that stage, for the reactors using ordinary or heavy water as moderator, there is the convenient possibility of using the motion of the water in bulk, which takes place by natural convection, if the core is provided with openings leading to a much greater mass of water or to an external heat exchanger.

Whenever this system cannot be used, or is found insufficient to reach the desired power and flux levels, the cooling fluid has to be forced through the reacting medium. The simplest case is:

(*a*) Gas in an open circuit. The only gas plentiful enough to be used for a single passage is air in which no high compression work has been invested, that is circulated at a low pressure. Advantages: extreme simplification of the cooling channels and of the disposal after passage (into a high chimney). No engineering and corrosion problems. Disadvantages: large-size blowers and ducts, fairly high power consumption.

The practice has shown that this system cannot compete with the natural convection mentioned above and is therefore applicable only to relatively low-flux reactors composed of graphite and natural uranium. The limitation of its efficiency comes simply from the fact that there are too few coolant molecules which can pass through the core in a given time.

(*b*) If used in a closed circuit, the gas can be compressed, thus increasing the number of passing molecules and the efficiency (better heat removal and lower power consumption). Fluxes of the order of 10^{13} become possible, so that this system can compete, to some extent, with the cooling by liquids; it presents the advantage of minimizing corrosion problems and it can stand high temperatures (but, on the other hand, it requires them). On the whole this sturdy, but somewhat clumsy, way of cooling is best suited for those research reactors which are built as a preliminary step towards industrial applications.

(*c*) Cooling by water: either ordinary or heavy water may be used. Advantages of H_2O as compared to D_2O: low cost, simplification of outside pumping and heat-exchanging devices, since leakage can be afforded. Advantages of D_2O: low neutron capture (important in systems where neutron economy is strict, above all in conjunction with natural uranium); elimination of the contamination risk (in reactors which already contain heavy water as moderator).

Both kinds of water present, as coolants, the common advantage of offering the highest number of heat-removing atoms per unit volume (as compared not only with compressed gas, but also—to a smaller but significant extent—with liquid metals); and the common disadvantage of requiring highly pressurized vessels and ducts, if any but the lowest working temperatures are to be adopted. Since in research reactors the accent is on high fluxes (reduced working volumes) rather than on high temperatures, the balance of advantages of water as a coolant is particularly favourable in the research reactor domain. For this reason we mention only very briefly:

(*d*) Cooling by liquid metals, to be used only if high temperatures are essential, or wherever it is necessary to avoid the presence of a moderating substance (as in the laboratory prototypes of fast-neutron reactors). Liquid sodium or sodium-potassium alloy (lower-melting, hence easier to handle, but less efficient as a heat remover) have been used so far; the use of bismuth is considered in some advanced projects.

2.5 Shielding

On the outer surface of the reflector neutron density, although much weaker than in the core, is still much too high to be safely approached by personnel; gamma-ray intensity is even less attenuated. Core and reflector must therefore be surrounded on all sides by a neutron—and gamma—absorbing medium. The first of these two aims is best achieved by a substance consisting of light-weight atoms, the second by a heavier one. The combined shielding may be achieved by two successive layers (say water followed by a metal), or by using a substance containing both kinds of atoms. Since heaviest metals are costly, the tendency is to use concrete (which contains, as light atoms, some H_2O and more O combined to Ca) loaded with iron or barytes. The heaviest loadings (concrete density up to 6) are costly and used only with the highest-flux reactors; in most cases densities of about 3.5. are sufficiently effective.

From a vast practical variety of shapes and thicknesses, the following general remarks can be abstracted:

(1) Reactors of zero or a few watts power require no protective shield;

(2) The core-and-reflector volume in research reactors fueled by natural uranium is so big that the radius of this volume is greater than the thickness of the concrete shield. If the concrete layer has to surround such a great inner volume, the total volume may become enormous (1000 m^3 or more) and the total weight of concrete may run into thousands of tons.

(3) In most up-to-date research reactors, however, the radius of the core-and-reflector volume is comparable to, or shorter than, the protective thickness. The total volume (overwhelmingly concrete) is therefore much smaller and within a small factor, is of the order of 100 m^3.

(4) The outer shape of the shield (and, therefore, of the whole reactor) should theoretically, be spherical but in practice is determined by the possibilities of construction. A near-cube is probably easiest to build, but the present tendency is towards octagonal (or dodecagonal) prisms.

(5) If the concrete contains some added boron, the necessary thickness is somewhat lower, which may result in a reduction of cost.

(6) In some H_2O-moderated and cooled research reactors the core is surrounded by a considerable bulk (of the order of 100 or 200 m^3) of water which serves as a first protective shield in some directions.

These orders of magnitude show the interest, from the economy point of view, of compact designs and, therefore, of enriched fuels.

A structural complication comes from the necessity of avoiding the excessive heating of the concrete. In high-power research reactors there usually is a layer of heavy metal (a few centimeters of iron or lead—"thermal shield") interposed between the reflector and the concrete. Air or water cooling of this layer is a simple problem, since no specifically nuclear difficulties are involved.

2.6 Controlling and Experimental Equipment

In all reactors, whether intended for research or not, the control of operation is based on the direct interference with the rate of production or (more often) the rate of disappearance of neutrons in the reacting core. The most frequently used device consists in moving a neutron-absorbing mass ("control rod") with respect to the core. In liquid-moderated types the level of moderator in the reacting tank can be varied; in compact types, motion of reflecting elements, or of the fuel itself can be very effective.

Such controlling devices may be operated by hand, or harnessed automatically to an instrument which measures the power level and, at any rate, arranged so as to stop the operation ("safety rods") if, for any accidental reason, the power level oversteps a pre-set allowed maximum. Their construction and coordination with radiation-measuring apparatus have by now reached a high degree of elaborateness and reliability; since their nature is the same in all research reactors, and their cost is never one of the major budget items, their technology is hardly relevant to our present enquiry. The same can be said of the radiation measuring apparatus itself which is standard electronics.

The situation is different with the experimental facilities. When choosing a reactor design, it must be remembered that the most powerful chain-reacting device is hardly of any use if no radiation can be taken out of the reacting volume, and no material specimen can be put into it or close to it. But, on the other hand, every facility to do so interferes with the reaction itself, increases the necessary amount of ingredients, decreases the efficiency of reflectors and shields and complicates the problems of cooling and of personnel safety. A balance has to be struck between these conflicting considerations, all of which have an incidence on the cost of the project.

Most of the experimental facilities take the shape of channels leading through the shield and the reflector towards the edge or the inside of the core. Most channels are associated with specialized equipment, according to their intended use, such as collimators and shutters for the radiation beams; special shielding plugs to be inserted after the necessary apparatus or material has been introduced inside the pile; layers of appropriate substances necessary for filtering the desired kind of radiation (such as bismuth used to obtain gamma-free beams of neutrons, or uranium which converts slow-neutron beams into fast ones); mechanical or pneumatic conveyor devices for subjecting samples to quick irradiations; thermostats for irradiation at a constant temperature.

Highest-flux regions of a reactor can hardly be reached otherwise than through these specially arranged channels (the term "beam hole" or "beam port" covers most of these, except for some very specialized types). Some use can also be made of openings normally used for the introduction and extraction of fuel; or a fluid substance to be irradiated may be circulated, instead of the coolant, through an isolated section of the cooling network. For irradiations requiring big volumes, cavities can be arranged in the shield; if filled with graphite or beryllia, they are called "thermal columns." Water-moderated and shielded reactors are particularly suitable for experimentation with bulky specimens.

The total number of beam holes and other irradiation openings in a research reactor should be at least of the order of 10; in less compact types this number may go as high as several dozen. As a representative example, we reproduce below the list of the main experimental facilities permanently attached to a modern high-flux reactor (CP5) in which a compromise was sought between compactness and availability of a conveniently wide experimental volume (dimensions across the opening are given in inches):

1 channel reaching to the center of core, 3 in.

7 channels reaching to the outer regions of core, 3 in.

2 beam holes, 12 in.

6 beam holes, 4 in., two of which positioned with a special regard to fast-neutron flux

2 beam holes across the reactor, passing near the edge of core, 6 in.

1 pneumatic through-channel, passing near the core, 2 in.

2 holes for biological irradiation, outer region, 8 in. × 12 in.

2 thermal columns, outer region, 60 in.

Some smaller facilities also are available, bringing the total number of experimental openings to about 50.

Ample space outside the reactor, close to the shield, should always be provided. The necessary floor space has been estimated at about 5 square meters per experiment. Since heavy shielding of apparatus is often necessary, the floor should be strong enough to support several tons per square meter.

3. PERFORMANCE DATA ON THE PRINCIPAL TYPES OF RESEARCH REACTORS

All figures quoted below aim at giving an idea of order of magnitude for the purpose of comparison. Precision is difficult, if only because the concepts such as the "average available flux," the "core volume," etc., have not yet been standardized. Fuller numerical details, together with sketches and plans, can be found in the current literature.

Each particular type can be mentioned only very briefly; we describe however in somewhat greater detail the two or three types which are likely to dominate the research reactor field in the near future.

At the time of writing, no details were available on Soviet research reactors.

3.1 Lowest-Energy Reactors

Assemblies of fuel, moderator and reflecting material in which no provision has been made for heat removal, can be run either without any shielding (power of the order of a few watts, flux close to the 10^7 range) or with some shielding which allows the operation at a few kilowatts. Such a "zero power" reactor can constitute either the easiest introduction to the reactor technology in general, or a first step towards the construction of some definite novel type. In the latter case, running at a very low power may be required so that the components do not become radioactive and can be approached and studied.

Historical specimens: the "first reactors" using graphite and natural uranium, such as "CP 1" (1942) in Chicago and "Gleep" (1947) in Harwell, England (the latter with some rudimentary cooling). With D_2O and natural uranium: "Zeep" in Canada (1945), "Zoé" in France (1948). In the present state of information and supply, it is unlikely that more such reactors will be built. On the contrary, the use of first-step "critical assemblies" is likely to develop (some past examples: "Lopo" built in 1944 at Los Alamos as a prelude to the development of the Water Boiler type; more recent critical experiments with plutonium solutions; "Dimple"—a D_2O and U assembly at Harwell).

A zero-power reactor requires appreciably (by a factor up to 2) less fuel and moderator than a full-scale reactor of a similar composition provided with cooling and experimental facilities.

3.2 Graphite and Natural Uranium

Principle

A mass of graphite (several hundred tons) serves as moderator and reflector; the mass is traversed by numerous (several hundred) channels through which fuel elements are introduced and the cooling gas (usually low-pressure air) is blown. Specimens: The X-10 reactor at Oak Ridge, Tenn. (1943); "Bepo" at Harwell (1948); Brookhaven, near New York (1950); research reactors being at present built in Belgium and Western Germany. Fuel: metallic U in cylindrical rods or cartridges, clad usually in Al, possibly Mg; the total amount of fuel in older versions is roughly of the order of 50 tons, whereas modern versions, thanks to improved quality of ingredients, may contain only 20 or 30 tons of fuel. Power: individual cases range between 3000 and 30,000 kw. Flux: around 10^{12} (highest value, reached at Brookhaven: about 5×10^{12}). Experimental facilities: very numerous and convenient, owing to the great bulk of the reactor and the ease of access to the centre of the core.

Comment

As enriched fuel and heavy water become available, it is unlikely that many more such reactors will be built in the future for research purposes alone, since they are far too costly in ingredients and cooling machinery. Graphite and natural U remain, however, of interest for power production, and pilot plants of this type may be provided with research facilities. It is also to be noted that most of the radioisotope production, for which high fluxes are not necessary, but great volumes available for irradiation are useful, takes place at present in reactors of this type.

3.3 Heavy Water and Natural Uranium

This type of chain-reacting medium has been of a considerable importance in the research reactor field. Its first representative ("CP3" of Argonne, near Chicago) was built in 1944 specifically for research purposes; subsequent development took place chiefly outside the United States. Specimens in existence or in project use a great variety of systems of cooling, covering a wide range of powers and fluxes, from the uncooled reactors, already mentioned, upwards:

1. Cooling by Unforced Circulation

Convection movement carries the bulk of heavy water, in a closed circuit, through an external heat exchanger.—Specimens: "CP3" (1944–1950); Kjeller, Norway (1951); Châtillon (1953, replacing the French uncooled reactor); Stockholm (1954).—Fuel: pieces of metal enclosed in aluminium tubes; total charge of U: about 2 or 3 tons.—Size of reacting core: a few cubic meters.—Reflector: graphite.—Power: about 100 kw per ton of uranium.—Flux: a maximum of 1 or 2×10^{12}. At this flux level the radiation-induced decomposition of D_2O is significant enough to necessitate the circulation of the gaseous atmosphere of the reactor tank through a catalytic recombination unit (this feature is found in all D_2O-moderated reactors above a certain power level).

A factor 3 or so in power and flux could probably be gained by realizing all the potentialities of this cooling system; such a D_2O and natural U reactor, still simple, might compete with the H_2O and enriched uranium systems (see below), in the 10^{12}–10^{13} flux region. If such a competition does take place, it will be governed by the availability and cost of D_2O and enriched U.

2. Cooling by Compressed Gas

The only specimen (Saclay, France, 1952) was the first reactor to be cooled by compressed gas and also the first D_2O-moderated reactor in which the coolant is brought to a high temperature. Fuel: about 3 tons of U in the form of metal cartridges clad with Al or Mg. Size of reacting core: about 6 cubic meters. Reflector: graphite. Coolant: N_2 or CO_2 gas under a pressure of up to 10 atmospheres. Maximum power: about 2000 kw, corresponding to a maximum flux of 8×10^{12}.

Gas cooling, as shown by the British plans for energy production, can probably be made 3 or 5 times more efficient, reaching the fluxes of a few times 10^{13}. For research purposes, however, cooling by water is probably more convenient at these flux levels.

3. Cooling by H_2O

Only specimen: "NRX" (Chalk River, Canada, 1947). Fuel: about 9 tons of uranium rods clad in Al.—Size of reacting medium: about 15 cubic meters.—Cooling: ordinary water flowing through tubular channels along the rods.—Reflector: graphite.—Power: 40,000 kw.—Flux: maximum 7×10^{13}; access to numerous regions in which flux is well above 10^{13}.

This very unique reactor offered for many years the highest flux in the world and still is remarkable for its numerous, large and convenient experimental facilities. It is however more costly than most modern reactors and its power is too high according to the safety standards valid for most places in which a research reactor is likely to be located. The great bulk of the reacting medium, although not likely to be reproduced in modern designs, is an advantage from the experimenter's point of view. In Canada reactor research is carried out in a single centralized establishment and in such conditions, and as long as enriched fuel is not readily available, the NRX design remains competitive.

4. Cooling by Forced Circulation of D_2O

A further development of the NRX type, with cooling by D_2O forced along the fuel rods, is nearing completion at Chalk River. This "NRU" reactor, with a power substantially higher than that of NRX, will produce significant amounts of plutonium; it will also serve as a prototype for power production. Most of its details are classified and it cannot be considered as belonging to the research reactor class. It is however noteworthy that such a multi-purpose reactor can offer fluxes not much smaller than those reached in the most efficient existing research reactors and that elaborate research facilities, mostly for reactor technology, have been provided in its design. Such a provision for research in non-research types of reactors may yet become an important future trend.

3.4 Heavy Water and Slightly Enriched Uranium

An interesting design recently completed in France ("EL3") is based on the use of a fuel containing about twice the natural amount of U^{235}. With this fuel, intermediate between natural and highly enriched, the characteristics of the proposed reactor fall between those of NRX and the highly-enriched type (see section below). There will be about half a ton of fuel in the form of metal cartridges; the total power, approaching 15,000 kw, will create a maximum flux of 10^{14} in the centre of an active volume of nearly 3 cubic meters. D_2O, under forced circulation, acts both as moderator and coolant.

Although the choice of these characteristics was dictated mainly by considerations of fuel supply, EL3, designed exclusively as a research reactor, may yet prove significant as a compromise between the modern trend towards low power and compactness, and the older, more spacious designs.

3.5 The Water Boiler

Principle

The fuel (highly enriched) is dissolved in ordinary water; this liquid core is contained in a small stainless-steel vessel surrounded by the reflector and shield.

Specimens

Los Alamos ("Supo," in operation since 1951).—North Carolina State College (since 1953).—University of Utah.—Armour Research Foundation (Chicago) Projects offered by several private companies. Fuel: about 1 kg of highly enriched U^{235} in form of uranyl sulfate. Moderator (and solvent medium): ordinary water. Size of core: about 15 liters. Cooling: ordinary water flowing through a system of tubes immersed in the core (no direct contact with solution). Reflector: blocks of beryllia, more often blocks of graphite. In at least one project, the core vessel is to be surrounded by an outer tank containing H_2O as reflector, the variation of water level being then used as the main controlling device. Shielding: thermal shield and heavy concrete. Experimental facilities: thermal columns (possibility of several); beam ports and experimental channels of all types including the all-the-way-through channel going through the core. In view of the small core volume, the water boiler is best suited for beam experiments.

Power

Supo is run at about 50 kw. More efficient cooling could push the power to 100 or 200 kw. As in D_2O moderated reactors (see above), provision must be made for the recombination of hydrogen and oxygen.

Flux

At 100 kw, about 3×10^{12}. Fast to slow ratio: favourable, because of moderation by H_2O.

Variant

In a project developed by North American Aviation Inc. the enriched fuel is in the form of U oxide mixed homogeneously with graphite powder; cooling is by D_2O circulating in a tubular coil. This design eliminates the recombination problem and some of the dispersion hazards; it is however less compact, more costly than that of a "conventional water boiler" and requires a somewhat higher power to produce the same flux.

Cost

Figures quoted in literature range between 100,000 and 500,000 dollars. The lowest figure seems to correspond to a minimum of experimental facilities; in more elaborate versions these facilities constitute the major cost item.

3.6 The Swimming-Pool

Principle

A single mass of ordinary water (100 to 200 m^3) held in a concrete tank serves as moderator, main reflector, coolant and first shield. The fuel assembly is attached to a steel framework which is suspended in the pool from a bridge spanning the pool width above the water level. The walls of the pool provide the residuary shielding.

Specimens

Oak Ridge ("Bulk Shielding Facility") in operation since 1951. Numerous reactors in construction, most of which are scheduled to operate in 1956: University of Michigan—University of Pennsylvania—Naval Research Laboratory (Washington)—Watertown Arsenal (Massachusetts)—Wright Air Force Base—Battelle Institute (Columbia, Ohio)—United Nations Conference (Geneva, August 1955)—As in the case of "water boilers," projects are offered by numerous American industrial companies, some of which are already acting as general contractors for reactors under construction.

Fuel

3 to 3½ kg (according to quality of reflector) of highly enriched U combined with Al in the way described in Chap. II.—Bulk of the assembled lattice: about 50 liters. Moderator: ordinary water (no separate container for the moderating volume, that is for the reacting core, is necessary).

Reflector

The pool water fulfills the main reflecting function. The efficiency is improved if the lattice is surrounded by graphite (see below) or by beryllia (a 10 cm thick BeO reflector can be obtained by putting, around the periphery of the fuel assembly, an outer layer of boxes similar in shape to fuel elements, but containing BeO instead of the U-Al combination).

Cooling

Temperature gradients resulting from the reaction taking place in the fuel plates produce a flow of water in the interstices between plates. Heat is thus drawn into the whole bulk of pool water whence it is dissipated through walls and by evaporation. This spontaneous heat removal is valid up to power levels of about 100 kw. To go beyond that, the pool water has to be circulated through an external heat exchanger connected with the pool volume through an inlet and outlet situated near the core. A factor 10 in power can thus be gained; intermediate power levels are technically unprofitable.

Flux

At 100 kw, inside the core (nearly unavailable for experimentation): about 2×10^{12}. At the surface of the core (available) 10^{12}. Fast flux at the core surface: about ¼ of the slow flux. At the higher power levels (recirculation of water), the fluxes are about 10 times higher.

Shielding and Experimental Facilities

In all Swimming Pools the core is immersed 5–7 meters deep in water which affords the shielding in the upward direction. The sideward shielding presents variations from one project to another, according to the intended use of the reactor. The first Swimming Pool (Oak Ridge) was designed mainly in order to observe the interaction of radiation with bulky items of material, which could be simply immersed in water. Instruments and equipment can also be immersed, if necessary. Water-proofed tubes leading to the vicinity of the core may also be provided. In the simplest version, the core can be set in a fixed position surrounded on all sides by several meters of water, and the tank can be imbedded in the ground. In later versions the core was made movable between a central position (for bulk experiments, as above), and one in which the core finds itself in the close proximity of a wall; the simple rectangular shape of the pool may in such a case be replaced by a more complicated one, affording a convenient corner. Numerous variants, in particular those proposed by Bendix Research Laboratories. The wall of the core-containing corner has then to be reinforced along the familiar lines (concrete thickness of the order of 1.5 or 2 meters). The usual beam holes and through channels can then be provided reaching through concrete and water to the immediate vicinity of the core.

Summary of Variants and Costs

It results from the published figures that the simplest version of the Swimming Pool (no recirculation, therefore power up to 100 kw, and full-depth immersion on all sides) may cost less than a well-equipped Water Boiler. Such a Pool is a simpler reactor suited for bulkier and less refined experiments than those performable with the Boiler.

In its most complicated variants, as yet unconstructed (recirculation, wallside-core facilities, available flux up to 10^{13} and possibly even more), the Swimming Pool will cost definitely more than the Boiler and will offer appreciably more varied research possibilities.

3.7 Heavy Water and Highly Enriched Fuel

Principle

D_2O used as moderator, coolant and first reflector.

Specimens

"CP5" at Argonne (Illinois), in operation since 1954; "E443" at Harwell, England, to operate in 1956. (The following data refer to CP5). Fuel: A minimum charge of 1.2 kg of U^{235} (about 90 per cent pure) alloyed and assembled with Al. Core volume: about 200 liters. Moderator and first reflector: about 5½ tons of D_2O in a single tank, forming a 60 cm layer around the core. Second reflector: a 60 cm layer of graphite around the tank. Cooling: convection flow through core and bulk circulation of D_2O through an external exchanger. Shield: About 150 cm of heavy concrete, lined on the inside with a few cm of lead. Experimental facilities: see the list given in Chap. II. Flux: at 1000 kw, more than 10^{13} at the maximum point inside the core; falls slowly to $\frac{1}{2} \times 10^{13}$ at tank edge and affords a vast experimental volume with about 10^{13}. Available fast (virgin) flux: about 10^{12}.—Cooling and other facilities are adequate for operation at 5000 kw (thus pushing the maximum towards 10^{14}), but the one-megawatt ceiling is observed for safety reasons.

Comment

The CP5 type provides a high (but not the highest) flux, with insistence on a large number of experimental facilities and a relatively low power. The future of this type depends on the possibility of running at higher powers (E443 is intended to run at 10 MW and reach 10^{14}) which may require a somewhat bigger fuel charge (2½ kg in E443).

3.8 Highest Fluxes

Principle

Although a D_2O-moderated reactor affords the best possibility of producing a very high slow flux, designers aiming at highest possible fluxes should not forget the claims of the fast-neutron research; here H_2O asserts itself again. As regards cooling at highest powers per unit volume, both waters are theoretically equivalent; in practice D_2O demands additional guarantees against pollution and loss by leakage, so that the already harassed designer may prefer to deal with H_2O. Water is used both for moderation and for cooling, but (in the highest-powered type) neither as a reflector nor as a shield.

Specimens

In the Materials Testing Reactor ("MTR", at Arco, Idaho), operating since 1952, the highest-flux principles have been pushed to the farthest limit as yet reached. Fuel: 4 kg of highly-enriched U assembled with Al in standard fuel elements. Moderator: As in Swimming Pool; the fuel, the moderator and the first reflector are contained in the same tank. Size of core: about 100 liters (there is room for extending the volume up to 170 liters). Cooling: H_2O forced through the tank; at 30 megawatts the flow rate is 75 m^3 per minute. First reflector: beryllia in blocks, pierced with channels for cooling; surrounds the core with a thickness of 30–40 cm. Second reflector: graphite (thickness of the order of 100–150 cm). Shield: 10 cm of steel and 270 cm of heavy concrete. Experimental facilities: usual types, some of which go through the highest-flux region. The Oak Ridge projects provide channels going through the core. Flux: (MTR at 30,000 kilowatts): maximum, situated in the reflector, 4×10^{14}; average available 2×10^{14}; fast (virgin), average: 1×10^{14}.

A preliminary reduced version ("LITR") has functioned at Oak Ridge since 1950. More ambitious reduced projects have been recently published by the Oak Ridge staff, and a powerful research reactor, falling however somewhat short of the MTR level, is at present in construction at Oak Ridge ("ORR"). A stronger version of MTR, which will be run at a substantially higher power, and will reach accordingly higher fluxes, is at present contemplated by the American AEC.

In ORR the power may reach 10,000 kw or more, and the available flux will be close to 10^{14}, within a small factor depending on the exact power.

According to the published figures, MTR is some 5 or 6 times more expensive than the ORR project; this may point to a "law of diminishing returns" as applied to the efficiency of the present design at highest powers and fluxes.

* * *

As we have already stated in connection with "NRU" (see Section C above), the great cost of research reactors offering very high fluxes may lead to a more widespread use of multi-purpose projects in which the reactor, built as a producer, or as a pilot stage of a technological development, is also provided with experimental facilities enabling it to be used for research purposes.

Such reactors lie outside the scope of the present report, since their design and economy are mainly conditioned by factors other than their usefulness for research. The same can be said of experimental assemblies seeking to explore entirely new trends in reactor development, usually with the ultimate aim of producing either useful power or transmuted fuels. In addition to their specific purpose, such assemblies can be useful for gaining information of a wider kind. Thus, for instance:

(1) In the Experimental Breeding Reactor (Arco, Idaho, 1951), run at 1400 kw, the chain reaction is propagated by fast neutrons, which enables the reactor to offer, at that power, a somewhat higher fast-flux than that reached in MTR.

(2) In the Homogeneous Reactor Experiment (Oak Ridge, 1953), a solution of enriched uranium salt circulates between the reacting core and an external heat exchanger at a high temperature and high pressure. This prototype, operating at 1000 kw, has given valuable information on the temperature dependence and other features of chain-reacting systems operating in hitherto unknown conditions.

Many more of such novel reactor concepts are today in various stages of design, construction or experimental running. Future types of pure research reactors will no doubt be developed from many of these beginnings; at this stage, however, we cannot give them here more than a passing mention, especially in view of the fact that most of their details are classified because of their very novelty.

4. FINAL CONSIDERATIONS AFFECTING THE CHOICE

4.1 Correlation with the Intended Programme

The institution may be ambitious and aim at the highest flux obtainable within the available budget, space and safety limitations; in such a case the research programme will be determined by the possibilities offered by that particular flux. Or, on the contrary, it may happen that the programme, whether limited or ambitious, is set beforehand and the flux value is chosen accordingly. In both cases the following brief summary of the flux-programme correlation will be valid:

At lowest fluxes (say, below 10^{10}), the reactor should be considered frankly as a zero pile, that is as one which requires neither protective shielding nor special precautions in approaching its components after shutdown. This accessibility makes it useful for such purposes as: teaching; demonstrations and studies of the chain reaction mechanism; study of the effect of unusual devices (cooling channels, controls, etc.) on reactivity; study of ingredients and lattices; study of the nuclear purity of materials; experimentation with various types of controls, reflectors and shields. As a source of neutrons, the "zero" power reactor can be used for studies of propagation and absorption of neutrons in bulky material assemblies, for instance for specimens of uraniferous media intended as cores for other types of reactors. On the whole, a lowest-flux reactor is either an object of study in itself or a step towards the design of a higher-power reactor; it is of small value as a tool for other domains of research. It can however produce some selected types of radioisotopes in quantities at least sufficient to offer an initiation to this domain of research.

At medium-low fluxes (lower or higher than 10^{11} by a small factor) shielding becomes necessary and the core is no longer easily approachable; some of the advantages of the zero-power reactor therefore disappear. Value as a tool, however, becomes appreciable first of all in biological research (where too intense a radiation is simply crudely destructive); also in many branches of radiochemistry and solid state research. Physical research has already been carried on at low fluxes for more than a decade and the main interest has shifted towards phenomena revealed at higher fluxes. Finally as sources of locally produced radioactive substances the medium-low powered reactors can be quite useful; in fact, for many kinds of isotope production fluxes beyond 10^{12} are simply unnecessary. In this connection we may note that about 70% of all radioactive species are short-lived enough to require the production on the spot. On the whole, the scientific resources offered by such reactors can be compared to those offered by a small flame for the study of heat or light: the more original the approach, the smaller may be the need for a stronger source.

The "normal research flux" at present is situated, within a small factor, around $\frac{1}{2} \times 10^{13}$ (and possibly closer to 10^{13} in a rather near future). This is the flux afforded not only by the modern enriched-fuel types such as the Water Boiler and the Swimming Pool, but also by the older and more laborious solutions on the lines of the Harwell, Saclay and Brookhaven reactors. They are most suitable for nearly all research items listed in Chapter I with the exception of those mentioned above as proper for the lowest-flux reactors and those belonging to the highest-flux domain.

This latter, beginning at nearly 10^{14}, can at present be approached only with the help of MTR; in the near future a few more research reactors either D_2O or H_2O moderated will come close to this region. It is already obvious that some types of radiation damage essential for the technology of future industrial atomic plants, can be studied only in this way. This may also be true of many other chemical and metallurgical problems. As research tools, highest-flux reactors will, therefore, be necessary chiefly in testing stations and technological, rather than purely scientific, institutions.

This situation may change; scientific work has already been started on subjects for which quite definitely the most intense tools are just good enough. This is particularly true of "higher-order phenomena," where the original intense source produces a substance or an effect which, in its turn, is used as source or source material for the investigated phenomenon (examples: research on heaviest transuranic elements; neutron optics involving several successive interactions with matter). The "normal" research domain may yet shift towards these higher fluxes; in the meantime the necessities of shielding, of precautions against radioactivation of apparatus, etc., make the highest fluxes a nuisance rather than a boon for most current types of research. The high running cost of a highest-flux reactor may also become an obstacle to its generalized use.

So far we have only compared reactors to other reactors, but the relative claims of other kinds of research tools should be considered as well. We may state without hesitation that, as a single tool capable of keeping a great number of research teams busy on a widely-varied programme, the normal-flux research reactor is without rival. The situation is somewhat different for a physical laboratory which considers building a reactor with a lower flux, or with a narrower programme in view (for example, for beam physics only). Such a tool is intrinsically *not* more valuable than a particle accelerator of a comparable cost. Since both reactors and accelerators can be used in a certain common domain comprising some lower-energy nuclear physics and the effects of radiation on matter, the choice is sometimes difficult to make on pure principle. The practical advantages of a reactor are: a higher intensity; the possibility of accommodating many experiments at the same time; easy operation and fewer stoppages. Against this, the accelerators offer: a more specifically quantitative action (constant and monochromatic radiation, as in precision Van de Graaff generators); a greater selectivity (radiation of only one kind, if desired; important in biophysics) and, finally, greater ease in charged-particle physics, as opposed to neutron physics (and for neutron-deficient, as opposed to neutron-excessive isotopes). As a tool for advanced and highly specialized physical research, for an institution working on a small budget, a cheap accelerator may prove to be a better investment than a cheap reactor. In most other cases, reactors will probably come first (with accelerators to supplement them), in an increasing measure as the atomic age advances.

4.2 Safety Considerations

Safety precautions needed in connection with the operation of a research reactor have to be considered from two different points of view: major risks in case of an accident, and minor risks resulting from the normal running.

Even in the less informed circles, it is fully realized nowadays that no research reactor resembles, even remotely, an atomic bomb. Exclusion of the possibility of a *nuclear* explosion does not, however, mean that explosions of what may be broadly termed "thermoelastic" type are unthinkable. Some research reactors contain, after all, hot or compressed fluids which make them *a priori* comparable to steam engines and boilers. If by mishap such a system runs wild, violent dislocation may occur.

With a proper design of the reactor it is possible to guarantee that, as a result of even the worst thinkable accident, blast damage will be limited only to the reactor itself, its building and a very small adjacent area. The "perimeter of unsafety" cannot however be based on this consideration alone, since even in a fairly unviolent accident fuel elements may be broken and their contents dispersed. The sudden spread of a cloud charged with radioactive dust, vapour and gas constitutes a very serious danger to a far wider area than that threatened with blast. The design of the reactor may be such that it would be unreasonable to exclude the possibility of such an accident. In that case all reasonable precautions must be taken to minimize the casualty rate among the operating personnel and, on the other hand, all other activities and occasions for sojourn (such as places of dwelling or work) must be excluded from a reasonably-estimated wide area.

The American Atomic Energy Commission has adopted this point of view for many large-power reactors. The assumption was made that one-half of the total mass of radioactive products accumulated in the reactor would escape and, on this basis, the radius of the excluded area is equal, in miles, to the square root of the total reactor power counted in tens of megawatts (example: for a 100 kw reactor power = $\frac{1}{100}$, therefore radius of danger area = $\frac{1}{10}$ mile or 176 yards). For a 1000 kw reactor, the diameter of the excluded area is very nearly 1 kilometer. The area thus excluded is far bigger than that which was actually found dangerously contaminated after the worst mishap which has, so far, happened in reactor history; the Chalk River accident of 1952. Even that accident should, however, be considered as comparatively mild compared to what might have happened in the worst possible case.

Since very few educational and research institutions can afford to evacuate the vicinity of their research reactors permanently and on so wide a scale, safety has to be ensured in some other way. It is always possible to design a *research* reactor so as to minimize:

(*a*) The risk of a runaway rise in power—by choosing a "self-stabilizing" system, that is, a material system in which a sudden increase in heating produces effects capable of stopping the nuclear reaction. A properly designed system of *ad hoc* safety devices and brakes also can be very effective.

(*b*) The risk of a violent dislocation in the case of such a runaway, by giving preference to designs which avoid the use of high temperatures, pressures and mechanical stresses;

(*c*) The risk of radioactive dispersal—by enclosing the reacting system in tight metallic envelopes or great bulks of water or concrete. (In at least one case the reactor building—that of "CP5"—maintained at a slightly lower-than-outside atmospheric pressure in order to minimize outward leakage risks).

The most current research reactor types—the Water Boiler and the Swimming Pool—are all very satisfactory from this point of view. In one particularly safety-conscious project (University of Michigan) it was found possible, after a careful study, to install a 1000 kw reactor within 500 feet of a great variety of university buildings. For the higher-power research reactors the demand on inherent safety will be increased (in this respect D_2O moderated designs present an advantage), but it may well happen that for the future highest-in-the-world fluxes (which may require designs incompatible with maximum inherent safety) it will be necessary to adopt the above-calculated exclusion areas without any mitigation; this already has been done for the MTR.

Quite apart from the possibility of an accident, the normal operation of a research reactor introduces many safety problems. Since the necessary precautions are the same for all kinds of reactors except the lower-power ones, they weigh little in the balance of arguments for and against a given type of reactor. It will be enough to recall that an institution contemplating reactor research will have to provide:

(*a*) A vast array of radiation-monitoring apparatus (counters, ionization chambers, film badges, etc.).

(*b*) Monitoring and health-safeguarding personnel comprising at least one full-time health physicist.

(*c*) Clothing, premises and containers for handling of radioactive material and waste.

(*d*) An elaborate set of rules for everyday behaviour and for periodic drill, which have to be followed by reactor operators and engineers, and by scientific workers using the facilities afforded by the reactor.

(*e*) A safety council, on the highest management level and vested with full enforcing powers, to see that the rules are applied and adapted as the changing conditions may require.

On the whole it can be said that the pedestrian question of safety in everyday operation requires rather more attention (from those responsible for the management of the institution), than the spectacular risks connected with the possibility of an accident. It also should be understood that all this safety materiel and routine constitute a sizable fraction of the running costs of a research reactor, and that if the institution is too small to afford them on a normal scale, this consideration may point towards the adoption of a low-power reactor.

4.3 Some Remarks on the Buildings for Research Reactors

The amount of floor space occupied by the reactor itself and by the experimental apparatus around it, is of the order of a few hundred square meters. As already stated, this floor must be suitable for supporting heavy loads. Height must be sufficient for some vertical manipulations (experimental apparatus and, in some types, fuel elements) and an overhead crane will always be necessary.

Existing buildings can sometimes be found to fill these specifications; the first Harwell reactors were erected in big hangars originally built for aircraft. The Naval Research Laboratory (Washington) found a warehouse (total floor space slightly over 1000 m^2 height 10½ m) to house its (probably uncooled) Swimming Pool and its auxiliary laboratories.

Several-story height is usually preferred with a great central hall and, sometimes, balcony-like rooms and booths for auxiliary services. A typical recent design, given in the "ORR" project, roughly approximates a cube with a 25-meter side (including the basement). Factory-type construction, with a steel frame and brick or concrete walls, is quite adequate.

The original tendency towards very big halls‡ seems to be tempered, in some modern designs, by the safety preoccupations. The CP5 hall, with its sealed-off atmosphere, already mentioned, has only 350 m^2 of floor area and it seems that the main hall of E443 will be even smaller; this means a greater degree of separation between the reactor itself and its auxiliary rooms. The same solution was adopted in Sweden, whose 300 kw research reactor was built in a deep excavation with a carefully calculated economy of floor space.

---

‡ Partly due to the great bulk of the early research reactors, using natural uranium.

Cooling machinery finds its natural place in the basement under the reactor. For air and gas-cooled reactors, such as Harwell or Saclay, separate outhouses or halls are necessary to house the blowing machinery. Disposal and handling of radioactive materials may require separate structures such as deactivation tanks or chimney stacks.

In several published detailed estimates, the cost of the building amounts to, roughly, 20% of the total project budget. This proportion was probably somewhat lower in the older reactors, in which the cost of the ingredients (fuel and moderator) was relatively higher.

4.4 Costs

An institution embarking on a research reactor project has to consider seriously the questions of cost, and yet if an attempt is made to compile cost data from the published literature, a contradictory picture is likely to result. It might be thought that projects already completed, with their full financial history, should afford a reliable basis for future estimates; in fact, figures referring to a given project may be presented in a wide variety of ways, according to the bookkeeping conventions adopted consciously or (often) unconsciously. No standardized interpretation of the published figures has, as yet, gained currency.

A *post factum* indication of what a given reactor has cost may be too low if it has failed to take into account such "free" items as the price of ground (the reactor may have been built on a reserve piece of ground belonging to the institution); administrative overhead; cooperation of scientific staff and of technical experts who have been "lent" to the project and in fact, owing to its greater urgency, tended to neglect for a while their other duties; miscellaneous supplies granted free or at reduced prices, from governmental or private sources connected in any way with the project. (This last category often includes the fuel). Such a subjective approach to accounting will result in an indication of the minimum sum on which the institution should be able to count, in addition to its normal resources.

An attempt at a comprehensive accounting may, on the contrary, reflect some special difficulties encountered by the project and not likely to recur in the future. Development costs, for instance, may be heavy in a pioneering project and less heavy in a subsequent imitation. The cost of rare ingredients (heavy water, processed fuel) may show a tendency to decrease. Contracting firms may reduce their margins, as their experience grows. For all these reasons the comprehensive cost indications may sometimes lead to excessive estimates.

The orders of magnitude estimated below represent a compromise between many contradictory indications found in the literature. An attempt was made to quote reasonably comprehensive figures; we feel that they may seem exaggerated to those accustomed to a more streamlined budgetary presentation.

A low-power reactor can be built nowadays on a budget of not more than $100,000 if enriched fuel is available (with natural uranium, the minimum amount of ingredients will cost many times that sum). This cheapness is due to the absence of heavy engineering (no cooling, very little or no shielding); no special building is necessary either.

Water-boiler, flux above 10^{12}: $400,000.

Swimming pool, flux 10^{14}, elaborate shielding: $800,000.

Elaborate research reactors giving many times 10^{13} (modern types, D_2O- or H_2O-cooled and moderated): $4 to 5 million.

It is interesting to compare these total costs with that of the enriched fuel; according to the published data, U^{235} can be counted at about $20 or $25 per gram. The cost of 1 to 3 kilograms invested in a modern research reactor cannot therefore constitute a major item.

Any formula attempting to link the cost to the flux should contain a fixed term and a flux-dependent term (not necessarily simply proportional). Both an obsolescent design and a design on the limit of the up-to-date engineering possibilities (as in MTR) lead to a heavy additional cost. For older reactors, indications found in literature often fall into the range of about $10 million (say, 5 to 20). Graphite-and-natural U reactors require a heavy initial investment in fuel, and their great size is reflected in the size and cost of the supporting engineering. Heavy-water-and-natural U reactors are more compact, but this is compensated by the high cost of the moderator. In both cases cooling is expensive both as regards the initial investment in machinery (and its housing) and the motive power.

Running costs, even more than investment costs, depend on the bookkeeping conventions and on the lavishness (or otherwise) which the institution is prepared to bestow on its reactor project. From the very scanty numerical data available in literature, the following rough indications can be deduced.

Operation and maintenance of a medium-flux university reactor (around 10^{12}): up to $100,000 per year (mobile equipment and personnel for the performance of experiments as distinct from operation not included).

Operation and maintenance of a somewhat more powerful facility, run round the clock or nearly, by a specialized personnel: around $200,000 per year.

At highest fluxes the cost of fuel and of heat removal becomes very important. The running cost, in present conditions, may reach the million-dollar-a-year range for a facility offering fluxes beyond 10^{14}. This heavy cost, as we have already mentioned, puts a limit on the use of highest-flux reactors in research institutions and makes more attractive, for most purposes, the use of somewhat less powerful types.

The Nuclear Reactor in Basic Science

By Arthur H. Snell,* USA

In this paper I shall concern myself with the scientific rather than the engineering aspects of nuclear reactors. This still leaves such a broad range of subject matter that I will proceed forthwith to shed large parts of it by pointing out that medical and radioactive tracer work are covered in other sessions of the Conference, and so indeed are many other scientific uses of the *products* of reactors. I believe that I can be most useful in this session if I speak mainly about the direct use of reactors in research, be it chemical, physical or biological, but omitting the therapeutic. In the pressure of time I have rather naturally used examples close to my own experience, and I am aware that this may make my paper regrettably provincial. My only hope is that speakers from other places will have found themselves under similar time difficulties, so that they may be equally provincial, and the whole thing will average out in the wide range of the Conference.

If we turn our attention first to chemistry, the first thing that strikes us, so strongly that it cannot be ignored, is the fact that reactors have given us a dozen new elements to play with. One of these, technetium, has certainly already been created by the pound, but it is still mixed with other fission products. Presumably separation will some day be undertaken, and it will be amusing to see what the bulk physical properties of the metal will be. It is probable that all isotopes of technetium are radioactive; naturally occurring terrestrial technetium has been sought but not found.[1] The optical spectrum is known from reactor-produced material, and surprisingly enough this spectrum is prominently displayed by some of the S-type variable stars.[2] Here is an observation that will have to be taken into account by theories of stellar evolution. Meanwhile, we should keep our eyes open for like revelations with respect to other new elements.

There is a whole wide range of work that is concerned with the rearrangements of atoms and radicals under the effect of radiation. Part of this is called radiation chemistry, and in its low-energy aspects radiation chemistry merges into photochemistry. Attention is focussed primarily upon chemical changes that result from the electronic excitation of molecules. In radiation chemistry, the reactor is actually not a good radiation source. The mixture of fast and slow neutrons, gamma rays and fast and slow electrons in the sample placed in a reactor often beclouds the issues under test, and in addition one has the nuisance of induced radioactivity to make the measurements more difficult. In fundamental studies of this kind, one can usually set up cleaner experimentation by using a cobalt gamma-ray source, an X-ray machine, or an electron accelerator. Then you can control the quality and quantity of your dosage accurately, and subsequently make ordinary laboratory measurements without worrying about mirrors, periscopes and shields.

In its high-energy aspects, radiation chemistry becomes "hot atom" chemistry. Here one is concerned not with free atoms or radicals that have energies just a few electron volts above the binding energies in molecules, but rather atoms and radicals that have acquired perhaps hundreds of electron-volts of energy, for example as the result of elastic collisions with fast nucleons, or recoil from nuclear emission. The interest is centered on flying atoms rather than electronic excitation. The hot atoms are slowed down in the material surrounding them, and the hot atom chemists are interested in their ultimate fate under various conditions. After slowing down, the final stages of energy loss probably are concerned with electronic de-excitation, and this is where hot atom chemistry merges into radiation chemistry. Reactors are involved in hot atom work because of the intimate connection of this subject with the Szilard-Chalmers reaction process. The interest here is two-fold. On the one hand, the Szilard-Chalmers reaction not only produces the hot atom through recoil from the emission of the capture gamma rays, but it rather neatly tags the hot atom at the same time, so it can help in the understanding of the hot atom processes. For example, in the reaction

$$C_2H_5Br + Br^* \text{ (hot)} \rightarrow C_2H_5Br^* + Br$$

one can measure how many hot atoms later recombine into the parent substance, a determination which would be impossible without the simultaneous radioactive tagging. High neutron intensities in reactors are not required for much of this work.

The other reactor interest in the mechanics of Szilard-Chalmers reactions lies in the practical demand toward improving the specific activity of (n,γ)-produced radioisotopes. Quite a lot of work has been done in this direction, and each element has its own problems. My impression is that the general results have been disappointing. The usual attack has been to irradiate the desired material in some organic form, and to collect by means of an inorganic extraction. In reactors there seems to be so much radiation decomposition of the organic material that the activated atoms are not the only ones thrown out of the organic molecules, and the equilibrium state is such that the Szilard-Chalmers enrichment is rather small. The higher the neutron flux, the lower is the pay-off. Inorganic separations have also been studied; for example, in separating activated bromide from irradiated bromate in solid form, enrichments by 20,000 have been obtained *for short irradiations*,[3] but when one activates for a half-life of the 36-hour bromine-82, the enrichment decreases markedly. For other elements there may be other tricks that can be used, so let us hope that some of them will be successful, because high specific activity from (n,γ) products remains a very desirable goal.

---

* Oak Ridge National Laboratory.

Radiation effects in polymer chemistry are not far removed from these subjects. Everybody knows that reactor irradiation hardens polyethylene. In other plastics the results are often deleterious. In some cases the molecular chains are merely broken down, and in others strength is improved by the induction of cross-linkages. There is work to be done in the understanding of these effects, and the applied interest is obvious.

The discussion of atomic displacement leads us finally to a consideration of the physical effects of reactor radiation in solids. This field so far has been little appropriated by the chemists, and is still called solid state physics.

The theory of crystalline solids, founded theoretically upon the wave mechanics of periodic lattices and experimentally so largely upon the classical observations on coloration in alkali halide crystals, has been corroborated and enlarged with a great enrichment of detail through the study of reactor radiation effects. Measurements with semiconductors have shown the conversion of *n*- and *p*-type materials through the effects of elastic collisions in producing displacements, and also conversion through the volume effect of atomic transmutation. A recent example of the latter concerns the bombardment of indium antimonide[4] in which neutron capture in the indium produced tin as a donor impurity, and changed the material from a *p*-type to an *n*-type semi-conductor. Coloration in quartz, introduced quickly by reactor radiations, has been found to fade slowly under prolonged bombardment.[5] Another interesting observation is that when diamonds are subjected to neutron irradiation, a set of new lines appears in the paramagnetic resonance spectrum as observed by microwave methods. These new lines do not result from X-ray irradiation. The lines are non-isotropic with respect to the crystal directions. They are non-annealing, and appear to come from interstitial atoms linked in pairs.[6]

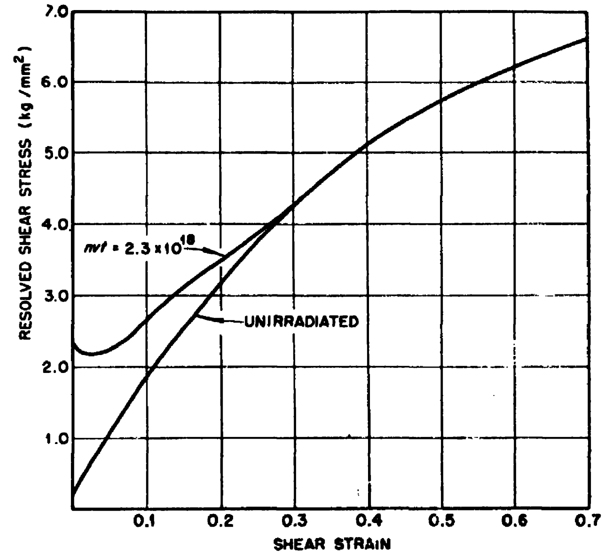

Figure 1. Stress-strain curves of copper crystals

One experiment may exemplify the uniqueness of the radiation damage approach in understanding metals. A typical stress-strain diagram is given for a copper single crystal in the lower curve of Fig. 1.[7] In the upper curve, the similar curve is shown for a crystal that has been radiation-hardened. The radiation hardening is known to be akin to alloy-hardening rather than to work-hardening, because (for one thing) after irradiation the crystal structure remains unchanged as indicated by X-ray diffraction. The hardening effect of the radiation is presumed to be connected with the migration of interstitial atoms to the regions of dislocation, where they serve as interlocking agents and restrain the dislocations against slippage. The initial high point at the upper yield point and the slight dip following it are presumed to originate in events at impurity centers, whereby the impurity center is surrounded by a cloud of interstitial atoms that have migrated to it, such that some extra stress is required to make the impurity center break loose and move through the metal. After this barrier has been overcome, the metal yields freely for a while as the impurity centers move. These migratory mechanisms are now under investigation in a conceptually simple but experimentally complicated way, in which the sample is kept at low temperature (20°K) during irradiation in the reactor. This should inhibit the migration of interstitials and thereby prevent radiation hardening so long as the sample is kept cold. On warm-up the interstitials can be expected to migrate, and if the above picture is correct the sample should harden after it gets to room temperature. Clearly the migration *rates* are capable of study in an experiment of this kind, and it is clear also that this kind of experiment could not have been done using alloys instead of radiation to provide the interstitials. It is also clear that fast neutron irradiation has been almost uniquely useful in providing uniform radiation through the body of the material; similar experiments carried out with charged particle beams would require thin-film targets and might be complicated by annealing effects from the local heating.

Many of the radiation effects in metals result from increased diffusion rates accompanying the introduction of vacancies.

Returning to chemistry again, there is another aspect in which the reactor is directly used, and that is analysis by neutron activation. The neutron capture cross sections and characteristics of the induced activity have to be in convenient ranges, but nearly thirty elements lend themselves to ultrasensitive detection by this means. As an example of the sensitivity attainable, I have stolen a few typical figures from a Harwell report (Table 1).[8] The figures apply to activation in a flux of 10^{12} neutrons per cm^2 per sec, and you will note that millionths of micrograms can be determined in the more favorable cases.

One of the neat things about this kind of analysis for very small traces is that chemical manipulations are made *after* activation, so one need not worry about extreme purity of reagents. However, there are some restrictions peculiar to the method. For example, there is no point in analyzing for arsenic through the As^{76} activity if selenium and bromine are also present, because they also can make As^{76} through the (n,p) and (n,α) reactions. So the methods of activation analysis have to be used with the awareness of pitfalls. The dangers of these troubles obviously increase if more sensitivity is sought by using higher neutron flux, and pre-contamination also becomes a proportionately greater hazard. Nevertheless, I have enough faith in the ingenuity of chemists to feel that they can get around various difficulties and push the sensitivity to even lower limits when they really want to do so.

Neutron activation analysis has been applied to a host of varied determinations: copper in aluminum, vanadium in oil, arsenic in hair, and gallium in meteorites, to mention only a few. Techniques will vary with the application; in one determination of arsenic in beans, for example, pre-contamination was forestalled by not opening the pods until the activation was finished.†

Table 1. Sensitivity of Neutron Activation Analysis under Reactor Flux of 10^{12} n/cm^2/sec

Element	*Radioactive product*		*Sensitivity of detection (micrograms)*
	Identity	*Half-life*	
Europium	Eu^{152}	9.2 hr	1.2×10^{-6}
Gold	Au^{198}	2.7 d	1.1×10^{-5}
Cobalt	Co^{60}	5.3 yr	1.5×10^{-5}
Vanadium	V^{52}	3.9 min	6.2×10^{-5}
Arsenic	As^{76}	26.8 hr	1.1×10^{-4}
Gallium	Ga^{72}	14.1 hr	3.1×10^{-4}

In nuclear physics experimentation, the reactor serves as a source of slow neutrons par excellence, but it has shortcomings in fast neutron work because of the very broad energy spectrum. In between, that is, in the range of units to hundreds of electron-volts, mechanical velocity selectors are either operating or are planned in nearly all countries possessing reactors, and the statistical work of measuring the widths, peak cross sections, and mean spacings of many resonances for comparison with various nuclear models is at present such a live subject as to comprise an extensive section of this Conference. I do not want to state that this kind of work is limited to reactors, because pulsed electromagnetic machines are becoming increasingly adapted to time-of-flight work, and they will probably outperform the rotating beam choppers before long so far as resolution and energy range are concerned. The choppers have one advantage which will probably remain for a while: they use such a small sample in the transmission cell that work with separated isotopes has been commonplace for some years now, whereas the pulsed accelerators still demand hundred-gram samples. Choppers will be able to work with radioactive samples, as has already been done with Xe^{135}.‡

The measurement of the radioactive decay of the neutron is a fundamental experiment that was lifted by the advent of nuclear reactors from the category of very difficult to the category of merely difficult. Angular correlation measurements between beta particle and recoiling proton are now nearing completion.[9] More and more work is needed on the absolute determination of the half-life of the neutron, because of its central position relative to considerations about the universality of the Fermi interaction. More and more different people should measure this half-life by as many different methods as can be dreamed up. It's not an easy quantity to determine accurately—I've tried it.

Mention of the angular correlation experiments in beta decay suggests the helium-6 recoil experiment,[10] in which the reactor was used to supply the required rather copious amount of the radioactive gas. You will recall the result that the tensor interaction was shown to prevail in beta decay processes involving Gamow-Teller transitions. A reactor supplied the radioactive gas for another recent neutrino recoil experiment, this one involving the electron-capture decay of argon-37.[11] Irradiation of about 100 grams of calcium oxide produced several curies of A^{37} by the Ca^{40} (n,α) reaction. This was sufficient to supply a pump-through experiment in which some of the gas was allowed to decay in a field-free volume at low pressure, with the result that an atomic beam of the recoils emerged from an aperture at one end. This beam was intense enough to be subjected to high-resolution spectrometry by magnetic deflection. (The recoils are charged because of Auger electron emission.) No nuclear gamma rays are emitted by argon-37, so one expected the recoils to be monoenergetic, and indeed one could run over the recoil line just as one runs over a conversion line in ordinary beta ray spectrometry. The line given by the singly-charged recoils is shown in Fig. 2 (there are other lines given by multiply-charged recoils, up to and including 7-charged ions), and the recoil energy is within one or two per cent just what would be expected from a two-body breakup in which the neutrino carries off the energy of the radioactive transition as previously known from other experimentation. Some of you may, like me, find this simple observation of neutrino emission particularly satisfying and pictorial. Incidentally, the recoil line has a considerable natural width, which is accounted for entirely by thermal motion. Recoil determinations like those of He^6 and A^{37} are examples of basic experiments that are aided by the abundant supply of reactor-produced radioisotopes.

---

† In the United States, neutron activation analysis has been organized as a service which can be obtained, for a fee, from the Oak Ridge National Laboratory through the Isotopes Division of the Atomic Energy Commission.

‡ See S. Bernstein, E. C. Smith, *et al.*, P/591, Volume 4, Session 16A2, these Proceedings.

There remains the detection of the free neutrino · the relating of a detection effect *here* with a source effect *there*. As you all know, a spectacular experiment has been carried out with slightly positive results using a Hanford reactor as the neutrino source,[12] and this experiment is in the course of further evolution. Detection is by means of the reaction $H + \nu \rightarrow n + \beta^+$, with delayed coincidences between the annihilation of the positron and the capture of the neutron in boron or cadmium after moderation. The reactor is called upon to provide neutrinos in excess of the 10^{11} or so of solar neutrinos that pass through every square centimeter of the earth per second although admittedly these neutrinos may turn out to be of the wrong kind, and therefore be unable to interfere with the observations. The experiment sets records in half a dozen directions: in the size of the detector and its sensitivity, in the forcing of coincidence techniques to the utmost as a discrimination against background, and in the elaborateness of the physical arrangements and the shielding. To my mind, the most impressive aspect is the fact that cross sections of the order of 10^{-44} cm^2 will probably be measured, whereas up to now cross sections like 10^{-33} cm^2 had been near the limit of detection; in other words, the experiment will be about 10^{10} or 10^{11} times more sensitive than any previously carried through.

Another sensitive neutrino experiment[13] is based upon radiochemical detection of an inverse beta process first suggested some years ago[14] in exactly this connection. The reaction is the inverse of the argon-37 electron capture, namely Cl^{37} $(\bar{\nu},e^-)A^{37}$. The experiment involves the separation of A^{37} from large volumes of carbon tetrachloride, and it has already been pushed to remarkable sensitivity.

Would it not be fun if, once we get a slight grip on neutrino experimentation, methods can be worked up to improve detection efficiencies until neutrino measurements come pretty well within our grasp! It sounds like a wild thought, but the possibility of detecting neutrons must have seemed equally wild when Rutherford suggested their existence in 1920, and look how easy they are now!

There are a variety of fundamental nuclear quantities that will require even more accurate measurement in the future, and reactors will be extensively used in the repeated re-measurement of such things as the electron-neutron interaction, the neutron-proton scattering lengths, and so on. Details of the fission process remain to be investigated with more and more refined techniques. The field of neutron diffraction, with its long-range and profound implications in the study of the magnetic structure of matter and in the crystallographic location of hydrogen atoms will not be pursued in this talk, inasmuch as more complete sessions on this subject are planned in this Conference. Let me add, however, that the recent theoretical work by Goodenough on superexchange in magnetic lattices, and the beautiful detailed experimental verification by Wollan and Koehler in neutron diffraction studies of perovskites will be worthy of the attention of people interested in this field.

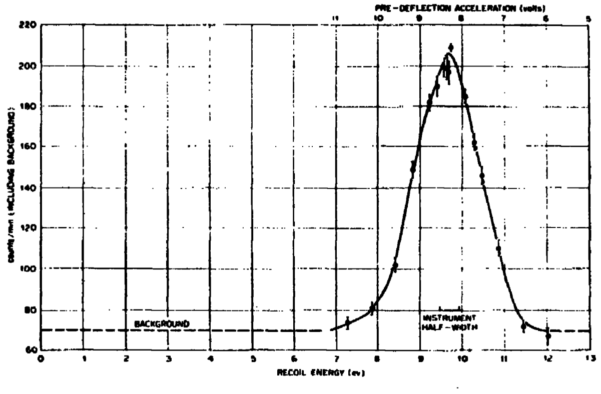

Figure 2. Singly-charged Cl^{37} neutrino recoils: magnet set at 3713 hp

I have so far been waxing enthusiastic about the possibilities of reactors in physics and chemistry, but one should also use one's perspective in pointing out serious limitations. For example, in the manufacture of positron-emitting or electron-capturing radioisotopes, the reactor is distinctly third-rate. A powerful cyclotron is in fact a much more versatile radioisotope source if variety is required. For fast neutron research, there is still nothing to equal an electrostatic generator delivering a beam of protons onto a thin target of lithium, tritium or vanadium. In the manufacture of trans-uranic elements, the reactor will soon be supplemented if not supplanted by accelerators employing multiply-charged heavy ions. On the other hand, reactors are sweet instruments to use because of their steadiness and their capability of supporting many simultaneous experiments.

What are the features of a research reactor that make it especially adaptable to the many kinds of experimentation for which it *is* pre-eminent? First of all, the experimenters will call for a high neutron flux. Modern requirements call for 10^{14} neutrons per cm^2 per second or better; certainly less than 10^{13} is undesirably low. High flux is essential for chemical work involving multiple neutron capture, such as has helped lead us into the realm of the trans-uranic elements, and it is mighty useful for neutron beam work of all kinds. Simultaneously with demanding high flux, the experimenters will ask for a low radiation background around the reactor. Several neutron beam holes will be required; they are most convenient if horizontal, and collimators of varied design will be

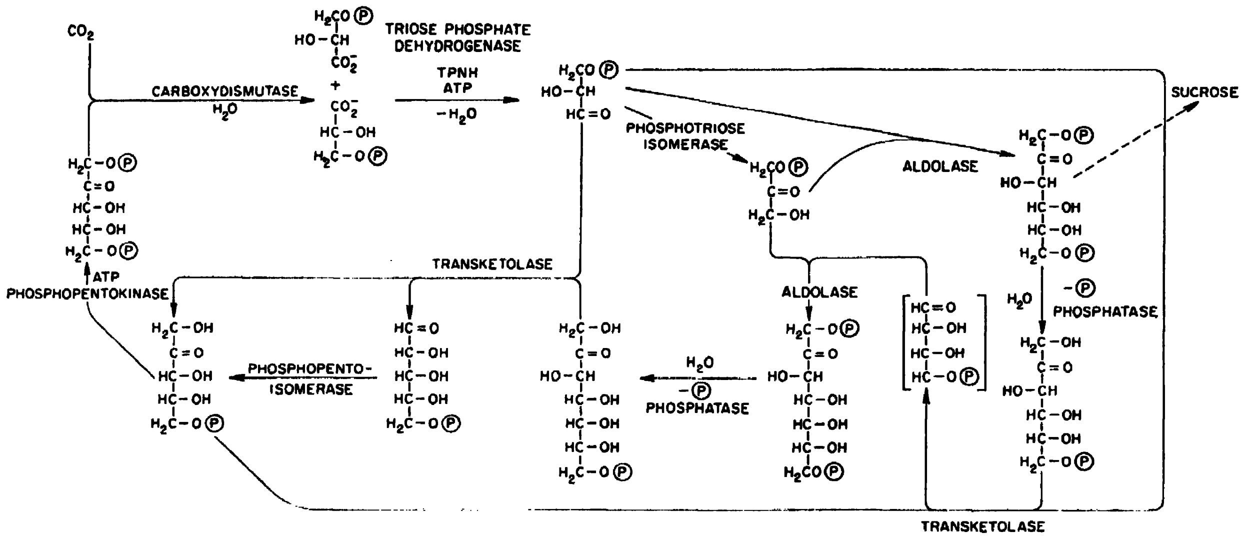

Figure 3. The path of carbon in photosynthesis

inserted by the experimenters. (The beam hole liners should be straight and true; there is nothing worse than a beam hole slightly out of round, or one that has a little obstruction somewhere in its depths.) The requirement of easy insertion and removal of activation samples is obvious. Whether or not to sacrifice beam hole space in favor of a thermal column can only be determined by the tastes and objectives of the experimental group. Finally, a rather strict operating schedule helps in the long-run to keep everybody happy.

The biologists have felt the disadvantages of the mixture of radiations accompanying direct exposure in reactors. My recollection is that for a few years following the start-up of the Oak Ridge graphite reactor in 1943, many survey experiments were made by animal exposure to establish mortality curves, tolerance levels and the like. After that, the interest concerning the action of radiation upon living cells became more detailed and basic, and the biologists retired from the reactor in favor of X-ray machines, cobalt gamma-ray sources, and D-D accelerators as yielders of purer types of radiation. Maybe they will later return to the reactor, but it looks as if that will be some time in the future. It is in fact a little hard for me to point to basic biology in which a reactor is currently used directly. The bulk irradiation of seeds to induce mutations might be cited, following which one plants the seeds and hopefully looks for a few beneficial mutations. However, I don't believe the reactor has been shown to have unique advantages over X-ray or gamma sources in this application.

Although the life-scientists may at present be reluctant to use the reactor directly, they are certainly using its products! One has only to look at the tracer sessions of this Conference to see that, or else one can look at the record of the Oxford Conference on Isotope Techniques in 1951, and any amount of current literature. Here I shall break my preliminary pledge not to attempt descriptions of tracer researches in order to illustrate the 1955 status of one of the most important investigations along this line—namely, that of photosynthesis. For this purpose I have filched a figure from a Berkeley report,[15] showing the path of carbon in photosynthesis (Fig. 3). This work was made possible mostly by the abundance of reactor-produced carbon-14. The carbon dioxide and water come together at the upper left, and under the action of light they enter into a most complicated mixture of cycles within cycles, yielding sugar (upper right) in some way that is not entirely apparent from the figure. (If you jump to the conclusion from the manner in which I discuss this topic that I don't know any biochemistry, you will be entirely right.) An important technique used to arrive at the design of this cycle was to introduce the carbon-14 in the CO_2 atmosphere around the plant, and then irradiate with light for only a short time. This, so to speak, started a wave of radioactive carbon into the cycle, and by examining the material at various subsequent times by the rapid methods of paper chromatography, one could identify the subsequent molecules roughly in the order of their appearance. The situation is probably even more complicated than is indicated in the figure, for a respiratory cycle (not shown) parallels the photosynthetic cycle, and the two have to some extent common paths. Looking at the complexity of the process, one is led to wonder whether nature has actually chosen the most efficient way of using the energy of sunlight. Maybe the average cabbage plant is not making the best use of its daylight hours, and when we have fuller knowledge and more perspective about photosynthesis and related processes, we can show the cabbage plant how it can grow into a ***super*** cabbage plant. Such an accomplishment would not only redound to the pride of the housewife when she serves cabbage for dinner, but it might hold out important hope for many people of the world who would like to have cabbage for dinner, but just don't have any at all.

If this superficial survey of the reactor in basic science has been a rambling one, the reason is that reactors have had and will continue to have far-reaching influences in many directions. We have touched on variable stars and polymers and neutrinos and I will leave you in the cabbage patch. I believe the journey has just begun.

REFERENCES

1. Boyd, G. E., *Technetium Activities at Mass 97*, Phys. Rev. *95*, 113–114 (1954); also unpublished work.
2. Merrill, P. W., *Spectroscopic Observations of Stars of Class S*, Astrophys. J. *116*, 21–26 (1952).
3. Boyd, G. E., Cobble, J. W., and Wexler, Sol, *Recoil Reactions with High Intensity Slow Neutron Sources: I. The Szilard-Chalmers Enrichment of 35.9 h* Br^{82}, J. Am. Chem. Soc. *74*, 237 (1952).
4. Cleland, J. W., and Crawford, J. H., *Radiation Effects in Indium Antimonide*, Phys. Rev. *93*, 894 (1954).
5. Levy, M., and Varley, J. H. O., *Radiation Induced Colour Centres in Fused Quartz*, Proc. Phys. Soc. *B68*, 223 (1954).
6. Griffiths, J. H. E., Owen, J., and Ward, I. M., *Paramagnetic Resonance in Irradiated Diamond and Quartz*, Nature *173*, 439 (1954).
7. Blewitt, T. H., Oak Ridge National Laboratory, private communication.
8. Smales, A. A., *Radioactivation Analysis*, Proceeding of Isotope Techniques Conference at Oxford, July, 1951, *II*, 162–171, London, Her Majesty's Stationery Office, 1952.
9. Robson, J. M., Chalk River Laboratories, private communication and Gordon Research Conference, 1955 (unpublished).
10. Rustad, B. M., and Ruby, S. L., *Gamow-Teller Interaction in the Decay of* He^6, Phys. Rev. *97*, 991 (1955).
11. Snell, Arthur H., and Pleasonton, Frances, Oak Ridge National Laboratory, 1955 (unpublished).
12. Reines, F., and Cowan, C. L., *Detection of the Free Neutrino*, Phys. Rev. *92*, 830 (1953).
13. Davis, Raymond, Jr., *Attempt to Detect the Anti-neutrinos from a Nuclear Reactor by the* $Cl^{37}(\bar{\nu},e^-)A^{37}$ *Reaction*, Phys. Rev. *97*, 766–769 (1955).
14. Pontecorvo, B., Chalk River Laboratory Report PD-205, 1948 (unpublished).
15. Bassham, James A., and Calvin, M., *Photosynthesis*, UCRL 2853 (1955).

Research Reactors

By E. Bretscher, J. V. Dunworth, H. J. Grout, G. J. Neary, and J. Wright,* UK

There has been published recently by the US AEC a very comprehensive account of research reactors (AECU-2900) and in addition there is to be presented to this conference, by Dr. Kowarski on behalf of UNESCO, a lengthy document which will take account not only of U.S. work but some of that in other countries. The present authors have had discussions with Dr. Kowarski on this paper.

Perhaps the first important point to note is that unlike the case of a power reactor there is no true economic basis on which to judge the merits of a research reactor since it is almost impossible to make precise calculations on the value to be attached to its facilities. In fact the nature of the facilities must depend to a very considerable extent on the location of the reactor and on the requirements of the potential user. A further point to bear in mind is that in some cases and, in particular in a University, a research reactor may be used for only 40 to 50 hours a week at the most. In this case low capital cost is likely to be a deciding factor. In the case of a reactor which is operating at high flux for an industrial or Government atomic energy authority it may well be that operating costs per annum can approach 50% of the total capital cost. In this case operating costs are clearly dominant. A further consideration is that there may be in certain cases a need for reactors which normally operate at low flux but which could operate at high flux for a very short time. No attempt will be made to draw any detailed conclusions on these points but they are worth noting.

It is one of the features of nuclear power that a great deal of information is required which can be obtained only from an experimental research reactor. Most of the nuclear constants necessary to evaluate reactor calculations have been obtained with the help of neutron beams from a pile, and little can be done on radiation effects on materials without the large fast fluxes available in a fairly high power research reactor. The chemistry of the all important transuranium elements could only be established after reactor produced specimens of these elements had been made available.

It has been clear for some time that one reactor is not suitable for all the above-mentioned tasks. The nuclear physicist requires undisputed access to high flux thermal and epithermal neutron beams, if possible without disturbance due to other work going on; the reactor engineer will wish to have many experimental loops in the reactor, so as to enable him to collect design information in the shortest possible time. As a rule his space requirements are very considerable, leading to special design problems. Metallurgists again depend on large facilities with enough space for temperature control of the samples, high fast neutron flux and large irradiation doses. If more advanced reactor information on shielding is required it is almost certain that a reactor has to be devoted to these problems. Though few reactors have been known to be built specially for biological work, it is well to consider the conditions which determine these particular features.

In view of the diversity of requirements by the various users, some indication as to what is wanted will be given below.

NEUTRON PHYSICS RESEARCH

The nuclear physicist is mostly interested in neutron *beams* coming from a radiator placed in the centre of the reactor. Almost all experimental arrangements profit from a high flux. Below are listed the most frequent uses of pile neutron beams at the moment:

(*a*) Time of flight experiments for the determination of nuclear data.

(*b*) Neutron diffraction work for investigation of lattice arrangements in crystals. Here high flux allows one to preselect a wavelength with a suitable crystal acting as monochromator and using the beam thus obtained much as the characteristic radiation from a suitable X-ray target.

(*c*) Monochromatisation with a crystal such as LiF, CaF_2, Be to obtain monoenergetic neutrons for nuclear studies or cold neutrons from filters.

(*d*) Free neutron beams for the study of neutron decay.

(*e*) Neutron total reflection from surfaces.

(*f*) Neutron capture gamma rays in various materials.

(*g*) Source of fission neutrons with the help of enriched materials.

With slightly enriched uranium a heavy-water or a light-water moderated reactor is of advantage as compared to a graphite pile, as for the same power the central flux is larger *and* the distance of the neutron radiator in the channel to the working point of the apparatus (rotor slit in *a*, crystal in *b* and *c*) is smaller. It is, however, generally easier to provide a large number of channels to the core in a graphite pile than in a liquid moderated system.

---

* Atomic Energy Research Establishment, Harwell.

Since many uses of neutron beams involve intensity measurements, it is necessary to avoid interference by control rods or highly absorbing samples placed in the reactor by other users as they may alter the local flux at the neutron radiator, whilst the total pile power is kept constant. Similar intensity disturbances have been observed where a channel goes through the centre and alterations are made in the opposite half of it. It is therefore from the experimental point of view essential and borne out in practice that the number of pile users should be restricted to avoid mutual disturbances.

The pile has in the past become a useful instrument as a *pile oscillator* to measure absorption cross sections, assay moderator materials for neutron absorption on a routine basis, calibrate neutron sources. Here the graphite pile has a definite advantage as its temperature coefficient is low when compared to that of a liquid moderated reactor. In addition, the neutron production through the photoeffect in deuterium causes complications which make the heavy-water pile oscillator an unattractive tool as its performance depends also on its previous history, and its useful sensitivity is low (unless the pile is run permanently at very low flux of about 10^9 or less).

SOLID STATE PHYSICS RESEARCH

Many different kinds of radiation are capable of displacing atoms in crystalline solids to produce interstitial atoms and vacancies, and the study of these lattice defects is of great interest to the solid state physicist.

Although fast neutron irradiations are easy to carry out experimentally, since large specimens can be used and there is little generation of heat in the specimens, fast neutron collisions introduce groups of displaced atoms and vacancies, and it is not usually very easy to calculate the number and distribution of defects in these groups. The electrical properties of semi-conductors are among the most sensitive to the presence of lattice defects, and large changes can be observed after short irradiations in fast neutron fluxes of 10^{10} to 10^{11} cm^{-2} sec^{-1}; similar concentrations of defects can be introduced by charged particle irradiations and the numbers and distributions of defects are more susceptible to calculation. Such sensitive properties are not, however, common and it is often desirable to be able to investigate simultaneously the changes in many physical properties (density, stored energy, thermal conductivity, electrical properties) so that fast neutron fluxes in the range from 10^{12} to 10^{14} cm^{-2} sec^{-1} are necessary. With this range of fluxes, greater concentrations of defects, than can readily be introduced by any other type of radiation, are easily attained, and the advantages of fast neutron irradiations are most obvious.

The space in which irradiations are carried out should have a high and uniform fast neutron flux coupled with a low thermal neutron flux. Thermal neutrons are troublesome because the impurities resulting from nuclear transmutations may cause unwanted changes of physical properties, and also because the induced activity may make handling difficult. These requirements may be met by surrounding the irradiation space with a uranium cylinder or fast neutron converter. In this way, irradiations can be carried out in the reflector of a reactor, where restrictions on space are usually less stringent and where the fast neutron flux in the absence of a converter would be low and would vary rapidly.

In many cases the defects are mobile at or below room temperature and it is therefore necessary to control the irradiation temperature. There is much to be gained by irradiating at the lowest possible temperature in order to freeze in the mobile defects, and reactor irradiations at −150°C have been reported.

Thus, although a cylinder of about one inch diameter is adequate to contain most of the specimens which might be used for the measurement of physical properties, the addition of some form of thermostat and a fast neutron converter, with its associated cooling, increased the minimum diameter of a useful experimental hole to about four inches.

CHEMICAL RESEARCH

The chemist's uses of a research reactor fall into two categories. In the first, the reactor is treated as a source of high thermal neutron flux for radioactivation analysis, chemical studies of the fission process, "hot-atom" chemistry, and similar radiochemical research. In the second category are uses of the reactor as a source of high-energy radiation, including basic studies in radiation chemistry and investigations of the chemical behaviour of future reactor systems.

Radiochemical studies are concerned with nuclear events and temperature control is seldom important. The chemistry is often conducted away from the reactor using irradiated specimens. Quantitative studies are simplified by the use of thermal neutron activation monitors, and it is often possible to arrange an internal measure of the dose received. The fast neutron and gamma radiation in a reactor core may be an embarrassment if it induces decomposition of the material or causes exchange between various chemical forms of an element. In this case a high-flux thermal column, more easily provided in an enriched-fuel reactor, has many advantages. Radiochemical techniques are so sensitive that large specimens are seldom required, and small diameter holes can be used. Means of inserting and removing specimens with the reactor operating enables a wider range of half-lives to be used in this work.

Radiation chemical studies make greater demands on reactor design. Thermal neutrons are less important, unless an element of high cross section is present, and the radioactivity induced by thermal neutron capture can be a serious embarrassment. High thermal neutron flux is only a means to an end—the attainment of high energy flux from fast neutrons and gamma radiation. A graphite-moderated reactor of large core size provides these conditions directly; in enriched-fuel, water-moderated reactors it is necessary to allow for appreciable amounts of power from uranium converters used in the experimental holes. Quantitative work is difficult because the chemical effects are not directly related to thermal neutron dose—the only readily measurable quantity—and results are very sensitive to the proximity of thermal neutron absorbers which alter the relation between that quantity and the energy deposition.

Though the chemical examination of irradiated material can give valuable data, the preparation of specimens and their handling under active conditions is time-consuming, and it is sometimes more convenient to devise apparatus for gas evolution studies, for taking samples during irradiation, or for using a flow system partly outside the reactor, so that a series of measurements can be made on a single specimen. Although radiation-induced processes usually have low temperature coefficients, the subsequent or accompanying reactions often call for close control of temperature. The needs for large specimens, for temperature control, and in some cases for uranium converters with their attendant cooling requirements, make the provision of large diameter holes essential. This is particularly true in "hot-loop" studies associated with future reactor systems since the research reactor provides only the radiation, and the other requirements (pressure, temperature, etc.) must be provided by the experimental equipment.

ENGINEERING RESEARCH

A high flux research reactor occupies an analogous place to the wind tunnels in aeronautical engineering; it provides a test bed on which engineers can test and develop new components and new assemblies for future power reactors and it would be as well to stress at this point the important part that "hot loops" in research reactors have played and will continue to play in the improvement of existing types and the development of new forms of power reactors.

In this work the engineer associates closely with scientists in the fields of physics, chemistry and metallurgy. The engineer is primarily concerned with design, development and operation of the hot active loops which are built into a research reactor for the purpose of investigating some new fuel element-coolant-moderator assembly.

The number of reactor fuel element-coolant-moderator variants, which must be explored and evaluated, is very large and to build prototype reactors for each variant would be too expensive; the "hot loop" however, although perhaps not providing all the answers, is an essential prerequisite before the prototype stage is decided upon.

A realistically designed "hot loop" can provide, if built into a research reactor of the appropriate high flux, a means of testing, developing and evaluating a very significant proportion of the parameters which will be encountered in the full scale prototype.

A serious incident can be caused in a reactor by the rupture of fuel element canning material with its consequent release of highly toxic and active fission products. Our aim throughout must be the production of a fuel element free from this trouble rather than the detection of fuel element failure. At the present stage the former cannot be guaranteed and it is accepted that detection at an early stage of failure is essential. This subject of engineering research can give handsome dividends in obtaining freedom from reactor shut-down.

BIOLOGICAL RESEARCH

The precise requirements in a reactor for biological research depend somewhat on the particular problem to be investigated but some general considerations are possible. In the first place it is usually desirable to carry out the actual exposures outside the reactor itself, in the region of the shield. In this way, possible high temperatures in the core are avoided and further it may be possible to arrange some shutter device between the reactor and the irradiation space. Interference with other research uses of the reactor is thereby lessened. Secondly a fast reactor is considerably more limited in its possible applications than is a thermal fission reactor. Usually the irradiation area that can be obtained with a fast reactor will be insufficient, and if slow neutrons are required, the thermal reactor is the only choice. It is quite possible with a thermal reactor to provide for fast neutron irradiations through conversion of the slow neutrons to fast neutrons in uranium external to the reactor. The fluxes required with a thermal reactor will next be considered.

Irradiation work with experimental animals and other biological specimens may be broadly divided into two main classes, acute and chronic. In acute work single doses of the order of a few hundred reps are common, and for practical reasons it is desirable to give such doses in not more than an hour and preferably in about ten minutes. In chronic work, doses of the order of ten reps per day and downwards are usual.

For acute doses of fast neutrons, a flux of about 10^8 fast neutrons/cm^2/sec is required. If the fast neutrons are to be produced through fission of uranium by slow neutrons, the required flux of the latter will be around 10^9. Such a flux at the inner edge of the shield of a natural uranium graphite moderated reactor is available at a power level of a few megawatts. If acute doses of slow neutrons are required, then a flux of about 5×10^9 would be suitable requiring a power level of around 10 megawatts. Neutron capture therapy, requiring slow neutron fluxes between 10^8 and 10^9 n/cm^2 sec would also be possible under these conditions. Adequate shielding from the reactor gamma radiation would be necessary, using lead or bismuth and slow neutron shutter containing boron. If fast neutrons were being used, then unwanted slow neutrons transmitted through the uranium would be absorbed in boron, and gamma radiation from the uranium (arising in fission from the fission products) absorbed in lead. Finally, some protective shield against the neutrons after passing the experimental animals would be required for the safety of operators. This shield might well consist of concrete plugs inserted into the hole through the main shield of the reactor. A vertical hole is likely to be most useful generally to permit a horizontal arrangement of animal cages. The size of hole should probably be at least a few feet square, to permit large numbers of small animals or individual larger animals such as pigs or goats to be irradiated.

For chronic work with fast or slow neutrons, fluxes about one thousandth of those mentioned above are needed, assuming that the irradiation is to be essentially continuous. The simplest way of obtaining such fluxes is to run the reactor at a power of a few kilowatts. If it is necessary for other reasons to run at power levels measured in megawatts, very careful design is necessary to attain the required low levels of irradiation in the experimental arrangement free from contaminating gamma radiation or fast neutrons from the reactor. Broadly speaking something amounting to a thermal column would be necessary. A large area is again desirable, to permit use of large numbers of animals; the area might well be sub-divided to enable different dose-rates to be studied concurrently. The external shielding requirements are more simply met than in an arrangement for the acute work; shields moving on runners may be satisfactory.

RESEARCH REACTOR FLUX RANGES

It is convenient to classify research reactors into a number of flux ranges:

High Flux Reactors: 10^{15} to 10^{13} n/cm^2/sec

Reactors of this type tend to be expensive to operate and the design of experiments is itself likely to involve a major effort. Such reactors are, therefore, likely to be of interest primarily to industrial and atomic energy organisations and the work with them is likely to be associated with fuel element technology and reactor corrosion problems. In most cases intense activities will have to be dealt with, and appreciable amounts of heat will be generated in the experimental apparatus. In many cases fairly elaborate precautions will have to be taken to ensure that no failure occurs in the experimental equipment. Such failure could cause considerable damage to the reactor as well as be a serious hazard in itself.

Two distinct types of high flux reactor can be discerned. In one case the reactor operates on natural uranium and a high flux of say 10^{14} may well involve a total power output of 100 Mw. Such a reactor is obviously a major project but it would be possible to recover an appreciable fraction of the expenditure by selling the plutonium by-product. A system which approaches this specification is the NRX reactor at Chalk River in Canada which was designed as long ago as 1944 by a joint Canadian-British-French team and which must still be considered as one of the finest research systems in the world.

The alternative type of system is based upon a small core of U^{235} and practically all experimental work is undertaken in a reflector around this core. In order to have an adequate flux over a reasonable volume in this reflector it is desirable to use a comparatively non-absorbing material. A very good example of this type of system is the MTR reactor which uses graphite in the outer regions of the reflector and beryllium close to the core. The UK is constructing two high flux systems with a similar specification but these will use heavy water rather than a solid for the high flux experimental region. This arrangement simplifies design of the reactor and will allow us to proceed more quickly. The same heavy water can be used as the cooling medium.

The UK reactors are essentially higher flux versions of the Argonne CP5 reactor.

Medium Flux Reactors: 10^{11} to 10^{13} n/cm^2/sec

The cost of reactors in this flux range is such that it is not particularly uneconomic to operate them at well below their normal rating. However, especially at the higher end of the flux range they do permit a reasonable range of experiments in physics and chemistry. It is our experience that the interest of physics and chemistry research staff drops off sharply as flux is reduced towards 10^{11} and becomes negligible below 10^{11}.

For fluxes of the order of 10^{11} to 10^{13} the amount of by-product plutonium becomes insignificant in a natural uranium research reactor while the consumption of U^{235} becomes insignificant in the U^{235} core reactor. Since the total cost of such reactors becomes relatively modest, it will not be worth while in many cases to design a complicated system using natural uranium to permit the carrying out of a large number of experiments at the same time and it is probable that research reactors in this flux range will tend to be based on the use of U^{235} in future.

The capital cost of D_2O will tend to become excessive for a medium flux system, and one will tend towards natural water for cooling.

In many cases the reactor will need only a small reflector surrounding the core. For these reasons the tendency would seem to be to surround the U^{235} core with a cube of graphite if a reflector is required.

The design of these lower flux systems affords a very wide field for individual features and this is a tendency which can already be discerned.

Low Flux Reactors: 10^9 to 10^{11} n/cm^2/sec

A reactor of this type requires virtually no cooling and about the only maintenance and operating problem is in connection with the electronic control circuits. The whole design of reactor including the shield can be exceedingly simple and cheap. Such systems are quite useful for many medical and biological experiments. They are of use also for measurements of the purity of reactor materials and for analytical investigations.

As enriched material was not available in the UK after the war, a simple graphite moderated system, known as Gleep, was constructed and this system has been in use 24 hours a day, seven days a week for the last eight years. In any future system in this flux range the UK would probably use slightly enriched uranium and a much purer graphite than was used in Gleep. This would result in a much smaller system with perhaps a three-metre cube of graphite or something a little larger. To reduce the size too far could be a disadvantage in that it would no longer be possible to have a reasonably large volume in the system at a moderately uniform flux. This can be important for biological work and oscillator type experiments.

Flux Up to 10^9

In carrying out zero energy experiments in connection with reactor design it is desirable to operate at such a flux that the fuel can be handled by hand after shutdown. In addition it is desirable to have no more than elementary shielding. These requirements can be met with a reasonably adequate sensitivity of measurement with fluxes not exceeding 10^9.

REACTOR COSTS

It would appear that the capital costs of the simple research reactor will be quite modest and even allowing for fuel and the cost of the building will not exceed between £100,000 and £200,000, unless the flux exceeds 10^{13}. Operating costs in this region will usually be small. In addition, relatively few safety precautions are needed with experiments and the design of experiments can be relatively simple and cheap. Above 10^{13} one begins to face major design problems in removing large quantities of heat, whilst the consumption of fuel becomes an important consideration. Costs of the order of two to three million pounds may be expected at a flux of 10^{14} with annual operating costs of perhaps £250,000 per year. For higher fluxes the cost will tend to increase in proportion.

CONCLUSION

A flux of 10^{13} can be obtained at a moderate capital cost of the order of £200,000 or less and with low operating costs. It will satisfy the needs of a large fraction of the research work which can be done in physics, chemistry, and biology. For the latter, in fact, smaller fluxes are adequate for much of the work. The nuclear energy industry, however, will demand expensive facilities for fluxes up to 10^{15} though much can be done with a flux of 10^{14}. Even so, operating costs may well be of the order of £250,000 per year or more.

Practical Experiences with the JEEP Reactor

By T. J. Barendregt, N. Hidle, A. Lundby, E. Sæland, and G. Trumpy,* Norway

The construction of the reactor installation, JEEP, at the Dutch-Norwegian Joint Establishment for Nuclear Energy Research (JENER), was started in 1948, at Kjeller, near Lilleström, Norway. The reactor became critical in the last days of July 1951, and has been in operation almost continuously since then. The main activity at Kjeller is related to the use of the reactor as a research tool and as an isotope producer. Many physicists and engineers from abroad have performed their own experiments with the reactor or have taken part in experiments with the institute staff, and we hope that the installation will still serve for a long time as a useful tool.

DESCRIPTION

JEEP (see Fig. 1) is a natural uranium heavy water moderated and cooled reactor.[1] The designed power level was 100 kw, but the actual level has gradually been increased to a maximum of 350 kw with a corresponding central thermal neutron flux of approximately $10^{12}/\text{cm}^2$ sec. The moderator water which is kept well below 100°C removes the generated heat from the fuel elements by natural convection. Heavy water is removed from the top of the reactor and circulated to an external heat exchanger where it is cooled by ordinary water before returning to the bottom of the tank. A closed circuit is chosen for the ordinary water, and this is cooled in a water-to-air heat exchanger. The heat energy is finally discharged to the atmosphere; a part however is used for heating the reactor building during the winter.

The reactor tank, 2 m in diameter, is surrounded by a graphite reflector 0.7 m thick. Cadmium plates, two for control and two for shut-off, are placed between the tank wall and the reflector. The plates, 35 × 130 cm, can be lowered into slots in the concrete floor below the reactor. A manually operated shim rod is placed in one of the six channels penetrating diametrically through the tank. Biological shield is ordinary concrete lined with cadmium on inner walls. Minimum concrete thickness is 2 m.

In addition to the above mentioned six channels, which pass through from one side of the concrete block to the opposite side, there is a thermal column and two channels extend through the graphite reflector on to the tank wall. This is a low number of openings for a research reactor of this kind. To ease the situation, both horizontal channels which normally contain neutron detectors and vacant fuel element holes in top of the tank are used for experimental set-ups.

The fuel is metallic uranium, canned in aluminium. Fuel elements spaced on a square lattice of 18 cm centre-to-centre distance, consist of two uranium rods 1 in. in diameter. The rods are comprised of 6½ individual uranium bars 11½ in. long. At present, the reactor is operated with 65 fuel elements, the maximum number being however, 76. The 65 elements have a total weight close to 2.3 tons. The total heavy water content in the system is 7 tons.

It might be of interest to note that the entire installation is built up from conventional and non-restricted materials and components. Aluminium used in rod construction, tank, and tubings is of an ordinary technically pure quality (2S). Steel used in pumps, valves, heat exchanger and tubings is of commercial quality with C, Cr, Ni and Mo content 0.05, 18, 9 and 1.5 per cent, respectively. All connections of stainless steel to aluminium in the circuit are electrically insulated to prevent corrosion. Gasket material is largely neoprene through the entire system.

Six separate neutron sensitive systems are located in the reactor. One is used for the main reference of power level. Three are used as shut-off channels; these will actuate the shut-off plates if the power should exceed a pre-set level. One is used for automatic control of power level. The last one is battery driven, and current from the detector passes directly to a galvanometer. This sixth system is installed to be able to see that the reactor shuts off in cases when the main current supply falls out. All neutron detectors are TPA ionization chambers with BF_3 filling.

FIRST START-UP OF REACTOR

The exact amount of uranium and heavy water needed to get the reactor critical was not known in advance. The first starting-up, therefore, had to be done very carefully. All 76 fuel elements were mounted in position in the reactor, a 100 mg Ra-Be source was placed close under the bottom of the reactor and heavy water was pumped in portions into the tank. BF_3 counters placed inside the reactor core gave counting rates which were plotted inversely against the height of heavy water. By extrapolation of the curve $1/c = f(H)$ to $1/c = 0$, a very good value for the critical water level was obtained. The Ra-Be source was

---

* Joint Establishment for Nuclear Energy Research, Kjeller near Lilleström.

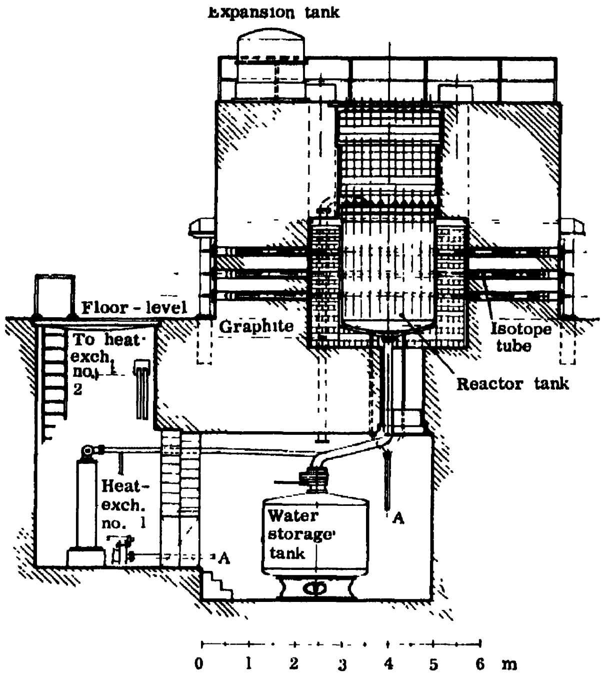

Figure 1. The Kjeller reactor

removed during the procedure when the multiplication factor was large enough to multiply the background neutrons to such an extent that they could be counted with the BF_3 counters. All cadmium plates were drawn out of the system during the start-up.

Critical water level in the tank was so low at the initial start-up that water did not reach up to the outlet tube for circulation. Fourteen fuel elements were therefore removed from the tank so that circulation level could be reached without the system having too much excess reactivity. Later, three elements have been reinserted to compensate for isotope loading.

Today the start-up is an easy routine procedure. It is done in the following manner. The neutron-sensitive instruments, which are calibrated in kw of power level, are switched to a sensitivity range where the background of neutrons can be detected. First, the two shut-off plates are withdrawn one at a time. Then the two control-plates are carefully taken out, also one at a time. Normally the reactor is still sub-critical after these operations due to the rather large shim rod in the lowest horizontal channel. The shim rod is then gradually withdrawn until criticality is reached. Pile period is watched very carefully during the entire procedure. The shim rod is withdrawn so far that the doubling time of the reactor is approximately 30 seconds. The power level is then allowed to increase until the desired operating level is reached. Control cadmium is then inserted manually to stabilize the level. The automatic control circuit can then be put into operation.

When the moderator is heated up, cadmium has to be taken out to compensate for the negative temperature coefficient. This is done with control plates in the first instance, and the shim cadmium is withdrawn step by step to keep the control plate in a practical working range.

When shutting down the reactor, even for short intervals, all the cadmium is reinserted, and starting-up has to proceed from the beginning. This rule is established to prevent the operators misjudging load changes.

REACTOR OPERATING EXPERIENCES

Since JEEP is our first installation of this kind, we are naturally very interested in gaining experiences with operation and maintenance of the reactor. To be able to follow the behaviour of the more important parts and equipment, we inspect fuel elements, reactor tank wall, pumps, valves and other accessible parts regularly. Some more details might be mentioned.

Inspection of fuel elements is carried out in a simple and in our opinion, effective way. The highly active fuel elements, accumulated dose up to 110 Mwd/ton uranium, are hoisted from the reactor into a lead coffin placed on top of the reactor shielding. This coffin is used for transporting burned fuel to the "cooling-down well," but for inspection, it is placed with the rod inside on top of a lead cylinder with an epidiascope built in. The fuel rod is then lowered from the coffin into the cylinder, passing the epidiascope on its way. An enlarged picture of the element can then be projected on to a screen. Turning the element and focusing the optical system can be done from a distance, i.e., by the inspector sitting in front of the screen. With this system, very small irregularities and also colouring effects on the canning can be discovered.

Although fuel elements in JEEP were made without knowing much about how to can uranium, very little trouble has arisen up to now. Five rods have been removed due to corrosion of canning material or "blister formation," but with today's knowledge, we probably would not have removed more than two of them. The corrosion attack on the canning which was serious enough to cause removal of elements was due to copper particles pressed into the canning surface giving local galvanic elements. Some general corrosion attack has been observed on non-treated canning surfaces. Fuel elements which have been anodically oxidized have shown remarkably little or no attack at all. New elements are now treated in this way. Blister formation (see Fig. 2) is probably due to moisture inside the canning reacting with uranium and resulting in uranium oxides or uranium hydrides in local spots. The result is an increased volume which can cause very sharp warts in the aluminium tubing. Several of these blisters have been formed, the largest has been up to approximately 3 mm high and 15 mm in diameter in the bottom. No burst of canning has occurred. All fuel elements are inspected twice a year, and according to the records, it seems as though most blisters stabilize on a reasonably small size, less than 1 mm high. Since blisters have also been found on fuel elements which have been stored, it is concluded that the effect is not primarily dependent on conditions in the reactor.

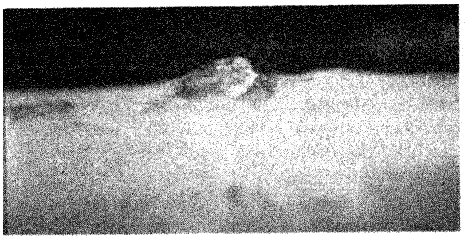

Figure 2. The picture shows one large, approx. 3 mm high, and one small blister on one of the active rods. The large blister is scratched on top when the element is extracted from the reactor, due to small clearance in the fuel element hole in top of tank. This rod was permanently removed because of the large blister. (Photograph is taken from the projected picture)

The inner wall of the reactor tank is inspected by means of a periscope. Fuel elements on the tank circumference are raised to make room for the periscope. No serious defects have been found in the welded tank structure. The walls are, however, tarnished with a grey aluminium oxide layer.

Since the initial start-up, the reactor has been checked for corrosion seven times. The corrosion effects in the reactor seem mainly to be a problem of heavy water contamination. Inspection of the valves, pumps, and heat exchanger of the heavy water system revealed corrosion attacks on the stainless steel material, which have resulted in the introduction of rust particles into the heavy water system.

Since the conductivity of the heavy water will give an indication of the dissolved impurities, the conductivity is measured regularly. Doubly distilled heavy water has a λ of about $1 \times 10^{-6}\Omega^{-1}$ cm^{-1} at 25°C, and the heavy water delivered by Norsk Hydro has an average $\lambda = 0.85 \times 10^{-6}\Omega^{-1}$ cm^{-1} at 25°C. The conductivity is slightly influenced by the power level at which the reactor is running, but its value was increased to $2 \times 10^{-5}\Omega^{-1}$ cm^{-1} at 25°C at the end of 1954. No data are available which can give a better explanation of this twentyfold increase of the conductivity of the heavy water, other than contamination by corrosion products.

As a comparison, the pD was determined. Doubly distilled heavy water with a so-called "apparent pH" of 6.2 was used as a standard. The apparent pH of the heavy water in the reactor system appeared to be slightly decreased to 4.8-5.0, which also indicates dissolved products in the heavy water. With diphenylbenzidine as a reagent, nitrate ions could be detected and a quantitative determination showed an amount of 10 mg/litre present. It is obvious that only a small percentage of this nitrate in the heavy water as free nitric acid would cause the lower pH. The elements listed in Table 1 were determined spectrographically in the residues obtained after distilling off the heavy water.

Due to the decomposition of the heavy water, D_2O_2 is present. During operation of the reactor, an average value of 10 mg D_2O_2/litre was obtained, but this amount decreases when the reactor is shut down for a longer period.

Table 1. Data of the Heavy Water in the JEEP System (January 1954)

1. Composition	99.8–99.85% D_2O
2. Conductivity	$17 \times 10^{-6}\Omega^{-1}$ cm^{-1} at 25°C
3. pD (apparent pH)	4.8–5.0
4. Nitrate	10 mg/litre
5. D_2O_2	18 mg/litre
6. Residue	50 mg/litre
Components of residue	
Al 9 ppm D_2O	Cr 0.1 ppm D_2O
Ca 0.05	Ni 0.15 ppm D_2O
Cu 0.15	B 0.05 ppm D_2O
Pb 0.9	Si 1.1 ppm D_2O
Fe 3.5	

On top of the reactor tank there is a layer of 1 m^3 of air, which is circulated over a catalyst to recombine the D_2-O_2 mixture, formed in the heavy water by irradiation. The content of D_2 in the air has been measured regularly. The amount increases continuously and the air is circulated to such an extent that the D_2-content is kept at about 0.5 per cent. The amount of recombined water is a linear function of the power at which the reactor is running. At a level of 250 kw the amount of recombined water is now 40 ml/hr.

Owing to the impurities present, the heavy water in the reactor system appeared to be radioactive. There is a close correlation between the specific activity of the heavy water in mc/ml and the level of the reactor. To obtain some idea of the elements which are responsible for the activity, Cu^{++}, Fe^{+++}, Ca^{++}, K^+, and Na^+ were added as carriers. From the analysis of the components it was found that approximately 70 per cent of the total activity was due to components of less than 4-hr half-lives, and 2.4 per cent to components with 24-hr half-lives. The contribution of more long-living components is of the order 1-2 per cent.

Although no precautions have been taken, no indications of serious corrosion attacks on the system have been observed. In order to reduce the decomposition rate at high power levels, however, plans have been made for building in a purification unit for the heavy water.

The heavy water circuit outside the main reactor shield is accessible when the reactor is shut down. Valves, pumps, flange connections, etc., in this system can then be checked quite often. In addition to the direct visual control, a leak detection system is installed. The detector which only needs a drop of water to set off an alarm, consists of two steel plates with a hygroscopic paper between. The paper is prepared with NaCl to act as a conductor when it becomes wet. The detector is coupled in series with a battery and an alarm relay. Detectors of this kind are placed all around the installation where leakages are likely to occur. The system has often proved to be very useful.

The circulation pump in the heavy water circuit is of a normal centrifugal type. The difficult problem when looking for a pump for expensive fluids like heavy water, is the shaft sealing. The sealing has to be tight, no lubrication is allowed, material choice is restricted, and low maintenance is required. In our case a standard rotating shaft seal is applied. The rotating seal itself is achieved with a ground carbon ring against a ground stainless steel ring. The system has proved to be good for our working conditions. During the four years of almost continuous operation, the shaft seal has been renewed only once. The reason for break-down was that an aluminium particle which had managed to enter between the carbon steel ring, had scratched the carbon ring so that water was able to leak out.

Valves used in heavy water lines are of a commercial available plug cock type. The valves are grease lubricated, the grease being of special quality non-soluble in water. The choice of these valves is not entirely to our satisfaction. Grease is loosened by the streaming water and is transported around in the system until it sticks to the wall somewhere. It does not cause much harm, but some trouble has arisen with the valves in a small diaphragm pump. We now believe that with the proper choice of material, diaphragm valves might prove to be better than the type used.

Gasket material used is mainly neoprene either as sheeted material or as standard O-rings. The material withstands fairly well the actual conditions outside the radiation field. O-rings are also used for tightening of fuel element holes. The rings are fitted in a slot under the top flange of the fuel element construction. The gasket should seal the hole by means of the element's own weight. The neoprene, however, becomes damaged rather soon in the radiation field; it hardens, turns brittle and loses its sealing effect.

Apart from the ordinary break down of electronic components, very few failures have occurred in the control installation. A water level indicator for the reactor tank was working on the principle of a float adjusting an iron core inside a solenoid, the solenoid being one branch of an inductive bridge. This indicator, however, did not function properly after about one year's operation. The float mounted on top of the tank under the top shielding is no longer accessible. We believe that the reason for not functioning is a broken lucite tube located inside the solenoid. This tube has probably caused the iron core to remain in a fixed position.

The wiring for one of two resistance thermometers recording reflector temperature is short-circuited somewhere inside the radiation shield.

Resistance thermometers are used throughout the entire installation. Thermometers situated in the reactor tank can be shown to be influenced by radiation. The effect is dependent on radiation intensity; no permanent change has been recorded.

EXPOSURE TO RADIATION

Members of the staff most exposed to radiation are the Reactor Operating personnel. Normally, the record over a three month period shows that the highest doses are approximately ⅓ of the accepted tolerance dose which corresponds to 300 mr per week. Personnel working constantly in the radiation field use pen-type gamma and neutron dosimeters and also film badges, whilst personnel working occasionally with radioactive materials wear only film badges. Blood checks of all personnel are made regularly.

One serious case of heavy contamination has occurred. About three kilos of uranium canned in aluminium had been inserted in an irradiation channel for three weeks, after which the experiment for which it was intended was completed. It had been checked after two weeks and found in good order, but when the uranium was to be removed from the channel, the canning had burst. Due to a rather high temperature in the uranium, it had oxidized strongly in the air, and quite a large amount was sprayed around, in the form of dust, when the channel was opened. All personnel were immediately evacuated from the building, and before men in protection clothing and masks were allowed to re-enter the building air samples were taken. Primarily the burst slug had to be removed. It was transferred to a container by means of long tongs, where it was soaked in oil to prevent more dust from escaping. Vacuum cleaners were then used for removing the major part of active dust which was located in the channel, and on the floor in front of the channel. The vacuum cleaners were so highly active that they were disposed of in concrete drums. The cleaning job was then commenced upon with brushes and water, the washing being continued day and night over the entire building, for four consecutive days. Most of the activity was then removed, but some was left in cracks in the concrete floor; after monitoring however, it was decided that the remaining activity was not dangerous. Liquid floor polish was then used for binding the dust in the cracks, the waxing of the floor being repeated several times.

REACTOR PHYSICS

One usually attempts to make most experiments with reactors as such immediately after starting them up (breaking-in period). As techniques and experience develop, however, previous experiments are revised and new ones added.

A number of physical experiments depend, furthermore, on the operation of the reactor as a whole. This is, for example, the case with reactor oscillator and danger coefficient experiments. Since they frequently have to be carried out at relatively low reactor power levels, one has to balance the available operating time between isotope production and measurements with high neutron fluxes on the one hand and low flux experiments on the other.

In heavy water moderated reactors complications arise under these conditions due to (*a*) the presence of long-lived photoneutrons, (*b*) the large nuclear temperature coefficient of heavy water, and (*c*) the xenon poisoning effect.

The reactor oscillator used in connection with JEEP is pneumatically operated.[2] The arrangement is easily moved in and out of any of the irradiation channels which run through the reactor. The effect of a sample on the reactivity is detected by integrating the first Fourier component of the signal from a boron coated ionization chamber placed near the reactor core. For practical and security reasons the reactor power level is reduced from a few hundred kw to a few kw when operating the oscillator. The background of long-lived photoneutrons will in this case tend to influence the reactor transfer function in such a way as to make reactor oscillator experiments ambiguous.[3] In order to be able to perform such experiments at power levels of one kw or less, it is necessary to wait several days after the power level is reduced.

The nuclear temperature coefficient of the heavy water in JEEP is about -2×10^{-4} per °C.[4] When the reactor has been running at full power level with a maximum cooling rate, the temperature of the heavy water is 20–30°C above the temperature of the surrounding air. The loss of reactivity in heating up (about 0.5%) cannot be tolerated in some experiments, e.g. when resonance integrals are measured with the reactor oscillator.[5] The power level and temperature have therefore to be reduced. Since it is hard to stabilize the temperature of the heavy water, one gets difficulties due to spurious changes in reactivity.

As compared to other natural uranium heavy water reactors JEEP has an unusually low ratio of uranium to heavy water. This reflects itself in the very long lifetime of neutrons in the reactor (nearly 2×10^{-3} sec.[6] As a result the stable period of the reactor is comparatively large even for several per cent excess reactivities. Together with the large nuclear temperature coefficient of the heavy water this makes the reactor relatively safe. At an operating level of 250 kw (maximum thermal neutron flux 7.54 cm^{-2} sec^{-1}) the xenon poisoning suppresses a reactivity of 2×10^{-3} after running the reactor for a few days. The build up after reactor shut down is negligible.

The reactor power level will be increased by at least a factor of two in the near future and the xenon effect will increase correspondingly.

NEUTRON PHYSICS RESEARCH

The JEEP has shown itself to be a very good tool for experiments in neutron physics, the only disadvantage being a shortage of experimental channels. For physical research the two "fast neutron channels" leading to the reactor tank wall, and two of the six "isotope channels" going all the way through the reactor are available. Further, there is the thermal column, but so far this has only occasionally been used for physical research. Most of the physical activities directly dealing with neutrons will be mentioned in the following.

Great emphasis is made upon neutron diffraction work, which at present is carried out with three different goniometers. The simplest one having its crystal sample irradiated by a "white" neutron beam was first used as a monochromator in the study of resonances, such as the 0.096 ev resonance in Sm.[8] Later, the temperature dependence of Bragg scattering has been particularly investigated. It has been shown that the magnetic scattering depends upon the temperature in the same way as the magnetization does, thus it disappears at the Curie point.[9] A detailed study of the "diffuse peaks" originating from magnetic inelastic scattering is being done. The cross section for this inelastic scattering has been determined, and shows a strong maximum at the Curie point.

The other two goniometers are solely applied to structural analysis, one of them being completely automatic in operation. The specimens studied on these goniometers are irradiated with monoenergetic neutrons from crystal monochromators. Among the studies made are:

The establishment of the CuH-structure by combined X-ray and neutron diffraction work, in which the hydrogen positions were determined by the study of CuD,[10] and also the verification of the short distance 2.53Å between the Al-atoms in Al_2Th.[11] A search for the reported anomalies in the scattered X-ray intensities from LiF, which were not found, indicating that the anomalies must be due to asymmetry of the electron clouds.[12] An investigation of the magnetic structure of pyrrhotite with Ni As-configuration.[12] At present combined X-ray and neutron diffraction work is done on single crystals of $Ca(H_2PO_2)_2$. By neutron diffraction the hydrogen positions of hexamethylene-tetramine and the oxygen positions of uranium-oxides are looked for.

Monochromatic neutrons scattered from a crystal were also applied to a measurement of the fission cross section of U^{235} up to 0.40 ev. A resonance at 0.28 ev was found.[13,14]

For low energy neutron work a mechanical monochromator has been built, consisting of a collimator and a steel rotor with 14 helical slits on a 9 m pitch helix.[15] The maximum angular velocity of 9000 rpm corresponds to 1350 m/sec for the neutrons. Some measurements of the Eu cross section were made with this instrument. A fast chopper, giving neutron pulses of 2 sec width at half maximum at a rotational speed of 12,000 rpm, is now ready for installation. The flight path and the detecting system are being prepared.

A method for the determination of fast neutron fluxes by the activities induced by threshold reactions has been established. Absolute neutron fluxes in the JEEP were determined by absolute counting of the induced beta-activity with a scintillation counter.[16]

The circular polarization of gamma-rays following polarized neutron capture is being investigated by measurement of the Compton scattering of the gamma-rays in magnetized iron. A few nuclear spin values have been determined in this way.[17]

ISOTOPE PRODUCTION AND RESEARCH

When the plans for the Kjeller reactor and its connected laboratories were drawn up, some provisional facilities for the preparation of radioactive isotopes were also included. It was felt at that time that a domestic production of radioactive isotopes might initiate and encourage the domestic use of isotopes. The experience of the past three years has shown that this idea was right. A number of interesting isotope applications could not have been carried out without a domestic isotope production. In addition, close cooperation between the research worker using the isotopes and the isotope production centre has in many cases proved essential for a positive result of the isotope investigations. This latter point seems to be of great importance for the smaller countries where relatively few scientists are familiar with the special techniques required in isotope applications and therefore need to discuss their intended methods, the specifications of the isotopes, safety precautions, etc.

As mentioned earlier, the JEEP became critical in July 1951. This did not mean, however, the immediate possibility of an effective isotope production. Because of desirable changes in the top shielding the reactor was shut down for about half a year after it had first started. Then followed the running-in period during which routine production of radioisotopes was impossible.

From January 1953 there has been a normal reactor operation and more than 1000 isotope shipments have since then been despatched from Kjeller to customers outside the institute. The rate of isotope shipments has been doubling every year. An important part of the shipments consisted of irradiated, non-processed material which was separated and distributed both in Europe and overseas by the pharmaceutical firm N. V. Philips-Roxane, Amsterdam. The direct shipments from Kjeller were mostly for the Scandinavian countries. Most current "carrier free" pile isotopes are being or will shortly be produced at Kjeller. As mentioned, the general devices for irradiating targets have until now been rather provisional. Three of the horizontal experimental channels have been reserved for isotope production making possible the simultaneous irradiation of about 60 standard cans, each enclosed in a 20 cm long graphite cylinder. In addition a vertical channel has been inserted in one of the vacant fuel rod positions and used for long time irradiations. At present the whole system is being reconsidered. In the future only vertical channels will be used for routine irradiations, because of the usefulness of the horizontal channels for research purposes. The isotope cans will be held in position by means of a long vertical aluminium stringer which can be moved to a desired position to permit the loading or unloading of the stringer by means of a pneumatic system.

Closely connected with the isotope production is the consultative work carried out by our institute in order to facilitate the industrial uses of radioisotopes. A number of industrial applications performed under this program will be described at the present conference.[18] The chemical separation methods used for the production of these isotopes are partly conventional, and partly new, e.g., for the separation of I^{131} from irradiated tellurium oxide and P^{32} from irradiated sulphur.[19] Another interesting study is the production of P^{33} by irradiating large quantities of sulphur at the outside of the reflector where a large space is available and where the ratio of the rate of formation of P^{33} and P^{32} is high due to a high proportion of thermal neutrons.

Concerning the pile neutron yield of threshold reactions a systematic study has been carried out especially for the (n,α) reactions.[21] This investigation shows that the yields of most threshold reactions earlier predicted and measured for unmoderated fission neutrons by Hughes apply well also for irradiations performed in the actual irradiation channels in the reactor core. Threshold reactions requiring very high neutron energies show, however, very reduced yields compared to those obtainable with fission neutrons. This is due to an obvious depletion of the very high energy part of the fission neutron spectrum in the irradiation channels.

The JEEP has also been used for investigating unknown isotopes or isotopes for which insufficient data exist. Several new fission isotopes have been discovered by irradiating uranium compounds and transferring the targets rapidly to an adjacent chemical laboratorium by means of a simple pneumatic system mounted in one of the horizontal channels.[22] The properties of the long-lived Nb^{94} produced by neutron irradiation of niobium have also been investigated.[23]

A large number of irradiations of plant material, especially seeds of different kinds have also been carried out both in the reactor core and at the outer surface of the reflector. Both genetic and physiological effects have already been studied.[24,25] As compared to X-rays the pile neutrons have been found very efficient in producing genetic effects, and some experiments also indicate that a different spectrum of mutations is obtained. In order to control the dose measurements which to a large extent were carried out by the ferrous-ferric system, the influence of the linear ion density on the radiation yield of this system was investigated. The additivity of the effects of simultaneous action of lightly and densely ionizing radiation was demonstrated. By exposing ferrous solutions to the nuclear fragments of different nuclear reactions and also to other types of radiations of known ion density the variation of the G value (Fe^{3+}/100 ev) with ion density was established.[25]

OPERATIONAL PROGRAM AND STAFF

Up to the present time, the reactor has been operated from Monday morning to Saturday morning, in three shifts. From this summer, however, continuous operation throughout the entire week in four shifts, will be put into effect. Since the reactor is used for both physics research and isotope production, it has proved most convenient to run experiments which need low or variable power level, during the day, and to operate on a maximum power level for isotope production and for high power level experiments the rest of the time.

In conclusion it might be mentioned that obvious limitations exist when a single reactor of this type shall serve as a research tool for 30 to 40 scientists and for isotope production. The JEEP has, however, within these limitations, proved extremely useful for both purposes.

REFERENCES

1. Dahl, O., and Randers, G., *Heavy Water Reactor at Kjeller, Norway*, Nucleonics 9: 5–17, (1951).
2. Grimeland, B., and Sunde, A., *The Pile Oscillator at Kjeller*, JENER Internal Report No. 36: (1954).
3. Lundby, A., *Effect of Photoneutrons on Transfer Function of a Heavy Water Reactor*, J. Nuclear Energy, 1: 53, (1954). JENER Report 33: (1954).
4. Lundby, A., *Temperature Measurements in JEEP*, JENER Report No. 32: (1954).
5. Eriksen, V. O., and Schmid, H., *Measurements of the Effective Resonance Integral of Uranium with the Pile-Oscillator*, Paper to be presented at this conference.
6. Lundby, A., and Holt, N., *Kinetic Behaviour of a Thermal Heavy Water Reactor*, Nucleonics 12: 22-5 (1954).
7. Eriksen, V. O. and Hälg, W., *Xe^{135} Poisoning of the JEEP*, JENER Report No. 17: (1953).
8. McReynolds, A. W., and Andersen, E., *Thermal Neutron Resonance of Sm*, Phys. Rev. 93: 195 (1954).
9. McReynolds, A. W. and Riste, T., *Magnetic Neutron Diffraction from Fe_3O_4*, Phys. Rev. 95: 1161 (1954).
10. Goedkoop, J. A., and Andresen, A. F., *The Crystal Structure of CuH*, Acta Cryst. 8: 118 (1955).
11. Andresen, A. F. and Goedkoop, A. J., *Neutron Diffraction Study of Al_2Th*, Acta Cryst. 8: 118 (1955).
12. Andresen, A. F., *Nyere Arbeider i Nöytrondiffraksjon på Kjeller*, Tids, skr. Kjemi, Bergv. og Met. 15: 47, (1955).
13. Popvic, D., *Energy Dependence of the U^{235} Fission Cross Section in the Low Energy Region*, J. Nuclear Energy, 1: 3, (1954).
14. Popvic, D., and Raisic, N., *Energy Dependence of the U^{235} Fission Cross Section*, J. Nuclear Energy, 1: 170, (1954).
15. Holt, N., *Mechanical Neutron Monochromator*, JENER Publication No. 7: 169 (1953).
16. Grimeland, B., *Absolute Measurements of Neutron Densities in the JEEP*, JENER Report No. 20.
    Grimeland, B., *Measurements of Fast Neutron Flux in the Centre of JEEP*, JENER Report No. 28.
17. Trumpy, G., *Circular Polarization of Gamma Rays Following Polarized Neutron Capture*, Nature 176: (to be published).
18. Been, U., and Sæland, E., *Some Industrial Uses of Radioisotopes in Norway*, Paper to be presented at this Conference.
19. Samsahl, K., and Taugböl, K., *Separation of Carrier-free Isotopes by Diffusion Methods*, paper to be presented at this Conference.
20. Westermark, T., *Production of P^{33} with Thermal Neutrons*, Phys. Rev. 88: 573 (1952).
21. Sæland, E., Lykaas, M., and Samsahl, K., *(n,α) –Yields for Pile Neutrons in Elements of Medium and High Atomic Number I.* JENER Report No. 23: (1954).
    Sæland, E., and Samsahl, K., *(n,α)— Yields for Pile Neutrons in Elements of Medium and High Atomic Number II*, JENER Report No. 27: (1955).
22. Pappas, A. C., *et al.* To be published.
23. Rollier, M., and Sæland, E., *Half-life and Beta Decay of the Long Lived Niobium-94*, Phys. Rev. 94: 1079 (1954). Act. Chem. Scand., 9: 57 (1955).
24. Ehrenberg, L., and Sæland, E., *Effects of Pile Radiation on Barley Seeds*, J. Nuclear Energy, 1: 150 (1954).
25. Mikaelsen, K., and Halvorsen, H., *Experiments on Respiration in Barley Seeds treated with Neutrons from an Atomic Pile*, Physiol. Plant., 8: (1955) in print.
26. Sæland, E., and Ehrenberg, L., *A Differential Dosimetry of Pile Radiations Using Fe^{2+} Oxidation*, Act. Chem. Scand., 6: 1133, (1952).
    Ehrenberg, L., and Sæland, E., *Chemical Dosimetry of Radiations giving Different Ion Densities. An Experimental Determination of G Values for Fe^{2+} Oxidation*, JENER Publication No. 8: (1954).

Experience with B.E.P.O.

By R. F. Jackson,* UK

DESCRIPTION

It is the purpose of this paper to discuss the development of experimental usage of B.E.P.O. from the date of its initial divergence in July, 1948, to the present day. It will be remembered the B.E.P.O. (the Harwell Pile) is a medium power graphite moderated experimental reactor containing 40 tonnes of uranium rods 0.9-in. in diameter on a 7¼-in. lattice pitch, the reacting core being 20-ft dia. × 20-ft long. The reactor is air cooled and normally runs at 6 Mw heat output corresponding to a central thermal flux in the graphite of $\sim 1.4 \times 10^{12}$ n/cm^2/sec. On the top face of the reactor are 22 vertical experimental holes 4 in. in diameter, 16 of which enter through a top thermal column, while on the side experimental face are 40 holes of which 23 penetrate to the opposite or control face, thus providing alternative experimental facilities, and a further proportion enter via the large side thermal column. There are in addition a limited number of large holes either 7¼-in. or 14½-in. square which extend to or below the reactor core. The unloading of the uranium charge is by a "dry" method and thus both the load and unload faces of the reactor have plugged holes corresponding to each core channel. The access thus provided to each end of the core has not only proved most valuable operationally but has allowed considerable use to be made of core channels for experimental purposes.

EXPERIMENTAL USAGE

A current analysis of the experimental utilisation of the 95 primary experimental holes is given below:

(*a*) 63 holes are in use: 12 for neutron beam experiments, 19 for isotope production, 9 for physics experiments, 9 for chemistry experiments, 6 for materials testing experiments, and 8 miscellaneous.

(*b*) 16 holes are obscured by the equipment in use on adjacent holes.

(*c*) 16 holes are currently available for use.

It will be seen that the utilisation of this considerable number of holes is very high, the small number of holes not in use generally reflecting their poor flux position or relative inaccessibility. Of the 22 vertical holes all are in constant use.

Experiments involving neutron beams such as neutron spectrometers, chopper monochromators, etc., are generally characterized by the bulk of the apparatus required external to the reactor and by problems of scattered radiation from the beam both as a health hazard and in respect of instrument background. The neutron source may variously be required from a position in the thermal column or from within the core, graphite blocks being suitably positioned in the hole. A neutron collimator usually occupies the last 3 or 4 feet of the hole and can with great advantage incorporate a neutron shutter. This enables adjustments to be made safely to the apparatus, eliminates unnecessary scattered radiation when the apparatus is not required and, not least important in a crowded experimental area, allows each beam in turn to be eliminated to find the culprit of a current radiation background! Some success is being obtained from a very simple water shutter for this purpose, the collimater section being flooded or emptied at will by a small reservoir bottle. The large size of the B.E.P.O. core has allowed this type of experiment to proceed at three levels on the experimental face—in the basement laboratory, at ground floor level and from cantilever platforms from the reactor face. Utilisation in depth has been obtained by bringing a beam away from the reactor face in an evacuated tube to a less congested floor area.

As B.E.P.O. provides the bulk of the radioactive isotope production of the United Kingdom these facilities occupy an important part in the programme. The large requirement for P^{32} and I^{131} is met by the irradiation of kilogram quantities of sulphur and tellurium in 3 of the vertical experimental holes in 3-in. dia. × 12-in. long containers; these are unloaded at weekly or fortnightly intervals during a reactor shut down. The greater proportion of the isotope production in B.E.P.O. is however for the irradiation of individual samples loaded into the standard 1-in. dia. × 3-in. long isotope can. As many as 500 samples may be in the reactor at one time and the great diversity of irradiation time or dosage and the considerable accuracy with which these are required has necessitated methods for loading and unloading these samples while the reactor remains at full power. This has been achieved by installing a 4-in. square horizontal experimental hole an irradiation "belt" comprising a continuous assembly of graphite blocks secured to a series of magnesium alloy link plates. A proportion of the graphite blocks have a cavity to contain an isotope can and the whole belt assembly is operated from a shielded mechanism at the face of the reactor and thus allowing samples to be inserted and withdrawn from the core at will. Six of these devices are now installed with a capacity of over 1000 samples. Requests for special irradiation conditions such as pure thermal flux, high fast flux, low temperature or for special objects such as piston rings are catered for as they arise. During the early operation of the reactor some 200 of the reflector lattice positions immediately surrounding the core were used for the irradiation of large quantities of KCl HNO_3 etc., for sulphur-35 and carbon-14 production. An interesting current application is the irradiation in an empty lattice position of some 14 kg of antimony in the form of 12-in. long cans. These, after some six months irradiation, are withdrawn and used in conjunction with hollow beryllium cylinders to produce a neutron source of some 10^{10} n/sec for a series of exponential experiments which had previously been conducted over a beam hole on the top face of the pile where the size of the apparatus and scattered radiation constituted a serious problem to other experimental usage on the top face. The neutron source so produced is built into a concrete plinth and can be turned off and on at will by removal or insertion of the Sb cans relative to the Be tubes. An alternative set of Sb cans is meanwhile being re-irradiated.

---

* Atomic Energy Research Establishment, Harwell.

The vertical 4-in. diameter experimental holes which extend down to the reactor centre line have proved invaluable for the type of chemistry and metallurgy experiment where repetitive use is to be made of an experimental assembly perhaps with glass and electrical connections to external apparatus. The apparatus can be assembled and tested externally in the vertical position (a series of working platforms at 8 ft. intervals are available at one end of the reactor for this purpose), it can then be transferred to the pile by means of the overhead crane without fear of stressing the assembly and, after irradiation, the remote control afforded by the use of the overhead crane in removing the assembly from the reactor and transferring it to a vertical mortuary hole allows several curies of activity to be handled without recourse to lead transfer vessels. These experiments are invariably designed to suit a standard 3¾ in. od aluminium guard tube and top plug assembly, the paraffin wax-borax-lead shot filling of the top plug allowing complete flexibility of the arrangement of pipes and leads passing through it. This coupled with some standardisation of the thermostatting arrangements has allowed wide use and re-use of the same apparatus with only minor modifications. Here again a limiting feature to the use of the vertical holes can be the bulk of the external apparatus associated for instance, with chemistry type experiments involving sampling or circulating techniques.

A useful facility which is being gradually extended is that of the pneumatically operated sample tube or "rabbit." In B.E.P.O. we have standardised on a 1½-in. bore tube in which is transmitted a cigar shaped sample carrier 1$^{15}/_{32}$-in. max. diameter made of moulded bakelite with chopped nylon filler, this material having the most satisfactory strength-temperature-activity characteristics of any yet tried. The cap of the carrier is secured by a three start moulded thread (for quick release) and the carrier is blown in the requisite direction by compressed air to give an average velocity of 25–30 ft/sec. The air vented from the system is discharged to the reactor or a suitable duct. One such device serves the reactor floor for general use, two travel some 100 feet to an adjacent hot chemistry laboratory while the fourth makes a 200-yard circuit to another building. A new circuit of 500 yards is now under construction and a run of ¾ mile is under active consideration.

There are two 7¼-in. square experimental holes which run the full length of the reactor parallel with the uranium channels and in substitution of two of them near the core axis. In one of these holes, both of which enjoy full air cooling, there is currently a 10-ft. length of air cooled hollow slugs of inner and outer uranium diameters of approx. 2⅝ in. and 3¼ in., the slugs being in 1 foot lengths canned in aluminium with longitudinal finning 5¼ in. in diameter. This considerable volume of fast flux (fast/thermal ratio approx. 4 times that in the lattice) is accessible from both ends of the reactor thus allowing two separate simultaneous uses. Vertical water cooled hollow slugs are available for use in top experimental holes, for instance one is used in connection with a liquid nitrogen cooled irradiation facility, and small hollow slugs 1¼-in. od × ⅝-in. id have from time to time been used in uranium channels.

The growing importance of the engineering scale loop experiment is illustrated in B.E.P.O. so far by three examples. A sodium loop was operated successfully for a year in a horizontal experimental hole, the second of the 7¼-in. square experimental holes on the core axis is currently occupied by a 48-ft. length of 6 in. dia × 14 s.w.g. stainless steel tube in which a gas cooled loop is being operated at the appropriate conditions of temperature and pressure and two further uranium channels have been replaced by a pressure water circuit. Again the space occupied by the external pumps, heat exchangers, shielding and control panels for loop experiments becomes a major problem, and as the operation of the reactor now becomes dependent upon the correct operation of the loop the integration of the loop control and safety circuits with those of the reactor becomes most important.

OPERATION

B.E.P.O. is one of the larger responsibilities of a Reactor Operations Group responsible for operating, maintaining and providing a close support design and workshop service to the Harwell research reactors. B.E.P.O., therefore, rates a full time operations engineer who is responsible in detail for the allocation and safe usage of the experimental facilities and for the operating programme. He is also responsible for all aspects of the operation such as uranium metal, operating methods and levels, technical records and operating staff. He has a shift staff of one engineer and two industrials per shift and a small daywork staff for active handling and housekeeping. The maintenance of B.E.P.O. is done to his operational requirements by a small section technically responsible to the Group maintenance engineer. A service of engineering design assistance to experimentalists is provided by a design engineer of equivalent status to the operations engineer. While a small B.E.P.O. safety committee exists for the purpose of reviewing the general safety principles involved in current experimental equipment and usage, the actual responsibility for the reactor safety must rest with the operations engineer. He is instructed to seek and obtain the second opinion of the design engineer in appropriate circumstances. The policy of operation of B.E.P.O. for the past 7 years has been to use the position of the shift engineer as a training ground in reactor engineering for young mechanical or electrical engineers (already with full professional qualifications) prior to their becoming available for more responsible positions in reactor operation, maintenance, design or research. Two years on the operating shift of an experimental reactor allows an engineer to acquire the "feel" of reactor kinetics and of problems of activity and shielding as well as giving him the opportunity of seeing and assisting in the application of a wide range of physics and engineering principles to reactor problems. This point of training is emphasized because the operation and design engineers are in a position to contribute materially to the experimental utilisation of the reactor by relating previous physics and engineering experience of the reactor to new circumstances or experimental requirements. They in fact represent the common stock of knowledge and experience in using that reactor.

While the general policy of operation is determined by an Establishment Management Committee the detailed weekly programme is worked out by the operations engineer at a weekly meeting at which reactor users stake their claims. During the early operation of the reactor, subject to guaranteeing a minimum pattern of operation to Isotope production, the small number and relative simplicity of experiments in progress resulted in a programme of frequent periods of shut down and lower power operation during the week to suit special requirements. This culminated in the standard weekly shut down from approximately 6 am to 6 pm on Monday to allow isotope handling, maintenance and rearrangement of experimental facilities. However, the increasing number of experiments which demanded steady maximum power, such as those involving counting or chemical rates of reaction, has resulted in a gradual change in programme so that between the weekly Monday shut downs a change of power has now become the exception rather than the rule. This has required changes in design and technique on the part of most pile users to make them as independent as possible of reactor shut downs for effecting experimental changes. The water shutters and belt irradiation stringers mentioned above are typical of this trend. We are at present looking ahead to a pattern of operation at which fortnightly or monthly shut downs only may occur, though with a reactor as convenient to use as B.E.P.O. and containing as many experimental facilities we are also very aware of the desirability of leaving the reactor programme open to the "little man" with the simple experiment or the man who has a new idea which he wishes to try quickly as well as operating to the advantage of the well organised major user.

Flux distributions through the core have been measured by search boron thermocouples in several radial and longitudinal positions with the reactor at power. These, carried out from time to time, indicate that remote from heavy absorbers, especially the control rods, flux distributions remain symmetrical and in good agreement with calculation. The central zone of the reactor is, however, heavily influenced by the control rods which, entering from the control face, may result in the horizontal centre of flux being displaced some 3 feet towards the experimental face with deviation from symmetry of up to ±30 per cent in flux on the central diameter. While the operations engineer can usually quote fluxes at a point to ±10 per cent and will measure them on demand, all experimentalists to whom flux or integrated dose is important take steps to monitor these individually. Flux distribution in the thermal columns, ion chamber holes, etc., have been plotted by indium foils at low power and an alternative standard method of measuring flux at high power is by observation of the β activity in small silica rods.

Proper reactivity control and accounting has always been regarded by the operations engineer and his shift staff as an important part of their duties. For simplicity of understanding by engineering and industrial staff alike we have always chosen to refer to the effect of a certain amount of excess reactivity in terms of the time for the power to double in magnitude (the doubling time) rather than the e-folding time and we have further adopted as our small unit of reactivity a millinile (or mn) equivalent to 10^{-5} in k (Harwell history relates an equivalence being drawn between the large "δ" represented by 1 per cent and the big delta of the Nile!). Over the first few years' operation of the reactor an attempt was made to follow the change of reactivity with integrated dosage resulting from the compounded effect of graphite clean up, plutonium build up and growth of samarium poison. This was attempted by a series of quarterly observations on the overall reactivity of the system making due allowance for minor changes in metal and experimental loading and adjusting all readings to standard conditions of temperature and pressure. This in turn precipitated most intensive efforts to calibrate the control rods and determine the graphite and uranium temperature coefficients and then to understand and explain the errors and difficulties encountered in these observations. Further, most careful measurements were made both by doubling time and control rod movement on the marginal change in reactivity associated with individual metal and equipment loading. In this way a detailed balance sheet was compiled at each quarterly reading from which the long term change in reactivity was deduced. Needless to say the observations, while conforming to the general form that would be expected were not of sufficient accuracy to enable any corroborative deductions to be made, for instance, of the samarium yield. They did however result in the development of a most reliable and accurate doubling time meter, in creating a reactivity accounting system and in educating the operations staff to the principles, methods and values involved. This latter aspect has probably been of greatest overall value, as an engineer can probably teach himself more about the neutron balance and kinetics of a reactor by a personally conducted experiment to calibrate a control rod followed by an attempt to relate this to his own predicted values than in any other way. Detailed observations on all reactivity changes are no longer attempted as these began to be restrictive of the very limited shut down time per week. The overall change of reactivity during a shut down is still measured and large changes of uranium loading and initial insertions of new apparatus are usually observed. In this way any major discrepancy is apparent and information on neutron economy of apparatus design is collected.

For several years the method of start up was manual, the operator raising the two banks of 12 shut off rods and then withdrawing the control rods to a position which, in view of his knowledge of the reactivity of the system, should result in a doubling time of some 10–15 seconds. Divergency was then first observed on an ionisation chamber in the range 0 1 kw and the reactor was then controlled to the required final power. Latterly however, a prototype automatic start up circuit has been in service which provides a velocity signal to the control rod drives proportional to the out of balance between the sum of a reactivity signal and a power signal to a demand power signal. This has operated without fault for two years and is being incorporated in more final form in a current control modification. To assist the measurement of reactor power under shut down and during start up conditions a self maintaining Sb-Be source has been provided. This comprises some 8 hollow beryllium cylinders ¾-in. id × 1¼-in. od × 12-in. long which contain an inner rod of antimony metal, the whole being robustly sheathed in aluminium. These tubes placed in 2 empty uranium channels at a mean flux position provide at equilibrium a neutron source strength of 5×10^8 n/sec thus effectively multiplying the spontaneous fission rate × 1000 and resulting in a shut down reactor power at $k = 0.98$ of approx. 0.5 watts. This can be observed by an ionisation chamber of low induced β-γ activity permanently situated in the thermal column.

From the aspect of operational safety B.E.P.O. is clearly a docile reactor. The maximum metal rating of less than 0.5 Mw/tonne results in a maximum uncooled rate of temperature rise of 2.5°C/sec and allows considerable time delay before serious metal temperatures result from excessive power. The failure of the suction cooling system results in a rise in atmospheric pressure in the reactor hence in an increase in the nitrogen absorbtion effect with loss of reactivity. In an experiment all cooling fans can be stopped instantly with the reactor at full power without serious temperature overshoot before restabilisation at reduced power. The maximum reactivity of the full core is ~1.4 per cent but rarely is more available than the 0.7–0.8 per cent required to satisfy the xenon and temperature effects.

The initial design of the reactor included an ingenious but complicated apparatus for the semi-automatic loading and simultaneous unloading of the uranium channels, new cartridges being inserted at one end as the active cartridges were discharged into a lead shielded magazine at the other face. This mechanism was never used operationally but was superceded by the simpler approach of manual discharge, using a flexible push rod, followed by visual observation of an empty channel and re-charge as required. While appearing unambitious, this simple approach, preferring the visual and manual sensibilities of the operator to a pre-ordained automatic sequence, has proved preferable in almost every application about the reactor. This is probably due to the frequency with which the unexpected happens in an experimental reactor and the greatly increased difficulty with which an "automatic" may be repaired if it contains within it an active component. B.E.P.O. has sponsored the development of most valuable X-ray techniques for the examination of unirradiated and irradiated fuel elements and also of a variety of instruments for the detection of activity in the effluent air stream and particularly for the unique detection of the fission products resulting from exposed uranium within the core. The scanning system now in use allows the air from every channel to be sampled individually for fission products once in 4 hours, and results in detection of cartridge sheath failures before these become visible to normal inspection. Before this system was installed one early failure remained unlocated for 48 hours and resulted in contamination of the channel from uranium oxide to an extent which so far prevents its further use for uranium loading.

The cooling air is drawn through both inlet and outlet filters with a stopping power down to some 5μ. These outlet filters are easily handled by operators in face masks and protective clothing. It is interesting to note that the outlet air duct from the face of the pile to the outlet filters is still quite accessible under shut down conditions, radiation levels being generally below tolerance except in sight of the pile structure, while the ducts and fans on the downstream side of the filters have scarcely risen above background level.

CONCLUSION

B.E.P.O. provided a very large volume of experimental flux coupled with extreme simplicity of use and lack of stringent safety requirements in respect of design and compatibility of experiments. It proved most adaptable and is an excellent training ground for engineering and experimental staff alike. Other experimental reactors will provide higher fluxes, but reactors like B.E.P.O. will continue to perform valuable functions for many years.

Materials Testing Reactor Experimental Program and Reactor Operation

By R. L. Doan* and J. R. Huffman,† USA

DESCRIPTION

The Materials Testing Reactor is a water-cooled, enriched-uranium thermal neutron reactor designed for the purpose of testing materials in high neutron fields. The fuel is in the form of approximately 3-in. × 24-in. plates of aluminum-clad uranium alloy which are assembled in groups of 18 to 19 plates with cooling spaces between them to form the fuel assemblies. Figures 1 and 2 show the cross section and the overall form of a fuel assembly. Water flowing through the interstices serves as both coolant and moderator.

The fuel assemblies can be loaded in any desired lattice configuration up to a 5 × 9 array. In practice not all of these lattice positions are occupied by fuel assemblies. Generally, a 3 × 9 array (a thin rectangular slab) has been chosen since it gives a virgin neutron flux in the three adjacent experimental beam holes. A 5 × 5 array, geometrically centered in the reactor, while giving a higher reactivity for a given uranium content, provides fewer beam holes having such high fast flux.

In the unused lattice positions and surrounding the lattice region, beryllium is placed as a reflector. These parts of the reactor are situated in an aluminum tank 54 in. in diameter. This tank is part of a well in the reactor structure through which water for cooling both the fuel and the reflector flows at a rate of 20,000 gpm to remove the 30,000 kw of heat produced by the reactor. Outside the tank there are a secondary reflector of graphite, an iron thermal shield, and a biological concrete shield, the outer dimensions of the whole forming essentially a cube approximately 34 feet on a side. The structure outside the tank is cooled by 1,700 pounds per minute of air which is pulled through the structure by compressors and discharged up a 250-ft stack.

The cooling water system consists of a seal tank, vacuum spray evaporators, a sump tank, pumps, and a high head tank. From this high tank the water is recirculated through flowmeters to the reactor tank. Heat is removed from this primary cooling system by another water stream which passes through the condensers in the spray evaporators to a forced-air-draft cooling tower.

To permit full use of the Materials Testing Reactor a large number of experimental openings have been provided. Spare positions in the lattice or positions in the beryllium reflector are available for experiments not requiring space larger than 3 × 3 × 36 in. About 17 beam holes penetrate the reactor structure radially to the reactor tank, some of them to the long sides of the lattice section. About 100 holes penetrate into the graphite region. Two pneumatic shuttle holes run beside the narrow side of the lattice section and four hydraulic shuttle holes run vertically adjacent to the lattice.

The control elements of the reactor are of three types: the fuel-cadmium shim rods, the beryllium-cadmium shim rods, and the regulating rods. The fuel-cadmium shim rods are so constructed that when fully raised to their upper limits, a section containing fuel in substantially the same form as the fuel assemblies resides in the core. When these shim rods are released by magnetic clutches, attached to the actuating members suspended from the reactor top plug, the rods fall to a lower position bringing their cadmium section into the fuel core. The beryllium-cadmium shim rods are similar to the fuel-cadmium shim rods except that in place of fuel there is a beryllium section which becomes a part of the reflector when these rods are raised. Bearings for all shim rods are located so that eight positions of the lattice may be occupied by either type of shim rod. Outside the lattice there are four positions into which the third type of control element, the regulating rod, may be fitted. These rods contain a cadmium section, but because of their size and location they exert a relatively small effect (<0.75 per cent $\Delta k/k$) on the reactivity. The regulating rods are actuated by motors on the reactor top plug and are subject to the commands of a servomechanism.

There are two separate servo channels, each associated with a regulating rod. Either channel may be used, the other acting as standby. The fine control of the reactor is accomplished with the regulating rod; the coarse control by means of the shim rods. Position indicators for the shim rods have been provided which read zero when the rods are fully inserted, and 30 inches when the rods are at the upper limit positions. The corresponding values for the regulating rods are zero and 22 inches.

A more detailed engineering description of the

---

* Manager, Phillips Petroleum Company, Atomic Energy Division, Idaho Falls, Idaho.

† Assistant Manager, Phillips Petroleum Company, Atomic Energy Division, Idaho Falls, Idaho.

MTR has been published elsewhere.[1] Figures 3, 4 and 8 serve to clarify the brief description given here.

OPERATION

Startup

The unique features of the MTR are thin-plate fuel assemblies, slab geometry, high specific power, and high excess reactivity. It is the first reactor having these features which has been operated above the flux range of 10^{14} thermal neutrons per square centimeter per second. Considerable care was therefore taken in bringing the reactor to criticality and to full power operation.

Criticality was attained on March 31, 1952 with 11 fuel assemblies and the contributions from part of the fuel in two shim rods. The assemblies contained 140 grams U^{235} and the shim rods 110 grams. They were loaded in the northeast corner of the lattice, the remaining lattice positions being filled with beryllium pieces or dummy fuel assemblies. With due precautions the full slab loading in a 3 × 9 array was attained and calibrations of all instruments and control rods were determined. The reactor power was increased in short steps from 1 Mw to 30 Mw with constant observation of the temperature rises in the water flowing through each fuel assembly. Full design power was reached on May 22, 1952. The MTR has been operating ever since with essentially no major shutdowns other than those required for reloading fuel and changing experiments.

From studies during the startup and early operation periods, several interesting characteristics of the reactor were observed. When a freshly loaded 3 × 9 core (140-gram assemblies) is first brought to power, the four fuel-cadmium shim rods, located in the center row, are only withdrawn 16½ inches of their full 30-in. travel. Flux mapping by means of cobalt wires indicated that the lower half of the reactor was carrying most of the load. As the reactor operated, the shim rods were gradually withdrawn and the vertical flux pattern gradually approached the cosine distribution normally expected. Several flux maps of the core were taken at various positions of the shim rods as the reactor burned fuel. Figure 5 shows three of these for the central fuel position (2-5) and for a corner position (1-1) in the 3 × 9 array. Since the MTR is designed to operate without exceeding the boiling point of water in the lattice (~250°F) the power levels of operation are restricted by the unusual peaking of neutron flux since the maximum-to-average plate temperatures are higher than for the normal cosine distribution.

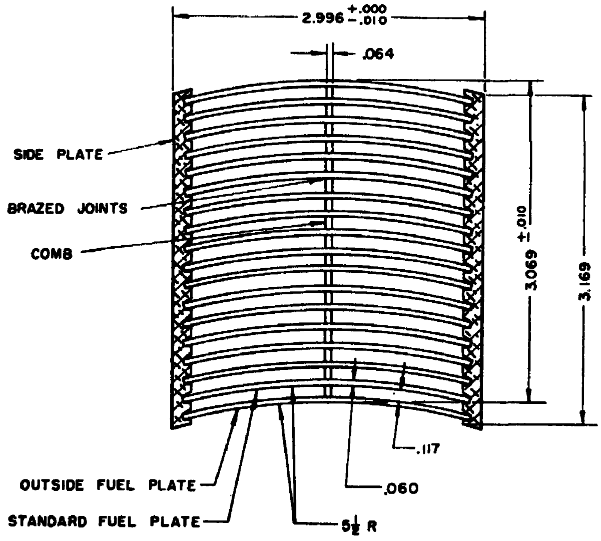

Figure 1. MTR cross section of fuel assembly

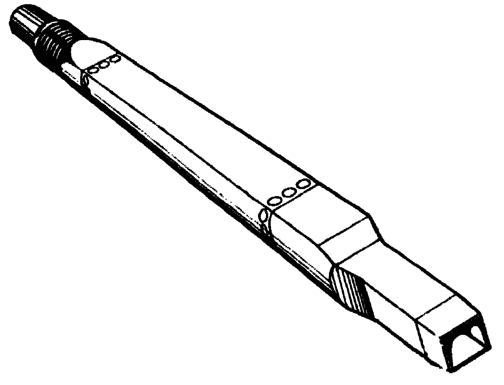

Figure 2. MTR fuel assembly

For a small heterogeneous reactor like the MTR, the relative value of each fuel assembly is difficult to calculate. The statistical weight of each fuel position was therefore determined experimentally by inserting poisons in the form of iron wires and measuring their effects on the reactivity. Similarly, a weighting of each position was obtained by measuring the heat output of each assembly. Figure 6 gives these results. At the time these data were taken there was an experimental opening in the reflector on the east side of the lattice, thus accounting for the low values on that side.

As indicated by the statistical weight and as verified experimentally, the center two fuel shim rods are twice as effective as the outer two rods.

Operating Cycles

When the MTR first started power operation in May 1952, 23 fuel assemblies and four fuel shim rods were loaded in a 3 × 9 configuration. The fuel assemblies contained 140 grams U^{235} each and the shim rods contained 110 grams U^{235} each, giving a reactor active mass of 3660 grams U^{235}. This loading (Charge 1) was operated at power until it shut down because of reactivity losses due to fuel depletion and buildup of fission product poisons (this is called a burn-out cycle). The total energy produced by Charge 1 was 376 Mwd (megawatt days), roughly equivalent to 12½ days at full power. The average fuel burnup was approximately 13 per cent.

The type of loading used for Charge 1 was continued for several subsequent cycles, but as the reactivity of the reactor was reduced by the increasing load of experiments, it became apparent that more reactivity was desirable. The fuel contents of the fuel assemblies and shim rods were increased 20 per cent to 168 grams

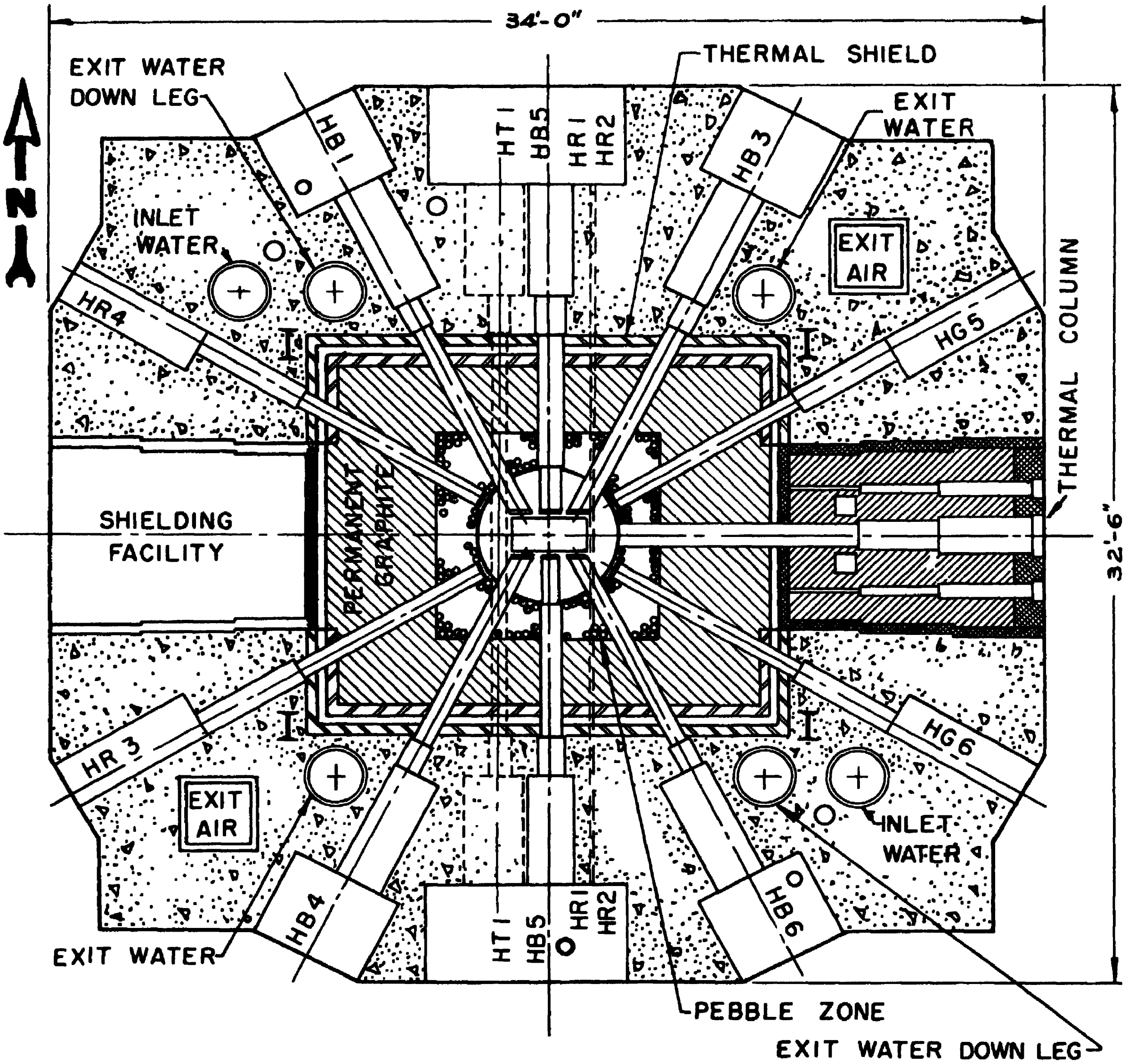

Figure 3. MTR horizontal section

and 132 grams, respectively. These fuel units produced a total energy of about 740 Mwd when loaded in a 3 × 9 core and operated in a burnout cycle. The average fuel burnup in these assemblies was about 21 per cent. This greatly reduced the number of new fuel assemblies required per month and consequently reduced the number of used assemblies that had to be chemically processed to recover the remaining U^{235}.

It also became apparent during the early phases of MTR operation that it was economically unwise to change shim rods every cycle because the cost of a shim rod was about ten times that of a fuel assembly. Therefore, starting with Charge 3, shim rods were used for two cycles each while fuel assemblies were used for only one cycle. In general, only two shim rods were changed each cycle. In order to take advantage of the higher statistical weights of the inner shim rod positions, the shim rods were placed in the 2-4 and 2-6 lattice positions for their first cycle in the reactor and in 2-2 and 2-8 positions for their second cycle. Since then the number of cycles shim rods are used has greatly increased, some having been in the reactor for as much as 5500 Mwd of operation. This operational procedure results in slightly less fuel burnup in fuel assemblies and shorter burn-out cycles, but is more economical.

A small increase in reactivity of the MTR with resultant increase in total energy per cycle was accomplished by reducing the thickness of the fuel assembly side plates from $\frac{3}{16}$ in. to $\frac{1}{8}$ in. The corresponding change in the aluminum-water ratio was 0.732 to 0.664.

In the burn-out cycles, which were used through Charge 14, the reactor was run at 30 Mw until it died a natural death, i.e., until no excess reactivity remained. This occasionally resulted in reactor shutdowns at inopportune times such as week ends or holidays. The lack of scheduled shutdown time became

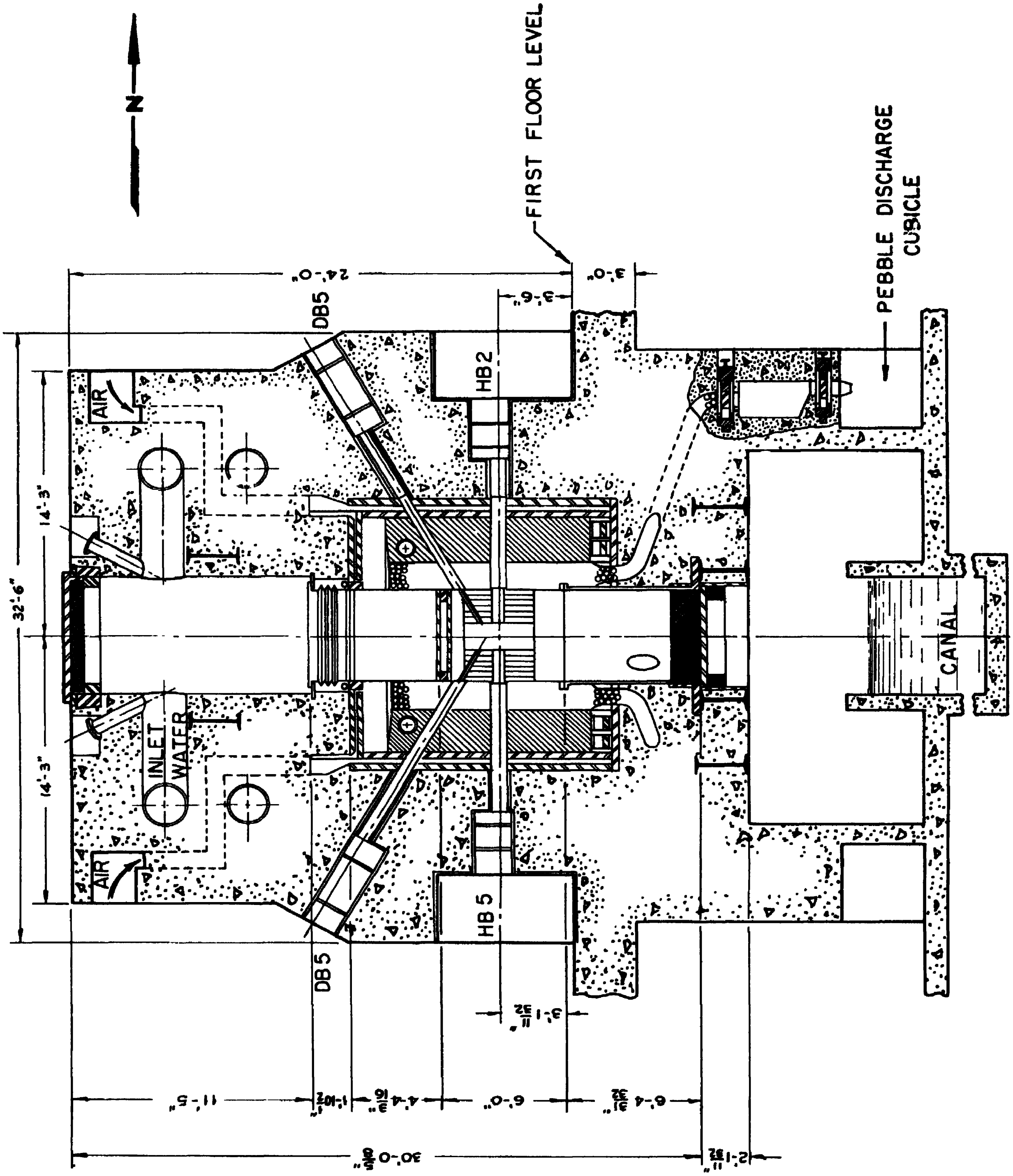

Figure 4. MTR north-south vertical section

more and more troublesome as the load of experiments and special maintenance work during shutdowns increased. This problem, and the fact that fuel burnup in the end positions of the 3 × 9 core was only half that at the core center, led to the adoption of the two-week cycle in June 1953. The two-week cycle involved a regularly scheduled shutdown every other Monday.

Use of the 168-gram fuel assemblies in a burn-out cycle had produced continuous power operation for about 23 days while with the two-week cycle only 12 days operation (two days shutdown) was desired. Thus only a partial loading of new fuel was required for each cycle and each fuel assembly was used for two or three two-week cycles. By starting the new assemblies in the high neutron flux (also high statistical weight) positions for succeeding cycles it was possible to eliminate largely the problem of uneven burnout and at the same time obtain maximum reactivity from a given loading. These procedures coupled with careful calculation of the fuel requirements for each cycle resulted in substantially higher average fuel burnups per assembly and associated economy. In 11 two-week cycles (Charges 12–25), in which shim rods were used about five cycles each, an average of about nine fuel assemblies were added each cycle. The average fuel burnup for these assemblies was about 31 per cent.

Although the two-week cycle was satisfactory in that it provided regularly scheduled shutdowns, the frequency of these shutdowns resulted in overloads of work. In the interest of obtaining a three-week cycle coupled with economical use of fuel, i.e., high burnup percentages, a 5 × 6 loading was tried for several three-week cycles. However, these loadings were not acceptable to the experimenters because of the reduced neutron flux in several of the larger irradiation facilities, principally the through hole (HT-1) and the three beam holes on the north side of the reactor. Therefore, the reactor was again loaded in the 3 × 9 core which provided the maximum flux "peaking" in the most useful experimental holes.

The number of experiments either loaded into the reactor or discharged, as well as the complexity of experiments, continued to increase. As a result of this the length of each shutdown became an appreciable part of the two-week cycle. Shutdowns of three to four days were not uncommon. In order to attain an economical three-week cycle the fuel content of the assemblies was increased to 200 grams of U^{235} each in May 1954. The reactor has been operating with a three-week cycle and a 3 × 9 loading since that time. A determination of average percentage fuel burnup per assembly has not yet been made from operating data. However, a fuel burnup per assembly of about 40 per cent is probably attained.

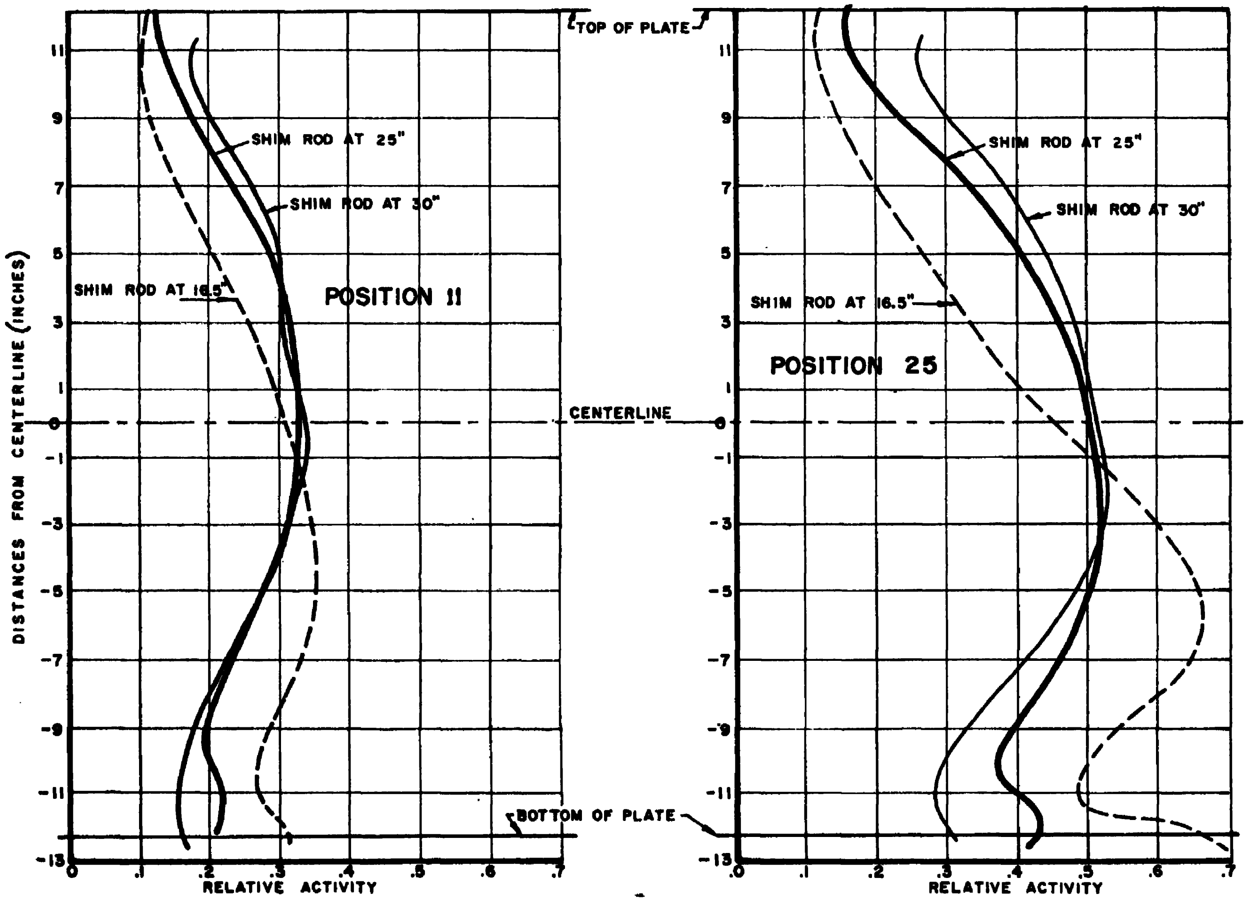

Figure 5. Vertical flux traverses in fuel assemblies

	1	2	3	4	5	6	7	8	9	
1	(.40)	(.44)	(1.04)	(1.11)	(1.05)	(.95)	(.88)	(.57)	(.38)	ϕ^2
	2.91	3.63	4.22	4.63	4.58	4.27	3.96	3.33	2.39	%
	.37	[.55]	[.73]	[.79]	.80	[.78]	[.70]	[.48]	[.27]	w
2	(.45)	(.62)	(.99)	(.92)	(1.00)	(.78)	(.73)	(.38)	(.23)	ϕ^2
	3.00	2.68	4.27	3.43	4.74	3.30	3.77	2.65	2.26	%
	[.43]	[.60]	[.78]	[.92]	1.00	[.92]	[.75]	[.52]	[.30]	w
3	(.47)	(.60)	(1.04)	(.98)	(1.02)	(.74)	(.57)	(.29)	(.19)	ϕ^2
	3.00	3.80	4.40	4.95	4.83	5.03	4.09	3.26	2.61	%
	.51	[.70]	.83	[.92]	.96	.91	.81	.57	.32	w

Figure 6. MTR statistical weights for poisons 3 × 9 lattice

Numbers in lattice position show measured relative statistical weight for that position. (W) Values in brackets were estimated from measured values. Values in parentheses were computed from temperature rise across assemblies (ϕ^2). Per cent of total power produced by each fuel assembly. (%)

The various changes in MTR operating cycles have made it possible for the MTR to better fulfill the needs of experimenters. They have also resulted in substantial economies due to reduction of the number of fuel assemblies and shim rods required per unit of power output. For example, the initial loading required approximately six fuel assemblies and one shim rod per 100 Mwd, while corresponding requirements are now about 1.5 and 0.1, respectively.

Mixed Loadings

To obtain the lowest operating costs under circumstances using mixed loadings of fuel assemblies, it is generally necessary to load the minimum number of new fuel assemblies for the specified megawatt days of operation. A method has been devised whereby this can be calculated.

For a fully depleted core which is just critical with all shim rods withdrawn, and for a given experimental load, the quantity of fuel remaining unburned has been found to be essentially a constant. Knowing the relative worth of a gram of U^{235}, the relative thermal neutron flux for each position in the lattice, and the average grams U^{235} burned up per megawatt day of operation, the quantity of new fuel required can be determined.

Figure 7 gives the relative weights for fuel and the relative fluxes for the 3 × 9 lattice positions. By trial and error methods, partially burned out fuel assemblies and new fuel assemblies are located in the 3 × 9 lattice until the proper loading is obtained. The only restriction is that new (200-gram) assemblies cannot be placed in positions where plate temperatures will exceed the boiling point of water, i.e., in positions of high flux. This restricts them to the outer positions of the lattice. If the experimental load is changed, corrections to the depleted mass of U^{235} can be made. Roughly, 100 grams U^{235} are equivalent to one per cent $\Delta k/k$.

Fission Breaks

The major activity in the process water in the initial stages of operation was due to Na^{24}. The activity two hours after leaving the reactor was: Mg^{56}, 78 dps/ml; Na^{24}, 276; long-lived, 10; and total 364 dps/ml. The Na^{23} content of the water can account for about 20 dps/ml, so that the majority of the Na^{24} activity is apparently coming from the $Al^{27}(n,\alpha)Na^{24}$ reaction, i.e., recoils from the action of the neutrons on the aluminum in the reactor. During these initial stages, the activity level near process water piping was about 50–100 milliroentgens per hour. After about one year of operation a section of piping was removed and

	1	2	3	4	5	6	7	8	9	
1	0.52	0.60	0.84	0.95	1.00	0.95	0.84	0.60	0.52	w
	0.73	0.88	0.97	1.00	1.08	1.00	0.97	0.88	0.73	ϕ
2	0.52	0.60	0.84	0.95	1.00	0.95	0.84	0.60	0.52	w
		S		S		S		S		
	0.73	0.88	0.97	1.00	1.00	1.00	0.97	0.88	0.73	ϕ
3	0.52	0.60	0.84	0.95	1.00	0.95	0.84	0.60	0.52	w
	0.73	0.88	0.97	1.00	1.08	1.00	0.97	0.88	0.73	ϕ

Figure 7. MTR statistical weights for fuel and relative fluxes 3 × 9 lattice

examined. Etching of the surface indicated that activity was "plating out" on the surface. Occasional spent fuel assemblies showed, by visual inspection under water, blemishes on the lower half of the outside concave fuel plate. No particular concern was raised since these were attributed to rubbing or scouring of the surface during handling procedures.

In the summer of 1954 the gross beta and gamma activity of the process water increased considerably and during the fall of 1954 suddenly increased to 40,000 dps/ml. Closer examination of the outside fuel plates showed a higher percentage of blemishes and disclosed some breaks through the aluminum cladding, thus permitting fission product escape into the water. These breaks and blemishes were discovered to be due to the bulging outward of the concave plates to the extent that they touched the surfaces of the fuel plates on the adjacent fuel assemblies. Thus higher temperatures existed on the aluminum surface, and possibly even melting, so that the cladding was destroyed. Pressure measurements were made to determine the differential pressures acting on the plates and it was discovered that forces existed which would cause the outer plates to bulge. Bench tests confirmed this fact. By slight adjustments in the dimensions of the lower end boxes on the fuel assemblies so that safe differential pressures were obtained, this difficulty has been eliminated. To provide a greater safety factor, the fuel plate and side plate thicknesses were also increased slightly.

The main consequence of this difficulty has been a greatly increased activity on the pipe walls of the process water system and in the MTR tank. Activities as high as three roentgens per hour were obtained at contact on the outside of tanks and pipes in the process water system, compared to 50–100 milliroentgens per hour. Activities as high as five to seven roentgens per hour were obtained inside the MTR tank where it is necessary to work in order to change a number of experiments. This activity of course died off to a great extent after the source of activity was removed from the system and normal operation was resumed; however, on a short-term basis it did create operating problems by limiting the working time in the MTR tank and the available time for maintenance of the process water system. During normal operation it causes no problems since all of the system is well shielded.

A second consequence has been the plating out of detectable quantities of U^{235} on parts of the reactor in the flux zone. This was confirmed by activation analysis on scrapings. Aluminum parts in the active zone of the reactor have an estimated amount of 6×10^{-7} grams U^{235} per square centimeter of surface. This is responsible for the present more or less constant activity level of 10,000 to 15,000 dps/ml in the process water. The burnout of this U^{235} will require considerable time but is no great problem if proper precautions are taken to flush the system for shutdown operations inside the reactor tank and for maintenance of the process water equipment.

Fission Break Monitoring

During the course of operation of the MTR, considerable experience has been gained in the reliability of fission break monitors. The high pressure ion chambers used at various spots in the water system have proven unsatisfactory. Their action is too slow to prevent contamination of the whole system and their background activity generally is too high because of dirt accumulation to permit their full sensitivity.

Considerable effort has been devoted to the development of new types of fission product monitors. A prototype of one of these types has been in operation for several months. This instrument relies upon the continuous isolation of fission product iodine activities using ion exchange resin columns. This is accomplished by passing a side stream from the water system first through a small cation column which removes virtually all activity due to cation fission products and any activity not due to fission products and, second, through an anion column upon which is collected essentially only fission product iodine, tellurium and molybdenum. The integrated activity on the anion column is viewed with a scintillation detector utilizing energy discrimination to bias out the gamma radiation due to all activities but those of 6.7-hr I^{135}. There results a device which exhibits sensitivity only to *fresh* fission product activities in the water stream, thus giving a measure of the rate of production of fission products. This offers a decided advantage in monitoring a recirculating water system since it allows the determination of recurring fuel ruptures with no interference from large quantities of long-lived fission products and other elements which may be present in the water. The device reaches equilibrium after a few hours on stream and from experience gained in the recent fission breaks indicates an improvement by a factor of several hundred in sensitivity to fission product activity.

MTR RESEARCH PROGRAM

The research program at the MTR is designed to take advantage of the unique characteristics of this reactor, principal among which are its very high neutron flux and the very high gamma intensity of its spent fuel assemblies. The major portion of the reactor program originates in laboratories external to the MTR that are carrying on research in connection with the United States Atomic Energy Commission reactor development activity, isotopes investigation or related studies. Sponsoring laboratories design and build their own equipment in consultation with the MTR project engineering organization, then send it to the MTR for installation in the reactor. Observations may sometimes be made during the course of irradiation; in other cases the irradiated specimens are returned to the sponsoring laboratories for detailed studies.

In addition to the sponsored experimental program, a substantial amount of research activity around the reactor originates with the MTR technical staff. Included in this are (1) a cross sections measurement program utilizing both a neutron fast chopper and a crystal spectrometer installed in two separate beam hole locations, (2) investigation of reactivity effects due to progressive burnup of fuel assembly components, utilizing a precision reactivity measurement facility, (3) investigation of metallurgical effects due to progressive burnup of fuel assembly components, (4) heavy isotopes studies, (5) investigation of film boiling and related effects, and (6) studies of higher order neutron reactions.

An increasing amount of research is being sponsored and paid for by private industrial concerns under the MTR commercial irradiation program. The major part of such work to date consists of gamma irradiation studies utilizing various geometrical arrays of spent fuel assemblies in which gamma intensities as high as thirty million roentgens per hour can be realized for short periods. As the fission product activity decays the available intensity decreases but even after several months the intensity still is of the order of 100,000 roentgens per hour. The supply of spent fuel assemblies is replenished at regular intervals from refueling operations in the reactor.

Effect of Irradiation on Physical Properties

As its name implies, the Materials Testing Reactor was designed primarily to serve as a facility for investigating the physical integrity of various materials and reactor components in the presence of highly intense reactor radiations. Some of this work takes the form of "before" and "after" experiments and some is in the nature of "in-pile" experiments in which certain observations are made while the specimens are in the reactor.

When fast neutrons or energetic fission fragments collide with metal nuclei, atoms are displaced from their lattice positions, resulting in changes in such physical properties as conductivity, creep rate, hardness, tensile strength, etc. The magnitude of the effect is dependent upon the integrated nvt, or number of neutrons incident on unit area of the specimen over the total exposure time. In some cases the changes brought about by fast particle bombardment can be annealed out at elevated temperatures, making it necessary for quantitative work to maintain rather close temperature control over experimental samples during the time they are exposed to reactor radiation.

Gamma rays and slow neutrons cause very little radiation damage in metals but may bring about large changes in the properties of certain organic liquids and plastics principally by ionization produced both directly and by excitation electrons. Again the effect is proportional to the total integrated dose. Beneficial effects can be produced in some instances by controlled dosages, as exemplified by the increase in strength, hardness and temperature resistance of certain plastics due to cross linking of the polymer.

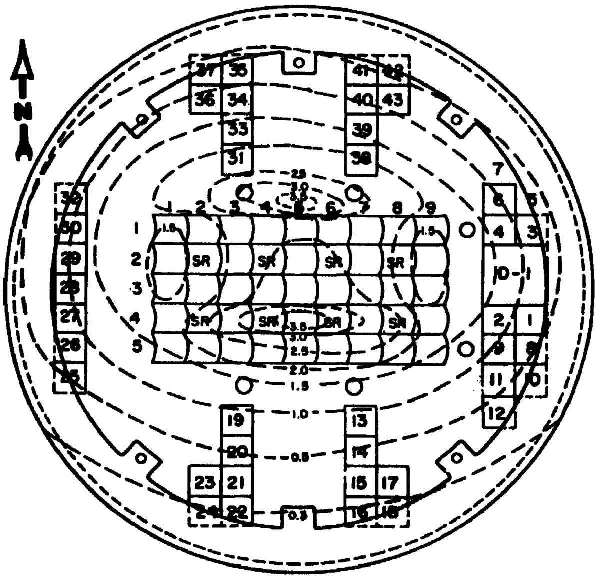

Figure 8. MTR reactor tank horizontal cross section maximum thermal flux values at midplane

The MTR makes an ideal facility for studying radiation damage since very high intensities of both fast and slow neutrons are available in a number of experimental positions in or near the reactor lattice. Fast neutron fluxes of 1 to 2 × 10^{14} and slow neutron intensities as high as 3 to 5 × 10^{14} are accessible both inside the core tank where it is necessary to leave the experimental samples throughout the fuel cycle and also through several hydraulic rabbit channels where capsules can be inserted and removed from the outside while the reactor is in operation. Several large beam holes are available in which elaborate engineered experiments can be installed for investigating radiation damage to specimens under various temperatures and pressures of coolant flow.

Figure 8 gives the thermal neutron flux values at the vertical midplane of the reactor for various positions

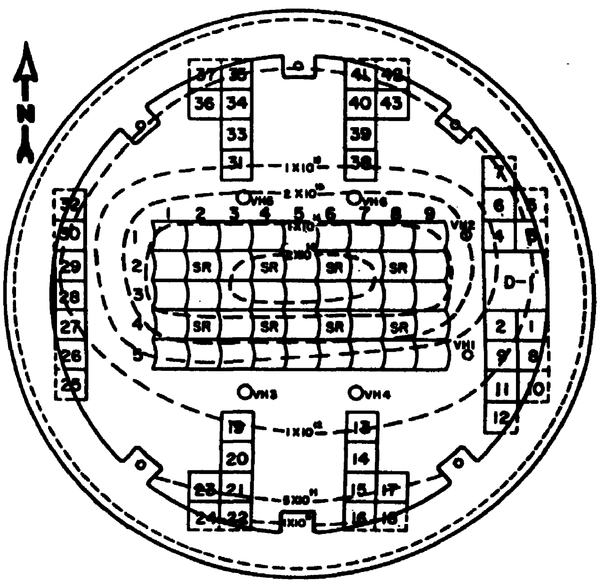

Figure 9. MTR reactor tank horizontal cross section fast neutron flux values at midplane

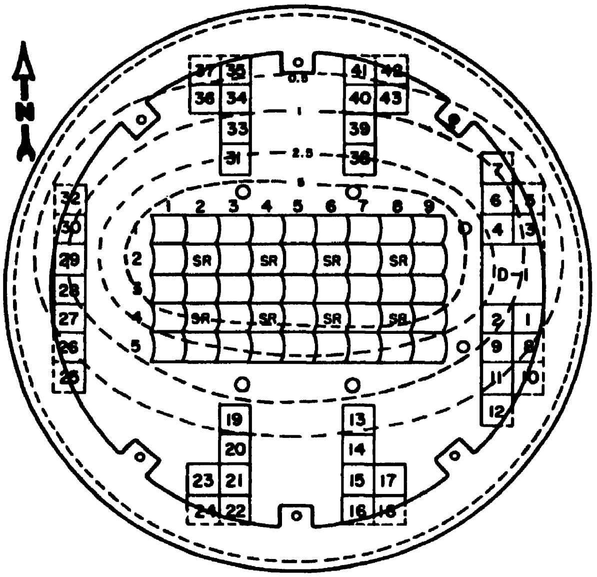

Figure 10. MTR reactor tank horizontal cross section gamma heat flux at midplane

inside the reactor tank. In the beryllium adjacent to the north and south faces of the lattice, fluxes of 3 to 5 × 10^{14} neutrons per square centimeter per second are obtained. Figure 9 is a similar map of the fast neutron flux contours.

The thermal neutron fluxes in the graphite zone, outside the reactor tank, vary from 5 × 10^{13} down to 1 × 10^{12} at the thermal shield. The fast fluxes outside the tank fall off very rapidly and are generally not considered useful. At the inside face of the thermal column the thermal fluxes are about 10^{11}; at the outer face eight feet farther out they are 10^7. The cadmium ratio, i.e., the ratio of thermal neutrons to epi cadmium neutrons, at the outer face of the thermal column is greater than 10^6.

High gamma-ray fluxes also exist in the MTR. In the lattice section they produce a heat evolution of fourteen watts per gram of absorbing material. Figure 10 is a contour map of this heat generation for positions inside the reactor tank.

Reactivity Measurement Facility

Because a cold clean reactor is required for most precise measurement of reactivity effects, the MTR itself is not suitable for such work. It does however provide an excellent medium for achieving rapid burnup of fissionable material in test specimens whose reactivity changes can then be determined precisely in a suitably designed reactor operating at zero power. Such a test facility, called the RMF, has been constructed and installed in the MTR canal.

The RMF consists of a rectangular vertical array of 30 MTR fuel assemblies with a large square opening in the center achieved by leaving out four fuel assemblies. One of the unusual features of this reactor is the marked variation in the sensitivity to fuel and poison at different positions in this test hole. This permits experiments to separate fuel and poison effects. Test specimens whose reactivity worth is to be measured are placed in this central opening and evaluated by determining the difference between the positions of a calibrated control rod with and without the specimen inserted in the reactor. Good stability has been achieved both with respect to temperature variations and geometrical perturbations when working with cold samples. No measurements have yet been made on irradiated samples. It is likely that some small temperature gradients will be set up by absorption of gamma radiation in the surrounding water, but this is not expected to be serious.

Non-Destructive Assay of MTR Fuel Assemblies

MTR fuel assemblies are not fabricated at the National Reactor Testing Station, but are supplied by an outside contractor. One of the inspection problems which arises when a new shipment arrives at the MTR is that of making an independent determination of the amount of fissionable material in each assembly. The assay must be non-destructive and must be sufficiently quantitative to be useful.

This problem has been solved successfully by utilizing a beam of thermal neutrons from the MTR. Each fuel assembly is placed in turn in the path of the neutron beam so that the direction of the beam is at right angles to the fuel plates. The resultant fission neutrons, after thermalization in paraffin wax, are measured by proportional counters placed on both sides of the fuel assembly. All of the measurements are relative to carefully determined standards. The relative precision with which the amount of fissionable material can be determined at various positions along the fuel assembly is of the order of ± 3 per cent.

Isotope Studies

The high neutron flux in the MTR greatly facilitates the study of isotopes produced from parent isotopes with low neutron cross section or by higher order neutron reactions with relatively short-lived intermediate isotopes of high cross section. Prolonged irradiation of transuranium isotopes has resulted in a wide variety of heavier nuclei, chief among which is the new element with atomic number 100 recently discovered by University of California scientists.

(n,p) reactions having such a low cross section as to pass unnoticed in reactors with a lower neutron flux may turn up unexpectedly in the MTR. A recent example of this is the inadvertent production of an unanticipated gamma activity in some nickelous oxide which was being irradiated in the reactor for the purpose of activation analysis. Investigation by scintillation counter analysis showed the activity to be due to 72-day Co^{58} which is produced by (n,p) reaction of Ni^{58} with an effective cross section estimated to be of the order of ten millibarns. The most important result of this observation is the possibility which it opens up for the production of substantial quantities of this gamma-emitting isotope in an essentially carrier-free condition which should prove to be exceedingly useful for a wide variety of tracer investigations.

Neutron Cross-Sections Studies

At two of the six main beam holes radiating out from the MTR active lattice are installed two major pieces of equipment for studying nuclear resonances. One is a neutron crystal spectrometer and the other a fast chopper velocity selector. The main components of both were fabricated by the Brookhaven National Laboratory based on equipment in successful operation there. The electronics control and measurement circuits were developed and built by the MTR staff.

The crystal spectrometer is equipped for remote manual and automatic operation. Using the 240 planes of a $\frac{3}{16}$-in. slab of natural NaCl in transmission, counting rates of 500,000 counts per minute at 0.07 ev, 12,000 counts per minute at 1 ev and 3,000 counts per minute at 10 ev have been obtained. For a detector system, two 24-in. × 2-in. diameter proportional counters filled to 40 cm mercury pressure with $B^{10}F_3$ are operated in parallel. An automatic data-taking system has been installed which records directly on an electric typewriter all significant data from the spectrometer in a form convenient for computation and permanent storage. These data include the arm angle, total monitor count, crystal position, sample identification, atomic number and atomic weight, and the total detector count. Among the more important results obtained with this equipment to date is the detection of a new tantalum isotope, Ta^{180}, by the Knolls Atomic Power Laboratory mass spectrometer group, to whom the resonance information was supplied with the suggestion that the search be made.

The fast chopper rotor spins at 6000 rpm and transmits neutrons for one microsecond out of every 1250. Energy values can be assigned to the detected neutrons by measuring the time required to travel the 30 meters from the rotor to the detectors. The drift tube is evacuated to the point which essentially eliminates the 40 to 50 per cent loss of neutrons which would occur in an equivalent air path between the chopper and detectors. The detector system consists of 28 aluminum-walled BF_3 proportional counters operating in parallel. The time-of-flight circuit consists of 100 consecutive channels following a variable time delay from the triggering light pulse. At present a one-microsecond channel width is being used but this can be modified by changing the mass oscillator frequency used to generate the timing sequence. The resolution obtained is of the order of 0.1 microseconds per meter.

Resonance parameters for silver, tantalum and several other isotopes have been determined in the course of checking out the equipment. New information that came out of this work included the splitting of the tantalum resonances at 24 ev and 35 ev.

Isotope Production

Because of its high neutron flux the MTR produces most of the high specific activity radioisotopes used in the USAEC program. Approximately 75,000 curies of Co^{60} have been produced to date, more than half of which had an average specific activity of 40 curies per gram or better. Certain samples have ranged as high as 90 curies per gram. Most of the high specific activity materials are employed in teletherapy equipment.

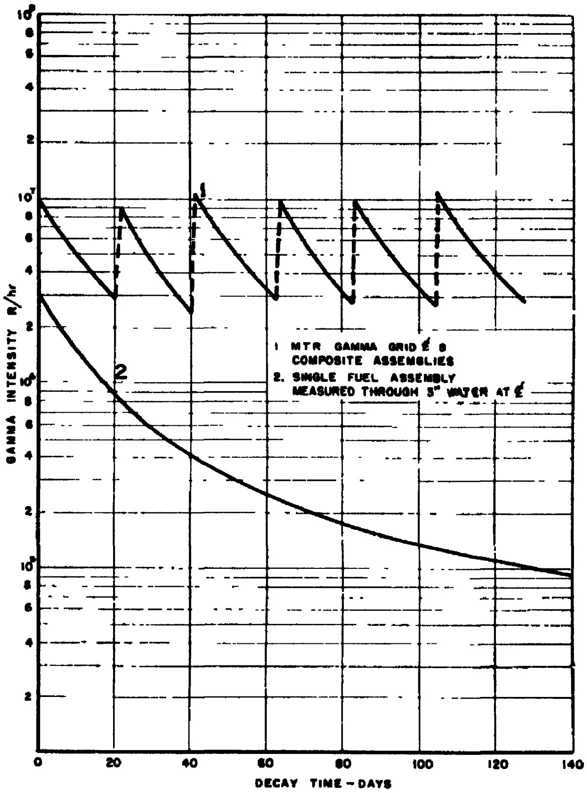

Figure 11. MTR gamma irradiation facility decay curves of spent fuel assemblies

Next to Co^{60}, the radioisotope most in demand for production in the MTR is Tm^{170}. The utility of radioactive thulium as a portable X-ray source was first pointed out by the Argonne National Laboratory. This isotope emits soft gamma rays of approximately 85 kev with a half life of 139 days. By mounting a small pellet of thulium metal or oxide at the "focal point" of a small lead-shielded source box and providing the box with a suitable shutter device, one has the radiation equivalent of an X-ray tube operating at 85 kev. The thulium source has two major advantages over the comparable X-ray equipment; one is lower cost and the other is portability. Since the thulium pellets needed for radiation sources are small, approximately $\frac{1}{8}$-in. diameter by $\frac{1}{8}$-in. long, several of them can be activated simultaneously in a relatively small space inside the reactor. They are encased in an aluminum capsule roughly one inch in diameter by one inch long which may be irradiated in any one of a number of locations in the water-cooled reflector adjacent to the reactor core. In the highest flux position a specific activity of approximately ten curies (equivalent gammas) per gram can be attained in one reactor fuel cycle of about three weeks.

Other isotopes that have been produced in the MTR include P^{32}, Na^{24}, Ce^{140}, Hg^{204}, Sb^{122}, Se^{75} and a number of transplutonium isotopes.

Gamma Irradiation Studies

MTR fuel assemblies after removal from the reactor constitute the most intense source of gamma radiation known. Stored in the canal underneath the reactor, they produce a brilliant Cerenkov glow in the surrounding water which can readily be seen with all the house and canal lights turned on. Neutron fields of the order of 10^4 neutrons per square centimeter per second are produced in the water immediately adjacent to the fuel assemblies newly removed from the reactor due to photo disintegration of the small amount of deuterium present in the water.

Gamma intensities as high as thirty to forty million roentgens per hour exist in the immediate neighborhood of fuel assemblies that have just been removed from the reactor. Both the intensity and spectrum of the gamma rays change rather rapidly during the first few weeks of storage due to fission product decay which approximately follows the Borst-Wheeler curves. Figure 11 shows the gamma intensity in roentgens per hour obtained as a function of decay time at three inches from the center of a fuel assembly and inside a grouping of fuel assemblies in the gamma facility in the MTR canal. The serrated line for the facility indicates the new loadings made each time assemblies are discharged from the reactor. By grouping the fuel assemblies into appropriate configurations during their storage period in the canal, several gamma irradiation facilities of very high radiation intensity are provided. These facilities have been extremely useful in a wide variety of investigations including radiation damage to organic liquids, plastics, glass, etc., cross-linking of plastic polymers, food sterilization, and the preservation of vegetables and meats.

REFERENCE

1. Huffman, J. R., *The Materials Testing Reactor*, Nucleonics 12: 20-6 (1954).

Research Program and Operating Experience on ORNL Reactors

By M. E. Ramsey and C. D. Cagle,* USA

The research programs at the Oak Ridge National Laboratory which make use of reactors or reactor products primarily use the two general-purpose research reactors. These are the normal-uranium, graphite-moderated reactor and the Low Intensity Testing Reactor. It is interesting that neither of these was built expressly as a long term research reactor but each has been adapted to this usage.

The research work involving usage of these reactors covers a wide range of fields in both pure and applied research including the following: basic studies of neutron and radiation properties, solid state structure and phase transitions by use of neutron spectroscopy, radiation damage of materials, radiation effects in chemistry, radioactivation analyses of trace impurities, biological effects of radiation, reactor development, and radiation monitoring development.

Another important usage of these reactors is the preparation of radioisotopes for world-wide usage.

Training of personnel in reactor technology is another important phase of the work. Two programs are devoted to this work. One is the Oak Ridge Institute of Nuclear Studies (ORINS) which concentrates on the uses of radioisotopes. The other is the Oak Ridge School of Reactor Technology which teaches the principles of reactor theory, design, and usage. In addition to these formal programs, faculty members from universities all over the United States do special research work at the reactors especially during the summer months.

This report describes these reactors and the research facilities available.

GRAPHITE REACTOR

The Oak Ridge National Laboratory's graphite-moderated, air-cooled, normal uranium reactor (Figs. 1 and 2) was built as the pilot plant for the plutonium-producing reactors which are at Hanford, Washington. Construction was started early in 1943, and critical loading was completed on November 4, 1943. This was the first reactor built that could be cooled and thereby operated at a reasonably high power level for long periods of time and was the second reactor built in this country. It was designed to operate at one megawatt power level, and its prime purposes were to furnish operating experience, reactor characteristics, and to provide small quantities of plutonium to aid in the development of chemical separation techniques to be used at Hanford. Since this is an air-cooled reactor, water-cooled fuel tubes of the Hanford type were simulated in some of the 4-in. square test holes.

The reactor core and reflector is a 24-ft cube of graphite built up of 4-in. square by 50-in. long blocks and contains 1248 fuel channels that are 1¾-in. squares with the diagonals vertical and horizontal. Also there are 22 horizontal 4-in. square holes that go all the way through and six that go half way through the graphite perpendicular to and between the fuel channels. Six vertical 4-in.-square holes penetrate to a depth of 17-ft-4-in. into the graphite. Ten instrument openings penetrate the shield up to the graphite. Two thermal column openings, two 14-in.-square biological specimen entrances, four 1.68-in. diameter holes through the central core, and a foil slot through the reactor center make up the remainder of the experiment facility openings (see Table I).

The reactor shield is a 7-ft thickness of concrete that surrounds the core with manifold spaces provided for the cooling air. Plugged sleeves set into the concrete provide access to the holes through the graphite. The inner-most and outer-most 1-foot thicknesses of the shield are normal structural concrete and aggregate and contain web-type steel reinforcing. The space between is filled with a special concrete mixture containing haydites, an expanded clay, to retain about 10 per cent of the make-up moisture as neutron shielding and barytes aggregate to increase its density. The shield was overdesigned and is still more than adequate at the present higher power level. The reactor does not have a thermal shield, but the concrete is insulated to some degree from the graphite by layers of asbestos and cellamite (see Fig. 3). A 10-in. high air passage across the top of the core between the graphite and the concrete was designed into the reactor but was closed off shortly after operation started to deflect more air through the fuel channels when it was found to be unnecessary.

The reactor coolant is atmospheric air that makes one pass through and is discharged to the atmosphere through a 200-ft stack. In order to remove the heat at the present 3.5 megawatt operating level, 120,000 cubic feet per minute of air is drawn through by two 900-horsepower suction fans. Rough fiber glass filters remove dust particles from the air at the inlet to the system and a combination of fine fiber glass and asbestos paper filters remove radioactive particles picked up from the reactor before the air reaches the suction fans.

---

* Oak Ridge National Laboratory.

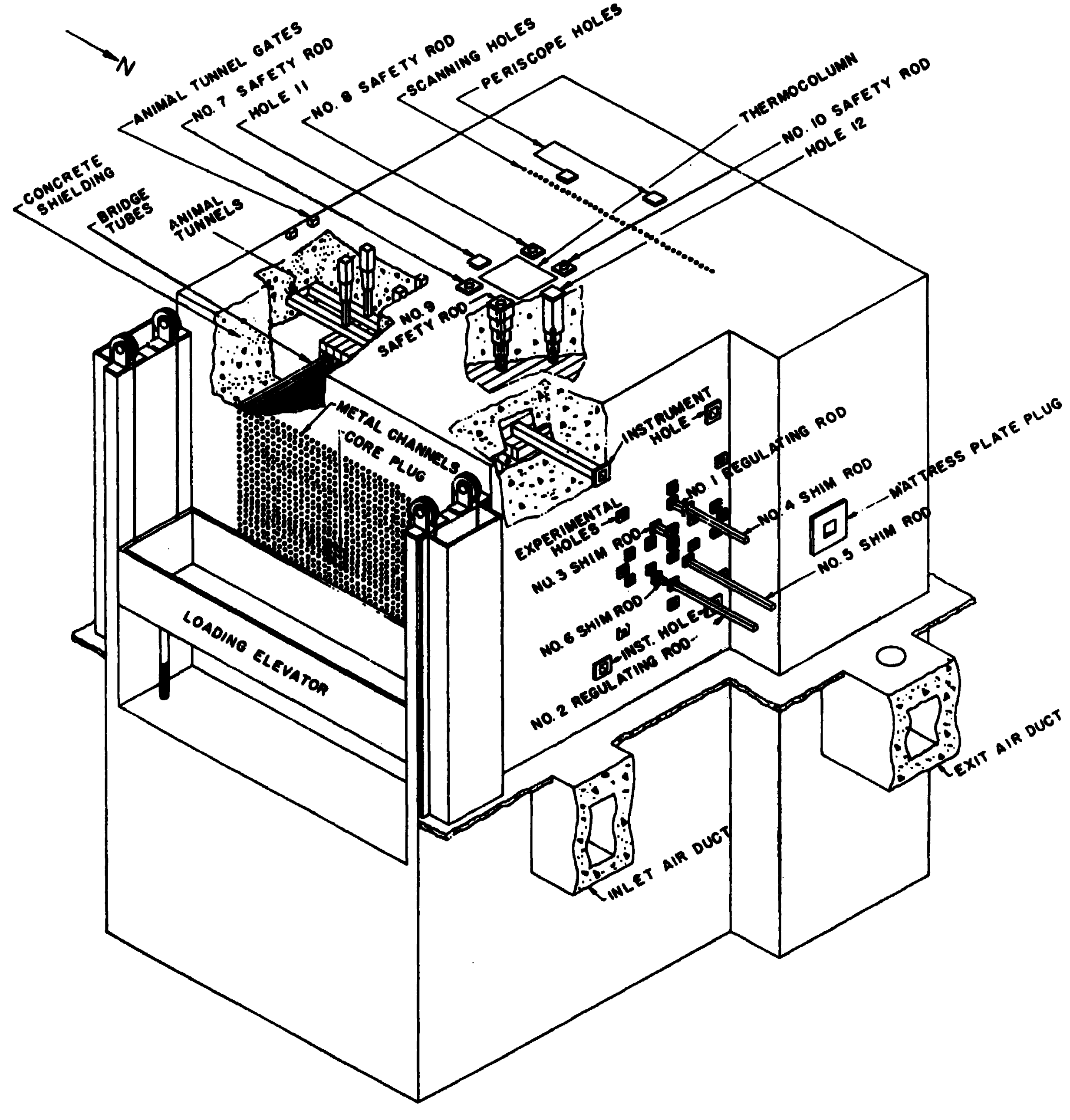

Figure 1. A cutaway sketch of the normal-uranium, graphite-moderated reactor

Five of the original eight shutdown rods are now in use (see Table II); three were removed to provide for experiments since they proved to be unnecessary. Three of the remaining rods enter vertical 4-in.-square holes from the top of the reactor. These rods are not of the original design. They are $3\frac{1}{2}$-in.-square hollow steel shells 8-ft long that contain a layer of $\frac{1}{16}$-in.-thick cadmium in the walls and a shield plug in the upper end. They are attached to steel cables that can be wound up on a windlass operated by electric motors through an electromagnetic clutch. The brake that holds the rod up in the operating position is on the electric motor so that if the power to the electromagnetic clutch is lost either by electrical power failure or by intentional interruption as for a normal shutdown, the windlass is made free to turn and allows the rod to fall into the core by its own weight. Full fall requires little more than one second.

The other two shutdown rods are $1\frac{3}{4}$-in.-square steel rods 200 inches long which contain 1.5 per cent boron. They enter two of the horizontal 4-in.-square holes which are sleeved down to 2-in. square with graphite. These two rods are driven by hydraulic motors for slow travel into or out of the reactor and can be made to travel the full distance into the reactor by a high pressure oil system within 4 seconds. This

Table I. Research Openings into Graphite Reactor

Kind of facility	*Number of facilities*	*Maximum thermal neutron flux*	*In-Cd ratio*	*Gamma flux*	*Approximate temperature*
4-in square horizontal	42 openings	3.6×10^{11} to 1×10^{12}	20	3×10^5 to 8×10^5 r/hr	35°C to 160°C
4-in. square vertical	3	8×10^{11}	20	6.7×10^5 r/hr	135°C to 140°C
1.68-in. diameter horizontal	4	1×10^{12}	20	9×10^5 r/hr	35°C
2¾ in. × ⅜ in. foil slot	1	1.1×10^{12}	20	9×10^6 r/hr	160°C
Unused fuel channels in core region	5	5.5×10^{11} to 1×10^{12}	20	4.5×10^6 to 9×10^5 r/hr	35°C
Unused fuel channels in reflector region	418	10^{10} to 3×10^{11}		10^4 to 3×10^6 r/hr	30°C to 40°C
14-in. square biological tunnel lead-lined	1	1.3×10^9	~70 Mn-Cd ratio	200 r/hr	25°C to 35°C
14-in. square biological tunnel bare	1	5×10^8	73 Mn-Cd ratio	3.4×10^3 r/hr	25°C to 35°C
5-ft square vertical thermal column	1	1.5×10^7	~10^6	135 r/hr at top of column	Room temperature
2½-ft square horizontal thermal column	1	5×10^9	130	1.2×10^4 r/hr	Room temperature
Unused 9-in. square ionization chamber holes	2	10^7 to 10^9	~70 Mn–Cd ratio	~5×10^3 r/hr	35°C

high pressure, 900 pounds per square inch, is maintained by two large weights pressing upon oil-filled cylinders and is kept from the drive mechanisms by normally open solenoid valves so that, if the electrical power fails or is interrupted by the shutdown switch, the valves open and allow the 900 psi pressure to hit pistons which operate rack and pinion drives to push the rods into the reactor.

Two other rods, identical to the hydraulic rods are used as regulating rods when the reactor is being operated manually. They are driven by electric motors and are not part of the shutdown system. Both rods have a fast speed in and out and one has a slow speed for fine control.

Within recent months an automatic control system has been developed which uses one of the hydraulic rods in the nearly out position as its control rod. The electrically driven regulating rods are still used to position the automatic control rod within its operating range. This arrangement tends to minimize distortion of the neutron flux pattern within the reactor core.

Up until recently a boron shot tube was kept for emergency or disaster shutdown use. This consisted of a hopper of boron-steel shot that could be released

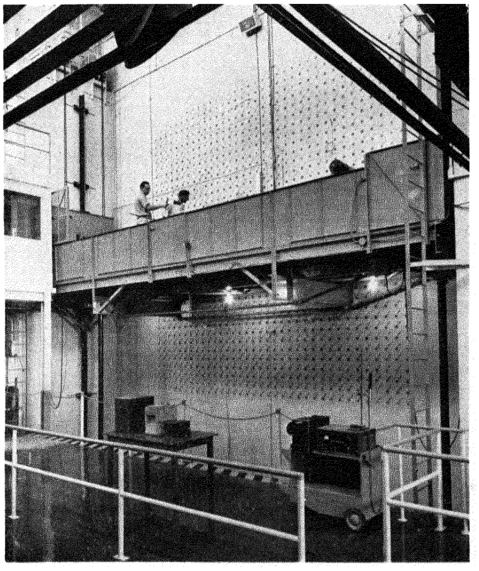

Figure 2. Fuel-charging side of the graphite reactor

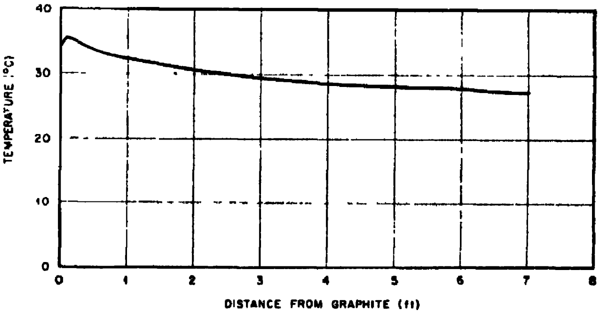

Figure 3. Temperature traverse through the concrete shield of the graphite reactor showing that gamma heating is not excessive nor is the temperature differential through the shield great enough to cause severe stresses

into the reactor core region by pulling a cable in the control room to release a plug in the bottom of the hopper. The hopper was within the top shield of the reactor and could not be easily inspected. Also there was no way to test the working of the apparatus on a routine basis. By accident the pull cable was pulled recently and the shot did not fall into the reactor. They were found to be rusted and stuck together. Because of this, authorization has been given to completely remove the equipment since any safety equipment that cannot be periodically checked cannot be trusted to operate. All other safety features can be checked.

When operation of the graphite reactor was first started, very low level neutron flux during startup was monitored with a counter and then by a gamma-compensated boron-coated ionization chamber as the power level rose to the kilowatt level. The practice of using the neutron counter was discontinued and only the ionization chamber retained. This is safe because the fuel loading is kept such that the excess reactivity is below the delayed neutron contribution and prompt critical is an impossibility. Three of the gamma-compensated chambers are now in use one is read by a galvanometer and used for startup and manual operation, a second for the automatic control and the third for vernier control while in manual operation or as a spare. These chambers are located in the shield of the reactor where they "see" a neutron flux of about 10^8 n/cm²-sec.

Three other non-gamma-compensated, boron-coated ionization chambers are used for the safety instrumentation to scram the reactor by way of electronic trips if the power level should be allowed to exceed 5.5 megawatts. It is not necessary that these chambers be gamma compensated because they are important only at a neutron level where the gamma contribution is negligible.

A second safeguard against power excursions is a system of boron-coated thermopiles whose composite signal which is proportional to the power level is fed to an electronic strip recorder containing a high level trip to initiate a scram at 6.0 megawatts.

The temperature of the aluminum jackets that enclose the uranium metal in the reactor must also be limited. This is accomplished by including in the loading fuel pieces having iron-constantan thermocouples attached to the jackets. Experience has shown that the hottest position in any fuel row is two feet past the center of the row in the direction of the air flow. At least forty such thermocouples are kept in the reactor at all times and positioned to give a good representation of the temperature distribution. The thermocouple having the highest reading supplies a signal to a single point strip recorder containing a high level trip to scram the reactor if the temperature exceeds 325°C. Actually the operator does not allow the temperature to exceed 280°C. It has been found that a standard power level of 3.5 Mw can generally be maintained year around without exceeding the safe temperature level.

The temperature of the graphite near (1 foot from) the center of the reactor is recorded but does not actuate any scram or alarm. Its value averages about 135°C.

Temperatures of the inlet and exit cooling air

Table II. Characteristics of Control and Shutdown Rods

	Type of rod		
	Control	*Horizontal shutdown*	*Vertical shutdown*
Number	2	2	3
Reactivity value	#1–0.57% $\frac{\Delta k}{k}$ #2–0.50% $\frac{\Delta k}{k}$	0.63% $\frac{\Delta k}{k}$	0.50% $\frac{\Delta k}{k}$
Material	1.5% boron steel	1.5% boron steel	Hollow steel shell containing layer of cadmium
Size and shape	1.75 in. square bar 19 ft long	1.75 in. square bar 19 ft long	3½ in. square hollow steel shell 8 ft long. Top end contains lead and masonite shield and bottom end has spring shock absorber
Method of operation	Direct electric motor driven	Hydraulic cylinder operates rack and pinion drive. Normal operation—pump. Emergency operation –accumulator	Gravity when latch solenoid is de-energized. Lifted out of reactor by electric motor
Travel (distance into reactor)	In: To within 5 ft of opposite side of graphite Out: To 1 ft outside graphite into concrete shield	In: To within 5 ft of opposite side of graphite Out: To 1 ft outside graphite into concrete shield	In: 4 ft below and 4 ft above reactor center Out: Just withdrawn from graphite
Speed of travel	#1: Max. in 6.9 in. per sec Max. out 6.9 in. per sec #2: Max. in 4.76 in. per sec Max. out 4.76 in. per sec Min. in 0.044 in. per sec Min. out 0.044 in. per sec	In: Normal—6 in. per second Emergency—full travel in 4 sec Out: 1 in. per sec	In: ~1 sec for full fall Out: ~10 sec
Guide tube	2¼-in. × 2¼-in. square slot milled into graphite blocks in 4-in. sq. hole	2¼-in. × 2¼-in. square slot milled into blocks in 4-in. square hole	Full size 4-in. square vertical hole

streams are measured for the purpose of heat power calculations by thermohms located in the inlet and exit air ducts. At one time the signal from a thermohm in the exit air duct was fed to a strip-recorder containing a high level trip to cause a scram. The scram feature has been removed as unnecessary since the lag in this temperature is too long to be of value in the event of a power excursion, and it served no other purpose.

A pitot tube in the inlet air duct sends a signal to oil manometers at the control desk and to a ring-balance circular chart recorder which scrams the reactor if the air flow drops too low. Another ring balance recorder shows the pressure drop across the reactor from pressure taps located in the inlet duct and in the exhaust manifold. This recorder also scrams the reactor if its reading falls too low.

The radioactivity of the exhaust air from the reactor is measured by an ionization chamber through which a continuous sample of the air passes. The signal from this ionization chamber is read on a strip recorder at the control desk and until recently would actuate a scram if the normal radioactivity level increased by a factor of three. Experience has shown that the reactor itself could not cause such a condition unless it experienced a violent power excursion or great loss of air flow, conditions, which if they occurred, would initiate a scram. Also the off-gas from experiments and equipment at the Low Intensity Test Reactor have been tied into the graphite reactor exhaust and it would be pointless to shut down the graphite reactor because of radioactivity from some other source. In the course of one operating day the reactor generates a total of about 500 curies of radioargon (A^{41}) from the 0.9 per cent argon present in the atmosphere. This is the major radioactivity in the exhaust air. There is a small amount of mixed fission product gases being evolved from small quantities of uranium oxide dust from defective fuel elements caught in cracks between graphite blocks.

The concrete shield at the exhaust end of the fuel channels would be damaged by the continual blast of hot air emerging from the channels if it were not protected. A one-inch thick wall of cellamite is spaced four inches from the inner face of the concrete to form a separate chamber which is cooled by a separate air stream. The pressure within this region as well as the air flow to it are monitored. If the negative pressure within the region becomes excessive, there is a possibility that the shield wall might collapse. To guard against this event, a negative pressure greater than 34 in. of water will cause the suction fans to be turned off. Loss of the fan suction shuts the reactor down by the other means described.

The hydraulic pressure accumulators which drive the horizontal shutdown rods into the reactor must be kept pumped up to contain a sufficient volume of oil at all times that the reactor is in operation. If a leak in the system should develop allowing the weights to fall to a minimum level, a switch actuated by the weight scrams the reactor while there is still enough oil left to accomplish the shutdown.

Table III. Automatic Reactor Scram Summary

Power level greater than 5.5 megawatts (ionization chambers)
Power level greater than 6.0 megawatts (boron-coated thermopiles)
Metal temperature greater than 325°C
Air flow less than 40,000 ft^3/min
Differential pressure across reactor less than 8 in. H_2O gage
Radiation at horizontal thermal column greater than 50 mr/hr
Any experiment requiring that the reactor be shut down for safety reasons

Frequently experiments are performed which can develop conditions which can injure personnel, the reactor, or expensive equipment if the reactor is not scrammed. Safeguard circuits from these experiments can be tied into the reactor scram circuits. Typical examples are:

1. One of the thermal column openings is shielded by a tank of water which, if accidentally drained, would allow about a 2-ft^2 beam of radiation to emerge from the reactor into a heavily frequented personnel area. To prevent this, a radiation monitor at the location scrams the reactor and sounds a siren.
2. A 4-in^2 horizontal hole contains a water-cooled hollow cylinder of enriched uranium aluminum alloy in which targets can be subjected to a high fast neutron flux. If the water flow were to fail the cylinder would probably melt and damage the reactor. The reactor is scrammed by a water flow recorder if the flow is lost.
3. A vertical 4-in^2 hole is used to expose capsules containing test fuels for homogeneous reactors to check both solution stability and corrosion of the capsule walls. If the pressure in the capsule becomes excessive due to unexpected behavior, the capsule may rupture causing contamination of equipment or even personnel with fission products. To prevent this, a pressure monitor on the capsule scrams the reactor to stop the pressure buildup.

Manual scram switches are located at the control desk, the exit doors of the building, and at the experiment locations. The control console is shown in Fig. 4.

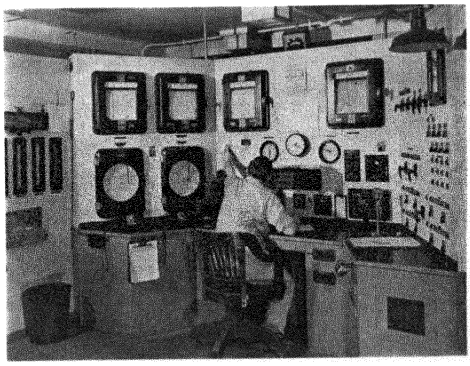

Figure 4. Control console of the graphite reactor showing operator throwing "scram" switch to shut the reactor down

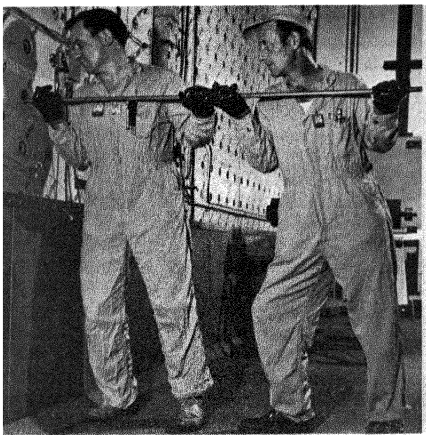

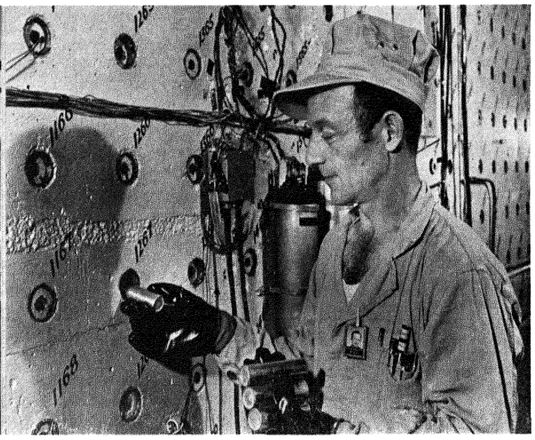

Figure 5. (Left) A closeup view of the fuel charging face showing operators pushing fuel elements from the reactor core

Figure 5a. (Right) Operator inserting fuel elements into a fuel channel. After being inserted by hand, they are cen'ered in the core by pushing them into place with measured steel rods

The reactor fuel is normal uranium metal in the form of 1.1 in.-diameter by 4-in. long slugs encased in a 35-mil thick 2-S aluminum jacket. These are charged into the fuel channels end-to-end to simulate long rods. The purpose of the segmentation is for ease in handling. Each slug weighs about 2½ pounds.

The fuel is inserted into the reactor by hand and positioned with measured rods while the reactor is shut down. Removal is accomplished by pushing it on through the graphite from which it falls through the air exhaust manifold to a chute which leads to a 20-ft deep water pit outside the reactor shield (see Figs. 5 and 5a).

All during the operation of the reactor an annoying number of fuel element failures have occurred and two full-scale attempts have been made to improve them. The first elements used were jacketed in 2-S aluminum cans having 20-mil thick walls, and the caps were sealed on by resistance welding. No bonding existed between the uranium and the aluminum. This type was used during 1943 and part of 1944. The next type had 35-mil thick 2-S aluminum walls with the caps arc-welded on in a helium atmosphere. Again the uranium and the aluminum were not bonded but were die-pressed to be in close contact. No failure of the first type of elements occurred but they were used only at low power and for only a short time. The second type came into use when the power level was increased from one megawatt to 3.6 megawatts. The failure rate of these elements was approximately one per month. Although this rate was not excessive enough to curtail operation, it did require constant vigilance to prevent damage to the reactor. The causes of failure were probably several, but the end result was always the same—bursting of the aluminum jacket allowing the rapid formation of uranium oxide which was carried away to some degree by the air stream causing contamination of the air exhaust system with fission products. The more serious result of failure is the possible sealing off of the channel by the swelling element jacket as the oxide volume increases. When the air flow ceases, other elements in the channel fail due to high temperature. This has occurred twice, once in 1947 and again in 1948. The first instance involved 13 elements and the second 5 elements. In both instances the fuel channel was so scarred by the discharging techniques that had to be used that they were not suitable for further use as fuel channels and were diverted to other usages. Since that time a weekly inspection of all fuel channels has prevented the recurrence of such multiple failures.

During 1952 the fuel was changed to a bonded type. This bond is an aluminum-silicon eutectic which fills the space between the aluminum jacket and the uranium metal. Its purpose is to separate the uranium from the aluminum and still provide good heat transfer. It also tends to slow the rate of a failure by minimizing the area of uranium that might be exposed to air if a tiny hole should develop in the aluminum jacket. Since one of the causes of failure in the unbonded elements was interaction between the uranium and the aluminum if the temperature were in the 200° to 300° range for long periods, it was hoped that the bonded elements could be operated above this temperature allowing the power level to be increased. This, however, has not proved to be true; the element jackets are now operating at a higher temperature relative to power level than before due to the better heat transfer from the uranium to the aluminum jacket through the bond under the thermocouple bead and failures occur at an objectionable rate above 300°C indicating that there is still sufficient contact between the aluminum and the uranium to cause trouble. With the unbonded elements the jacket temperature could be operated continuously at 245°C without experiencing serious failure rates.

The power level at this temperature averaged 3.6 megawatts with frequent operation at 4.0 megawatts. With the bonded elements, experience has shown that 285°C as shown by the thermocouple should not be exceeded for long periods. The average power level now is 3.5 megawatts to stay below this limit. The gain has been only in the frequency of failure rate which is less than half that with the unbonded elements. A temperature traverse along the length of a fuel channel is shown in Fig. 6.

The quantity of normal uranium required for critical loading was almost exactly 30 tons. The present loading is 54 tons to provide sufficient excess reactivity for the benefit of experiment and radioisotope target materials in the reactor as well as to provide for the poisoning effect of the Al-Si bonding material in the present elements (see Figs. 7 and 8).

The reactor is operated on a round-the-clock basis with the only routine shutdown being from 5:00 am to about 3:30 pm each Monday. The continuous operation is necessary for the varied experiments being conducted as well as for a routine production of radioisotopes. The percentage operating time since the reactor first attained critical loading is in excess of 90 per cent. During the routine shutdown, each fuel channel is inspected for any evidence of failure, changes in research equipment made, radioisotope targets are removed and inserted, and required maintenance performed. Close scheduling is required to accomplish this work in the allotted time and planning always starts each Thursday for the following Monday.

Other shutdowns are scheduled as required for emergency maintenance, of course, and shutdowns for special research or radioisotope production work are sometimes arranged with the permission of other research personnel using the reactor.

At the standard operating power level of 3.5 megawatts the maximum thermal neutron flux is 1.1×10^{12} n/cm^2-sec. Up until 1952 the power level was generally kept as high as possible without exceeding the temperature limitation of the fuel jackets. This caused several different power levels to be existing even during the course of one day ranging from 3.4 to 4.2 megawatts and caused a lot of extra work for the research personnel in normalizing their data. This was a case of doing something just because it had always been done and was a hangover from the old plutonium production days when it was required to operate at the highest power level possible. The present operation at a standard power level has somewhat simplified the work of the research personnel but even now very precise work has to be specially monitored at the exact facility being used.

Due to the size of the reactor and the placement of the regulating rods slow fluctuations of greater than one per cent can take place in one day in any one location without any change in the over-all power output of the reactor. As the temperature of the coolant (atmospheric air) increases from shortly after daylight until about 2:30 or 3:00 pm, when the peak temperature usually occurs, the regulating rods move outward to compensate for the over-all temperature rise in the reactor. This causes the peak flux in the reactor to move toward the center of the reactor in the direction the rods are traveling. The opposite effect begins shortly thereafter until about 10:00 pm after which nearly a stationary flux pattern exists until daylight. For this reason, research personnel needing precise neutron flux control prefer data taken at night unless they have automatic compensation in their equipment which many have at present.

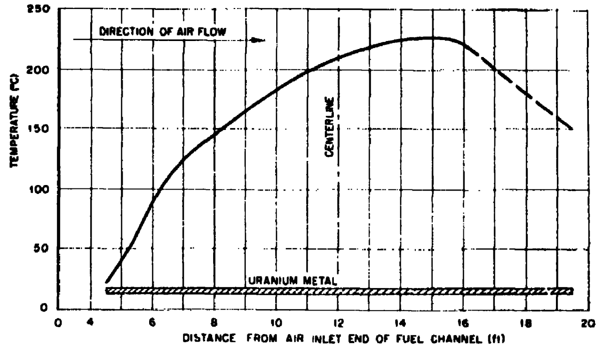

Figure 6. Temperature traverse through a fuel channel showing that the peak temperature is downstream from the reactor center

Also, due to having two general purpose pneumatic exposure tubes and a vertical hole through which relatively large samples (up to 18 in. long by 2½ in. in diameter) can be inserted and removed without shutting down, many brief flux fluctuations occur all during the day as these facilities are used. Announcements five minutes prior to such fluctuations by way of a public address system gives each research man time to prepare for them or raise objections to their being done. Another such fluctuation occurs during a major regulating rod adjustment which must be made at any time the two regulating rods become unbalanced as much as 10 inches. This occurs due to having fine control movement on only one rod. When this rod has been moved inward or outward 10 inches farther than the one-speed rod, they are re-balanced by moving one in one direction and the other in the other direction simultaneously. At best, some fluctuation occurs and this, too, is announced five minutes ahead of time. The balancing procedure minimizes distortion of the flux pattern in the reactor. This technique need only be used during manual operation. While the reactor is in automatic control, the rods can be adjusted to be an even distance out at all times.

Since the total poisoning value of the five shutdown rods is only 2.7 per cent $\Delta k/k$ the loading is limited to half this value for the cold reactor. Due to the low power density, roughly 600 watts per cubic foot, the xenon-135 poisoning is not severe, only 0.2 per cent $\Delta k/k$. The combined temperature coefficients amount to 0.4 per cent $\Delta k/k$, making a total of 0.6 per cent $\Delta k/k$. An allowance of about 0.3 per cent $\Delta k/k$ is cancelled by the regulating rods to provide flexibility of

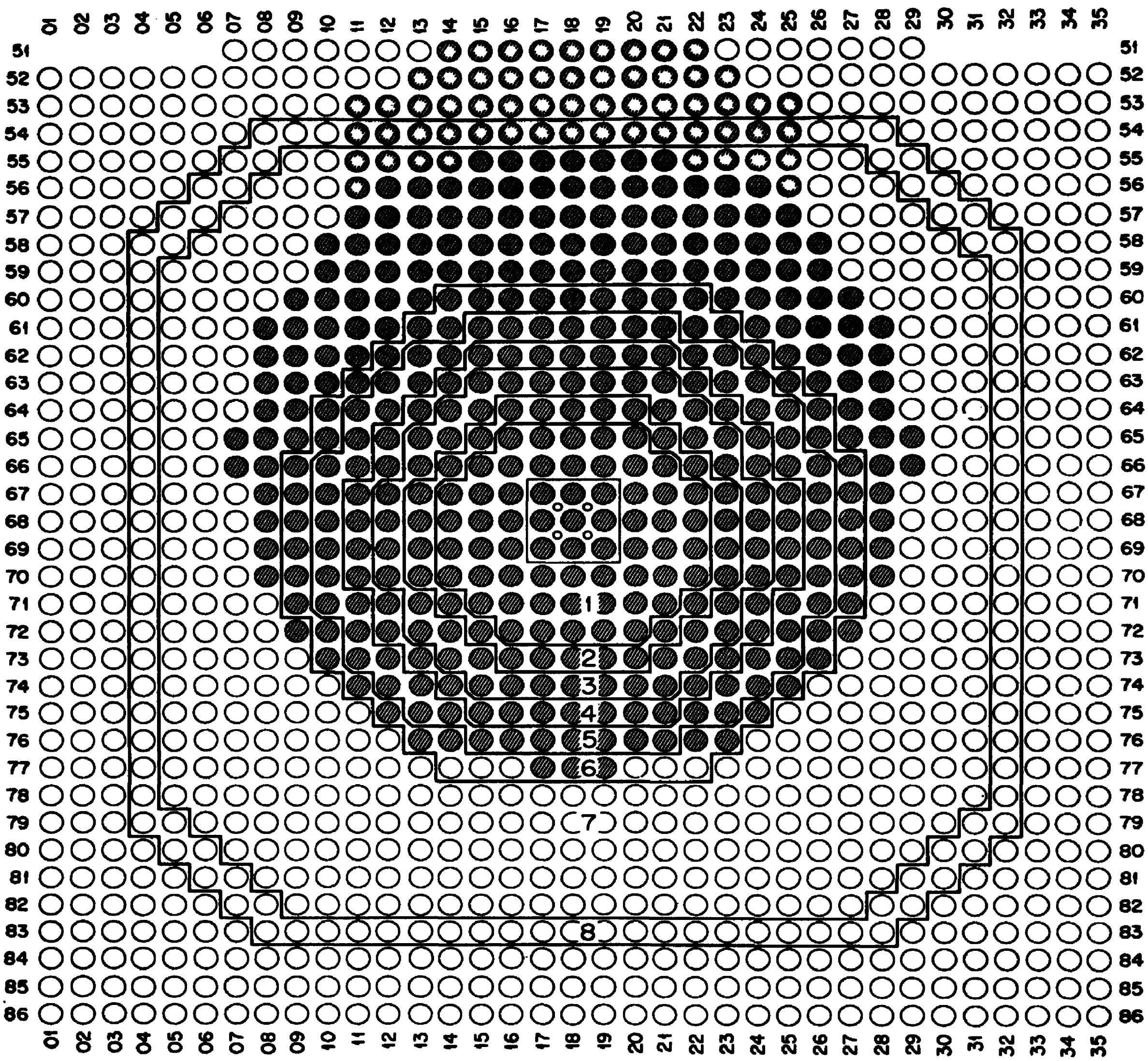

ORIGINAL LOADING

◎ 30 ELEMENT ROWS TO PROVIDE HIGHER NEUTRON FLUX IN VERTICAL THERMAL COLUMN

● 65 ELEMENT ROWS

Figure 7. First operating fuel loading of 35.7 tons of normal uranium. The 30-element rows at the top were to provide a higher neutron flux in the vertical thermal column

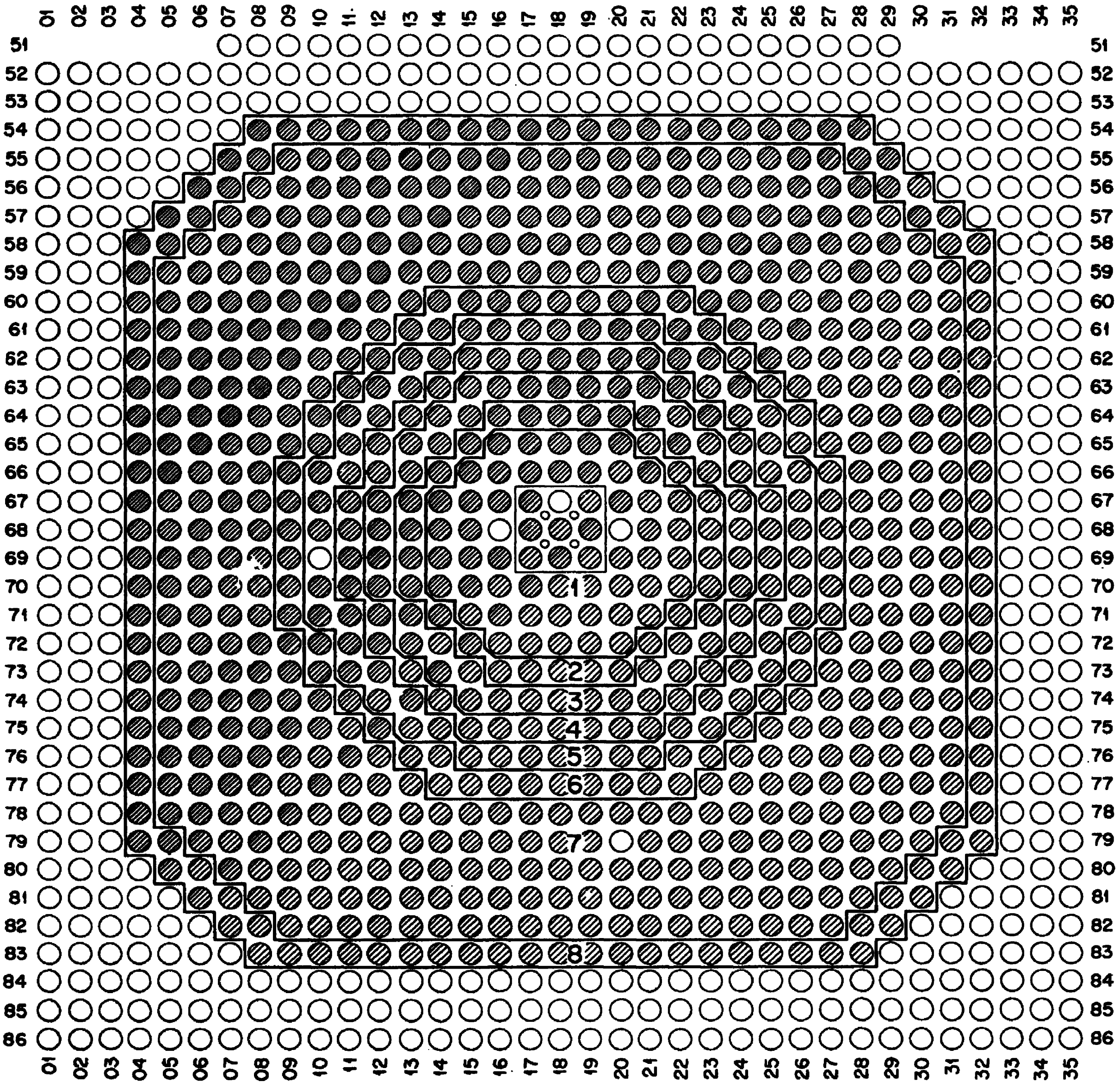

Figure 8. The present fuel loading pattern of the graphite reactor showing a much expanded core size and shorter rows at the center to depress the temperature in that region. This loading consists of 54.1 tons of normal uranium

Zone	*Channels*	*Slugs*	*Zone*	*Channels*	*Slugs*
1	60	41	5	58	54
2	26	45	6	54	54
3	42	51	7	438	54
4	38	51	8	114	47

control and for experiments of a temporary nature. Another 0.5 per cent $\Delta k/k$ is used by permanently installed experiment facilities giving a total of approximately 1.4 per cent $\Delta k/k$ excess reactivity for the clean cold reactor. The only possibility of prompt critical occurring is during startup and this is prevented by a careful slow startup procedure which requires fifteen minutes.

Table IV. Summary of Graphite Reactor Information

Size of graphite	24 ft × 24 ft × 24 ft-4 in. high
Thickness of concrete shield	7 ft 0 in.
No. of fuel channels	1248
No. of 1.6-in. diameter holes through central part of core	4
Type of fuel	normal uranium
Dimension of aluminum-clad fuel element (slug)	1.1 in. diameter by 4.1 in. long
Weight of uranium metal per slug	1170 grams
Thickness of aluminum cladding	0.035 in
Bonding material between Al and U	Al-Si eutectic
No. of fuel channels containing fuel	821
24-slug rows	10
41-slug rows	51
45-slug rows	23
47-slug rows	115
51-slug rows	79
54-slug rows	543
No. of 4 in² openings	56
No. of horizontal through holes (4 in²)	22
No. of horizontal half holes (4 in²)	6
No. of vertical holes (4 in²)	6
No. of 4 in² horizontal through holes used for control and shutdown rods	4
No. of 4 in² horizontal openings for experimental and target exposures	47
No. of 4 in² vertical holes for shutdown rods	3
No. of 4 in² vertical holes for experiments and target exposures	3
Other experiment facilities	14
Total reactivity value of shutdown rods	2.7% $\Delta k/k$
Total reactivity value of control rods	1.1% $\Delta k/k$
Approximate amount of reactivity absorbed by experiments and radioisotope samples	0.5% $\Delta k/k$
Weight of uranium in reactor	54.11 tons
Maximum thermal neutron flux at 3.5 Mw	1.1×10^{12}
Cadmium ratio	20
Average gamma photon energy	0.9 Mev
Maximum gamma photon flux (at average energy of 0.9 Mev)	5.13×10^{11} γ/cm²-sec
Maximum gamma dose rate	9.2×10^{5} r/hr
Ratio of gamma flux to thermal neutron flux	0.50
Standard reactor power level	3.5 megawatts
Average graphite temperature at center of reactor	~135°C
Average metal temperature at hottest region	~270°C
Average neutron flux (based upon power level and amount of fuel)	5.0×10^{11} n/cm²-sec
Ratio of maximum thermal neutron flux to average thermal neutron flux	2.24
Volume of active portion of reactor	5933.4 ft³
Power density inside active portion	587.5 watts/ft³
Volume of coolant air	120,000 ft³/min
Negative pressure inside reactor	~29 in. H_2O gage
Operating metal temperature coefficient	−0.29 inhour/°C
Operating graphite temperature coefficient	−0.77 inhour/°C
Barometric pressure coefficient	−0.38 inhour/mm Hg
Xenon poisoning coefficient	−25 inhours/1000 kw

SPECIAL RESEARCH EQUIPMENT AT THE GRAPHITE REACTOR

1. Neutron Spectrometers

Three neutron spectrometers are in use (Figs. 11 and 12). Two are operated by the Physics Division and one by the Chemistry Division. The primary beams of neutrons from collimators set in 4-in. square openings range from about ½-in. square to an inch square. This beam consists of neutrons of all energies from about 0.03 ev to more than 10 Mev and cannot be used. From this beam a crystal set in its path scatters the neutrons at angles inversely proportional to their energy. By using a second collimator, neutrons of about 0.07 ev (about 1Å wave length) are obtained. These are used in much the same way as X-rays in studying crystal structures, crystal transitions at

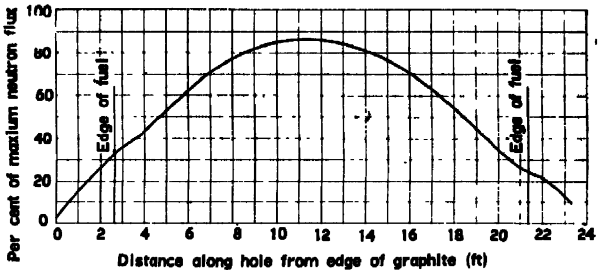

Figure 9. A typical thermal-neutron traverse through one of the 4-in. square experiment holes

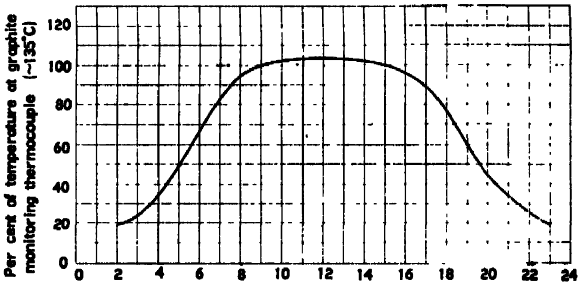

Figure 10. A typical temperature traverse through a 4-in. square hole showing a flattening at the center

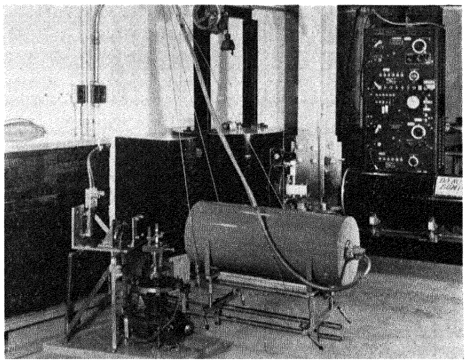

Figure 11. A view of two neutron spectrometers showing the external shielding required to keep the background neutron count low

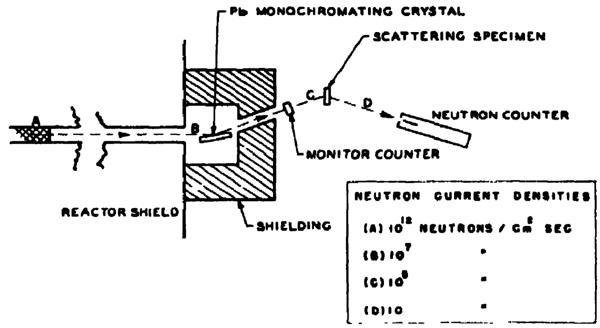

Figure 12. A schematic sketch of a neutron spectrometer with the parts named

different temperatures (using heaters or refrigerants), and the location of nuclei in crystals. Neutrons are particularly useful in studying crystals containing hydrogen, deuterium, or tritium since they are scattered by nuclei rather than by shell electrons.

2. Vertical Low Temperature Exposure Facility—Hole 12

Operated by—Solid State Division
Thermal neutron flux—8 × 10^{11} n/cm²-sec
Gamma—6.7 × 10^5 r/hr

This is a newly installed facility that is cooled by a helium refrigerator. The lowest temperature that can be obtained in the exposure chamber is about 18°K. The maximum sample size that can be accommodated is 1-in. in diameter by 24 in. in length. It will be used to study radiation damage without annealing occurring.

3. Horizontal Low Temperature Facility—Hole 52-N

Operated by—Solid State Division
Thermal neutron flux—3.6 × 10^{11} n/cm²-sec
Gamma—3 × 10^5 r/hr

The horizontal low temperature facility has been in operation since 1952. The exposure chamber can be cooled to 115°K by a stream of helium gas passing through a liquid nitrogen heat exchanger. The maximum size of samples is ⅞-in. diameter by 5 in. in length.

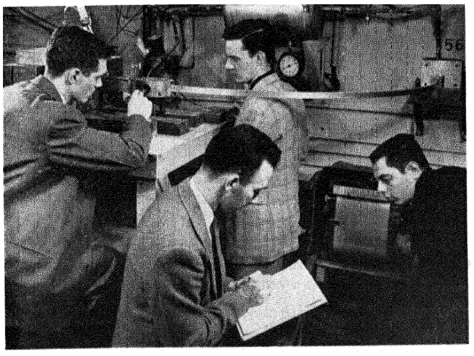

Figure 13. The external parts of the fast pneumatic tube

4. Water-Cooled Fast Neutron Exposure Facility—Hole 51-North

Operated by—Solid State Division
Neutron fluxes:
Thermal—5.5 × 10^{11} n/cm²-sec
Fast—8 × 10^{11} n/cm²-sec
Gamma—5 × 10^5 r/hr
Temperature in exposure chamber—~25°C

The fast neutron source is a water-cooled hollow cylinder made of aluminum-clad, enriched uranium-aluminum alloy. The maximum sample size is 1½-in. diameter by 11 inches long. Samples are inserted and removed by a chain conveyor.

5. Water-Cooled Horizontal Exposure Facility—Hole 19

Operated by—Solid State Division
Thermal neutron flux—8.5 × 10^{11} n/cm²-sec
Gamma—7 × 10^5 r/hr
Temperature in exposure chamber—~30°C
Maximum sample size—1¼-in. diameter × 8 inches long

Samples are inserted and removed by water pressure and are cooled by water flow.

6. Vertical Water-Cooled Facility—Hole 10

Operated by—Reactor Operations Department for general usage by all research divisions and radioisotope production.
Thermal neutron flux—7 × 10^{11} n/cm²-sec
Gamma—5.7 × 10^5 r/hr
Temperature in exposure chamber—30°C (controlled)
Maximum sample size—2½-in. diameter × 1 foot long

Samples for short exposure are tied onto waxed linen cords. Long exposures are done in aluminum cans with upright bails which are lowered to the bottom and retrieved with grappling hooks. Reactor shutdown is not required for insertion or removal. Samples are stored in six-place rotating magazine shield over hole.

7. Fast Pneumatic Tube—Hole 56-North (see Fig. 13)

Operated by—Physics Division
Thermal neutron flux—3.6 × 10^{11} n/cm²-sec
Gamma—3 × 10^5 r/hr
Temperature of exposure chamber—~50°C
Maximum sample size—5/16-in. thick by 13/16-in. wide by 1¼-in. long

Samples are inserted into and removed from the reactor by CO_2 pressure. Exposure time can be less than one second. Removal time is less than one second. Equipment operates automatically, exposure being controlled by timing mechanism.

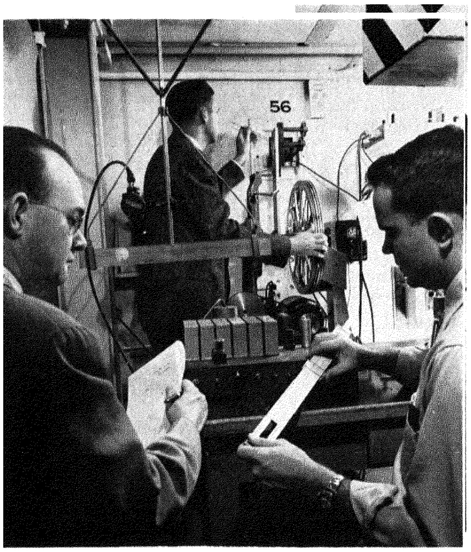

Figure 14. The oscillator used in making neutron absorption measurements. The drive mechanism was made from a washing machine

8. General Usage Pneumatic Tubes—Hole 22-South

Operated by—Reactor Operations Division for use by all research divisions and for radioisotope production.

Thermal neutron flux—6.5×10^{11} n/cm²-sec

Gamma—$\sim 5 \times 10^6$ r/hr

Temperature of exposure chamber ~80°C

Maximum sample size:

Large tube—¾-in. diameter × 2¼-in. long.

Small tube—7/16-in. diameter × 2-in. long.

Ordinarily samples are discharged to a storage shield to await pickup. Samples from the large tube can also be made to travel through a shielded tube to a laboratory room for quick analyses. Samples are inserted into and removed from the reactor by CO_2 pressure.

9. Fuel Channel Pneumatic Tube—Channel 2079

Operated by—Reactor Operations Department for use by all research divisions and for radioisotope production.

Thermal neutron flux—5.5×10^{11} n/cm²-sec.

Gamma—$\sim 4.5 \times 10^6$ r/hr

Temperature of exposure chamber—~50°C

Maximum sample size—⅞-in. diameter × 3⅜-in. long.

This tube utilizes one of the two fuel channels that were made unusable for fuel by removal of a multiple fuel rupture. Access is through a hole drilled through the concrete shield opposite the charging face. Samples are inserted and removed by CO_2 pressure and stored in a eight-place magazine shield.

10. Oscillator—Hole 56-South (see Fig. 14)

Operated by—Physics Division

This facility is a four-in. square hole which contains a boron-coated ionization chamber beside which a small beryllium oxide boat containing a specimen can be oscillated. The current through the ionization chamber will be inversely proportional to the neutron absorption of the specimen. By oscillating the specimen, a wave-form voltage change will be introduced in the circuit whose amplitude will be proportional to the neutron absorption cross section. By using some material whose cross section is well known, such as gold, for a standard, the neutron absorption cross section of any material may be determined.

11. Stringer Holes—Hole 13 and Hole 14 (see Fig. 15)

Operated by—Reactor Operations Department for use by all research divisions and for radioisotope production.

Thermal neutron flux—1×10^{11} to 9×10^{11} n/cm²-sec

Gamma—10^4 to 8×10^6 r/hr.

Temperature in exposure regions—~35°C to ~160°C

Maximum sample size ¾-in. diameter by 3 in. long

These facilities are stringers or trains of connected 4-ft long graphite trays that extend all the way through two 4-in.- square horizontal holes. Each tray accommodates 36 targets and the two holes accommodate a total of 389 targets. Reactor shutdown is required for removal or insertion of materials, so the minimum exposure time is one week.

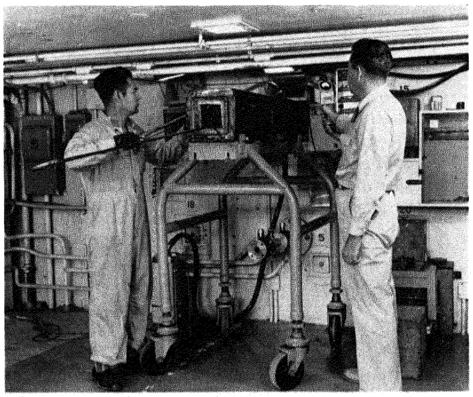

Figure 15. A view of operators removing radioisotope targets from a "stringer" hole. Notice the vacuum cleaner which removes dust from the graphite tray as it is withdrawn from the reactor through a lead shield

12. "Doughnut" Holes—Fuel Channels 1768, 1867, and 1968 (see Fig. 16)

Operated by—Either the research divisions or by the Reactor Operations Department depending upon the material inserted.

Neutron fluxes:
  Thermal—4 × 10^{11} n/cm²-sec
  Fast—2.2 × 10^{11} n/cm²-sec, > 0.5 Mev
Temperature in exposure chamber—~40°C
Maximum sample size—½ in. diameter × 11 in. long

These are fuel channels in the center of the core region which each contain seven 4-in. long hollow aluminum-clad normal uranium cylinders. Targets are tied to either iron or aluminum wires of measured length to center them in the uranium. Removal is accomplished by winding the wire up on a shielded windlass. Reactor shutdown is required for removal or insertion.

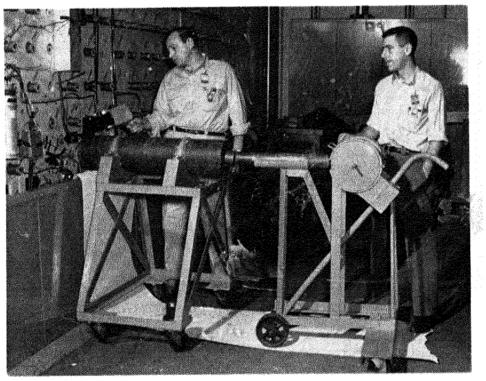

Figure 16. Research sample being removed from a charging face hole. The specimen is pulled into a shield by an attached wire which is rolled up on a lead-shielded windlass

13. Vertical Thermal Column (see Fig. 17)

Operated by—Primarily the Physics Division with minor use by other divisions.
Neutron Fluxes:
  Thermal—7 × 10^{7} n/cm²-sec at top of column.
  Fast—negligible
  In-Cd ratio—~10^{6}
Gamma—~135 r/hr at top of column
Average gamma energy—~3 Mev
Temperature—Room temperature at top of column.

This thermal column is a stack of graphite blocks in a 5-ft square (at the bottom) hole through the roof of the reactor shield centered over the reactor core. The top is shielded by a 5-ft square tank of water with lead and cadmium around the sides. Materials to be irradiated or radiation shield configurations to be tested are lowered through the water to the bottom of the tank.

14. Horizontal Thermal Column—Opposite Fuel Charging Side (see Fig. 18)

Operated by—Physics Division
Neutron Fluxes:
  Thermal—5 × 10^{9} n/cm²-sec
  Fast—In-Cd ratio is 130
Gamma—1.2 × 10^{4} r/hr
Temperature—Room temperature

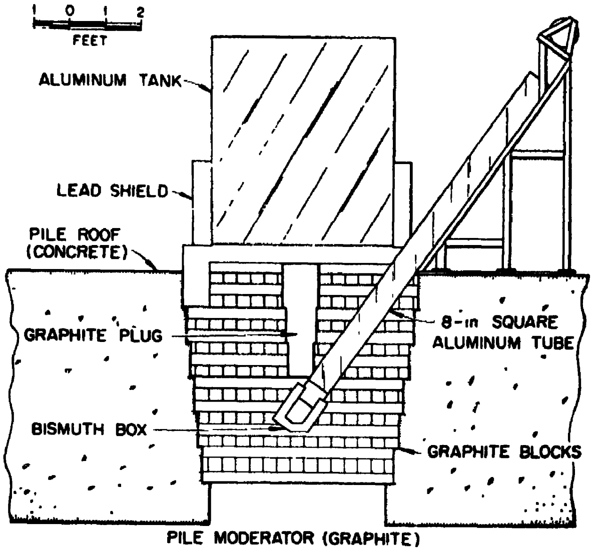

Figure 17. A sectional sketch of the vertical thermal column showing the inclined biological tunnel

This thermal column opening is not used as a thermal column but as a lid tank for shielding tests. The opening through the reactor shield contains a 2-S aluminum tank which can be filled with water to act as a radiation shutter. A concrete-shielded water tank just outside the hole normally acts as the biological shield when the shutter tank is empty. Shielding configurations are built up in the outer tank and checked for attenuation efficiency.

15. Inclined Biological Tunnel (see Fig. 17)

Operated by—Biology Division and Reactor Operations Department
Neutron Fluxes:
  Thermal—1 × 10^{9} n/cm²-sec
  Fast—negligible
  In-Cd ratio—10^{5}
  Gamma—360 r/hr
Temperature—Room temperature
Maximum specimen size—7 in. × 3 in. × 3 in.

This biological tunnel was built in order to lower the gamma to neutron ratio for biological exposures beyond the value of the facilities built into the reactor shield. It is a slanted shield plug through the graphite in the thermal column and the exposure chamber is enclosed with a 4-in. thick layer of bismuth metal. Specimens are put into a graphite box which is affixed to the lower end of the tunnel. Movement of the plug is done by a hoist.

16 Lead-Lined Biological Tunnel

Operated by—Biology Division and Reactor Operations Department
Neutron Fluxes:
  Thermal—1.3 × 10^{9} n/cm²-sec
  Fast—Mn-Cd ratio is 70
Gamma—200 r/hr
Temperature—~25°C
Maximum specimen size—24 in. long × 12 in. wide × 10 in. high.

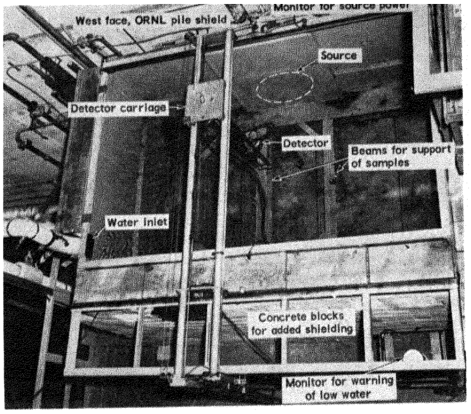
West face, ORNL pile shield
Monitor for source power
Source
Detector carriage
Detector
Beams for support of samples
Water inlet
Concrete blocks for added shielding
Monitor for warning of low water

Figure 18. Looking down into the lid tank at the horizontal thermal column opening. An enriched uranium source plate between the tank supplies fast neutrons and shield configurations to be tested are assembled in the outer tank

This biological tunnel was built into the reactor shielding at the time of construction. It is located in the shield above the reactor so that neutrons and gamma radiation entering it come primarily through the bottom of the exposure chamber and are filtered through a 4-in.-thick layer of lead. A ventilating system pulls fresh air from outside the reactor through the exposure chamber and into the reactor coolant stream. Specimens are rolled into the chamber on trays by means of push rods. A series of three lead gates, only one of which can be opened at a time, shield the operator. A concrete barricade outside the reactor shield provides further protection. Specimens can be inserted and removed while the reactor is operating.

17. Bare Biological Tunnel

Operated by—Biology Division and Reactor Operations Department

Neutron Fluxes:

Thermal –5 × 10^8 n/cm^2-sec

Fast -Mn-Cd ratio is 73

Gamma—∼3400 r/hr

The bare biological tunnel was built into the reactor shielding at the time of construction. It is similar to the lead-lined tunnel in all aspects except for the lead lining. Since it is located farther from the vertical centerline of the reactor than the lead-lined tunnel, its neutron flux is lower.

18. Other Equipment

Other more temporary equipment is built at the experiment openings as desired and frequent exposure of materials or equipment is made inside the 4-in. square holes and in uncharged fuel channels. Some examples are shown in Figs. 19, 20, 21, and 22.

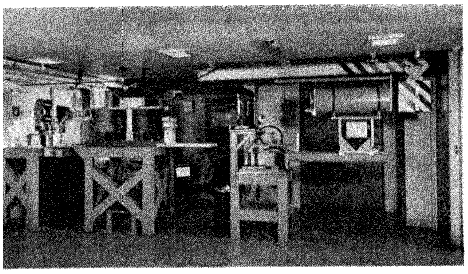

Figure 19. Equipment at a neutron collimator for performing a Stern-Gerlach experiment with neutrons

LOW INTENSITY TESTING REACTOR

The Low Intensity Testing Reactor (LITR) is probably the only operating reactor that was built from left-over test parts. Originally the tank that contains the reactor core was a mock-up assembly for measuring the water flow and mechanical characteristics of the Materials Testing Reactor (MTR) which is now operated at the National Reactor Test Station by the Phillips Petroleum Company for the AEC (see Fig. 23). Since this installation was not intended to be permanent, all portions of the reactor tank except that surrounding the core were made of ordinary steel. The section containing the core is of 3-S aluminum since tests of actual flow through the coolant shells of actual beam hole thimbles had to be made. The hydraulic tests were completed in 1949 and a mockup of the beryllium reflector to be used in the MTR was built into one quadrant of the core tank with only a minimum thickness of beryllium surrounding the remainder of the core. With this assembly, a criticality test and neutron distribution measurement was made in 1950.

After these tests were completed, the need for a training reactor for the operating personnel of the MTR was recognized and conversion of the test mockup to a low power temporary reactor was completed on March 2, 1951 (see Fig. 24). The maximum power level was to be 500 kilowatts.

The conversion consisted of the following:

1. Painting the inside of the steel portions of the reactor tanks and some external piping to inhibit rusting.

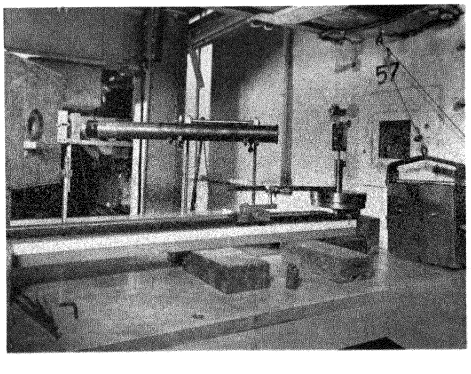

Figure 20. Neutron collimator used by the Oak Ridge School of Reactor Technology (ORSORT) for performing short experiments. The setup shown is for an experiment in the diffraction of neutrons with a crystal

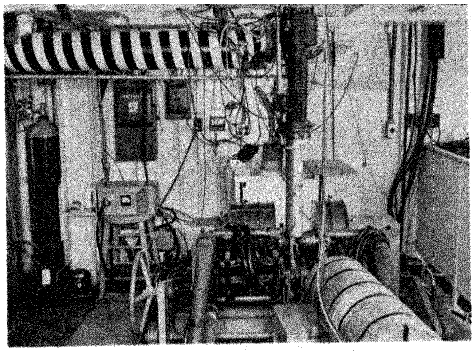

Figure 21. The external-field polarization of In^{115} nuclei. Neutrons from a collimator are polarized by a magnetic field and used to measure the degree of polarization of the In^{115} nuclei

2. Stacking a permanent beryllium reflector held in place by a sheet aluminum housing (Figs. 25 and 26).

3. Providing access holes for the various ionization chambers used for control (Fig. 27).

4. Adding an additional shim-safety rod to the two used for the criticality test.

5. Surrounding the reactor tank with a concrete block shield and extending the beam holes through the shield. Also providing shielding for the holes (Fig. 28).

6. Replacing the 20,000 gallon per minute water system with a smaller one to provide a flow up to 300 gallons per minute and providing a heat exchanger.

7. Enclosing two sides and the top of the reactor with rooms for shelter of experiments and operating personnel.

8. Providing a special radioactive waste water disposal system including two retention ponds.

9. Permanentization of the reactor control room and the control instrumentation (Fig. 29).

During the time that the reactor was being used for training, it was seen that conversion to a research and radioisotope producing reactor would require only slight modification and would not be excessively expensive. This further modification included only increasing the cooling capacity and making the shield thicker. This was completed and operation at a power level of 1.5 megawatts began on April 25, 1952. This was raised to 3 megawatts on September 2, 1953, by further thickening the shielding on the exit water line from the reactor.

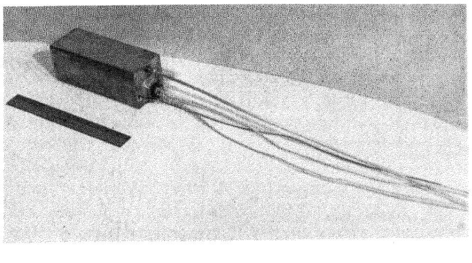

Figure 22. A typical experiment can be used in the 4-inch square holes. Lead wires to furnaces, and thermocouples or other metering devices are brought out of the reactor through serpentine openings through the shield plugs

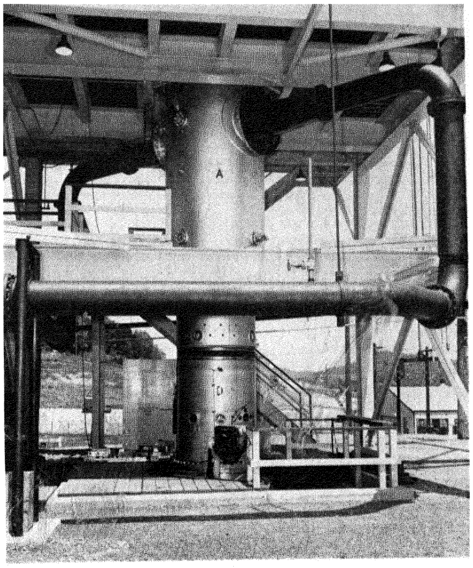

Figure 23. The original bare mockup of the materials testing reactor (MTR) which was later converted to the reactor now known as the low intensity testing reactor (LITR)

The LITR is a heterogeneous light water cooled, light water moderated, beryllium reflected enriched uranium reactor. The size of the core that contains the fuel plates is roughly 2 ft high by 9 in. wide by 2 ft long and contains about 3400 grams of U^{235}. The fuel assemblies are roughly 3-in. square pipes which contain sixteen 24⅝-in. long plates each consisting of a layer of an aluminum and enriched uranium alloy sandwiched between layers of aluminum. Two walls of the pipe are also fuel plates making a total of eighteen plates per element. The total thickness of each plate is about 60 thousandths of an inch. They are separated about a tenth of an inch apart by spacers to allow passage of water for cooling. The water between the plates is also the neutron moderator. The plates are curved laterally on a 5.5-in. radius to strengthen them and to define the direction of thermal deformation.

The shim-safety rods are actually special fuel elements. Their total length is 13 ft 7½ in. The lowermost section is made of stainless steel to provide weight and to withstand the impact of hitting the shock absorber when the rod falls. The bottom end is cylindrical and acts as a piston in the water-filled shock absorber shell to lessen the force of impact upon the bottom of the tank. Above the stainless steel portion is an aluminum section containing fuel

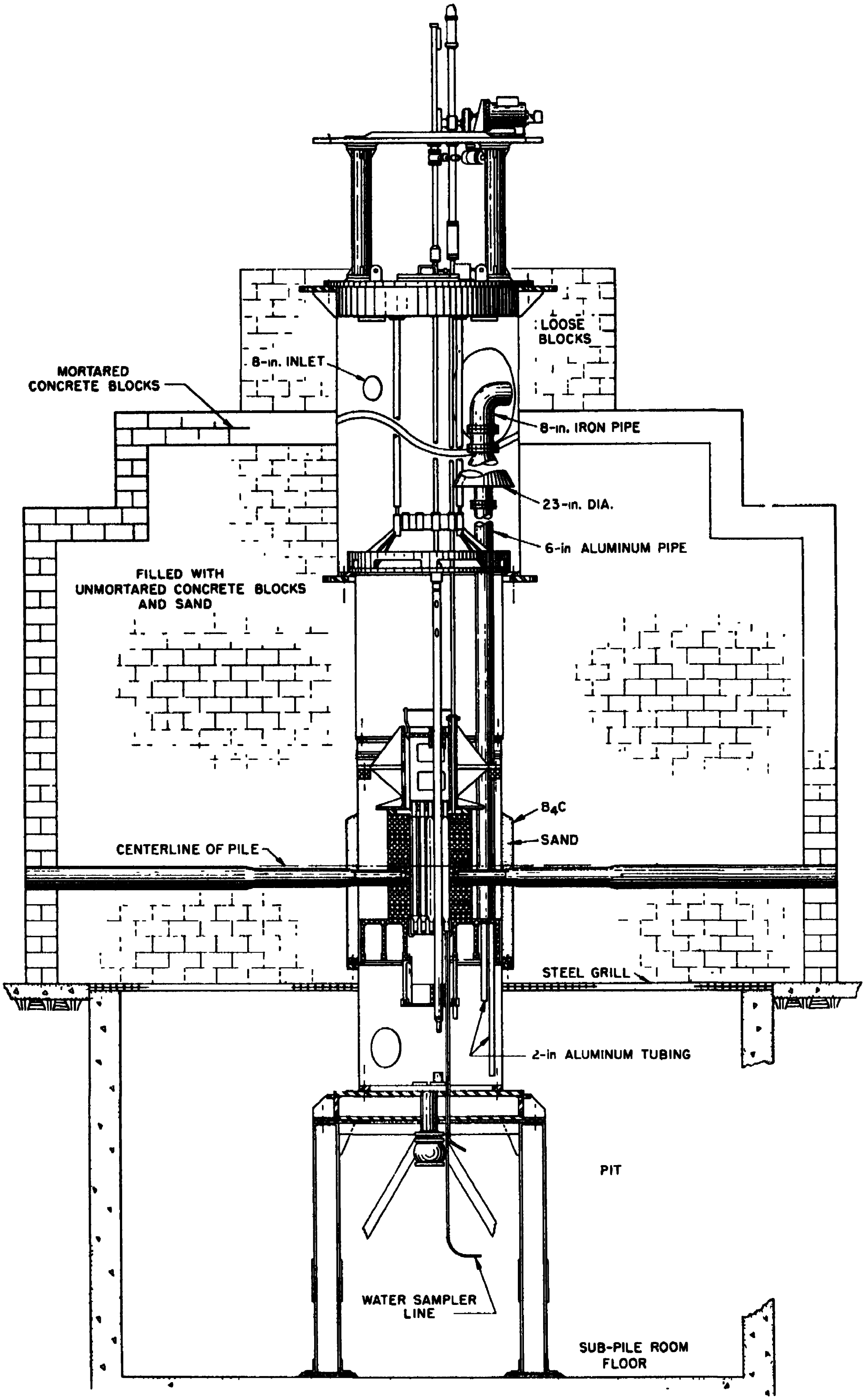

Figure 24. Sectional drawing of the LITR showing the reactor tank, core, beam holes, shielding and internal water lines

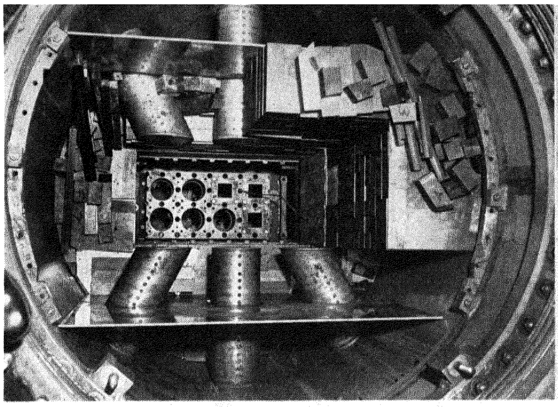

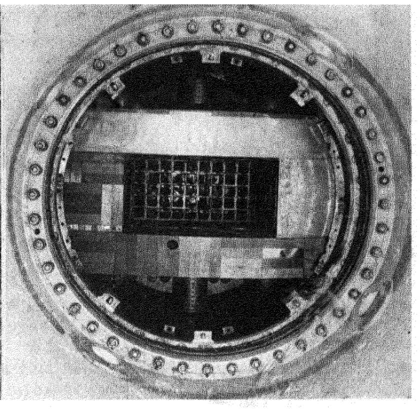

Figure 25. (Left) A view of the LITR core space with the permanent beryllium being stacked around the beam hole thimbles
Figure 26. (Right) A view of the LITR core space with the stacked beryllium in place prior to being covered with the sheet aluminum housing

plates. The fuel plates are in the core when the rod is fully withdrawn into the operating position. Immediately above the fuel plates is a shell of cadmium metal sheathed with aluminum. The cadmium is in the core when the rod is in the down position. Above the cadmium is a further extension of the aluminum section and the top of the rod is a nickel-plated steel block mounted on a spring-loaded ball and socket joint which is keyed to limit its movement to tilting only. This steel top allows the rod to be lifted by an electromagnet which hangs from the top cover of the tank on a drive shaft. Above the cadmium section and below the fuel section there are slots in each of the four sides. These eight slots are about 12-in. long and about 1-in. wide. Their purpose is to allow water to flow over the cadmium and fuel.

The regulating rod used by the automatic control is a hollow-diameter cylindrical shell that contains strips of cadmium metal between two layers of aluminum. It does not enter the core but operates in the reflector.

The reactor tank which is 26 ft $9\frac{13}{16}$ in. high is actually five hollow cylinders stacked to form a single tank. The two top sections are carbon steel. The next section is a stainless steel expansion ring. Next is a 3-S aluminum section which contains the beam hole thimbles and encloses the reactor core. Last is another carbon steel tank. The bottom of the tank is a hollow carbon steel disc which in the MTR contains lead for shielding but in the LITR is empty. The tank is supported both at the bottom and top by steel beams and thermal expansion is absorbed by the expansion ring.

The support for the core and reflector is an aluminum casting which is anchored to the tank wall. Centered in the casting is a removable 45-place grid that supports the bottom of the fuel elements and removable beryllium pieces. Eight of the 45 holes in the grid are large enough for the shim-safety rods to pass through. All but three of these are narrowed with adapters to hold the bottoms of fuel elements or beryllium pieces. Hanging below this grid is a bearing support for the shim-safety rods. Shock absorbers for the rods sit upon the bottom of the tank. A permanently stacked beryllium reflector made up of beryllium blocks whose maximum size is 2 in. by 2 in. by 8 in. is built up around the core to a height of 41 in. and enclosed on all sides by an aluminum housing. The minimum thickness of this stacked

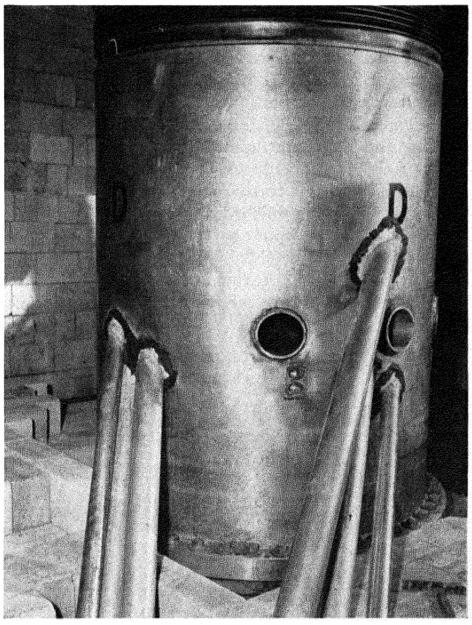

Figure 27. The ionization chamber access tubes before being covered with shielding

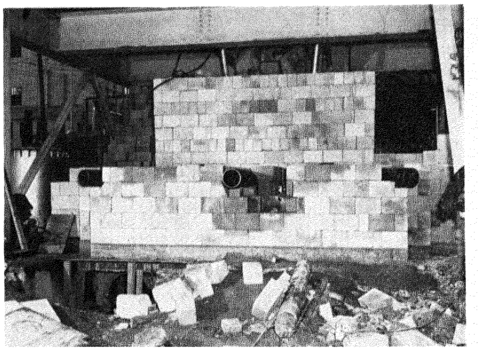

Figure 28. The stacking of the unmortared concrete block shielding. The large pipes are the beam hole tubes

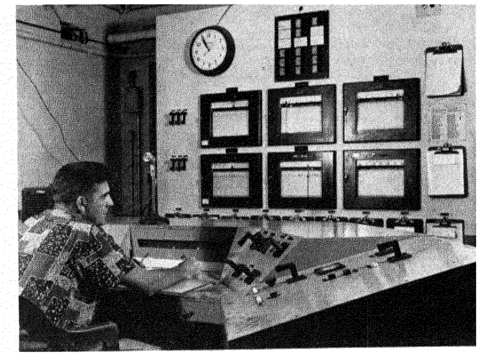

Figure 29. The LITR control console; the power level recorders are behind the console

beryllium is 8 in. and occurs on the sides where the beam holes enter. It is formed around the beam hole thimbles which terminate at the core itself (Fig. 25). Since no provision was made for forced cooling of the beryllium in the stacking, the power level is limited to the present 3 megawatt level because of nuclear heating in this region which is about 0.4 watt per gram at 3 megawatt power level. At the ends of the core the stacked beryllium goes to the tank wall itself to provide a better path for neutrons to the ionization chamber thimbles which are terminated outside the tank wall. This beryllium contains two vertical holes to accommodate regulating rods used by the automatic power control. Only one of these holes is used for this purpose. The other is used for exposure of targets.

A second grid assembly fits over the tops of the fuel elements to further assure their being vertically aligned and holds the upper bearings for the shim-safety rods. This grid assembly must be removed in order to have access to the core for fuel replenishing. Figure 30 shows the finished core as it was for 500 kw operation with the upper assembly of grids removed and suspended at one side of the tank.

The hollow, flanged carbon steel disc known as the top plug which fits into the top of the tank to form a water seal also serves as a support for drive motors and shafts for the shim-safety rods and the regulating or control rod (see Fig. 31). Four support columns hold a horizontal steel frame below the top plug. This frame contains guide bearings for the rod shafts. At the corners of the frame are sockets which fit over aligning pins anchored to a heavy steel ring which in turn, is anchored to the flanged junction of the top tank and the smaller tank immediately under it. The guide frame is spring mounted on the columns from the top plug so that actual aligning is done by the aligning pins in the tank. Four upright columns on the top plug support a platform upon which are mounted two of the shim-safety rod drive motors and the drive motor for the regulating rod. The third shim-safety rod drive motor which is not standard is mounted upon the top plug itself and requires a gear train to approximate the drive speed of the other two.

The shield around the reactor tank is built up of unmortared concrete blocks (see Fig. 28) except for the outermost 1 foot layer which is of mortared concrete block covered with a layer of smooth concrete stucco. The minimum thickness is 10½ feet. All cracks in the unmortared block are filled with sand. A layer of boron-carbide impregnated plastic was spaced at a 3-in. distance around the core tank and the

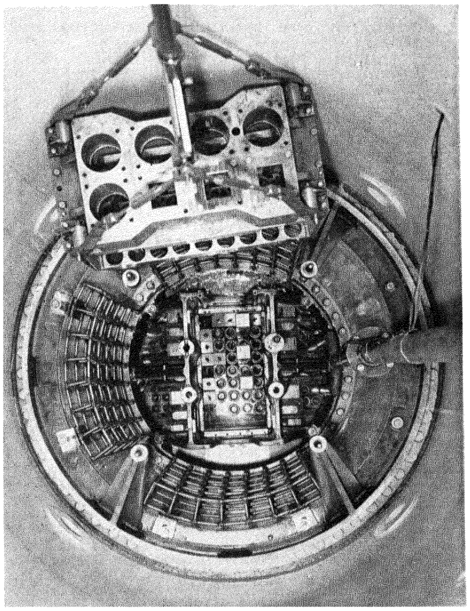

Figure 30. Looking down into the reactor tank as assembled for 500 kw operation. The return water line from the bottom section is now 8 inches in diameter. The upper assembly of grids hangs from a bracket at top of the tank. The shaft it hangs by is a removable handling tool

3-in. space was filled with sand. The plastic has been destroyed by radiation leaving a layer of boron and carbon. The boron reduces the number of capture gammas born in the shield. Radiation through the shield in the beam hole rooms is less than 5 mr/hr at full power.

The water cooling system has a total volume of about 13,000 gallons. Usually only 10,000 gallons is used. About 4000 gallons is in the reactor tank, and another 4000 gallons is in a 7000-gallon tank in series with the reactor. This second tank serves as a reservoir, a degassing tank, and a hold-up tank to allow decay of short-lived radioactivities such as N^{16}. The remaining 2000 gallons is in the lines, heat-exchangers, pumps, strainers, filter, and demineralizer. The water is recirculated through the system at a rate of 1200 gallons per minute and no purging is done except in unusual circumstances.

Two 75-horsepower 1500-gpm electrically driven centrifugal pumps are used to circulate the water. Only one pump is used at a time and the other is kept in standby. In order to know that they are in working order they are used alternately for about one week periods. These pumps have stainless steel impellers and cast carbon steel housings.

Two water to air heat exchangers remove the heat from the water (see Fig. 32). These are made up of banks of finned aluminum tubes over which air is blown by propellers operated by 40- and 10-horsepower two-speed electric motors. They were designed to dissipate 2 megawatts of heat during the hot summer days (90°F), so a water-to-water shell and tube heat exchanger must be used during the summer to remove the other 1 megawatt at the present power level. The shell and tube heat exchanger is used during very cold weather to add heat to the system during shutdowns to prevent freezing. This is done by passing steam through the shell.

Since all the piping in the system is mostly either aluminum or carbon steel, enough iron hydroxide and aluminum hydroxide builds up in the water to impair visibility through the 20 feet of water in the reactor tank so that shutdown work in this region (fuel renewal, etc.) becomes very difficult. Originally the water was purged during every shutdown to improve clarity. The installation of a cellulose fiber bypass filter has completely eliminated the water clarity difficulty and actually provided greater visibility than was possible with the purging technique. Up to 400 gallons per minute can be bypassed through the filter. The life of the filter media is 6 to 8 weeks; then it begins to disintegrate. A lucite viewing plate is provided in the filter housing so that the beginning of disintegration can be seen and the media changed before it becomes distributed through the cooling system.

In order to minimize corrosion of the aluminum parts of the reactor, the pH of the water must be maintained between 5.5 and 6.5 and the specific resistance greater than 250,000 ohms. These conditions are maintained by use of a bypass demineralizer which is a system of three ion exchange resin columns capable of handling a flow of 14 gallons per minute. The three columns are in series. The first is a cation exchanger and the second is an anion exchanger, the purpose of these two being to remove most of the foreign materials from the water. The third column is a mixed bed unit which further dresses up the water and has an effluent of better than 2,000,000 ohms specific resistance. In removing ions from the water, the columns remove practically all the radioactivity from the water and thus minimize shielding for the system. The reason for not using only a mixed bed unit is that

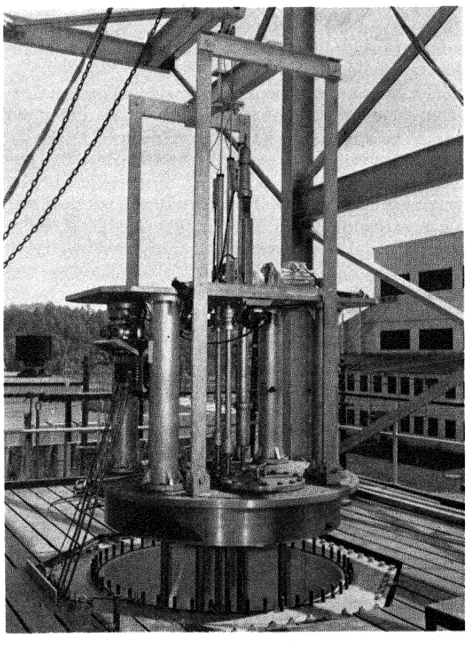

Figure 31. A view of the top plug partially elevated. The lead wires to the shim rod and regulating rod drives are still connected. This area is now enclosed

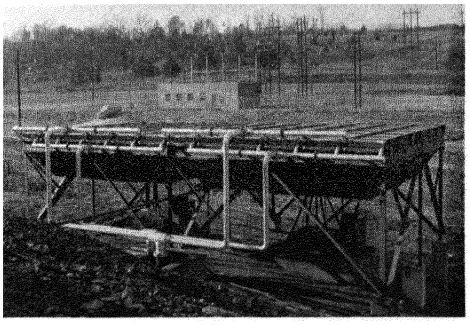

Figure 32. The water-to-air heat exchangers used for removing heat from the reactor cooling water

the anion exchange resin is more subject to radiation damage than the cation. By using separate primary columns, which are easily replaced, or regenerated, the life of the mixed bed resins is much prolonged with respect to regeneration and especially with respect to radiation damage to the anion component of the mixed bed. The water flow through the demineralizer is from the exit line from the air-water heat exchangers to the suction side of the circulating pumps.

Where the water lines pass through areas frequented by personnel, they are shielded by either lead or barytes concrete blocks.

The path of the water through the system is thus: Beginning at the storage tank it moves to the pump and all but the 200 to 400 gallons per minute which goes to the filter goes on through the water-to-air heat exchangers. The portion that goes through the filter bypasses the heat exchangers. After passing through the water-to-air heat exchangers all the water goes through a strainer and part or all can be passed through the shell-and-tube heat exchanger. From this point 14 gallons per minute is bled to the demineralizer and returns to the low suction side of the pump. After the shell and tube heat exchanger all the water collects into one 8-in. diameter aluminum pipe and rises to the top of the reactor tank. Just before it reaches the tank it passes a radiation monitor which shows a measure of the radioactivity of the water on a recorder in the control room. The orifice for measuring the water flow is also in this region. The water then enters the top of the reactor tank and flows downward through the core. Below the core it enters the exit water line which rises inside the tank beside the core and emerges from the tank near the top. This arrangement makes a "U" trap of the reactor tank itself and limits the amount of water that can be lost from the tank in the event of an external leak. From the top of the reactor tank the exit water line descends directly to the storage tank.

Instrumentation for the reactor controls and safeguards uses the signals from four ionization chambers and a fission chamber. When the reactor is just being started up, the neutron flux in the region where the chambers are located is very low and must be monitored by the fission chamber. This is a small counter tube whose inside surface is plated with uranium enriched in U^{235}. In order to keep the fission rate in the chamber in the range of the counter circuit, the chamber is mounted on a chain drive by which it can be moved farther from the reactor core as the neutron flux increases. The counting rate recorder contains contacts that require that it be showing at least two counts per second but not be off scale in order for the shim-safety rods to be moved upward from the core. During the time that the fission chamber counter is the only instrument showing a reading, the shim rod drive mechanism is limited by a timer so that the drive can be on only one second out of four.

The next instruments that begin reading as the neutron flux increases are what are known as the Log N meter and the period meter. The Log N recorder has a logarithmic scale and becomes operative when the power level is only 1/1,000,000 of the maximum power level. The period meter shows the rate of rise of the Log N. The signal to this instrumentation is from a gamma-compensated boron-coated ionization chamber which can be adjusted only during reactor shutdown. Startup limitations are imposed by both the period and the Log N meters. The period meter limits initial startup rate to greater than a 30-second period during simultaneous withdrawal of the shim rods. A period as short as 7 seconds is allowed for single rod withdrawal, and a 5-second period causes automatic insertion of the rods by the drive. A one-second period causes the magnets to release the rods allowing them to fall into shutdown position. The Log N recorder contains contacts which drop out restrictions and add others as the power level increases. At 1/1,000,000 of full power, it gives permission to continuously withdraw all three rods simultaneously and then requires that this permission be relinquished between $\frac{1}{1000}$ and $\frac{1}{100}$ of full power. It also requires that the period be longer than 30 seconds when $\frac{3}{100}$ of full power is reached in manual operation or that the automatic control has begun operating if in automatic; otherwise a reversal of the rod drive is initiated. It also requires that the power level be greater than $\frac{1}{100}$ of full power when automatic control begins operating; otherwise the input demand to raise the power by the automatic control cannot be increased. When the reactor power falls below $\frac{1}{1000}$ of full power in the event of a shutdown, a contact on the Log N resets the automatic control demand to $\frac{1}{100}$ of full power to prepare for startup.

The automatic control ionization chamber is not gamma compensated so it is not used until the power level is at least $\frac{1}{100}$ of full power. As soon as its output is greater than a set bias, it becomes effective and the automatic control takes over. This is set to occur at $\frac{1}{100}$ of full power. This chamber is boron-coated for neutron detection and is not capable of being adjusted, position wise, unless the reactor is shut down. The automatic control instrumentation uses the regulating rod to either raise or lower the reactor power so that the chamber output balances an input demand signal. The regulating rod is limited to 0.25 per cent $\Delta k/k$ and cannot initiate an unsafe condition. If a positive period develops in the reactor that cannot be handled by the regulating rod, the control instruments insert the shim rods. The reverse condition cannot happen, i.e., the instruments cannot initiate withdrawal of the shim rods. In order to keep the regulating rod in its most effective position, half inserted, the operator must make small infrequent adjustments of shim rod position.

Two identical power monitors are used for power levels above 1 per cent of full power. These take signals from boron-coated non-gamma-compensated ionization chambers which can be adjusted only during reactor shutdown. These chambers give signals to two linear recorders which show the power level from 1 per cent to 150 per cent of full power. On each recorder

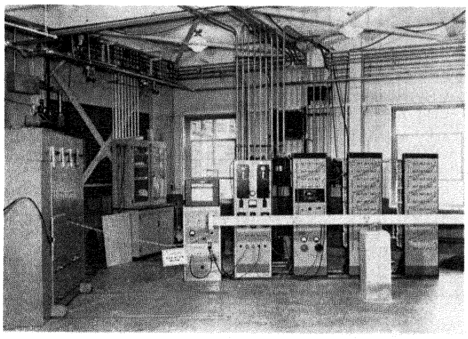

Figure 33. The chopper type neutron velocity selector used for cross-section measurements in the *dE/E* neutron region. The beam strength for these neutrons is 2×10^{12} n/cm^2-sec

are contacts which cause a slow reduction of power by way of the automatic control if the reading exceeds 110 per cent of full power and a fast reduction by shim-safety rod insertion if 120 per cent is exceeded. The output from these chambers is also fed to the magnet power control and causes a reduction in magnet current as the power level increases. At 145 per cent of full power, the magnet current is sufficiently reduced to cause the magnets to release the rods to cause a full shutdown of the reactor. This is the same system that the period meter operates through to cause a scram at a 1-second period.

The temperature differential to determine power by heat output is measured by thermocouples in wells in the inlet and exit water lines to the reactor. The water flow measurement for this determination is measured by a calibrated manometer across an orifice in the inlet water line. All other instrumentation is calibrated from the heat output.

Other instrumentation includes monitoring or provisions for monitoring the following: (1) radioactivity of the inlet water line, (2) radioactivity and temperature of the effluent from individual fuel elements, (3) pH and specific conductivity of the water system and of the effluent from the demineralizer, (4) power load on the pumps and heat exchanger blowers.

EXPERIMENT FACILITIES IN THE LITR

The experiment openings and core spaces in the LITR are similar to but less in number than those of the MTR. Six horizontal beam holes with internal thermal neutron fluxes ranging from 8×10^{12} to 3×10^{13} n/cm^2-sec go through the concrete shield and up to the core within the tank as shown in Fig. 25. These have an internal diameter of 6 inches for the portion within the reactor tank and change to 7 inches and then 8 inches in diameter in going outward to provide for stepped shield plugs to minimize radiation streaming along the plugs. The beam holes are used primarily for the exposure of materials, either static as in the case of crystal damage or dynamic as in the case of circulating loops of homogeneous reactor fuels. One beam hole is more or less permanently occupied by a chopper-type neutron velocity selector used for cross section measurements as shown in Fig. 33 while the other beam holes are devoted to less permanent usages. Figures 34 and 35 show the method used to remove shield plugs from beam holes. The wide "T" handle on the tool is provided to allow the operators to stand outside the beam from the hole as the plugs are removed. Two horizontal pneumatic tubes are available which can accommodate samples up to $\frac{3}{8}$-in. in diameter by $1\frac{7}{8}$-in. long.

In the core some of the removable beryllium pieces can be replaced with experiment equipment if the neutron absorption by the experiment is not excessive. In the spaces which correspond to shim-safety rod positions in the MTR but are not used as such in the LITR, access tubes can be inserted through the unused shim-safety rod holes in the top plug and on into hollow beryllium pieces in the core. These provide for irradiating small targets or pieces of equipment in thermal neutron fluxes up to 4×10^{13} n/cm^2-sec. Three removable beryllium pieces have been replaced with vertical trays made of a magnesium-aluminum alloy to provide multiple spaces for irradiating small targets in thermal neutron fluxes up to 2×10^{13} n/cm^2-sec. Four $3\frac{3}{8}$-in. diameter vertical holes outside the reactor tank provide up to only 4×10^{11} n/cm^2-sec and are used primarily for ionization chamber development.

Experiments performed in the LITR require more rigid instrument monitoring than those in the Graphite Reactor because of the nuclear heat damage in the event of loss of coolant to the experiment equipment. This generally involves an automatic power reduction or shutdown of the reactor. For this reason, practically

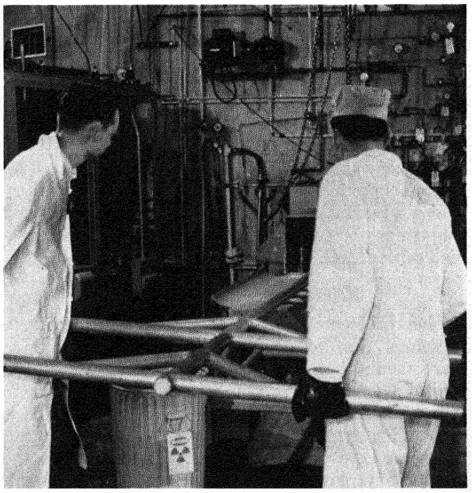

Figure 34. A view of operators removing a beam hole shield plug. The wide "T" handles on the tool permit the operators to stand outside the radiation beam from the hole

all experiments other than simple target irradiations in the water-cooled core must be equipped to send automatic signals to the reactor safety circuits in the event of excessive heat or other undesirable condition.

Operation of this reactor has for the most part been uneventful as far as the reactor behavior itself is concerned. The instrumentation has performed as designed and the control system has operated as planned. Only the usual types of instrument failures have occurred such as broken or shorted wires, tube burnout, and relay failure. Duplication of necessary functions in the instrumentation and fail-safe features have, however, prevented these from being serious.

The only really perplexing problem arose during operation at the 1000 kw power level early in the life of the reactor. This was the appearance of bubbles rising out of the core accompanied by minor power fluctuations. It was finally discovered that the water circulating pump then in use was designed to be an acid pump and was built to draw air in through the shaft seals to prevent loss of acid. This air dissolved into the water and was released as bubbles when the water was heated in passing through the core. Since the flow rate was only 300 gallons per minute, its velocity through the core was not sufficient to prevent the bubbles from rising countercurrent to the flow and causing the power fluctuations.

Reactors of this type lose fission product gases to the water from pores in the fuel element plates when operated at high powers. This does not cause a serious problem but does require that the top of the water storage tank be connected to the off-gas system since this is the only place in the system where gas can collect. Also a small amount of the water is dissociated when passing through the core and would cause an explosive mixture of hydrogen and oxygen to collect in the top of the storage tank if it were not continuously purged.

Two other lower power reactors of the LITR type are being operated as sources for shielding studies by the Physics Division. These, however, are not general purpose reactors and are usually not available for uses by other research divisions.

The Geneva Conference Reactor being operated by personnel from the Oak Ridge National Laboratory is also a reactor of this type. It, however, relies upon convection for coolant flow and cannot operate at a high power level.

CONTAMINATION CONTROL

The problems involving radiation hazards to personnel are, of course, common to both these reactors and are present where any reactor, particularly a research reactor is operated. Where there is frequent removal of materials from a reactor it is very difficult to prevent some contamination spread and some exposure of personnel to radiation.

At the graphite reactor it has been found necessary to carefully wipe all handling tools with moist cloths as they are withdrawn from experiment holes or fuel channels. Tools or pieces of equipment that cannot be wiped are drawn past a vacuum opening to remove any particles that might have been picked up within the reactor (Fig. 15). Every tool removed from the reactor is placed on paper spread upon the floor.

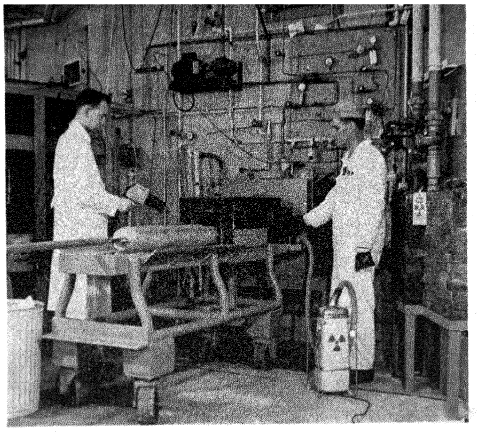

Figure 35. Lead shield for the beam hole shield plugs. The vacuum cleaner is used throughout any removal of plugs or experiment pieces to clean up radioactive dust

At the LITR it is in most cases impossible to use the wiping technique due to the high radiation coming from any open beam hole (up to 100 r/hr) until the tools have been removed to one side. For this reason they must be carefully handled and laid upon paper until they have been decontaminated. The inside of beam holes at the LITR are not subject to an internal suction as the ones at the graphite reactor are except for the outer one foot so when a shield plug is pushed into a hole too fast, radioactive dust is blown out by the expelled air. Vacuum cleaners and suction lines from the off-gas system are used as much as possible to minimize this condition.

After any work is performed at any beam hole in either reactor or at the fuel channels in the graphite reactor, the area is carefully cleaned by mopping and thoroughly checked by radiation detecting instruments. This is in addition to the continuous radiation monitoring that is always done while any such work is in progress.

At the top of the LITR during work in the core, long handling tools, shields, and submarine lights must be frequently inserted and removed. Since the water in the reactor is radioactive, all these items must be rinsed with fresh demineralized water as they are withdrawn.

In order to keep down the spread of radioactive dust that is not concentrated enough or not radioactive enough to be read with portable radiation detection equipment, two procedures are used. One is the use of the smear technique in which small areas (about 100 cm^2) are rubbed with a piece of absorbent paper about 1½ in. in diameter and the paper counted by standard beta-gamma and alpha counters. The other method is the use of X-ray films which are taped to surfaces and take radioautographs of radioactive particles. The use of the films shows the presence of imbedded particles which cannot be found by the smear technique.

In order to guard against the exposure of personnel to radiation without their knowledge, it has been found unwise to rely upon the voluntary warning from personnel handling radioactive materials, so radiation monitoring instruments that sound a loud alarm bell when the radiation exceeds 7½ mr/hr are located in or near all work areas in the reactor buildings. Constantly operating air activity monitors which sound loud alarms are located about the buildings.

OPERATING AND SERVICE PERSONNEL

The Reactor Operations Department, a part of the Operations Division, is responsible for the operation and maintaining of the Graphite Reactor and the LITR. In addition to the two reactors, this department also operates a water demineralizer plant, a hydrogen liquefier, and does the handling work for a canal in which most of the radioactive materials from other sites are unloaded and stored. The personnel in the department consist of five technical men, one secretary and twenty non-technical men. The five technical men are the department superintendent, two department supervisors who report to the superintendent, and two day-shift supervisors who report to one of the department supervisors. The other department supervisor serves as liaison between the Reactor Operations Department and the various research groups and aids in the preparation and operation of experiments in the two reactors. Four of the non-technical men are shift foremen and supervise the other non-technical men during 24-hr per day operation. The foremen are in direct charge of the operation of the reactors at all times. Although they have not had formal technical training, they have had sufficient training in the operation of the reactors to be competent in all physical phases of the work.

Repair work and equipment revision is done by the maintenance departments which also service other equipment and buildings.

In order to have standard radiation and contamination control, the personnel that handles the monitoring is also a central service group. These people check all work involving radiation in the reactor buildings or elsewhere to see that personnel do not become exposed to dangerous amounts of radiation and that all radioactive contamination is removed from equipment and work areas.

Research Program and Operating Experience on ANL Reactors

By W. H. McCorkle and W. H. Zinn,* USA

Argonne National Laboratory and its predecessor, the Metallurgical Laboratory of the University of Chicago, have had 13 years of experience using the nuclear reactor as a tool for research. In a brief review, only a few of the techniques which have been developed can be mentioned. Most of the research accomplished directly with the reactor, as distinguished from the use of radioisotopes, has made use of the neutron flux of the reactor and, thus, has not been an application in which the reactor is unique. In most cases, however, the nuclear reactor is superior to any other neutron source because of the magnitude of the neutron flux and because of its steady availability.

GRAPHITE REACTOR

From 1942 until 1954, the original graphite reactor (named Chicago Pile 2, or CP-2) was used continuously. The reactor had no cooling other than leakage of heat from its surface and, therefore, was limited to a continuous power of not more than 10 kw. A catalog of experiments which were performed first with this reactor would be very extensive, but of course as other reactors with higher flux were made available the effectiveness of the low power graphite machine was exceeded in many applications. For some, the usefulness of the graphite reactor remained unique, and the description here will be limited to these experiments.

Danger Coefficients

The graphite reactor has consistently performed well in the so-called danger coefficient experiments. Two applications of this method will be mentioned.

Uranium metal and graphite which are routinely produced for reactor use must have carefully controlled purity. The usual methods of chemical analysis are used by the manufacturers of these special materials to control the quality of their products. In accepting these materials for reactor construction, there has been considerable question regarding the adequacy of the analytical methods, especially for trace amounts of high cross-section elements such as boron. The graphite reactor easily can be arranged to provide a check on representative samples of either graphite or uranium. Stringers of graphite are so arranged that they can be pushed into or out of the reactor and, by substituting the samples to be tested for samples of standard quality and measuring the effect on the reactivity of the reactor, a sensitive test of the purity of the materials is obtained. This use of the reactor has saved a sizable amount in analytical costs and has guaranteed that the materials to be used in reactor construction fully meet the specifications.

A graphite reactor which is not operated at any appreciable power is particularly suitable for such work because adequate volume is available in the core and because of the very great stability of the system. Temperature effects do not disturb the reactivity and the only troublesome perturbation is due to changes in atmospheric pressure. Atmospheric pressure changes can be handled by appropriate corrections to the reactivity measurements or can be entirely eliminated by using a gas-tight container on the reactor and sealing off the test space from the general reactor atmosphere.

The danger coefficient type of measurement also has been made with the graphite reactor to obtain estimates of the long-term reactivity changes in an operating reactor. In this measurement, a fuel element which has had long irradiation is compared for its effect on the reactivity of the graphite reactor with an identical sample which has not received long irradiation. The relative effect on the reactivity of the reactor is interpretable in terms of a substitution of plutonium for U^{235} in the test sample and in terms of the accumulation of fission products in the test sample. Results of this nature are reported in a Geneva Conference Paper by Spinrad, Carter, and Eggler.[1]

Source Intercalibration

The intercalibration of neutron sources is a matter of considerable consequence to experimenters who depend upon the absolute measurement of neutron flux. The history of neutron flux standardization is fairly long but essentially is based upon several neutron sources of the radium-beryllium type whose absolute yield of neutrons has been measured. Frequently it is necessary to intercalibrate such a standardized neutron source with others. The graphite reactor has been very useful for this and has made possible intercalibrations with an accuracy of approximately 1 per cent.[2] This method of intercalibrating the sources is similar to the danger coefficient measurement except that the reactor is made slightly subcritical. The sources are interchanged in a fixed position in the reactor core. The neutron intensity as measured by an ionization chamber which is far distant from the source is directly proportional to the strength of the source. The method works exceptionally well if the sources emit neutrons of the same spectrum; where the spectrum differs markedly, a small correction for neutron energy difference is necessary.

---

* Argonne National Laboratory.

Source for Exponential Experiments

The sub-critical pile or exponential pile method of determining the buckling of various combinations of reactor materials is a well-established experimental technique. The low-power graphite reactor, operated at about 10-kw power, has been a splendid source of neutrons for such experiments. The neutrons are led to the exponential experiment by a thermal column which is part of the top shield of the reactor. At the power indicated, irradiations of about 10 minutes are sufficient to give ample intensity using small indium foils as detectors in the exponential experiment.

HEAVY-WATER REACTORS

Argonne National Laboratory also has had a number of years of experience with heavy water-moderated research reactors. The first of these was placed in operation in 1944 and is briefly described by W. H. Zinn.[3] This reactor had a maximum neutron flux of 10^{12} n/cm^2/sec for the first six years of its existence; by changing from natural uranium fuel elements to enriched uranium fuel elements, its neutron flux was raised to 4×10^{12} n/cm^2/sec for the remaining four years of operation. This reactor was primarily used in two ways. First, there evolved a whole series of experiments in neutron optics; and secondly, the so-called pile oscillator, a natural outgrowth of the danger coefficient techniques, was developed and brought into wide use as a tool for the measurement of absorption cross sections.

Neutron Diffraction

For the study of neutron interactions in the thermal and the resonance regions, a variety of devices which produce a more or less monochromatic beam have been developed. The simplest of these is the filtering technique in which the Bragg reflection of neutrons from the polycrystals of a bar of graphite, for instance, are used to deflect out of the main beam all but the long wave length neutrons. These so-called "cold" neutrons represent the most successful technique evolved so far for measurements in the low energy neutron regions.

The diffraction of neutrons by a single crystal first was demonstrated with the intense collimated beam from the heavy water reactor, and the use of a crystal monochromator for the investigation of neutron resonances is a well-established technique.

Mirror Reflection and Other Neutron Optics Experiments

The highly collimated beam has been used to study the total reflection of neutrons from mirrors, leading to a technique which has been very fruitful in studying the phase of scattering. The use of magnetized mirrors has opened up a considerable area of research, as has the polarization of a collimated beam of neutrons in a passage through magnetized materials. The neutron-electron interaction has been studied by means of a collimated beam and such beams have been most useful in the study of scattering resonances. A highly collimated beam of neutrons and a pair spectrometer have given important information on the spectrum of capture gamma rays. Examples of the experimental arrangements for typical experiments with neutron beams are included in a subsequent section concerning the present program with the heavy water-moderated, enriched uranium reactor (CP-5).

Pile Oscillator

The oscillator which was used to the greatest extent with the first heavy water reactor (CP-3, CP-3′) has been described by Langsdorf.[4] The apparatus is so arranged that the sample under investigation is moved from a point at the center of the reactor to a point at the edge of the core in a cyclic fashion. The detector, which is a boron-coated ionization chamber, is located at the outside of the reactor tank. The signal from the ionization chamber is measured by a resonant or selective electronic circuit. The absorption cross section of the sample is directly related to the amplitude of the oscillating electrical signal. When used with CP-3, the oscillator had a limit of accuracy of 0.001 cm^2 of thermal absorption cross section. This permitted the detection, for instance, of as little as 25 micrograms of boron. Absorption cross sections of most elements of the periodic table have been measured with this apparatus. Difficulty is encountered only in those elements where moderation or overwhelming scattering enter as disturbing effects.

OPERATING EXPERIENCE WITH THE CP-5 REACTOR

Continued improvement in reactor technology and demands for a higher neutron flux led to the construction of a new, enriched uranium, heavy water-moderated reactor, CP-5. The reactor has been in use a little over one year. No difficulties whatsoever in the normal operation of the reactor have been experienced. The following comments are made to illustrate some of the operating procedures which have been given special attention in order to insure continuous and trouble-free operation.

Excess Reactivity for Operation

The matter of the amount of excess or flexible reactivity which must be available in the reactor in order to permit operation is of importance both from the point of view of the routine control and of safety. The CP-5 reactor requires a maximum of 7 per cent $\Delta k/k$ at 30°C when freshly loaded with fuel. This amount of reactivity is easily controlled with the shim-safety rods of the reactor. This amount of excess reactivity also is not sufficient to lead to any serious trouble if any considerable fraction of it were actually applied to the reactor. This conclusion follows from a study of the effects of excess reactivity on a light water-moderated reactor having fuel plates similar to those used in the CP-5 reactor. The results of the light water study are recorded by J. R. Dietrich.[5] The application of the results of the light water-moderated experiments to the heavy water case involve a calculation of the reactivity coefficient for steam voids in the heavy water reactor. It is easily seen that only a small amount of steam would have to be formed in the fuel elements of CP-5 in order to reduce reactivity by an amount larger than 7 per cent $\Delta k/k$. Because of the long lifetime of the neutrons for the heavy water reactor, the possibility of obtaining a short enough period to damage the fuel plates is considered very remote.

Fuel Handling and Inventory

Fuel elements are removed from the reactor by drawing them upwards through the shield into a lead cask weighing approximately eight tons. They are discharged into pipes placed in concrete below grade. Because of the small number of fuel elements and the infrequent replacement required, the handling of the fuel has been a very simple matter.

The inventory of fuel required to keep the reactor in operation depends somewhat on the cycle of loading fuel in the reactor and sending it to chemical processing. An estimate of the amounts required is included in reference 3.

Heavy-Water Handling

A question of considerable importance in the operation of a research reactor, moderated with heavy water, is the amount of difficulty or effort required to cope with the fact that heavy water is an expensive material. The loss of heavy water can be held to a very low figure. Present experience in the CP-5 reactor indicates that heavy-water losses are essentially nil. A certain consumption of heavy water occurs in deuterating the resin beds which are necessary in order to maintain the purity of the water. For instance, the resin bed (volume = 0.5 ft^3) is quickly exhausted after the initial startup. In CP-5, the first bed had to be replaced in two months. A second bed was exhausted after four months of operation. The third bed, however, has been in operation almost a year and is maintaining conductivity of the water at a satisfactory level of 0.33 micromho. This history indicates that the initial cleanup of the system makes a considerable demand for fresh resin and therefore constitutes a loss of the heavy water which is used for deuterating the resins. The flow rate through the resin column is 4 gpm, which suffices to keep the seven tons of heavy water at a pD value of 6.5. The long-lived activity of the reactor water due to dissolved material, under these circumstances, is almost negligible. Pipes six inches in diameter carrying 1000 gpm directly from the operating reactor show an activity level of 1.5 r/hr at the surface, but this is all short-lived activity associated with oxygen and nitrogen activation. After shutdown of the reactor, it is possible to approach all parts of the cooling system immediately for direct maintenance.

The isotopic quality of the water shows no appreciable deterioration with time. The heavy water was loaded into the reactor and cooling system without special conditioning of the interior surfaces. Initially, the isotopic purity of the heavy water was 99.6 per cent and after one and a half years the isotopic purity is 99.56 per cent. Most of this decrease occurred on the initial loading. In connection with the question of isotopic purity and the loss of heavy water, it is pertinent to cite the experience of the Laboratory in operating the CP-3 reactor over a period of ten years. For a good part of the ten years, the techniques of handling the heavy water, especially in maintaining purity, were not as well developed as they are at the present time. Nevertheless, the heavy water which originally had an isotopic ratio of deuterium to hydrogen of 99.85 per cent had a ratio of 99.65 per cent when it was removed. During all of this time, the heavy water was circulated through a heat exchanger which was cooled by light water. From time to time, the heat exchanger was tested for leaks and those found were repaired. Also, from time to time, leaks which permitted atmospheric air to enter the reactor occurred. Nevertheless, the fact that there has been only this small depreciation in the quality of the heavy water indicates that it is a very easy matter to maintain isotopic purity.

Similarly, it has been possible to take the heavy water once it has been heavily contaminated with dissolved material and clean it up to a point where it fully meets reactor standards, and it has been possible to do this while maintaining continuous operation of the reactor. For instance, at one period, the heavy water in the CP-3 reactor showed a very high accumulation of dissolved material, principally aluminum. The water was purified by continuous distillation and by passing it through ion exchange resins. In the ten years of operation of the CP-3 reactor, the losses due to all causes were less than 1 per cent per year, and this without any extensive precautions to prevent loss and without many of the construction techniques designed to minimize loss which have been incorporated in the design of later heavy-water reactors.

Helium System

In CP-5, the free space above the heavy water in the reactor is pressurized with helium at 2½ inches of water pressure. This helium prevents the free entry of atmospheric air into the reactor when the upper plugs are removed for the insertion of fuel elements or experimental thimbles. The purity of the helium is normally 99 per cent or better and the fact that the acidity of the reactor water is maintained at a pD value of 6.5 indicates that the formation of nitric acid from nitrogen is essentially prevented by the purity of the helium gas. Also, this helium is circulated by means of a blower at the

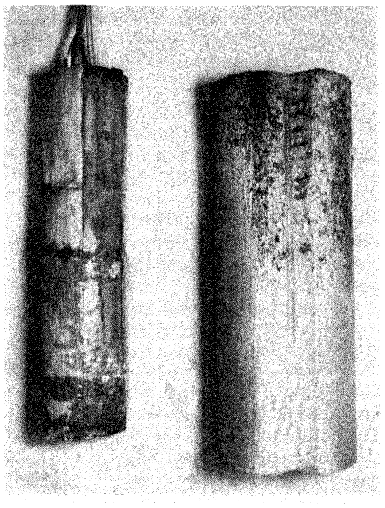

Figure 1. Corrosion of ion chamber in beam hole

rate of 4 cfm through a catalyst chamber for the purpose of recombining any deuterium and oxygen formed by disassociation due to neutron bombardment. At a power level of 1 Mw, deuterium is formed at the rate of 0.02 liter/minute. This small amount of disassociated gas is easily recombined by the catalyst.

Corrosion in Humid Air

The formation of nitric acid by neutron irradiation, while not a problem inside the reactor, has been a matter of concern in the beam holes which enter regions of high flux. Figure 1 is a photograph of an ionization chamber and beam hole plug which were exposed to the reactor radiation while air with high humidity was supplied to the hole. The corrosion of the steel of which the ionization chamber and plug were constructed is extensive. Because of this effect, the work area surrounding the reactor is supplied with conditioned air for which the relative humidity is held to 50 per cent. Where possible, beam hole plugs, collimators, and equipment are constructed of stainless steel or other materials for which corrosion is not to be expected.

RESEARCH PROGRAM WITH CP-5

In the following paragraphs descriptions of a few typical arrangements for experiments in physical research, reactor engineering, biology research, and teaching of reactor science are given. No attempt is made to relate all the work undertaken with the CP-5 reactor, nor are any results given. The descriptions of experiments are not meant to give details adequate for analysis of performance but rather are meant to indicate the scale of equipment required in addition to the reactor. The various pieces of equipment illustrated in the following have been developed by members of the Metallurgy, Chemistry, Physics and Reactor Engineering Divisions of Argonne National Laboratory. Detailed descriptions are available in the appropriate journals.

Crystal Spectrometer

One of the unique uses to which a research reactor can be put is the provision of an intense collimated beam of thermal and epi-thermal neutrons for use in connection with crystalline diffraction. No other neutron source so far has proved satisfactory for diffraction work. The experimental arrangement, which is typical of reactor installations, is shown in Fig. 2. A collimator tube is inserted in one of the

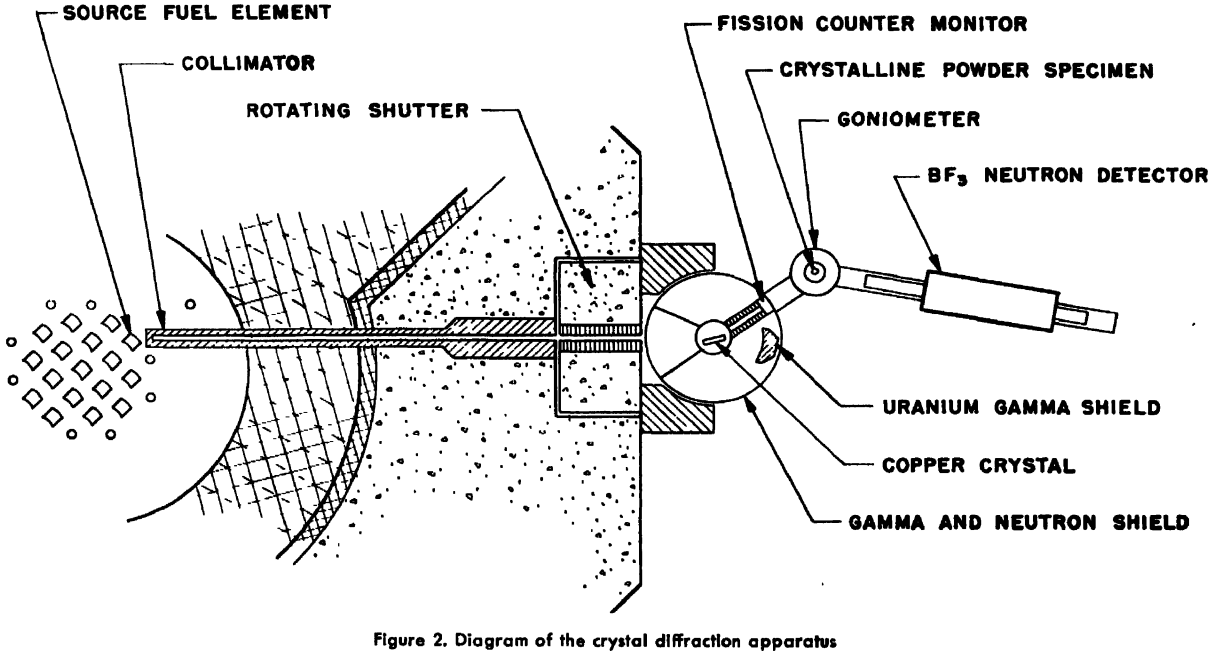

Figure 2. Diagram of the crystal diffraction apparatus

horizontal beam holes which permits neutrons from a fuel element and the adjacent moderator to fall on the first crystal. The collimator opening has dimensions of 1.5 in. by 2.5 in. and therefore the beam of radiation falling on the first crystal is extremely intense. Shielding of this intense beam is one of the major technical difficulties encountered. The diffracted beam from the first crystal leaves its local shield and falls on the sample under study. The sample usually is in the form of a crystalline powder which is packed into a cylindrical sample holder. The neutrons diffracted by the crystalline powder sample are detected by the means of a large BF_3 proportional counter, which is rotated automatically about the powder sample.

The detection of the diffracted neutrons also is recorded automatically so that the experimenter need not be present while the data are collected. The shield surrounding the first crystal is made up of a combination of iron, pressed wood, and paraffin. The direct gamma-ray beam is interrupted by a block of uranium. Although the reactor power is held constant to better than 1 per cent, it does not follow that the neutron intensity emitted from a particular spot of a particular fuel element will be constant to the same degree. Insertion of experiments into thimbles, operation at various times of the xenon poisoning cycle, and operation at various temperatures all bring about situations in which different amounts of reactivity must be absorbed by the regulating rods. The variations in the position of the regulating rods cause variation in the neutron flux at any particular fuel element. In most experiments, therefore, it is found necessary to incorporate a monitor in such a position in the apparatus so that it records the fluctuations in intensity of the primary beam. In the diffraction apparatus illustrated, this is done with the part of the beam which is diffracted by the first crystal.

Assay of Fissionable Isotopes by Fission Counting

The identification of fissionable isotopes which can be produced only in very small quantities has been greatly aided by the development of techniques of operating a fission chamber in very high neutron flux. In order to determine the fission rate, it is necessary to know the number of fissionable nuclides, the fission cross section, and the neutron flux. The product of the fission cross section and the neutron flux can be obtained by using a standard sample of the material under investigation. Thus, a determination of the fission rate in a high neutron flux gives a sensitive measure of the amount of fissionable material in an unknown sample. The success of the technique depends almost entirely on the ability to construct an ionization chamber in which the relatively low counting rate due to fission of the scarce isotope is not obscured by other types of disintegration caused by direct reactor radiation or due to fission of uranium present as impurity in the materials of construction of the ionization chamber. Figure 3 indicates the design of a fission chamber which has been used in a thermal column neutron flux as high as 10^{11} n/cm²/sec. The principal material of construction is Lucite, which is remarkably free of uranium contamination. Conducting surfaces are provided by coating the Lucite with a silver paint. The ionization chamber is provided with a means for quickly and rapidly changing the sample by remote handling. This is necessary because irradiation of the chamber and of the sample in high neutron flux makes them sufficiently radioactive so that direct handling is impossible. The ionization chamber shown, with a suitable amplifier, has been used to measure the amounts of the heavy isotopes when the amount present in the sample was no more than 10^{-10} gm. Where the amount of fissionable nuclide has been known by other means, α-particle counting for instance, the chamber has been used very effectively to determine fission cross sections.

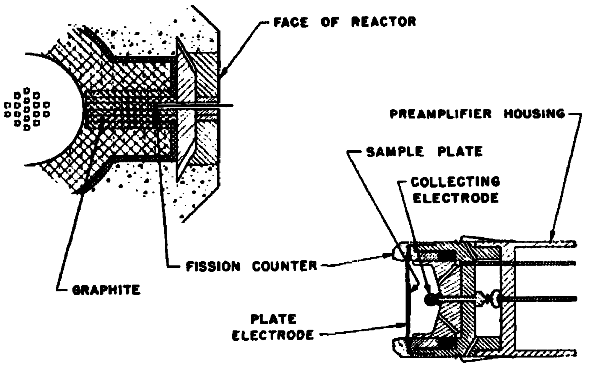

Figure 3. Ionization chamber for fission counting and high neutron flux

Fast Chopper

The measurement of neutron interactions as a function of energy is of continuing interest. The research reactor has contributed in a powerful way to this subject through the use of devices for interrupting a neutron beam with high frequency. The fast chopper used with CP-5 is shown diagrammatically in Fig. 4. A large diameter beam hole is fitted with a collimator. The exit aperture consists of 7 slits, each 2 in. by 0.04 in., and the inlet aperture consists of one slit, 9 in. by 2¼ in. The reactor end of the collimator looks directly at one of the fuel elements. At the pile face, the beam is interrupted by means of a cylindrical metal rotor which rotates about a vertical axis at 15,000 revolutions per minute. The rotor is equipped with slits 0.025 in. wide. Detector stations are located at 25 meters and at 60 meters from the rotor. The

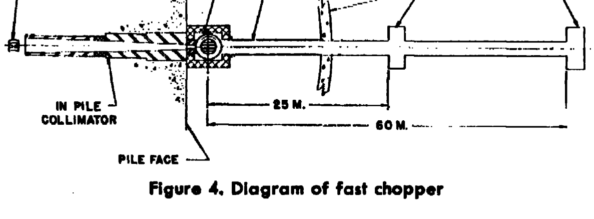

Figure 4. Diagram of fast chopper

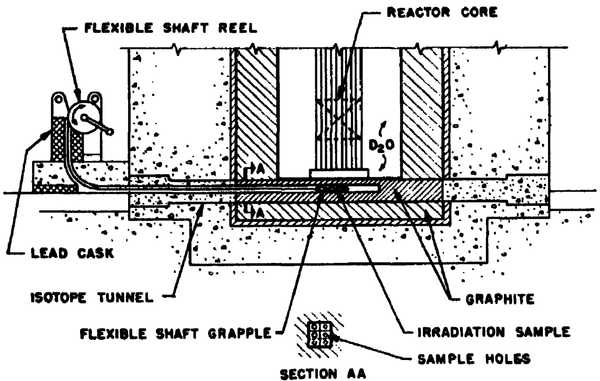

Figure 5. Diagram of the irradiation tunnel beneath the reactor

detector is a liquid scintillator. The use of a long flight path makes it possible to make measurements in the 1000-electron volt region. Ordinarily, the neutrons are counted in 100 time-of-flight channels. Counting simultaneously in so many channels permits the collection of data at a very rapid rate. For the 60-meter flight path, the resolution is 0.02 microsecond per meter.

Radioisotope Production

The routine production of radioisotopes is done by inserting suitable target material in either vertical thimbles or into the isotope tunnels which give access to the neutron flux below the reactor tank. Insertion and removal of samples into the vertical thimbles which pass close to the core, and hence into the highest neutron flux, is done best with the reactor shut down. If attempted while the reactor is operating, there is the leakage of a very intense beam of radiation from the thimbles which, if it does not present a health hazard, gives high background for all experiments. Removal of samples with the reactor operating also is unwise because of the possible effect on the reactivity. Samples to be manipulated while the reactor is operating are inserted into either vertical thimbles in the graphite zone or into the isotope tunnels. Figure 5 shows the arrangement which is used to place samples under the reactor and remove them into a lead cask. Each sample enters a hole in the graphite and is manipulated by means of a gripping tong operated by a flexible shaft. The neutron flux in one of these holes is 2×10^{12} n/cm^2·sec.

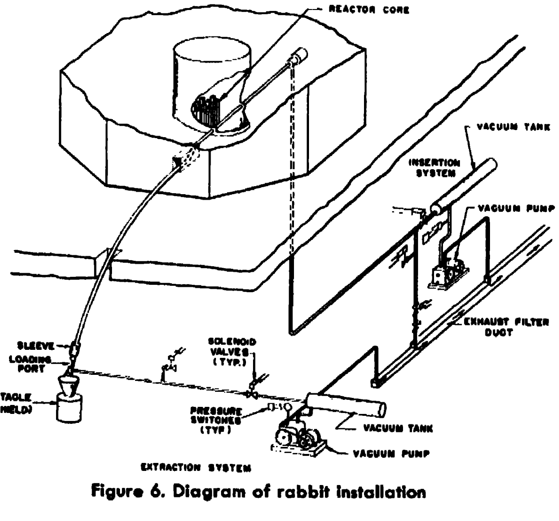

Figure 6. Diagram of rabbit installation

Activation of Materials of Short Half-Life

In order to give short measured irradiations and to quickly retrieve a sample from the reactor, the "rabbit" shown in Fig. 6 is used. A vacuum is used to suck the irradiation capsule, which is light weight plastic, into position next to the core. A vacuum also is used to quickly suck it out of the reactor and eject it into a lead cask. Any activated air is delivered to the building exhaust system. The diameter of the rabbit tube is so sized that the effect on the reactivity of the reactor of any sample the tube can accommodate is not of consequence. Irradiation of very large objects is carried out in the thermal columns. Such irradiations are never routine because of the large amount of induced radioactivity of the sample and the handling difficulty this radioactivity presents.

Gamma-Ray Spectrometer

The fact that the research reactor is equipped with beam holes which pass through the core from side to side of the reactor makes it possible to construct a gamma ray spectrometer which has unique features. Figure 7 illustrates the installation. The source of gamma rays is a small plate or wire which is placed in the through beam hole at the point of highest neutron flux. Capture gamma rays from this source are led out of the beam hole to a large bent quartz crystal. The diffracted gamma rays from the crystal are detected by a number of sodium iodide scintillators. Because the source is isolated in a beam hole containing only air, capture gamma rays from materials in the neighborhood of the source are absent and thus cannot obscure the source gamma rays. Also, because the source is isolated, scattered reactor gamma rays should not reach the crystal. The availability of high neutron flux permits the use of a source of low mass, also diminishing the intensity of scattered gamma rays. It is expected that with this equipment a resolution of 1 per cent at 1 Mev will be obtained. The instrument is designed to cover the range of gamma ray energy from 20 kev to several Mev.

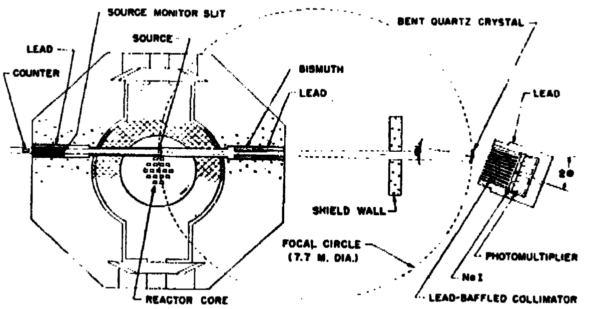

Figure 7. Gamma-ray spectrometer installation

Reactor Engineering

Two examples of apparatus which is used for fuel element development are given. These examples are selected rather than others, such as circulating loops, because of their uniqueness.

Water Autoclave

In the development of fuel elements for use in water-cooled power reactors, the corrosion of the fuel element in the water is perhaps the most difficult problem. A great deal of corrosion information on materials of construction is obtained from laboratory studies using autoclaves with static water or loops in which the water is circulated over the test specimens. It is desirable, however, to subject fuel element test specimens to the complete reactor environment before making a definitive decision concerning the usefulness of any particular material. In many cases, the jacket must be relied upon to provide a non-corroding barrier between the water and the fissionable material. Tests on the consequences of imperfections in this jacket are important and should be carried out under conditions simulating the actual reactor conditions. The autoclave shown in Fig. 8 is one of a number of such facilities which are used in CP-5 to follow the history of test specimens as a function of burnup of the fissionable material. A test specimen, whether in the form of a plate or a rod, has a small thickness, usually no more than one-eighth of an inch. This small thickness is used because to achieve an increased rate of burnup, enrichment of the samples with U^{235} is used. Self-protection does not produce a serious distortion of the burnup rate in samples of this thickness unless the enrichment is raised above 20 per cent. The samples may be of any length up to approximately 16 inches. Actually, a number of samples are exposed together.

These autoclaves are installed in the region of the reactor just outside of the fuel elements, and therefore are located in the region of highest neutron flux. Because the samples are small, the total heat generation also is small. The burnup rate can be increased by higher neutron flux since the surface heat flux is 15 $cal/cm^2/sec$, but it cannot be increased by higher enrichment because of the flux distribution within the sample. Increasing the burnup rate with higher flux would demand forced convection, including a fairly complicated circulating loop. These points indicate that the program of irradiation studies would benefit most by making the autoclave as simple as possible. The one shown in Fig. 8, which permits obtaining about 0.2 per cent burnup of the total atoms of the sample per 1000 hours of exposure, is an example of an inexpensive apparatus which requires a minimum of attention. The sample is supported inside a stainless steel tube of outside diameter 0.75 in. having a wall thickness of 0.049 in. It is designed for a pressure of 1500 psi, but is usually operated in the neighborhood of 800 psi. This tube is filled about two-thirds of its length with water and the gas space above is pressurized with helium gas. The pressure of this space is carefully measured and recorded and the reactor shutdown rods are interlocked with this pressure so that a too high or too low pressure will sound an alarm and shut down the reactor. The heat transfer rate cited above, of course, will cause local boiling on the surface of the sample. The pressure tube just mentioned is immersed in water in a second tube

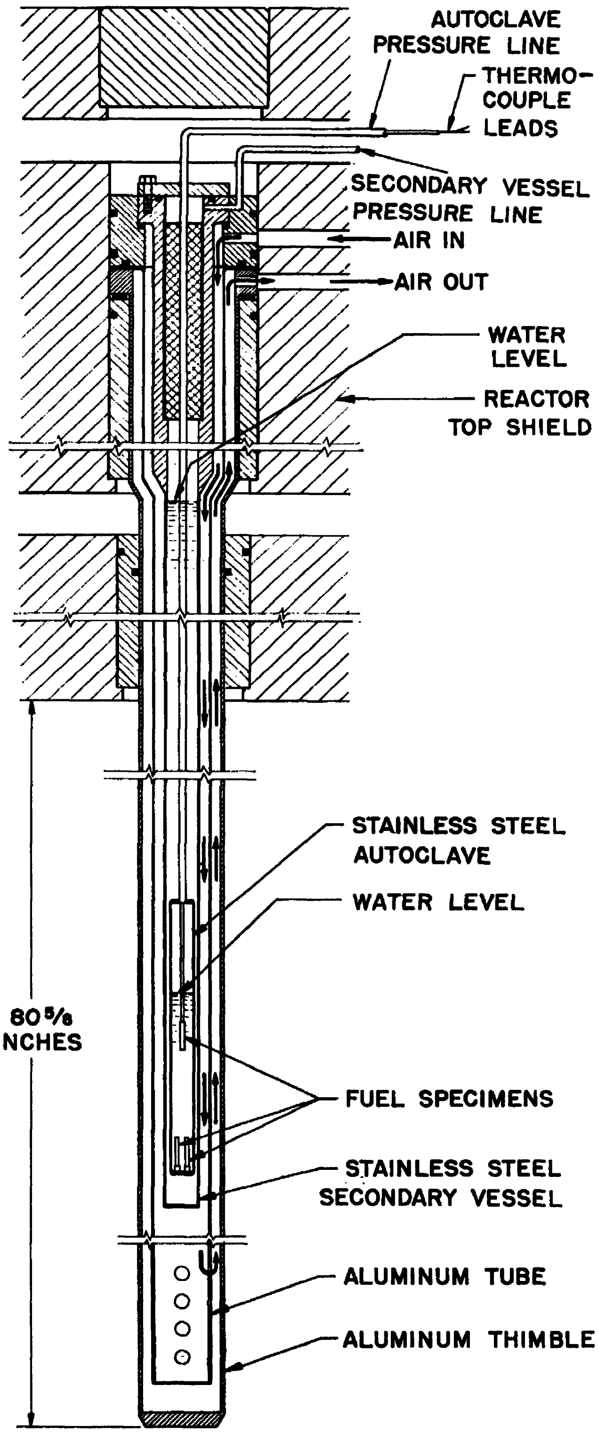

Figure 8. Pressurized water autoclave

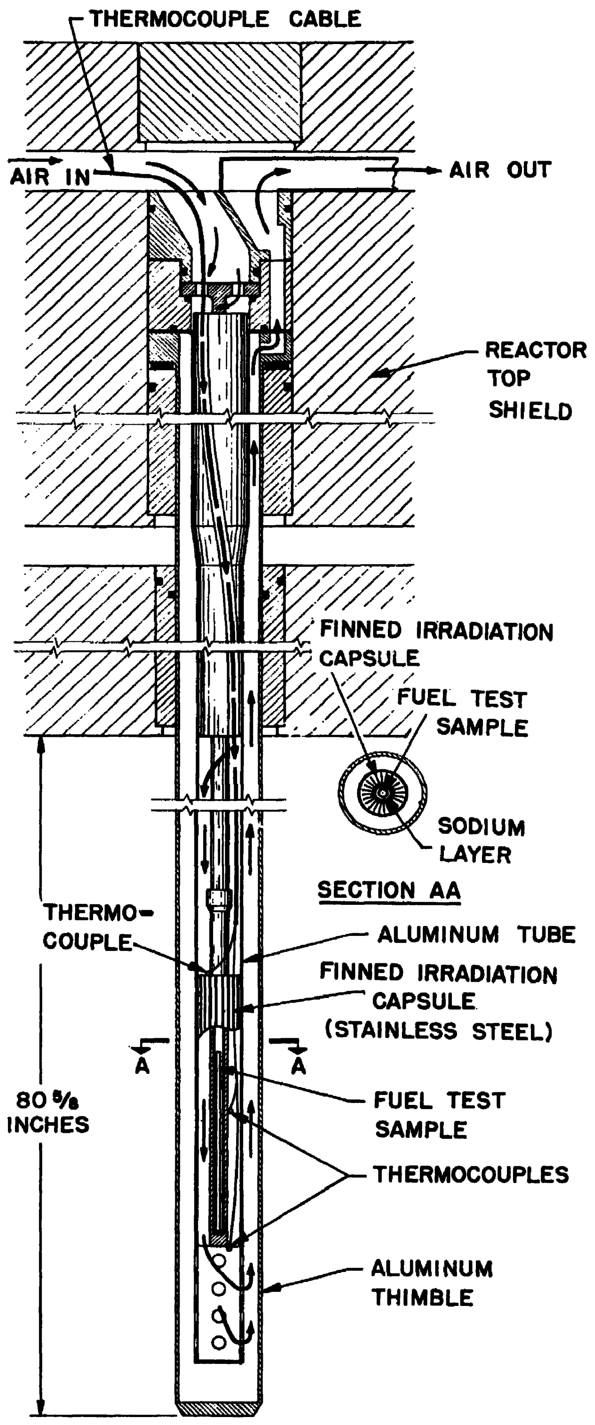

Figure 9. High temperature irradiation apparatus

which surrounds it. The water in the second tube is pressurized to only 400 psi in the same way as the water in the inner autoclave. The heat is removed by convective circulation of the water in the annulus between the two stainless steel tubes. The water in the second stainless steel tube also provides a convenient shield to prevent neutrons streaming through the hole in the reactor through which the whole assembly is inserted. The assembly is inserted in one of the standard aluminum thimbles provided in the reactor and is cooled by the small amount of air flow which is provided for each of the thimbles, namely, about 20 cfm. These autoclaves are easily installed and removed from the reactor.

High-Temperature Exposure of Fuel Samples

In contrast to the development of fuel elements for water reactors, where the operating temperature of the fuel element is limited by the fact that it is cooled with water, the development of fuel specimens for sodium-cooled or gas-cooled reactors is not restricted similarly. The apparatus sketched in Fig. 9 was evolved to permit exposure of fuel specimens to the highest neutron flux of the research reactor while permitting the temperature of the specimen to reach high values. Here again, the emphasis is on an apparatus which is inexpensive to construct and which requires little attention. As was cited earlier, the use of enriched fuel requires that the thickness of the specimen be small. The specimen in this work is usually a rod or a plate of a thickness of approximately one-eighth of an inch. A typical example would be a thin rod 14 in. long and 0.15 in. in diameter. In order to obtain simplicity of construction and operation, it is most convenient to use air as the coolant. The problem then is to get the heat generated in the sample to the air, and this obviously calls for the provision of an extended surface. The fuel sample is placed inside a finned capsule made of stainless steel. The space between the fuel sample and the inside of the finned tube is filled with carefully purified sodium and is welded shut. A vacant space is left at the top inside the finned tube for the accumulation of any gases which may be emitted from the fuel sample. Eighty cubic feet per minute of air are drawn over the finned tube. The total heat removed from the sample is 5 kw. In a typical case, the thermal flux at the surface of the sample is 24 cal/cm^2/sec. Under these circumstances, the burnup rate is approximately 0.27 per cent of the atoms of the fuel specimens per thousand hours of exposure. Thermocouples are attached to the root of the fins. Temperatures as measured by these thermocouples and the total power generated lead to an estimate of the sample temperature. It is, for instance, relatively easy to adjust the conditions so that the highest temperature in the sample is just below the α-β transition temperature of uranium.

Biological Research

The thermal column of the reactor readily can be adapted to the irradiation of small animals. The maximum size opening within the thermal column is 16 in. by 16 in., but it is unlikely that the flux within the thermal column will be used directly for animal irradiation because of too great intensity. For experiments in which the effects of fast neutrons are to be studied and are to be compared with the effects of gamma-ray irradiation alone, the apparatus shown

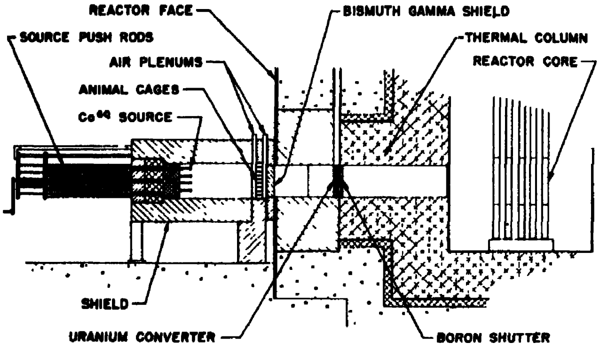

Figure 10. Fast neutron exposure chamber

in Fig. 10 has been used. In the construction of the reactor, a slot was provided in the shield extending from the inner side of the movable shutter on the thermal column to the top of the reactor shield. Into this slot, an apparatus has been placed which can lower a uranium converter plate into the full beam from the thermal column. When not required, the converter plate can be drawn up into the slot and is thus shielded. Thermal neutrons from the thermal column strike the converter plate and are converted on a one-for-one basis to fast neutrons of fission energy. The thermal neutron flux at the converter plate is 1.5×10^{10} n/cm^2/sec. These fast neutrons are used to irradiate small animals which are placed in plastic containers some distance beyond the converter plate. By keeping the animals some distance from the converter plate, a uniform irradiation field for the small animals is attained. Because the intensity of fast neutrons is quite high, an extensive shield must be built around the irradiation areas. The intensity of fast neutrons emitted from the converter plate can be altered by means of boron shutter which, by rotation, permits various amounts of the thermal neutrons to fall on the converter plate. With this apparatus, it is possible to give lethal doses of fast neutrons in short times of the order of one hour. During the time of exposure, the animals must be furnished with conditioned air by blowers. The gamma irradiation of the animals is carried out in the same place by means of cobalt-60 sources which can be varied in number in order to achieve the appropriate dose rate. With this apparatus, an extensive program of the irradiation of mice has been carried out to determine the additivity of gamma and fast neutron dosage and to study the consequences of fast neutron irradiation in contrast to gamma irradiation.

The direct radiation from the reactor generally is not used in biological experiment. Both gamma and photoneutron sources for use elsewhere in biological experiments, however, are manufactured by irradiating suitable materials in the reactor.

Instruction

The CP-5 reactor is being used in the instruction of students in the fundamentals of reactor technology. The teaching done with the reactor concerns the study of the machine itself and its use in experiments designed to illustrate techniques of measurement.

Operating Characteristics

Space does not permit a detailed description of all of the instruction exercises which can be done on an operating reactor. The following are typical of some which have been found to be interesting and informative.

Of basic importance is the flux distribution in the reactor. This is measured by stringing cobalt wires in various thimbles, making an irradiation, permitting time for the decay of short-lived activities and then the wire is scanned with a counting apparatus which gives the intensity point by point along the wire. With this technique, scanning of the neutron flux in any accessible portion of the reactor is done quickly and with minimum effort.

The calibration of a control rod is a basic procedure in the operation of a reactor. This is done by choosing a particular rod for calibration, usually the regulating rod, and by measuring the positive reactor period produced by displacing the rod a known amount from its critical position. Thus the reactivity value per unit length of the rod at tha. position is obtained. By varying the set position of the rod, a complete calibration curve is obtained. Once a rod has been calibrated, it can be used for making other reactivity measurements such as the temperature coefficient of reactivity. This is done by finding the critical position for one temperature, heating up the reactor, and again finding the critical position with the calibrated rod.

Experimental Techniques

A very instructive measurement which should be familiar to all reactor technologists is the measurement of high neutron flux. This involves the irradiation of gold foils in a standard pile and in the high flux in the reactor. A suitable calibration of a counter and associated absorbers permits counting of the highly activated foil and leads to a direct comparison of a standard pile flux with the high flux of the reactor.

An interesting exercise is the determination of the disadvantage factor for a lattice of natural uranium plates in light water. The apparatus for this experiment consists of an aluminum box which holds seven uranium plates in water. Copper foils are placed throughout the assembly, including the uranium

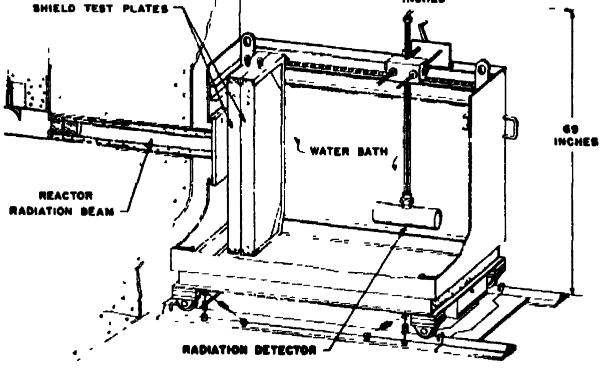

Figure 11. Shield test apparatus

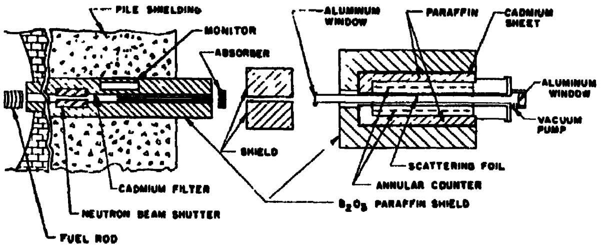

Figure 12. Annular scattering chamber

plates, and the whole box is irradiated in the thermal neutron flux of the thermal column. The induced radioactivity of the foils gives the neutron flux throughout the lattice and permits calculation of the disadvantage factor.

Basic measurements in shielding are carried out in an apparatus which is placed before one of the beam holes in the reactor. A beam of reactor radiation is allowed to come out of the beam hole and strike shielding plates which are installed in a large tank of water which rests against the pile face. A scanning device with thermal neutron or fast neutron or gamma-ray detectors can be moved about in the tank of water to obtain a plot of intensity back of the test plate. Figure 11 is a schematic diagram of the setup. From the data obtained, removal cross sections for the material of the test plate are calculated Also, observations are made of the intensity of the capture gamma rays.

To give training in the techniques of cross-section measurements, the annular counter scattering apparatus is used. This is illustrated in Fig. 12, which shows how a highly collimated beam of reactor radiation is scattered by a thin foil. The scattered neutrons are detected by an ionization chamber which surrounds the position of the foil. Experiments on self-protection are done and the properties of scattering resonances determined. Figure 13 is a photograph of the work space around the reactor, showing the annular scattering chamber and the shield test apparatus.

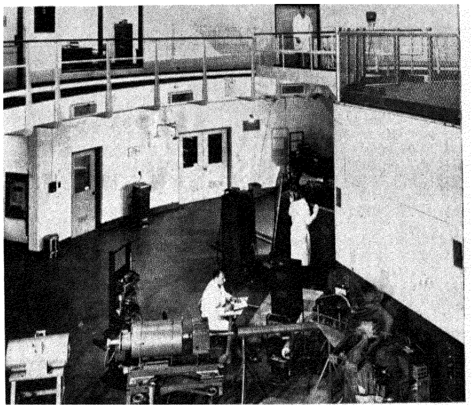

Figure 13. Reactor work space

REFERENCES

1. Spinrad, B. I., Carter, J. C. and Eggler, C., P/835, *Reactivity Charges and Reactivity Lifetimes of Fixed Fuel Elements in Thermal Reactors*, Session 20A.2, Vol. 5, these Proceedings.
2. Hughes, D. J., *International Neutron Source Calibrations*, Nucleonics, 12: 26 (December, 1954).
3. Zinn, W. H., P/861, *Design and Description of ANL Reactors CP-3, CP-3' and CP-5*, Session 10A.1, Vol. 2, these Proceedings.
4. Langsdorf, A. S., Jr., *The Thermal Neutron Reactor as a Device for Measuring Neutron Cross Sections*, AECD-3194 (July 13, 1951).
5. Dietrich, J. R., P/481, *Experimental Determinations of the Self-Regulation and Safety of Operating Water-Moderated Reactors: Results and Motion-Picture Records*, Session 6.2, Vol. 13, these Proceedings.

Observations on Operation, Training and Research Experiences with the Raleigh Research Reactor

By Clifford Beck,* USA

DESIRED PATTERN OF OPERATION

It was intended from the time of the original conception of a "university research reactor" for North Carolina State College[1] that the project should coincide as nearly as possible with the normal pattern of training and research in universities. In major part it has been possible to achieve this objective. Two policies were adopted at the outset which have contributed greatly to this success: (1) that all portions of the reactor facility itself and all phases of the associated training programs in nuclear engineering would be so selected as to lie outside the bounds of secrecy and restricted information, and (2) that the Atomic Energy Commission and other federal government funds would not be sought for capital investment in the facility, in order that complications of governmental auditing and any possible tendency toward "outside" control of the program could be avoided.

On the other hand, it is currently required by law that ownership of the uranium in the reactor core be retained by the Atomic Energy Commission as well as certain responsibilities for ascertaining that specified standards of safety in reactor operation are maintained. To achieve this, it is necessary that periodic inspection visits be made and periodic reports and records be filed. These procedures are somewhat contrary to usual university practices, though clearly they are necessary and desirable because of the unusual hazards and other factors involved. Even though not customary all these relationships have moved on a very high plane of amiability, cooperation and, apparently, mutual satisfaction.

STAFF RELATIONSHIP

The reactor was designed and the associated Nuclear Engineering Training Program was organized within the Physics Department, where the entire program is administered. It should be noted, however, that Chemical, Mechanical or Electrical Engineering Departments, etc. (or even an entirely new department in the college) would constitute equally acceptable homes for a reactor project provided a core of qualified staff members was assembled there.

Within the Physics Department, students may register either in the Nuclear Engineering Curriculum[2,3] or in the parallel curriculum in Engineering Physics. Staff members in the department primarily responsible for supervision of the reactor and for instruction in the specially developed courses in nuclear technology, also assist in meeting departmental obligations for teaching standard courses in physics. Thus, the four staff members experienced in atomic energy activities not only guide reactor operation and teach the core nuclear courses in the Nuclear Engineering Curriculum, but also join the other ten members of the staff in regular instructional duties in physics.

Included in the departmental duties is the obligation to direct graduate students in Nuclear Engineering in thesis research investigations, most of which involve use of the reactor in one way or another. Other members of the staff, as well as those with reactor experience, participate in directing these projects. Thus, in this respect the reactor does function in such customary patterns of departmental training and research procedures, as would be followed, for example, with an infrared spectrograph or a Van de Graaff accelerator.

In addition to the four senior scientific staff members, there are four others, at the research-associate, graduate-student level who play a major role in keeping the reactor in operation.

These two groups, of about six equivalent full-time staff members, plus a director, would comprise an acceptable minimum staff for operation of the reactor as a separate project (not as a part of some standard department) *if* routine use of the reactor in instructional and minor staff research programs should comprise its only application. In fact however, the reactor has a much wider potential usefulness than this; it can serve as the hub of a research program of greater diversity and more challenging interest than could be provided within any one department.

To encourage and serve these wider potential interests (studies as divergent as genetics and polymerization, activation analysis and nuclear thresholds, etc.) the reactor staff must be more than a technical organization functioning solely to provide neutrons and irradiation services to interested customers. It will be discovered at once that almost every "outside" group interested in using the reactor needs the sympathetic and cooperative assistance of a responsible member of the reactor staff in developing a plan of the anticipated investigation which uses the reactor to maximum advantage. Thus, most "outside" research projects develop into a teamwork partnership involving a member of the reactor staff and the "outside" scientist.

---

* North Carolina State College.

This is as it should be. Within a university, the caliber of scientists having sufficient training and experience to be responsible for operation of a research reactor would hardly be interested in routine service irradiations and isotope production. On the other hand, the reactor can be effectively used in research investigations in many different divisions of the university, though the scientists in these scattered divisions would usually not be sufficiently acquainted with reactors to plan to use one with maximum effectiveness. Clearly the solution is to effect a partnership as indicated above.

This indicates at once one qualification of over-riding importance for staff members of university research reactors, and one challenging aspect of university research reactor programs which might not have been anticipated. *The challenging aspect:* The amazing potentiality of the reactor for attracting scientists from almost every scientific discipline into mutually satisfactory and intellectually fruitful partnerships with the reactor staff. Such research partnerships, which break across department and school barriers, may have intrinsic values of far-reaching significance, aside from the worth of the objectives directly pursued. The reactor is a potent catalyst for promoting such cooperative endeavors.

The *important qualification* of reactor staff members referred to above, obviously is an alert, interested and cooperative attitude toward scientists from "outside" groups who have potential interest in using the reactor. No other tool is known which has such widely applicable versatility. To realize its fullest potential the cooperative interest of the staff should match the versatility of the instrument.

Extension of this idea leads to another, related, observation: The administrative machinery should be sufficiently informal and flexible to permit the reactor staff to negotiate working arrangements with other scientists with a minimum of red tape, approvals and bookkeeping. One might expect *a priori* that this would always be the case in a university, where the primary attention would be on a "scientific search for truth." Unfortunately, however, even in a university, distorted emphases and misguided objectives do arise which may erect artificial barriers in the pathway of scientific collaboration between different groups. These difficulties can largely be avoided by judicious planning and management, but the pattern for achieving this may vary greatly from one university to another.

To some extent, therefore, it is concluded, the reactor can fit into regular university patterns for training and research. However, primarily because of safety factors which require continued contact with governmental health and safety agencies, and because of the large potential versatility of the reactor which implies an obligation to make it widely accessible to scientists from all areas of the institution, operation of a reactor imposes some requirements which are not customary to university campuses.

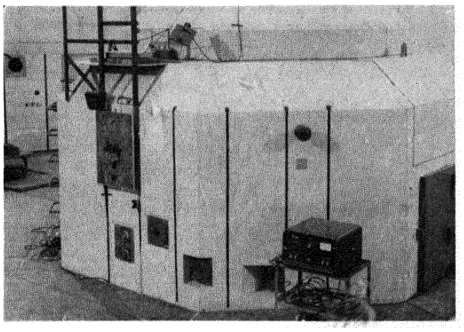

Figure 1. The shield assembly of the Raleigh Research Reactor

THE REACTOR AS A TRAINING TOOL

In four distinct ways the Raleigh Research Reactor (Fig. 1) has been used effectively in strengthening and enriching the experiences of students in Nuclear Engineering.

1. A Reactor Laboratory course, consisting of eighteen or so experiments on reactor characteristics and usages, has been developed. Advanced students may register for this course as they would, for example, for a laboratory course on X-ray techniques. One experiment is performed each week, with the students working in team groups of eight or ten members. The practical experiences of reactor operation and behavior obtained from these exercises greatly enhances the student's understanding of reactor principles and concepts presented elsewhere in the curriculum in reactor theory courses.

Typical experiments are:[4] (*a*) a simulated approach to criticality; (*b*) measurement of reactor periods; (*c*) control rod calibration; (*d*) build-up and decay of gamma activity in the reactor core; (*e*) temperature coefficient of the reactor; (*f*) power calibration by heat balance (see Fig. 2).

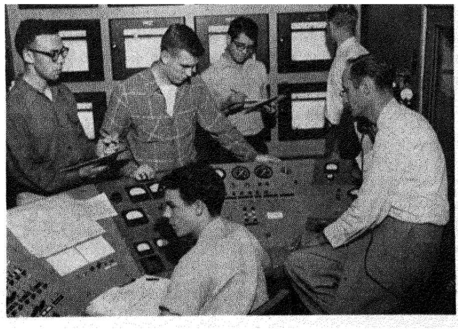

Figure 2. Students in the reactor experiments course studying thermal methods of power calibration

2. Many of the graduate students in the department choose thesis research projects which deal with further investigation of reactor characteristics or utilization of the reactor as a source of radiation. Valuable incidental experience on reactor operation and behavior is gained in the course of these studies.

Typical projects are: (*a*) preparation and properties of barytes concrete for reactor shielding; (*b*) tests of solutions of the two-group reactor equations; (*c*) instruments for measuring liquid level in the reactor core; (*d*) fast neutron response of organic phosphors; (*e*) a test of two-group control rod theories; (*f*) branching ratio of the B^{10} (n,α) reaction; (*g*) time transients in the automatic control system of the reactor; (*h*) thermal calibration of reactor operating levels.

3. Part-time student assistants in the department, in many cases, are scheduled to participate in reactor operation and research as part of their assigned departmental duties. The experiences involved are incidentally of value to the student as well as useful to the department.

4. The physical existence of the reactor facility on the campus exerts an intangible but significant influence in inspiration, motivation and stimulation of the imagination of students and staff. This important factor in the training process is further enhanced by the variety and challenge of research studies in progress around the reactor.

Thus, the reactor is indeed a tool of essential importance in the training program of students in Nuclear Engineering.

THE REACTOR AS A RESEARCH TOOL

An enriched uranium, homogeneous fuel, water-boiler type reactor is probably the most completely satisfactory type of training and research reactor for producing thermal neutron fluxes up to 10^{12}. In safety, cost of construction and operation, small size of fuel investment, and high adaptability and flexability in research it is unmatched by any other type. On the other hand, there are certain types of research, e.g., radiation damage in metals, which require fluxes higher than 10^{12} and, for these, reactors of some other type must be used.

The versatility of the 10 kw water-boiler reactor, and its adaptation to the research requirements of a university campus are shown by the variety of experiments in progress. Typical ones are listed below:

1. Effect of Neutron Energy on Production of Bromine Isomers

When bromine-79 is irradiated with neutrons, two gamma emitting isomers are formed, one having a half-life of 18 min, one 4.4 hr. A study is in progress to determine whether the ratio of isomers formed is dependent on neutron energy. This is quite simply done by exposing samples of bromine at different positions along the axis of the thermal column. The n_s/n_f ratio varies from ~1 near the core to about 10^5 near the end of the column. Analyses of activities measured for samples of bromine exposed to neutrons at various positions are now being made.

2. Activation Analysis

By measuring the characteristic radioactivity of materials exposed to neutrons, the reactor may be used as a chemical analysis instrument of unmatched sensitivity. It has been suggested that more than half of the elements, and in some cases to a sensitivity of 10^{-11} grams, can be detected and measured by activation analysis.[5]

In a cooperative study with the staff of the Animal Industry Department, a method is being developed for using the Raleigh Research Reactor to measure the manganese content of blood serum by activation analysis. This study is typical of numerous other similar applications.

3. Effect of Reactor Radiation on Textile Fibers and Other Organics

Several studies are in progress on the effects of radiation on textile fibers and other organic materials. The factors which influence these effects, and improved methods of detecting the effects, are also being sought. The reactor staff is cooperating with the Textile School of the College, with the National Bureau of Standards, with the Office of Ordnance Research and with various industrial groups on several such studies. Among other devices, changes in infrared spectra and changes in mechanical moduli by resonance vibration are being studied as means of ascertaining the effects caused by radiation.

4. Porosity of Ceramic Layers

In collaboration with the Ceramics Department, studies of the porosity of thin layers of ceramics to fission product gases are being studied. The ceramic layers are placed on uranium wafers and the fission gases are produced *in situ* by neutron irradiation. The subsequent emergence of the gases from the sandwich under various conditions is measured by observation of the associated radioactivity.

5. Neutron Slowing-Down Lengths in Water-Metal Mixtures (Fig. 3)

The distance a fission neutron travels in becoming thermalized in a given reactor is an important factor in determining the physical characteristics of the reactor. In practical reactors, which are composed of assorted materials, it is often very difficult to estimate the slowing-down lengths in the combination of materials present. The experiments described here are intended to establish empirical values of slowing-down lengths of neutrons in certain water-metal mixtures, for comparison with theoretical predictions of these values.

A beam of thermal neutrons from the reactor is allowed to bombard a thin metal plate of U^{235} (4 in. × 4 in. × 0.020 in.) located at the outer surface of the reactor shield. The plate is situated in the center of one side of a four-foot cubical tank placed against the reactor shield. The fission neutrons produced in the U^{235} plate spread radially in all directions, including some in the forward direction into the cubical tank. The tank is filled with water and chosen amounts of the selected metal, in the form of thin sheets (4 ft × 4 ft × ⅛ in.). Neutron slowing-down lengths are measured in the tank contents, by means of appropriately placed foils, as the ratio of metal to water in the tank is increased (by the addition of more metal plates) from zero to 1:1.

Experiments are in progress on water-iron and water-aluminum mixtures. These will be extended to include water-zirconium mixtures as well.

6. Neutron Diffraction

At 10 kw power level, the thermal neutron flux at the core surface is about 2.5×10^{11}. This is an adequate intensity for various studies of structural and magnetic properties of materials by neutron diffraction. A diffraction spectrometer, using a copper crystal monochromater, is now in construction.

7. Radiation Effects on Insects; Assorted Biological Experiments

In cooperation with the Biological and Genetic Departments, a wide variety of radiation effects on physiological and hereditary characteristics of plants and small animals can be carried out. To some extent, by judicious placing of the specimens, and utilization of appropriate shielding materials, the separate effects of gamma, slow and fast neutrons can be partially identified.

Numerous other experiments have been visualized[6] which have not been attempted thus far. The inaccessibility of various types of experiments (e.g. metal damage, ultra-high dose rates of biological materials for very short times, etc.) to reactors having fluxes of 10^{12} or less does not result in a dearth of interesting and useful research studies within reach of such low-power reactors. On the contrary, there are still many untried experiments in almost every field of science, even in nuclear physics, where the useful explorations with a low-powered reactor are less abundant than in most fields.

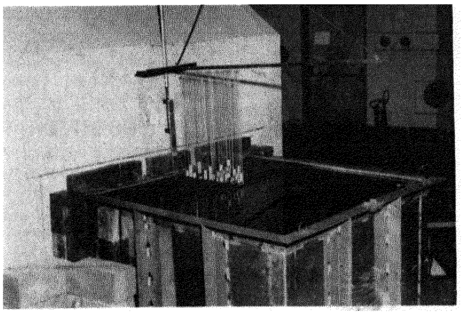

Figure 3. Apparatus beside the reactor shield for studying slowing-down lengths of fission neutrons in water-metal mixtures

Perhaps it is worthy of observation again, as clearly indicated in the list of experiments above, that abundant opportunities will emerge from reactor utilization for team partnerships in research which involve a member of the reactor staff in cooperation with a member of an "outside" department. If there is some dearth of research projects in "pure" nuclear physics accessible to a low-power reactor, there is undoubtedly over-compensation for this deficiency in the abundance of applied physics projects available through joint endeavors with scientists in other areas of study.

REFERENCES

1. Beck, Clifford K., *Proposal of a Nuclear Reactor at North Carolina State College*, NCSC Bulletin, July 7 (1949).
2. Beck, Clifford K., *Training Program in Nuclear Engineering*, NCSC Bulletin (1950).
3. Beck, Clifford K., *Undergraduate Nuclear Engineering Curriculum at North Carolina State College*, Nucleonics, Vol. 9, No. 5, pp. 18–27, November (1951).
4. A laboratory manual is now in preparation.
5. Leddicotte, George and Reynolds, S. A., *The Determination of Trace Elements by Neutron Radioactivation Analysis*, Oak Ridge National Laboratory, Report #52-12-155. June 15 (1953).

The Need for Basic Research in an Atomic Energy Program

By Thomas H. Johnson,* USA

As we strive to develop the uses of atomic energy for the benefit of mankind surely there is no phase of our endeavor where one nation can assist another more effectively, or where the magnitude of the tasks more cogently challenges the cooperation of scientists on a world scale than in basic research. Just as the present achievements of each country have been augmented by scientists from many nations, so research into nature's laws and materials, wherever it is done, will continue to advance the welfare of everyone.

Much remains to be done. Within a generation the growth of fundamental knowledge can be expected to affect profoundly all phases of atomic technology and even to reorient our thoughts towards radically new methods of releasing nuclear energy. From the training engendered by basic research activities there will also arise the manpower to put new ideas to practical use. Any nation intending to benefit from technical advances, whether in atomic energy or in other fields, might best prepare itself by promoting basic research within its own borders as a means of possessing the scientists who will be able to understand the significance of new advances, wherever they are made.

The scope of the research tasks which are before us can be seen only in the imagination of each individual, but we all know the nature of the problems which now challenge investigators everywhere. We also know how quickly a new discovery can enlarge the visible horizon and shift the emphasis of the search. At the moment several areas can be delineated where further investigation will clearly lead to practical benefits. It seems certain that uranium ores are in sufficient abundance to supply the world's power needs for centuries, but further studies in geology and geochemistry are needed before we can predict systematically and reliably where the high grade deposits are located. Developments in chemistry and chemical engineering are needed to recover uranium more economically from low grade sources and with benefit of coproducts. Examples of such sources are the ores of other metals, uraniferous phosphates from which fertilizers can be produced, combustible lignites and oil bearing shales. An important element of the cost of atomic power is in the separation of uranium from the raw material and in the recovery of plutonium and uranium from spent fuel. Significant economies can yet be expected from chemical and metallurgical developments related to these materials.

The expansion of knowledge of neutron cross sections and new computational methods for using such data will improve the design of power reactors. A better command of basic chemistry will help us overcome corrosion and lead to the choice of better materials that can be used at higher temperatures in a reactor. In this respect we are also deficient in understanding the effects of radiation on chemical rates and equilibria. Moreover we have insufficient knowledge of the effects of radiation on solid materials, or indeed of solid materials in the absence of radiation.

In the more basic areas where the practical consequences are more difficult to predict we still lack a satisfactory understanding of the force which binds neutrons and protons in the nucleus, and of the statistical laws which govern the nuclear ensemble. Until we understand the nucleus we cannot expect to understand fission.

In the basic scientific fields of chemistry and metallurgy further exploration cannot fail to contribute to the more effective utilization of atomic energy. Many of the elements are still new to the chemist and of the 70-odd metallic elements only a few have come into industrial use on a scale to pay for thorough metallurgical investigation. The recent developments of fluorocarbons and of zirconium and titanium suggest that still other important materials are yet to come. Moreover the investigations in neither chemistry nor metallurgy have dealt adequately for our present needs with high temperature properties.

In addition, there are many unexplored uses of neutrons and other radiations and of radioactive materials which will lead to increased knowledge in fields of biology, meteorology, geology, chemistry, and engineering, to more effective treatment of diseases, to better industrial processes and controls, and to many miscellaneous economies and improvements.

Everyone has his own view of the future and I do not speak in this respect for all American scientists, least of all for the scientists of the world. I have presumed to refer to these matters because the magnitude of the research effort in which we are now engaged in the United States of America may lend some interest to what we believe is in sight for the future. The same reasoning suggests that an exposition of the United States Atomic Energy Commission's actual program in basic research is an appropriate topic for this conference.

The total expenditures for research and development in the United States are estimated at 4.7 billion dollars annually, including operating costs and plant additions. About half of this amount is spent by the federal government. Recent studies by the National Science Foundation estimate 7 per cent of the federal expenditures for research and development are for basic research. If this figure also applies to privately supported research the total spent for *basic* research in the United States of America is about $330,000,000 annually or slightly less than 0.1 per cent of the gross national product. The total for research and development is about 1.2 per cent of the gross national product. The federal government's share for research and development is 3½ per cent of the federal budget and the government's share of the basic research is ¼ of one per cent of its total budget. The Atomic Energy Commission spends about a third of the government's total of $150 million for basic research.

---

* Director, Division of Research U. S. Atomic Energy Commission.

The role of the federal government and its various agencies in the support of research has been extensively reviewed recently. Of the 56 departments and agencies of the Executive Branch of the government, 20 report funds for research and development but seven departments account for 98 per cent of the total. A recent executive order encourages each agency to conduct basic research in areas which are closely related to its mission and directs the National Science Foundation to assume increasing responsibility for providing support for general-purpose basic research through grants and contracts. Funds available to the Science Foundation for such support now amount to $20 million annually.

Despite the support now given to research by the federal government, a Commission which is studying the organization of the Federal Government has recently recommended that still greater federal support be given to basic and medical research.

In the atomic energy program it is difficult to draw any meaningful distinction between basic and applied research. The measurement of a neutron cross section may be needed for the design of a reactor but it is also interesting as a test of the cloudy crystal ball model of the nucleus, and a single individual may be conducting research with both interests in mind. We therefore find a lot of basic research going on in many of the development and production facilities of the Commission and there is hardly a laboratory working for or supported by the Commission which does not have contact with or responsibility for some phase of production or development. However, it is meaningful to point out that basic research is recognized in the law and in the organization of the Commission as an independent activity and funds are allocated for this purpose to the Divisions of Physical Research and of Biology and Medicine. Research supported by these Divisions must relate in a general way to the development or use of atomic energy but the specific application of the results need not be foreseen or recognized. These funds can be used for studying nuclear forces, or for developing a chemical process of possible future use.

About two-thirds of the funds available for physical research are used to support the more basic parts of the programs of the large laboratories. These are operated for the exclusive use of the Commission by private contractors. One-third of those funds are used to support physical research contracts in private laboratories, mainly in the universities. Because of differences in indirect costs about the same number of scientists are employed under university contracts as in the basic programs of the large laboratories. In all about 2400 scientists are employed with funds administered by the Research Division.

The largest of the national laboratories is operated at Oak Ridge, Tennessee, by the Carbide and Carbon Chemicals Company. Its program in the physical sciences includes the production and distribution of stable and radioisotopes, research with the various reactors and accelerators in neutron physics and nuclear structure, and all phases of chemistry and metallurgy.

The laboratory has among its facilities a large air cooled graphite reactor, and two light water moderated reactors. It is just building its fourth reactor which, however, will be the first specifically designed for research and development. Oak Ridge also has two Van de Graaff accelerators, a high current 86-in. cyclotron and a 63-in. cyclotron for the acceleration of heavy ions. It has an electronic computer, a spectroscopic laboratory, excellent facilities for hot chemistry experiments and radiation caves for studying solids exposed to radiation. In conjunction with the Oak Ridge Laboratory and with use of its facilities, the Oak Ridge Institute of Nuclear Studies, a corporation of southern universities, promotes research by university personnel in the field of atomic energy.

The Argonne Laboratory, operated by the University of Chicago and located near Chicago, studies problems of nuclear structure and neutron physics using its excellent new heavy water reactor, its 60-in. cyclotron and a Van de Graaff accelerator. It has an electronic computer and will soon add another.

The Argonne also has excellent facilities for radiation and radiochemistry, for spectroscopy, and for all phases of metallurgical investigation. This laboratory operates the reactor training school for foreign students. It is also studying the design of a high energy accelerator which will be of interest to physicists throughout the midwest region. In the formation of its policies and programs it is advised by a Council of Participating Institutions representing fourteen midwest universities.

Third largest of the Commission's laboratory programs for basic research is at Brookhaven, on Long Island about sixty miles from New York City. This Laboratory is operated by a corporation representing nine northeastern universities, called Associated Universities, Inc. Its program in the physical sciences is almost entirely devoted to basic research with its large air-cooled graphite reactor, its 3 billion volt proton synchrotron, its 60-in. cyclotron, its Van de Graaff accelerator and its numerous other facilities for physics, chemistry, and metallurgy. Brookhaven is also building a 25-billion electron volt proton synchrotron of the alternating gradient variety. A large fraction of the Brookhaven program is manned by university personnel on short term leave from their home institutions.

Fourth in order of basic program size is the Radiation Laboratory of the University of California, which is operated by the University, entirely at the Commission's expense, but with some privately owned facilities. Its research program, like that of Brookhaven, is largely basic and makes use of the 6 billion electron volt bevatron, the 184-in. cyclotron, which will soon be modified to generate 700 Mev protons, a 300 Mev electron synchrotron, and a 30 Mev proton linac. It also has under construction a linear device for the acceleration of heavy ions. The laboratory has excellent facilities and a distinguished program in radiochemistry. A considerable exchange of personnel, interests, and the use of facilities takes place between the Radiation Laboratory and the Departments of Chemistry, Physics and Biology of the University.

The fifth Commission-owned laboratory is operated by the State College at Ames, Iowa. Its principal programs are in basic chemistry and metallurgy but it also carries on research in nuclear and solid state physics. Here too one finds extensive exchange of interests, personnel and the use of facilities with the departments of the college.

The Los Alamos Laboratory in New Mexico is operated for the Commission by the University of California. In addition to other assignments it carries on basic work in nuclear physics and radiochemistry. This laboratory has a variable energy cyclotron, three Van de Graaff accelerators, and two reactors. It makes extensive use in its basic program of scientists on short term leave from universities and other laboratories of the Commission.

Besides the work in the large laboratories university scientists participate in the program by carrying on research projects in their own laboratories under contract with the Atomic Energy Commission. It is estimated that these contracts employ the equivalent of 1000 full time professional scientists and 1600 students. The actual number of scientists participating in these projects is much greater than this number since many give only a fraction of their time.

In selecting projects for support the policy is to find people who want to do what the Commission wants done, or in many instances, to determine whether the Commission has sufficient interest to support what the institution proposes to do. Many of the problems in the field of atomic energy are of academic interest and there has been a happy marriage of interests between the Commission and the university scientists under these contracts. Usually only a part of the costs of the work is borne by the Commission. Typically, the university continues to pay the full academic year salary of scientists of professorial rank, it supplies laboratories, and other facilities, and it pays part of the administrative costs. The Commission, on the other hand, supplies enough money, without designating the purposes for which it will be used, to pay for supplies and equipment, stipends for graduate student assistants, the salaries of postdoctoral research associates, three months' salary for the professorial staff if they spend full time on the project during the summer, and a part of the indirect administrative costs. The aim is not to impose upon the university projects unsuited to its academic program, nor to relieve it of its normal burden of research support in the particular department, but to supply extra funds for extra work which at the same time reinforce the university in carrying out its responsibility to train students and to expand basic knowledge.

Under the contract program in the physical sciences nearly 350 projects are operating in more than 100 universities and colleges. Some of these are supported jointly by the Office of Naval Research. Ninety-five of these projects are in nuclear and high energy physics, and most of these make use of some electronuclear device which has been supplied by the government. A count of the machines involved in the university projects shows 7 electron synchrotrons in energies ranging from 80 Mev to 1.5 Bev, 5 meson producing synchrocyclotrons, 14 cyclotrons operating below the meson threshold, 6 betatrons ranging from 20 to 300 Mev, 7 electron or proton linacs ranging from 10 to 700 Mev, and 20 Van de Graaff accelerators. In addition two linacs for the acceleration of heavy ions are under construction.

Although accelerators are numerous, reactors for research at university sites have not yet come into widespread use. The uncertain hazards of operating a reactor on a university campus and the restrictions on the use of fissionable material imposed by the original atomic energy law have been the principal restraints. One such reactor of the "water boiler" type has been in use for about a year at the North Carolina State University in Raleigh, North Carolina. The first university Swimming Pool Reactor has just received its fuel elements at Pennsylvania State University and another reactor of this type designed for higher power is under construction at the University of Michigan in Ann Arbor. Several other reactors are being designed and funds have been raised for their construction. Except for a special medical reactor at the University of California in Los Angeles no government funds have been required in this program.

Interest in the university reactor usually centers in the engineering department, although physicists, chemists, biologists, geologists, metallurgists and medical personnel find uses for the neutron beams or the irradiation facilities. When all of the manifold research possibilities are considered a reactor seems to be a very desirable facility for a university. Its presence there is also usually calculated to attract to the staff nuclear engineers and scientists who can inspire the teaching program with the result of training more students who will be able to take active roles in the atomic energy program after graduation.

The problem of disseminating scientific information in a basic research program of the magnitude of ours is naturally difficult. In the United States the results of basic research are unclassified and publication in the open literature is encouraged. However, there is no substitute for face to face discussion, and distances in the United States are great. For example, it is further from Columbia University in New York to the University of California in Berkeley than from London to Bagdad. Nevertheless, topical conferences are frequent and the average scientist spends a fair fraction of his time in travel usually at the expense of the government. In supporting travel to foreign conferences, the rule has been about one traveler per year from each major division of the Commission's laboratories, or when in the judgment of the Director the travel is likely to result in short cuts which will compensate the time and expense of the trip. Another device for dissemination, supported extensively by the government, is the compilation of data such as the neutron cross section book, the tables of nuclear data, and tables of isotopes. Compilation needs urgently to be done in high temperature chemistry and metallurgy and we are now organizing for it. The more effective exchange of information in these fields on an international scale would help everyone, and point up where more research is needed. In projects such as these the scientists of the world can most effectively cooperate to their mutual benefit.

In planning and administering the basic research program of the Commission we have taken as a guiding principle that the scope and magnitude of the problems we are facing exceed by far the present capability of our scientists and facilities to deal with them. Every available scientist of competence and every facility not otherwise engaged has been drawn into the program, and every means has been sought to make their work more effective. It is our hope that out of this conference relations will develop between our scientists and those of the other countries which will reinforce all of our endeavors in the basic research which is still needed to adapt atomic energy to the peaceful uses of mankind.

Record of Proceedings of Session 8A

THURSDAY AFTERNOON, 11 AUGUST 1955

Chairman: Mr. C. N. Watson-Munro (Australia)
Vice-Chairman: Mr. H. Staub (Switzerland)
Scientific Secretaries: Messrs. C. A. Sastre and A. Salam

PROGRAMME

P/946 Report on research reactors .... L. Kowarski
P/484 The nuclear reactor in basic science .... A. H. Snell
P/401 Research reactors .... E. Bretscher *et al.*
DISCUSSION
P/888 Practical experiences with the JEEP reactor .... T. J. Barendregt *et al.*
DISCUSSION
P/762 Experience with B.E.P.O .... R. F. Jackson
DISCUSSION
P/485 Materials testing reactor experimental program and reactor operation .... R. L. Doan and J. R. Huffman
DISCUSSION

8A.1. Survey Papers on Reactor Types

Mr. L. KOWARSKI (UNESCO) presented paper P/946.

Mr. A. H. SNELL (USA) presented paper P/484. Part of his presentation, in which he discussed some material in more detail than in the paper, follows:

There are a few basic absolute nuclear experiments that will bear almost indefinite repetition by various and successively refined techniques. The measurement of the electron-neutron interaction is an example; another is the determination of the neutron half-life and the associated beta-proton angular correlation. In view of the very substantial contribution to the study of the neutron decay that was produced yesterday by the Soviet physicists, it seems fitting that the recent results of Robson of the Chalk River Laboratories should be mentioned here, and I have his permission to bring them to your attention. Instead of measuring the explicit angular distribution of the beta particles and the recoiling protons, as the Soviet physicists are doing, Robson chose to obtain the same information by an alternative method of measuring the shape of the beta-ray spectrum at a selected angle relative to the proton recoil. His experimental arrangement is shown in Slide 1.

The neutron beam comes in from the bottom and proceeds upwards. Half-way up, it passes through a hollow electrode and an aperture in this electrode allows the protons to recoil to the right in a defined direction. The beta particles go to the left and their angle is defined by the cone of acceptance of this magnetic lens spectrometer that is used to measure the shape of the beta spectrum. Coincidences are taken between the proton counts and the beta particle counts, properly delayed to allow for the proton time of flight.

Robson's results are given in Slide 2 as experimental points; the results are summarized here with the line of best fit shown solid and the dotted lines indicating the shape of the spectrum that would be obtained on various hypotheses of the fundamental beta interaction. The angular interval between the beta rays and the protons is between 145 and 175 degrees. Casting the results in the form of the determination of the coefficient, which is often called α, in the equation that describes the electron-neutrino angular correlation, Robson derives for α the value 0.086 ± 0.120, whence the beta interaction for the neutron decay is concluded to be slightly more than half tensor in nature and slightly less than half scalar.

Reactors can produce substantial amounts of A^{37} by irradiating calcium, and some of this was recently used in another recoil experiment. A^{37} is an electron-capturing radionuclide with no gamma rays, so the only mechanism that can give nuclear recoil is neutrino emission. The energy carried off by the neutrino is known to be 816 ± 2 kev, whence one deduces that in a two-body breakup the recoiling Cl^{37} atom will have an energy of 9.66 ± 0.05 ev.

With A^{37} produced in the reactor, one can set up an experiment which I will sketch briefly. There is a chamber containing A^{37} at low pressure so that some recoils come out from the aperture at one end, and these can be put through a magnet so that the recoils go around and are simply put through a magnetic spectrometer. In fact, it is possible to measure the recoils under resolutions comparable to that of a good beta ray spectrometer. Monochromatic lines are indeed found. I will show you one in a minute. First,

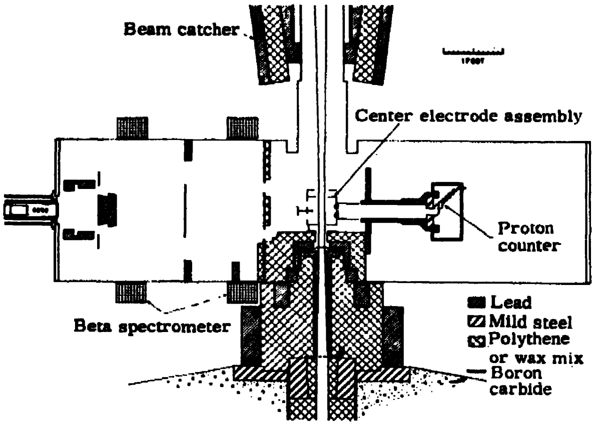

Slide 1

however, I should like to add that before the recoils go through the spectrometer, one can add a voltage to them. The way in which the results I will show you were taken was to hold the deflecting field constant and to vary the voltage applied to the source volume.

Slide 3 shows two determinations of the neutrino recoils in A^{37}. The results are both cast in terms of the recoil energy abscissa scale. You will note that the zero will be far over to the left. By centering the peaks one sees that the recoil energy in this determination is 9.63 ± 0.05 ev. Thus we see that the momentum conservation in neutrino emission is confirmed experimentally within a precision of about 1%.

Reactors are the only machines in our possession that can give neutrino fluxes big enough to make neutron detection barely possible with advanced techniques, and it may be that reactors have an extended future in neutrino experimentation. Let me cite the Los Alamos experiment of Reines and Cowan, which was aimed at the detection of free neutrons. You will recall that they used an 11 cubic foot liquid scintillator near the Hanford reactor and looked for the reaction: proton plus a neutrino going to a neutron plus a positron. In a sense, it is the inverse of the beta decay of the neutron. Coincidences were taken between the annihilation pulse of the positron and the large pulse obtained when the neutron was captured in cadmium dissolved in the scintillator liquid. A suitable time delay was introduced to take account of the slowing-down time of the neutron, and appropriate pulse height selection was added. With this arrangement, the slightly positive effect 0.4 ± 0.2 appropriate coincidences per minute was observed with the reactor on as compared with the reactor off.

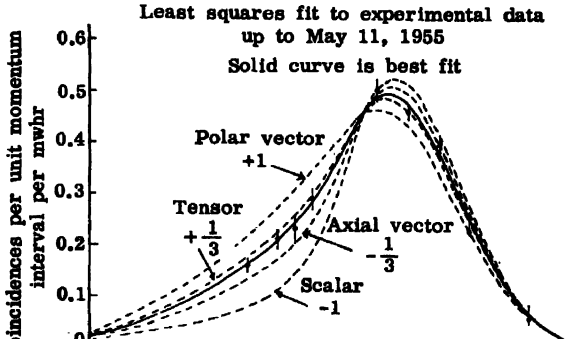

Slide 2

Dissatisfied with this rather marginal result, Reines and Cowan are revising their experiment, and they have sent me some slides that show their new arrangement.

In Slide 4, you see the ends of five rectangular tanks. The three larger ones (1, 2, 3) contain the liquid scintillator; they measure about 2 feet deep by about 8 feet long by about 6 feet wide. The smaller intervening tanks contain hydrogen—simply in the form of water, I believe. What is supposed to happen is that a neutrino being captured in the hydrogen will give rise to a positron, which, in turn, is annihilated. The annihilation quanta go in opposite directions, and so one looks for coincidences—taking advantage of this 180 degree effect—in the scintillators above and below the hydrogen liquid. The tanks below are simply to double the sensitivity of the apparatus. This 180 degree effect is the main change that Reines and Cowan are introducing in their new experiment. From there on, it goes like the old experiment, namely, that another coincidence is required between the positron

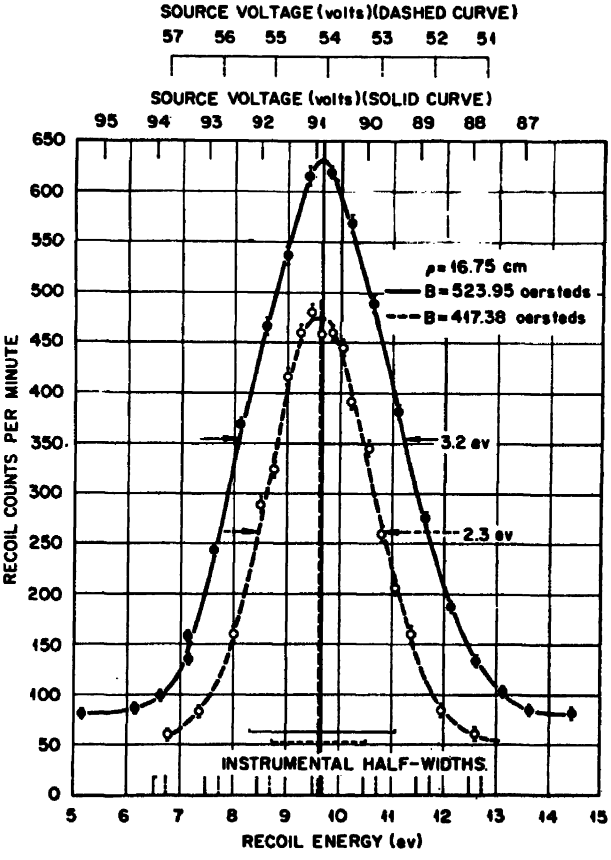

Slide 3. Energy spectrum of singly-charged neutrino recoils of A^{37} (two determinations)

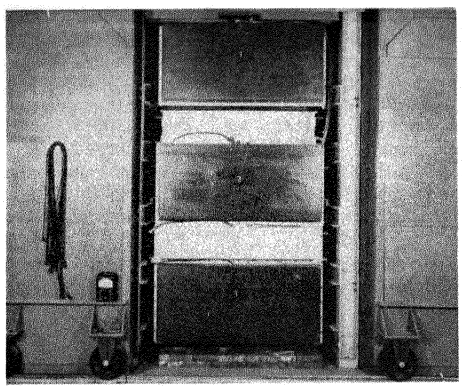

Slide 4

effect and the delayed neutron capture in cadmium, which is also present. Note the lead doors which can be brought in from the sides to complete the shield around the assembly.

Slide 5 shows one of the scintillator tanks by itself.

Slide 6 shows the connections to the scintillator tubes on the ends of the tanks.

Slide 7 on this subject shows the inside of one of the scintillator tanks. You see the white reflecting layer all around the bottom and sides. You are looking at the array of 55 five-inch photo-multiplier tubes, which are present on each end of the three tanks. Reines and Cowan will have this apparatus set up in a few months, and I think we may rather confidently expect from them good evidence of the detection of free neutrinos within a year.

Mr. E. Bretscher (UK) presented paper P/401.

DISCUSSION OF P/946, P/484 AND P/401

The Chairman: There are quite a number of questions in connection with these three papers on experimental reactors. I should like to make it clear at the outset that quite a few of these questions are concerned with the relative costs of reactors. I should not like to see this session becoming involved in a long argument over the relative costs of reactors, when, very often, two different things are being discussed; the cost of nuclear materials, experimental and post-irradiation facilities, and so forth, is included in one case but not in the other. I should therefore like to caution delegates not to get involved in trying to compare two reactors which do not include the same facilities.

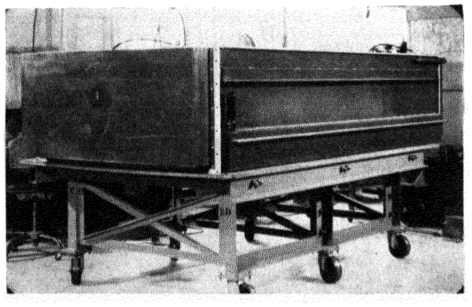

Slide 5

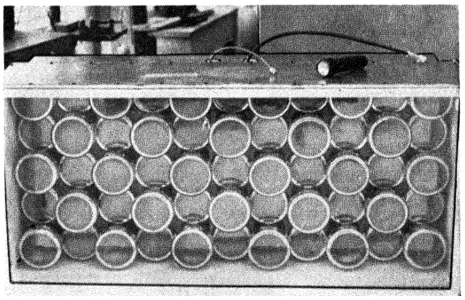

Slide 6

Mr. R. L. Doan (USA): This is a general comment directed to Mr. Kowarski's paper. It is therefore of general interest rather than specific. Mr. Kowarski calls attention to the high cost of the MTR with its thermal flux maximum of 3.5×10^{14} in comparison with that of the Oak Ridge Research Reactor of about 10^{14}, and draws the conclusion that this may represent some sort of law of diminishing returns with respect to the higher flux reactors. My comment is this: that rather than representing the law of diminishing returns, the relatively high cost of the MTR with respect to the ORR represents what one learns by experience. There is about four years difference in the design and construction of these reactors. We now believe that we know how to build a reactor of the MTR type with approximately the same maximum thermal neutron flux over a much larger volume of irradiation space at a considerably lower cost than the original MTR cost.

The Chairman: I think Mr. Doan has made the

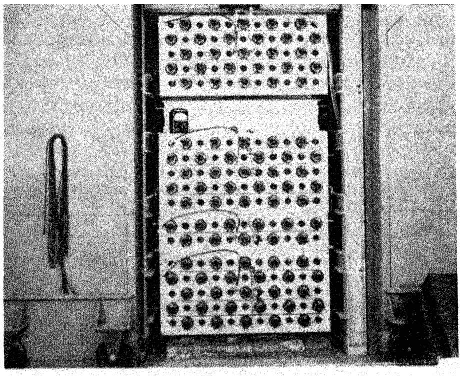

Slide 7

point about the MTR quite clear and I do not think we will ask Mr. Kowarski to comment further.

Mr. B. Buras (Poland): I should like to ask Mr. Kowarski what he thinks about the formula mentioned in his paper, that "the radius of the exclusion area is equal, in miles, to the square root of the total reactor power in tens of megawatts." How does he fit this formula to the experiments on runaway referred to yesterday?

Mr. Kowarski (UNESCO): I have not given much thought to this formula. I only tried to reproduce it as accurately as I could. I hope I reproduced it correctly.

The Chairman: I do not know whether one of the United States representatives who was present at these particular experiments would like to comment.

Mr. W. H. Zinn (USA): I could comment that the formula does not apply particularly to a case where there are no fission products built up in the reactor. Of course, the experiment we saw yesterday had no fission products built up, so it would not have made any sense to try and verify the formula. The general impression, however, that one obtains from the experiment we saw yesterday is that the formula would have provided adequate exclusion space.

Mr. D. S. Billington (USA): I should like to amplify the remarks of Mr. Snell in connection with the possibility of doing radiations at 20°K. Since this is a somewhat unique facility, I should just like to mention briefly of what it consists. It is a cylindrical aluminum Dewar 10 cm in diameter and 6 m long located in a vertical hole in the Oak Ridge Graphite Reactor. This Dewar is an integral part of a helium refrigerating system composed of a recirculating compression expansion system built by the Arthur D. Little Company at Cambridge, Mass. The cooling capacity of this unit is 340 watts at 20°K. It has been found useful to employ helium as the exchange gas for cooling, and it may be of interest to know that we have raised the pressure up to one atmosphere. Blewitt, Coltman, Cleland, Howe and Fielder and others were responsible for the design and construction of the Dewar.

I should like to show one slide which shows the data they have obtained.

Slide 8 illustrates that the radiation induced resistance increase of copper single crystals at this temperature is about two to four times the rate that you would obtain with liquid nitrogen. The other thing is that the curve is linear for this relatively short exposure of 3×10^{17}.

The Chairman: Mr. Zinn would like to make a few remarks about the proposals to increase the flux of the CP-5.

Mr. Zinn (USA): I believe the Chairman had my question in mind when he cautioned us against introducing questions which would cause comparisons in reactor costs. Actually I am interested in not having research reactors over-priced, and that is the basis for my question. I notice that Mr. Bretscher estimates that the cost of construction of a 10^{14} flux reactor might be between £2 and £3 million. The CP-5 reactor which is similar to the one to which he was referring could be operated at a flux of about 8×10^{13}, and I have the cost since it is in operation. The reactor costs £794,000. The heavy water required—14,000 lb at the United States price of $28 per lb—would add £140,000. If one estimates that a reactor of that kind could be kept going with 10,000 grams of U^{235} and this material is priced at the United States price of $25 per gram, this adds another £90,000. The total comes out at £1,024,000, about one-half of Mr. Bretscher's estimate. I was wondering if this represents additional facilities, or whether it represents the fact that in the United Kingdom it costs more to build a reactor.

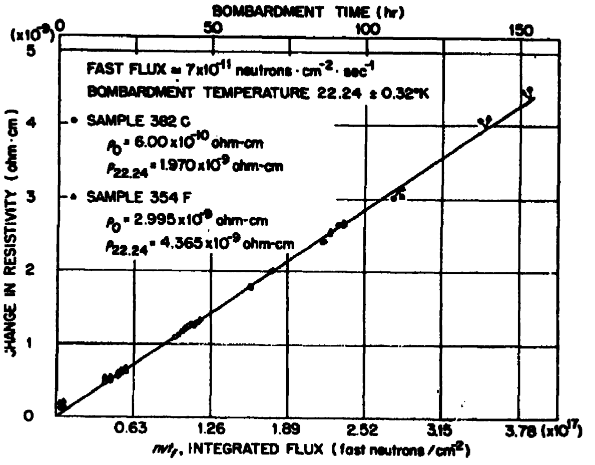

Slide 8

Mr. Bretscher (UK): I am very happy to hear that your reactors are cheaper, but, disregarding the heavy water, ours costs £1,250,000, which includes the laboratory. If the fuel is not as cheap as your $25 per gramme, then it reaches the region which I have stated. Perhaps one needs to go into more detail, but I cannot give you a closer breakdown. We could say that the flux is supposed to be 10^{14} or a little more in the centre, which is just a shade above yours, but I do not want to push the price difference on this.

Mr. H. J. Gomberg (USA): Mr. Kowarski assures me that his comment about cost was provocative, and this particular fish is rising to the bait. Some question was raised about the comparative cost of the reactor in Switzerland and the University of Michigan reactor. I checked with him, and he agreed that he was referring to the $300,000 stated for the reactor installed here. I should like to point out as a word of caution, possibly to the Swiss delegation, that this cost does not include the erection of a building with basic laboratory facilities, the erection of a tank, shield, or beam hole facilities and the thermal column; also water cooling equipment will have to be added if the Swiss reactor is to operate at one megawatt or about 10^{13} neutron flux. I think the words of the Chairman are well taken. If we talk about the same things, we shall arrive at about the same cost, and it turns out that if we were to separate out our costs for the facilities that are on display here in Geneva we come to just about the same basic figure as applies to the equivalent Michigan facilities. There is no bargain reactor, I am afraid. If you are going to have the reactor and the necessary facilities, it is going to cost something to put it up.

The CHAIRMAN: There are a lot of other questions regarding costs of reactors, but I propose to leave them out because I do not think any useful purpose would be gained by discussing them further. I am therefore going to ask Mr. Dunworth to say a few words about zero-energy systems, without regard to cost.

Mr. J. V. DUNWORTH (UK): Mr. Kowarski and I have just been having a word on zero-energy systems, and I think we are largely in agreement. We were a little troubled by the suggestion that zero-energy experiments are of short-term interest only for securing engineering data. Actually, I believe that zero-energy experiments may be of much wider interest, and I should like to draw attention, for example, to the work carried out by Mr. Shepherd and his team on the ZEPHYR. In the thermal reactor field, and looking at matters on a wider basis, pulsed zero-energy systems or pulsed exponential experiments are of value. We have, for example, the work of von Dardel in Sweden. We have also the work on transient conditions carried out by Zinn. Despite the fact that it did reach a very high power level, I think fundamentally it was a zero-energy system.

The CHAIRMAN: Mr. Weinberg of the United States would like to say a few words about the design of future systems.

Mr. A. M. WEINBERG (USA): I should like to speak of the question of the future of the present generation of research reactors. Since research reactors are expensive scientific instruments, it is always important, it seems to me, in considering the design elements which go into the reactor, to have an eye to the future potentiality of the reactor. It seems to me, therefore, that one must always keep very much in mind the possibility of ultimately increasing the power or of ultimately increasing the flux, or of doing both. I think it is clear from the history of practically every research reactor that has been built that there has always been a strong pressure developed mostly by the technological people towards increasing the power of the reactor. The Oak Ridge Graphite Reactor, for example, started at 400 kw and now runs at 4000 kw. A similar thing applies even with some reactors which have not yet been built, such as the Oak Ridge Research Reactor which started on paper as a 5000-kw reactor but is now scheduled to be a 20,000-kw reactor. The issue that is involved here, of course, is that of having somehow a cooling system which is adequate and having shielding which is adequate and, curiously enough, in many cases making certain that the reflector system is adequately cooled. There are numerous cases in point, in which the ultimate limitation on the power of a research reactor was actually the cooling of the reflector.

The other point I wanted to mention was the following: in many cases it is possible to increase the slow neutron flux substantially without changing the power simply by going from unenriched operation to enriched operation. This has been done already by the Argonne Laboratory in CP-3. I imagine it will be of considerable interest to those countries which have embarked on unenriched reactor systems and which are now faced with the possibility of acquiring sufficient enriched material to power the same reactor.

Mr. J. J. WENT (Netherlands): Mr. Bretscher has stressed the evident importance of hot loops of new types in a reactor instead of building a prototype reactor. Does he agree with me that if it is possible to reduce considerably the dimensions of such a reactor it is worthwhile building a small prototype reactor immediately, instead of a hot loop?

Mr. BRETSCHER (UK): The reactor is required to obtain a high flux for experiments, material testing and such things, and I do not see how a small reactor could do all that. Perhaps I misunderstood the question? A small prototype reactor would not test the endurance of a fuel element.

Mr. WENT (Netherlands): My idea was using a small prototype high-flux reactor, not a zero-energy reactor.

The CHAIRMAN: I know of some loop experiments running an order of cost of a quarter of a million dollars, but in some cases it would be better to build a separate high-flux reactor running with the fuel element in question, rather than to carry out the test in a high-flux reactor that is existing. I think it depends upon the test that is being carried out, and the relative economies.

Mr. WIRTZ (West Germany): May I address a question to Mr. Bretscher? Take the case that there would be no enriched uranium and no heavy water available in great amounts—I know that is not the case at the moment—and take further the case that a research reactor with great flux, $> 10^{13}$, is wanted. Would you prefer to build a separation plant to get enriched uranium or a heavy water plant to get heavy water? The cost of the separation plant should be considered of minor importance—I know that is not the case, of course, for the moment—for the answer to this question. The question looks more to future development.

Mr. BRETSCHER (UK): I would have preferred Mr. Dunworth to answer this question.

Mr. DUNWORTH (UK): I think, fortunately, it should be possible in future to purchase either one or the other from some source. Obviously, in Britain immediately after the war we decided we would have to use natural uranium and graphite since other materials were in short supply. If one wished to have high flux one had no alternative but to have a large pile of high output, which in fact we built for other purposes. But I am afraid there is no straight answer to your question, because obviously one would not wish to build either a diffusion plant or a heavy water plant solely to enable one to have a research reactor. I am sorry if I seem to dodge the question, but I do not really think either answer is a correct one.

8A.2. General Principles and Practical Experience

Mr. N. HIDLE (Norway) presented paper P/888.

DISCUSSION OF PAPER P/888

Mr. DOAN (USA): In reading the paper, I have noted that during start-up of the JEEP reactor, the pile period is entirely under the control of the operator. He brings it to where he thinks it is safe. Do you also have automatic shut-down instrumentation based on the pile period so that if the period gets too short the reactor shuts down automatically?

Mr. HIDLE (Norway): We have no instrument for shutting down because of short periods. The shut down system only reacts on the absolute level of the reactor.

The CHAIRMAN: For a reactor of this order of power, I think that would be quite satisfactory.

Mr. R. F. JACKSON (UK) presented paper P/762. There was no discussion.

Mr. J. R. HUFFMAN (USA) presented paper P/485.

DISCUSSION OF PAPER P/485

Mr. MUMMERY (UK): Would Mr. Huffman give the reactivity breakdown associated with xenon poison, with the fission products and the depletion effects for 20% burn up, and the sort of excess reactivity which he thinks a reactor of this kind should have?

Mr. HUFFMAN (USA): As I remember, the 20% total recovery in the reactor is broken down as follows: 4.9% for xenon and samarium poisoning; 4.7% for overriding xenon in case you have an accidental shut-down; of the order of 5 to 7% excess reactivity for experimental work and there is of the order of 5 to 7%, I think, for normal fuel depletion and gross fission products poisoning. As to how to answer how much reactivity you should have in an experimental reactor, that is difficult to say. Actually, as we have increased the fuel content in order to get better operating cycles, I think we have about 20% excess k available for reactors for certain experiments occasionally. We have had no difficulty operating this reactor with of the order of 5 to 7% excess k. Of course, when the experiment does not need it, we do not put it in.

Mr. H. J. GROUT (UK): Would Mr. Huffman like to comment on the relative advantages and disadvantages of light and heavy water as a moderator in high flux research reactors using enriched uranium, particularly where these research reactors are to be used for material testing and engineering loop work? Further to that question, would Mr. Huffman please say whether the beryllium reflector surrounding the core of the MTR reactor is absolutely essential in this class of reactor for it to be a success, and also give some actual dimensions of the maximum flux, which was indicated to be about 3.5×10^{14}. In other words, over what volume would this very high flux extend?

Mr. HUFFMAN (USA): I do not know whether I can answer this question of heavy water and light water reactors, but it is my personal opinion that the light water moderated reactor gives a fast flux which you would not obtain with the heavy water moderated reactor unless you put in converters. This high fast flux also acts somewhat as a reservoir for the thermal flux which you want to use nearby. This high fast flux is needed to back the total flux, because there is less flux when you put a large loop into a heavy water moderator. I am not really good enough in physics to answer this question, but I feel it does give you the high fast flux in addition to the high thermal flux.

With regard to the second question, regarding the beryllium reflector in the MTR, as is given in our paper we started out with a beryllium reflector. Actually this is now of the order of 3-in. around the core and most of the other reflectors positions are filled up with aluminum in which experiments are being conducted. It is cheaper to use aluminum than to bore beryllium for a particular experiment. I would believe a beryllium reflector is not at all necessary for this type of reactor, certainly not more than three inches is necessary around the actual core. As regards the flux, I should repeat that the fluxes in this pile as I give them are unperturbed. As soon as you put a major experiment in you lose because of the poison associated with the experiment. A maximum of 3.5×10^{14} occurs in the beryllium right close to the core or the active uranium; about three inches out of the uranium rectangle slab face you get 3.5×10^{14} flux. I doubt if this is over an area of more than two to three inches in depth and probably of the order of one foot in height, so that you do not have in this reactor large spaces with high flux. You must sacrifice the space to get the flux.

Mr. WEINBERG (USA): I wish to raise again the points which Mr. Huffman has mentioned, that you have a sort of complementarity in the reactor. If you wish to get high fast flux you must sacrifice space and if you wish space you have to sacrifice high fast flux. I should point out another matter, though, that the total number of neutrons which are available for experiments is always $(k - 1)/k$ multiplied by power. It is true that in the heavy water system $k - 1$ is on the whole somewhat higher than it is in the light water system. On the other hand, as my earlier remarks implied, it is at least my impression that it is easier to run a light water reactor at very high power than it is to run a heavy water reactor at very high power and that, therefore, in considering the question of the total number of neutrons available for experimental purposes, the light water systems seem perhaps to have a very small advantage. On the whole I would caution the audience, however, not to be doctrinaire in the matter. Both reactors have advantages and disadvantages and in all cases the difference between having a reactor and not having a reactor is far more important than the difference between having a heavy water reactor or a light water reactor.

Mr. J. Pelser (Netherlands): This is a question concerning the use of 20% enriched uranium in materials testing reactors. Is it possible to obtain the same values for fast and thermal fluxes at the same power levels and possibly also the same built-in reactivity when using 20% enriched uranium, and what changes in construction, if it is possible, eventually would be made?

Mr. Huffman (USA): I would like to refer this question on the design of the MTR to Mr. Weinberg.

Mr. Weinberg (USA): I would like to have an opportunity of referring to this question at tomorrow's session,* at which this issue will be discussed. I might simply say that so far as we can see it seems entirely feasible to run high flux reactors with 20% enriched uranium, but we will touch upon this matter tomorrow in my paper.

---

* Session 9A.

Session 9A

RESEARCH REACTORS, DESCRIPTIONS

LIST OF PAPERS

Page

P/623 A heavy-water research reactor . . . . A. I. Alichanov *et al.* 331

P/387 The Saclay reactor: two years of experience in the use of a compressed gas as a heat transfer agent . . . . J. Yvon 337

P/915 Description of the Swiss research reactor . . . . F. Alder 351

P/860 The Brookhaven reactor . . . . M. Fox 353

P/488 Design and description of water boiler reactors . . . . L. D. P. King 372

P/621 The experimental nuclear reactor with ordinary water and enriched uranium . . . . Y. G. Nikolaev 392

P/622 A 2000-kilowatt thermal power nuclear reactor for research purposes . . . . Y. G. Nikolaev 399

P/490 The Materials Testing Reactor and related research reactors . . . . A. M. Weinberg *et al.* 402

P/489 The swimming pool reactor and its modifications . . . . W. M. Breazeale *et al.* 420

A Heavy-Water Research Reactor

By A. I. Alichanov, V. V. Vladimirski, S. J. Nikitin, A. D. Galanin, S. A. Gawrilow, and N. A. Burgow, USSR

1. PURPOSE

The heavy-water reactor of the Academy of Sciences, USSR, was designed in 1947, installed in 1948 and put into operation in April 1949. The main purpose of the reactor was to perform physics experiments with the reactor itself (critical experiments) and with the neutron beams from it. Beside this, it was intended to use the reactor for the production of radioactive isotopes, for biological research and for research in the field of radiation chemistry and metallophysics.

The theory of heavy-water reactors is significantly different from that of the graphite reactors: the comparatively small size of the system and the high multiplication-factor, the comparatively small number of collisions necessary for slowing down the neutrons, the presence of secondary neutrons from the $D(\gamma,n)$ reaction and the sharp change of the medium properties at the border between the reactor and the graphite reflector. The high cost of heavy water makes it necessary to determine the optimal size of a heavy-water reactor with a great accuracy. On the other hand, the use of the liquid moderator allows an easy change of arrangement of the uranium rods within the reactor. This made it possible to perform a series of critical experiments with uranium rods of different diameter and with several values of the lattice spacing.

2. DESIGN OF THE REACTOR

The heavy water is contained in a thin-walled tank (1) (see Figs. 1, 2) made out of aluminium sheets 3–3.2 mm thick. The tank is 175 cm in diameter and 195 cm high. The slightly conical bottom of the tank is supported by the graphite reflector. The bottom and cylindrical part of the reflector are 100 cm thick. The graphite reflector is surrounded by hermetical outer tank (3), which is usually evacuated. Provision has been made for demounting and replacing the aluminium tank.*

The uranium rods (4) are suspended from a rotating plate (7) above which the lead shield (5) carrying four slit-shutters (6) is located. The outer hermetical tank is closed in the upper part by a stainless steel cover (8) which has four slit-gaskets for replacement of uranium rods. By opening the slit-shutters (6) and moving the rotating plate, it is possible to bring any of the uranium rods under the slit and remove it without demounting the upper shield of the reactor. The rotating plate has a number of additional holes, which permit one to make a number of rod arrangements. When a part of uranium rods is removed there is no necessity for closing the free holes in the rotating plate, as the shielding and the tightness of the apparatus is not affected. Two types of rotating plate were manufactured: one of them has two sets of holes, corresponding to square-lattice spacings equal to 115 and 138 mm and is provided below with a 60 cm thick graphite reflector, the other plate has no reflector and the holes form a 90 mm square lattice. The uranium rods are 160 cm long and their lower ends are 5 cm above the bottom of the reactor tank.

The heat is removed by circulating the heavy water (see Fig. 3). The heavy water enters the reactor tank at the bottom through the pressure pipe (9) and is drained off in the upper part of the reactor. The drain pipe (10) runs along the axis of the reactor and goes out through the inlet pressure tube. From the drain pipe the heavy water passes through the circulating pumps (11) to the heat exchanger (12) and returns to the reactor. The uranium rods are cooled by natural convection, the circulating velocity of the heavy water within the reactor being low. The choice of such a circulating system sets the power level of the reactor at 500 kw.

There are two circulating pumps each having a peak pumping rate 25 m^3/hour. Usually one of the pumps is operated. The pumps are tightened by rings of soft plastic and by an additional rubber gasket, which when the pump is not operated closely tightens the shaft of the pump. The leakage of heavy water does not exceed 10 gm per day. The heat exchangers, where heavy water is cooled by ordinary water, are made of stainless steel.

When the reactor is not in operation the heavy water is kept in the storage tank (13).

Helium is kept above the heavy water and is circulated by means of gas blowers (14). The shafts of the gas blowers have no gaskets as the rotor of the driving motor is located in the helium atmosphere and is separated from the stator by an isolating gas-tight cap. The circulating helium carries away the detonating mixture, which is recombined by means of an apparatus (16) with palladium-catalyst, deposited on aluminium oxide.

Original language: Russian.

* The tank was replaced once in 1953.

The reactor is provided with four cadmium control rods, which may be used for manual or automatic control. A remote precision device is provided which permits measuring by means of selsyns the position of the control rods accurately within 0.1 mm (corresponding to the introduction of 0.1 mg of boron into the reactor). The positions are transmitted to the control desk. The control rods are driven by means of a rack and pinion. The motors (17) and the selsyns are placed outside the gas tight reactor tank; the rotation is transmitted by means of a bent shaft with a rubber pipe-junction packing. Beside the control-rods there are two emergency rods, which fall when the current through the electromagnet holding them ceases. A device for a rapid emergency draining of the heavy water from the reactor is provided.

The level measurement and the automatic control are performed by means of ionization chambers lined with boron and supplied with dc amplifiers. The starting of the reactor at low power-levels is controlled by BF_3 counters with integrating circuits.

The concrete side shield of the reactor (18) has a thickness of 2.5 m. There is a number of channels (19) for irradiation and for the letting out beams. Three channels extend through the graphite reflector and reach the tank of the reactor. These channels penetrate the reflector through thin-walled steel mantles which are welded into the wall of the outer tank. All channels (19) are closed by interchangeable screw plugs inside of which the collimators defining the emerging beams can be mounted. In the upper cover of the reactor there is an opening through which passes a thin-walled (2 mm) aluminium channel (21) with a diameter 9 cm. This channel serves to let out a beam for irradiation and for other experimental purposes. Besides this there is a number of vertical channels for putting instruments and irradiated samples into the reflector and into the shield. In the side shield there is a graphite thermal column (20) of 1.4 × 1.4 m cross section.

The reactor is provided with a level gauge with an absolute accuracy of 2 3 mm and with a relative

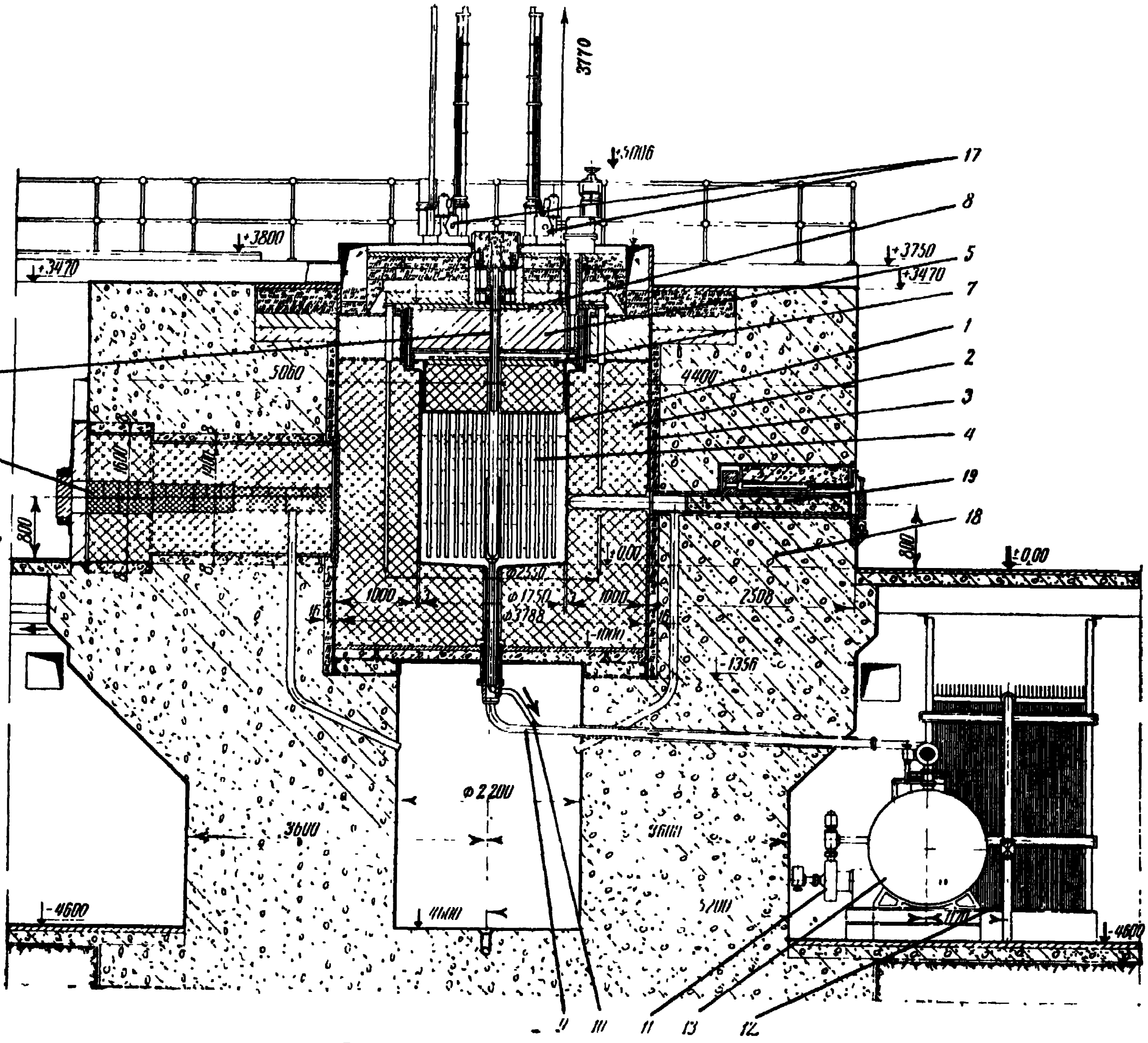

Figure 1. Longitudinal cross section of the apparatus

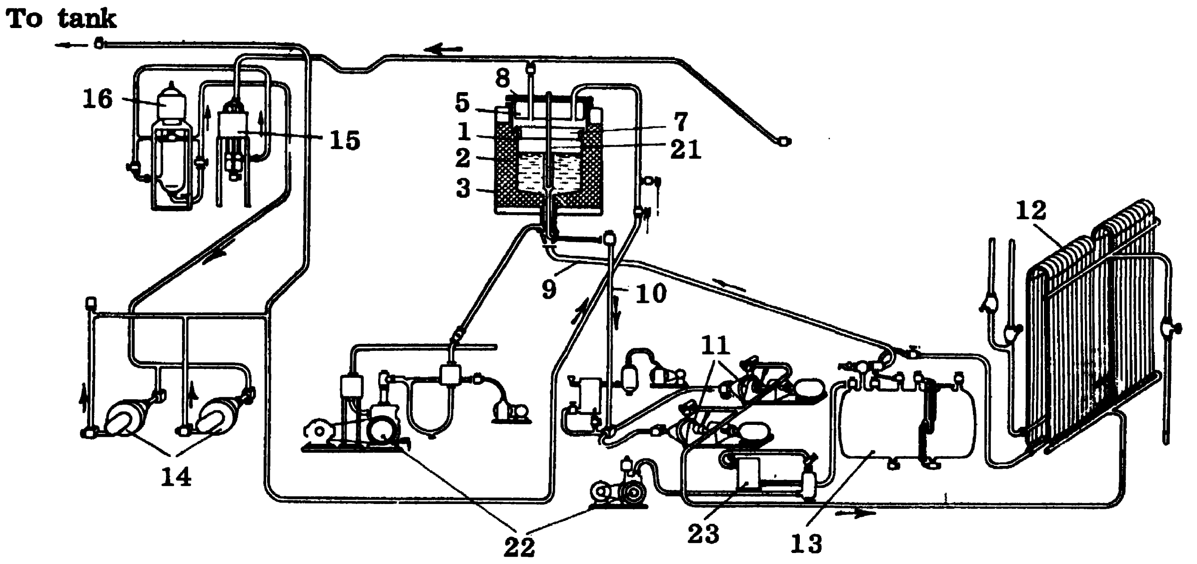

Figure 3. The scheme of the installation

LEGEND TO FIGURES 1, 2 AND 3

1. Aluminium tank
2. Graphite reflector
3. Hermetical outer steel tank
4. Uranium rods
5. Lead shield cover
6. Slit-shutters
7. Rotating plate
8. Stainless steel cover
9. Pressure pipe
10. Drain pipe
11. Circulating pump
12. Heat exchanger
13. Storage tank
14. Gas blower
15. Condenser
16. Recombination apparatus
17. Drives of the control recombination rods
18. Side shield
19. Side experimental channel
20. Graphite thermal column
21. Vertical experimental channel
22. Vacuum pumps
23. Liquid nitrogen trap

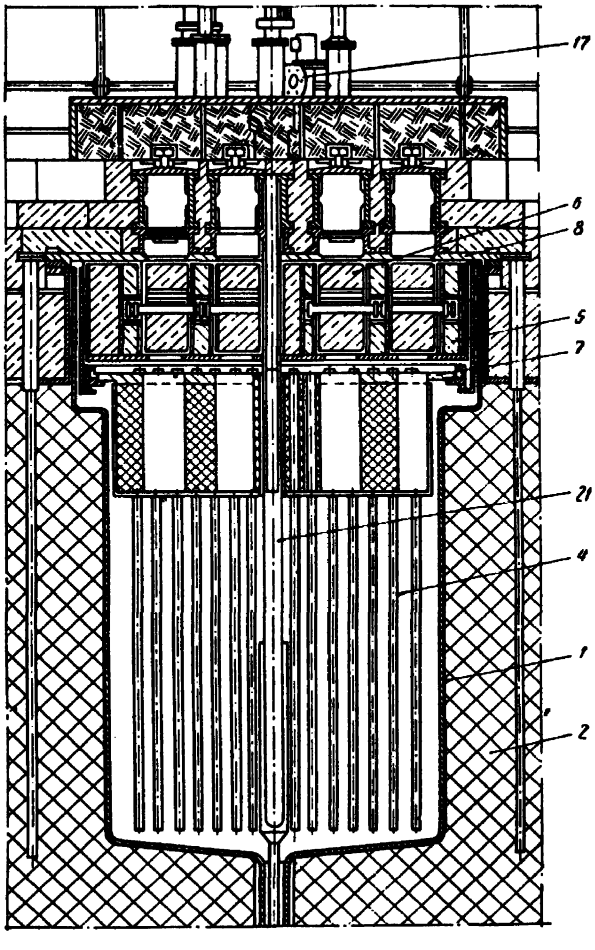

Figure 2. Cross section showing the location of the slit-shutters

accuracy of 0.2 mm. The temperature of the heavy water at the input and output of the reactor, the temperature of the reactor envelope, of the graphite and shield; the circulation-rate of heavy water, of the gas and the consumption-rate of the cooling water, the pressure within the reactor and within the side-reflector are all measured. Special care was given to the measurement of the detonating gas mixture concentration. All the vessels and pipes for heavy water and helium were tested for vacuum tightness. Drying after servicing is performed by evacuation, heavy water is frozen out in liquid nitrogen traps.

3. CRITICAL EXPERIMENTS AND THE VERIFICATION OF REACTOR THEORY

The critical volume was measured with different arrangements of uranium rods in the reactor. Besides this, for three arrangements of the rods, a detailed investigation of the neutron density distribution along the radius and the axis of the reactor was performed. The density distribution allows the direct determination of the Laplacian of the reactor for a given lattice. For the purpose of comparing the computed and experimental data, it is convenient to use the value of the Laplacian, as it does not depend on the details of the construction and is the main parameter determining the dimensions of the reactor. Because of this the results of the critical experiments were used for obtaining the experimental value of the Laplacian. All the constructive features of the reactor must be accounted for as corrections. The most important corrections are due to the nontotal reflection of the neutrons in the upper part of the reactor due to the presence of an additional amount of aluminium (the outlet tube and the central experimental channel) and leakage through the reflector in the vicinity of the horizontal experimental channels. In a number of cases the active core of the reactor did not approach the vessel envelope and a need arose to account for the effect of the heavy water layer on the reflector properties. In the lattices with 115 and 138 mm spacing one central rod was absent (the location of the central experimental tube and of the outlet tube). In the 90 mm lattice two central rods were absent.

All critical experiments were performed with the temperature of heavy water equal to 20–23°C. The level of the heavy water within the reactor, corresponding to its critical size in the absence of the control rods, was determined. Experiments on the neutron density determination were carried out at a power level of the order of 100 watts. The density measurements were carried out by means of dysprosium and gold detectors and also by means of the reactivity change method. The experimental curve was approximated by the function $\cos \alpha_z(z - z_0)$ by the least square method; the radial distribution was approximated by $AJ_0(\alpha_r r) + BN_0(\alpha_r r)$. The presence of the function N_0 is connected with the loss of neutrons in the centre where the outlet and the experimental tubes are located. The experimental value of the Laplacian is determined as $\alpha^2 = \alpha_r^2 + \alpha_z^2$. The results of some critical experiments and their treatment are given in Table 1.

The calculation methods are given in reports by A. D. Galanin.[1] In the calculations of the Laplacian from the constants the following data on the materials in the reactor were used: mean number of the secondary neutrons for natural uranium, disregarding impurities, $\eta = 1.33$; fast fission factor, $\epsilon = 1 + 1.7 \times 10^{-2}\rho$ where ρ = radius of the rod in cm.

The resonance absorption was calculated using the expression

$$\psi = -\ln \varphi = \frac{\alpha\rho^{3/2} + \beta\rho^2}{a^2 - 0.94S_U - 0.96S_{Al}}$$

where a is the lattice-spacing, $S_U = \pi\rho^2$ the uranium area, and S_{Al} the aluminium area.

The values of the constants α and β in the expression for φ were taken from the experiments of N. A. Burgow.

For the thermal cross-sections the following values, referred to the standard boron cross section σ_a = 700 barn, were used: uranium cross-section σ_a = 7.1 barn, σ_S = 9.0 barn; heavy water (per molecule) σ_a = 0.001 barn; slowing down constant τ_0 = 139 cm²

$$\tau = \frac{\tau_0}{1 - 0.54\dfrac{S_U}{a^2} - 1.6\dfrac{S_{Al}}{a^2}}$$

graphite, L = 50 cm, τ = 370 cm²; and aluminium σ_a = 0.28 barn.

Comparison of the Laplacian obtained by different methods show a satisfactory agreement between the experimental data and those computed from the measured values of η, φ, τ and the cross-sections. The experimental errors and the errors of the theoretical computations are so large that it is impossible to improve materially the accuracy of the values of the constants measured earlier. It is only possible to say that an increase of the resonance absorption by 10%, with a simultaneous increase of the multiplication coefficient by 0.8% would lead to some improvement of the agreement of the results. The multiplication coefficient may be increased by altering the fast fission factor, the effect of fission by intermediate neutrons, the constant η etc. It is impossible to make such an alteration, however, as with the values of the constants taken the discrepancy lies within the limits of experimental error. In any case, the comparison of the calculated and the measured critical volumes shows that the errors in the calculated values of the multiplication coefficient do not exceed 1% and, most important, it considerably increases confidence in the theory.

FURTHER OPERATION OF THE REACTOR

The considerable excess reactivity of the reactor made it possible to use in normal operation an unusual arrangement of uranium rods. In the central part of the reactor a cylindrical region was left free of uranium rods, the so-called "pit." The diameter of the pit was 60 to 70 cm, depending on operation conditions.

As the radius of the pit considerably exceeds the slowing down length of neutrons in heavy water, an almost pure thermal neutron spectrum was obtained in its centre. The location of the pit in the centre of the reactive zone provides a high neutron density nearly coinciding with the peak density. The experimental channel in the centre of the pit allows the introduction into the neutron field of samples without breaking the tightness of the reactor and to let out beams of thermal neutrons in the vertical direction. This arrangement proved rather convenient for a wide range of experiments. When needed, it was possible to alter the neutron spectrum. For the purpose of irradiation by fast neutrons a "neutron converter," a water cooled uranium cylinder, was introduced into the experimental channel. Within the cavity of the neutron transformer a powerful flux of fast neutrons was obtained.

A considerable negative temperature coefficient makes the reactor quite safe in operation. After heating-up and reaching the stationary concentration of Xe^{135} the reactor was able to operate indefinitely with switched-off or fully removed control rods. The self-regulation of the power due to the negative temperature coefficient excludes the possibility of accidents due to failure of the controlling devices. If all control rods are removed from the shut down reactor, the power rapidly rises to 700–1000 kw, then falls gradually and reaches a value determined by the heat removal.

The temperature coefficient of the reactor was determined by measuring the displacement of the automatic control rod during heating and cooling of the reactor. The effect of the control rods was calibrated by standard boron samples. The temperature coefficient equals 14×10^{-5} degree^{-1}; it is determined by a number of effects which are difficult to distinguish experimentally (the change of moderator density, the change of σ_a with energy, the change of the resonance capture by higher levels with change of the metal temperature). By measuring the poisoning of the reactor the value of the capture cross-section of Xe^{135} was determined: $\omega/\sigma = 2.6 \times 10^{-19}$ cm² ± 15%, where ω is the yield of Xe.

Table 1

Diameter of the uranium rods, cm	2.8	2.8	2.8	2.2	2.2	2.2
Thickness of the aluminum canning, cm	0.1	0.1	0.1	0.1	0.1	0.1
Spacing of the square lattice, cm	11.5	13.8	16.26	9	12.7	6.3
Number of rods	120	120	86	272	107	292
Critical level in the reactor, cm	131	120	148	118.5	174.5	181.6
Length of the uranium rods cm	160	160	160	162.5	162.5	162.5
Critical volume of heavy water, including the side and bottom layers of water, m³	3.09	2.78	3.52	2.764	4.175	4.104
Volume of the active zone, m³	2.02	2.64	3.28	2.52	2.86	A part of the volume is occupied by 9 cm lattice
Laplacian, measured by neutron density distribution, m⁻²	8.1 ± 0.5	—	6.8 ± 0.3	8.0 ± 0.5	—	—
Laplacian, calculated from critical dimensions by the effective boundary conditions method m⁻²	7.9	7.6	6.5	7.9	7.0	3.0
Laplacian, calculated from the critical dimensions by numerical solution of the cylindrical problem m⁻²	—	—	—	8.0 ± 0.1	7.4 ± 0.15	
Laplacian, calculated from the values of the constants m⁻²	8.3 ± 0.5	7.6 ± 0.4	6.7 ± 0.4	8.4 ± 0.6	7.4 ± 0.4	4.0 ± 0.0
The multiplication coefficient, calculated from the values of the constants	1.214	1.244	1.258	1.195	1.241	1.071

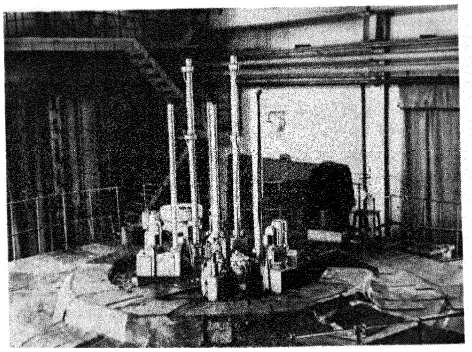

Figure 4. General view of the top of the reactor

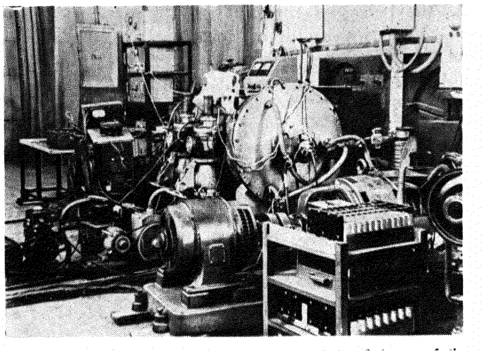

Figure 5. Arrangement for the investigation of the β-decay of the neutron

The continuous peak power is 600 kw, the usual power level, when operating for the purpose of irradiation of samples and neutron beam research equals 350–500 kw. At this power the thermal neutron density in the centre of the reactor reaches the value 2×10^{12} cm^{-2} sec^{-1}. In the beams emerging from the reactor it equals to 10^7 cm^{-2} sec^{-1}. When operating with automatic control, the power is held constant with an accuracy ±0.3%. A number of measurements on the reactor were performed at a lower power. In particular, all measurements of the cross sections and of the number of secondary neutrons by the reactivity method were carried out with a power of the order 20–500 watts. The automatic control of the reactor at such a low power level was achieved by introducing an ionization chamber inside the reflector through the side channel.

The thermal operating data of the reactor are given in Table 2.

Table 2

Temperature of heavy water at the inlet of the reactor	20–43°
Temperature of heavy water at the outlet of the reactor	38–65°
Heavy water circulation rate	21 m^3/hour
Cooling water consumption	40–60 m^3/hour
Excess pressure of the gas in the reactor	0.1–0.45 atm
Circulating rate of the gas	80 m^3/hour
Detonating mixture content	0.05%

The radiation level outside the side shield equals one tolerance dose. On the top of the reactor the radiation level when operating at full power reaches 50 doses. The background in the reactor room is mainly determined by the scattered radiation, penetrating through the upper cover and the experimental channels on the side.

Several physics investigations were performed with the reactor. Some of them will be presented in separate reports to the conference.[2–8]

At present improvements on the reactor are planned. The power level and the shielding will be increased. It is proposed to raise the thermal neutron flux inside the reactor to 2×10^{13} cm^{-2} sec^{-1}.

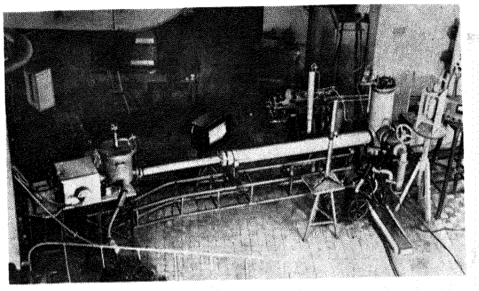

Figure 6. Experimental arrangement for the study of scattering of neutrons by ortho- and para-deuterium

REFERENCES

1. Galanin, A. D., P/664, *Application of the Method of Effective Boundary Conditions for Calculating the Critical Dimensions of Reactors*, P/666, *The Thermal Coefficient in a Heterogeneous Reactor*, Session 23A, Vol. 5, these Proceedings.
2. Alichanov, A. I., Vladimirski, V. V. and Nikitin, S. J., P/658, *Number of Fission Neutrons for One Captured Thermal Neutron in U^{233}, U^{235} and Pu^{239}*, Session 18A, Vol. 4, these Proceedings.
3. Burgov, N. A., P/660, *Number of Fission Neutrons for One Captured Thermal Neutron for Natural Uranium*, Session 18A, Vol. 4, these Proceedings.
4. Spivak, N. E. and Sosnovsky, A. N., P/650, *Investigation of the Decay Neutron*, Session 6A, Vol. 2, these Proceedings.
5. Nikitin, S. J. and Smolyankin, V. T., P/643, *Scattering of Slow Neutrons by Ortho- and Para-Deuterium*, Session 6A, Vol. 2, these Proceedings.
6. Dolin, P. I. and Ershler, B. V., P/679, *Radiolysis of Water in the Presence of H_2 and O_2 Under the Action of Reactor Irradiation, Fission Fragments and X-Rays*, Session 12B, Vol. 7, these Proceedings.
7. Vladimirski, V. V., Sokolovsky, W. W. and Radkevich, I. A., P/641, *A Neutron Selector with the Mechanical Interrupter*, Session 17A, Vol. 4, these Proceedings.
8. Girshfeld, S. V., P/648, *The Study of Delayed Neutrons Emitted by Uranium-233 as a Result of Irradiation by Thermal Neutrons*, Session 16A, Vol. 4, these Proceedings.

The Saclay Reactor: Two Years of Experience in the Use of a Compressed Gas as a Heat Transfer Agent

By J. Yvon,* France

I. PURPOSE

The first studies for the Saclay reactor began in 1949. The main lines of the program to be carried out were set in August of that year. We must go back to that period, which may well seem lost in the past to those who have followed the day to day development of our concepts and the progress of our knowledge regarding atomic reactors, in order fully to appreciate the atmosphere of doubt and uncertainty in which decisions were taken which were to commit the C.E.A. (Commissariat à l'Energie Atomique—French Atomic Energy Commission) to several years of work along the lines then laid down.

Reactor Zoe, with a charge of uranium oxide and a heavy water moderator, then was operating with great regularity ever since it had gone critical, on December 15 of the year before: this bore witness to the good nuclear quality of the materials in use, as well as to the purity of the uranium oxide, of the graphite used in the reflector, of the aluminum cladding and of the vessel. The power level, which had been brought up progressively to a few kilowatts, had enabled the supervisory personnel to become familiar with the operation of a device of that type, to control the reactor, to adjust the power level, to effect heavy water transfers, and to produce radionuclides. At the same time, a physical study of the reactor,[1] of the neutron flux and of its kinetics, brought our knowledge, which until then had been purely theoretical, into the realm of the concrete and practical.

The French uranium production, which had, until then, been very small, did not warrant anything but a heavy water reactor. Fortunately, the heavy water requirements were met, as they had been for reactor Zoe, by purchasing a fraction of Norway's production. Nevertheless, the amount of heavy water available was not known with any great accuracy, and remained limited. It appeared reasonable to provide for a reactor which could go critical with only 5.8 tons of heavy water.

Uranium oxide, which is not too suitable for a good utilization of the neutrons, had been given up. This meant that the C.E.A. chemists had to set up the production of ingots of pure uranium. The metallurgists had to learn how to turn ingots into uranium rods of acceptable mechanical quality, then to clad them.

The objective was to produce, in the new reactor, neutron fluxes far more intense than those delivered by Zoe. This intense production of neutrons is necessarily attended by the evolution of large amounts of heat inside the reactor. This would have to be taken care of in order to make an abundance of neutrons available to the research workers.

In this aspect, the C.E.A. could make a free choice. This choice was between several processes dependent on the nature of the fluid to be used for the purpose of removing the heat (primary fluid) and various types of circulation: (1) bulk circulation of heavy water, (2) forced circulation of heavy water along the rods, (3) air circulation under atmospheric pressure, (4) compressed gas circulation.

The efficiency of methods 1 and 3 seemed too low. The second method was better than the last in efficiency, but a higher outlet temperature of the primary fluid could be expected with 4. A reactor operated on such a principle could indeed be an advance model for future reactors designed to produce a hot fluid: this would be the beginning of the application of atomic fission to the production of utilizable power.

The use of compressed gas faced the engineers with greater problems, both from the standpoint of circulating the primary fluid and from that of making an accurate estimate of the neutron economy. Before any decision was made, they had given more time to that concept than to others. Thus, instinctively they advocated the solution of which they had made a more painstaking study, which, in the end they knew better. It was this solution that was adopted.

The primary fluid circulates along the uranium slugs, inside aluminum tubes. These are submerged in heavy water. The circulation system is so designed that the hot gases do not heat the heavy water. The tubing is strong enough to withstand an internal pressure of 10 atmospheres at least. The aluminum vessel which contains the heavy water has no other load to resist but that due to the weight of the liquid itself, the surface of which remains at atmospheric pressure.

Another solution would have been using thin tubing and placing the whole of the reactor in a gas tight and resistant envelope. It would have had to house the

---

Original language: French.

* Chief, Reactor Design Department, Commissariat à l'Energie Atomique.

reflector as well, and thus be fairly large. The arrangement actually used is more preferable:

Every unit in the fluid-tight tubing system kept under pressure can be taken apart and serviced, overhauled or replaced without any great difficulty; the means of access required by the experimenters in order to make use of the reactor's radiation, the installation of the control rods and plates, and the recombination system for the heavy water, present no greater difficulty than in a reactor entirely at atmospheric pressure.

It should be noted that these advantages might lose some of their value in a reactor not so clearly experimental in design and purpose.

The pressure resistant tubing, arranged vertically in the reactor, is fed from the top by manifolds which are somewhat critical to make. They require a certain minimum distance between the centers of two neighboring uranium rods. On the other hand, it was desired to develop a high power compatible without excessive power production by each individual rod, they had to be mounted very close to one another, in order that there would be as many of them as possible in the allocated space. These contradictory requirements were met by a compromise solution: the lattice used was hexagonal, with a distance of 151 mm between centers. The computations led to a 26 mm diameter for the rods.

Allowing for the indispensable tubing, the lattice so obtained is far from being the optimal one for uranium and heavy water.

The project was designed for a power of 1500 kw. Nevertheless, only 1000 kw were announced publicly.

The reactor was quickly built and went critical on October 27, 1952.

It is now understood that, in order to develop power with a uranium and heavy water reactor, a good technique is the use as a primary fluid, of heavy water kept in the liquid phase, despite the rise in temperature, by suitable pressurizing. This solution is not very compatible with the use throughout of aluminum, the only structural metal available in 1949. The reactor builders of 1949 did not give much thought to such a technique. It is now clear that they had neither the knowledge, nor the means, required.

II. DESCRIPTION[2]

Active Section

Vessel

The heavy water vessel is a cylinder, 2 m in diameter, 2.50 m high. The thickness of its walls is 3 mm, that of its flat bottom 6 mm. The net capacity after deduction of space taken up by the elements which are submerged in the water, is 7 m^3, but the critical volume is substantially smaller. The vessel is made of 99.5% pure aluminum.

Fuel Assemblies

The mass of uranium used in the reactor amounts to 3 tons. The fuel rods, which are vertically arranged, are 136 in number, and form an hexagonal lattice, so centered as to have a pitch of 151 mm.

In order to facilitate the manufacture of the vessel and internal reflector, feeding cold gas to the cells and removal of the warm gas are effected through the upper part. Thus, circulation is of the "hair pin" or "loop" type.

A "cell" can schematically be described as follows: the axial part is taken up by a uranium rod surrounded by a shielding tube. This assembly is housed in another tube which, in turn, is directly submerged in the heavy water. The cold gas goes down between the outer tube and the shielding pipe, it then travels up again, along the uranium rod. During its downward flow, it cools off the moderator, in which 5% of the total power is developed, while the uranium is cooled off during the upward run.

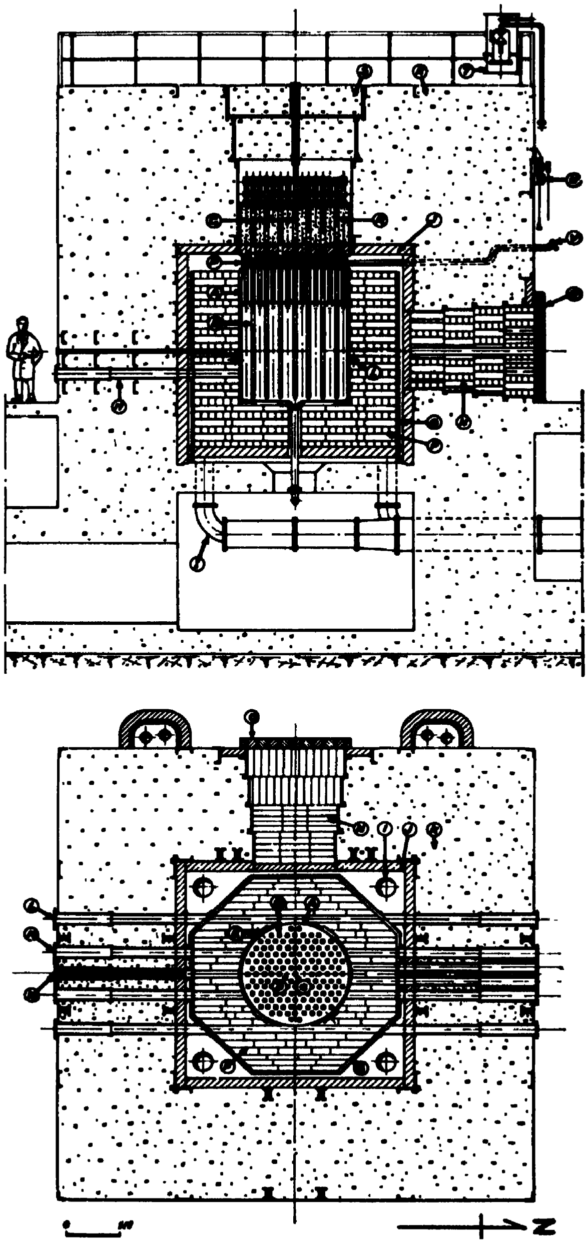

Figure 1. Vertical and horizontal cross sections of the reactor

Heat transfer, between the ascending and the descending flows, is reduced by the presence of a 1 mm thick gas layer trapped between the two intermediate tubes, forming a thermal screen. This gas layer provides very satisfactory insulation: during the downward travel, coolant fluid temperature thus does not go up by more than 3°C.

Each rod is made up of several slugs. They rest on "shelves" which, in turn, are held by the screening tubes. The cladding metal is magnesium.

Each cell is fed an amount of gas proportional to the power developed, so that the outlet temperatures are the same for all the cells. This adjustment is made by means of valves which can be operated from above once the reactor is shut down and uncovered. The valve operating rods are hollow to house thermocouples.

Reflector and Shielding

A graphite reflector surrounds the vessel laterally and extends under the bottom. The existence of a reflector above the heavy water would have been desirable, but constructional difficulties made this impossible. Externally, the graphite mass is shaped like an octagonal prism. The minimum thickness is 0.90 m. It is made up of 3700 140 mm square bricks, and weighs 57 metric tons. Each of these bricks has been machined to a tolerance of 0.05 mm.

Protection is provided by a double cast iron and concrete shield.

The thermal shield, which alone stops 90% of the radiation, completely lines the inside surface of the concrete shield. It consists of cast iron slabs 20 cm thick, laid side by side, with suitable clearance between them for expansion. The weight of the cast iron used in the thermal shield is 160 tons.

The biological shield consists of a 2.25 m thick concrete wall made more compact by vibration treatment. The specific gravity thus achieved is about 2.35.

The top of the reactor is closed by a very heavy assembly which serves as a rest for the vessel, as well as for various control and safety devices.

This assembly which, by reason of its shape, we shall call "the tubular block" is made up of two 2-m square steel plates connected by a bundle of tubes 70 mm in diameter. The fuel rods go through these tubes. The thickness of the tubular block is one meter, its weight 17 tons, making it the heaviest single part in the reactor.

The lower plate, which is made of steel, 200 mm thick, continues the thermal screen.

The space available between the tubes and sheets is filled up with concrete containing barites (barium sulfate) and boron carbide. Pouring of the concrete (this is a fairly delicate operation, despite the appearance and large dimensions of the piece) was done very carefully, so that its contraction would cause no dimensional changes in arrangement of the tubes.

The fairly large empty spaces which are left, particularly in the suspensions of the fuel, in order to permit carbon dioxide circulation, make the tubular block anything but a perfect protective shield. The protection which it does afford makes it possible, none the less, to reach the cell heads when the reactor is shut down. During operation production is completed by a stack of barite containing concrete slabs, the total thickness of which is 1.50 m.

Controls

The ionization chambers in use on this reactor can be divided into three categories, according to their function: (*a*) power chambers, (*b*) leak detection chambers, (*c*) health protection chambers.

The data supplied by each of them can be read on the control panel. The power chambers are sensitive to slow neutrons. Each of them consists of an array of parallel electrodes covered with a boron layer. There are four power chambers, housed in channels through the concrete and thermal shield. These channels do not extend into the graphite. Their position is fixed and their sensitivity is varied by means of sets of resistors inserted in the electrical circuits. Three chambers operate simultaneously. The fourth is kept in reserve. They supply the following data, by direct reading: (*a*) power P, (*b*) power variation ΔP, (*c*) reactivity $\Delta P/P\ \Delta t$.

One of them is directly connected to a light spot galvanometer.

The reactivity is adjusted by means of two cadmium plates which can be moved vertically between the vessel and the reflector. By acting in zones of different neutron fluxes, they afford means of varying the reactivity. Each plate consists of a cadmium sheet 0.7 mm thick, 300 mm high, sandwiched between two aluminum sheets.

These plates are remotely operated from the control console by means of an electronic device which, by now, is of a conventional type. They hang from metal tapes which pass over pulleys and wind on the drums of a mechanical assembly attached to the outside wall of the reactor. The speed of plate displacement is 30 mm per second. Their position is shown at the control console, but the operator acts more on the indications from the power chambers or on the reactivity than on the position of the plates. Since several months, this painstaking work has been simplified by an automatic control device.

The control plates are supplemented by two plates known as the "start-up plates" which can also be moved vertically between the vessel and reflector. These are more efficient than the others. They are loaded with boron carbide and their surface is double that of the adjusting plates.

A certain number of interlocks have been provided to rule out human error. The first start-up plate, for instance, can be raised only if the safety rods are at the top of their travel and the control plates at the bottom. The second start-up plate can be pulled up only if the first already is at the top of its travel. The control cannot be raised until the two start-up plates are all the way up.

The start-up plates can be lowered at will by means of a control knob, but they automatically go down with the safety rods. The speed of descent of the starting plates is, in each and every case, equal to that at which they go up.

The reactor is provided with two safety rods, each of which can shut it down. Each of the rods is controlled by an individual mechanism, but the release is always simultaneous. They consist of a metal tube closed at both ends, which contains a cadmium cylinder 45 mm in diameter, 1.20 m long and 0.7 mm thick. They hang from a metal tape, and move vertically in tubes which plunge in the heavy water. The tapes wind on assemblies located outside the reactor.

They fall under the action of gravity, thus with linear acceleration, for the first half of their travel, and then under uniform deceleration for the second half. This is achieved by means of an oil dash-pot. The time of fall is 4 seconds for 2.30 m travel. This is relatively long, due to the inertia of the metal parts operated by the rods. It can be claimed, however, that full efficiency is achieved 2.5 seconds after release, since speed reduction is greatest over the last few centimeters of rod travel.

The rods are held in their uppermost position by an electromagnet which releases them when it is de-energized.

A certain number of interlocks have been provided between the safety rods and other elements. Thus, for instance, the safety rods can be raised only if the start-up plates are at the bottom of their travel, and the ionization chambers and their amplifiers energized. The safety rods also rule out the operation of the heavy water pump as long as they are not fully pulled up. They can be dropped at will by the operator (push button on the control panel). However, they can drop automatically under various circumstances, in case of a power failure for instance, where the reactor power level exceeds a certain value and when the controls cease to operate.

Experimental Provisions

The experimental provisions can be classed arbitrarily into four groups of devices which are: a central channel going vertically through the active core, 9 horizontal channels which penetrate into the reflector as far as the vessel, a thermal column and, finally, an array of some 40 vertical channels on the outside of the reflector.

The central channel is an aluminum tube 57 mm in diameter. It contains a second tube, 50 mm in diameter. The purpose of this arrangement is protection against the fall of heavy objects. Normally this channel is closed by a steel plug.

Heavy Water Circuit

The heavy water circuit includes, outside the reactor, a tank located in the basement, the dimensions of which are adequate for it to hold the whole of the heavy water in the circuit. Connection between the reactor and this tank is by a conduit 100 mm in diameter, normally closed by a valve known as the "safety valve," since opening it would shut down the pile if this ever were necessary.

The heavy water circuit, as a whole, is made very tight, not only to avoid heavy water losses, but also in order that this critically important liquid be not polluted by atmospheric humidity. As a matter of fact, this last mentioned point is of such importance that the whole circuit is placed under a helium atmosphere kept at a slightly positive pressure in order categorically to rule out any and all entry of atmospheric air.

Attention has already been drawn to the fact that the vessel actually is very fragile. In view of this, the positive helium pressure is limited to 30 gm/cm^2. One may well wonder what would happen if one of the tubes in which the gas circulates under a pressure of several atmosphere were to fail. In the absence of any safety device, it is quite plain that, in such a case, the vessel would explode. In order to rule out this risk, two safety valves have been provided, the diaphragm of which is so thin (a few microns thick) that it will burst in case of any accidental pressure surge. The ducts between them and the reactor are of such a diameter that the pressure in the vessel would not exceed 30 gm/cm^2, even if a plunger should really break. Before heavy water is placed in the circuit, it is necessary to dry it thoroughly, which is done by circulating the air in that loop over silica gel cartridges. This drying operation takes several days.

The heavy water is transferred back to the reactor from the storage tank by a low output volumetric pump (1500 liters an hour). The output has been limited on purpose, in order to keep the increase in the reactivity under control. As a safety measure, an automatic timer has been provided in the electrical circuit of the pump in order to limit the duration of its operation to 30 sec, and to keep the operator attentive throughout the critical period of pumping heavy water.

The weight of heavy water in the reactor can be computed from the indications of a glass tube gauge of more or less conventional design. It is mounted on the side of the reactor. Due to the deformation of the reactor vessel under the combined actions of pressure and temperature, the data so obtained are not too accurate.

Recombination Circuit

Heavy water, as is well known, is decomposed under neutron bombardment. In order to avoid an accumulation of deuterium and oxygen, the atmosphere above the reactive medium is constantly being pumped off, the gases then passing over a catalyst which recombines the elements.

The catalyst is made up of a palladium layer on an alumina support. It is located between two flame arrestors in order to rule out the propagation of an explosion throughout the loop, should a rapid reaction develop inside the catalyst.

Alumina will hold water, even after prolonged autoclave treatment. Before use, therefore, it is necessary to make a H_2O/D_2O exchange. This operation is carried out in the laboratory.

Before it goes through the catalyst, the gas first is cooled off in a heat exchanger. The condensed heavy water vapors return to the reactor by gravity.

The reconstituted heavy water is released by the catalyst as a vapor, since the reaction is an exothermal one. A second cooler condenses this steam, and the condensate goes back to the vessel by gravity. Proper progress of this operation is ensured by watching the temperature in the catalyst, and continuously checking on the oxygen and deuterium content of the gas on either side of it.

The gas output (40 cubic meters per hour) is so adjusted that the deuterium content cannot exceed 1.5%. Should it accidentally exceed 3%, an alarm will be released. In view of the fact that the explosive threshold is around 8%, the safety margin seems to be adequate.

Compressed Gas Circuit

We have already said that the uranium rods are cooled by compressed gas circulation. This necessarily implies the evolution of gas in a closed circuit. Let it be remembered that the gas is distributed between the cells according to their power; in order to clarify matters, let it be pointed out that the peripheral cells only develop 55% of the power generated in the central one. The throttling of these cells thus doubtless is of interest, since blower power, which is already very large, varies as the third power of the output.

As it comes out of the reactor, the hot gas goes through a first exchanger cooled by water circulation. It then comes to three blowers, two of which operate together (the third is kept as a standby). It then goes to a second exchanger. After going through an output meter, the gas returns to the reactor. Its average pressure in the reactor is 8 atm absolute, and its circulation rate 70 t/hr.

In the Fall, for a power level of 2000 kw, the temperatures are approximately as follows: 30°C at the reactor intake, 130°C at the outlet. While the second figure is too low for energy recovery and electricity production, it is sufficient to heat the building. This point became manifest at once and a summary study showed that the cost of the additional facilities needed to make use of this heat could be amortized in less than a season, by the fuel economy it would bring about.

Accordingly, the functions of the three heat exchangers are as follows:

Exchanger I is used to heat the building during the winter time;

Exchanger II has the dimensions required to absorb the whole of the power developed in the reactor;

Exchanger III is designed to recover the power of the blowers since, in fact, all the electrical energy supplied to the engines is stored up in the gas in the form of heat, but for a few losses.

In case of need, the gas may be stored in a 7 cubic meter sphere, under a pressure of 30 atmospheres. A two stage diaphragm compressor makes it possible to transfer the gas from the loop to the sphere or vice-versa. Before gas is transferred back to the loop, the latter must be freed of all air. A vacuum pump has been provided for the purpose. The residual pressure being of the order of one cm Hg, there remains a little air, with the argon which it contains, showing its presence by the activity of the channels and machines. This activity raises no serious problem at all.

The blowers are of the centrifugal type and rotate at 9600 rpm. Each of them requires close to 400 kw. Since the two machines always operate in parallel, it can be seen that cooling the reactor requires a power of some 800 kw, which is not by any means negligible when compared with the amount of power developed in the uranium.

The blowers are of a duel originality: while their features are similar to those of the last rotor in a multistage centrifugal compressor, the use of one single rotor having such features had never been considered until now and, in addition, the drastic fluid tightness requirements raised the issue of the shaft gland, which is particularly difficult due to the relatively high speed of rotation.

We know that, while the drop of the safety rods, for all practical purposes, stops the nuclear reaction instantaneously, the existence of delayed neutrons still prolongs it for a few moments at a reduced rate. In addition, the fission products accumulated in the uranium bring about a release of heat which continues for a relatively long time.

These two phenomena added to each other release so much heat that five minutes after the safety rods have been dropped the power level still is a few hundredths of its rated value.

In view of this, it is indispensable, in the event of a power failure, that cooling off be kept up for a relatively long time, lest the uranium be overheated. To this end, a heavy flywheel is keyed on the drive shaft of the engines which operate the blowers. Its inertia is such that, five minutes after a current cut-off, the gas flow still is at 10% of its nominal rated value.

This is time enough to start automatically a standby power plant.

The exchangers consist of bundles of loop-shaped tubes. The gas circulates inside the tubes, the water outside and at right angles to their axes.

All these assemblies are linked by ducts made of carbon steel, 300 mm in diameter. This makes up a fairly extensive circuit, and the couplings—although their number has been reduced to a minimum—are relatively numerous (several hundreds).

In view of the danger of activation of the gas, it was necessary to minimize the leaks to the utmost. Our objective was not to exceed an hourly loss of 0.001 of the gas contained in the circuit. Thanks to the extreme care in making and assembling of the parts, this aim was met and even exceeded a little.

The significance of these figures will be the better understood once it is realized that a leak of 1% of the output is commonly allowed for steam circuits in thermal plants, even of the most modern types.

Water Circuit

The cold water is supplied by a drip type free air cooler housed in a 30 m high tower which acts as a stack.

The cold water is collected in a vessel which presents a suitable pressure head with respect to the installation, permitting gravity flow through the exchangers. These are thus fed for a while after any power failure. The water temperature drops 8°C in the open air cooler, summer and winter, but its absolute value obviously varies according to the season. The reactor power, as a consequence, thus depends on the atmospheric conditions.

Air Circuit

The purpose of the air circuit is to cool off the graphite and the cast iron thermal shield. The air is pumped in through filters and flows between the graphite and an aluminum liner, then goes down between the aluminum liner and the thermal shield. It is then aspirated by fans, which makes it possible to maintain a certain negative pressure inside the reactor, and thus to rule out any escape of active gases to the room. This air is removed by a 30 m stack. The cool air which comes in at the base of the reactor might freeze the heavy water in the piping, were it not that provision has been made for recirculating hot air when the outside temperature falls below +5°C.

The power developed in the graphite is about 16 kw, while 4 kw are developed in the cast iron. Thus, the cooling of these assemblies poses no critical problem.

There are three fans, but only two of them operate together. Jointly, they deliver 10,000 cubic meters of air.

An ionization chamber is at the base of the stack, in order permanently to monitor the activity of the air which comes out of it.

Some Details

By way of conclusion, let us mention some of the difficulties which were overcome in building this reactor. The main one, without a doubt, was the requirement that perfect tightness be achieved at all points, which is particularly exacting on so extensive a circuit as this one. The tightness of the blower shaft glands raised a difficult problem. Finally, in order to achieve maximal internal cleanliness of the heavy water or carbon dioxide, piping required mounting precautions which were truly unusual for an assembly of such a size. These same precautions of cleanliness also had to be taken in the machining and piling up of the graphite, which led us to install it last, after the reactor block was completed.

It should be mentioned, for this is an important point which applies to all reactors, that an effort was made at the cost of what were at times serious complications, to make most parts subject to disassembly, so that repairs could be carried out when and as needed. This point, which has also been stressed by the Canadian engineers, after the accident with the NR reactor, must constantly be borne in mind by reactor builders, and it will have to be carried still further in projects to come.

III. RELATION BETWEEN THE NEUTRON FLUX AND THE THERMAL POWER LEVEL

Problem

The power level of the Saclay reactor can be determined by measuring the flow and temperature rise of the compressed gas.

Another way of computing it is from the neutron flux throughout the reactor, and the cross sections and energy released in the fission process.

It struck us as being worth while to find out whether the two methods of evaluation are in agreement. There are many intermediate stages in such a study. It provides us with an opportunity of reviewing a whole series of phenomena.

Flux at the Center of the Pile

Most flux measurements give relative values. The thermal flux at the center of the core will serve as a standard, to which the other determinations will be referred.

The reactor lattice is a regular hexagonal centered one. One of the nodes in the lattice coincides with the axis of the reactor. The relevant plunger, with a diameter of 57 mm contains no uranium. It communicates with the atmosphere and is accessible to detectors or small ionization chambers.

This is where the thermal neutron flux is at its maximum, serving as a reference for all the determinations we make. To this end, a thin detector of known weight, made up of copper or manganese, is irradiated to saturation. The beta activity of this detector then is measured by means of a "4π" counter.[3] Measurements of the cadmium ratio give an evaluation of the effect of fast neutrons, i.e., of those having an energy greater than 0.6 ev.

The cadmium ratio, as measured with care for an indium detector, has been found to be 3.65.

Ultimately, the following integral is obtained:

$$\int_0^{0.6\text{ev}} \sigma_c(v) v N(E)\, dE \tag{1}$$

It will be assumed that, for the energy range under consideration, the detector behaves according to a $1/v$ law. If $\bar{v}$ be the average velocity, the above expression will become:

$$\sigma_c(\bar{v}) x \bar{v} \int_0^{0.6\text{ev}} N(E)\, dE \tag{2}$$

It is customary to call:

$$\phi = \bar{v} \int_0^{0.6\text{ev}} N(E)\, dE$$

the thermal neutron flux. The evaluation of this flux requires a knowledge of the cross section of the detector, as well as of the average velocity.

As to the average velocity, it is usually assumed that:

1. The velocity distribution follows Maxwell's law. Although this is not accurately true between 0.1 and 0.6 ev, this does not entail any appreciable error.
2. The temperature which defines the distribution is that of the moderator.[4]

It is obviously impossible to measure the central flux every time a relative measurement is taken. Fortunately, it proved possible to take advantage of the proportional relationship between the readings of a boron fluoride counter and the central flux.

The slowing down flux of neutrons can be deduced approximately from the cadmium effect of indium. Assuming that the energy distribution law is of the dE/E form, and that it extends to 2 Mev, the following value is found, which applies, at least, to the middle region of the central channel:

$$\frac{\text{flux of neutrons undergoing moderation}}{\text{thermal flux}} \simeq 1$$

The flux of neutrons having an energy greater than 1.1 Mev, was measured. For convenience, we shall call it the fission neutron flux. To do this, a small chamber was made, using low capture elements. It was lined with very pure thorium, containing less than 5×10^{-6} parts of uranium. It was arbitrarily assumed that the spectral distribution was the same as that of a fission spectrum. The fission cross section of thorium was weighted for this spectrum and estimated at 0.078 barn. Finally, the following estimate was arrived at:[5]

$$\frac{\text{fission flux at center}}{\text{thermal flux at center}} = 3 \times 10^{-2}$$

3. Neutron distribution: The value of the neutron flux at the center of the reactor is obtained by an absolute measurement. It should be completed by a knowledge of the fluxes in the whole of the reactor as given by relative measurements. Starting from the premise that the reactor is truly symmetrical, the distribution along all but one of the seven rods in the meridian half-plane was measured.

In a first series of measurements, continuous determinations were made of the activity in copper strips[6] which had been stuck along the uranium rods. In another series, the uranium in the rods itself served as a detector. These last mentioned measurements, which rest on a very simple principle, unfortunately had to be discontinued:

The over-all distribution is represented by:

$$\cos\frac{z}{H}\, x f\left(\frac{r}{R}\right) \qquad (3)$$

The plane of maximum vertical density is at level 73 ± 1 cm, 0 being defined by the lower ends of the rods. The sine law applies up to the heavy water level. From above that level on, the density is approximately constant. A coarse estimate may be made for an extrapolation length of 3 or 4 cm.

The radial distribution is given by:

$$J_0\left(j\frac{r}{R}\right), \quad R = 132 \pm 2 \text{ cm} \qquad (4)$$

for the first four rods from the axis. Thereafter, the flux decreases less rapidly than would appear from the above law, and it reaches a maximum in the graphite at 10 cm from the vessel.

Equation 4, when extrapolated to $r = 0$ does not give the flux in the central plunger, because the latter does not contain any uranium.

Thus, the knowledge of two ratios is required for our work:

$$\frac{\text{maximum flux in the central plunger}}{\text{maximum flux, as extrapolated from the distribution at the surface of the rods}} = 1.52$$

$$\frac{\text{the average of flux (3)}}{\text{maximum of flux (3)}} = 0.325 \pm 0.012$$

In addition, the average flux in uranium is smaller than the flux at the surface of the cartridges. The ratio between these fluxes has been measured, not at the Saclay reactor, but rather by placing, in the axial channel of the Zoe reactor, some uranium slugs of various diameters. This may cause a certain error, since the thickness of the air layer is 14.5 mm in the Saclay reactor, rather than 19.5 mm in the Zoe reactor. In addition, the uranium rod lattice is not the same in both reactors. Be that as it may, the result obtained is as follows:[7]

$$\frac{\text{flux at the surface of the uranium}}{\text{average flux in the uranium}} = 1.23 \pm .03$$

The measurements are carried out with a gold foil detector. The neutrons having energies under 0.6 ev were eliminated.

Let it be noted, for the sake of completeness, that, in the gas layer which surrounds the cartridges, the flux decreases as one goes from the heavy water to the uranium. A detector was attached to a slug, while another one was stuck onto the outside tube of the concentric thermal screen. This gave the following ratio:

$$\frac{\phi(2.75)}{\phi(1.4)} = 1.10 \pm 0.02$$

The complete set of measurements gives the following result:

$$\frac{\text{maximal thermal flux}}{\text{average thermal flux in the uranium}} = 3.8$$

4. Reactor power, as computed from the flux: The fission energy,[8] without allowance for the neutrons, was taken to be 185 Mev ± 5.

To this one must add the energy developed by neutron capture, namely some 7 Mev.

The foregoing paragraphs enable us to compute the number of fissions due to thermal neutrons. They take place in U^{235}. To these, we must add the fissions brought about, in the same nuclide, by epicadmium neutrons. A fission chamber which contained natural uranium and depleted uranium, and which had been made for other work, by operating on neutrons from the reactor, showed this ratio to be $1/60$. One should also allow for the fissions brought about by the fission neutrons in U^{238}. Here, the measurements carried out on fission neutrons in the central channel of the reactor or near the well of the vessel are not usable because the fission flux drops too rapidly from the uranium to the moderator. It was preferred to deduct the percentage of these fissions from the fast multiplication factor ϵ, which from the literature is 1.03. The percentage of these fissions then would be:

$$\frac{\nu}{\nu - 1} (\epsilon - 1) = 5\%$$

Thus, the total amount of heat generated by thermal fission is equivalent to 204 Mev.

The conclusion of all these estimates and the computations is:

A power of 1 kw corresponds to a thermal flux, at the center, of 4.2×10^9 cm^{-2} sec^{-1}, within 15%.

5. Measurement of the heat production is much simpler. The fluid is carbon dioxide under a pressure of 6 atmospheres. A flowmeter which operates on a venturi provided with water pressure gauges, gives the mass flow. The temperature rise of the gas in the reactor, some 100°C, is measured without any difficulty. The gas can be treated as a perfect gas. Its specific heat is known.

To the measured value, the heat removed by the secondary circuit, some 2%, should be added.

However, these measurements are not carried out in a power range suitable for flux measurements. This power is in the neighborhood of 1000 kw when these heat power measurements are made. The heavy water level is higher than when the fluxes are measured, and the ionization chamber no longer is in the horizontal plane where the flux is maximum, as is the case under low power, which tends to give a too low flux valve. On the other hand, the flux gradient between the active zone and its periphery is reduced, a phenomenon whose effect is the opposite of the former one. These sources of errors have not yet been properly evaluated. They have not been taken into account.

The final result is that the power as estimated from the fluxes is greater by 11% than the measured heat power. This is no striking disagreement. It is felt, however, that it would be well to investigate the relevant phenomena more closely.

IV. STUDY OF THE REACTIVITY

Components of the Reactivity

A reactor comprises, on the one hand, some elements which can not be modified, such as: the nature of the moderator, the reflector, and the maximum number of uranium rods; and, on the other hand, variable elements such as the level of the moderator, if heavy water is used, the position of the adjusting or trim plates, the temperature, the condition of the fuel, etc. The reactivity components to be reviewed here are these essentially variable ones. The variations of reactivity with which they are associated are, on the whole, of the order of 1%. Reactor operation requires profound knowledge of these variations.

Most of the components of the reactivity can be studied by means of relative measurements, either at a non-critical level by measuring the neutron flux developed in the reactor by spontaneous sources, or by following the growth of power slightly above the critical level.

Absolute measurements can be made according to Nordheim's formula.[9] The use of Nordheim's formula assumes a proper knowledge of the percentages of delayed neutrons produced in the reactor, as well as of the relevant periods. In the case of a heavy water reactor, not only the fission neutrons, but also those produced in the heavy water by the photons must be taken into consideration.

Raievski[10] developed a method which is less exacting, since all it requires is an accurate knowledge of the total percentage (β) of delayed neutrons.

The reactivity variation is modulated with a frequency which ranges from 0.15 to 10 c/sec. This brings about a flux modulation, the amplitude of which is connected with that of the reactivity by a formula given here in an approximate form:

$$\left| \frac{\delta_n}{n} \right|^2 = \frac{\delta k^2}{\beta^2 + \tau^2 \omega^2}$$

The amplitude of the flux variations is measured as a function of the frequency ω. This gives, respectively, τ, the average life time of the delayed neutrons, and δk, the amplitude of the reactivity variation.

The average life time of the neutrons in the Saclay reactor has thus been found to be 1.00 ± 0.2 msec.

The technique just outlined has the advantage of being applicable when the power level is high.

This makes it possible to determine the effect of the control plates on the reactivity, first for small displacements and then by integrating for any displacement.

Some Results

The following data are of some interest as to their order or magnitude.[11] The heavy water, in the glass level gauge, stood at division 1794 mm.

	$\delta k \times 10^5$
Increase of 1 mm in the level of the heavy water	6.6
Lowering of one control plate	− 240
Lowering of two control plates	− 480
Lowering of one safety rod	−1860
Lowering of two safety rods	−3150
Nitrogen-filled compressed gas circuit, pressure rise of 5 atmospheres	− 580
1° increase in the uranium temperature (uniform, at low power)	−1.25

The substantial depression in reactivity due to the compressed nitrogen, which was expected, soon led to the use in its place of carbon dioxide. This had two advantages: (1) heavy water saving, and (2) the avoiding of a rapid power surge following a severe nitrogen leak.

The heating of the heavy water also gives rise to a loss of reactivity:

$$10^5\delta k = -12.64(T - 17) - 0.227(T - 17)^2$$

A rise from 17° to 40° of the temperature of the heavy water entails a loss of reactivity of approximately 0.004.

The loss of reactivity due to poisoning by fission products led to the following results:

The reactor, after a week's rest, started at a power of 800 kw, showed, after a few hours, a loss of reactivity of 0.0045. This was due to xenon poisoning. A computation made with the known constants, allowing for the fact that the xenon percentage is higher at the center of the reactor, gives a higher figure: 0.0055.

The long term reactivity loss was checked after a period of 3.6×10^6 kw of operation, i.e., 41 Mw-day per ton of uranium. A loss of reactivity of 0.012 was observed. Computation of long term poisoning mostly involves the samarium. The computed loss does not exceed 0.006. The disagreement in the results gives reason to believe that there has been a case of accidental poisoning.

We can not readily analyze these results in greater detail. We trust the Geneva conference will supply us with more accurate data regarding poisoning phenomena by fission products and thus will enable us better to interpret our findings.

V. HEAT TRANSFER

The Various Techniques in Use

The heat generated in a reactor is extracted by circulating a fluid which, either through a rise in its temperature or a change of state, removes this energy as it is being generated.

The heat appears mostly in the uranium, but also in the moderator, the reflector and the protective shield.

Resort may be had to various fluids in order to remove the heat released in the various components. However, the main problem is the uranium: the fluid which removes the heat released in the uranium is called the primary fluid.

If the primary fluid leaves the reactor at a sufficiently high temperature, the energy stored in it may be used to drive a thermal engine, whether it be directly or through a heat exchanger, in which latter case the energy first is transferred from the primary fluid to another one which is more easily handled: this new fluid is the "industrial" fluid.

In all solutions which offer an acceptable efficiency, the primary fluid circulates in a closed circuit. Its flow is effected by pumps.

The primary fluids which have particularly received attention up until now have been water, molten sodium or uranium-bearing solutions for the homogeneous reactors, or again, compressed gases. Each has its advantages and drawbacks, depending on the moderator, the nature of the fuel, and the risks one is prepared to incur: all this decides which one is to be preferred.

We do not have in France such an experience with, or even knowledge of, these methods, as would enable us to make forecasts regarding the future of each of them. Let us express the opinion that each appears

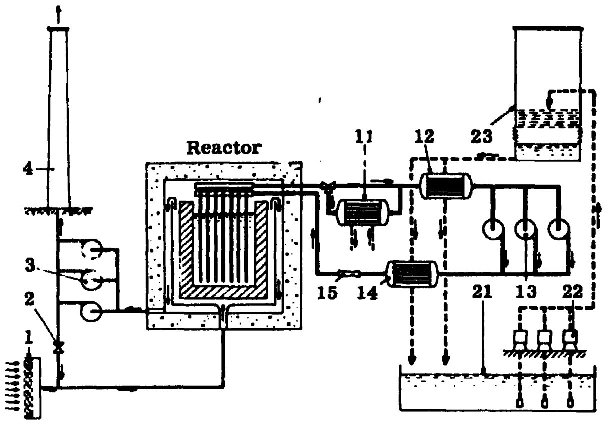

Figure 2a. Cooling circuit schematic. Air: 1. filter; 2. by pass; 3. fans. Nitrogen: 11. heat exchanger for heating building; 12. main heat exchanger; 13. blowers 14. auxiliary heat exchanger; 15. venturi. Water: 21. pool; 22. pumps; 23. cooling tower

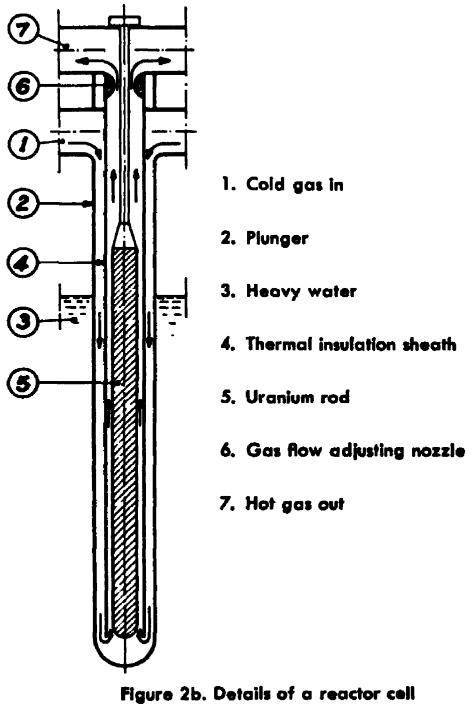

Figure 2b. Details of a reactor cell

perfectly sound, and that the triumphs of one or the other will require several generations of reactors (one generation is the time from design to routine operation, i.e., about 5 years).

As we review the history of the automotive industry we find that many concepts which had been imagined by its pioneers, only to be dropped because of practical difficulties, came back into favor later, as soon as the condition of industrial development provided means of implementing them.

Comparisons between the development of the automotive industry and that of atomic energy may not seem in order because the former developed in small shops while the latter was immediately taken over by powerful state organizations. However, if we were to imagine that the means available to us tomorrow have to remember those of today, we would be underestimating the industrial development of the coming half century.

The drawbacks of the compressed gases are obvious: poor thermal capacity, poor thermal conductivity, high viscosity. Some advantages are no less obvious, such as their ease of handling and low corrosion effects.

Choice of the Gas

The following ten tasks are required of the primary gas:

1. Chemical stability at the operating temperature.
2. Adequate heat capacity.
3. Adequate thermal conductivity, low viscosity.
4. Availability.
5. Chemical inactivity with respect to the conduits and cladding.
6. Same lack of activity with respect to the uranium, should a cladding be broken.
7. The molecules are dissociated by the radiation produced by a reactor in operation. The free radicals thus formed may produce, by recombination, unexpected and undesirable products. At first sight, it would seem that these drawbacks will not be smallest if the molecules are very simple.
8. The free radicals must not contribute too much to corrosion.
9. Low neutron absorption.
10. The activity created by this absorption must be short lived and weak.

Obviously, there is no gas which is best from every possible standpoint. Our first projects had caused us to consider helium and nitrogen. Helium was rejected for reasons of availability. Nitrogen was to contain but a very small quantity of argon, which is troublesome by reason of its intense activity. A nitrogen of satisfactory quality was used for some time. It seemed to offer no drawbacks.

By reason of its capture cross section, nitrogen finally was given up and carbon dioxide used in its place. The main problem was whether carbon dioxide (CO_2) would be stable.† Following the release of some 5×10^6 kwh, no untoward chemical phenomenon developed. It should be pointed out, however, that our physicists and chemists, who were taken up by other tasks, have not as yet given all the attention they should to these problems.

The substitution of one gas for another, in a compressed gas piping network, presents no great difficulty. Thus, it might seem easy to carry out tests with a variety of gases. However, the blowers used to move the gas cease to be suitable once the physical properties of that gas are changed. This is why helium, which might have been fed into the device for a short period of operation, has not been tried until now.

Nuclear Requirements

The primary fluid is made to circulate through the reactor around the uranium slugs through plungers (tubes closed at their lower extremity) made of "Brillalumag" alloy. In order to reduce neutron losses in the metal of the plungers and of the double walled shield which is used with them as an accessory (see description of the reactor), it became necessary to limit the thickness and diameter of these parts.

In the gas, the neutrons move practically without any collisions. Some of them cover long straight paths through the gas. Thus, they have a regrettable tendency to migrate from the regions where the flux is intense, where they are very useful, to those where the flux is moderate, where they are less useful.

These rapid changes invalidate the equations which give the diffusion of the neutrons in the multiplying media. This must bring about at least an increase and anisotropy in the migration length: it has proven impossible, to date, to assign a numerical value to this anisotropy.

A phenomenon which is better known, both theoretically and experimentally, is the reduction of the thermal neutron flux when moving from the surface of the moderator to that of the uranium. This tends to bring down the thermal utilization factor.

It will be understood, therefore, that these phenomena were carefully taken into account in the design of the reactor, and that an id of only 57 mm was used for the plungers.

The gas channels are all the narrower as, in the plungers, the gas goes through each cross section twice, first on the way down, when it cools off the heavy water, then on the way up, when it cools off the uranium.

The descending channel has a width of 6.5 mm, the ascending one 4.4 mm.

Thermal Requirements

In designing the reactor, a certain number of requirements relative to the temperatures had to be considered. When the primary fluid operates a steam engine through a boiler, it is necessary to use the high temperature calories for the purpose of vaporizing the industrial water at a suitable temperature. Calories of a poorer grade are used to warm up the water, taken off from the condenser, to the boiler temperature.

---

† Everybody, nowadays, knows the very important part played by the compressed gases, particularly carbon dioxide, in British designs.

There would be an excess of calories of medium quality if the primary fluid entered the reactor at ambient temperature. This leads to feeding the primary fluid to the reactor at a temperature not greatly different from that at the outlet.

The Saclay reactor is but a preliminary study, in preparation of actual power-producing installations. It was desired to learn how to produce a warm fluid without endeavoring to transform the heat into mechanical energy: the power is removed from the compressed gas, at the reactor outlet, in plain cold water-fed heat exchangers.

Furthermore, there is an exchanger between the blowers and the reactor, the purpose of which is to cool off the gas which has again been heated up by going through the machines. Thus, the gas enters the reactor at a temperature around 25°C.

During its downward motion, the gas warms up at the contact of the heavy water, in which 5 to 8% of the total power is released. The heavy water thus is kept at a fairly low temperature, which reduces the risks of plunger and vessel corrosion by it.

The solution, taken as a whole, is an elegant one: the heavy water is insulated from the hot gases formed at the contact of the uranium, the heat which develops therein is removed without the need for a special device, the piping does not go through the bottom of the vessel, the design of which is extremely simple, and pipes can be taken out without having to expose the mechanics to radiation, since all critical parts have been arranged above the tubular block, away from the active region.

This completely rules out the need for heavy water circulation. It would appear that this simplification would not necessarily remain in a more elaborate and careful design: the heavy water must circulate in such a fashion that its purity can be kept up consistently by filtration and extraction, on suitable resins, of the salts produced by corrosion. In addition, with the help of an exchanger provided in the heavy water circuit, its temperature can be adjusted independently from that of the primary fluid. This provides an additional means of adjusting the reactivity.

The next requirements to be met are those pertaining to the slugs. Some are easy to visualize: the cladding temperature must remain lower than the temperature of chemical attack of the cladding metal by the primary fluid, no spot in the uranium must reach the temperature of its transformation from the α to the β phase. Preliminary tests have made it possible to determine the temperature which can be withstood by the uranium cladding assembly without suffering cracks or even deformations due to thermal strains.

But such requirements do not allow for the fissions which take place inside the uranium, and which may bring about additional difficulties, either by altering the structure of the metal, or by modifying its thermal conductivity. These phenomena can be studied only inside the reactor or in a reactor specialized for work on slugs. This brings a new factor into the picture, namely, the flux to which the cartridges are exposed.

Finally, the manner in which the slugs may be treated is determined by the time it is proposed to keep them in the reactor. Only a long period of experimentation will indicate the rules to be adopted in order to make the best possible use of the potentialities of these slugs.

Speed of Gas, Output and Temperature Distribution

The ducts are narrow, and the full elements must be kept at a relatively low temperature. The 1000 to 2000 kw released in the pile can only be removed by a high speed of gas circulation.

Different fuel elements do not generate the same amount of heat, since the fission rate, which parallels the neutron flux, decreases from the axis of the vessel to its walls. Thus, it is advisable to adjust the flow plunger by plunger, the maximal flow being for those closest to the axis.

This adjustment, at the Saclay reactor, is achieved by throttling the gas duct at the plunger outlet. The rule adopted has been that the temperature rise should be the same in all plungers. Accordingly, the temperatures are lower in the rods having a lower power load. Consequently, the requirements are not so strict for the slugs in the peripheral plungers. Logically, these slugs should be allowed to stay longer in the reactor.

The same type of comment applies to the various slugs in a given plunger, but it is impossible to remove the slugs separately: they are all subject to the same irradiation time.

Below is a set of results regarding the temperature and flow of the nitrogen. A certain number of uranium rods had been provided with thermocouples inserted between the uranium and the cladding. These gave a close approximation of the cladding temperature. However, they made the slugs more fragile. The slugs so equipped were removed from the reactor when it was placed in operation:

Thermal power	800 kw
Absolute circuit pressure at rest	8.9 atm
Nitrogen flow	66 tons/hr
Nitrogen inlet temperature	24°C
Outlet temperature	70°C
Maximum cladding temperature	126°C
Heavy water temperature	30°C

These data make it possible to estimate the temperatures with the reactor operating at different powers, according to proportionality, from the temperature of the industrial water used to cool off the gas in the exchangers. The heavy water level and other secondary factors must be taken into consideration as well.

Where carbon dioxide replaces the nitrogen, the pressure is reduced in such a way as to keep the same mass flow. The temperature differential between the cladding and the industrial water then goes up about 15%, the industrial water temperature, heavy water level and reactor power being kept fixed.

In the central channels, for the output indicated, the average speed (it increases from the inlet to the outlet) is 50 m/sec. At these high speeds, the fluid exerts considerable mechanical action on the light thermal screen and the suspension from which the slugs hang. Final design was adopted only after a number of tests.

During the first months of operation, the power of the reactor had been kept at some 1000 kw, lest the slugs be brought up to unduly high temperatures. Improvements were made in the slugs, and reactor power is no longer limited by concern over the slugs, but rather by the amount of reactivity available. This limit, which is probably partly due to an accidental poisoning, will in turn be pushed back: the slugs will then be used in a manner more in line with their potential rating.

The slugs are the most delicate elements found in a reactor, but they can be perfected even while the reactor is in operation. Its design must not be so rigidly set as to impede such improvements.

Let it be noted that the improvements carried out concern only mechanical resistance: the heat exchange surfaces have suffered no important alteration.

Pressure Drops

The high speed of the fluid entails important pressure drops. Here are a few data pertaining to nitrogen, which will provide the reader with order of magnitude:

Total pressure drop	2.5 atm (measured) 2.0 atm (computed)
Pressure drop along the uranium	0.6 atm (computed)
Pressure loss at the elbow	0.09 atm (computed)
Pressure loss in the manifolds and tubular block, up to the uranium	0.04 atm (computed)

These pressure losses are the cause of the large electrical power required to operate the blowers: this is 800 kw. This sizable consumption has to do with the experimental nature of the reactor; it must not be allowed to foster undue pessimism regarding the development of the compressed gas technique.

The carbon dioxide-nitrogen comparison, presented in the above paragraph, and which is in favor of nitrogen, is a thermal, but neither a nuclear nor a chemical comparison, and it bears only on a specific case: the blowers designed for nitrogen have first been applied, unchanged, to carbon dioxide. An adaptation of the blowers to carbon dioxide mostly in the vanes will give it the advantage. This is a consequence of its larger molecular weight.

Fluid Tightness

The manifold, piping and exchanger couplings, the valves, as well as the bearing of each blower can be the seats of leaks. In the reactor itself, the only couplings are those of the manifolds and those placed at the head of the plungers. The latter had to be modified following some tests. The design of the whole system now is right.

The piping used for over-all circulation, the exchangers and the valves, are steel parts, of greater weight than those mentioned above. This also raises design problems. The whole is housed in a ventilated cellar, which is inaccessible during reactor operation.

The couplings on the blower casings have been polished with particular care. The rotor is shaft-end mounted. Thus, there is only one bearing to be lubricated. It is located outside the stator. The gland between the movable and fixed assemblies consists of special rings placed under spring load, soaked on the outside in a slight excess pressure of oil. This device does not allow the oil to enter the blower. In case of failure, suitable sling rings recover such oil as might have filtered through. The rings heat up: a certain amount of oil circulation removes the heat so developed. The oil pressure, which is related to that present in the system, and its output, are carefully regulated. An indispensable precaution is a change of rings at reasonable intervals, determined by the number of hours of operation. This device, which is a little critical, rules out the possibility of oil getting into the circuit.

In this fashion, there is no gas leak at all in the blowers. They can be reached while the reactor is in operation, but the radiation emitted by the gas, which goes through the stator, makes it necessary not to stay for any length of time in their immediate vicinity.

VI. THE PHILOSOPHY OF THE PHYSICS RESEARCH CONDUCTED WITH THE SACLAY REACTOR

Extensive mention has been made of the work program developed around the reactor, with the object of acquiring better knowledge of this device, and of the general principles suggested by this study of a particular situation.

The work is made somewhat difficult by the need of operating the reactor consistently in order to produce the radioisotopes and excess neutrons needed for various experiments. A certain amount of time was given the reactor specialists while it was placed in operation, after which they have had to make do, in order to complete their research, with the few available spots in a heavy schedule. It is impossible to turn the reactor over to them under well defined conditions, since the experimental channels are loaded with various samples or taken up by equipment.

This point being made, let us see the spirit in which the research carried out on reactor radiation was conducted, in the field of reactor physics, which research is of a less technical, and more truly scientific, nature, than the study of the reactor itself.

In the first place, such research entails the measurement of a certain number of well defined magnitudes, best exemplified by the cross-sections. A series of measurements of the fission and scattering cross-sections was undertaken, and the work was carried out on the fissile or fertile materials available to us. Being done with reactor neutrons, it was limited to thermal neutrons and to neutrons having slightly higher energies than those.

In view of the date on which the work was undertaken, there was no hope of obtaining results which would be unknown to all physicists. At least, they had the merit, for the most part, of never having been published. There could be no question, for us, of remaining unaware of fundamental data, in so far as we were in a condition to measure them. To be sure, we felt that, some day, the wraps of secrecy around atomic energy physics would be lifted. But, at any rate, our physicists had to prepare themselves for more difficult tasks, to train and equip for more original work. The field to be covered, at any rate, has now just been touched upon.

But the physics of reactor neutrons does not merely deal with well defined magnitudes. While nuclear physics is cartesian, that of the scattering and moderation of neutrons is largely empirical. Even before any original, or at least unpublished, measurements were undertaken, we first had to learn what use to make of the numerical data published in official documents which were most useful but brief, at times couched with all the dryness of administrative regulations. This is a situation in which theoretical work preceded experimental research. The latter bore mostly on thermal neutrons. Results have been obtained which we believe to be more accurate, on occasion, than those published in the older literature. In particular, they offer a possibility of refining our computation of the reactivity, but they do not form an integrated whole: we have to proceed with caution if we are to bring these innovations into an over-all structure which may, on occasion, seem illogical, but which, at least, is efficient.

The two above paragraphs most certainly do not dispose of the question of reactor physics. However, what has been stated sufficiently illustrates the trends which we followed.

Pure physics, or more exactly that which does not deal with reactors, such, for instance, as the study of crystal lattices, has not been the object of a comparable effort. It must wait until the art of the reactor makers has progressed enough to make liberal amounts of neutrons available.

VII. PROSPECTS OFFERED BY THE USE OF COMPRESSED GASES

The future of compressed gases is in reactors which are designed to operate a thermal machine.

In a reactor meant exclusively for the production of plutonium, an attempt is made at removing the heat as conveniently as possible: i.e., the fluid enters the reactor at the lowest possible temperature. One of the fundamental data pertaining to the fluid then is its temperature rise in the reactor.

However, when the reactor drives the turbines through a heat exchanger, the temperature which is of most interest is the average temperature of the fluid. This temperature, on the one hand, defines the thermal efficiency to be expected of the turbines and, on the other hand, serves as a reference for all the temperatures in the reactor, more particularly those of the slugs.

A given type of slugs can stand certain temperatures, allowing for the neutron flux and duration of operation. The question is that of finding out to what extent the mean fluid temperature can approach these limits, an approach which has the advantage of turbine efficiency, but the drawback of increasing the power needed for the forced circulation of the fluid (pumping power), thus of losing at one end what is gained at the other.

It should be noted that the pumping power is not entirely wasted, since it is recovered in the form of heat in the fluid.

Let us consider, in order to simplify matters, a reactor having identical channels subjected to the same neutron flux.[‡] These are cylindrical channels, of the simple flow type, and contain concentric uranium slugs. Outside the reactor, the fluid circuit includes piping, the major part of which is in the exchangers and a pump. The resistance of the circuit to the passage of gas thus has a certain well defined value.

Let T_m be the absolute mean temperature of the primary fluid. This temperature is the same in the reactor itself, where the gas warms up, and in the heat exchangers, where it cools off. T_c is the temperature in the condenser.

The efficiency, defined as the ratio of the power available on the turbine shaft to that released to the industrial fluid by the primary fluid, can be written:

$$\eta\left(1 - \frac{T_c}{T_m}\right)$$

The second factor is the thermodynamic efficiency. The former, smaller than one, expresses the imperfections in the system made up of the exchangers, boilers, turbines and condenser.

It is assumed that the cladding can stand a maximum temperature T_g, set, either by the possibility of an attack of the cladding by the primary fluid, or by concern for the slug itself.

Without specifying the thermal power at which the reactor must operate, the mean fluid temperature can be chosen so that the usable power be as large as possible. The result is that it must be the geometric mean of the temperatures T_c and T_g.

$$T_m = \sqrt{T_c T_g}$$

The same idea then is applied to the flow. The efficiency of the setup as a whole, i.e., the ratio of the available useful power to the thermal power released in the reactor then is given by the simple expression:

$$\eta\left(1 - \sqrt{\frac{T_c}{T_g}}\right)$$

These expressions which are not strictly accurate because the derivatives of Reynolds' number, occurring as a low power in the formula for the useful power, and the derivative of Prandtl's number with respect to the temperature, have been left out, but they are none the less good enough approximations to be retained. They seem to be remarkably independent of the nature of the primary fluid.

[‡] A survey by G. B. Meleze, Engineer at the C.E.A.

The third stage of the work concerns the ratio of the diameter of the channel to that of the slug, in order once more to make the useful power maximum (one must make sure that the secondary parameters are so chosen as not to be meaningless).

In addition, it is assumed that there is a temperature level which the uranium may not exceed without a risk. In order to make the best possible use of the uranium, it is desirable that when the cladding reaches its limiting temperature, the same should happen with the uranium. This condition defines the rod diameter and the useful power.

The temperature excess of the uranium over the cladding temperature is written for the hottest layer:

$$T_u - T_g = 100\pi\tau \frac{P}{M} a^2$$

in which a is the radius of the rod, P/M the average power per unit mass and τ a coefficient which would be proportional to its thermal conductivity if the temperature of the cladding were the same as that of the surface of the uranium. In fact, the uranium is hotter than the cladding due to the imperfection of the contact between the two metals. The factor of 100π has been chosen to adjust the order of magnitude of τ and make it close to one.

In this fashion, one determines the radius of the rod a, which appears to be a characteristic length set by the properties of the materials and their temperatures:

$$a = 3.5 \times 10^{-3} \frac{\rho_u}{\tau} \frac{T_u - T_g}{T_c} \frac{1}{\sqrt{\frac{T_g}{T_c}}\left(\sqrt{\frac{T_g}{T_c}} - 1\right)^2} \times (\eta T_c)^{-1/2} \frac{1}{\rho C^{3/2}} \left[\frac{K\Lambda}{\left(\frac{kN}{PR}\right)^3}\right]^{1/2} \quad (5)$$

where the symbols are as follows: ρ_u specific gravity of the uranium, ρ absolute mean specific gravity of the primary fluid, C specific heat under constant pressure, Λ Darcy's coefficient, K ratio of total resistances to circulation of primary fluid to the resistance encountered in the reactor, N, P, R, Nusselt's, Prandtl's and Reynolds' numbers, respectively, k a factor giving, for instance, the improvement in the heat transfer, as achieved by the use of fins.

The useful power per mass unit of uranium is given by:

$$\frac{P_u}{M} = \frac{2.1 \times 10^{-3}}{\tau} \frac{\eta T_c}{a^2} \frac{T_u - T_g}{T_c} \left(1 - \sqrt{\frac{T_c}{T_g}}\right) \quad (6)$$

One must strive to have small radii, which is done, in the case of a gas, by increasing the pressure and improving the heat exchange. The classical gases seem to be closely equivalent. Computation further shows that one can obtain values that are reasonable from the nuclear standpoint for the various magnitudes which this method makes it possible to choose on the basis of thermoaerodynamic considerations.

Equation 5 applies to the problem of an imaginary reactor in which all the channels are identical. A complete study then consists of finding out how much flow each channel should receive in order to achieve the best possible efficiency. The Saclay solution of throttling the outlets of the peripheral channels is better than nothing, but still causes a waste of power. Two approaches are possible and can be used jointly: the first one consists of equalizing the energy released in the various cells as much as possible. The second consists of feeding the peripheral channels on the one hand, and the central ones on the other, independently.

The first method leads to the establishment of an irregular lattice, either as to dimensions or as to loading. The central area lattice will not be so good as that of the periphery. This presupposes a measure of "lavishness" in the use of reactivity. By following the second course, it is obvious that, for reasons of simplicity, the general fluid pressure is not the magnitude which will be altered. But a hotter gas will then flow through the peripheral channels. A provision may be made, for instance, to have the gas come out of all the channels at the same temperature, but feeding the peripheral channels with warmer gas. This will entail a certain measure of design complication in the fluid circuit and in the exchangers and blowers.

More exhaustive studies show that it is perfectly possible, in the near future, to build a thermal plant in which the "furnace" would be a graphite reactor loaded with natural uranium, having carbon dioxide as its primary fluid. The difficulty of making long pipes sufficiently pressure resistant while using a low capture material then leads to the use of a pressure vessel.

In another direction, it also seems possible to make use of the technique used at Saclay, namely the heavy water, natural uranium, and tubular structure, in order to produce utilizable power, in a reactor of moderate dimensions, the pressure being less than that in a pressurized water reactor, but greater than that found in a graphite reactor.

REFERENCES

1. Kowarski, L., J. de Physique, *12*, p. 751, (1951).
2. From Martin, R., *Cours de Génie Atomique du C.E.A.*, (1955); V. also: La revue Atomes, Paris, April 1955; Kowarski, L., Nucleonics, p. 8, August 1954; Le Meur, E., la Technique Moderne, June 1953.
3. Cohen, R., *Mesure absolue d'activités β et application à la détermination des densités neutroniques*, Paris, 1952.
4. Galula, M., Jacrot, B. and Netter, F., J. de Phys., *16*, p. 232, (1955).
5. Hubert, P., C.E.A., (1955), unpublished.
6. Raievski, V. and Pellé, M., J. de Phys., *14*, p. 463, (1953).
7. Zaleski, P., C.E.A., (1955), unpublished.
8. Meem, J. L., Holland, L. B. and McGammon, G. M., ORNL 1537, p. 25 (1954).
9. Nordheim, L. W., Pile Kinetics, 70, p. 115 (1946).
10. Raievski, V., C.R. 237, p. 1513 (1953).
11. Jacrot, B., Netter, F. and Raievski, V., rapport C.E.A. 215, (1953).

Description of the Swiss Research Reactor

By F. Alder, W. Hälg, and W. Zünti, Switzerland

The Swiss research reactor is still in the project stage. The detailed plans, however, are in a fairly advanced state and the realization may begin before the end of this year.

1. SITUATION

The reactor site is located at the right border of the Aare River, in the community of Würenlingen, 30 km from Zurich. The main building, covering about 1200 m^2, will house the reactor proper and most of the associated equipment, while the departments of physics, chemistry, metallurgy, isotopes, the workshops and the administration are accommodated in smaller separate houses. At a later time a "hot-lab" shall be added.

The swimming pool reactor shown in Geneva will be again erected in a modified form at the same location.

2. THE REACTOR

Our aims called for a low temperature research reactor, using natural uranium as fuel, and heavy water as moderator and coolant. The aluminium clad uranium rods are arranged in a square lattice with 208 lattice positions inside a cylindrical aluminium tank of 220 cm diameter and 240 cm height. The tank is surrounded at the sides and the bottom by a graphite reflector of 75 cm thickness. At the design power of 10 megawatt the maximum thermal neutron flux is expected eventually to reach 2.5×10^{13} n/cm^2-sec.

3. THE SHIELD

The lateral shielding consists of a boral-lined iron wall of 10 cm thickness, 80 cm of limonite + boron concrete, and 160 cm of hematite concrete of a density of 3.5 gm/cm^3. The first element of the top shield is a shallow tank of 25 cm height, filled with ordinary water, followed by 45 cm of iron and 140 cm of hematite concrete. Above the iron shield, space is provided for an additional layer of 20 cm of a material which will minimize the residual activity in the room containing the drive mechanism of the control rods and other equipment.

4. CONTROL RODS

All control and safety rods consist of cadmium clad cylinders inserted vertically into the core from the top. For the manual or automatic control of the power level of the reactor, two rods are provided, each controlling 0.5% of reactivity. Actually, only one of them may be used at a time, the other serving as a standby. There are six safety rods. On release of magnetic clutches they drop into the core. Four of the safety rods, controlling about 4% of reactivity, are used as shim rods in order to compensate Xe-poisoning, etc. The velocity of withdrawal is limited to a low value.

5. IRRADIATION FACILITIES

The core is traversed by four vertical channels of 12 cm diameter and by five channels of 7 cm diameter, all of them in lattice point positions. This arrangement provides for an easy installation of high temperature loops for testing fuel elements, the associated equipment being located in the basement. All horizontal channels pierce the graphite reflector and end at the reactor core with the exception of a 7 cm diameter radial through-channel and two 15 × 15 cm tangential channels. There are radial channels of 50 × 50 cm, 25 × 25 cm, but most of them are of 12 or 7 cm diameter.

6. THE COOLING SYSTEM

The maximum heat flux at the surface of the uranium amounts to 60 w/cm^2; cooling by forced flow is a necessity. A careful study was made of the relative merits of systems with a complete separation of the moderating heavy water and the cooling heavy water, and of systems combining the two functions. A solution of the second type was adopted.

Cold water from the heat exchanger enters the tank, acts as moderator, reaches the top of the uranium rod through an outer annular space, then flows downward along the rod with a velocity of 1.2 to 2.5 m/sec, depending on rod position. The warm water, 50°C at maximum, leaves the lower compartment through the central tube, proceeds to the pump and the heat exchanger.

This system allows a wide variation of the heavy water level. It is safe in case of a power failure on account of the great heat capacity. It is economic: the aluminium weight is low, the external cooling circuit needs 0.8 tonnes of heavy water compared to 9 tonnes within the core.

The fuel elements are replaced from the top without loss of helium-gas. The flow-confining aluminium tubes also can be replaced, a valuable feature in case of severe rod distortion. The gaskets are placed above the top iron shield.

The gas space in the top of the syphon has to be kept under control. This is not considered as a serious draw-back, because this feature can be incorporated neatly in a detector-system of fuel element failure.

The pumps and heat exchangers, the purifier unit, the heavy water storage tank and the gas recombination unit are all located in the basement.

The graphite reflector and the thermal shield also need cooling, which is provided by air at slightly less than atmospheric pressure. The air is filtered at the inlet, and is filtered again before entering the blowers, which are located at the base of a 70-meter stack.

The Brookhaven Reactor

By Marvin Fox,* USA

DESIGN CONCEPTS

The first large-scale nuclear reactor, designed and built specifically to support fundamental research programs, was constructed at the Brookhaven National Laboratory directly after World War II. The design was based upon the experience gained with the Oak Ridge and Hanford reactors during the war years, and was chosen because of the ready availability of its primary materials, reactor-grade graphite and normal uranium metal. It was deemed necessary to design and build the reactor in a minimum period so that it would be available for research projects without delays due to development programs on untried design concepts. The reactor was the first built in the United States under nonmilitary control; being handled by a nonprofit, educational and research corporation under contract with the United States Atomic Energy Commission.

The reactor concept was based upon a requirement for large research areas adjacent to the reactor, and this influenced the choice of the large volume, graphite-moderated core. A design criterion was a maximum central neutron flux of 5×10^{12} n/cm^2 sec, and this called for a power level of about 28,000 kw; which was much higher than for any gas-cooled reactor existing at that time. The removal of this heat dictated a novel air flow pattern through the graphite core and a novel fuel element design providing large heat transfer surfaces. A high density, iron-loaded concrete was developed as a shielding material in order that adequate attenuation, to insure low backgrounds for research purposes, would be achieved through a maximum thickness of five feet. The horizontal control and regulating rods were positioned along the diagonals of the graphite structure so that the research areas, external to the shield, would not be usurped by operating mechanisms.

A further requirement, which made itself felt throughout the design, had to do with the fact that the reactor was located in the neighborhood of very high population density. It was extremely important to minimize the possibility of contamination due to fission product escape from the fuel elements. This requirement led to the particular design of our fuel element which in turn had a great effect on the shield design, and also dictated the elaborate leak detection system incorporated in the structure.

The variety and placement of all the research facilities were patterned to afford the flexibility required by research and development in all fields of science, with participation of the Brookhaven National Laboratory staff, academic institutions, industry, and hospitals. The diverse interests of all these research groups were anticipated, both as to variety and numbers, such that the utilization of the reactor, at the present time, is impressive.

DESIGN PROBLEMS AND THEIR TREATMENT

Graphite

The graphite used in the Brookhaven reactor was obtained from war surplus stocks. The records on these stocks were not good enough to assure the quality of the graphite, so that a program was established to measure the neutron diffusion parameters for the several batches of material. However, the engineering design and construction schedule could not wait for the results of the measurements. Hence a decision had to be made on the size of the graphite moderator on the basis of very meager information on the neutron diffusion parameters. In order to introduce a safety factor to take care of the possibility of poor graphite quality, it was decided to make the graphite moderator overly large; a 25-ft cube. It turned out to be unnecessary because the quality was good. Thus the Brookhaven reactor has a 4.5-ft reflector around the core which would not have been called for in the design if adequate information had been available. Undoubtedly, the graphite cube would have been designed no larger than a 21-ft cube if the neutron parameters had been known. This fact, of course, had a sizable effect on the costs of construction.

The graphite structure is of great complexity; consisting of 60,000 individual pieces of stock, machined to 0.001 inch tolerances, and fitted together like a three-dimensional puzzle. The complexity arises from the great array of holes or channels extending through the structure in four directions (three coordinate directions and one diagonal) to accommodate the fuel channels, experimental holes, control rods, and the multiplicity of experimental facilities, and also from the pattern of bidirectional coolant flow through the fuel channels. There were 3000 engineering drawings on the graphite structure alone. One half of the graphite structure and the base plate on which it was supported were constructed to be movable ±0.5 inch in order that it would be possible to vary the central gap width (see P/488, this Session). This was done so that a proper balance could be established between the loss of neutrons from the gap and the aerodynamics of the coolant flow through the gap. The gap width was permanently set after the reactor was in operation.

---

* Brookhaven National Laboratory. Including work by R. O. Bolt, N. P. Shiells, California Research Corporation; J. B. Trice, Oak Ridge National Laboratory, Carbide and Carbon Chemicals Company; J. E. Binns, L. B. Borst (presently affiliated with New York University), G. J. Dienes, J. J. Floyd, D. H. Gurinsky, W. L. Kosiba, H. J. Kouts, R. W. Powell, W. W. Pratt (presently affiliated with Pennsylvania State University), A. C. Rand, Brookhaven National Laboratory Associated Universities, Inc.

Control and Safety Systems

Under a subcontract, the control and safety system was developed and engineered by the Servomechanisms Laboratory of the Massachusetts Institute of Technology. By the then-existing standards, it was a very elaborate system with complete integration in operation. It was desired that each of the control rods should have an independent source of energy for shutdown purposes in case the electrical power supply fails, and this led to the flywheel-hydraulic pump-hydraulic motor-variable speed transmission on each of them. This system has been absolutely trouble-free.

The first of two manually-operated, auxiliary shutdown systems makes use of boron-steel balls which are dropped into four separate tubes in the graphite structure. The operating mechanisms for this system are imbedded in the shield and are connected by cables to levers beside the operating console. The four shot wells have a total effectiveness of less than 1 per cent in excess reactivity.

The second auxiliary safety system, also manually operated, employs a liquid poison, trichlorobenzene. This flows from a storage tank outside the shield into a series of eleven tubes in the graphite structure when a series of diaphragms are punctured by a lever operation. This system is also capable of about 1 per cent *k* in control.

The Coolant System and Meteorology

Because of the importance of preventing contamination from getting into the air coolant stream and being released from the effluent stack, it was deemed imperative to install high efficiency filters on both the inlet and exhaust streams. This, again, was an innovation at that time. The inlet filters are of higher efficiency than those on the exhaust side because no very high efficiency filter media, capable of withstanding the 500°F exhaust air temperature, were available. The filter media on the inlet side were changed after four years of operation because of a high pressure drop across them, but the original media on the exhaust side are still in service.

A very stringent condition was imposed upon the maximum permissible radiation levels arising from the gaseous effluent from the stack. The specifications were that on the Brookhaven site the radiation level due to this source should not exceed 5 milliroentgens per day and for offsite areas not more than 0.5 milliroentgens per day. Since it was calculated that about 7000 curies of A^{41} would be discharged from the stack each day, it was felt necessary to establish a meteorology program in conjunction with reactor operations. This program and the results are described in P/567, Volume 9 of these Proceedings.

Besides this, a series of twenty background monitoring stations, situated in all directions from the reactor out to a distance of about twenty-five miles, was established to obtain a continuous record of the radiation levels surrounding the site.

It should be stated that the specified radiation level maximums have never been reached so that the reactor has never been shutdown for meteorological reasons alone.

Geology

The Brookhaven National Laboratory is situated in an area on Long Island where the local ground water supports everyday living in a very direct ground-to-home and ground-to-industry way. Thus, it is very important that the Laboratory operation does not contaminate the ground water. A condition was imposed that not more than two curies of activity per year would be permitted to be discharged into the ground water on the site. This led to a geology and hydrology program of investigation of the local parameters by the United States Geological Survey. Its report, based upon four years of study and investigation, will soon be published.

CONTROL SYSTEM

The control of the reactor can be broken down as follows: (1) control of the rate at which neutrons (and heat) are generated; (2) control of the temperature at various points inside the reactor by the use of an air-cooling system; (3) control of internal damage to the reactor due to corrosion, differential expansion, and radioactive contamination; and, (4) control of hazards to personnel due to radioactive byproducts and radiation leakage. However, this section is limited to a discussion of item (1).

Control of Neutron Flux

The control of the neutron flux is essential for the following reasons: (1) to provide a constant neutron flux which is necessary for many research uses; (2) to avoid costly damage to the fuel elements due to high temperature or to thermal shock; (3) to avoid a catastrophe in which the temperatures would be so high as to damage the reactor structure itself (this danger is, however, minimized by the negative temperature coefficient of the reactor); and (4) to avoid other kinds of damage which would result from operation under unsafe conditions.

Control Elements

The reactivity of the reactor is determined primarily in three ways:

1. Control Rods

The control rods contain enough poison, with a good safety factor, to bring the reactor subcritical whenever they are inserted. They are used to override the changing effects; such as fission product poisons and temperature coefficients of the fuel and moderator. In addition, the rods provide control for the ever-changing in-pile experimental load.

The control rods are operated either manually, as during startup, or instrumentally, as by the constant flux regulator during level operation. Another case of instrumental operation is that of an emergency shutdown, when all rods are inserted as rapidly as possible.

Two of the control rods are electrically driven for fine control; the rest are driven by hydraulic variable-speed transmissions. Failure of electric power is provided for by storage of energy in a flywheel coupled to each hydraulic drive.

2. In-pile Experimental Items

There are many experiments which go into the reactor for the purpose of capturing neutrons. Among these are experimental loops which circulate various chemicals, pieces of cobalt for gamma sources, and furnaces or refrigerators for controlling the temperature of certain specimens. Most of these in-pile experimental items are poisons and affect the reactor in the same way as control rods.

3. Fuel Loading

The reactivity is also determined by the amount of fuel loading. By changing the loading, the reactivity can be varied within safe limits to meet research requirements and to permit operation with a minimum of control rod in the reactor.

Startup

The reactor is started up by withdrawing control rods. During startup, the behavior of the reactor is similar to that of an amplifier with positive feedback. Removal of poison from the reactor is analogous to increasing the gain of such an amplifier.

There is a position of the rods for which the reactor is said to be critical. When this condition exists, any existing neutron population will continue unchanged. If the rods are further inserted, the reactor becomes subcritical and the population dies off exponentially to a stable level. If the rods are pulled out beyond the critical position, the reactor becomes supercritical and the population grows exponentially until rods are inserted to stop the increase.

Instrumentation†

The neutron instruments used during startup are described in order of decreasing sensitivity.

1. Counting Rate Meter‡

The neutron level before startup of the reactor is about a factor of 10^9 lower than the normal operating level. In order to read this low neutron level, a fission chamber is inserted into the reactor as far as the outer fuel elements. There the neutron density is sufficient to give about one pulse of ionization a second. These pulses result from the fission of the U^{235} with which the plates are coated. As shown in Figs. 1 and 2, the pulses of current are amplified, passed through a discriminator which rejects the pulses of lower energy (not due to fission) and feeds the fission pulses—now of equal energy—into a logarithmic rate circuit.

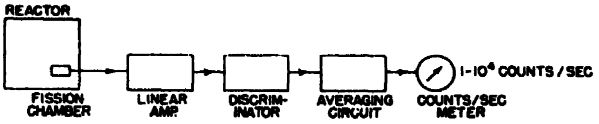

Figure 1. Counting rate system

At the withdrawal of each control rod, the counting rate rises to a new level. At the rate of 10^4 counts a second, the indicator is reading full scale and a relay acts to withdraw the chamber into a region of lower flux to prevent too much activation of the metal and burn-up of the U^{235}. Before 10^4 counts a second, however, the reactor has become critical and the level is rising exponentially so that the period meter can be used.

2. Period Meter§

In starting up the reactor, it is just as important to know the rate at which the level is rising as to know the level itself. Since very high rates of rise are possible and since the rise is exponential, it is conceivable that, even at very low level, the power may be rising so fast that by the time a level has been reached which can be recognized as dangerous, it is too late for the operator or safety controls to stop the rise before serious damage is done. It is important, therefore, to recognize a dangerous rate. This is done by the period meter, which responds as:

$$\frac{d}{dt}\log n$$

Since the neutron density is rising as:

$$n = n_0 e^{t/T}$$

$$\frac{d}{dt}\log n = \frac{1}{T}$$

The deflections of the period meter are, therefore, inversely proportional to the reactor period, *T*. It will

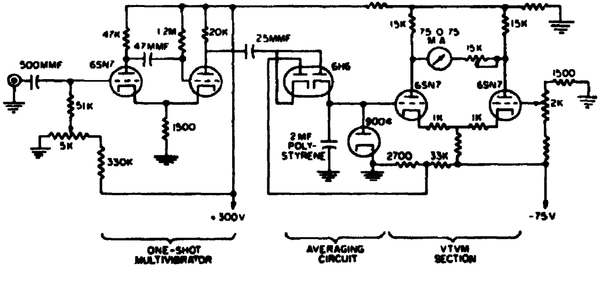

Figure 2. Counting rate circuit

---

† The initial instrumentation for measurement and control of radiation was designed and procured by the Servomechanisms Laboratory of the Massachusetts Institute of Technology.

‡ The counting rate circuit is based on a design of P. R. Bell and W. Jordan of the Oak Ridge National Laboratory, Carbide and Carbon Chemicals Company.

§ The basic amplifier circuit was developed at the Oak Ridge National Laboratory by P. R. Bell and W. Jordan.

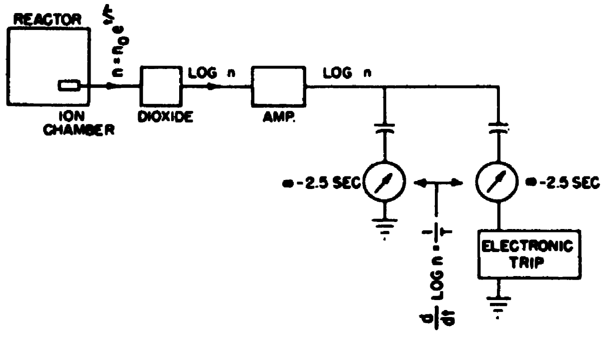

Figure 3. Period system

be seen that the reactor period is the time required for the reactor level to increase by a factor of *e*.

As shown in Figs. 3 and 4, the period system employs an ionization chamber, boron-lined so it will be sensitive to neutrons (which split boron atoms into two highly ionizing particles). The dc component of the current from the chamber is fed into a diode with negative plate voltage. The resulting change in plate voltage is proportional to the logarithm of the signal current and, hence, to the logarithm of the neutron level. (This behavior of a diode with retarding plate voltage has been known since the early days of work in thermionic emission, and is due to the Maxwellian distribution of the energies of the emitted electrons.) The voltage signal is then amplified and differentiated to give an output current inversely proportional to reactor period. The output current operates an indicator, as well as an electronic trip circuit.

The ionization chamber is actually two chambers in one. They have a common collector and one, being boron-lined, is sensitive to neutrons and gamma rays; while the other, being uncoated, is sensitive only to gamma rays. It is found that, by proper angular positioning of the chamber, the signal current due to gamma rays in the two halves may be made to balance out. Thus, the background signal due to previous operation of the reactor may, during a shutdown, be eliminated so that the period meter will, during a startup, present us with an early and accurate reading.

If the high voltage is supplied to the chamber from a bridge circuit, as shown in Fig. 4, the bridge may be balanced so that the noise from the two halves of the chamber, due to voltage fluctuations, will cancel out.

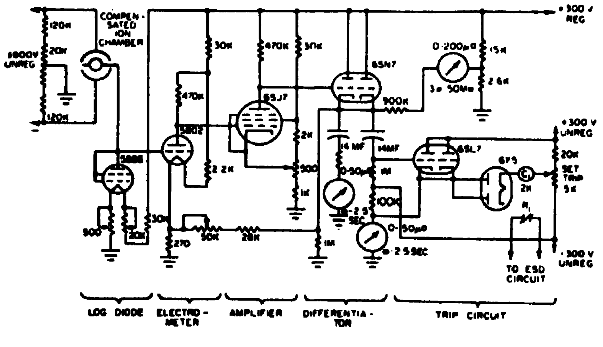

Figure 4. Period system

This gives more reliable operation than the use of a regulated high voltage supply.

In the period trip circuit, a standard type of feedback differentiator is used which provides enough power to operate a plate circuit relay while maintaining the desired high speed of response. The diode in series with the relay coil gives a suppressed-zero action and, consequently, a more stable trip point.

In Fig. 4, the means for applying test signals are not shown. These consist of circuits for applying known currents to the input in order to calibrate the amplifier, and a circuit for applying test signal current at the grid of the trip circuit which may be increased until the relay trips. The trip point can then be read off the meter directly in seconds of reactor period.

There are three period systems, each with a trip, and with their emergency shutdown relays so wired that if two or more circuits trip, the reactor will shut down.

3. High Level Power Indicator

In practice, the power level is allowed to rise on a constant, safe period until the megawatt region is reached. At a power about a factor of 10^6 below the operating level, indications are first obtained on a sensitive galvanometer which is connected to a boron-lined ionization chamber in the reactor. By means of a shunt, the range of this galvanometer may be changed by the operator so as to follow the rise of power up to the operating level. Recently, this galvanometer has been replaced with a sensitive dc amplifier of the chopper type, with the advantage of ruggedness, so that complicated protective devices are no longer necessary (see Fig. 5).

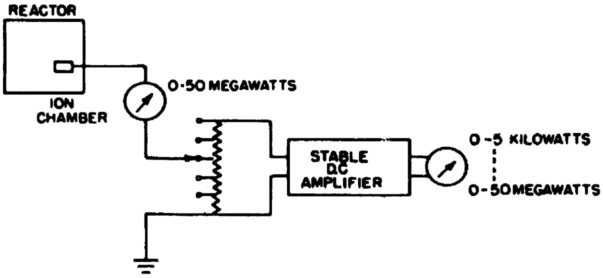

Figure 5. High level power indicator

4. High Level Power Controller

For high level constant power operation, a simple on-off type of servo is provided. A recorder-controller actuates one of the regulating rods by means of mercury switches. The signal to the controller is essentially the difference between two voltages: the voltage drop resulting from the flow of chamber current through a resistor, and a fixed comparison voltage which determines the set point.

This simple device is adequate since the response of the reactor to small rod motions is rather slow. It holds the power to about 0.5 per cent.

5. High Level Trips

In order to insure that the reactor shuts down if a certain level is exceeded, three boron-lined ionization chambers are provided; each connected so that its

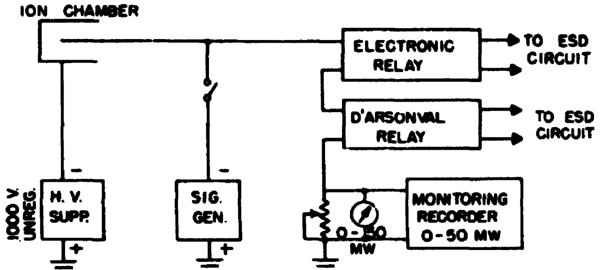

Figure 6. High level trips

signal current flows in turn through an electronic relay, through a d'Arsonval relay, and through the common shunt of a power meter and a power recorder. One of the three trip circuits is shown in Fig. 6.

The procedure for setting the high level trips is as follows: With the reactor operating at a known power level, the power meter and power recorder are calibrated by varying their shunt until they read this power. With the key of the signal generator closed, the simulated power is then raised to the desired trip value by increasing the current contribution from the signal generator. The two trip circuits are then adjusted until they just trip.

The electronic relay (Fig. 7) is a 2-tube amplifier which energizes an emergency shutdown relay. Because of the suppressed-zero design, the full current is maintained through the relay coil until the reactor power is within a few per cent of the trip point, then drops rapidly. This, by insuring full contact pressure during normal operation, diminishes the chance of an accidental trip. At the same time, it makes the trip point more accurate.

The signal from the ionization chamber causes the grids of both stages to go negative so that the electronic relay is fail-safe with respect to most tube and circuit failures.

The purpose of the d'Arsonval relay is to back up the electronic relay with a simpler device. It has the disadvantages, however, of being slower and of not having fail-safe contacts.

A three-point recorder is connected in turn to each of the three recorder shunts to monitor the signals to the three trip circuits. As in the case of the period circuits, the relays of the high level trips are wired so that the reactor will not shut down unless at least two out of three relays drop.

Avoidance of Accidental Emergency Shutdowns (ESD)

While a very few accidental ESD's have been caused by operational mistakes, most have been due to instrument failure. Wherever possible, the instrument systems are designed to fail safe. This makes for a safe reactor, but one which is susceptible to accidental shutdown.

One obvious means for reducing the number of accidental ESD's is to make the instruments more reliable. In the case of the high level and period trips, this was done by use of zero-suppression. A program of contact cleaning also helped.

The hard-to-maintain contacts of the ESD lockout switches were eventually replaced with a banana plug type. The use of an independent power supply for instruments only has been a help in preventing shutdowns due to loss of instrument power. Along the same lines, it is planned to segregate on certain circuit breakers all the instruments which can cause an ESD and to eliminate all other loads from these circuits. It is also planned to install an automatic transfer switch so that in the event of an instrument power failure the instrument load will be transferred to the commercial mains. Since all the circuits which will trip on momentary power failure are self-setting, the control rods will move in only a short distance and the reactor power will drop only about one per cent.

As mentioned above, the ESD relays for the three period trips, the three electronic relays, and the three d'Arsonval relays are specially connected. Each of these relays has two sets of contacts through which the main ESD contactor is energized. These contacts are connected so that the ESD contactor will remain energized unless at least two relays drop. This connection has proved to be the most potent factor in the reduction of accidental ESD's.

Theory of Coincidence-Connected Trips

Each group of three trips has a small but finite probability of failing to act when called upon; i.e., it is not completely fail-safe. Each group also has a small but finite probability of causing an accidental ESD, owing to "safe" failures. The object is to reduce drastically, by coincidence-connected relays, the latter probability without seriously increasing the former.

Let $P =$ the chance that one circuit will be in a tripped condition at some instant. The chance that a certain pair of circuits will both be in a tripped condition at the same instance is P^2. Now P is very small, since special efforts have been made to prevent accidental trips, and if a momentary trip does occur, the circuit resets itself. P^2, therefore, is negligible.

The chance that some pair of circuits will both be in a tripped condition at the same instant and that the reactor will accidently shut down is $3P^2$, still negligibly small.

How much safety has been sacrificed? Let $p =$ the chance of some one circuit failing to act when called

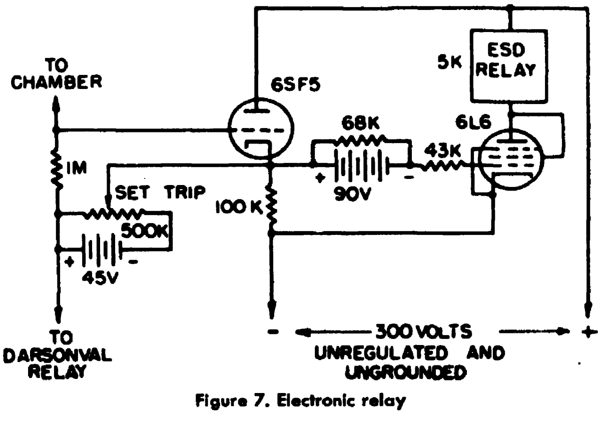

Figure 7. Electronic relay

upon. This is small because the circuits are almost completely "fail-safe," and because of routine maintenance and monitoring by the operators. The chance of the reactor failing to shut down in an emergency is just the chance of some pair of circuits simultaneously failing to act when called upon. This is $3p^2$. Now, if the same three circuits were not coincidence-connected, the chance of the reactor failing to shut down in an emergency would be p^3; that is, the chance of simultaneous failure of all three circuits; therefore, in the coincidence-connection of the relays, the chance of failing to shut down has been increased by a factor of 3. While this is a large factor, it is applied to a quantity which is already exceedingly small.

It would be possible, of course, by increasing the number of circuits, to compensate for the loss of safety due to the coincidence-connection. In the case of the Brookhaven reactor, this was deemed unnecessary.

FUEL ROD LEAK DETECTION METHODS

The Brookhaven reactor contains about fifty metric tons of normal uranium in the form of some thirteen hundred individual fuel elements. The fuel elements are the subject of P/828, Volume 9, these Proceedings. The uranium rods are covered with aluminum tubes which serve to prevent the escape of fission products and to prevent chemical action of the uranium. The integrity of the aluminum containers against leaks is of vital importance and it is essential that any leaks which do occur are detected without delay. Detection methods must be highly sensitive and reliable to assure good operational practices. There are several leak detection methods used at Brookhaven.

Exhaust Air Monitor

This instrument is an ionization chamber, located in a small holdup tank, into which a stream of the filtered exhaust air passes and stays for a few seconds. In normal operation the predominant radioactivity associated with this air is A^{41}. In the case of a fuel element failure there is added to this background activity that due to xenon and other gaseous fission products.

Exhaust Air Filter Monitor

A small side stream of unfiltered exhaust air is drawn off and separately filtered. This filter is constructed so that it forms a portion of an ionization chamber. Since all atmospheric dust is removed by high quality inlet filters, any particulate matter originating in the reactor will be held up on this filter. The ionization chamber routinely yields a signal due mainly to the A^{41} radioactivity of the exhaust air. In the event of a fuel element failure, the activity due to the particulate matter held up on the filter medium is added to the background activity and creates a signal.

Probes

The probe consists of an oil-soaked bundle of steel wool attached to the end of a steel rod. This is inserted through the wall of the exhaust air ducts in a position before the air encounters the exhaust filters. The steel wool will pick up some particulate matter if any is present. This operation is done once every hour to establish backgrounds and any increase of activity is readily ascertained.

Helium System

This is a very complicated mechanical-electrical system for determining which of the thirteen hundred fuel elements has failed when a failure is detected. Communication with each of the individual elements is achieved with this system through an aluminum (0.125-in. diameter) capillary tube welded to the end of each of the aluminum containers. These capillary tubes pass from the ends of the fuel channels through fixed conduits terminating at the outside face of the reactor shield on top of the reactor. Groups of these tubes are connected to twenty-seven separate manifold chambers and each manifold is pressurized with a static pressure of helium at 1 psig. The helium in the fuel element serves: (1) to indicate a leak by a drop in pressure; (2) to prevent oxidation of the uranium metal and also other chemical reactions; and, (3) as a good gaseous heat transfer medium.

The helium pressure in each manifold is monitored automatically and continuously by recording instruments sensitive to the loss of only a few cubic centimeters of gas. When one of the manifolds indicates a low pressure due to a leaking fuel element, the leaker is located by connecting the individual fuel element capillary tubes to pressure monitors, through a permanent system of valves. Almost all the leaks develop gradually so that the escaping helium prevents the oxidation of the uranium until the time the leak is detected. When the leakage rate is determined to be small the fuel element is allowed to remain in the reactor under special surveillance until the rate increases beyond allowable limits. In this way, the fuel element lifetime may be extended considerably and it can be discharged at a convenient shutdown rather than immediately.

THE REACTOR SHIELD

It has been mentioned that one of the original design concepts was that the shield be no thicker than five feet. The development of a high density concrete was chosen as the most likely material to provide the desired characteristics. In 1947, only very fragmentary information existed on the attenuation properties of the reactor shields at Oak Ridge and Hanford. At that time, a reactor shield was thought of to include: (1) a dense, metallic inner section to absorb 99 per cent or more of the primary gamma-ray heat incident on the shield (this section is usually designated as the thermal shield and requires cooling); (2) a high, stable hydrogen content to provide for the slowing down of fast neutrons by elastic collision; and (3) a high density constituent effective in absorbing the residual primary and secondary gamma rays, and in slowing down fast neutrons by inelastic collision.

In 1946, L. B. Borst, at Oak Ridge, made the suggestion that a "loaded" or "heavy" concrete, containing hydrated metallic ores, might serve to provide the characteristics of (2) and (3), above. It would have the advantage, too, of economical fabrication as a monolithic, poured material.

At the outset, it was established that the density of the mixture should be about twice that of ordinary concrete in order to hold the thickness to five feet or less. Such a density could not be achieved using only hydrated metallic ores, so it was necessary to include a dense metallic constituent. Thus, attention was confined to a mixture containing only cement, crushed limonite ($2Fe_2O_3 \cdot 3H_2O$) as the fine constituent, and scrap iron punchings as the coarse constituent. A specific gravity of 4.5 demanded approximately equal volumes of limonite and iron scrap pieces. Various mixtures were poured in an effort to effect a workable combination at least the equal of ordinary concrete as a structural material. Tests demonstrated that a workable mixture of high compressive strength, satisfying all the design criteria, was achieved with:

	lb	*ft*^{3}
Portland cement (10 bags)	940	4.8
Crushed limonite	1880	8.4
Iron punchings	4100	8.4
Water (36 gallons)	300	4.8
Retarding, plasticizing admixture	15	—

A six-inch thick iron thermal shield was adopted for the inner section of the shield structure, and it was decided to use this as one side of the forms into which the heavy concrete would be poured. A large quantity of three-inch thick iron plate, surplus to the war effort, was located, and this was used for building the forms. Hence the shield configuration was: 6 inches of iron plate; 4 feet, 3 inches of heavy concrete; and 3 inches of iron plate as the outside face of the forms. Obviously, the use of 3-in. plate on the outside was unnecessary: its availability as surplus material dictated its use.

Physical Properties

1. Density—280 to 300 pounds/ft^3. The total iron content is about 70 per cent of the gross weight and the weight ratio of iron to hydrogen is about 120.
2. Specific heat—averaged, about 0.164.
3. Thermal conductivity—averaged, about 0.0085 cal/sec cm^2 °C.
4. Coefficient of expansion—about 16×10^{-6}/°C.
5. Modulus of elasticity—about 3.5×10^6 psi.

Attenuation Properties

Measurements on the attenuation characteristics for both neutrons and gamma rays were made at Brookhaven and at Oak Ridge. For a thermal reactor the shield thickness is generally determined by the gamma attenuation length, which is somewhat longer than for the neutrons leaking into the shield.

In the gamma-ray measurements, two kinds of detectors were used: one, nondirectional to receive the radiation emerging through the shield in all directions, and the second, collimated so that only the forward direction, more energetic component of the radiation was detected. Using the collimated detector, the attenuation length is about 9.2 cm, and in the uncollimated case it is about 7.9 cm. The corresponding over-all attenuation factors for the total five-foot thickness is $e^{16.5} = 10^{7.2}$, and $e^{19.3} = 10^{8.4}$.

The attenuation length for reactor neutrons is about 6.5 cm. The corresponding attenuation factor for the five-foot thickness of the shield is $e^{23.5} = 10^{10.2}$.

Costs

It is meaningless to attempt to compare the costs of different kinds of reactors or their individual components. Likewise, it is difficult to compare costs for reactors built at different times and under different conditions. Thus, the cost of the Brookhaven reactor shield cannot be compared even with the cost of another of the same type, such as the Oak Ridge graphite reactor. As an example, the graphite structures in the Brookhaven and Oak Ridge reactors are almost identical in overall size (a 25-ft cube versus a 24-ft cube), yet the Brookhaven shield is 58 × 38 × 35 feet in over-all dimensions whereas the Oak Ridge shield is 47 × 38 × 35 feet. The extra length in the Brookhaven shield is dictated by the fuel element design.

The only sensible comparison of costs should concern itself with the costs per square foot of shield, without any built-in special facilities. The costs per square foot of the bare Brookhaven shield in place, including the six-in. thermal shield of iron plate, are about seventy-five dollars.

EXPERIMENTAL FACILITIES

The over-all dimensions of the reactor shield are approximately fifty-eight feet (length) by thirty-eight feet (width) by thirty-five feet (height). One of the ends is reserved for the operational loading and unloading of the fuel elements. Actually, this operational face is also used in connection with the production of long half-life radioisotopes; such as cobalt-60, which is accomplished in some of the unfilled fuel channels. The other five faces of the box are research areas where all the experimental facilities are located.

A pattern of thirty horizontal beam holes extends through the graphite core and the opposite shielding walls, in the direction perpendicular to the fuel channels (see Figs. 8 and 9). These holes, four-inch squares in the graphite, are spaced three feet apart horizontally and four feet apart vertically. They are used either for neutron beam or inpile irradiation types of experiments, It was originally thought that only about ten of these holes could be used on each face at any one time because of space limitations. Actually, about twenty of the thirty on each face are in almost constant use.

The top face of the reactor was designed to accommodate experiments requiring large areas of neutrons leaking out of the reflector; such as the thermal column. The top shield is built in the form of interlocking blocks, each four feet square (see Fig. 10). When one of them is removed, an opening of this size right down to the top of the reflector is provided.

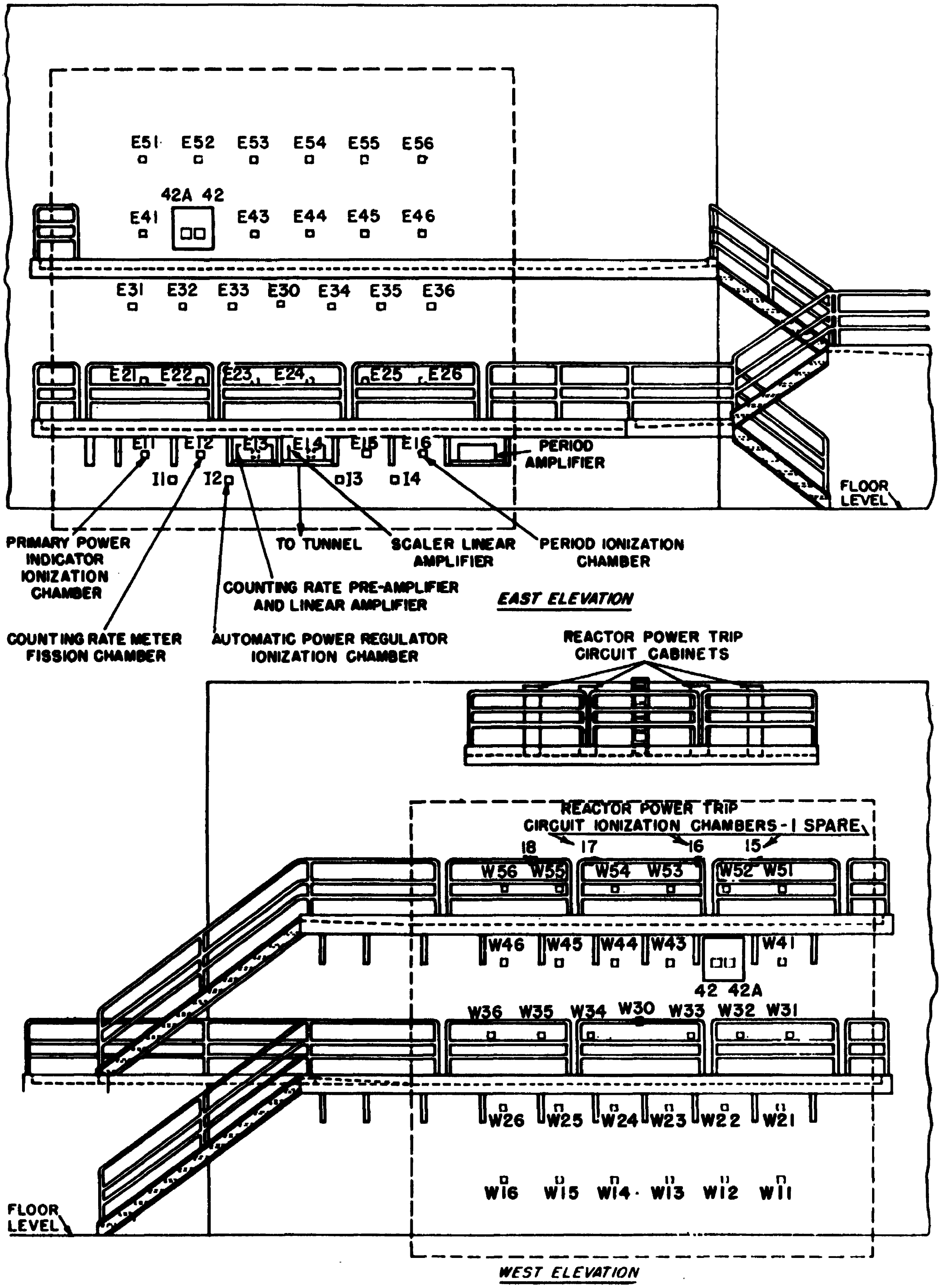
E51 E52 E53 E54 E55 E56
42A 42
E41 E43 E44 E45 E46
E31 E32 E33 E30 E34 E35 E36
E21 E22 E23 E24 E25 E26
E11 E12 E13 E14 E15 E16
I1 I2 I3 I4
PERIOD AMPLIFIER
FLOOR LEVEL
PRIMARY POWER INDICATOR IONIZATION CHAMBER
TO TUNNEL
SCALER LINEAR AMPLIFIER
PERIOD IONIZATION CHAMBER
COUNTING RATE PRE-AMPLIFIER AND LINEAR AMPLIFIER
EAST ELEVATION
COUNTING RATE METER FISSION CHAMBER
AUTOMATIC POWER REGULATOR IONIZATION CHAMBER
REACTOR POWER TRIP CIRCUIT CABINETS
REACTOR POWER TRIP CIRCUIT IONIZATION CHAMBERS - 1 SPARE
18 17 16 15
W56 W55 W54 W53 W52 W51
W46 W45 W44 W43 W41
42 42A
W36 W35 W34 W30 W33 W32 W31
W26 W25 W24 W23 W22 W21
W16 W15 W14 W13 W12 W11
FLOOR LEVEL
WEST ELEVATION

Figure 8. Location of experimental facilities

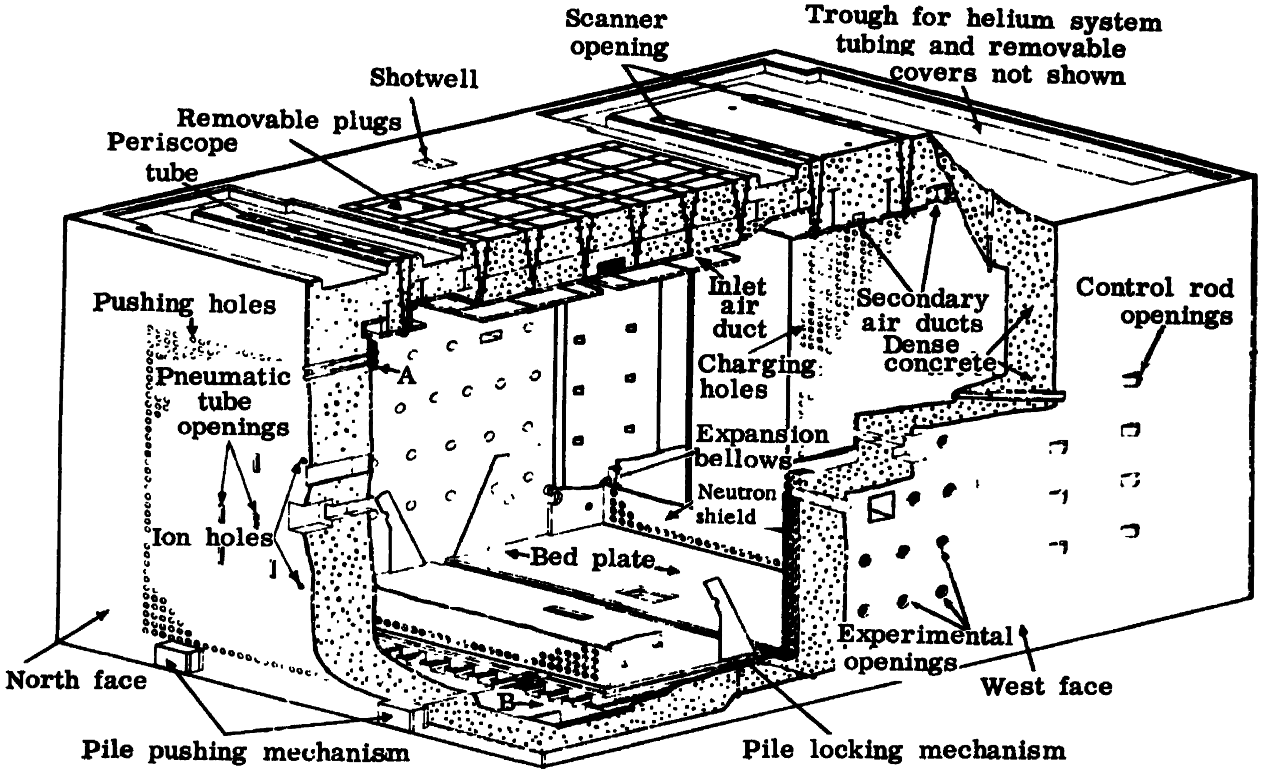

Cutaway isometric view of shield

Figure 9. (A) Thermal shield which lines both plenum chambers; (B) floor grill and east-west channels omitted to show I-beams; (C) airtight membrane, restraining springs not shown; and (D) balconies not shown

There are five experiments here, using six of the four-ft square positions.

The bottom face of the reactor is accessible by means of two tunnels built underneath the graphite structure. Figure 11 shows the steel liners, forming these tunnels, being set in the foundation. The larger tunnel is two feet square in cross section and has an exposure window three by two feet in area. The smaller tunnel is one-foot square in cross section and has a window three feet by one foot in area. A small, flat car moves on rails in the bottom of each tunnel and can be loaded through openings in the floor of the building on both sides of the reactor. These tunnels were built to provide for the irradiation of live animals, as well as large size instruments or equipment. Leads can be taken out of the tunnels from the experiments to monitoring or recording meters in the reactor room.

The sixth face, opposite the loading and unloading face, is used primarily for the production of radioisotopes and to provide service irradiations of special targets. Eleven special tubes, parallel to the fuel channels, terminate at this face. Some of them are used to convey samples pneumatically into and out of the core. Others can be used manually to insert samples of special nature, with or without monitoring leads connected to them. The fuel channels are also accessible through this face. A twelve-inch square removable section of the graphite core, parallel to the fuel channels and including the central fuel channel, provides for a beam experiment extending over a distance of up to one hundred feet: it is here that the fast chopper is installed.

There is a wide variety of devices built into the reactor for doing irradiations of specialized character. Most of the specialization comes by way of requirements for controlled ambient temperatures. The graphite and air temperatures in the reactor range between 50 and 200°C. Two of the four-in. square beam holes have each been provided with water-cooled irradiation chambers to yield a controlled temperature of 30°C. These are built so that samples can be inserted or removed while the reactor is in operation. A third such beam hole has a chamber cooled by liquid nitrogen to provide an ambient temperature of −190°C; this, also, can be operated independent of shutdowns. A fourth beam hole has a furnace installed to provide elevated temperatures up to 500°C. A fifth beam hole contains a foil slot for irradiating thin samples and is operable independent of shutdowns. A sixth beam hole is used for the target conveyor, which can handle some three hundred separate samples, at one time, in an endless loop. Samples can be inserted and removed from this facility also while the reactor is operating.

One of the fuel channels has a chamber for the irradiation of gaseous samples, pumped into the reactor and out by a special system without requiring a shutdown. Still other holes in the reactor have controlled temperatures in the range of 50 to 70°C,

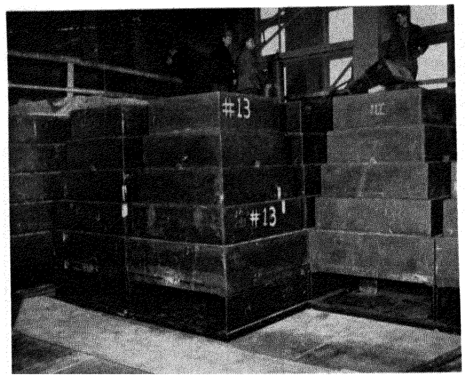

Figure 10. Interlocking and removable shielding blocks installed on the top face

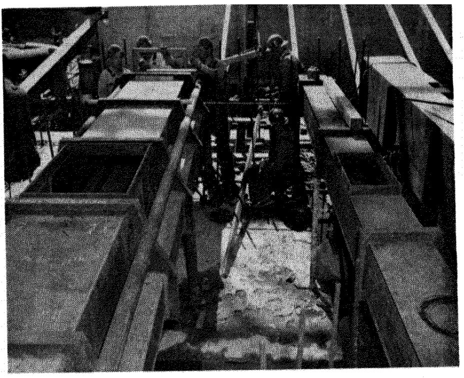

Figure 11. Steel liners being installed in foundation of the Brookhaven reactor to provide irradiation tunnel facilities on bottom face

provided by air-cooling. With regard to cross sectional area, the largest object which has ever been irradiated in the core of the reactor was a sixteen-in. diameter piston ring.

THE OPERATING SCHEDULE AND PHILOSOPHY

For a reactor supporting a large program of research, the most productive schedule of operations is that of full power operation continuously, or nearly so. In this way, data can be taken around the clock, providing the equipments are set up to operate and record data automatically over long periods of time. There are about fifteen experiments at the Brookhaven reactor which are conducted in this manner, having research personnel in attendance essentially during the day shift only. Several others have personnel in attendance on either a two or a three-shift basis. All the other experiments devote the day shift only to data taking.

The operating schedule includes a shutdown of the reactor at approximately ten-day intervals. These occur on alternate Tuesday and Friday evenings at the end of the day shift. The Tuesday evening shutdowns are usually of short duration, only a few hours, to allow for changes in experimental equipment and the insertion or removal of irradiated samples being done in facilities which require a shutdown. The Friday evening shutdown is usually of short duration, also, but may extend over twelve hours or more to permit more extensive work to be done and also to accomplish fuel element changes in the loading. All shutdown work is scheduled very carefully in advance.

The demands of the research people for high neutron fluxes of constant magnitude dictates an operating procedure calling for the presence of almost no control rods in the reactor at equilibrium conditions. Experimenters do not like to have a source of neutrons in close proximity to a control rod because the flux is decreased by its presence and varied by its motion. Hence, it is important to achieve a balance between the fuel loading and the neutron-absorbing materials as represented by the experimental equipment. In other words, it is important that the excess reactivity, at equilibrium conditions, be of minimum value. In routine practice, the excess reactivity taken up by the control rods of the Brookhaven reactor is hardly ever greater than 0.05 per cent k. Indeed, the balance is so tightly held that often the reactor operates at full power with no excess reactivity—this means that at such times all sixteen control rods are fully withdrawn from the reactor.

It is important that the operations staff has as its guiding criteria, one of safety and one of making it easy for the performance of research. The second criterion may, at times, be incompatible with a good operating record, however, it is not often so—as a matter of historical record, the Brookhaven reactor operates more than 90 per cent of the time. The important elements of the operating staff which have to be imbued with the spirit of cooperation with the research staff are those at the top level in charge of the reactor and those who come in contact with the research people by way of rendering some service necessary to the conduct of the research.

THE OPERATIONS STAFF

The character of the Reactor Operations Division is tailored precisely to meet the demands of the reactor and the research programs. The supervisors and operators are divided into five shift groups which are responsible for the shift operations. Besides, there are: (1) an instrument group responsible for maintenance and development work on all electronic equipment; (2) a maintenance group responsible for all other maintenance on the reactor and operation of the staff machine shop; (3) a research coordination group which handles all problems of the research people as they affect the scheduling and physical changes required, as well as of the radioisotope work; (4) a fuel element group which fabricates the new fuel elements and prepares the shipments of burned out fuel elements for processing; (5) an administrative and clerical staff in charge of records, fuel element inventory and control, and outside contacts; and (6) a meteorological group responsible for problems pertaining to the discharge of the gaseous effluent from the reactor.

All members of the division who are involved with actual work on the reactor are trained to be very versatile in all functions so that they may be used in all phases of the work. They understand radiation problems and are able to use radiation instruments.

The total staff comprises about fifty persons. The annual payroll, including insurance and retirement benefits, vacation and sickness allowances, and shift and overtime bonuses, amounts to about 285,000 dollars at the present time.

STARTUP AND SHUTDOWN PROCEDURES AND THEIR EFFECT ON FUEL ELEMENT LIFE

In the early history of the Brookhaven reactor, the startup and shutdown procedures were of a pattern to insure an over-all safe operation. The period trip circuits would not permit a period shorter than three seconds, although in practice the startup periods used were in the range of 20 to 40 seconds. There was little or no concern about a relationship between fuel element life and modes of startup or shutdown.

An early research program required a number of closely spaced, full power operating intervals, followed by short, shutdown intervals. Immediately following this type of operation, it was noticed that some fuel element failures would occur. It was decided that the failures were due to a combination of two causes: (1) thermal stresses on the fuel elements resulting from severe temperature cycling; and (2) high power densities in some of the fuel elements due to the reduction in core size by the presence of control rods. As more and more experience was gained, it became evident that these effects could be minimized by simple restrictions to our operations procedures.

In order to prevent severe temperature cycling of the fuel elements, restrictions were put into effect on both the startups and shutdowns. The startup rate of power increase is limited to prevent a temperature rise greater than 2°C/min. The shutdowns are controlled, by cutting the coolant flow, to prevent a cooling rate greater than 2°C/min. Along with these conditions, the control system has been modified so as to eliminate faulty shutdowns due to false signals or electronic failures (see Control System above).

Inordinately high power densities are avoided in startups by approaching the full power level gradually. The full power level is reached only after the short-lived fission products build up considerably, so that very little control rod effect on power density remains. Only eighteen fuel elements have failed in the entire Brookhaven reactor history, and none at all during the past year.

MEASURED FLUX PATTERN AND SPECTRA

In a large reactor, such as this one, with an extensive research program changing from month to month, it is somewhat meaningless to specify the flux pattern or spectrum throughout the volume of the graphite structure. Generally, when an experiment requires precise information of this sort, measurements are made at the position of the equipment at the time of the experiment. Extensive measurements have been made in two experimental holes, E-13 and E-25, and the data follow.

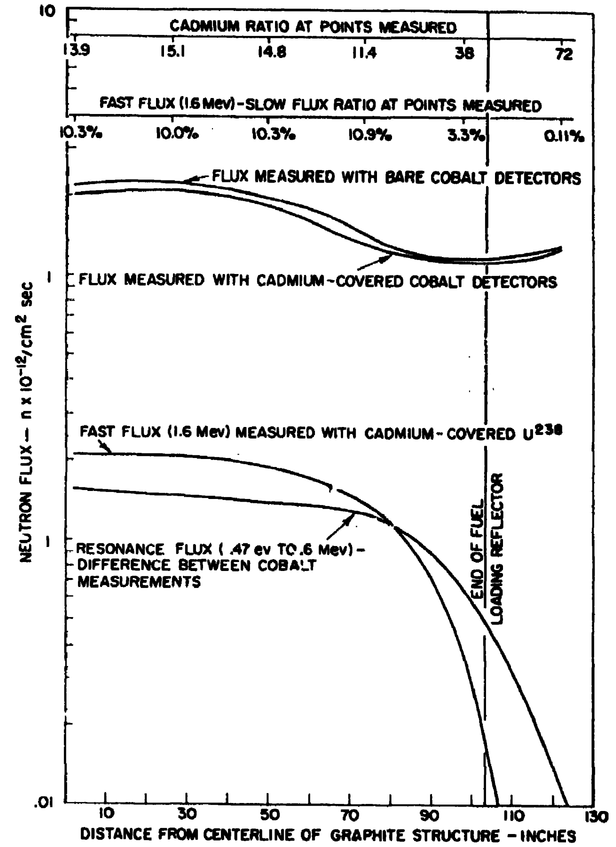

Figure 12. Neutron flux measurements in experimental hole E-13, power level 26 megawatts

A plot of the variation of the slow, resonance, and fast neutron fluxes, as a function of the distance from the center line of the graphite core in E-13, appears as Fig. 12. The resonance flux between 0.47 ev and 0.6 Mev is taken as the difference between the fluxes measured with cobalt detectors, with and without cadmium coverings. The fast neutron flux above 1.6 Mev is obtained from cadmium-covered U^{238} detectors. The cadmium ratios and the fast flux-slow flux ratios are displayed. The cobalt cross sections used in these evaluations were 34.2 barns for the thermal activation cross section and 41.2 barns for the resonance activation cross section. Other measurements with cadmium-covered Np^{237} detectors indicate that the ratio of fast flux above 0.6 Mev to slow flux is 25 per cent.

Calorimeter measurements indicate that the gamma-ray flux averaged at an energy of 1 Mev is about 40 per cent of the slow neutron flux. This means that at a slow neutron flux of $4 \times 10^{12}/cm^2$-sec, the gamma-ray flux, averaged at 1 Mev, would be $1.6 \times 10^{12}/cm^2$-sec. Using the conversion factor of 1.9×10^9 to convert from gamma flux to roentgen dosage, this gives about 3×10^6 r/hr. This value compares with the rough rule which applies to this type of reactor which says that the gamma dosage in r/hr is the square root of the slow neutron flux in n/cm^2-sec. This rule gives 2×10^6 r/hr for comparison with the above number.

LISTING OF LONG-TERM EXPERIMENTAL EQUIPMENTS

Physics Department

Four crystal spectrometers, slow chopper, fast chopper, three radiation damage study facilities, fast neutron converter, thin-lens β-ray spectrograph, experiment on lattice structure of crystals, neutron detection experiment, nuclear isomer studies, magnetic domain experiment.

Chemistry Department

Two crystal spectrometers, low temperature irradiation facility.

Reactor Department

Two crystal spectrometers, shielding experiment.

Nuclear Engineering Department

Lattice experiments, in-pile loop, creep experiment, neutron diffusion studies.

Biology Department

Thermal column, studies on biological specimens.

Medical Department

Neutron irradiation therapy facility.

Guests from Other Institutions

Three crystal spectrometers, three in-pile loop experiments, He^6 decay experiment.

SOME EFFECTS PRODUCED IN GRAPHITE BY NEUTRON IRRADIATION IN THE BROOKHAVEN REACTOR

Introduction

When graphite was first considered for use as a moderator in reactors, E. P. Wigner pointed out that the bombardment of graphite by neutrons would result in knocking out atoms from their lattice sites and that a change in the physical properties of the material should be expected. The initial theoretical work was extended by F. Seitz[1] whose calculations showed that the number of carbon atoms displaced in graphite in slowing down a single fission neutron (2 Mev) to thermal energies is of the order of 1870.

The earliest experimental work on the effect of radiation on the properties of graphite was performed by a group under the direction of Franck and Burton.[2] The effect of neutron bombardment on the c-axis (distance between hexagonal planes) was first studied by Zachariasen.[2] The work of these investigators confirmed the existence of the so-called "Wigner effect." Since graphite is an important moderator, the effect of radiation on its properties has been studied intensively at many of the laboratories in the United States of America, in Canada, and in the United Kingdom. The list of investigators[2] is so long and their contributions so extensive that this paper does not attempt to enumerate them.

The present paper is the result of a study of the effect of neutron bombardment on three properties of graphite; i.e., physical dimensions, crystal dimensions (c-axis), and heat content. Since the changes in these properties have been shown by previous investigators to depend on temperature of irradiation as well as on exposure, the experiments were carried out over a range of irradiation temperatures.

Experimental Procedure

Three types of samples were used in this study. The first set consisted of one-half inch diameter cylinders, approximately four inches long. These were used primarily for physical expansion measurements. The long axis of the specimen was parallel to the axis of extrusion of the graphite bar. Subsequently, these will be called E samples. These samples were irradiated in experimental holes which are parallel to and between the fuel bearing channels. The second type of sample was used for heat content and crystal expansion and was obtained from the containers in which the E samples were irradiated and were either one inch in diameter by one-inch long cylinders, or one-inch cubes. These will be referred to as EC samples. The third set of samples consisted of parts of a solid cylinder (the whole cylinder would be about one inch in diameter and one-half to three-quarters of an inch in length). These will be referred to as C samples, which were obtained by means of a coring tool inserted into an empty fuel channel, and used for heat content measurements. The first two types of samples differ from the last in one important way; namely, that for the same integrated flux (usually given in terms of thermal neutrons) the percentage of fast neutrons bombarding the specimen is much greater in the case of the C (cored) samples.

Method of Measurement

1. Heat Content

The sample for this measurement, which as indicated above, was small, was placed in the center of a cylindrical brass furnace, 4.25 inches inside diameter by 29.5 inches long. The space between the sample and the inner wall was filled with the insulating material, "Santocel." The brass cylinder was quickly raised to the desired temperature, either 200 or 400°C, and this temperature was maintained constant by means of a thermocouple attached to the midpoint of the brass cylinder furnace. The temperature of the sample was measured as a function of time by means of a thermocouple imbedded in the specimen. After allowing the furnace and specimen to cool to room temperature, the procedure was repeated. The latter establishes the base heating curve for the specimen in its environs.

Table I. Stored Energy

Sample number	*Average irradiation temperature °C*	*nvt* × *10²⁰*	*Maximum temperature reached °C*	*Energy released on heating cal/g*	*Furnace temperature °C*
C-1	55	1.13	281.8	53.6*	200
C-2	65	1.61	228.0	24.0	200
C-3	150	1.66	200.0	00.0	200
C-4	65	1.61	400.5	—†	400.5
EC-5	60	1.19	234.0	24.9*	200
EC-6	60	1.19	400.5	43.9*	400.5

* Values of stored energy calculated by J. Chernick. Other values calculated, using approximate method outlined previously.

† No calculation done on Sample No. C-4.

2. Crystal Expansion

Portions of the EC and C samples were taken before and after the heat content experiments and polished through 4/0 emery paper. These were then mounted on the sample holder of a North American Phillips high angle spectrometer and a trace of the 002 peak was taken. From the angular measurement of the center of the peak, the value of the *d* spacing, and therefore, the interplanar distance of the 002 planes (*c*-axis) was calculated.

3. Physical Dimensions

The E samples, which were the only ones used for this measurement, were provided with squared ends. They were measured before and after irradiation by means of a Sheffield Comparator and gauge blocks on a 3.98000 inch gauge length. As a rule, thirteen individual readings were taken across the ends of the cylinder.

Results

A few representative examples of temperature-time plots are presented in Figs. 13–18. The upper curve in these figures is obtained on the first heating of the irradiated sample; whereas, the lower curve is the result of the second heating of the same sample. Most of the irradiated samples showed an increase in heat content. This increase in heat content will be referred to as stored energy. Figures 13 through 15 are the plots obtained on samples which showed a maximum, medium, and no stored energy when heated to 200°C. One of the samples, which had been heated to 200°C (see Fig. 14), was then heated to 400°C to obtain Fig. 16. Figures 17 and 18 were obtained by heating adjacent samples to 200 and 400°C, respectively.

The calculated values of stored energy, given in Table I, were obtained from the experimental heating curves by a mathematical analysis of the heat flow of this experiment.[¶] The stored energy may also be roughly calculated as the product of the temperature rise (i.e., the difference between the temperature at which the first heating curve deviates from the second heating curve and the maximum temperature attained) and the average specific heat of graphite, 0.25 to 0.30. The sharper the peak for the maximum temperature, the better is this approximation. Values calculated in this manner agree reasonably well with those calculated by Chernick, but are apt to be lower. For example, in Fig. 13, the temperature difference is about 152°C. Thus, the energy released is approximately 45 cal/gm, which compares favorably with the calculated value of 53.6 cal/gm.

The results obtained on the physical growth and *c*-axis measurements are given in Table II and Fig. 19 and Table III and Fig. 20, respectively.

Discussion

The data, in the previous section, show some of the interesting changes in physical properties which occur upon displacing atoms by means of reactor irradiation. It is well known that radiation effects can be annealed out by heat treatment at elevated temperatures.[3] The recovery or healing of the lattice is due to the migration of the radiation induced defects out of the crystal, their mutual annihilation or aggregation into less effective clusters. It is qualitatively clear, however, that the changes produced by an exposure at a given temperature depend upon two competing processes; namely, the rate of damage production and the rate of annealing. At very low temperature, annealing is minimized and defect production depends upon the rate of bombardment and is expected to vary linearly with total integrated flux. At temperatures where ap-

Table II. Physical Growth

Sample number	*Average irradiation temperature °C*	*nvt* × *10²⁰*	*Change in length in 3.98000 inch gauge length sample due to irradiation (inches)*	*Per cent of growth*
E-1	50	1.18	+0.00696	0.18
E-2	55	1.19	+0.00671	0.17
E-3	65	1.20	+0.00545	0.14
E-4	85	1.21	+0.00525	0.13
E-5	120	1.20	+0.00371	0.093

[¶] We are indebted to J. Chernick, of the Brookhaven National Laboratory, for this calculation.

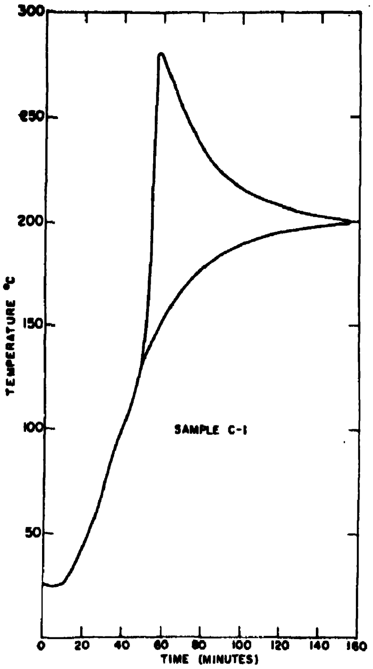

Figure 13. Time vs temperature plot of a graphite sample in a furnace held at 200°C: temperature of irradiation, 55°C

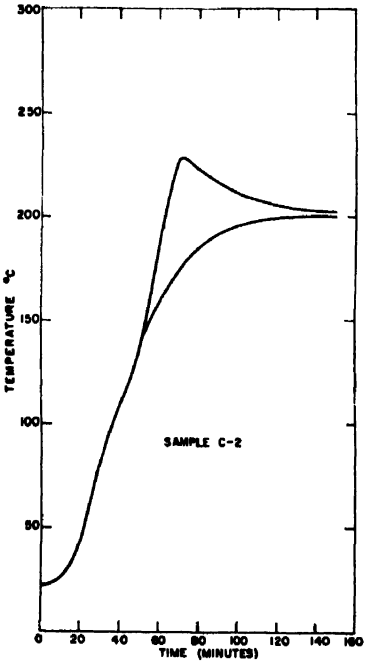

Figure 14. Time vs temperature plot of a graphite sample in a furnace held at 200°C: temperature of irradiation, 65°C

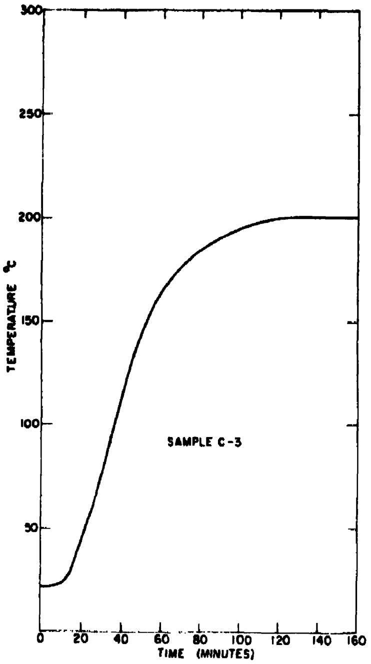

Figure 15. Time vs temperature plot of a graphite sample in a furnace held at 200°C: temperature of irradiation, 150°C

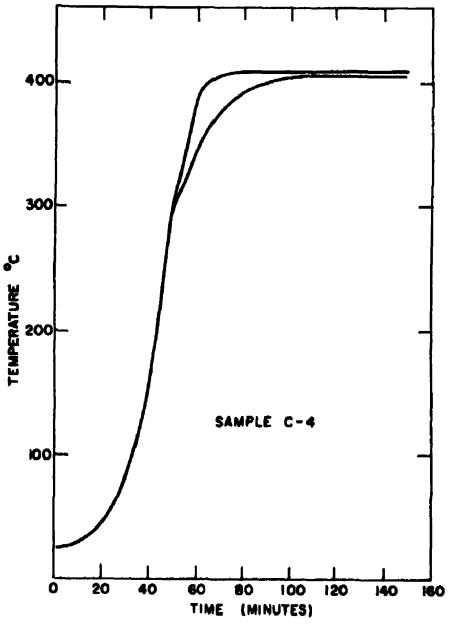

Figure 16. Time vs temperature plot of a graphite sample in a furnace held at 400°C temperature of irradiation, 65°C. Some of the stored energy of this sample was released in a furnace held at 200°C

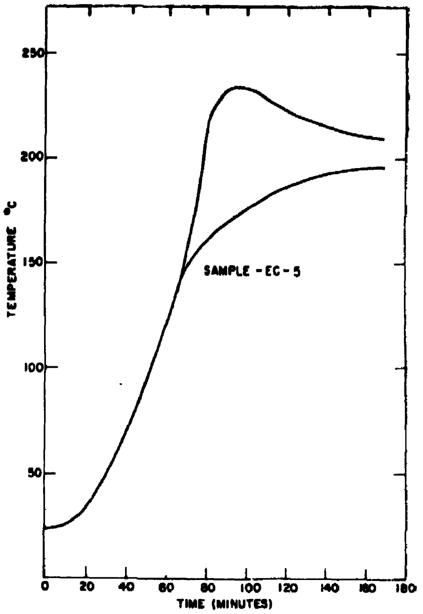

Figure 17. Time vs temperature plot of a graphite sample in a furnace held at 200°C: temperature of irradiation, 60°C

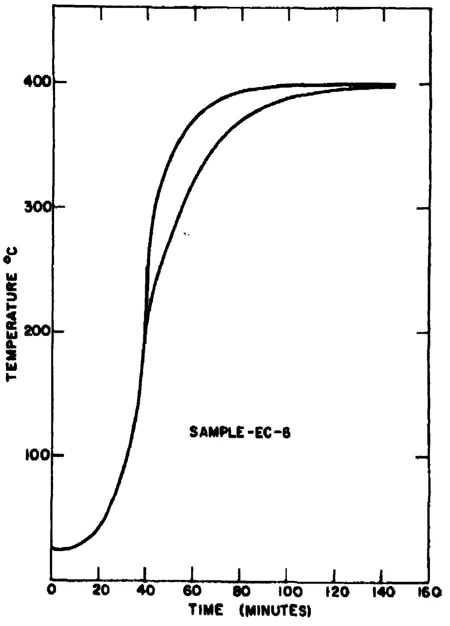

Figure 18. Time vs temperature plot of a graphite sample in a furnace held at 400°C temperature of irradiation, 60°C

Table III. *c*-Axis Growth

Sample number	*Average irradiation temperature °C*	*nvt* × *10*^{20}	*C-axis after irradiation (angstroms) °C*	*Per cent c-axis expansion* *
EC-4	50	1.18	6.821	1.8
EC-5	60	1.19	6.802	1.6
EC-7	130	1.20	6.735	0.54
EC-8	50	1.18	6.817	1.7
EC-9	60	1.19	6.802	1.5
EC-10	85	1.21	6.775	1.1
EC-11	130	1.20	6.753	0.81

* Calculation based on *c*-axis = 6.699 angstroms for non-irradiated graphite.

preciable annealing takes place, a typical growth curve, characterized by a steadily decreasing slope, is expected when defect concentration, or an associated change in physical property is plotted against integrated flux. Such curves have been published for various metals.[4,5] Thus, radiation effects are expected to approach a limiting value at any given temperature whenever annealing is important, and, since annealing is a thermally activated process, the amount of attainable damage will be a more sensitive function of the temperature of exposure than of the integrated flux.

According to the data presented, graphite exhibits a behavior which is quite similar to other crystalline materials and follows the above-outlined general pattern. Each physical property measured is briefly discussed below.

1. Stored Energy

Although the data, presented in Table I, are meager, it is obvious that the extent of damage, as determined by the stored energy measurement, is not linear with exposure (integrated flux). Rather, as pointed out above, the data suggest that the amount of stored energy is more dependent on the temperature of exposure than on the integrated flux at these levels of exposure. The fact that more energy is released on heating to 400°C shows that annealing is an activated process.

2. Physical Growth

Similar trends are shown by the physical growth data, of Table II. Expansion decreased with temperature of exposure, as shown in Fig. 19; again, in agreement with the ideas presented above.

3. *c*-axis Growth

c-axis, or crystallite expansion, parallels, in general, changes in gross physical dimension with one important difference. *c*-axis expansion is of the order of a factor of 9 larger than gross physical expansion over the range of exposures and temperatures covered in these experiments. Crystallite expansion is probably due to the presence of interstitial atoms since far larger strains are associated with these defects than with vacant lattice sites.[6,7] The difference between crystallite expansion and physical expansion is probably attributable to the porosity of graphite; i.e., there is considerable room for crystallite expansion without a correspondingly large change in the over-all dimensions of the specimen.

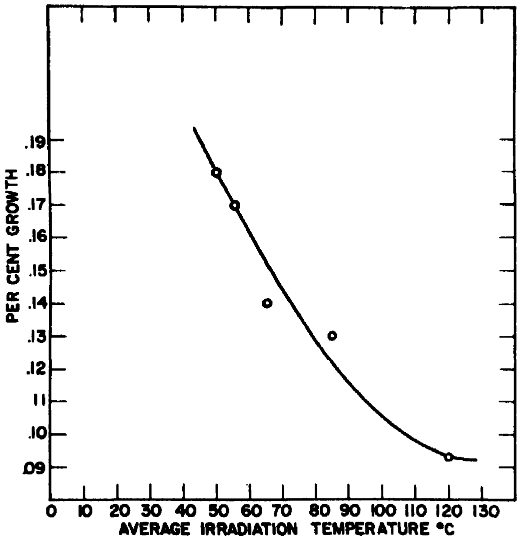

Figure 19. Per cent growth vs average irradiation temperature of graphite samples: integrated flux 1.2 × 10^{20} neutrons/cm^2

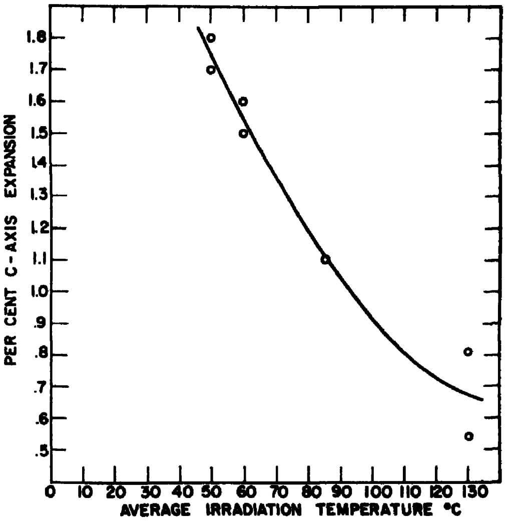

Figure 20. Per cent c-axis expansion vs average irradiation temperature of graphite samples: integrated flux 1.2 × 10^{20} neutrons/cm^2

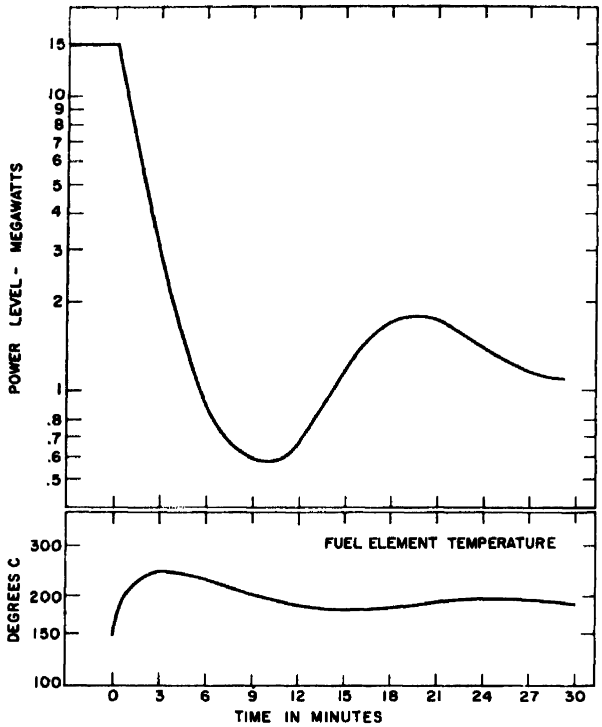

Figure 21. Behavior of reactor following a loss of coolant (with control rods locked out)

EXPERIMENT TO DETERMINE BEHAVIOR OF REACTOR UPON LOSS OF COOLANT

A controlled experiment was performed to determine the behavior of the reactor under the very improbable circumstance of having the control system fail at the same time the power supply to the coolant system fails. This set of conditions might permit the reactor to continue to operate after the flow of cooling air ceases. In order to do this experiment, all the safety trip circuits, which would tend to shutdown the reactor because of violation of safe operating conditions, were locked out.

Just prior to the experiment, the reactor had been operating routinely at a power level of about 26,000 kw in equilibrium with the xenon poison. The power level was reduced to 15,000 kw where equilibrium was again established, so that the temperature of the fuel elements dropped to 100°C below the routine operating temperature. At this point, the cooling fans were shut down manually. The control rods, of course, did not move. The metal temperature and the power level were then followed for a period of thirty minutes. A plot of these data appears as Fig. 21.

It is seen that the fuel element temperature rose abruptly and that the power level decreased rapidly. Obviously, the reactor went subcritical due to the combination of negative temperature and barometric coefficients. It is difficult to analyze these data quantitatively to determine how much each effect contributes to subcritical condition. The initial slope of the power level curve indicates a period of about 110 sec or a Δk of 26 inhours. The negative barometric pressure in the reactor due to the cooling fans is 90 mm Hg. If the pressure changed instantaneously by this amount, when the fans are turned off, the contribution from this source, alone, would be about 30 inhours. In contrast to this, an instantaneous rise of about 55°C in the average metal temperature would, by itself, account for the initial period. The temperature data, plotted in Fig. 21, are not actually the temperature of the uranium metal but the temperature of one of the fins on a fuel element. This must lag behind the actual metal temperature considerably in time at the beginning of the experiment. Hence, it must be left to intuitive judgment to assess the contributions from the two effects. Probably the greater contributions at the beginning come from the barometric effect. This underscores the wisdom of a process design for such reactors calling for a less-than-atmospheric operating pressure to insure this safety feature.

The cyclic behavior of the power and temperature data that followed is interesting and understandable in terms of the negative temperature coefficients which contribute alone during this part of the experiment.

SOME ASPECTS OF THE HISTORY OF THE OPERATIONS

Summarized in Table IV is a history of all the emergency shutdowns (ESD) which have occurred since the reactor was put into operation at high power levels after the initial investigative period. It is apparent from this analysis and record that changes and improvements in the instrumentation and control system design have significantly increased the reliability and stability of the operation.

Table V is a summary of the safety experience of the reactor operations prepared for US Atomic Energy Commission official files.

CONSTRUCTION COSTS

The construction costs of the Brookhaven reactor are useful only as an historical record, and cannot be used in any comparative manner. It must be recalled that the design and construction took place before the birth of even the small-scale reactor industry as it exists at this time. There was almost no experience upon which to rely so that the whole endeavor may only be represented to be a laboratory-scale research equipment project. Much of the material used in the construction was obtained from war surplus stocks and the designs were executed to accommodate these items. A number of components in the design were first attempts so that there were high development costs which would not appear in designs of the present, which make use of some of these same developments. In addition, a number of finished components had to be removed, reconstructed, and reinstalled in order to meet the operating specifications.

The construction costs on the reactor, the reactor building, and the air-cooling system, including the fan house with blowers, filters, air ducts, and air cooling equipment totaled about 16 million dollars. The control system alone totaled 1.5 million dollars, of which

Table IV. Emergency Shutdown History of the Brookhaven Reactor

	1951‡	*1952§*	*1953*	*1954¶*	*1955*	*Total*
Personnel mistakes						
Error in operating procedure*	4	3	3	4		14
Error in judgment*				1		1
Inattention while near trip points†	9		1			10
Accidental pushing of ESD button*	2	1				3
Short circuit*				1		1
Equipment failure						
Fluctuation or loss of commercial power*	3	6	5	3	1	18
Fluctuation or loss of ac instr. power*	3	4	3	1		11
Fluctuation or loss of dc instr. power*						0
Failure of air compressor*		1				1
Failure of blower motor†		1		1		2
Instability or inaccuracy of instr.*		1		2		3
Instability or inaccuracy of trip point*	16					16
Vacuum tube failure*	2					1
Contact failure*		2	2			4
Short circuit*		2	1	1		4
Leakage of oil or air*		1	1			2
Failure of test equipment*				1		1
Loss of fixed poisons†	1					1
All causes—totals each year	38	23	17	14	1	93

* ESD during permissible process conditions.

† ESD during prohibited process conditions.

‡ Time at which High Level Trips were improved.

§ Time when protective guards were installed over ESD buttons.

¶ Time when ESD circuits were made self-resetting on occasions of false signals.

Table V. Safety Experience of the Brookhaven Reactor Operations

United States Atomic Energy Commission Safety Experience—Reactors and Critical Facilities to December 31, 1954

1. Designation of reactor or facility—BNL 2. Location—Upton, New York Date—March 18, 1955
3. Type (critical, research, production, power)—Research 4. Design power (kw heat)—28,000
5. Brief description of reactor or facility and associated control and safety equipment—Graphite-moderated, air-cooled, normal uranium heterogeneous fueled; moderator—25 ft cube; 8 inch lattice; 55 tons fuel; 16 horizontal control rods (2 regulating, 14 shim) individually powered; 4 boron shot wells and liquid trichlorobenzene system; maximum flux 5 × 10^{12} n/cm^2-sec; manual startup; automatic power level regulation.

	*Aug.-Dec. 1950**	*1951†*	*1952*	*1953*	*1954*
6. Time operated					
kw hours	2.58 × 10^8	1.24 × 10^8	1.67 × 10^8	1.80 × 10^8	1.86 × 10^8
total operating hours	918	6717	7688	7401	7691
time approaching critical		0.25 per cent	0.25 per cent	0.25 per cent	0.25 per cent
time, critical to full power	—	1 per cent	1 per cent	1 per cent	1 per cent
7. Average number of persons—(operators, research staff, and others in reactor building during operations)	120	130	140	150	150
8. Accidents involving over-exposure of persons or radioactive contamination of property as defined in AEC Manual, Sec. 0502, Par. 031a-1(e):					
on-site—	0	0	0	0	0
off-site—	0	0	0	0	0
9. Other accidents involving property damage—in excess of $5000 per accident—	0	0	0	0	0
10. Number of startups—	50 (?)	283‡	160	83	54
11. Number of scrams—	5	72	21	22	15
Due to personnel failures:					
Inattention—	0	17	3	5	4
Accidental activation of controls—	2	4	1	0	0
Other	0	0	0	1	0
Due to equipment failures:					
Fluctuation or loss of power supply—	0	6	9	8	4
Electrical failures—	3	41	6	4	4
Mechanical failures—	0	3	1	2	2
Other	0	1	1	2	1

* Time devoted mainly to critical loading, full loading, and startup experiments.

† Operation limited to 10,000 kw during early part of year.

‡ Mainly due to startup experiments.

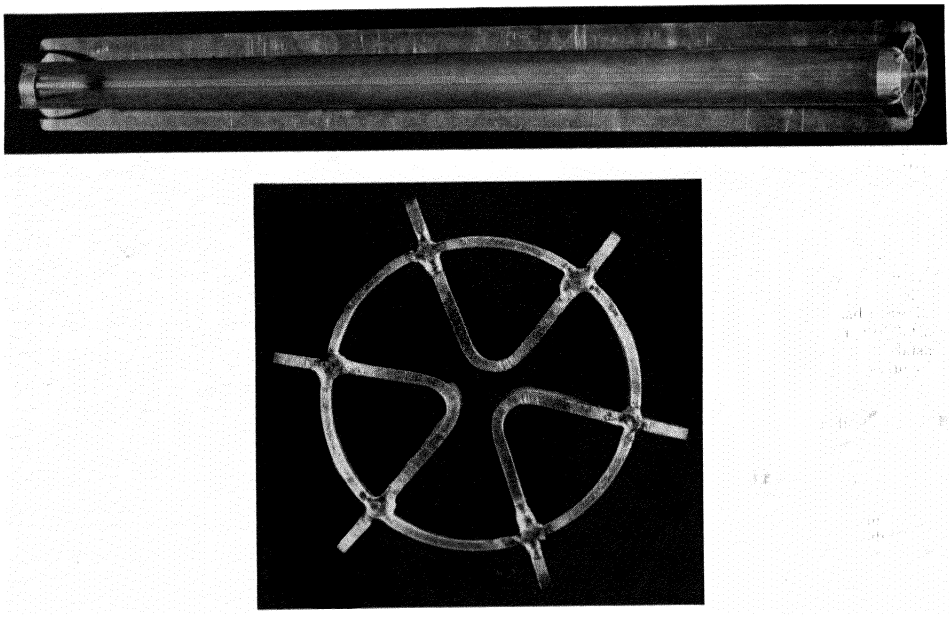

Figure 22. Design and assembly of fuel element to be used in the reloading of the Brookhaven reactor with enriched U^{235}

more than half were development costs. The shield costs added up to another 1.5 million dollars, with high development costs and unnecessarily high fabrication costs due to the use of surplus materials. Included in the shield costs are those of many special features required by the built-in experimental facilities. The graphite machining and erection costs, exclusive of the cost of the graphite, totaled 1.6 million dollars due to the complexity of the structure required by the installed experimental equipment. The air cooling system came to 3.8 million dollars and included high development costs on the bidirectional flow pattern, special blowers and filters, and some reconstruction costs. The leak detection system totaled 0.5 million dollars with high development costs. The fuel element costs of 0.3 million dollars included high development costs, but did not include the cost of the uranium metal. All the special experimental facilities, elevators, air conditioning, and other special features totaled about 1 million dollars.

PLANS FOR REFUELING THE REACTOR

A development and testing program has been in progress for about one year now, with the objective of converting the fuel from the present normal uranium to highly enriched U^{235}. Theoretical studies indicate that about fifty kilograms of U^{235}, distributed over approximately the same number of fuel channels as at present, will serve to increase the maximum central thermal neutron flux from its present level of 5×10^{12}/cm²/sec to about 3×10^{13}/cm²/sec. The power level for this higher flux is calculated to be 20 megawatts instead of the present 30 megawatts.

The fuel elements under development are fabricated from MTR type fuel plates. Each plate will be 2.25 inches wide by 24 inches long by 0.060 to 0.080 inch thick, and will contain only 3 to 4 grams of U^{235} imbedded in an aluminum matrix and clad with aluminum. These plates are bent along the axis of the long dimension into a 60 degree angle. Three such bent plates are then held together at each end by welds to a thin ring (see Fig. 22). There will be eight assembled fuel elements in each fuel channel of the loading and about 5000 will be required. These new fuel elements will provide much less impedance to the flow of air through the fuel channels than do the present elements and the pumping power required to drive the cooling air through the reactor will be greatly reduced. It is anticipated that the pumping power will be only 1000 kilowatts in contrast with the present demand of 5000 kilowatts.

Although the MTR type fuel plates have never been operated in other than a water-coolant medium at low temperatures, the tests, so far, indicate that they can be used with air cooling at much higher temperatures with the expectation of good service life and high burnout of the contained U^{235}. Failures which lead to the escape of fission products are expected to be much less frequent than with the solid rod, natural uranium fuel elements. In fact, the whole operation of the Brookhaven reactor will be much simpler when the reloading has been accomplished.

The change of fuel will have a marked effect on all the neutron physics aspects of the reactor. This is due to the removal of the U^{238} which represents a very great poison in the core. The neutron generation time, at the present time about 1.5 milliseconds, will be about 6 milliseconds. This means that every poison will have a larger reactivity effect than now, and that the response to excess reactivity will be more sluggish. The control rods will represent about 14.8 per cent in excess reactivity in contrast with the 4.3 per cent with the present loading. It should also be stated that the shield will require no modifications to take care of the increased flux.

ACKNOWLEDGEMENTS

References to other material on the details of design and construction of the Brookhaven reactor appearing in the proceedings of the conference include:

A. The theory and reactor physics design is treated in P/606 by I. Kaplan *et al.*, Session 21A, Volume 5, these Proceedings.

B. The technology and fabrication of the fuel elements is described in P/828 by D. H. Gurinsky *et al.*, Session 18B.2, Volume 9, these Proceedings.

C. The variation of effluent concentrations from an elevated stack is the subject of P/567 by M. E. Smith, Session 23B.3, Volume 9, these Proceedings.

REFERENCES

1. Seitz, F., Discussions of the Faraday Society, *5*, 271 (1949).
2. An excellent historical review is given by Seitz, F., Phys. Today, *5*, No. 6, p. 6 (1952).
3. For general reviews, see: Slater, J. C., J. Appl. Phys. *22*, 237 (1951); Dienes, G. J., Ann. Rev. Nucl. Sci. *2*, 187–219 (1953).
4. Marx, Cooper, and Henderson, Phys. Rev. *88*, 106 (1952).
5. A. W. Overhouser, Phys. Rev. *90*, 393 (1953).
6. Dienes, G. J., Phys. Rev. *86*, 228 (1952); *87*, 666 (1952).
7. Chipman, Warren, and Dienes, J. Appl. Phys. *24*, 1251 (1953).

Design and Description of Water Boiler Reactors

By L. D. P. King,* USA

I. INTRODUCTION

It is the purpose of this paper to give a brief survey of the origin, design, and operating characteristics of water boiler type reactors. Through long usage the name "Water Boiler," in the reactor field, has become associated with small enriched homogeneous reactors. Basically the water boiler consists of a container filled with enriched uranium and water solution surrounded by a neutron reflector, a set of control rods to adjust the criticality, and usually a gas handling system.

The first need of a water boiler type assembly arose early in 1943 when it became necessary to know the critical-mass of homogeneous solutions of U^{235} in various concentrations and moderating media. The purpose of this assembly was not only to provide critical mass data but also to provide experience in the operation and control of an enriched chain reacting assembly. This unit soon became known as Lopo (low power) since it was operated at essentially zero power in order to simplify the overall design.

As a result of the successful operation and experience gained from Lopo, it seemed desirable to construct a power unit to be used as a strong neutron source for various experiments. This first power water boiler called Hypo (high power), was put into operation in December of 1944. After 14,000 kilowatt hours of operation it was decided to redesign this reactor in order to make it a more useful research tool.

The rebuilt reactor known as Supo has been used up to power levels of 45 kw with peak thermal fluxes of 3.7×10^{10} neutrons/cm^2/sec/kw. This model of the water boiler began operation in 1950 and is in use at the present time after about 200,000 kilowatt-hours of running time. This reactor has been found to be a very versatile and reliable research tool.

From the data accumulated on Supo, it appears that with some redesign this model of the water boiler can produce substantially higher flux levels. A more radical design proposal known as the Test Tube Reactor appears to have some promising features.

The Atomic Energy Research Department of North American Aviation Inc. has constructed two water boiler type reactors. A one-watt unit designated as WBNS (Water Boiler Neutron Source), went into operation in April, 1952. A 500-watt reactor was completed in November, 1953 as a neutron source for the Livermore Research Laboratory in California.

The North American Aviation group also has design proposals for two 50-kilowatt reactors; one is a general research unit which will be constructed for the Armour Research Institute at Chicago, the second is especially designed for medical research.

The North Carolina State College has had a 10-kilowatt water boiler in operation since September, 1953. This reactor is used in the university research program, especially for the training of students in reactor technology.

II. TESTED WATER BOILER DESIGNS

A. Zero Power Reactor, Lopo, Los Alamos, 1944

This reactor was really a critical assembly experiment using enriched uranyl sulphate solution in water. The zero power operating level was chosen after considering a power model in order to eliminate shielding requirements and minimize possible troubles which might arise in connection with radiation effects on the solution. These potential difficulties were concerned with holding uranium in solution, the gas evolution from decomposition products produced by the fission process, and the contamination of the solution by the fission products themselves.

The design of Lopo was based on the requirement that a minimum amount of uranium should be used. This necessitated the use of a good reflector and the use of materials throughout which had a minimum neutron absorption. It was also required that there be an accurate control of reactivity and the entire system be as simple as possible consistent with safety.

Uranyl sulphate was chosen in preference to uranyl nitrate since it has a lower neutron cross section and has a larger uranium solubility. Table I lists the components of the homogeneous mixture used in Lopo which soon became known as "soup."

Calculations indicated that beryllium oxide would make an excellent reflector and that a 1-ft diameter sphere would be the proper size to minimize the uranium requirements for a 7 per cent to 15 per cent enriched solution. Corrosion studies showed that stainless steel (type 347 18-8) would be a satisfactory material to contain the solution.

The schematic design of Lopo is shown in Fig. 1. Control of reactivity was accomplished by means of a 34-in. long cylinder of cadmium ¾ in. in diameter. The rod could be moved remotely in a vertical direc-

---

* Los Alamos Scientific Laboratory. Including work by Los Alamos Scientific Laboratory Water Boiler Groups; Harold M. Busey, Los Alamos Scientific Laboratory; R. Philip Hammond, Los Alamos Scientific Laboratory; Atomic Energy Research Department of North American Aviation; Nuclear Reactor Project at North Carolina State College; Paul R. Kasten, Oak Ridge National Laboratory.

Table I. Lopo Solution Composition

Element	*Grams*	*Moles*	*σ_a barns per atom*
U^{235}	580	2.47	640
U^{238}	3378	14.19	12.1
S	534	16.66	0.45
O	14,068	880.4	0.0009
H	1573	1561	0.31
Stainless steel (sphere and re-entrant tube)	1100	20	—

$UO_2SO_4 \cdot 2\frac{1}{2}H_2O + H_2O$ = 15 liters
Density 1.348 at 39°C
U^{235} concentration 14.67 per cent

tion and set to within 0.5 thousandth of an inch. An additional cadmium rod was used as a shutdown safety. In order to eliminate temperature effects the entire apparatus was enclosed in a thermostated enclosure.

The solution could be dropped into a subcritical geometry below the sphere when not in use. Numerous safety features were incorporated in the design of the solution handling system, shown in Fig. 2, so as to eliminate accidental loss of solution.

Since this was the first chain reaction with enriched material, many precautions were taken while approaching the critical condition. Five independent neutron detectors placed in different positions were used to determine the multiplication of a 200-millicurie radium beryllium source placed at the center of the sphere. A zero or no multiplication reading was obtained by filling the sphere with distilled water. Fig. 3 illustrates how far in advance the critical mass can be estimated by a judicious placing of the detectors and source. The abscissa are normalized reciprocal counting rates.

Reactivity was increased by first removing solution, then adding and thoroughly mixing some more concentrated solution to the conical pan. The new soup was then raised each time to a definite level in the pipe above the sphere. The critical mass with 14 per cent enriched uranium, for the geometry used, was found to be 565.5 grams of U^{235} at 39°C.

Several measurements were made to better understand the operating behavior of Lopo.

1. The control rod calibration was determined by comparing rod position with known additions of U^{235}. The entire rod was equivalent to 11.3 grams of U^{235} which was later determined to be $6.2 \times 10^{-3} \Delta k/k$.

2. The absolute criticality of the system or the relation between Δk and ΔM is of primary interest. (k is the reproduction constant and M the total mass of uranium in the system.) For very small changes these quantities can be considered proportional. This proportionality constant was determined by measuring the effect on control rod position when a liquid-filled plastic bubble was moved within the sphere. The bubble was filled with a boron solution of equivalent nuclear properties except for the absence of a fissionable material. The absolute criticality was determined as $5.48 \times 10^{-4} \Delta k/k$ per gram of U^{235}.

3. The temperature coefficient at 39°C was determined as 0.55 grams U^{235}/°C or a $\Delta k/k$ of 6.2×10^{-3} per degree centigrade, by varying the temperature of the entire reactor system and observing the effect on the control rod position.

4. The effective fraction of delayed neutrons (γf) and the mean prompt neutron lifetime (τ_p) were determined by a special experiment. A cadmium absorber connected to a crank on an electric motor was jerked in and out of the reflector at such a repetition-rate that the delayed neutron intensity had no time to decay but merely produced a steady background, while the fast neutrons were able to follow the fluctuations. From an absolute calibration of the reactivity effect of the cadmium for all crank positions and from

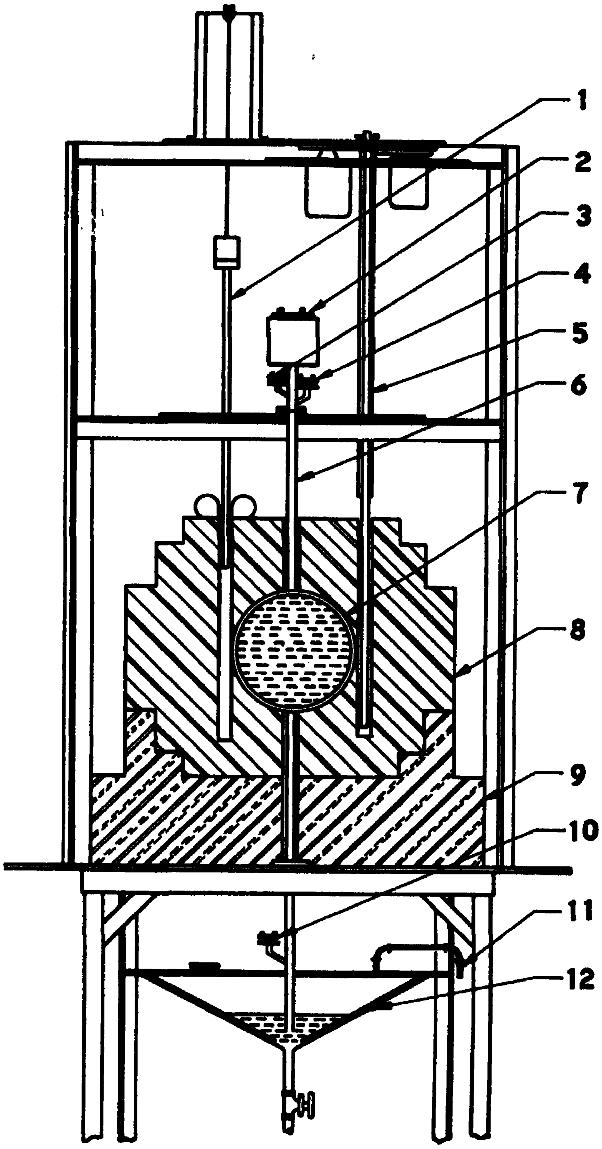

Figure 1. Cross section, LOPO: (1) Cd safety curtain; (2) overflow; (3) safety electrode; (4) level electrode; (5) Cd control rod; (6) upper pipe; (7) stainless steel sphere containing enriched uranyl sulfate (UO_2SO_4); (8) BeO reflector; (9) graphite reflector; (10) level electrode; (11) air pipe; (12) dump basin

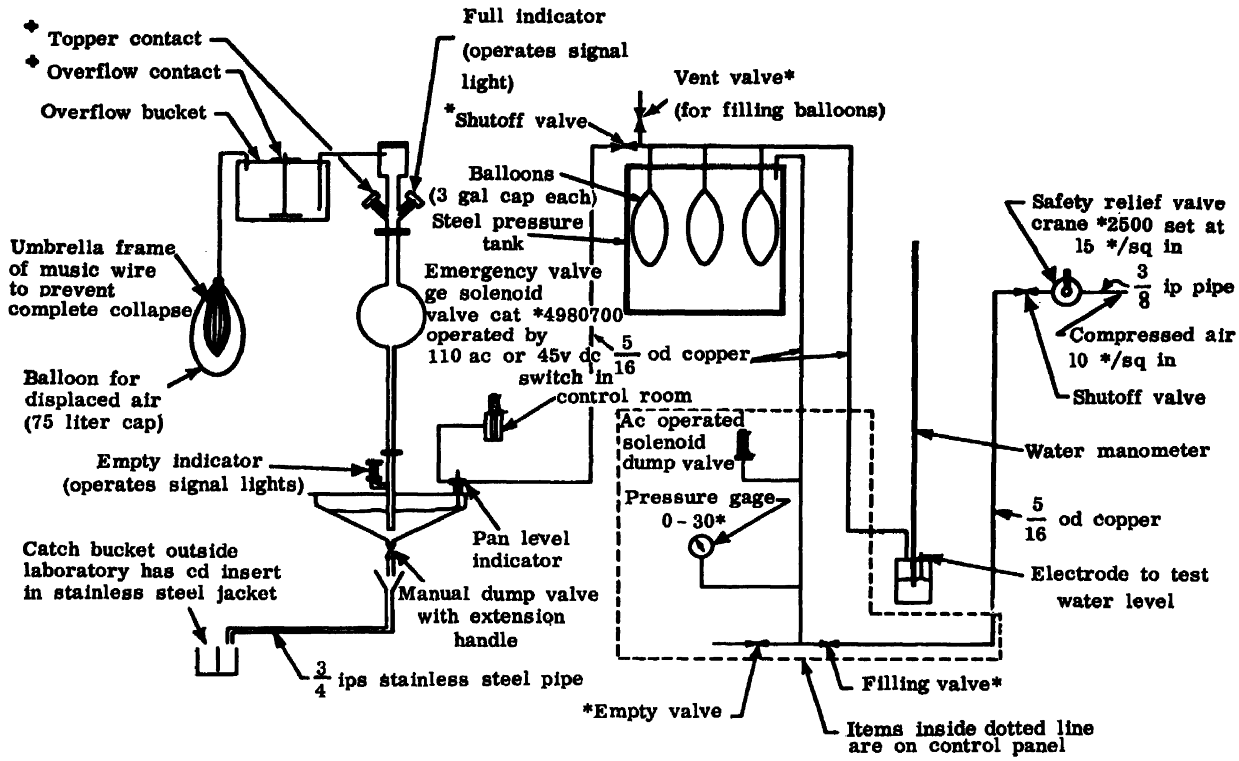
✦ Topper contact
✦ Overflow contact
Overflow bucket
Full indicator (operates signal light)
*Shutoff valve
Vent valve* (for filling balloons)
Balloons (3 gal cap each)
Steel pressure tank
Umbrella frame of music wire to prevent complete collapse
Emergency valve ge solenoid valve cat *4980700 operated by 110 ac or 45v dc switch in control room
5/16 od copper
Balloon for displaced air (75 liter cap)
Safety relief valve crane *2500 set at 15 */sq in
3/8 ip pipe
Compressed air 10 */sq in
Shutoff valve
Water manometer
Ac operated solenoid dump valve†
Empty indicator (operates signal lights)
Pressure gage 0-30*
Pan level indicator
5/16 od copper
Electrode to test water level
Catch bucket outside laboratory has cd insert in stainless steel jacket
Manual dump valve with extension handle
3/4 ips stainless steel pipe
Filling valve*
*Empty valve
Items inside dotted line are on control panel

Figure 2. LOPO solution system. Fluid handling system: note, * = hoke needle valve; † = opens solenoid dump valve automatically; electrical connections not shown

the measurements of the counting rates of the gated counters at various phase angles, the value of γ/f was determined as 0.0086. For high crank velocities the prompt neutron lifetime can be determined by the phase lag between the counting rates and the absorber position. A value of 135 ± 20 microseconds was determined.

5. The theoretical relation between excess reactivity (Δk) and reactor period (T) is given by the equation

$$\Delta k/k = \tau_p/T + \sigma_f \sum_i \frac{q_i \tau_i}{T + \tau_i}$$

where the q_i and τ_i are the respective amplitudes and periods of the delayed neutron fractions relative to the total number f. Substituting experimental values for Lopo and the known delayed neutron periods gave

$$\Delta k/k = \left[\frac{135}{T} + \frac{626}{T + 0.62} + \frac{6287}{T + 2.2} + \frac{62{,}600}{T + 31.7} + \frac{24.420}{T + 80.2}\right] \times 10^{-6}$$

This equation correctly predicted the periods of the reactor for known excess reactivity values.

6. Short time fluctuations of the neutron intensity when Lopo was run at critical, were studied by means of a fast recording counter and by a circuit which permitted adjusting counting gate widths and times between gates. These variations were found to be much larger than for an ordinary Poisson fluctuation.

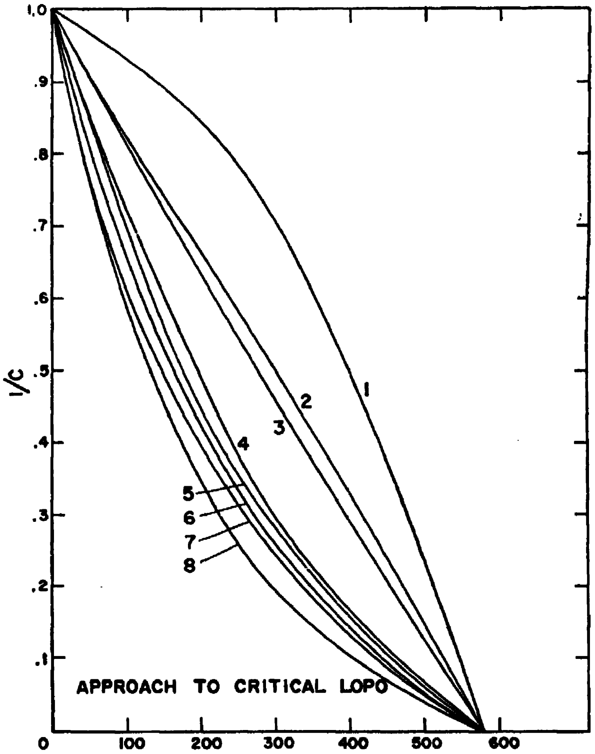

Figure 3. Grams U^{235} in sphere: (1) Mn foils at sphere center; (2) U^{235} chamber 3 in. from center; (3) Mn foils at node of 3rd harmonic; (4) BF_3 + Cd + Ch_2 outside reflector, BF_3 + Cd outside reflector; (5) U^{238} chamber against outer sphere surface; (6) BF_3 chamber outside reflector; and (7) In foils 3 in. from sphere surface; (8) In + Cd foils 3 in. from sphere surface

Table II

Material	*Size of reflector*	*Critical mass, grams U^{235}*
BeO	3 ft mock sphere	572 ± 2
BeO-graphite	2 ft BeO cube surrounded by 1½ ft of graphite shell	573 ± 2
Graphite-BeO	18-in. graphite cube surrounded by 1 ft of BeO shell	735 ± 10
Graphite-tuballoy slugs	4 ft cube of graphite and 20 slugs of tuballoy 2½ in. diameter, 2¼ in. long placed 12 cm from edge of sphere	740 ± 10
Graphite	4 ft cube graphite	760 ± 10
H_2O-tuballoy slugs	5 ft diameter cylinder, 5 ft high with 63 tuballoy discs 2¼ in. × 2½ in. spaced equally on a spherical surface 20 cm in radius	1100*
H_2O	5 ft cylinder, 5 ft high	1200*

* Extrapolation estimates.

7. Neutron distribution measurements taken in the sphere and reflector were found to check theoretical predictions.

8. Tests were made on several reflector materials to compare their relative effectiveness. The results are shown in Table II.

B. Power Water Boiler, Hypo, Los Alamos, 1944–1949

The construction of this reactor was based on the satisfactory operation of Lopo and the fact that such a reactor due to its small size can produce strong neutron fluxes at moderate power. An operating level of one kilowatt was originally chosen because: (1) the cooling requirements were simple; (2) bubbling or frothing due to gas evolution from the solution decomposition products was not expected to be serious; (3) not much additional enriched material was required and; (4) neutron fluxes of the order of 5 × 10^{10} were expected.

The general design was influenced by that of the low power experiment. The principle modification consisted in eliminating the hydrostatic control and poor geometry storage system, a precaution which no longer seemed necessary after the experience gained in the operation of Lopo. The new design features for increased power operation were numerous: (1) a change of solution from uranyl sulphate to uranyl nitrate since an extraction method for the removal of fission products was known only for the latter at that time; (2) installation of additional control rods for greater operational flexibility; (3) introduction of a horizontal one-in. pipe or "glory hole" through the sphere to permit access to the highest neutron flux; (4) addition of a water cooling and an air flushing system; (5) construction of a gamma ray and neutron shield; (6) the addition of a graphite thermalizing column; (7) the use of a 1/16-in. thick stainless steel sphere instead of the 1/32-in. thickness used in Lopo to provide for the possibility of a greater corrosion rate when operating at higher fluxes and temperatures.

A simplified section through Hypo is shown in Fig. 4. The numbers in this figure point out the following components: (1) one-foot diameter core sphere, (2) thin walled stainless steel safety drip pan around beryllium oxide, (3) secondary solution catcher at base of graphite, (4) heat exchanger, (5) "glory hole" irradiation port through core, (6) removable graphite sections for experimental work.

Figure 5 shows details of the sphere assembly. After initial operation it was found that the 157 inches long cooling coil shown would permit operation at 5.5 kilowatts without exceeding the normal operating temperature of 85°C. This was somewhat higher than expected and indicated that the bubbles formed during operation did not decrease the effective heat exchanger surface area. As shown in Fig. 5, the solution level was maintained several centimeters below the top of the sphere in order to provide a space for solution expansion and a larger surface area for the release of gas bubbles. Because of the explosive nature of the hydrogen and oxygen mixture released by radiolysis and the highly concentrated radioactive gases produced in the solution, a means of diluting and flushing-out these gases was required. Approximately 50 cm³/sec of filtered air was admitted through the level indicator tube and discharged to a stack.

An adjustable contact type level indicator was required to determine the solution level. A fixed bubble tube served as a solution addition tube and an absolute level indicator. Initially only distilled water was added to replace the decomposition products; but after several hundred kilowatt hours of operation it was observed that the reactivity of the solution had increased considerably. Chemical analysis of the solution indicated a 30 per cent deficit in the original nitrogen content. The uranyl nitrate was apparently gradually being converted into basic nitrate and the free nitrate carried off in the flushing air. At this time it seemed desirable to remove the large drain tube shown in Fig. 4 and replace it with a small tube running to the top of the reactor. A rapid dump tube did not seem necessary. The removal of this pipe eliminated a possible trap for precipitation products and the new ¼-in. od. tube made it possible to make additions to the solution during reactor operation. These were made about every 35 kw-hr of operation in the ratio of water to acid of 1.4:1. About 6 cm³ of water plus acid were required per kw-hr of operation.

The reactivity was controlled by 3 vertical cadmium rods. Two of these had continuous selsyn position control and one had only an in or out position. These rods are outside and tangential to the sphere surface

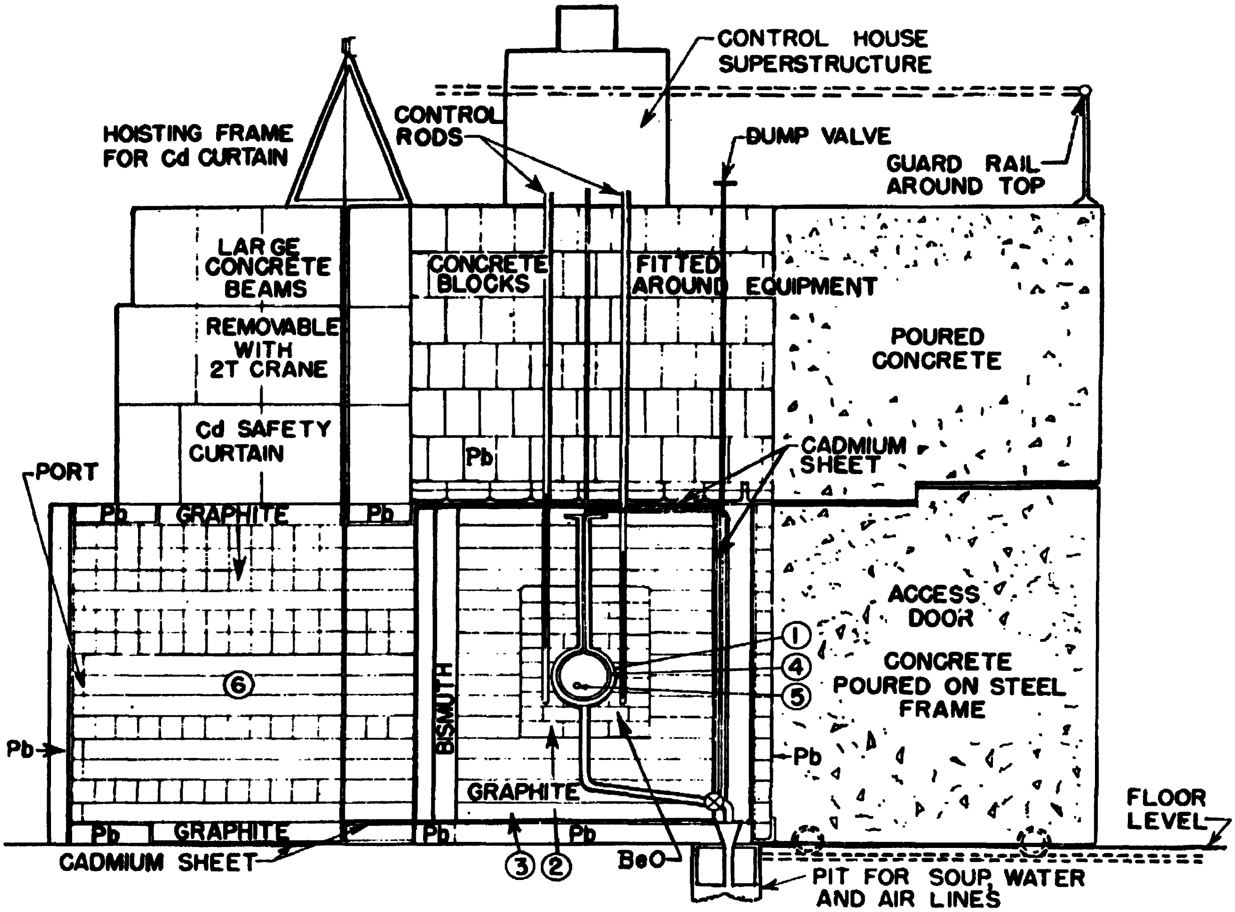

Figure 4. Hypo

as shown in Fig. 4. Cadmium sheet 3 in. wide by 30 in. long is contained in the lower portion by an aluminum frame. An automatic control unit attached to one of the rods was used to eliminate small drifts in neutron intensity due to convection and currents and bubble formation in the core.

Approach to critical was done in a manner similar to that used in Lopo. Since rather good estimates of the critical mass could be made beforehand, a considerable amount of U^{235} could be added initially. The solution composition for Hypo is shown in Table III. The critical mass was found to be 808 grams of U^{235}. The normal operating mass was 870 grams U^{235}. This additional material was required in order to have sufficient Δk to override the negative temperature coefficient of $2.6 \times 10^{-4} \Delta k/k$ per °C and have some excess k for experimental purposes. The absolute calibration of the reactor was determined to be approximately $2 \times 10^{-4} \Delta k/k$ per °C.

The thermal flux at the center of the "glory hole" was measured with small calibrated Mn foils. It was found to be 5×10^{10} neutrons/cm²/sec/kw.

Table III. Hypo Solution Composition

Element	*Grams*	*Moles*	*σ_a barns per atom*
U^{235}	869.6	3.7	640
U^{238}	5341	22.44	12.1
N	731	52.2	1.75
O	13,780	860	0.0009
H	1312	1302	0.31
Stainless steel sphere and cooling coil	3000	55	—

$UO_2(NO_3)_2 \cdot 6H_2O + H_2O$ = 13.65 liters
Density = 1.615
U^{235} concentration 14.5%

The radioactive fission-product gases produced in Hypo were blown by a stream of air through a long tube whose axis was a negatively charged wire. The various gases deposited their solid radioactive daughters upon the wire in a manner proportional to their half-lives. By cutting the wire into sections and analyzing each one for several fission products the fraction of the fission product chains swept out of the water boiler during normal operation was determined. These values are shown in Table IV.

C. High Flux Water Boiler, Supo, Los Alamos, 1950–1955

This model of the water boiler resulted from rather extensive changes in the Hypo model. Higher neutron fluxes were desirable as well as more research facilities.

The modifications were made in two parts. The first phase, begun in April, 1949 and completed in February, 1950, improved the experimental facilities

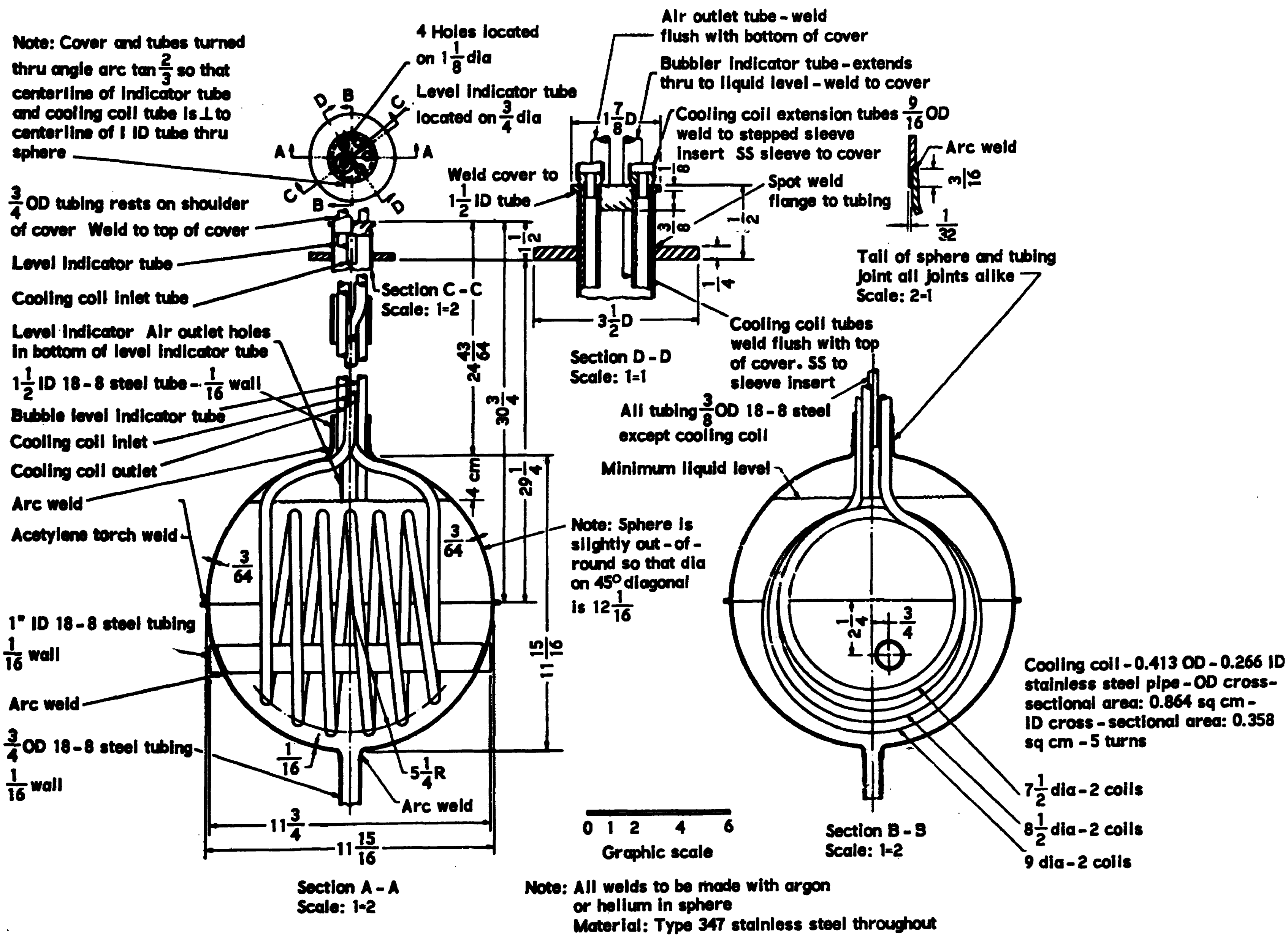
Note: Cover and tubes turned thru angle arc tan $\frac{2}{3}$ so that centerline of indicator tube and cooling coil tube is ⊥ to centerline of 1 ID tube thru sphere
4 Holes located on $1\frac{1}{8}$ dia
Level indicator tube located on $\frac{3}{4}$ dia
A
B
C
D
$\frac{3}{4}$ OD tubing rests on shoulder of cover Weld to top of cover
Level indicator tube
Cooling coil inlet tube
Section C - C Scale: 1=2
Level indicator Air outlet holes in bottom of level indicator tube
$1\frac{1}{2}$ ID 18-8 steel tube - $\frac{1}{16}$ wall
Bubble level indicator tube
Cooling coil inlet
Cooling coil outlet
Arc weld
Acetylene torch weld
1" ID 18-8 steel tubing $\frac{1}{16}$ wall
Arc weld
$\frac{3}{4}$ OD 18-8 steel tubing $\frac{1}{16}$ wall
$\frac{3}{64}$
$\frac{1}{16}$
$5\frac{1}{4}$R
Arc weld
$11\frac{3}{4}$
$11\frac{15}{16}$
Section A - A Scale: 1=2
$\frac{1}{2}$
$24\frac{43}{64}$
$30\frac{3}{4}$
4 cm
$29\frac{1}{4}$
$11\frac{15}{16}$
Note: Sphere is slightly out-of-round so that dia on 45° diagonal is $12\frac{1}{16}$
Weld cover to $1\frac{1}{2}$ ID tube
Air outlet tube - weld flush with bottom of cover
Bubbler indicator tube - extends thru to liquid level - weld to cover
$1\frac{7}{8}$D
Cooling coil extension tubes $\frac{9}{16}$ OD weld to stepped sleeve insert SS sleeve to cover
$\frac{1}{8}$
$\frac{3}{8}$
$\frac{1}{2}$
$\frac{1}{4}$
Spot weld flange to tubing
$3\frac{1}{2}$D
Section D - D Scale: 1=1
Cooling coil tubes weld flush with top of cover. SS to sleeve insert
All tubing $\frac{3}{8}$ OD 18-8 steel except cooling coil
Arc weld
$\frac{3}{16}$
$\frac{1}{32}$
Tail of sphere and tubing joint all joints alike Scale: 2=1
Minimum liquid level
$2\frac{1}{4}$
$\frac{3}{4}$
Cooling coil - 0.413 OD - 0.266 ID stainless steel pipe - OD cross-sectional area: 0.864 sq cm - ID cross-sectional area: 0.358 sq cm - 5 turns
$7\frac{1}{2}$ dia - 2 coils
$8\frac{1}{2}$ dia - 2 coils
9 dia - 2 coils
Section B - B Scale: 1=2
0 1 2 4 6
Graphic scale
Note: All welds to be made with argon or helium in sphere
Material: Type 347 stainless steel throughout

Figure 5. Hypo sphere assembly

Table IV. Estimated Fractions of Fission-Product Chains Swept Out of Water Boiler During Normal Operation

			Per cent swept out						
Mass no.	*Fission gas*	*Important solid members of chain*	*>75%*	*50–75%*	*25–50%*	*10–25%*	*1–10%*	*<1%*	*<1%*
83	1.9 hr Kr		x						
85	4.6 hr Kr		x						
	~10 yr Kr		x						
87	75 min Kr	6.3×10^{10} yr Rb	x						
88	3 hr Kr	17.5 min Rb	x						
89	2.6 min Kr	15 min Rb							
		55 d Sr		x	x				
90	33 sec Kr	30 yr Sr							
		60 hr Y					x	x	
91	9 sec Kr	9.7 hr Sr							
		57 d Y						x	
(92)	3 sec Kr	2.7 hr Sr							
		3.5 hr Y							x
(94)	1.4 sec Kr	20 min Y							x
95	2 sec Kr	11 hr Y 35 d Cb							
		65 d Zr							x
97	Kr	17 hr Zr							
		75 min Cb							x
133	5.3 d Xe		x						
135	9.2 hr Xe	2×10^4 yr Cs	x						
	10 min Xe	2×10^4 yr Cs	x	x					
137	3.4 min Xe	35 yr Cs		x	x				
138	17 min Xe	33 min Cs	x						
139	41 sec Xe	85 min Ba					x		
140	16 sec Xe	12.8d Ba							
		40 hr La				x	x		
141	1.7 sec Xe	18 min Ba 28d Ce							
		3.5 hr La							x
143	1.3 sec Xe	33 hr Ce							
		13.8 d Pr							x
(144)	Xe	275d Ce							
		17 min Pr							x
(145)	1 sec Xe	1.8 hr Ce							
		4.5 hr Pr							x

and increased the neutron flux. The second phase, begun in October, 1950 and completed in March, 1951, increased the thermal neutron irradiation facilities, improved the reactor operation, and removed the explosive hazard in the exhaust gases.

The first group of alterations consisted of the following:

(1) The space around the reactor was increased by enlarging the building so that experiments could be carried out on all four sides instead of on only two.

(2) The construction of a second thermal column was made possible by eliminating a removable portion of the reactor shield. This made available a neutron beam and irradiation facilities on a previously unused face of the reactor.

(3) The entire spherical core assembly was replaced:

(*a*) Three 20-foot long, $\frac{1}{4}$-in. O.D., 0.035-in. wall stainless steel tubes replaced the former single cooling coil. This increased the operating power level from 5.5 kw to a maximum of 45 kw. A factor of three higher heat transfer coefficient than predicted by theory is believed to be primarily due to fluid agitation from radiolytic-gas-bubble evolution.

(*b*) A new removable level indicator and exit gas unit was installed in the sphere stack tube. The stack tube itself was made more accessible for future modifications.

(*c*) External joints were not welded, but unions or flare fittings were used to simplify the removal of the sphere or permit pipe replacements.

(*d*) An additional experimental hole was run completely through the reactor tangent to the sphere. This $1\frac{7}{16}$-in. id tube supplements the 1-in. id "glory hole" running through the sphere.

(4) The beryllium portion of the reflector was replaced by graphite. The all-graphite reflector gives a more rapid and complete shutdown of the reactor and eliminates the variable starting source produced by the (γ,n) reaction on beryllium. A 200 millicurie RaBe source placed in the reflector is used as a start-up neutron source.

(5) Two additional vertical control rods were added which move into the sphere volume in reentrant thimbles. These consist of about 120 grams of sintered B^{10} in the form of $\frac{9}{16}$-in. rods about 18 inches long. These rods gave the additional control required by the change to an all-graphite reflector. Previously observed shadow effects were eliminated by the internal position of the rods and by the location of the control chambers under the reactor.

Table V. Effectiveness of Control Rod Materials*

Material	*Comments*	*Grams U^{235} equiv.*	*Est. % $\Delta k/k$*
Cadmium	0.015-in. cadmium 18 in. long wrapped on 0.595 od brass tube with $\frac{1}{16}$-in. wall. Inside length tube 17¾ in. Weight cadmium 71.7 gm; weight brass tube 183.3 gm.	~39	1.3
Cadmium	0.015-in. cadmium wrapped on ½-in. polystyrene rod.	~39	1.3
Cd + paraffin	Above brass tube filled with 46.5 grams of paraffin.	~26	.87
B_4C	Density of B_4C 1.33 weight B_4C hand tamped 73.3 grams.	~53.5	1.8
B_4C + Cd	Same cadmium sleeve as above.	~58	1.9
B^{10}	95.5% B^{10} material in above brass holder 68 grams B^{10}.	~68.5	2.3
B^{10}	Same as above.	~73.5	2.4
B^{10}	92.5 grams B^{10} tamped into brass holder as above but 18⅛ in. long inside.	~78.5	2.6
B^{10}	Sintered 95.5% B^{10} plugs 0.555 in. diameter overall length 17.9 in. B^{10} density 1.73; actual weight B^{10} 116.5 grams.	~80.2	2.67
B^{10} + Cd	Above stainless tube plated with about 0.003 mil cadmium*	~82.2	2.74

* These are actual rods in use.

(6) The reactor solution was changed from 15% U^{235} enriched uranyl nitrate to one of 88.7% enrichment. This makes possible the continued use of a low uranium concentration in the solution with the poorer all-graphite reflector. The gas evolution produced by nitric acid decomposition is greatly reduced, due to the lower total nitrogen content.

(7) The entire inner reactor shield was improved to permit higher power operation with a low neutron leakage and also to increase the neutron-to-gamma-ray intensity in the thermal columns. Cadmium was replaced by B_4C + paraffin and additional steel shielding was added.

Table V lists the observed effectiveness of various control rod materials which were tested in order to determine which material would be used for the internal rods of Supo.

After operating the reactor with the above modifications for about 10,000 kw-hr at a power of 30 kw the following (second group) alterations were made:

(1) The original south thermal column was completely rebuilt with improved shielding to provide many more irradiation facilities.

(2) A recombination system was constructed to handle the "off" gases from the reactor. The use of a closed circulating gas system with a catalyst chamber of platinized alumina removed any explosive hazard in the exhaust gases due to the presence of hydrogen and oxygen. The operating characteristics of the reactor have been greatly improved by returning directly back to the reactor as water all but a very small fraction of the gases produced.

(3) A shielded solution-handling system was constructed to simplify the handling of routine solution analysis and for the removal or change of the entire reactor solution.

Figures 6 and 7 are vertical cuts through the north-south central plane of the reactor. The reflector, two thermal columns and general type of shielding are shown. The two special transverse experimental holes can be seen. The location of the recombination system in the reactor shield is indicated.

Figure 8 is a schematic layout of the recombiner system. Gas produced in the reactor, primarily hydrogen and oxygen, is carried by the circulating air in the system first through a vertical condenser in the sphere stack. This condenser, which occupies the space previously used for the level indicator, removes most of the water and acid vapor, as well as solution spray. From here the air passes through a stainless steel wool trap to capture fission fragments and entrained uranium before entering the blower. The blower feeds the gas into one of two interchangeable catalyst chambers containing platinized alumina pellets. Here all the hydrogen and oxygen are recombined and the gas leaving the catalyst chamber contains the water vapor formed. A second condenser reduces the temperature of the gas leaving the catalyst chamber to about the same temperature as that of the gas leaving the first condenser. Any excess pressure produced in the circulating system can be bled into a 150-ft exhaust stack. The circulation rate (100 liters/minute) is such that the hydrogen concentration is kept below the detonation limit at all points of the system.

Figure 9 is a bottom and side view of the sphere, showing the internal parts. The three nesting cooling coils are arranged so that turns are separated by about 1 inch through the volume, except in the uppermost 5 cm where there is no solution. The re-entrant thimbles for the B^{10} control rods can be seen. The location of the "glory hole" in the final assembly is indicated.

Figure 10 shows the sphere assembly in position with the reflector partially constructed. The small tube out of the bottom is used for solution addition or removal and for routine sampling. This view is from the new thermal column cavity looking south.

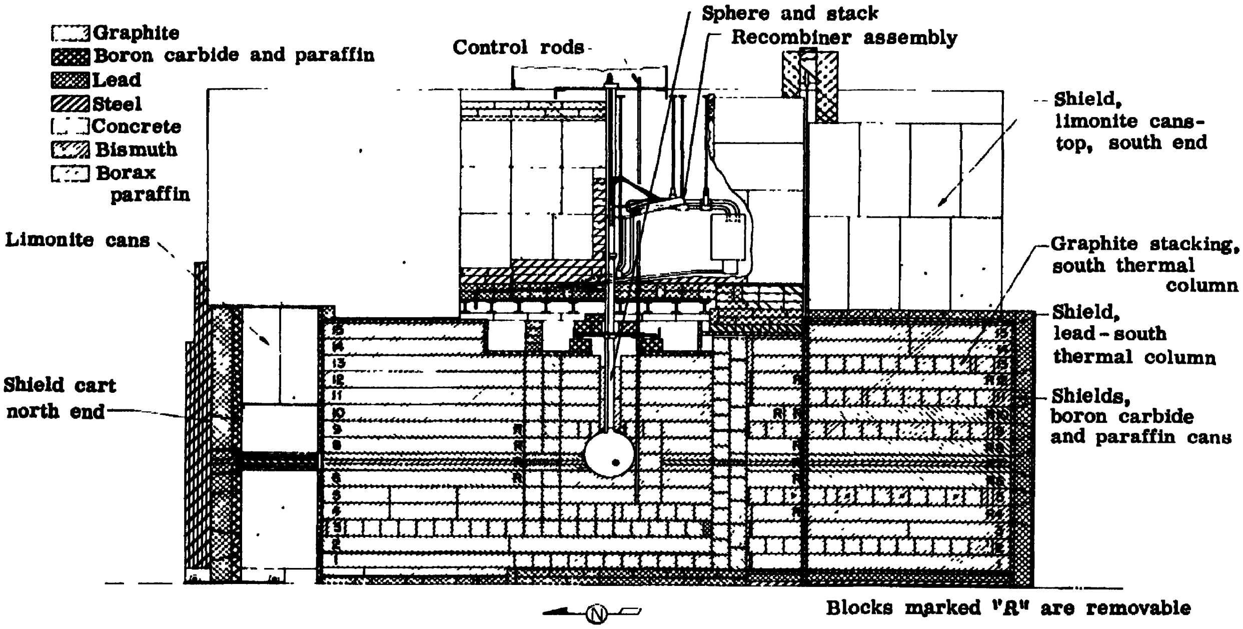
Graphite
Boron carbide and paraffin
Lead
Steel
Concrete
Bismuth
Borax paraffin
Control rods
Sphere and stack
Recombiner assembly
Shield, limonite cans-top, south end
Limonite cans
Graphite stacking, south thermal column
Shield, lead-south thermal column
Shield cart north end
Shields, boron carbide and paraffin cans
N
Blocks marked "R" are removable

Figure 6. North-south vertical section of water boiler (Supo model)

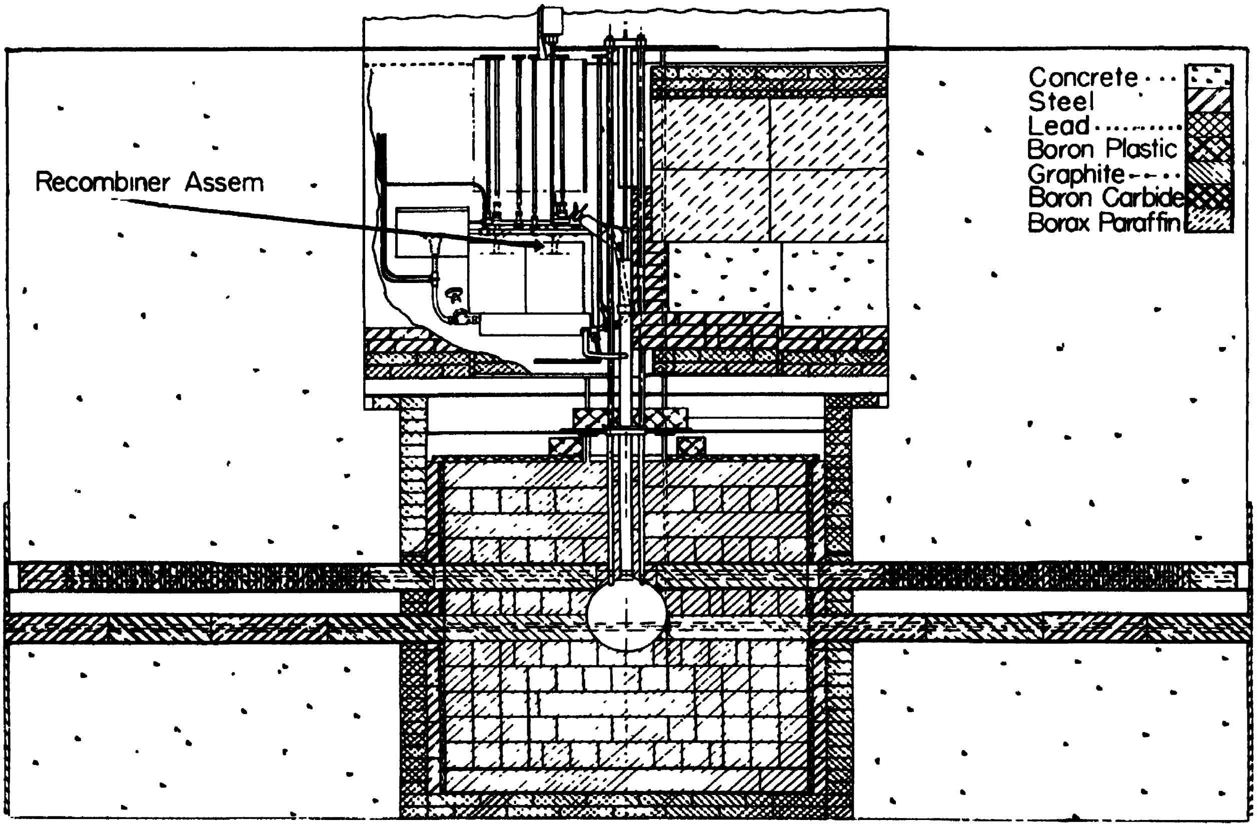

Figure 7. East-west vertical section of water boiler (Supo model)

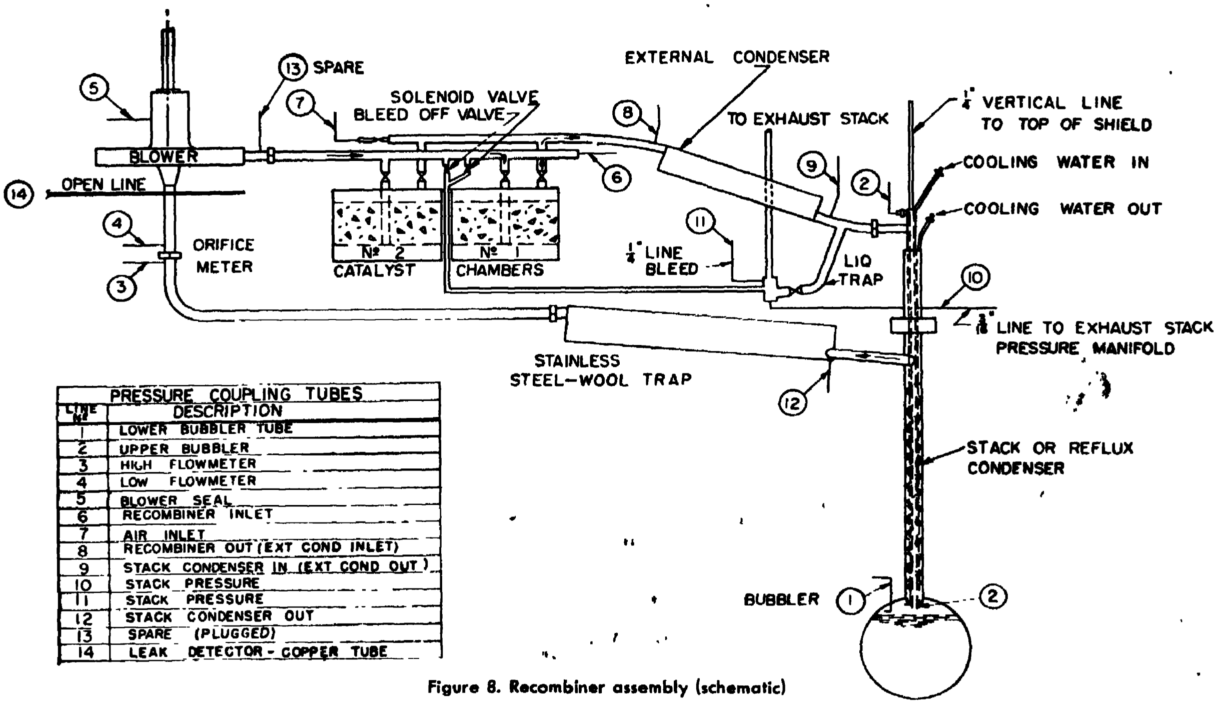

PRESSURE COUPLING TUBES	
LINE Nº	DESCRIPTION
1	LOWER BUBBLER TUBE
2	UPPER BUBBLER
3	HIGH FLOWMETER
4	LOW FLOWMETER
5	BLOWER SEAL
6	RECOMBINER INLET
7	AIR INLET
8	RECOMBINER OUT (EXT COND INLET)
9	STACK CONDENSER IN (EXT COND OUT)
10	STACK PRESSURE
11	STACK PRESSURE
12	STACK CONDENSER OUT
13	SPARE (PLUGGED)
14	LEAK DETECTOR - COPPER TUBE

Figure 8. Recombiner assembly (schematic)

The bismuth pier across the south thermal column is in the background, and a portion of the shield for the north column can be seen under construction in the foreground.

An exterior view of the reactor is shown in Fig. 11. This photograph is a general view of the south face showing the multiple irradiation ports into the south thermal column. The entire control mechanism is in the small rectangular structure shown on top of the reactor.

The peak thermal flux available in the "glory hole" is 3.7×10^{10} n/cm²/sec/kw. Figure 12 illustrates Hypo and Supo neutron distributions through the "glory hole." The curves in Fig. 13 compares the neutron fluxes and cadmium ratios existing in the

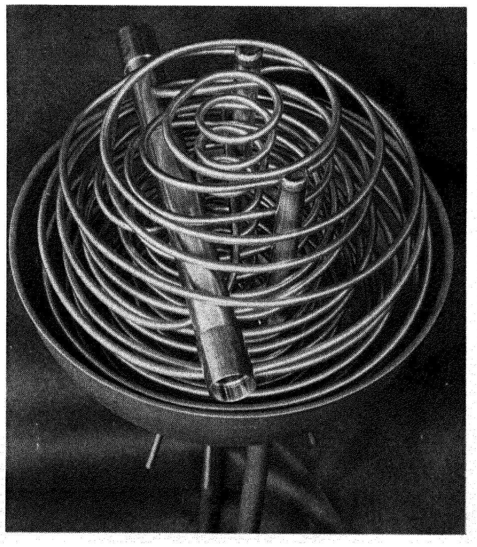

Figure 9. Supo sphere details

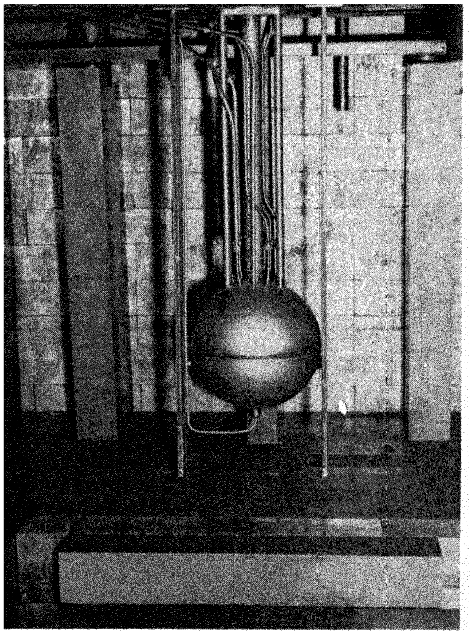

Figure 10. Supo core assembly

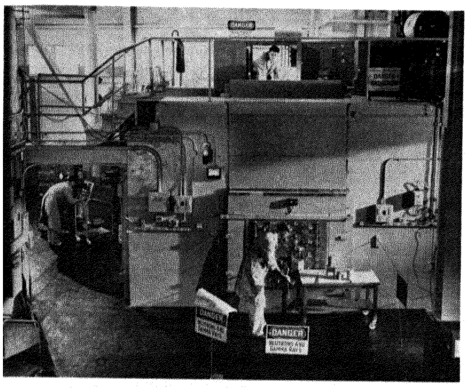

Figure 11. South face—Supo

"glory hole" and tangent hole. The curves in Fig. 14 shows the thermal fluxes and cadmium ratios existing in the north thermal column from the sphere face to the outer shield.

Nuclear plates have been used to measure the neutron spectra emerging from the sphere with energies over 1 Mev. These can be roughly approximated by a fission spectrum. Calculations made from fast beams emerging from the north thermal column give the following fast flux values above 1 Mev in units of n/cm²/sec/kw: (1) at the sphere surface 6.5×10^{10}, (2) at the bismuth column 1.5×10^9 and

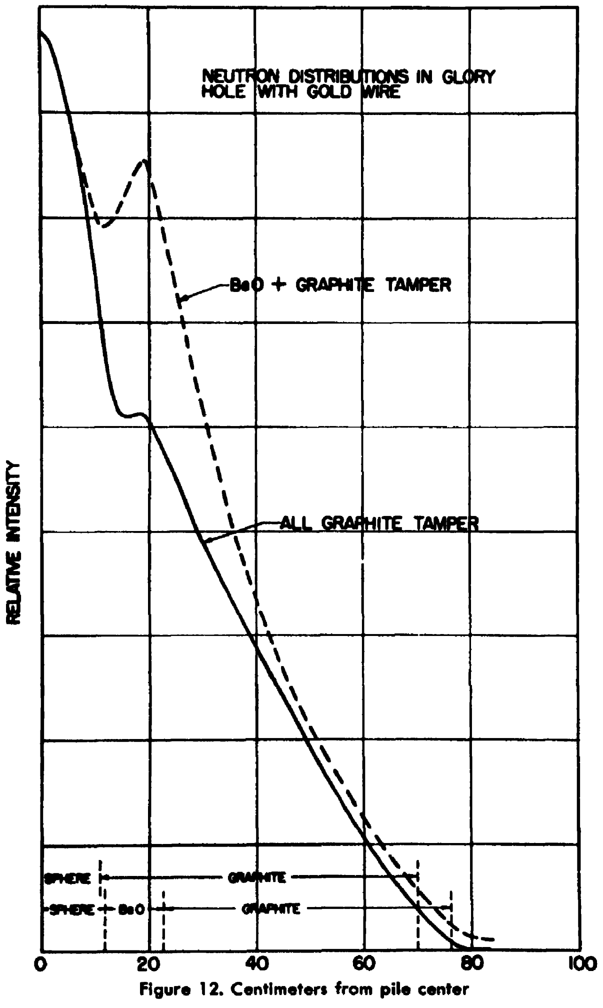

Figure 12. Centimeters from pile center

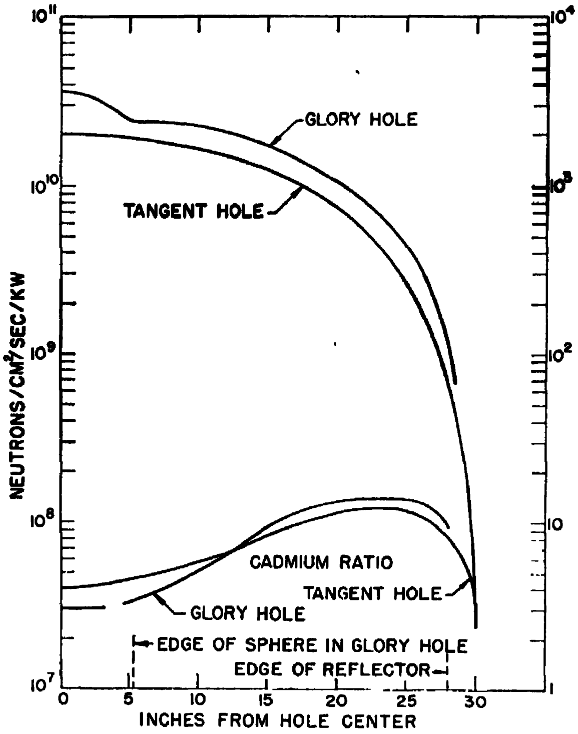

Figure 13. Supo distributions

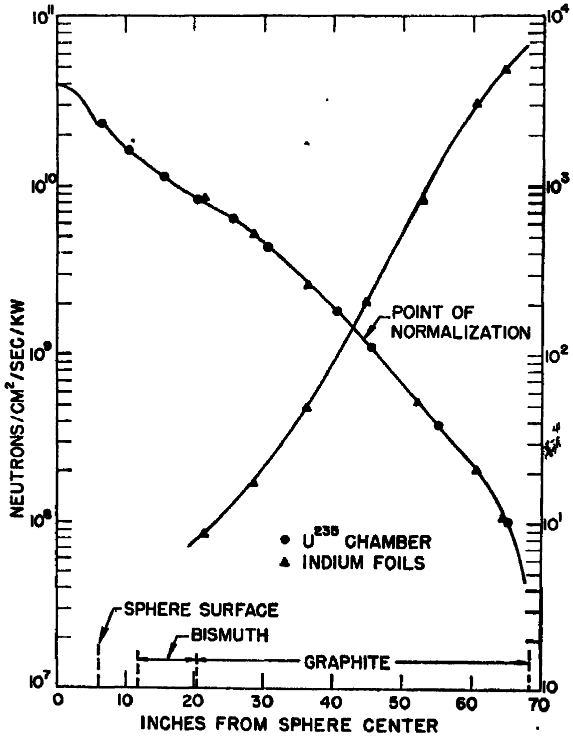

Figure 14. Supo north thermal column

(3) at a graphite face 1 ft in front of the bismuth column 4.4×10^7. A multiple U^{235} disc neutron converter when placed in the "glory hole" produces almost pure fission spectrum neutrons. With a 5-ft long, 1-in. id collimator, fast external beams of 6×10^5 n/cm^2/sec/kw have been obtained with such a source.

The reactor can readily be started and stopped for short time intervals. Power levels ranging from a fraction of a watt to 45 kw have been used. An automatic level control operating from a neutron sensitive ionization chamber is used almost exclusively due to its convenience and ability to remove small fluctuations.

For high stability operation of 0.1% or better, which has been required for a few precision experiments, the power level is limited to about 30 kw. This limitation appears to be imposed by the gas circulation rate in the recombination system and the capacity of the catalyst chamber, rather than by the rate of bubble formation in the solution or the cooling capacity of the main reactor heat exchanger.

Power levels in excess of 35 kw increase the hydrogen concentration to more than 10% in the circulating gas and may increase the catalyst bed temperature above 500°C. The combination of these factors is believed to ignite the hydrogen and oxygen gas mixture in the catalyst chamber and produce small pressure fluctuations. These fluctuations produce power variations which cannot be completely compensated for by the automatic level control.

Figure 15 illustrates the effect of temperature, and bubbles from solution decomposition, on the liquid level. Estimates of bubble depth are also shown. These measurements were made during initial operation with a pointer-type level indicator.

The large net negative operating coefficient of this reactor is illustrated in Fig. 16 for various powers. It is seen that as the power level is increased, the coefficient increases substantially up to the boiling point where it loses meaning. The true temperature coefficient has been masked by an additional bubble or power coefficient. The effective decrease in solution density due to this coefficient still further increases the inherent stability and safety of this type of reactor core.

The response of Supo to sudden reactivity changes has been studied to obtain information on the power coefficient of reactivity and to separate the effects of core temperature rise and decomposition gas formation upon the reactor behavior. Reactivity was added to the reactor by ejecting a neutron absorber out of the core region, the effectiveness of the absorber being known as a function of time. A reactivity change of about 0.4% Δk was added in about 0.1 sec. The average life time of the prompt neutrons was determined as about 1.7×10^{-4} sec, assuming an effective fraction of delayed neutrons equal to 0.0085. Initially following a reactivity addition, reactivity decrease was due primarily to decomposition gas formation, at least 10% of the potential gases appearing as such within 0.2 sec. The decrease in reactivity corresponding to gas formation was initially always about 5 times the decrease attributable to core temperature rise. It therefore appears that gas formation has a very influential effect upon the safety aspects of water boiler type reactors. As the gas bubbles left the core region, reactivity decrease due to core temperature rise increased in relative importance.

Table VI. Constants and Properties of Supo

Max. power: 45 kw heat   Max. power density: 2.8 kw/liter
Max. thermal flux: 1.7×10^{12} n/cm^2/sec
Est. max. intermediate: 2.8×10^{12} n/cm^2/se
Est. max. fast: 1.9×10^{12} n/cm^2/sec
Uranium: 88.7% U^{235}
Critical mass: 777 gm U^{235}
Operating mass: 870 gm U^{235}
Solution density: 1.10; pH <2
Solution volume: 12,700 cm^3
Pile dimensions:
  External size: 15 × 15 × 11 feet high
  Core: 12-in. diameter stainless steel sphere
  Moderator: Water 12 liters
  Reflector: Graphite 55-in. cube
  Thermal columns: (1) 42 inches wide, 64 inches high, 68 inches to sphere center. (2) 60 inches wide, 64 inches high, 95 inches to sphere center.
Shielding:
  8½-in. bismuth pier in thermal columns.
  ½ in. of B_4C + paraffin; 2 inches steel, 4 inches lead, 5 feet normal concrete.

Typical running conditions, 25 kw power level:	
Gas circulation rate	100 l/min
Catalyst chamber drop	2.2 in. H_2O
Reflux condenser drop	4.5 in. H_2O
Max. system pressure	3.1 in. H_2O
Exhaust line pressure	3.2 in. H_2O
Catalyst bed temperatures:	
Inlet region	467°C
Middle region	438°C
Outlet region	369°C
Reactor solution temperature	75°C
Reflux condenser water:	
Flow	0.17 gal/min
Temperature in	3.5°C
Temperature out	20°C
After condenser water:	
Temperature in	20°C
Temperature out	28°C
Air temperatures:	
Out of reflux condenser	15°C
Into catalyst chamber	45°C
Into after condenser	211°C
Into reactor sphere	33°C

Radiolytic gas production:
  Hydrogen plus oxygen: 0.44 liters/min/kw
  Nitrogen decomposition: 2.5 cm^3/min/kw

The compilation in Table VI summarizes some of the constants and properties of Supo:

D. One-Watt Solution Type Reactor, North American Aviation 1952–1955

This water boiler type reactor has been constructed by North American Aviation Inc. It is designated as WBNS (Water Boiler Neutron Source) and operates at a one-watt power level with a maximum thermal flux of 4×10^7 neutrons/cm^2/sec. It uses an enriched uranyl nitrate solution encased in a cylinder of graphite 5 ft in diameter and 5 ft high.

E. A 500-Watt Solution Type Reactor, North American Aviation 1953–1955

This reactor has been built by N.A.A. for Livermore Research Laboratory in California. The general design is similar to the one-watt unit except that it uses an enriched uranyl sulphate solution and has a completely closed cycle sweep gas and recombination system. The maximum thermal flux is 2×10^{10} neutrons/cm^2/sec.

The above two reactors have been described in detail in a report entitled Solution Type Research Reactors, which is a part of the Information Package for the International Conference at Geneva, and will therefore not be described any further.

F. A 10-Kilowatt Research Water Boiler, North Carolina State College 1953–1955

This reactor is notable in being the first such device not to be owned and operated by a national government. The purpose of the reactor was not to make many original contributions to reactor technology. Rather, the construction was aimed at providing as simply and quickly as possible a safe flexible nuclear reactor with the maximum adaptability to instructional and research purposes. Although the general designs of numerous components have been borrowed from the successful Los Alamos Supo model water boiler, this reactor has some different features.

The reactor core is placed below ground level in the center of a 57-ft diameter room. This room, in turn, is in the center of the building. On three sides are laboratories for instruction and research. On the fourth is an observation room and the control room. A cylindrical core using a uranyl sulfate solution enriched to about 90% with U^{235} is used. The cylinder is made of stainless steel (347 type 18-8) with an inner diameter of 10¾ in. and 11 in. height; the wall thickness is 1/16 in. Four internal hairpin type cooling coils, shown in Fig. 18, are used to dissipate the heat developed in the core. Fourteen liters of solution fill the core to a height of 9.9 in. A volume of 0.9 liters is left above the solution to allow for frothing and solution expansion. About 848 grams of U^{235} are required for normal operation. The core is surrounded by a graphite reflector in the form of a five-ft cube.

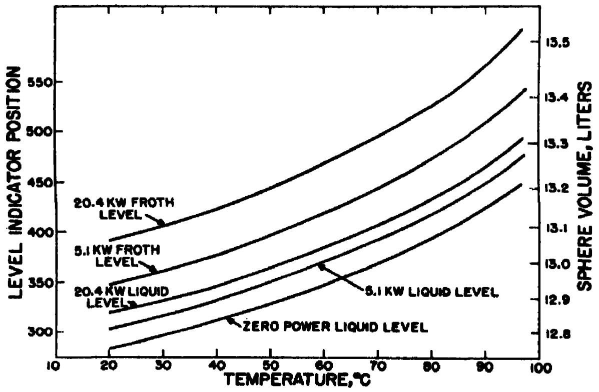

Figure 15. Supo levels

The shield consists of four to six inches of lead around the graphite followed by heavy barite type concrete. The outer shield is in the form of an octagon about 17 ft in diameter and 12 ft high. Numerous exposure facilities exist, including a thermal column, a central vertical re-entrant thimble extending into the core, and access ports from all eight faces of the octagonal shield (see Fig. 17).

A recombination unit similar to that in Supo is used. No decomposition products other than hydrogen, oxygen and fission product gases are produced. Since some air is bled into the system, however, a small amount of gas is discharged after a time delay to the atmosphere by means of a stack. Control of reactivity is maintained by four vertical rods. Two of these are internal and made of boron. Two are tangential cadmium strips.

Figure 19 shows Dr. Beck explaining the operation of the control console to two students.

During the first ten months of operation the reactor was operated at 100 watts or less. Effort during this period was devoted to the determination of the reactor characteristics, calibration of instruments and auxiliary apparatus, and the development of satisfactory operating and experimental procedures.

When the reactor was first run at about 400 watts for one hour with widely varying core temperatures, a decrease in reactivity was observed. This loss first appeared when the temperature of the fuel had been lowered to 11°C. The total loss of reactivity amounted to 40 grams U^{235} equivalent.

The loss of reactivity was established to be due to a partial precipitation of uranium, the pH of the solute having changed from the normal 2.3 to 1.3.

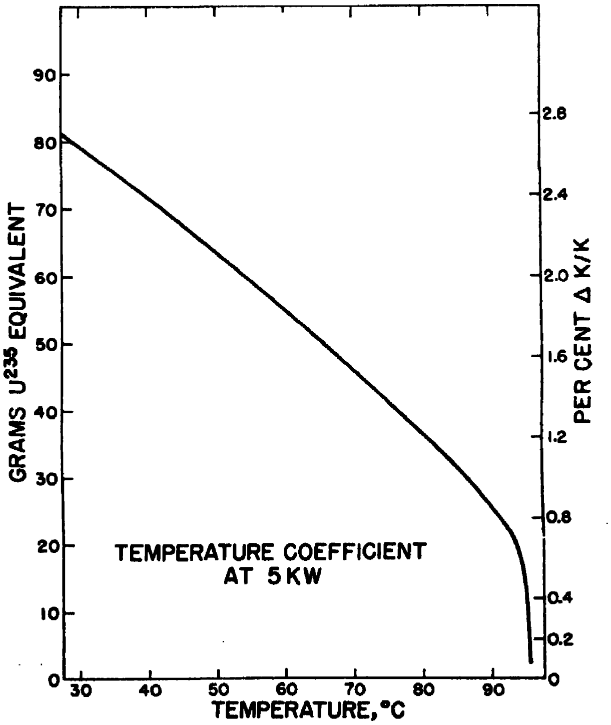

Figure 16. Temperature coefficient at 5 kw

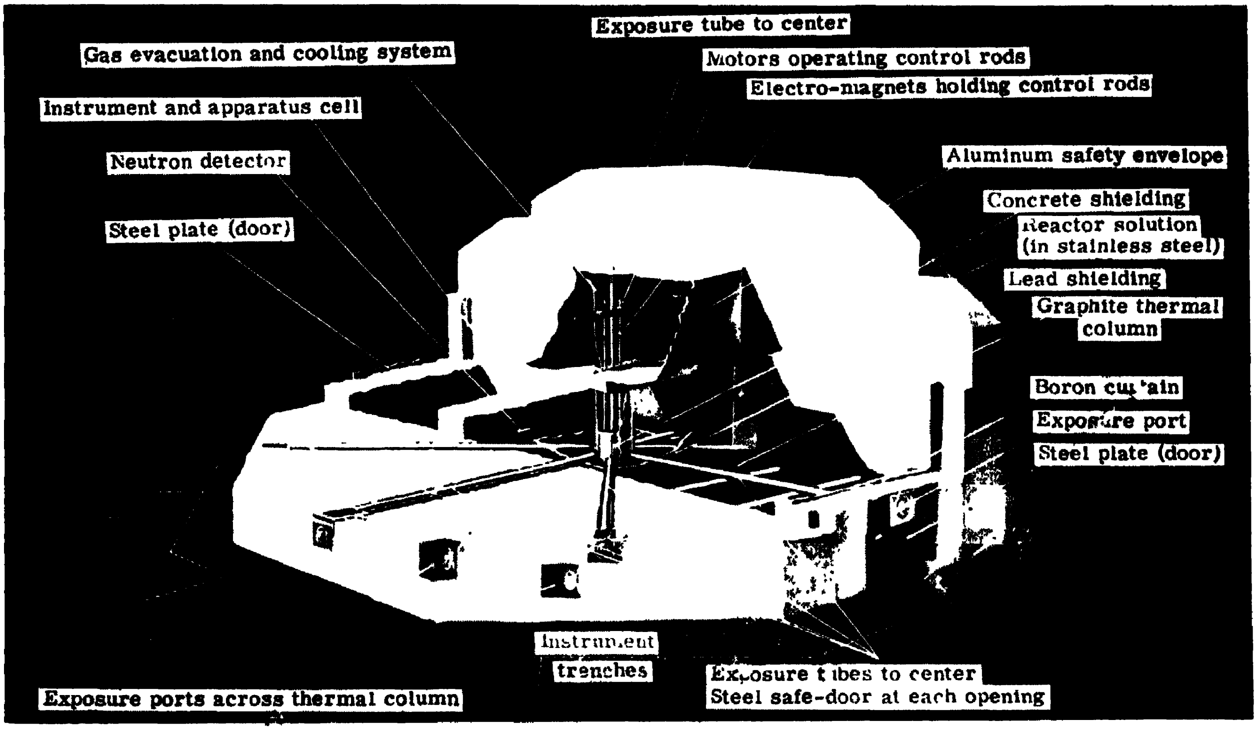
Exposure tube to center
Gas evacuation and cooling system
Motors operating control rods
Electro-magnets holding control rods
Instrument and apparatus cell
Neutron detector
Aluminum safety envelope
Concrete shielding
Steel plate (door)
Reactor solution (in stainless steel)
Lead shielding
Graphite thermal column
Boron curtain
Exposure port
Steel plate (door)
Instrument trenches
Exposure tubes to center
Steel safe-door at each opening
Exposure ports across thermal column

Figure 17. Raleigh reactor, North Carolina State College

The precipitate was dissolved in 7 days by the addition of cupric sulfate and ferrous sulfate to the solution along with temperature cycling and bubbling to assist stirring.

The equilibrium operating conditions at temperature are normally such that the hydrogen peroxide concentration reaches an equilibrium value due to the presence of the fission product radiations and does not continue to build up. When, however, the reactor is shut off and the temperature is dropped, one can get an excess of hydrogen peroxide which reacts with the uranyl ion producing UO_4 as a precipitate. After operating at 10 kilowatts and 80°C for example one cannot cool the solution much below 40°C without having a precipitate form. The addition of $CuSO_4$ and $FeSO_4$ catalyzes the decomposition of hydrogen peroxide.

III. WATER BOILER DESIGN PROPOSALS

A. 50 Kilowatt Medical Reactor, North American Aviation Inc.

A homogeneous, water solution type nuclear reactor has been designed to provide radiations for medical research and experimental therapy.

The enriched uranyl sulphate fuel-moderator solution is contained in a spherical core tank, surrounded by a graphite reflector and a dense-concrete shield. The reactor is cooled by recirculated chilled water. Stainless steel is used to fabricate all reactor components which come in contact with the fuel solution or reactor atmosphere. Radiolytic and fission gases produced during reactor operation are handled in a closed-cycle system. No discharge of radioactive effluents are required during operation.

Section views of the proposed reactor are shown in Figs. 20 and 21. Neutron and gamma radiation tubes, isotope production tubes, a fission-gas gamma radiation source, and two thermal columns comprise the experimental facilities. The columns contain flexible arrangements for providing large cross-section, intense beams of gamma rays, thermal neutrons, and fast neutrons, either singly or together. Tables VII and VIII give the calculated radiation intensities expected.

Figure 22 is a schematic diagram of the proposed gas circulation and recombination system. It differs from the Supo design in that the main gas stream does not sweep the reactor core region and the gas is pumped by means of water injection.

A similar core design proposal for a general type research reactor with different radiation facilities will be constructed by North American Aviation Inc. for the Armour Research Institute of Chicago, in the fall of 1955.

B. Supo Model II, Los Alamos

A study of the operating characteristics of Supo Model I has indicated that with some design modifications substantially higher fluxes could be made available.

Only such changes have been considered in this design which are known to improve the performance either due to direct experimentation or from extrapolation of known data.

The gas disposal by means of a tall exhaust stack as used in Supo offers some difficulties in highly

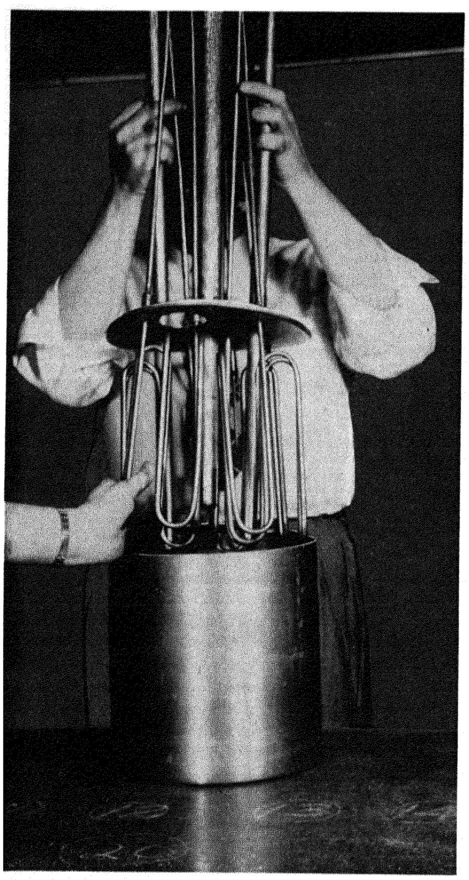

Figure 18. NCSC reactor core

Figure 19. NCSC reactor console

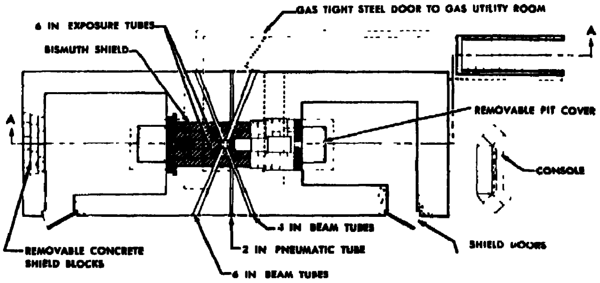

Figure 20. NAA medical reactor, top view

populated locations. This problem can be eliminated either by the recombination of the nitrogen by well known nitrogen fixation methods or using a uranyl sulphate solution as is in use at North Carolina State.

The present flux limitations of Supo are due to (1) the gas circulation rate in the recombination system, (2) the capacity of the catalyst chamber, (3) the capacity of the heat exchanger, and (4) the effectiveness of the shielding. These restrictions can

Table VII. Calculated Radiation Intensities Available at the Shield Face of the Thermal Neutron Facility

Use	*Thermal neutron intensity rep/min/kw*	*Thermal neutron flux n/cm²/sec/kw*	*Fast neutron intensity rep/min/kw*	*Fast neutron flux n/cm²/sec/kw*	*Gamma ray intensity rep/min/kw*
Patient therapy					
Direct beam	3 2	3.8×10^7	0.6	1.3×10^5	0.1
Penumbra	—		0.03	6.5×10^3	3×10^{-3}
Shadow	—		7×10^{-4}	1.5×10^2	3×10^{-4}
Animal research	1.2	$1\ 4 \times 10^7$	0.009	2×10^3	0.005

Table VIII. Calculated Radiation Intensities Available from the Gamma and Fast Neutron Facility at a Distance Eight Feet from the Reactor Core Center

Use	*Description of facility*	*Gamma ray intensity rep/min kw*	*Fast neutron intensity rep/min kw*	*Fast neutron flux n/cm²/sec/kw*
Patient therapy	21 inches water no lead	1.3	0.086	1.9×10^4
Animal research	33 inches water no lead	0.50	0.0036	8×10^2
Animal research	8 inches lead	0.002	10	2.2×10^6

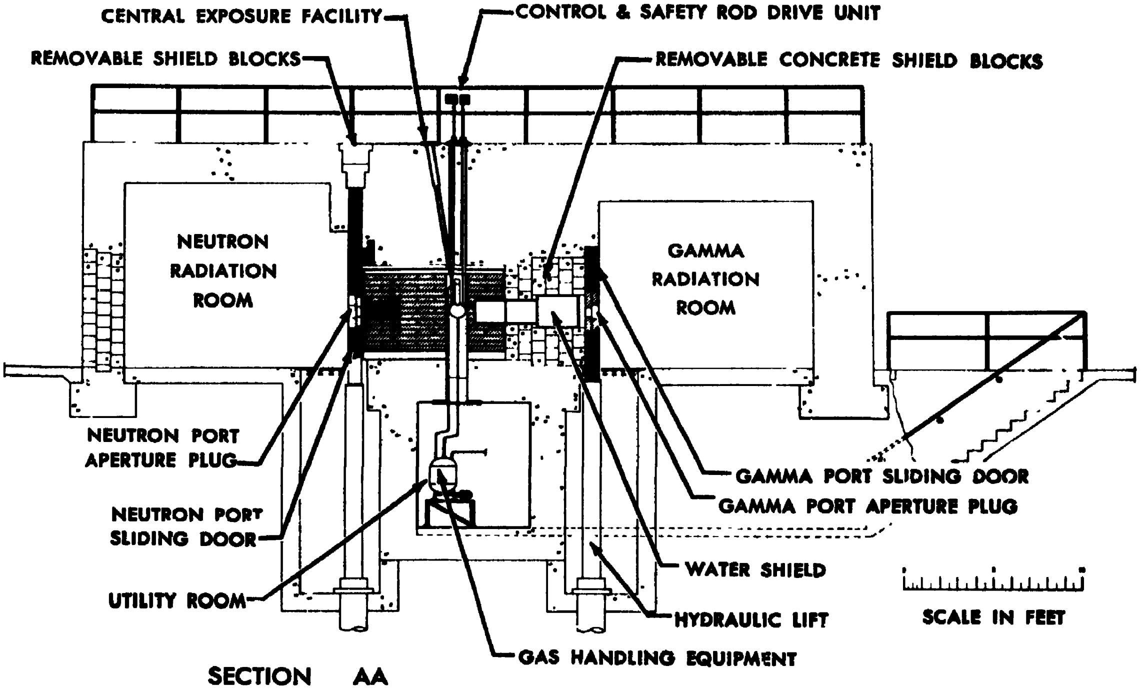

Figure 21. NAA medical reactor, side view

easily be removed by increasing the size and capacity of the necessary components.

Instabilities and reactivity loss due to bubble formation probably present the real flux limitations. Extreme bubble formation was produced in Supo by permitting the solution to boil with no water flow through the main heat exchanger. With the reactor producing 5 kw of steam in the reflux condenser of the recombination system (Fig. 8) the inherent reactor power fluctuations were found to be ±5%. These operating conditions correspond to a release of 290 liters of vapor per minute as compared to 13 liters per minute of radiolytic gas at a normal 30-kilowatt operating level.

Figure 23 compares power coefficients for normal operation with appreciable radiolytic gas production to the 5-kilowatt boiling condition when most of the gas is water vapor. An extrapolation of the radiolytic gas production curve makes it appear feasible to run water boiler type reactors at substantially higher power densities.

Figure 24 is a schematic sketch of a proposed Supo type research reactor which incorporates improvements in the overall shield geometry and port facilities.

The spherical geometry used on Los Alamos Water Boilers was originally based on the desire to minimize the active material required for critical experiments. When power operation was begun, the upper half of the sphere was no longer completely filled with solution in order to provide appreciable surface area for the escape of gas bubbles. A cylindrical rather than a spherical shape has numerous advantages for the upper portion of the reactor vessel. (1) The free solution surface can be increased, which provides a more favorable geometry for the escaped bubbles. (2) The circulating gas can be vented more efficiently at lower velocities, which reduces entrained liquid in the gas stream. (3) Excess volume for emergency

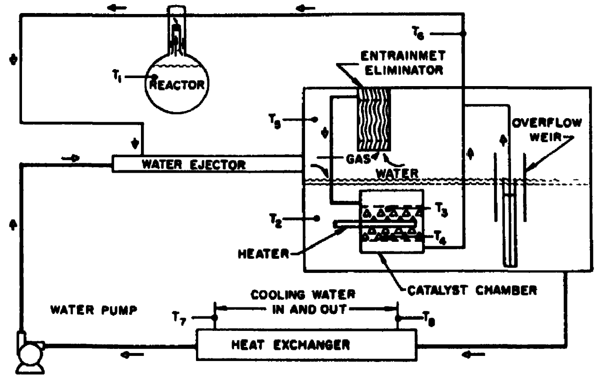

Figure 22. NAA wet gas handling system

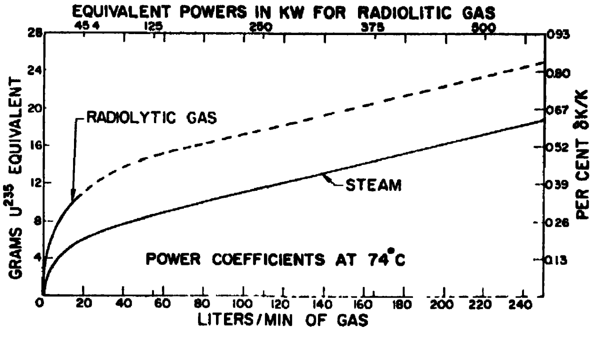

Figure 23. Power coefficients at 74°C

expansion can be easily supplied above the solution. (4) Neutron shielding and vertical access facilities can be more easily provided. Figure 25 shows a Supo type reactor design which incorporates these features.

Both the reflux and after condenser of the recombination system are included in the reactor vessel shell. The solution-gas interface of Supo I is 410 cm^2 when at full operating temperature of 88°C; this area has decreased to 245 cm^2 when operating at 30 kw. The cylindrical geometry of Supo II has three times this area which does not decrease for an increase in power.

The total heat exchanger surface area has been increased by about a factor of seven over that in Supo I. Cooling the wall of the reactor vessel contributes about 25% to this area increase and prevents the heating of the reflector by conduction now observed.

Effort has been made to prevent entrainment of solution spray into the gas circulating system. Early experience on Supo, before the recombination system was installed, has shown that adequate washback features are essential or uranium can be lost by caking onto available surfaces. The present design of Supo I where continuous washdown by condensation occurs in the reflux condenser has been found entirely satisfactory for the gas flows used. The design of Fig. 25 is believed to offer a better geometry even with the factor of 20 increase in the gas circulation rate. The neutron shielding above the reactor is supplied by part of the cooling water system and the entire reactor assembly can be easily removed from the top.

Since the recombination system shown in Fig. 8 was the first use of a catalyst chamber for recombining gases from a homogeneous reactor, numerous features were provided to determine the operation behavior and causes of failure if failure should occur. With the experience gained from the operation of this system, one can now make some simplifications with confidence.

Figure 26 is a schematic layout of a simplified recombination system which has more than ten times the capacity of the old system. The changes and essential features are: (1) the spare catalyst chamber is not necessary and actually has been removed from Supo I; (2) pressure coupling tubes 5 through 14 (Fig. 8) are not essential; (3) the external condenser can be included in the reactor; (4) the liquid trap can be removed or combined with a sampling tube if the nitrogen is recombined or a solution such as uranyl sulfate is used which produces no excess gas; (5) a single bubble tube for occasional level checking or gas sampling is desirable; (6) some means for measuring the flow rate of the circulating gas is advantageous in order to be able to shut the reactor off before high hydrogen concentrations have accumulated in case of stoppage in the gas circulation; (7) a blower with an all-welded case using a canned-rotor motor is known to give completely trouble-free service for the life of the bearings used. High grade ball bearings should last for several years of continuous operation and it is quite simple to design the bearings for easy replacement.

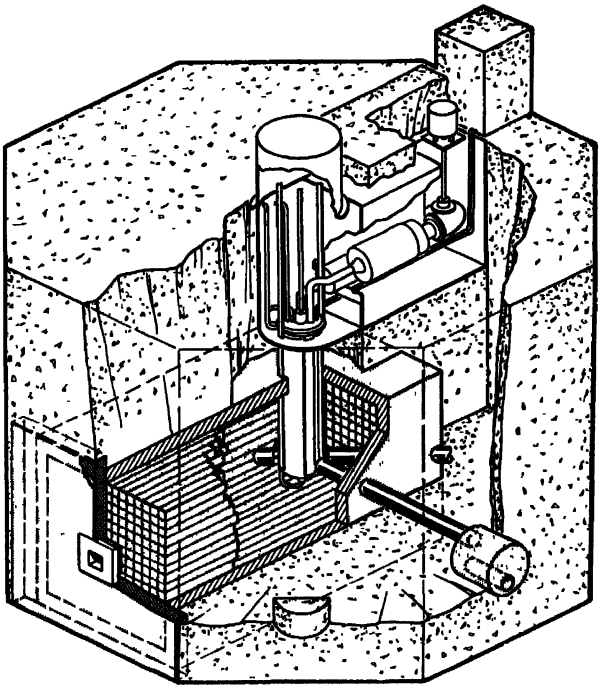

Figure 24. Schematic, Supo II

Operation of Supo I has shown that the following features are desirable in a catalyst chamber; (1) the chamber should be designed to prevent the catalyst bed temperature from exceeding 500°C during full power operation to prevent possible ignition of the gas; (2) an explosion trap on the inlet side of the unit is desirable to prevent flashback or burning at any point outside of the catalyst bed if the hydrogen concentration increased due to an accident; (3) cooling facilities on the chamber surface should be provided to avoid heating the surrounding shield.

Figure 27 illustrates a possible design for a catalyst chamber which incorporates these features. This unit has a gas handling capacity 20 times greater than that used on Supo I. The re-entrant thimbles shown are thermocouple wells. A shift in the hot zone from the outside towards the center gives an indication of a loss in catalytic activity. No such shift has yet been observed in the Supo I system.

The entire recombination system becomes a very strong gamma ray source due to fission deposition on the walls of the components and from the circulating gas itself. The gas circulating in Supo I for example, had a gamma activity of 2000 curies/liter. A very high gamma ray to neutron ratio can be made available for irradiation purposes by supplying irradiation facilities which "see" a portion of the recombination system.

C. Test Tube Reactor, Los Alamos

This reactor design is a more radical modification of the water boiler type reactor than that given above. A schematic drawing of the reactor proposal is shown

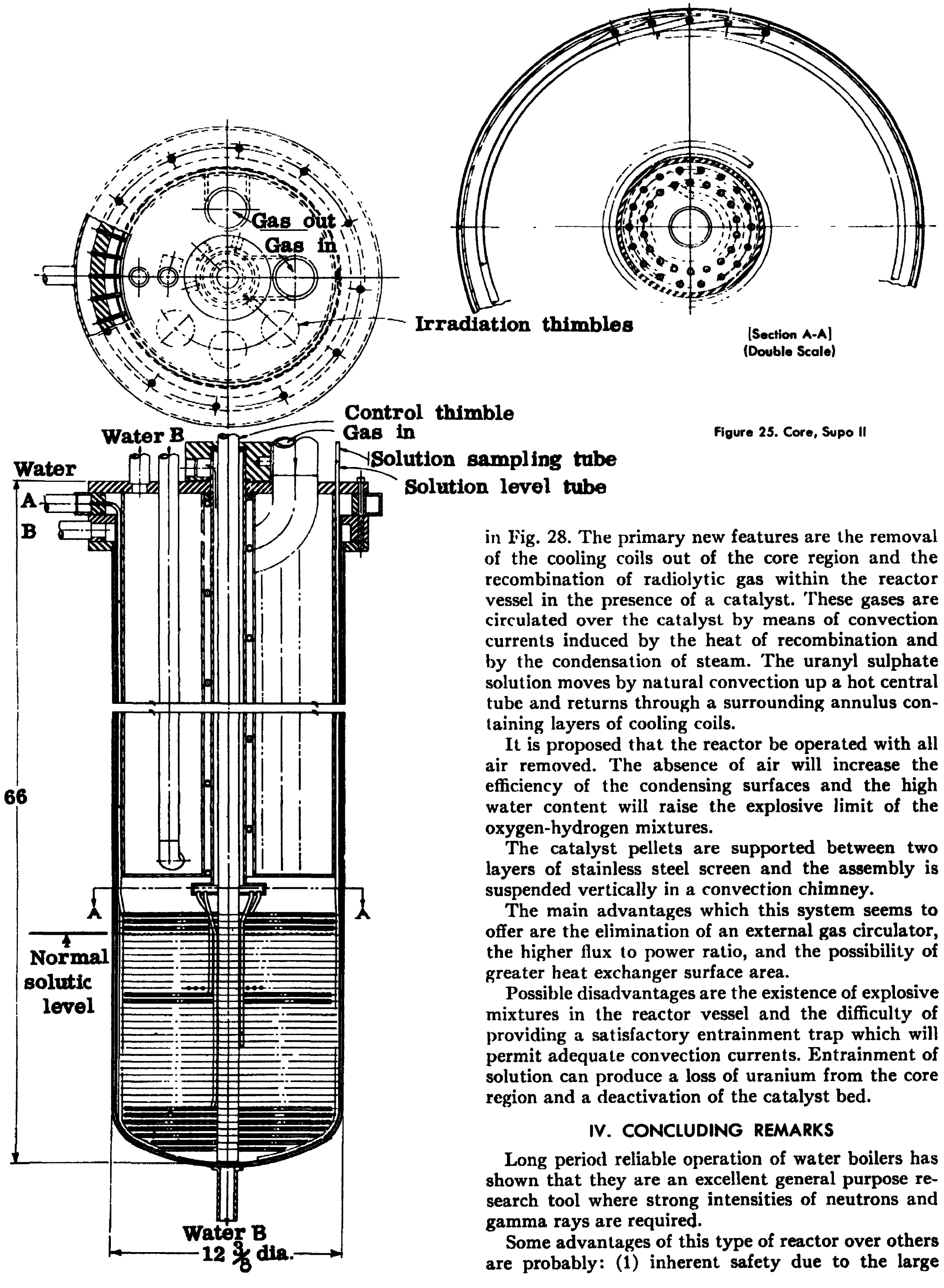

Figure 25. Core, Supo II

in Fig. 28. The primary new features are the removal of the cooling coils out of the core region and the recombination of radiolytic gas within the reactor vessel in the presence of a catalyst. These gases are circulated over the catalyst by means of convection currents induced by the heat of recombination and by the condensation of steam. The uranyl sulphate solution moves by natural convection up a hot central tube and returns through a surrounding annulus containing layers of cooling coils.

It is proposed that the reactor be operated with all air removed. The absence of air will increase the efficiency of the condensing surfaces and the high water content will raise the explosive limit of the oxygen-hydrogen mixtures.

The catalyst pellets are supported between two layers of stainless steel screen and the assembly is suspended vertically in a convection chimney.

The main advantages which this system seems to offer are the elimination of an external gas circulator, the higher flux to power ratio, and the possibility of greater heat exchanger surface area.

Possible disadvantages are the existence of explosive mixtures in the reactor vessel and the difficulty of providing a satisfactory entrainment trap which will permit adequate convection currents. Entrainment of solution can produce a loss of uranium from the core region and a deactivation of the catalyst bed.

IV. CONCLUDING REMARKS

Long period reliable operation of water boilers has shown that they are an excellent general purpose research tool where strong intensities of neutrons and gamma rays are required.

Some advantages of this type of reactor over others are probably: (1) inherent safety due to the large

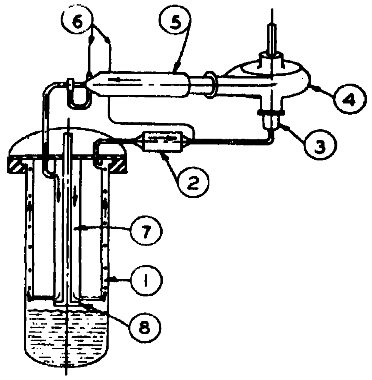

Figure 26. Schematic gas system: (1) spray condenser; (2) steel wool entrainment trap; (3) flow meter; (4) centrifugal pump; (5) catalyst chamber; (6) sampling tubes; (7) reflux condenser; and (8) solution baffle

negative temperature and power reactivity coefficients; (2) small size along with low power and uranium requirements for comparable fluxes; (3) no replacement of burned out fuel elements; (4) low cost and simplicity of design core; (5) ease of rapid shut downs and start ups; and (6) automatic removal of fission gases from core.

The chief disadvantage is the flux limitation. Even with the new designs mentioned above, stable operation with fluxes much in excess of 10^{13} neutrons/cm^2/sec are not likely. Most types of experiments can, however, be adequately carried out with such fluxes.

The main difference in the new water boiler designs described is the method of handling the radiolytic gas. The Supo system of Fig. 8 has been proven to be satisfactory, whether the wet gas system shown in Fig. 22 or the internal recombiner of Fig. 28 are satisfactory can only be demonstrated by actual test. These tests must be made under high flux reactor operation since the problems to be answered are: (1) whether with high density bubble formation there is any effect on the catalyst or any loss of uranium from entrainment and (2) whether the explosive gas mixture in the reactor core affects the operation or safety of the reactor.

Water boiler designs for pressurized high temperature operation have not been considered here. These may offer some advantages by reducing the bubble formation and permitting internal recombinations by the back reaction between hydrogen and oxygen. The use of heavy water as a moderator also has some advantages but no such unit has yet been constructed.

REFERENCES

Section II-A

1. Kerst, D. W., *et al.*, "Water Boiler," LA-134 (LASL 1944).
2. Helmholtz, L. and Friedlander, G., "Physical Properties of Uranyl Sulfate Solutions," MDDC-808 (LASL-1944).
3. LASL, "An Enriched Homogeneous Nuclear Reactor," *Rev. Sci. Inst. 22*, 489 (1951).
4. deHoffmann, F., *et al.*, "Criticality of Water Boiler and Effective Number of Delayed Neutrons," AECD-3051, (LASL 1944).
5. King, L. D. P. and Schreiber, R. E., "Distribution and Power Measurements in the Water Boiler," AECD-3054 (LASL 1944).
6. Hughes, D. J., Dobbs, J., Cohn, A., and Hall, D., "Delayed Neutrons from Fission of U^{235}," *Phys. Rev. 73*, 111 (1948).
7. Carter, R. E., Hinton, J. D., King, L. D. P., and Schreiber, R. E., "Water Reflector Measurements for a Water Boiler," LA-241 (LASL 1945).
8. Hinton, J. D. and King, L. D. P., "Experimental Determination of the Diffusion Length for C Neutrons in BeO," LA-160 (LASL 1944).
9. deHoffmann, F., "Intensity Fluctuations of a Neutron Chain Reactor," MDDC-382 (LASL 1946).
10. deHoffmann, F., "Formula for Water Boiler Fluctuations," LAMS-336, (LASL 1946).
11. deHoffmann, F., "Relative Effectiveness of Delayed Neutrons in the Water Boiler," LA-471 (LASL 1945).

Section II-B

1. King, L. D. P., *et al.*, "High Power Water Boiler," LA-394 (LASL 1945).
2. Katcoff, S., "Sweeping of Radioactive Gas from a Homogeneous Reactor," MDDC-293 (LASL 1946).

Section II-C

1. King, L. D. P., "Los Alamos Homogeneous Reactor—Supo Model," AECD-3287 (LASL 1951).

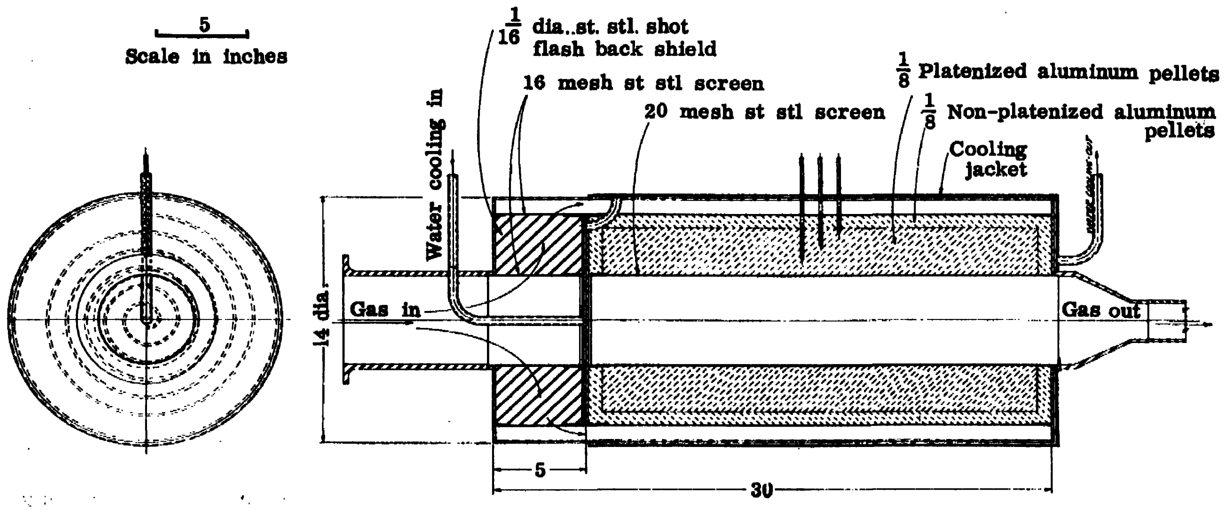
5
Scale in inches
$\frac{1}{16}$ dia..st. stl. shot flash back shield
16 mesh st stl screen
20 mesh st stl screen
$\frac{1}{8}$ Platenized aluminum pellets
$\frac{1}{8}$ Non-platenized aluminum pellets
Cooling jacket
Water cooling in
Water cooling out
14 dia.
Gas in
Gas out
5
30

Figure 27. Catalyst chamber, Supo II

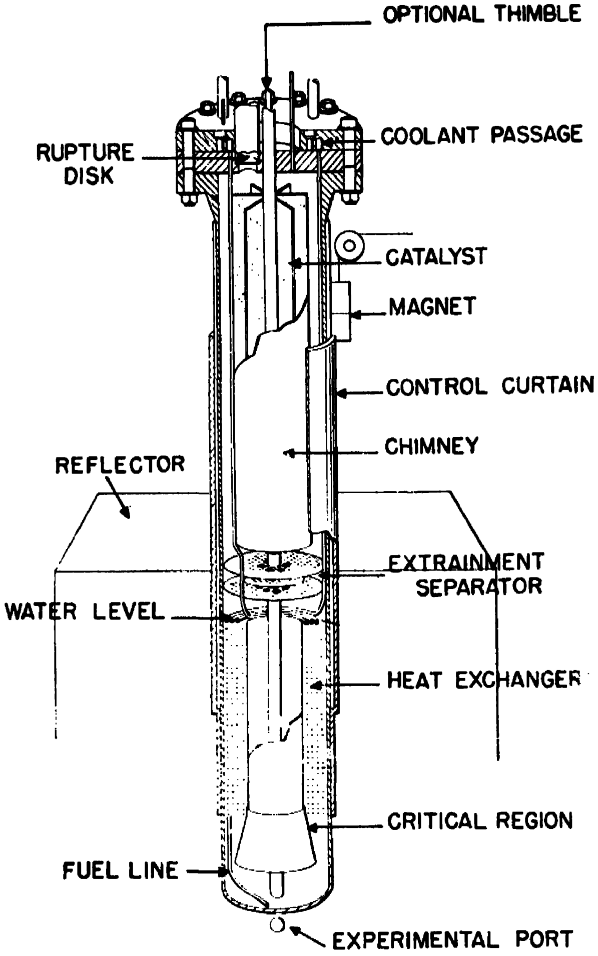

Figure 28. Test tube reactor

2. King, L. D. P., Hammond, R. P., Leary, J. A., Bunker, M. E. and Wykoff, W. R., "Gas Recombination System for a Homogeneous Reactor," *Nucleonics 11(9)*, 25 (1953).
3. Evans, J. E., King, L. D. P., and Schulte, J. W., "Solution Handling System for a Homogeneous Reactor," *Nucleonics 11(1)*, 67 (1953).
4. Evans, J. E., "Fast Neutron Spectra from the Water Boiler," LA-1395 (LASL 1951).
5. Kasten, P. R., "Reactor Dynamics of the Los Alamos Water Boiler," Chem. Eng. Progress Symp. Series No. 11, *Nuclear Eng. Part 1, Vol. 50* (1954).
6. King, L. D. P., "Research With a Low Power Reactor," Proc. University Research Reactor Conference, AECU-2900 (1954).
7. Brennan, J. T., Payne, S. H., Carter, R. E., Langham, W. H., "The Biological Effectiveness of Thermal Neutrons on Mice," *Nucleonics 12(2)*, 48 (1954) (A calibration of neutron and gamma intensities in Supo thermal column).
8. Busey, H. M., "Composition, Decontamination of Radioactive Gas Mixtures," *Nucleonics 12(5)*, 9 (1954).
9. Durham, F. P., "Radiolytic Gas Bubbling Improves Convective Heat Transfer in Supo," *Nucleonics 13(5)*, 42 (1955).

Section II-D

1. Remley, R. E., "Operation of the North American Aviation Water Boiler Neutron Source," *Science 119*, 3079 (1954).
2. Chalker, R., "Design and Construction of Water Neutron Source," *Science 119*, 3079 (1954).

Section II-E

1. Shortall, J. W., Flora, J. W., Graham, R. H., and Shelton, A. V., "Description and Start-up of a Water Boiler Reactor," LRL-136, (1954).
2. Flora, J. W., Shortall, J. W., and Drummond, W. E., "Temperature Effect on Reactivity of the CR and D Water Boiler," LRL-148, (1954).
3. Shortall, J. W., Flora, J. W., Graham, R. H., and Strain, E. J., "Power Calibration of the Water Boiler Reactor," LRL-149, (1954).
4. Flora, J. W., Shortall, J. W., and Strain, E. J., "Operating Characteristics of the Water Boiler," LRL-151, (1954).
5. Flora, J. W. and Shortall, J. W., "Experimental Facilities of the Water Boiler," LRL-152, (1954).
6. Shortall, J. W., Flora, J. W., and Drummond, W. E., "Biological Shield Evaluation of the Water Boiler," LRL-154, (1954).

Section II-F

1. Beck, C., *et al.*, "Further Design Features of the Nuclear Reactor at North Carolina State College," AECU-1986 (1952).
2. Beck, C., and Staff, "Temporary Loss of Reactivity Due to Precipitation of Fuel in the Raleigh Research Reactor," R-NCSC-88 (1954).

Section III-A

1. North American Aviation, Inc., "Nuclear Reactor for Medical Research," NAA-AER-1180 (1955).
2. North American Aviation, Inc., "Solution Type Research Reactor," NAA-AER-1023 (1954).

Section III-B

1. King, L. D. P., "Evaluation of the Los Alamos Water Boiler as a Research Tool," to appear in *Nucleonics* (1955).

Section III-C

1. Busey, H. M. and Hammond, R. P., "Test Tube Reactor," to appear in *Nucleonics* (1955).

Abbreviations

LASL Los Alamos Scientific Laboratory operated for US Atomic Energy Commission by University of California, Los Alamos, New Mexico.

NAA North American Aviation, Inc., Atomic Energy Research Department, Downey, California.

LRL Livermore Research Laboratory of the US Atomic Energy Commission operated by California Research and Development Company, Livermore, California.

The Experimental Nuclear Reactor with Ordinary Water and Enriched Uranium

By Y. G. Nikolaev,* USSR

The purpose of this report is to give a description of a thermal-neutron research reactor. Light water is used for moderating, heat-exchanging and as reflector material. The fuel elements contain 10% enriched uranium.

The reactor serves for the study of the passage of neutrons and γ-rays through shielding materials, for radioactive isotopes production and for various investigations in physics.

The following basic results obtained in experiments with a zero energy version of the reactor and with the reactor itself during its initial operation will be presented: the critical mass dependence on the lattice spacing, the thermal and resonance neutron density distributions in the active core and in the reflector, the thermal neutron density distribution within a lattice cell, the effect of temperature and the reactivity effect of the control rods.

The reactor active core is of quasi-cylindrical form. Its diameter and height are, respectively, $\sim$40 and 50 cm.

The reactor fuel loading expressed in U^{235} amounts to $\sim$3.5 kg.

The reactor is designed with the object to make possible the production of neutrons and γ-ray beams sufficiently intense to carry out the above mentioned experiments at relatively low power levels (of the order of several hundred kw).

DESCRIPTION OF THE REACTOR CONSTRUCTION

In Figs. 1–10 drawings and photographs of the reactor and some of its parts are presented.

The central part of the reactor structure is a water-filled aluminium tank with a 500 mm diameter tube welded to its bottom. The active core of the reactor is located inside this tube. To facilitate reactor fuel loading and unloading operations, the core is subdivided into 32 units. Of these, 24 contain 16 fuel elements each; the remaining 8 units each contain 15 fuel elements; in addition, these units contain tubes in which control and safety rods are placed.

The units are fixed at the top and bottom of the active core by means of guide grids.

Aluminium and aluminium alloys are used as structural materials in the active core and for canning the fuel elements.

The fuel elements, which are in the form of cylinders of 9 mm outer diameter and 500 mm active height, are arranged vertically and form a square lattice of $\sim$18 mm spacing.

The tubes containing control and safety rods rise above the water level in the aluminium tank and are fastened to the tank top cover. On the same cover plate are also mounted the guides for the wires and the electro-magnets of the safety rods. In the side reflector are six tubes containing ionization chambers.

In order to prevent a loss of intensity of the neutron beam, there is no water reflector in the beam exit region.

The reactor radiation shielding is composed of cast-iron and water. The arrangement of the different shielding layers is shown in Figs. 7 and 9.

During the loading, unloading of repair operations

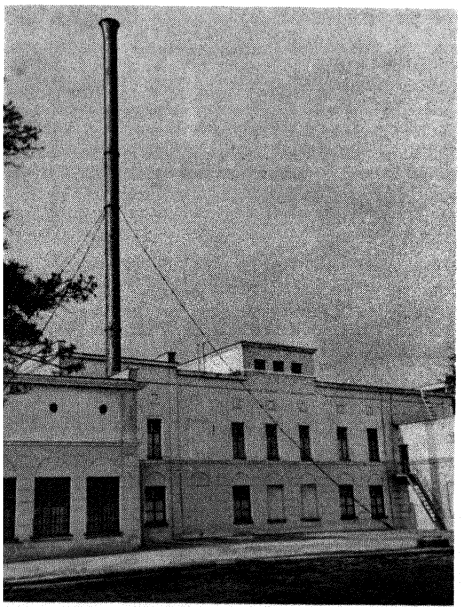

Figure 1. Front view of the reactor building

Original language: Russian.

* This paper has been prepared on the basis of the materials available at the Academy of Sciences of the USSR.

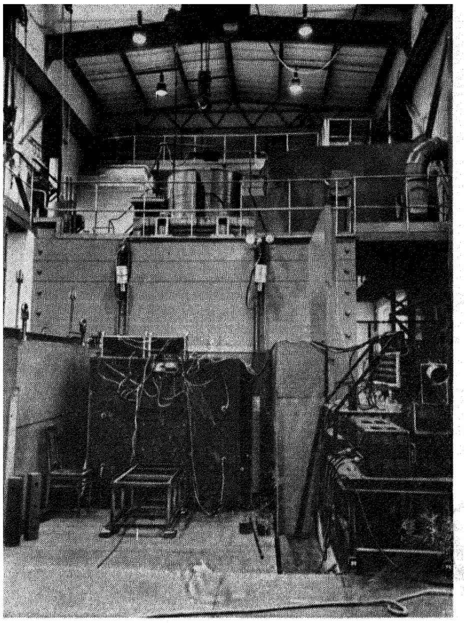

Figure 2. North view of the reactor

in the active core, protection against the residual radiation is provided by an approximately 3.5 m thick layer of water above the active core.

In the direction of the neutron and γ-ray beam which is let out from the active core (the northern direction) a part of the stationary lateral shielding has been removed.

In the resulting opening, extending inward to the reactor active core, shielding plugs can be placed. A shielding plug is mounted in a steel box mounted on a movable truck. The truck can be moved on rails with the help of a winch. When the box is moved away, protection against the radiation of the shut-down reactor is provided by two cast iron plates which are let down. Such an arrangement makes it possible to test the shielding properties of materials, to irradiate considerable amounts of substances in the immediate vicinity of the reactor active core and also to let out narrow beams of neutrons and γ-rays.

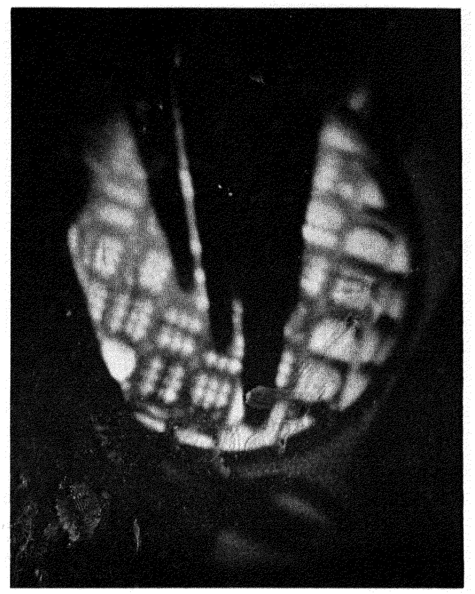

Figure 4. The phosphorescence of the core at 10 kw power level (photographed through a water-layer)

Several holes are provided in the top shielding above the experimental box through which detectors connected to various control instruments are introduced.

On the southern side of the reactor there is a special adjoining basement in which the centrifugal pumps of the closed circulation circuit and the heat-exchanger are located. The basement is covered with a floor consisting of bitumen-filled tanks and cast-iron plates which serve as a protection against the radioactivity of the circulation circuit water. The controls of the circulation circuit valves protrude out of the shielding.

On the eastern side of the reactor, storage surrounded by concrete shielding is provided for units unloaded from the core.

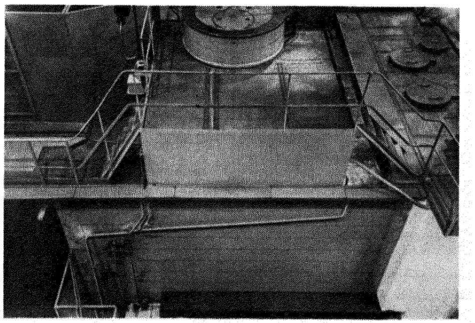

Figure 3. South view of the reactor

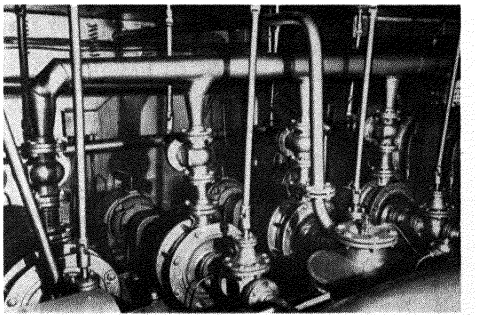

Figure 5. The reactor pump system

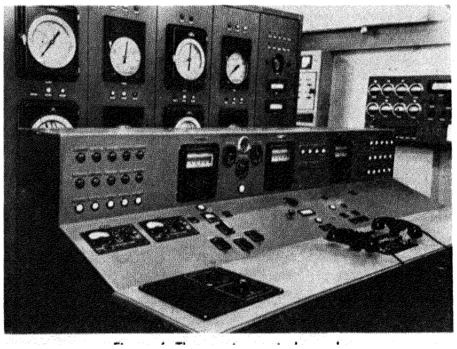

Figure 6. The reactor control panel

On the western side of the reactor there are special balconies on which the motor drives of the control and safety rods are mounted.

Figure 11 shows the flow diagram of the reactor installation. The heat developed in the core is taken over by the water circulating in a closed primary circuit and transferred in the heat exchanger to the continuously flowing water of the secondary circuit. (The circulation of water is indicated by arrows in Fig. 11.)

A part of the water flow from the circulation pumps head collector goes to the deaerator, where explosive mixture produced during the water passage through the core is removed.

The tightness of the fuel element cannings is monitored by measuring activity of the water in the circulation circuit. The damaged element can be located by checking the activity of water taken at the outlet of each unit. No case of fuel element damage occurred during the whole period of the reactor operation.

Listed below are the main operating characteristics of the reactor at a power level of 300 kw:

1. Rate of water flow through the active core: 240 m^3/hour.
2. Rate of water flow in the deaerator circuit: 20 m^3/hour.
3. Rate of water flow in the secondary circuit: up to 50 m^3/hour in summer time.
4. Water temperature before entering the core: 30°C.
5. Water temperature rise in the reactor core: $\sim$1°C.
6. Temperature of the outer surface of a fuel element: not more than 70°C.

The design of the ventilation system completely excludes any possibility of radioactive gases or vapours penetrating to working rooms. All air spaces adjacent to the reactor central structure in which air can be either activated or contaminated with radioactive gases or vapours are under suction and well ventilated. Air contaminated with radioactive gases or vapours is exhausted through a ventilation stack.

A special reactor sewer has been provided, made in such a way that all water containing radioactive contaminations is discharged into two buried decay-tanks. The amounts of radioactivity contaminated water discharged are very small. The discharging takes place periodically.

The reactor is equipped with control instruments permitting control of all parameters important for the reactor operation. Besides that, the temperature operation conditions of motors and stuffing-boxes of

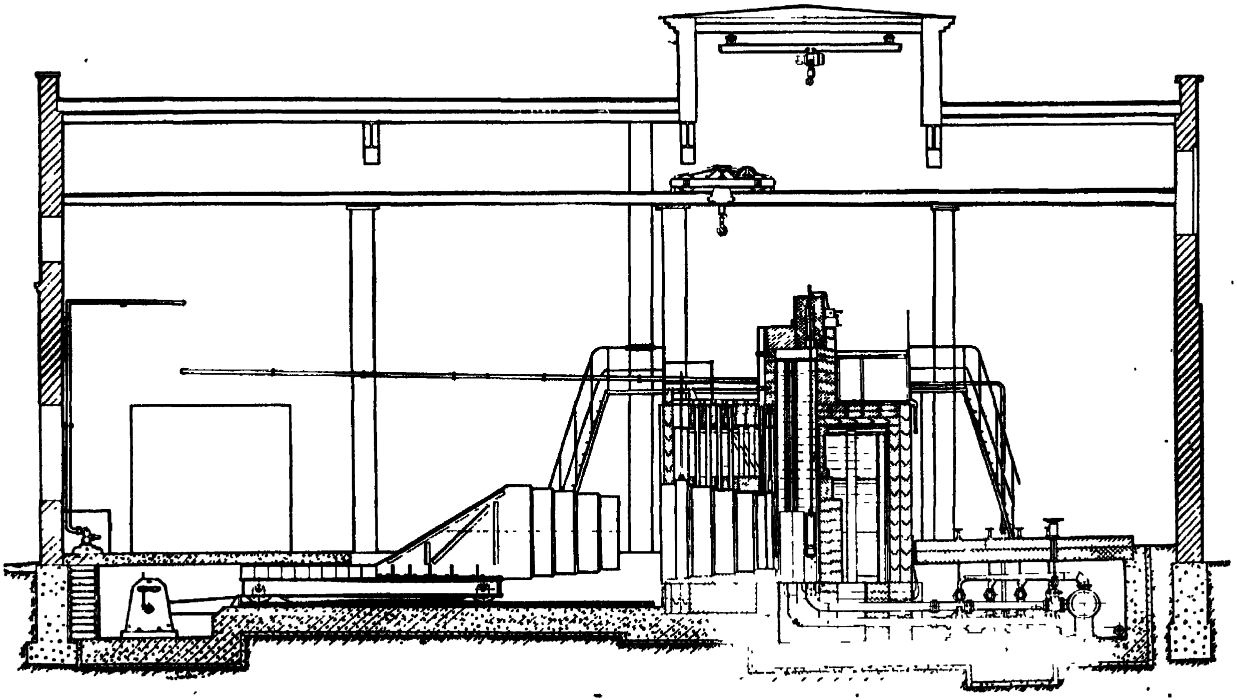

Figure 7. Section of the reactor

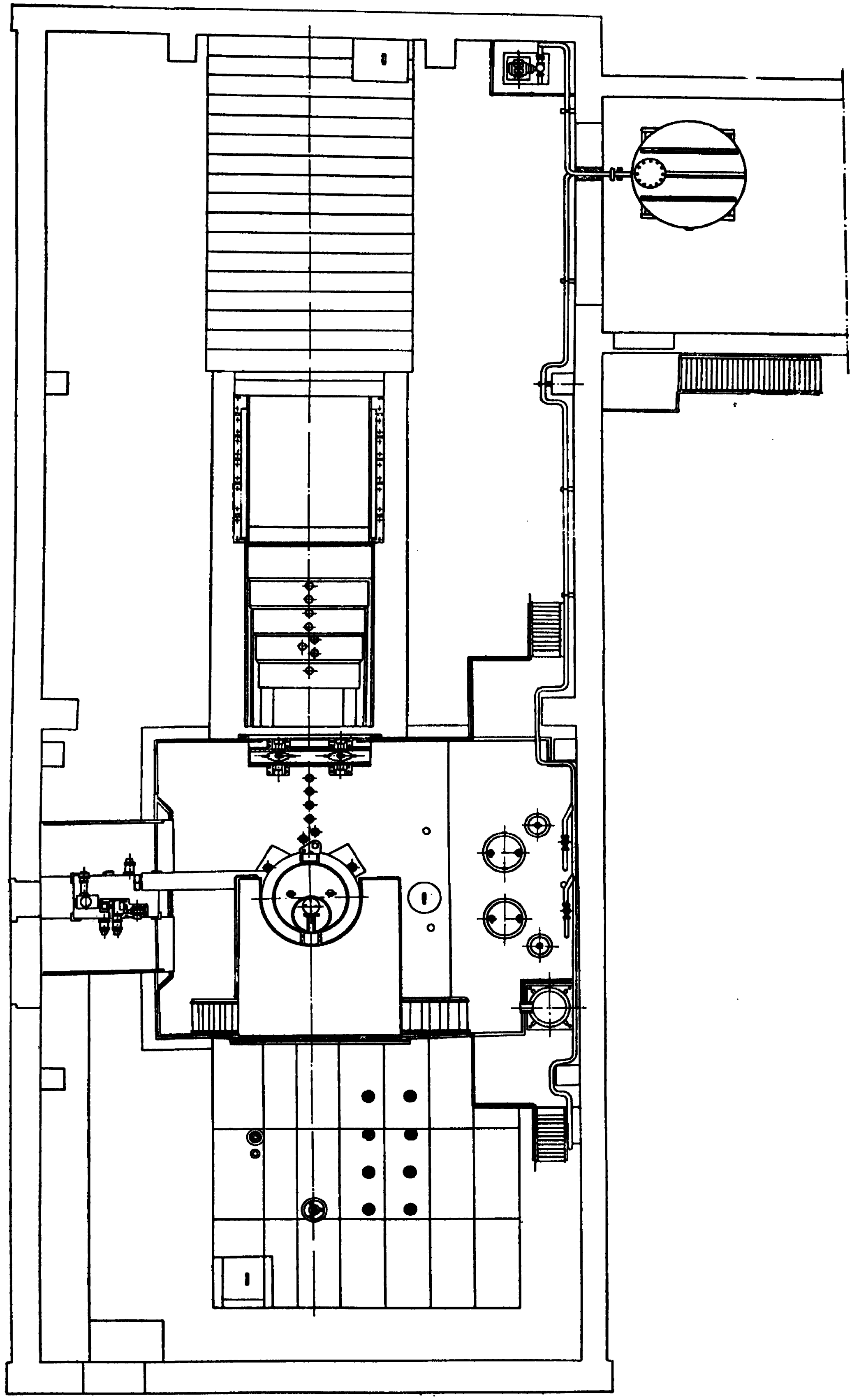

Figure 8. Plan view of the reactor

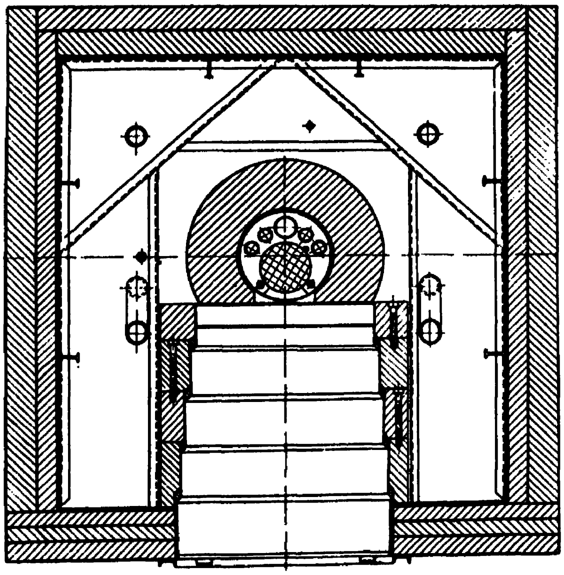

Figure 9. Horizontal section of the reactor

the circulation pumps are monitored by resistance thermometers; very simple indicators make possible the detection of leakage occurrence in any part of the circulation circuit. Dose-meters permit to check the radiation safety of the working rooms and to monitor the activity of the air exhausted through the ventilation stack and the activity of the water continuously flowing in the secondary circuit to detect leakage in the heat-exchanger tubes.

Six ionization chambers are provided for measuring reactor power level. Two of them, called "start-up" chambers are filled with gaseous BF_3 and are used during the reactor start-up and low power level operation. The remaining "work" chambers have a layer of solid boron carbide on their electrodes and are used during reactor operation at high power levels.

Pile control is accomplished by means of 4 control

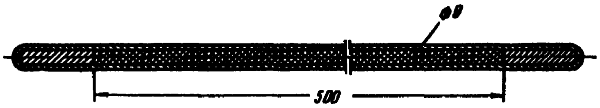

Figure 10. Fuel element

rods, three of which are made of boron carbide and one of steel. The steel rod is used as the regulating element operated by the automatic system for maintaining a pre-set power level. The system includes an ionization chamber, a galvanometer, a potentiometer-type control for setting the power level, an electronic and a servo-amplifier, a control rod motor drive and the control rod itself. The ionization chamber current passes in series through the galvanometer and the power level control. When a deviation of the power level from the set value in either sense occurs, a positive or negative signal appears accordingly at the output of the power level control device. This signal is amplified successively by the electronic and servo amplifiers up to an amplitude sufficient for the operation of the control-rod motor drive.

To ensure reactor safety, three rods of boron carbide are used. During reactor operation the safety rods are raised and clutched to electromagnets. On the arrival of the emergency signal the magnets are de-energized and the safety rods fall freely into the core. The time interval between the arrival of the emergency signal and the completion of the safety rods plunge is ~0.5 sec.

The emergency system is triggered automatically in the following cases:

1. The pre-set power level is exceeded by 20%.
2. The start-up velocity is intolerably high.
3. The water flow in the primary circuit drops.
4. The current is cut off in the circulation pumps motors.

Subcritical operation is used for maintaining very low power levels, necessary for instance when measurements in the first layers of an experimental shielding

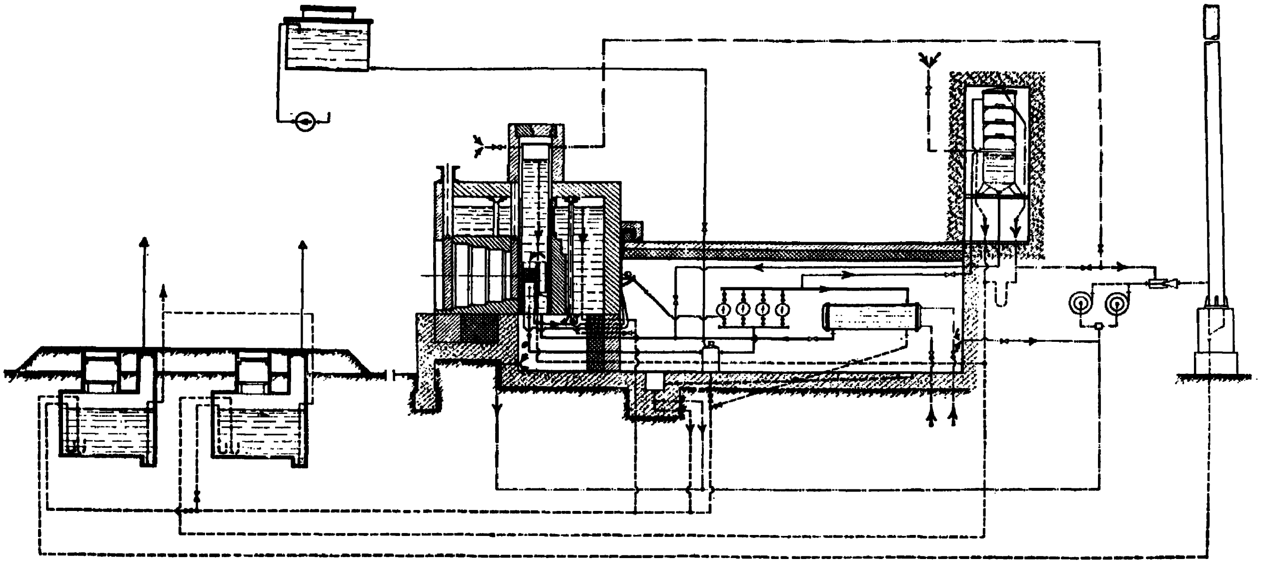

Figure 11. Flow diagram of the reactor

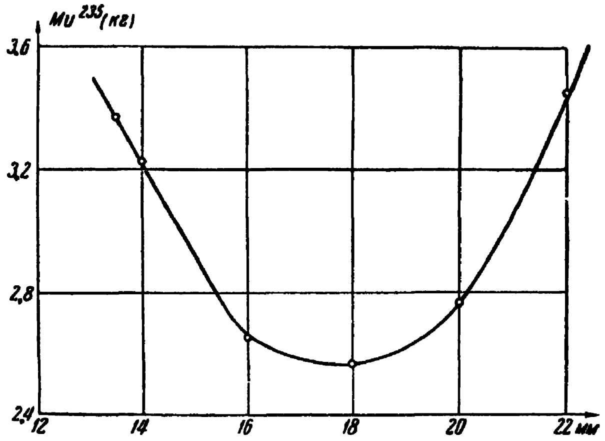

Figure 12. Dependence of the critical fuel loading on the lattice spacing

are done. During this operation a photoneutron source is introduced into the core.

Unloading of units from the reactor and their transportation to the storage is accomplished with the aid of a special lead container.

REACTOR MAIN PHYSICAL PARAMETERS

The study of the physical parameters of the reactor was carried out during its design, construction and initial operation.

At first all the principal parameters (critical uranium loading, effect of control rods, etc.) were computed by the multi-group method. However, the experience in theoretical analysis of enriched-uranium, light-water, reactors, available by that time, indicated that calculations based on the multi-group method might in the present case lead to errors of the order of 30% in the critical mass and control rod effect values. To increase the precision of the computed values, detailed experiments were carried out with a zero energy model. In these experiments actual fuel elements were used.

Plotted in Fig. 12 is the experimental dependence of the critical uranium loading (expressed in U^{235} isotope) on lattice spacing obtained in experiments with the reactor model.

As seen from Fig. 12, the minimum critical uranium loading (2.6 kg) corresponding to the chosen fuel element design is achieved when the lattice spacing is 18 mm. This value of the lattice spacing was adopted for the reactor. The curve in Fig. 12 is valid when there are no structural materials in the core and in the reflector; the thickness of the water reflector is >15 cm and the form of the active core approaches a round cylinder.

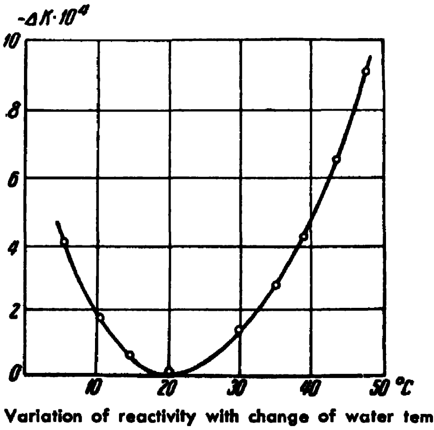

Figure 13. Variation of reactivity with change of water temperature

The introduction of structural materials into the core, the removal of a part of the side reflector and some deviations from the optimum form of the core have lead to an increase of the minimum critical uranium loading up to ~3.2 kg. In practice the uranium loading is ~3.5 kg. Consequently the mean thermal neutron flux in the reactor core is for instance $\sim 2 \times 10^{12}$ neutrons/cm²/sec at 300-kw power level.

The difference between the minimum and the actual uranium loading arises from the necessity of compensating for the changes in reactivity occurring during reactor operation.

As called for by the reactor design, the U^{235} depletion and the samarium poisoning are compensated in the course of reactor operation by adding appropriate numbers of fuel elements. The reactivity excess is needed only for overcoming the temperature effect, the xenon poisoning and the change in reactivity due to experiments.

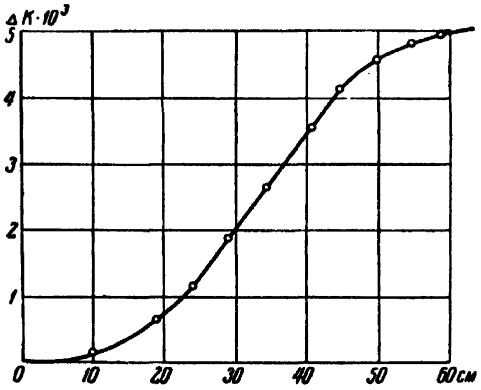

Figure 14. Reactivity compensated by an iron rod

The change in the reactivity as function of the water temperature in the core is shown in Fig. 13. Under operating conditions the water temperature in the core may fluctuate between 20 and 30°C; correspondingly the compensation of the temperature effect requires an excess in reactivity of $\Delta k \sim 0.001$.

The reactivity loss due to xenon poisoning in the reactor, as a rule, does not exceed the value $\Delta k \sim 0.02$. The possible change in reactivity due to the carrying out of experiments is less than $\Delta k \sim 0.01$.

To compensate the above-mentioned reactivity changes a reactivity excess $\Delta k \sim 0.03$ is available. The four control rods compensate together a reactivity excess $\Delta k \sim 0.04$. Figure 14 shows how the reactivity compensated by the iron rod depends on the depth the rod penetrates into the core. Together the three safety rods can compensate $\Delta k \sim 0.04$.

Figure 15 gives the macroscopic thermal and

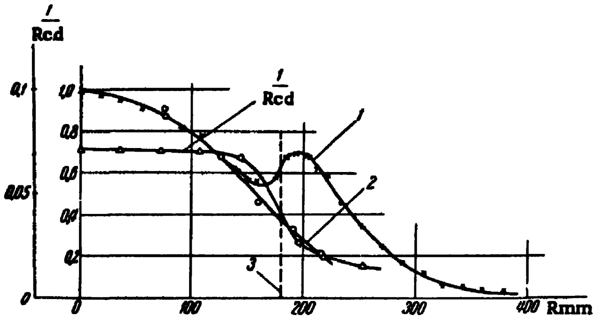

Figure 15. Thermal and resonance neutron distributions along the core radius: (1) thermal neutrons; (2) resonance neutrons; and (3) core boundary

resonance neutron density distribution along the radius of the core. The neutron density was measured by the activation method. As activation materials, copper was used for thermal neutrons, and indium, for resonance neutrons.

Figure 15 shows also the cadmium ratio for the Cu^{63} isotope measured in different points of the core and reflector. It is seen from Fig. 15 that the fraction of the epithermal region neutron captured by an absorber whose absorption cross-section obeys the $1/v$ law amounts to ~5%. Because of this, epithermal neutron induced fission can be in the first approximation neglected in calculations of the multiplication factor. Figure 16 represents the variation of the neutron density within a lattice cell as measured by the activation method.

The computed value of the multiplication factor in the lattice is $k_\infty = 1.56$.

It was assumed in the multiplication factor calculations, that the thermal neutrons in the core have a Maxwell spectrum with the neutron gas temperature exceeding that of the core by ~100°C. The computed value of the thermal utilization factor is $\theta = 0.81$.

The above-mentioned value of the neutron gas temperature in the core was obtained by comparison of neutron absorption in cadmium and boron. These substances were mounted in an air space in the center of the active core. Small deviations in the form of the neutron distributions from the Maxwell law affect but slightly the results of the calculation so they were not investigated.

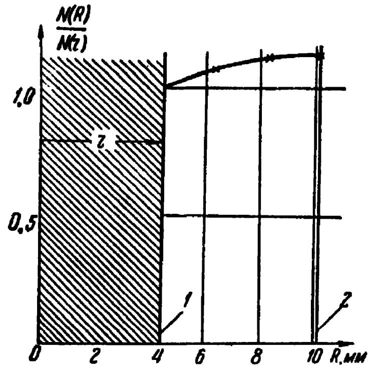

Figure 16. Thermal neutron distribution within a lattice cell: (1) fuel element boundary; and (2) effective cell radius

In a special series of experiments the fission-neutron age in a medium corresponding to the reactor core was measured. For the chosen lattice spacing and with the principal structural materials introduced, $\tau = 40$ cm^2.

The calculated value of the thermal neutron diffusion length in the core is $L \sim 1.5$ cm. The unimportance of the value L^2 as compared with the age ($\tau/L^2 \approx 26$) which is characteristic of all light-water reactors results in a very "hard" energy distribution of the neutrons leaving the core (in contrast to the case of graphite and heavy-water thermal reactors).

In the study of reactor shielding materials and in many neutron physics experiments the main interest lies precisely in the fast neutrons. This consideration was taken into account when the reactor was designed.

The reactor radiation shielding reduces the neutron and γ-ray flux leaving the core down to a value ≤ 0.01 of the tolerance dose.

A 2000-Kilowatt Thermal Power Nuclear Reactor for Research Purposes

By Y. G. Nikolaev, USSR

The project described in this paper is that of a thermal nuclear reactor designed for experimental purposes, and to be used in a wide variety of research in nuclear physics, radiochemistry and biology.

The neutrons are moderated by ordinary water, which is used as a coolant at the same time. Uranium enriched up to 10% is used as fissionable material.

For experimental work in the field of nuclear physics, radiochemistry and biology and for the production of radioactive isotopes, the reactor is provided with horizontal and vertical experimental holes and with a thermal column. The project provides for the construction of special cells equipped with manipulators necessary for work with radioactive substances.

The basic drawings of the reactor project are attached to this paper and it gives a list of some of the experiments for which the reactor may be used.

The reactor project was designed on the basis of experience gained in construction and operating the reactor described in P/621. That paper contains in detail the characteristics of the reactor as acquired by tests on a zero energy model and later on the reactor.

The reactor, according to the project, is designed to have a power of 2000 kilowatts. The operating loading of uranium-235 will be equal to 4.5 kg. The maximum and average neutron fluxes in the reactor core are equal to 2×10^{13} thermal neutron/cm^2-sec and $\sim 1 \times 10^{13}$ thermal neutron/cm^2-sec, respectively.

DESCRIPTION OF THE REACTOR CONSTRUCTION

Figure 1 shows the reactor core construction. To facilitate loading and unloading, the core is composed of 52 units. Most of them contain 16 fuel elements each. Nine units contain 15 fuel elements each, and have tubes for the insertion of control and safety rods. In the lower and upper parts of the core these units are fixed by means of the guide lattices.

The fuel elements are rods coated with aluminium tubes with an outside diameter of 10 millimetres. The working length of the fuel elements is 500 millimetres. They are placed vertically in the reactor core and form a square lattice with a spacing of ~17.5 millimetres.

As shown in Fig. 1 the vertical experimental holes, as well as the tubes for the insertion of ionization chambers, and the horizontal hollow cylinders forming the outer part of the horizontal experimental holes are situated in the water reflector of the reactor.

It is possible to remove and replace the horizontal cylinders in case they develop leaks. The reflector space may also be used for other purposes, as for instance mounting of additional vertical holes, etc.

Horizontal and vertical sections through the reactor are shown in Figs. 2 and 3. The reactor core, as indicated in Fig. 2, is enclosed within an aluminium tank filled with water. The shielding against radiation consists of layers of cast iron, water and concrete. The position of these separate layers of shielding is indicated in Figs. 2 and 3. A layer of water surrounding the core protects operating personnel from radiation during loading, unloading and repair works in the central part.

As was mentioned above, the reactor is provided with horizontal and vertical holes for experimental purposes, and with a thermal column, to allow research in the fields of nuclear physics, radiochemistry and biology, and to produce radioactive isotopes.

The horizontal holes are provided with turning shielding gates, handled by remote control.

The reactor core is separated from the thermal column by a bismuth shield for the attenuation of γ-rays. The unloading of units from the reactor core and their transfer to storage is done in a special lead container.

In the reactor building are cells for working with radioactive substances by means of manipulators.

Figure 4 shows the reactor flow diagram. Heat generated in the core and carried away by water circulating in the primary closed circuit is transferred in the heat exchanger to water flowing in the secondary circuit. The flow of water is indicated by arrows (see Fig. 4). The explosive gas that is generated in the

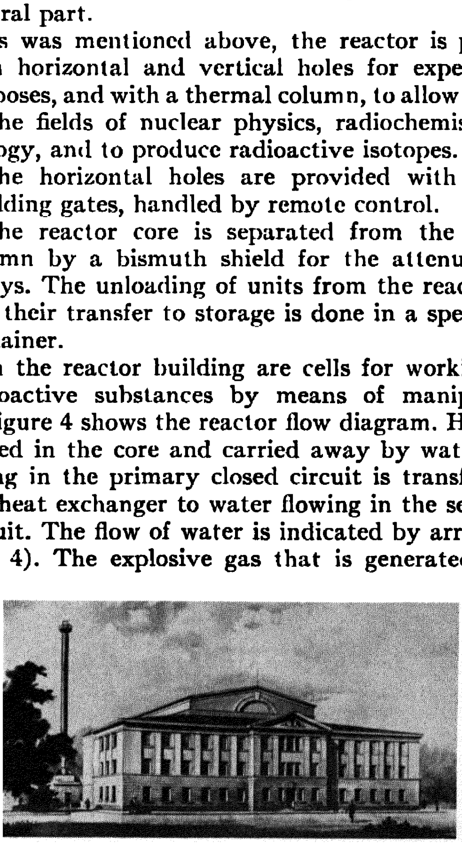

Front view of the building housing reactor

Original language: Russian.

water during reactor operation is removed in the de-aerator.

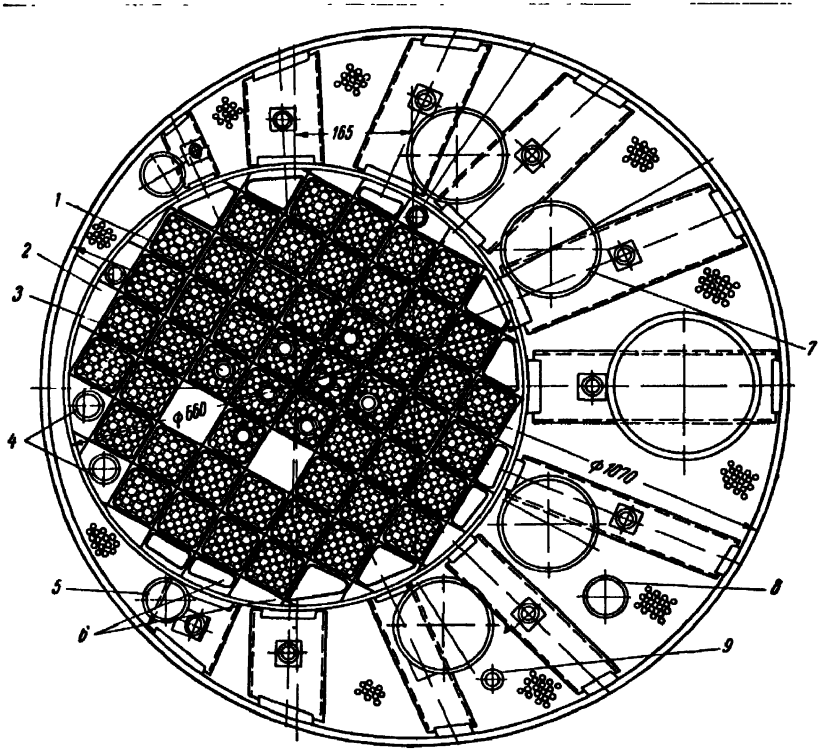

Figure 1. Reactor active core: (1) lattice; (2) supporting plate, (3) safety and control rods; (4) experimental holes; (5) channel for the starting ionization chamber; (6) plugs; (7) channel for the working ionization chamber; (8) overflow pipe; and (9) level indicator channel

The basic operating parameters of the reactor for a power of 2000 kilowatts are given below:

1. Flow of water in the primary circuit: 900 m^3 per hour.
2. Flow of water in the secondary circuit: 250 m^3 per hour.
3. Average water temperature in the active core: 35°C.
4. Maximum rate of heat transfer through the surface of fuel elements 3.8×10^5 kcal/m^2 per hour.
5. Maximum surface temperature of fuel element: 90°.

Radioactive gases and steam are pumped out through the reactor ventilation system from every volume where they accumulate. Air mixed with radioactive gases and steam is ejected into a ventilation stack. Water containing radioactive admixtures goes to holding tanks. If necessary it is afterwards purified in the adsorption installation.

The power level of the reactor is controlled by means of six ionization chambers. Two "starting" chambers are filled with BF$_3$ gas and are used for the start-up procedure or when the reactor is at low power level. Four "working" chambers have a coat of boron carbide on the electrodes and are used when the reactor is operated at high power levels.

Reactor control is effected by means of nine rods, eight of which are of boron carbide and one of steel. Three boron rods are used as safety rods, and with their aid the reactor may be stopped quickly. Five other boron rods compensate for reactivity reserve that is necessary if the reactor is to work for a prolonged time at a high power level. The steel rod is used to keep the power at a given level.

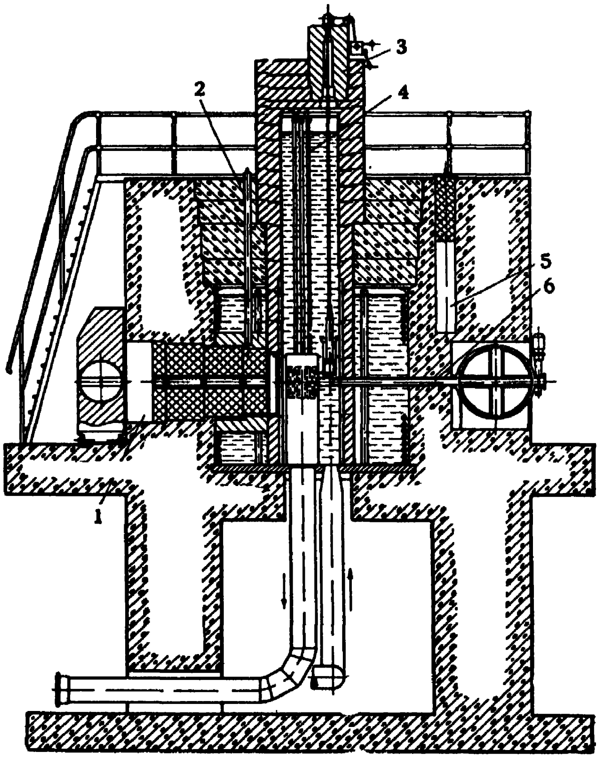

Figure 2. Vertical section of the reactor: (1) thermal column; (2) vertical hole; (3) lead container; (4) control rod tubes; (5) biological hole; and (6) horizontal hole

SOME EXPERIMENTS THAT CAN BE PERFORMED WITH THE REACTOR

1. Measurements of cross sections of nuclei for interaction with monochromatic neutrons. This can be made by means of mechanical selectors of resonance and thermal neutrons and with neutron monochromators of various types (either crystal or mechanical). Appropriate apparatus may be installated at the reactor horizontal holes.
2. Neutron optics investigations (experiments with mirrors and polarized neutrons) may also be made at the horizontal holes of the reactor.
3. Studies with the aid of magnetic and scintillation spectrometers of neutron capture γ-rays.
4. Research work that requires a powerful beam of fission neutron. A hole, where thermal neutrons may be converted into fast neutrons, has been reserved for this kind of work.

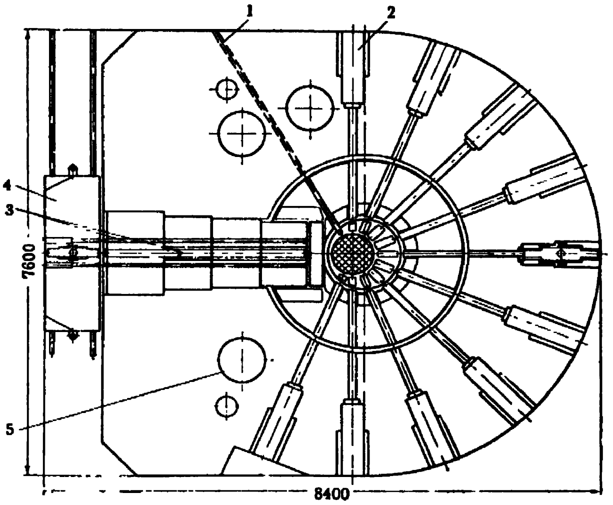

Figure 3. Horizontal section through the reactor: (1) experimental hole (curved); (2) horizontal hole; (3) thermal column holes; (4) thermal column shielding; (5) storage for radioactive materials

5. Neutronographic research in which neutron beams are applied for the study of the structure of substances. The equipment for such studies may be installed at a horizontal beam hole.

6. Measurement of the neutron characteristic of a substance (diffusion and slowing down lengths), measurement of the effective number of neutrons generated in the process of fission, of the resonance integrals and cross sections of various elements and isotopes. For these measurements, made usually in a prism, either one of the beams or the reactor thermal column may be also used.

7. Short intensive irradiations of samples with the purpose of studying radioactive isotopes with short half-life. Such work may be carried out in the special curved channel with pneumatic operation.

8. Irradiation of various materials to study its effect on their properties.

9. Production of radioactive isotopes that may be used in various fields of science and engineering. Vertical holes can be used for the last two problems. If necessary samples can be cooled during irradiation.

10. Studies of irradiation effects on living organisms. A vertical hole of large diameter, located in the reactor shielding, may be used for this purpose.

The maximum intensity of the total flux of neutrons at the outer end of the experimental holes will be equal to $0.5–1 \times 10^9$ neutrons/cm^2-sec.

The intensity of the neutrons in the thermal column hole may be increased several times by placing the measuring equipment nearer to the core of the reactor.

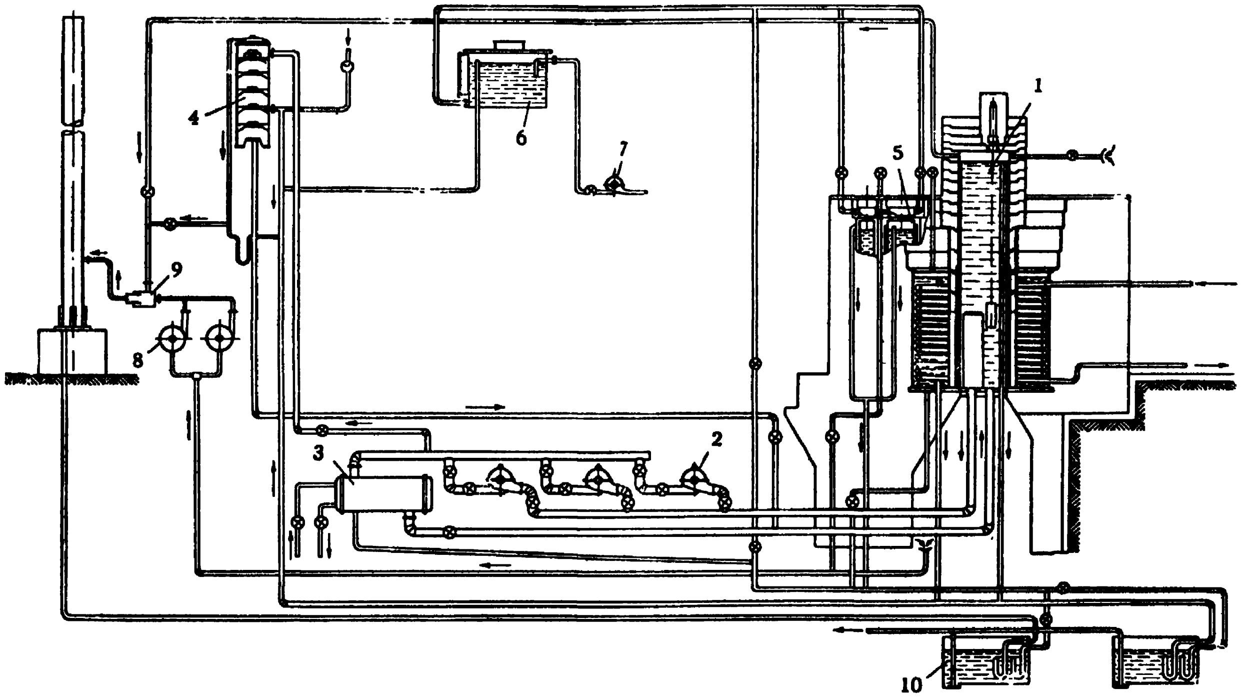

Figure 4. Reactor flow diagram: (1) reactor; (2) centrifugal pump; (3) heat exchanger; (4) de-aerator; (5) storage; (6) water tank; (7) pump; (8) ventilator; (9) air ejector; (10) holding tank

The Materials Testing Reactor and Related Research Reactors

By Alvin M. Weinberg, Thomas E. Cole,* and Marvin M. Mann,† USA

This paper will be concerned with H_2O-moderated and cooled, enriched research reactors with plate-type fuel elements. Such reactors have been called MTR-type reactors after their prototype, the Materials Testing Reactor, which has operated since March 31, 1952. At least four MTR-type reactors in various power ranges from 10 kw to 30,000 kw have been built by the US, and many others are under design or construction. These are summarized in Table I.

It will be our purpose to discuss the basic design principles and problems of MTR-type reactors. For a general engineering description of the reactor the reader is referred to an article by J. R. Huffman.[1] Included in the discussion will be some consideration of the usefulness of 20% enriched uranium in MTR plate-type reactors.

BASIC DESIGN PRINCIPLES

As nuclear technology matures, its central problems pass from nuclear physics to questions of metallurgy and chemistry. This is natural in a thermodynamic technology: the central issue is not how to ignite the nuclear fire but rather how to maintain the integrity of the system under extreme conditions of temperature and radiation. The extensive testing of materials under radiation which a power development would involve quickly led to the realization at Oak Ridge National Laboratory in 1945 that a neutron source in which both fast and slow fluxes were maximal would be required. The Materials Testing Reactor was built to meet this need.

The MTR was designed and built as a joint enterprise of the Oak Ridge and Argonne National Laboratories. Located at the National Reactor Testing Station in Arco, Idaho, it is operated by the Atomic Energy Division of the Phillips Petroleum Company. The detailed architect-engineering was done by the Chemical Plants Division of the Blaw-Knox Construction Company, and the construction contractor was the Fluor Corporation.

The underlying aim of the MTR design was to achieve as high fast (>1 Mev) and slow neutron flux as possible. The availability of enriched fuel in the United States made it possible to aim at flux levels about an order of magnitude higher than would have been possible with unenriched uranium. The enriched reactors are small, which means that power per unit volume (or volume specific power) could be made very high; and, because there is much "spare k" in such systems, the fuel can be dispersed very finely which means that power per unit mass of fuel (or fuel specific power) could also be made very high.

Both specific powers—volume and fuel—must be maximized in order to maximize simultaneously both the fast and the slow flux. Since power output is proportional to fission rate,

$$P \sim M\sigma_f\phi_t$$

where P = total power, M = mass of U^{235}, σ_f = slow neutron fission cross section, ϕ_t = thermal flux,

$$\phi_t \sim P/M \tag{1}$$

which shows that the slow neutron flux is proportional to the power output per kilogram of U^{235}.

Thus to achieve maximum thermal flux it is necessary to maximize the heat transfer from each gram of uranium fuel; that is, to provide as much heat transfer surface as possible to each atom of U^{235}. In MTR-type reactors this is done by disposing the fuel in parallel aluminum plates and cooling each surface vigorously with a stream of rapidly flowing water. The extreme dilution of the fuel is made possible because the fuel is enriched, and so relatively large amounts of diluent can be tolerated without reducing the multiplication constant too much. The specific heat transfer area in the MTR, 100 cm²/gm U^{235}, is about 13 times higher than the specific heat transfer area in an unenriched reactor like NRX at Chalk River, Canada, with 1.73 cm radius, unenriched uranium rods. This is basically the reason for the order of magnitude thermal flux advantage in the MTR-type reactor.

The fast neutron flux is of two kinds: the virgin or uncollided flux, ϕ_v, and the moderated fast flux, ϕ_m. This latter flux has a dE/E spectrum, while the uncollided flux has the fission neutron energy distribution. For radiation damage experiments in non-fissionable materials it is the very fast ϕ_v which is important; for experiments with neutron time-of-flight spectrometers it is the dE/E flux, ϕ_m, which is most needed.

Both ϕ_v and ϕ_m are proportional to the volume specific power: for the number of neutrons produced per cm³, q, is proportional to P/V where V is the reactor volume, and the virgin flux, ϕ_v, is

$$\phi_v = \frac{q}{\Sigma_0} \sim \frac{1}{\Sigma_0}\frac{P}{V} \tag{2}$$

---

* Oak Ridge National Laboratory.

† Savannah River Plant.

while the moderated fast flux per unit energy interval is

$$\phi_m(E) = \frac{q}{\Sigma_s \xi E} \sim \frac{1}{\Sigma_s \xi E} P/V \tag{3}$$

In these equations Σ_0 is the macroscopic total cross section for fission neutron energy, and $\Sigma_s \xi$ is the slowing down power at energy E.

Equations 1, 2, and 3 show that to achieve a maximal fast and slow flux it is necessary to maximize both P/M, the fuel specific power and P/V, the volume specific power.

In the early design of the MTR it was proposed that the fuel elements be cooled by H_2O, and arranged in a lattice with space between the lattice elements filled with heavy water. Since the fuel specific power is independent of the lattice pitch, such a "diluted reactor" would have the same slow flux as MTR. However, as pointed out by E. P. Wigner, the volume specific power in such a reactor is lower than in the MTR, and therefore the dilution entails a severe loss in fast flux. This was the main reason for "squeezing the heavy water" out of the original MTR design and using H_2O as both coolant and moderator.

The small size of the MTR, required to get high fast flux, makes it difficult to perform many experiments directly in the lattice. However, the "infinite" multiplication constant of the MTR is so high, about 1.6, that at 30 Mw there are available, for experiments *outside* the reactor core, as many neutrons as in a graphite reactor ($k \sim 1.04$) operating at 300 Mw. This point is sometimes overlooked—the fuel region of the MTR has a volume of only about 100 liters—but in the inner beryllium reflector and the outer graphite reflector there are about 4000 liters of space at an average thermal flux above 10^{13} neutrons per cm^2 per second, and about 20,000 liters of space at an average thermal flux above 10^{12} neutrons per cm^2 per second.

PROBLEMS IN DESIGN OF MTR

General Description

How the dual requirements of high fuel specific power and high volume specific power were met in the MTR may be seen from the accompanying diagram of the internal lattice (Fig. 1). The uranium is disposed in parallel aluminum plates, 20 mg of U^{235} per cm^2. Each plate is a sandwich with 0.5 mm U-Al alloy as the "meat" and 0.5 mm thick Al "bread" on either side. Eighteen parallel plates are assembled into a "fuel element" (Figs. 2 and 3); the 3 mm space between the plates is filled with the cooling and moderating H_2O. There is room in the active lattice for as many as 45 fuel elements in a 9 × 5 array; the positions not occupied by fuel are filled with Be metal reflector pieces. The fuel elements, stacked side by side, occupy a position 6.25 m below the top of a 9.1 m deep water well; coolant flow is downward through the fuel array and Be reflector at a rate of 1260 liters per second (310 liters per second through Be and 950 liters per second through fuel). A vertical section of the reactor is shown in Fig. 4.

The active lattice is surrounded by a closely fitting Be reflector which is pierced with holes through which flows water required for cooling the beryllium as seen in Fig. 5. Of the total power, 28,800 kw is generated in the fuel elements and 1200 in the beryllium. The entire assembly, active lattice and Be reflector, is contained in an aluminum tank which is pierced by numerous experimental ports. Outside the tank is a graphite reflector in which 10^{13} fluxes are available.

Shim control for the reactor is provided by eight Cd rods which enter the lattice from above. The rods have the same cross section as the fuel elements; the bottom portion of four of the rods is an active fuel element, and the bottom portion of each of the remaining rods is Be so that lifting a rod removes cadmium and inserts fuel or reflector. Regulating rods of cad-

Table I. MTR Type Reactors Built or Proposed

Reactor type	*Power*	*Maximum slow flux*	*Location*	
			Built	*Proposed*
Materials Testing Reactor	30,000 kw	4×10^{14} n/cm^2/sec	Arco, Idaho	
Oak Ridge Research Reactor	20,000 kw	2×10^{14} n/cm^2/sec	ORNL, Oak Ridge	Westinghouse
Low Intensity Testing Reactor	3,000 kw	4×10^{13}	ORNL, Oak Ridge	University of California Radiation Laboratory Los Alamos
Swimming Pool Reactor	10–1000 kw	2×10^{11}–2×10^{13}	ORNL, Oak Ridge Bulk Shielding Facility Geneva, UN Demonstration Pennsylvania State University	Battelle Memorial Institute American Machine and Foundry Naval Research Laboratory University of Michigan Washington State College Vanderbilt University Brookhaven Medical Center

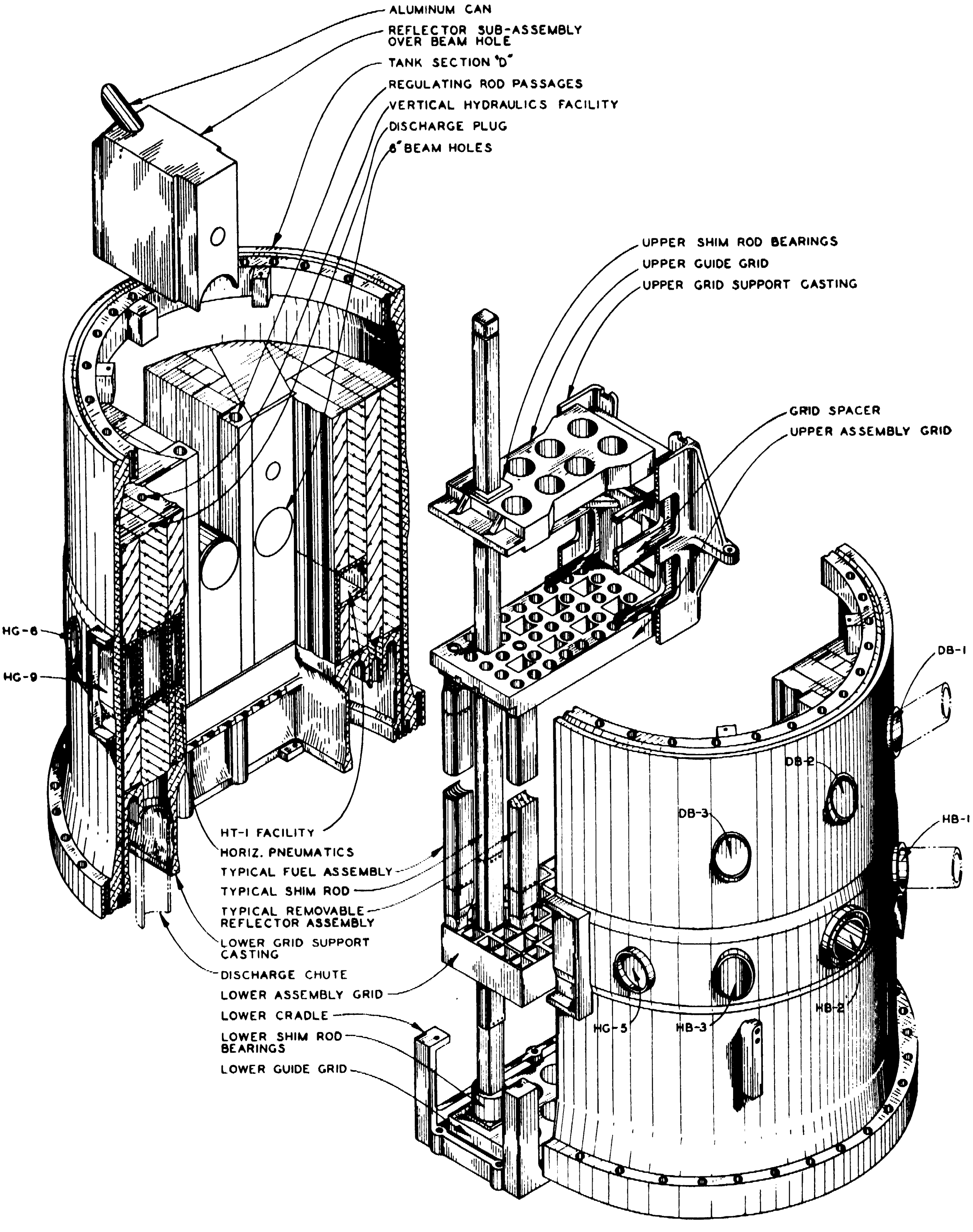

Figure 1. Pictorial cross section, reactor tank

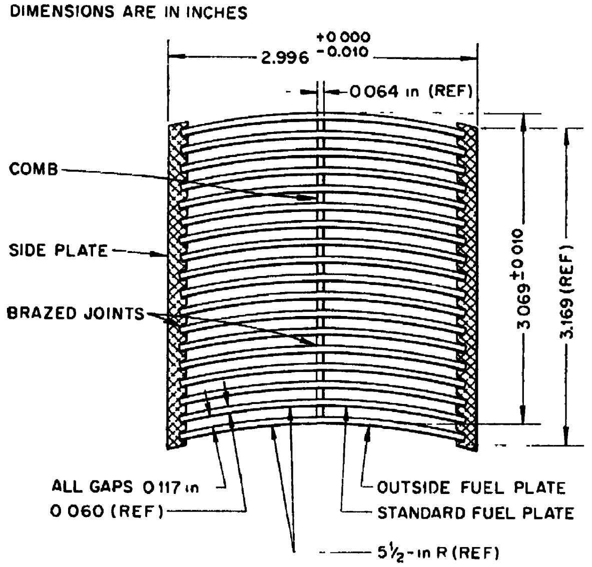

Figure 2. Cross section of MTR fuel assembly

mium are provided in the Be reflector for automatic control.

The nuclear composition of the MTR core is summarized in Table II.

Reactor Physics

Since the MTR was the first high-powered enriched reactor built, there were numerous questions centering around the criticality of the system. To settle these questions many critical calculations and experiments were done on mocked-up MTR-type lattices with various reflector arrangements.

Table II. Specifications of Active Portion of MTR

Volume aluminum/volume water	0.73
U^{235} concentration,* gm/liter	35.8
Active-plate thickness, cladding included, mm	1.5
Width × length of active portion of plates, cm	6.5 × 60
Thickness of uranium-aluminum alloy layer, mm	0.5
Thickness of cladding, each layer, mm	0.5
U^{235} in active plates, gm/cm²	0 020
Distance (gap) between active plates, mm	3
Number of plates per assembly	18
U^{235} per assembly, gm	140
Possible number of assemblies in reactor	37
Possible number of shim safety rods in reactor	8
Number of regulating-rod locations	4

* The U^{235} concentration in a portion of the reactor made up of normal fuel assemblies is actually 35.8 grams per liter. An over-all average U^{235} concentration of the reactor is smaller because of the presence of the shim safety rods. If all the shim safety rods were in the "in," or absorbing, position, the average U^{235} concentration of the active portion of the reactor would be about 29.2 grams per liter.

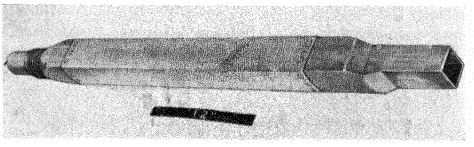

Figure 3. Typical MTR fuel element

All of the criticality calculations on the MTR were done by standard two- and three-group theory.[2] The success of such calculations, which are essentially schematic, depends on proper choice of constants, most particularly the fast transport mean free paths, λ_{tr}, in lattice and reflector. These were determined by the usual weighting formula

$$\lambda_{tr} = \frac{\int \frac{dE}{\xi \Sigma_{tr} \Sigma_s E}}{\int \frac{dE}{\xi \Sigma_s E}}$$

where Σ_{tr} and Σ_s are the macroscopic transport and scattering mean free paths, respectively.

The age which was used for the Al-H_2O mixtures was measured to In resonance energy by L. D. Roberts and T. E. Fitch,[3] and corrected by calculation to 0.025 ev as described by Nancy M. Dismuke and M. Ruth Arnette.[4] The results are shown in Fig. 6. The age calculated by the usual transport theory expression for the second moment in water mixtures is also shown in Fig. 6.

The nuclear constants which were finally chosen are summarized in Table III. They apply, of course, only to the MTR composition given in Table II.

Three series of critical experiments to check the calculated two-group critical masses were performed in 1946 and in 1948 under the general supervision of M. M. Mann and A. B. Martin. The experiments were performed with a variety of reflectors: H_2O, D_2O, Be, and unreflected. The critical masses of some representative arrays compared with calculated values are given in Table IV. The arrangement for D_2O and H_2O-reflected experiments is shown in Fig. 7.

The beryllium experiments were performed in the same tank, but Be was stacked in place of the D_2O (Figs. 8 and 9). The active lattice in the Be experi-

Table III. MTR Nuclear Constants, Two-Group Model

	Active portion	*Reflector* *2 % water–98 % Be*
Temperature	290°K	
Diffusion coefficient, thermal	0.269 cm	0.86 cm
Diffusion coefficient, epithermal	1.32 cm	0.64 cm
Age to thermal	64 cm²	91 cm²
Diffusion area	3.9 cm²	531 cm²
Total macroscopic cross section	0.070 cm⁻¹	0.00163 cm⁻¹
Total macroscopic cross section of U^{235}	0.054 cm⁻¹	
Multiplication constant, infinite media	1 612	

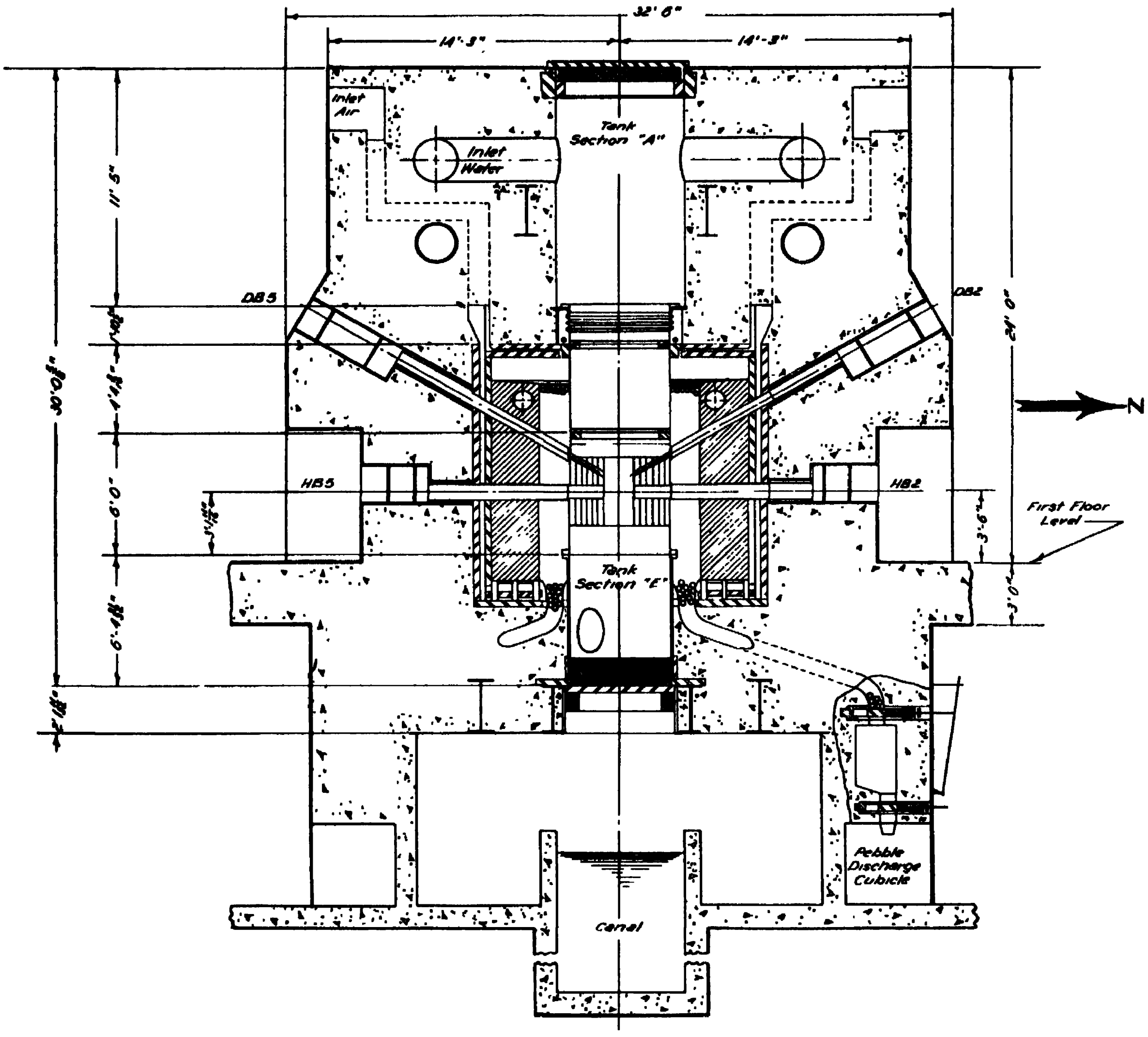

Figure 4. MTR north-south vertical section

ments was roughly square, while in the D_2O experiments it was cylindrical.

The physical data for the D_2O and H_2O reflector experiment were as follows: concentration of U^{235} = 35.6 grams/liter of reactor volume; height of active portion = 70 cm (no reflector, top and bottom).

The simple two-group calculations, as seen in Table IV, agree well with the observed critical masses. While at first sight this might appear surprising, considering the crudeness of the two-group approximation, it should be remembered that most of the neutrons leak into the reflector as fast neutrons, since τ/L^2 in the lattice is about 18. Hence if the ratio of fast mean free paths in reactor and reflector is properly adjusted, the leakage out of the reactor will be well reproduced, and the critical mass would be expected to be well estimated even by one-group theory.

Table IV. Critical Masses in Kilograms of U^{235}

Reflector	*Volume ratio Al/H_2O*	*Observed*		*Calculated, two-group*
		Gross	*Corrected for empty control rod ports, etc.*	
D_2O	0.88	2.48	2.40	2.64
D_2O	0.76	2.23	2.15	2.43
Be	0.76	1.54	1.42	1.54
H_2O	0.76	3.29	3.22	3.34
H_2O	0.66	2.82	2.72	3.04

Two points emerged immediately from these measurements: one, Be was the best reflector, being even better than D_2O; however, some of this advantage arises because the Be was stacked directly against the lattice with an Al tank separating the D_2O reflector from the core. Two, in all experiments with "good" reflectors the fundamental neutron mode is overwhelmed by the transients arising from the reflector. In all these cases there is a very steep rise in flux in the reflector, reaching as much as one and one-half times the average core neutron density in the case of a very narrow slab reactor reflected by Be. This is seen in Fig. 10 which gives the measured distribution in a typical Be-reflected assembly.

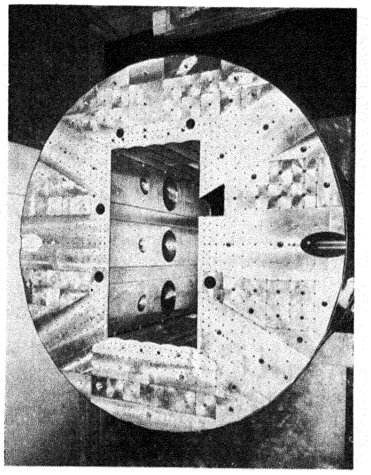

Figure 5. Beryllium assembly

Table V lists some observed flux ratios for two typical assemblies. Assembly No. 1 had a core 22.5 × 22.5 cm in cross section and 66 cm in height, containing 1.21 kg of U^{235} at a fuel concentration of about 40 grams of U per liter of reactor volume. The Al/H_2O volume ratio in the core was 0.65. The core was bare on top and bottom, but it was reflected by a minimum of 30 cm of Be on all sides. The minimum critical mass for the array described above was found to be 1.07 kg. The lateral measurement was made along a perpendicular bisector of the side of this reactor; a measurement also was made along a diagonal.

Assembly No. 2 had a core 11 cm × 51 cm in cross section, containing 1.35 kg. The height of the reactor, reflector thickness, fuel concentration, and the Al/H_2O volume ratio in the core were the same as for the square assembly. The minimum critical mass of this thin-slab assembly was found to be 1.28 kg.

The ratio of the peak thermal neutron flux to the thermal neutron flux at the center is an indication of the maximum slow neutron flux, for a given operating level, which the assembly will provide for experimental purposes. The ratio of the thermal neutron flux at the edge of the core to that at the center is a measure of the maximum heat production per unit volume to be expected in the core. The extent to which the thermal neutron flux holds up in the reflector is of interest in planning experiments which will make use of this flux.

Table V. Relation between Thermal Neutron Flux ϕ_{th} at Certain Horizontal Midplane Locations in the Reactor and That at Center of Core

Assembly no.	$\frac{\phi_{th}\ (peak)}{\phi_{th}\ (center)}$	$\frac{\phi_{th}\ (edge)}{\phi_{th}\ (center)}$	*Position in reflector at which ϕ_{th} falls to center value, measured in cm*	
			From center of core	*From edge of core*
1 (lateral)	1.32	1.19	26.5	15
1 (diagonal)	1.16	1.13	25	9
2 (lateral)	1.42	1.24	22	16.5
2 (longitudinal)	0.90	0.85		

The first critical experiments were performed with clean geometry; i.e., the reflector was unpierced by holes and the lattice was a regular geometric figure. Since actual research reactors have control rods, experimental holes, etc., it was necessary to measure the effect of such perturbations on the reactivity of the reactor. This was done in later experiments by maintaining the unperturbed reactor critical with uniformly distributed gold or silver wires of known absorption cross section. After the holes or control rods are in place, as shown in Fig. 11, the reactor is sub-critical unless an amount of poison, $\Delta\Sigma$, is removed. The equivalent reactivity loss entailed by the perturbation is then very nearly

$$\frac{\Delta k}{k} = \frac{\Delta\Sigma_a}{\Sigma_R'}$$

where Σ_R is the total absorption cross section of the reactor, having the smaller cross section, and k in the denominator is the multiplication constant after the perturbation is introduced. Equivalent reactivity losses reported in subsequent tables were measured in this way.

In the MTR reflector there are numerous very large holes (15 cm in diameter), and it was necessary to determine how much loss in reactivity was caused by these holes. The loss of reactivity (measured in equivalent $\Delta k/k$) found in these experiments is given in Table VI.

Table VI. Effect of Experimental Holes in the MTR Critical Assemblies

Assembly no.	3	5	6
Reactor dimensions (cm)	71 × 11 × 66	71 × 17 × 66	71 × 22.5 × 66
Critical mass (kg)	1.94	2.94	3.95
Σ_R (cm²)	4118	6240	8384
Poison, Σ, (cm²)	303	1140	1848
Total Σ (cm²)	4421	7380	10,232

Effect of the Holes in $\Delta k/k$ (%) where k is the k of the Reactor with solid Reflector

Holes extending to reactor-reflector interface			
6-in. hole on edge	1.17	0.75	0.49
6-in. hole in center	2.20		0.86
8-in. hole in center	4.80	2.84	1.71
Holes beginning 15 cm from reactor			
6-in. hole on edge	0.17	0.12	0.08
6-in. hole in center	0.34		0.13
8-in. hole in center	0.68	0.40	0.22
Holes extending to reactor, water-filled			
6-in. hole on edge	0.90	0.65	0.42
6-in. hole in center			0.84
8-in. hole in center	3.88	2.45	1.53
Holes beginning 15 cm from reactor, water-filled			
6-in. hole on edge		0.08	0.06
6-in. hole in center	0.24		0.06
8-in. hole in center	0.37	0.23	0.11

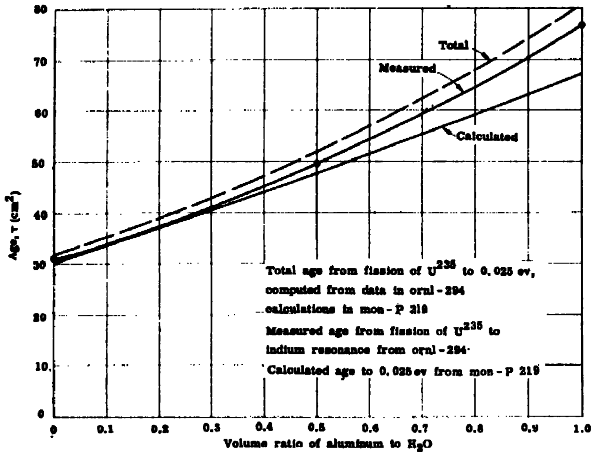

Figure 6. Age, τ fission neutrons in H_2O-Al mixtures

A more important effect of holes is that the neutron flux is lowered in them. An example of this is seen in Fig. 12. For these experiments the Be reflector was surrounded by a 30 cm graphite layer to simulate the outer graphite reflector of the MTR.

Control Rod Effectiveness

A number of experiments were carried out to study the effectiveness of control rods of various sizes in the four kg mock-up of the MTR. They were performed in the following way: the uniform poison in the "clean" core (before the control rod is inserted) is adjusted until the assembly is just critical. The control rod is inserted and the amount of uniformly distributed poison in the core is reduced until the assembly is just critical. When the experiment involves no change in the amount of concentration of fuel in the core, the percentage change in k, i.e., $\Delta k/k$, is given simply by $\Delta\Sigma/\Sigma_R$ where $\Delta\Sigma$ is the change in uniform poison and Σ_R is the total cross section of the active portion of the core after the rod is inserted. In experiments which entail the removal of fuel *and* the insertion of a control rod the k of the clean core, k_1, is calculated, the k of the active portion of the core after insertion of the rod, k_2, is calculated, and $\Delta k/k$ is then given directly by $(k_1 - k_2)/k_2$.

The Cd control rods tested in these experiments were essentially replicas of those designed for the MTR insofar as dimensions and composition are concerned. They were in the form of hollow cylinders of square 8¼ cm × 8¼ cm cross section, 66 cm long, and were filled with water to duplicate the conditions that would be found in the MTR.

For use in the MTR it was planned for these rods to be attached at one end of the fuel assemblies so that as a rod was withdrawn fuel was inserted in its place and vice versa. Therefore the measurement of interest was the effect of the rod versus fuel in the same position. The percentage changes in reactivity of the active portion of the core when these rods were inserted in place of fuel in the locations indicated in Fig. 13 are shown in Table VII.

Table VII

Rod	$\Delta k/k$ (%)
Cd at *A*	7.3
Cd at *A* and *B*	20.7

It was also observed that the reactivity change due to the removal of 180 grams of fuel from a central position such as *A* amounted to about 3%.

At first glance a comparison of the effect of a single rod at *A* with the effect of rods at both *A* and *B* indicates that the effect of a rod at *B* (a position of

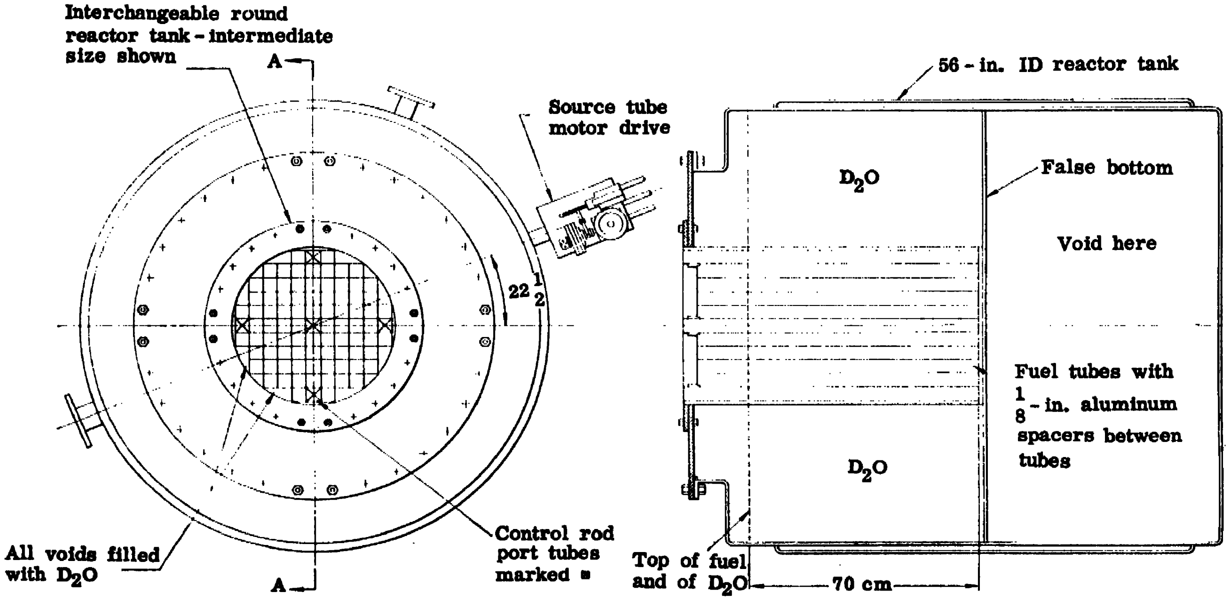
Interchangeable round reactor tank - intermediate size shown
A
Source tube motor drive
22½
All voids filled with D₂O
A
Control rod port tubes marked ■
56 - in. ID reactor tank
D₂O
False bottom
Void here
Fuel tubes with ⅛ - in. aluminum spacers between tubes
D₂O
Top of fuel and of D₂O
70 cm

Plan

Section A - A

Figure 7. Assembly for D_2O reflector

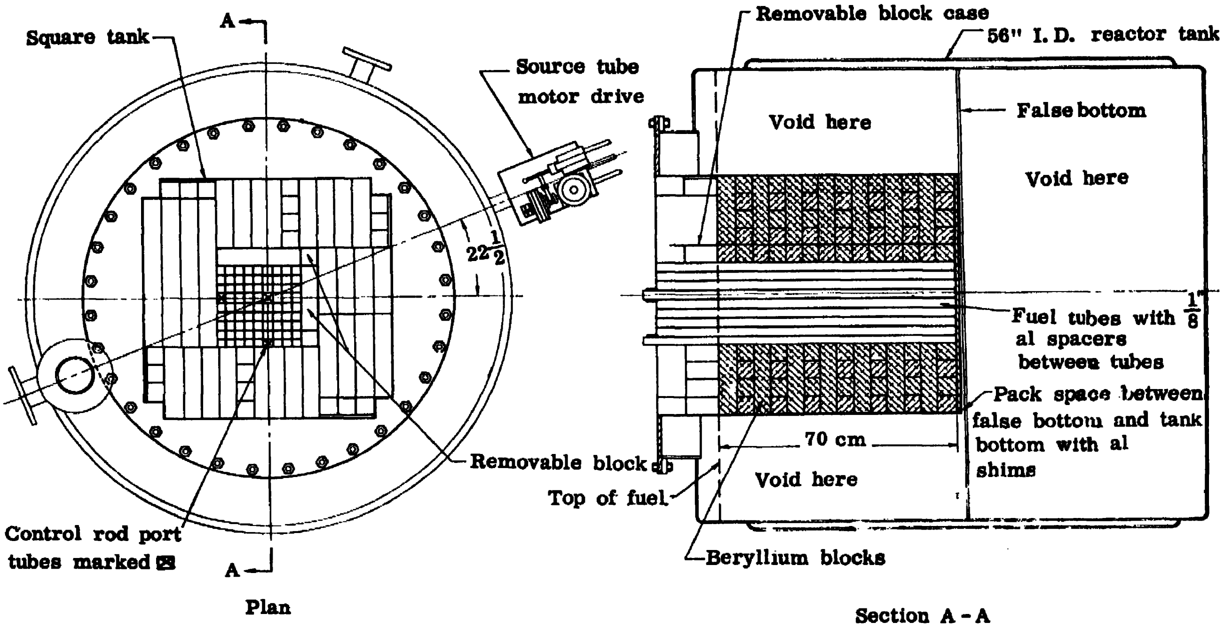

Figure 8. Assembly for beryllium reflector

relatively low statistical weight) is greater than the effect of a similar rod at *A* (a position of relatively higher statistical weight). It is apparent, however, that this anomaly comes about as a result of the change in neutron flux distribution caused by the introduction of the first rod at *A*. The neutron flux is depressed in this region and the statistical weight distribution in the core is shifted in such a way that the maximum is now in the vicinity of position *B*. Hence it is true that the second control rod, introduced at *B*, has a greater effect on the asymmetrical core than the control rod at *A* has on the clean pile.

Temperature Coefficient

Increase in water temperature of the MTR has two important effects: one, the ratio of U to H_2O is increased because the water expands and is ejected. This tends to increase the thermal utilization and the leakage. Of the two, leakage is the more important and imposes an over-all negative temperature coefficient on the MTR.

Two, the thermal diffusion length is increased, in addition to the afore-mentioned density effect, because both the absorption cross section and the proton scattering cross section decrease with increase in neutron temperature. This also contributes to the negative temperature coefficient. The over-all temperature coefficient, for uniform heating, as measured in the LITR, was found to be -0.013% $\Delta k/k$ per °C at water temperatures between 36°C and 54°C.

Gamma-Ray Heating

Another important practical question which is common to all highly enriched, high-powered reactors is the determination of the heat production due to gamma-rays and neutrons in the reflector. This is difficult to calculate because the gamma-ray sources are never known in detail, and the geometry is usually too complicated to allow a reliable calculation to be made. For this reason a method had to be used which allowed the heat production rate in the reflector to be measured, although the total power of the critical assembly was kept at a watt.

The method is based on application of the Bragg-Gray principle. The ion current produced in small ion chambers (filled with CO_2 or He rather than air so there would be no recoil protons from $N(n,p)$ reactions) was measured in the reflector. The power production in the medium in which the chamber is immersed is simply obtained by measuring the ion current, calculating the energy loss per unit volume in the chamber, and multiplying by the ratio of stopping power of reflector material and ion chamber gas. This method is the same one used originally by L. H. Gray to measure the total gamma energy emitted per second by radioactive substances, and it was used with great success in the MTR design. For example, it was found in this way that the heat production at the Be-graphite interface outside the reactor tank was about 1.0 watt per cm^3 of graphite for a reactor power level of 30 Mw.

Shielding

The MTR was the first chain reactor to rely heavily on water as a shield; the reactor core is located near the bottom of a deep well filled with water. To verify the adequacy of water as a shield measurements of the gamma-ray and neutron attenuation in the water were performed on the Low Intensity Test Reactor (LITR) which is a low-powered replica of the MTR. The thermal neutron attenuation above the lattice, measured with indium foils, is shown in Fig. 14; the measured gamma-ray attenuation is shown in Fig. 15.

The bottom of the top plug is 5.95 m above the lattice center line. As seen in Fig. 15, at this point the gamma-ray dose is about 2×10^{-3} mr/hr when the reactor runs at 270 watts. At full power, 30,000 kw, the gamma-ray dose would be about 220 mr/hr, compared with the 40-hour per week tolerance of 7.5 mr/hr; this necessitates incorporation of additional lead shielding in the top plug.

The neutron attenuation by the water, on the other hand, is much more than ample. At 30×10^3 kw the central slow neutron flux is about 3.5×10^{14}; the slow neutron tolerance is 1750 neutrons/centimeter^2/second for a 40-hour week so that an attenuation of 2×10^{11} is required. As seen in Fig. 14, this attenuation is achieved in about 300 cm.

Control

The requirement of very large available excess reactivity coupled with a relatively short generation time, encountered for the first time in the design of the MTR control system, led to considerable effort to establish criteria and develop instruments for the control of reactors capable of very short periods. This work was carried out at Oak Ridge National Laboratory under the direction of H. W. Newson during 1946 and 1947; and the results still serve as a basis for control design, although more detailed work has subsequently been done at ORNL as well as at several other locations.

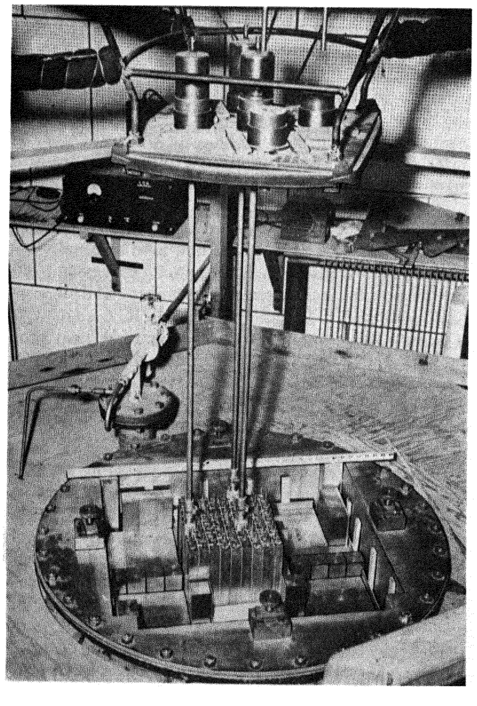

Figure 9. Reactor assembly; beryllium reflector

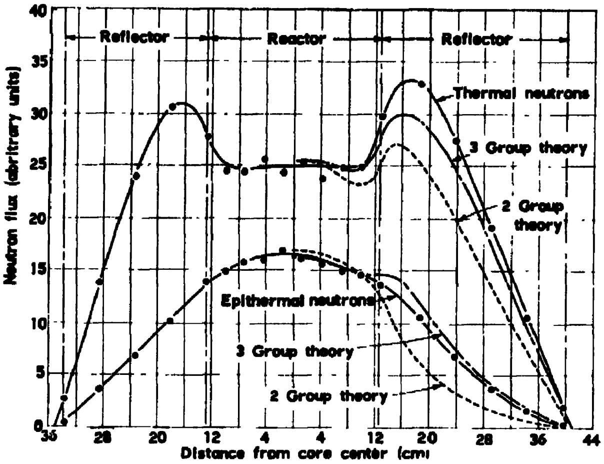

Figure 10. Radial neutron distributions: beryllium reflector

Table VIII lists MTR reactivity requirements.

As can be seen from Table VIII the control rods must be capable of controlling 30 40% in reactivity if a reasonable margin of safety is to be provided for possible overloading of fuel and changes in experiments.

In the case of a complete shutdown following steady operation of the MTR, Xe^{135} poisoning reduces reactivity initially at a rate of about 9% per hour; a maximum reduction of 39% is reached about 10 hours after shutdown. It was not considered practicable to provide sufficient excess reactivity to override the peak poisoning and therefore it is necessary that startup time be held to a minimum following an accidental or short shutdown. The buildup and decay of Xe in addition to the sensitivity of the small highly enriched reactor to changes in and near the core leads to a situation where the position of the control rods for criticality varies over a wide range. The above factors requiring short startup time with variable rod position for criticality led to the conclusion that safety analysis should be based on the rate of rod withdrawal; i.e., on rate of change of *k*, rather than on rod position.

Knowing the time response of the safety system from ion chamber to control rod and the tolerance of the reactor for temporary overloads, one can calculate a rate of change of *k* (rod speed) which will not damage the reactor if startup is made by withdrawing all control rods at their maximum rate. The MTR rod drive mechanism is designed so that a maximum rate of

Table VIII. Minimum Excess Reactivity Built into the MTR

Source of reactivity loss	*Amount* $\Delta k/k$ *(%)*
$Xe^{135} + Sm^{149}$ (steady-state)	4.9
Xe^{135} ½ hour override	4.7
Fuel depletion + low cross-section fission products	7.0
Temperature	0.8
Others (experiments, beam holes, etc.)	1.5
Total	18.9

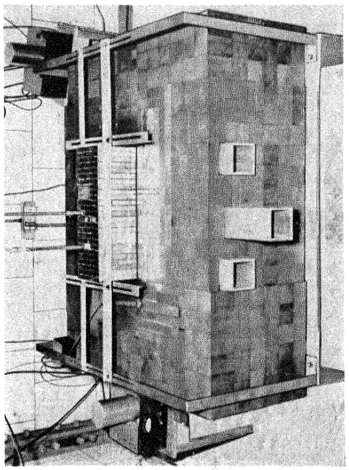

Figure 11. Critical assembly: simulated MTR structure

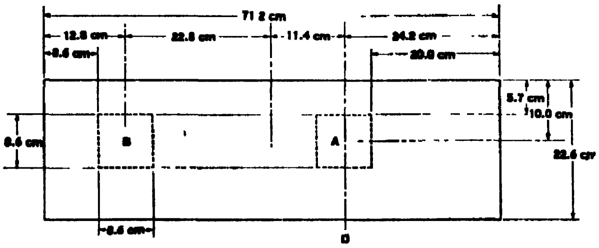

Figure 13. Test positions of large Cd rods in the core of the 4-kg mockup assembly

change of about 0.1% $\Delta k/k$ per second is the maximum for all rods withdrawing simultaneously. This rate allows complete withdrawal of the rods in six minutes and could lead to a reactor period no faster than about $\frac{1}{30}$ second as the reactor reaches the safety trip level. The response time of the MTR safety system is sufficiently fast to protect the reactor from damage under this situation. This fast rate of rod withdrawal is not normally available unless the reactor power level is at least 300 watts and therefore in a range where period-measuring instruments can reliably exert some control. The fast rate is available, however, when a rapid restart is necessary following an accidental or short shutdown as the power level in the Be-reflected MTR does not decay below 300 watts for a number of hours following shutdown. Startup after shutdown of long duration is more leisurely, as the problem of overriding Xe is not present and in general the requirements of the experimentalists is such as to make a slow startup desirable in any case.

In a reactor with characteristic high excess reactivity and relatively short generation time (4×10^{-5} to 2×10^{-4} seconds) it is asserted that provision must be made to monitor the flux level at all times. In a highly enriched reactor spontaneous fission from U^{238} does not contribute sufficient neutrons to allow easy reliable detection of the flux level under shutdown conditions, and therefore it is necessary to include a radium-beryllium or similar source to bring the flux to a readable level. In the MTR a piece of natural antimony was built into the Be reflector. After initial operation of the reactor this serves as a gamma source which, with the Be, provides a sufficient neutron source due to the photoneutron effect. Pulse-type fission chambers are used as detectors at these low levels primarily because of their high discrimination against the gamma background from previous

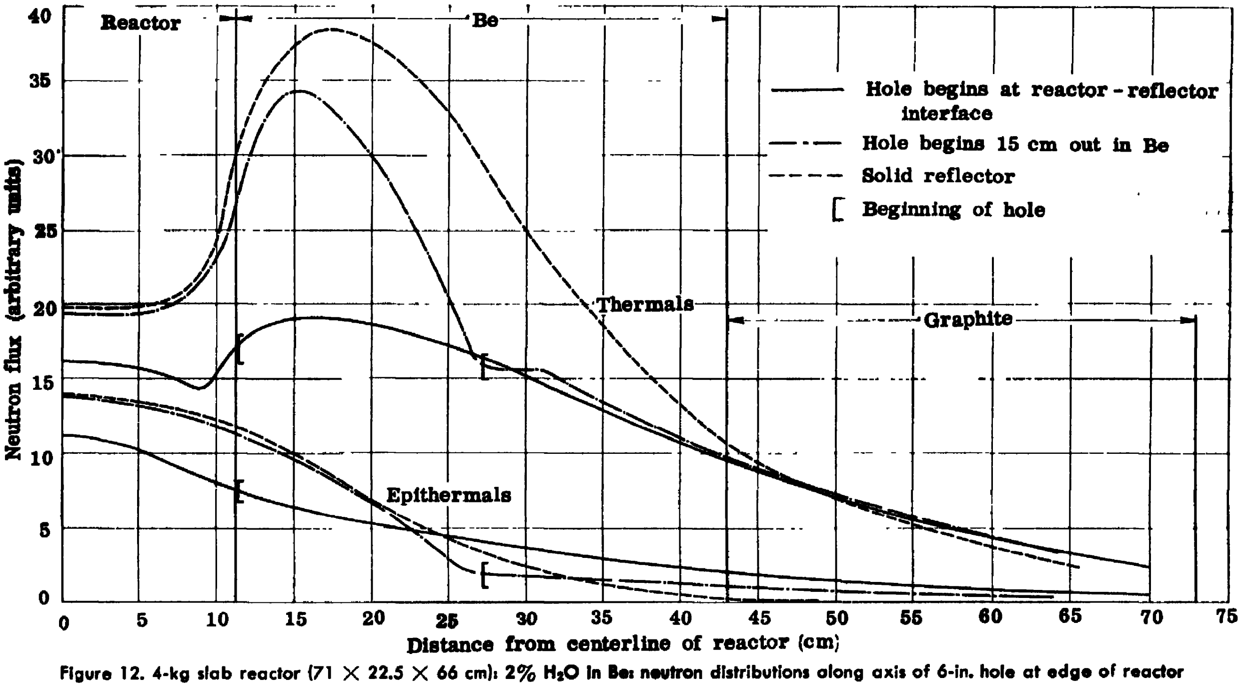

Figure 12. 4-kg slab reactor (71 × 22.5 × 66 cm): 2% H_2O in Be: neutron distributions along axis of 6-in. hole at edge of reactor

Table IX. Instruments Used in Various Power Ranges

Full power 1		
10^{-2}	Power	Range of servo, linear power instruments, and recorders
Lower limit of servo and power instruments 10^{-5}	Period	Restart region—maximum rod withdrawal speeds necessary; operation supervised by log N and period meter
Lower limit of log N and period meter (10^{-6}) 10^{-11}	Counter	Cold-start region; fission-rate meter is only instrument available through major portion of region; only intermittent rod speed available; cold reactor normally becomes critical below 10^{-6}; strictly manual control up to about 10^{-6}
Lower limit of count-rate meter	Source	No rod withdrawal permitted in this range. Source must be used to get over 10^{-11}

operation. In addition, the simplicity, ruggedness, and low voltage requirements lead to high reliability.

Nuclear instrumentation at power levels near full power can be made quite simple, fast, and reliable since substantial currents can be obtained from ion chambers; also, a variety of conventional instruments are in range to read heat power, etc. For this reason, the primary fast-acting safety of the MTR is based on safety shutdown when a given neutron flux (in excess of normal full power) is exceeded.

The control rods, as previously mentioned, are supported by individual electromagnets. The current to each magnet is supplied by vacuum tube amplifiers so arranged that a signal from any one of three ionization chambers will reduce the current in all magnets. This will release the rods which then fall into the reactor under the influence of gravity. This "auctioneer" type of circuit lends itself very well to safety action in that a number of signals can be supplied to a single bus which in turn feeds a signal to the multiple-rod system. In this manner a degree of "safety-in-numbers" is obtained.

Nuclear instrumentation on the MTR is shown in block form in Fig. 16. Three ionization chambers are provided for level safety action through individual preamplifiers and Sigma Amplifiers. The Sigma Amplifiers "auction" the signals to the highest bidder. In addition, two channels are provided with chambers compensated against the gamma background from the reactor to give a wide range, 10^6, presentation on a logarithmic scale. These channels also provide a shutdown signal if the reactor period becomes faster than one second. Table IX gives the relationship between power level and instrumentation.

In order to minimize shutdown due to misoperation, drifts in the electronic circuitry, and changes in neutron flux distribution the "fast" safety channels are adjusted so that the reactor flux must be considerably outside of the normal operating range before safety action occurs. The measured level must exceed the normal level by a factor of about 1.5 before the level safety channels will cause a shutdown; the period must be as fast as one second before a period trip will occur.

Dependence on vacuum tubes in such a system leads to the probability of failure; however, vacuum tubes were chosen rather than relays because they can more easily be monitored to determine their condition. While a relay is probably more reliable, it is very difficult to predict whether or not it will operate the *next* time. The vacuum tube circuits are monitored at various points so as to inform the operator of any trouble in a particular circuit, and sufficient channels are provided to allow operation with one channel out of service.

In addition to the "fast" shutdown through the electronic circuits, a so-called slow shutdown is also provided for signals not requiring high-speed response. These signals are collected by means of relays and act by removing the ac power supply from the amplifiers which supply current to the magnets.

In normal startup and operation the general principle may be stated: for increase in reactivity (rod withdrawal) the instruments and the operator must agree that withdrawal is proper; for decreases (rod insertion) either the operator or the instruments may initiate the action. In order to withdraw rods if the period is faster than 30 seconds the operator must operate a by-pass switch in addition to the withdrawal switch. For periods faster than 7 seconds permission is taken away from the operator to withdraw rods at all. If the period becomes faster than 5 seconds the rods are run in under motor drive until the situation is corrected. The interlocks described, with a number of others not mentioned here, are designed to help the operator in starting and operating the reactor by guarding against misoperation which might cause an accidental shutdown with loss of operating time.

The stability of this type reactor is very good; however, in the higher powered versions small disturbances in reactivity due to changes in water temperature, small mechanical displacements caused by the high-velocity water flow, experiments, etc., lead to variations in neutron flux which are undesirable in many experiments. For this reason a servo system is provided for automatically regulating reactor power level as measured by an ionization chamber. The

MTR servo can hold the flux to within about 1% of the requested level over the range from 1% of full power to full power. This automatic regulating system was developed and tested with a reactor simulator (analog computer). Tests subsequently performed with the system in control of the LITR proved the worth of this technique.

Control systems on other reactors of this family follow the same general pattern. The lower powered reactors such as the ORNL Swimming Pool are much less bothered by Xe buildup; hence adequate control is afforded with much less equipment even though this means that accidental shutdowns are more likely than in the MTR. These shutdowns are not serious as the low-powered reactor can be restarted as soon as the difficulty has been remedied.

ENGINEERING PROBLEMS OF THE MTR

Heat Transfer

The power output of the MTR is determined by the performance of the water as a heat transfer agent. The design water flow velocity is about 10 meters per second in the active lattice, and this implies a nominal heat transfer coefficient $h = 0.9$ calories/centimeter^2/second/°C. The average film drop is about 27°C, and the temperature rise is about 6.1°C.

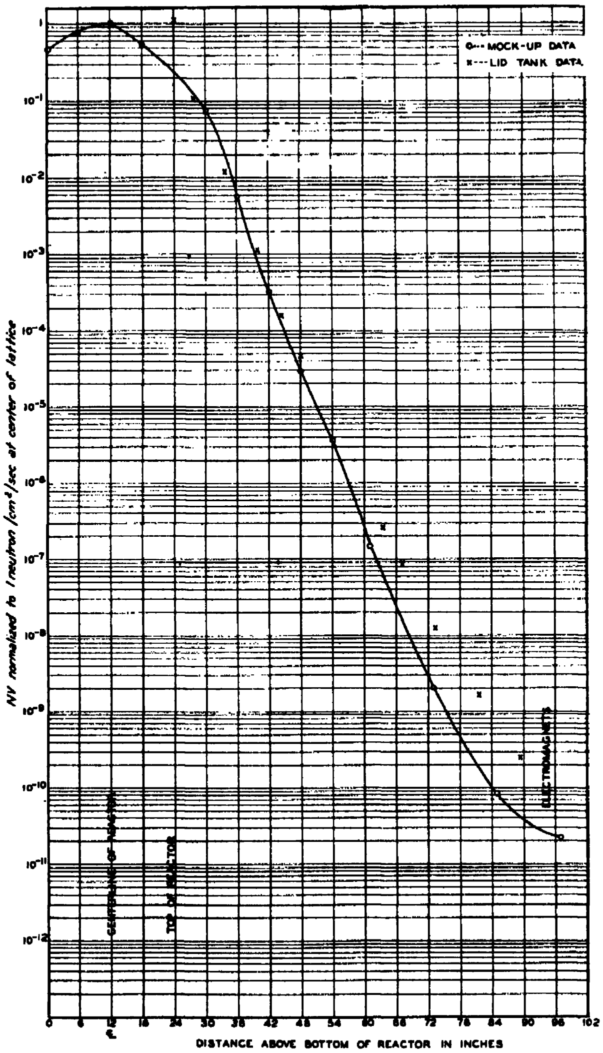

Figure 14. Neutron attenuation in water above reactor lattice: o = mock-up data, x = lid tank data

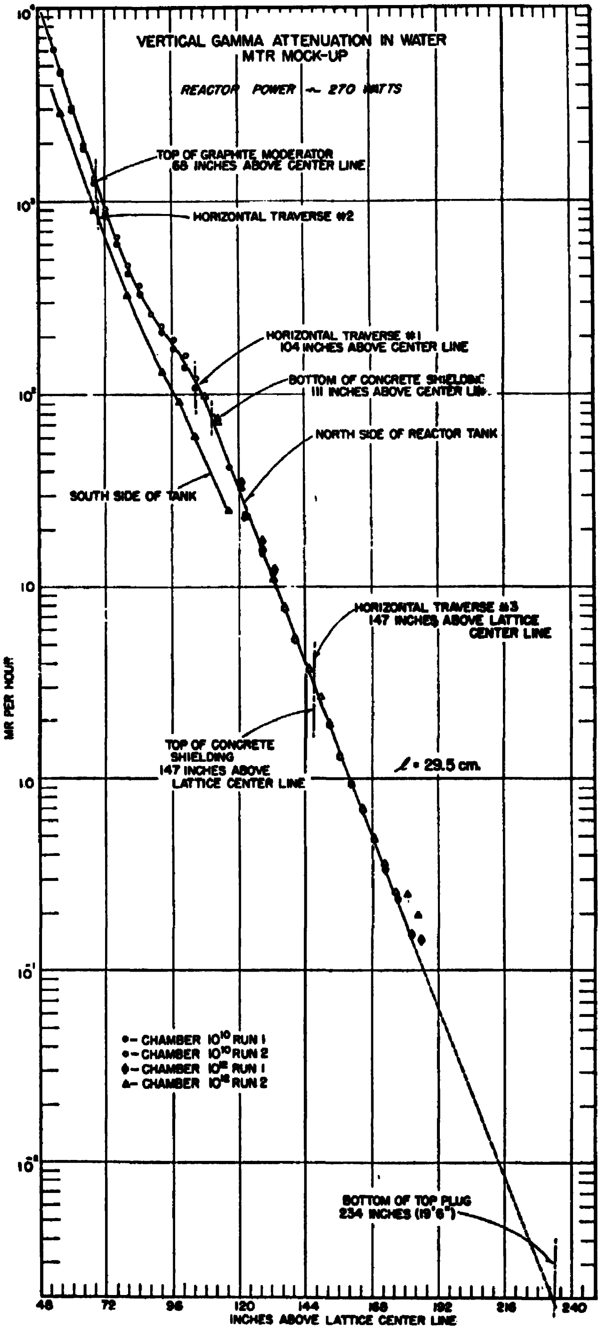

Figure 15

These are nominal, average figures. The actual performance of the reactor is limited by the local hot spots which arise wherever the neutron flux is high. Such high points in the neutron density occur wherever there is less than the normal absorption cross section. The most serious such places are at the corners of the

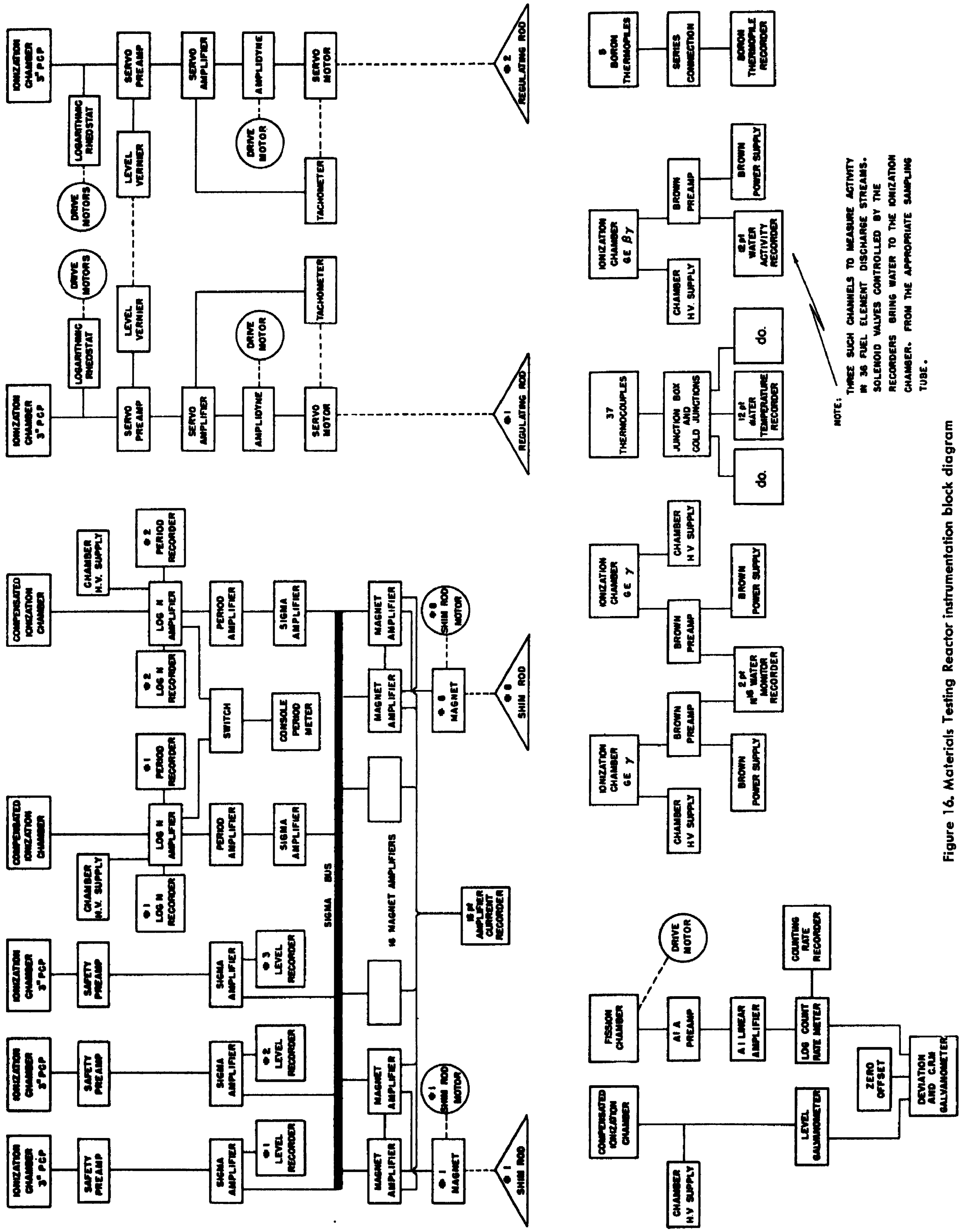

Figure 16. Materials Testing Reactor instrumentation block diagram

lattice where a uranium-bearing assembly is surrounded on two sides by Be, in which the neutron lifetime is relatively very long, and between the top and bottom sections of the Cd shim rods where there is a dead layer of water. The neutron flux peaking in this layer of water tends to persist in the active portion of the shim rods, and hot spots are likely to occur there.

The cooling of the Be reflector, in which 1200 kw is generated at 30,000 kw total power, is in some ways more difficult than cooling the main lattice. For in order to maintain the excellent neutron-reflecting properties of the Be, it is necessary to keep the water content of the Be as low as possible. The aim in the MTR was to keep the average water content of the Be below 2% by volume; engineering compromises increased this to 4.2% by the time MTR went into operation.

Fuel Elements

The fuel elements in MTR-type reactors were developed after several years of experimentation with a variety of configurations at the Oak Ridge National Laboratory. The plates of the elements are curved in order to increase their rigidity; the MTR elements as they are now routinely produced can withstand a differential pressure of approximately 15 pounds from inside to outside without buckling the outside curved plates sufficiently to give trouble. The actual method of fabrication is described by Boyle, "MTR-Type Fuel Elements" (P/953, Session 18B.2, Volume 9, these Proceedings).

Mechanical Design

It was decided early in the design of the MTR that the control and shim rods would be operated from above (Fig. 1). This means that the rod drives must be decoupled from the rods whenever the top plug is removed, as the rod drive mechanism is mounted on the top plug.

The rods are fairly long, and it is of utmost importance that cooling clearance be maintained as they pass through the lattice. The rods pass through bearings in the upper and lower guide grids which position the fuel elements; these upper and lower guide grids are attached directly to the reactor tank. The stratagem of hanging these two members from the same rigid structure insures the integrity of the control rod clearances, and is one of the most important mechanical design features of MTR.

The MTR control rods are of two main classes, the shim-safety rods and the regulating rods. All rods in the reactor are designed to lower the reactivity of the reactor when they are inserted.

The shim-safety control rods, as their name implies, serve the purpose of providing control of reactivity during operation and safety action when required. There are places for eight shim-safety rods running through the active lattice; two different types are used as mentioned previously—Cd-U rods in the active core and Cd-Be rods in the reflector. In the fully inserted positions the lower end of the rods rests in shock absorbers (dash pots) located in the plug closing the bottom of the tank. The rods are raised from this position by means of individual electromagnets on the bottom of the lifting shafts; these shafts extend through seals in the top plug to the motor drive mechanism. The magnetic clutch provides for safety action of the rods; removing the exciting current from the magnet allows the rods to fall by gravity into the reactor and thus reduce the reactivity. Initial acceleration of several g is obtained when full flow of coolant is present due to hydraulic forces on the rods.

The regulating rods are designed to provide for automatic regulation of the reactor flux level. There are positions for four such rods in the Be reflector. Two locations are normally in use and are selected depending on the shape and location of the active lattice in the 45 position grid. These rods have cadmium as the neutron absorber; the location is so chosen as to limit the effect of a given rod to less than the delayed neutron fraction in order that failure of the automatic regulating system cannot in itself make the reactor super-prompt critical. The rods are mechanically connected to a support shaft extending through the top plug and drive through a rack and pinion drive by a low inertia servo-motor. Shock absorbers are mounted on the drive mechanism and serve to dissipate the kinetic energy of the rod and motor should it overtravel at high speed.

Another important feature of the MTR is the fact that the design makes it possible to replace the tank and active portion of the reactor without dismantling the major portion of the graphite or of the shielding. This would, of course, be a major undertaking and would probably consume several weeks, even with careful planning. To this end the materials within the highly active zone of the reactor have been chosen in part for their lack of long-lived induced activities. For example, aluminum has been used instead of stainless steel in this zone. The design is such as to allow the reactor to be dismantled under water piece-by-piece. For this reason the Be pieces have been kept small. This high degree of flexibility makes it possible to insert another type of reactor (of identical external dimension) in the hole left by the removal of the present one. This also allows for replacement in the event of damage or failure in operation.

Not only the tank is removable by this means but also the graphite reflector adjacent to the tank. The main problem in the design of the graphite reflector was the fact that graphite expands under radiation bombardment and temperature increase. The solution was to divide the graphite into two zones, a pebble zone which is adjacent to the reactor tank, and a permanent graphite zone which is 3.65 m by 4.25 m and 2.84 m high.

The pebble zone is a volume 2.22 m square by 2.74 m high. It surrounds the reactor tank and is filled by some 700,000 graphite pebbles 2.54 cm in diameter. The pebbles rest on a base plate and are free to expand upward. In this way any expansion due to radiation effects or temperature increase will merely raise the level of the balls without exerting undue stress on the tank wall or the permanent graphite. Two discharge chutes in the pebble support plate can be opened into a discharge bin, thus allowing easy removal of the pebbles at any time. Easy removal of the pebbles also makes for relatively easy removal of tank sections. Furthermore, since the pebbles are in the highest flux region of the graphite reflector, any radiation damage will affect them first.

The physical removal of the spent fuel elements and recharging of the reactor is accomplished through 6 m of water, using long-handled tools by means of which an assembly can be lifted out of its socket and moved across the top of the lattice to a position over a vertical hole through the Be beneath which is a water-filled discharge tube leading, through locks to minimize loss of water, to a deep canal beneath the reactor. This hole through the Be is filled with a Be plug during reactor operation. New assemblies are loaded into the spaces left by old ones by lowering them through the water from the top of the tank.

OTHER MTR-TYPE REACTORS

The Swimming Pool

As has been mentioned in the introduction, many research reactors embodying the parallel plate, H_2O-cooled and moderated idea have been built in the United States.

The simplest of all these reactors are the swimming pools. In these reactors, a detailed description of which is given by W. M. Breazeale, "The Swimming Pool Reactor and Its Modifications," Volume 2, Session 9A, P/489, these Proceedings, water shielding is used on all sides. The reactor is immersed in a tank from which the name Swimming Pool is derived. Figure 17 is a curve of the gamma-ray attenuation in H_2O, measured perpendicular to one face of an H_2O-reflected swimming pool reactor. Figure 18 gives similar data for neutrons.

The only cooling available in the original Swimming Pool is natural convection, and the reactor was designed to run at 10 kw. Over the years the power level of the Oak Ridge National Laboratory Swimming Pool has been increased; it now runs routinely at 100 kw and it has been run for short times at 1000 kw with only convective cooling. At this high power level the N^{16} formed by O^{16} $(n,p)N^{16}$ is carried to the surface of the pool by the warm water and is a radiation hazard. To overcome this, horizontal jets of water above the reactor core disperse the water which has been convected out of the reactor. This mixing action prevents the N^{16}-bearing water from reaching the Swimming Pool surface until the N^{16} with its seven-second half-life has decayed.

The LITR

The Low Intensity Test Reactor (LITR) was originally a hydraulic and mechanical mock-up of the MTR. After the hydraulic tests were concluded, the LITR was loaded with active elements and converted into a reactor. It has operated routinely at a power of 1500 kw since May 1952 and 3000 kw since September 1953.

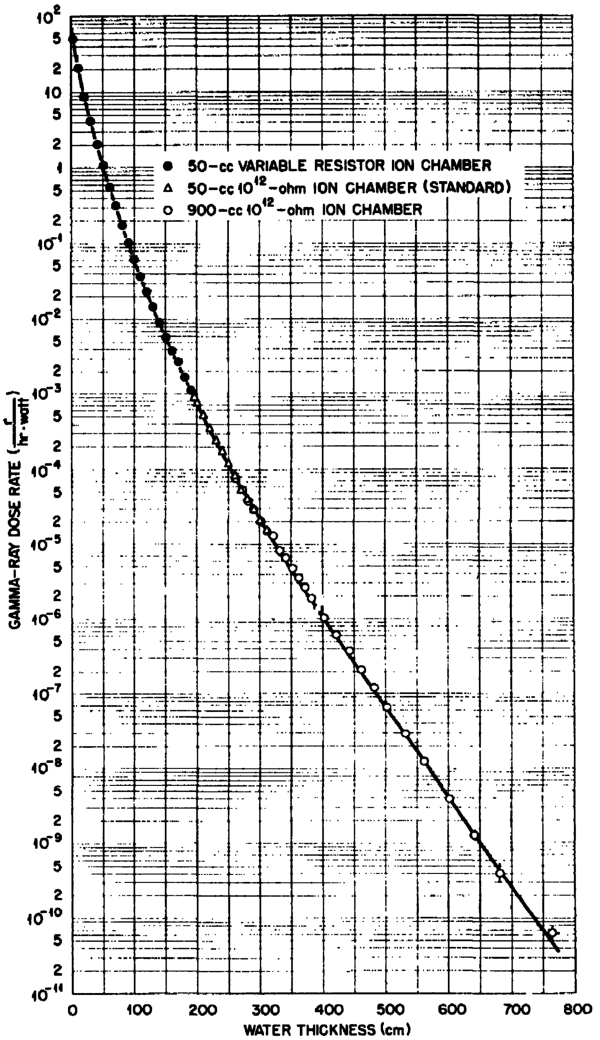

Figure 17. Gamma-ray dose rate as a function of distance from the Bulk Shielding Reactor

The LITR is a replica of the MTR except that the Be reflector, instead of being carefully machined and fitted together, consists of loosely stacked blocks. The cooling system of the LITR consists of two fan driven water-to-air radiators, each rated at 1000 kw at an inlet H_2O temperature of 49°C and an inlet air temperature of 32°C. These radiators are supplemented on hot summer days by a tube and shell heat exchanger using plant process water as a secondary coolant. The recirculated reactor water gives up its heat in these radiators and then flows back into the reactor. The exit water from the reactor is held up in a 2.6×10^4 liter surge tank in order to allow most of the N^{16} activity to decay before the water enters the pumps and radiators.

The LITR is one of the cheapest reactors per unit of flux. Its total cost to date has been approximately

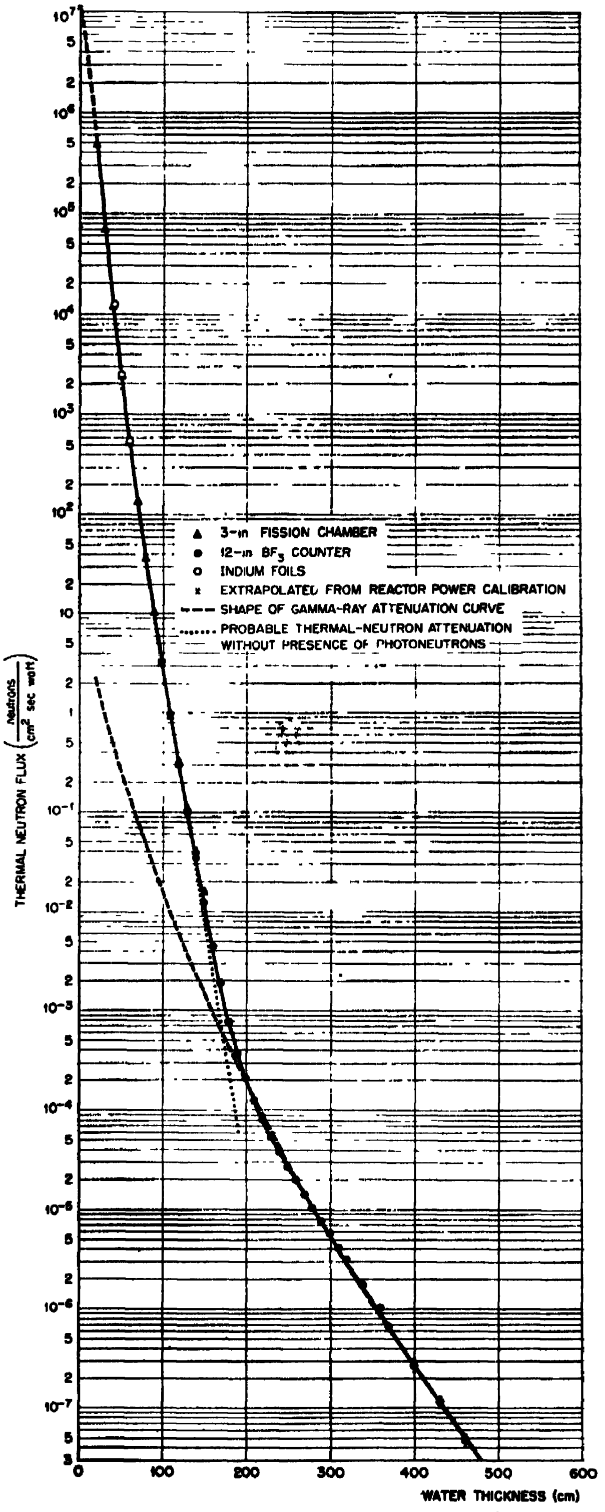

Figure 18. Thermal-neutron flux as a function of distance from the Bulk Shielding Reactor

$1.1 × 10^6 of which about $0.5 × 10^6 was the cost of the Be metal in the reflector.

The Oak Ridge Research Reactor

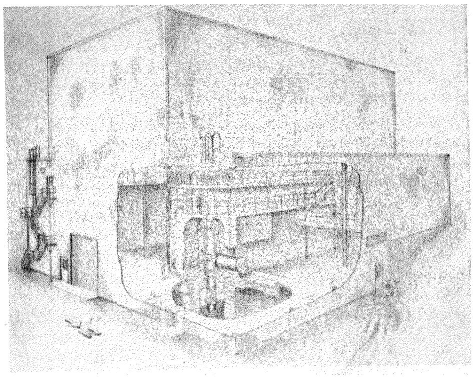

Figure 19 ORNL research reactor project

The Oak Ridge Research Reactor (ORR) (Figs. 19 and 20) is an attempt to rationalize the MTR design by further increasing the accessibility to the very high flux of the active lattice. The somewhat awkward control rod drive arrangement in the MTR with the rods entering from above is replaced by a bottom control rod drive system. The top of the ORR core is therefore more easily accessible for experiments. Since ORR is designed to complement existing facilities at ORNL, it is not provided with the large low flux space described on the MTR.

In order to further increase accessibility, ORR is built in a modified swimming pool. There will be large experimental ports on two sides of ORR for large loop experiments, and one entire reactor surface, with entry from above, is available for irradiation-type experiments. The remaining vertical face of the reactor surface is shielded with water and concrete and is fitted out like the MTR with horizontal beam holes.

ORR will be cooled by 758 liters of water per second passing through the lattice. This cooling water is separated from the shielding tank water of the pool by an aluminum tank. The entire reactor is so designed that it can be completedly removed and replaced if necessary, though the induced activity in the vicinity of the core will cause this to be a major operation.

The power rating of ORR is 20 × 10^3 kw; it is estimated to cost $3.5 × 10^6.

A new principle of catastrophe containment will be tried at ORR. The building will be semi-tight; i.e., it can be maintained at a negative pressure relative to the outside greater than 1.27 cm of H_2O; this will involve a purge rate of about 2300 liters of air per second. This air, after being washed, will be sent through the Laboratory's main 76 m stack. It is estimated that this "purge and wash" system can dissipate the products of a reactor "meltdown" in which the volatile fission products are released, without danger to the inhabitants of the surrounding countryside.

Reactors with 20% Enriched Material

Up to this point all of the reactors which have been described use highly enriched U^{235} as fuel. The use of

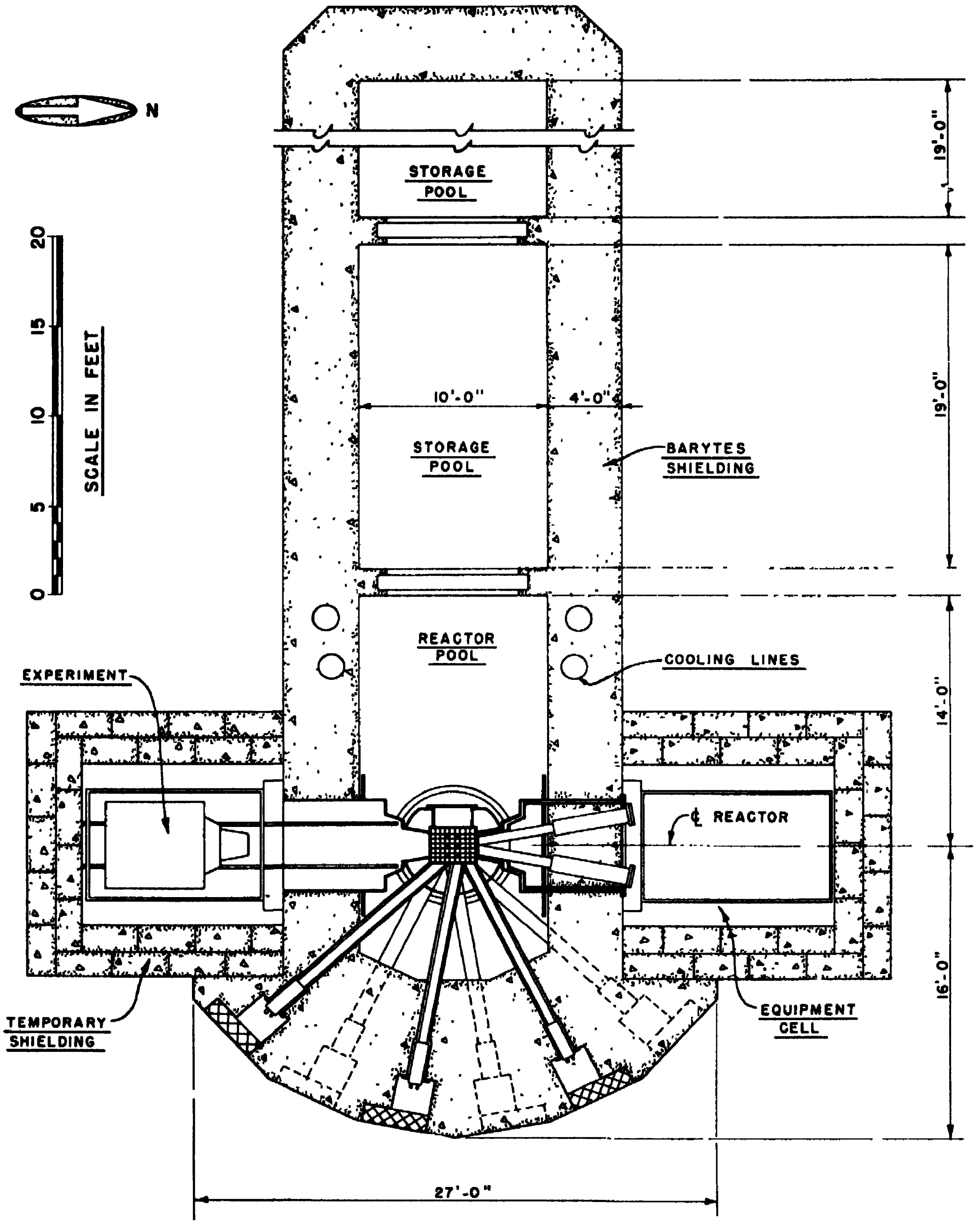

Figure 20. Reactor and pool structure, horizontal section

20% enriched fuel introduces some metallurgical problems, since the U-Al alloy in Al is difficult to fabricate in the highly concentrated combination required with 20% reactors. Nevertheless a technique using a compact of UO_2 in Al for making "meat" material in fuel plate sandwiches has been devised at ORNL and is being described in detail in E. J. Boyle's paper, "MTR-Type Fuel Elements," P/953, Session 18B, Volume 9, these Proceedings.

A little work has been done on reactors of this type using 20% enriched material; preliminary results indicate that the critical mass does not increase significantly over that obtained using highly enriched material. This was verified in some experiments performed at the ORNL Swimming Pool. For example, a lattice containing 23 fuel elements arranged in a 4×5 array with the three odd elements on one side had a critical mass of approximately 3560 grams with full water reflector on all sides. These fuel elements contained 170 grams of U^{235} per element at an enrichment of 20%. A similar experiment with highly enriched elements which contain 140 grams per element went critical with approximately 3460 grams.

At first sight it may seem surprising that there is so little difference between the 20% enriched elements and the fully enriched elements. However it must be remembered that the 20% elements contain more uranium per element than the others; hence the thermal utilization is better by about 4%. The resonance absorption is of course larger in the 20% reactor because there is more U^{238}, but the layer of UO$_2$ in the fuel elements is about 0.6 mm thick. This is sufficiently thick to cause the first few U^{238} resonances to be strongly self-absorbed, and therefore the resonance absorption is much less than it would be in a truly dispersed U^{238}-H$_2$O mixture.

CONCLUSION

The MTR-type closely packed water-moderated and cooled research reactors have proved to be extremely useful irradiation sources. Such reactors have less space than do heavy water reactors, but this is the price that must be paid for their very high fast flux. The MTR-type reactors are extremely versatile—many different lattice configurations are possible. Experience has shown that this versatility in some degree eases the experimental difficulties associated with irradiations in very small space.

REFERENCES

1. Huffman, J. R., Nucleonics *12*, 4 (1954).
2. Glasstone, S. and Edlund, M. C., *The Elements of Nuclear Reactor Theory,* D. van Nostrand Company, Inc., New York (1952).
3. Roberts, L. D. and Fitch, T. E., *Slowing Down Distribution to In Resonance of Fission Neutrons from a Point Source in Two Mixtures of Aluminum and Light Water, 1 :1 and 1 :2 by Volume,* ORNL-294, Oak Ridge National Laboratory (1949).
4. Dismuke, N. M. and Arnette, M. R., *Age to Thermal Energy (.025 ev) of Fission Neutrons in* H_2O*-Al-Mixtures*, Mon P-219, Oak Ridge National Laboratory (1946).

The Swimming Pool Reactor and Its Modifications

By W. M. Breazeale, R. G. Cochran,* and K. O. Donelian,† USA

The aluminum-uranium alloy fuel elements, originally developed for the Materials Testing Reactor, can be used in a variety of installations. These range from the design involving an assembly of such elements suspended in an open pool of water to one in which the assembly is contained in a closed cylinder and cooled by forced circulation.

The MTR type elements consist of Al-U alloy plates 7½ cm wide and 60 cm long clad in Al and brazed into a fuel element approximately 7½ cm square and 60 cm long. The number of plates can vary from 5 to 19 per element; the choice depending on the heat transfer surface required. The thickness of the plates is determined by the amount of uranium to be carried in one fuel element and has varied from 0.150 cm to 0.250 cm. Because of the lesser amount of aluminum, the elements with fewer plates require the smaller critical mass, but the power handling capacity is correspondingly reduced.

In the pool type facility the required number of elements are placed vertically in an aluminum grid, or indexing plate, and immersed in a pool of light water.[1,2] A simple arrangement of reactor and pool is shown in Fig. 1. The water acts as moderator, coolant and biological shield. With convection cooling only, an active lattice consisting of twenty 10-plate elements can be operated at a power level of several hundred kilowatts without boiling. In fact, the maximum practical operating power level probably will be determined by the rate of rise of the N^{16} activity to the surface of the pool rather than by heat transfer considerations. Experiments with jet diffusers[3] which break up the rising column of activated water above the core and diffuse it in a horizontal direction demonstrate a substantial reduction in the surface activity when the reactor power level exceeds several hundred kilowatts.

If higher operating powers are required, it is necessary to use forced cooling. A funnel can be fitted over the bottom of the grid and water from the pool drawn through the fuel elements, passed through a heat exchanger and finally returned to the pool. By drawing the water downward, the N^{16} activity is moved further from the surface of the pool after which it partially decays while passing through the heat exchanger. The heat exchanger must be shielded; about 60 cm (2 feet) of ordinary concrete being sufficient when the reactor power is 1000 kw.

The critical mass depends on the aluminum to water ratio and the reflector material. If the Al/H_2O ratio is 0.5 and the active lattice is surrounded on all six sides by a water reflector, the critical mass is in the neighborhood of 3.3 kilograms of U^{235}. Replacing the water on the four vertical sides by graphite or beryllium reduces the critical mass to about 2.2 kg. These quantities are for fuel enriched to about 90%. Decreasing the U^{235} enrichment to 20% results in only a slight increase in the critical mass, *provided* the total amount of aluminum in the lattice is not increased. It appears that this may be accomplished by using a powder metallurgy technique in fabricating the plates in place of the aluminum-uranium alloy process.

Characteristics of a typical lattice with a given loading are as follows:

Type	Thermal
Power	100 kilowatts
Fuel loading	2.75 kilograms U^{235}
Average thermal neutron flux	0.8×10^{12} n/cm^2-sec
Average epicadmium flux	2×10^{12} n/cm^2-sec
Average fast flux (> 1 Mev)	0.3×10^{12} n/cm^2-sec

At a constant power level, the average fluxes are inversely proportional to the U^{235} loading.

The pool water forms the neutron and gamma shield above the reactor. The absorption of neutrons is much greater than the absorption of gammas and hence the depth required is determined by gamma shielding considerations. Close to the reactor, the attenuation length for fission gammas is about 20 cm but, due to hardening of the spectrum, this increases to nearly 40 cm at a distance of six meters from the reactor. Correspondingly, at a power level of 100 kilowatts, five meters (16½ ft) of water and at 1000 kilowatts six meters (19½ ft) are required to reduce the dose rate at the surface to 7.5×10^{-3} r/hr. The fact that at high powers the depth of water required for shielding increases rapidly with the power level, means that shielding rather than cooling considerations set an effective upper limit to the power level at which an open pool reactor facility can be conveniently operated. This upper limit beyond which the water becomes too deep for convenient operation probably is somewhere in the neighborhood of 2000 kilowatts.

It is possible to reduce somewhat the depth of water required for shielding and still preserve the flexibility of this type of active lattice by supplying lead caps on the tops of the individual fuel elements.

---

* The Pennsylvania State University.

† Nuclear Development Associates.

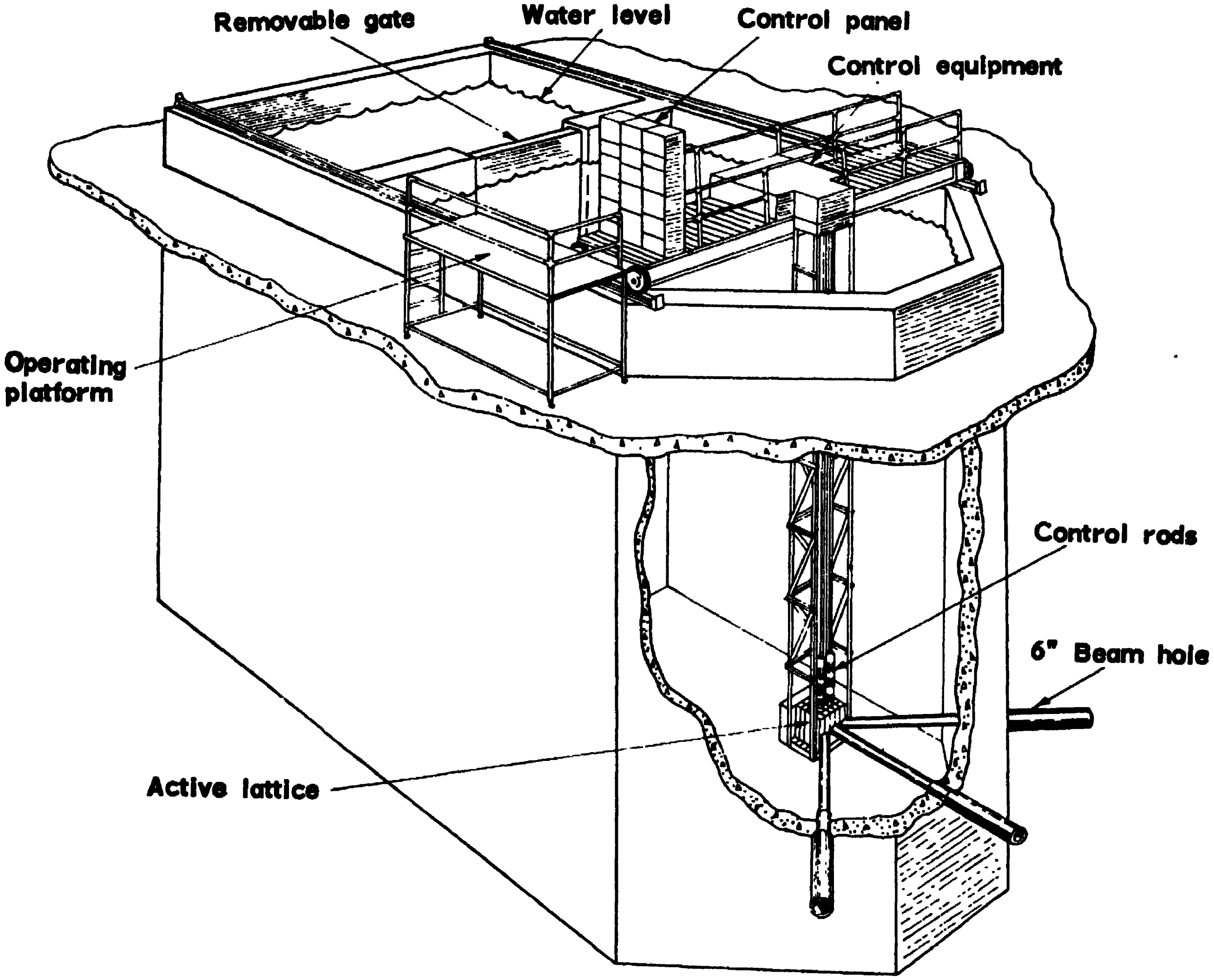

Figure 1. Open pool reactor

In order to permit circulation of cooling water, the caps must consist of a series of offset steps. If the average thickness of these caps is 7½ cm, the gamma intensity at the surface is reduced by a factor of about four.[4]

The use of light water for the moderator permits the smallest size active lattice and provides the highest ratio of fast neutron flux to thermal flux. This is particularly important to experimenters who are interested in carrying on radiation damage experiments requiring fast neutrons. Also the design is extremely simple since the same water serves as moderator, coolant and shield. It has been shown that active lattices of the size discussed above have a negative coefficient of reactivity with respect to steam voids formed in the core. Experiments have demonstrated that if the reactor is left on a rising period, corresponding to excess reactivities less than two per cent, the reactor will simply boil. The steam formation prevents the average power level from increasing to more than a megawatt or two. Thus the accidental introduction of excess reactivities of the order of two per cent would not injure the lattice.

The control and safety system, originally developed for the Materials Testing Reactor, has been modified into a standard package for use with this type of reactor. A description has been published.[5] The control system is a relatively simple "on-off" servo which receives a signal from a compensated‡ ion chamber. The servo motor drives a stainless steel absorbing rod worth 0.5 per cent in reactivity.

The safety system provides three or four boron carbide filled absorbing rods, worth 2% to 3% each in reactivity, depending on location in the lattice, and which are dropped into the reactor to shut it down. These rods are suspended from electromagnets which in turn are excited by vacuum-tube power amplifiers.

---

‡ A "compensated" chamber contains two sensitive volumes or cups of approximately equal size connected in opposition. One cup is coated with boron; the other is not. Thus the current collected from the first cup is proportional to the neutron plus gamma flux and the current from the second proportional to gammas only. The net current is then that due to the ionization caused by the neutron flux alone. With careful adjustment of the compensation, the output of current from the compensated chamber can be made proportional to the neutron flux over a range approaching 10^6 even in the presence of a strong gamma flux from the fission products.

The bias applied to the grid of these amplifiers is determined by the current from an uncompensated ion chamber. Increasing the neutron flux results in a decrease in the magnet current and at a predetermined point the absorbing rods are released. A differentiating circuit connected to a compensated ion chamber provides a signal proportional to the reactor period, (the time derivative of the neutron flux). If this signal is larger than some predetermined amount, indicating that the reactor is on a dangerously fast period, the circuit also acts to release the safety rods. This action is effective from 0.001 per cent of full power to full power.

Designers in the United States have used the "standard" reactor and control system outlined in the foregoing section as the basis for a number of low-cost research reactor facilities to operate in the power range up to a megawatt or two. Construction of some of these facilities has already been completed. Although, in general, the reactor and control system are the same, a wide variety of shielding and experimental equipment designs have been introduced. Description of several representative designs follows.

I. LARGE OPEN POOL REACTORS

The Bulk Shielding Facility

This is at the Oak Ridge National Laboratory.[6] This facility was completed in 1953 and is the original of all open pool reactors. The facility consists essentially of a pool 6 meters (20 ft) wide, 12 meters (40 ft) long and 6 meters (20 ft) deep in which the active lattice is immersed. The main use has been to determine the characteristics of various shielding arrangements. Normal operating power level is 100 kw but short time experiments have been run at appreciably higher levels.

The Pennsylvania State University Facility

This facility, with the exception of the "hot" laboratory wing, is essentially completed. Eventual operation at a power level of 1000 kw will provide an average thermal neutron flux approaching 10^{13} nv. The facility consists of the following parts:

The reactor and controls which are similar to those discussed earlier and which will be on exhibition at the Geneva meeting.

The pool and shield are similar to those in Fig. 1. The pool is 9 meters (30 ft) long, 4½ meters (15 ft) wide, and 7.2 meters (24 ft) deep and is placed endwise in the side of a hill so that earth forms the shielding on three sides. The side through which the beam holes extend is protected by a high-density concrete shield (not shown in Fig. 1) about 1 meter (3½ ft) thick poured against the pool walls. The pool is equipped with a removable gate which divides it into two sections making it possible to drain one-half of the pool while the active lattice is stored in the other half. The rear half of the pool also serves as a "canal" for storage of radioactive samples.

The building, shown in Figs. 2 and 3, consists of the reactor room 18 meters (60 ft) long, 10½ meters (35 ft) wide and 10½ meters (35 ft) high, a two floor office and shop wing and a second similar wing housing a "hot" laboratory. Two shielded enclosures or "caves" with concrete walls and ceilings two feet thick are provided on the ground floor of the "hot" laboratory wing where they rest on bed rock. These caves will be equipped with manually operated, remote handling equipment, stainless steel drip pans, drains to a waste hold-up tank and other apparatus necessary in such a facility.

Experimental facilities, in addition to the "hot" laboratory, include a transportable graphite thermal column, fast and slow pneumatic rabbits, and other irradiation facilities.

Construction (with the exception of the "hot" laboratory where detailed cost estimates have been prepared) is essentially completed. Records indicate the following costs:[7]

	$
Design	14,352
Present building	134,483
Pool and shield	32,450
Utilities, roads and fencing	26,675
Reactor and control	76,000
Experimental facilities	24,000
Future "hot" lab and equipment (estimate)	155,000
	462,960§

The facility will be used both for instruction and research. The projected research program includes neutron diffraction studies, neutron and gamma spectroscopy, radio-activation analysis, short-lived radioisotope production, radiation damage studies, radiation chemistry, biochemistry and biology.

The Naval Research Laboratory Reactor Facility

This facility was designed by the staff of the Naval Research Laboratory. It is expected that construction of this facility will be completed in 1956.[8] This facility differs from the Pennsylvania State University design in two important respects. First, the pool walls are entirely above the level of the ground floor (Fig. 4) and therefore are much thicker to provide the necessary shielding from gamma rays. Second, the reactor core can be moved into a slot at one end of the pool (Fig. 5) where it will be surrounded on three sides by a graphite reflector. A graphite thermal column and five beam holes radiate from this position.

When the active lattice is in position adjacent to the thermal column and beam holes, empty positions in the grid can be filled with graphite shapes canned in aluminum which have the same outline as the fuel elements. Thus, any space between the active lattice and the thermal column can be taken up with graphite and neutron absorption in water reduced to a minimum. At the operating power level of 100 kilowatts, the heating of the graphite by fast neutrons and

---

§ Does not include uranium or the cost of any experimental equipment.

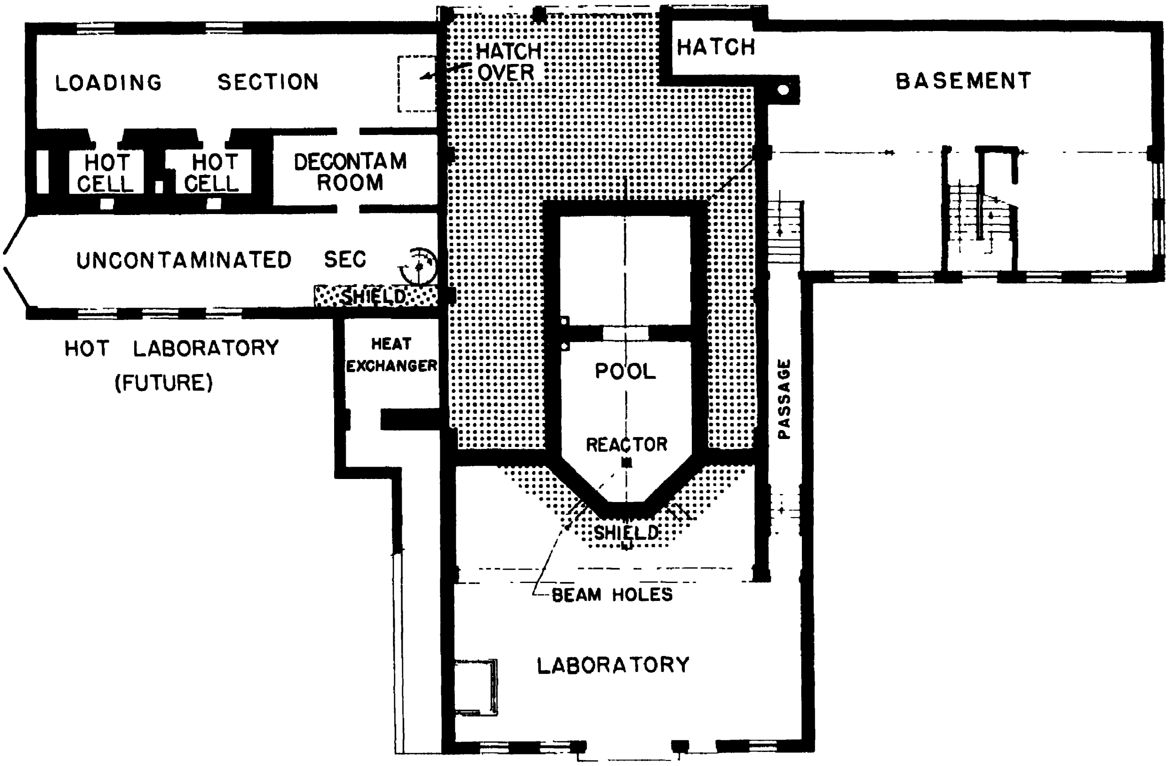

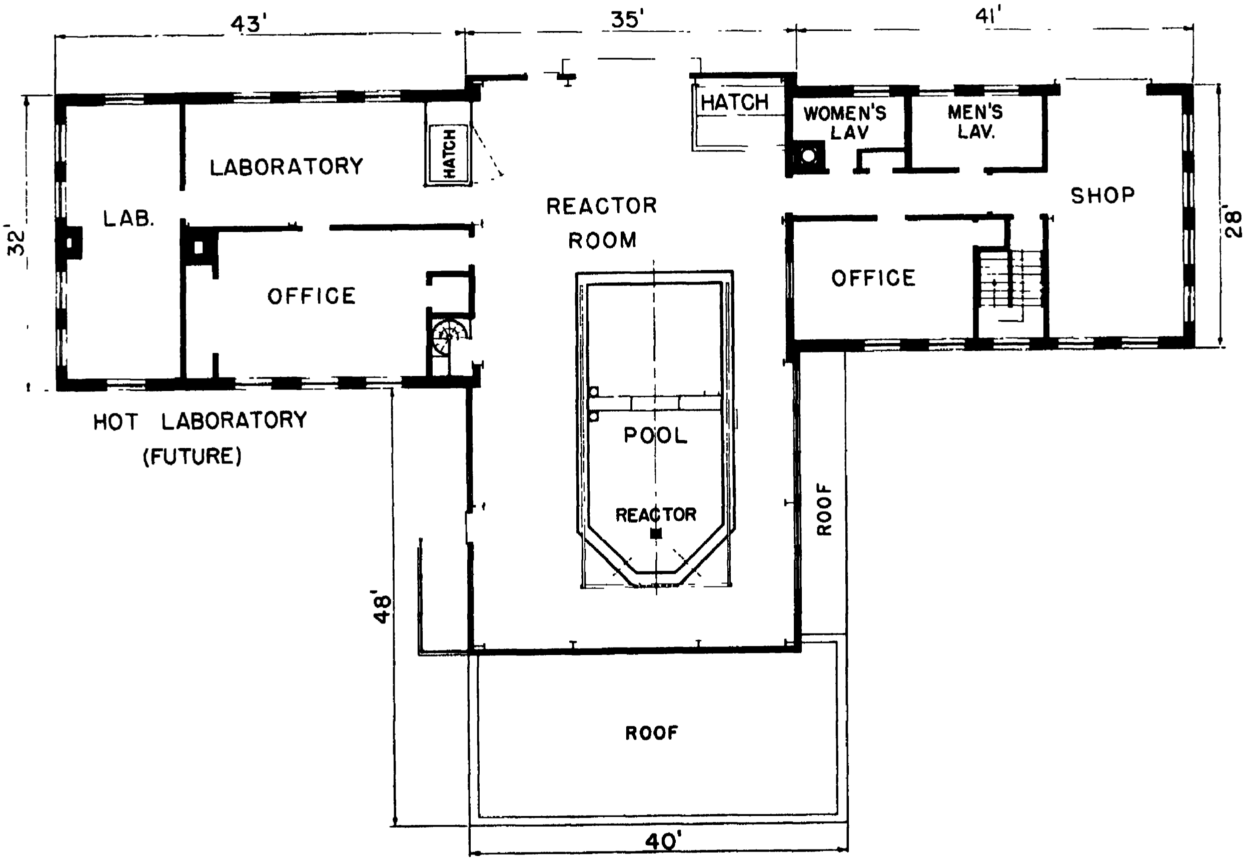

Figure 2. (At top) The Pennsylvania State University reactor facility: basement and laboratory
Figure 3. (At bottom) The Pennsylvania State University reactor facility: main floor

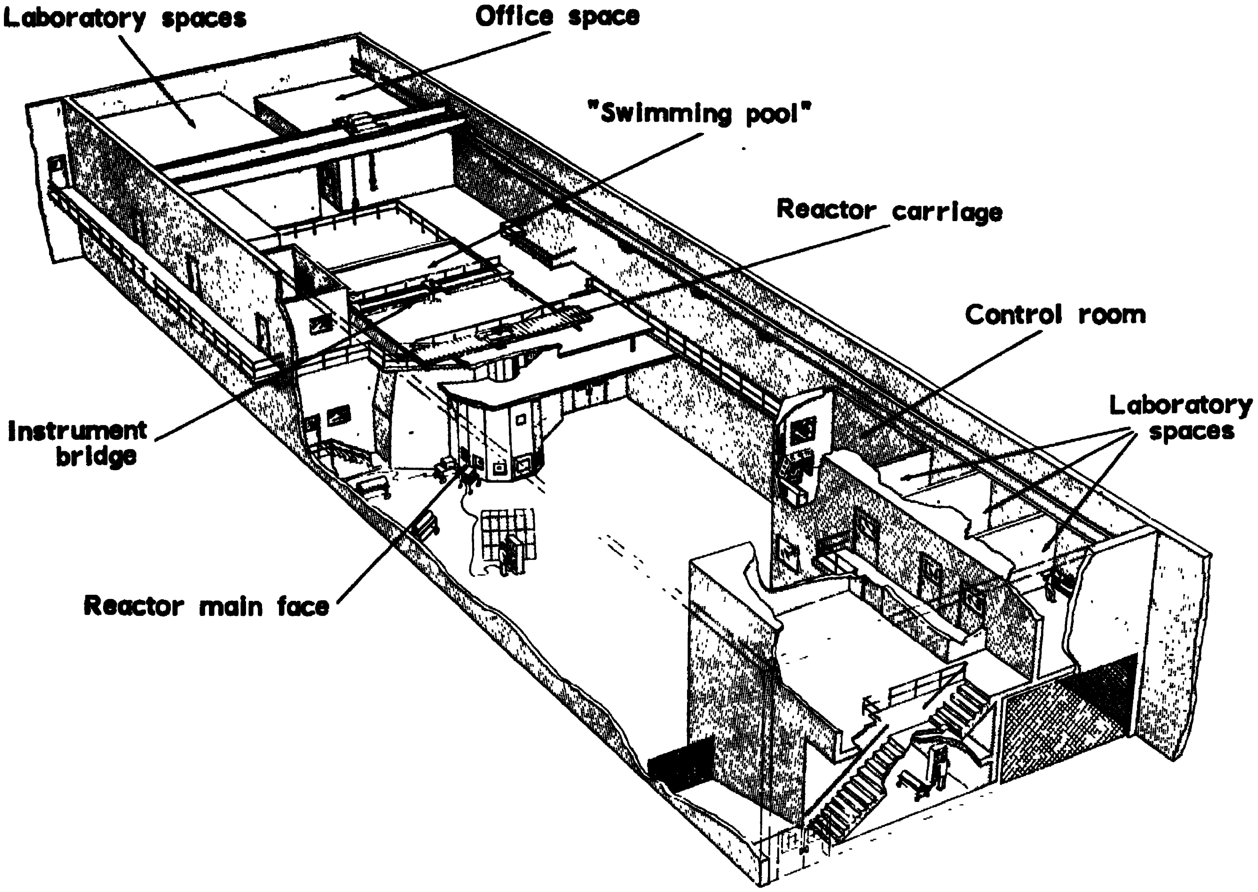

Figure 4. Proposed NRL research reactor facility

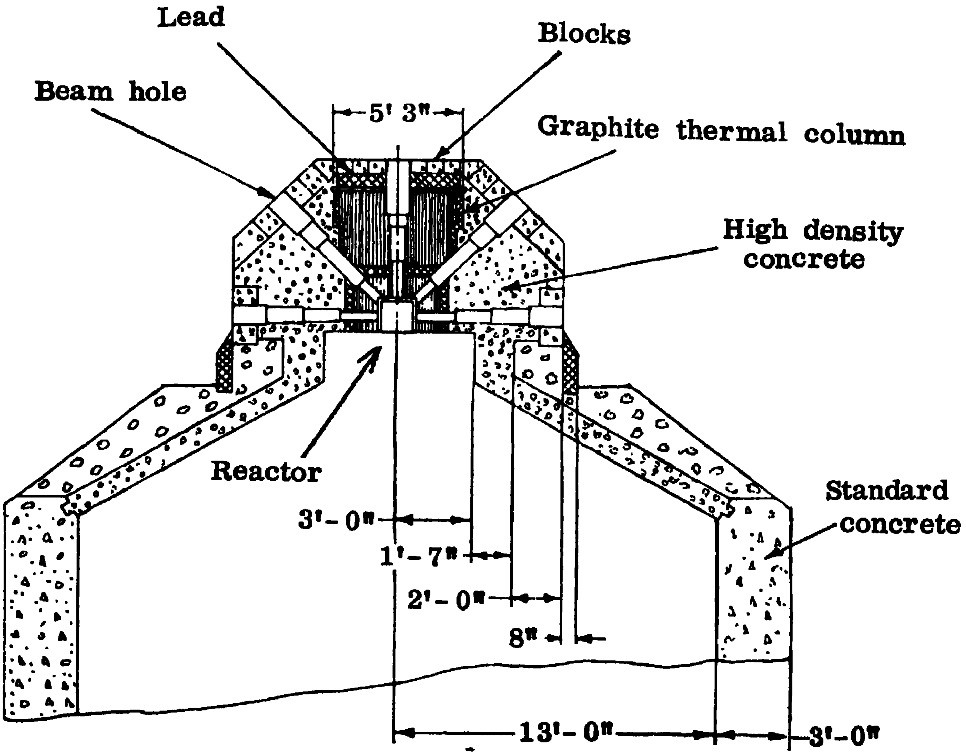

Figure 5. Naval Research Laboratory reactor

gammas is sufficiently small so that no especial cooling is required. The average heat dissipated in a canned graphite reflector piece against the active lattice is in the neighborhood of 0.02 watts/cm^3 and in the thermal column behind 15 cm of canned graphite pieces is well under 0.01 watt/cm^3. It is expected that this heat will be conducted to the faces of the reflector pieces or thermal column and dissipated in the pool water.

Normally the core will be operated in the location adjacent to the thermal column where it will furnish neutrons for the usual experimental program. The reactor can be moved out into the pool making it possible to carry out transmission and absorption measurements through large samples of materials. In this position the active lattice can be either entirely water reflected or partially graphite reflected. The latter is accomplished by placing aluminum cans filled with graphite in the empty holes in the bottom grid around the active lattice.

Research reactors somewhat similar to the Penn State design, except that the pool is above ground, are being built by the University of Michigan (designed by Babcock and Wilcox Company) and Battelle Memorial Institute (designed by American Machine and Foundry Company). Completion of both is scheduled for 1956.

II. REACTORS IN SMALL OPEN POOLS

Reactor for Metallurgical Research

This reactor was designed by the Bendix Aviation Corporation. This facility is an example of a design in which the active lattice is suspended in a concrete tank of light water.[9] The facility is intended primarily for use as a source of neutrons for neutron diffraction experiments and general irradiation work. No bulk shielding work is planned and, unlike the facilities described previously, the reactor itself cannot be moved.

A three-dimension sketch of the reactor and tank is shown in Fig. 6. The inner diameter of the tank is approximately 3 meters (10 ft) and is determined by the requirement that there be sufficient water between the active lattice and tank walls to keep the latter from becoming seriously activated. The tank walls provide the bulk of the gamma shielding. Opposite the core, the walls are 1.5 meters (5 ft) thick and are made up of 30 cm of ordinary concrete and 120 cm of very dense concrete. This latter contains as aggregate a mixture of limonite ore, magnetite ore and iron punchings which produces a density approaching 4.4 grams/cm^3. Six and one-half meters (21 ft) of water above the active lattice provides the shielding in the vertical direction and is sufficient to reduce the gamma radiation to 2×10^{-3} r/hr at the surface with a reactor power of 1000 kw.

The annular depression extending part of the way down inside the shield provides a space for underwater storage of active materials including the fuel elements. Thus the reactor core can be completely unloaded, the tank drained and personnel can enter the tank should internal repairs become necessary.

The tank holds only 75,000 liters of water, as opposed to 350,000 liters or more in the larger pools, and hence its heat storage capacity is not great. Forced circulation cooling is employed at all power levels above a few kilowatts so that the heat will be dissipated in the external heat exchanger. This is necessary to insure that the tank water remains at a reasonable temperature.

No firm date for the construction of this facility has yet been set.

A similar facility is now being designed for the AEC's Livermore, California, laboratory. The chief innovation in the Livermore facility is the addition of two graphite thermal columns extending from opposite sides of the tank to the reactor core.

III. REACTORS WHICH ARE COMPLETELY ENCLOSED

Medical Research Reactor

This reactor was designed by Nuclear Development Associates. Early experiments by L. E. Farr, M.D., Chairman of the Medical Department at Brookhaven National Laboratory, using neutrons from the Brookhaven graphite pile indicated that beneficial effects may be obtained by neutron bombardment of malignant tumors in which boron has been concentrated. The facility to be described here incorporates special features which are important to such medical and biological research. It provides a strong source of neutrons which can be adjusted over the energy range from thermal to about 8 kev thus permitting the treatment of deep-seated tumors as well as those near the surface. In addition, the gamma rays at the treatment locations are strongly attenuated. The design

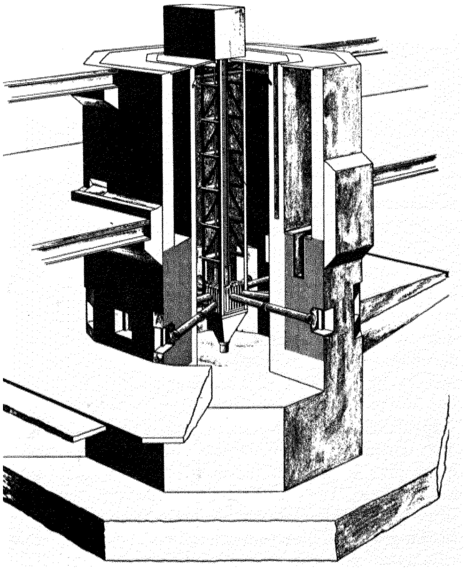

Figure 6. Reactor for metallurgical research

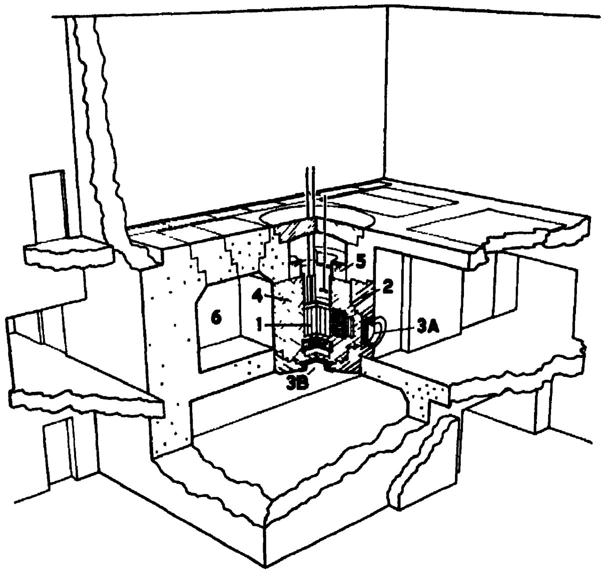

Figure 7. Perspective of medical research reactor

also provides two animal cells where animals may be subjected to neutron irradiation and an experimental hole intended for instrument development work.

A three-dimension sketch of the reactor and associated facilities is shown in Fig. 7.¶ The reactor, consisting of the usual assembly of aluminum-uranium fuel elements, is reflected on all sides (except the top) by 100 cm of graphite. It is cooled and moderated with light water. The demineralized cooling water flows through the core *1* in two passes and then through the primary heat exchanger *5* installed at the top of the active lattice. Grid positions not required for fuel are filled with close fitting aluminum clad graphite blocks thus keeping the amount of water between the active lattice and reflector to a minimum. A cast-iron top plug, through which the control and safety rod actuators pass, can be removed to provide access to the core. The well left by the removal of the top plug when filled with water provides sufficient biological shielding against fission product gammas after a few hours decay, to enable personnel to work safely from a position above the water. The control and safety system is similar to that discussed earlier in this paper.

When the reactor power is 1000 kw, the heat generated by gammas and neutrons in the portion of the graphite reflector next to the active lattice is 0.5 watt/cm^3 and some type of forced cooling is indicated. (The heat generation decreases more or less exponentially according to $e^{-0.17x}$, where x is the distance in centimeters from the face of the active lattice.) Water cooling of the graphite is undesirable because of the absorption of neutrons in the water channels. Air cooling does not involve appreciable neutron loss but does require that the surface temperature of the graphite be kept below 210°C to prevent oxidation. Air drawn from the outside is forced through channels machined in the graphite. The total air flow is 110 cubic meters per minute and the increase in temperature is 75°C. Activity produced in the air is largely the argon-41 isotope with a half life of 1.8 hours. When the average reactor power is 20 kilowatts, about half a curie of this activity is formed in 24 hours. The activated air is exhausted up a stack.

The reactor and cooling system are designed for peak powers of 1000 kw, although the operating cycle will be such that the long-time average power level will be somewhat lower, depending on demands of the research program. The fuel loading is 2.5 kilograms of U^{235}. Details of the reactor and primary cooling system are shown in Fig. 8. Forced convection cooling is employed at all times regardless of the reactor power level.

Details of some of the special features peculiar to the facility's use for medical work follow (see Fig. 7). Two neutron therapy ports, *3A 3B* (thermal columns of graphite and D_2O) are supplied. These ports are 50 cm in diameter, 95 cm long and penetrate approximately 50 cm into the graphite. Bismuth curtains are used to slow the fast neutrons by inelastic collisions and to attenuate the gamma rays as much as possible without materially reducing the neutron flux. After leaving the core, the neutrons pass through the following materials.

Material	*Thickness*
Graphite	15 cm
Bismuth	35 cm
D_2O	Variable from 0 to 15 cm
Graphite	35 cm
Bismuth	10 cm

When the D_2O tank is filled, the neutron flux is essentially thermal. Draining the tank reduces the moderation so that about half the flux is in the thermal

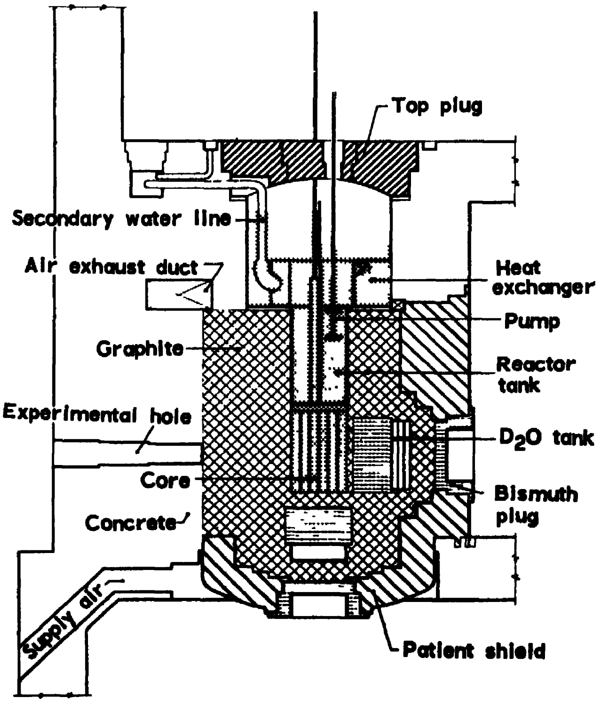

Figure 8. Section through medical research reactor

region and the rest rather uniformly distributed over the energy range up to 8 kev. For deep-seated tumor bombardment a boral shield at the treatment port removes the thermal neutrons and the patient receives practically his entire dose in epi-thermal neutrons. With the reactor power level at 1000 kw and the D_2O tank filled, the thermal neutron flux emerging from the port is about 5×10^{10} nv. The corresponding fast neutron dose and the gamma dose are about 20 rem per minute each. Removing the D_2O completely raises the fast neutron dose to 70 rem per minute.

¶ Numbers shown in italics correspond to parts in this figure.

The therapy ports pass through a "patient" shield *2* which replaces the concrete on the bottom and the side where the ports are located. The side shield begins at the outer surface of the graphite reflector *4* and consists of 56 cm of steel, lead and boron impregnated plastic laminations in the following order; 0.6 cm steel, 10 cm lead, 17.5 cm laminated lead and borated plastic, 10 cm lead, 17.5 cm laminated lead and borated plastic and 0.6 cm steel. It is designed to minimize the whole body irradiation while permitting a maximum neutron flux at the desired location. The fast neutron dose at the outside of this shield is about 2 rem per minute and the gamma ray dose 10^{-2} rem per minute. The bottom shield is somewhat lighter and the dose rates through this shield are approximately ten times as great.

The two rooms for full scale irradiation of animals *6* are separated from the reactor only by the graphite reflector. At full power the thermal neutron flux entering these cells is approximately 10^{11} nv and the gamma ray intensity in the neighborhood of 10^5 rem. The walls of the rooms are high-density concrete 1½ meters thick and form part of the biological shield for the reactor. The number and location of such rooms and of the treatment ports may be changed to provide other design geometries which may be desired.

The design work described above was performed under a contract with the Brookhaven National Laboratory. Construction has not yet been authorized.

REFERENCES

1. Breazeale, W. M., *The Swimming Pool—A Low Cost Research Reactor*, Nucleonics, Vol. 10, No. 11, p. 56, November (1952).
2. Abernathy, F. H., *et al.*, *Low Cost Reactor*, ORNL CF 52-11-125.
3. Cochran, R. G., *et al.*, *Reactivity Measurements with the BSR*, ORNL 1682.
4. Experiments by C. E. Clifford, *et al.*
5. Cole, T. E., *Control System for a Low Cost Reactor*, Nucleonics, Vol. 11, No. 2, p. 32, Feb. (1953).
6. Breazeale, W. M., *The Bulk Shielding Facility*, ORNL-991.
7. Richardson, L. A. and Gillan, G. N., *Nuclear Research Reactor*, Engineering News-Record, Vol. 154, No. 14, p. 47, April 7 (1955).
8. Krause, E. H., *NRL Research Reactor*, "Nuclear Engineering—Part I," Chemical Engineering Progress Symposium Series, Vol. 50, No. 11, p. 203 (1954).
9. O'Connor, J. J. and Foster, L. S., *Reactor for Metallurgical Research*, "Nuclear Engineering—Part II," Chemical Engineering Progress Symposium Series, Vol. 50, No. 12, p. 59 (1954).

Record of Proceedings of Session 9A

FRIDAY MORNING, 12 AUGUST 1955

Chairman: Mr. J. J. Went (Netherlands)
Vice-Chairman: Mr. W. Zunti (Switzerland)
Scientific Secretaries: Messrs. J. A. Goedkoop and A. Milojevic

PROGRAMME

P/623	A heavy-water research reactor	A. I. Alichanov
P/387	The Saclay reactor: two years of experience in the use of a compressed gas as a heat transfer agent	J. Yvon
P/915	Description of the Swiss research reactor	F. Alder *et al.*
	Discussion	
P/860	The Brookhaven reactor	M. Fox
P/488	Design and description of water boiler reactors	L. D. P. King
	Discussion	
P/621	The experimental nuclear reactor with ordinary water and enriched uranium	Y. G. Nikolaev
P/622	A 2000-kilowatt thermal power nuclear reactor for research purposes	Y. G. Nikolaev
P/490	The Materials Testing Reactor and related research reactors	A. M. Weinberg *et al.*
	Discussion	

Mr. V. V. Vladimirski (USSR) presented paper P/623, except for the part on exponential experiments, which was presented in session 21A.

Mr. J. Yvon (France) presented paper P/387.

Mr. W. Zünti (Switzerland) presented paper P/915.

DISCUSSION OF PAPERS P/623, P/387, P/915

The Chairman: We will now have a discussion on these three papers. First of all, there are a few questions directed to Mr. Vladimirski.

Mr. M. V. Lichtenberger (USA): I should like to address a question to the author of the first paper. What means are used to keep the heavy water clean and at the desired pH or pD?

Mr. Vladimirski (USSR): Purification of the heavy water is accomplished by distillation only, but since the composition of the heavy water changes little, we do this very rarely. The reason for the constancy of the chemical composition is that there is a layer of an inert gas, helium, over the heavy water.

Mr. W. H. Zinn (USA): I note in a footnote in the paper prepared by Mr. Vladimirski and his associates that the tank had to be replaced once in 1953. Would he care to comment on what occasion there was this necessity for replacing the tank and if this operation caused much difficulty?

Mr. Vladimirski (USSR): The reason for replacing the reactor tank was a small accident, which I can tell you about in detail.

In 1953 we noted an increase in the activity of the gas. Analysis showed the presence of fission products in the helium, which indicated failure of the uranium rod covering. We decided to replace the uranium rods. After the reactor had cooled, all the uranium rods were withdrawn and two of them proved to have damaged canning. One of the rods had expanded somewhat and would not come out through the top plate. During attempts to pull it out, it broke and damaged the bottom of the reactor tank. The rod was finally removed through the central experimental tube, the diameter of which was large enough to permit withdrawal of the rod. After this incident, the top cover (shield) of the reactor was demounted and the aluminum tank was replaced. In fabricating the reactor, we prepared two new replacement tanks. Some difficulty was encountered in disconnecting the bottom packing under the reactor, where the gamma activity reached 700 microroentgen per second. Appropriate protective measures were taken and the work was quickly accomplished.

Mr. Zinn (USA): I should like to thank Mr. Vladimirski for his explanation for the reason that all of us who operate research reactors or other reactors worry about just such incidents. Although one has made provision for taking care of them, it is only when they happen that one really finds out what it takes to cope with them.

Mr. D. G. Hurst (Canada): I would be interested if Mr. Vladimirski could give some details of the modifications they plan to make to the heavy water reactor.

I think he spoke of future plans to get higher flux without raising the power. We would be interested in having these details.

Mr. **Vladimirski** (USSR): After reconstruction, we plan to use not ordinary uranium but uranium enriched to 2 per cent. A much smaller quantity of uranium—approximately 250 kg—will be used in the modified reactor. Cooling of the uranium will be more intensive, inasmuch as the uranium elements will be made in the form of rings which will be cooled from both outside and inside. The total power of the reactor will be increased to about 3 megawatts. The thermal neutron flux is expected to increase approximately tenfold. Appropriate measures will be taken to detect dangerous variations of the neutron flux in each channel. Cooling of the uranium elements will be accomplished by forced flow rather than by natural circulation, as is the case in the present reactor.

Mr. B. I. **Spinrad** (USA): Inasmuch as the power to which a reactor will rise during an excursion depends not only upon the amount of reactivity but the rate at which it is added, I should like to ask the following question of Mr. Vladimirski. What is the maximum rate of withdrawal of the regulating rods in terms of per cent change in reactivity per unit time and what limits this rate?

Mr. **Vladimirski** (USSR): The total reactivity of the four control rods amounts to about 1 to 1.5 per cent, depending on the level of the heavy water. The rods can be withdrawn in about half a minute. I am sorry I cannot be more precise, I just don't recall the exact figures.

Mr. V. O. **Eriksen** (Norway): I should like to put a question to Mr. Vladimirski. Has he measured the mean lifetime of thermal neutrons in the reactor and is there any difference in this mean lifetime if you fill the "thermal pit" inside the reactor with uranium?

Mr. **Vladimirski** (USSR): Obviously if the uranium rods are in the region of the "thermal pit" the lifetime of the thermal neutrons is much shorter. Precise measurements of the neutron lifetimes in heavy water were not made and in our work we relied on the reports of Moon *et al.*, published in Canada.

The **Chairman**: There are two questions directed to the paper of Mr. Yvon.

Mr. C. K. **Beck** (USA): The problem was mentioned of the necessity to eliminate argon from the circulating carbon dioxide gas. My first question relates to the problem of activity build-up due to other impurities such as dust which accumulate in the routine operation of the gas-handling equipment.

The second question relates to the consequences in case a fuel element should rupture. Have such instances occurred? What levels of activity were reached, and how was the carbon dioxide gas cleaned up after such fuel element rupture?

Mr. **Yvon** (France): In reply to the first question, we have indeed noted when we disassembled the tubing the presence of dust and in particular traces of what were probably iron particles. But the activity of this dust is not troublesome either during shutdown or in the vicinity of the blowers when the pile is in operation.

I regret that I can contribute nothing instructive in reply to the second question, because we have had no cases of rupture; the situation has not arisen.

Mr. R. **Liljeblad** (Sweden): In the system with compressed gas, Mr. Yvon said that they could not get it quite tight. I wonder if it would not be possible to get it tight if all joints were welded and if the motors for the blowers are included in the high-pressure system with only so much tightening between the motors and the blowers that you have no direct circulation between the cool gas of the motors and the hot gas in the blowers.

Mr. **Yvon** (France): I believe it is possible to achieve perfect tightness of the system. However, in the case of an experimental pile, the method we adopted has the advantage that the equipment is easy to disassemble.

The **Chairman**: Finally, there is a question on the paper presented by Mr. Zünti.

Mr. H. J. **Grout** (UK): I should like to put a question to Mr. Zünti about the proposed Swiss research reactor. He states that this is a 10 megawatt reactor and that 9 metric tons of heavy water are required in the reactor core while the external cooling circuit needs 0.8 tons. Would he like to comment on how this very low figure of 0.8 tons has been achieved for a heat dissipation of 10,000 kilowatts, and on special heat exchangers?

Mr. **Zünti** (Switzerland): We will make use of aluminum heat exchangers of a very careful design. I think it is possible to have this low figure.

Mr. D. H. **Gurinsky** (USA) presented paper P/860.

Mr. L. D. P. **King** (USA) presented paper P/488.

DISCUSSION OF PAPERS P/860 AND P/488

Mr. R. F. **Jackson** (UK): I should like to ask Mr. Gurinsky what experience they have had with burst cartridges, and whether this has influenced their decision to go to a new design of fuel charge; and further, when they have adopted this new charge, what are the relative running costs of fuel burnup and pumping power compared with their old charge arrangement?

Mr. **Gurinsky** (USA): I am not sure that I can answer that question completely. Our experience with the fuel has been that we have had three bursts which permitted fission product activity to appear in the exhaust ducts. However, this does not mean there have not been any other leaks detected. These other leaks were of such small size that no fission products appeared in the exhaust chamber. I think it can be said that the decision to go to the enriched fuel element is not based on difficulties with our present fuel element; rather, it is due to the pressure applied to the operating people by the research people to get higher and higher fluxes. No reactor is good the day it is built as far as its flux is concerned.

With respect to the costs of operation, if one does not figure in the initial cost of the U^{235}, it is expected that the pumping power will be somewhat reduced, and if new fans are installed there will be a further reduction in the actual operating cost; but these costs are all interdependent on the extent to which we redesign the pumping system.

Mr. ERIKSEN (Norway): My question is more or less similar. It is: How often do you observe ruptures of your canning in the Brookhaven Reactor, and what is the main reason for them?

Mr. GURINSKY (USA): The frequency of appearance of leaks is higher in the central region, which is the high flux region, and this, we think, is due to the higher heat flux to begin with. Secondly, it is due to the much higher flow of gas. I would say fully 50 per cent of the material now in the reactor is the same material which went into the reactor. That does not mean that the other 50 per cent leaked; there were other reasons for removal.

Mr. Y. G. NIKOLAEV (USSR) presented papers P/621 and P/622.

Mr. A. M. WEINBERG (USA) presented paper P/490. Towards the end of his presentation he made the following statement regarding the use of 20% enriched uranium in MTR-type fuel elements.

I am happy to be able to state to this Conference that I have just received information from my country that sample UO_2-aluminum 20 per cent enriched fuel elements of the type which will be available to foreign countries have now been tested both in the LITR and in the MTR. The LITR tests, which are at a flux of about 2×10^{13}, have run to a total nvt of $8\frac{1}{2} \times 10^{19}$. The tests in the MTR, which are at a flux of 2×10^{14}, have now run to a total nvt of 30×10^{19}. No failures have been encountered in either case. 15×10^{19} corresponds to 10 per cent burn-up.

DISCUSSION OF PAPERS P/621, P/622 AND P/490

Mr. MUMMERY (UK): In Mr. Nikolaev's first paper, P/621, he showed a curve of the variation of reactivity with change of water temperature. I must confess that, at first sight, I do not really understand the shape of the curve. I am wondering if, in fact, this curve represents the effective temperature, neglecting the effect on the slowing down area in the reactor.

Mr. NIKOLAEV (USSR): In reply to this question, I should like to say that this non-monotonous variation of the reactivity with temperature would appear to result from the opposing effects of temperature on the coefficient of thermal utilization of neutrons on the one hand and the neutron age (the value of τ) on the other. It must be borne in mind that the curve was plotted for the case where approximately 1 per cent of the reactivity was compensated by the control rods.

Mr. B. I. SPINRAD (USA): In P/621, Mr. Nikolaev showed a curve of a flux distribution in a lattice cell of the reactor. I noticed, however, that there were no points within the fuel rod itself. I am wondering if he did experimental work in this regard or whether he used theory for his work. If the latter is the case, what type of theory was used?

Mr. NIKOLAEV (USSR): No measurements of the variation of thermal neutron flux were made inside the fuel elements. The variation was calculated using conventional diffusion theory with the necessary corrections. The value of the coefficient of thermal utilization of neutrons, θ, was found to be 0.81 for this lattice spacing.

Mr. MUMMERY (UK): With regard to the second paper, P/622, and the achievement of a power level of 2000 kilowatts from the reactor, I should like to ask if this means that the uranium used in the fuel element will be combined in an alloy in order to achieve a large amount of irradiation.

Mr. NIKOLAEV (USSR): In reply I should like to say that in contrast to the fuel elements used in the United States reactors, the elements used in both the reactors actually operating, and in the planned reactor, consist of uranium and uranium oxide with magnesium.

Mr. GROUT (UK): My question is for Mr. Weinberg. In connexion with the beryllium reflector or experimental space around the MTR reactor, Mr. Huffman mentioned yesterday* that considerable modifications had been made to the reflector and that some sections of it had been replaced by aluminium. Could Mr. Weinberg state what these modifications were and why they were made?

Mr. WEINBERG (USA): I think that Mr. Huffman was referring to the so-called removable part of the beryllium reflector. The number of lattice spaces available in the MTR is forty-five. In actual operation not all of these are filled with fuel. The remaining spaces are filled with what we call beryllium-A pieces, which have the same over-all dimensions as fuel but are made of beryllium. I believe that this is the beryllium which Mr. Huffman referred to as removable.

Mr. P. SCHMID (Switzerland): I should like to ask Mr. Weinberg what kind of slowing down theory is suited for criticality calculations of beryllium-reflected MTR-type reactors.

Mr. WEINBERG (USA): We have had very good luck, as it were, with the simple two- and three-group diffusion theory. I believe that the main reason for this is that most of the neutrons which escape into the reflector in a reactor of this sort are fast neutrons. From this point of view one might expect that a one-group model would be fairly adequate. The trick in getting good results, of course, depends upon establishing the correct over-all boundary conditions for the fast group of neutrons. This means that one gets good results if one carefully computes the average mean free path for fast neutrons in the reflector and in the lattice.

---

* P/485, session 8A.

Mr. N. S. Kalitsin (Bulgaria): I have a question regarding the two reactors described by Mr. Nikolaev. If I understood him correctly, he said that radioactive air from these two reactors will be discharged into the atmosphere. What is the level of radioactivity of this air, and will it not be dangerous to the population in the vicinity?

Mr. Nikolaev (USSR): The air will not be dangerous, since the level of activity will not be high. The figures for the operating reactor refer to the activity of argon, which does not exceed a few hundredths of a curie per hour. In the case of the planned reactor, the level of activity will be higher and will amount to a few tenths (of a curie per hour).

Session 10A.1

RESEARCH REACTORS, DESCRIPTIONS (Continued)

LIST OF PAPERS

P/620 Reactor for physical and technical investigations..........................G. N. Kruzhilin 435
P/402 The experimental facilities of E.443........................H. J. Grout and F. W. Fenning 449
P/861 Design and description of ANL reactors (CP-3, CP-3′, and CP-5).............W. H. Zinn 456

Reactor for Physical and Technical Investigations

By G. N. Kruzhilin,* USSR

1. INTRODUCTION

The reactor for physical and technical investigations (RPT) was designed to be a source of neutrons for physical experiments and for testing fuel elements for new nuclear power reactors. The heat output of the reactor is 10,000 kw. The maximum intensity of the thermal neutron flux in the centre of the core is approximately 8 × 10^{13} neutrons/cm^2 per sec. Graphite and water are used as moderators, enriched uranium as fuel. Two beams of neutrons emerge from the surface of the core, two other beams from the reflector. Five channels of large diameter contain "loops." The latter have independent cooling circuits and are designed for testing the elements of constructions (fuel element units) of nuclear power reactors on full scale and under true operating conditions. Six channels of smaller diameter are designed for experimental fuel elements and for irradiation of samples with fast and thermal neutrons and gamma rays. The graphite column serves to produce an intensive thermal neutron beam. The reactor has a biological shield for the safety of the personnel. A hot laboratory, with special shielding for the safety of the personnel and remote control and manipulators has been provided. It enables one to conduct chemical and metallographic investigations of fuel elements and samples irradiated in the RPT, and of highly radioactive materials.

The reactor went into operation in April 1952 and is working successfully at the present time.

I. I. Gurevich and S. M. Feinberg suggested the physics design of the reactor.

P. E. Nemirovsky did the calculations of critical mass and shielding of the reactor.

M. I. Pevzner and M. K. Romanovsky determined the physical parameters of the reactor.

S. A. Skvortsov and others worked out the thermal aspects of the installation.

A number of USSR Ministries participated in the engineering part of the design and the fuel elements.

V. V. Goncharov, G. N. Kruzhilin and E. N. Babulevich were in charge of starting and running the reactor.

When the design of the RPT reactor was in the initial stage of preparation, the reactor was meant to be used for obtaining intensive neutron flux and for irradiating samples of various materials and small fuel elements of future power reactors. For this purpose an installation was designed with a water moderator and with water as a coolant. The core of the reactor had the shape of a cylinder, 45 cm in height and 45 cm in diameter. The lattice consisted of vertically arranged cylindrical rods (0.5 cm in diameter) of enriched uranium (15% U^{235}). In the horizontal plane, the lattice was square, with 1.5 cm spacing. A current of water was to flow over the lattice with a velocity of 3 m per sec to obtain a heat output of 10,000 kw. The maximum neutron flux was expected to be about 1.1 × 10^{14} neutrons/cm^2/sec in the centre of the core and nearly 2 × 10^{14} neutrons/cm^2 per sec in the central cavity filled with water.

To find the constructive and hydrodynamic characteristics of this reactor, a full scale model (Fig. 1) was constructed, with a circulation in the circuit of 2000 cubic metres of water per hour. A core with a mobile part (Fig. 2) was set up, the purpose of this mobile part being to adjust reactivity and ensure safety.

This test model operated in the course of the spring of 1950. Some time later, in the summer of the same year, a number of other tests were put into operation. On these, the fuel elements, in actual size and placed in the water flow, were heated electrically. The behaviour of fuel elements under heat flows up to 8.10^6 kcal/m^2 per hour, with a water velocity of up to 12 m per sec, were investigated in these tests.

As the work of designing nuclear power reactors was being conducted on a growing scale, the programme of testing the designs of fuel elements had to be considerably extended. It became necessary to provide the designed reactor with a possibility for testing, in actual size and under true operating conditions, the

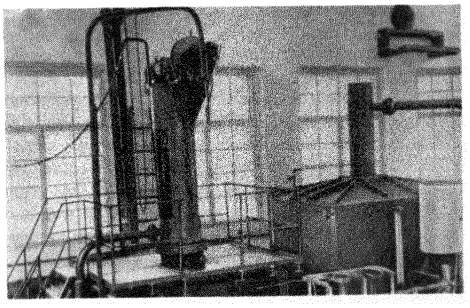

Figure 1. Test model

---

* The paper was prepared on the basis of the data available at the Academy of Sciences of the USSR.
Original language: Russian.

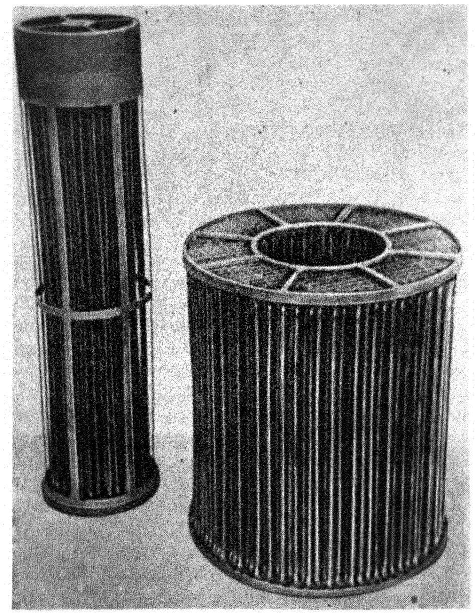

Figure 2. Mobile and stationary parts of the core

fuel elements of future power reactors with water (under high pressure), liquid-metal, and air cooling.

For this purpose it was necessary to make channels with independent circulation circuits, which later on were given the name "loops." It is difficult to arrange these channels in such a small reactor with a water moderator, as they would occupy a considerable part of the core. It was then decided that the reactor should be designed with a graphite moderator, and that water moderator would be used only partly.

The new design led to larger dimensions of the core, in which it was much easier to find place for the "loops." The work on the reactor with a water moderator had been continued for other purposes.†

The engineering design of the reactor with graphite and water moderator was completed in September 1950, and at once the preparations for the construction and the setting up of the installation were started. The manufacture of the fuel elements, which underwent prolonged thermal tests, on tightness of the canning and physics tests, was completed in March 1952. Initial operations of the reactor were carried out in April 1952, after which it was ready for use. For half a year the reactor worked at comparatively small power (10–30 per cent of the design power) and was used exclusively for physics experiments. At that time, full-power operation of the reactor was not economical since the "loops" were not ready for use. In December 1952, when the first "loop" for testing fuel elements of power reactors with high pressure water cooling was completed, the reactor started operating at full power, equal to 10,000 kw. Later on two "loops" were installed whose purpose was to investigate constructional elements of reactors, with water cooling under high pressure, and with liquid-metal cooling, respectively; still later two other "loops" were put in for testing under operating conditions fuel elements of nuclear power reactors with air and water cooling.

Concurrently with the operation of the "loops," experimental physics investigations have been carried out. Two mechanical velocity selectors for the measurement of neutron cross sections were installed at the neutron beam channels. A γ-spectrometer for investigating thermal neutron capture γ-ray spectra and an installation for studying the electron-proton angular correlation in the β-decay of the neutron were also built. A graphite column, with a set of neutron counters forming a system insensitive to the scattering of neutrons in samples under investigation, has been used for improving measurements of neutron absorption cross sections and resonance integrals. There is also a number of other installations for physics investigations at the reactor beam holes.

Samples of constructional materials (stainless steel, aluminium and others) have been placed in the channels of the reactor in order to investigate how their mechanical, electrical and thermal properties, their microstructure and corrosion resistance change when they are intensively irradiated by fast and thermal neutrons and γ-rays.

When the hot laboratory,‡ provided with special shielding and manipulators for working with highly radioactive materials, was put into operation, a systematic study was started of the properties of materials which had been irradiated for a long time in the reactor.

During the three years of its operation the installation proved its reliability and stability. Only one more or less significant accident took place, when the cooling coil of the shell bottom broke and the reactor did not operate for eight days. On another occasion, the reactor went out of commission on account of damage to the fuel elements. With the improvement of the technological methods of their manufacture and testing, the number of breakdowns decreased. Thirty fuel elements went out of commission in the years 1952–1953 and only seven elements in the year 1954.

More often, and for longer periods of time, the pile had to be shut down in order to install new "loops" or to replace the experimental fuel elements.

In the "loops," experimental types of fuel elements are investigated. All the time the need arises to investigate new cooling conditions and new designs of fuel element units.

---

† See the report by Y. G. Nikolaev: "Experimental Nuclear Reactor with Ordinary Water and Enriched Uranium," P/621, session 9A.

‡ See reports by N. F. Pravdyuk "Hot Metallographic Laboratory" (P/673, session 8B) and by G. N. Yakovlev and others "Hot Analytical Laboratory" (P/677, session 10B, volume 7, these Proceedings).

2. CORE AND REFLECTOR

The core and the reflector of the reactor consist of layers of graphite, which form a cylinder 240 cm in height and 260 cm in diameter. The central part of the graphite, pierced by a system of vertical cylindric channels 54 mm in diameter, forms the core, which is a cylinder of one meter in height and one meter in diameter. There are altogether 37 channels, forming a square lattice with a 14 cm spacing, which contain the fuel assemblies. The side and top graphite reflectors are 80 cm thick and the bottom reflector 60 cm. Through the top reflector run the channels, filled with water, whereas the side and bottom reflectors consist entirely of graphite.

The graphite had a density increased to 1.8 gm per cm³. The "age," τ, of neutrons from a Po + Be source in the graphite, with empty channels, measured with a resonance gold detector (energy 4.85 ev) is about 342 ± 25 cm², and the diffusion length for the thermal neutrons about 52 cm.

As mentioned before, the fuel elements are placed in aluminium tubes. The fuel elements are hollow cylinders containing enriched uranium and clad with aluminium.

The outer tube together with the fuel element form a field tube. Water enters the annulus between the tube and the outer surface of the element, and then returns through the internal duct of the fuel element. Therefore, not only the graphite but also the water in the annulus and in the internal duct of the elements serve as moderator. In the cell of the lattice of 14 × 14 cm² cross section per 1 cm of length there is $\omega_C = 173$ cm³ of graphite with a slowing down power of $\omega_C\xi\Sigma_S{}^C =$ 11.20 cm² and $\omega_H = 6.6$ cm³ of water with a slowing down power of $\omega_H\xi\Sigma_S{}^H = 9.50$ cm².

Consequently, the slowing-down power of water constitutes about 46% of the total slowing-down power of the core.

3. MULTIPLICATION CONSTANT OF THE LATTICE

Table 1 shows the total absorption areas ($\omega\Sigma_C$) of the components of the core.

Table 1. Total Absorption Areas of the Components of the Core

Material	*Absorption area in cm²*	*Absorption area in cm², taking account of the neutron distribution*
Graphite	0.058	0.078
Water	0.139	0.175
Aluminium	0.021	0.028
Fuel Element	3.55	3.55
	3.77	3.83

Figure 3 shows the distribution of the thermal neutron flux in the lattice cell. Part of the thermal neutrons is generated in the graphite, another part in the water inside and outside of the fuel element. In accordance with the distribution of slowing down power, about 46% of the total number of thermal neutrons is generated in the water.

The dashed line in Fig. 3 shows the distribution of the thermal neutron density when there is no water in the fuel assembly and graphite temperature is 20°C.

The following values were found for the thermal utilization: In the lattice without water, at room temperature: 0.97; in the lattice with water, at room temperature: 0.92; in the lattice with water at operating temperature: 0.925.

The resonance absorption of neutrons in U^{238} in the hollow slug is rather large because slowing down neutrons enter in it not only from its outer surface but from the inner surface as well. On the other hand, the neutron, after falling on the outer surface of the element, passing through the uranium layer and entering the water-filled internal duct of the fuel element, may leave the resonance energy interval by colliding with a proton. According to calculations carried out with a semi-empirical equation, the resonance escape probability is equal to:

In the lattice without water: 0.865 ± 0.015.

In the lattice with water: 0.91 ± 0.01.

The fast fission factor in fuel elements with highly enriched metal is not large, about 1.003.

The multiplication constant K_∞ of the lattice in the core is now found to be:

For the lattice without water at room temperature, 1.59 ± 0.03.

For the lattice with water at room temperature, 1.59 ± 0.03.

For the lattice with water at operating temperature, 1.57 ± 0.03.

In order to verify these calculations, experimental determination of the multiplication constant of neutrons with these fuel elements were made before the construction of the reactor was begun. Measurements were done in a graphite prism of 2 × 2 × 3 metres. A wide beam of thermal neutrons fell on the front surface of this prism. Inside the prism were the ele-

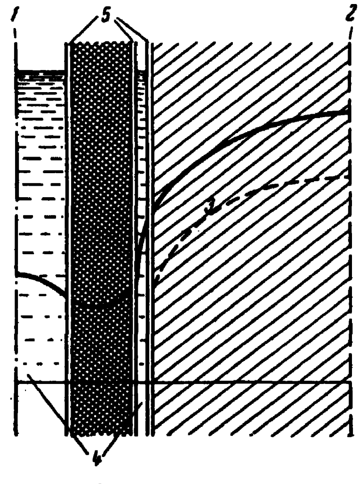

Figure 3. Distribution of the thermal neutron flux in the lattice cell: (1) axis of the channel; (2) outer boundary of cell; (3) graphite; (4) water; (5) aluminum

ments under investigation as well as known absorbers (boron, for example). By determining the variation in the flux of thermal neutrons in the prism it was possible to verify the results of the calculations. They turned out to be in satisfactory agreement with the experimental data. Deviations were within the limits of experimental error.

While the reactor is in operation equilibrium concentrations of Xe^{135} and Sm^{149} are formed. This causes a decrease of K_∞ of the lattice from 1.57 to 1.51 at maximum power.

These values refer to the initial ratio of uranium isotopes. During operation of the reactor, the isotope composition is changed and K_∞ changes accordingly. These changes will be examined later.

4. AGE OF NEUTRONS AND DIFFUSION LENGTH

The critical dimensions of the reactor depend on the age of neutrons $\sqrt{6\tau}$ and the diffusion length of thermal neutrons L. The lattice of the reactor under consideration contains a comparatively small number of non-elastically scattering nuclei. Therefore, their contribution to the value of τ may be neglected. According to calculations, the value of τ in graphite with a density of $\gamma = 1.8$ gm/cm^3 is about 285 cm^2. As was indicated above, water in the lattice contributes considerably to the slowing down power. It also greatly reduces the value of τ. However, this latter effect is somewhat weaker than the effect of the increase in slowing down power. This is because of the relatively small effect of the water in the energy range of $E > 0.1$ Mev, as a result of the rapid decrease in the neutron scattering cross section of hydrogen.

Calculation gives the following values of τ for fission spectrum neutrons:

For a solid graphite core: 285 cm^2.

For a graphite core with ducts filled with water and lead models of the fuel elements: 220 cm^2.

Experimental values for τ, obtained in the graphite moderator of the reactor with a Po + Be source of neutrons and a cadmium-covered ionization chamber, are in satisfactory agreement with these calculated values. On this basis, we can assume that the values calculated for τ for a source with fission spectrum are not far from the truth.

The squared diffusion length L^2 of the thermal neutrons in the lattice was calculated theoretically and found to be approximately equal to 65 cm^2. No experimental determination of this value in the lattice was undertaken. Since, however, the value L^2 turns out to be several times less than τ, the inaccuracy in the value of L^2 has a comparatively weak influence on the critical dimensions. In the side and bottom reflectors (assuming the "loops" and the ducts of the control system removed and replaced by graphite plugs so that they become solid graphite layers) the quantities τ and L^2 are equal to 285 cm^2 and 2700 cm^2, respectively. In the top reflector, which is pierced by ducts filled with water, the values of τ and L^2 differ sharply from those above and are approximately:

$$\tau \approx 150 \text{ cm}^2$$

$$L^2 \approx 350 \text{ cm}^2$$

5. CRITICAL DIMENSIONS OF THE REACTOR

With the above-mentioned values for the constant of neutron multiplication in the core and the migration lengths at our disposal, we were able to calculate the critical dimensions. The calculation was done for a homogeneous reactor with material parameters K_∞, τ and L^2, corresponding to the parameters of the heterogeneous lattice under consideration. Conventional multi-group methods of calculating critical dimensions were applied to this homogenized system. Two difficulties arise when these methods are employed: firstly, the cylindrical form of the core leads to partial differential equations; secondly, the solution of the problem becomes more cumbersome as the number of groups increases.

This led us to the following method of calculation: for a spherically symmetrical core, surrounded by a spherical reflecting layer, a two-groups approximation was used. Then, in order to determine the error resulting from the small number of groups, calculations with four and six groups were carried out. In this way corrections for the two-groups method were determined.

Then, in order to determine the effect of deviation from the spherical form, that is, to find the transition coefficient from the spherical form to the cylindrical, partial differential equations were solved for the cylindrical core in two-groups approximation. Table 2 below shows that these corrections were comparatively small.

Table 2. Critical Radii, cm

	Reactor without water	*Reactor with water*
Spherical reactor:		
(*a*) In two-group approximation	48	48
(*b*) In four-group approximation	50.5	45.5
(*c*) In six-group approximation	50.8	45
Cylindrical reactor in two-group approximation ($2R = H$)	45.5	40.9

The treatment of the core as if it were homogeneous may raise legitimate doubts because of the relatively small number of fuel rods in the core, 37 only. Therefore, the applicability of this homogenization had to be verified. For this purpose critical dimensions for an essentially heterogeneous lattice were determined.§

In these calculations every fuel element is considered as a line source of fast neutrons and also as a line sink of thermal neutrons placed in the infinitely extended slowing down medium. If we write I_k for the fast neutron flux emitted by the kth element, and by i_k the flux of thermal neutrons absorbed by the same element, then $I_k = \nu_\theta i_k$, where ν_θ is the number of fast neutrons emitted by the element per absorption of a thermal neutron. In this way we obtain a system of linear equations, the number of which is equal to the number of fuel elements in the core of the reactor. Actually, the number of different equations is considerably smaller because of the symmetrical arrangement of the elements. In the case under consideration, a system of eight equations is obtained.

---

§ For details see S. M. Feinberg's paper "Heterogeneous Methods of Reactor Calculations. Survey of Results and Comparison with Experiments," P/669, session 23A, volume 5, these Proceedings.

It is convenient to choose the number ν_δ as the unknown quantity. For a given number and arrangement of fuel elements one can, with this system of equations, determine the value of ν_δ for which the determinant of the system of homogeneous linear equations is zero. This value of ν_δ can then be compared with the value of ν_δ obtained by calculation for the homogeneous core. The difference between these values of ν_δ was found to be approximately 0.03. From this it follows that the homogeneous method is quite satisfactory for the reactor under consideration. In addition to the verification of the applicability of the homogeneous method, the method of heterogeneous calculation of critical dimensions opens the possibility to investigate more accurately the distribution of heat generation in the fuel elements of the core and, in particular, enables one to calculate the effects produced by disturbing the periodicity of the lattice (for instance, the effect of removing a single fuel element or replacing it by a neutron-absorbing rod). With the homogeneous method such effects can be calculated only very roughly.

As an example, Fig. 4 shows the distribution of the density of thermal neutrons in the system consisting of 24 multiplying and 6 absorbing rods with a hollow cell in the centre, calculated with the heterogeneous method.

When comparing the calculated values of the critical mass with the experimental ones, it is necessary to make allowance for the presence in the actual core and reflector of a number of absorbing elements of construction. In the system without water these increase the critical mass by 8% and in the system containing water by 7%. Table 3 shows calculated and experimental values of the critical mass.

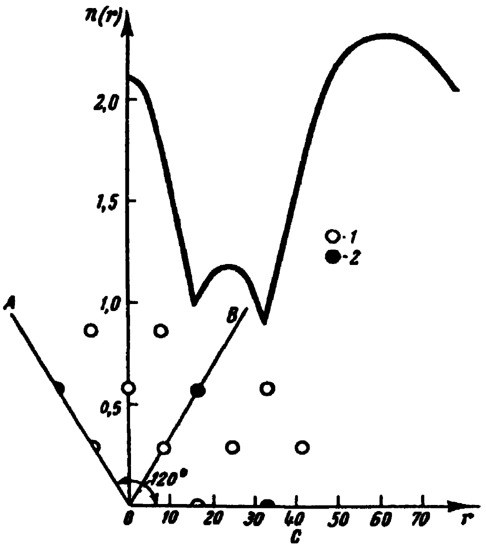

Figure 4. Thermal neutron flux along symmetrical directions OA, OB and OC; (1) uranium rods; (2) absorbing rods

Table 3. Calculated and Experimental Values of the Critical Mass

	Experimental	*Calculated*
1. Critical mass for the lattice without water	35 elements	33 elements
2. Critical mass for the lattice with water (water level equal to upper level of the core)	23.5 elements	25 elements

It is seen that when the channels are filled with water the critical mass is considerably reduced, which is due mainly to a considerable reduction in the migration length of the neutron.

The discrepancies between the calculated and experimental values of the critical mass show the accuracy of calculation.

6. FISSION BY EPITHERMAL NEUTRONS, CADMIUM RATIO

On the basis of the above-mentioned calculations, one may assume that the neutron capture in U^{235} and, consequently, also the fission of the latter are caused by thermal neutrons only. Actually, of course, a certain fraction of neutrons is captured by U^{235} during the moderation process. It is obvious that if a large number of fissions were due to the slowing down neutrons, then calculations which take into account fission by thermal neutrons only may be significantly in error. The ratio of the number of neutrons captured during the slowing down process to the number of neutrons captured in the thermal region, is in first approximation given by:

$$\beta = \alpha \frac{\sigma_{235}{}^{p}}{\sigma_{235}{}^{T}} = \frac{1}{\xi} \cdot \frac{\Sigma_c{}^{T}}{\Sigma_s{}^{z}} \cdot \frac{\sigma_{235}{}^{p}}{\sigma_{235}{}^{T}}$$

where ξ is the logarithmic energy loss; $\sigma_{235}{}^{p}$ is resonance integral of U^{235}; $\sigma_{235}{}^{T}$ is capture cross section for thermal neutrons of the same isotope; $\Sigma_c{}^{T}$ is total macroscopic capture cross section of thermal neutrons in the lattice; and $\Sigma_s{}^{z}$ is total macroscopic scattering cross section of a neutron in the moderation process.

If the absorption cross section varies according to the $1/v$ law then:

$$\frac{\sigma_p}{\sigma_T} = \frac{1}{\sigma^T} \int_E^\infty \sigma(E') \frac{dE'}{E'} = \frac{1}{\sigma^T} \int_E^\infty \sigma^T \frac{v^T}{v'} \frac{dE'}{E'} = 2 \sqrt{\frac{E_T}{E}}$$

For the mixture of water and graphite $(1/\xi)(\Sigma_c{}^{T}/\Sigma_c{}^{z})$ is found to be 0.185. Consequently, if the capture cross section of U^{235} on an average would obey the $1/v$ law (which in reality is only approximately true) then $\beta \approx 0.185 \times 2 \sqrt{E_T/E}$. Assuming that $E_T = 1/40$ and $E = 0.4$ ev, which corresponds to the upper limit of resonance absorption of neutrons in cadmium, we find for the fuel element:

$$\beta_{Cd} = 0.092$$

When calculating β_{Cd} in graphite or an empty duct it is necessary to multiply the above-mentioned figure by the ratio of the density of thermal neutrons in the fuel element to the density in graphite, equal to 0.75.

In order to verify the correctness of this estimate, a copper detector was used to determine the cadmium ratio, i.e., the ratio of the activity of the detector covered with cadmium to the activity without cadmium cover. In one of the central ducts of the reactor we found the value 0.107. The deviation of the capture cross section of copper from the $1/v$ law is known; taking into account this deviation we find that the cadmium ratio for a $1/v$ cross section is equal to 0.057. This value can be considered as sufficiently close to the value $0.092 \times 0.75 = 0.069$ calculated above if we take into account the fact that the neutron spectrum in the core is somewhat softer than in the infinite lattice.

In the system without water the cadmium ratio of the copper detector is found to be 0.133.

If the energy range above 0.1 ev is considered as epithermal, then the number of collisions with capture in U^{235} (which is proportional to $2\sqrt{E_T/E}$) increases by a factor of 2. Therefore, for the whole epithermal spectrum, the number of fissions in U^{235} is approximately 9%.

On the basis of this examination we can conclude that in the case under consideration the calculations of critical size made assuming complete absence of U^{235} fission in the epithermal region are still sufficiently accurate.

7. SPATIAL DISTRIBUTION OF NEUTRON FLUX IN THE REACTOR

The vertical distribution of the neutron flux in the reactor was studied in the channel of an automatic shim rod by means of a copper detector for thermal neutrons. Figure 5 shows the variation of the neutron flux in the core and reflector.

As is seen from Fig. 5, there is a considerable asymmetry with respect to central plane of the core. This asymmetry is explained by a difference in the properties of the top and bottom reflectors. The mean life of thermal neutrons in the bottom reflector is seven times larger than that in the top reflector. As was explained before, this is due to the presence in the top reflector of a considerable amount of water in the cooling channels.

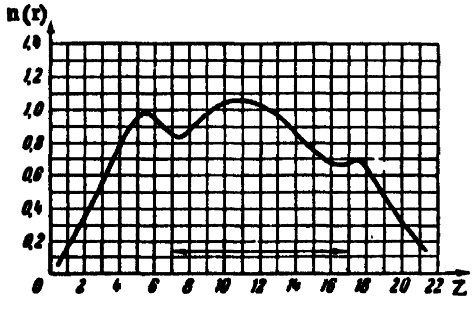

Figure 5. The neutron flux at different levels of the reactor. The core is indicated by a double arrow

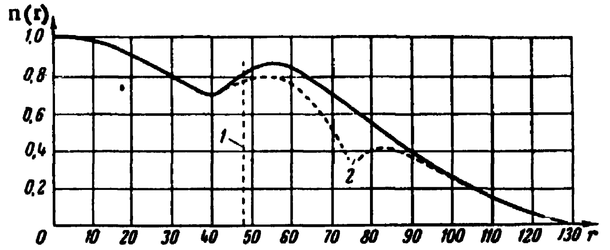

Figure 6. Distribution of the flux of thermal and epithermal neutrons along the radius of the "homogenized" reactor; (a theoretical curve): (1) border of the active zone, (2) location of a "loop"

The distribution of the neutron flux along the radius of the core was found in the process of calculating critical dimensions. Figure 6 shows a theoretical variation in the flux of thermal and epithermal neutrons along the radius of the "homogenized" reactor.

It is seen from Fig. 6 that a considerable increase in the density of thermal neutrons is observed in the side reflector. This is a result of a marked difference in the mean lives of thermal neutrons in pure graphite and in the lattice of the core. However, the side reflector contains the "loops" and a large number of control and safety rods. The presence in the side reflector of this rather large amount of neutron absorbing constructional materials decreases the mean life of neutrons and, consequently, their density. The dashed line in Fig. 6 gives a schematical picture of the decrease in thermal neutrons flux due to the absorption in the steel jacket of a "loop."

8. CONTROL AND SAFETY SYSTEM

Control of the nuclear chain reaction and shut down of the reactor in the case of emergency are effected through a system of neutron-absorbing rods that are operated by hand or by automatic drives. The rods may be operated automatically by signals from ionization chambers. Figure 7 shows the arrangement of control rods and "loop" channels.

Two rods for automatic control are placed in the side reflector. When these rods are completely immersed in the apparatus, K_{eff} is reduced by 0.001. This is sufficient for sustaining the power of the reactor at the required level and for compensating minor, accidental fluctuations of reactivity.

Three manual and three slowly moving automatic absorbing rods made of boron carbide are situated between the fuel channels of the core.

Each of these rods changes K_{eff} by 0.015, so that the total effect of all six rods is equal to 0.10. These rods take up the bulk of the excess reactivity of the reactor and secure a reactivity reserve for Xe^{135} poisoning and for overcoming the "iodine dip" during a short shut down of the pile; they also secure the necessary reserve of reactivity for the slow processes of the burn up and poisoning of the fissionable material.

In order to shut down the system rapidly in the case of an emergency, two systems of safety rods were provided for in the original design; they came

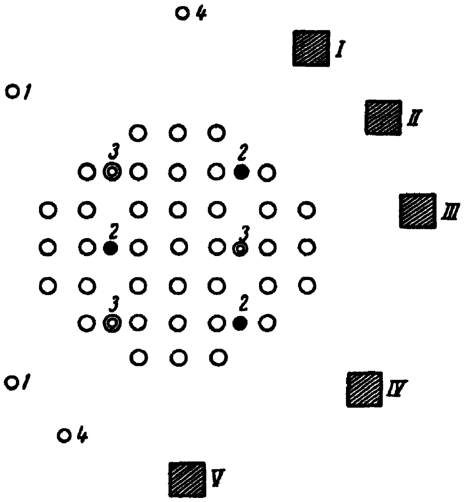

Figure 7. Arrangement of control rods and "loop" channels: (1) rods for automatic control; (2) shim rods, manual; (3) shim rods, automatic; (4) safety rods. "Loop" channels: (I) with gas cooling; (II) with high pressure water cooling; (III) with liquid metals cooling; (IV) with medium pressure water cooling; and (V) with high pressure water cooling

into action simultaneously but operated with different velocities. The three for the fast safety rods were situated on the border between the active zone and the reflector. They were cadmium rods, producing rather small changes (~0.15%) in K_{eff}, but operating very rapidly through a pneumatic system. Not more than 0.02 sec passed between the moment when the signal came from the ionization chamber and the moment when the rod reached its lowest position. These rods were incorporated because it was feared that the reactor reactivity might sharply change as a result of air bubbles being sucked in into the flow of cooling water. Simultaneously with these rods two other rods of a slowly-operating safety system came into operation. These rods reached their extremely lowest position in 0.4 sec, but produced a much larger change in K_{eff} equal to ~0.01. In the course of operation of the reactor it turned out that there was no need for the fast safety rods. Therefore, these rods were dismantled (they are not shown in Fig. 7).

9. TEMPERATURE EFFECT, BURNING UP AND SLOW POISONING

As the reactor heats up the multiplication parameters of the lattice change and the reactivity decreases. The temperature in the graphite layer at peak power of the reactor reaches 470°C, while the temperature of the neutron gas increases to 800°K. Owing to these temperature changes in the lattice of the reactor two effects of opposite signs appear which to a certain extent compensate each other. The diffusion length of graphite increases approximately to 60 cm. The penetrability of water for thermal neutrons is also changed considerably. As is well known, changes of the neutron energy are accompanied by great changes in the neutron scattering cross section of the water molecule. As a result of the increase in the diffusion lengths of graphite and, particularly, of water, the neutron flux become more uniformly distributed in the lattice cell and the thermal utilization increases. On the other hand, the migration length of neutrons M increases; resonance capture in U^{238} increases as a result of Doppler broadening of the resonance levels; the number of neutrons produced per neutron absorbed, ν, decreases slightly because of interference of fission and capture levels in U^{235}. According to measurements done, the temperature coefficient of K_{eff} is about 6.7×10^{-5}/°C of temperature of the graphite layer at room temperature.

As a result of the considerable power density of the reactor, poisoning by Xe^{135} and Sm^{149} decreases the reactivity considerably, and, when the system is shut down, a large "iodine dip" occurs. At design power this poisoning results in changing K_{eff} by -0.04, and the bottom of the "iodine dip" is lower than the stationary level of reactivity by -0.045. The minimum of the reactivity is reached approximately 9 hours after the system is shut down. A typical reactivity variation curve is shown on Fig. 8.

Another reason leading to a considerable, although slow decline in the reactivity of the reactor is the burn up and slow poisoning of the fuel elements, that is, the changing of the isotope composition of metal as a result of the nuclear chain reaction. During design power operation K_{eff} decreases by about 7×10^{-4} per day, according to measurements.

10. NEUTRON BEAMS

The thermal graphite column has a cross section of 1.0 × 1.0 m and is 2 m in length. This column leads into a special laboratory room (see Fig. 9). It gives a broad beam of thermal neutrons with an intensity of about 10^7 n/cm² per sec.

Two neutron beams of 100 mm in diameter emerge from the active zone (Fig. 9). One of these has been designed for installing a mechanical velocity selector with a large flight path, the other for miscellaneous neutron measurements.

In addition there is a neutron beam of 60 mm in diameter coming from the centre of the side reflector.

In both beams with 100 mm diameter, the density of the thermal neutron flux at the point where they emerge is 10^9 n/cm² per sec; in the beam emerging from the centre of the side reflector it is 10^8 n/cm² per sec.

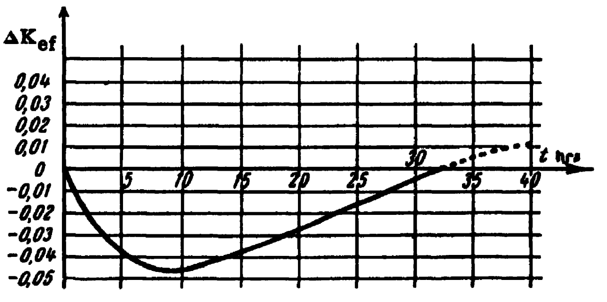

Figure 8. Drop in reactivity after the reactor is shut down (time after shutdown on the abscissa)

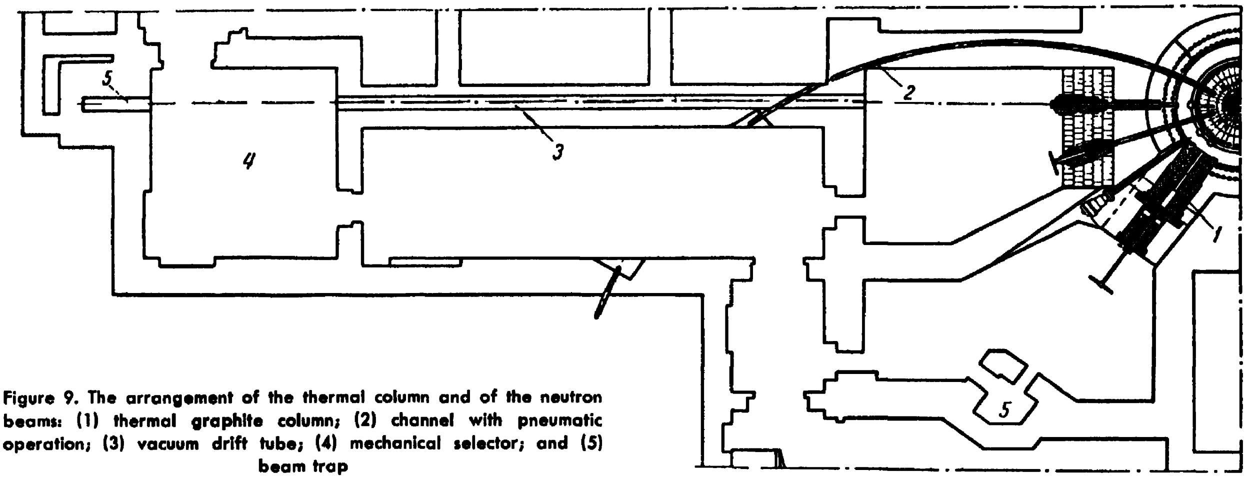

Figure 9. The arrangement of the thermal column and of the neutron beams: (1) thermal graphite column; (2) channel with pneumatic operation; (3) vacuum drift tube; (4) mechanical selector; and (5) beam trap

Figure 10 shows the spectral composition of neutrons in the beam emerging from the core, measured by means of a mechanical selector.

In the same figure the Maxwell spectrum of the neutron gas at a temperature 480°K, corresponding approximately to the temperature of the graphite, is shown by a dotted line. Apparently, the spectrum of neutrons in the beam differs only slightly from that in the core.

The beam holes are provided with remotely-controlled shutters, so that the work on neutron beams does not interfere with the running of the reactor. One of the shutters is shown in Fig. 11. It is mounted with its axis horizontal and perpendicular to the axis of the beam. When the shutter is turned through 90°, by remote operation of its electric drive, the neutron beam is intercepted by layers of paraffin and lead.

While the shutter is in an intermediate position, samples can be placed in it for irradiation in a weak neutron flux.

11. SHIELDING

To protect the personnel from the biologically dangerous effects of neutron and γ-radiations from the core, the reactor is surrounded by shielding.

Side shielding is formed by: the graphite reflector, 80 cm thick; an iron shell, 2.5 cm thick; a concrete shield, 320 cm thick, with specific gravity 2.4 gm/cm^3.

The total radiation behind the side shielding (when the beam holes are shut) is not more than 0.1 of the maximum permissible dose, which ensures not only the safety of the personnel, but also provides a comparatively low harmful background for physics experiments.

The top shielding of the reactor is formed by: the graphite reflector, 80 cm thick; an additional graphite layer above the reflector, 150 cm thick; a lead layer, 40 cm thick; and a top iron slab, 20 cm thick.

When the fuel channels and the irradiation channels are closed, the total neutron and γ-radiation over the top slab is about 0.2 of the maximum permissible dose.

When fuel assemblies are removed from the reactor after prolonged irradiation, there is a very high activity in the main hall. Therefore, the main hall has concrete walls 130 cm thick; the operations are performed by remote control.

There is considerable activity of oxygen and other forms of induced activity in the initial circulation circuit and its pumps. They are therefore shielded by concrete walls and floors 100 cm thick. In the laboratory spaces which receive neutron beams, the walls and floors have a thickness of 100 cm.

12. ENGINEERING ASPECTS OF THE REACTOR

The flow diagram is shown in Fig. 12.

The reactor is cooled by distilled water in a closed circuit: water from tank (1) is pumped by centrifugal pumps (2), and enters the distributor (3) under pressure. From this tube the water enters the fuel assemblies (4) and cooling channels of the reflector (5), then it enters the horizontal collector (6) and heat-exchangers (7) and returns to tank (1). The cooling channels and connecting tubes with the collectors are made of aluminium alloy. All other elements of the distilled water circuit: pipe-lines, fittings, heat-exchangers, tank and pumps, are made of stainless steel.

To cool the primary circuit, river water is led through pipe-line (8) to the heat-exchangers (7); then it is released back into the river. River water is also used to cool the concrete slab below the reactor and on the side.

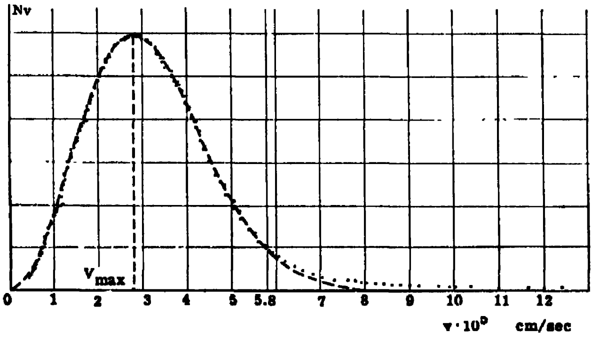

Figure 10. The spectral composition of the neutrons in a beam: $v_{max} = 2.8 \times 10^5$ cm/sec ($E = 0.041$ ev); $T = 480$°K. The dotted line shows Maxwell distribution: $f(v) = Av^{2}e^{-v^{2}/v^{2}_{max}}$

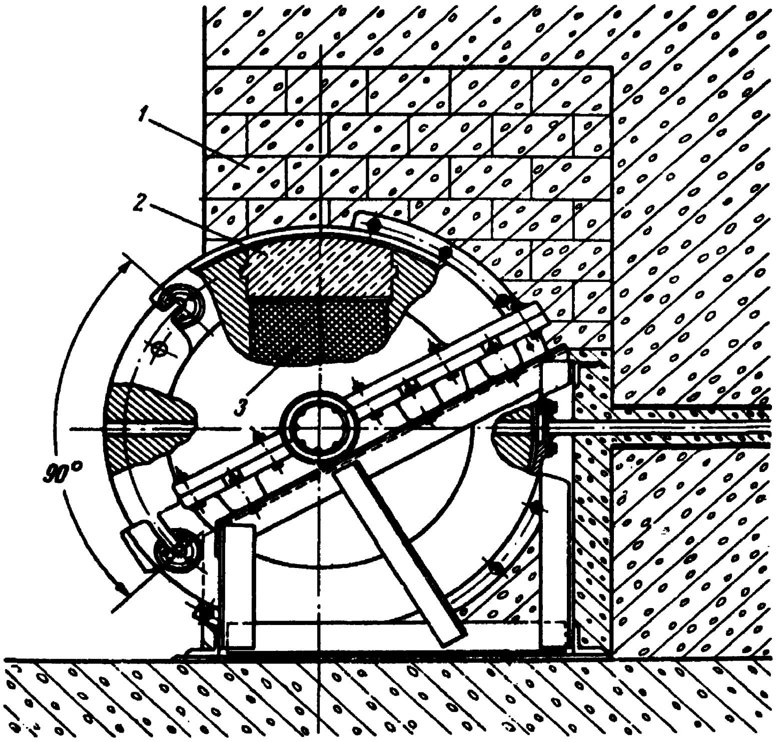

Figure 11. Beam hole shutter: (1) shielding bricks; (2) lead; and (3) paraffin

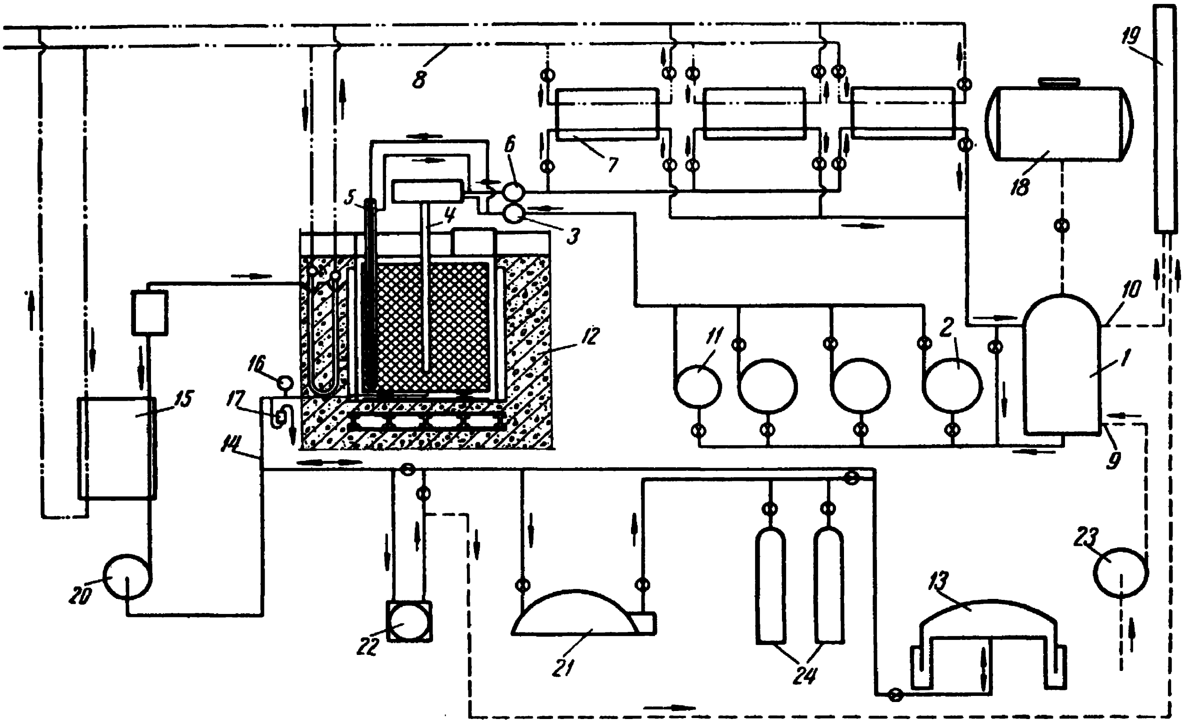

Figure 12. Flow diagram: (1) degassing tank; (2) centrifugal pumps; (3) distributor; (4) fuel assembly; (5) cooling channels in the reflector; (6) collector; (7) heat-exchangers; (8) pipe-line for river water; (9) air-pipe; (10) pipe-line to the ventilation stack; (11) emergency pump; (12) reactor shell; (13) gas holder; (14) helium pipe-line; (15) gas cooler; (16) water detector; (17) water lock; (18) emergency supply of distilled water; (19) ventilation stack; (20) gas blower; (21) compressor; (22) vacuum pump; (23) ventilator; and (24) helium storage

Tank (1) is under atmospheric pressure. It is used for two purposes: as a reserve capacity for the primary circuit and as a separator for the explosive gas mixture, which is formed in the reactor by disintegration of water under the influence of radiation. From the tank the fire-damp is removed by a flow of air which is supplied through the air-pipe (9) and then discharged to the ventilation stack through the pipeline (10).

Special attention has been given to the reliability of the cooling. In connection with this, three pumps, two working and one in reserve, are attached to the primary circuit. The pumps are driven by alternating current motors. Each of the two working pumps is fed from an independent local supply so that any failure of the supply results in stopping of only one pump. If both pumps would break down, two smaller emergency pumps (11) with direct current motors are automatically switched on; these motors are fed by a storage battery. It stands to reason that if this occurs, the emergency protection of the reactor starts operating automatically. No such damages have occurred during operation of the installation.

In order to monitor the cooling of the fuel assemblies, individual flow meters were installed in the cooling lines. When the amount of water flowing through the channels is decreased or increased by a definite amount, the reactor shuts down automatically.

The graphite layers of the reactor are stacked inside a hermetic steel vessel (12). To cool the graphite, the vessel is filled with helium. The helium pressure in the apparatus exceeds atmospheric pressure by 20-50 kg/m^2 and is controlled by the gas-holder (13). The helium system (14), is also used for drying the graphite if water penetrates into it as a result of leakage in one of the cooling channels or some accident during repair work. During operation of the reactor moisture is removed in the form of steam and condenses in the heat-exchanger (15) of the helium circuit. A detector (16) stops the reactor when water appears in the graphite. It is attached to the section of helium circuit adjoining the bottom of the reactor. Drainage of water from the vessel is through a water lock (17) which prevents flooding of the reactor in case the wall of a cooling channel is broken. The defective channel can be detected by putting pressure on it.

The reactor is serviced only from the top. Installing of channels, loading of the fuel elements and other parts, as well as unloading, are done from the top. Unloading is done by a bridge crane with remote control; the parts that are removed from the reactor are lowered in storage cells located next to the reactor in the concrete shielding.

As shown on Fig. 13, the fuel assemblies of the reactor have the form of a field pipe.

The fuel element itself is shown on Fig. 14. It has a form of a tube with aluminium cladding inside and outside. The aluminium canning has end pieces that center the fuel element in the channel. Also, halfway the length of the fuel element a belt with ribs assists in centering it.

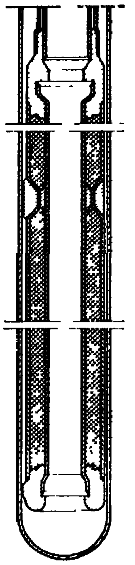

Figure 13. (Left)
RPT fuel assembly

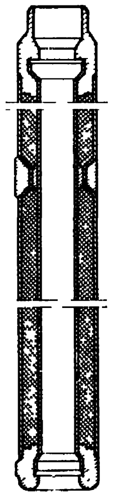

Figure 14. (Right)
Fuel element

The control rods are suspended from cables connected with motor drives. The channels in which they move are also in the form of field pipes and are part of the primary cooling circuit.

Thirteen ionization chambers have been installed to monitor the operation of the reactor. Among these, two chambers filled with boron trifluoride, are for working at very small starting power. All the other chambers have electrodes coated with boron carbide and are for working at high power. Some of them are attached to the control rod circuit, others to the emergency circuit.

The current from the chambers attached to the control rod circuit passes first through the sensitive galvanometer showing pile power, and then through a potentiometer. Deviation of the chamber current

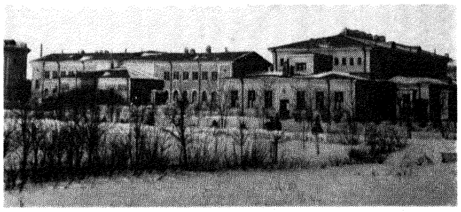

Figure 15. General view of the reactor buildings and the "hot" laboratory

Figure 16. Reactor building

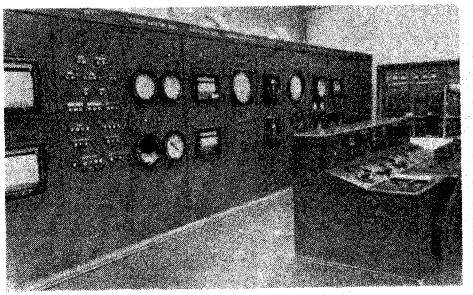

Figure 17. Control panel and shield

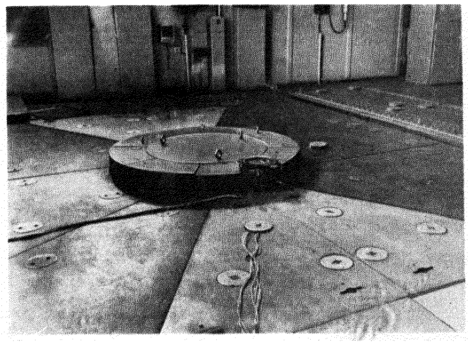

Figure 18. Top view of reactor: the top shielding of the reactor is seen

from the set value creates a difference voltage on the outlet terminals of the potentiometer, which is then successively stepped up by multistage electronic and servo amplifiers until it reaches the power required for the electric drive of the control rods.

The current from chambers attached to the emergency circuit is amplified and leads to the switching on of the emergency protection of the apparatus if the set value is exceeded by a definite amount.

The installation is shut down automatically if any of the working parameters deviate from the standard, or if any failure occurs. Automatic shutdown occurs: (*a*) if the pressure of the primary circuit before the reactor drops by 10%; (*b*) if the pressure of the primary circuit after the reactor drops by 20%; (*c*) if the outlet temperature of cooling water reaches 65°C; (*d*) if the pressure of river water on entering drops below 1.5 atm; (*e*) if the amount of the distillate in any of the fuel assemblies changes by more than 4%; (*f*) if the control rod is completely in; (*g*) if power fails on one of the mains supplying the plant; (*h*) if any of the experimental circuits (loops) fails.

The principal specifications of the reactor are given in Table 4.

Table 4. Principal Characteristics of RPT

1. Power	10,000 kw
2. Total flow of primary coolant water	250 m^3 per hour
3. Pressure of water on entering the core	12 atm
4. Pressure of water on leaving the core	8.5 atm
5. Temperature of water on entering	20°–30°C
6. Temperature of water on leaving (average)	55°–65°C
7. Flow of water through each fuel channel	6.0 m^3 per hour
8. Velocity of the water in the channels	5.5 m per sec
9. Power of one channel, maximum	400 kw
10. Heat flux, maximum	2×10^6 kcal/m^2 per hour
11. Temperature of water in fuel channel, maximum	70°C
12. Temperature of graphite	up to 470°C
13. Temperature of the side walls of the reactor vessel	up to 200°C
14. Flow of river water	up to 400 m^3 per hour

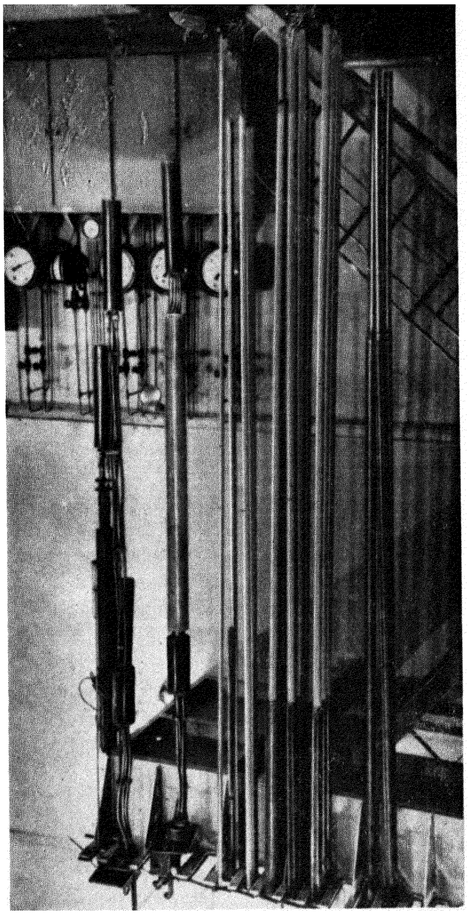

Figure 19. Platform with suspended spare fuel and experimental assemblies, and ionization chambers

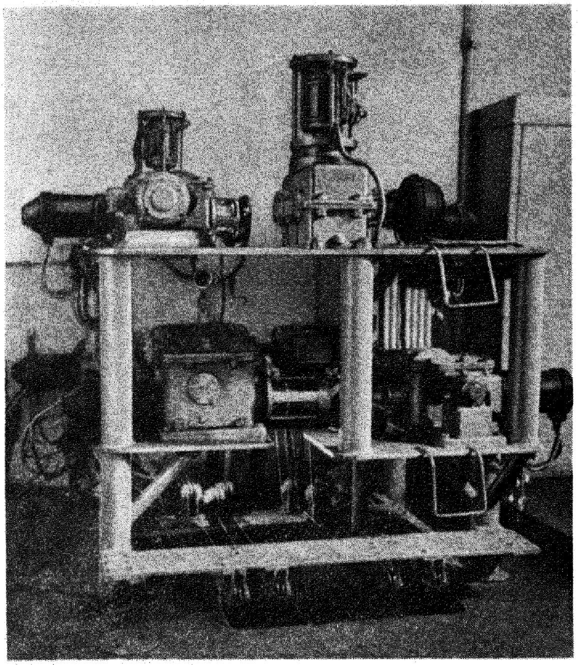

Figure 20. Table with the electric drives of the control rods

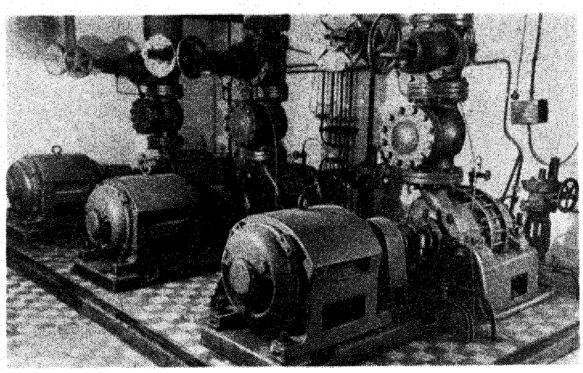

Figure 21. Main circulation pumps of the installation

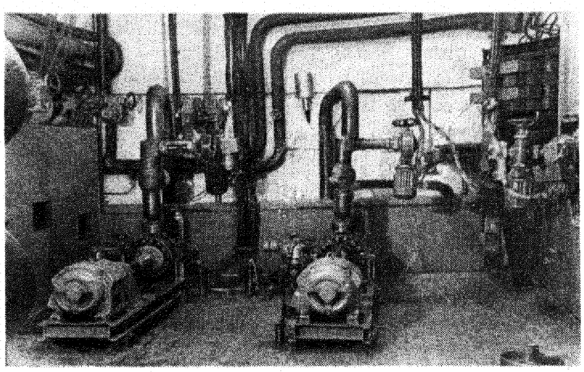

Figure 23. High pressure circulation pumps of the "loop" with water cooling

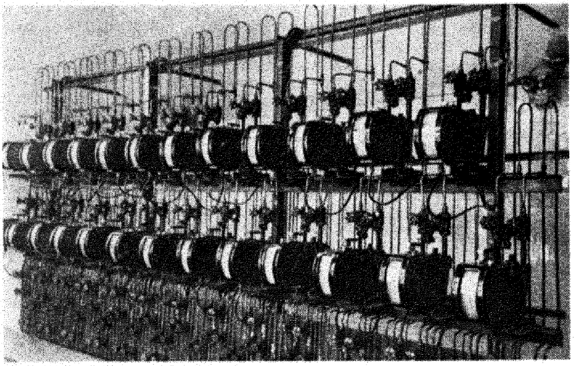

Figure 22. Shield with meters registering flow through the cooling channels of the reactor

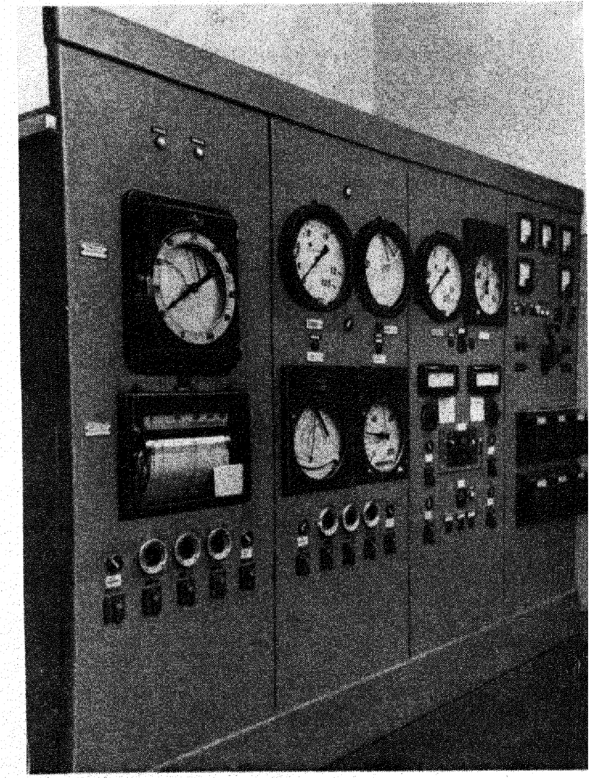

Figure 24. Panel of loop no. 3 with water cooling

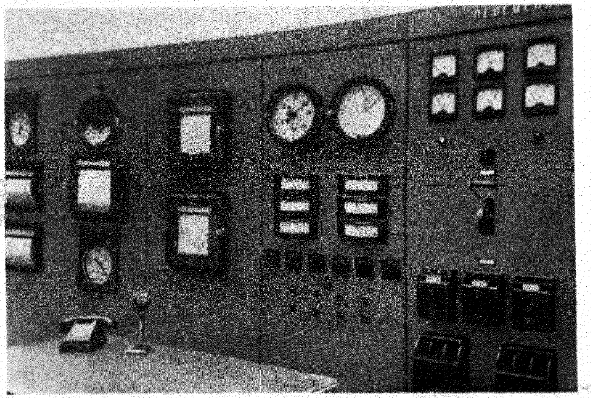

Figure 25. Panel of loop with metal cooling

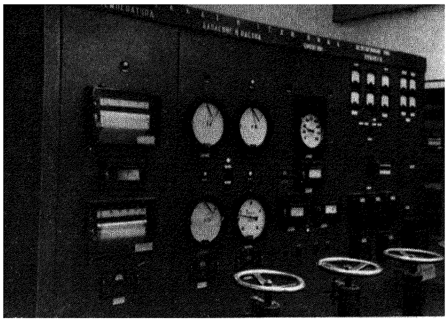

Figure 26. Panel of loop no. 2 with water cooling

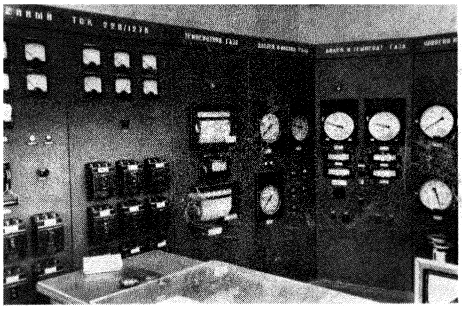

Figure 28. Panel of loop with air cooling

During the whole period of running, that is, in the course of more than three years, the reactor worked quite normally and steadily. There was not a single serious disturbance. Of the minor disturbances we may mention the following:

1. On several occasions there was water leakage from the fuel assemblies. In the original fuel elements the centering ribs were 2 mm thick. As a result of the vibration of the fuel element in the water flow through the channel, the channel wall was completely worn away by these ribs after 4–5 months. To avoid this, it was found necessary to turn the fuel elements through 15° after every two months of operation. On the new fuel elements the ribs are 10 mm thick and, in addition, they are provided with centering sprockets on a suspended pipe; at the present time the wearing away of the wall is not observed at all.
2. There were three occasions when water began to leak from the assembly at the place of the bottom weld.
3. There were seven occasions when the fuel elements went out of commission as a result of being squeezed to the wall of the outer tube. This led to a reduction of the water flow over a part of the surface of the element, and boiling began on it; this was shown by the appearance of blisters typical for the erosion of the aluminium surface through boiling. By raising the water pressure in the apparatus by 2 atm it was possible to eliminate these damages.

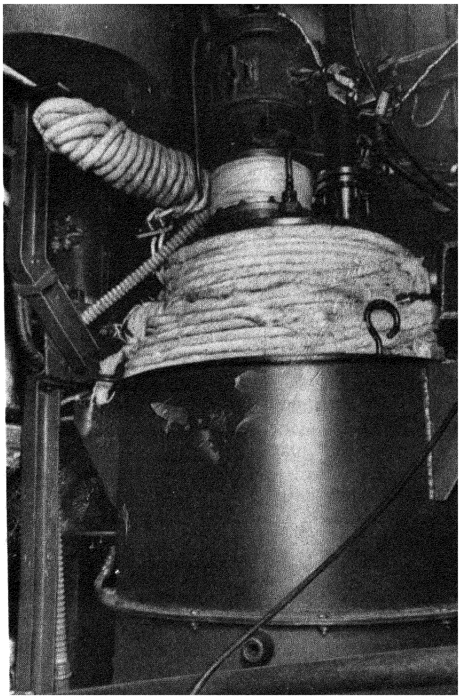

Figure 27. Loop with metal cooling: view of tank with melted metal and vertical pump

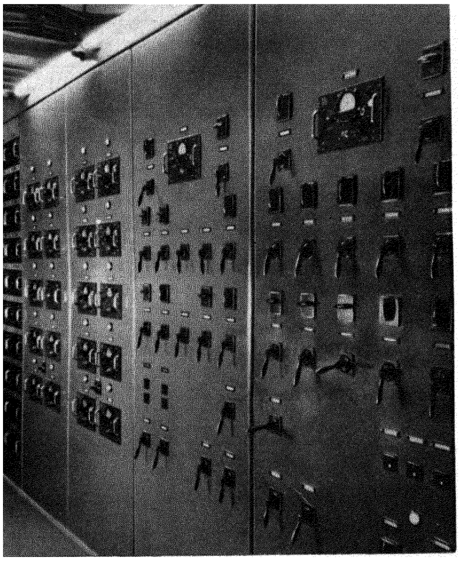

Figure 29. Control panel for general γ-activity and gas activity in the rooms

4. A considerable number of assemblies went out of commission in the first period of exploitation as a result of constructional defects.

The fuel elements and parts of the fuel assemblies can be examined in the cutting compartment located next to the reactor. This compartment is equipped with a universal cutting lathe, manipulators and an optical system. Cutting and examination operations are carried out by distant manipulation.

There were several occasions when test pieces broke, both in the experimental circuits (loops) and in the experimental channels in the main circuit. This caused a considerable contamination of water by radioactive substances. Such a possibility was taken into consideration when the apparatus was designed; next to the reactor building one for water decontamination was designed and constructed. Four settling basins with a holding capacity of 40 cubic metres each and two decontaminating absorption columns are installed in this building. Water contaminated with radioactive substances is at first discharged into the settling basins. As the need arises, but not within 30 days, this water is released from the upper part of the settling tank and passed through the decontaminating absorption columns; then it is mixed with the water flowing from the heat-exchangers and through the pipeline discharged into the river. This discharge is kept under constant supervision, the discharged water always being kept at an activity lower than the tolerance value.

All compartments of the plant are ventilated, the air being exchanged 10-20 times an hour. The ventilation system is arranged in such a way that an underpressure is constantly maintained in the spaces where gas activity may appear as a consequence of failures in the air-tightness of the main or experimental circuits. The space between the reactor shell and the concrete shield is also ventilated, which prevents the penetration of radioactive air into the service compartments. Under normal conditions of operation this gap is the principal source of gas (argon) activity, which reaches up to 4 curie per hour.

From the ventilation system the air is discharged into the stack 60 metres tall.

13. EXPERIMENTAL CIRCUITS (LOOPS)

In the experimental "loops," fuel elements of various construction as well as fuel assemblies are tested under actual operating conditions. Usually, such tests are preceded by comprehensive tests of samples in installations without irradiation. Naturally, the tests carried out in the loops are of principal importance.

For instance, one of the loops with water cooling served for the selection of the fuel elements as well as the channels for the atomic electric station. Three different constructions were tested after they had been successfully and thoroughly examined without irradiation. During testing in the RPT one of them proved to be altogether unsatisfactory, a second required improvements, while a third worked quite reliably for a long time; this latter construction was chosen for the reactor of the power station. In the process of testing, certain defects of the design were discovered and eliminated. After that one of the assemblies of a series manufactured for the reactor of the power station was tested in the same loop. Altogether, 20 elements for the atomic electric station have been tested in this loop.

The loops are autonomous circuits. Each of them is provided with complete operating and emergency equipment, has its own control panel and is served by a special group of personnel. The connection with the personnel servicing the reactor is as follows: The engineer in charge of the loop, when he wants to change the operation of his loop, or switch over the equipment in conformity with the instruction, must consult the engineer on duty of the reactor. In addition, as was already mentioned, the reactor will shut down if a number of working parameters of one of the loops deviate from the standard.

The Experimental Facilities of E.443

By H. J. Grout and F. W. Fenning,* United Kingdom

With the existing facilities at Harwell it is not possible to achieve neutron fluxes greater than 1.5 × 10^{12} thermal neutrons per cm^2 per second. Many aspects of nuclear reactor development and the need for radioisotopes of higher specific activity called for considerably higher neutron fluxes for experimental purposes.

Several possible types of experimental reactor were therefore considered, the final choice being a heavy water cooled and moderated reactor with nearly pure U^{235} fuel. The two general considerations leading to this decision are contradictory in some respects but were the need to limit the heat to be disposed of at a given neutron flux level and the desirability of spreading the neutron flux achieved over as large a volume as possible.

The objectives finally agreed upon were:

1. That the reactor should make available thermal neutron fluxes up to 10^{14} n/cm^2 sec.
2. That the reactor should be capable of producing the equivalent of 30,000 curies/annum of CO^{60} at high specific activity.
3. That the reactor should be capable of maintaining a limited number of loops for testing fuel systems for advanced types of reactor.
4. That the reactor should cost no more than £2 × 10^6 including site development, adjacent laboratories and offices and heavy water.

GENERAL CONSIDERATIONS OF EXPERIMENTAL FACILITIES

Experience with BEPO indicates the need for three general types of facility. These are

1. Beams of Neutrons

These require some collimation in the shield, a means of cutting off the beam without shutting down the pile, space adjoining the reactor face. Examples of this type of requirement envisaged for E.443 are a high speed chopper type monochromator used in

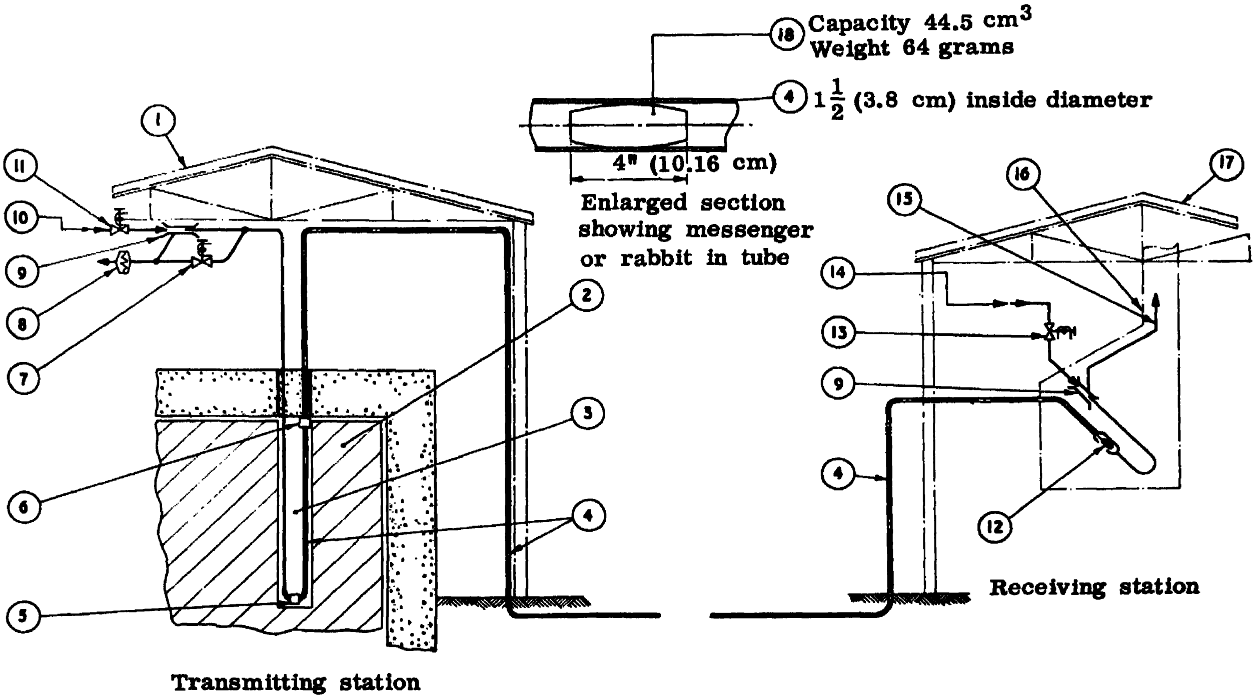

Figure 1. 220 rabbit installation. Description: (1) reactor building; (2) reactor; (3) experimental hole; (4) rabbit or messenger tube; (5) "in reactor" position switch; (6) "transit in reactor" switch; (7) solenoid exhaust valve; (8) filter before discharging air to building; (9) air injection; (10) air supply 30 psig; (11) solenoid air injection valve; (12) receiving station; (13) air injection valve (return to reactor); (14) air supply 30 psig (return to reactor); (15) air exhaust to stack; (16) laboratory fume cupboard; (17) laboratory building; (18) rabbit or messenger

---

* Atomic Energy Research Establishment, Harwell, Berks.

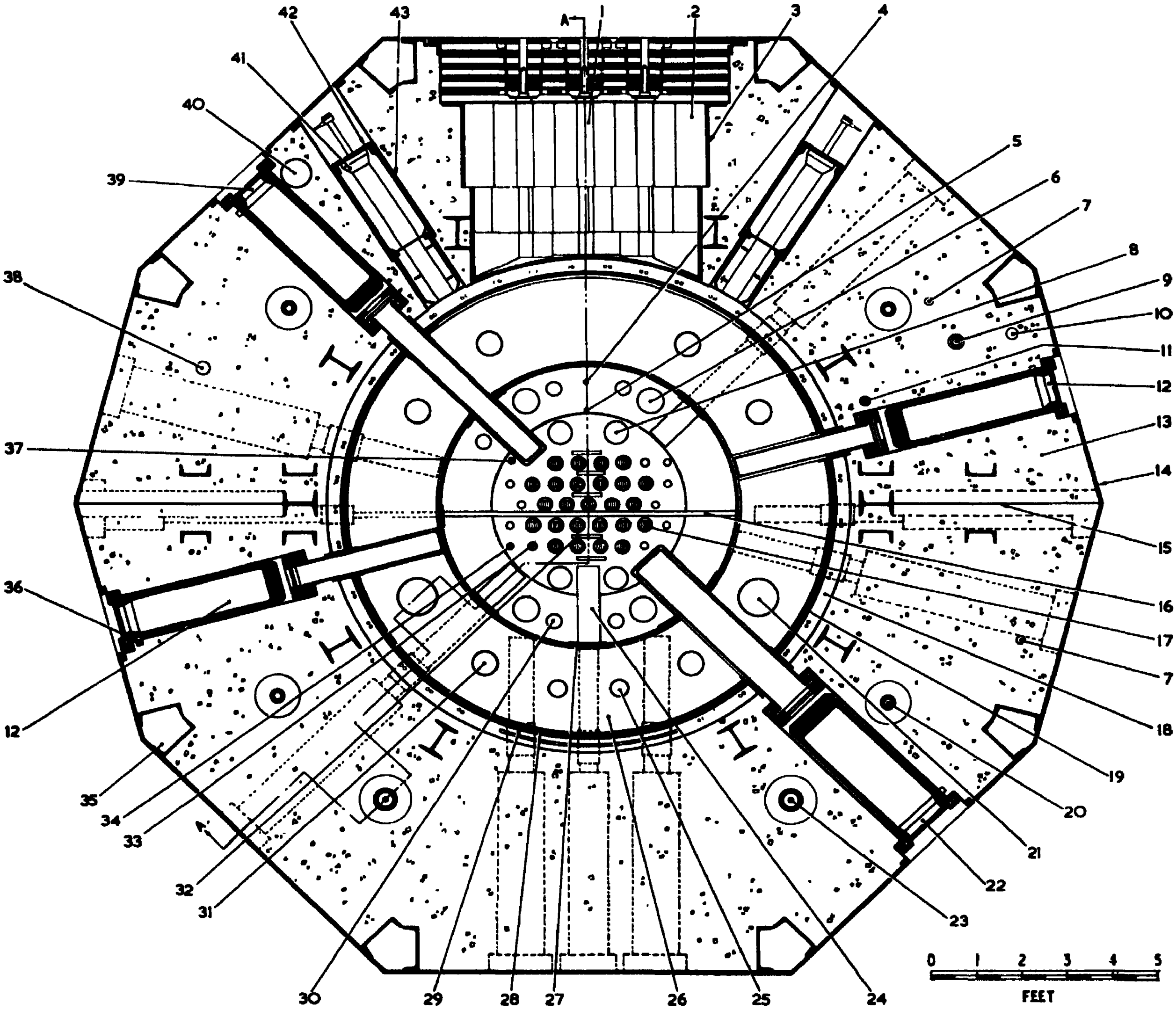

Figure 2. Reactor E.443: section in plan at half-depth of reactor core. Description: (1) thermal column; (2) thermal column graphite reflector; (3) thermal column boral lining; (4) 1 in. heavy water overflow pipe; (5) 1 in. aluminium tank drain pipe; (6) 7 in. heavy water outlet pipe; (7) 2 in. helium supplementary expansion line; (8) 6 V vertical experimental facility; (9) 2 in. anti-syphon weir pipe; (10) 3 in. helium balance line; (11) 1 in. anti-syphon weir pipe; (12) 6 HGR horizontal experimental facility; (13) concrete biological shield; (14) outer casing plates; (15) top structure; (16) 2 ton horizontal experimental facility; (17) fuel element; (18) lead shield with cooling coils; (19) steel tank; (20) 3 in. mortuary hole; (21) 10 VGR vertical experimental facility; (22) 10 H horizontal experimental facility; (23) 6 in. mortuary hole; (24) 4 H horizontal experimental facility; (25) 4 VGR vertical experimental facility; (26) graphite reflector; (27) aluminium tank; (28) lead thermal bond; (29) boral lining in steel tank; (30) 4 V vertical experimental facility; (31) 6 VGR vertical experimental facility; (32) coarse control rods with drive; (33) safety rod with drive; (34) 2 V vertical experimental facility; (35) service station; (36) CO_2 purge connection; (37) fine control rod with drive; (38) $3\frac{1}{2}$ in. air suction manifold interconnector; (39) 6 H horizontal experimental facility; (40) helium expansion main; (41) ion chamber fittings; (42) ion chamber plug; and (43) ion chamber liner

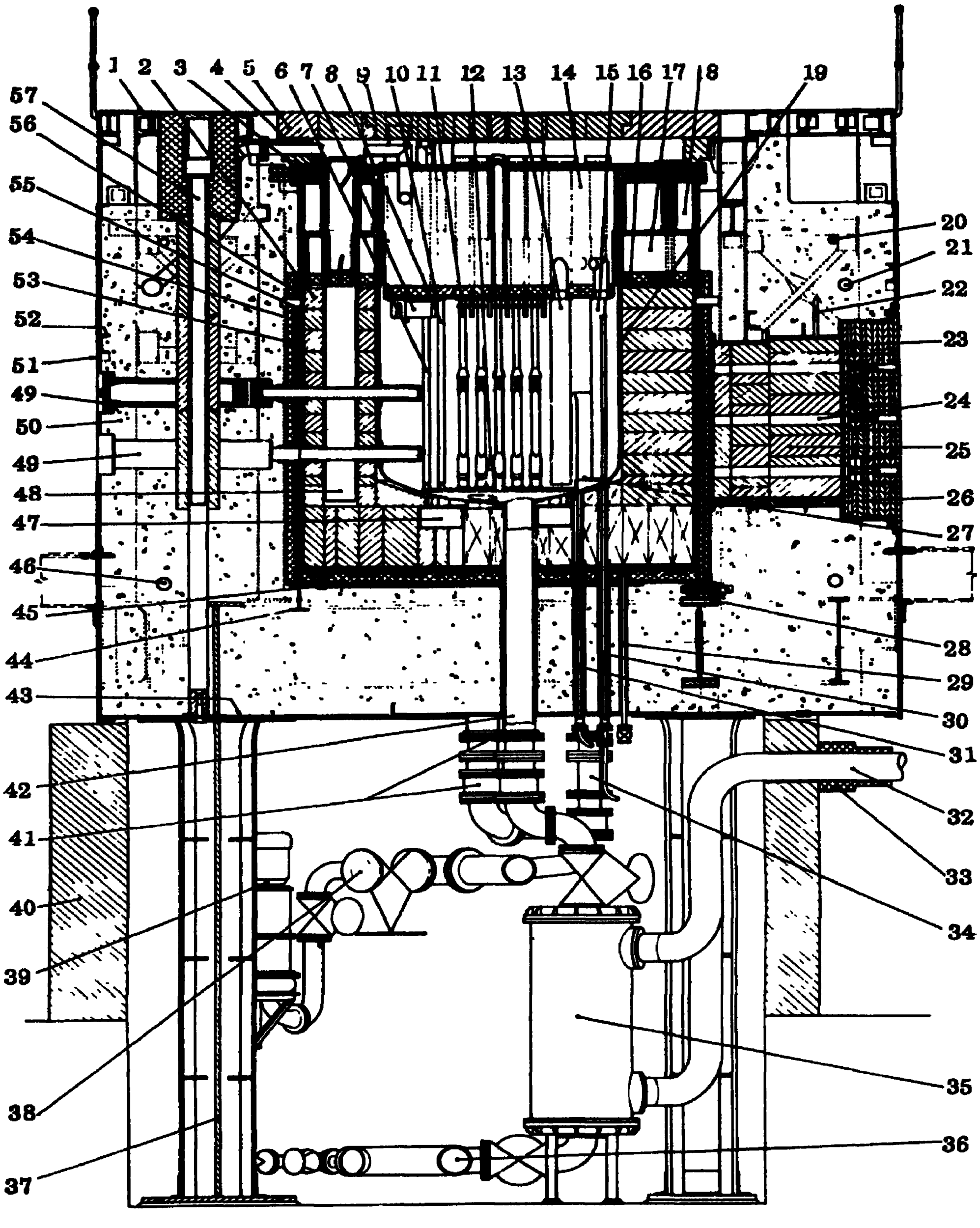

Figure 2a. Reactor E.443: section in elevation

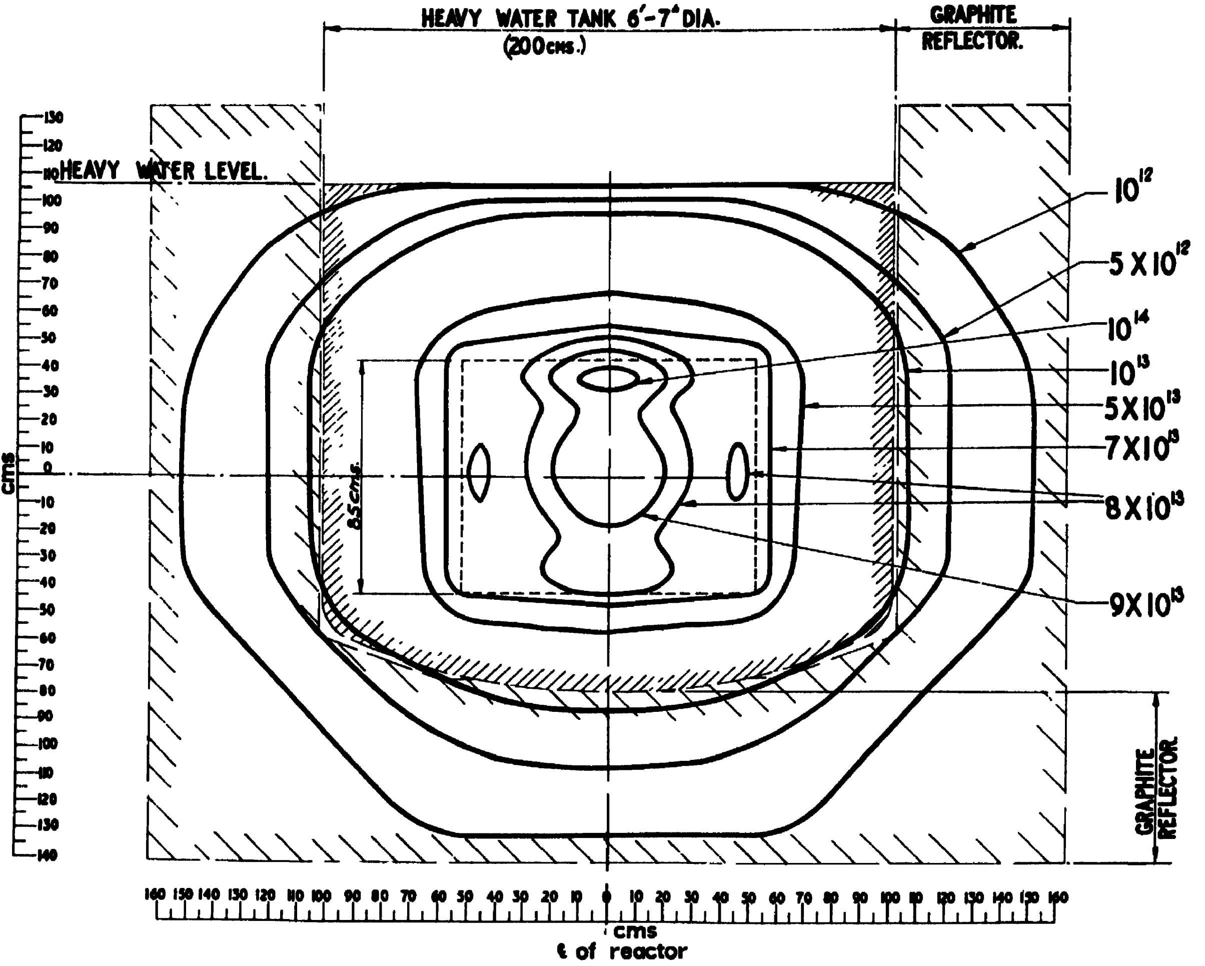

Figure 3. Undisturbed thermal flux distribution n/cm²/sec in E.443

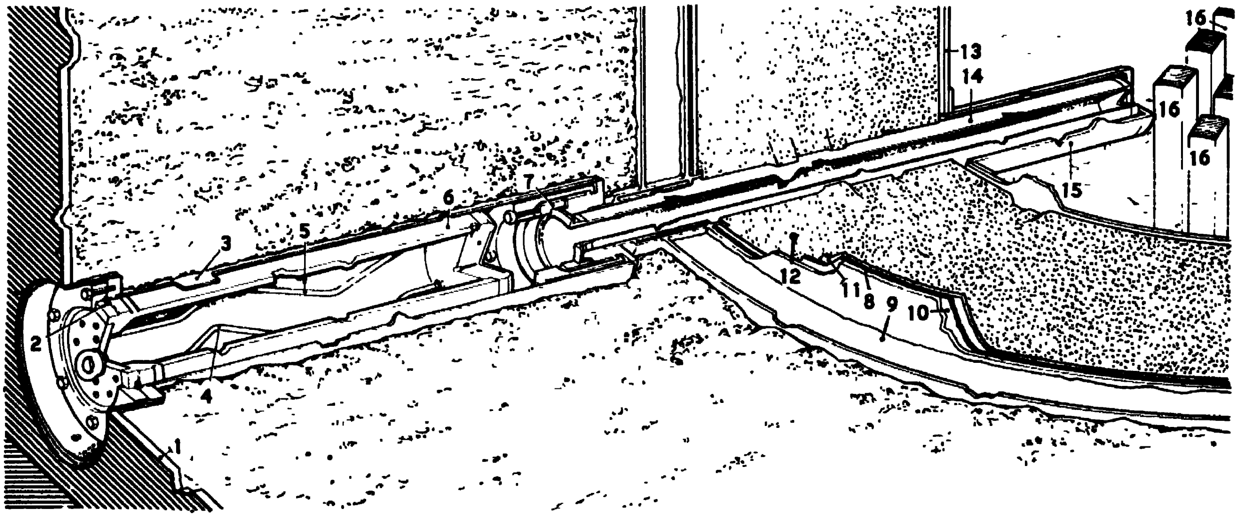

Figure 4. Reactor E.443: 6 in. horizontal experimental hole entering heavy water. (1) Steel facing on outside concrete biological shield; (2) gas sealing of shield plug; (3) steel liner tube in concrete shield; (4) shielding plug tip water cooling line; (5) CO_2 purge line; (6) biological shielding plug (concrete filling not shown); (7) aluminium liner tube sealing arrangement; (8) steel vessel; (9) lead thermal shield; (10) boral sheet; (11) lead; (12) graphite; (13) heavy water tank; (14) aluminium liner tube 6 in. inside diameter (removable); (15) fixed re-entrant aluminium tube from heavy water tank; and (16) fuel elements

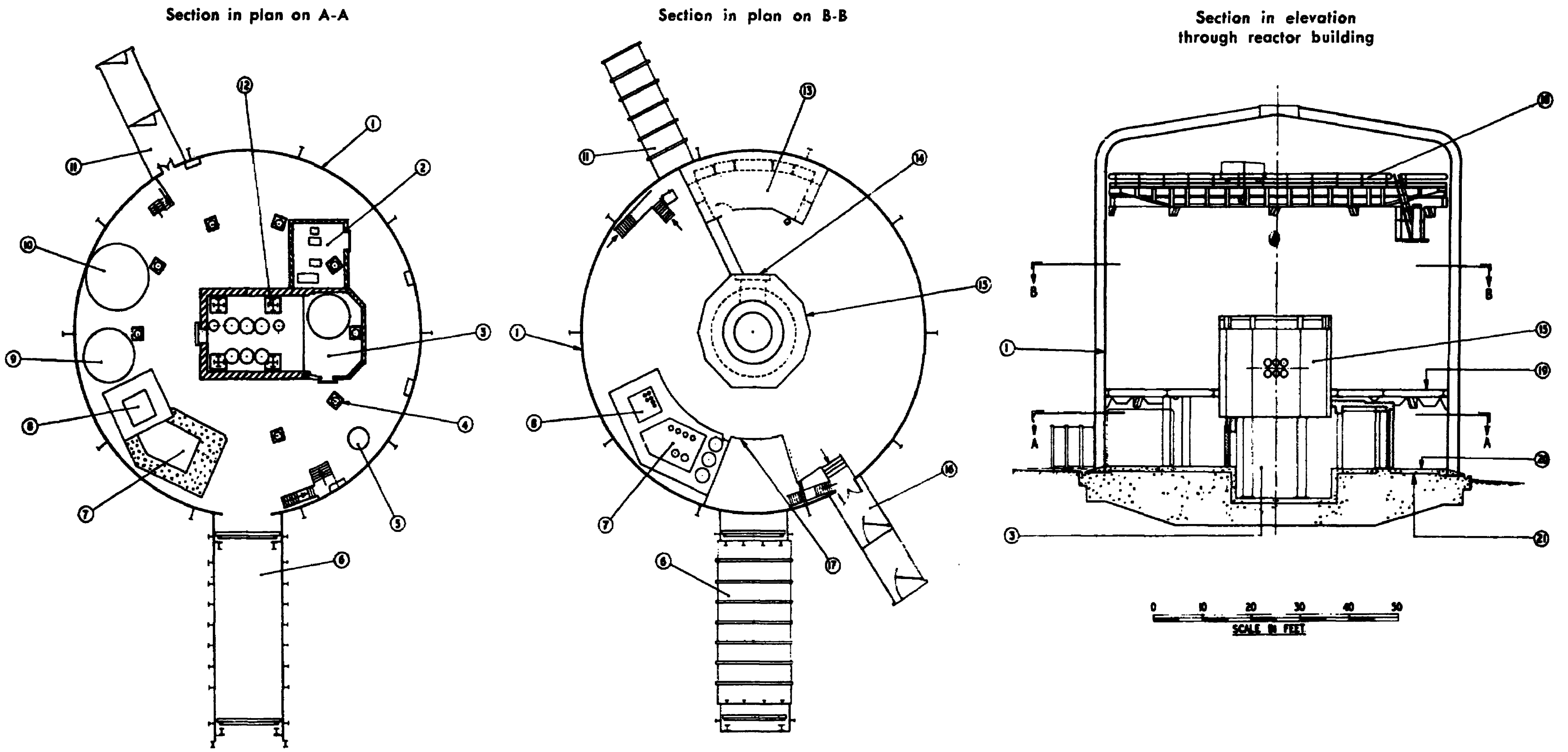

Section in plan on A-A

Section in plan on B-B

Section in elevation through reactor building

Figure 5. Reactor E.443: reactor building with plant layout. (1) Pressurized steel building 70′-0″ diam.; (2) thermal shield cooling water plant room; (3) heavy water plant room; (4) columns; (5) helium gasholder capacity 100 cu. ft.; (6) vehicle air lock with two air tight doors; (7) irradiation facilities storage block; (8) fuel element storage block; (9) helium gasholder capacity 500 cu. ft.; (10) expansion vessel capacity 1000 cu. ft.; (11) emergency personnel exit; (12) reactor column supports; (13) control room (on first floor); (14) thermal column on reactor; (15) reactor; (16) personnel air locked entry from laboratories; (17) line of opening in first floor for vehicle loading, etc.; (18) 20-ton crane; (19) first floor level; (20) ground floor level; (21) steel diaphragm

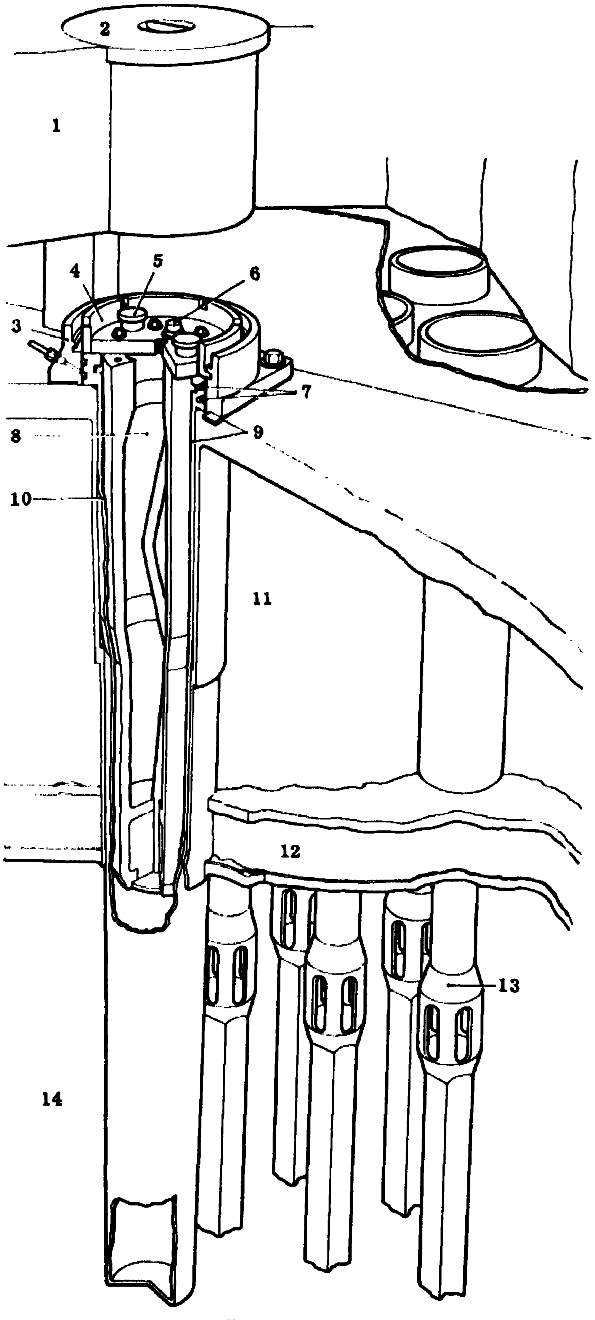

Figure 6. Reactor E.443: 6" dia. vertical experimental hole in heavy water. (1) Mild steel reactor top plate; (2) removable plug; (3) adaptor; (4) retaining ring; (5) shield plug locking control; (6) experimental hole purge connector; (7) aluminium liner tube sealing rings; (8) biological shielding plug (concrete filling not shown); (9) aluminium liner tube; (10) stainless steel liner tube in biological shield; (11) biological shield; (12) lead thermal shield; (13) fuel elements; (14) heavy water

conjunction with a 50 m flight path and a crystal spectrometer. The holes intended for such purposes are horizontal, the shield holes opening out to large diameter half-way through the biological shield, thereby giving space in which to fit a collimator fitted with a suitable shutter.

2. Irradiations without Close Control

These are the simplest requirements to fulfil. Included in this category is the preparation of radioisotopes where the parent material is stable in the temperature and radiation conditions available. For this purpose small diameter vertical holes and some horizontal holes are available. Their design is simple, providing only for small heat production in the irradiated specimen. This heat is removed by the reactor cooling circuits without special provision. No permanent allocation of space in the reactor building is required, but a shielded container is required for periodic discharge of irradiated material.

3. Irradiations in Which Close Control of Environment Is Required

These are by far the most difficult facilities to supply and operate. They include the use of holes for solid state studies, radiation chemistry studies and experimental fuel element testing. They usually require control of temperature or neutron spectrum thereby necessitating special heat removal circuits or furnaces and considerable space adjacent to the reactor for control and recording instruments. Usually the reliability of such experimental work must be as good as the reliability of the reactor itself. Clearly the maximum possible space inside the reactor and easiest access from outside the shield are desirable. In attempting to achieve these in E.443 as many large diameter vertical holes as possible have been planned and have been made removable. Limitations referred to later have restricted the number of holes accessible to both ends and these are horizontal. Provision is made for up to 1 Mw of heat to be disposable from all these facilities.

The location at Harwell imposes requirements of safety which it was decided to meet by containing within a steel pressure type building. This inevitably reacts back on experimental facilities through the cost of extra space inside such a building. Thus an early requirement for some vertical holes to pass right through the reactor and be accessible at both ends was finally abandoned because of the additional cost.

Other limitations on experimental facilities arise from the reactivity required to operate with them and the need for control devices to cover the variation in reactivity during operation. Here again, flexibility has been sought so that many facilities requiring large reactivity are optional and when conditions are favourable absorber control plates can be replaced by experimental holes.

General Description of Reactor

The reactor core consists of up to 2.5 kg of U^{235} in the form of uranium-aluminium alloy plates arranged in boxes to form an approximate cylinder of length 60 cm and equivalent diameter 86 cm. This cylinder is in the centre of a cylindrical aluminium tank 2m in diameter and 2 m in height. The elements are cooled by forced upward flow of D_2O which overflows the

Table 1. Experimental Facilities of E.443

General description	*Dimensions*	*No.*	*Reactivity loss due to empty facility %*	*Maximum thermal flux in empty facility n/cm²/sec*
Fixed horizontal round tubes				
(*a*) Entering D_2O reflector	10 in. diam.	1	0.5	8×10^{13}
	6 in.	1	0.2	8×10^{13}
	4 in.	6	0.6	7×10^{13}
(*b*) Entering graphite reflector only	6 in.	10		1.5×10^{13}
Fixed, horizontal oval tube passing right through D_2O reflector	4 in. × 2 in.	1	0.4	8×10^{13}
Removable, vertical round tubes				
(*a*) Entering D_2O reflector	6 in. diam.	4	0.8	8×10^{13}
	4 in.	5	1.2	5×10^{13}
	2 in.	9	0.5	9×10^{13}
(*b*) Entering graphite reflector only	6 in.	6		0.4×10^{13}
	4 in.	2		0.4×10^{13}
	10 in.	2		0.4×10^{13}
Fixed horizontal rectangular tube passing right through bottom graphite reflector	8 in. × 12 in.	2		$\sim 1 \times 10^{13}$
Thermal column of graphite containing square holes	5 ft × 5 ft 4 in. × 4 in.	1 9		10^{12} 10^{12}

top of the elements to become the reflector before passing out to a heat exchanger for cooling and recirculating. Outside the aluminium tank is a graphite reflector of 60 cm thickness on the sides and bottom. The graphite is in turn contained in a steel tank which is helium filled. Outside this tank is a biological shield of concrete except for a 1.5 m square section occupied by a thermal column with appropriate shielding at the outside.

Below the reactor is a plant room containing pumps and a heat exchanger for the D_2O. The total heat removal catered for is 10 Mw from the core, 1 Mw from all experimental facilities.

The experimental facilities consist of aluminium tubes entering graphite or D_2O vertically or horizontally, details being given in the table below and in the attached drawings.

External Facilities Attached to the Reactor

Owing to the need for containment the space available within the reactor hall is extremely limited, and therefore additional facilities have been provided adjacent to the main entrances. An open building 106 ft long × 33 ft wide and provided with a 20-ton crane, change room facilities and extensive services for power, light, ventilation and the disposal of active effluents will be used for the examination of irradiated material. A deep pond sunk in the floor will allow of under-water examinations and also the dismantling of activated equipment.

Remote controlled power heads in shielded rooms will be installed to facilitate the dismantling of both active and contaminated equipment in preparation for detailed examination.

List of Experimental Facilities

Table 1 indicates all the facilities which can be made available, though not necessarily all at once. Included in the table are estimates of the reactivity loss associated with the installation of particular holes, but of course the inclusion of equipment in those holes may add to or subtract from this. The flux figure quoted is the maximum thermal flux likely to be available in the facility before any equipment is installed in it.

All holes may be purged and sealed with CO_2 to reduce A^{41} activity in handling experimental equipment in and out during shut-down.

Design and Description of ANL Reactors (CP-3, CP-3', and CP-5)

By W. H. Zinn,[*] USA

PART I: HEAVY WATER REACTOR, CP-3 AND CP-3'[†]

Heavy water was first used as a moderator in a nuclear chain reaction in a research reactor built during the war at the Argonne Laboratory of the Metallurgical Project of the Manhattan District. This reactor became known as CP-3. It began operation on May 15, 1944. With one change of fuel elements, it was kept in continuous operation for ten years at which time it was taken out of service. When taken out of service, it was still in excellent operating condition and probably could have continued to serve usefully for many more years.

The reactor consists of an aluminum tank of diameter 6 ft into which are suspended a maximum of 136 natural uranium metal rods, 6 ft long and of diameter 1.1 in. Figure 1 gives the general arrangement of the rods in the tank, and Fig. 2 shows that the uranium rods are spaced in a square lattice of 5⅜-in. pitch. The aluminum tank wall is $^3/_{16}$ of an inch thick and is surrounded by a graphite reflector of 2-ft thickness. A water-cooled gamma ray shield made of Pb-Cd alloy and a 7 ft 8-in. thick concrete layer complete the shielding. The top of the reactor is closed by a shield made up of laminated blocks of wood and steel. The fuel rods are constructed as shown in Fig. 3. The aluminum jacket of thickness 0.035 in. is drawn down onto the uranium rod by a die to give a close fit for better heat transfer.

Heat released from the uranium rods is transferred by natural convection to the bulk moderator in the tank. Suction of hot heavy water from the top of the reactor and return of cooler water through a pipe at the bottom of the aluminum tank is the method of cooling. Figure 4 is a schematic diagram of the fluid systems of the reactor. The heavy water pumped from the reactor tank is forced through a heat exchanger where it is cooled with light water.

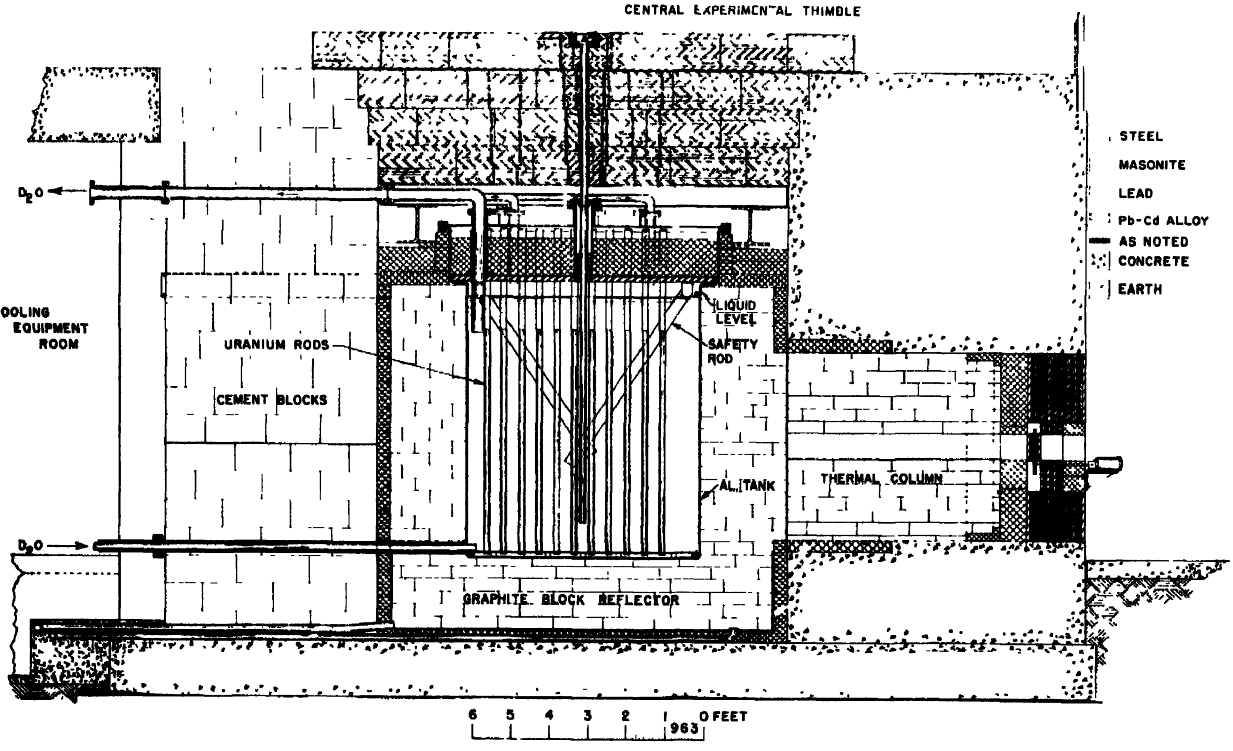

Figure 1. Vertical section of natural uranium heavy water research reactor

---

[*] Argonne National Laboratory.

[†] Including work by H. V. Lichtenberger, A. Langsdorf, W. H. McCorkle, and A. Wattenberg, Argonne National Laboratory.

The space above the moderator in the tank is flooded with helium gas, which is pumped through a catalyst chamber to recombine any deuterium gas which may be generated. Control of the reactor is by means of four swinging arm type control rods as illustrated in Fig. 1. The shafts which rotate the control rods are brought to the exterior of the biological shield where the mechanisms for providing the motion are situated.

Experimental facilities are provided as shown in Fig. 5. Nine openings at the mid-plane of the reactor pass through the shield and terminate at the aluminum tank wall. One of these openings, which is 6 ft in rectangular cross section, is filled with graphite, thus providing a thermal column. For irradiation of samples and for the generation of neutron beams of the maximum intensity, thimbles are provided through the upper shield. The principal one is a $4\frac{5}{8}$-in. diameter hole which passes down through the central axis of the reactor. Any of the fuel element holes also can be adapted for experimental use by the installation of a thimble.

At an operating power of 300 kw, the maximum neutron flux for this reactor is 10^{12} n/cm^2/sec.

After six years of uneventful operation, it was observed that there was a small amount of fission product activity in the circulating heavy water. The heavy water is purified by being continuously pumped through ion exchange resins and the fission product activity first became evident in the resin bed. It was obvious that a fuel element jacket had failed. Therefore, in 1950, the original fuel elements which had been installed in 1944 were removed, and it was found, indeed, that one had defects in the aluminum jacket. Figure 6 is a photograph of the damaged part of this fuel element. It is not clear from examination of the rod whether the penetrations of the jacket were due to pitting of the aluminum due to corrosion or were due to imperfections originally present in the aluminum. From the fact that there are a number of the holes clustered in one area, it can be concluded that it was a pitting type corrosion which caused the failure and it is conceivable that this corrosion was initiated by some kind of inclusion in the aluminum jacket.

In refueling the reactor in 1950, due to the availability of enriched uranium it was decided to replace all of the rods with quite similar rods in which the core material was 2% uranium-aluminum alloy. The critical amount of uranium was 3.8 kg of U^{235} enriched to at least 90%. This change in fuel element had the twofold advantage of eliminating any future difficulty with the corrosion of uranium metal, since in its corrosion properties the uranium-aluminum alloy would act about the same as aluminum itself, and, also, removing U^{238} from the reactor gave increased neutron flux. The maximum neutron flux in the rebuilt machine was 4×10^{12} n/cm^2/sec for a power of 300 kw. At this power, many years of operation on one set of fuel rods is possible.

This research reactor, CP-3 and CP-3′, provided

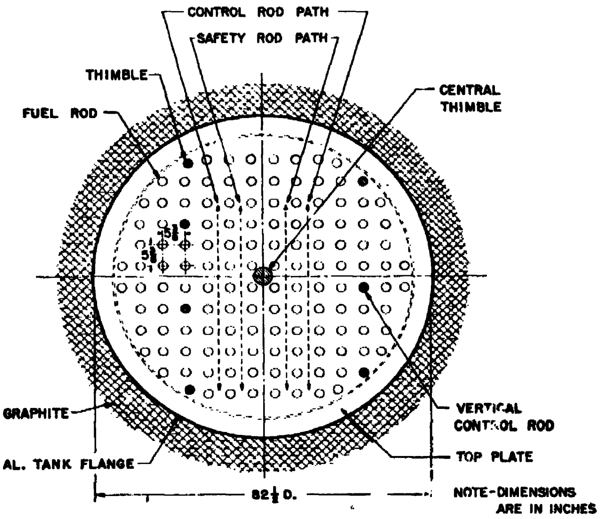

Figure 2. Lattice of natural uranium heavy water research reactor

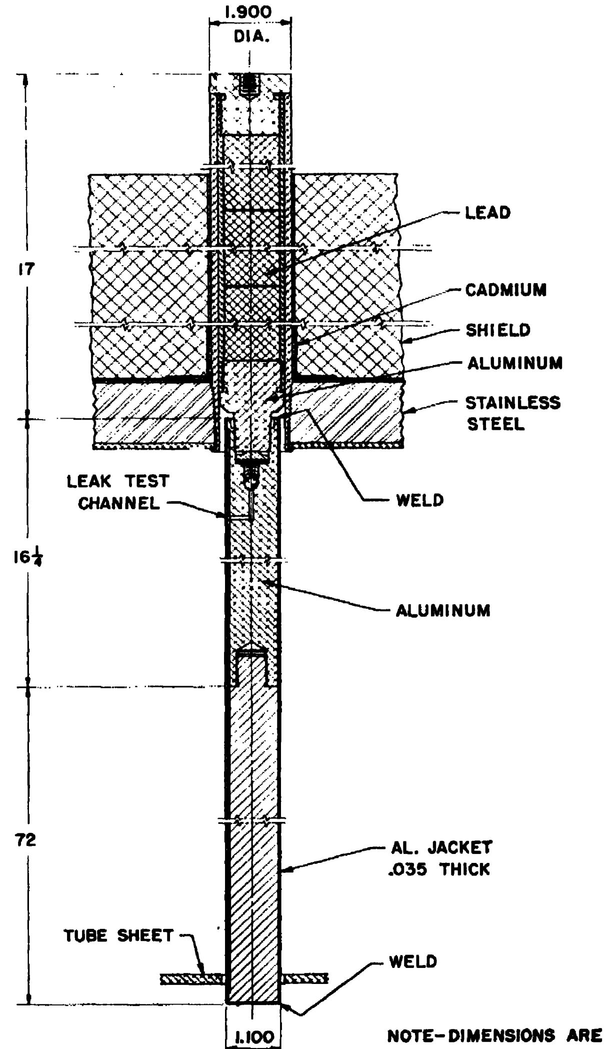

Figure 3. Natural uranium fuel rod

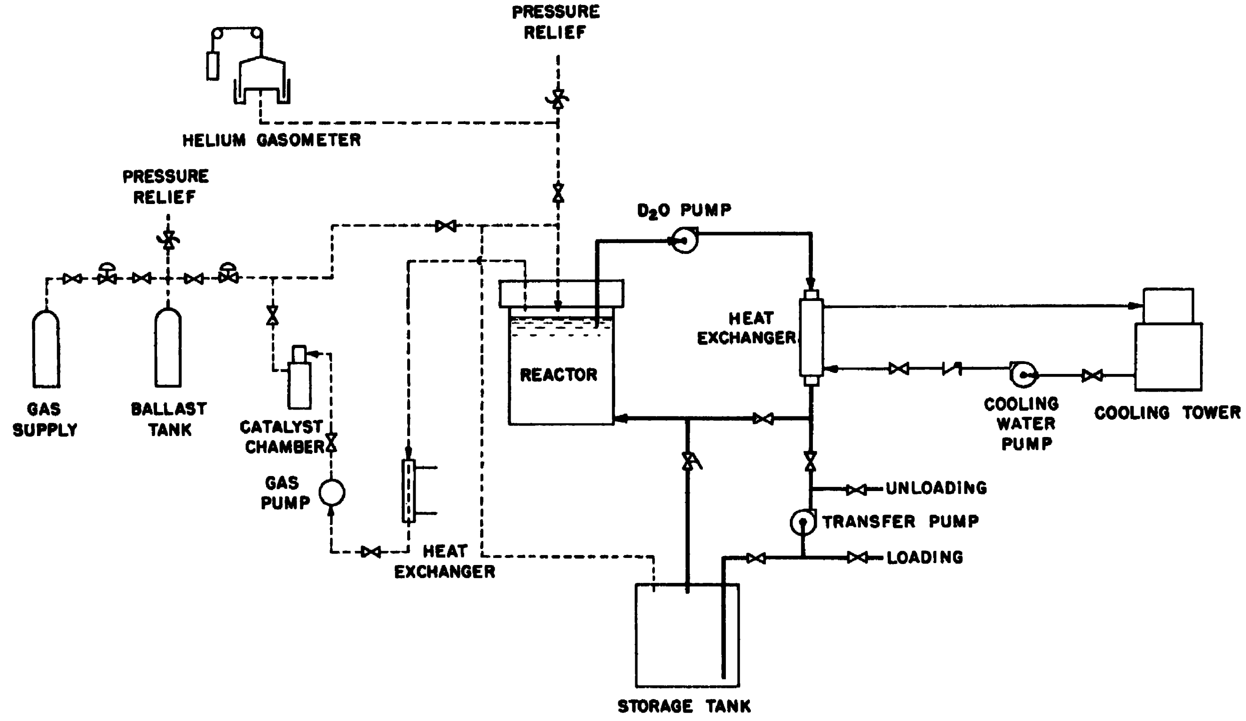

Figure 4. Natural uranium heavy water research reactor flow diagram

an excellent facility for work with neutron beams. The various choppers were developed with this reactor, and the initial work on crystalline diffraction was performed with it as the source of neutrons. Investigations on the polarization of neutrons and many aspects of resonance neutron physics were first investigated with beams from this machine. It is extremely simple and safe to operate, and it is highly recommended, especially in the form in which enriched uranium metal or uranium oxide is used as fuel, for research laboratories in which the capital investment in the reactor is to be held to a minimum.

PART II: ARGONNE RESEARCH REACTOR, CP-5[‡]

In the period of 1949, Argonne National Laboratory was faced with the problem of making a choice of reactor type for a research reactor to be located in the immediate vicinity of its principal laboratories. In making the choice, a number of requirements had to be considered, some of which were conflicting. A review of the Laboratory's program and the facilities available to the Laboratory elsewhere indicated that the machine to be constructed should primarily provide beams of neutrons for physics experiments. This was so because radioisotopes were available from the radioisotope distribution facilities of the USAEC and because the Laboratory was engaged with the Oak Ridge National Laboratory in the construction of the Materials Testing Reactor, whose principal function would be to provide facilities for engineering tests on fuel components for future reactors. Although it was recognized that the principal function of the research reactor was to be the provision of neutron beams, it was desired that the reactor would be used in other ways, such as basic studies on the phenomenon of radiation damage, engineering testing of fuel samples, and the manufacture of radioisotopes which, because of half-life or special conditions, could not be obtained otherwise. For these purposes, a sizable volume of neutron flux was a necessary requirement.

A consideration of major consequence was the probable cost of the operation of the machine. While the Laboratory had a historic interest in neutron physics and while it was expected that for a considerable period of time neutron physics would be one of the main interests of the research program, it was not deemed to the best interests of the research program to construct a reactor for which the operating cost would be a significant burden.

The Laboratory had had experience with a graphite-moderated reactor and with a heavy water, natural uranium reactor. Analysis indicated that the best compromise among the factors indicated above would be obtained for a reactor moderated with heavy water in which the fuel was enriched uranium. It thus was a natural successor to the heavy water reactor with which many years of successful experience had been had. This design yields the maximum neutron flux for a given power and thus provides for economy of operation, since it is the reactor power which basically determines the operating cost. In selecting the reactor design, a decision had to be made as to the actual

---

[‡] Including work by G. A. Anderson, T. Brill, O. W. Childs, J. A. DeShong, J. J. Dickson, E. E. Hamer, J. M. Harrer, L. C. Livesey, B. I. Spinrad, S. Untermyer, J. T. Weills, and J. M. West, Argonne National Laboratory.

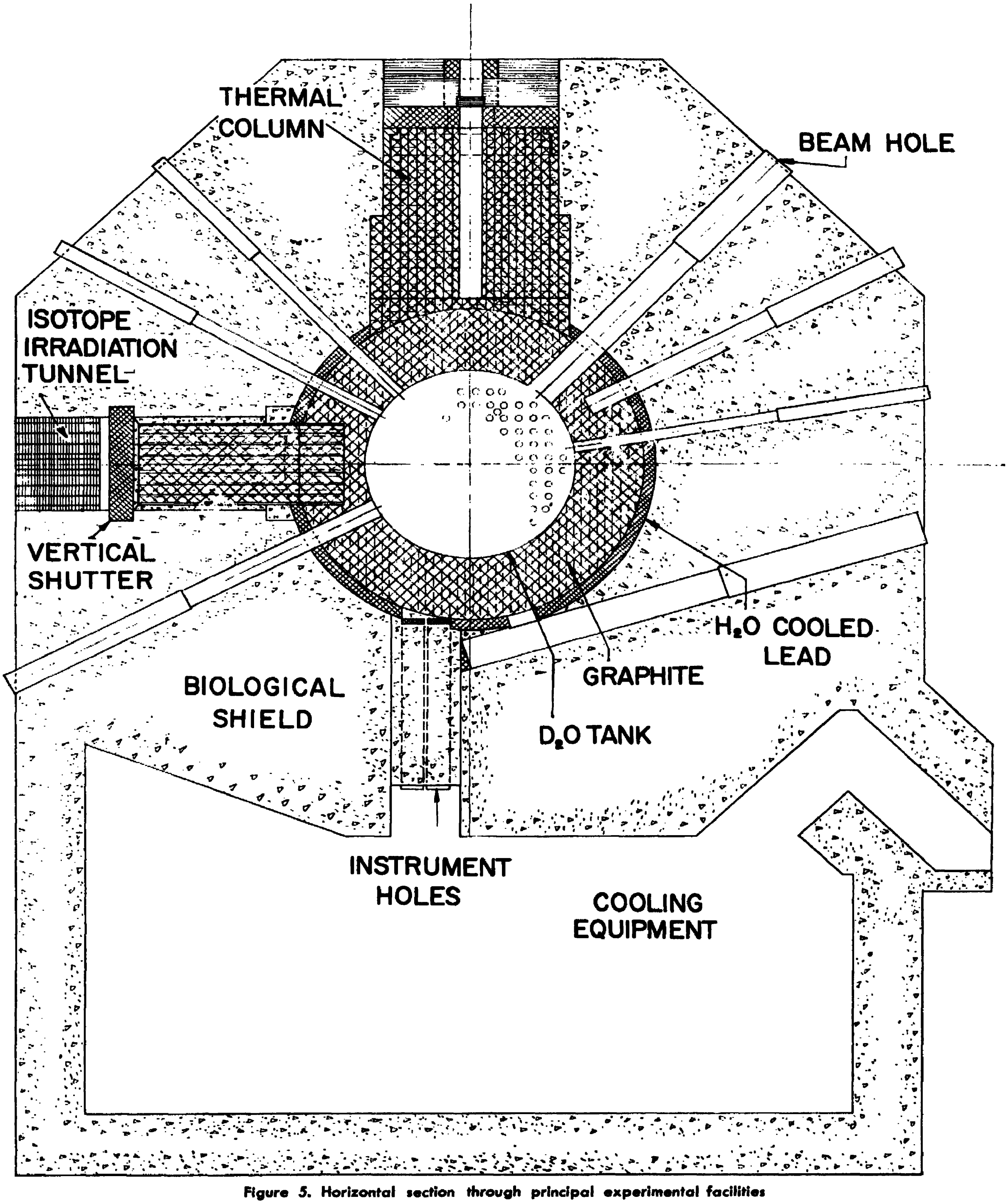

Figure 5. Horizontal section through principal experimental facilities

operating power. In this, the location of the reactor in a metropolitan area had to be taken into account. Since at that time it was the policy of the USAEC to require essentially unoccupied area surrounding a reactor of a magnitude dependent upon the power, a limitation had to be accepted. As a design evolved, however, it developed that the design power was essentially set by consideration of the consequences of certain malfunction of the reactor upon shutdown, to be discussed later, rather than upon operating power.

The machine, which was first put into operation in February, 1954, was fundamentally designed for a power of 4000 kw. So far, it has been operated at a nominal 1000 kw but increases in the routine power level to the 4000 kw figure are scheduled.

A preliminary description has been published by S. Untermyer[1] and by J. T. Weills.[2]

In the present paper, some of the experience resulting from a year's operation is given as well as a brief description of the facility. As a result of this experience, it can be said that the reactor fully meets the design specifications set for it. The neutron beams produced are not exceeded in intensity by beams from any other reactor in the USA, and it has been gratifying to find that the reactor lends itself quite well to engineering-type experiments. In the general management and operation of the machine no difficulty whatsoever has been experienced.

Fuel Element

The heat producing element of the reactor is an aluminum-uranium alloy plate jacketed on both sides with aluminum. Since the U^{235} mass required for the reactor is small, no problem exists in the concentration of the uranium in the uranium-aluminum alloy. Choice of the number of fuel elements was made on the basis of volume of neutron flux desired, geometrical limitations in the arrangement of the fuel tubes, and heat transfer requirements. Figure 7 is a sketch of a single fuel element. Figure 8 shows the arrangement of 17 of these in a lattice of spacing 6 inches. The spacing was determined by the feasibility of constructing the holes through the shield through which the fuel elements are inserted in the reactor. Since it is easy to vary the amount of uranium incorporated in the fuel plate and the number of plates in a fuel element, the reactor core has a great deal of flexibility. This flexibility is made use of mainly to adjust the reactivity to compensate for the burnup.

Heat Transfer

For operation at 1000 kw, the heat flux is so low that no problem exists. For operation at 4000 kw, a fuel element with 12 uranium-bearing plates is required. Sixteen fuel elements are the minimum permitted for operation at this power. Each fuel element has a heating area of 9100 cm². The average heat flux is 6.5 cal/cm²/sec and the maximum about 9.8 cal/cm²/sec. The water velocity is 1.6 m/sec and the film coefficient is 0.2 cal/cm²/sec/°C, hence the maximum film temperature drop is 49°C. The temperature rise of the

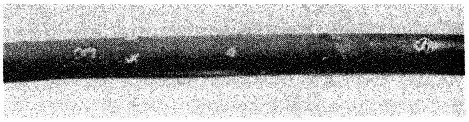

Figure 6. Damaged portion of fuel element

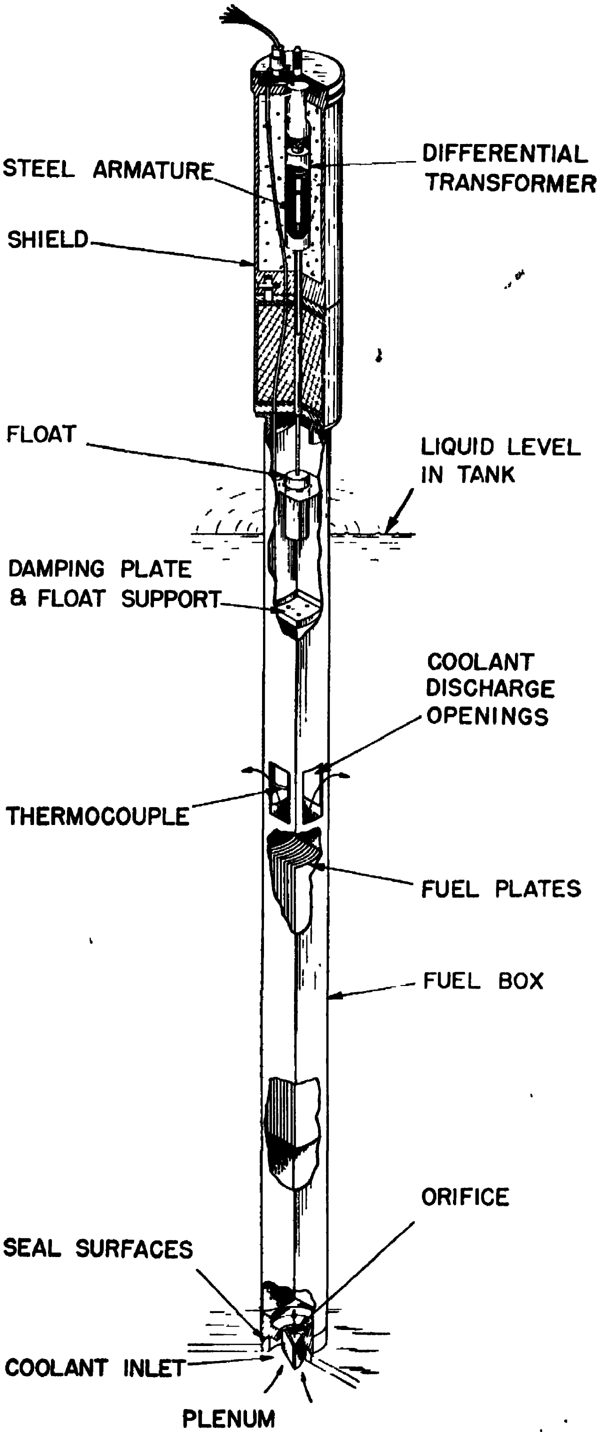

Figure 7. Fuel element

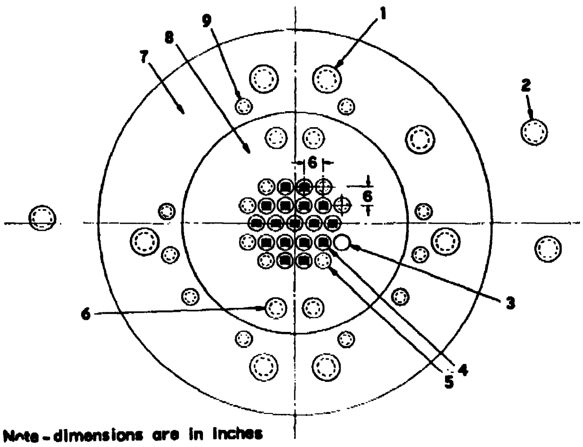

Figure 8. Fuel elements and experimental thimbles: (1) 5¾ dia. exp. thimble holes in graphite; (2) 6 dia. storage holes for radioactive samples; (3) Regulating rod; (4) Fuel elements: (5) 3⅛ dia. exp. thimble holes in D_2O; (6) 4 dia. exp. thimble holes in D_2O; (7) Graphite zone; (8) D_2O zone; (9) 3$\frac{3}{16}$ dia. exp. thimble holes in graphite

water in a fuel element is 12.6°C for a pumping rate of 1200 gpm. With an inlet temperature of 40°C, film boiling is just avoided.

Fuel Inventory

A matter of considerable importance in the management of a research reactor is the amount of enriched U^{235} which must be committed in order to keep the reactor in operation. Also, the cost of fabricating new fuel elements and of chemical recovery of unburned fuel is not a negligible operating cost. Loss of reactivity and the lowering of flux due to poisoning by long-lived fission products determine the frequency of replacement of the fuel. So far in the operation of the Argonne Research Reactor, it has been the practice to limit the average depletion to 15% and the maximum for any fuel element to 30%. Experience may indicate how these percentages can be improved.

The fuel inventory is dependent on the power level. It also depends on the purely technical matter of the frequency with which new fuel elements are supplied by the fabricator and the frequency of shipment of irradiated elements to chemical recovery.

At a power level of 1000 kw, it will be most convenient to place receipt and shipment of fuel on a yearly basis. At the start of the year the reactor is loaded with only 12 elements containing a total of 1680 gm of U^{235}. This provides excess reactivity for xenon poison, temperature coefficient, experimental apparatus and for the first two months of operation. Successive additions of the remaining five fuel elements carries the operation through the year, at which time most of the fuel is removed. Allowing two months for cooling before shipping of irradiated elements, a total average inventory of 2700 gm is sufficient.

Operation at 4000 kw requires at least 16 fuel elements, as was indicated in the section on heat transfer. A fuel element contains 132 gm U^{235} and is replaced when it has been depleted to 100 gm. Partial replacement is made at monthly intervals at which time one quarter of the fuel charge, consisting of the most highly depleted elements, is replaced. If receipt of new fuel elements and shipment to chemical processing is on a yearly basis, a total of 13.0 kg will be committed to the operation of the machine. If these manufacturing operations are on a twice yearly basis, the committed inventory becomes 7.5 kg.

A calculation of the critical size of this reactor, using uranium enriched to only 20%, indicates that it will increase by a factor of 1.8. Inventories would be increased correspondingly. These inventory figures strongly suggest that where the supply of enriched uranium is limited this machine is ideally suited, since it provides high neutron flux with the least inventory.

Flow Diagram

Figure 9 is a diagrammatic representation of the fluid systems of the reactor. Heavy water pumped into the distribution plenum at the bottom of the tank passes through orifices in the bottom of the fuel elements, through the fuel elements and discharges into the tank. The flow in each fuel element is measured by a float arrangement, as well as the temperature rise by thermocouples in the plenum and the exit port in each fuel element.

The heavy water discharged from the reactor tank is pumped through a heat exchanger where the heat is discarded to a light-water cooling system. The heat exchanger is provided with double tube sheets to lessen the possibility of mixing of the two kinds of water.

The level of water in the reactor tank is maintained constant by means of an overflow pipe installed at a fixed height. A small constant flow is maintained through this overflow pipe. A tank is so installed that the heavy water reflector above the core can be dumped quickly. The tank arrangement, however, is such that it is not possible to expose the actual fuel elements. The heavy water handling system is installed in the basement underneath the heavy floor of the main workroom. It is easily accessible and can be inspected during operation. Purity of water is controlled by pumping a side stream through ion exchange resins.

Reactor Helium System

The atmosphere over the heavy water in the reactor tank is helium gas at a positive pressure of 2½ inches of water. This pressure is maintained by a gas supply system and a neoprene diaphragm gas holder. The gas space over the heavy water in the reactor is connected by a large diameter pipe to a holdup space of volume 1000 ft^3. The end of the pipe connecting the reactor gas space to the holdup volume is sealed with a rubber diaphragm which bursts at a pressure of 1 psi. This is purely a safety measure which ought to vent the products of reaction if a hydrogen-air explosive mixture were by any chance acquired over the heavy water, or if by any chance steam were formed. The consumption of helium in this system is low, being no more than 1000 ft^3 at atmospheric pressure

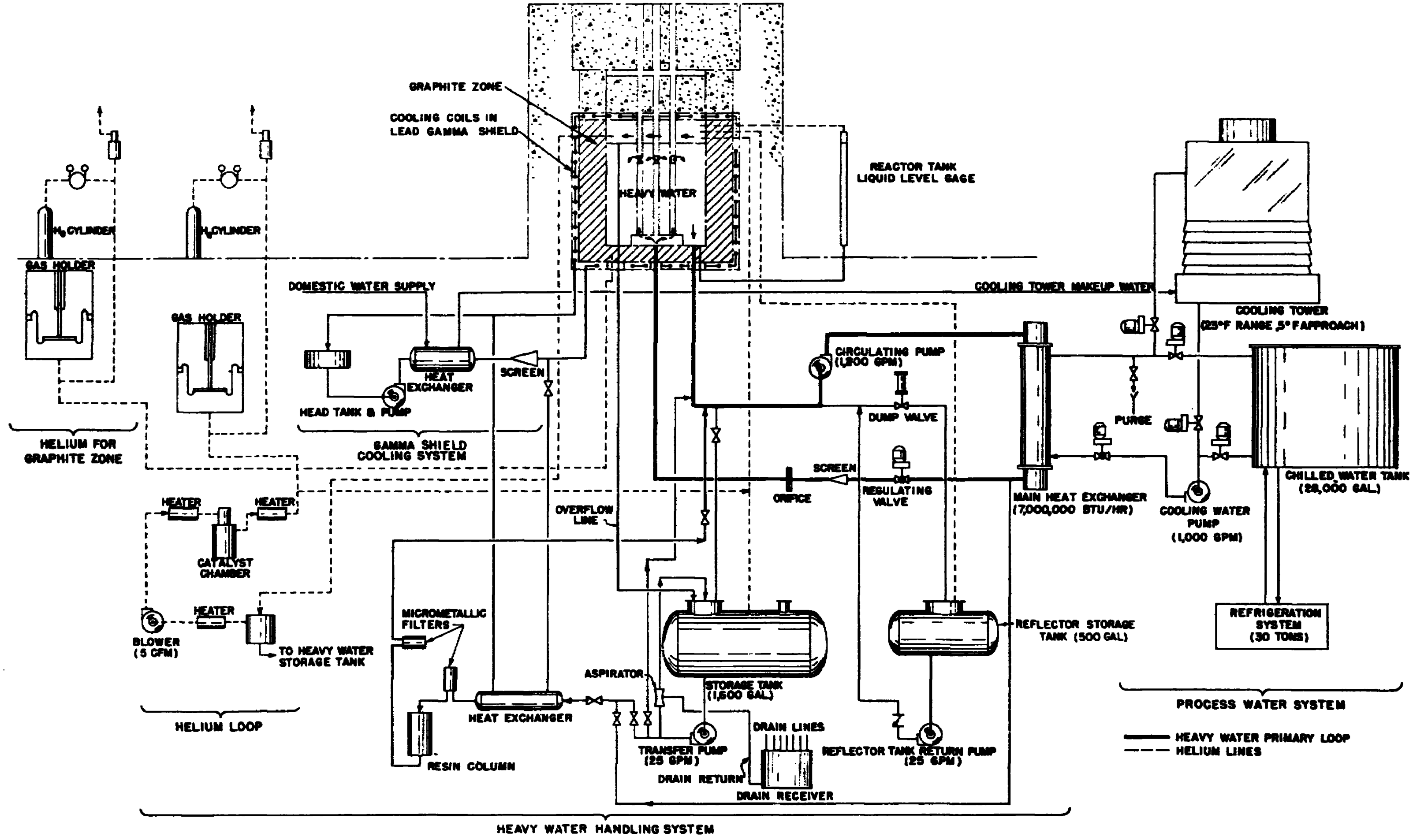
GRAPHITE ZONE
COOLING COILS IN LEAD GAMMA SHIELD
HEAVY WATER
REACTOR TANK LIQUID LEVEL GAGE
H_2 CYLINDER
H_2 CYLINDER
GAS HOLDER
GAS HOLDER
HELIUM FOR GRAPHITE ZONE
DOMESTIC WATER SUPPLY
HEAT EXCHANGER
SCREEN
HEAD TANK & PUMP
GAMMA SHIELD COOLING SYSTEM
COOLING TOWER MAKEUP WATER
COOLING TOWER (25°F RANGE, 5°F APPROACH)
CIRCULATING PUMP (1,200 GPM)
DUMP VALVE
PURGE
SCREEN
ORIFICE
REGULATING VALVE
MAIN HEAT EXCHANGER (7,000,000 BTU/HR)
COOLING WATER PUMP (1,000 GPM)
CHILLED WATER TANK (28,000 GAL.)
OVERFLOW LINE
HEATER
HEATER
CATALYST CHAMBER
HEATER
BLOWER (5 CFM)
TO HEAVY WATER STORAGE TANK
HELIUM LOOP
MICROMETALLIC FILTERS
ASPIRATOR
STORAGE TANK (1,500 GAL.)
REFLECTOR STORAGE TANK (500 GAL.)
REFRIGERATION SYSTEM (30 TONS)
PROCESS WATER SYSTEM
HEAVY WATER PRIMARY LOOP
HELIUM LINES
HEAT EXCHANGER
RESIN COLUMN
TRANSFER PUMP (25 GPM)
DRAIN LINES
REFLECTOR TANK RETURN PUMP (25 GPM)
DRAIN RETURN
DRAIN RECEIVER
HEAVY WATER HANDLING SYSTEM

Figure 9. Argonne research reactor flowsheet

per month. Purity is normally maintained at 99% in order to reduce any argon activity in the leakage.

H_2O Cooling

The light water cooling system has a pumping capacity of 1000 gallons per minute. It is standard in all respects with the exception of the fact that a large tank which can hold specially chilled water has been introduced as a parallel side stream. At those times when burnup has reduced the amount of available reactivity, the chilled water is used to reduce the temperature of the reactor system and thus gain reactivity. It is mainly useful to extend the period of time during which shutdown can persist without being trapped by the growth of shutdown xenon. While it has been used in some cases, only extended experience will indicate if its usefulness justifies the cost of installation.

Mechanical Arrangement

The basic element of the reactor is an aluminum tank, 6 ft in diameter and 9 ft 7 in. high. Since the aluminum tank is surrounded by a graphite reflector, the thickness of the tank wall is a compromise. The thickness of the bottom of the aluminum tank also had to be controlled because the neutron flux in the graphite below the tank was to be used. The wall thickness of the aluminum tank is ⅜ inch. Figure 10 is a photograph of the inside of the aluminum tank. Figures 11 and 12 give further details. The fuel elements are installed in the central portion of the tank, leaving a heavy water reflector on all sides and top and bottom. The heavy water reflector not only acts to reduce the critical mass of the reactor but provides the volume for the experimental facilities. In order that the facilities can make use of the highest neutron flux, they must extend through that part of the reflector which lies just outside the core. Therefore, as is shown in the photograph of the inside of the reactor tank, re-entrant tubes are welded into the wall of the reactor tank so that the horizontal beam holes can extend to the edge of the core. Similarly, the four holes which extend directly through the reactor from side to side pass through the region of D_2O reflector close to the core. At the top of the reflector in the aluminum tank, there is installed a gridwork which provides mechanical strength both for the support of the cantilevered ends of the internal beam holes and the hinges of the shim-safety rods. Supporting the protruding ends of the beam holes is quite an important item since there is a high probability that experimenters will wish to place plugs of bismuth or lead or graphite at such locations and when the beam hole has a diameter of 12 inches, the weld stress becomes very great. The graphite surrounding the reactor tank is installed so that there is a minimum space of one inch between the interior edge of the graphite and the outer wall of the aluminum tank. The graphite is further held in position by a thin aluminum sheet. In this way, the aluminum tank, if it should become damaged, can be removed by first removing the main top shield plugs of the reactor. Because of the radioactivity involved, this would not be a simple operation, but provision to make it possible is incorporated in the basic design of the machine. The graphite has been installed with as few cracks in the radial direction as possible so that the conduction of heat is outward to the inner wall of the biological shield, which is water-cooled. The water-cooled gamma shield was constructed by erecting a steel tank on the outside of which a layer of lead brick of thickness 3½ in. was installed. Leaded into these bricks are copper cooling coils through which distilled water is circulated. Boral sheet was fastened with screws on the inside of the steel tank. The boral consists of boron carbide mixed with a small amount of aluminum and sheathed on both sides with a thin layer of aluminum, the total being one-quarter of an inch thick. The highly thermalized neutrons are absorbed by the boral without giving rise to penetrating gamma rays. The suppression of these capture gamma rays in this manner is necessary if the biological shield thickness is to be kept small. The graphite is fitted closely to the boral and the remaining cracks are filled by pouring in lead. In addition, the atmosphere of the graphite space is helium gas. This necessitates sealing all of the space enclosing the graphite. This graphite zone is operated at a helium pressure of 2½ in. of water, negative with respect to the atmosphere. Therefore, leakage around beam holes and other places where the seal may not be perfect is leakage of room air into the graphite-helium system. A periodic purging of the system maintains the purity of the helium. About 2000 cubic feet of helium at atmospheric pressure is used per month. The helium atmosphere for the graphite is thought to be necessary to prevent excessive heating of the graphite when the reactor is operated at highest power.

A matter of considerable concern in the design of a heavy water reactor is the arrangement of the upper shield. The upper shield must provide the working deck for the installation and removal of fuel elements. Therefore, at some times work must be done above the reactor with lead coffins weighing perhaps ten tons. The shield must be so arranged so that no mismanagement of this coffin can damage the reactor.

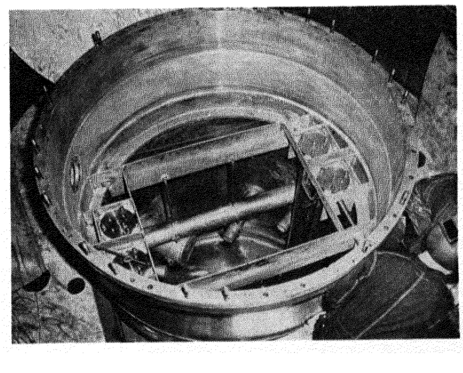

Figure 10. Interior of reactor tank

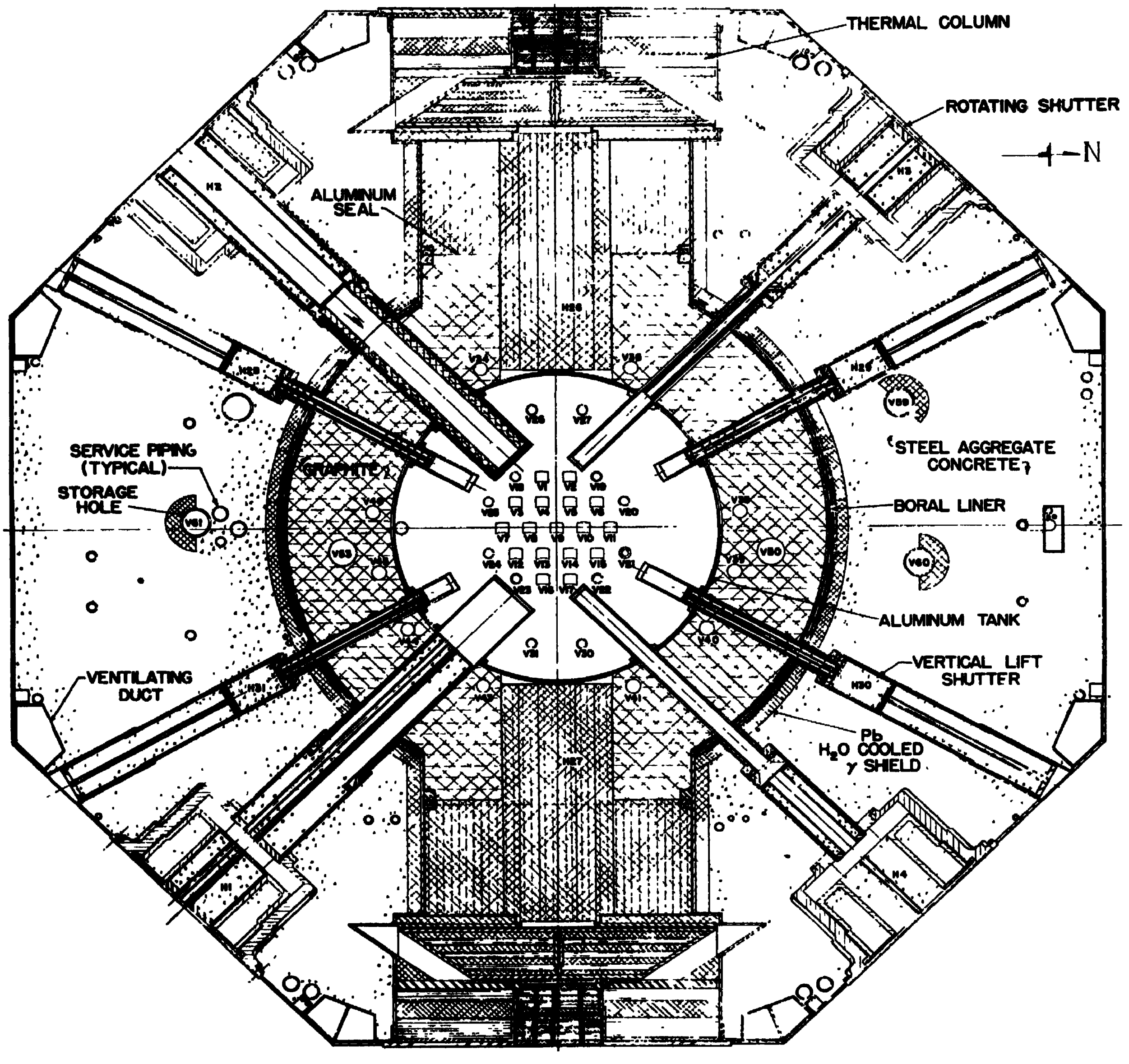

Figure 11. Section through principal beam holes

In the design of this reactor, this has been accomplished by splitting the upper shield into two parts. The lower part, weighing eight tons, is carried inside the aluminum vessel. The gasket which seals this plug in the reactor tank is at the top of the plug and therefore accessible. Temperature expansion of the tank merely raises this plug. The second part of the shield is in the form of a large circular disk which spans the aluminum tank and graphite reflector. Any blow struck to the top of this disk is transmitted to the concrete shield and could not put stress on the reactor vessel. This means, however, that the shield plugs above the fuel elements also have to be divided in two. Each of them is sealed into its appropriate top shield plug by means of a neoprene "O" ring. The "O" ring for the lower plug is placed as far as possible from the radiation field to prevent deterioration of the material. The fact that the reactor consumption of helium is low indicates that these "O" ring seals are very successful. The fuel element plug in the lower shield also acts as a weight to keep the fuel element seated in the plenum chamber.

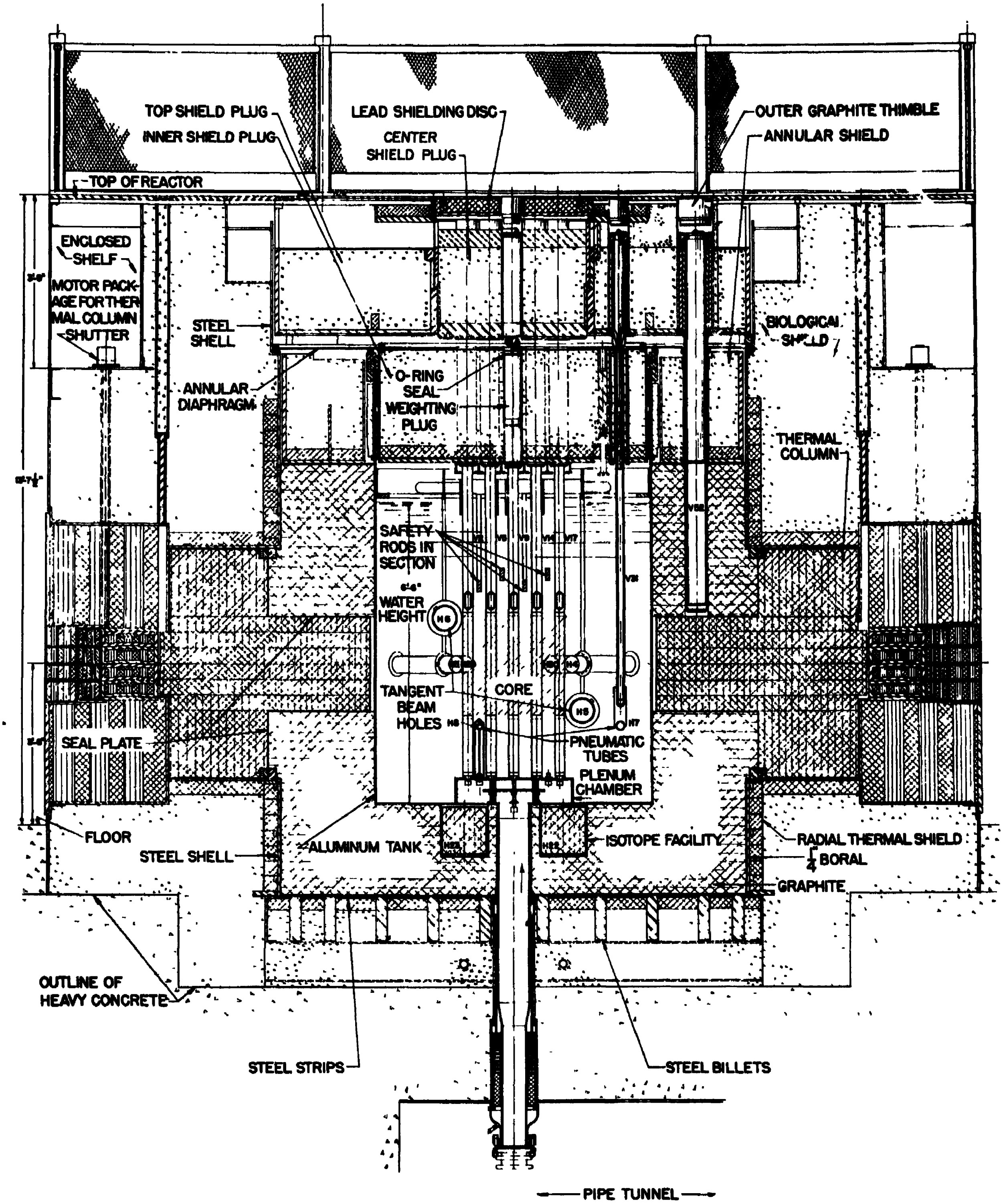

Figure 12. Elevation of research reactor

The construction of the thermal columns has been a matter of special concern. Consideration of possible experiments indicated that there should be a space made available which should have a minimum diameter of 16 in. The graphite in this space must be adjustable and removable in order to make cavities of size to fit the experiments. Therefore, an aluminum liner was so arranged that it separates the graphite of the thermal column from the graphite of the remainder of the reflector. Whereas the main biological shield of the reactor is made of concrete in which the aggregate is steel punchings of graded sizes and in which the sand is magnetite, the shield over the thermal column face is made of lead, pressed wood, and iron. To provide access to the 16-in. diameter space, adjustable doors are provided and since these are very heavy, they are motorized. Figure 11 shows that the minimum thickness of biological shield is 56 in. For a horizontal beam hole, the distance of the outerface of the shield to the point of highest neutron flux is only 103 in. The greatest flexibility for the beam hole is obtained if this distance is kept small, because for some experiments this distance will be just as important as the maximum neutron flux in determining what flux is available to experiments outside the shield. In placing the shield, great care has been used to provide additional density in those places where it has been necessary to leave holes. By doing this, local leaks in the shield have been avoided.

For a machine in which the neutron beams can be very intense, it is highly desirable to provide in the shield some means of attenuating the beam. The experimenter will find many occasions for adjusting his apparatus and unless a reasonably convenient method is provided for shutting off the beam, he will either make his adjustments and risk overexposure or demand that the reactor be shut down. No easy solution to this problem exists. Two solutions have been used in this design. For the two 12-in. diameter beam holes and for two of the 4-in. diameter ones, a section of the biological shield 1.5 ft thick has been arranged in the form of a drum which can roll on its side. The drum is of sufficient diameter so that on one side of the center an opening can be made of the same size as the beam hole. A collimator installed in such a beam hole is divided into two parts. A fixed part is on the reactor side of the drum and another section is in the hole in the rotating drum. The drum is positioned accurately enough so that the drum can be rotated from the closed to the open position and the collimator will still be in accurate alignment. For experiments which have electric wires or fluid-carrying pipes connected to them and which are to be installed in such a beam hole, there is provided in the back of the rotating drum a recess to which access is provided both to the top of the reactor and to the basement below the reactor. Connection is made by reaching through the open hole in the drum and then the radiation leakage spaces around the wires or pipes reaching into the reactor are sealed off by rotating the drum. In this way, the background in the room around the reactor is reduced. In the second type of beam hole shutter a block of absorbing material is moved in a vertical channel so that it can come down and completely block the beam hole. This vertical channel is placed deep in the biological shield and is quite effective in interrupting the beam. It also demands that the collimator be installed in two sections. All of the beam shutters are electrically operated and are provided with signal lights showing their open and closed positions. The outer surface of the biological shield is a heavy steel plate which has been provided in order to give a convenient and solid place to fasten experimental equipment.

Another feature of all openings penetrating the shield which is designed to reduce work room radiation is worth mentioning. These openings will ordinarily be filled with air, and the argon in the air in these beam holes will become highly radioactive. Near the outer edge of the biological shield each beam hole is connected to a high velocity ventilating system. This tends to sweep the irradiated argon out of the beam hole; in fact, normally there is a suction of room air into the beam hole past the face of the pile.

All of the facilities of the reactor are arranged so that it is possible to bring the normal laboratory services to them. Slots have been placed in the biological shield which permit bringing power and fluid lines to the top of the reactor, and in the top shield raceways have been left so that utilities can be distributed to the thimbles which pass into either the heavy water region or the graphite region. For instance, a number of the experiments now installed in the vertical thimbles of the reactor are air-cooled by suction with fairly large capacity blowers. The pipes carrying this air are concealed in the biological shield and go to the basement area where the blowers are placed. Because of the care that has been taken in installing the raceways for utilities, the exterior surfaces of the reactor are remarkably free of projections as is shown in Figs. 13 and 14.

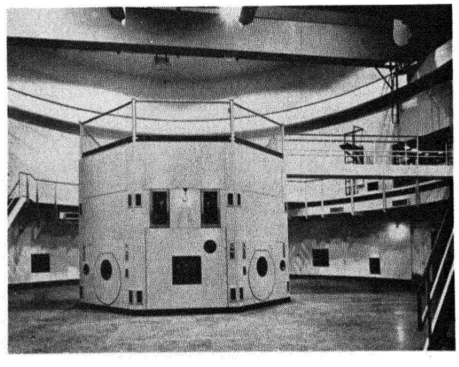

Figure 13. Reactor and work space around it

Control System

Control of reactivity of the reactor is incorporated into three systems. Large amounts of reactivity are handled by four shim-safety rods. Each of these shim-safety rods is a plate of cadmium jacketed in aluminum. As a safety rod, each bar is arranged so that it can fall into the reactor from its all-out position into its position of maximum effectiveness in a time of 0.35 second. A strong spring provides initial acceleration. Each rod subtracts between 8% $\Delta k/k$ and 12% $\Delta k/k$ depending on its location; therefore in normal operation any one of these shim-safety rods would shut down the reactor. In being raised to add reactivity, the shim-safety rod is moved at a slow speed which is variable within limits by the operator. Each of these rods is of the swinging arm type. The hinge is supported on the grid mentioned earlier which is welded in the reactor vessel. The rod is moved by means of a shaft which is inserted through the biological shield and terminates in the drive mechanism which is installed in a recess in the face of the pile. The shim-safety rod

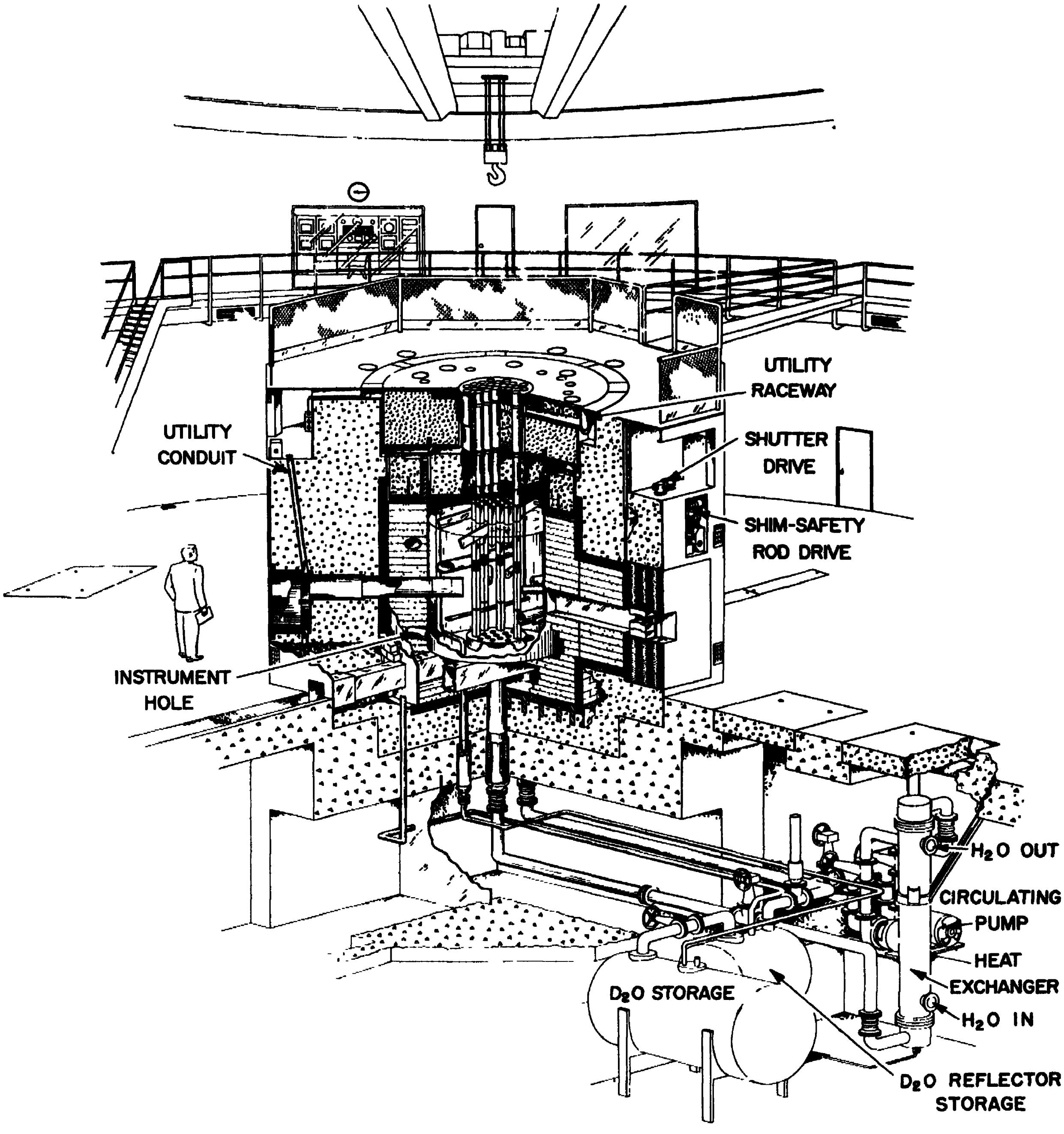

Figure 14. Pictorial assembly and research reactor

can be removed for replacement by withdrawing the shaft and lifting the whole rod through a plugged opening in the upper shield. This is illustrated in Fig. 15. This type of construction of the shim-safety rods has a number of unique advantages. The rods are fast since the circular motion needed for effective action extends over only a short arc. No special provision for cooling need be provided since the rods lie within the moderator water in the upper reflector. Because the penetration through the biological shield is always closed by the shaft no leakage of radiation whatsoever to the outside takes place. Finally, because it is a rotary motion, no space outside the pile itself is required for a framework to house the drive mechanism. Many years of experience with this type of control system indicates that it is of superior performance. The shim-safety rod system is the one used to add reactivity for temperature coefficient; a moderator temperature change from 30 to 50°C reduces reactivity by 0.8%. Reactivity loss due to operating xenon, which is about 3½%, and reactivity loss due to burnup, which may vary between 1 and 2%, also are compensated for by the motion of the shim-safety rods. The removal and insertion of experiments from time to time causes changes in reactivity of the machine of 1 or 2% and this is usually balanced by the motion of the shim-safety system.

Running control of the reactor is automatic and is done with a regulating rod which is inserted in a thimble entering the heavy water reflector vertically. The total reactivity under control by the regulating rod is limited to not more than 0.4%. Because the lifetime of neutrons in this machine is 1.5×10^{-3} second, it follows that no motion of this regulating rod can impart to the reactor a dangerously short period. Therefore this regulating rod is permitted to operate quite rapidly. The automatic control system moves the regulating rod about a fixed point in such a way as to keep the power measured with ionization chambers constant to better than 1%. Also with this regulating rod, startup of the reactor is done automatically. The rod itself consists of a cylinder of cadmium enclosed in aluminum; alternately, it could be a cylinder of cobalt since it would provide a convenient source of this important activated material. The third method of controlling reactivity is the dumping of the heavy water reflector over the fuel element core. This takes a time of about 15 seconds and removes 3½% $\Delta k/k$.

This reactor, it is believed, has a very large degree of inherent safety. This judgement is based on the experiments on the self-limitation of a water-cooled reactor, which are being reported at the Geneva Conference.[3] Estimates of the reduction in reactivity due to the formation of steam in the spaces between the fuel plates indicate that very large amounts of reactivity would be subtracted as the water is expelled from the space between the fuel plates. Because the lifetime of this reactor is about twenty times longer than the lifetime of the light water reactor in which the experiments were done, no amount of

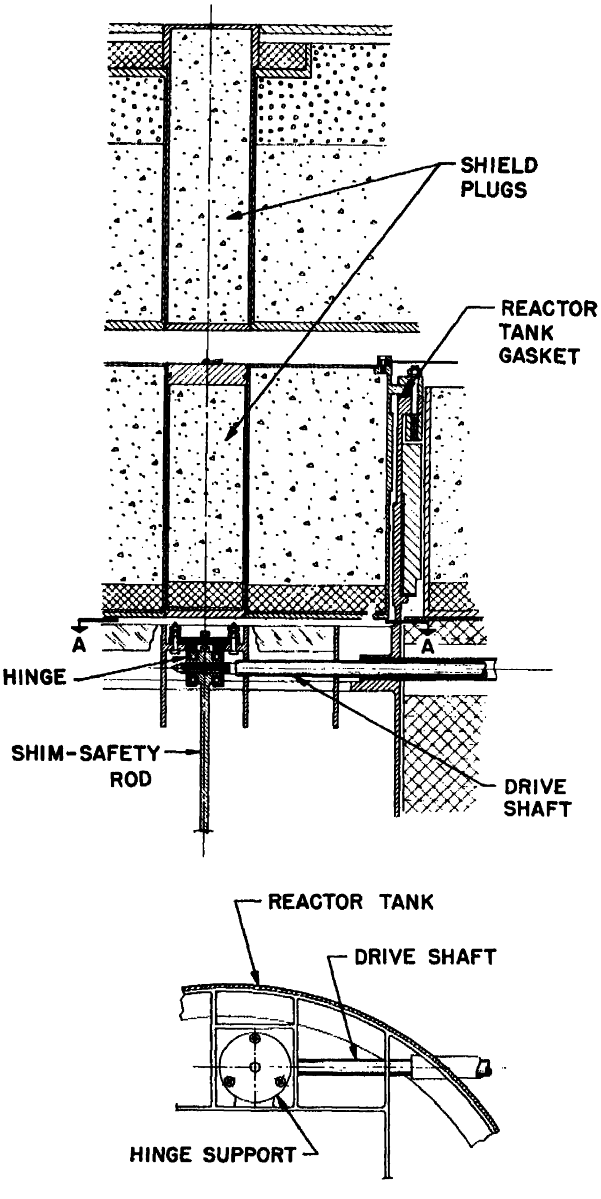

SECTION AA

Figure 15

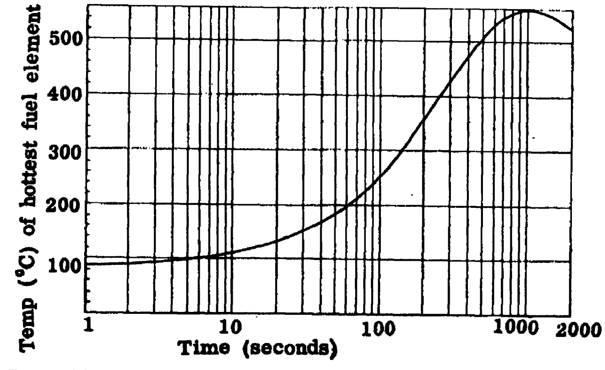

Figure 16. Heating of fuel elements after shutdown from 2000 kw; no water or helium in reactor tank

reactivity which is available in ordinary use can give the heavy water reactor a period which would result in a power excursion of any consequence. Normally, the reactor is loaded in such a way that at no time is the excess reactivity more than about 6%. If this all were added suddenly, the formation of steam in the fuel plates would limit the power excursion to a value for which melting of the fuel plates is not to be anticipated.

The experiments on the self-limitation of the water-cooled reactor were done after the building for the Research Reactor had been designed and was under construction. The building is of the gas-tight type of construction. It is made of reinforced concrete, the method of erection being by the continuous slip form process. This is why the cross section of the building through the reactor area is circular. Tests have shown that the building is adequately gas-tight and that in the event of the emission of a quantity of radioactive gaseous material, the building would provide very effective barrier against hazardous leakage. Figure 18 is a photograph of the building exterior. Although the self-limitation features of the reactor are such that there is no likelihood that an excursion would melt the fuel plates, it is apparent that a large rupture in the aluminum reactor vessel such as the destruction of a large beam hole would cause the loss of all heavy water and that the shutdown fission product heating of the fuel plates might raise the aluminum to the melting point. Mockup experiments with electrical heating have been done on this point and the results are shown on Fig. 16. This figure indicates that at 2000 kw operation the replacement of the heavy water by air will still not lead to the melting of the aluminum plates due to the shutdown fission product heating. Experiments with a helium atmosphere indicate that the aluminum plates might just not melt even if the operation were 4000 kw. For operation at 4000 kw, however, a water spray system is required in order to guarantee that the loss of the heavy water would not be followed by the melting of the plates and the emission of the fission gases. The spray system consists of a series of nozzles which are installed on the lower side of the top shield of the reactor over the fuel elements. A tank of heavy water pressurized with gas is available to provide pressure for this spray cooling. It is seen from Fig. 16 that the spray cooling need be continued only for a limited period of time, but of course it could be continued indefinitely by switching to the light water mains. The gas-tight building provides further assurance that such an event could not lead to the discharge of radioactive gas to the environs. As a result of the inherent safety of the reactor and the nature of the building, it is believed that this facility possesses the largest degree of protection against mishap so far devised for a high flux reactor.

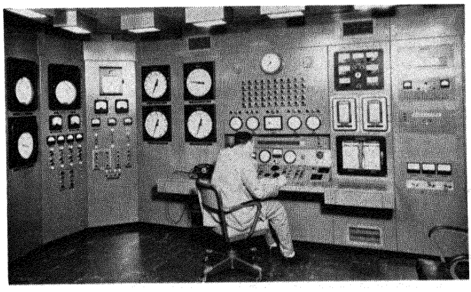

Figure 17. Control room

All of the control operations of the reactor, including the manipulation of all valves, pumps, and flow systems, is centralized in a control room. It is a feature of the control system that all vacuum tubes and electronic components are collected in this one place. An enunciator board provides visual indication for the malfunctioning of any of 50 points of the system. Figure 17 is a photograph of the control room.

Experimental Facilities

Two thermal columns are provided since experience had indicated that these are very versatile facilities. They can be used to provide beams of thermal neutrons with high cadmium ratios. Also, they provide places in which fairly large objects, up to 16 in. in diameter, can be irradiated. Eight beam holes on a horizontal plane are provided, all with the central axis at the same height from the working floor. This permits a certain amount of flexibility in moving apparatus from one beam hole to another without having to reconstruct the apparatus supports. Two holes are provided, $5\frac{3}{4}$ inches in diameter, which pass straight through the reactor from face to face of the shield. These can be used either as the source of a tangent beam, which does not look directly in the reactor core, or they can be used for the installation of engineering-type experiments in which the through hole is very useful for the passage of pipes for the cooling fluid. Two tubes going through the edge of the core are provided to enable the quick irradiation of samples. These tubes are furnished with a helium gas system which carries a cartridge in or out of the reactor in a very short time. The top of the reactor is provided with a number of openings which carry aluminum tubes or thimbles into the heavy water or into the graphite. Any unused fuel positions also can be equipped with thimbles for irradiation purposes. Normally, 11 vertical thimbles are available in the heavy water zone and 17 in the graphite zone. Beneath the reactor, there are two tunnels which pass from side to side through the graphite reflector. These have proved to be very convenient places for irradiating materials when the highest flux is not required. The cadmium ratio in this position is about 2000. Ionization chambers for the normal operation of the machine are installed in eight tubes which enter the graphite zone of the reactor horizontally. These are reserved exclusively for reactor operation.

Available Neutron Flux

Measurements have been made on the neutron flux in all parts of the machine when it is operated at 1000

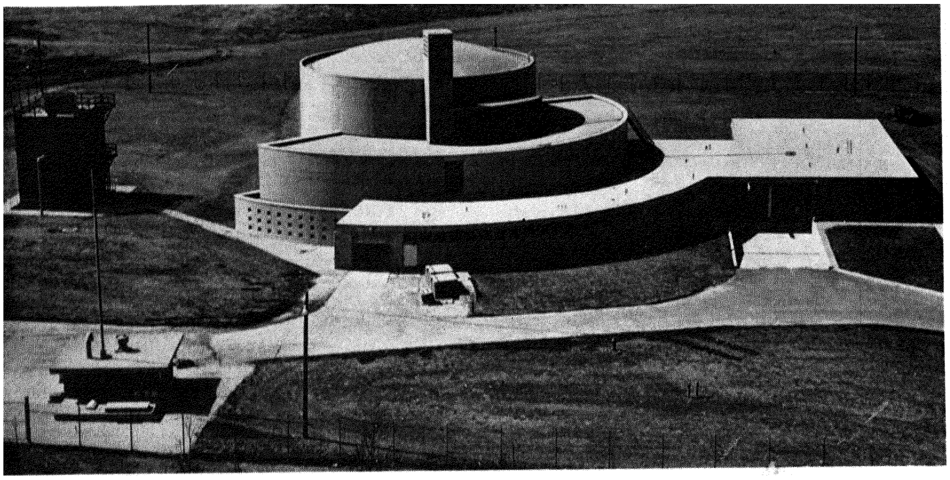

Figure 18. Reactor building

kw. As was expected, the thermal neutron flux rises a small amount in the moderator just outside of the core.

Where fast neutron flux is required for experiments, it is provided by installing a fuel element in which the uranium bearing plate has been formed into a cylinder. A thimble extending from outside the shield passes through the middle of the cylindrical fuel element and provides a fast flux approximately equal to the thermal flux at the fuel element.

Table I gives the thermal neutron flux at typical places in the reactor.

Table I

	Neutron flux (n/cm²/sec)	
Location	1000 kw	4000 kw
Vertical D_2O thimble	1.7×10^{13}	6.2×10^{13}
Vertical graphite thimble	6.5×10^{11}	2.6×10^{12}
Thermal column	2×10^{12}	8×10^{12}
Horizontal beam hole	1.5×10^{13}	6×10^{13}
Isotope tunnel	1.2×10^{12}	4.8×10^{12}

Of greatest interest to experimenters is the magnitude of the flux which can be obtained at points outside the shield. The fact that this shield has been made as thin as practical is of considerable assistance here. For instance, at 1000 kw by opening the thermal column to its full width and installing an appropriate collimator a thermal neutron flux of 6×10^9 n/cm²/sec is obtained in the room. A strong fast flux for experiments is obtained by interposing an uranium converter plate in this beam. Installation of a collimator tube with a slit 0.25 inches wide and a length of 106 inches in one of the horizontal holes produces a collimated beam in the room of intensity 3.4×10^8 n/cm²/sec.

Cost

Costs for the reactor and all of its auxiliaries were accumulated during construction. The major part of the cost of the whole facility is in the building and the auxiliary laboratories. The reactor, exclusive of building, cost $1,051,000. This does not include the cost of the seven tons of heavy water but does include the $15,000 fabrication cost for a set of fuel elements. The cost cited does include plugs for the experimental openings, collimators and other special thimble arrangements. It also includes a fuel coffin, an electrically operated truck, and other handling tools. The largest single component of cost, $403,000, was the erection of the biological shield, the installation of the graphite, and the installation of the reactor tank.

Operation

No manual manipulations are required to keep the reactor operating in a steady fashion. A normal operating crew consists of a supervisor and two control room operators. This staff also prepares samples for irradiation and removes and ships all irradiated samples. Electric power consumption by the reactor and its auxiliaries is only 80 kw and the consumption of other supplies is negligible. Because of the large heat capacity of the tank of heavy water, it is possible to dispense with pumps or other machinery for shutdown cooling. Thus operators are not required to be in attendance if the machine is taken out of service for a short time.

REFERENCES

1. Untermyer, S., *Plans for the New Argonne Research Reactor, CP-5*, Nucleonics, *12*: 12-15 (January 1954).
2. Weills, J. T., *A Description of the Argonne National Laboratory Research Reactor CP-5*, Chemical Engineering Progress Symposium Series No. 11, Nuclear Engineering, Part I, 50: 213-227 (1954).
3. Dietrich, J. R., and Zinn, W. H., P/481, *Experimental Determinations of the Self-Regulation and Safety of Operating Water-Moderated Reactors: Results and Motion Picture Records*, Volume 13, session 6.2, these Proceedings.

Record of Proceedings of Session 10A.1

FRIDAY AFTERNOON, 12 AUGUST 1955

Chairman: Mr. M. Oliphant (Australia)
Vice-Chairman: Mr. L. Kowarski (UNESCO)
Scientific Secretaries: Messrs. D. J. Littler and I. Ulehla

PROGRAMME

P/620 Reactor for physical and technical investigations............... G. N. Kruzhilin
P/402 The experimental facilities of E.443............. H. J. Grout and F. W. Fenning
DISCUSSION

Mr. G. N. Kruzhilin (USSR) presented paper P/620.

Mr. F. W. Fenning (UK) presented paper P/402.

DISCUSSION OF PAPERS P/620 AND P/402

Mr. H. Brooks (USA): This question is addressed to the Soviet paper, P/620. What is the fast flux and the epithermal flux available in this reactor?

Mr. Kruzhilin (USSR): The thermal-neutron flux has been measured experimentally at 8×10^{13} with a minimum charge of uranium-235. In later testing operations, with a large load of structural materials, the uranium-235 charge was increased, so that the maximum flux, of course, fell somewhat. In practice, we use a flux of 4 to 5×10^{13}. A question was asked about the fast neutron flux. Unfortunately, I do not have this figure.

Mr. A. M. Weinberg (USA): I should like to address this question to the Soviet paper. Are there any particular provisions made for gas-tight containment for the RPT reactor? I am referring to the fact that both in the United States and in the United Kingdom the strong trend is towards putting reactors of high power into buildings which are essentially gas-tight. I am asking whether, in the Soviet Union, the same practice is encountered.

Mr. Kruzhilin (USSR): Research reactors in the Soviet Union are built without gas-tight housing. The reactor I described also has no gas-tight housing.

Mr. P. W. Mummery (UK): I should like to ask Mr. Kruzhilin a question. I noted with interest that in the plan of this reactor his loop experiments appear in the reflector outside the core. Presumably the reason for this is that he considers the flux there as adequate, and the effect of reactivity is much smaller than if it were in the core. Is this correct?

Mr. Kruzhilin (USSR): The reflector affords greater possibilities of installing the loops and the thermal-neutron flux is adequate for the purposes of the research in which we are engaged.

Mr. H. Kronberger (UK): I should like to ask a question about the fuel elements and the vibration. Is this vibration caused by fluctuations in the pump or by the design of the coolant channel? If it is the former, would not a buffer tank have solved the problem?

Mr. Kruzhilin (USSR): The vibration I mentioned is of a local nature and is confined to the fuel rod channel. The fuel elements are installed in this channel in a vertically suspended position and in conditions conducive to vibration. The cause of the vibration is the flow of water through the channel.

Mr. J. M. Harrer (USA): I should like to direct a question to Mr. Fenning. We are interested in the enclosure of his reactor, the steel pressure-type building. I should like to know if he would care to comment on the specifications to which it is being built, or what tests it has been given or will be given before he goes into operation with the reactor.

Mr. H. J. Grout (UK): This pressure-type building is being built to British standard code 1500. It will be tested to full working pressure by air and we shall also conduct a leak test on the completed structure.

PEACEFUL USES OF ATOMIC ENERGY:

Proceedings of the International Conference in Geneva, August 1955.

The following is a complete listing of the sixteen volumes which comprise this publication, together with the main subjects covered by each volume.

VOLUME 1

The World's Requirements for Energy: The Role of Nuclear Power

World Energy Needs
Capital Investment Required for Nuclear Energy
The Role of Thorium
The Role of Nuclear Power in the Next 50 Years
Education and Training of Personnel in Nuclear Energy
Economics of Nuclear Power

VOLUME 2

Physics, Research Reactors

Special Topics in Nuclear Physics
Fission Physics
Research Reactors
Research Reactors and Descriptions

VOLUME 3

Power Reactors

Experience with Nuclear Power Plants
Fuel Cycles
Design of Reactors for Power Production
Power Reactors, Prototypes

VOLUME 4

Cross-Sections Important to Reactor Design

Equipment and Techniques Used in Measuring Cross-Sections Important to Reactor Design
Cross-Sections of Non-Fissionable Materials: Delayed Neutrons
Cross-Sections of Fissionable Materials
Properties of Fissionable Materials

VOLUME 5

Physics of Reactor Design

Integral Measurements
Resonance Integrals
Fission Product Poisoning
Criticality in Solutions
Zero Energy and Exponential Experiments
Zero Energy Experiments on Fast Reactors and Reactor Kinetics
Reactor Theory

VOLUME 6

Geology of Uranium and Thorium

Occurrence of Uranium and Thorium
Prospecting for Uranium and Thorium

VOLUME 7

Nuclear Chemistry and the Effects of Irradiation

The Fission Process
Facilities for Handling Highly Radioactive Materials
Chemistry of Fission Products
Heavy Element Chemistry
Effects of Radiation on Reactor Materials
Effects of Radiation on Liquids
Effects of Radiation on Solids

VOLUME 8

Production Technology of the Materials Used for Nuclear Energy

Treatment of Uranium and Thorium Ores and Ore Concentrates
Production of Metallic Uranium and Thorium
Analytical Methods in Raw Material Production
Production Technology of Special Materials

VOLUME 9

Reactor Technology and Chemical Processing

Waste Disposal Problems
Metallurgy of Thorium, Uranium and their Alloys
Fabrication of Fuel Elements
Liquid Metal Technology
Chemical Aspects of Nuclear Reactors
Chemical Processing of Irradiated Fuel Elements
Waste Treatment and Disposal
Separation and Storage of Fission Products

VOLUME 10

Radioactive Isotopes and Nuclear Radiations in Medicine

Isotopes in Medicine and Biology
Therapy
Diagnosis and Studies of Disease

VOLUME 11

Biological Effects of Radiation

Modes of Radiation Injury and Radiation Hazards
Mechanisms of Radiation Injury
Protection and Recovery
Genetic Effects
Human Implications

VOLUME 12

Radioactive Isotopes and Ionizing Radiations in Agriculture, Physiology, and Biochemistry

Isotopes in Agriculture
Radiation-induced Genetic Changes and Crop Improvement
Tracer Studies in Agriculture
Animal Physiology
Plant Biochemistry
General Biochemistry

VOLUME 13

Legal, Administrative, Health and Safety Aspects of Large Scale Use of Nuclear Energy

Legal and Administrative Problems
Reactor Safety and Location of Power Reactors
Safety Standards and Health Aspects of Large Scale Use of Atomic Energy

VOLUME 14

General Aspects of the Use of Radioactive Isotopes: Dosimetry

Isotopes in Technology and Industry
General Uses, Production and Handling of Radioactive Isotopes
Dosimetry

VOLUME 15

Applications of Radioactive Isotopes and Fission Products in Research and Industry

Radioactive Isotopes in Research
Radioactive Isotopes in Control and Technology
Fission Products and their Applications

VOLUME 16

Record of the Conference

Opening of the Conference and the Presidential Address
International Co-operation in the Peaceful Uses of Atomic Energy
Closing Presidential Address

SALES AGENTS FOR UNITED NATIONS PUBLICATIONS

Editorial Sudamericana S.A., Alsina 500, Buenos Aires.

AUSTRALIA

ARGENTINA

H. A. Goddard, 255a George St., Sydney; 90 Queen St., Melboufne.
Melbourne University Press, Carlton N.3, Victoria.

AUSTRIA

B. Wüllerstorff, Markus Sittikusstrasse 10, Salzburg.
Gerold & Co., Graben 31, Wien.

BELGIUM

Agence et Messageries de la Presse S.A., 14-22 rue du Persil, Bruxelles.
W. H. Smith & Son, 71-75, boulevard Adolphe-Max, Bruxelles.

BOLIVIA

Librería Selecciones, Casilla 972, La Paz.

BRAZIL

Livraria Agir, Río de Janeiro, Sao Paulo and Belo Horizonte.

CAMBODIA

Papeterie-Librairie Nouvelle, Albert Portail, 14 Avenue Boulloche, Pnom-Penh.

CANADA

Ryerson Press, 299 Queen St. West, Toronto.
Periodica, Inc., 5112 Ave. Papineau, Montreal.

CEYLON

Lake House Bookshop, The Associated Newspapers of Ceylon, Ltd., P. O. Box 244, Colombo.

CHILE

Librería Ivens, Casilla 205, Santiago.
Editorial del Pacifico, Ahumada 57, Santiago.

CHINA

The World Book Co., Ltd., 99 Chungking Road, 1st Section, Taipeh, Taiwan.
Commercial Press, 211 Honan Rd., Shanghai.

COLOMBIA

Librería América, Medellín.
Librería Nacional Ltda., Barranquilla.
Librería Buchholz Galería, Bogotá.

COSTA RICA

Trejos Hermanos, Apartado 1313, San José.

CUBA

La Casa Belga, O'Reilly 455, La Habana.

CZECHOSLOVAKIA

Ceskoslovensky Spisovatel, Národni Trida 9, Praha 1.

DENMARK

Einar Munksgaard, Ltd., Norregade 6, Kobenhavn, K.

DOMINICAN REPUBLIC

Librería Dominicana, Mercedes 49, Ciudad Trujillo.

ECUADOR

Librería Científica, Guayaquil and Quito.

EGYPT

Librarie "La Renaissance d'Egypte," 9 Sh. Adly Pasha, Cairo.

EL SALVADOR

Manuel Navas y Cía., 1a. Avenida sur 37, San Salvador.

FINLAND

Akateeminen Kirjakauppa, 2 Keskuskatu, Helsinki.

FRANCE

Editons A. Pedone, 13, rue Soufflot, Paris V.

GERMANY

Elwert & Meurer, Hauptstrasse 101, Berlin-Schoneberg.
W. E. Saarbach, Gereonstrasse 25-29, Köln (22c).
Alexander Horn, Spiegelgasse 9, Wiesbaden.

GREECE

Kauffmann Bookshop, 28 Stadion Street, Athens.

HAITI

Librairie "A la Caravelle," Boîte postale 111-B, Port-au-Prince.

HONDURAS

Librería Panamericana, Tegucigalpa.

HONG KONG

The Swindon Book Co., 25 Nathan Road, Kowloon.

ICELAND

Bokaverzlun Sigfusar Eymundssonar H. F., Austurstraeti 18, Reykjavik.

INDIA

Orient Longmans, Calcutta, Bombay, and Madras.
Oxford Book & Stationery Co., New Delhi and Calcutta.
P. Varadachary & Co., Madras.

INDONESIA

Pembangunan, Ltd., Gunung Sahari 84, Djakarta.

IRAN

"Guity", 482 Avenue Ferdowsi, Teheran.

IRAQ

Mackenzie's Bookshop, Baghdad.

ISRAEL

Blumstein's Bookstores Ltd., 35 Allenby Road, Tel-Aviv.

ITALY

Librería Commissionaria Sansoni, Via Gino Capponi 26, Firenze.

JAPAN

Maruzen Company, Ltd., 6 Tori-Nichome, Nihonbashi, Tokyo.

LEBANON

Librairie Universelle, Beyrouth.

LIBERIA

J. Momolu Kamara, Monrovia.

LUXEMBOURG

Librairie J. Schummer, Luxembourg.

MEXICO

Editorial Hermes S.A., Ignacio Mariscal 41, México, D.F.

NETHERLANDS

N.V. Martinus Nijhoff, Lange Voorhout 9, 's-Gravenhage.

NEW ZEALAND

United Nations Association of New Zealand, C.P.O. 1011, Wellington.

NORWAY

Johan Grundt Tanum Forlag, Kr. Augustsgt. 7A, Oslo.

PAKISTAN

Thomas & Thomas, Karachi.
Publishers United Ltd., Lahore.
The Pakistan Cooperative Book Society, Dacca and Chittagong (East Pak.).

PANAMA

José Menéndez, Plaza de Arango, Panamá.

PARAGUAY

Agencia de Librerías de Salvador Nizza, Calle Pte. Franco No. 39-43, Asunción.

PERU

Librería Internacional del Peru, S. A., Lima and Arequipa.

PHILIPPINES

Alemar's Book Store, 749 Rizal Avenue, Manila.

PORTUGAL

Livraria Rodrigues, 186 Rua Aurea, Lisboa.

SINGAPORE

The City Book Store, Ltd., Winchester House, Collyer Quay.

SPAIN

Librería Bosch, 11 Ronda Universidad, Barcelona.
Librería Mundi-Prensa, Lagasca 38, Madrid.

SWEDEN

C. E. Fritze's Kungl. Hovbokhandel A-B, Fredsgatan 2, Stockholm.

SWITZERLAND

Librairie Payot S.A., Lausanne, Genève.
Hans Raunhardt, Kirchgasse 17, Zurich 1.

SYRIA

Librairie Universelle, Damas.

THAILAND

Pramuan Mit Ltd., 55 Chakrawat Road, Wat Tuk, Bangkok.

TURKEY

Librairie Hachette, 469 Istiklal Caddesi, Beyoglu, Istanbul.

UNION OF SOUTH AFRICA

Van Schaik's Bookstore (Pty.), Ltd., Box 724, Pretoria.

UNITED KINGDOM

H.M. Stationery Office, P. O. Box 569, London, S.E. 1 (and at H.M.S.O. Shops).

UNITED STATES OF AMERICA

International Documents Service, Columbia University Press, 2960 Broadway, New York 27, N. Y.

URUGUAY

Representación de Editoriales, Prof. H. D'Elía, Av. 18 de Julio 1333, Montevideo.

VENEZUELA

Librería del Este, Av. Miranda No. 52, Edf. Galipan, Caracas.

VIET-NAM

Papeterie-Librairie Nouvelle, Albert Portail, Boîte Postale 283, Saigon.

YUGOSLAVIA

Drzavno Preduzece, Jugoslovenska Knjiga, Terazije 27/11, Beograd.
Cankarjeva Zalozba, Ljubljana, Slovenia.

Orders and inquiries from countries where sales agents have not yet been appointed may be sent to: Sales and Circulation Section, United Nations, New York, U.S.A.; or Sales Section, United Nations, Palais des Nations, Geneva, Switzerland.